MINERALOGY, GEOCHEMISTRY, PETROLOGY AND PETROGENESIS OF THE MEYDAN-ZILAN (ERCIS-VAN, TURKEY) AREA VOLCANIC ROCKS

A thesis submitted for the degree of
Doctor of Philosophy

by Mehmet ARSLAN

B.Sc., Selcuk University(Konya, Turkey)

Department of Geology & Applied Geology

University of Glasgow

January 1994

ProQuest LLC.
789 East Eisenhower Parkway
P.O. Box 1346
Ann Arbor, MI 48106 – 1346

THESIS DECLARATION

The material presented in this thesis is the result of research carried out between November 1990 and January 1994 in the Department of Geology and Applied Geology, University of Glasgow, under the supervision of Professor B.E. LEAKE.

This thesis is based on my own independent research and any published or unpublished material used by me has been given full acknowledgement in the text.

Mehmet ARSLAN

January, 1994

I certify that Mehmet ARSLAN has undertaken the bulk of the work involved in this thesis. Specifically; background geology, sample preparation, examinations and analyses, and their interpretation. I have assisted with advice and help of a general, technical, conceptual nature, as would be expected in the course of normal Ph.D. supervision and advice. Mehmet ARSLAN has written the thesis himself, and is responsible for its content.

Professor B. E. LEAKE

ACKNOWLEDGEMENTS

I would like to start by thanking the Turkish Ministry of Education for giving me the opportunity to undertake this degree and providing funding for my research.

Many thanks go to my supervisor Professor B. E. Leake for his patience, encouragement and helpful supervision throughout my research. I am also greatly indebted to the academic and technical staff in the Glasgow University, Geology&Applied Geology Department for all their assistance: Dr. C. Gribble, Prof. M. Russell, Dr. B. Bell, Dr. T. Dempster, Dr. C. Farrow, Dr. J. Harris, Dr. C. Braithwaite, J. MacDougall, Pete, Dugie, Murdo, William, Alan, Jim, Douglas, Archie, Roddy, John and Robert.

I am indebted to Dr. B. Bell for his help with volcanic petrology, to Dr. R. Ellam for help with strontium isotope geochemistry, to Dr. T. Fallick for help with oxygen isotope geochemistry, and Dr. C. Farrow for help with computing. I am also very grateful to Prof. H. Bas for introducing me this field and his supervision throughout my research in Turkey.

Thanks to R. Morrison for logistic support, R. McDonald who helped with microprobe analyses, J. Gallagher for running major and trace element analyses, and to M. MacLeod, D. Turner and W. Higginson for their assistance in the geochemistry laboratory, to J. Gilleece and A. Jones supplied thin section and polished sections, to Tracy for analyzing REE samples on ICP-MS, and Ann and Julie for their assistance in the isotope geology unit laboratories at SURRC.

Thanks also to all post grads, Huseyin, Veysel, Bulent, Kerim, Rona, Campbell, Helen, David, Paul, Vojtech, Ali, Gary, John, Robert, Richard, Ahmed, Abudrahman, Daud, Esam, Amar, Zafer, Chris, Mark, Shuang at the department, and to the Turkish Students' Society for social support during my stay in Glasgow.

I would finally like to express my thanks to my mother Elif and father Hidayet, brother Nihat and sisters Saadet and Fatma for all the understanding, support and love they have shown me over the years.

CONTENTS

Page No

LIST OF FIGURES

Page No

CHAPTER 1

CHAPTER 2

CHAPTER 4

CHAPTER 5

CHAPTER 6

CHAPTER 7

LIST OF TABLES

Page No

CHAPTER 3

CHAPTER 4

CHAPTER 5

CHAPTER 6

CHAPTER 7

LIST OF PHOTOS

Page No

CHAPTER 3

CHAPTER 4

ABSTRACT

The stratigraphy in the area starts with the Upper Miocene Kizildere formation containing carbonates, sandstone, tuff and tuffite, followed by Pliocene-Quaternary volcanic rocks. The sediments have been studied in some detail.

The volcanic rocks are divided into three main suites; (1) a calcalkaline suite consisting of Kizildere lavas, andesite, trachyandesite, dacite, agglomerate, ignimbrite, rhyolite dome and dykes, pumice and the Gurgurbaba lava; (2) the Meydan alkaline suite containing alkali olivine basalt, hawaiite, mugearite, benmoreite and trachyte; (3) a transitional suite containing the Aladag lava and the Zilan lava. All of these suites have characteristic mineralogical and chemical compositions.

(1) In the calcalkaline suite, andesite, trachyandesite and dacite show a variety of petrographical disequilibrium textures reflecting contamination and magma mixing processes. The crystallization conditions obtained from different mineralogical assemblages range 786-1074°C and fO_2=1.56-1.98 for andesite, 1015-1089°C for trachyandesite, 724-828(±75)°C, fO_2=1.71-1.76 and P=5.08-8.90(±0.5) kbar for dacite. Ignimbrites indicate high temperature emplacement with moderate to strongly welded textures, and crystallization conditions of 750-921°C and fO_2=1.42-2.29. A rhyolite dome and dykes also show evidence of disequilibrium textures. Mineral thermobarometers for the rhyolite dome and dykes gave 750-850°C, fO_2=2.21-2.29 and P=3-3.5 kbar. Pumice tephra formed as pyroclastic fall and surge by mainly Plinian- and Phreatoplinian-type explosive productions.

(2) The Meydan alkaline lavas show evolution from alkaline olivine basalt to trachyte, with lack of ilmenite and alkali feldspar indicating relatively high oxygen fugacity. Mugearite and trachyte show disequilibrium textures as a result of magma mixing and disequilibrium crystallization. Olivine-liquid thermometers yielded crystallization temperatures of 1142-1248(±40) for alkali olivine basalt, 1025-1141(±40) for hawaiite, 1037-1085(±40) for mugearite, and 913-964(±40) for benmoreite. Coexisting magnetite and ilmenite in trachyte gave values of 825-1056°C and fO_2=1.28-1.38 relative FMQ.

(3) In the transitional suite, the Aladag lava formed under low and falling oxygen fugacity, and at probably 869-1017°C and 14 kbar. Crystallization temperature in the Zilan lava ranges between 1073 and 1095°C.

Plagioclase $\delta^{18}O$ values(7-9‰) in the Meydan alkaline lavas suggest a contribution from ^{18}O-rich continental crust during the evolution of the rocks. The degree of contamination is large for the evolved rocks.

Furthermore, the variation of $^{87}Sr/^{86}Sr$(0.7048-0.7056) in the Meydan suite is evidence of open-system processes. $^{87}Sr/^{86}Sr$ values from the most primitive samples are close to those characterizing an enriched mantle source. The $^{87}Sr/^{86}Sr$(~0.7050) of the basaltic magma suggest that it may have undergone some interaction with crust prior to its emplacement into a crustal magma chamber. Small Sr-isotopic variations in the Meydan suite suggest fractionation proceeded with assimilation of crustal rocks. Although isotopic data contradicts with an AFC process in the evolution of the calcalkaline suite, minor amounts of contamination have occurred in differentiated rocks. O- and Sr-isotope covariations suggest a two stage process of (a) source contamination controlled by hydrous flux from a subducted slab which gives rise to a large range of Sr isotopes, and (b) followed by crustal contamination and fractional crystallization.

In the Meydan alkaline suite, mugearite, benmoreite and trachyte magmas were modified by open-system fractionation and replenishment with increasing fractional crystallization as a result of a long period in the magma chamber. Crystal fractionation was the main factor controlling the variations in bulk compositions. Hawaiites have been derived from an alkali olivine basalt parent by fractionation of an augite-dominated assemblage at high pressure. Olivine and titanomagnetite fractionations are also evident. Plagioclase and apatite fractionations were significant in the more evolved rocks. Generally, alkali olivine basalt represent fractionated liquids derived from reservoirs at upper mantle levels. The degree of partial melting for the near-primary basalt samples was calculated as between 4% and 12%. The basaltic lavas are interpreted as large degree melts of a mantle source enriched in LILE, LREE and $^{87}Sr/^{86}Sr$.

Parental magma of the Meydan lavas may have undergone medium to high pressure fractionation of olivine, augite and titanomagnetite, followed by low pressure olivine, augite, plagioclase and titanomagnetite fractionation. The chemical variability of the rocks is controlled by open system fractionation and crustal contamination±magma mixing. The enrichments in Ba and depletions in Nb are most likely the result of fluid metasomatism of mantle material. Therefore, the chemical and isotopic variation of the Meydan alkaline lavas reflect derivation from a variably enriched subcontinental lithosphere.

Andesite, trachyandesite and dacite(medium-K suite) are cogenetic and related to each other by mainly fractional crystallization and lesser contamination±magma mixing during the evolution of crustal magma chambers. Geochemical variations from andesite to trachyandesite reflect fractional crystallization(and contamination±mixing) within the mid to

lower crust whereas variations from trachyandesite to dacite resulted from upper crustal processes. Hornblende-dominated fractionation was the dominant process in the evolution of the suite. Trachyandesite and dacite formed by low pressure fractional crystallization and magma mixing. Lower crustal contamination was significant in causing the compositional variation from parent magma to andesite. The lower crustal contribution to parental magma is probably a partial melt of subducted-slab derived material. Therefore crustal differentiation controlled their eruptive compositions but the extent of contamination was limited. Contamination involved incorporation of partial melts of crustal wall rock, producing selective enrichments in certain incompatible elements. Moreover, upper crustal contamination caused significant enrichments of Rb and Th in evolved magmas. Mineralogical and petrochemical data suggests disequilibrium due to magma mixing which is also supported by mass balance modelling. Thus magmas behaved as open-system in the evolution of trachyandesite and dacite. Parental magma of the suite may have resulted from greater fluxing of mantle by subducted slab-derived fluids. The composition of this parental magma has been subsequently affected by crustal processes.

In high-K suite(ignimbrite, rhyolite dome and dykes, pumice tephra, and Gurgurbaba lava), chemical variations indicate the involvement of fractional crystallization, magma mixing, crustal melting, and the complexing of volatiles and incompatible elements during magmatic degassing. Generally, the rocks are non-minimum melts. The geochemical data points to an origin by fractional crystallization of a hybrid magma with mantle and crustal components. Differentiation of liquids involved biotite, amphibole, plagioclase±K-feldspar, and Fe-Ti oxides. Pumice represent the most fractionated liquids. Bulk magmas of the Gurgurbaba lava and pumices were compositionally stratified in a magma chamber that shows a capping layer of crystal-poor rhyolitic magma underlain by relatively crystal-rich rhyolitic liquids. Sudden fluctuations in the volatile and chemical budget during explosive eruptions have promoted brief periods of rapid crystallization along the magma chamber walls. The parental magmas of the suite may have been derived as partial melts of intermediate to transitional high-K calcalkaline, metaigneous rocks in the continental crust. These source material may have been derived from enriched subcontinental lithosphere.

The thesis contains microprobe analyses of olivine, augite, opx, plagioclase, K-feldspar, hornblende, kaersutite, biotite, magnetite and ilmenite, chemical analyses of sedimentary and volcanic rocks, REE analyses of rocks, whole-rock $^{87}Sr/^{86}Sr$, $\delta^{18}O$ of mineral separates, and a new geological map of the area.

CHAPTER 1. INTRODUCTION

1.1. INTRODUCTION

Eastern Anatolia is a high region with more than half of the area lying at an elevation of about 1500 m. The late Cenozoic history of the region is dominated by volcanism which shows wide variation in space, time, and eruptive products. Alpine orogenesis in the area is considered to be result of the convergence of the African and European plates.

Collision zone volcanism in Eastern Anatolia is thought to have begun in the late Miocene(Innocenti *et al.*, 1976), and forms part of a volcanic province that occupies a zone 900 km long from eastern Turkey through Armenia into northeast Iran. The province attains its maximum width of 350 km in eastern Anatolia where it extends in a SW-NE direction from the Arabian foreland to the Kars Plateau on the Armenia border.

The volcanic rocks of Eastern Anatolia range in composition from calcalkaline to moderate-strongly alkaline types. Alkaline volcanic rocks are dominated by basanite, olivine basalt, hawaiite and more differentiated types whereas calcalkaline rocks are represented by various types of andesite, dacite, rhyolite and their pyroclastic rocks, ignimbrite and agglomerate.

The large volume of volcanic rocks makes Eastern Anatolia one of the few places in the world where it is possible to study variations in lava composition more or less continuously across most of the width of an active continent-continent collision zone. This research centres around the Meydan volcano north of Lake Van and covers about 350 km^2(Figure 1.1).

1.2. THE AIM OF THE RESEARCH

The aim of this research is to map the sequence of different volcanic rock types in the area, identify their mineralogical, petrographical, geochemical and isotopic characteristics, and use all the information, integrated together, to deduce the petrogenesis of the rocks, their sources, and the magmatic processes that have operated. An important aspect will therefore include consideration of current theories of petrogenesis of volcanic rocks and computer modelling of the magmatic evolution.

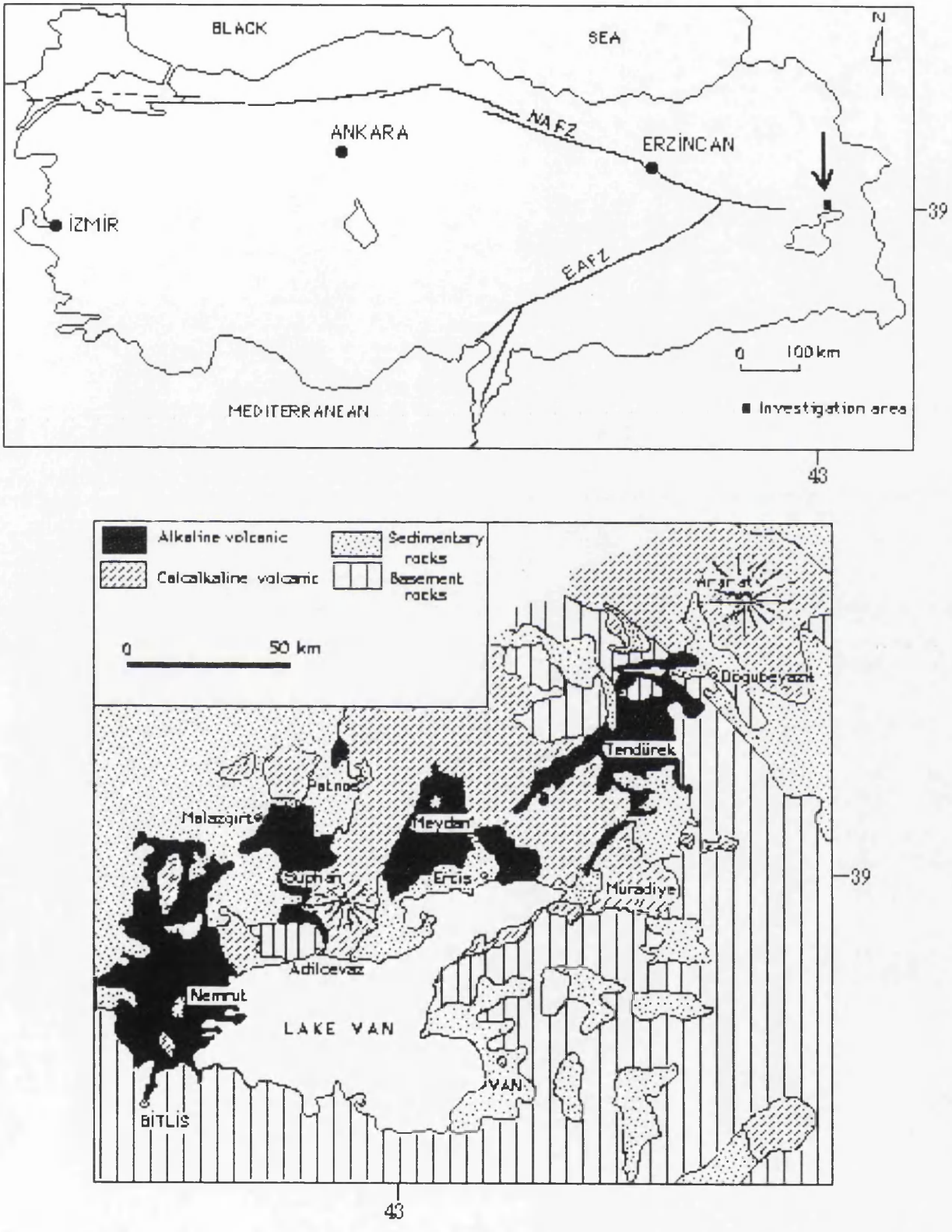

Figure 1.1. Location map of the investigated area. The geological sketch map of the region is from Innocenti *et al.* (1976).

1.3. PREVIOUS WORK

Previous studies in Eastern Anatolia include those of Blumental(1958) who described the regional setting within Turkey and presented a general work on the region. He gave a general map, delimiting areas of Lower Red tuffs, andesites, later basalts and surrounding sediments in Ararat region.

Agrali(1966) gave a detailed account of the geology and coal resources of Ercis-Zilan area. Altinli(1966) described the volcanism, orogeny and tectonism in the region as a part of producing the Van section of the geological map of Turkey at a scale of 1:500 000.

Ozpeker(1973) investigated petrologically and volcanologically the Nemrut volcano , especially on the basis of Maxcon(1936)'s early studies.

Ongur *et al.* (1974) investigated the geothermal potential of the Zilan valley and surrounding areas, and the geological evolution of the region.

Lambert *et al.* (1974) described a suite of lavas from Mount Ararat in terms of chemical petrology and petrogenesis. They recognized two distinct series(low Y and high Y) and discussed a subduction mechanism for the origin of the volcanics, and suggested a lithospheric shear zone theory.

Innocenti *et al.* (1976) contributed geological and volcanological data on the geotectonic evolution of Eastern Anatolia from Miocene to present, and studied in detail what happens when converging plate motions continue after the continental collision.

Saroglu and Guner(1979) considered the Caldiran fault and its part continuation as the Tutak fault. They prepared a morphotectonic map of the present investigation area. They showed the presence of strike-slip faults and emphasized the region as an earthquake zone. Turkunal(1980) compiled a summary of the geology of Eastern and Southeastern Anatolia.

Innocenti *et al.* (1980) described the geological and volcanological features north of Lake Van. They contributed to an interpretation of the deformation suffered by the Eurasian mass in a sector of maximum compression with particular emphasis on the significance of associated volcanism. Furthermore, in this study the mineralogy and petrology of volcanic rocks were given in detail.

Gulen(1980 and 1982) studied the Sr, Nd and Pb isotope systematics of the Mount Ararat and Suphan volcanic rocks, and deduced significant crustal contamination for the Suphan rocks but with no significant crustal contamination for the Ararat suites.

Saroglu and Guner(1981) outlined factors which effected the evolution of Eastern Anatolia. Taskin(1984) studied geology of perlite areas

around Meydandagi(Van-Ercis), Harmantepe village(Bitlis-Adilcevaz) and Koseler village(Agri-Patnos).

Karamanderesi *et al.* (1984) investigated the Zilan valley (Van-Ercis) in terms of possible geothermal potential, and studied the detailed geology of the area.

Guner(1984) studied the stratigraphy, geomorphology and evolution of Nemrut volcano. Saroglu and Yilmaz(1984) worked on the neotectonics of Eastern Anatolia and related igneous activity.

Tokel(1984) investigated crustal deformation mechanisms and the petrogenesis of young volcanic rocks in Eastern Anatolia. In this work, he applied Turcotte's(1983) model for Eastern Anatolia, and schematized possible deformation mechanisms during Neogene. In addition new ideas were suggested on the origin of volcanic rocks.

Aktimur(1986) made a geological and tectonic investigation of the Van-Ercis area using Landsat-4 TM(thematic mapper) pictures, and provided data for studies being carried out on the geothermal power resources of the region.

Guner and Saroglu(1987) studied Quaternary volcanism in Eastern Anatolia and its importance in terms of geothermal power. They investigated the stratigraphy and evolution of the major Quaternary volcanoes; Agri, Nemrut, Suphan and Tendurek.

Yilmaz *et al.* (1987) described the geology of the Solhan area with a view to understanding the environmental conditions during the initiation of the young volcanism within the general geological frame work of eastern Anatolia. They studied the volcanic sequence in the Solhan region together with the surrounding rock groups, and discussed their relative timing and the tectonic evolution of the region. Besides the petrographic investigation of volcanic rocks, and interpreting geochemical data he also noted the genetic meaning and importance of the volcanism which started to develop in the initial stage of neotectonism. He concluded that these volcanic rocks represent the first alkaline volcanic activity in Eastern Anatolia.

Yilmaz(1990) petrographically and geochemically compared the young volcanic rocks of western and eastern Anatolia, and concluded that the volcanic evolution of these two regions followed a similar pattern producing highly contaminated calcalkaline lavas at the beginning and evolving towards uncontaminated alkaline lavas at the end.

Ercan *et al.* (1990) reviewed previous work and provided data about common Quaternary and Neogene volcanic rocks in eastern and southeastern Anatolia. From geochemical, petrographical and other data they interpreted the genesis of volcanics in terms of plate tectonics.

Pearce *et al.* (1990) presented new geochemical, isotopic and isotopic age data for the Neogene collision volcanics of eastern Anatolia, and used the data to re-examine the nature and cause of compositional variations in space and time within the province. Having first placed the volcanism into its neotectonic and regional geological framework, they described the volcanology and petrology of the areas and then examined the major element, trace element and isotopic characteristics of the rocks, and deduced the petrogenesis and tectonic significance of the data.

1.4. SAMPLING AND ANALYTICAL METHODS

Sampling involved collection of fresh unweathered specimens from various localities taking particular care to ensure that the samples were clean. Samples were collected as widely as possible from different levels.

Thin sections have been analysed for mineral assemblages, proportions of minerals and matrix, rock texture and grain size distribution. For the grain size investigation, the microscope had a calibrated eye-piece micrometer. Throughout the study, modal analyses were made using a polarizing microscope with a Swift automatic point counter unit attached to its stage. The accuracy of the results depends largely on the numbers of minerals to be counted, the grain size of the mineral constituents and the degree of alteration and crystallization of minerals.

Chemical analyses were made by XRF analysis for both major and trace elements. The principle and practice of X-ray fluorescence are well documented(e.g., Norich and Chappell, 1977; Jenkins and De Vries, 1967) and the application to the determination of major and trace elements in geological samples have been described(Leake *et al.*, 1969; Harvey *et al.*, 1973). The first step consists of reducing the size of the samples into small, typically 0.8x0.5 cm chips and then crushing down to 100 mesh for major elements and 250 mesh for trace elements. Conventional wet chemical analysis determined the FeO, H_2O and CO_2 .

Individual mineral analyses were carried out using a Cambridge Instrument Microscan 5 electron microprobe. This machine analyses the X-rays generated by an electron beam striking a finely polished and carbon coated thin sections(90μ thick). Each element produces a characteristic X-ray energy spectrum which is measured by a solid state detector for a counting time of 100 seconds. The total spectrum is processed by an on-line Data General Corporation Nova 2 microcomputer using a program developed by C.M. Farrow.

Details of analytical techniques including isotope studies are given in Appendix 1.

CHAPTER 2. GEOLOGICAL SETTING

2.1. NEOTECTONICS OF THE EASTERN ANATOLIA

The Eastern Anatolian Collision Zone is characterized at present by a plateau, a reflection of thick(50 km) continental crust, and diffuse, shallow seismicity which is indicative of active deformation(Pearce *et al.*, 1990). Tectonic movement of most of Anatolia is taking place to the west by right-lateral strike slip along the North Anatolian Fault(NAF) combined with left lateral strike slip along the East Anatolian Fault(EAF)(Nowroozi, 1972; McKenzie, 1972; Rotstein and Kafka, 1982; Jackson and McKenzie, 1984)(Figure 2.1). Current rates of slip are about 0.9 cm a^{-1} for the NAF and 0.2 cm a^{-1} for the EAF; these rates combine to give a westward movement rate for the Anatolian plate of 0.5 cm a^{-1} (Pearce *et al.*, 1990). The NAF and EAF(McKenzie, 1976) have been active since the mid-late Miocene(Ambraseys, 1970; Tatar, 1975; Ketin, 1976) and show a well-developed surface expression up to 1 km wide, with associated pull-apart basin(Hempton, 1982; Hempton and Dewey, 1983). Tectonic slip along these faults cannot remove much of the strain induced by the Arabian convergence of 1.4 cm a^{-1}(Dewey *et al.*, 1986) and other processes must therefore be active in accommodating the crustal shortening, such as crustal thickening or diffuse, distributed strike-slip faulting(Saroglu *et al.*, 1980; Yilmaz *et al.*, 1987).

The Eastern Anatolian Collision Zone(EACZ) region is cut by a complex of faults which are either SE-trending with a dominantly right-lateral strike slip displacements such as the Varto, the Caldiran and the Balik Golu Faults or NE to NNE-trending with dominantly right-lateral strike slip displacement such as the Malazgirt and Kagizman Faults. Faults of either set may have subordinate vertical displacements, often with a thrust sense(the Varto fault: Tchalenko, 1977). Some E-W trending faults with a mainly thrust displacement are also present, in particular the fault bounding the northern margin of Mus Basin, and its continuation into Lake Van(Pearce *et al.*, 1990). There is relatively minor folding of post middle Miocene strata north of the Bitlis Thrust Zone which is associated with ramp structures on thrusts. In general, however, there is no coherent network of linked faults and folds north of the Bitlis Thrust Zone and no obvious direct link between the North Anatolian and the Main Recent Fault of the Zagros(Tchalenko, 1977).

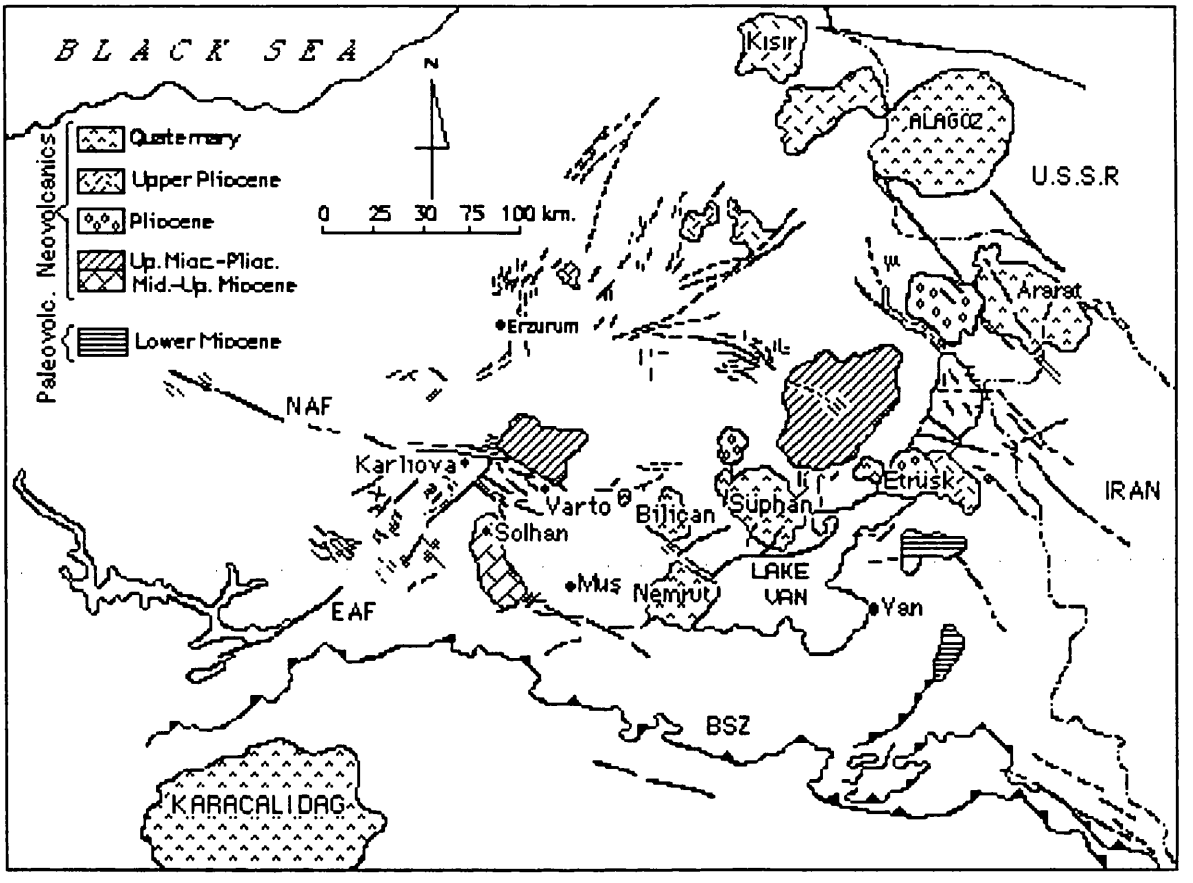

Figure 2.1. The tectonic map of Eastern Anatolia together with areal distribution of the products of the main volcanic centres. BSZ-Bitlis Suture Zone, NAF-North Anatolian Fault, EAF-East Anatolian Fault.

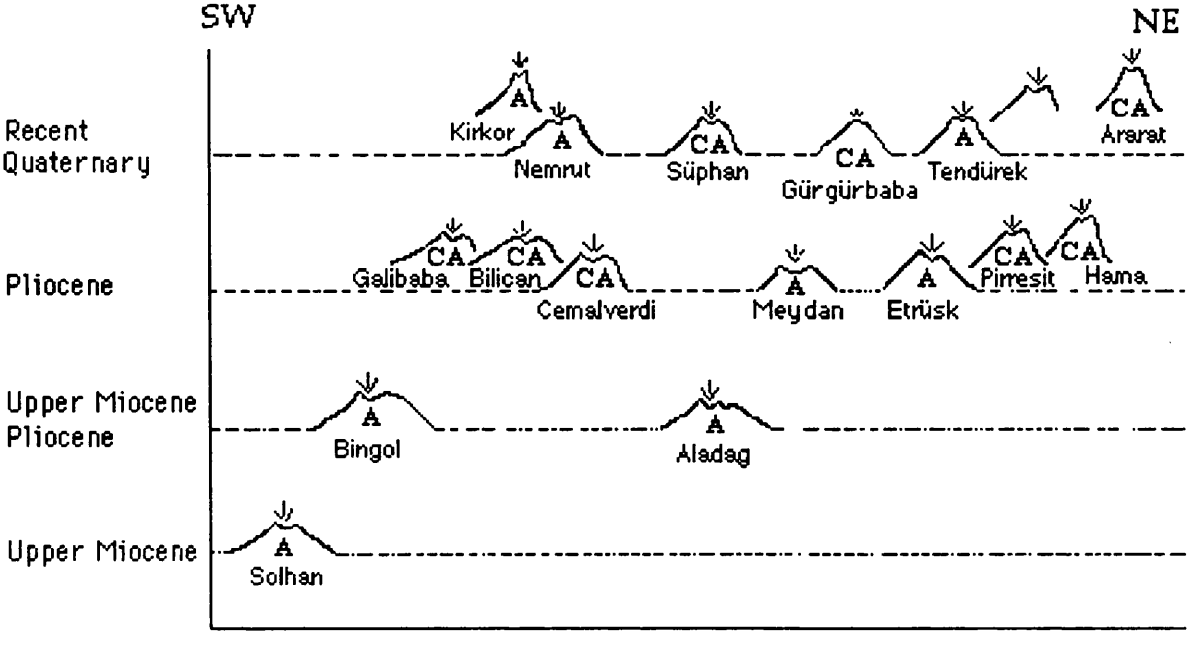

Figure 2.2. The main volcanic centres in Eastern Anatolia with their possible age relations(adapted from Yilmaz et al., 1987). The possible place of Meydan and Gurgurbaba volcanoes within this province from the investigated area. The geochemical nature of the volcanism is shown as either A-alkaline or CA-calcalkaline.

Normal faults and fissures in the EACZ are minor features compared with the other faults. N-S fissures control the morphology of the Karacalidag volcano on the Arabian foreland and fed the youngest, post-caldera eruptions of Nemrut, implying minimal E-W extension in the foreland and the southern margin of the EACZ(Pearce *et al.*, 1990). Two other volcanic edifices with N-S elongation are seen to the east of Cildir Golu on the northern margin of the Kars Plateau, indicating minor extension in this region. The Akcakale Graben, a small rift structure with N-S normal faults, which is located to the SW of Karacalidag, is another indicator of E-W extension, although this rift appears to act, at least in part, as a transfer structure between some of the outer thrusts of the Arabian foreland sedimentary sequence. The only normal fault- dominated structure in EACZ is the Baskale Graben east of Lake Van on the border between Turkey and Iran(Pearce *et al.*, 1990).

2.2. PRE-COLLISIONAL GEOLOGY OF EASTERN ANATOLIA

The Eastern Anatolian Collision Zone is characterized geologically by three terranes separated by suture zones containing melanges, accretionary complexes and flysh-molasse basins. The southernmost terrane is the para-autochthonous Arabian foreland which is made up of an almost continuous stratigraphic sequence of mainly shelf sediments of early Palaeozoic to Miocene age resting on a Precambrian basement. At its northern margin, termed the Foothills Structural Belt, the sedimentary rocks have experienced foreland-type thrusting and folding. The central terrane is the Bitlis Massif, an allochthonous terrane of Palaezoic metamorphic rocks, predominantly metasediments(Hall, 1976). The northern terrane is the Pontide belt which comprises a metamorphic basement of Palaezoic age overlain by Mesozoic shelf sediments which are in turn overlain by volcanosedimentary complexes of late Cretaceous and Eocene age, assumed, on the basis of their calcalkaline composition and continous linear character, to be subduction related(Peccerillo and Taylor, 1976). The Black Sea is thought to have formed as a marginal basin behind this Pontide arc. The Pontide Terrane experienced folding towards the end of the Eocene(Brinkman, 1976) and granitoid intrusion from the late Eocene to early Miocene.

Rocks of the Arabian foreland are seperated from the Bitlis Massif by a complex imbricated zone, the Bitlis Suture Zone, which contains ophiolitic and island arc assemblages of probably late Cretaceous age(Robertson and Aktas, 1984). Mafic lavas overlain by middle Eocene pelagic chalks within this zone show that an oceanic realm existed between

Arabia and the Bitlis microcontinent at that time, although the lavas are of transitional geochemical affinity, possibly indicating that they formed part of the crust of a small, extensional basin rather than a major ocean(Robertson and Aktas, 1984). No subduction related volcanic rocks younger than late Cretaceous have yet been identified within the Bitlis Suture Zone. Neogene strata, mainly volcanic rocks, obscure the contact between the Bitlis Massif and the Pontide Terrane. The limited exposure that does exist suggests that the pre-Neogene geology of this zone dominated by an accretionary complex of Eocene or younger age(Sengor and Yilmaz, 1981).

The Pontide Terrane is the product of northward subduction from the beginning of the late Cretaceous to the end of the Eocene. It clearly must have accommodated a large part of the convergence between Arabia and Eurasia during the Palaegone since there is little evidence for subduction of this age in the Bitlis Suture Zone(Pearce *et al.*, 1990). Collision of the Bitlis Massif with the Pontide Terrane to form the Pontide Suture Zone probably took place in the late Eocene, terminating the calkalkaline volcanism and causing the folding and subsequent granite plutonism in the Pontide Terrane (Sengor and Yilmaz, 1981).

2.3. TIMING OF THE COLLISION EVENT

The age of the initial contact between the northern edge of Arabia and the Anatolia-Pontide-Caucasus margin of Eurasia has not yet been concluded accurately. The minimum proposed age of 12 Ma(Sengor and Kidd, 1979; Sengor and Yilmaz, 1981) is based on: (1) The age of the transition from carbonate to flysch-molasse sedimentation seen in the passive margin sedimentary section that is preserved in the thrust belt south of the ophiolites of the BSZ; (2) The abrupt cessation of marine sedimentation throughout Eastern Anatolia at this time; (3) the cessation at this time of subduction related calcalkaline volcanism and plutonism in the Karkas-Jebel e Barez region of the Zagros to the east.

The maximum proposed age of late Eocene(Robertson and Aktas, 1984; Michard *et al.*, 1984) marks the end of subduction related calcalkaline volcanism in Eastern Anatolia, both in the Pontide volcanic province in the north and in the volcanic sequences within the BSZ in the south. It is generally agreed that an earlier, late Cretaceous ophiolite emplacement event seen in the foreland thrust belt south of the Bitlis Suture Zone(Hall, 1976), in the Southern Zagros(Hallam, 1976) and Oman(Gealy, 1977) does not require that the Arabia-Eurasia collision took place at that time, although it does require collision between the Arabian margin and an

ophiolitic forearc. The resumption of carbonate dominated sedimentation over the ophiolitic melange in the Arabian foreland south of the Bitlis Suture shows that the passive margin was essentially re-established during the Palaegone prior to the main collision event(Pearce *et al.*, 1990).

A further constraint on the age of initiation of the collision can also be obtained from the amount of convergence since collision. An estimate, made on the basis of the degree of crustal thickening(taken as 50%) multiplied by the width of the collision zone yields a value of 250-300 km(Pearce *et al.*, 1990).This estimate does not take account lateral slip which is assumed, from the limited total offset on the North Anatolian Fault(about 85±5 km: Sengor and Kidd, 1979), to make only a small contribution to the accommodation of the convergence. A similar value for the convergence is obtained by matching the Cretaceous ophiolites of the foreland margin with the possible equivalent complexes in Troodos-Hatay-Baer Bassit region of the Eastern Mediterranean that have experienced the late Cretaceous, but not the Neogene, emplacement event. At current convergence rates in the direction of maximum shortening of about 1.5 cm a^{-1} (Dewey *et al.*, 1986), collision would have to have started about 20 Ma ago(Pearce *et al.*, 1990).

While it is a common consequence of collision for turbiditic clastics to be deposited in a basin floored by the flexurally loaded continental lithosphere of the impinging passive margin, it is difficult to envisage how, at a yearly convergence rate of 1 cm or more, the initiation of crustal thickening could have been much older than the change from shallow water marine to orogenic clastic sedimentation(commonly flysch at the base) that is observed in the oldest thrust sheets nearest to the suture. It is possible , however, that the continents had made or almost made, contact at the end of Eocene and that eastern Anatolia in the Oligocene and early Miocene was marked by low angle subduction that generated little or no arc volcanism, while steeper subduction along the same margin in Iran continued to generate calcalkaline magmatism into the Miocene(Pearce *et al.*, 1990).

2.4. EVOLUTION OF COLLISION-RELATED VOLCANISM

In Eastern Anatolia, collision volcanism is found mainly at Karacalidag, the Mus Basin, Nemrut, Suphan, Bingol, Tendurek, Ararat and the Kars Plateau(Figure 2.1).

In the southern part, on the Arabian foreland, post-Pliocene volcanism has formed the complex basaltic shield of Karacalidag. This

volcano is fed by N-S trending fissures(Sengor, 1976) parallel to the nearby Akcakale Graben.

The central part between the latitudes of Erzurum and the southern edge of Lake Van, may contain the earliest collision volcanism. Yilmaz *et al.* (1987) proposed a stratigraphic age of ?middle to late Miocene for the initiation of volcanism in the Solhan-Mus district southwest of Erzurum, and Innocenti *et al.* (1976) suggested volcanism began in the Upper Burdigalian(early Miocene) (Figure 2.2). However, apart from one isolated early-middle Miocene isotopic date (13.1 Ma) published by Innocenti *et al.* (1976) from a lava near the Iranian border, the oldest set of isotopic ages(8.3-6.0 Ma) have been obtained by Innocenti *et al.* (1982b) from the Cat area south of Erzurum. The age of initiation of volcanism still requires confirmation. Innocenti *et al.* (1976) proposed that an initial calcalkaline phase of volcanism related to northward subduction took place before about 6 Ma, forming a broad volcanic belt parallel to the Bitlis Suture Zone. According to their model, continued volcanism in the same area gave more alkaline volcanic rocks with ages of 6-0 Ma in response to extensional tectonics. This concept of an early subduction related calcalkaline event is, however, by no means a consensus view(e.g., Sengor and Kidd, 1979; Pearce *et al.*, 1990).

The northern zone is dominated by the Kars Plateau, which covers an area of approximately 500 km^2 with an average elevation of 1.5 km. The volcanic sequence has been described by Innocenti *et al.* (1982b) as comprising lava flows with subordinate ignimbrite units and intercalated sediments giving ages from 6.9±0.9 to 1.3±0.3 Ma and comprising an early Aras lower sequence(7-4 Ma), followed by a Plateau sequence(4-2 Ma) and finally by scoriaceous spatter cones of Pleistocene age. Most of the plateau overlies shallow water sediments of Oligocene age which in turn probably overlie the Pontide Terrane over most of its area.

CHAPTER 3. STRATIGRAPHY

3.1. INTRODUCTION

The studied area is covered by Neogene-Quaternary volcanic rocks, associated with marine and continental sediments of the same age. Although the basement is not observed in the area, it probably extends outside the area investigated and comes in contact with units of the Bitlis Suture Zone(BSZ), in the south.

In the area investigated, the observed stratigraphy starts with a volcanosedimentary sequence consisting of limestone, sandstone, marl, lava flow, tuff and tuffite, and then follows the products of a continental type of volcanism until today. Volcanism is represented by three evolutionary cycles; early calcalkaline rocks, alkaline rocks and young calcalkaline rocks. Each of these cycles has its own petrological and geochemical characteristics.

The Aquitanian-Late Burdigalian sediments underlying the volcanic rocks do not contain any volcanic material. It has therefore been concluded that volcanic activity in the area started post Late Burdigalian(Innocenti *et al.*, 1980). In addition, the Serravalian age of the initiation of the volcanism has been confirmed by K-Ar dating on calcalkaline rocks, giving an age of 13.1 Ma(Innocenti *et al.*, 1976).

In the area studied, the stratigraphic sequence can be defined as follows in two sub-areas(Table 3.1). These sequences are given in the light of field observations and recorded radiometric ages.

3.2. ALTERED ANDESITE

The lowest lava underlying the Kizildere formation is characteristically brownish red and extensively hydrothermally altered. The lava covers a small area east of Gecekoyagi Tepe and underlies the alluvium of Zilan Dere. The lava is andesitic in composition but do not exhibit lava flow features due to heavy alteration.

3.3. KIZILDERE FORMATION

The formation consists of volcanic lava flows, tuffite(tuff and sediment), tuff, marl interbeds, clayey limestone, limestone and sandstone. It covers a large area in the northeast of the studied area. The main locations where it is observed very well are near Magara village, in the south of Gelintasi Tepe, Kavak Tepe, Dimso Tepe and the south of Tavsan Tepe.

The Kizildere Formation changes from carbonated clastics to sandstone containing mainly volcanic material, tuffite and tuff.

Table 3.1. Stratigraphic sequences in two sub-areas.

ZILAN VALLEY AREA		MEYDAN AREA	
Lithology	*Thickness (m)*	*Lithology*	*Thickness(m)*
Alluvium	0-75	Colluvium and alluvium	0-75
Old alluvium	0-50		
Travertine	5-30	Gurgurbaba lava; *massive grey- cream rhyolite and black-brown obsidian, and perlite in some areas* *5.75±0.55 Ma and 0.48-0.99 Ma(Ercan et al., 1990)*	0-500
Zilan lava	20-40	Pumice and tuff	0-50
Ignimbrite; *4.8-5.9 Ma(Innocenti et al., 1980)*	0-175	Rhyolite dome and dyke;*perlitic and vesicular*	0-250
Agglomerate	0-60		
Aladag lava	200-350	Meydan Lavas: Trachyte	50-375
		Benmoreite	0-100
Dacite ; *5.7Ma(Innocenti et al., 1976)*	150-300	Hawaiite	50-150
Trachyandesite	75-200	Mugearite	125-250
Andesite	50-200	Alkali olivine basalt; *6.2 Ma and 4.4±0.43 Ma (Innocenti et al., 1976 and 1980)*	50-200
		Ignimbrite	50-175
Kizildere Lavas: Andesite; *grey- pink, altered*		Aladag lava	200-350
Basaltic andesite; *reddish brown and slightly altered*			
Andesite; *grey and altered*			
Andesite; *reddish brown, and showing columnar joints*			
Kizildere Formation; *sandstone, marl, clayey limestone, limestone, tuff and tuffite*	400-450		
Altered andesite; *bordeaux and hydrothermally altered*	0-60		

In addition, it contains lava flows varying in composition from basaltic andesite to andesite. Therefore the formation reflects a volcanosedimentary feature implying a significant volcanic activity at the time of sedimentation.

According to field observations and geological cross-sections, the thickness of the unit is about 450-500 m. In the investigated area the basement of the unit is not observed. However, in the northeast, outside of the area studied it overlies unconformably the Gergili formation(Karamanderesi *et al.*, 1984) and granodiorite.

The lower members of the formation are lavas and sediments with dominant volcanic clasts whereas at the upper levels, mainly sandstone and clayey limestone together with volcanic material are observed.

In Magara village, the formation is dark grey or black fragmented and altered, overlaid by pumice and tuff, and layering is not well developed. In this location, the bottom part of the unit is represented by black fractured limestone with 10-15 cm thick layers and then dark grey-black hard limestone with 20-30 cm thick layers and having thin secondary calcite veins. This limestone level passes into greenish purple sandstone. The upper part of sandstones is carbonate cemented and well laminated, exhibiting fragmented and altered exposures.

In the south of the area, massive, homogeneous, cream limestone crops out at the base. Above this limestone, clayey limestone and sandstone are present.

South of Gelintasi Tepe the unit is in contact with altered lavas, and is cut by NNW-SSE trending fault which has caused vertical fractures in the limestone. The lithologies comprise dark grey, hard and partially crystallized limestone and brown-green sandstone. The limestones contain abundant microfossils which can even be seen macroscopically. Some limestones have thin yellowish brown coloration which may have formed by alteration and in part hydrothermal from lava flows on top of the limestones. Where heavily developed the alteration has destroyed the original rock texture.

In Kavak Tepe region, the unit underlies with altered tuffites, and crops out as sandstone and limestone. The limestone is dark grey and well bedded and overlies the dark brown-bordeaux of heavily altered basal andesitic lava which has a spherical alteration surface.

Around Tavsan Tepe, sandstone and tuffite occur. West of Hasanaptal village , the formation is well exposed and extends through the Attepe region. At Attepe, it is represented by hard limestone with 25-30 cm layers, clayey limestone and sandstone. South of Ilgi Tavlasi, 1m of dark grey-grey sandstone is present.

The formation contains the following microfossils within the lower limestones: *Miogpsinoides, Lepidocyclina, Miliolidae, Bryozoa*. These fossils give a Burdigalien age(Karamanderesi *et al.*, 1984).

Limestones in the upper part of the formation contain the following fossils: *Miliolidae, Amphistegina, Miogypsina, Lepidocyclina, Victoriellidae, Gypsina, Herostegina, Ratalidae, Globigerinidae, Alge, Austrotrillina, Elphidium*. These fossils give a Middle Miocene age(Karamanderesi *et al.*, 1984).

All these fossils indicate that the formation formed in a shallow marine environment.

3.3.1. TUFF AND TUFFITE

White, greenish white, cream and yellow tuff and tuffites form thick sequence at the base of the Kizildere Formation. Generally ,fresh parts of the tuffite are white in colour but an extensive alteration to clays is characteristic.

The sequence is typically observed around the Varikani plain, Binok Dere and extends to the north of the area. Despite the alteration to clay minerals, transparent fine crystals of quartz can be seen. Tuffites are exposed around Dimso Tepe and are overlaid by dacite flows in the north. Tuffites underlying the dacite flows are much compacted and contain varying size of large clasts, at about 7-10% in the whole rock.

Within the tuffite unit, beds of marl 15-20 cm thick and very thin limestone layers are also present.

3.3.2. LAVA FLOWS

One of the significant features of the Kizildere Formation is presence of different types of calcalkaline lavas varying from basaltic andesite and andesite to rhyolite.

Rhyolites are largely at the basal levels of the Kizildere Formation whereas the andesitic lavas are present in the upper levels of the formation. All of them have suffered from alteration producing clay and carbonate minerals. Four main lava flows were recognised; hyalorhyolite, two different andesites and a basaltic andesite.

Hyalorhyolite occurs south of Hudud Dere as a laminated grey to pink or pale red glassy lava containing a much glassy matrix and a small amount of crystals.

Carbonated andesites crop out the south of Dimso Tepe and northwest of Tavsan Tepe. They are columnar jointed greenish brown and

reddish brown lavas with phenocrysts of feldspar and mafic minerals but the rocks are commonly altered to carbonates.

Andesites occur south of Dimso Tepe, south of Kuzubulak Lake and southeast of Sirakayalar Tepe and Kurttepe. Their characteristic colour is grey-pinkish purple. In some places, these andesite flows cut carbonated andesite flows. Compared with carbonated andesite, the andesite has less phenocrysts but more matrix.

Basaltic andesite is observed only the west of Dimso Tepe. Generally it is reddish brown and brownish black, with large phenocrysts of mafic minerals. The flow is overlain by dacite in the north of the area.

3.3.3. ALTERED AND SILICIFIED TUFFITE

An altered and silicified yellow to red-brown tuffite unit is present at the top of sandstones and limestone, typically the west of Kavak Tepe, Menekse Dere, Koycuk village and Berrus Tepe.

The original rock structure and texture has been destroyed by the hydrothermal alteration and weathering. The freshest parts of the rock are white with feldspar altered to clay minerals, mainly kaolin. The unit weathers smoothly except where thin(<1 cm) silicified veins intersect each other.

At Berrus Tepe and around Koycuk village, the tuffite is unbeded, extremely silicified and has a conglomeratic resting on it in which there are clasts slicified after deposition.

The tuffite is overlaid by a andesite flow in the west and a trachyandesite flow in the east.

3.4. ANDESITE

Andesites are generally dark grey-black and brownish red and occur observed around Kohkalesi Tepe where there is laminated flow banding, particularly in the eastern part of Kohkalesi Tepe. Transition to thick lava flows overlain by tracyhandesite flow which are chemically transitional to upper lavas of andesite.

Brownish red andesites also occur northeast of Kardogan village where at the base is an agglomerate unit 15 m in thick bedding followed upwards by 4 m of dark grey to black andesite and then the main brownish red andesite about 75 m overlain by the Aladag lava in the west and an ignimbrite flow in the east.

3.5. TRACHYANDESITE

Trachyandesites crop out along both west and east side of the Zilan stream. They are brownish grey to grey but fresh surfaces are generally grey.

East of the Zilan stream, they overlie silicified tuffites and sediments of the Kizildere Formation and underlie dacite flows. Macroscopically, their colour and presence of elongated hornblende phenocrysts are notable. Around Purnisin Dere, the basal levels are dark brown and black and flow banding is absent and.

In the west, they cover large area around Misir Tepe and Kale Tepe. The colour changes from pink-brownish to red. At Misir Tepe, agglomeratic bands containing andesitic clasts of small blocks and lappili 2-4 cm are present. Therefore some explosive action producing agglomerates occurred during the eruption of the trachyandesite lava which is itself transitional to andesite. At Kurttepe, laminated flows are occur.

3.6. DACITE

Dacite lavas occur in two zones, one at Omeraga Tepe and to the east and the other at the Alikalesi Tepe region in the west. They are commonly dark grey and grey or brownish red due to alteration.

In the eastern zone, they crop out along Kardogan Sirti and in the west lie above ignimbrite and andesite. A few metres of agglomerate is present at the base. At Omeraga Tepe, a basal agglomerate is also present and well developed flow structures, laminated like flow banding(25-30 cm thick). Clasts in the agglomerate are relatively large, reaching 10 cm and have almost rounded edges. South of Sakiran Tepe dacites overlie sandstone levels of the Kizildere Formation, and show flow folding. In the Zilan valley, the dacites are faulted and post-fault hdyrothermal fluids caused intense alteration so that the original texture and mineralogy are transformed with the formation of clay minerals, and silicification.

In the western zone, the dacites cover large areas around Alikalesi Tepe and Kohkalesi Tepe. On the hill, columnar jointing occurs. Porphyritic texture containing laths of feldspar and hornblende are characteristic. They overlie trachyandesites and underlie rhyolite and obsidian of the Gurgurbaba volcano. Their areal distribution, flow direction and morphological shape suggest that dacites in this zone may have been erupted in situ, and flowed to the south from a hidden feeder.

3.7. ALADAG LAVA

In the northern part of the studied area grey trachytic lavas cover large areas and extend outside the area investigated. They appear to have came from outside of the present area, possibly from the Aladag range.

Near Goktas village in the northwest, the lavas are whitish grey and contain many feldspar phenocrysts. The lava flows have laminated flow banding, flow folding and columnar jointing and are overlain by mugearites, and cut by 1-1.5 m diabase dykes trending NW-SE or N-S, and a rhyolite dyke.

Around Magara Dere, the lavas are overlaid by ignimbrite and hawaiite flows.

3.8. AGGLOMERATE

Poligenetic heterogeneous agglomerates underlie ignimbrite flows at near Dimso Tepe. Both their distribution and thickness(50 m) are limited. Clast sizes vary from a few cm to 1 m in diameter and the compositions are andesitic and dacitic. Clasts form 60-70% of the rock and are cemented by 30-40% white-cream tuffaceous matrix.

Clasts and matrix are hydrothermally altered with silicification and the presence of jasper nodules up to 10 cm. Some large blocks(75cm-1m in diameter) are significantly rounded, and some of the large blocks themselves contain clasts, implying reworking of old agglomerate.

3.9. IGNIMBRITE

Ignimbrite flows cover large areas in the northeast of the area and extend outside the studied area. They are best exposed to the west of Evbeyli village, Semikayalari Sirti, northwest of Kuzubulak Golu, southeast of Isbasi village and Demek Tepe. There were three main phases distinguished by composition, welding, colour and structural featured. The lowest ignimbrite is black, glassy and closely horizontally fractured and showing plate cleavage. Above this flow, there is a white-yellowish cream tuffaceous ignimbrite which shows some sedimentary structures namely parallel lamination, slightly graded bedding and cross bedding. Above second flow, upper ignimbrite is present with less glass except at very top.

Among these ignimbrite flows , unwelded tuffs are present. Tuffs show longitudinal transition to the main ignimbrite flows. Generally, the thickness of whole ignimbrite flow unit varies from place to place from about 75 m down to zero. Generally, this ignimbrite unit has elongated glass and pumice fragments, lithic fragments such as metamorphic

rocks(metasedimentary) and volcanic lavas, alignment of feldspar crystals and blocky structure.

West of Evbeyli village a thick(50 m) ignimbrite has a flow breccia at the base with abundant angular sedimentary lithic fragments. The top is much welded and exhibits alignment of glassy fragments and crystals. Lithic clasts of volcanic lavas are also present.

East of Magara village the unit overlies the Aladag lava. Two distinctive layers are seen on the hill; the lower is dark grey-black, strongly welded and shows typical compaction welding structure with accompanying columnar jointing. The upper layer is pale grey to whitish cream , poorly welded and contains some glassy fragments.

At Semikayalari Sirti, fiamme texture and elongated glassy pumice fragments and the matrix are both cream coloured. NW of Kuzubulak Golu, ignimbrites are generally black and contain many glassy fragments. In this area the ignimbrite unit overlies dacite in the north and andesite in the south. The base of the unit is a 5 m agglomerate.

Ignimbrite flows extend to the southeast of the area. They are characteristically exposed at Demek Tepe, overlying agglomerates which are above hawaiite flows.

3.10. ALKALI OLIVINE BASALT

Alkali olivine basalts are one of the dominant volcanic lavas in the Meydan alkaline association, and were the first alkaline products derived from volcanic centres situated southwest of the area.

They are black or dark grey and generally massive lava flows.They crop out in the southwest of the area, around Pinarli, Gumusoluk and Gultepe villages. Since they are mainly covered by pumice and tuffs, they are not well exposed. Furthermore, as they also grade into hawaiite flows they are not easily mapped.

These lavas flowed to form a plateau dependent on the paleotopography of the area forming thick massive lavas in small valleys and thin layered lavas on slopes. Commonly there are vesicles at the bottom and, or the top of flows. Near Gumusoluk village, flow layering(5 to 10 cm thick), small minor folding and the presence of phenocrysts of olivine and pyroxene are very characteristic near the bottom of the lava.

Around Pinarli village alkali olivine basalts are exposed where covering pumice and tuff were eroded. Later faults have caused flows by showing fractures and brecciated structures(e.g. at Pinarli Tepe).

3.11. HAWAIITE

Hawaiite lavas form the second most voluminous rock within the alkaline association and are represented by two main volcanic eruption centres located in the southwest at Topsini Tepe and Kartepe, and in the northeast at Kucuk Deveci Tepe. Other hawaiite areas also occur but they were fed from vents, outside of the studied area.

Hawaiites are represented by both black or dark grey lava flows and brownish red pyroclastic products such as scoria and lapilli, especially around volcanic cones. Plateau lava flows cover large areas in the north and southeast parts of the area.

One of the main Kartepe-Topsini Tepe centres is located southwest of the Meydan caldera. Both lava flows and pyroclastics are present. Lavas are black in colour and massive. Red-brown pyroclastics are also common as scoria and lapilli. In some places, they form thin layers of reddish brown soil cover. At Topsini Tepe, lavas are seen as layered flows and have vesicles in the lower zones. In addition blocky parts and spherical flow surfaces occur. Hawaiites overlie alkali basalts in the south, and underlie with late trachytes of the Meydan volcano.

The Kucuk Deveci volcanic centre, north east of the Meydan caldera, also exhibits typical eruption centres with hawaiite lava flows, scoria, lapilli and bombs. At the base agglomerate consisting of hawaiitic clasts is present while the upper parts contain mainly pyroclastic products. The same type of basal agglomerate level is also seen at Sait Tepe and passes into lava flows upwards.

Around Goktas village is another volcanic centre which is slightly ellipsoidal in shape and about 150 m in diameter. Pyroclastic rocks with characteristic reddish brown colour are common. In the same locality, a mixture of blocks, lapilli, scoria and bombs are present. These pyroclastics could be an indicator of an old parasitic volcanic conduit now filled.

In the north of the area lavas form a horizontal plateau overlain by thin pumice deposits are well seen in the stream beds of Mirza Dere, Boga Dere and Yayla Dere. In this region the hawaiites overlie mugearites and contain many vesicles at the contact. At Maruf Tepe and Kottepe thin lava flows overlie a perlitic rhyolite dome. The contact with the rhyolite is an agglomerate which includes clasts with vesicles. On the east side of the hill(out of the area) pyroclastics appear again and may indicate a relict volcanic centre.

At Semikayalari Sirti, hawaiite flows overlying mugearites are massive and thick(150 m) but the basal parts on the valley side exhibit well developed flow lamination and vertical jointing.

In the studied area, the presence of small volcanic centres from which basaltic rocks were erupted and the field relationships suggest that alkaline volcanism started primarily as fissure eruptions and then continued by the central Meydan volcano producing more differentiated rocks.

3.12. MUGEARITE

Mugearites are quite distinctive rock types black-dark grey and reddish brown in colour, with large feldspar crystals reaching 1-2 cm and common vesicles. They are exposed very well at Kuyruk Tepe, Kottepe, Meydan Tepe, Cayirbicen Dere, Kocagavur Dere, Huseyin Dere and around Goktas village.

The mugearite flows can be divided into two layers. At the bottom, mugearites are greenish grey or black in colour, contain large tabular plagioclase crystals, less vesicles, and show exfoliation structure. The higher layers are reddish brown to black and contain large lath-shaped plagioclase crystals and numerous vesicles.

Between Amca Tepe and Kottepe the mugearites have a 2 m basal of agglomerate and are cut by small rhyolite dykes.

In the north of the area, around Goktas village, mugearites form thick flows overlying the Aladag lavas. They exhibit exfoliation structures or onion-skin type weathering 50-70 cm in diameter. Similarly at Semikayalari Sirti, they show the same type of spherical blocks and are highly vesicular and reddish brown in colour. North of Cayirbicen Dere, the bottom 15 m of the lavas is greenish grey, massive, less vesicular and lacking large feldspar crystals. Generally, mugearite flows are almost horizontal and their flow was controlled by the paleotopography. Mugearites overlie ignimbrite flows in the east, the Aladag lava in the north, and underlie with hawaiite flows in the west.

3.13. BENMOREITE

Benmoreites are dark green to black and sometimes yellowish brown on the surface. They occur as a dome at Basri Tepe, NE of the Meydan caldera.

They are restricted to a small area(600 m^2), commonly altered, rarely vesicular and compared with the mugearites, feldspar crystals are small. The benmoreite is overlain by rhyolite and obsidian flows of the Gurgurbaba volcano which limit the benmoreite exposure in the east of the dome. In the west the benmoreite dome is surrounded by trachytic lavas of the Meydan volcano.

From the above the evolution of the benmoreite dome should have taken place after the first eruption stage of Meydan.

3.14. TRACHYTE

Trachytes within the Meydan alkaline association appear to be homogeneous rock type, less vesicular, grey to dark grey or rarely pinkish brown and occur along the west side of the Meydan volcano and in the north.

West of Meydan Deresi, trachytes form thick flows trending to the south with cooling joints and laminated flows at the base. These laminated flows are well seen east of Cinpinari where laminates vary between 10-20 cm in thickness. The upper part of the lava exhibits cream or whitish grey spherical weathering. Trachytes are overlain by a thin pumice and tuff cover.

Along the west wall of the Meydan caldera, trachytes are observed as following from bottom to top: At the bottom they are dark grey and mainly covered by blocks fallen from the upper zones. In the middle zones, pinkish grey layers are present together with grey-black layers containing large feldspar crystals, and lava flow direction is to the west and southwest. In the upper zone, around Kurttepe, they are fractured and spheroidally altered. North of Meydan Tepe and surrounding areas, they also form thin flows following mugearites and overlie mugearites.

Since the trachytes represent the latest evolved product of the Meydan volcano, the in high west wall formed by trachytes gives a clue to the internal morphology of the volcano.

3.15. THE ZILAN LAVA

In the area studied the Zilan lava is the youngest basalt of the alkaline suite. They are generally dark grey-black, sometimes pinkish black massive 40 m lava from that underlie alluvial deposits within the Zilan valley at Attepe and near Hasanaptal village.

They are aphyric with columnar jointing. Lava flows showing a NE trend extend along the Ilica stream bed as underlying old alluvial deposits of the stream where indicates that the flow came from a volcanic centre in the northeast, probably Hudavendigar. The lava was controlled by the paleotopography and a major fault trending NE.

3.16. RHYOLITE DOME AND DYKES

In the studied area, rhyolites form a dome at Maruf Tepe and dykes to the south of Kottepe. They are vesicular, generally grey, whitish grey and cream, and sometimes perlitic, with minor crystals of feldspar and mafic minerals set in glass.

Between Maruf Tepe and Kottepe, the rhyolites are vesicular, porphyritic, sometimes perlitic, often heavily altered with a tuffaceous cover on top. Rhyolites extend through Goktas village and to the east as a result of dome structure.

At Maruf Tepe they form three layers with glassy part at the base , a middle resistive, pinkish grey in colour and more crystalline layer with flow banding 5 to 10 cm thick and at the top are perlitic and tuffaceous rhyolite. These are covered by hawaiite flows on the summits of Maruf Tepe and Kottepe. These rhyolites overlie mugearite flows in the north and the east.

Maruf Tepe with a dome structure is thought to be the eruption vent for rhyolites which thin to the east and finally disappear underneath hawaiite flows.

South of Kottepe rhyolites occur as dykes cutting mugearite flows. Four dykes trend NW-SE and N-S. These dykes are related to the rhyolite dome and evolved at the same time. Another important rhyolite dyke which extends out of the area occur north of Goktas village. Although these dykes show similar features with rhyolite flows, the dykes are more crystalline and have glassy outer zones due to rapid cooling in contact with the country rock.

3.17. PUMICE AND TUFF

South of the studied area, pyroclastic deposits(mainly pumice and sometimes perlitic tuff) show a wide distribution with an almost flat topography in a E-W direction, the old basin of Lake Van. They are common around Doganci and Yetisen villages and along the Ercis-Patnos road.

This pyroclastic unit shows features of both pyroclastic fall and surge. Generally pumice deposits in the west reflect pyroclastic fall whereas tuffs in the east exhibit surge features. The deposition of pumice in the old basin of Lake Van resulted in interbedded lake sediments especially at the bottom of the pumice deposits. These pyroclastic deposits form valley fills and thin covers on slopes and hills. They sometimes show almost horizontal bedding depending on the paleotopography with sloping inclination on hillsides.

Pumice deposits are generally whitish grey, grey and sometimes yellowish cream due to weathering. The clast size is mainly less than 6 cm and large clasts(10 cm) are rare. Deposits do not have a characteristic sequence since they show local changes in both thickness and depositional features. However, the lower parts are composed of a main coarse pumice and the upper parts comprise fine pumice and tuff. Each of these parts exhibits significant depositional features within itself. In the main pumice deposits, there is no distinctive grading but slightly zonal changes are

present. They contain lithic fragments in various size. In addition, large rounded fragments of basaltic and trachytic rocks can be seen in the upper levels around Pinarli village. The deposits are generally thick in valleys and thin on slopes. Perlitic tuffs, sometimes containing fine pumice clasts, are observed as thin covers in the north and south east of the area. The tuffs can have thin bedding and cross bedding, indicating a pyroclastic surge feature. They were later redeposited within stream beds by recent events.

Two typical quarries were examined for depositional and stratigraphical features of these deposits: In the first quarry near Ercis-Patnos road, the lower part is a more than 10 m containing volcanic clasts varying from a few mm up to 10 cm. The pumice clasts are mainly 2-5 cm but less than 10 cm in diameter. The upper part is a 1 m fine tuffaceous pumice composed of small pumice clasts (<1cm) and common volcanic fragments of the same size. In addition there are small lenses of coarse pumice(2-3 cm in clast size). At the top 25-50 cm of soil occur. In the second quarry located at the NW of Kocapinar village the bottom more than 2 m part contains the pumice which shows slight grading with clasts smaller than 2 cm. The upper 3 m layer is composed of thin(4-10 cm) beds of perlitic tuff with some cross bedding.

3.18. GURGURBABA LAVAS

The Gurgurbaba lavas are composed of grey-black rhyolite, black-brown obsidian flows and grey perlite layers, all within the half dome structure of the Gurgurbaba and the Coban hills. Since they evolved within the dome, the distribution of rhyolite, obsidian and perlite is irregular and intricate, and is difficult to map separately. The lavas are the youngest calcalkaline rocks in the investigated area.

Rhyolites are variable in appearance from grey to reddish brown, white, cream and sometimes greenish grey and are poorly vesicular at Gurgurbaba and Coban Tepe. Flow banding and flow folding on a small scale is common.

West of Gurgurdere, the rhyolites are reddish grey and sometimes black and pass upwards into obsidian layers with lineation along the flow direction of the lava. West of the Zilan stream the lava forms an arch shape above pumice deposits. They form about 50 m sequence of rhyolite mainly at the bottom and obsidian at the top with irregular obsidian bands, lenses or blocks. Perlitic layers are not common within flows but flow folding and banding occur north of Afgan village. North of Cagdas village, again the base is rhyolite and the upper part is obsidian and perlitic obsidian.

Obsidian is well seen within the small stream beds to the south of Gurgurdere, Cataydere and Pisviran dere ranging from 20 cm to 2 m within flows. On the weathering surfaces of the obsidian, lineation indicating flow direction is observed.

From field observations, the Gurgurbaba lava containing rhyolite and obsidian flows are thought to have evolved mainly along a fissure extending from Gurgurbaba Tepe to Coban Tepe. In addition, at least 5 lava flow cycles have followed each other after the pumice deposits.

3.19. TRAVERTINE

Travertines occur associated with a fault in the west of Isbasi village, in the Zilan valley. They form a small area of about 300 m^2 in contact with the alluvial deposits of Ilica Dere. A NE-SW fault has provided the fissures along which hot springs travel to the surface.

Travertines are generally yellow, brownish yellow and rarely cream and white. They are formed as irregular thin beds depending on hot spring flow direction being to the southeast. At the base pebbles of alluvium are cemented within these deposits. In the east travertines sit on top of limestone and sandstone of Kizildere formation.

3.20. OLD ALLUVIUM

Old alluvial deposits of the Magara and Ilica streams cover large areas along Zilan valley and extend almost parallel to young alluvial deposits and form terraces. They contain various sizes of volcanic rocks. Generally, around Magara village boulders and sometimes half rounded blocks indicate a high energy environment. The deposits also contain small black lenses of probably organic materials, and yellowish brown tuffaceous materials.

3.21. ALLUVIUM

Alluvial deposits associated with existing streams are observed along the Zilan valley, in the south of Cagdas village and within the Meydan caldera. Compared with the old alluvium, they are composed of smaller sized pebbles and in some places redeposited materials of old alluvium. Their thicknesses change from a few meters to a hundred meters.

Photo 3.1. Dacite (D) showing vertical columnar jointing, and underlying tuff deposits of Kizildere Formation (KF) around Kurugol (at ca. 5820-4325), view towards NW. Cream, yellow, much compacted tuffs form a thick sequence at this location.

Photo 3.2. A close up view of tuff on the east side of Sirakayalar Tepe (58025-44500). Tuffs contain varying size (mm up to a few cm) of rock fragments at about 7-10% of whole rock. Bedding is not well developed. Hammer is c. 25 cm long, and arrow indicates way up.

Photo 3.3. Andesite showing laminated flow banding (5-10 cm spacing) in the south of Kale Tepe (51250-32700), view towards SW.

Photo 3.4. Dacite showing almost vertical columnar jointing in Kasderesi (53275-45025), view towards NE. The flow overlies sedimentary rocks of Kizildere Formation.

Photo 3.5. A view around the Zilan valley towards N. At the top of the hill in the middle ground is an almost flat lying ignimbrite (Ig) underlain by the Kizildere Formation (KF). In the foreground are terrace deposits (mT) and present day alluvial deposits (m) of the Zilan river, around Cakirbey village.

Photo 3.6. Polygenetic heterogeneous agglomerate on the northwest side of Demek Tepe (at ca. 58125-34600), view towards E. Clasts vary from a few cm to block size and comprise 60-70 % of the rock. Bedding is not developed.

Photo 3.7. A view from Meydan caldera toward N. Mugearite flows (M) of the Meydan suite form north flank of the caldera around Meydan Tepe. The flows are almost flat or inclined gently to N. In the foreground is the caldera base.

Photo 3.8. A view from Meydan caldera towards W. Trachyte (T) of the Meydan suite forms a thick flow on the west flank of the caldera, around Kurttepe, and formed a topographic high on the pre-caldera Meydan volcano. In this section the lava varies in colour and morphology.

Photo 3.9. A view from SW of Cayirbicen towards NE (Kosehasan Tepe). The succession, from bottom to top, comprises: ignimbrite (Ig), mugearite (M) and hawaiite (H) flows of the the Meydan suite.

Photo 3.10. A view around Goktas village, towards SW. From bottom to top, Aladag lava (T^A), mugearite (M), rhyolite (R), and hawaiite (H) at Maruf Tepe. The rhyolite forms a dome structure cutting the mugearite flow.

Photo 3.11. Rhyolite dykes (R) cutting mugearite (M) lava of the Meydan suite in the south of Kottepe, view towards NW. The dyke trends nearly N-S. At the summit, almost flat lying hawaiite (H) of the Meydan suite crops out.

Photo 3.12. Cream-grey dacite (D), and overlying dark, glassy rhyolite of Gurgurbaba lava (R^G) on the east side of Alikalesi Tepe. The dacite does not show obvious flow layering; the upper and lower contacts indicate that the flow is almost flat-lying.

Photo 3.13. Pumice deposits on the Ercis-Patnos road side (38025-33250), view towards NE. The deposits are poorly graded and show local changes in both thickness and depositional features. The lower part (A) is composed of a coarse pumice, and the upper part (B) comprises fine pumice clasts.

Photo 3.14. Pumice deposits on the Ercis-Patnos road side (38250-32875), view towards N. The lower part (A) is normally-graded, and the upper part (B) is composed of mainly fine pumice forming thin flat layers.

Photo 3.15. A close up view from the lower part of the pumice deposits (38025-33250). Pumice clasts vary from a few mm up to 10 cm (average 2-5 cm). There is no distinctive grading but slight zonal changes are present. The deposits also contain xenoliths of trachybasalt(black). Arrow indicates way up.

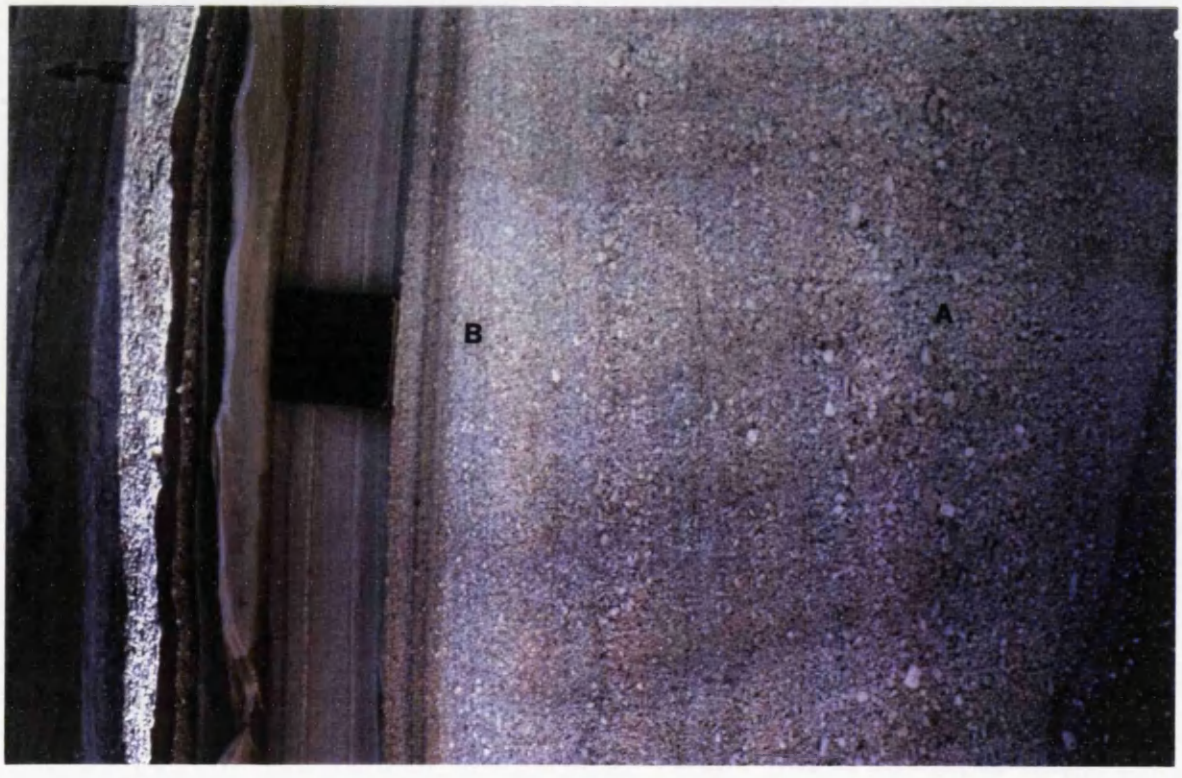

Photo 3.16. A close up view from the lower pumice deposits (at 38250-32875). Lower part shows slight grading from a coarse (A) to relatively fine (B) pumice levels. Section A is a normally-graded sequence of coarse material, whereas the upper part of the sequence (B) comprises finely laminated material. A return to coarse material occurs above (B). Arrow indicates way up.

Photo 3.17. Rhyolite dome at Gurgurbaba Tepe, view from Kurttepe towards E. The dome is one of the main volcanic structures in the area, and consists of glassy Gurgurbaba lavas. The formation of the dome disturbed the Meydan caldera in the foreground.

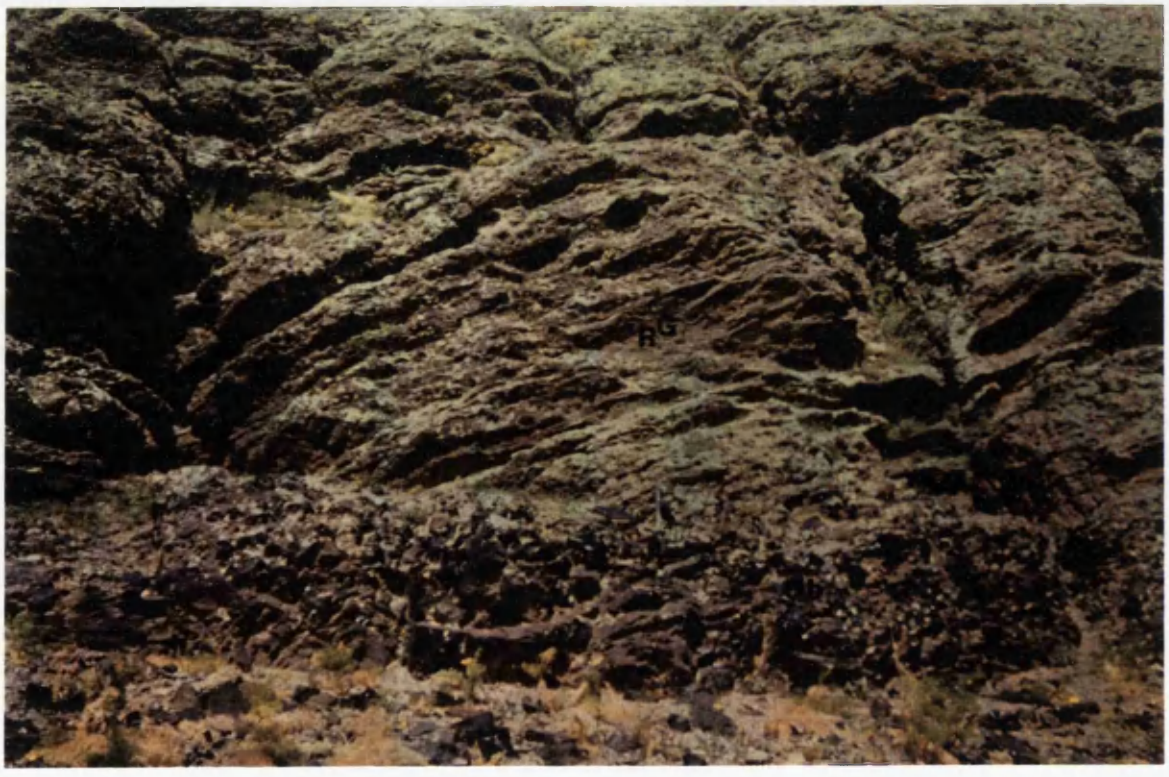

Photo 3.18. A close up view of the Gurgurbaba lava (R^G) (43775-38650), view towards NE. Black-brown obsidian (Ob) about 1 m at the base passes up into grey-reddish laminated rhyolite (R^G) flows.

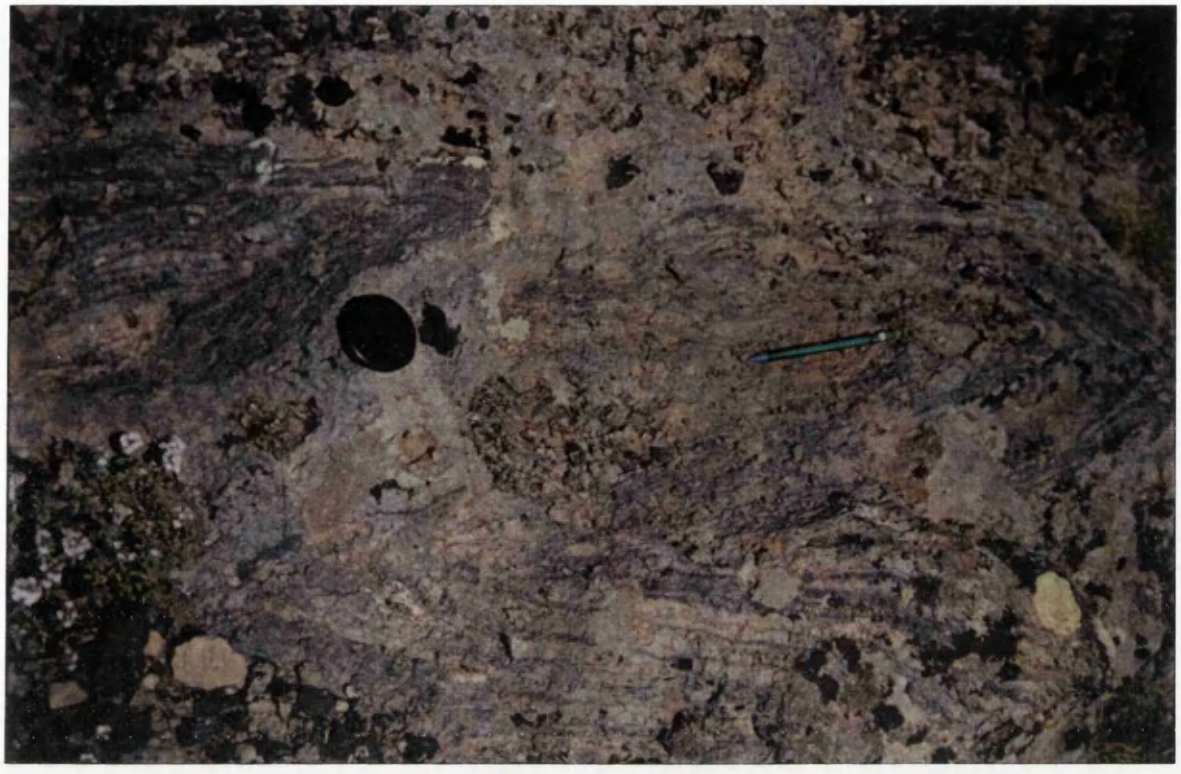

Photo 3.19. A close up view of the Gurgurbaba lava (43750-38675) showing small scale flow folding. The folding is highlighted by the more glassy(dark) layers. Lens cap is 50 mm across.

Photo 3.20. Perlitic parts of the Gurgurbaba lava (49950-40850). Devitrification of glassy rhyolite produced the perlitic portions. Flow folding is still preserved within the flow.

Photo 3.21. White-weathering travertine in the west of Isbasi village (58250-36875), view towards W. Travertine covers a small area(~300 m^2) and was deposited within a fracture zone which gave rise to hot springs at the Earth's surface.

Photo 3.22. Old alluvium (terrace deposits) of the Zilan river (57050-36025), view towards N. The deposits contain cobbles of various sizes of mainly volcanic lithologies, lenses of organic and tuffaceous materials.

CHAPTER 4. PETROGRAPHY

4.1. INTRODUCTION

This chapter defines the main sedimentary and volcanic rock types found in the Meydan-Zilan area in terms of their mineralogy and petrography, and particularly considers the volcanic rocks. The mineral chemistry of phenocrysts within the lavas is discussed in order to establish the nature of the phases involved in the magmatic processes(e.g., fractional crystallisation, crustal contamination, and possibly magma mixing) and to characterise the lavas.

Polished sections of representative samples of each volcanic rock were analysed by electron microprobe to determine the compositions of all major minerals. Cores of crystals were analysed to investigate the composition of phases which might have been involved in fractional crystallization.

One of the major uses of analyses of igneous rocks is to test hypotheses of fractional crystallization of observed phases from parental magmas to derive differentiates. Since fractionation takes place at a range of depths in the crust, or upper mantle it is necessary to determine the composition of phases which have crystallized under both high and low pressure conditions. The assemblages found in lavas may not be high pressure phases, as these may have already been removed from the magma at depth by resorption or by crystal settling. Evolved lavas may have assemblages which are dominated by crystallization on or near the Earth's surface and it is difficult to determine the nature of their high pressure phases.

Cores of large zoned crystals are more likely to be relics of higher pressure crystallization and may approximate to the composition of extracted phases. This is almost certainly the case for megacrysts in basic magmas which include highly Mg-rich olivines and aluminous clinopyroxenes.

4.2. KIZILDERE FORMATION

4.2.1. CARBONATES

4.2.1.1. PETROGRAPHY

Generally, the carbonates are biomicrites, biomicrosparites and biosparites according to the classification sheme of Folk(1962). They show a transition from almost pure carbonates up to those with a high terrigenous content. They commonly contain variable amounts of marine microfossils(see Chapter 3).

Biomicrite contains 10-20% of microfossils that may be recrystallized or replaced by sparry calcite. In addition, detrital quartz, a few feldspars, clay minerals, patchy areas or grains of oxidised opaque minerals and veinlets of calcite, or less commonly ferroan dolomite or rarely iron oxide, are present. The veinlets vary from microscopic to megascopic and are up to a few mm wide in some samples. The shape of veinlets is variable, including irregular, branching and net-like forms. There are some microstylolites resulting from pressure dissolution during later burial, or tectonic pressure(Wanless, 1979). Partial dissolution and replacement by silica(chalcedony) is also observed.

Biomicrosparites include 15-30% microfossils that are mainly recrystallized or replaced by sparry calcite. They may also contain subhedral ferroan dolomite, 2-5% of subangular fragments of siltstone(quartz+mica), quartzite, glauconite and detrial quartz as mono-, or polycrystalline grains one of which includes zircon. In some samples, minor feldspar, biotite and muscovite are observed. There are also subhedral crystals of dolomite enclosed in fine calcite crystals(MA-109). Even some of these dolomites are partially replaced by fine-grained silica. Silica(chalcedony) and calcite can also occur as pore or cavity filling. Silicification can be earlier than calcite development. It seems that first calcite formed and then was overgrown by dolomite in the pores. Stylolites sometimes mark grain boundaries with dark colour. Thin iron-oxide veins indicate late fluid interaction. In the rocks, quick burial produced rapid compaction, because large bioclasts in several mm occur cemented together. Neomorphism and silicification of bioclasts(e.g., silicified mollusc fragments) are very characteristic.

Biosparites contain 60-70% of marine microfossils that are recrystallized or replaced by sparry calcite, forming a medium grained mosaic. A few detrital grains of quartz, volcanic ash and oxidised opaque grains are also present. The rocks appear to be well sorted, and reflect a high energy environment.

Dolomitic carbonates are also present. These are finely crystalline with a mosaic texture made up of subhedral to euhedral dolomite crystals. Pores are filled by clay or silica(calcedony). However, a few spherical cavities

contain large rhombs of calcite and dolomite(MA-111). The rock formed as a result of replacement of microsparite. In some samples, gypsum is also present as a primary sediment and, or, cavity filling. It is thought that volcanic activity in the region provided heat which drove the circulation required for replacement.

4.2.1.2. DIAGENESIS

The analyses of fabrics and their paragenesis display variations in these carbonates. However, a diagenetic sequence has been proposed. It is believed that the bulk of the present fabrics are secondary in origin.

The microscopic investigation of the carbonates shows that they have undergone differential diagenesis which has resulted in the development of new fabrics. The carbonates range from almost complete preservation of their original fabric to complete obliteration of the primary fabric by diagenesis. The newly formed fabrics have different compositions and crystal characteristics from the primary ones.

Biomicrite is of primary origin. This assumption is based principally on the fact that it has a very fine texture, and has not been found replacing other fabrics. The carbonate portion of the biomicrite originated through primary chemical or biochemical precipitation. Biomicrites are thought to have been the parent rocks for other carbonates(biomicrosparites, biosparite, and dolomitic carbonates). Neomorphism(Folk,1965) is suggested as the main diagenetic process in the development of these carbonates. Biomicrosparite and biosparite are considered to be products of neomorphism. Dolomitic carbonate has resulted from both replacement and metasomatism.

4.2.1.2.1. NEOMORPHISM

Neomorphism is a term proposed by Folk(1965) to describe the products of both inversion and recrystallization processes. The effect of neomorphism can be patchy as well as pervasive. The resultant fabric can be finer(degrading) or coarser (aggrading). In the carbonates examined, aggrading neomorphism yielded coarse microspar, and recrystallization or replacement of microfossils.

The change in the fabric of biomicrite is obviously of an aggraditional nature as the texture can be seen to be altered gradually from its assumed original shape through stages in neomorphism to a relatively coarse crystals in varying size. The newly formed fabric suggests that the gradational nature in the crystal size is possibly a consequence of neomorphism. Locally, relatively coarse crystals are present. These have been produced by neomorphism, but they are probably replacing cavity cement which could

have been either primary dolomite or replacive after calcite and, or, gypsum.

4.2.1.2.2. METASOMATISM

Metasomatism is a very widespread phenomenon in carbonate rocks which results mainly in dolomitization and calcitization.

Dolomite is common in the carbonate intervals in the Kizildere formation. The occurrence of gypsum may indicate that gypsum played an important role in bringing about dolomitization. In the dolomitization of calcite, neomorphism is assumed to have operated with metasomatism, possibly simultaneously in some instances.

4.2.1.3. CARBONATE FORMATION MODEL

It is suggested that carbonates were formed in a quiet water shallow marine environment. Most coarse grains are bioclasts but this environment also received various amounts of terrigenous material(mainly clay) and volcanic material during deposition of the carbonate. It is believed that there were at least three stages in the formation of the carbonates involving neomorphism, silicification and dolomitization.

The rate of evaporation in addition to the availability of the concerned elements is, however, suggested to be the major factor determining the formation of carbonates. Volcanic activity has at the same time provided material and thermal heat for the occurrence of dolomite with the Mg coming from hydrothermal fluids.

4.2.2. SANDSTONES

4.2.2.1. PETROGRAPHY

Detailed petrographic investigations of sandstones from the Kizildere formation were undertaken. Generally, the rocks are feldspar and lithic greywackes(Pettijohn *et al.*, 1973) with small proportions of angular quartz. The matrix in some samples equals or exceeds the volume of the detrital grains (ranging from 20% up to 65%). The rock fragments, which range in size from 0.5 to 2 mm, are often angular and subangular volcanic lava fragments, tuffaceous material with abundant plagioclase, and occasionally quartzite.

Epidote(clinozoisite), K-feldspar, calcite, and chlorite occur and opaque minerals(magnetite and hematite, pyrite) are found in minor amounts. Detrital muscovite and biotite are present in some samples. Detrital chlorite, including a deep green variety, may also be present in minor amounts. Clay minerals are common in the matrix, and include both detrital and authigenic components. Accessory apatite and zircon are

present in some samples. Although the rocks show variations in the abundance of components, the main components are the matrix(20-65%), plagioclase(10-25%), quartz(3-25%), carbonates(5-30%), lithic fragments(5-15%), opaques(2-15%).

Generally, the rocks are mineralogically immature, suggesting deposition close to a source area with little reworking from the source area of limited physical and chemical alteration.

Some of the rocks show transitions towards mudstone with increasing proportions(75-80%) of fine matrix. In these, banding of fine grained and coarse grained parts can even be seen microscopically. Coarse-grained bands contain patchy or composite grains of calcite(60%), quartz(10%) and altered lithic fragments(7%) within a clay and fine-grained quartz matrix. Conversely, fine-grained bands are made of only clay(60%) and quartz(25%), rare muscovite(1%) and patchy areas of clay+muscovite display alignments.

In some samples, there is an abundance of feldspar(30%) and lithic particles in a matrix consisting of a fine-grained intergrowth of sericite and chlorite together with some silt-sized quartz, and feldspar. Some of samples have volcanic quartz, volcanic rock fragments, and zoned and, or, broken crystals of plagioclase.

Some of the samples are calc-arenaceous containing up to 50% carbonate grains(mainly calcite and rare dolomite). They are developed presumably in carbonate producing areas where there is a large influx of terrigenous clastics. In the rock, calcite forms angular discrete crystals or patchy areas of pore filling, and dolomite is in discrete grains or associated with calcite.

From these descriptions it is clear that there are substantial variations in the greywackes. These variations are related both to formation and to changes in the source material, diagenesis and secondary alterations.

4.2.2.2. DESCRIPTION OF THE FRAMEWORK GRAINS

The more abundant framework grains in the greywackes are described below and include quartz, feldspar and lithic fragments. A brief summary of the matrix is also given.

QUARTZ

Quartz occurs as subangular to very angular fragments. It is generally of monocrystalline grains sometimes with strongly undulose extinction, and rarely as polycrystalline aggregates with sutured crystal interfaces. Quartz grains derived from volcanic rocks are typically monocrystalline with uniform extinction.

FELDSPAR

Feldspar is generally twinned plagioclase, but in some samples minor K-feldspar is also present. Grains are subangular and commonly display alteration into sericite and clay(kaolinite±illite), sometimes with patchy calcite. Some grains are completely replaced by calcite, perhaps these were a more calcic plagioclase and the released calcium now appears in the rock as replacement patches of calcite, indicating the compled action of CO_2. Alteration and weathering are ubiquitous throughout the sequence but the main effects are sericitization and, or, saussuritization of the plagioclase.

LITHIC FRAGMENTS

Lithic fragments are of volcanic, metasedimentary and sedimentary types. Volcanic rock fragments are altered(chloritized) and, or, devitrified glassy tuffaceous and lava fragments. Tuff fragments are yellowish brown. Lava fragments are subangular, cosisting of microlites and brown glass. The metamorphic fragments are commonly quartzite. In some samples, metapelite fragments, containing biotite+chlorite+quartz and fine opaques, are also present in minor amounts. The sedimentary fragments are siltstone, mudstone and carbonate.

THE MATRIX

The matrix is a microcrystalline intergrowth of fine-grained quartz and feldspar with small amounts of chlorite, muscovite+sericite and clay(particularly kaolinite) minerals, and is, in places, replaced by patchy carbonate. Micas make patchy areas with slight internal alignment.

4.2.3. TUFF AND TUFFITE

4.2.3.1. PETROGRAPHY

Tuffs are lithified deposits of ash grains whereas tuffites contain up to 75% of pyroclasts. Generally, tuffs vary from crystal to lithic tuffs(Schmid, 1981; Le Maitre, 1989) with the former being commonest. Crystal tuffs consist of 15-20% phenocrysts of mainly plagioclase and quartz, rare sanidine and biotite. Some samples may contain lithic(10-15%) and vitroclastic(5-10%) fragments. The matrix is fine-grained consisting of abundant quartz, some clay(particularly kaolinite), and accessory apatite and zircon. The mode is plagioclase(7-10%), sanidine(3%), quartz(60-80%), clay(3-7%), biotite(2%) and opaques(3-5%).

Plagioclase phenocrysts are subhedral to anhedral crystals. They may display albite twinning and continuos or discontinuous zoning. Some of them are embayed and a few altered to clay minerals . Sanidines are subhedral crystals, and commonly show alteration into clay minerals but crystal outline is still preserved with carlsbad twinning. They may also be

replaced by very fine-grained quartz. Quartz phenocrysts are angular crystals, in some cases with abundant embayments. They commonly have patchy extinction, internal cracks filled by the matrix or occur as aggregates of interlocked grains. Biotites are variably altered to chlorite.

Lithic fragments are of quartz rich rocks, possibly fine-grained sandstone with interlocked quartz grains. Vitroclastic fragments are irregular yellowish or brownish particles, and show alteration into quartz and chlorite.. These particles are sometimes drop-like. In some cases, vitroclastic fragments are devitrified and display spherulites.

The groundmass contains interlocked fine grains of quartz, and clay minerals which fill spaces between grains of quartz. Clay forms patchy areas. In some cases, the groundmass may have been glassy but altered into a microcrystalline matrix . There may be small spherulites of alkali feldspar or quartz. In addition, some opaques are present. Argillization and silicification are probably the commonest types of alteration in the groundmass.

Tuffs are generally crystal tuffs and lack a vitroclastic fraction. This may be interpreted to be the result of the glassy fine fraction becoming elutriated during the emplacement processes. However, various factors can effect a high crystal concentration in volcanoclastic aggregates(Cas and Wright, 1987); (a) eruption of highly crystallised magmas, (b) physical fractionation and sorting processes associated with pyroclastic eruption and transportation processes, and (c) epiclastic reworking and redeposition.

4.2.3.2. MINERAL CHEMISTRY

4.2.3.2.1. FELDSPAR

Feldspars of the tuffs are commonly andesine with some labradorite(Figure 4.1). They may display compositional variations from core to rim(Table 4.1).

Generally, phenocrysts are andesine with a composition of An_{50-32}. Some of them have labradorite cores, and show normal zoning with a composition varying from An_{48-54} in the core to An_{34-35} in the rim, or An_{44} in the core changing to An_{32} in the rim. Microlites have similar compositions to the phenocrysts withAn_{50-35}.

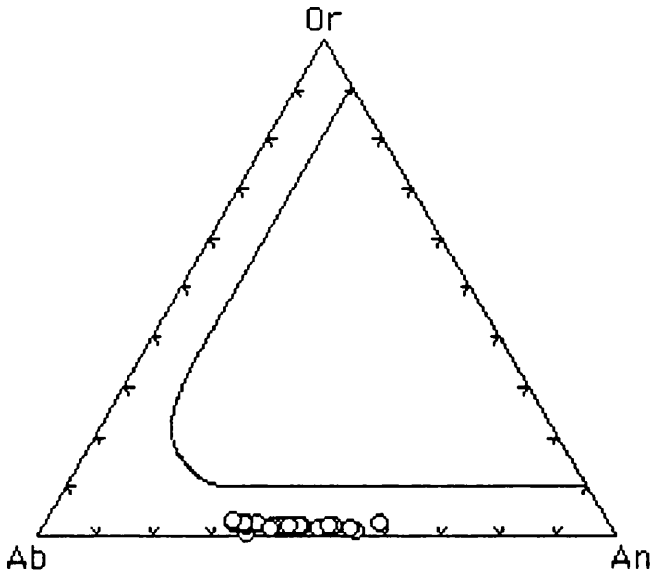

Figure 4.1. Ternary Or-Ab-An plot of feldspars in the tuffs.

4.2.3.2.2. BIOTITE

Biotites in the tuffs are phlogopite-annite rich types(Figure 4.2), with an end member composition between phlogopite(53-60) and annite(22-26). Generally, they have homogeneous compositions(Table 4.2), with a $Mg/(Mg+Fe^{+3}+Fe^{+2})$ ratio of 0.63-0.70 and Ti content of 0.43-0.48(TiO_2=3.75-4.36 wt.%).

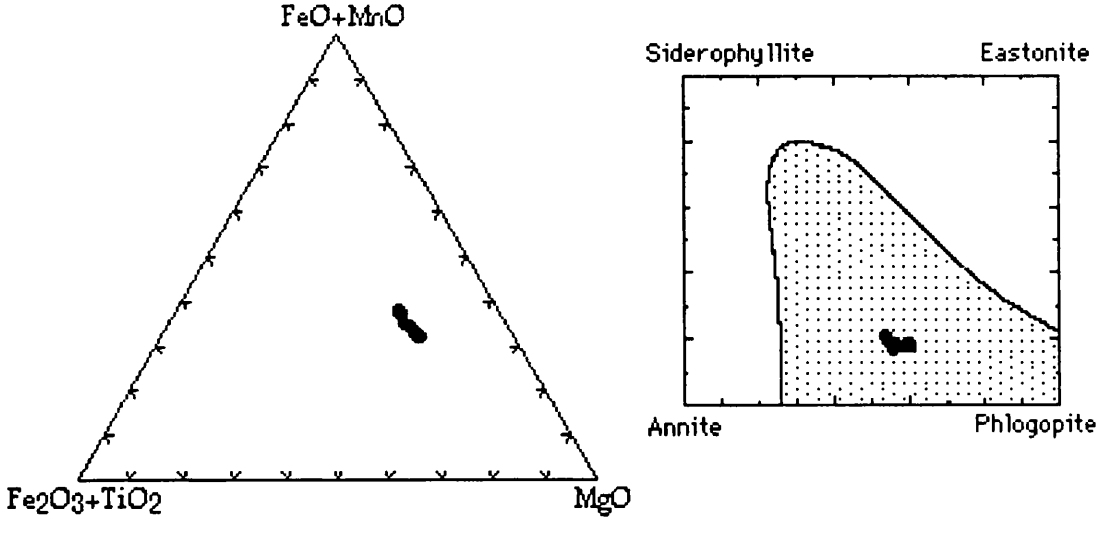

Figure 4.2. Compositional variations and the principal components of biotite compositions in the tuffs. The shaded field is that in which most natural biotites lie(after Deer *et al.*, 1992).

4.2.3.2.3. FE-TI OXIDES

Magnetite and ilmenite are common oxide minerals in the tuffs. Generally, they have homogeneous compositions, but occasionally are altered or oxidised. Magnetites contain traces of V, according to qualitative analyses.

Table 4.1. Representative analyses of feldspars in tuff.

Sample	MA-184 Pheno core	MA-184 Pheno rim	MA-184 Pheno core	MA-184 Pheno rim	MA-184 Pheno	MA-184 Pheno	MA-184 Micro pheno	MA-184 Pheno core	MA-184 Pheno rim	MA-184 Pheno	MA-184 Micro-lite
SiO_2	55.83	56.47	54.25	59.27	59.28	60.34	58.57	56.12	59.02	57.35	55.13
TiO_2	0.00	0.00	0.01	0.00	0.02	0.00	0.00	0.01	0.03	0.02	0.04
Al_2O_3	27.08	26.57	28.60	25.72	25.32	24.91	26.43	27.35	25.00	26.46	27.15
FeO*	0.25	0.23	0.16	0.09	0.18	0.21	0.17	0.27	0.24	0.24	0.20
MnO	0.00	0.00	0.00	0.07	0.01	0.02	0.01	0.00	0.00	0.03	0.00
MgO	0.08	0.14	0.06	0.06	0.03	0.14	0.11	0.16	0.01	0.10	0.10
CaO	10.13	9.01	10.93	6.52	6.99	6.52	8.08	9.01	6.45	8.68	9.89
Na_2O	5.73	6.34	4.93	7.24	6.88	7.39	6.63	6.07	7.20	6.20	5.17
K_2O	0.29	0.36	0.19	0.45	0.36	0.54	0.32	0.31	0.56	0.32	0.39
P_2O_5	0.03	0.00	0.00	0.05	0.06	0.03	0.03	0.00	0.00	0.00	0.08
Cr_2O_3	0.00	0.04	0.00	0.00	0.02	0.00	0.02	0.11	0.00	0.00	0.01
NiO	0.20	0.02	0.00	0.00	0.04	0.00	0.00	0.04	0.02	0.00	0.00
Total	99.62	99.18	99.13	99.47	99.19	100.10	100.34	99.45	98.53	99.40	98.16
Formula on the basis of 32 oxygens											
Si	10.10	10.24	9.87	10.72	10.65	10.74	10.44	10.14	10.79	10.34	10.03
Ti	0.00	0.00	0.00	0.00	0.00	0.00	0.00	0.00	0.00	0.00	0.01
Al	5.77	5.68	6.13	5.27	5.36	5.23	5.55	5.83	5.17	5.62	5.93
Fe^{+2}	0.04	0.04	0.02	0.01	0.03	0.03	0.03	0.04	0.04	0.04	0.03
Mn	0.00	0.00	0.00	0.01	0.00	0.00	0.00	0.00	0.00	0.01	0.00
Mg	0.02	0.04	0.02	0.02	0.01	0.04	0.03	0.04	0.00	0.03	0.03
Ca	1.96	1.75	2.13	1.26	1.35	1.24	1.54	1.75	1.26	1.68	1.96
Na	2.01	2.23	1.74	2.54	2.40	2.55	2.29	2.13	2.55	2.17	1.86
K	0.07	0.08	0.04	0.10	0.08	0.12	0.07	0.07	0.13	0.07	0.09
P	0.01	0.00	0.00	0.01	0.01	0.01	0.00	0.00	0.00	0.00	0.01
Cr	0.00	0.01	0.00	0.00	0.00	0.00	0.00	0.02	0.00	0.00	0.00
Ni	0.03	0.00	0.00	0.00	0.01	0.00	0.00	0.01	0.00	0.00	0.00
Total	20.05	20.07	19.96	19.95	19.89	19.97	19.96	20.03	19.97	19.97	19.96
An	48.52	43.11	54.45	32.35	35.19	31.76	39.51	44.26	31.99	42.79	50.18
Ab	49.73	54.85	44.45	65.00	62.64	65.10	58.62	53.92	64.68	55.32	47.49
Or	1.68	2.04	1.10	2.64	2.17	3.14	1.87	1.83	3.32	1.89	2.33

FeO* is total iron as FeO.

Table 4.2. Representative analyses of biotites in tuff.

Sample	MA-184 pheno core	MA-184 pheno	MA-184 micro-pheno	MA-184 pheno	MA-184 inclusion in plag.	MA-184 pheno core	MA-184 pheno rim
SiO_2	37.25	36.56	37.99	37.35	37.16	37.25	37.64
TiO_2	4.14	4.14	4.22	3.88	4.36	4.06	4.00
Al_2O_3	14.27	13.92	14.53	13.97	14.39	14.58	14.51
Fe_2O_3	2.28	2.59	2.18	2.43	2.38	2.07	2.15
FeO	11.65	13.18	11.11	12.41	12.14	10.56	10.99
MnO	0.09	0.23	0.15	0.12	0.21	0.14	0.15
MgO	15.89	15.05	16.44	15.61	15.85	16.29	16.13
CaO	0.04	0.10	0.01	0.15	0.06	0.09	0.00
Na_2O	0.93	0.88	0.78	0.73	0.96	0.85	0.61
K_2O	8.71	8.79	8.99	8.21	8.64	8.75	8.91
P_2O_5	0.02	0.01	0.03	0.01	0.03	0.00	0.00
Cr_2O_3	0.00	0.00	0.01	0.00	0.01	0.00	0.00
NiO	0.04	0.05	0.03	0.14	0.04	0.09	0.00
Total	95.31	95.60	96.47	95.01	96.23	94.73	95.09
Formula on the basis of 22 oxygens							
Si	5.52	5.47	5.54	5.61	5.47	5.52	5.56
Ti	0.46	0.47	0.46	0.44	0.48	0.45	0.45
Al	2.49	2.45	2.50	2.48	2.49	2.55	2.53
Fe^{+3}	0.26	0.29	0.24	0.28	0.26	0.23	0.24
Fe^{+2}	1.44	1.65	1.35	1.56	1.49	1.31	1.36
Mn	0.01	0.03	0.02	0.02	0.03	0.02	0.02
Mg	3.51	3.35	3.57	3.27	3.48	3.60	3.55
Ca	0.01	0.02	0.00	0.02	0.01	0.01	0.00
Na	0.27	0.26	0.22	0.21	0.27	0.25	0.18
K	1.65	1.68	1.67	1.57	1.62	1.65	1.68
P	0.00	0.00	0.00	0.00	0.00	0.00	0.00
Cr	0.00	0.00	0.00	0.00	0.00	0.00	0.00
Ni	0.01	0.01	000	0.01	0.00	0.01	0.00
Total	15.60	15.66	15.57	15.46	15.62	15.59	15.54
$Mg^{\#}$	0.67	0.63	0.69	0.64	0.67	0.70	0.69
Phlog.	58.28	55.90	59.52	53.29	56.76	59.95	59.15
Annite	23.97	27.47	22.57	25.41	24.39	21.80	22.62

Fe^{+3} is calculated by ratio according to Schumacher(1991).
$Mg^{\#}=Mg/(Mg+Fe^{+3}+Fe^{+2})$

4.2.4. LAVA FLOWS

4.2.4.1. HYALORHYOLITE

4.2.4.1.1. PETROGRAPHY

Hyalorhyolites are hyalocrystaline to hypocrystalline porphyritic with 10- 15% phenocrysts of plagioclase, sanidine, quartz, and occasionally biotite and accessory zircon. Groundmass is microcrystalline and, or, devitrified glass, consisting of mainly quartz, and sanidine. The mode is quartz(50-60%), sanidine(10-15%), plagioclase(7%), biotite(2%), opaques(3%) and glass(20-25%).

Plagioclase phenocrysts are subhedral, corroded or rarely resorbed. They exhibit discontinuous and oscillatory zoning, and albite twinning. Some are corroded and contain embayments of groundmass minerals. They are commonly alterated to calcite, especially in calcic cores. Sanidine phenocrysts are subhedral corroded crystals whereas quartz phenocrysts are anhedral, rounded, fragmented crystals with rare pyramidal crystals commonly corroded. Rare biotite microphenocrysts are subhedral and altered to chlorite layers between relic biotite layers. Biotites may also be surrounded by quartz grains.

The groundmass is felsitic and fine-grained, and shows early spherulitic and late devitrification texture being mainly quartz and needle-like sanidine. Patchy areas of opaques and calcite related to hydrothermal solutions and thin veins of tridymite occur. Generally, the felsitic texture indicates a very high degree of undercooling. Crystal form is totally suppressed, and the constituent minerals form a very fine-grained mosaic. Felsitic texture represents a combination of very slow diffusion and growth rates; crystal growth was little more than sufficient to reorganize the glass structure into crystalline order, more or less in situ(Shelley, 1993).

4.2.4.2. BASALTIC ANDESITE

4.2.4.2.1. PETROGRAPHY

Basaltic andesite is hypocrystalline with minor amount of glass, and 5-7 % phenocrysts of olivine+cpx and lesser plagioclase. The groundmass is intersertal consisting of mainly plagioclase, cpx+opx, opaque grains and minor olivine. The mode is plagioclase(70-75%), cpx+opx(7-10%), olivine(3%), opaque(3-5%) and glass(<3%).

Olivine phenocrysts are subhedral-anhedral, internaly cracked, rarely skeletal shapes and altered into iddingsite and chlorophaeite. Some of them are enclosed by opx. Cpx phenocrysts are subhedral prisms or composite grains with complex and simple twinning, sector and concentric zoning and may contain abundant iddingsite. Sector zoning involves different faces of a

crystal growing with differing compositions(Nakamura, 1973; Dowty, 1976) and develops most commonly when crystal growth is relatively fast as described by Carpenter(1980), and Smith and Lofgren(1983). However, the idea that different growth speeds for each crystal face contribute to sector zoning is not supported in the recent literature(e.g., Reeder and Grams, 1987). Plagioclase phenocrysts are subhedral laths with albite twinning, discontinuous or rare oscillatory zoning, and sieved cores which may include iddingsite and thick overgrowth rims.

The groundmass is intersertal with minor glass which is altered to yellowish brown palagonite. Between plagioclase laths are cpx+opx often intergrown, magnetite±ilmenite and iddingsite.

4.2.4.3. ANDESITIC LAVAS

4.2.4.3.1. PETROGRAPHY

Andesitic lavas are hypocrystalline, porphyritic with 15-30% phenocrysts of mainly plagioclase with hornblende and biotite. Microphenocrysts of the same minerals, quartz, cpx and magnetite±ilmenite also occur. The groundmass is fine-grained or microlitic consisting of plagioclase, pseudomorphs of hornblende±biotite, opaque grains, accessory apatite and zircon. The rock mode is plagioclase(60-80%), hornblende+biotite(5-10%), quartz(3-5%), cpx(2%), magnetite±ilmenite(5-7%).

Plagioclase pheno- and micro-phenocrysts are subhedral laths or fragmented, corroded, rarely resorbed crystals with albite twinning and common oscillatory or discontinuous zoning and may include hornblende, biotite, apatite or opaque oxide grains. Some phenocrysts are sieved with a thin overgrowth rim. Generally, they have been altered into sericite, clay and calcite preferentially in the cores of the phenocrysts sometimes replacing the whole crystal with calcite. Quartz is generally anhedral, or rounded with common embayments, internal cracks, opaque inclusions and sometimes thin rims of fine-opaques. Hornblendes are subhedral prisms or pseudomorphs, generally being completely or partially replaced by iron-oxides, chlorite, sericite and quartz, and often enclosed by an opaque rim or partially mantled by biotite, or cpx. They contain inclusions of apatite and opaque minerals, and may form clusters with plagioclase and opaques. Biotites are subhedral to anhedral, slightly altered to chlorite and largely replaced by calcite and epidote. Phenocrysts may be corroded and have rims of opaque minerals. Cpx grains or aggregates occur in some samples.

The groundmass is fine-grained containing mainly plagioclase and hornblende pseudomorphs, opaques, minor glass, secondary calcite and

quartz. In microlitic types, plagioclase laths may show subparallel arrangement. Generally, saussuritization is very characteristic with calcite, sericite, epidote, chlorite and clay minerals in the rocks.

4.2.4.3.2. MINERAL CHEMISTRY

4.2.4.3.2.1. FELDSPAR

Feldspars in the andesitic lavas vary from abundant andesine to rare labradorite(Table 4.3; Figure 4.3). Generally, phenocrysts and microphenocrysts of plagioclase are characteristically andesine(An_{30-49}) with both normal and reverse zoning. Two normally zoned phenocrysts vary from An_{39-40} in the core to An_{29-32} in the rim, and An_{40-45} in the core to An_{32-41} in the rim. Two reversely zoned phenocrysts vary from An_{31} in the core to An_{46} in the rim, and An_{38} in the core to An_{44} in the rim.

Microlites in the groundmass are commonly andesine(An_{41-50}) and some labradorite(An_{53-62}).

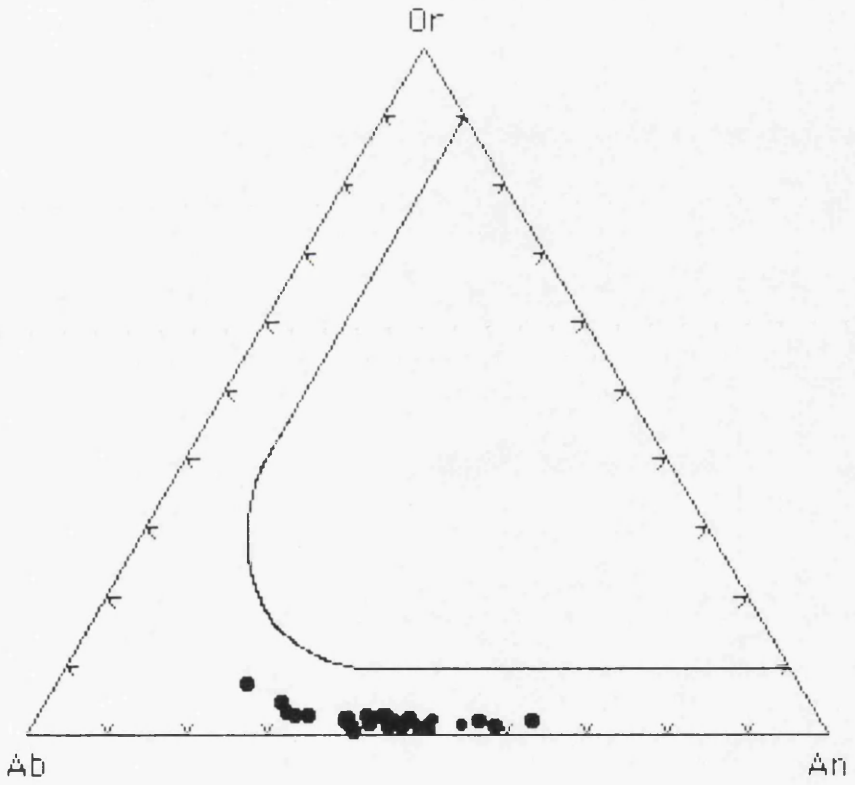

Figure 4.3. Ternary An-Ab-Or plot of feldspars in the andesites.

4.2.4.3.2.2. HORNBLENDE

Slightly zoned magnesio-hornblendes(Leake, 1978) have $Mg/(Mg+Fe^{+3}+Fe^{+2})$ ratios ranging from 0.65 to 0.68(Table 4.4; Figure 4.4). Phenocrysts may have slightly Fe-rich rims with a $Mg/(Mg+Fe^{+3}+Fe^{+2})$ ratio varying from 0.68 in the core to 0.66 in the rim. Generally, they contain Ti 0.12-0.15(TiO_2=1.09-1.38 wt.%) and there is no significant zoning. On the

variations plots(Figure 4.5), total Al versus Al[4], Ti and Na display almost linear correlations with decreasing $Mg(Mg+Fe^{+3}+Fe^{+2})$ ratio.

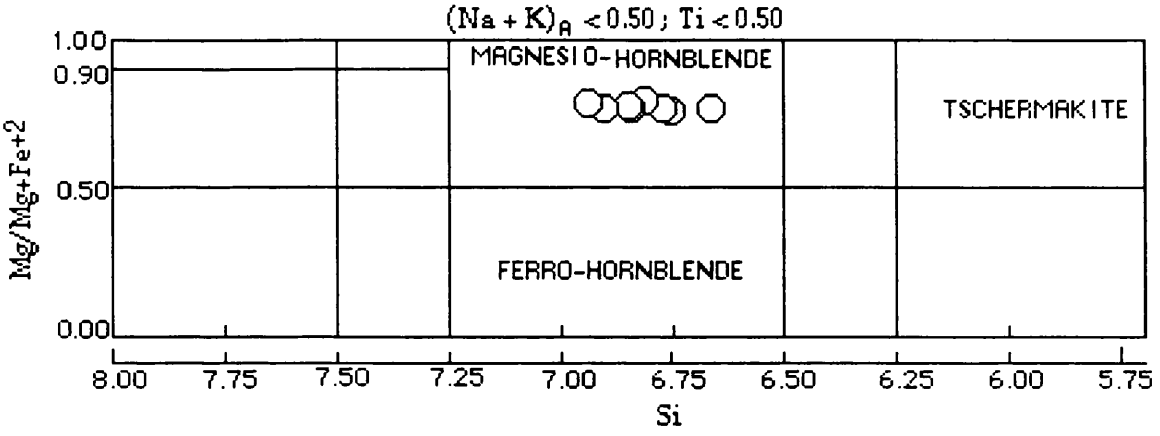

Figure 4.4. Classification and nomenclature of andesite hornblendes, according to Leake(1978).

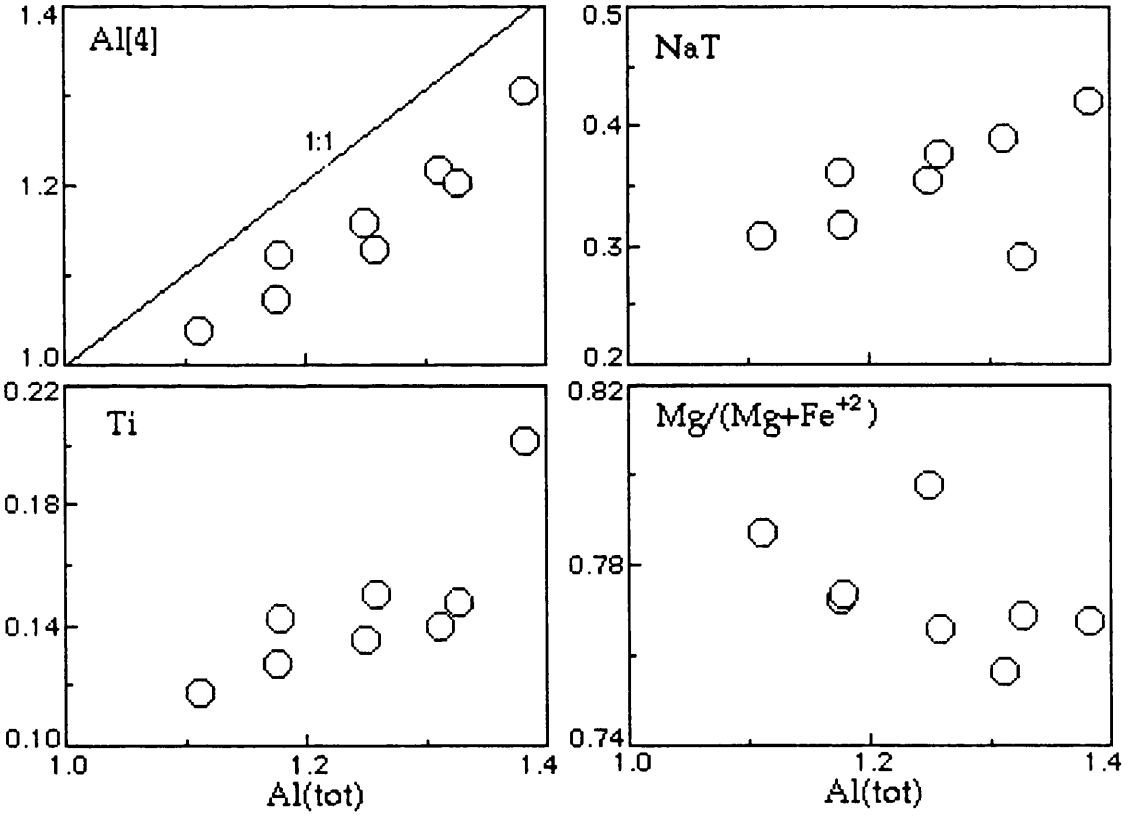

Figure 4.5. Plots of total Al versus tetrahedral Al[4], Ti, Na and $Mg/(Mg+Fe^{+2})$ ratio in the formula units of hornblendes from the andesites.

4.2.4.3.2.3. BIOTITE

Biotites have $Mg/(Mg+Fe^{+3}+Fe^{+2})$ ratios between 0.58 and 0.70 and are phlogopite-annite rich types(Table 4.5; Figure 4.6), with end member compositions between phlogopite(45-60) and annite(22-30). Generally, they are homogeneous, except for few phenocrysts with Fe-

rich[Mg/(Mg+Fe^{+3}+Fe^{+2})=0.60] rims and magnesian(0.69) cores. Generally, biotites have Ti 0.43-0.54(TiO_2=3.84-4.84 wt.%) but show no zoning in Ti.

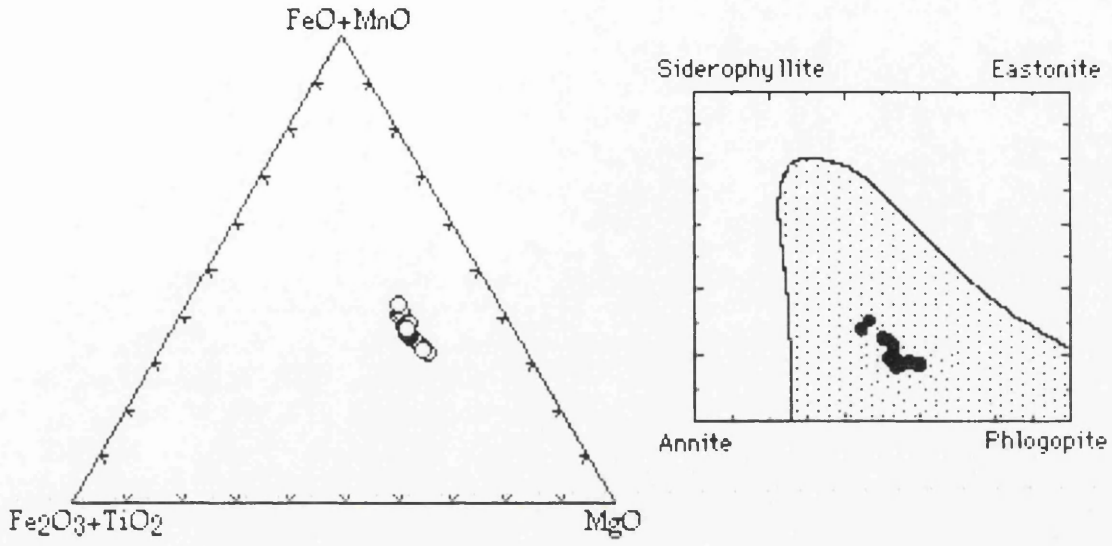

Figure 4.6. Compositional variations and the principal components of biotite compositions in the andesites. The shaded field is that in which most natural biotites lie(after Deer *et al.*, 1992).

4.2.4.3.2.4. FE-TI OXIDES

Magnetite is the commonest iron-oxide mineral but some ilmenite is observed(Table 4.6; Figure 4.7). They display almost homogeneous compositions. Magnetites are slightly Ti-rich types with a TiO_2 content from 2.27 up to 6.79 wt.%. There is significant amount of V. Ilmenites have a TiO_2(33.74-39.50 wt.%) and MgO(1.74-1.95 wt.%).

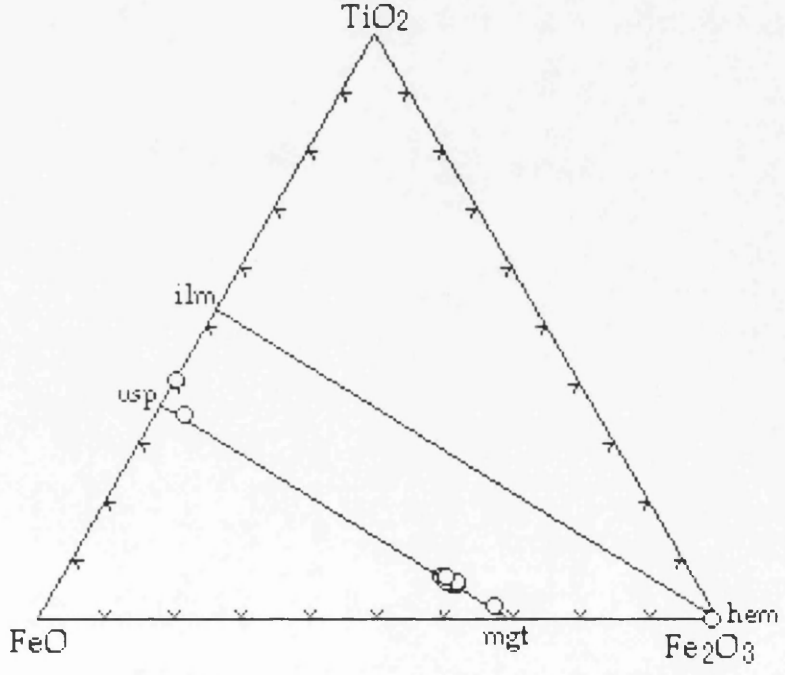

Figure 4.7. Compositions of iron-titanium oxides in andesites.

Table 4.3. Representative analyses of feldspars in the andesites.

Sample	MA-199 Pheno core	MA-199 Pheno rim	MA-199 Pheno core	MA-199 Pheno rim	MA-199 Pheno core	MA-199 Pheno rim	MA-199 Micro pheno	MA-199 Micro-lite	MA-193 Pheno core	MA-193 Pheno rim	MA-193 Micro-lite
SiO_2	55.37	57.97	58.66	60.73	60.76	57.16	59.43	56.57	56.40	57.27	55.18
TiO_2	0.00	0.00	0.04	0.04	0.02	0.00	0.11	0.07	0.07	0.00	0.08
Al_2O_3	27.67	26.40	26.16	25.10	24.99	27.51	25.49	27.13	26.86	27.06	28.10
FeO*	0.23	0.24	0.13	0.16	0.13	0.18	0.17	0.64	0.25	0.25	0.29
MnO	0.00	0.00	0.00	0.03	0.00	0.00	0.00	0.00	0.00	0.00	0.00
MgO	0.14	0.13	0.14	0.19	0.03	0.10	0.05	0.09	0.09	0.07	0.16
CaO	10.07	8.31	8.01	6.02	6.35	9.58	7.01	9.25	9.06	9.04	11.39
Na_2O	5.59	6.69	6.76	7.55	7.57	5.84	7.30	6.36	5.91	6.14	5.28
K_2O	0.26	0.42	0.48	0.89	0.57	0.45	0.53	0.57	0.41	0.35	0.27
P_2O_5	0.00	0.00	0.09	0.02	0.05	0.00	0.00	0.07	0.00	0.00	0.02
Cr_2O_3	0.00	0.01	0.00	0.00	0.08	0.00	0.00	0.00	0.00	0.00	0.01
NiO	0.00	0.00	0.00	0.00	0.00	0.00	0.00	0.00	0.00	0.01	0.00
Total	99.33	100.17	100.47	100.73	100.55	100.82	100.19	100.75	99.05	100.19	100.78
Formula on the basis of 32 oxygens											
Si	10.04	10.38	10.45	10.81	10.82	10.19	10.66	10.19	10.23	10.26	9.80
Ti	0.00	0.00	0.01	0.01	0.00	0.00	0.02	0.01	0.01	0.00	0.01
Al	5.91	5.57	5.49	5.18	5.16	5.78	5.30	5.66	5.74	5.71	6.09
Fe^{+2}	0.04	0.04	0.02	0.02	0.02	0.03	0.03	0.09	0.04	0.04	0.04
Mn	0.00	0.00	0.00	0.00	0.00	0.00	0.00	0.00	0.00	0.00	0.00
Mg	0.04	0.04	0.04	0.05	0.01	0.03	0.01	0.03	0.02	0.02	0.04
Ca	1.96	1.60	1.53	1.13	1.19	1.83	1.33	1.76	1.76	1.74	2.17
Na	1.96	2.32	2.33	2.56	2.57	2.02	2.50	2.18	2.08	2.13	1.82
K	0.06	0.10	0.11	0.20	0.13	0.10	0.12	0.13	0.09	0.08	0.06
P	0.00	0.00	0.01	0.00	0.01	0.00	0.00	0.01	0.00	0.00	0.00
Cr	0.00	0.00	0.00	0.00	0.01	0.00	0.00	0.01	0.00	0.00	0.00
Ni	0.02	0.00	0.01	0.01	0.00	0.00	0.00	0.00	0.00	0.01	0.00
Total	20.02	20.04	20.00	19.97	19.93	19.98	19.98	20.09	19.98	19.99	20.07
An	49.24	39.80	38.54	29.05	30.59	46.33	33.67	43.25	44.74	43.96	53.51
Ab	49.24	57.71	58.69	65.81	66.07	51.14	63.29	53.56	52.85	54.04	44.95
Or	1.52	2.49	2.77	5.14	3.34	2.53	3.04	3.19	2.41	2.00	1.52

FeO* is total iron as FeO.

Table 4.4. Representative analyses of hornblendes in the andesites.

Sample	MA-193 micro-core	MA-193 micro	MA-193 micro	MA-193 micro	MA-193 pheno-rim	MA-193 pheno	MA-193 pheno	MA-193 micro
SiO_2	47.09	45.58	47.48	48.46	48.10	47.89	46.96	47.81
TiO_2	1.15	1.83	1.38	1.09	1.33	1.26	1.29	1.38
Al_2O_3	6.78	7.98	7.37	6.57	6.99	7.41	7.70	7.92
FeO*	12.67	13.06	12.85	12.95	13.49	13.21	13.95	13.96
MnO	0.60	0.41	0.33	0.52	0.74	0.49	0.59	0.54
MgO	14.80	14.49	14.99	15.40	15.08	15.36	14.44	14.66
CaO	11.23	11.32	11.45	11.54	11.65	11.22	11.56	11.71
Na_2O	1.27	1.48	1.35	1.11	1.15	1.28	1.39	1.06
K_2O	0.47	0.52	0.60	0.48	0.41	0.42	0.63	0.58
P_2O_5	0.00	0.34	0.07	0.01	0.01	0.05	0.02	0.07
Cr_2O_3	0.00	0.02	0.10	0.00	0.02	0.01	0.00	0.03
NiO	0.12	0.08	0.00	0.00	0.00	0.00	0.00	0.00
Total	96.18	97.11	97.97	98.13	98.97	98.60	98.53	99.72
Formula on the basis of 23 oxygens								
Si	6.93	6.69	6.87	6.96	6.88	6.84	6.78	6.80
Al(IV)	1.07	1.31	1.13	1.04	1.12	1.16	1.22	1.20
Al(T)	1.18	1.38	1.26	1.11	1.18	1.25	1.31	1.33
Al(VI)	0.10	0.08	0.13	0.07	0.05	0.09	0.09	0.12
Ti	0.13	0.20	0.15	0.12	0.14	0.14	0.14	0.15
Fe^{+3}	0.51	0.55	0.46	0.57	0.59	0.67	0.57	0.62
Mg	3.24	3.17	3.23	3.30	3.21	3.27	3.11	3.11
Fe^{+2}	1.040	1.06	1.09	0.98	1.02	0.91	1.11	1.04
Mn	0.08	0.05	0.04	0.06	0.09	0.06	0.07	0.06
FMT	13.11	13.10	13.10	13.10	13.11	13.13	13.10	13.10
Ca	1.77	1.78	1.77	1.78	1.79	1.72	1.79	1.78
NaM4	0.12	0.12	0.12	0.12	0.10	0.15	0.11	0.12
NaT	0.36	0.42	0.38	0.31	0.32	0.36	0.39	0.29
NaA	0.24	0.30	0.26	0.19	0.22	0.20	0.28	0.18
K	0.08	0.09	0.11	0.09	0.08	0.08	0.11	0.11
SumA	0.32	0.39	0.37	0.28	0.30	0.28	0.39	0.29
$Mg^{\#}$	0.68	0.66	0.67	0.68	0.67	0.67	0.65	0.65

Fe^{+3} is calculated by estimation according to Spear and Kimball(1984).
$Mg^{\#}=Mg/(Mg+Fe^{+3}+Fe^{+2})$

Table 4.5. Representative analyses of biotites in the andesites.

Sample	MA-199 micro	MA-199 pheno-core	MA-199 pheno-rim	MA-199 pheno	MA-199 pheno	MA-193 micro	MA-193 pheno	MA-193 pheno	MA-193 micro
SiO_2	37.83	38.16	37.25	38.04	37.96	37.26	37.00	37.31	34.48
TiO_2	4.02	4.26	4.14	4.19	3.89	4.39	4.61	4.59	3.97
Al_2O_3	15.23	14.52	14.80	14.76	14.99	14.24	14.29	14.12	13.76
Fe_2O_3	2.17	2.27	2.82	2.62	2.58	2.42	2.50	2.57	3.17
FeO	11.06	11.56	14.40	13.35	13.18	12.32	12.76	13.10	16.14
MnO	0.02	0.10	0.20	0.16	0.20	0.17	0.31	0.20	0.25
MgO	16.76	16.67	14.22	15.53	14.71	16.06	15.79	15.50	15.02
CaO	0.06	0.03	0.01	0.08	0.12	0.06	0.08	0.07	0.57
Na_2O	0.72	0.71	0.68	0.99	0.84	0.87	0.66	0.58	0.52
K_2O	9.12	9.20	8.75	8.78	8.66	8.75	8.23	8.90	8.41
P_2O_5	0.00	0.00	0.11	0.00	0.00	0.01	0.07	0.04	0.35
Cr_2O_3	0.00	0.00	0.00	0.04	0.03	0.06	0.00	0.01	0.00
NiO	0.01	0.01	0.05	0.00	0.00	0.00	0.08	0.04	0.00
Total	97.00	97.49	97.43	98.54	97.16	96.61	96.38	97.03	96.64
Formula on the basis of 22 oxygens									
Si	5.48	5.52	5.46	5.51	5.54	5.47	5.44	5.49	5.21
Ti	0.44	0.46	0.46	0.46	0.43	0.48	0.51	0.51	0.45
Al	2.60	2.48	2.56	2.52	2.58	2.46	2.47	2.45	2.45
Fe^{+3}	0.24	0.25	0.31	0.29	0.28	0.27	0.28	0.30	0.36
Fe^{+2}	1.34	1.40	1.77	1.62	1.61	1.51	1.57	1.61	2.04
Mn	0.00	0.01	0.02	0.02	0.03	0.02	0.04	0.03	0.03
Mg	3.62	3.59	3.11	3.26	3.20	3.51	3.46	3.40	3.38
Ca	0.01	0.01	0.00	0.01	0.02	0.01	0.01	0.01	0.09
Na	0.20	0.20	0.19	0.28	0.24	0.25	0.19	0.17	0.152
K	1.69	1.70	1.64	1.62	1.61	1.64	1.54	1.48	1.43
P	0.00	0.00	0.01	0.00	0.00	0.00	0.01	0.00	0.05
Cr	0.00	0.00	0.00	0.00	0.00	0.01	0.00	0.00	0.00
Ni	0.00	0.00	0.01	0.00	0.00	0.00	0.01	0.01	0.00
Total	15.61	15.61	15.54	15.58	15.53	15.62	15.53	15.45	15.65
$Mg^{\#}$	0.70	0.69	0.60	0.63	0.63	0.66	0.65	0.64	0.58
Phlog.	60.28	59.85	51.80	54.23	53.32	57.26	53.07	50.33	44.57
Annite	22.33	23.30	29.45	26.87	26.80	24.64	24.08	23.87	26.88

Fe^{+3} is calculated by ratio according to Schumacher(1991).
$Mg^{\#}=Mg/(Mg+Fe^{+3}+Fe^{+2})$

Table 4.6. Representative analyses of Fe-Ti oxides in the andesites.

Sample	MA-199	MA-193	MA-193	MA-193	MA-193	MA-193	MA-193	MA-199	MA-199
	micro	micro	micro	incl. in amph.	micro	micro	micro	micro	micro
SiO_2	0.27	0.52	0.28	0.52	0.63	0.26	0.36	0.16	0.24
TiO_2	5.62	5.72	5.83	2.27	5.84	5.92	6.21	39.50	33.75
Al_2O_3	1.61	1.74	1.39	0.55	1.30	1.72	1.80	0.06	0.19
FeO*	82.70	82.96	84.01	86.26	83.81	83.90	83.99	56.99	61.56
MnO	0.47	0.56	1.75	0.48	1.01	0.60	0.81	0.63	0.28
MgO	1.26	0.99	0.19	0.09	0.25	0.68	1.03	1.95	1.74
CaO	0.06	0.32	0.06	0.76	0.33	0.00	0.07	0.03	0.02
Na_2O	0.08	0.35	0.15	0.46	0.10	0.00	0.38	0.27	0.26
K_2O	0.02	0.00	0.00	0.00	0.01	0.03	0.00	0.03	0.00
P_2O_5	0.00	0.00	0.05	0.00	0.07	0.00	0.05	0.00	0.00
Cr_2O_3	0.12	0.05	0.09	0.09	0.16	0.05	0.10	0.00	0.07
NiO	0.00	0.00	0.00	0.00	0.10	0.00	0.13	0.00	0.00
Total	92.21	93.21	93.80	91.48	93.61	93.16	94.93	99.62	98.11
Formula on the basis of 32 oxygens for magnetites and 6 oxygens for ilmenites									
Si	0.01	0.02	0.01	0.02	0.02	0.01	0.01	0.00	0.01
Ti	0.16	0.16	0.17	0.07	0.17	0.17	0.17	0.73	0.63
Al	0.07	0.08	0.06	0.03	0.06	0.08	0.08	0.00	0.01
Fe^{+3}	1.59	1.58	1.59	1.83	1.56	1.56	1.57	0.55	0.74
Fe^{+2}	1.07	1.04	1.09	0.96	1.12	1.12	1.05	0.62	0.54
Mn	0.02	0.02	0.06	0.02	0.03	0.02	0.03	0.01	0.01
Mg	0.07	0.06	0.01	0.01	0.01	0.04	0.06	0.07	0.06
Ca	0.00	0.01	0.00	0.03	0.01	0.00	0.00	0.00	0.01
Na	0.01	0.03	0.01	0.03	0.01	0.00	0.03	0.01	0.00
K	0.00	0.00	0.00	0.00	0.00	0.00	0.00	0.00	0.00
P	0.00	0.00	0.00	0.00	0.00	0.00	0.00	0.00	0.00
Cr	0.00	0.00	0.00	0.00	0.01	0.00	0.00	0.00	0.00
Ni	0.00	0.00	0.00	0.00	0.00	0.00	0.00	0.00	0.00
Total	3.00	3.00	3.00	3.00	3.00	3.00	3.00	2.00	2.00
Mn/Mg	0.29	0.33	6.00	2.00	3.00	0.50	0.50	0.14	0.16
sp	3.99	4.25	1.21	0.55	1.60	4.26	4.33		
mg-chr	0.21	0.09	0.00	0.00	0.00	0.00	0.15		
mg-fer	3.73	1.76	0.00	0.00	0.00	0.00	1.76		
trev	0.00	0.00	0.00	0.00	0.35	0.00	0.43		
herc	0.00	0.00	2.21	0.75	1.67	0.02	0.00		
chr	0.00	0.00	0.15	0.15	0.28	0.08	0.00		
mt	83.19	84.97	87.25	95.13	86.74	86.24	83.79		
usp	8.89	8.93	9.19	3.43	9.36	9.39	9.53		

Fe^{+3} is calculated by normalization according to Schumacher(1991).

4.3. ANDESITE

4.3.1. PETROGRAPHY

The rock is hypocrystalline porphyritic with 25-50% phenocrysts of plagioclase, clinopyroxene, orthopyroxene, amphibole, biotite, including microphenocrysts of plagioclase, amphibole, biotite, orthopyroxene, few quartz and opaque oxides. The groundmass contains plagioclase, orthopyroxene, amphibole, biotite, opaque grains and some glass. Accessory apatite and zircon are present. The mode is plagioclase(60-75%), clinopyroxene(7%) and amphibole(5-10%), opaque oxides(5%), orthopyroxene(3-5%), biotite(3%) and quartz(2%). Accessory apatite occurs in both the groundmass and other minerals.

Plagioclase pheno- and micro-phenocrysts are subhedral platy laths and rarely resorbed and fragmented crystals. They commonly display sieve texture with mottled extinction or patchy zoning(Vance, 1965) and inclusions of pale brown glass, sometimes with an overgrowth rim around the sieved zone which may be separated from the cores by a dark grey zone of "clouded" plagioclase charged with micron-sized melt inclusions. These textures bear a marked resemblance to the sieve-textured or dusty crystals produced experimentally on dissolution of plagioclase in the system Di-An-Ab (Tsuchiyama, 1985). Rarely, plagioclase phenocrysts display asymmetry in which part of the crystal has suffered substantial corrosion while other margins remain uncorroded. Plagioclases show discontinuous and sometimes oscillatory zoning, and albite twinning, especially in unsieved crystals. Some phenocrysts are surrounded by pyroxene and opaque grains. Clusters of plagioclase may be enclosed by hornblende and opaque grains as well. Phenocrysts may contain inclusions of pyroxene, apatite, biotite and opaque grains, and may be slightly altered to sericite or carbonate.

Orthopyroxene and clinopyroxene are subhedral and either discrete or associated together. Clusters of pyroxenes include opaques and, or, plagioclase laths. A few phenocrysts of cpx have spongy texture with opaque oxide inclusions. Orthopyroxenes form around vesicles as radiating crystals and with cpx form coronas on quartz, or enclose quartz. They are altered into bastite and chlorite around rims or as patchy areas.

Hornblendes are subhedral, but often pseudomorphed by opaques, pyroxene, feldspars and quartz or simply rimmed by opaque minerals. They also form clusters or coronas on quartz. The most common hornblende breakdown gives cpx+opx+plagioclase+magnetite+ilmenite. These textures are easily distinguished from synneusis intergrowths which involve oscillatory-zoned plagioclase and resemble the"gabbroic-type" amphibole replacement structure(Stewart, 1975; Garcia and Jacobson, 1979). The modal

abundances of breakdown products vary substantially, especially cpx/opx ratios, and in rare cases cpx may be absent, presumably because of breakdown outside the stability field of cpx, and points to the complexity of amphibole decomposition reactions(Eggler, 1972a; Helz, 1973). In some cases, simple twining may be preserved due to epitaxial replacement by pyroxenes.

Biotites are subhedral-anhedral(or resorbed) with common reaction rims or breakdown products. They are surrounded by fine grained opaques or completely replaced by opaques and quartz. They sometimes contain plagioclase and may be enclosed by clusters of plagioclase. Breakdown of biotite forms opaque oxides or a granular intergrowth of opx+ilmenite+magnetite±K-feldspar. The lack of cpx and plagioclase and increased abundances of K-feldspar and ilmenite, distinguishes these breakdown products from those of amphibole. Apatite and opaque oxides occur as inclusions.

Quartz is anhedral, partly resorbed and rounded or fragmented with common embayments and internal cracks. Some of them are enclosed by clinopyroxene grains. Reaction coronas of cpx generally occur a short distance away(a few mm) from the edge of quartzs suggesting nucleation within the boundary layer melt.

The groundmass is microcrystalline to microlitic, pilotaxitic and glassy, and contains mainly plagioclase and some opx and opaque oxides. Microlites may show subparallel arrangement, resembling trachytic texture. Opaque grains may form clusters.

4.3.2. MINERAL CHEMISTRY

4.3.2.1. FELDSPAR

Phenocrysts and microphenocrysts are mainly andesine and labradorite with compositions varying from An_{32} to An_{74}(Table 4.7; Figure 4.8). Generally, they show reverse zoning or have more calcic rims around a sieved zone. These pheno- and micro-phenocrysts range from An_{54} in the core to An_{65} in the rim, but one crystal had an An_{47} core varying to an An_{71} rim. However, a few phenocrysts are normally zoned from An_{68} in the core to An_{56} in the rim, or An_{44} in the core varying to a more sodic rim(An_{36}).

Microlites in the groundmass are commonly labradorite with a composition ranging between An_{54} and An_{70}. Rarely, andesine(An_{40}) laths are also present. Inclusions of plagioclase within other mafic silicates are andesine(An_{47-50}).

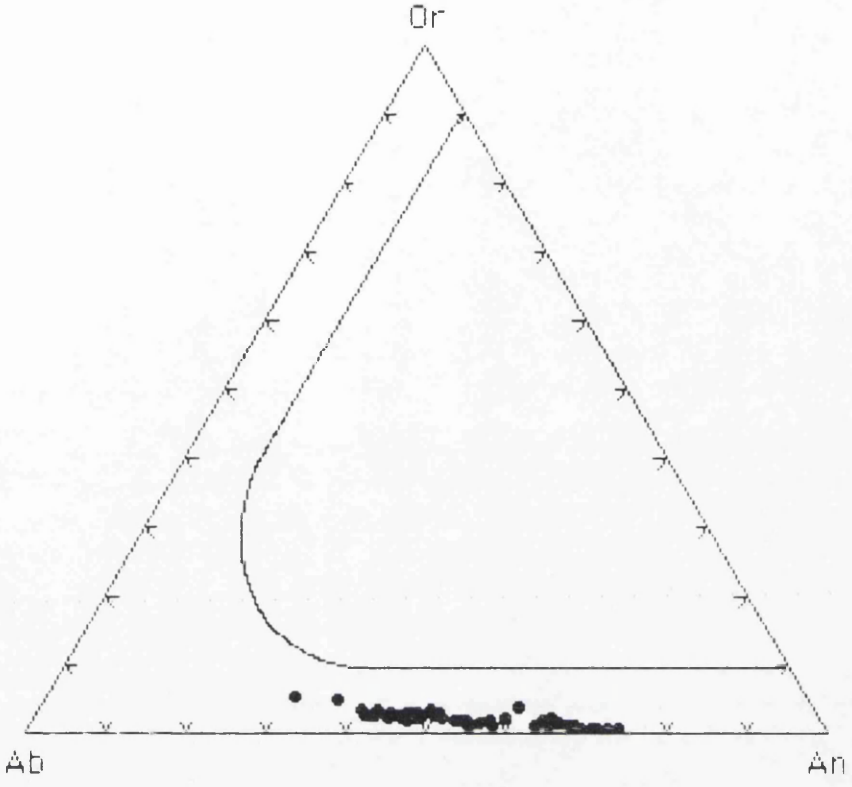

Figure 4.8. Ternary An-Ab-Or plot of feldspars in the andesite.

4.3.2.2. BIOTITE

Biotites are typically phlogopite(54-60)-annite(14-28) rich types(Table 4.8; Figure 4.9) with $Mg/(Mg+Fe^{+3}+Fe^{+2})$ ratios varying from 0.63 to 0.68 and Ti 0.50-0.60 Biotites have relatively high-TiO_2(4.73-5.44 wt.%) and uniformly Mg-rich compositions suggesting crystallization from liquids of restricted composition.

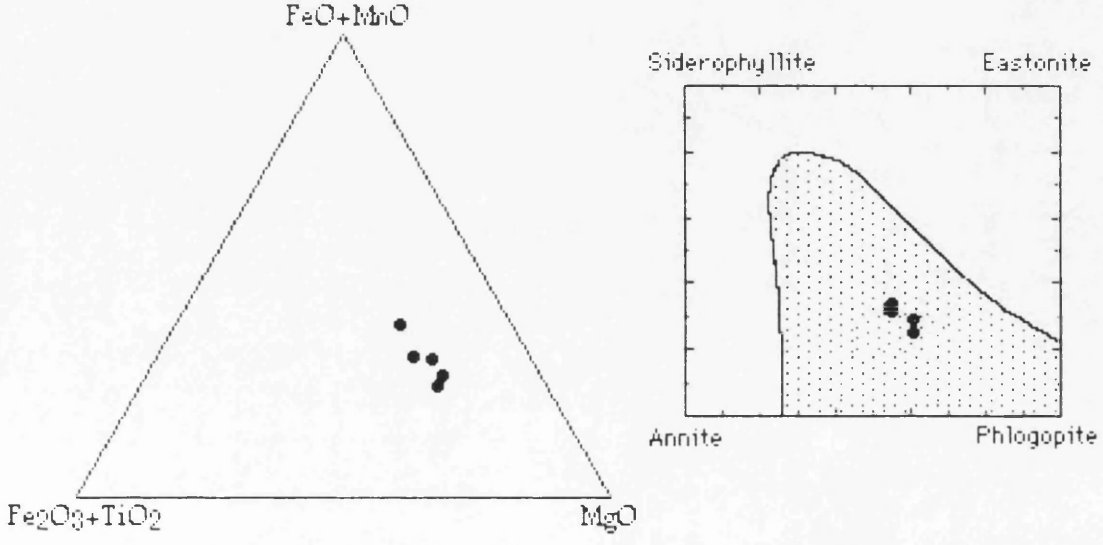

Figure 4.9. Compositional variations and the principal components of biotite compositions in the andesite. The shaded field is that in which most natural biotites lie(after Deer *et al.*, 1992).

4.3.2.3. PYROXENE

Pyroxenes are augite and orthopyroxene(Figure 4.10), according to the classification of Morimoto *et al.* (1988). Generally, they are homogeneous(Table 4.9; Figure 4.11).

Augites have a composition varying from $Wo_{41}En_{46}Fs_{13}$ to $Wo_{44}En_{42}Fs_{14}$, a $Mg/(Mg+Fe^{+3}+Fe^{+2})$ ratio between 0.74 and 0.78, and TiO_2 of 0.32-0.74 wt.%. Orthopyroxenes are $Wo_3En_{72}Fs_{25}$ with a $Mg(Mg+Fe^{+3}+Fe^{+2})$ ratio of 0.76. The distribution of Mg and Fe between augite and orthopyroxene suggest equilibrium between the two phases.

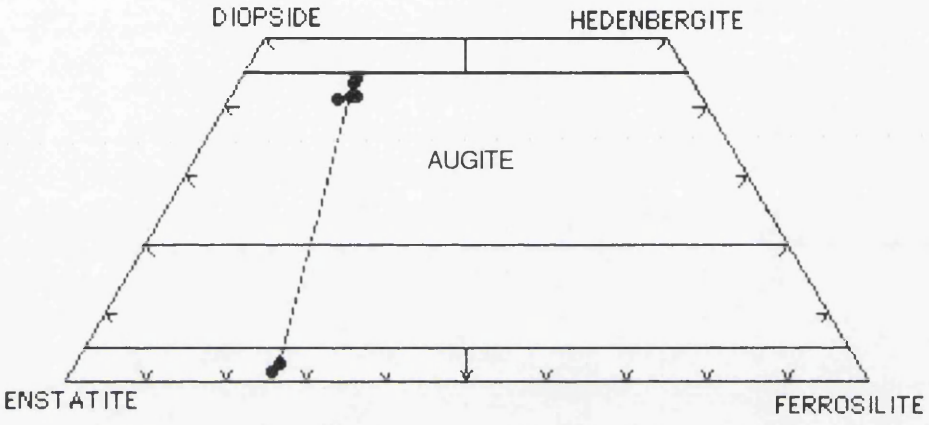

Figure 4.10. Ternary Wo-En-Fs plot of pyroxenes in the andesite. Tie line projects to the Wo-En join at about Wo_{92}.

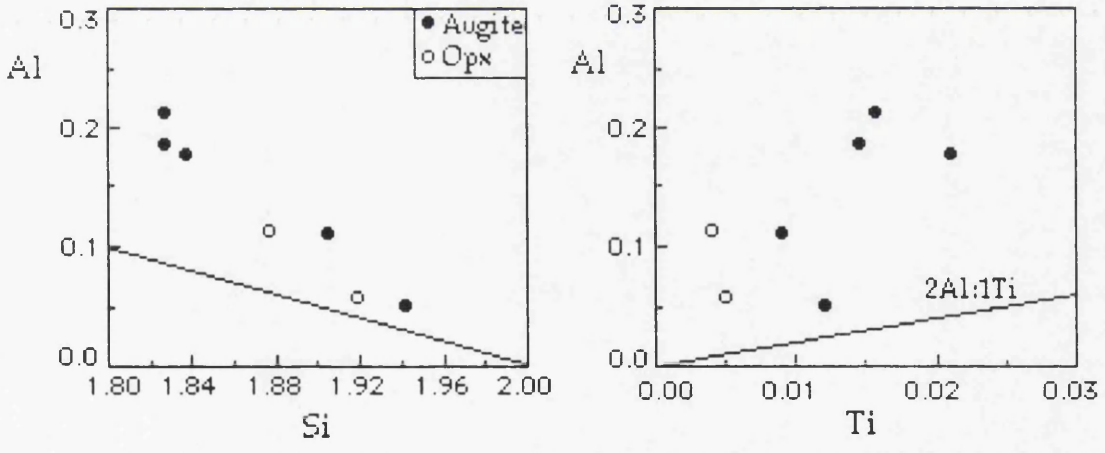

Figure 4.11. Plots of total Al versus Si and Ti contents per formula units for augites and orthopyroxenes in the andesite.

4.3.2.4. FE-TI OXIDES

Magnetite is the common oxide with some ilmenite and ulvospinel(Table 4.10; Figure 4.12) all of which have homogeneous compositions.

Magnetites are typically Mg-rich(MgO 1.82 to 3.65 wt%) types with a TiO_2 content from 5.23 up to 16 wt.% and significant trace amounts of V.

Ilmenites have a small proportion of $MgTiO_3$. They contain TiO_2(43.87 wt.%) and MgO(3.19 wt.%). Mg and Mn partitioning in coexisting magnetite and ilmenite suggests equilibrium between these two coexisting phases(Bacon and Hirschmann, 1988).

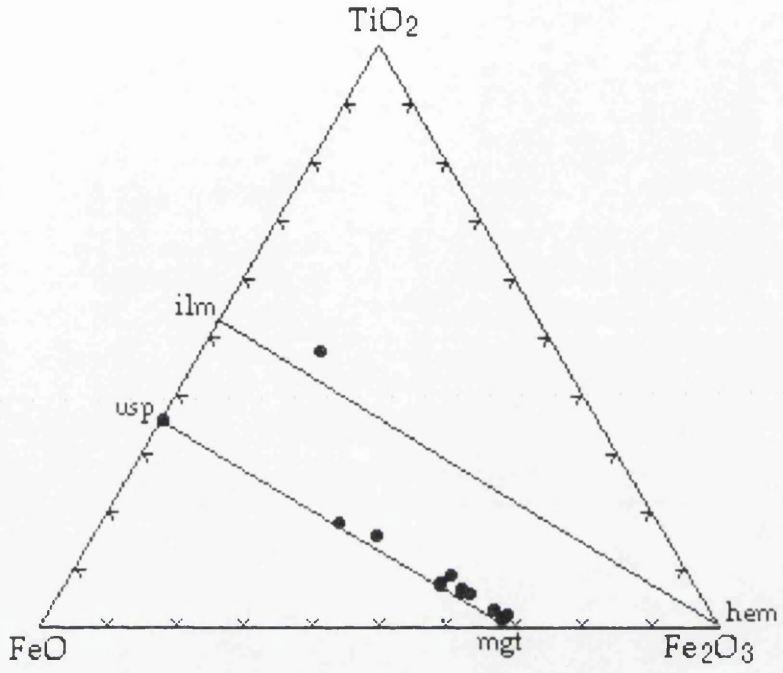

Figure 4.12. Compositions of Fe-Ti oxides in the andesite.

4.3.3. GEOTHERMOMETRY AND GEOBAROMETRY

Geothermobarometry calculations in the andesite were made on the basis of two pyroxene thermometry(Kretz, 1982) and Fe-Ti oxide thermometry(Anderson and Lindsley, 1985).

Coexisting augite and orthopyroxene microphenocrysts gave solvi temperatures ranging between 1013°C and 1074°C. However, coexisting Ti-rich magnetite and ilmenite pairs in the groundmass gave a temperature of 786-834°C, and a fO_2 of 1.56-1.98 relative to FMQ buffer(Figure 4.13). Temperatures obtained from magnetite-ilmenite pairs are sufficently low to suggest sub-solidus cooling temperatures.

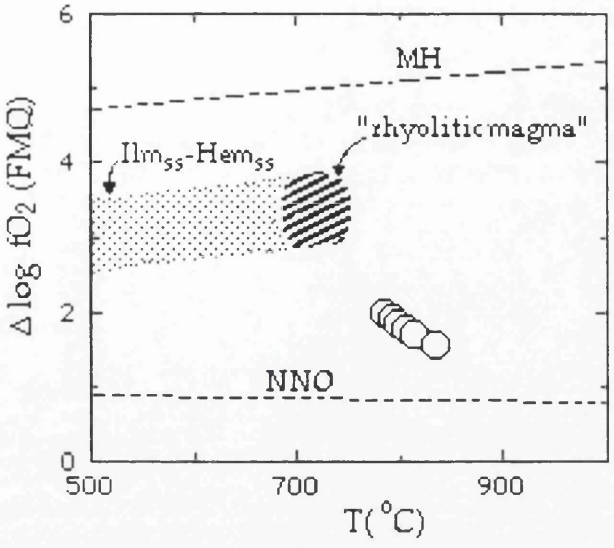

Figure 4.13. Oxygen fugacity relative to FMQ(Δlog fO_2) plotted against temperature for the andesite. Oxygen fugacity and temperature were calculated according to Anderson and Lindsley(1985). The field labelled Ilm_{ss}-Hem_{ss} represents the coexisting ilmenite and hematite solid solutions(Spencer and Lindsley, 1981).

Table 4.11. Representative analyses of groundmass glass in the andesites.

Sample	MA-120 Glass	MA-120 Glass	MA-120 Glass	MA-120 Glass	MA-148 Glass	MA-148 Glass
SiO_2	79.38	73.83	74.03	71.59	51.12	57.47
TiO_2	0.26	0.26	0.18	0.43	0.12	0.09
Al_2O_3	10.35	13.38	14.27	13.44	29.19	25.78
FeO*	0.65	0.56	0.69	0.67	0.78	0.82
MnO	0.05	0.06	0.00	0.00	0.03	0.00
MgO	0.15	0.09	0.35	0.07	0.02	0.23
CaO	1.67	1.83	2.33	1.41	12.68	9.63
Na_2O	3.36	3.63	4.42	2.25	3.73	5.07
K_2O	1.81	3.10	2.98	5.26	0.14	0.66
P_2O_5	0.05	0.16	0.23	0.16	0.07	0.00
Cr_2O_3	0.00	0.00	0.00	0.00	0.03	0.07
NiO	0.04	0.00	0.00	0.00	0.00	0.00
Total	97.77	96.90	99.48	95.28	97.91	99.82

FeO* is total iron as FeO.

Table 4.7. Representative analyses of feldspars in the andesites.

Sample	MA-120 Micro-pheno	MA-120 Micro-lite	MA-120 Pheno core	MA-120 Pheno rim	MA-120 Inclus. in bio	MA-120 Pheno core	MA-120 Pheno rim	MA-120 Pheno	MA-148 Pheno core	MA-148 Pheno rim	MA-148 Micro-pheno
SiO_2	49.25	51.57	55.98	56.64	56.26	51.22	53.88	50.28	55.35	50.54	56.79
TiO_2	0.10	0.02	0.02	0.00	0.00	0.01	0.05	0.00	0.05	0.00	0.00
Al_2O_3	30.89	29.69	27.12	26.15	27.42	30.29	28.64	32.05	27.74	30.94	27.05
FeO*	0.74	0.86	0.28	0.21	0.36	0.38	0.44	0.66	0.16	0.61	0.22
MnO	0.02	0.04	0.00	0.00	0.00	0.00	0.00	0.00	0.01	0.00	0.01
MgO	0.08	0.13	0.09	0.11	0.00	0.02	0.08	0.13	0.16	0.04	0.14
CaO	14.43	13.18	9.60	8.59	9.64	13.78	11.50	15.46	9.54	14.33	9.11
Na_2O	3.23	3.88	5.71	6.14	5.68	3.44	4.85	2.97	5.50	3.20	6.07
K_2O	0.15	0.26	0.44	0.53	0.46	0.19	0.24	0.11	0.51	0.16	0.45
P_2O_5	0.10	0.09	0.00	0.00	0.04	0.00	0.06	0.00	0.02	0.00	0.08
Cr_2O_3	0.02	0.01	0.03	0.00	0.09	0.06	0.06	0.00	0.00	0.11	0.07
NiO	0.11	0.01	0.01	0.00	0.06	0.00	0.00	0.00	0.07	0.00	0.03
Total	99.17	99.74	99.28	98.37	100.01	99.39	99.80	101.66	99.21	99.93	100.02
Formula on the basis of 32 oxygens											
Si	9.11	9.44	10.15	10.33	10.13	9.38	9.78	9.06	10.15	9.16	10.21
Ti	0.01	0.00	0.00	0.00	0.00	0.00	0.01	0.00	0.01	0.00	0.00
Al	6.73	6.40	5.80	5.62	5.82	6.54	6.13	6.81	5.78	6.74	5.73
Fe^{+2}	0.12	0.13	0.04	0.03	0.05	0.06	0.07	0.10	0.03	0.01	0.03
Mn	0.00	0.01	0.00	0.00	0.00	0.00	0.00	0.00	0.00	0.00	0.00
Mg	0.02	0.04	0.02	0.03	0.00	0.01	0.02	0.04	0.05	0.01	0.04
Ca	2.86	2.59	1.86	1.68	1.86	2.71	2.24	2.99	1.88	2.84	1.75
Na	1.16	1.38	2.01	2.17	1.98	1.22	1.71	1.04	1.95	1.15	2.11
K	0.03	0.06	0.10	0.12	0.11	0.05	0.06	0.03	0.12	0.05	0.10
P	0.02	0.01	0.00	0.00	0.01	0.00	0.01	0.00	0.00	0.00	0.01
Cr	0.00	0.00	0.00	0.00	0.01	0.01	0.00	0.00	0.00	0.02	0.01
Ni	0.02	0.00	0.00	0.00	0.01	0.00	0.00	0.00	0.01	0.00	0.01
Total	20.09	20.06	20.00	20.00	19.99	19.98	20.02	20.06	19.99	20.05	20.02
An	70.62	64.28	46.86	42.32	47.09	68.09	55.87	73.65	47.60	70.30	44.19
Ab	28.64	34.24	50.62	54.66	50.13	30.65	42.64	25.61	49.37	28.46	53.28
Or	0.74	1.48	2.52	3.02	2.78	1.26	1.49	0.74	3.03	1.24	2.53

FeO*is total iron as FeO.

Table 4.8. Representative analyses of biotites in the andesites.

Sample	MA-120 pheno	MA-120 pheno	MA-148 pheno	MA-148 pheno	MA-148 pheno
SiO_2	37.37	37.19	36.02	36.13	38.59
TiO_2	5.44	4.74	5.10	5.44	4.73
Al_2O_3	14.06	14.15	13.13	14.82	15.77
Fe_2O_3	2.05	2.59	2.21	1.61	1.82
FeO	10.44	13.21	11.27	8.22	9.26
MnO	0.18	0.16	0.32	0.19	0.26
MgO	16.61	14.94	20.08	19.15	19.86
CaO	0.00	0.08	0.21	0.12	0.02
Na_2O	0.88	0.52	0.71	0.90	0.82
K_2O	9.03	8.55	7.67	8.00	7.69
P_2O_5	0.02	0.05	0.00	0.03	0.01
Cr_2O_3	0.00	0.00	0.00	0.08	0.05
NiO	0.00	0.00	0.02	0.00	0.00
Total	96.08	96.18	96.74	94.69	98.88
Formula on the basis of 22 oxygens					
Si	5.47	5.49	5.25	5.29	5.39
Ti	0.60	0.53	0.56	0.60	0.50
Al	2.43	2.46	2.26	2.56	2.60
Fe^{+3}	0.23	0.29	0.24	0.18	0.19
Fe^{+2}	1.28	1.63	1.38	1.01	1.08
Mn	0.02	0.02	0.04	0.02	0.03
Mg	3.62	3.29	4.36	4.18	4.13
Ca	0.00	0.01	0.03	0.02	0.00
Na	0.25	0.15	0.20	0.25	0.22
K	1.69	1.61	1.43	1.49	1.37
P	0.00	0.01	0.00	0.00	0.00
Cr	0.00	0.00	0.00	0.01	0.01
Ni	0.00	0.00	0.00	0.00	0.00
Total	15.57	15.48	15.75	15.61	15.51
$Mg^{\#}$	0.71	0.63	0.73	0.78	0.76
Phlog.	60.35	53.80	54.29	60.19	54.26
Annite	21.28	26.70	17.11	14.51	14.19

Fe^{+3} is calculated by ratio according to Schumacher(1991).
$Mg^{\#}=Mg/(Mg+Fe^{+3}+Fe^{+2})$

Table 4.9. Representative analyses of pyroxenes in the andesites.

Sample	MA-148	MA-148	MA-148	MA-148	MA-148	MA-148	MA-148
	Opx	Cpx	Cpx	Opx	Cpx	Cpx	Cpx
	micro	micro	micro	micro	micro	micro	micro
SiO_2	51.60	49.27	49.28	52.87	52.19	49.47	50.91
TiO_2	0.15	0.74	0.52	0.20	0.43	0.56	0.32
Al_2O_3	2.67	4.05	4.29	1.38	1.21	4.91	2.54
FeO*	15.99	9.19	8.47	15.62	9.19	8.37	7.99
MnO	0.37	0.26	0.31	1.13	0.29	0.20	0.30
MgO	26.25	14.77	14.52	27.67	15.40	14.33	15.79
CaO	1.43	19.95	20.74	0.82	20.64	21.03	19.80
Na_2O	0.28	0.62	0.88	0.18	0.24	0.55	0.42
K_2O	0.00	0.00	0.00	0.04	0.00	0.01	0.03
P_2O_5	0.09	0.03	0.00	0.07	0.08	0.14	0.08
Cr_2O_3	0.16	0.16	0.25	0.03	0.06	0.37	0.15
NiO	0.05	0.00	0.02	0.01	0.00	0.07	0.06
Total	99.04	99.04	99.28	100.02	99.73	100.01	98.39
Formula on the basis of 6 oxygens							
Si	1.88	1.84	1.83	1.92	1.94	1.83	1.90
Ti	0.00	0.02	0.01	0.01	0.01	0.02	0.01
Al	0.11	0.18	0.19	0.06	0.05	0.21	0.11
Fe^{+3}	0.13	0.14	0.18	0.10	0.05	0.12	0.08
Fe^{+2}	0.36	0.14	0.08	0.37	0.24	0.14	0.17
Mn	0.01	0.01	0.01	0.03	0.01	0.01	0.01
Mg	1.42	0.82	0.80	1.47	0.85	0.79	0.88
Ca	0.06	0.80	0.82	0.03	0.82	0.83	0.79
Na	0.02	0.04	0.06	0.01	0.02	0.04	0.03
K	0.00	0.00	0.00	0.00	0.00	0.00	0.00
P	0.00	0.00	0.00	0.00	0.00	0.00	0.00
Cr	0.00	0.00	0.01	0.00	0.00	0.01	0.00
Ni	0.00	0.00	0.00	0.00	0.00	0.00	0.00
Total	4.00	4.00	4.00	4.00	4.00	4.00	4.00
$Mg^{\#}$	0.74	0.75	0.75	0.76	0.75	0.75	0.78
Wo	2.83	41.67	43.39	1.57	41.72	44.12	41.05
En	71.99	42.92	42.25	73.46	43.31	41.84	45.52
Fs	25.18	15.41	14.36	24.97	14.97	14.04	13.43

Fe^{+3} is calculated by normalization according to Schumacher(1991).
$Mg^{\#}=Mg/(Mg+Fe^{+3}+Fe^{+2})$

Table 4.10. Representative analyses of Fe-Ti oxides in the andesites.

Sample	MA-148 Magnet. micro	MA-148 Magnet. micro	MA-120 Magnet. micro	MA-120 Magnet inclus.	MA-120 Magnet. micro	MA-148 Magnet. micro	MA-120 Magnet. micro	MA-120 Magnet. micro	MA-120 Ilmenite
SiO_2	0.27	0.26	0.19	0.23	0.26	0.30	0.35	0.40	0.40
TiO_2	2.12	3.10	15.99	5.65	8.51	1.25	6.52	6.35	32.65
Al_2O_3	2.36	0.90	0.79	2.68	1.73	2.63	1.44	3.51	2.15
FeO*	88.33	85.28	71.19	80.52	78.32	86.28	80.13	78.68	58.42
MnO	0.69	0.58	1.05	0.47	0.23	0.78	0.47	0.24	0.18
MgO	2.04	1.63	1.83	2.31	3.65	1.88	2.76	1.86	0.64
CaO	0.20	0.08	0.03	0.06	0.07	0.55	0.00	0.06	0.00
Na_2O	0.36	0.28	0.00	0.06	0.19	0.12	0.00	0.04	0.31
K_2O	0.00	0.00	0.02	0.02	0.00	0.03	0.02	0.00	0.00
P_2O_5	0.02	0.06	0.03	0.00	0.00	0.48	0.00	0.00	0.00
Cr_2O_3	0.09	0.15	0.13	0.07	0.08	0.04	0.17	0.24	0.16
NiO	0.00	0.00	0.11	0.00	0.00	0.00	0.10	0.00	0.06
Total	96.48	92.32	91.36	92.07	93.04	94.34	91.96	91.38	94.97
Formula on the basis of 32 oxygens for magnetites and 6 oxygens for ilmenite									
Si	0.01	0.01	0.01	0.01	0.01	0.01	0.01	0.02	0.01
Ti	0.06	0.09	0.47	0.16	0.24	0.03	0.19	0.18	0.63
Al	0.10	0.04	0.04	0.10	0.08	0.11	0.06	0.16	0.06
Fe^{+3}	1.79	1.77	1.00	1.56	1.44	1.76	1.53	1.44	0.67
Fe^{+2}	0.88	0.95	1.33	1.01	1.01	0.91	1.02	1.08	0.58
Mn	0.02	0.02	0.03	0.02	0.01	0.02	0.02	0.01	0.004
Mg	0.11	0.09	0.11	0.13	0.20	0.10	0.16	0.11	0.02
Ca	0.01	0.00	0.00	0.00	0.00	0.02	0.00	0.00	0.00
Na	0.03	0.02	0.00	0.00	0.01	0.01	0.00	0.00	0.02
K	0.00	0.00	0.00	0.00	0.00	0.00	0.00	0.00	0.00
P	0.01	0.00	0.00	0.00	0.00	0.02	0.00	0.00	0.00
Cr	0.00	0.00	0.00	0.00	0.00	0.00	0.01	0.01	0.00
Ni	0.00	0.00	0.00	0.00	0.00	0.00	0.00	0.00	0.00
Total	3.00	3.00	3.00	3.00	3.00	3.00	3.00	3.00	2.00
Mn/Mg	0.18	0.22	0.27	0.15	0.05	0.20	0.13	0.10	0.20
sp	5.17	2.13	2.41	5.59	4.35	6.00	3.61	8.84	
mg-chr	0.13	0.24	0.26	0.11	0.13	0.07	0.29	0.41	
mg-fer	5.98	7.38	11.50	8.72	18.63	4.80	13.63	2.57	
trev	0.00	0.00	0.45	0.00	0.00	0.00	0.34	0.00	
mt	85.77	85.59	54.22	76.69	63.29	87.32	71.66	77.97	
usp	2.96	4.67	31.17	8.89	13.61	1.82	10.47	10.20	

Fe^{+3} is calculated by normalizaton according to Schumacher(1991).

4.4. TRACHYANDESITE

4.4.1. PETROGRAPHY

The rock is hypocrystalline porphyritic textured with interstitial groundmass, and contains phenocrysts of plagioclase, quartz, hornblende and biotite, with microphenocrysts of the same minerals and orthopyroxene- clinopyroxene and rare opaque oxides. The groundmass is very finely crystallized and microlitic with plagioclase, opx+cpx, rare sanidine, and accessory apatite with little or no volcanic glass. The mode is plagioclase (50-65%), opx+cpx(7-10%), amphibole (7-10%), biotite (5%), quartz (3%), sanidine (2%) and opaque oxides (3-5%).

Plagioclase phenocrysts and microphenocrysts are subhedral or rarely corroded, and occur in clusters. They commonly have sieve-texture, sometimes with a thin overgrowth rim(Figure 4.14). Generally, unsieved crystals show albite twinning and oscillatory zoning. Some phenocrysts contain internal cracks. Plagioclase may include apatite needles. Sanidine may occur as acicular crystals in the groundmass.

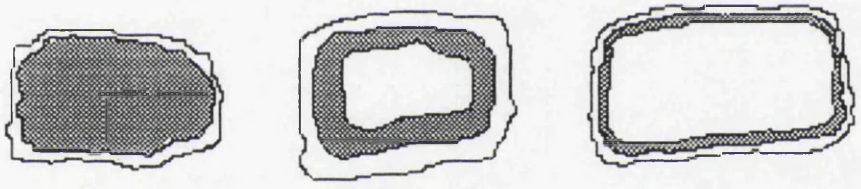

Figure 4.14. Three types of sieve-texture observed in plagioclase phenocrysts. Shaded area represents sieved region; (a) and (b) in the core, (c) at the margin of the phenocryst.

Quartz has irregular or rounded shapes with internal cracks and seems to be xenocrysts with common embayments caused by dissolution. Some are enclosed by pyroxene micrograins, resembling a corona texture. The corona is interpreted as forming by diffusion controlled growth of pyroxene in a dissolution boundary layer on quartz(Sato, 1975) induced by magma mixing.

Hornblendes are subhedral to anhedral "ghost like" crystals and fresh hornblendes are rare; usually they are replaced by opaques and fine silicates(quartz and opx), as a consequence of amphibole breakdown. These features indicate a disequilibrium with melt. In some cases, amphiboles have only thin opaque reaction rim surround an original core. Hornblende also forms crystal clots together with plagioclase.

Biotites are subhedral and are also pseudomorphed by opaque oxides with patchy areas of preserved biotites. Similar reaction products of biotites in dacites were interpreted by Nixon(1988a) as resulting from dehydration

above the biotite stability limit as result of magma mixing.

Ortho- and clinopyroxene are subhedral single grains or aggregates. In one large cpx enclosed by amphibole pseudomorphs, there is embayment of plagioclase in patchy areas. In some samples, small grains of cpx form coronas on quartz.

The groundmass contains plagioclase and rare sanidine needles, opaques and opx+cpx and pseudomorphed of amphibole and biotite micrograins. Microlitic and trachytic texture with sub-parallel arrangement of laths may occur.

There is therefore abundant textural evidences for disequilibrium, probably brought up by magma interaction or mixing. In some samples, it is evident that there is a heterogeneous rock texture, in which two distinct areas with different grain sizes and mineral compositions occur, reflecting incomplete magma mixing.

4.4.2. MINERAL CHEMISTRY

4.4.2.1. FELDSPAR

Phenocrysts(Table 4.12; Figure 4.15) are mainly andesine(An_{50-39}) with reverse zoning or with a calcic overgrowth rim around a sieved core. The composition changes from An_{42-44} in the core to An_{65-75} in the rim.

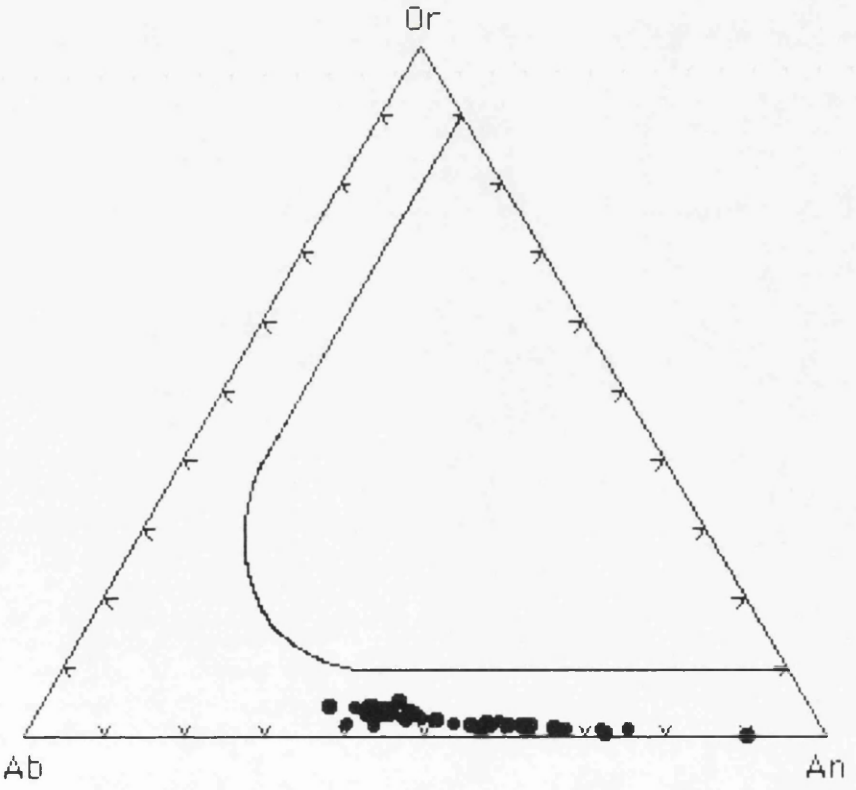

Figure 4.15. Ternary An-Ab-Or plot of feldspars in the trachyandesites.

However, there are also a few normally zoned andesines(An_{46} in the core varying to An_{39} in the rim), and bytownite phenocrysts with a composition varying from An_{89} in the core to An_{66}, or An_{71} in the core varying to An_{67} in the rim. Microphenocrysts of plagioclase are also andesine(An_{36-41}) and common labradorite(An_{57-72}).

Microlites in the groundmass are generally labradorite with a composition ranging from An_{54} to An_{62}. There are also some andesine(An_{41}).

The presence of sieved texture, calcic overgrowths and reverse zoning in the plagioclase phenocrysts, a varied range of compositions in different crystals and more calcic groundmass relative to phenocrysts reflect disequilibrium conditions. These relationships have been interpreted as the result of magma mixing(Kuno, 1950; Anderson, 1976; Nixon and Pearce, 1987; Kolisnik, 1990), or basic and acidic magma interaction(Stimac and Pearce, 1992).

4.4.2.2. PYROXENE

Augites(Table 4.13; Figure 4.16) have a composition ranging from $Wo_{46}En_{47}Fs_7$ to $Wo_{40}En_{48}Fs_{12}$, and a $Mg/(Mg+Fe^{+3}+Fe^{+2})$ ratio from 0.88 to 0.80. Some of phenocrysts display zoning with Fe-rich rims; the composition varies from $Wo_{43}En_{49}Fs_8$ in the core to $Wo_{40}En_{48}Fs_{12}$ in the rim, with the $Mg/(Mg+Fe^{+3}+Fe^{+2})$ ratio varying from 0.87 to 0.81, or a composition from $Wo_{46}En_{47}Fs_7$ in the core varying to $Wo_{44}En_{47}Fs_9$ in the rim with a $Mg/(Mg+Fe^{+3}+Fe^{+2})$ ratio from 0.87 to 0.85 in the rim. Generally, augites are Ti-poor types with a TiO_2 content below 1 wt.%(0.17-0.96 wt.%) which reveals a subalkaline host rock(Kushiro, 1960; Le Bas, 1962). Some of them are chromian with a Cr_2O_3 content 0.55-0.86 wt.%.

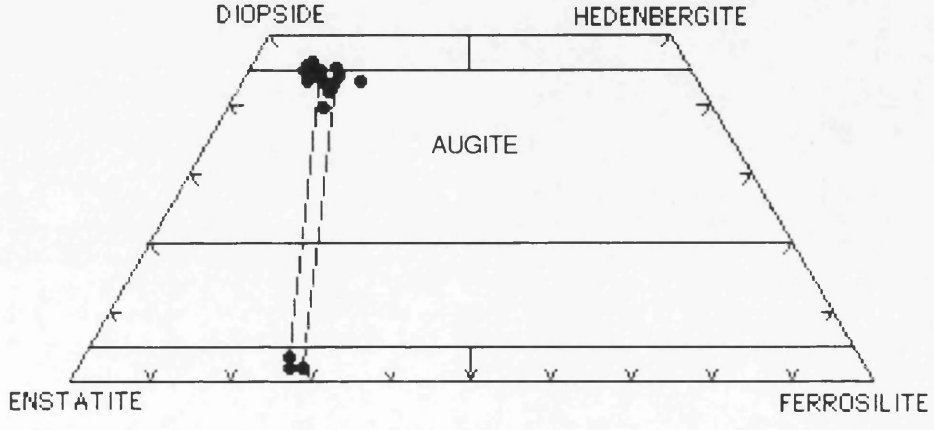

Figure 4.16. Ternary Wo-En-Fs plot of pyroxenes in the trachyandesite. Tie lines project to the Wo-En join at about Wo_{70-73}.

Orthopyroxenes have a composition ranging from $Wo_2En_{66}Fs_{32}$ to $Wo_3En_{71}Fs_{26}$, and a $Mg/(Mg+Fe^{+3}+Fe^{+2})$ ratio from 0.69 to 0.74. Figure 4.17 shows the opx and cpx crystallized in equilibrium. Augite and orthopyroxene assemblages that have Mg/(Mg+Fe) ratios >24% are present in andesites(Kuno, 1966; Nakamura and Kushiro, 1970a), and presumably crystallized at lower temperatures than the pyroxenes of basalts(Huebner, 1980).

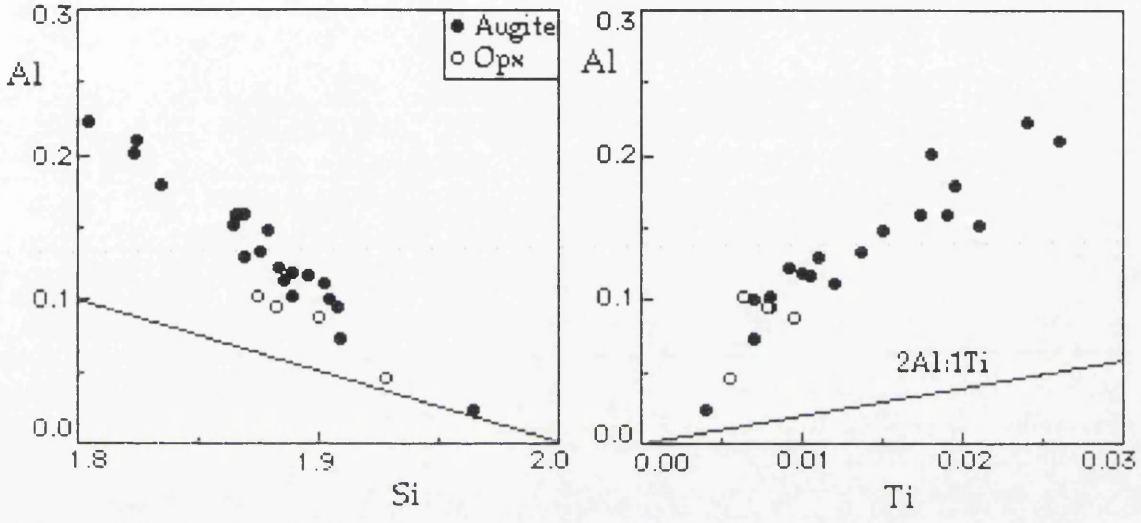

Figure 4.17. Plots of total Al versus Si and Ti contents per formula units for augites and orthopyroxenes in the trachyandesite.

4.4.2.3. HORNBLENDE

Hornblendes are mainly magnesio-hastingsites and a few magnesio-hornblendes(Table 4.14; Figure 4.18), according to the classification of Leake(1978). Generally, they are homogeneous and have two distinct compositions.

Magnesio-hornblendes have a $Mg/(Mg+Fe^{+3}+Fe^{+2})$ ratio between 0.52 and 0.57, Ti 0.15-0.16 and Si of 6.71-6.84 per formula units. Magnesio-hastingsites have a $Mg/(Mg+Fe^{+3}+Fe^{+2})$ ratios from 0.70 to 0.74, and are rich in Mg and Ti relative to magnesio-hornblendes with Ti of 0.28-0.37 and Si of 5.88-6.10 per formula unit. They are therefore titanian magnesio-hastingsites. On the variation plots(Figure 4.19), there is good correlation between total Al versus tetrahedral Al[4] and Ti per formula units.

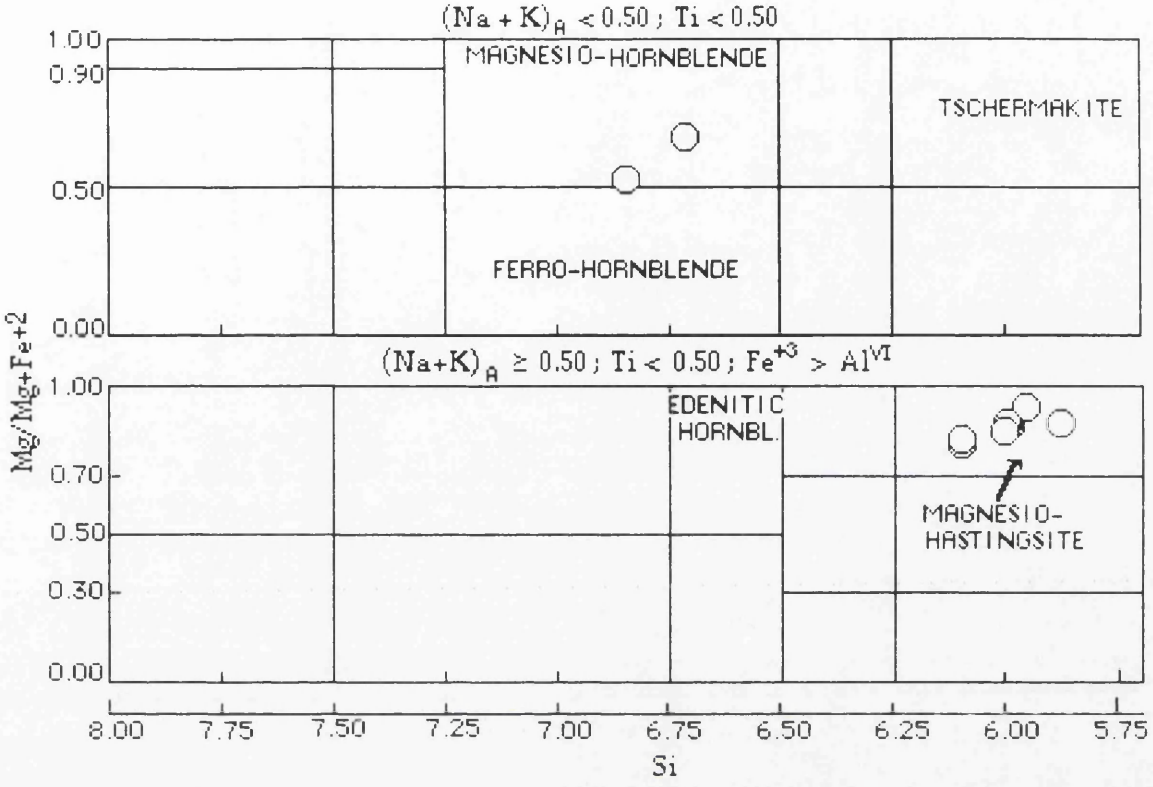

Figure 4.18. Classification and nomenclature of hornblendes in the trachyandesites, according to Leake(1978).

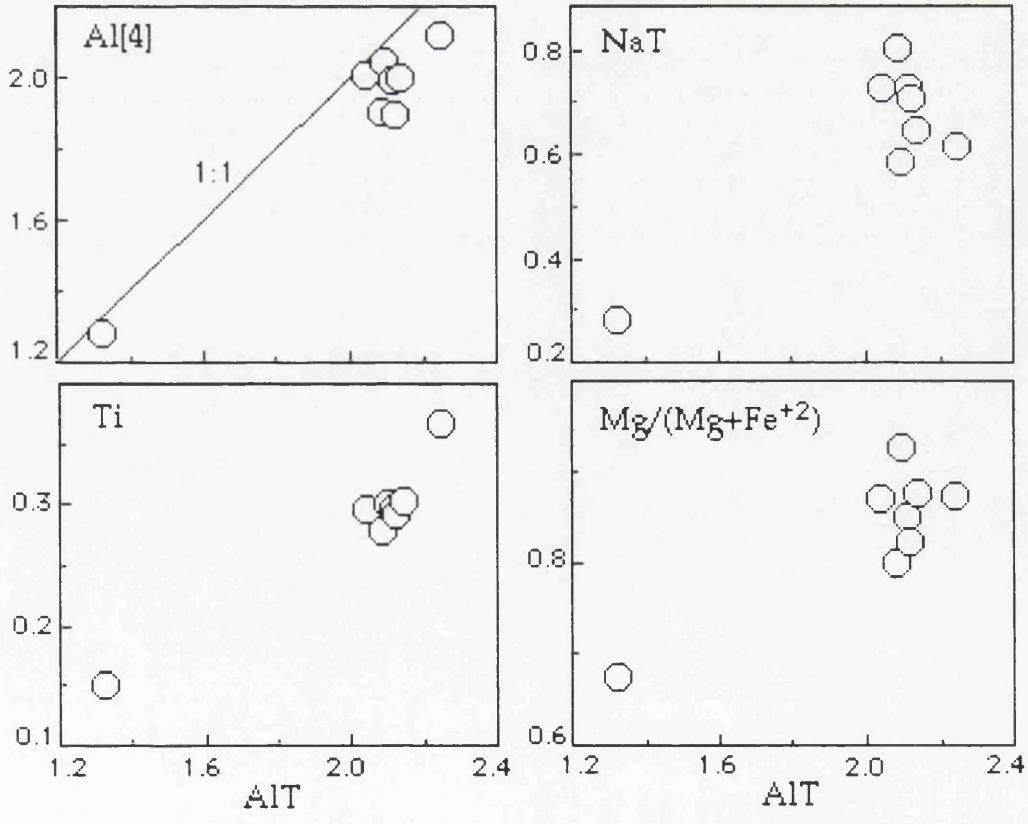

Figure 4.19. Tetrahedral Al[4], Ti, NaT and Mg/(Mg+Fe^{+2}) ratio plotted against total AlT per formula unit of hornblendes in the trachyandesite.

4.4.2.4. BIOTITE

Biotites are phlogopite(70-75)-annite(11-15) rich types, being high in Mg(Table 4.15; Figure 4.20) with $Mg/(Mg+Fe^{+3}+Fe^{+2})$ ratios varying from 0.80 to 0.86, and Ti from 0.50 to 0.69 per formula unit. Trace element contents are very low and insignificant. Generally, analyses of biotite show relatively high-TiO_2(4.56-6.33 wt.%) and uniform Mg-rich compositions suggesting crystallization from basic liquids of restricted composition.

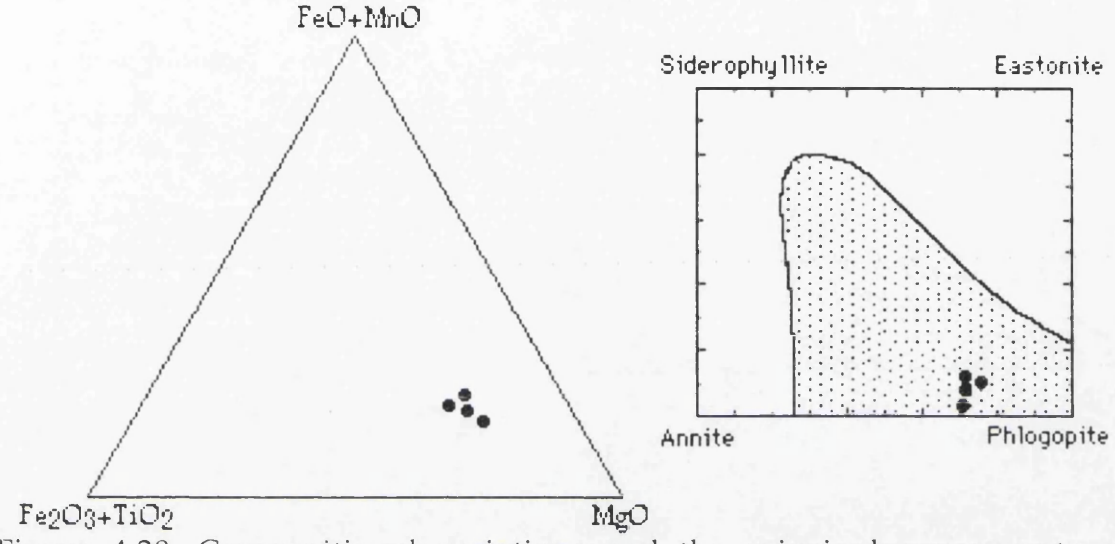

Figure 4.20. Compositional variations and the principal components of biotite compositions in the trachyandesite. The shaded field is that in which most natural biotites lie(after Deer *et al.*, 1992).

4.4.2.5. FE-TI OXIDES

Magnetite is the common oxide mineral together with rare ilmenite, both being homogeneous(Table 4.16;Figure 4.21).

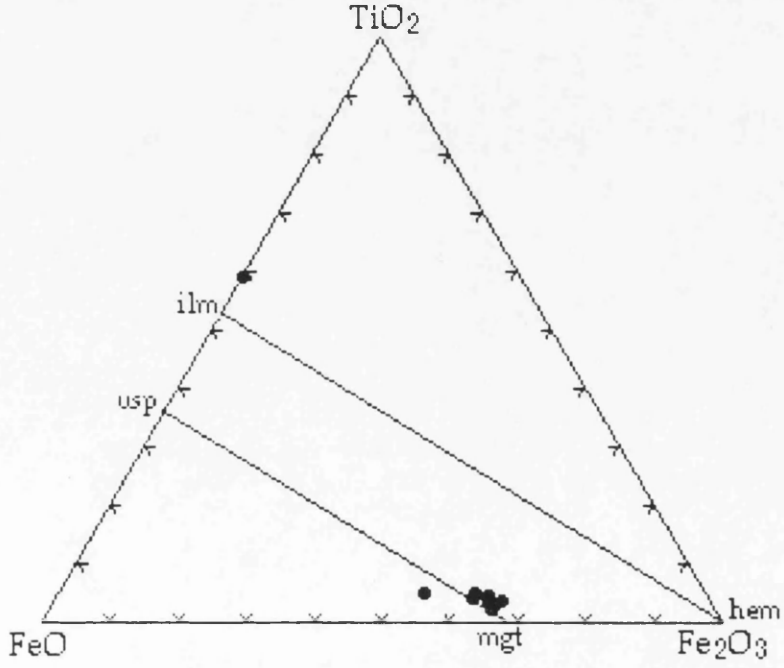

Figure 4.21. Compositions of Fe-Ti oxides in the trachyandesites.

Magnetites are slightly Ti-rich with TiO_2 varying from 2.21 up to 4.33 wt.%. A few individual grains contain exsolved ilmenite. Ilmenites are almost stoichiometric with 3.83-3.93 wt.% of MgO. Mn and Mg partitioning between magnetite and ilmenite suggests disequilibrium for the two coexisting phases(Bacon and Hirschmann, 1988).

4.4.3. GEOTHERMOMETRY AND GEOBAROMETRY

Since magnetite displays exolution lamellae of ilmenite, they were not used for geothermometry. Two pyroxene geothermometer gave a solvi temperature between 1015°C and 1089°C(Table 4.17), according to the method of Kretz(1982).

Water contents of >4 wt.%, temperatures of <1050 °C, and pressure of 2-10 kbars are required for amphibole to be stable in andesitic melts(Allen and Boetcher, 1978; Eggler, 1972a; Eggler and Burnham, 1973; Cawthorn and O'Hara, 1976; Helz, 1973). In addition, oxygen fugacity measurements of hornblende bearing andesites are at or above Ni-NiO buffer(Haggerty, 1976).

Table 4.17. Coexisting two pyroxene compositions and calculated solvi temperatures, according to Kretz(1982).

	Opx	Cpx	Opx	Cpx	Opx	Cpx	Opx	Cpx
Wo	0.035	0.425	0.020	0.447	0.019	0.437	0.017	0.425
En	0.714	0.471	0.710	0.480	0.721	0.480	0.676	0.470
Fs	0.233	0.104	0.251	0.073	0.241	0.084	0.285	0.115
T(°C)	1067		1015		1045		1089	

Table 4.18. Representative analyses of groundmass glass in the trachyandesite.

Sample	MA-143 Glass	MA-143 Glass	MA-132 Glass	MA-132 Glass	MA-132 Glass
SiO_2	53.79	57.91	54.05	64.46	81.92
TiO_2	0.00	0.07	0.09	0.28	0.23
Al_2O_3	27.76	25.62	28.22	18.64	11.06
FeO*	0.91	0.73	0.78	0.51	0.35
MnO	0.00	0.02	0.08	0.00	0.00
MgO	0.07	0.13	0.00	0.03	0.10
CaO	11.02	8.73	11.04	3.03	1.61
Na_2O	4.80	5.91	4.76	11.74	2.48
K_2O	0.50	0.77	0.46	0.07	2.90
P_2O_5	0.00	0.18	0.03	0.05	0.13
Cr_2O_3	0.06	0.00	0.00	0.02	0.00
NiO	0.00	0.08	0.00	0.00	0.00
Total	98.91	100.16	99.51	98.83	100.78

FeO* is total iron as FeO.

Table 4.12. Representative analyses of feldspars in the trachyandesite.

Sample	MA-143 Pheno core	MA-143 Pheno rim	MA-143 Pheno core	MA-143 Pheno rim	MA-143 Micro-lite	MA-143 Mega core	MA-143 Mega rim	MA-132 Micro-lite	MA-132 Micro-pheno	MA-132 Pheno core	MA-132 Pheno rim
SiO_2	58.08	51.26	57.35	51.30	53.01	55.88	52.53	51.93	57.72	56.91	50.12
TiO_2	0.01	0.00	0.07	0.02	0.00	0.02	0.00	0.02	0.05	0.00	0.07
Al_2O_3	26.44	30.16	26.16	30.14	28.95	27.70	29.23	29.57	26.46	26.69	31.13
FeO*	0.16	0.47	0.70	0.52	0.85	0.27	0.64	0.63	0.26	0.21	0.71
MnO	0.06	0.00	0.01	0.00	0.00	0.06	0.00	0.02	0.08	0.01	0.04
MgO	0.13	0.23	0.05	0.10	0.01	0.07	0.08	0.18	0.14	0.00	0.09
CaO	8.63	13.49	8.75	13.17	12.08	9.84	12.31	12.63	8.29	9.39	14.69
Na_2O	6.18	3.77	5.57	3.60	4.39	5.13	4.17	4.12	6.18	5.51	2.64
K_2O	0.62	0.28	0.87	0.21	0.30	0.45	0.31	0.26	0.81	0.58	0.19
P_2O_5	0.00	0.00	0.04	0.00	0.00	0.00	0.03	0.00	0.02	0.00	0.00
Cr_2O_3	0.08	0.14	0.00	0.05	0.00	0.01	0.00	0.05	0.00	0.00	0.00
NiO	0.00	0.00	0.00	0.01	0.00	0.00	0.00	0.09	0.00	0.00	0.00
Total	100.39	99.80	99.57	99.12	99.59	99.43	99.30	99.50	100.01	99.30	99.68
Formula on the basis of 32 oxygens											
Si	10.37	9.37	10.36	9.41	9.67	10.10	9.61	9.51	10.36	10.22	9.11
Ti	0.00	0.00	0.01	0.00	0.00	0.00	0.00	0.00	0.01	0.00	0.01
Al	5.56	6.50	5.57	6.52	6.23	5.90	6.30	6.38	5.60	5.75	6.80
Fe^{+2}	0.02	0.07	0.11	0.08	0.13	0.04	0.10	0.09	0.04	0.03	0.11
Mn	0.01	0.00	0.00	0.00	0.00	0.01	0.00	0.00	0.01	0.00	0.01
Mg	0.04	0.06	0.01	0.03	0.00	0.02	0.02	0.05	0.04	0.00	0.03
Ca	1.65	2.64	1.69	2.59	2.36	1.91	2.41	2.48	1.60	1.84	2.92
Na	2.14	1.34	1.95	1.28	1.55	1.80	1.48	1.46	2.15	1.95	0.95
K	0.16	0.07	0.20	0.05	0.07	0.11	0.07	0.06	0.19	0.13	0.04
P	0.00	0.00	0.01	0.00	0.00	0.00	0.00	0.00	0.00	0.00	0.00
Cr	0.01	0.02	0.00	0.01	0.00	0.00	0.00	0.01	0.00	0.00	0.00
Ni	0.00	0.00	0.00	0.00	0.00	0.00	0.00	0.00	0.00	0.00	0.00
Total	19.99	20.07	19.91	19.99	20.03	19.89	20.01	20.06	19.99	19.95	19.98
An	41.77	65.19	44.01	66.17	59.30	50.00	60.86	62.00	40.61	46.94	74.68
Ab	54.18	33.08	50.78	32.65	38.94	47.12	37.37	36.50	54.57	49.74	24.30
Or	4.05	1.73	5.21	1.28	1.76	2.88	1.77	1.50	4.82	3.32	1.02

FeO* is total iron as FeO.

Table 4.13. Representative analyses of pyroxenes in the trachyandesite.

Sample	MA-143 Cpx micro-core	MA-143 Cpx micro-rim	MA-143 Cpx micro	MA-143 Cpx micro	MA-143 Cpx pheno	MA-143 Cpx pheno	MA-132 Opx micro	MA-132 Opx micro	MA-132 Cpx pheno core	MA-132 Cpx micro	MA-132 Cpx micro
SiO_2	52.43	50.67	49.32	52.05	51.80	52.15	52.58	51.98	52.42	50.95	51.17
TiO_2	0.27	0.70	0.88	0.40	0.39	0.30	0.29	0.24	0.44	0.64	0.33
Al_2O_3	1.73	3.66	5.21	2.80	2.64	2.41	2.27	2.42	2.62	3.71	2.86
FeO*	4.78	7.06	6.84	4.88	4.58	4.10	16.91	19.80	4.54	5.75	4.94
MnO	0.25	0.33	0.21	0.05	0.16	0.17	0.64	1.27	0.09	0.20	0.06
MgO	17.76	16.89	16.16	16.65	16.55	17.28	26.56	24.57	16.64	16.32	16.52
CaO	21.87	19.35	20.08	22.43	22.55	22.56	1.01	0.87	22.34	21.37	22.31
Na_2O	0.30	0.31	0.62	0.53	0.64	0.44	0.40	0.35	0.55	0.44	0.37
K_2O	0.02	0.00	0.00	0.00	0.01	0.06	0.00	0.00	0.00	0.00	0.00
P_2O_5	0.04	0.03	0.22	0.00	0.02	0.05	0.06	0.00	0.01	0.00	0.01
Cr_2O_3	0.53	0.21	0.36	0.64	0.67	0.84	0.04	0.00	0.86	0.33	0.55
NiO	0.00	0.07	0.00	0.00	0.03	0.06	0.03	0.02	0.03	0.05	0.03
Total	99.98	99.28	99.90	100.43	100.04	100.42	100.79	101.52	100.54	99.76	99.15
Formula on the basis of 6 oxygens											
Si	1.91	1.87	1.81	1.89	1.89	1.89	1.88	1.88	1.90	1.87	1.88
Ti	0.01	0.02	0.02	0.01	0.01	0.01	0.01	0.01	0.01	0.01	0.01
Al	0.07	0.16	0.22	0.12	0.11	0.10	0.10	0.10	0.11	0.16	0.12
Fe^{+3}	0.10	0.08	0.13	0.10	0.12	0.11	0.14	0.16	0.07	0.09	0.10
Fe^{+2}	0.05	0.14	0.08	0.05	0.02	0.02	0.36	0.44	0.07	0.08	0.05
Mn	0.08	0.01	0.01	0.00	0.00	0.01	0.02	0.04	0.00	0.01	0.00
Mg	0.96	0.93	0.88	0.90	0.90	0.93	1.42	1.32	0.90	0.89	0.91
Ca	0.85	0.76	0.79	0.87	0.88	0.88	0.04	0.03	0.87	0.84	0.88
Na	0.02	0.02	0.04	0.04	0.04	0.03	0.03	0.02	0.04	0.00	0.03
K	0.00	0.00	0.00	0.00	0.00	0.00	0.00	0.00	0.00	0.00	0.00
P	0.00	0.00	0.01	0.00	0.00	0.00	0.00	0.00	0.00	0.00	0.00
Cr	0.02	0.01	0.01	0.02	0.02	0.02	0.00	0.00	0.02	0.01	0.02
Ni	0.00	0.00	0.00	0.00	0.00	0.00	0.00	0.00	0.00	0.00	0.00
Total	4.00	4.00	4.00	4.00	4.00	4.00	4.00	4.00	4.00	4.00	4.00
$Mg^{\#}$	0.86	0.81	0.81	0.86	0.87	0.88	0.74	0.69	0.87	0.84	0.86
Wo	43.31	39.81	41.78	45.37	45.76	45.19	1.96	1.69	45.50	43.86	45.36
En	48.91	48.33	46.77	46.85	46.73	48.14	71.51	66.36	47.14	46.60	46.71
Fs	7.78	11.86	11.45	7.78	7.51	6.67	26.53	31.95	7.36	9.54	7.93

Fe^{+3} is calculated by normalization according to Schumacher(1991).
$Mg^{\#}=Mg/(Mg+Fe^{+3}+Fe^{+2})$

Table 4.14. Representative analyses of amphiboles in the trachyandesite.

Sample	MA-143 Mag,-hasting. micro-pheno	MA-143 Mag,-hasting. micro-pheno	MA-143 Mag,-hasting. microph. opaqued	MA-143 Mag,-hasting. microph. opaqued	MA-143 Mag,-hasting. micro-pheno	MA-132 Mag,-hasting. -----	MA-132 Mag,-hasting. -----	MA-132 Mag.-hornbl. -----	MA-132 Mag.-hornbl. -----
SiO_2	42.03	41.82	41.87	40.87	41.48	41.56	40.46	42.31	43.51
TiO_2	2.56	2.67	2.74	2.68	2.79	2.79	3.35	1.29	1.31
Al_2O_3	12.20	12.34	12.51	11.82	12.38	12.57	13.13	5.75	7.28
FeO*	11.43	10.27	11.57	10.62	10.41	10.41	10.65	18.15	17.19
MnO	0.14	0.03	0.15	0.17	0.10	0.16	0.14	0.43	0.52
MgO	14.93	15.15	15.37	15.86	16.17	15.59	15.12	11.22	12.58
CaO	11.52	11.80	11.51	11.51	11.89	11.83	11.79	10.39	9.39
Na_2O	2.86	2.50	2.62	2.57	2.11	2.32	2.18	0.75	0.94
K_2O	0.68	0.78	0.75	0.68	0.78	0.78	0.85	0.59	0.98
P_2O_5	0.05	0.02	0.01	0.00	0.05	0.13	0.00	0.09	0.00
Cr_2O_3	0.00	0.05	0.02	0.02	0.05	0.02	0.03	0.02	0.04
NiO	0.06	0.00	0.00	0.10	0.08	0.02	0.02	0.00	0.00
Total	98.46	97.43	99.12	96.90	98.29	98.18	97.72	90.99	93.74
Formula on the basis of 23 oxygens									
Si	6.10	6.10	6.01	5.99	5.96	6.00	5.88	6.84	6.72
Al IV	1.90	1.90	1.99	2.01	2.04	1.99	2.12	0.00	1.28
Al T	2.09	2.12	2.12	2.04	2.10	2.14	2.25	1.12	1.32
Al VI	0.19	0.23	0.12	0.04	0.05	0.14	0.13	0.00	0.04
Ti	0.28	0.29	0.30	0.30	0.30	0.30	0.37	0.16	0.15
Fe^{+3}	0.45	0.40	0.67	0.66	0.84	0.64	0.67	0.00	0.62
Mg	3.22	3.30	3.29	3.47	3.46	3.56	3.27	2.77	2.89
Fe^{+2}	0.94	0.85	0.72	0.64	0.41	0.62	0.63	2.51	1.60
Mn	0.02	0.00	0.02	0.02	0.01	0.02	0.02	0.06	0.07
FMT	13.10	13.07	13.11	13.12	13.08	13.08	13.08	13.47	13.37
Ca	1.79	1.84	1.77	1.81	1.83	1.83	1.84	1.84	1.55
Na M4	0.11	0.08	0.12	0.07	0.09	0.09	0.09	0.00	0.08
Na T	0.80	0.71	0.73	0.73	0.59	0.65	0.61	0.24	0.28
Na A	0.69	0.62	0.60	0.66	0.50	0.56	0.53	0.00	0.21
K	0.13	0.14	0.14	0.13	0.14	0.14	0.16	0.12	0.19
Sum A	0.82	0.76	0.74	0.79	0.64	0.70	0.69	0.12	0.40
$Mg^{\#}$	0.70	0.73	0.70	0.73	0.73	0.74	0.72	0.52	0.57

Fe^{+3} is calculated by estimation according to Spear and Kimball(1984).
$Mg^{\#}=Mg/(Mg+Fe^{+3}+Fe^{+2})$

Table 4.15. Representative analyses of biotites in the trachyandesite.

Sample	MA-132 pheno	MA-132 pheno	MA-132 micro	MA-132 pheno	MA-143 pheno
SiO_2	37.99	37.09	38.31	38.75	37.12
TiO_2	5.14	6.33	4.56	4.72	4.89
Al_2O_3	14.25	13.02	14.06	12.33	13.72
Fe_2O_3	1.22	1.32	1.45	1.03	1.39
FeO	6.20	6.71	7.41	5.23	7.05
MnO	0.14	0.07	0.03	0.03	0.05
MgO	20.21	19.46	19.70	20.80	21.69
CaO	0.07	0.05	0.01	0.00	0.14
Na_2O	1.07	0.87	0.67	0.61	0.94
K_2O	9.04	9.11	9.39	9.14	9.39
P_2O_5	0.00	0.00	0.02	0.02	0.00
Cr_2O_3	0.00	0.00	0.06	0.00	0.02
NiO	0.00	0.05	0.02	0.00	0.00
Total	95.33	94.08	95.69	92.66	96.40
Formula on the basis of 22 oxygens					
Si	5.48	5.53	5.53	5.71	5.35
Ti	0.56	0.69	0.50	0.52	0.53
Al	2.42	2.23	2.39	2.14	2.33
Fe^{+3}	0.13	0.14	0.16	0.11	0.15
Fe^{+2}	0.75	0.82	0.90	0.64	0.85
Mn	0.02	0.01	0.00	0.00	0.01
Mg	4.34	4.21	4.24	4.56	4.66
Ca	0.01	0.01	0.00	0.00	0.02
Na	0.30	0.24	0.19	0.18	0.26
K	1.66	1.69	1.73	1.72	1.73
P	0.00	0.00	0.00	0.00	0.00
Cr	0.00	0.00	0.01	0.00	0.00
Ni	0.00	0.01	0.00	0.00	0.00
Total	15.67	15.56	15.65	15.59	15.88
$Mg^{\#}$	0.83	0.81	0.80	0.86	0.82
Phlog.	70.95	70.13	70.67	75.19	72.95
Annite	12.20	13.58	14.92	10.61	13.30

Fe^{+3} is calculated by ratio according to Schumacher(1991).
$Mg^{\#}=Mg/(Mg+Fe^{+3}+Fe^{+2})$

Table 4.16. Representative analyses of Fe-Ti oxides in the trachyandesite.

Sample	MA-143 Magnet. pheno	MA-143 Magnet. micro	MA-143 Magnet pheno	MA-143 Magnet. pheno	MA-132 Magnet. micro.	MA-132 Magnet. micro	MA-143 Ulvosp. pheno	MA-132 Ilmenit. micro	MA-132 Ilmenit. micro
SiO_2	4.89	0.58	0.20	0.61	0.24	0.65	0.31	0.17	0.16
TiO_2	4.33	3.96	3.39	2.21	4.33	3.55	34.92	53.68	43.87
Al_2O_3	1.75	1.91	2.48	2.42	8.29	1.52	0.23	2.47	0.52
FeO*	77.03	85.21	85.94	83.37	78.64	83.60	56.47	37.10	46.49
MnO	0.09	0.51	0.47	0.23	0.64	0.70	1.55	0.05	0.75
MgO	1.53	1.52	2.03	1.11	3.86	1.44	3.83	3.93	3.19
CaO	0.13	0.05	0.04	0.08	0.04	0.02	0.06	0.03	0.08
Na_2O	0.38	0.00	0.57	0.29	0.05	0.36	0.15	0.10	0.19
K_2O	0.22	0.05	0.01	0.03	0.00	0.06	0.00	0.00	0.02
P_2O_5	0.00	0.00	0.00	0.00	0.00	0.00	0.00	0.00	0.00
Cr_2O_3	0.20	0.23	0.17	0.14	0.12	0.24	0.05	0.03	0.04
NiO	0.00	0.00	0.05	0.05	0.05	0.00	0.00	0.00	0.00
Total	90.55	94.02	95.35	90.54	96.26	92.14	97.57	97.56	95.31
Formula on the basis of 32 oxygens									
Si	0.18	0.02	0.01	0.02	0.01	0.02	0.01	0.00	0.00
Ti	0.12	0.11	0.09	0.06	0.11	0.10	0.97	1.00	0.84
Al	0.08	0.08	0.11	0.11	0.34	0.07	0.01	0.07	0.02
Fe^{+3}	1.33	1.64	1.73	1.73	1.41	1.70	0.04	0.00	0.31
Fe^{+2}	1.14	1.03	0.89	0.97	0.89	0.96	1.70	0.77	0.69
Mn	0.01	0.02	0.01	0.01	0.02	0.02	0.05	0.01	0.02
Mg	0.09	0.08	0.11	0.06	0.20	0.08	0.21	0.15	0.12
Ca	0.01	0.00	0.00	0.00	0.00	0.00	0.00	0.00	0.00
Na	0.02	0.00	0.04	0.02	0.00	0.03	0.01	0.00	0.01
K	0.01	0.00	0.00	0.00	0.00	0.00	0.00	0.00	0.00
P	0.00	0.00	0.00	0.00	0.00	0.00	0.00	0.00	0.00
Cr	0.01	0.01	0.00	0.00	0.00	0.01	0.00	0.00	0.00
Ni	0.00	0.00	0.00	0.00	0.00	0.00	0.00	0.00	0.00
Total	3.00	3.00	3.00	3.00	3.00	3.00	3.00	2.00	2.00
Mn/Mg	0.11	0.25	0.09	0.17	0.10	0.25	0.24	0.07	0.17
sp	5.15	4.56	5.52	5.79	18.28	3.64	0.99		
mg-chr	0.40	0.37	0.25	0.22	0.19	0.38	0.14		
mg-fer	5.83	4.25	5.62	0.66	3.07	4.70	4.20		
trev	0.00	0.00	0.15	0.16	0.15	0.00	0.00		
mt	80.51	84.78	83.66	89.81	72.23	85.87	0.00		
usp	8.11	6.03	4.81	3.36	6.09	5.41	94.67		

Fe^{+3} is calculated by normalization according to Schumacher(1991).

4.5. DACITE

4.5.1. PETROGRAPHY

Dacites are generally hypocrystalline and porphyritic containing about 20-35% of both phenocrysts and microphenocrysts of mainly plagioclase, biotite, brownish-green hornblende, and rare anorthoclase and quartz in lesser amounts. Phenocrysts represent pre-eruptive crystallization at low degree undercooling. The groundmass is fine-grained and, or, glassy with plagioclase microlites, quartz, biotite, amphibole and opaque oxides, and accessory sphene, zircon and apatite. The mode is plagioclase(50%), biotite(10%), opaque oxides(7%), amphibole(5%), quartz(3%), alkali feldspar(<2) and accessories(2%).

Plagioclase phenocrysts and microphenocrysts are subhedral to anhedral with zoning, especially oscillatory zoning in some phenocrysts, and albite twinning. Phenocrysts may have embayments of glass with spongy texture, and also show sieve texture especially around the margins or in the core, indicating a dissolution effect. Despite the dissolution, they may still preserve oscillatory zoning and twinning. Embayments of glassy inclusions are seen commonly in the inner parts and sometimes an overgrowth rim encloses this embayed core. In addition, partially resorbed phenocrysts display thin overgrowth rims suggesting that the dissolution may have taken place as result of magma mixing, presumably in the magma chamber before eruption. Phenocrysts may include hornblende, biotite, opaque oxide and apatite.

Quartz crystals are anhedral or rounded shapes with common internal cracks and embayments filled by groundmass material. The embayment of quartz may be a disequilibrium growth form or a solution effect due to decrease in pressure or increase in temperature as magma rose to the surface. Donaldson and Henderson(1988) pointed out that solution at a crystal surface should actually be inhibited by an embayment, on the basis of experimental studies. Embayment can also result from unstable primary growth. If an embayed crystal has sharp corners and edges, and if a zone of inclusions follow the shape of the embayments, then primary disequilibrium growth rather than corrosion is the cause(Donaldson and Henderson, 1988). In the case of the studied samples, embayments are more likely to be the result of dissolution.

Subhedral biotites are partly or completely pseudomorphed by opaque minerals. They form clusters with amphibole, plagioclase and opaque oxides. Fresh biotites may contain opaque oxide and apatite inclusions. A few biotites show corona texture and are partially enclosed by hornblende, indicating magma mixing. Some phenocrysts include opaque oxides along

the cleavages and, or, around the rim of biotite, presumably formed as a result of reaction between biotite and melt.

Amphiboles are subhedral to anhedral sometimes with simple twinning, and occur as aggregates of partially altered grains, or pseudomorphed due to amphibole breakdown. They also form clusters with plagioclase laths. In some samples, amphibole is replaced by fine-grained opaque oxides and silicates, indicating an amphibole breakdown rather than alteration products. Some of them may preserve patchy areas of primary amphibole in the core.

The groundmass varies between glassy and fine grained representing high degrees of undercooling. The same minerals of phenocrysts and microphenocrysts are abundant, relative to volcanic glass which fills space between plagioclase laths. In some samples, microlites of plagioclase may show subparallel arrangement. In the fine-grained groundmass, quartz and plagioclase microlites are present with minor glass. Moreover, some samples display heteregeous textural patterns in which dark areas containing less microlites and light areas containing abundant microlites are in the same sample.

4.5.2. MINERAL CHEMISTRY

4.5.2.1. FELDSPAR

The dacite feldspar is mainly andesine and oligoclase with a few labradorites and anorthoclases(Table 4.19; Figure 4.22).

Phenocrysts are commonly andesine(An_{30-50}) and some labradorite(An_{50-60}). They display both normal and reverse zoning, and sieved phenocrysts have a thin calcic overgrowth rim(An_{60}), relative to the sodic core(An_{36}). Normally zoned phenocrysts have a composition from An_{42-49} in the core varying to An_{29-44} in the rim. Reversely zoned phenocrysts have a composition ranging from An_{32-45} in the core to An_{39-57} in the rim. Microphenocrysts(An_{28-51}) have similar compositions to phenocrysts. Microlites are mainly andesine to oligoclase with a composition ranging from An_{26} to $_{50}$, and a few labradorites(An_{53-64}). In addition, a few anorthoclases($An_{17}Ab_{60}Or_{23}$) are also present.

The reverse zoning and calcic overgrowth rims may be an indicative of magma mixing, and the presence of reversely zoned and normally zoned plagioclase phenocrysts in the same samples may again suggest magma mixing or interaction which are also consistent with disequilibrium textures in plagioclase phenocrysts as discussed later.

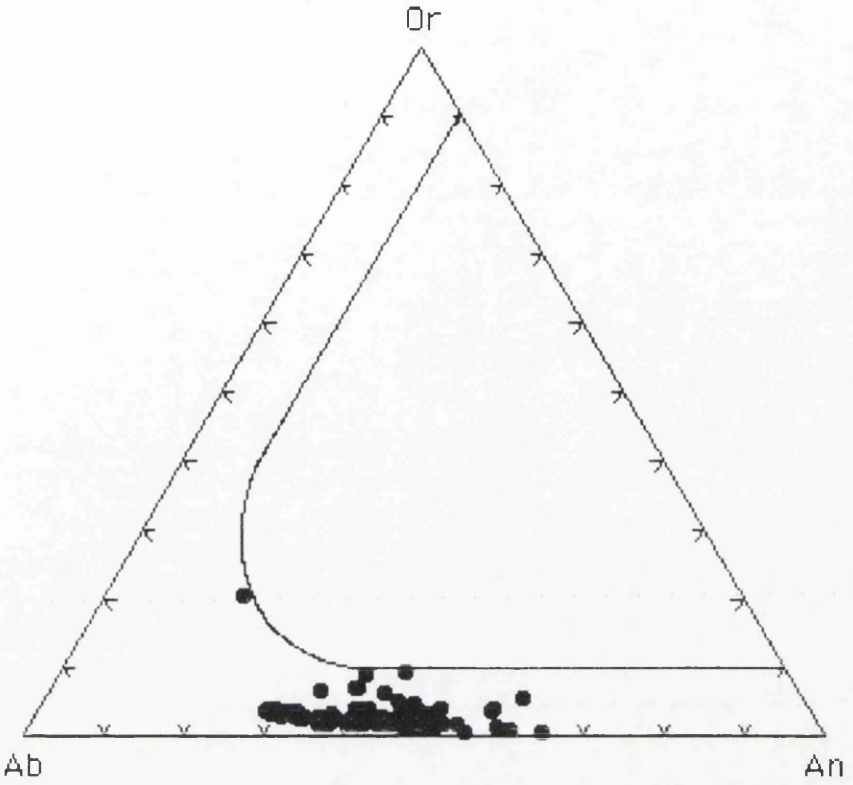

Figure 4.22. Ternary An-Ab-Or plot of feldspars in the dacites.

4.5.2.2. HORNBLENDE

Hornblendes are mainly tschermakitic hornblende, magnesio-hornblende, magnesio-hastingsite, and a few magnesio-hastingsitic hornblende and edenite(Table 4.20; Figure 4.23), according to the classification of Leake(1978). The compositional changes from core to rim appear to be insignificant. Generally, phenocrysts of hornblende are tschermakitic hornblende, magnesio-hornblende, and rarely magnesio-hastingsite. Some phenocrysts of magnesio-hastingsite are slightly zoned; the rim is richer in Mg than the core, with $Mg/(Mg+Fe^{+3}+Fe^{+2})$ ratio varying from 0.68 to 0.71. Microphenocrysts of hornblende are tschermakitic hornblende, magnesio-hornblende, magnesio-hastingsite and magnesio-hastingsitic hornblende. A few microcrysts of tschermakitic hornblende have sodic rims changing to magnesio-hastingsitic composition. Furthermore, some almost opaque amphiboles are edenitic hornblende.

Tschermakitic hornblendes have $Mg/(Mg+Fe^{+3}+Fe^{+2})$ ratios between 0.61 and 0.73 with Ti 0.16-0.28 , Na 0.53-0.61, and Si 6.29-6.45 per formula unit. Magnesio-hornblendes have $Mg/(Mg+Fe^{+3}+Fe^{+2})$ ratios from 0.56 up to 0.74 with Ti 0.11-0.21, Na 0.41-0.67, and Si 6.33-6.98 per formula unit.

Magnesio-hastingsites have $Mg/(Mg+Fe^{+3}+Fe^{+2})$ ratios from 0.68 up to 0.71 with Ti 0.27-0.34, Na 0.66-0.77, and Si 6.11-6.21 per formula unit. Magnesio-hastingsitic hornblendes have $Mg/(Mg+Fe^{+3}+Fe^{+2})$ ratios from 0.68 to 0.70 with Ti 0.20-0.27, Na 0.64-0.70, and Si 6.25-6.36 per formula unit.

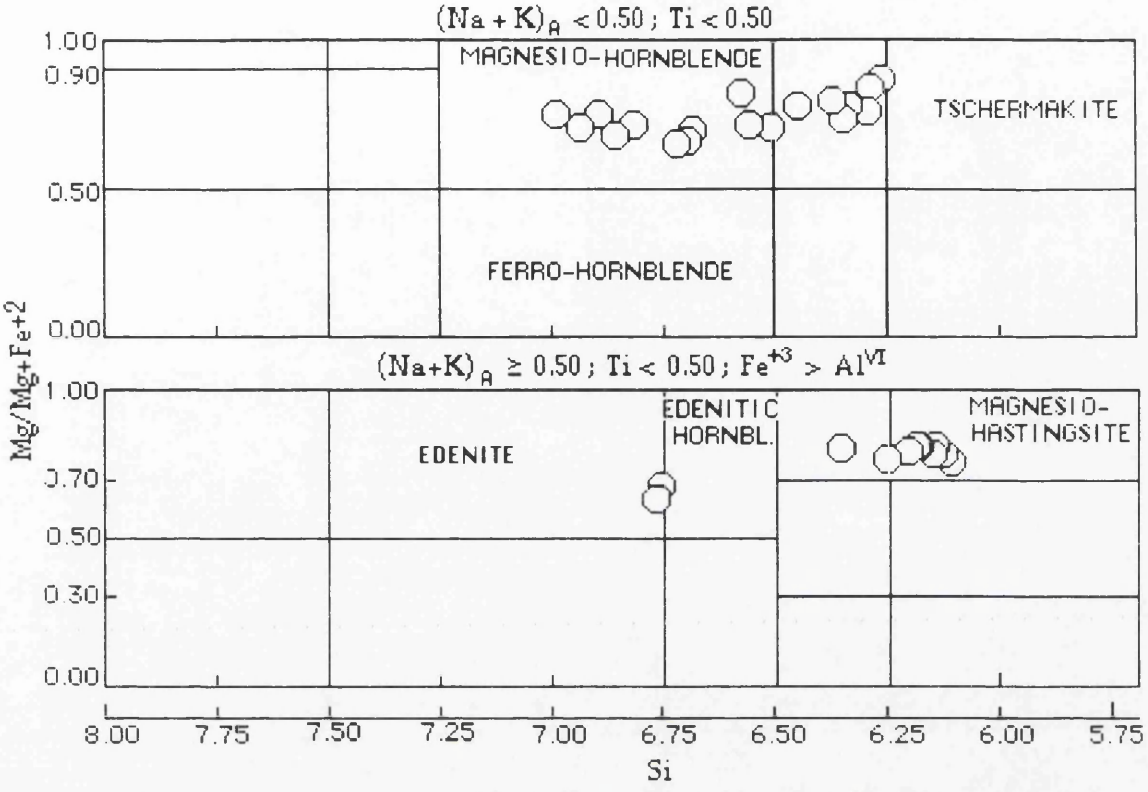

Figure 4.23. Classification and nomenclature of hornblendes of the dacites, according to Leake(1978).

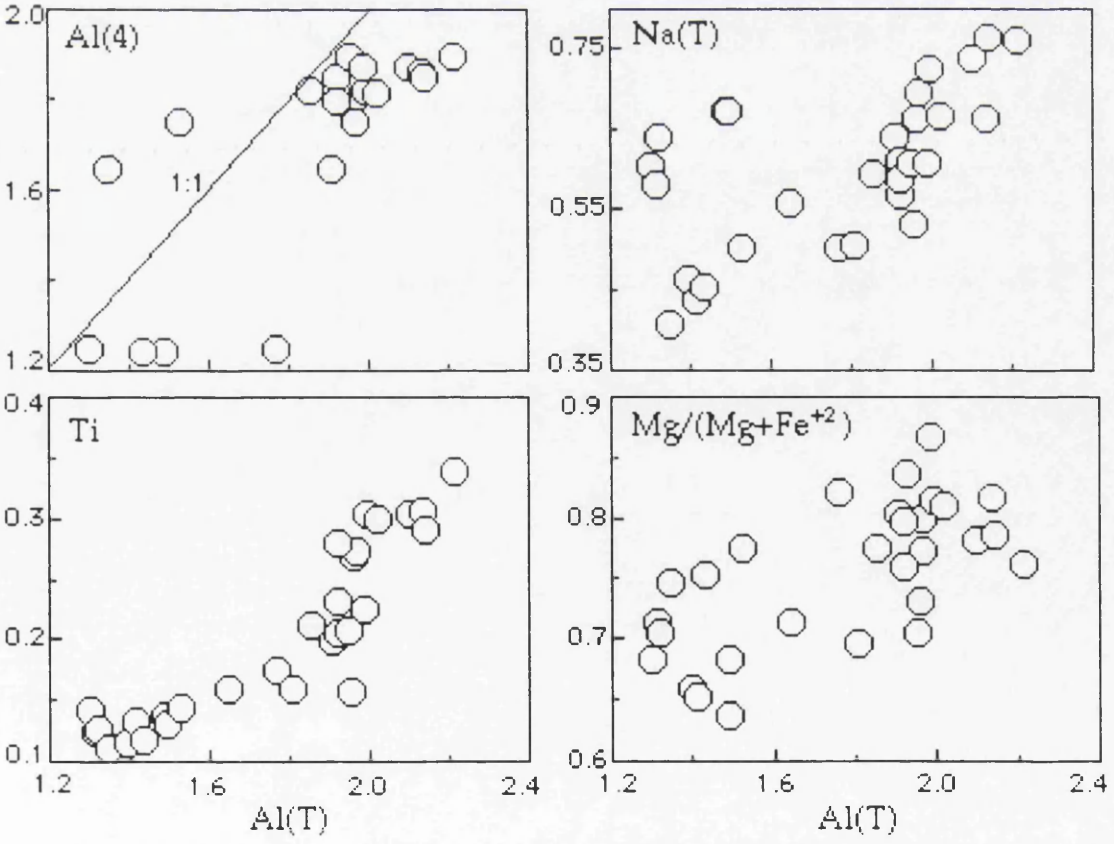

Figure 4.24. Tetrahedral Al(4), Ti, Na(T) and Mg/(Mg+Fe^{+2}) ratio plotted against total Al(T) of hornblendes in the dacites. Values are in the formula unit.

In addition, edenites have $Mg/(Mg+Fe^{+3}+Fe^{+2})$ ratio about 0.76 with Ti 0.14, Na 0.60-0.67, and Si 0.76 per formula unit.

On the variation plots(Figure 4.24), it is seen that there is a good correlation between total Al versus Na and Ti but only a poor correlation of tetrahedral Al and $Mg/(Mg+Fe^{+2})$ ratio.

4.5.2.3. BIOTITE

Biotites are phlogopite(40-69)-annite(16-35) rich types with a moderate to slightly high Mg contents(Table 4.21; Figure 4.25).

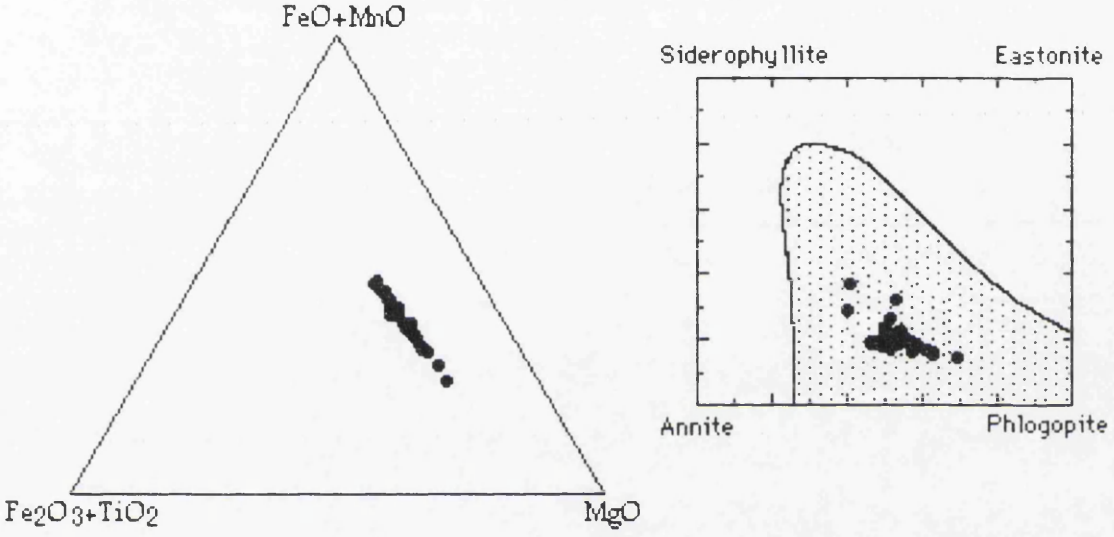

Figure 4.25. Compositional variations and the principal components of biotite compositions in the dacites. The shaded field in which most natural biotites lie(after Deer *et al.*, 1992) is also shown.

Generally, biotites have $Mg/(Mg+Fe^{+3}+Fe^{+2})$ ratios varying from 0.53 to 0.78 with Ti 0.39-0.48, Al 2.38-2.68, Na 0.12-0.55 and K 1.36-1.77 per formula unit(Figure 4.26). Trace element contents are very low or absent. Some of the phenocrysts and microphenocrysts display significant compositional variation from core to rim. In these biotites, $Mg/(Mg+Fe^{+3}+Fe^{+2})$ ratio in one sample varies from 0.53 in the core to 0.71 in the rim, or in another sample from 0.61-0.66 in the core to 0.68-0.78 in the rim, indicating a relatively Mg enrichment the rims. Furthermore, the core appears to be rich in Al and Na and the rim is rich in Ti and K(Figure 4.27).

Highly Mg-rich biotites in the dacites may represent crystallization from basic liquids. Moreover, Mg-rich rims relative to the cores may be as a result of basic-acid magma interaction or mixing, as suggested earlier.

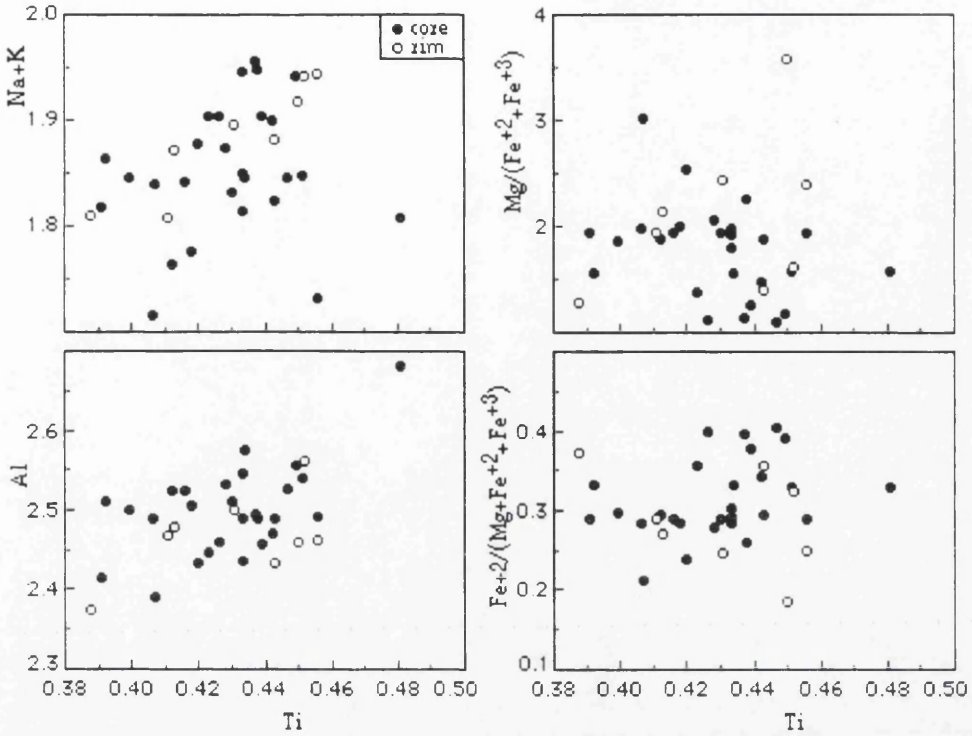

Figure 4.26. Plots of Ti versus major element and ratios of biotites in the dacites. The values are per formula unit.

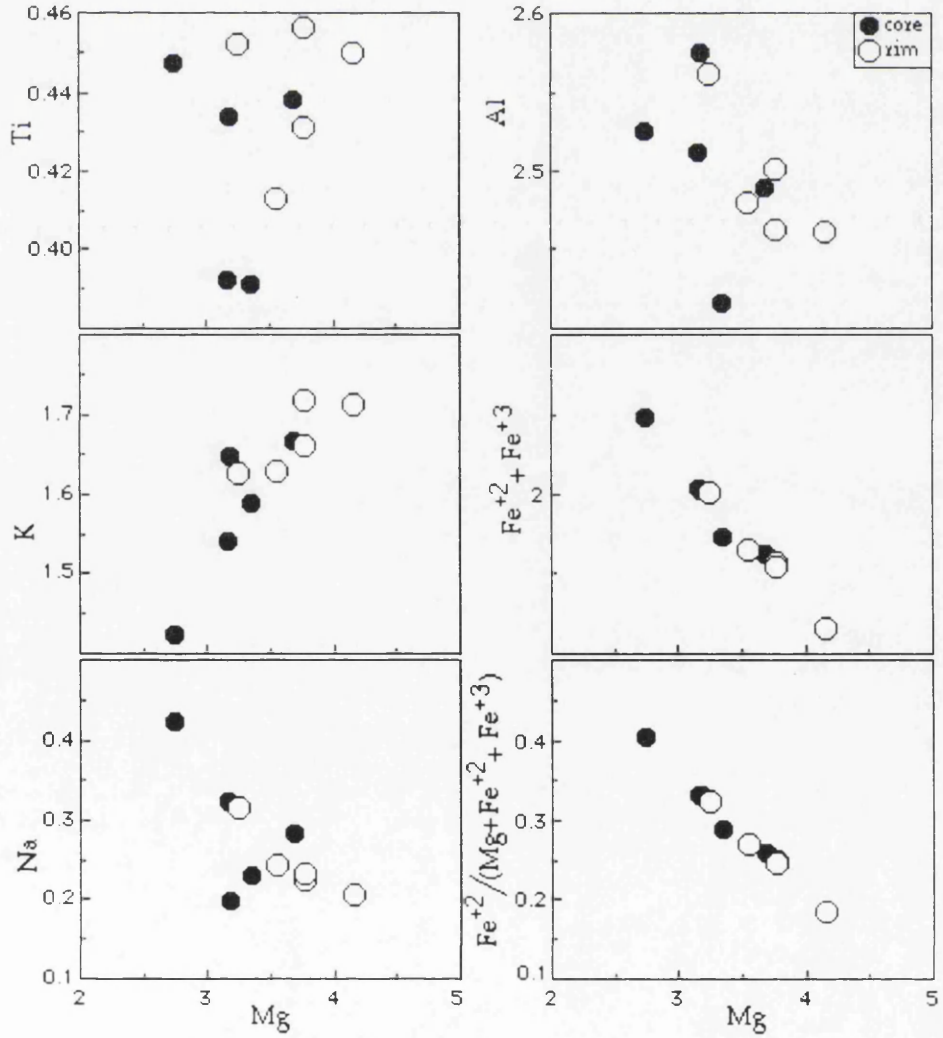

Figure 4.27. Variation plots showing compositional changes from core to rim in the zoned biotites of dacites. Values are per formula unit.

4.5.2.4. OTHER SILICATE MINERALS

In one sample, orthopyroxene occurs with a composition varying from $Wo_2En_{64}Fs_{34}$ in the core to $Wo_2En_{78}Fs_{20}$ in the rim thus displaying reverse zoning with the $Mg/(Mg+Fe^{+3}+Fe^{+2})$ ratio varying from 0.65 in the core to 0.80 in the rim. In addition, Ca and Na increase whereas Ti, Al and Mn decrease from core to rim(Table 4.22).

Sphene microcrysts occur in some samples. The sphene contains small amount of Al and Fe(Table 4.22) with Al_2O_3(1.37 wt.%) and FeO*(1.78-1.89 wt.%). The Fe/Al ratio of sphene is approximately 1, as is typical for volcanic sphenes(e.g., Cundari, 1979; Giannetti and Luhr, 1983; Luhr *et al.*, 1984; Worner and Schimincke, 1984; Nakada, 1991). The stability of sphene in magmas has been discussed by several authors(Verhoogen, 1962; Carmichael and Nicholls, 1967; Lipman, 1971; Wones, 1989), who noted that it is stable in oxidized magmas. Because the occurrence of sphene is sensitive to f_{O2}, its presence as a phenocryst allows constraints to be placed on f_{O2} in the magma chamber(e.g., Nakada, 1991). However, experimental results of partial melting at high pressure and temperature(Yoder and Tilley, 1962; Helz, 1973; Hellman and Green, 1979; Green and Pearson, 1986a, 1986b, 1987) show that sphene is stable in hydrous silicic melts of high-Ti content regardless of f_{O2}.

4.5.2.5. FE-TI OXIDES

Magnetite is the main oxide mineral with sparse ilmenite in some samples(Table 4.23; Figure 4.28). Generally, both they have homogenous compositions. Magnetites are slightly Ti-rich types with TiO_2 between 4.51 and 7.12 wt.%, Al_2O_3(1.12-6 wt.%), MnO(0.14-0.90 wt.%), MgO(0.92-1.85 wt.%), CaO(0-0.46 wt.%) and Na_2O(0.02-0.47 wt.%). Trace elements are very low or absent but qualitative analyses indicate that there are trace amounts of V.

Ilmenites are almost stoichiometric with a small proportion of $MgTiO_3$. with TiO_2(44.31 wt.%), Al_2O_3(0.13 wt.%), MnO(0.89 wt.%), MgO(2.65 wt.%) and Na_2O(0.23 wt.%). TiO_2 and MgO contents of ilmenites in the dacites are similar to those of common felsic rocks(Haggerty, 1976). The distribution of Mg and Mn between magnetite and ilmenite suggests equilibrium between two coexisting phases(Bacon and Hirschmann, 1988).

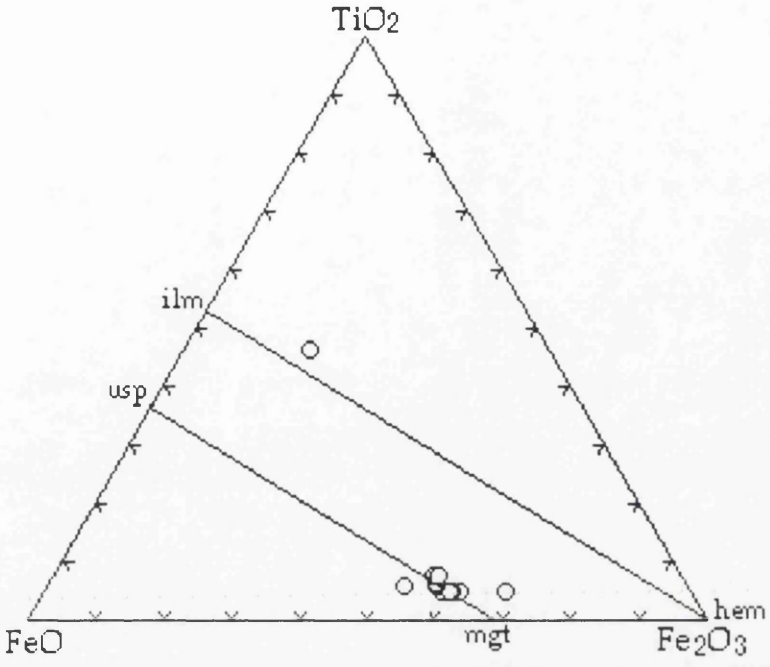

Figure 4.28. Compositions of iron-titanium oxides in the dacites.

4.5.3. TEXTURAL EVIDENCE FOR MAGMATIC PROCESSES

Dacites display a variety of disequilibrium textures. Plagioclase exhibits abrupt shifts to a more calcic composition and sieve texture. Quartz is similarly rounded and embayed. Hornblende and sometimes biotite are rimmed or replaced by fine-grained opaque minerals and silicates. Generally, magma mixing is accepted to be the dominant process leading to the eruption of intermediate composition rocks(Eichelberger, 1978; Grove and Donnelly-Nolan, 1986).

Fine scale plagioclase zoning is thought to be controlled by the interplay of growth and diffusion rates in compositional and thermal boundary layers(unrelated to magma mixing) surrounding individual crystals(Sibley *et al.*, 1976; Kuo and Kirkpatrick, 1982; Loomis, 1982; Pearce and Kolisnik, 1990). Rounded interfaces are a common feature of plagioclase and have been interpreted as dissolution surfaces that formed during episodes of plagioclase resorption(Nixon and Pearce, 1987; St. Seymour *et al.*, 1990; Kolisnik, 1990; Pearce and Kolisnik, 1990). This interpretation is also in accord with the experimental evidence of Tsuchiyama(1985). The combination of a rounded or ragged discontinuity(resorption surface) truncating underlying zones followed by a shift to a more calcic composition and subsequent normal zoning has been observed in many studies of plagioclase zoning in andesitic and dacitic rocks(Nixon and Pearce, 1987; Pearce *et al.*, 1987; St. Seymour *et al.*, 1990; Kolisnik, 1990; Blundy and Shimizu, 1991). This general pattern has been attributed to shifts in temperature and melt composition attending magma mixing(Nixon and

Pearce, 1987; Kolisnik, 1990).

Generally, sodic plagioclases are partially sieve textured but some are entirely sieve-textured. Sieved and unsieved crystals may occur side by side. Sieved zones are intergrown plagioclase and glass with highly variable morphology. Most sieved crystals have clear thin overgrowths. A sieved texture forms when sodic plagioclase is immersed in a melt that is in equilibrium with more calcic plagioclase(Lofgren and Norris, 1981; Tsuchiyama, 1985; Glazner *et al.*, 1988 and 1990). Alternatively, sieve texture may form in plagioclase by rapid growth during episodes of undercooled crystallization(Hibbard, 1981; Anderson, 1984). Kuo and Kirkpatrick(1982) described sieved crystals compatible with both origins. Coarse sieve textures may result from the rapid ascent of magmas(Nelson and Montana, 1992).

Several criteria may be used to distinguish between these hypotheses; rapid growth textures should not disturb underlying zones and may lead to skeletal crystal terminations. Resorption should truncate underlying zones and progress inward from crystal margins along cracks and grain boundaries. Compositional information is also critical in distinguishing between resorption and rapid growth. If a sieve texture represents the reaction of sodic plagioclase to more calcic compositions by preferential dissolution of the sodic component(Tsuchiyama and Takahashi, 1983), analyses of the sieved region should be more calcic than those of the underlying zones. Conversely, plagioclase formed rapidly by undercooling should be more sodic than underlying zones(Smith and Lofgren, 1983). The widespread occurrence of similar sodic shifts and strong normal zoning at crystal rims in calc-alkaline rocks(Smith and Lofgren, 1983; Barbarin, 1990; Blundy and Schimizu, 1991) suggest that recycling of mafic derived plagioclase into more silicic magmas is both common and widespread.

Recently, Stimac and Pearce(1992) suggested that the large degree of thermal and chemical disequilibrium induced by the interaction of mafic and felsic magma is recorded by textures and mineral assemblages; disequilibrium resulted in (1) simple dissolution, (2) partial reaction progressing inward from crystal margins, (3) local internal melting of crystals and (4) formation of mantles or coronas by diffusion-limited reactions in dissolution boundary layers at the margin of crystals.

4.5.4. GEOTHERMOMETRY AND GEOBAROMETRY

Coexisting magnetite-ilmenite pairs which are in equilibrium were used as a geothermometer following Anderson and Lindsley(1985). They gave temperatures ranging between 822°C and 828°C, and f_{O2} between 1.71 and 1.76 relative to FMQ buffer(Figure 4.29).

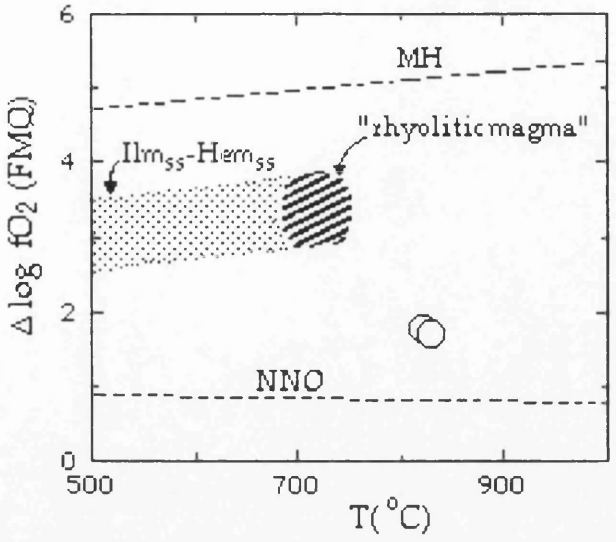

Figure 4.29. Oxygen fugacity relative to FMQ(Δlog f_{O2}) plotted against temperature for the dacites. Oxygen fugacity and temperature were calculated according to Anderson and Lindsley(1985). The field labelled Ilm_{ss}-Hem_{ss} represents the coexisting ilmenite and hematite solid solutions(Spencer and Lindsley, 1981).

The estimated temperatures of 724-793(±75)°C with the geothermometer of Blundy and Holland(1990) were obtained from sodic core of plagioclase phenocrysts(mainly sieved) and coexisting hornblende. The magma is thought to have had stable hornblende, biotite, quartz, plagioclase, sphene and Ti-rich magnetite, all of which are required to use the geobarometer based on the Al content of hornblende(Johnson and Rutherford, 1989). The calculated pressure ranges from 5.08(±0.5) to 8.90(±0.5) kbar(Table 4.24).

Experimental data for dacites(Ritchey and Eggler, 1978; Merzbacher and Eggler, 1984; Rutherford *et al.*, 1985; Rutherford and Devine, 1986; Rutherford and Devine, 1988) and data from other hornblende dacites(Ewart, 1979; Grove and Donnelly-Nolan, 1986; Smith and Leeman, 1987; Nixon, 1988a) suggest that the dacites evolved under oxidizing conditions(0.5-2 log units above Ni-NiO) at depths greater than 7 km and contained at least 4.5 wt.%, and possibly as high as 7 wt.% water. Furthermore, experiments on hornblende dacites(Merzbacher and Eggler, 1984; Rutherford *et al.*, 1986; Rutherford and Devine, 1988) indicate pressures greater than 2 kbars(~7 km at > 4.5 wt.% water and X_{H2O}=0.67) are required for hornblende to become a liquidus phase, whereas experiments by Sekine *et al.* (1979) constrain the minimum total pressure at which hornblende becomes a liquidus phase to be >1.5 kbars. Merzbacher and Eggler(1984) estimated that Mt. St. Helens dacites contained up to 6 wt.% water prior to eruption. Blake(1984) estimated that ~7 wt.% was an upper

limit in magma chambers at <3 kbars pressure because volatile oversaturation would initiate an eruption at higher water concentrations. Assuming fractionation at <3 kbars pressure, 7 wt.% water is an upper limit for these dacites(e.g., Romick *et al.*, 1992).

Table 4.24. Calculated pressures in dacites, based on the Al-content of hornblende according to Johnson and Rutherford(1989).

Sample No	Phase Type	$Mg^{\#}$	Al_2O_3(wt.%)	Al^T(pfu)	P ± 0.5(kbar)
MA-122	micropheno	80.29	11.21	1.91	7.60
	micropheno	73.06	10.93	1.96	7.81
	micropheno	70.44	11.37	1.95	7.78
MA-123	micropheno	74.67	7.94	1.35	5.23
	micropheno	69.68	10.67	1.80	7.17
	micropheno	75.32	8.46	1.43	5.60
MA-125	pheno	68.24	8.77	1.49	5.85
	micropheno	71.35	7.71	1.31	5.09
	micropheno	65.82	7.97	1.40	5.45
MA-185	micropheno	71.38	9.49	1.64	6.49
	micropheno	75.90	11.14	1.92	7.66
	micropheno	77.19	11.49	1.96	7.85
	pheno	76.17	12.95	2.21	8.90
MA-187	micropheno	82.22	11.25	1.92	7.67
	micropheno	80.91	12.56	2.02	8.08
	micropheno	78.51	12.56	2.14	8.61

$Mg^{\#}$ =100xMg/(Mg+Fe^{+2})
Al^T is total Al per formula unit(pfu)

Table 4.25. Representative analyses of groundmass glass in the dacites.

Sample	MA-187 Glass	MA-185 Glass	MA-185 Glass	MA-185 Glass	MA-125 Glass	MA-125 Glass	MA-123 Glass	MA-123 Glass	MA-122 Glass
SiO_2	67.17	64.43	67.78	74.43	66.85	74.64	73.53	75.73	77.27
TiO_2	0.10	0.10	0.15	0.11	0.22	0.18	0.12	0.12	0.15
Al_2O_3	19.20	17.69	16.73	12.87	18.33	13.71	13.79	13.18	12.57
FeO*	0.34	0.29	0.56	0.36	1.25	0.89	0.69	0.71	0.12
MnO	0.00	0.10	0.00	0.03	0.02	0.00	0.05	0.01	0.00
MgO	0.00	0.06	0.13	0.08	0.31	0.31	0.07	0.23	0.08
CaO	3.86	0.68	2.32	1.62	4.31	2.08	1.61	1.37	1.62
Na_2O	6.78	3.78	5.46	4.72	3.88	3.78	4.38	3.83	4.31
K_2O	1.16	9.56	3.25	2.41	3.10	3.65	2.97	3.42	1.60
P_2O_5	0.14	0.24	0.02	0.16	0.14	0.11	0.09	0.16	0.02
Cr_2O_3	0.00	0.06	0.00	0.00	0.00	0.07	0.00	0.04	0.00
NiO	0.02	0.05	0.04	0.00	0.08	0.02	0.09	0.00	0.00
Total	98.77	97.04	96.44	96.79	98.49	99.44	97.39	98.80	97.74

FeO* is total iron as FeO.

Table 4.19. Representative analyses of feldspars in the dacites.

Sample	MA-122	MA-122	MA-123	MA-123	MA-123	MA-125	MA-125	MA-185	MA-185	MA-187	MA-187
	Pheno core	Pheno rim	Micro-lite	Pheno core	Pheno rim	Micro-pheno	Micro lite	Pheno core	Pheno rim	Pheno core	Pheno rim
SiO_2	57.46	55.58	62.74	59.01	56.56	55.43	55.51	60.75	53.62	59.01	52.36
TiO_2	0.03	0.00	0.05	0.03	0.05	0.00	0.04	0.00	0.02	0.01	0.03
Al_2O_3	26.20	27.66	22.62	25.58	27.69	27.11	26.54	24.46	29.21	25.76	29.67
FeO*	0.13	0.25	0.26	0.22	0.19	0.28	0.77	0.18	0.34	0.19	0.45
MnO	0.00	0.02	0.11	0.00	0.00	0.00	0.05	0.00	0.00	0.00	0.01
MgO	0.06	0.13	0.02	0.06	0.04	0.14	0.30	0.13	0.17	0.07	0.10
CaO	8.19	10.20	6.15	7.37	9.78	9.66	11.03	6.23	11.37	7.58	12.56
Na_2O	6.46	5.39	6.05	7.16	5.72	5.68	4.30	7.70	5.10	6.90	4.47
K_2O	0.34	0.24	1.10	0.55	0.29	0.55	0.62	0.61	0.15	0.60	0.19
P_2O_5	0.00	0.02	0.00	0.08	0.11	0.03	0.15	0.05	0.03	0.00	0.00
Cr_2O_3	0.00	0.00	0.03	0.03	0.00	0.03	0.09	0.09	0.00	0.00	0.08
NiO	0.13	0.00	0.05	0.00	0.01	0.00	0.00	0.00	0.01	0.00	0.00
Total	99.00	99.49	99.18	100.09	100.44	98.91	99.40	100.20	100.02	100.12	99.92
Formula on the basis of 32 oxygens											
Si	10.39	9.99	11.21	10.61	10.12	10.10	10.09	10.81	9.71	10.55	9.53
Ti	0.00	0.00	0.01	0.00	0.01	0.00	0.01	0.00	0.00	0.00	0.01
Al	5.59	5.97	4.76	5.33	5.84	5.82	5.69	5.13	6.23	5.43	6.37
Fe^{+2}	0.02	0.04	0.04	0.03	0.03	0.04	0.12	0.03	0.05	0.03	0.07
Mn	0.00	0.00	0.02	0.00	0.00	0.00	0.01	0.00	0.00	0.00	0.00
Mg	0.02	0.04	0.01	0.02	0.01	0.04	0.08	0.03	0.05	0.02	0.03
Ca	1.59	2.00	1.18	1.40	1.88	1.89	2.15	1.19	2.21	1.45	2.45
Na	2.27	1.91	2.10	2.45	1.98	2.00	1.52	2.66	1.79	2.39	1.58
K	0.08	0.06	0.25	0.12	0.07	0.13	0.14	0.14	0.03	0.14	0.05
P	0.00	0.00	0.00	0.01	0.00	0.01	0.02	0.01	0.00	0.00	0.00
Cr	0.00	0.00	0.01	0.00	0.00	0.01	0.01	0.01	0.00	0.00	0.01
Ni	0.02	0.00	0.01	0.00	0.00	0.00	0.00	0.00	0.00	0.00	0.00
Total	19.96	20.00	19.58	19.98	19.95	20.03	19.84	20.00	20.08	20.00	20.08
An	40.35	50.38	33.43	35.27	47.84	47.01	56.43	29.82	54.84	36.43	60.04
Ab	57.61	48.11	59.49	61.71	50.38	49.75	39.90	66.67	44.42	60.05	38.73
Or	2.04	1.51	7.08	3.02	1.78	3.24	3.67	3.51	0.74	3.52	1.23

FeO* is total iron as FeO.

Table 4.20. Representative analyses of hornblendes in the dacites.

Sample	MA-122	MA-123	MA-125	MA-185	MA-185	MA-185	MA-185	MA-187	MA-187	MA-187	MA-187
	Mag.-hast. hbl.	Mag. hbl.	Eden. hbl.	Tsch. hbl.	Mag. hbl.	Mag. hbl.	Mag.-hast. hbl.	Mag. hast.	Mag. hast.	Tsch. hbl.	Mag. hast.
	micro	micro	pheno	pheno	micro	micro	micro	pheno core	pheno rim	micro core	micro core
SiO_2	44.09	48.53	46.26	43.94	45.02	44.64	43.14	42.11	42.76	43.34	42.75
TiO_2	1.84	1.03	1.28	2.09	1.03	1.44	2.50	3.10	2.80	2.57	2.47
Al_2O_3	11.21	7.94	7.54	11.82	7.96	9.49	11.49	12.95	11.69	11.25	11.47
FeO*	11.75	12.70	15.11	10.38	17.06	14.59	12.36	11.61	11.00	10.99	12.68
MnO	0.13	0.44	0.58	0.14	0.63	0.38	0.09	0.18	0.11	0.16	0.23
MgO	15.03	14.51	13.60	15.98	12.10	13.30	14.47	14.06	15.29	15.14	14.49
CaO	11.27	10.77	11.82	11.34	11.34	11.20	11.15	10.99	11.28	11.26	10.90
Na_2O	2.29	1.46	2.14	2.20	1.60	1.95	2.48	2.71	2.58	2.08	2.35
K_2O	0.36	0.44	0.41	0.40	0.77	0.59	0.42	0.49	0.53	0.47	0.55
P_2O_5	0.08	0.05	0.00	0.10	0.02	0.04	0.05	0.01	0.06	0.15	0.04
Cr_2O_3	0.15	0.90	0.05	0.10	0.03	0.03	0.01	0.01	0.00	0.00	0.10
NiO	0.02	0.01	0.00	0.12	0.09	0.00	0.00	0.03	0.00	0.06	0.06
Total	98.22	98.78	98.79	98.61	97.65	97.65	98.16	98.26	98.10	97.47	98.09
Formula on the basis of 23 oxygens											
Si	6.35	6.98	6.75	6.26	6.69	6.56	6.25	6.11	6.18	6.29	6.21
Al(4)	1.65	1.02	1.25	0.74	1.31	1.44	1.75	1.89	1.82	1.71	1.79
Al(T)	1.91	1.35	1.30	1.99	1.40	1.64	1.96	2.21	1.99	1.92	1.96
Al(6)	0.26	0.33	0.06	0.25	0.09	0.20	0.22	0.32	0.18	0.21	0.17
Ti	0.20	0.11	0.14	0.22	0.12	0.16	0.27	0.34	0.30	0.28	0.27
Fe^{+3}	0.56	0.43	0.39	0.64	0.58	0.51	0.50	0.41	0.48	0.54	0.65
Mg	3.23	3.11	2.96	3.39	2.68	2.91	3.12	3.04	3.29	3.27	3.14
Fe^{+2}	0.86	1.09	1.45	0.59	1.54	1.28	1.00	0.99	0.85	0.80	0.89
Mn	0.02	0.05	0.07	0.02	0.08	0.05	0.01	0.02	0.01	0.02	0.03
FMT	13.12	13.13	13.07	13.12	13.09	13.11	13.12	13.13	13.12	13.12	13.14
Ca	1.74	1.66	1.85	1.73	1.81	1.76	1.73	1.71	1.75	1.75	1.70
NaM4	0.14	0.21	0.08	0.14	0.10	0.13	0.14	0.16	0.14	0.13	0.16
NaT	0.64	0.41	0.60	0.61	0.46	0.56	0.70	0.76	0.72	0.59	0.66
NaA	0.50	0.19	0.52	0.46	0.36	0.43	0.55	0.58	0.59	0.45	0.50
K	0.07	0.08	0.07	0.07	0.15	0.11	0.08	0.09	0.09	0.09	0.10
SumA	0.57	0.27	0.59	0.53	0.51	0.54	0.63	0.67	0.68	0.54	0.60
$Mg^{\#}$	0.70	0.67	0.62	0.73	0.56	0.62	0.68	0.68	0.71	0.71	0.67

Fe^{+3} is calculated by estimation according to Spear and Kimball(1984).
$Mg^{\#}=Mg/(Mg+Fe^{+3}+Fe^{+2})$

Table 4.21. Representative analyses of biotites in the dacites.

Sample	MA-187 micro-core	MA-187 micro-rim	MA-187 micro-core	MA-187 micro-rim	MA-187 pheno-core	MA-185 pheno-core	MA-123 micro	MA-123 pheno	MA-123 inclus.	MA-122 pheno
SiO_2	36.78	37.33	38.98	38.41	38.32	35.69	38.83	38.06	37.94	37.04
TiO_2	4.01	4.14	3.54	4.17	3.83	3.94	3.82	3.97	3.79	4.01
Al_2O_3	14.46	14.26	13.95	14.54	14.16	14.32	14.61	14.54	14.67	14.40
Fe_2O_3	3.34	2.13	2.34	1.62	2.03	3.18	2.27	2.47	2.43	2.63
FeO	17.01	10.89	11.95	8.24	10.33	16.22	11.60	12.61	12.42	13.40
MnO	0.15	0.09	0.08	0.00	0.10	0.37	0.07	0.02	0.08	0.14
MgO	12.46	17.24	15.30	19.46	17.39	12.59	15.30	15.99	15.91	13.97
CaO	0.23	0.04	0.08	0.01	0.04	0.00	0.24	0.01	0.03	0.23
Na_2O	1.47	0.79	0.81	0.74	0.69	0.58	0.81	0.83	0.76	1.01
K_2O	7.54	9.19	8.48	9.34	9.05	9.18	8.33	8.53	8.74	8.16
P_2O_5	0.00	0.06	0.00	0.00	0.00	0.00	0.20	0.06	0.00	0.01
Cr_2O_3	0.05	0.00	0.05	0.00	0.00	0.00	0.00	0.11	0.02	0.00
NiO	0.14	0.00	0.00	0.00	0.00	0.02	0.03	0.01	0.00	0.00
Total	97.64	96.16	95.56	96.53	95.94	96.09	96.11	97.21	96.79	95.00
Formula on the basis of 22 oxygens										
Si	5.45	5.47	5.73	5.52	5.59	5.40	5.65	5.53	5.53	5.54
Ti	0.45	0.46	0.39	0.45	0.42	0.45	0.42	0.43	0.42	0.45
Al	2.53	2.46	2.42	2.46	2.43	2.56	2.51	2.49	2.52	2.54
Fe^{+3}	0.37	0.24	0.26	0.18	0.22	0.36	0.25	0.27	0.27	0.30
Fe^{+2}	2.11	1.33	1.47	0.99	1.26	2.05	1.41	1.53	1.52	1.68
Mn	0.02	0.01	0.01	0.00	0.01	0.05	0.01	0.00	0.01	0.02
Mg	2.75	3.76	3.35	4.17	3.78	2.84	3.32	3.46	3.46	3.11
Ca	0.04	0.01	0.01	0.00	0.01	0.00	0.04	0.00	0.00	0.04
Na	0.42	0.23	0.23	0.21	0.20	0.17	0.23	0.24	0.22	0.29
K	1.43	1.72	1.59	1.71	1.68	1.77	1.55	1.58	1.63	1.56
P	0.00	0.01	0.00	0.00	0.00	0.00	0.02	0.01	0.00	0.00
Cr	0.01	0.00	0.01	0.00	0.00	0.00	0.00	0.01	0.00	0.00
Ni	0.02	0.00	0.00	0.00	0.00	0.00	0.00	0.00	0.00	0.00
Total	15.58	15.69	15.45	15.68	15.60	15.66	15.41	15.55	15.57	15.52
$Mg^{\#}$	0.53	0.71	0.66	0.78	0.72	0.54	0.67	0.66	0.66	0.61
Phlog.	40.34	62.72	55.23	69.13	62.98	47.35	54.30	54.76	56.58	50.60
Annite	30.91	22.22	24.22	16.42	21.00	34.23	23.10	24.24	24.77	27.25

$Fe^{+3}$is calculated by ratio according to Schumacher(1991).
$Mg^{\#}=Mg/(Mg+Fe^{+3}+Fe^{+2})$

Table 4.22. Representative analyses of pyroxene and sphene in the dacites.

Sample	MA-187 Opx core	MA-187 Opx rim	MA-185 Sphene	MA-185 Sphene
SiO_2	50.60	53.65	28.11	28.44
TiO_2	0.32	0.31	34.80	35.20
Al_2O_3	3.81	2.66	1.37	1.36
FeO*	21.47	12.94	1.78	1.89
MnO	0.44	0.33	0.00	0.08
MgO	22.56	28.85	0.05	0.03
CaO	0.84	1.21	25.75	25.97
Na_2O	0.29	0.32	0.14	0.05
K_2O	0.00	0.04	0.00	0.00
P_2O_5	0.00	0.00	0.00	0.10
Cr_2O_3	0.12	0.13	0.00	0.00
NiO	0.00	0.13	0.00	0.00
Total	100.45	100.57	92.00	93.12
Formula on the basis of 6 oxygens for pyroxene and 4 oxygen for sphene				
Si	1.86	1.89	0.80	0.80
Ti	0.01	0.01	0.75	0.75
Al	0.17	0.11	0.05	0.05
Fe^{+3}	0.12	0.10	----	----
Fe^{+2}	0.54	0.28	0.04	0.05
Mn	0.01	0.01	0.00	0.00
Mg	1.24	1.52	0.00	0.00
Ca	0.03	0.05	0.79	0.78
Na	0.02	0.02	0.01	0.00
K	0.00	0.00	0.00	0.00
P	0.00	0.00	0.00	0.00
Cr	0.00	0.00	0.00	0.00
Ni	0.00	0.00	0.00	0.00
Total	4.00	4.00	2.43	2.43
Mg#	0.65	0.79		
Wo	1.71	2.34		
En	63.62	77.62		
Fs	34.67	20.04		

Fe^{+3} is calculated by normalization according to Schumacher(1991).

Table 4.23. Representative analyses of Fe-Ti oxides in the dacites.

Sample	MA-122 Magnet. Micro	MA-122 Magnet. Micro	MA-123 Magnet. Micro	MA-123 Magnet. Inclusion	MA-123 Magnet. Micro	MA-125 Magnet. Micro	MA-187 Magnet. Micro	MA-187 Ilmenite Micro
SiO_2	0.28	0.60	0.56	0.63	0.69	0.44	0.68	0.31
TiO_2	4.74	5.47	4.77	4.84	4.80	6.13	7.07	44.31
Al_2O_3	3.72	4.24	2.06	2.02	1.99	1.91	1.12	0.13
FeO*	82.36	80.15	85.94	83.43	86.08	80.79	79.30	49.19
MnO	0.66	0.72	0.47	0.52	0.56	0.14	0.55	0.89
MgO	1.28	1.91	1.01	1.03	0.92	1.17	1.33	2.65
CaO	0.21	0.46	0.06	0.01	0.12	0.14	0.13	0.04
Na_2O	0.51	0.31	0.20	0.20	0.24	0.30	0.50	0.23
K_2O	0.01	0.00	0.04	0.00	0.01	0.02	0.00	0.05
P_2O_5	0.09	0.43	0.01	0.00	0.05	0.10	0.00	0.00
Cr_2O_3	0.09	0.08	0.09	0.02	0.01	0.09	0.02	0.05
NiO	0.06	0.09	0.02	0.02	0.00	0.00	0.00	0.01
Total	93.92	94.46	95.23	92.72	95.47	91.23	90.70	97.86
Formula on the basis of 32 oxygens for magnetites and 6 oxygens for ilmenite								
Si	0.01	0.02	0.02	0.02	0.03	0.02	0.03	0.01
Ti	0.13	0.15	0.13	0.14	0.13	0.18	0.20	0.83
Al	0.16	0.19	0.09	0.10	0.09	0.09	0.05	0.00
Fe^{+3}	1.58	1.44	1.62	1.60	1.61	1.53	1.52	0.33
Fe^{+2}	0.97	1.04	1.05	1.06	1.05	1.08	1.06	0.69
Mn	0.02	0.02	0.01	0.02	0.02	0.01	0.02	0.02
Mg	0.07	0.08	0.06	0.06	0.05	0.07	0.08	0.10
Ca	0.01	0.02	0.00	0.00	0.01	0.01	0.01	0.00
Na	0.03	0.02	0.01	0.01	0.02	0.02	0.04	0.01
K	0.00	0.00	0.00	0.00	0.00	0.00	0.00	0.00
P	0.00	0.01	0.00	0.00	0.00	0.00	0.00	0.00
Cr	0.00	0.00	0.00	0.00	0.00	0.00	0.00	0.00
Ni	0.00	0.00	0.00	0.00	0.00	0.00	0.00	0.00
Total	3.00	3.00	3.00	3.00	3.00	3.00	3.00	2.00
Mn/Mg	0.29	0.25	0.17	0.33	0.40	0.14	0.25	0.20
sp	7.54	8.60	4.88	4.97	4.73	4.83	2.89	
mg-chr	0.00	0.00	0.15	0.03	0.02	0.16	0.03	
mg-fer	0.00	0.00	1.01	1.38	0.81	2.50	5.73	
trev	0.18	0.28	0.07	0.05	0.00	0.00	0.00	
herc	1.11	1.77	0.00	0.00	0.00	0.00	0.00	
chr	0.14	0.13	0.00	0.00	0.00	0.00	0.00	
mt	84.00	80.68	86.68	85.99	87.14	82.64	79.74	
usp	7.03	8.54	7.22	7.59	7.30	9.88	11.62	

Fe^{+3} is calculated by normalization, according to Schumacher(1991).

4.6. THE ALADAG LAVA

4.6.1. PETROGRAPHY

The Aladag lava is hypocrystalline and porhyritic containing 10-15% of megacryts and phenocrysts. The rock has a characteristic mineralogical assemblage of abundant megacrysts and phenocrysts of plagioclase and anorthoclase with microphenocrysts of alkali feldspar, clinopyroxene, orthopyroxene, biotite and opaque oxides. The groundmass is microcrystalline and contains sanidine laths and needles, plagioclase, quartz, accessory apatite and zircon. The volume percentages of minerals are approximately plagioclase 45%, anorthoclase 25%, sanidine 7%, quartz 3, clinopyroxene 4%, orthopyroxene 5%, biotite 2%, opaque oxides 5% and accessories 2%.

Plagioclase and anorthoclase megacrysts and phenocrysts are generally subhedral crystals with corroded rims, and have a common sponge-like texture and are embedded in glass, quartz micrograins and, or sanidine needles. Anorthoclase shows cross-hatched twinning with a core containing inclusions of microphenocryts as well as apatite. In some of the euhedral anorthoclase megacrysts, plagioclase crystals with fine albite twining are present in the core. Some phenocrysts also have sieve-like rims. They form also glomerophyric clusters with orthopyroxene.

Pyroxenes are commonly subhedral, and rarely resorbed or altered into chlorites and brownish pseudomorphous materials around their edges or within internal cracks. They may also form fragmented crystals having internal cracks. Phenocrysts of pyroxene include some apatite and zircon inclusions.

Biotite microphenocrysts are subhedral to anhedral and are associated with fine quartz or glass, and show embayment texture.

4.6.2. MINERAL CHEMISTRY

4.6.2.1. FELDSPAR

Representative analyses of feldspars are presented in Table 4.26. These range from oligoclase to sanidine(Figure 4.30). Feldspar megacrysts are generally anorthoclase $An_{15-20}Ab_{67-71}Or_{10-18}$ with a rim of $An_{20-21}Ab_{69-73}Or_{6-11}$. Megacrysts of plagioclase are oligoclase $An_{15-38}Ab_{9-57}Or_{5-16}$ with normal zoning with an average rim of $An_{10}Ab_{65}Or_{25}$. Minor sanidine phenocrysts show a composition range $An_{2-3}Ab_{38-44}Or_{53-60}$ with the edges being more sodic and potassic.

Phenocrysts of feldspar have a similar composition to the megacrysts. They show a composition range $An_{17-31}Ab_{63-70}Or_{6-14}$ with reverse zoning with a more calcic rim, $An_{39}Ab_{56}Or_5$. However, some of them have more

potassic rims with $An_{10}Ab_{58}Or_{32}$. In addition, the composition of microphenocrysts have a composition range from $An_{23}Ab_{67}Or_{10}$ to $An_{26}Ab_{64}Or_{10}$.

Feldspars in the groundmass are mainly sanidine with a composition range $An_{3-4}Ab_{38-52}Or_{47-60}$. Microlites of oligoclase are $An_{17-21}Ab_{72-75}Or_{6-9}$.

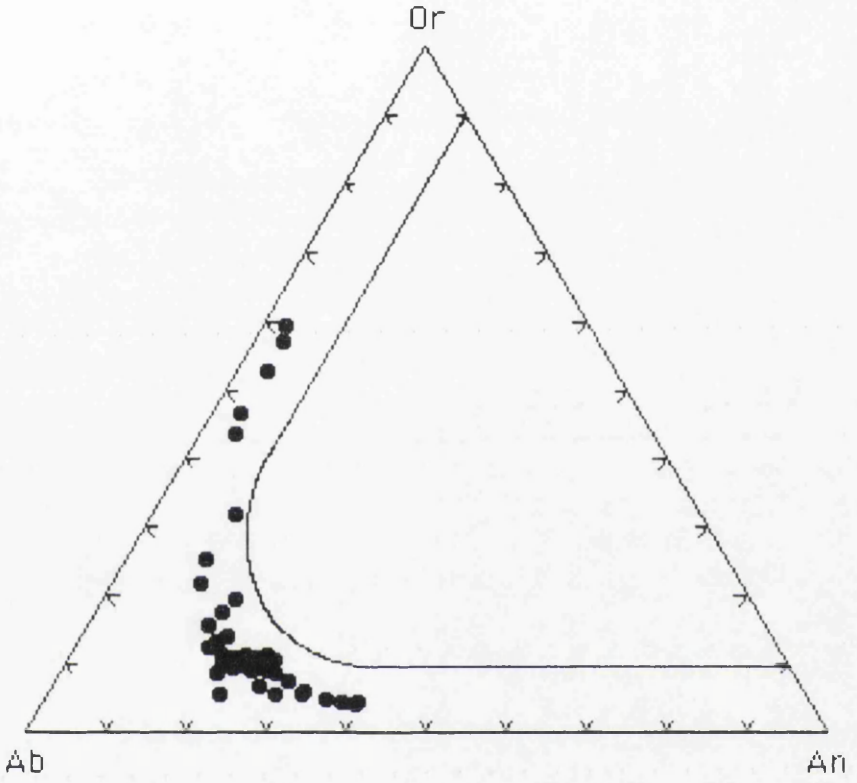

Figure 4.30. Or-Ab-An diagram of feldspars in the Aladag trachytes.

4.6.2.2. PYROXENE

The pyroxenes are augites and orthopyroxenes the later being enstatite according to classification of Morrimoto *et al.* (1988)(Figure 4.31; Table 4.27).

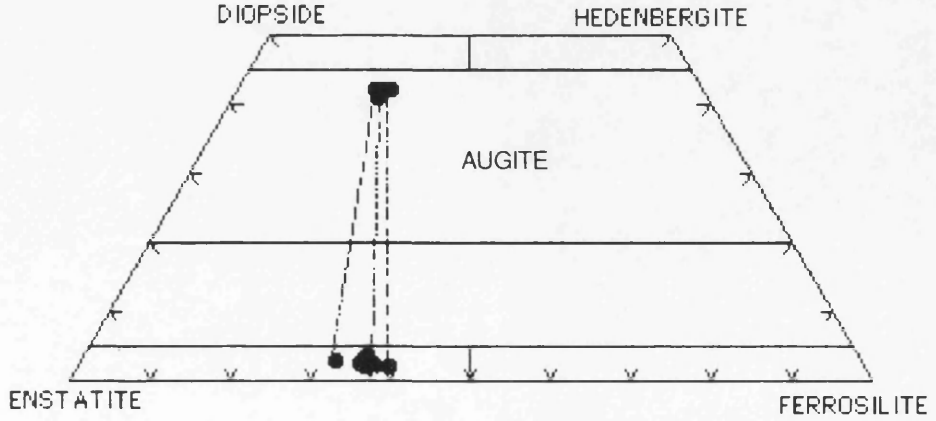

Figure 4.31. Pyroxene nomenclature of the Aladag trachytes on the Wo-En-Fs ternary plot. The tie lines intersect the Wo-En join at about between Wo_{75} and Wo_{80}.

The augites have a narrow compositional range of $Wo_{41-42}En_{38-40}Fs_{16-18}$ with an average composition of $Wo_{42}En_{40}Fs_{18}$, and are relatively low in Ti and Al, and high in Ca and Mg compared to those of alkaline volcanic rocks.

It has been suggested that octahedral Ti and Al in clinopyroxenes from alkali rocks are present as the hypothetical titanium pyroxene $CaTiAl_2O_6$(Yagi and Onuma, 1967; Ross *et al.*, 1970; Barberi *et al.*, 1971; Gibb, 1973). In the plots of total Al versus Ti and Si versus Al in terms of atoms per 6 oxygens, there is not a good correlation between Ti and Al in augites(Figure 4.32). If substitution is exclusively of the titanium pyroxene, they should cluster along the line of slope 2.0(i.e. 2Al for each Ti); but present augites have a general excess of Al over Ti.

Kushiro(1960) and Le Bas(1962) suggested that the amount of Al and Ti entering clinopyroxene depended on the degree of alkalinity of the parent magma. Furthermore, they showed that clinopyroxenes from non-alkaline rocks commonly have less than 1%TiO_2 whereas alkaline rocks have more. According to these features, clinopyroxenes in the Aladag trachytes closely resemble non-alkaline suites which is not compatible with their other geochemical characteristics. However, the Al and Ti contents of clinopyroxene are a reflection of the low silica activity(Verhoogen, 1962; Brown,1967) and the conditions of crystallization(Barberi *et al.*, 1971).

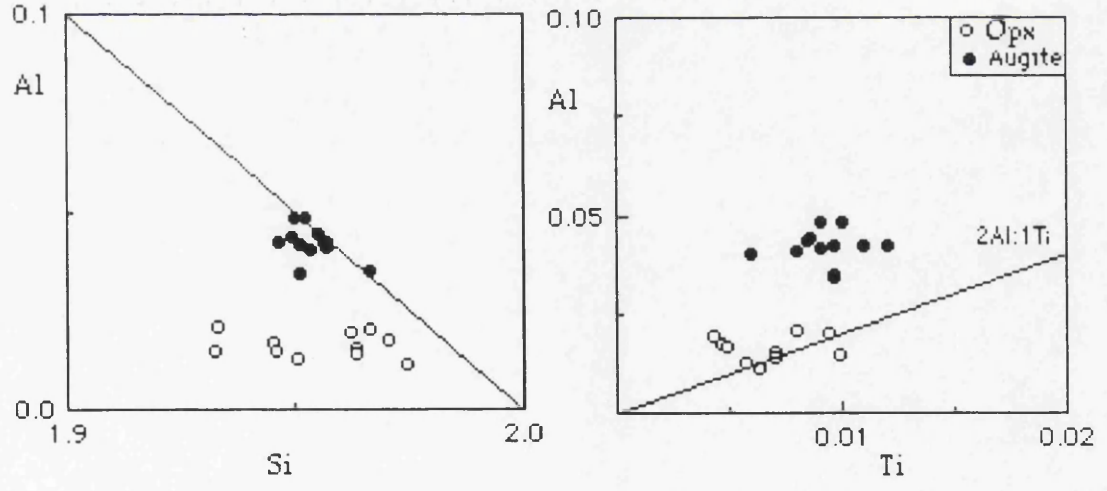

Figure 4.32. Plots of total Al against Si and Ti calculated on the basis of 6 oxygens for clino- and orthopyroxenes of the Aladag trachytes.

Orthopyroxenes, averaging $Wo_3En_{62}Fs_{35}$, occur in the groundmass. MnO content varies from 0.88 to 1.17 wt.% with the core being richest in MnO, and CaO is less than 1.5 wt.%. Ca is generally related to the temperature of crystallization(Deer *et al.*, 1978). From the investigation of the synthetic $MgSiO_3$-$CaMgSi_2O_6$ system by Atlas(1952), and later Schairer

and Boyd(1957), the orthopyroxenes in the Aladag trachyte which have a maximum Ca of 0.058 on the basis of 6 oxygens is consistent with 1000°C and a pressure of about 14 kbar(Boyd and England, 1965). Orthopyroxenes are enriched in Mg relative to the augites and this kind of relationship may indicate non-equilibrium between two pyroxenes.

The presence of two coexisting pyroxene phases, augite and orhopyroxene, and the absence of subcalcic augite in the Aladag trachyte indicates a rather slow rate of cooling. Gibb(1973) suggested that the nature of pyroxene is dependent on the major chemical characteristic of the magma; augite being related to Si and opx to the Fe content. Other factors, especially variations in water pressure may have had an important influence on the crystallization of Ca-poor pyroxenes in the Aladag trachyte. Initially, high P_{H2O} at depth would favour the formation of orthopyroxene(e.g., Nicholls, 1971). The influence of high magmatic water pressure on the nature of pyroxenes has also been discussed by many authors. Crystallization under low and falling oxygen fugacity is vital to the production of tholeiitic type pyroxenes from alkali magma(Barberi *et al.*, 1971).

4.6.2.3. FE-TI OXIDES

In the Aladag trachytes, the dominant opaque mineral is magnetite. In addition, some ilmenite is present(Figure 4.33). Representative analyses of these minerals are given in Table 4.28.

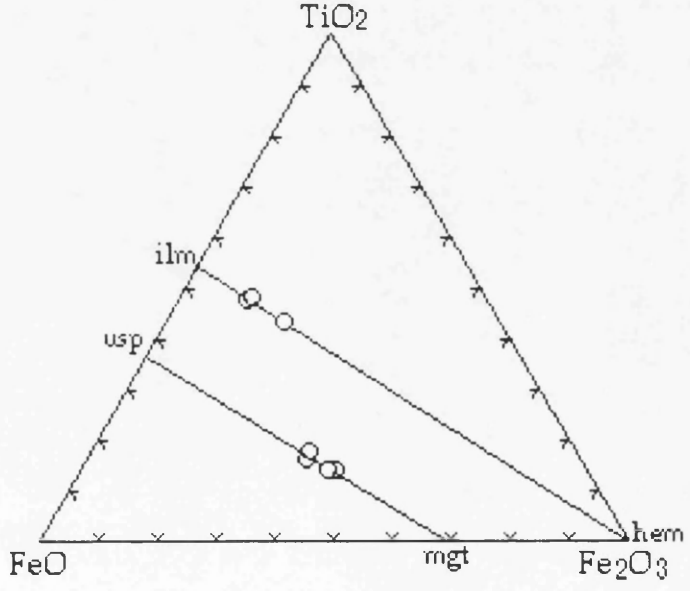

Figure 4.33. Compositions of iron-titanium oxides in the Aladag trachyte.

Magnetites are characteristically Ti-rich, containing a range of TiO_2 between 13 and 17 weight percent. They have Al_2O_3 content ranging from 0.34 up to 1.61 weight percent. NiO and Cr_2O_3 are quite low, between 0.03 and 0.08 for NiO, and 0.04-0.09 percent for Cr_2O_3.

Ilmenites have a Ti content between 1.21 and 1.32, and a Fe^{+2} content between 1.57 and 1.67 in the formula units. The Mn content is high relative to magnetites and varies from 0.54 to 1.39 wt.%.

Partitioning of Mg and Mn between Ti-rich magnetite and ilmenite grains in the Aladag trachytes indicates equilibrium between these coexisting phases(Bacon and Hirschnann, 1983).

4.6.3. GEOTHERMOMETRY AND GEOBAROMETRY

Geothermometry calculations in the Aladag trachytes were made on the basis of two feldspar thermometry, two pyroxene thermometry and Fe-Ti oxide thermometry.

The feldspars of the Aladag trachyte have been related to a geothermometer based on synthetic ternary feldspar compositions and thermodynamic data(Fuhrman and Lindsley, 1988). The tie lines(Figure 4.34) indicate that sanidine is in equilibrium with sodic plagioclase and anorthoclase, and these feldspars fall on a solvus temperature between 825 and 900°C. However, more calcic plagioclases appear to be in disequilibrium with sanidine, and reveal a solvus temperature below 825°C. The disequilibrium in more calcic plagioclase is also confirmed with its corroded or dusty appearance as described by Tsuchiyama(1985). Experimental results on dissolution of plagioclase at 1 atm(Tsuchiyama, 1985) showed that the rate of partial dissolution depends on magma temperature and is extremely slow at low temperature; 100-1000 yr are necessary for a dusty zone of 100μm width to form even at 1000°C in a dry melt. However, fH_2O may be great importance.

Magnetite and ilmenite were used in a geothermometer following Andersen and Lindsley(1985). From magnetite-ilmenite pairs a temperature between 869 and 1017°C was obtained(Table 4.29; Figure 4.5) which is consistent with the temperatures obtained from the feldspars.

Augite and orthopyroxene phenocryts were also used as a geothermometer following the method of Kretz(1982). Coexisting two pyroxenes gave relatively high solvus temperatures above 1000°C(Table 4.30).

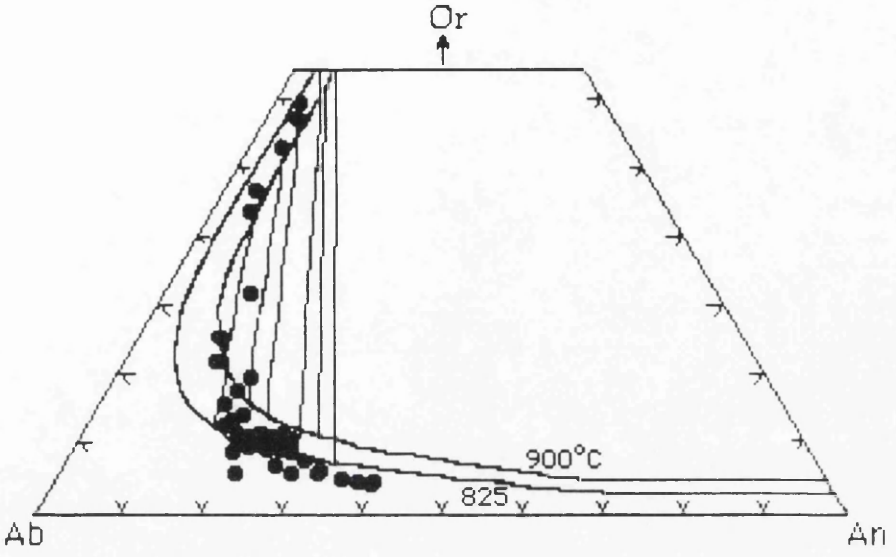

Figure 4.34. Ternary feldspar plot of the Aladag trachyte. Solvi and tie lines for feldspars coexisting in equilibrium are shown for 825°C at 1 kbar and 900°C at 0.5 kbar(Fuhrman and Lindsley, 1988).

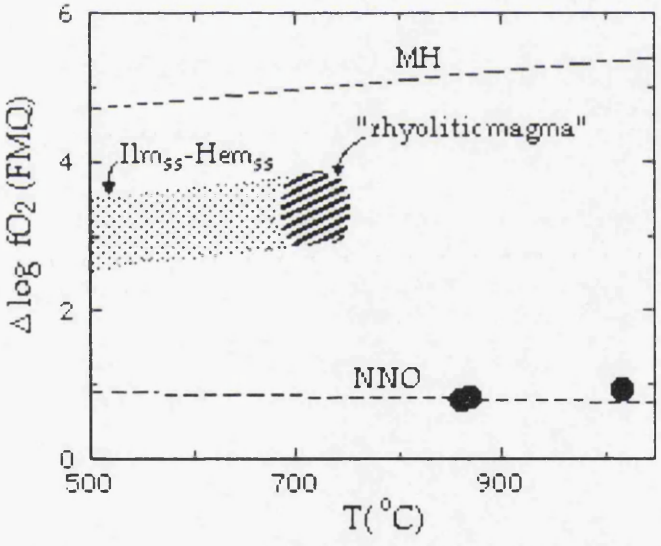

Figure 4.35. Oxygen fugacity relative to FMQ(Δlog fO_2) plotted against temperature for the Aladag trachyte. The field labeled Ilm_{ss}-Hem_{ss} represents the coexisting ilmenite and hematite solid solutions(Spencer and Lindsley, 1981).

Table 4.29. Calculated temperatures and f_{O2} for coexisting Fe-Ti oxides in the Aladag lava.

	MA-55A				MA-61	
	magnetite	ilmenite	magnetite	ilmenite	magnetite	ilmenite
SiO_2	0.27	0.27	0.46	0.28	0.29	0.25
TiO_2	13.71	48.65	13.65	47.49	16.94	43.28
Al_2O_3	1.41	0.13	1.61	0.22	0.35	0.32
Fe_2O_3	41.18	11.97	40.36	11.75	34.78	19.67
FeO	40.12	41.15	42.03	38.79	42.54	35.97
MnO	0.84	1.34	0.77	1.39	1.20	0.54
MgO	0.52	0.89	1.22	1.22	0.76	0.95
CaO	0.02	0.01	0.01	0.00	0.06	0.00
Total	98.07	104.40	100.11	101.15	96.93	100.97
Mn/Mg	0.89	0.86	0.39	0.65	0.88	0.32
Xusp	0.40	------	0.39	------	0.50	------
Xilm	------	0.88	-------	0.89	------	0.81
T(°C)	869		860		1017	
$\Delta\log f_{O2}$	0.83		0.77		0.93	

Note: The $\Delta\log f_{O2}=f_{O2}$ relative to FMQ, ulvospinel(Xusp), and ilmenite(Xilm) contents were calculated according to Schumacher(1991). The $\Delta\log f_{O2}$ and temperatures were calculated according to Andersen and Lindsley(1985).

Table 4.30. Coexisting pyroxenes and calculated solvus temperatures according to Kretz(1982).

	Opx	Cpx	Opx	Cpx	Opx	Cpx	Opx	Cpx
Wo	0.027	0.414	0.028	0.407	0.024	0.410	0.024	0.419
En	0.629	0.409	0.623	0.417	0.620	0.420	0.629	0.412
Fs	0.315	0.177	0.317	0.176	0.327	0.170	0.316	0.169
T(°C)	1045		1065		1061		1037	

Table 4.26. Representative microprobe analyses of feldspars in the Aladag lava.

Samp. No	MA-55A Pheno core	MA-55A Pheno core	MA-55A Micro-lite	MA-55A Mega core	MA-55A Mega rim	MA-61 Micro pheno	MA-61 Pheno core	MA-61 Pheno rim	MA-61 Pheno ----	MA-61 Micro-lite
SiO_2	63.41	58.92	64.72	64.41	63.29	61.89	57.81	61.13	64.77	71.77
TiO_2	0.09	0.15	0.00	0.10	0.11	0.11	0.04	0.01	0.18	0.20
Al_2O_3	22.02	25.75	21.81	21.94	22.92	23.35	26.11	23.69	19.00	15.39
FeO*	0.46	0.36	0.47	0.34	0.41	0.30	0.32	0.42	0.22	0.46
MnO	0.00	0.01	0.03	0.00	0.00	0.00	0.00	0.03	0.01	0.00
MgO	0.03	0.04	0.06	0.05	0.04	0.00	0.06	0.10	0.09	0.08
CaO	3.73	7.77	3.40	3.29	4.31	5.23	8.12	5.53	0.52	0.50
Na_2O	7.90	6.71	8.25	7.26	7.91	7.19	6.47	7.42	4.16	4.48
K_2O	2.48	0.84	2.24	3.36	1.77	1.82	0.83	1.55	10.04	6.42
P_2O_5	0.00	0.00	0.00	0.00	0.00	0.00	0.00	0.00	0.00	0.00
Cr_2O_3	0.00	0.00	0.00	0.00	0.05	0.07	0.00	0.06	0.00	0.07
NiO	0.00	0.01	0.00	0.08	0.00	0.02	0.07	0.05	0.03	0.00
Total	100.12	100.56	100.98	100.83	100.81	99.98	99.83	99.99	99.02	99.37
Formula on the basis of 32 oxygens										
Si	11.30	10.51	11.41	11.39	11.18	11.04	10.41	10.94	11.86	12.71
Ti	0.01	0.02	0.00	0.01	0.01	0.01	0.01	0.00	0.03	0.03
Al	4.62	5.41	4.53	4.57	4.77	4.91	5.54	4.99	4.10	3.22
Fe^{+2}	0.07	0.05	0.07	0.05	0.06	0.05	0.05	0.06	0.03	0.07
Mn	0.00	0.00	0.00	0.00	0.00	0.00	0.00	0.00	0.00	0.00
Mg	0.01	0.01	0.02	0.01	0.01	0.00	0.02	0.03	0.03	0.02
Ca	0.71	1.48	0.64	0.62	0.82	1.00	1.57	1.06	0.10	0.10
Na	2.73	2.32	2.82	2.49	2.71	2.49	2.60	2.57	1.48	1.54
K	0.56	0.19	0.50	0.76	0.40	0.42	0.19	0.35	2.35	1.45
P	0.00	0.00	0.00	0.00	0.00	0.00	0.00	0.00	0.00	0.00
Cr	0.00	0.00	0.00	0.00	0.01	0.11	0.00	0.00	0.00	0.01
Ni	0.00	0.00	0.00	0.01	0.00	0.00	0.01	0.01	0.00	0.00
Total	20.02	20.00	19.99	19.93	19.96	19.92	20.04	20.03	19.98	19.14
An	17.77	37.11	16.19	16.11	20.79	25.62	35.95	26.59	2.57	3.12
Ab	68.16	58.08	71.13	64.34	69.06	63.75	59.69	64.53	37.68	49.84
Or	14.07	4.81	12.68	19.55	10.15	10.63	4.36	8.88	59.75	47.04

FeO* is total iron as FeO.

Table 4.27. Representative microprobe analyses of pyroxenes in the Aladag lava.

Sample	MA-55 Opx	MA-55 Opx	MA-61 Opx	MA-61 Opx	MA-61 Cpx	MA-61 Cpx	MA-61 Cpx	MA-61 Cpx
SiO_2	53.02	52.66	51.77	53.01	52.22	51.93	52.28	51.76
TiO_2	0.28	0.26	0.30	0.34	0.32	0.34	0.29	0.43
Al_2O_3	0.33	0.36	0.47	0.46	0.95	1.10	0.94	0.95
FeO*	21.71	21.69	22.47	21.72	10.91	10.79	10.33	10.28
MnO	1.17	1.09	1.05	1.04	0.53	0.59	0.63	0.55
MgO	22.51	21.97	22.15	22.34	14.09	13.99	14.34	14.04
CaO	1.40	1.41	1.22	1.23	20.57	20.45	20.13	20.58
Na_2O	0.11	0.24	0.26	0.18	0.39	0.36	0.56	0.55
K_2O	0.00	0.04	0.00	0.01	0.01	0.00	0.00	0.01
P_2O_5	0.00	0.07	0.00	0.00	0.08	0.01	0.00	0.00
Cr_2O_3	0.00	0.11	0.03	0.00	0.00	0.00	0.04	0.07
NiO	0.00	0.00	0.00	0.00	0.01	0.00	0.00	0.01
Total	100.53	99.90	99.72	100.33	100.08	99.56	99.54	99.23
Formula on the basis of 6 oxygens								
Si	1.96	1.96	1.93	1.97	1.95	1.95	1.96	1.95
Ti	0.01	0.01	0.01	0.01	0.01	0.01	0.01	0.01
Al	0.01	0.02	0.02	0.02	0.04	0.05	0.04	0.04
Fe^{+3}	0.05	0.05	0.11	0.04	0.06	0.06	0.07	0.08
Fe^{+2}	0.62	0.63	0.59	0.63	0.28	0.28	0.26	0.24
Mn	0.04	0.03	0.03	0.03	0.02	0.02	0.02	0.02
Mg	1.24	1.22	1.23	1.24	0.78	0.78	0.80	0.79
Ca	0.06	0.06	0.05	0.05	0.82	0.82	0.81	0.83
Na	0.01	0.02	0.02	0.01	0.03	0.03	0.04	0.04
K	0.00	0.00	0.00	0.00	0.00	0.00	0.00	0.00
P	0.00	0.00	0.00	0.00	0.00	0.00	0.00	0.00
Cr	0.00	0.00	0.00	0.00	0.00	0.00	0.00	0.00
Ni	0.00	0.00	0.00	0.00	0.00	0.00	0.00	0.00
Total	4.00	4.00	4.00	4.00	4.00	4.00	4.00	4.00
$Mg^{\#}$	63.73	63.21	62.67	63.66	68.83	68.74	70.03	69.87
Wo	2.77	2.83	2.42	2.46	41.88	41.89	41.40	42.38
En	61.90	61.41	61.13	62.05	39.93	39.88	41.00	40.20
Fs	35.33	35.76	36.45	35.49	18.19	18.23	17.60	17.42

Fe^{+3} is calculated by normalization according to Schumacher(1991).
$Mg^{\#}=100xMg/(Mg+Fe^{+3}+Fe^{+2}+Mn)$

Table 4.28. Representative microprobe analyses of Fe-Ti oxides in the Aladag lava.

Sample No	MA-55A Magnetite	MA-55A Ilmenite	MA-55A Magnetite	MA-55A Magnetite	MA-61 Ilmenite	MA-61 Magnetite
SiO_2	0.27	0.27	0.46	1.53	0.23	0.28
TiO_2	13.71	48.65	13.64	15.23	43.28	16.94
Al_2O_3	1.41	0.13	1.61	1.35	0.32	0.35
FeO*	77.18	51.93	78.35	73.53	53.65	73.84
MnO	0.84	1.34	0.77	0.77	0.54	1.20
MgO	0.52	0.89	1.12	0.47	0.95	0.76
CaO	0.02	0.01	0.01	0.13	0.00	0.06
Na_2O	0.49	0.00	0.00	0.52	0.20	0.36
K_2O	0.02	0.00	0.02	0.00	0.00	0.00
P_2O_5	0.00	0.04	0.00	0.00	0.00	0.07
Cr_2O_3	0.10	0.02	0.00	0.09	0.05	0.04
NiO	0.03	0.06	0.03	0.08	0.06	0.08
Total	94.59	103.34	96.01	93.70	99.28	93.98
Formula on the basis of 32 oxygens for magnetites and 6 oxygens for ilmenites						
Si	0.01	0.01	0.02	0.06	0.01	0.01
Ti	0.39	0.88	0.38	0.44	0.81	0.49
Al	0.06	0.00	0.07	0.06	0.01	0.01
Fe^{+3}	1.17	0.22	1.13	0.98	0.37	1.00
Fe^{+2}	1.27	0.83	1.31	1.36	0.75	1.36
Mn	0.03	0.03	0.02	0.03	0.01	0.04
Mg	0.03	0.03	0.06	0.03	0.03	0.04
Ca	0.00	0.00	0.00	0.00	0.00	0.00
Na	0.03	0.00	0.00	0.04	0.01	0.03
K	0.00	0.00	0.00	0.00	0.00	0.00
P	0.00	0.00	0.00	0.00	0.00	0.00
Cr	0.00	0.00	0.00	0.00	0.00	0.00
Ni	0.00	0.00	0.00	0.00	0.00	0.00
Total	3.00	2.00	3.00	3.00	2.00	3.00
Mn/Mg	0.89	0.85	0.39	0.96	0.32	0.88
sp	3.61		4.47	3.60		1.04
mg-chr	0.00		0.00	0.0		0.09
mg-fer	0.00		3.39	0.000		4.65
trev	0.11		0.10	0.33		0.33
herc	0.25		0.00	0.49		0.00
chr	0.18		0.00	0.18		0.00
mt	71.89		67.91	65.98		61.53
usp	23.96		24.13	29.41		32.36

Fe^{+3} is calculated by normalization according to Schumacher(1991).

4.7. IGNIMBRITE

4.7.1. PETROGRAPHY

The ignimbrites vary in texture, mineralogy, degree of welding and compaction from trachytic to rhyolitic types. Generally, they contain a mixture of rock fragments, crystals, glass shards and glassy pumice fragments. In most cases, especially at the base of the unit, eutaxitic fabrics with intense welding, compaction and alignment of flattened glassy pumice fragments and elongated-curved glass shards are very characteristic. The vitroclastic fraction ranges from abundant to zero. The ignimbrites commonly display moderate to strongly welded textures which indicate high temperature emplacement.

Generally, the rocks are medium to coarse grained, crystal rich and well sorted. Internal parts of the unit may show a foliation which is accentuated by the presence of centimeter-scale fiamme.

The average crystal size is a few mm and may be finer towards the top of the unit. The erupted crystals include abundant fresh plagioclase(20-30%), alkali feldspar(5-7%) and biotite. In addition, resorbed augite, a little olivine, opaque minerals, quartz, amphibole, accessory apatite and zircon are present in lesser amounts(Table 4.31). All phenocryst phases are commonly fragmented. Quartz crystals are sparse and isolated.

Feldspar crystals are variable from phenocrysts to microlites, and are embedded in a glassy matrix. They form as subhedral laths and fragmented clusters. They are also observed in glassy pumice fragments. Feldspars are plagioclase, anorthoclase and sparse sanidine. Some of them have spongy texture. A few anorthoclase phenocryts show granophyric texture with intergrown quartz. Occasionally, they show sericitic alteration. Plagioclase phenocrysts are normally zoned, sometimes with superimposed low amplitude oscillatory zoning, and multiple twinning, and contain inclusions of biotite, apatite and glass. Glass inclusions within them are $An_4Ab_{62}Or_{34}$. Clots and intergrowths of subhedral to euhedral zoned plagioclase in more mafic samples suggest accumulation of early magmatic calcic plagioclase. In rare cases plagioclase phenocryts have small corroded cores surrounded by normally zoned feldspar. Some plagioclase phenocrysts have suffered two periods of partial resorption, producing mottled, high An zones. This interpretation contrasts with that of Chappell(1978) that these features are characteristic of restite felspar.

Biotites are large(2-3mm), euhedral to subhedral red brown plates, and some are slightly chloritised. They contain opaque oxide and apatite, or plagioclase inclusions. Some of them exhibit deformation texture due to compaction of the rock. Augite occurs as subhedral and rarely anhedral

microphenocryts in glomeraporhyritic clots which suggest accumulation of this phase during differentiation. Opaque oxides are common as equant grains. In addition, zircon is present, generally associated with opaque minerals.

The vitroclastic fraction is composed of glass shards, flattened or curved and rarely chloritized pumice fragments commonly moulded around crystals. The glassy matrix has an apparent discontinuous or continuous lamination caused by compaction and welding of original pumice fragments. In some cases, the glassy matrix shows devitrification and recrystallization textures which produced a fine-grained groundmass.

Ignimbrites generally vary in their crystal contents. This reflects the the degree of crystallization before eruption, and for crystal-rich types it probably implies significant crystallization in high level or shallow crustal chamber. Furthermore, the high phenocryst content of the ignimbrites indicates extensive crystallization prior to eruption. Microgranitoid clasts have a similar composition to the average ignimbrite. Thus it may concluded the magma reached high levels in a largely liquid state but was preceded by earlier magma which crystalized. Quartz and clinopyroxene appear to have crystallized first, followed by plagioclase, then biotite, and lastly K-feldspar at lower pressure.

Table 4.31. Descriptive petrographic features of the ignimbrites.

Rock type	Phenocrysts	Groundmass	Fabrics developed
Rhyolite ignimbrite	Quartz Anorthoclase Sanidine(sparse) Plagioclase Biotite plates Augite	microcrystaline quartz and feldspar minor biotite, ilmenite, magnetite, accessory apatite, zircon	devitrified glass shards, pumice fragments, compaction foliation and aggregates of plagioclase and augite
Trachyte ignimbrite	Anorthoclase Sanidine Plagioclase Quartz(sparse)		

4.7.2. LITHIC CLASTS IN IGNIMBRITES

Lithic clasts up to 1.5 cm are common being usually angular fragments of country rock, derived from the walls and roof of the magma chamber at high levels. They include volcanic rocks(basaltic and rhyolitic), microgranitoids, and metasedimentary rocks.

The volcanic rock fragments include plagioclase±sanidine,

clinopyroxene, abundant opaque oxides, quartz and a glassy matrix. Some of them display porphyritic and microlitic textures, and have calcic plagioclase(An_{53}) and chromian augite($Wo_{37}En_{48}Fs_{15}$ and Cr_2O_3=0.253 wt.%)(Table 4.32).

Table 4.32. Microprobe analyses of mineral compositions in lithic fragments of the ignimbrites.

	Volcanic rock fragments				Granitoid fragments	
	Plag. Pheno	Plag. Microlite	Augite	Augite	Albite	Albite
SiO_2	54.28	54.50	50.76	51.79	65.83	67.26
TiO_2	0.12	0.09	0.76	0.57	0.04	0.02
Al_2O_3	27.62	27.64	2.42	1.85	20.87	19.99
FeO*	0.79	0.73	9.06	8.72	0.17	0.12
MnO	0.00	0.02	0.22	0.17	0.00	0.00
MgO	0.21	0.24	16.18	16.95	0.00	0.00
CaO	10.77	10.96	17.91	17.91	0.22	0.18
Na_2O	4.84	5.13	0.42	0.28	10.29	10.95
K_2O	0.51	0.50	0.00	0.01	1.18	0.92
P_2O_5	0.00	0.04	0.08	0.01	0.00	0.00
SO	0.07	0.02	0.04	0.00	0.05	0.02
Cr_2O_3	0.00	0.01	0.25	0.21	0.00	0.00
CoO	0.01	0.02	0.01	0.01	0.01	0.00
NiO	0.04	0.02	0.03	0.03	0.00	0.00
Total	99.26	99.92	98.14	98.51	98.66	99.46
	An 53.49	52.60	Wo 37.57	36.98	An 1.06	0.85
	Ab 43.54	44.51	En 47.22	48.68	Ab 91.99	93.96
	Or 2.97	2.88	Fs 15.21	14.34	Or 6.95	5.19

FeO* is total iron as FeO.

Microgranitoid fragments are also present with an equigranular texture and a mineral assemblage of albite(Ab_{91-93}) and quartz(Table 4.32). In addition, some of them exhibit granophyric intergrowths of K-feldspar and quartz. This granophyric texture indicates a rapid cooling at lower pressures from near eutectic compositions and hence are typical of high level intrusions. It is therefore concluded that the granitic fragments present in the ignimbrites were derived from high level intrusions.

Metasedimentary rock fragments, interpreted as regional metamorphic rocks, contain quartz, biotite, muscovite, chlorite and clay minerals. In samples MA-57 and 63, one of metasedimentary fragments contains

radiating muscovites. They are rare but are of major interest as they represent restite or readjusted restite material(White and Chappell, 1977). Another interpretation of such fragments is that they are country rock xenoliths genetically unrelated to the magma.

4.7.3. MINERAL CHEMISTRY

4.7.3.1. FELDSPAR

The ignimbrites have feldspars varying from oligoclase to anorthoclase represented by $An_{10-38}Ab_{58-78}Or_{4-22}$(Figure 4.36). Representative compositions of feldspars are presented in Table 4.33.

All the plagioclase whether phenocrysts, microphenocrysts or microlites have a composition $An_{20-38}Ab_{58-70}Or_{4-8}$. Some the large crysts are normally zoned with An_{38} in the core and An_{18} at the rim. Some of them also exhibit antiperthitic intergrowths(Smith and Brown, 1988). In addition, they may also have more potassic rims showing transition to anorthoclase. Embayed crysts of plagioclase have a composition An_{22} in the core ranging to An_{19} at the rim. Inclusions of unzoned plagioclase in mafic minerals, especially in clinopyroxene, are more calcic with labradorite(An_{53}), and corroded.

Anorthoclase phenocrysts are unzoned and have an average composition of $An_{13}Ab_{67}Or_{20}$. Some of them may have a slightly more potassic rim with Or_{22}. Microlites are still more potassic with $An_6Ab_{67}Or_{27}$.

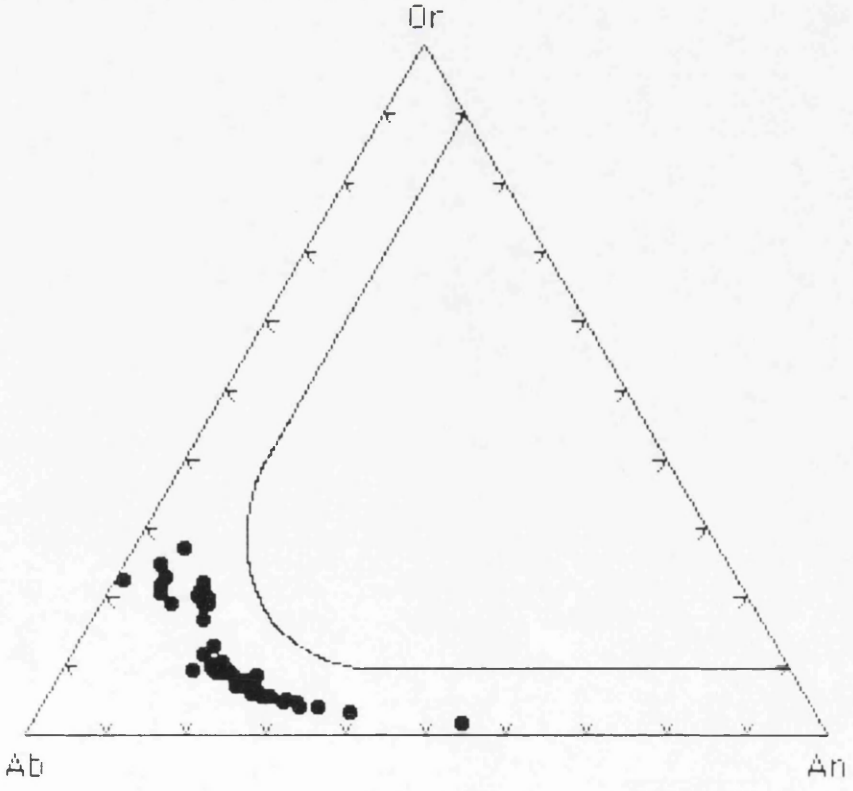

Figure 4.36. Ternary Or-Ab-An plot of feldspars in the ignimbrites.

4.7.3.2. BIOTITE

Biotites(Table 4.34; Figure 4.37) are phlogopite-annite rich types with $Mg/(Mg+Fe^{+3}+Fe^{+2})$ ratios varying from 0.66 to 0.70. They are extraordinarily rich in TiO_2 ranging from 5.48 to 6.75 wt.%. It is known that biotite commonly has up to a few wt.%(1-5) of TiO_2 and less than 1wt.% of CaO(e.g., Foster, 1960a, 1960b; Deer *et al.*, 1962a). Furthermore, biotite in igneous rocks often contains more Ti and Ca than biotite in metamorphic rocks(Rimsaite, 1964; Velde, 1969), and Ca is assumed to occupy interlayer sites(Deer *et al.*, 1962a; Rimsaite, 1964; Guidotti, 1984; Speer, 1984).

In most cases, the phenocrysts of biotite in ignimbrite have higher Ti than the microphenocryts. Inclusions of biotite within other minerals is rather Mg-rich with an average $Mg/(Mg+Fe^{+3}+Fe^{+2})$ ratio 0.68. Some of the phenocrysts have a relatively Na-rich core(0.36 percent in the formula unit).

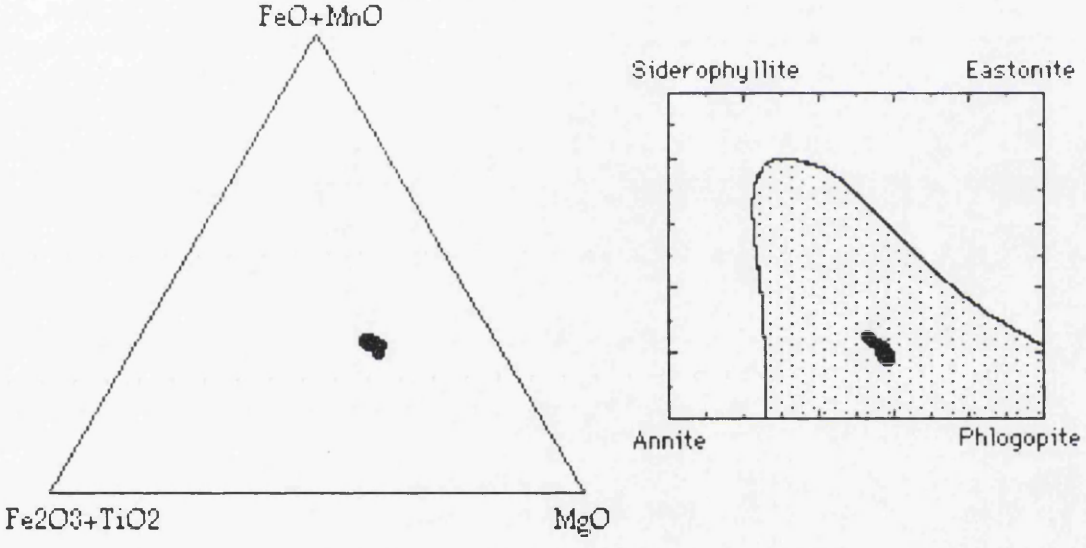

Figure 4.37. Compositional variations and the principal components of biotite compositions in the ignimbrites. The shaded field in which most natural biotites lie(after Deer *et al.*, 1992).

The Ti substitution in natural biotite has been investigated by many authors(Guidotti *et al.*, 1977; Dymek, 1983; Labotka, 1983; Brigatti *et al.*, 1991). The Ti in biotite is located in octahedrally coordinated sites, and its substitution is coupled with substitution of Al for Si(Robert, 1976; Guidotti, 1984; Hewitt and Wones, 1984; Abrecht and Hewitt, 1988), sustitution of O for OH(Bohlen *et al.*, 1980) or octahedral vacancies(Dymek, 1983).

In Figure 4.38, various plots are used to investigate Ti enrichment in the biotite of the ignimbrites. There is no clear relationship between Al and Ti, which implies that Ti-Tschermak's substitituion was not important. On the Ti versus $Mg/Fe^{+3}+Fe^{+2}$ ratio , a significant negative correlation is seen by a decrease in Mg with increasing Ti. However, a positive correlation of Ti

versus (K+Na) and $Fe^{+2}/Mg+Fe^{+3}+Fe^{+2}$ ratio plots is present. The substitution of Ti for octahedral cations is a companied principally by vacancies in octahedral sites or substitution of O for OH with subordinate Ti-Tschermak's substitution. Thus, substitution of Ti+ a vacancy is more important than substitution of O for OH in the biotite of ignimbrite. In addition, Brigatti *et al.* (1991) pointed out that Ti + a vacancy substitution is more significant in magnesium biotite than in iron biotite, and brings about an increase inTi.

A positive trend of $Fe^{+2}/(Mg+Fe^{+3}+Fe^{+2})$ ratios with Ti contents has been considered to be controlled by crystal chemical factors(as biotite co-exists with Ti-rich phases such as ilmenite or titanomagnetite). Generally, substitution of larger Fe^{+2} ions for Mg compensates for the misfit resulting from the substitution of smaller Ti^{+4} ions in octahedral sheets of biotite(Dallmeyer, 1974; Guidotti *et al.*, 1975 and 1977; Shau *et al.*, 1991).

Ti content of synthetic phlogopite increases with increasing temperature, as demonstrated in hydrothermal experiments by Robert(1976) and Tronnes *et al.* (1985). Olesch(1979) showed thet the extend of clintonite solid solution in phlogopite increases with temperature. The extend of solid solution for both Ti and Ca in biotite generally increases with increasing temperature(Shau *et al.*, 1991).

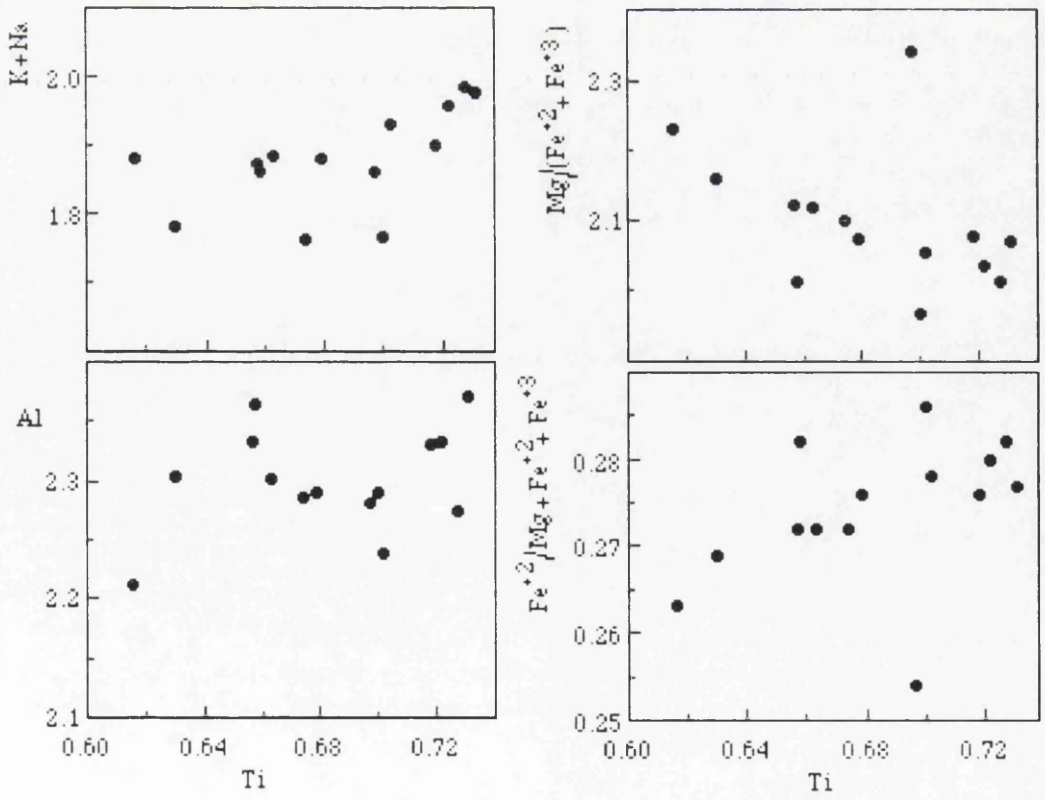

Figure 4.38. Ti versus main element and ratios of biotites in the ignimbrites. Element values are in per formula unit.

As a conclusion, it can be suggested that the Ti-rich biotite in the ignimbrites indicates a very high temperature of crystallization. Moreover, the most important petrological factors affecting biotite chemistry are temperature of crystallization, rock acidity and alkalinity and the presence of other Fe-Mg minerals, but factors, such as fH_2O and fO_2, can cause more limited variations(De Pieri *et al.*, 1978; Lyakhovich and Lyakhovich, 1987; Brigatti and Gregnanin, 1987).

4.7.3.3. PYROXENE

The pyroxenes are augite according to the classification of Morrimoto *et al.* (1988), with little compositional variations(Figure 4.39).

They have a compositional range from $Wo_{37}En_{48}Fs_{15}$ to $Wo_{44}En_{40}Fs_{16}$. The significant feature is the low TiO_2 content(less than 1 w.t.% in all samples) with Ti between 0.01 and 0.03 in the formula unit, and relatively high Al with between 0.04 and 0.11 in the formula unit(Figure 4.40) which is significant for subalkaline rock types(Le Bas, 1962).

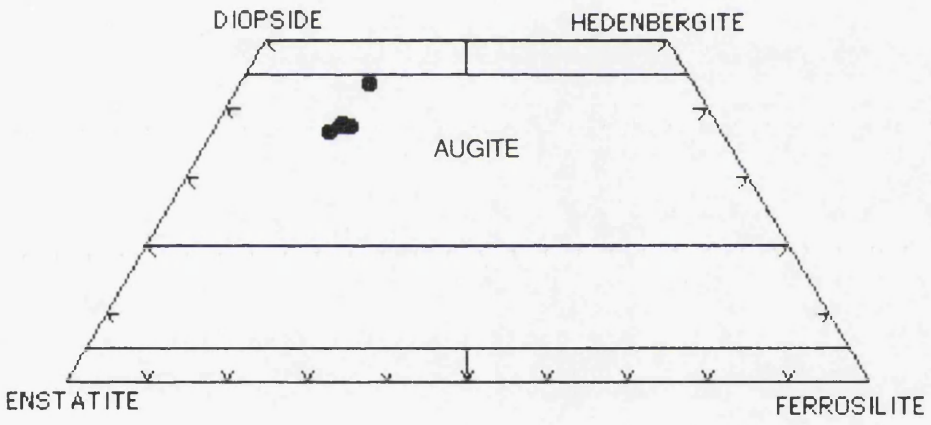

Figure 4.39. Ternary Wo-En-Fs plot of pyroxenes in the ignimbrites.

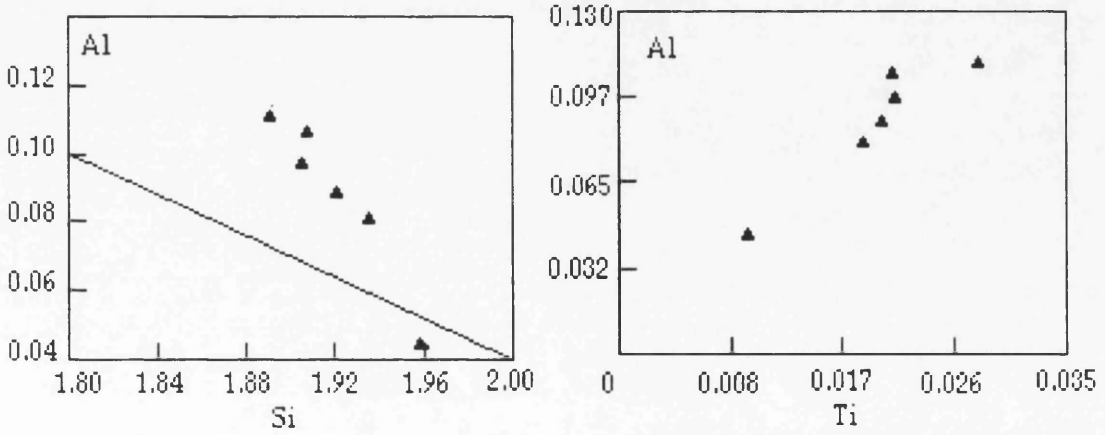

Figure 4.40. Plots of Si and Ti versus Al content in the formula unit of augites in the ignimbrites.

The presence of low Ti in augites contrasts with biotites which have extremely high Ti contents. This may be due to early crystallization of augites within a shallow magma chamber, and following accumulation of this phase during differentiation. The presence of the most calcic plagioclase(An53) inclusions within augite phenocryts supports this interpretation. Representative analyses of augites are given in Table 4.35.

4.7.3.4. FE-TI OXIDES

The two main oxide minerals are ilmenite which is common and magnetite which is less common(Figure 4.41). Both of them have almost homegeneous compositions with unzoned grains(Table 4.36).

Magnetites are Ti-rich types with a TiO_2 content between 10 and 25 weight percent. They contain total FeO between 60 and 74%, Al_2O_3 from 0.8 to 2%, MnO 1.33 to 2.17%, MgO 0.82 to 1.24% but Ni and Cr are very low or absent. Magnetite inclusions within other mineral phases(e.g., biotite) have relatively low TiO_2(~5 wt.%).

Ilmenites are almost stoichiometric $FeTiO_3$(Figure 4.42), with a small solid solution toward geikielite($MgTiO_3$) and minor Cr and Al and MnO between 1.96 and 2.66%. Qualitative analyses indicate that a significant amount of V is present in ilmenites. The distribution of Mg and Mn between the Ti-rich magnetite and the ilmenite grains in the ignimbrites indicates equilibrium between these coexisting phases(Bacon and Hirschmann, 1988).

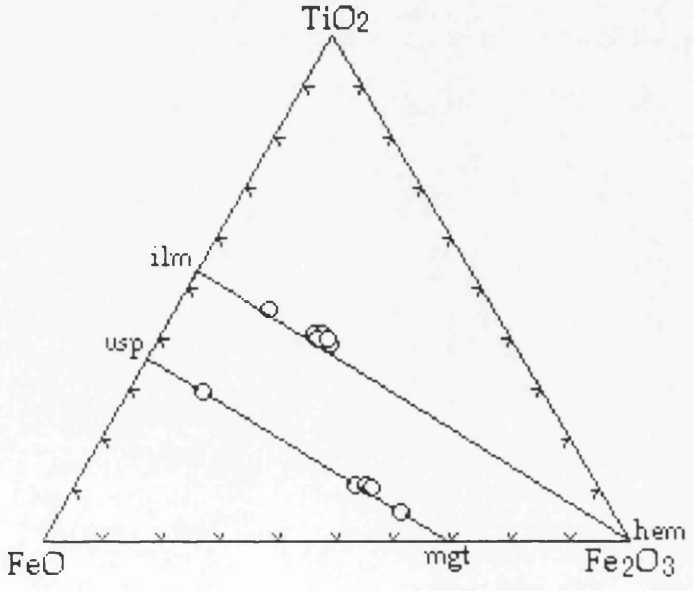

Figure 4.41. Compositions of iron-titanium oxides in the ignimbrites.

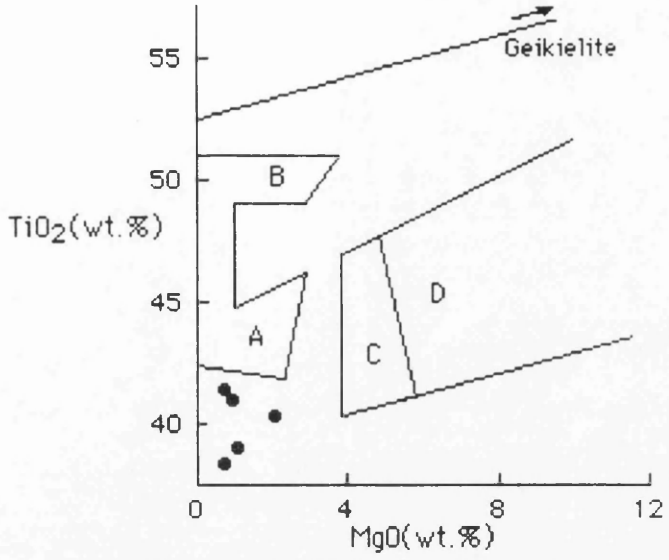

Figure 4.42. Plot of MgO versus TiO_2 for ilmenites in the ignimbrites. Typical fields of ilmenite compositions are from Haggerty(1976), A from felsic rocks; B from tholeiitic rocks; C from alkali basaltic rocks; D from kimberlites.

4.7.4. GEOTHERMOMETRY AND GEOBAROMETRY

Ignimbrite feldspars are illustrated on a ternary isotherm plot based on synthetic ternary feldspar compositions and the thermodynamic data of Fuhrman and Lindsley(1988)(Figure 4.43). On the plot, alkali feldspars, mainly anorthoclase, fall in the temperature field between 750 and 900°C. However, plagioclases in disequilibrium with anorthoclase indicate a temperature below 750°C.

In the ignimbrites, co-existing Ti-rich magnetite and ilmenite can be used as a geothermometer. Following Anderson and Lindsley(1985), magnetite and ilmenite phenocrysts give a temperatures between 846 and 921°C, and fO_2 between 1.42 and 2.29 relative to QFM buffer(Table 4.37; Figure 4.44).

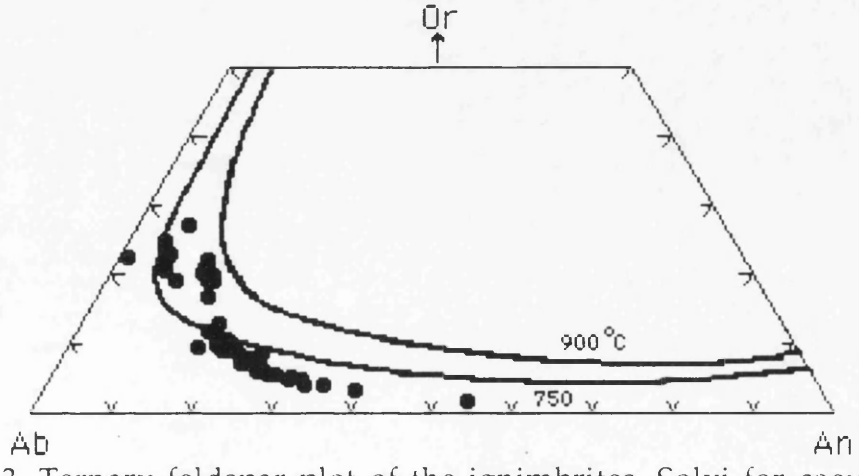

Figure 4.43. Ternary feldspar plot of the ignimbrites. Solvi for coexisting in equilibrium is shown for 750°C at 1 kbar and 900°C at 0.5 kbar(Fuhrman and Lindsley, 1988).

In the metamorphic rock fragments within the rocks, the presence of muscovite+quartz assemblage reveals a maximum pressure of about 6.5 kbar and a maximum temperature of 725°C for the stability field of this assemblage(Chatterjee and Johannes, 1974). In addition, the absence of the high grade assemblage; sillimanite-orthopyroxene in the metamorphic fragments provides an upper pressure limit of about 10 kbar(Hensen and Green, 1973) for the origin of these fragments.

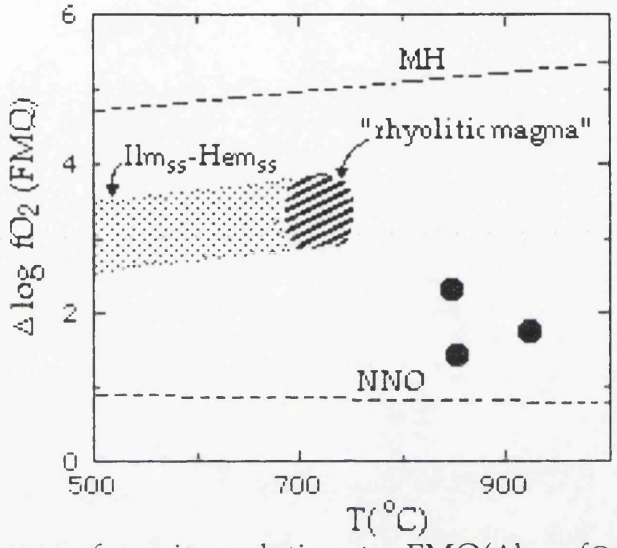

Figure 4.44. Oxygen fugacity relative to FMQ(Δlog fO_2) plotted aganist temperature for the ignimbrites. The field labeled Ilm_{ss}-Hem_{ss} represents the coexisting ilmenite and hematite solid solutions(Spencer and Lindsley, 1981).

Table 4.37. Calculated temperatures and fO_2 for coexisting Fe-Ti oxides in the ignimbrites.

	MA-63		MA-74		MA-229	
	magnetite	ilmenite	magnetite	ilmenite	magnetite	ilmenite
SiO_2	0.33	0.15	0.65	0.14	0.43	0.37
TiO_2	11.16	40.34	5.52	39.05	10.61	45.07
Al_2O_3	2.10	0.11	1.13	0.16	0.66	0.12
Fe_2O_3	49.16	25.67	53.46	28.23	51.62	15.63
FeO	38.77	32.58	33.08	30.47	39.52	37.53
MnO	1.47	1.97	0.80	2.27	1.61	2.21
MgO	1.38	2.09	0.28	1.05	0.29	0.58
CaO	0.03	0.01	0.32	0.02	0.04	0.01
Total	102.94	102.94	95.23	101.40	104.79	101.53
Mn/Mg	0.61	0.53	1.64	1.23	3.15	2.19
Xusp	0.31	-------	0.18	-------	0.29	-------
Xilm	-------	0.72	------	0.72	-------	0.84
T(°C)	921		846		853	
Δlog fO_2	1.73		2.29		1.42	

Note: The Δlog fO_2=fO_2 relative to FMQ, ulvospinel(Xusp), and ilmenite(Xilm) contents were calculated according to Schumacher(1991). The Δlog fO_2 and temperatures were calculated according to Anderson and Lindsley(1985).

Table 4.33. Representative microprobe analyses of feldspars in ignimbrites.

Sample No	MA-63 Micro. core	MA-63 Pheno core	MA-63 Pheno core	MA-63 Pheno rim	MA-63 Micro-lite	MA-63 Micro. core	MA-63 Inclus. in px	MA-74 Pheno core	MA-74 Pheno rim	MA-74 Micro-lite
SiO_2	63.89	66.50	57.18	62.25	53.74	64.38	54.41	63.95	61.96	62.12
TiO_2	0.18	0.15	0.09	0.16	0.08	0.18	0.13	0.15	0.10	0.07
Al_2O_3	20.99	18.40	26.06	21.79	27.56	20.95	27.67	21.35	23.51	23.19
FeO*	0.33	1.13	0.52	0.35	0.75	0.27	0.64	0.37	0.38	0.09
MnO	0.02	0.00	0.00	0.00	0.01	0.00	0.00	0.11	0.03	0.00
MgO	0.11	0.15	0.15	0.08	0.12	0.03	0.15	0.10	0.02	0.10
CaO	2.33	0.13	7.89	3.75	11.11	2.25	10.32	2.57	5.03	4.62
Na_2O	7.69	8.74	6.57	8.04	5.16	7.67	4.91	7.54	8.06	8.05
K_2O	3.59	3.90	0.63	1.77	0.35	3.62	0.71	3.41	1.27	1.37
P_2O_5	0.16	0.00	0.00	0.01	0.07	0.00	0.00	0.02	0.01	0.01
Cr_2O_3	0.00	0.00	0.02	0.00	0.05	0.00	0.00	0.00	0.02	0.05
NiO	0.05	0.05	0.00	0.00	0.08	0.04	0.09	0.00	0.00	0.00
Total	99.34	99.15	99.11	98.20	99.08	99.39	99.03	99.57	100.39	99.67
Formula on the basis of 32 oxygens										
Si	11.47	11.96	10.37	11.27	9.84	11.54	9.94	11.45	11.00	11.05
Ti	0.02	0.02	0.01	0.02	0.01	0.02	0.02	0.02	0.01	0.01
Al	4.44	3.90	5.57	4.65	5.95	4.42	5.96	4.51	4.92	4.87
Fe^{+2}	0.05	0.17	0.08	0.05	0.12	0.04	0.09	0.06	0.06	0.06
Mn	0.00	0.00	0.00	0.00	0.00	0.00	0.00	0.01	0.00	0.00
Mg	0.03	0.00	0.04	0.02	0.03	0.01	0.04	0.03	0.01	0.03
Ca	0.45	0.02	1.53	0.73	2.18	0.43	2.02	0.49	0.96	0.88
Na	2.68	3.05	2.31	2.82	1.83	2.66	1.74	2.62	2.78	2.78
K	0.82	0.89	0.14	0.41	0.08	0.83	0.16	0.78	0.29	0.31
P	0.02	0.00	0.00	0.00	0.01	0.00	0.00	0.00	0.00	0.00
Cr	0.00	0.00	0.00	0.00	0.01	0.000	0.00	0.00	0.00	0.00
Ni	0.01	0.01	0.00	0.00	0.01	0.01	0.01	0.00	0.00	0.00
Total	19.99	20.04	20.06	19.98	20.08	19.97	20.00	19.97	20.04	20.02
An	11.37	0.60	38.44	18.37	53.26	11.01	51.46	12.67	23.79	22.18
Ab	67.78	76.83	57.92	71.26	44.76	67.91	44.33	67.27	69.05	69.97
Or	20.85	22.56	3.63	10.37	1.98	21.07	4.20	20.05	7.16	7.85

FeO*is total iron as FeO.

Table 4.34. Representative microprobe analyses of biotites in the ignimbrites.

Sample	MA-63	MA-63	MA-74	MA-74	MA-74	MA-74	MA-74	MA-74
	Pheno	Pheno	Micro	Micro	Pheno	Micro	Micro	Pheno
SiO_2	36.87	36.41	37.49	37.79	37.61	37.76	37.47	36.99
TiO_2	6.07	6.42	6.41	5.98	6.01	6.36	5.99	6.61
Al_2O_3	13.07	13.29	13.04	12.97	13.30	13.29	13.74	13.18
Fe_2O_3	2.24	2.21	2.32	2.26	2.21	2.08	2.29	2.32
FeO	11.44	11.25	11.84	11.55	11.26	10.64	11.68	11.81
MnO	0.34	0.38	0.36	0.46	0.38	0.26	0.42	0.34
MgO	15.65	15.43	16.07	16.18	15.75	16.45	15.53	15.70
CaO	0.04	0.13	0.00	0.00	0.00	0.00	0.02	0.03
Na_2O	0.85	1.09	0.98	0.81	0.86	1.06	0.91	1.20
K_2O	8.62	8.35	8.89	8.82	8.74	8.42	8.59	8.81
P_2O_5	0.00	0.07	0.00	0.00	0.01	0.00	0.04	0.06
Cr_2O_3	0.00	0.00	0.02	0.00	0.00	0.05	0.00	0.00
NiO	0.00	0.05	0.00	0.00	0.05	0.03	0.08	0.00
Total	95.19	95.08	97.42	96.82	96.18	96.40	96.76	97.05
Formula on the basis of 22 oxygens								
Si	5.48	5.42	5.46	5.52	5.53	5.49	5.47	5.41
Ti	0.68	0.72	0.70	0.66	0.66	0.69	0.66	0.72
Al	2.29	2.33	2.24	2.33	2.30	2.28	2.36	2.27
Fe^{+3}	0.25	0.25	0.25	0.25	0.24	0.23	0.25	0.25
Fe^{+2}	1.42	1.39	1.44	1.41	1.38	1.29	1.43	1.44
Mn	0.04	0.05	0.04	0.05	0.05	0.03	0.05	0.04
Mg	3.46	3.42	3.48	3.52	3.44	3.57	3.38	3.42
Ca	0.01	0.02	0.00	0.00	0.00	0.00	0.00	0.00
Na	0.25	0.31	0.28	0.23	0.25	0.29	0.26	0.34
K	1.63	1.58	1.65	1.64	1.64	1.56	1.60	1.64
P	0.00	0.01	0.00	0.00	0.00	0.00	0.00	0.01
Cr	0.00	0.00	0.00	0.00	0.0 0	0.00	0.00	0.00
Ni	0.00	0.00	0.00	0.00	0.00	0.00	0.01	0.00
Total	15.51	15.51	15.56	15.52	15.48	15.48	15.48	15.56
$Mg^{\#}$	0.67	0.67	0.67	0.68	0.68	0.70	0.67	0.67
Phlog.	57.75	56.24	58.10	58.65	57.40	57.37	56.32	57.07
Annite	23.68	23.01	24.03	23.49	23.02	20.82	23.76	24.08

Fe^{+3} is calculated by ratio according to Schumacher(1991).
$Mg^{\#}=Mg/(Mg+Fe^{+3}+Fe^{+2})$

Table 4.35. Representative microprobe analyses of pyroxenes in the ignimbrites.

Sample	MA-63	MA-63	MA-63	MA-63	MA-63	MA-63
	Cpx core	Cpx core	Cpx rim	Cpx core	Cpx rim	Cpx core
SiO_2	52.06	50.91	50.37	50.98	50.77	51.79
TiO_2	0.36	0.77	0.99	0.73	0.76	0.57
Al_2O_3	1.01	2.20	2.53	2.00	2.42	1.85
FeO*	8.37	9.10	9.68	8.93	9.06	8.72
MnO	1.22	0.27	0.31	0.23	0.23	0.17
MgO	14.02	16.06	15.71	16.15	16.18	16.95
CaO	20.96	18.38	18.01	17.89	17.91	17.91
Na_2O	0.67	0.54	0.69	0.53	0.42	0.28
K_2O	0.09	0.05	0.00	0.02	0.00	0.01
P_2O_5	0.01	0.00	0.00	0.00	0.08	0.01
Cr_2O_3	0.00	0.20	0.09	0.29	0.25	0.21
NiO	0.00	0.00	0.00	0.06	0.03	0.03
Total	98.77	98.48	98.38	97.81	98.11	98.50
Formula on the basis of 6 oxygens						
Si	1.96	1.91	1.89	1.92	1.91	1.93
Ti	0.01	0.02	0.03	0.02	0.02	0.02
Al	0.04	0.09	0.11	0.09	0.11	0.08
Fe^{+3}	0.07	0.08	0.10	0.06	0.04	0.03
Fe^{+2}	0.19	0.20	0.20	0.22	0.24	0.24
Mn	0.04	0.01	0.01	0.01	0.01	0.01
Mg	0.78	0.89	0.88	0.91	0.91	0.94
Ca	0.84	0.74	0.72	0.72	0.72	0.72
Na	0.05	0.04	0.05	0.04	0.03	0.02
K	0.00	0.00	0.00	0.00	0.00	0.00
P	0.00	0.00	0.00	0.00	0.00	0.00
Cr	0.00	0.01	0.00	0.01	0.01	0.01
Ni	0.00	0.00	0.00	0.00	0.00	0.00
Total	4.00	4.00	4.00	4.00	4.00	4.00
Mg#	0.75	0.76	0.74	0.76	0.76	0.78
Wo	43.70	38.27	37.79	37.66	37.58	36.98
En	40.65	46.49	45.85	47.28	47.22	48.68
Fs	15.65	15.23	16.36	15.06	15.20	14.34

Fe^{+3} is calculated by normalization according to Schumacher(1991).
$Mg^{\#}=Mg/(Mg+Fe^{+3}+Fe^{+2})$

Table 4.36. Representative microprobe analyses of Fe-Ti oxides in the ignimbrites.

Sample	MA-74 Pheno Magnet.	MA-229 Pheno Magnet.	MA-63 Pheno Ilmenite	MA-63 Micro Ilmenite	MA74 Micro Ilmenite	MA-74 Micro Ilmenite	MA-74 Pheno Ilmenite
SiO_2	0.47	0.43	0.15	0.22	0.29	0.18	0.14
TiO_2	25.95	10.61	40.34	40.94	41.39	38.38	39.05
Al_2O_3	0.79	0.66	0.11	0.15	0.02	0.25	0.16
FeO	60.77	85.97	52.42	55.56	58.99	57.31	55.88
MnO	2.17	1.61	1.97	2.66	2.45	2.27	2.27
MgO	0.82	0.29	2.09	0.95	0.69	0.71	1.05
CaO	0.29	0.04	0.01	0.01	0.00	0.00	0.02
Na_2O	0.01	0.35	0.28	0.27	0.00	0.03	0.16
K_2O	0.01	0.02	0.02	0.02	0.01	0.02	0.01
P_2O_5	0.48	0.00	0.00	0.00	0.00	0.00	0.08
Cr_2O_3	0.11	0.00	0.06	0.09	0.00	0.05	0.05
NiO	0.02	0.00	0.04	0.00	0.00	0.00	0.00
Total	91.89	99.98	97.49	100.87	103.84	99.20	98.87
Formula on the basis of 32 oxygens for magnetites and 6 oxygens for ilmenites							
Si	0.01	0.01	0.00	0.01	0.01	0.01	0.00
Ti	0.77	0.28	0.76	0.75	0.74	0.72	0.73
Al	0.04	0.03	0.00	0.00	0.00	0.01	0.00
Fe^{+3}	0.33	1.39	0.48	0.49	0.50	0.55	0.53
Fe^{+2}	1.68	1.18	0.61	0.64	0.67	0.64	0.63
Mn	0.07	0.05	0.04	0.05	0.05	0.05	0.05
Mg	0.05	0.06	0.08	0.03	0.02	0.03	0.04
Ca	0.01	0.00	0.00	0.00	0.00	0.00	0.00
Na	0.00	0.02	0.01	0.01	0.00	0.00	0.01
K	0.00	0.00	0.00	0.00	0.00	0.00	0.00
P	0.02	0.00	0.00	0.00	0.00	0.00	0.00
Cr	0.00	0.00	0.00	0.00	0.00	0.00	0.00
Ni	0.00	0.00	0.00	0.00	0.00	0.00	0.00
Total	3.00	3.00	2.00	2.00	2.00	2.00	2.00
Mn/Mg	1.50	3.15	0.05	1.59	2.00	1.83	1.24
sp	3.25	1.67					
mg-chr	0.31	0.00					
mg-fer	4.97	0.18					
trev	0.09	0.00					
mt	23.64	81.43					
usp	67.74	16.76					

Fe^{+3} is calculated by normalization according to Schumacher(1991).

4.8. MEYDAN ALKALINE ASSOCIATION

4.8.1. GENERAL CHARACTERISTICS OF THE ASSOCIATION

The Meydan alkaline volcanic rocks are dominated by alkali olivine basalt and hawaiites which were first described by Innocenti *et al.* (1976 and 1980). The alkaline character of the Meydan association is reflected in its mineralogy, which displays a degree of evolution from primitive alkali olivine basalt with mineral compositions close to those that would be in equilibrium with a mantle peridotite source, to trachyte containing kaersutitic amphibole and two pyroxenes(Table 4.38).

Table 4.38. The petrographic characteristics of the rock types in the Meydan alkaline association.

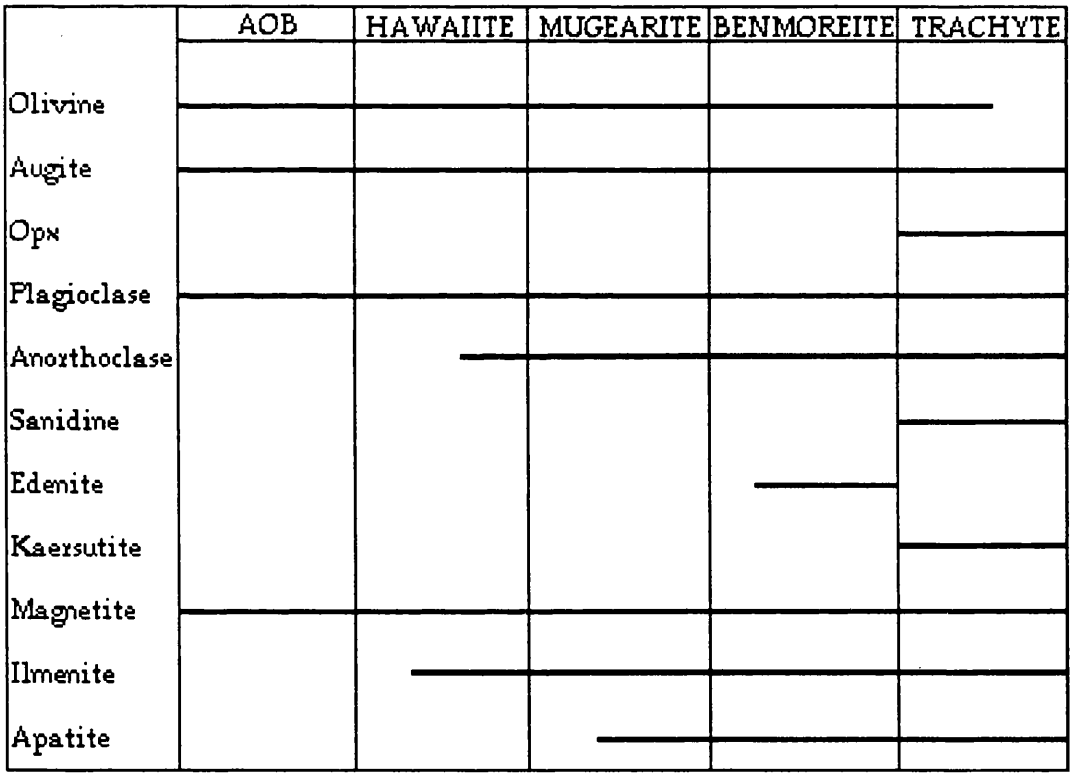

AOB=Alkali olivine basalt

In the alkaline rocks, olivine was the first crystallising phase. It continued to crystallise from the basalts through to the trachytes. Its composition varies from Fo_{92} to Fo_{40}. Olivine is often altered and more abundant in the basaltic rocks. Pyroxene was the second crystallising phase, varying from pink titanaugites in the basalts and hawaiites to salite-ferrosalite in mugearite, but with primary orthopyroxene in the trachytes. Both alkali olivine basalt and hawaiite contain augite phenocrysts up to 2mm in length. Plagioclase is a common crystallising phase with varying compositions in all rock types. The plagioclase in the groundmass varies

from about An_{72} to An_{58} in the alkali olivine basalts and hawaiites, with anorthoclase dominating in the benmoreites and trachytes. The trachytes also contain some groundmass sanidine. Titanomagnetite is the main oxide mineral. In addition, some spinel occurs associated with olivine. Other significant mineralogical features are the lack of ilmenite and the Na-rich alkali feldspar. All of these features point to a high oxygen fugacity.

Megacrysts are very rare in the alkali olivine basalt and hawaiite samples, but they are very common in the mugearites, benmoreites and trachytes. The plagioclase megacrysts of the mugearites are particularly characteristic in both texture and composition, reflecting different magmatic conditions.

Sometimes, alkaline volcanic rocks contain abundant ultramafic nodules or xenoliths. However, the Meydan alkaline suite have distinct lack of such nodules. Only one of the hawaiite samples, (MA-36), contains a gabbroic xenolith with cognate crystals of olivine and plagioclase.

4.8.2. ALKALI OLIVINE BASALT

4.8.2.1. PETROGRAPHY

Alkali olivine basalt is a distinctive rock type. It varies from slightly vesicular to massive. Generally, the vesicular samples are hyalophitic, whereas the massive ones are holocrystalline or hypocrystalline containing about 5-10% of phenocrysts of olivine, clinopyroxene and sometimes plagioclase, and rare anorthoclase. Generally, they are predominantly olivine-rich, usually with clinopyroxene and, or plagioclase as subordinate phenocryst phases. Oxide microphenocrysts have been observed in several samples. Samples, MA-27 and 64 are very rich in olivine(probably due to olivine accumulation) with clinopyroxene and a few phenocrysts of oxides. In some samples, the phenocryst proportion may reach up 20-30%(MA-15). They are generally microcrystalline with microlites. In the phenocrysts, rare plagioclases indicate that olivine and augite crystallisation took place earlier than plagioclase. The mode of minerals is plagioclase(70-80%), anorthoclase(1%), olivine(5-15%), clinopyroxene(7-10%) and opaque oxides(5-7%).

The olivine phenocrysts and microphenocrysts are commonly subhedral, sometimes euhedral, and less commonly skeletal, crystals. They are often inverted to iddingsite or rarely chlorophaeite. They generally have iron rich opaque rims. Microphenocrysts of olivine are almost granular. Their irregular internal cracks are typical. Some of phenocrysts are embayed by groundmass crystals. They also show alteration to iddingsite spreading along internal cracks. Phenocrysts have semi-opaque iddingsitized rims whereas microphenocrysts with yellowish brown colour in the groundmass show a common alteration forming iddingsite. They occasionally show simple twinning, and form aggregates of fine granules. The alteration of olivine is often complete so that pseudomorphs are common, and alteration products are rather diverse as described by Deer *et al.* (1982). The presence of thin iddingsite rims on phenocrystic olivine and common iron-rich olivine in the groundmass suggest that the iddingsite may have formed during post-extrusive deuteric alteration. In addition, the presence of chlorophaeite mineraloids indicates a lower oxidation state for the evolution of the rock.

Clinopyroxene occurs as euhedral or subhedral microphenocrysts and phenocrysts in all samples. They contain inclusions of plagioclase needles and olivine grains. They are rarely zoned and sometimes corroded, indicating that they were either not in equilibrium with the magma, or were dissolving. Some of cpx has simple twinning and partings. In the

groundmass subhedral pyroxene crystals sometimes are jacketed by small plagioclase laths, forming subophitic texture.

Plagioclase phenocrysts are euhedral to subhedral, normally zoned, sometimes intergrown with olivine, sometimes with inclusions of cpx, iron oxide, olivine and abundant apatite which may be arranged around the crystal rim in large corroded grains. Some large plagioclase phenocrysts contain clinopyroxene strips and blobs lying along the albite lamellae. This feature implies that there is melt reaction with early formed plagioclase phenocrysts. This network form of the cpx in the plagioclase could have resulted from a partial melting reaction and subsequent growth of clinopyroxene in the holes. In some samples phenocrysts of anorthoclase are also present, showing a sponge-like texture and corroded rims. They indicate a disequilibrium with the groundmass. Core regions of the crystals are filled by groundmass minerals.

The groundmass is commonly intergranular and rarely intersertal or subophitic and composed of mainly plagioclase laths, granules of olivine and clinopyroxene, and opaque oxides with accessory apatite as inclusions. Plagioclase laths are also set in fine grained clinopyroxene, olivine and iron opaque minerals. Almost equgranular plagioclase laths, olivine and clinopyroxene grains exhibit intergranular texture. Spaces between plagioclase laths are filled by olivine, clinopyroxene and opaque oxides. Compared with olivine, clinopyroxene is fine grained. Clinopyroxene and olivine occasionally form spherical aggregate clusters. Plagioclase laths may form subparallel arrangement, or aggregates.

In the rock, small vesicles contains late crystallisation products such as calcite or zeolite showing radiating crystals. Some of the rocks show important alteration products of calcite and chlorite.

4.8.2.2. MINERAL CHEMISTRY

4.8.2.2.1. OLIVINE

The olivines in the alkali olivine basalt are the most Mg-rich types in the alkaline association. They have composition ranging from Fo_{88} to Fo_{58}(Figure 4.45). Generally, there is a tendency towards lower Fo contents in holocrystalline varieties. In addition, phenocrysts are more Mg-rich than microcrysts in the groundmass phase(Figure 4.45). Representative olivine analyses are given in Table 4.39.

Phenocrysts of olivine have a composition varying from Fo_{88} to Fo_{75}. Some of them are slightly zoned with composition Fo_{75-77} in the core varying to Fo_{60-63} in the rim. Most of phenocrysts have thin iddingsite(Fo_{59}) rims. Olivines in the groundmass are typically Fe-rich with composition varying from Fo_{64} to Fo_{58}(Figure 4.45).

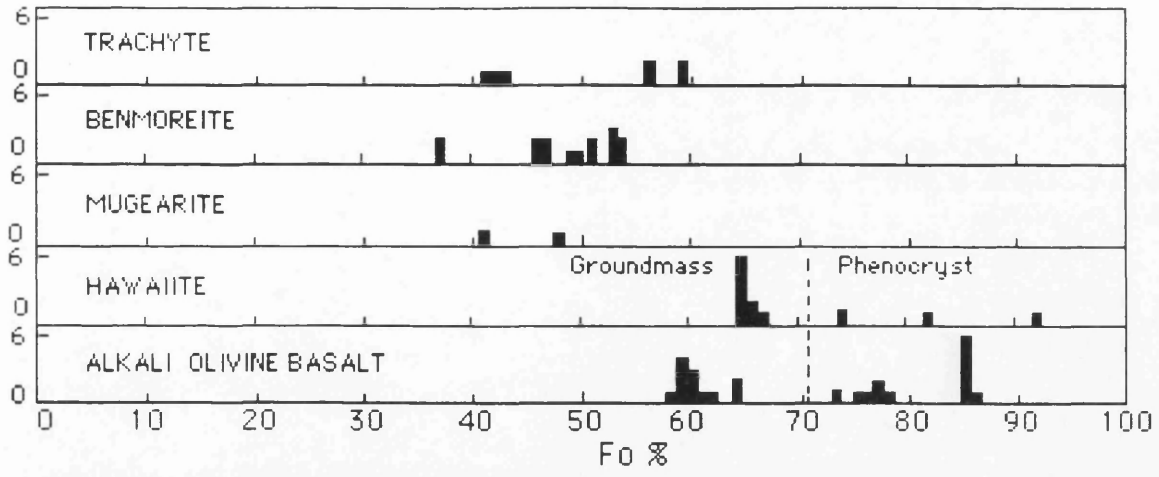

Figure 4.45. Histogram of analysed olivine compositions in the each rock type of the Meydan alkaline association.

4.8.2.2.2. CLINOPYROXENE

The clinopyroxene of the alkali olivine basalt is augite with high CaO and MgO, and falls on the line dividing diopside and augite fields(Figure 4.46), according to pyroxene classification of Morimoto *et al.* (1988). Representative augite analyses are given in Table 4.40.

Generally, they have homogeneous compositions with unzoned crystals. However, phenocrysts and microphenocrysts are relatively CaO rich with a composition of $Wo_{45}En_{38}Fs_{17}$. Groundmass augites are represented with a composition $Wo_{45}En_{37}Fs_{18}$. Typically, some clinopyroxenes are chromian with Cr_2O_3 =0.01- 0.05 wt.%.

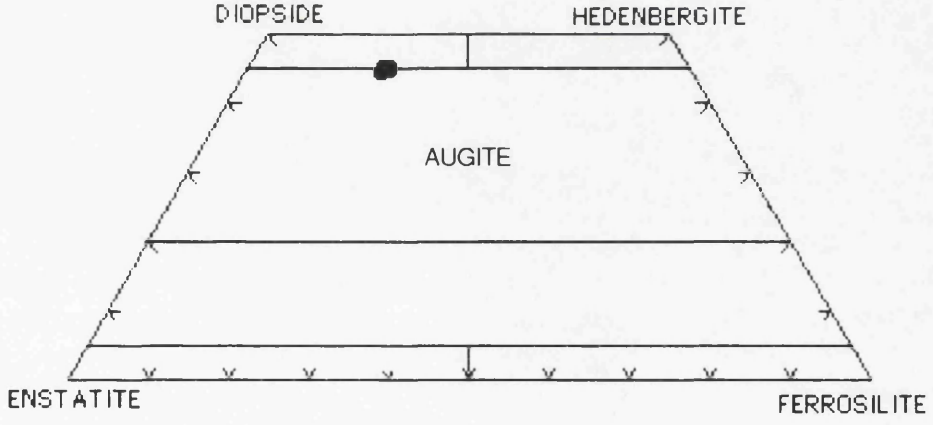

Figure 4.46. Pyroxene nomenclature of alkali olivine basalts.

Augites have relatively high contents of Ca, Ti and Al(Figure 4.47). These features are in agreement with their high content of $CaTiAl_2O_6$ and other non-quadrilateral components. In all samples, TiO_2 is higher than 1wt.%(between 2 and 3 wt.%) and Al_2O_3 is between 3 and 5 wt.%, reflecting the alkaline nature of the rocks. It is known from literature that the

compositions of the clinopyroxenes vary according to the chemistry of their host lavas. Clinopyroxene from alkali basalts are Al and Ti-rich but Si-poor with respect to clinopyroxenes from tholeiites(Kushiro, 1960; Le Bas, 1962; Verhoogen, 1962).

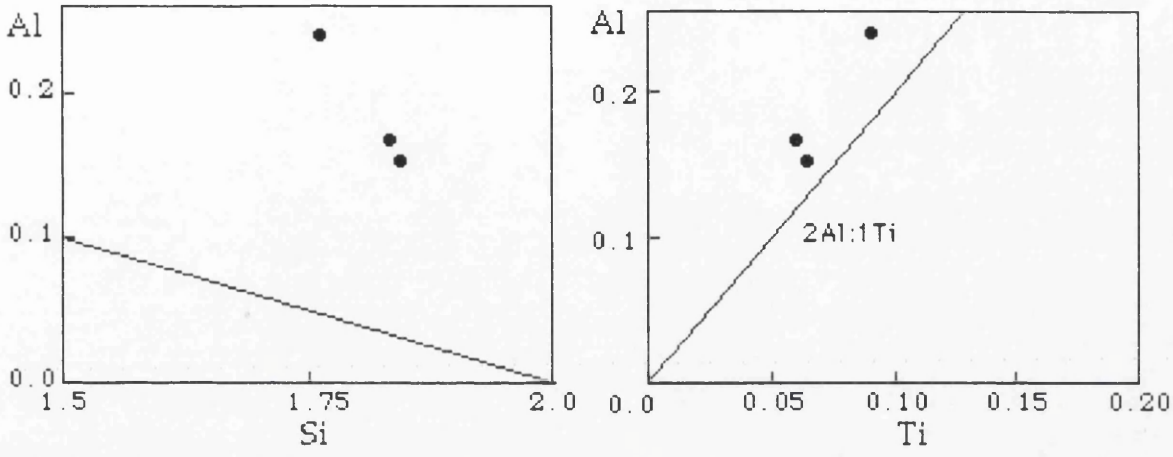

Figure 4.47. Plots of total Al versus Si and Ti contents calculated on the basis of 6 oxygens for pyroxenes of alkali olivine basalts.

4.8.2.2.3. FELDSPAR

Alkali olivine basalts have An_{51} to An_{79} plagioclase(Figure 4.48). Representative analyses are given in Table 4.41.

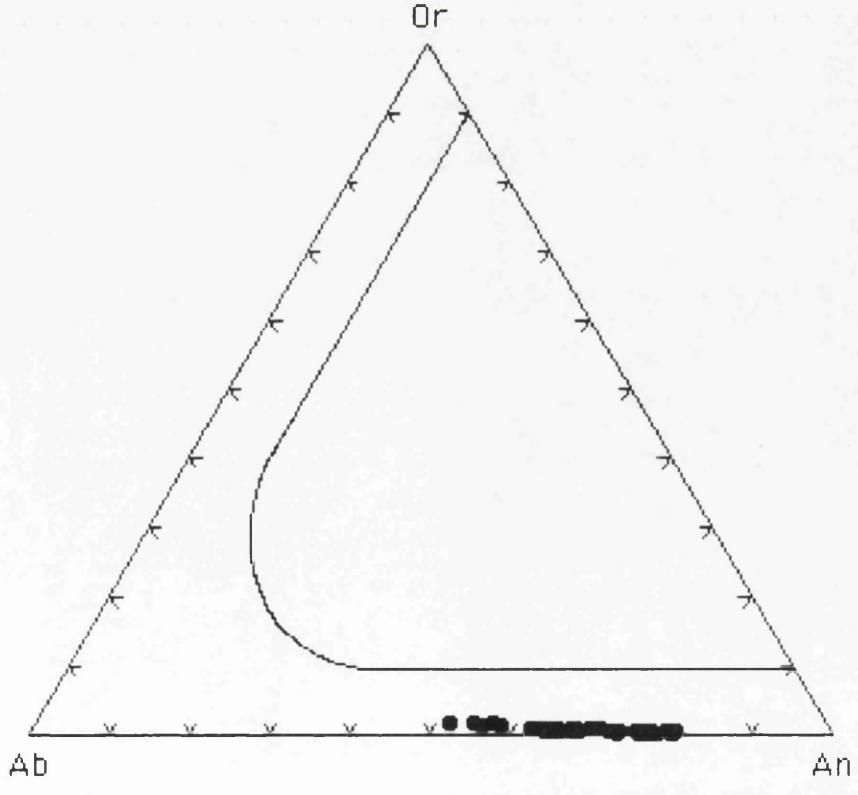

Figure 4.48. Or-Ab-An ternary diagram of feldspars in alkali olivine basalts.

Megacrysts of plagioclase are generally bytownite and reversely zoned with An_{71} in the core ranging to An_{79} in the rim. However, phenocrysts range from An_{62} to An_{79}. They are normally zoned with An_{78-79} in the core and An_{75-70} in the rim. In addition, some phenocrysts have a more sodic rim with An_{58}. Microphenocrysts have compositions similar to phenocrysts, with a range between An_{68} and An_{70}. Groundmass laths are generally labradorite with a composition range between An_{51} and An_{67}. In some samples corroded grains of plagioclase of composition An_{26-38} are found. These are usually in reaction relationship with the surrounding matrix.

4.8.2.2.4. FE-TI OXIDES

In alkali olivine basalts, magnetite is the main oxide mineral with homogeneous compositions(Figure 4.49). Representative analyses of magnetites are given in Table 4.42.

They are characteristically Ti-rich types with a TiO_2 content varying between 21% and 25 wt.%. They also have high MgO between 2% and 4 wt.%, and Al_2O_3 between 1 and 2 wt.%. They show a transition towards ulvospinel with Usp_{57} and Mt_{23}. NiO and Cr_2O_3 contents are very low. However, qualitative analyses indicate that there is a significant amount of V in all analysed magnetites.

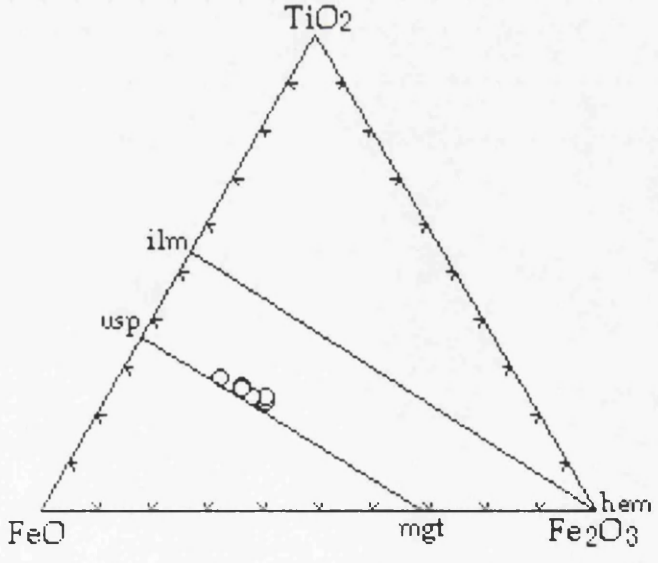

Figure 4.49. Compositions of iron-titanium oxides in the alkali olivine basalt.

Table 4.39. Representative microprobe analyses of olivines in alkali olivine basalts.

Sample	MA-20 Micro core	MA-20 Pheno core	MA-20 Micro rim	MA-22 Pheno rim	MA-22 Pheno core	MA-22 Micro core	MA-22 Micro core	MA-22 Pheno core
SiO_2	35.47	39.20	36.61	37.95	37.98	36.16	35.83	38.21
TiO_2	0.01	0.01	0.00	0.05	0.00	0.11	0.05	0.05
Al_2O_3	0.40	0.00	0.56	0.00	0.00	0.11	0.00	0.01
FeO*	31.68	14.14	28.91	22.69	22.79	33.19	31.69	20.77
MnO	0.72	0.15	0.45	0.35	0.49	0.77	0.75	0.27
MgO	25.06	45.13	26.55	38.51	38.84	29.88	31.07	40.18
CaO	0.56	0.20	0.68	0.20	0.12	0.45	0.38	0.20
Na_2O	0.31	0.15	0.29	0.32	0.17	0.08	0.27	0.14
K_2O	0.16	0.00	0.11	0.01	0.00	0.00	0.03	0.00
P_2O_5	0.09	0.00	0.13	0.05	0.05	0.08	0.12	0.05
Cr_2O_3	0.01	0.00	0.03	0.00	0.00	0.12	0.00	0.00
NiO	0.04	0.18	0.09	0.07	0.11	0.08	0.01	0.02
Total	94.51	99.16	94.41	100.20	100.55	101.03	100.20	99.90
Formula on the basis of 4 oxygens								
Si	1.03	0.99	1.05	0.99	0.99	0.99	0.98	0.99
Ti	0.00	0.00	0.00	0.00	0.00	0.00	0.00	0.00
Al	0.01	0.00	0.02	0.00	0.00	0.00	0.00	0.00
Fe^{+2}	0.77	0.30	0.69	0.49	0.49	0.76	0.72	0.45
Mn	0.02	0.00	0.01	0.01	0.01	0.02	0.02	0.01
Mg	1.08	1.70	1.13	1.49	1.50	1.21	1.27	1.55
Ca	0.02	0.01	0.02	0.01	0.00	0.01	0.01	0.01
Na	0.02	0.01	0.02	0.02	0.01	0.01	0.01	0.01
K	0.01	0.00	0.00	0.00	0.00	0.00	0.00	0.00
P	0.00	0.00	0.00	0.00	0.00	0.00	0.01	0.00
Cr	0.00	0.00	0.00	0.00	0.00	0.00	0.00	0.00
Ni	0.00	0.00	0.00	0.00	0.00	0.00	0.00	0.00
Total	2.97	3.01	2.95	3.02	3.02	3.01	3.02	3.01
$Mg^{\#}$	0.58	0.85	0.62	0.75	0.75	0.62	0.64	0.77
Fo	54.35	84.24	56.60	74.11	73.91	60.26	61.75	76.43
Fa	39.45	14.96	35.15	24.89	24.89	38.44	36.15	2.47

FeO* is total iron as FeO.

$Mg^{\#} = Mg/(Mg+Fe^{+2})$

Table 4.40. Representative microprobe analyses of pyroxenes in alkali olivine basalt.

Sample No	MA-22 Microphenocore	MA-22 Microphenocore	MA-22 Microphenorim	MA-22 Phenocrystcore	MA-22 Microphenocore
SiO_2	48.21	47.64	47.38	48.25	46.02
TiO_2	2.52	2.04	2.64	2.27	3.17
Al_2O_3	3.13	3.72	4.09	3.39	5.32
FeO*	10.10	9.81	9.64	9.65	10.13
MnO	0.29	0.17	0.25	0.26	0.16
MgO	12.32	13.01	12.53	12.82	12.33
CaO	20.82	20.86	20.89	21.17	20.95
Na_2O	0.98	0.70	0.69	0.80	0.73
K_2O	0.03	0.03	0.00	0.01	0.00
P_2O_5	0.13	0.08	0.01	0.05	0.08
Cr_2O_3	0.00	0.00	0.00	0.00	0.05
NiO	0.00	0.04	0.00	0.00	0.00
Total	98.53	98.10	98.12	98.67	98.94
Formula on the basis of 6 oxygens					
Si	1.84	1.81	1.81	1.83	1.74
Ti	0.07	0.06	0.07	0.06	0.09
Al	0.14	0.16	0.18	0.15	0.24
Fe^{+3}	0.09	0.13	0.10	0.12	0.14
Fe^{+2}	0.22	0.18	0.21	0.18	0.18
Mn	0.01	0.01	0.01	0.01	0.01
Mg	0.70	0.74	0.71	0.72	0.70
Ca	0.85	0.85	0.85	0.86	0.85
Na	0.06	0.05	0.05	0.06	0.05
K	0.00	0.00	0.00	0.00	0.00
P	0.00	0.00	0.00	0.00	0.00
Cr	0.00	0.00	0.00	0.00	0.00
Ni	0.00	0.00	0.00	0.00	0.00
Total	4.00	4.00	4.00	4.00	4.00
$Mg^{\#}$	0.68	0.70	0.70	0.70	0.68
Wo	45.18	44.62	45.38	45.30	45.41
En	37.22	38.71	37.85	38.15	37.17
Fs	17.61	16.67	16.77	16.55	17.42

Fe^{+2} is calculated by normalization according to Schumacher(1991).
$Mg^{\#} = Mg/(Mg+Fe^{+3}+Fe^{+2})$

Table 4.41. Representative microprobe analyses of feldspars in alkali olivine basalts.

Sample	MA-20 Mega core	MA-20 Micro-lite	MA-20 Pheno core	MA-20 Micro-pheno	MA-20 Pheno core	MA-22 Pheno core	MA-22 Pheno rim	MA-22 Micro-lite
SiO_2	49.85	48.76	49.07	50.28	48.49	50.89	51.85	54.19
TiO_2	0.08	0.01	0.10	0.07	0.10	0.11	0.05	0.15
Al_2O_3	30.97	31.34	31.09	30.88	31.73	30.16	29.90	27.43
FeO*	0.42	0.66	0.72	0.66	0.48	0.57	0.59	0.91
MnO	0.00	0.00	0.07	0.01	0.03	0.02	0.06	0.00
MgO	0.42	0.18	0.15	0.05	0.13	0.23	0.17	0.17
CaO	14.16	14.77	14.45	14.16	15.27	13.22	12.81	10.12
Na_2O	3.23	2.95	3.26	3.33	2.74	3.85	4.09	5.11
K_2O	1.11	0.13	0.22	0.19	0.12	0.16	0.20	0.33
P_2O_5	0.01	0.00	0.00	0.00	0.00	0.00	0.00	0.00
Cr_2O_3	0.00	0.10	0.05	0.04	0.00	0.02	0.03	0.04
NiO	0.02	0.00	0.06	0.00	0.00	0.04	0.00	0.01
Total	99.27	98.90	99.24	99.67	99.09	99.27	99.75	98.46
Formula on the basis of 32 oxygens								
Si	9.17	9.03	9.08	9.22	8.97	9.35	9.47	9.95
Ti	0.01	0.00	0.01	0.01	0.01	0.02	0.01	0.02
Al	6.71	6.85	6.78	6.68	6.92	6.53	6.44	5.94
Fe^{+2}	0.06	0.10	0.11	0.10	0.07	0.09	0.09	0.1
Mn	0.00	0.00	0.01	0.00	0.01	0.00	0.01	0.00
Mg	0.11	0.05	0.04	0.01	0.04	0.06	0.05	0.05
Ca	2.79	2.93	2.86	2.78	3.03	2.60	2.51	1.99
Na	1.15	1.06	1.17	1.18	0.98	1.37	1.45	1.82
K	0.03	0.03	0.05	0.04	0.03	0.04	0.05	0.08
P	0.00	0.00	0.00	0.00	0.00	0.00	0.00	0.00
Cr	0.00	0.01	0.01	0.01	0.00	0.00	0.01	0.01
Ni	0.00	0.00	0.00	0.00	0.00	0.01	0.00	0.00
Total	20.05	20.06	20.13	20.04	20.06	20.07	20.05	20.00
An	70.35	72.98	70.09	69.44	74.93	64.89	62.63	51.25
Ab	28.99	26.23	28.64	29.49	24.38	34.16	36.19	46.77
Or	0.66	0.69	1.27	1.07	0.69	0.95	1.18	1.98

FeO* is total iron as FeO.

Table 4.42. Representative microprobe analyses of Fe-Ti oxides in alkali olivine basalts.

Sample	MA-22	MA-22	MA-22	MA-22	MA-22	MA-22	MA-22
	Micro	Micro	Micro	Micro	Micro	Micro	Micro
SiO_2	0.23	0.25	0.33	0.18	0.29	0.27	0.18
TiO_2	21.53	21.38	21.37	22.15	23.85	25.45	22.41
Al_2O_3	2.49	2.11	2.15	2.09	1.49	1.32	1.25
FeO*	68.05	68.15	68.47	68.43	65.38	64.22	68.20
MnO	0.74	0.72	0.69	0.63	0.55	0.75	0.63
MgO	3.30	3.51	3.76	3.52	3.23	2.24	2.33
CaO	0.29	0.09	0.09	0.14	0.11	0.09	0.04
Na_2O	0.27	0.08	0.15	0.39	0.26	0.20	0.27
K_2O	0.00	0.00	0.00	0.00	0.00	0.04	0.00
P_2O_5	0.00	0.04	0.05	0.06	0.04	0.00	0.01
Cr_2O_3	0.13	0.14	0.03	0.07	0.11	0.17	0.16
NiO	0.10	0.00	0.07	0.05	0.00	0.04	0.00
Total	97.13	96.47	97.16	97.71	95.31	94.79	95.48
Formula on the basis of 32 oxygens							
Si	0.01	0.01	0.01	0.01	0.011	0.01	0.01
Ti	0.58	0.59	0.58	0.60	0.67	0.72	0.63
Al	0.11	0.09	0.09	0.09	0.06	0.06	0.06
Fe^{+3}	0.72	0.71	0.73	0.72	0.59	0.48	0.68
Fe^{+2}	1.34	1.37	1.35	1.34	1.44	1.55	1.45
Mn	0.02	0.02	0.02	0.02	0.02	0.02	0.02
Mg	0.18	0.19	0.20	0.19	0.18	0.13	0.13
Ca	0.01	0.03	0.00	0.00	0.00	0.00	0.00
Na	0.02	0.01	0.01	0.03	0.02	0.01	0.02
K	0.00	0.00	0.00	0.00	0.00	0.00	0.00
P	0.00	0.00	0.00	0.00	0.00	0.00	0.00
Cr	0.00	0.00	0.00	0.00	0.00	0.00	0.00
Ni	0.00	0.00	0.00	0.00	0.00	0.00	0.00
Total	3.00	3.00	3.00	3.00	3.00	3.00	3.00
Mn/Mg	0.12	0.12	0.10	0.10	0.10	0.19	0.15
sp	7.51	6.52	6.56	6.31	4.92	4.64	4.02
mg-chr	0.27	0.29	0.06	0.13	0.25	0.40	0.34
mg-fer	17.37	20.59	22.32	20.35	21.79	14.48	14.49
trev	0.43	0.00	0.28	0.20	0.000	0.17	0.00
mt	33.03	30.47	29.26	30.48	22.74	23.19	35.33
usp	41.39	42.13	41.52	42.53	50.29	56.58	45.81

Fe^{+3} is calculated by normalization according to Schumacher(1991).

4.8.3. HAWAIITE

4.8.3.1. PETROGRAPHY

Hawaiites have similar texture and mineral composition to alkali olivine basalts. They vary from holocrystalline to hypocrystalline types with 5-7% of phenocrysts of olivine and clinopyroxene, plagioclase and occasionally anorthoclase, and opaque oxides. Megacrysts are very rare. The rocks around eruption centres are vesicular or scoriaceous and have microlitic texture with a brownish oxidised matrix. Generally, the holocrystalline types are fine grained and have intergranular texture. The mode of minerals is plagioclase(60-70%), anorthoclase(3-5%), olivine(5-7%), clinopyroxene(5-10%) and opaques(5-10%).

The phenocrysts are set in a matrix of olivine, clinopyroxene and feldspar. These phenocrysts are sometimes set in a fine-grained, ophimottled groundmass as illustrated by MacKenzie *et al.* (1982). The rocks also show closely seriate-texture in some samples. Ophimottled texture in the rock indicates the simultaneous growth of clinopyroxene and plagioclase.

Phenocrysts of plagioclase are subhedral and show albite and carlsbad twinning, and normal zoning. They contain abundant inclusions of glass and groundmass minerals, and accessory apatite. Opaque oxide inclusions may be concentrated near the margin of the phenocrysts. Some of the large crystals have sieve texture and corroded rims, and sometimes sponge-like textures in microphenocrysts. Tsuchiyama(1985) showed that heating above the plagioclase liquidus causes solution of plagioclase phenocrysts and rounding of shapes. Since An% of the phenocryst is less than the An% of the plagioclase in equilibrium with the melt, the corroded surface becomes very rough and finely indented to form a sieve texture which is filled with magma, and in which the plagioclase reacts to become more calcic. It is also possible to achieve solution by decompression as magma rises towards the surface(Pearce *et al.*, 1987), in which case there would be no evidence that corrosion was accompanied by a change in the composition of the magma.

Anorthoclase phenocrysts are subhedral, and rarely fragmented with irregular and resorbed shapes. Some of them, for example in sample MA-29B, show well formed thin lamellae twinning along which strips or blobs of clinopyroxene are seen. This feature is very similar to the one in alkali olivine basalts, and resulted from a partial melting reaction and subsequent growth of cpx in the holes. Large anorthoclase crystals showing this melting feature also may have thin overgrowth rims, probably formed after equilibrium with the coexisting melt. Phenocrysts also contain opaque oxide grains.

Clinopyroxene phenocrysts and microphenocrysts are subhedral and commonly show partings or internal cracks, and rarely zoning and simple twinning. They are also present as embayed crystals. They contain fine granular inclusions of opaque oxides, sometimes with an arrangement around their margin indicating a reaction product or disequilibrium growth rather than solution.

Phenocrysts and microphenocrysts of olivine are subhedral to anhedral with internal cracks and thin iddingsite rims, and are rarely skeletal. They also form aggregates of irregular shapes. Embayed crystals with opaque oxide inclusions are also present.

The groundmass is mainly plagioclase, olivine, clinopyroxene and opaque oxide micrograins. However, in some samples clinopyroxene and olivine are common in the groundmass. Olivine and clinopyroxene are difficult to distinguish due to the fine grain size but the pinkish birefringence colour of clinopyroxene is very characteristic. Plagioclase is seen as laths showing albite twinning or as needle-like crystals. Clinopyroxene rarely encloses bladed plagioclases or forms radiating needles and may be altered to chlorite. Olivine is often altered to iddingsite. Opaque iron oxides are seen as equant grains, and enclose both clinopyroxene and plagioclase laths.

In some samples of hawaiites, for instance MA-29B, a single xenocryst of quartz occurs with resorbed shape and irregular cracks and is surrounded by radiating needles of clinopyroxene indicating a reaction rim. The reaction of quartz with basic magma produces pyroxenes, usually as a fine-grained aggregate encrusting the margin of xenocrysts as described by Shelley(1993). In addition, some samples(e.g., MA-36 and 117) exhibit heterogeneous groundmass textures having rich parts with dark colour and poor parts with light colour in opaque oxides. In one of the scoriaceous types(MA-36), a gabbroic xenolith containing olivine and plagioclase was also observed.

4.8.3.2. MINERAL CHEMISTRY

4.8.3.2.1. OLIVINE

Olivines in the hawaiites(Table 4.43) are Mg-rich types with closely similar compositions to those of alkali olivine basalts(Figure 4.45). Phenocrysts have a composition between Fo_{86} and Fo_{73}. Some of them show slight zoning with Fo_{83-74} in the core varying to Fo_{70-60} in the rim. Generally, they have thin iddingsite rims adjoining a composition between Fo_{60} and Fo_{67}. Occasionally, olivine with Fo_{92} is present, especially in scoriaceous samples. The groundmass olivines have homogeneous compositions but are more Fe-rich relative to the phenocrysts. They have a composition ranging from Fo_{68} to Fo_{58}.

4.8.3.2.2. FELDSPAR

Hawaiites have plagioclase compositions(Table 4.44) varying from bytownite, through labradorite to andesine with sparse anorthoclase(Figure 4.50).

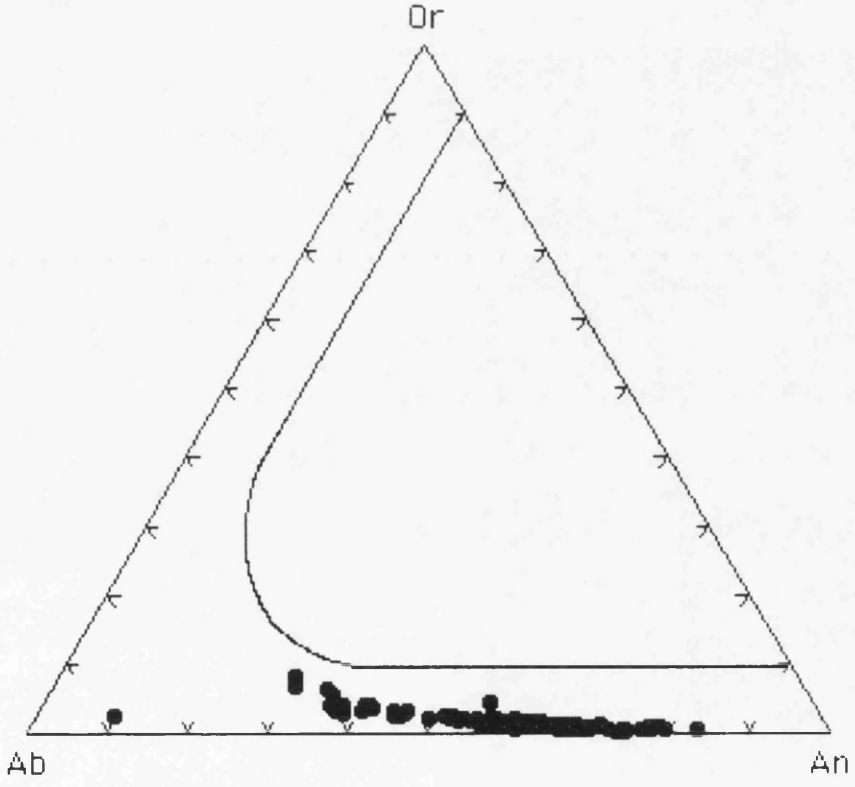

Figure 4.50. Ternary Or-Ab-An diagram of feldspars in the hawaiites.

Megacrysts of plagioclase are labradorite with a composition between An_{61} and An_{52}. Some of them, corroded or embayed, show slightly reverse zoning with An_{56-57} in the core varying to An_{61-60} in the rim. However, some of them have more sodic rims with An_{36}. These compositional changes in the megacrysts provide evidence about crystallisation conditions.

Loomis(1982) showed that a reduced undercooling or a build-up in volatiles may produce reverse zoning in plagioclase. In addition, reverse zoning may also result from magma mixing. However, normally zoned crystals show that equilibration is generally much slower than the rate of crystallisation.

Phenocrysts of plagioclase are mainly labradorite(An_{51-69}) and rarely bytownite(An_{70-84}). Labradorite phenocrysts are normally zoned with a composition An_{57-60} in the core varying to An_{53-55} in the rim. However, some labradorite phenocrysts are reversely zoned with An_{54} in the core and An_{65} in the rim. Generally, bytownite phenocrysts are reverselly zoned with An_{78} in the core varying to An_{82} in the rim, or An_{71} in the core changing to An_{77} in the rim. Sparse phenocrysts of andesine have a composition varying from An_{34} to An_{49}. It is evident that they show also reverse zoning with An_{36-41} in the core ranging to An_{63-65} in the rim.

Microphenocrysts of plagioclase are commonly labradorite with compositions similar to phenocrysts. They have a composition between An_{59} and An_{70}. Some of them exhibit normal zoning with An_{65} in the core and An_{62} in the rim but no reverse zoning.

Microlites of plagioclase are generally labradorite with a composition ranging from An_{50} to An_{70}. In addition, some more sodic laths(andesine) are present with a composition between An_{30} and An_{45}. Furthermore, inclusions of plagioclase within mafic minerals, especially clinopyroxene, are also andesine with An_{35-45}.

4.8.3.2.3. CLINOPYROXENE

The clinopyroxene of hawaiites is mainly augite and rare diopside(Figure 4.51), according to classification of Morimoto *et al.* (1988). Representative analyses are given in Table 4.45.

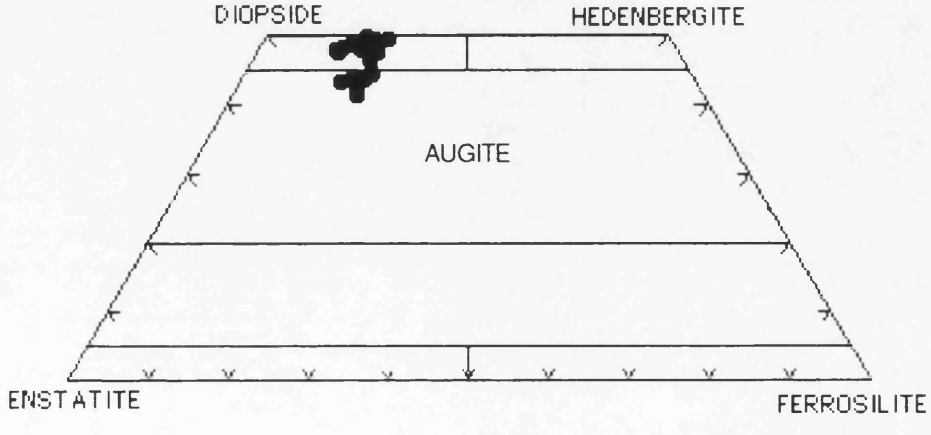

Figure 4.51. Pyroxene nomenclature of hawaiites on the Wo-En-Fs ternary plot(Morimoto *et al.*, 1988).

Augites are almost homogeneous with a composition ranging only from $Wo_{44}En_{44}Fs_{12}$ to $Wo_{41}En_{43}Fs_{16}$. They have a $Mg/(Mg+Fe^{+3}+Fe^{+2})$ ratio between 0.72 and 0.78. Generally, augites have lower contents of Ti and Al compared with those in alkali olivine basalts. TiO_2 content is between 1.1 and 1.8 wt.%, reflecting the alkaline nature of the rocks(Kushiro, 1960; Le Bas, 1962; Verhoogen, 1962). Al_2O_3 content is between 3.9% and 6.4 w.t%. They have low contents of Cr and Ni.

Diopsides occur without augite in only one of the samples(MA-140). They have a compositional range of $Wo_{48-49}En_{40-38}Fs_{12-13}$. They are Ti and Al-rich relatively to augites. On the Ti versus Al plot, it is significant that there is positive relationship with increasing Ti and Al contents from augites towards diopsides. However, on the Si versus Al plot, there is a negative trend with decreasing Al content from diopsides towards augites(Figure 4.52).

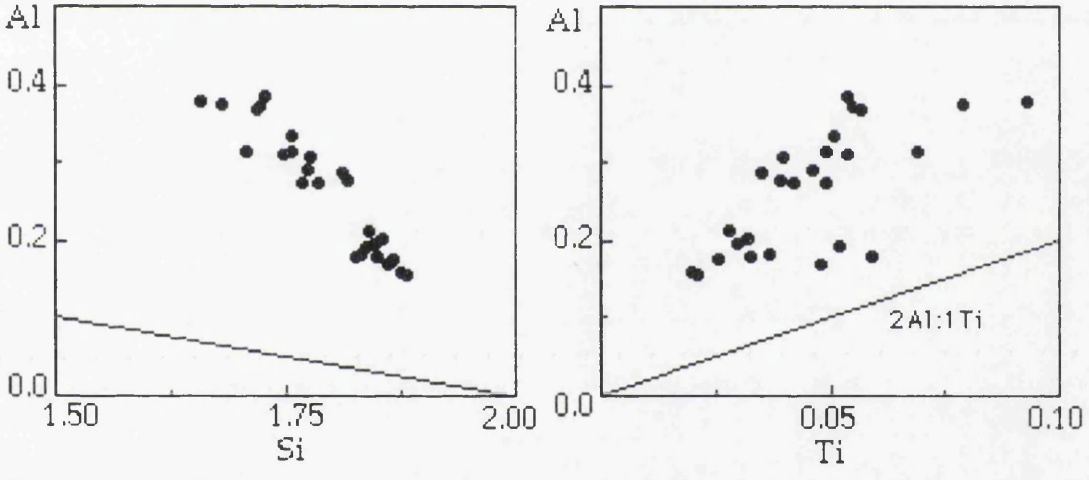

Figure 4.52. Plots of total Al against Si and Ti per formula unit for pyroxenes of the hawaiites.

4.8.3.2.4. FE-TI OXIDES

Magnetite is the main oxide mineral with spinel and ilmenite also present in some samples(Figure 4.53). Representative analyses of oxides are given in Table 4.46.

Magnetites are Ti-rich types with a TiO_2 content between 12% and 20 wt.% which is lower than Ti in the magnetites in the alkali olivine basalts. They generally have high Al_2O_3 contents between 1% and 9 wt.%, showing transition towards ulvospinel(usp21-39). MgO contents are also high varying between 1% and 6 wt.%. NiO(0-0.2wt.%) and Cr_2O_3(0-0.1 wt.%) contents are very low.

Spinels are generally pleonastes with significant hercynite being sp_{54-59} and $hercynite_{19-25}$. They have a TiO_2 content between 1.5 and 1.7 wt.%. Al_2O_3 is about 49% and MgO is about 14 wt.%. MnO is about 0.2 wt.%. NiO and Cr_2O_3 contents are quite low and insignificant.

Ilmenites have TiO_2 contents of about 45 wt.%, MgO about 2%, MnO about 0.5 wt.%, and very low NiO and Cr_2O_3 contents.

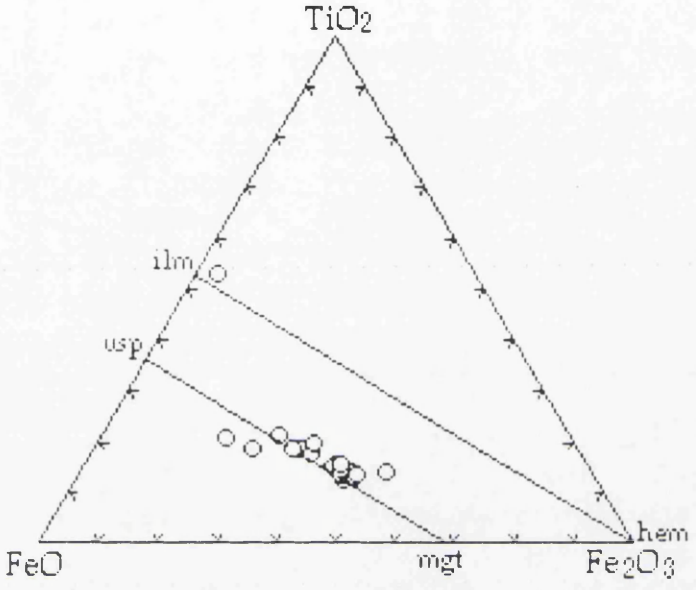

Figure 4.53. Compositions of iron-titanium oxide minerals in the hawaiites.

Table 4.43. Representative analyses of olivines in the hawaiites.

Sample	MA-36 Micro core	MA-40 Pheno core	MA-40 Pheno rim	MA-40 Micro ----	MA-40 Micro ----	MA-37 Micro ----	MA-37 Pheno core	MA-166 Pheno core	MA-117 Micro ----
SiO_2	39.45	37.19	37.51	36.40	36.13	36.01	36.33	38.92	35.98
TiO_2	0.06	0.00	0.00	0.07	0.09	0.09	0.01	0.00	0.05
Al_2O_3	0.17	0.00	0.05	0.09	0.08	0.00	0.09	0.00	0.00
FeO*	16.97	23.66	27.05	30.11	29.78	31.29	30.54	17.23	29.53
MnO	0.62	0.48	0.62	0.82	0.85	0.79	0.73	0.27	0.80
MgO	42.67	36.92	35.05	31.93	32.01	31.90	31.89	43.38	33.05
CaO	0.38	0.19	0.26	0.26	0.32	0.39	0.36	0.06	0.33
Na_2O	0.14	0.18	0.38	0.27	0.21	0.17	0.37	0.26	0.17
K_2O	0.03	0.00	0.00	0.01	0.00	0.00	0.00	0.00	0.00
P_2O_5	0.04	0.00	0.03	0.12	0.14	0.18	0.09	0.12	0.08
Cr_2O_3	0.00	0.00	0.07	0.01	0.00	0.00	0.02	0.00	0.10
NiO	0.07	0.12	0.05	0.05	0.06	0.03	0.00	0.17	0.01
Total	100.60	98.74	101.07	100.14	99.67	100.85	100.43	100.41	100.10
Formula on the basis of 4 oxygens									
Si	0.99	0.99	0.99	0.99	0.99	0.98	0.98	0.99	0.97
Ti	0.00	0.00	0.00	0.00	0.00	0.00	0.00	0.00	0.00
Al	0.01	0.00	0.00	0.00	0.00	0.00	0.00	0.00	0.00
Fe^{+2}	0.36	0.53	0.60	0.68	0.68	0.71	0.69	0.37	0.67
Mn	0.01	0.01	0.01	0.02	0.02	0.02	0.02	0.01	0.02
Mg	1.6	1.47	1.38	1.29	1.30	1.29	1.28	1.64	1.34
Ca	0.01	0.01	0.01	0.01	0.01	0.01	0.01	0.00	0.01
Na	0.01	0.01	0.02	0.01	0.01	0.01	0.02	0.01	0.01
K	0.00	0.00	0.00	0.00	0.00	0.00	0.00	0.00	0.00
P	0.01	0.00	0.00	0.00	0.00	0.00	0.01	0.00	0.00
Cr	0.00	0.00	0.00	0.00	0.00	0.00	0.00	0.00	0.00
Ni	0.00	0.00	0.00	0.00	0.00	0.00	0.00	0.00	0.00
Total	3.00	3.01	3.02	3.01	3.01	3.02	3.01	3.02	3.02
$Mg^{\#}$	0.82	0.74	0.70	0.65	0.66	0.64	0.65	0.82	0.67
Fo	80.50	72.51	68.74	64.02	64.06	62.37	63.26	81.78	66.67
Fa	18.50	26.59	30.46	34.78	34.44	35.23	34.84	18.22	33.33

FeO* is total iron as FeO.
$Mg^{\#}=Mg/(Mg+Fe^{+2})$

Table 4.44. Representative analyses of feldspars in the hawaiites.

Sample	MA-40 Mega core	MA-40 Mega rim	MA-37 Micro core	MA-37 Micro-lite	MA-49A Pheno core	MA-36 Pheno rim	MA-166 Pheno core	MA-117 Pheno core	MA-117 Micro core	MA-140 Micro-lite
SiO_2	58.10	50.78	51.56	53.10	47.91	56.94	48.16	55.14	52.22	48.50
TiO_2	0.00	0.02	0.15	0.14	0.02	0.02	0.00	0.13	0.11	0.00
Al_2O_3	25.25	30.15	29.95	28.75	32.43	25.42	31.34	27.47	29.79	31.66
FeO*	0.21	0.34	0.76	0.61	0.42	0.40	0.41	0.40	0.98	0.61
MnO	0.03	0.07	0.00	0.00	0.04	0.00	0.01	0.00	0.00	0.00
MgO	0.00	0.11	0.09	0.12	0.22	0.17	0.19	0.00	0.14	0.16
CaO	7.22	13.13	12.85	11.49	15.89	7.65	14.97	9.90	13.06	15.05
Na_2O	6.74	3.75	3.96	4.91	2.24	6.70	2.85	5.47	3.86	2.99
K_2O	0.75	0.28	0.34	0.27	0.13	0.71	0.05	0.40	0.29	0.08
P_2O_5	0.00	0.00	0.01	0.00	0.00	0.00	0.00	0.09	0.00	0.00
Cr_2O_3	0.03	0.02	0.01	0.05	0.10	0.02	0.06	0.01	0.02	0.00
NiO	0.04	0.09	0.03	0.04	0.02	0.00	0.16	0.00	0.01	0.05
Total	98.37	98.74	99.71	99.48	99.42	98.03	98.20	99.01	100.48	99.10
Formula on the basis of 32 oxygens										
Si	10.57	9.35	9.40	9.65	8.83	10.40	8.99	10.04	9.48	8.98
Ti	0.00	0.00	0.02	0.01	0.00	0.00	0.00	0.02	0.01	0.00
Al	5.43	6.54	6.44	6.17	7.05	5.47	6.90	5.90	6.37	6.91
Fe^{+2}	0.03	0.05	0.12	0.09	0.06	0.06	0.06	0.06	0.15	0.09
Mn	0.00	0.01	0.00	0.00	0.01	0.00	0.00	0.00	0.00	0.00
Mg	0.00	0.03	0.03	0.03	0.06	0.05	0.05	0.00	0.03	0.05
Ca	1.43	2.59	2.52	2.24	3.14	1.49	2.99	1.93	2.54	2.99
Na	2.38	1.35	1.40	1.74	0.80	2.36	1.03	1.93	1.36	1.07
K	0.18	0.06	0.08	0.06	0.03	0.17	0.01	0.09	0.07	0.02
P	0.00	0.00	0.00	0.00	0.00	0.00	0.00	0.02	0.00	0.00
Cr	0.00	0.00	0.00	0.01	0.01	0.00	0.00	0.00	0.00	0.00
Ni	0.00	0.01	0.00	0.00	0.00	0.00	0.02	0.00	0.00	0.01
Total	19.99	19.99	20.01	20.00	19.99	20.00	20.07	19.99	19.99	20.11
An	35.84	64.75	63.00	55.45	79.09	37.06	74.19	48.86	63.98	73.28
Ab	59.65	33.75	35.00	43.07	20.15	58.71	25.56	48.86	34.26	26.23
Or	4.51	1.25	2.00	1.48	0.76	4.23	0.25	2.28	1.76	0.49

FeO* is total iron as FeO.

Table 4.45. Representative analyses of clinopyroxenes in the hawaiites.

Sample	MA-166	MA-40	MA-40	MA-40	MA-37	MA-49	MA-49	MA-140	MA-140
	Micro	Micro core	Micro rim	Micro	Pheno	Micro	Micro	Pheno core	Pheno rim
SiO_2	48.80	48.90	48.31	48.50	48.53	50.42	49.46	47.22	46.49
TiO_2	1.69	1.09	1.35	1.21	1.82	0.78	0.91	1.65	1.89
Al_2O_3	3.80	5.28	6.11	6.42	4.33	3.53	3.90	6.62	7.05
FeO*	8.72	8.99	8.79	8.45	8.47	7.49	8.63	6.83	6.70
MnO	0.45	0.24	0.19	0.19	0.17	0.07	0.26	0.22	0.13
MgO	14.28	14.25	12.75	13.28	13.11	15.26	14.60	12.99	13.45
CaO	18.93	18.84	19.85	19.71	21.78	21.01	20.72	22.88	22.87
Na_2O	0.61	0.85	0.86	0.94	0.76	0.57	0.34	0.78	0.62
K_2O	0.07	0.01	0.00	0.00	0.04	0.00	0.02	0.01	0.03
P_2O_5	0.19	0.00	0.00	0.00	0.00	0.07	0.00	0.18	0.03
Cr_2O_3	0.06	0.03	0.02	0.02	0.08	0.11	0.13	0.03	0.26
NiO	0.05	0.00	0.03	0.04	0.06	0.03	0.04	0.00	0.00
Total	97.65	98.48	98.26	98.76	99.15	99.34	99.01	99.41	99.52
Formula on the basis of 6 oxygens									
Si	1.84	1.83	1.80	1.79	1.82	1.88	1.85	1.75	1.72
Ti	0.05	0.03	0.04	0.03	0.05	0.02	0.03	0.05	0.05
Al	0.17	0.23	0.27	0.28	0.19	0.15	0.17	0.29	0.31
Fe^{+3}	0.11	0.10	0.11	0.13	0.12	0.09	0.10	0.15	0.18
Fe^{+2}	0.16	0.18	0.17	0.14	0.14	0.13	0.17	0.06	0.03
Mn	0.01	0.01	0.01	0.01	0.01	0.00	0.01	0.01	0.00
Mg	0.80	0.79	0.72	0.75	0.73	0.84	0.81	0.72	0.74
Ca	0.76	0.76	0.81	0.80	0.87	0.83	0.83	0.91	0.91
Na	0.04	0.06	0.06	0.07	0.06	0.04	0.02	0.06	0.04
K	0.03	0.00	0.00	0.00	0.00	0.00	0.00	0.00	0.00
P	0.01	0.00	0.00	0.00	0.00	0.00	0.00	0.01	0.00
Cr	0.00	0.00	0.00	0.00	0.00	0.00	0.00	0.00	0.01
Ni	0.00	0.00	0.00	0.00	0.00	0.00	0.00	0.00	0.00
Total	4.00	4.00	4.00	4.00	4.00	4.00	4.00	4.00	4.00
$Mg^{\#}$	0.75	0.74	0.72	0.74	0.73	0.78	0.75	0.77	0.78
Wo	41.19	41.08	44.51	43.87	46.58	43.65	43.20	49.26	48.75
En	43.22	43.21	39.77	41.11	38.99	44.09	42.33	38.89	39.88
Fs	15.59	15.71	15.72	15.02	14.43	12.26	14.47	11.85	11.37

Fe^{+3} is calculated by normalization according to Schumacher(1991).
$Mg^{\#}=Mg/(Mg+Fe^{+3}+Fe^{+2})$

Table 4.46. Representative analyses of Fe-Ti oxides in the hawaiites.

Sample	MA-37 Pheno	MA-40 Micro	MA-166 Micro	MA-117 Pheno rim	MA-117 Micro	MA-117 Inclus.	MA-140 Micro	MA-140 Micro	MA-49 Micro
SiO_2	0.24	0.13	0.53	0.20	0.21	0.42	0.47	0.17	0.22
TiO_2	10.29	12.01	17.81	1.49	11.80	14.26	13.13	14.52	45.09
Al_2O_3	13.38	4.85	1.83	49.35	8.36	4.23	3.23	2.10	0.03
FeO*	67.16	74.40	69.04	36.76	71.32	72.67	73.99	74.56	48.29
MnO	0.37	0.47	0.66	0.24	0.67	0.54	1.04	1.03	0.48
MgO	5.44	2.43	4.10	13.44	3.59	3.26	2.05	2.52	2.16
CaO	0.01	0.01	0.24	0.01	0.03	0.12	0.56	0.14	0.02
Na_2O	0.07	0.04	0.25	0.40	0.34	0.41	0.38	0.33	0.00
K_2O	0.01	0.00	0.04	0.01	0.00	0.01	0.01	0.04	0.00
P_2O_5	0.05	0.03	0.03	0.00	0.00	0.04	0.04	0.05	0.02
Cr_2O_3	0.04	0.27	0.13	0.10	0.05	0.13	0.03	0.07	0.02
NiO	0.00	0.07	0.04	0.03	0.08	0.08	0.01	0.01	0.04
Total	97.06	94.71	94.70	102.03	96.45	96.17	94.94	95.54	96.37
Formula on the basis of 32 oxygens for magnetites and 6 oxygens for ilmenite									
Si	0.01	0.01	0.02	0.01	0.01	0.02	0.02	0.01	0.01
Ti	0.26	0.33	0.49	0.03	0.31	0.39	0.36	0.40	0.87
Al	0.53	0.21	0.08	1.57	0.35	0.18	0.14	0.09	0.01
Fe^{+3}	0.93	1.11	0.91	0.38	1.04	1.04	1.10	1.11	0.25
Fe^{+2}	0.98	1.18	1.22	0.45	1.06	1.15	1.17	1.18	0.78
Mn	0.01	0.01	0.02	0.01	0.02	0.02	0.03	0.03	0.01
Mg	0.27	0.13	0.22	0.54	0.19	0.17	0.11	0.14	0.08
Ca	0.00	0.00	0.01	0.00	0.00	0.00	0.02	0.01	0.00
Na	0.00	0.00	0.02	0.02	0.02	0.03	0.03	0.02	0.00
K	0.00	0.00	0.00	0.00	0.00	0.00	0.00	0.00	0.00
P	0.00	0.00	0.00	0.00	0.00	0.00	0.01	0.00	0.00
Cr	0.00	0.01	0.00	0.00	0.00	0.00	0.00	0.00	0.00
Ni	0.00	0.00	0.00	0.00	0.00	0.00	0.00	0.00	0.00
Total	3.00	3.00	3.00	3.00	3.00	3.00	3.00	3.00	2.00
Mn/Mg	0.04	0.11	0.09	0.01	0.11	0.09	0.29	0.23	0.13
sp	31.01	12.70	5.35	54.63	20.44	11.16	8.70	5.68	
mg-chr	0.04	0.47	0.26	0.00	0.08	0.22	0.05	0.13	
mg-fer	0.82	2.93	24.73	0.00	1.67	10.35	5.22	11.37	
trev	0.00	0.25	0.18	0.06	0.25	0.28	0.04	0.03	
herc	0.00	0.00	0.00	24.70	0.00	0.00	0.00	0.00	
chr	0.00	0.00	0.00	0.11	0.00	0.00	0.00	0.00	
mt	52.89	63.61	36.27	19.20	59.15	54.00	63.41	57.78	
usp	15.22	20.05	33.23	1.30	18.41	23.99	22.58	25.01	

Fe^{+3} is calculated by normalization according to Schumacher(1991).

4.8.4. MUGEARITE

4.8.4.1. PETROGRAPHY

The mugearites are hypocrystalline and significantly porphyritic with 10-25% plagioclase megacrysts, and a mode of plagioclase(60-70%), anorthoclase(5-7%), clinopyroxene and olivine(15-25%), amphibole(<1%), opaque oxides(10%) and accessory apatite. The phenocrysts are mainly plagioclase with minor anorthoclase, clinopyroxene, and a few amphiboles. In addition, microphenocrysts of plagioclase, olivine, titanomagnetite and a few ilmenites are present. The matrix is plagioclase, clinopyroxene, Fe-Ti oxides and a little olivine.

Plagioclase megacrysts are subhedral, corroded and embayed. They can reach up to 1 cm. They show well developed oscillatory and rarely convolute and sector zoning, and large lamellae albite twinning. Oscillatory zoning shows discontinuities due to twinning. Megacrysts are formed as either single crystals or as interlocking megacryst clusters. In most cases, the twinning cuts of common zoning(Figure 4.54). They contain abundant glass inclusions giving the crystal sponge-like texture, with cpx and opaques±olivine and sometimes apatite inclusions. Internal cracks within the crystals are significant and probably indicate release of earlier high pressure. Occasionally, inclusions of opaque oxides are ordered along the rim or in the core of the crystals. The large dimensions of the plagioclases perhaps indicate a long period of cooling of the magma rather than rapid chilling.

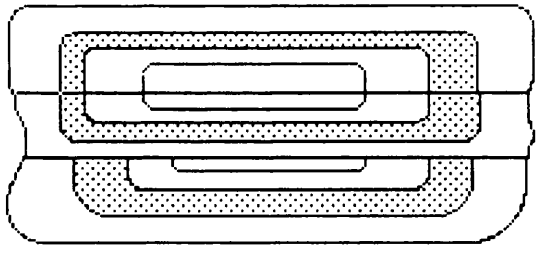

Figure 4.54. A sketch of plagioclase megacryst illustrating relationship between oscillatory zoning and common twinning. Independently zoned crystals joined through synneusis, as suggested by Vance(1969). However, Dowty(1980b) expressed doubts about synneusis, pointing out that apparently independent zonal patterns could be an artefact of oblique sections of either simply zoned crystals or twins resulting from epitaxial nucleation of one crystal on the other.

Clinopyroxene phenocrysts are elongated prismatic in shape and show slight zoning and simple twinning. Olivine microphenocrysts are subhedral and generally altered to iddingsite.

The groundmass is fine-grained with a trachytic texture of plagioclase laths, some anorthoclase, granular Fe-Ti oxides, clinopyroxene and some iddingsite. Ilmenite is one of the earlier constituents of the magma to crystallise and associated with pyroxene. Generally, plagioclase laths are enclosed by granules of cpx, olivine and opaque oxides, with some skeletal olivines and rare orthopyroxene. All these minerals are set in a dark matrix, with a yellowish brown alteration(chlorophaeite) of olivine and, or clinopyroxene. This alteration is common around vesicles in the rock.

Some of the samples(e.g., MA-54) indicate late stage hydrothermal alteration products. These products such as calcite and micaceous mineraloids form in thin cracks or around vesicles forming concentric rings. In addition, a cpx crystal is enclosed by needle-like crystals of prehnite and fine grained quartz. A similar texture in which anorthoclase microphecrysts interlocking each other are enclosed by fine grained quartz crystals is significant and may represent a xenolith as a whole.

4.8.4.2. MINERAL CHEMISTRY

4.8.4.2.1. OLIVINE

Most of the olivines in mugearites(Table 4.47) vary from Fo_{48} to Fo_{41}(Figure 4.45). Generally, they are unzoned with homogeneous compositions.

Microphenocrysts range from Fo_{48} to Fo_{46}, with slight normal zoning(Fo_{47-44}). Groundmass olivines are $Fo_{42\pm1}$. Generally, MnO content changes between 0.3% and 0.6 wt.%, and trace element contents(NiO and Cr_2O_3) are quite low between 0 and 0.2 wt.%.

4.8.4.2.2. FELDSPAR

The feldspar in mugearites(Table 4.48) ranges from An_{62} to An_{22}(Figure 4.55).

The megacrysts are mainly labradorite and some andesine with a composition between An_{62} and An_{38}. They show both reverse and normal zoning in the same samples. The reverse zoned crystals have a composition An_{53} in the core varying to An_{59} in the rim, or An_{48} in the core changing to An_{53} in the rim. The normally zoned crystals show a composition ranging from An_{62-60} in the core to An_{51-47} in the rim, or An_{55-53} in the core varying to An_{47-45} in the rim. Generally, the megacrysts show complex oscillatory zoning and have abrupt increases or decreases of An% between which gradual variation either with increasing or decreasing An% occurs(Figures 4.56 and 4.57).

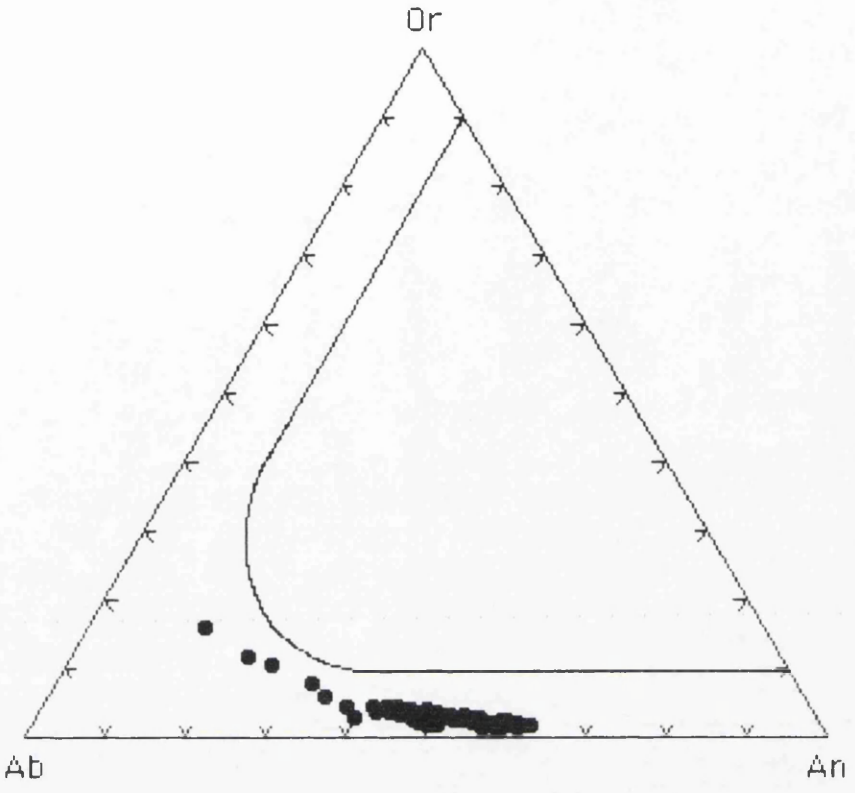

Figure 4.55. Or-Ab-An diagram of feldspars in mugearites.

Phenocrysts and microphenocrysts are unzoned An_{55} to An_{44}, microlites are An_{50} and An_{22}, and the groundmass contains $An_{55\text{-}61}$ with some anorthoclase An_{14} $Or_{17}Ab_{69}$.

The largest megacrysts are generally oscillatory or reversely zoned from An_{48} to An_{53}, or from An_{53} to An_{59}. These variations could result from;

a) polybaric fractional crystallisation and fluctuations in water pressure during magma ascent(Yoder *et al.*, 1957),

b) magma mixing of plagioclase-phyric, compositionaly diverse magmas,

c) the incorporation of crustal plagioclase xenocrysts.

The two main features that characterise oscillatory zoning are: abrupt changes which usually mark a sudden outwards increase in An%(reverse zoning) and which may feature corrosion of the underlying crystal surface; gradual changes of An%(either reverse or normal) in the plagioclase deposited between successive sharp breaks. The An% change at sharp boundaries varies from small to large(33% for one crystal); the gradual changes are always small(less than 10%).

Abrupt compositional changes require abrupt changes in the dynamic conditions of crystallisation, and most researchers now advocate magma mixing. Nixon and Pearce(1987) showed that repeated injection of fresh, hot,

basic magma into a chamber of already differentiated and cooled magma can repeatedly cause resorption of already crystallised plagioclase(Figure 4.56).

The more gradual changes in oscillatory zoning are best interpreted in terms of local effects of disequilibrium crystallisation(Loomis, 1982). Liquidus-solidus curves for pure anhydrous plagioclase are depressed by the presence of other components. Water alone can depress the curves by several hundreds of degrees, and the shape of the curves change too.

Reverse zoning forms if undercooling decreases or residual components adjacent to the crystal face increase; normal zoning forms if undercooling increases or the residual components decrease. The changes are likely to be small and transient. Loomis(1982), for example, shows that the build-up of volatiles next to the crystal eventually leads to a density gradient that will in turn cause local convection. This convection will readjust the chemical composition of the magma next to the crystal; repeated convection will cause oscillations in plagioclase composition(Figure 4.56). Anderson(1984) suggests that the alternative mechanism of liquid shearing for interrupting the build-up of chemical gradients next to the crystal. He proposes that the crystal-liquid interface is sheared twice daily by tidal pulses.

Oscillatory zones are usually euhedral in character and the resorption surfaces associated with abrupt changes in composition cut across previous crystal faces and zoning patterns. However, not all embayments are the result of resorption; some result from dentritic growth, as demonstrated by convolute oscillatory zone patterns that parallel embayment surfaces.

As a result it is suggested that oscillatory zoning in plagioclase megacrysts from the mugearites is caused by combination of magma mixing and disequilibrium crystallisation(Figure 4.57), as described by Stamateloulou-Seymour *et al.* (1990).

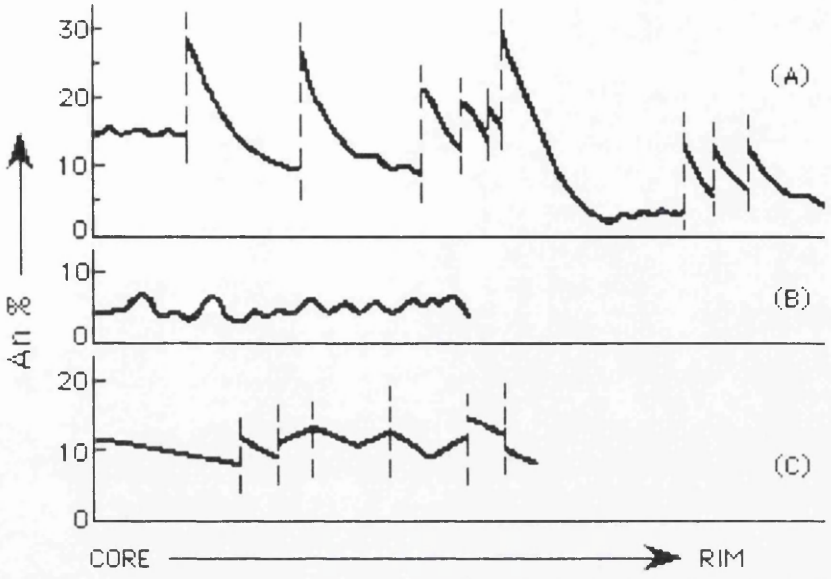

Figure 4.56. Schematic illustration of typical oscillatory zoning profiles from core to rim(After Shelley, 1993). (A): Repeated major sharp reversals due to magma mixing caused by injection of fresh basic magma, as described by Nixon and Pearce(1987). (B): Small irregular oscillations due to local disequilibrium crystallisation, as described by Loomis(1982). (C): Complex oscillatory zoning due to combinations of magma mixing and disequilibrium crystallisation, as described by Stamatelopoulou-Seymour *et al.* (1990).

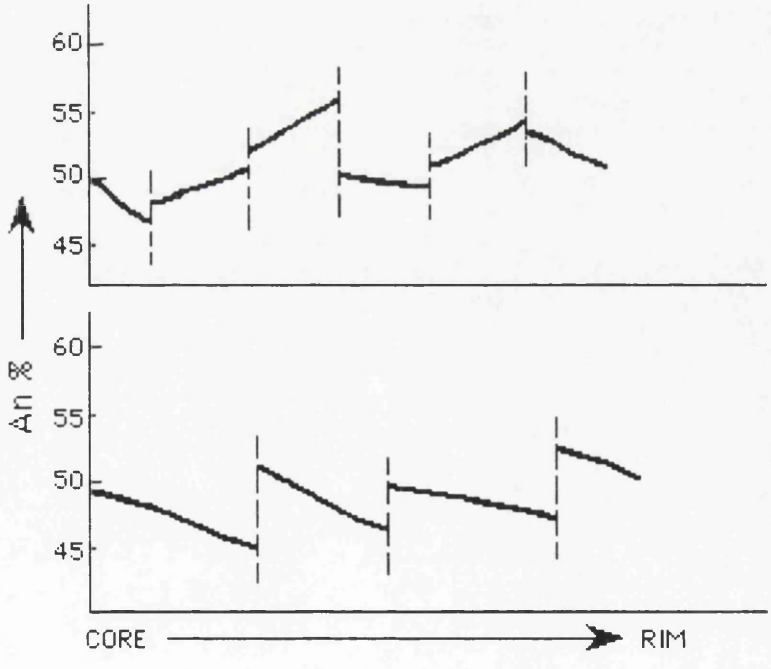

Figure 4.57. Schematic illustration of oscillatory zoning profiles of two plagioclase megacrysts from the mugearites, based on the An% from core to rim. The profiles reflects the complex oscillatory zoning, probably caused by combinations of magma mixing and disequilibrium crystallisation.

4.8.4.2.3. CLINOPYROXENE

The clinopyroxenes of the mugearites are mainly augite, some diopside and hedenbergite(Figure 4.58), according to the classification of Morimoto *et al.* (1988). They are generally homogeneous types but in some samples, they show compositional changes with Mg-rich core and Fe-rich rim. Representative analyses are given in Table 4.49.

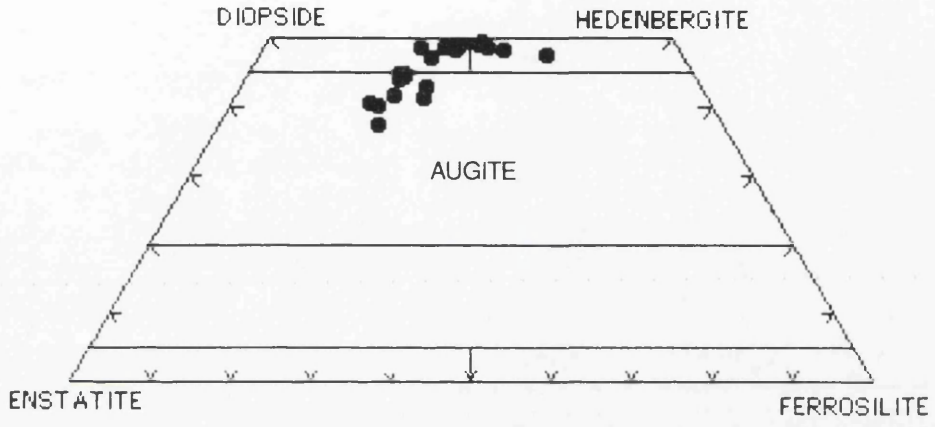

Figure 4.58. Pyroxene nomenclature of mugearites on the Wo-En-Fs ternary plot(Morimoto *et al.*, 1988).

Augites have a composition varying from $Wo_{45}En_{36}Fs_{19}$ to $Wo_{41}En_{42}Fs_{17}$, and $Mg/(Mg+Fe^{+3}+Fe^{+2})$ ratio between 0.65 and 0.72. They are typically titanian types with a TiO_2 content between 1% and 3 wt.%. Groundmass augites are richer in TiO_2(2-3 wt.%) than phenocrysts. In addition, groundmass augites have Al_2O_3 content between 3.2 and 4.7 wt.% whereas phenocrysts are relatively poor in Al_2O_3 content(2.7-2.9 wt.%). Generally, augites have MnO between 0.22 and 0.35 wt.%., Na_2O changes between 0.49 and 0.83 wt.%. and trace elements (e.g., NiO and Cr_2O_3) are low.

Diopside and hedenbergite occur in some samples(e.g., MA-54). Diopsides have a composition varying from $Wo_{49}En_{27}Fs_{24}$ to $Wo_{49}En_{32}Fs_{19}$, and $Mg/(Mg+Fe^{+3}+Fe^{+2})$ ratio between 0.53 and 0.63. They are also Ti-rich types with a TiO_2 content between 1.5 and 2.4 wt.%. Al_2O_3 content is quite high between 6 and 9 wt.%, relative to augites(Figure 4.59). MnO is between 0.10 and 0.30 wt.%, Cr_2O_3 and NiO are very low. Some of them display very significant zoning with a diopsitic core($Wo_{49}En_{27}Fs_{24}$) varying to more iron rich rim($Wo_{50}En_{23}Fs_{27}$), or a composition $Wo_{47}En_{32}Fs_{21}$ in the core ranging to $Wo_{48}En_{17}Fs_{35}$ in the rim. Hedenbergites are represented with a composition of $Wo_{49}En_{25}Fs_{26}$, and $Mg/(Mg+Fe^{+3}+Fe^{+2})$ ratio between 0.43 and 0.48. Both diopsides and hedenbergites contain a significant Na_2O content varying between 0.6 and 1.6 wt.%.

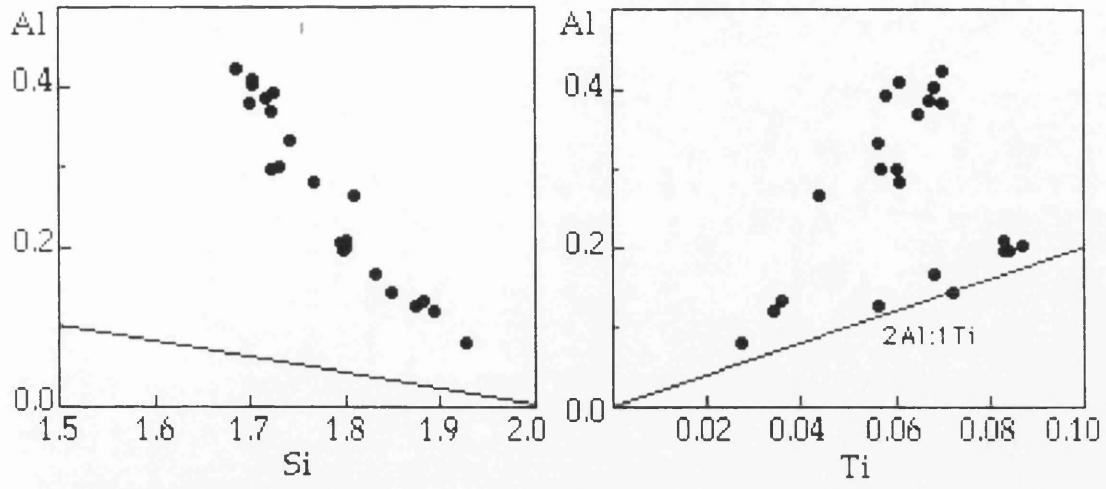

Figure 4.59. Plots of total Al against Si and Ti contents in the formula units from the clinopyroxenes of the mugearites.

4.8.4.2.4. FE-TI OXIDES

In the mugearites, Ti-rich magnetites(Table 4.50) are present with a TiO_2 content between 22% and 29 wt.%, although each grain is almost homogeneous.

Magnetites are also rich in MgO with 1.3 to 2.5 wt.%. Al_2O_3 is between 0.7 and 2.7 wt.%. MnO content is low but in some samples it reaches up to 1 wt.%. Generally, magnetite compositions show transition towards ulvospinel with Usp_{84-70}(Figure 4.60).

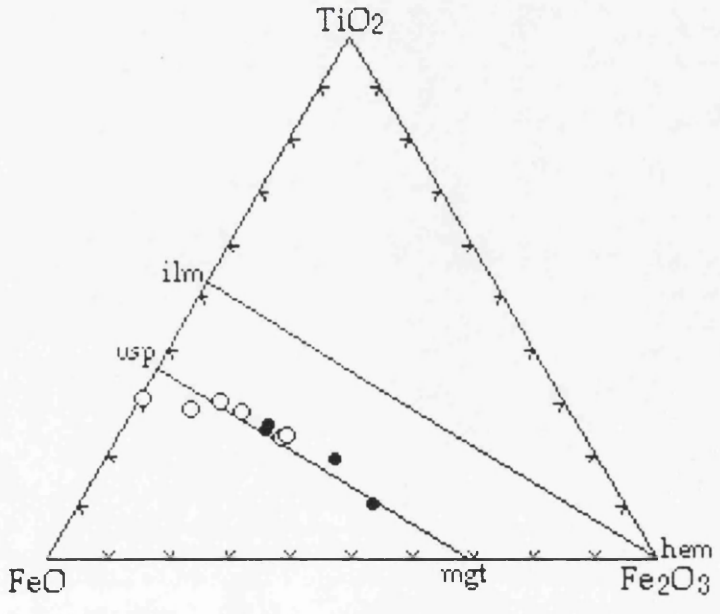

Figure 4.60. Compositions of iron-titanium oxides in the mugearites. Solid circles represent inclusions in plagioclase megacrysts.

Table 4.47. Representative analyses of olivines in the mugearites.

Sample	MA-53 Microphe. Iddingsite	MA-53 Microphe. Iddingsite	MA-53 Microphe. Iddinsite	MA-53 Microphe. core	MA-53 Microphe. rim	MA-53 Iddingsite	MA-53 Iddingsite
SiO_2	32.82	28.10	31.15	30.90	30.77	31.49	30.94
TiO_2	0.09	0.34	0.07	0.18	0.00	0.07	0.57
Al_2O_3	0.41	0.36	0.59	0.53	0.43	0.21	0.29
FeO*	39.84	44.37	38.47	38.61	40.73	37.67	40.08
MnO	0.38	0.46	0.38	0.40	0.29	0.50	0.47
MgO	20.97	17.40	19.49	19.28	17.68	19.40	16.87
CaO	0.49	0.53	0.47	0.44	0.52	0.42	0.65
Na_2O	0.20	0.08	0.23	0.35	0.07	0.38	0.05
K_2O	0.02	0.02	0.00	0.01	0.00	0.04	0.06
P_2O_5	0.08	0.10	0.07	0.11	0.05	0.09	0.03
Cr_2O_3	0.07	0.00	0.03	0.00	0.00	0.00	0.03
NiO	0.15	0.00	0.04	0.00	0.08	0.06	0.00
Total	95.52	91.76	90.99	90.81	90.62	90.33	90.04
Formula on the basis of 4 oxygens							
Si	0.99	0.91	0.98	0.96	0.95	0.98	0.96
Ti	0.00	0.01	0.00	0.00	0.00	0.00	0.01
Al	0.02	0.01	0.02	0.02	0.02	0.01	0.01
Fe^{+2}	0.99	1.20	1.01	1.03	1.12	1.01	1.11
Mn	0.01	0.01	0.01	0.01	0.01	0.01	0.01
Mg	0.93	0.84	0.91	0.92	0.87	0.93	0.83
Ca	0.02	0.02	0.01	0.01	0.02	0.01	0.02
Na	0.01	0.01	0.01	0.02	0.00	0.02	0.00
K	0.00	0.00	0.00	0.00	0.00	0.00	0.00
P	0.02	0.03	0.02	0.02	0.03	0.02	0.02
Cr	0.00	0.00	0.01	0.00	0.00	0.00	0.01
Ni	0.00	0.00	0.00	0.00	0.00	0.00	0.00
Total	2.99	3.03	2.98	2.99	3.02	2.99	2.98
$Mg^{\#}$	0.48	0.41	0.47	0.47	0.44	0.48	0.43
Fo	48.17	40.88	47.15	46.94	43.50	47.69	42.56
Fa	51.83	59.12	52.85	53.06	56.50	52.31	57.44

FeO* is total iron as FeO.
$Mg^{\#}=Mg/(Mg+Fe^{+2})$

Table 4.48. Representative analyses of feldspars in the mugearites.

Sample No	MA-47 Micro-lite	MA-53 Mega core	MA-53 Mega mid	MA-53 Mega rim	MA-53 Mega core	MA-53 Mega rim	MA-53 Pheno core	MA-54 Pheno core	MA-54 Pheno rim	MA-54 Micro-lite	MA-54 Micro-lite
SiO_2	54.44	54.40	52.57	54.36	51.77	54.67	56.09	62.40	54.90	51.70	54.12
TiO_2	0.09	0.14	0.09	0.13	0.11	0.07	0.12	0.14	0.16	0.14	0.15
Al_2O_3	28.07	27.11	28.16	27.35	29.22	27.74	27.20	22.53	28.08	29.34	27.58
FeO*	0.74	0.66	0.61	0.64	0.69	0.64	0.60	0.48	0.91	0.97	0.98
MnO	0.00	0.04	0.05	0.00	0.00	0.01	0.00	0.00	0.03	0.02	0.00
MgO	0.21	0.13	0.17	0.10	0.15	0.00	0.12	0.00	0.07	0.12	0.09
CaO	11.27	10.46	11.70	9.72	12.44	9.91	9.25	2.99	10.37	12.27	10.39
Na_2O	5.30	5.22	4.33	5.40	4.28	5.16	5.86	7.56	5.51	4.24	5.45
K_2O	0.52	0.51	0.37	0.56	0.37	0.61	0.59	3.00	0.35	0.24	0.39
P_2O_5	0.00	0.00	0.00	0.00	0.00	0.00	0.00	0.00	0.00	0.00	0.01
Cr_2O_3	0.00	0.04	0.00	0.08	0.00	0.00	0.00	0.00	0.00	0.00	0.00
NiO	0.03	0.00	0.07	0.05	0.00	0.05	0.02	0.01	0.00	0.05	0.00
Total	100.67	98.71	98.12	98.39	99.03	98.86	99.85	99.11	100.38	99.09	99.16
Formula on the basis of 32 oxygens											
Si	9.75	9.86	9.62	10.04	9.48	10.10	10.22	11.34	9.87	9.48	9.84
Ti	0.01	0.02	0.01	0.02	0.02	0.01	0.02	0.02	0.02	0.02	0.02
Al	6.02	5.90	6.19	5.74	6.31	5.82	5.55	4.62	5.95	6.34	5.91
Fe^{+2}	0.11	0.10	0.10	0.10	0.11	0.10	0.12	0.07	0.14	0.45	0.15
Mn	0.00	0.01	0.01	0.00	0.00	0.00	0.00	0.00	0.00	0.00	0.00
Mg	0.06	0.04	0.05	0.03	0.04	0.00	0.03	0.00	0.02	0.03	0.02
Ca	2.12	2.07	2.34	1.92	2.44	1.96	1.66	0.58	1.99	2.41	2.02
Na	1.81	1.87	1.57	1.92	1.52	1.85	2.19	2.67	1.92	1.51	1.92
K	0.11	0.12	0.09	0.13	0.09	0.14	0.18	0.70	0.08	0.06	0.09
P	0.00	0.00	0.00	0.00	0.00	0.00	0.00	0.00	0.00	0.00	0.00
Cr	0.00	0.00	0.00	0.09	0.00	0.00	0.01	0.00	0.00	0.00	0.01
Ni	0.00	0.00	0.02	0.01	0.00	0.01	0.01	0.00	0.00	0.00	0.01
Total	19.99	19.99	20.00	19.99	19.99	19.99	20.03	19.99	20.00	19.99	19.99
An	52.00	50.08	57.37	46.86	59.61	48.24	44.73	14.68	49.50	60.09	49.63
Ab	44.21	45.26	38.41	46.76	37.15	45.48	51.23	67.59	47.62	37.54	47.09
Or	2.82	2.89	2.15	3.22	2.14	3.54	3.40	17.73	1.98	1.39	2.24

FeO* is total iron as FeO.

Table 4.49. Representative analyses of clinopyroxenes in the mugearites.

Sample	MA-47 Micro	MA-47 Micro	MA-53 Micro	MA-53 Pheno	MA-53 Incl. in plag.	MA-54 Pheno core	MA-54 Pheno rim	MA-54 Pheno core	MA-54 Pheno rim
SiO_2	47.87	48.47	48.74	49.54	49.24	43.68	43.13	47.17	43.54
TiO_2	3.10	2.47	1.92	1.25	2.54	2.26	2.40	1.53	1.87
Al_2O_3	4.61	3.82	2.81	2.97	3.23	8.35	9.20	5.88	7.09
FeO*	11.56	11.40	11.30	9.95	14.11	12.97	14.44	11.93	18.90
MnO	0.29	0.26	0.32	0.28	0.35	0.21	0.23	0.30	0.47
MgO	12.15	12.73	12.88	14.50	12.03	8.34	7.33	10.16	5.12
CaO	21.23	21.23	19.60	19.35	19.65	21.13	21.40	21.15	20.37
Na_2O	0.70	0.83	0.65	0.63	0.49	1.22	1.25	1.29	1.65
K_2O	0.00	0.05	0.05	0.01	0.00	0.00	0.01	0.06	0.04
P_2O_5	0.00	0.12	0.00	0.00	0.04	0.00	0.05	0.04	0.07
Cr_2O_3	0.00	0.00	0.09	0.14	0.11	0.00	0.00	0.03	0.00
NiO	0.00	0.00	0.10	0.01	0.08	0.00	0.03	0.01	0.13
Total	101.51	101.38	98.46	98.63	101.87	98.16	99.47	99.55	99.25
Formula on the basis of 6 oxygens									
Si	1.78	1.81	1.86	1.86	1.84	1.69	1.65	1.78	1.70
Ti	0.09	0.07	0.06	0.04	0.07	0.07	0.07	0.04	0.05
Al	0.20	0.17	0.13	0.13	0.14	0.38	0.42	0.26	0.33
Fe^{+3}	0.12	0.12	0.09	0.11	0.07	0.21	0.23	0.18	0.28
Fe^{+2}	0.23	0.23	0.27	0.20	0.37	0.21	0.23	0.20	0.34
Mn	0.01	0.01	0.01	0.01	0.01	0.01	0.01	0.01	0.02
Mg	0.67	0.70	0.73	0.81	0.67	0.48	0.42	0.57	0.30
Ca	0.84	0.83	0.80	0.78	0.79	0.87	0.88	0.86	0.85
Na	0.05	0.06	0.05	0.05	0.04	0.09	0.09	0.09	0.12
K	0.00	0.00	0.00	0.00	0.00	0.00	0.00	0.00	0.00
P	0.00	0.00	0.00	0.00	0.00	0.00	0.00	0.00	0.00
Cr	0.00	0.00	0.00	0.01	0.00	0.00	0.00	0.00	0.00
Ni	0.00	0.00	0.00	0.00	0.00	0.00	0.00	0.00	0.00
Total	4.00	4.00	4.00	4.00	4.00	4.00	4.00	4.00	4.00
$Mg^{\#}$	0.66	0.67	0.67	0.72	0.60	0.53	0.51	0.60	0.33
Wo	44.81	44.19	42.07	40.73	41.22	49.12	49.71	47.18	47.80
En	35.67	36.86	38.45	42.45	35.10	26.96	23.68	31.52	16.71
Fs	19.52	18.50	19.48	16.82	23.68	23.92	26.61	21.30	35.49

Fe^{+3} is calculated by normalization according to Schumacher(1991).
$Mg^{\#}=Mg/(Mg+Fe^{+3}+Fe^{+2})$

Table 4.50. Representative analyses of Fe-Ti oxides in the mugearites.

Sample No	MA-53 Inclusion in cpx.	MA-47 Magnetite	MA-47 Magnetite	MA-47 Magnetite	MA-54 Magnetite	MA-54 Magnetite
SiO_2	0.33	0.27	0.28	0.34	7.94	3.37
TiO_2	22.32	27.15	29.40	22.54	24.64	24.99
Al_2O_3	2.75	1.39	0.73	0.55	2.87	1.51
FeO*	70.86	66.47	65.98	70.52	54.48	60.52
MnO	0.41	1.04	0.98	0.91	0.06	0.46
MgO	2.49	2.73	1.33	2.01	0.20	0.24
CaO	0.19	0.05	0.13	0.05	0.97	0.43
Na_2O	0.31	0.17	0.28	0.37	0.42	0.15
K_2O	0.01	0.00	0.00	0.03	0.13	0.07
P_2O_5	0.00	0.00	0.00	0.00	0.07	0.00
Cr_2O_3	0.33	0.13	0.08	0.15	0.07	0.00
NiO	0.05	0.00	0.05	0.12	0.05	0.05
Total	100.05	99.40	99.24	97.59	91.92	91.79
Formula on the basis of 32 oxygens						
Si	0.01	0.01	0.01	0.01	0.31	0.13
Ti	0.59	0.73	0.81	0.62	0.71	0.72
Al	0.11	0.06	0.03	0.02	0.13	0.07
Fe^{+3}	0.69	0.46	0.35	0.73	0.00	0.24
Fe^{+2}	1.41	1.54	1.67	1.44	1.75	1.77
Mn	0.01	0.03	0.03	0.03	0.01	0.02
Mg	0.13	0.15	0.07	0.11	0.01	0.01
Ca	0.01	0.00	0.01	0.00	0.04	0.02
Na	0.02	0.01	0.02	0.03	0.03	0.01
K	0.00	0.00	0.00	0.00	0.01	0.00
P	0.00	0.00	0.00	0.00	0.00	0.00
Cr	0.01	0.00	0.00	0.01	0.00	0.00
Ni	0.00	0.00	0.00	0.00	0.00	0.00
Total	3.00	3.00	3.00	3.00	3.00	3.00
Mn/Mg	0.08	0.20	0.04	0.27	1.00	2.00
sp	8.17	4.69	2.65	1.68	2.65	2.80
mg-chr	0.65	0.286	0.19	0.29	0.00	0.00
mg-fer	9.87	18.34	9.30	13.95	0.00	0.00
trev	0.19	0.00	0.23	0.49	0.00	0.28
herc	0.00	0.00	0.00	0.00	12.75	4.10
chr	0.00	0.00	0.00	0.00	0.24	0.00
mt	38.84	18.23	19.72	38.47	0.00	23.10
usp	42.28	58.46	67.91	45.12	84.36	69.72

Fe^{+3} is calculated by normalization according to Schumacher(1991).

4.8.5. BENMOREITE

4.8.5.1. PETROGRAPHY

The benmoreites are generally altered rocks. They are holocrystalline to hypocrystalline varieties with intergranular or pilotaxitic groundmass, and porphyritic textured containing about 10-30% mega- and phenocrysts. Megacrysts of plagioclase are about 10%. Phenocrysts include plagioclase, anorthoclase, some olivine, clinopyroxene, a few orthopyroxenes and amphiboles. Microphenocrysts(<0.2mm) are variably present and contain plagioclase, equant titanomagnetite, ilmenite(as isolated grains and exolution lamellae in magnetite) and red-brown iddingsite interpreted as pseudomorphs after olivine. The mode of minerals is plagioclase(65-70%), anorthoclase(5%), opaque oxides(7-10%), olivine(3-5%), cpx(5-7%), opx(<3%), and amphibole(<1%). These pheno- and microphenocrysts are set in a seriate-textured groundmass, and sometimes occur in a matrix of small, slightly aligned plagioclase laths and small grains of clinopyroxene. The groundmass composition is similar to the microphenocryst assemblage. In addition, opaque iron-oxides and accessory apatite are present.

Plagioclase phenocrysts form generally subhedral laths, sometimes in aggregates with glomeraphyric texture. They show carlsbad-albite twining, normal and oscillatory zoning. They may have internal cracks filled by brownish-red alteration products, and contain inclusions of olivine(iddingsite) and granules of opaques.

Anorthoclase phenocrysts are commonly subhedral showing carlsbad, albite, and cross-hatched twinning. They also form aggregates with plagioclase. Some of the microphenocrysts exhibit corroded textures and, or reaction rims which are enclosed by fine-grained opaques. In addition, some of phenocrysts have thin overgrowths of plagioclase, representing a disequilibrium with the melt.

Olivine pheno- and micropheno-crysts are subhedral with rare sector zoning(MA-6C), common alteration to iddingsite or rarely chlorophaeite but some cores are usually preserved from alteration. Pyroxene microphenocrysts are subhedral and mostly clinopyroxene with rare orthopyroxene. Amphibole phenocrysts form euhedral to subhedral, with a characteristic thin opaque rim. Simple twinning and apatite inclusions are common.

The groundmass is mainly plagioclase and anorthoclase in a trachytic texture.

4.8.5.2. MINERAL CHEMISTRY

4.8.5.2.1. OLIVINE

The phenocrysts and microphenocrysts of olivine are Fo_{54} to Fo_{51}, or rarely Fo_{47}. The groundmass has homogeneous iron-richer olivines Fo_{54} and Fo_{35}(Figure 4.45; Table 4.51) which are generally replaced by iddingsite. Generally, olivines have MnO contents varying from 0.8% to 1wt.%.

4.8.5.2.2. FELDSPAR

The feldspars vary from abundant An_{46-27} plagioclase to sparse $An_{21}Ab_{64}Or_{15}$ anorthoclase(Figure 4.61; Table 4.52).

Megacrysts are generally An_{35} up to An_{46}; some show normal zoning from An_{39} to An_{36}. Phenocrysts and microphenocrysts are commonly An_{30} to An_{33} while microlites in the groundmass are commonly An_{27-30} and rarely An_{30-33}. In addition, anorthoclase laths with $An_{21}Ab_{64}Or_{15}$ are present.

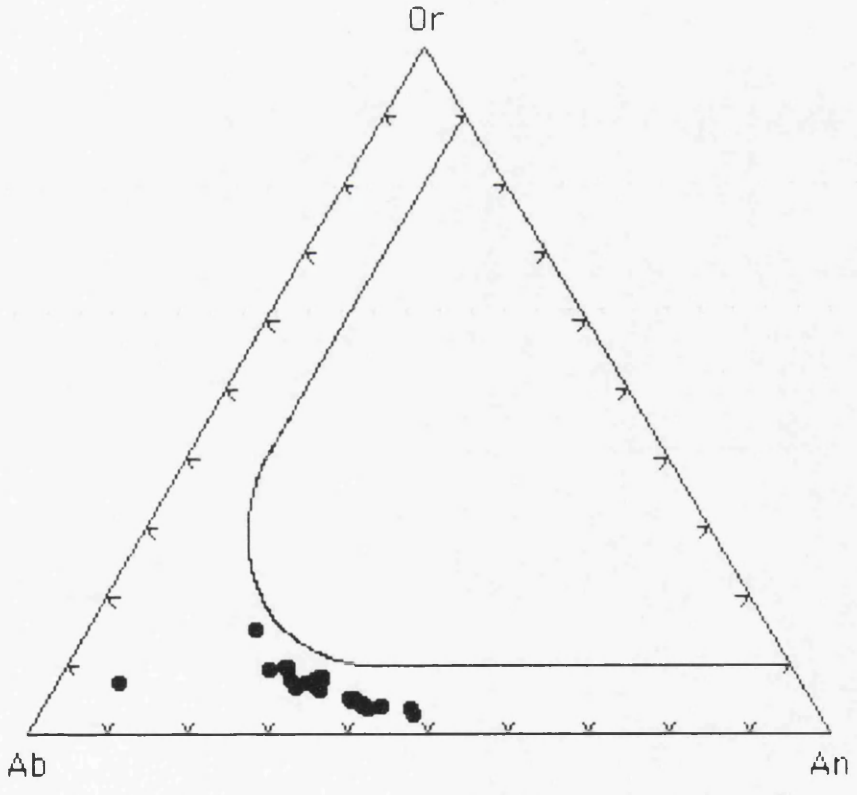

Figure 4.61. Ternary Or-Ab-An diagram of feldspars in benmoreites.

4.8.5.2.3. CLINOPYROXENE

The clinopyroxene is augite(Figure 4.62; Table 4.53), according to Morimoto *et al.* (1988).

Phenocrysts and microphenocrysts of augite have a composition between $Wo_{38}En_{39}Fs_{23}$ and $Wo_{41}En_{40}Fs_{19}$, and $Mg/(Mg+Fe^{+3}+Fe^{+2})$ ratio between 0.64 and 0.69. Groundmass augites have similar compositions to

those of the phenocrysts, with $Wo_{39}En_{39}Fs_{22}$. Generally, augites have TiO_2 between 0.9% and 1.2 wt.%, Al_2O_3 between 1.5% and 2.9 wt.%, MnO 0.4-0.5 wt.% and Na_2O varying from 0.3 up to 1wt.%. Some phenocrysts display slight compositional changes from core($Wo_{39}En_{39}Fs_{22}$) to rim($Wo_{40}En_{40}Fs_{20}$). The core is rich in Al_2O_3 and TiO_2, and poor in MgO whereas the rim is relatively rich in MgO, poor in TiO_2 and Al_2O_3(Table 4.53). In all augite compositions, Cr_2O_3 and NiO are quite low or insignificant. On the plots of Ti versus Si and Al in the formula units, it is significant that there is an excess of Al for both Si and Ti contents(Figure 4.63).

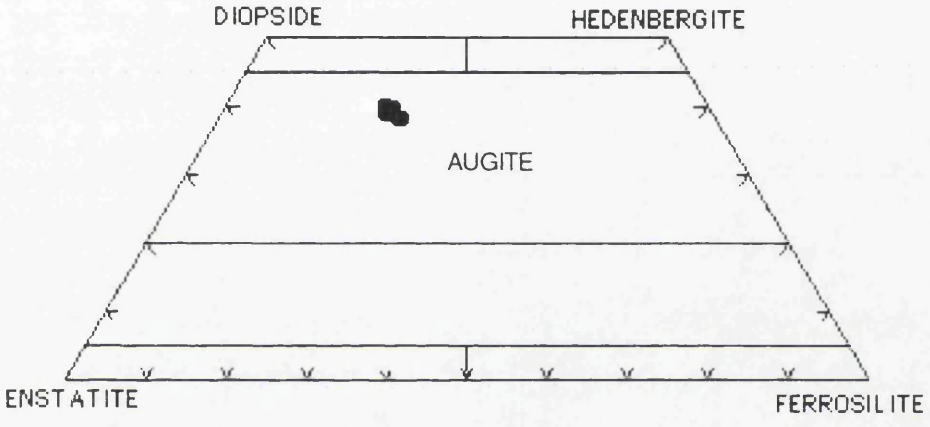

Figure 4.62. Pyroxene nomenclature of benmoreites on the Wo-En-Fs ternary plot(Morimoto *et al.*, 1988).

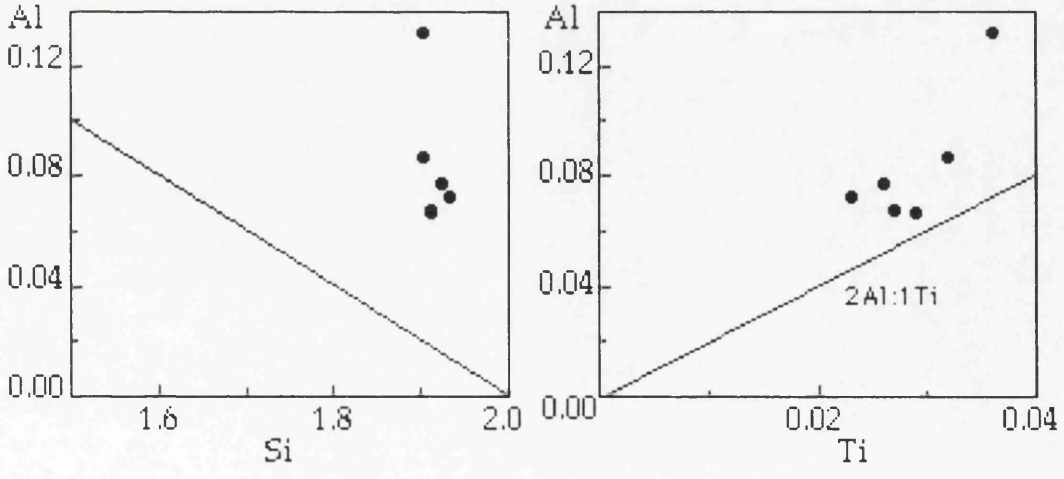

Figure 4.63. Plots of total Al versus Si and Ti contents in the formula units for clinopyroxenes of benmoreites.

4.8.5.2.4. FE-TI OXIDES

The oxide minerals are mainly homogeneous magnetite and rare ilmenite(Figure 4.64; Table 4.54).

Magnetites are typically Ti-rich (TiO_2 23% to 25 wt.%). They are also rich in MgO(1.6-3.2 wt.%) and Al_2O_3(1.7-2.6 wt.%), indicating a compositional transition towards ulvospinels. Qualitative analyses show a significant V content. Ilmenites have MgO up to 3 wt.%, and MnO varying between 0.5 and 0.7 wt.%.

The distribution of Mn and Mg between Ti-rich magnetite and ilmenite grains may indicate equilibrium between these phases(Bacon and Hirschmann, 1988). On the basis of oxide thermometry(Anderson and Lindsley, 1985), the magnetite-ilmenite geothermometer provides a temperature between 890 and 1017°C, and fO_2 between -0.96 and -1.01 relative to QFM buffer.

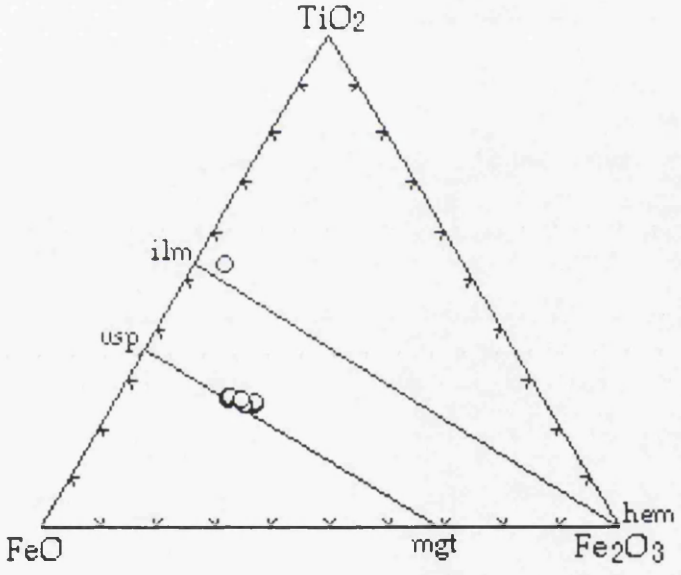

Figure 4.64. Compositions of iron-titanium oxide minerals in the benmoreites.

Table 4.51. Representative analyses of olivines in the benmoreites.

Sample	MA-35 Microph. core	MA-35 Ground-mass	MA-35 Iddingsite	MA-35 Pheno core	MA-35 Ground-mass	MA-35 Pheno Iddingsit	MA-35 Inclusion in plag.	MA-35 Microph. core
SiO_2	34.73	34.26	33.92	35.15	34.51	32.53	33.57	34.95
TiO_2	0.03	0.06	0.02	0.02	0.07	0.14	0.63	0.11
Al_2O_3	0.06	0.08	0.14	0.02	0.03	0.23	0.32	0.01
FeO*	40.42	43.57	39.56	38.67	40.80	40.76	39.74	38.50
MnO	0.97	1.03	0.94	0.85	0.99	0.84	0.66	0.89
MgO	24.21	21.49	21.67	25.70	23.73	20.58	19.47	25.93
CaO	0.35	0.37	0.26	0.29	0.37	0.47	0.52	0.32
Na_2O	0.19	0.28	0.27	0.32	0.20	0.50	0.38	0.49
K_2O	0.08	0.02	0.00	0.05	0.03	0.05	0.08	0.00
P_2O_5	0.16	0.00	0.16	0.00	0.09	0.11	0.13	0.00
Cr_2O_3	0.02	0.00	0.01	0.00	0.00	0.03	0.01	0.00
NiO	0.00	0.00	0.00	0.00	0.06	0.00	0.00	0.00
Total	101.22	101.16	96.95	101.07	100.88	96.24	95.51	101.20
Formula on the basis of 4 oxygens								
Si	0.98	0.99	1.00	0.99	0.98	0.98	0.99	0.98
Ti	0.00	0.00	0.00	0.00	0.00	0.00	0.01	0.00
Al	0.00	0.00	0.01	0.00	0.00	0.01	0.01	0.00
Fe^{+2}	0.98	1.05	0.98	0.91	0.97	1.03	1.01	0.90
Mn	0.02	0.03	0.02	0.02	0.02	0.02	0.02	0.02
Mg	1.02	0.92	0.96	1.07	1.01	0.92	0.88	1.09
Ca	0.01	0.01	0.01	0.01	0.01	0.02	0.02	0.01
Na	0.01	0.02	0.02	0.02	0.01	0.03	0.02	0.03
K	0.00	0.00	0.00	0.00	0.00	0.00	0.00	0.00
P	0.00	0.00	0.00	0.00	0.00	0.01	0.02	0.00
Cr	0.00	0.00	0.00	0.00	0.00	0.00	0.00	0.00
Ni	0.00	0.00	0.00	0.00	0.00	0.00	0.00	0.00
Total	3.02	3.02	3.00	3.02	3.01	3.02	2.98	3.03
$Mg^{\#}$	0.51	0.46	0.49	0.54	0.51	0.48	0.46	0.55
Fo	51.05	46.20	48.80	53.67	50.30	46.85	46.20	53.98
Fa	48.95	53.80	51.20	46.33	49.70	53.15	53.80	46.02

FeO* is total iron as FeO.
$Mg^{\#}=Mg/(Mg+Fe^{+2})$

Table 4.52. Representative analyses of feldspars in the benmoreites.

Sample	MA-35 Micro-lite	MA-35 Mega-core	MA-35 Mega-core	MA-35 Micro-lite	MA-35 Mega	MA-35 Micro-pheno	MA-35 Mega	MA-35 Micro-lite	MA-35 Micro-lite
SiO_2	59.48	58.18	57.48	60.69	58.11	59.48	57.36	59.14	61.15
TiO_2	0.09	0.21	0.09	0.19	0.13	0.19	0.20	0.11	0.24
Al_2O_3	23.88	25.16	26.19	23.86	25.64	24.86	27.40	24.47	22.84
FeO*	0.80	0.42	0.50	0.56	0.47	0.62	0.44	0.73	1.13
MnO	0.00	0.05	0.00	0.00	0.00	0.00	0.01	0.00	0.08
MgO	0.17	0.20	0.20	0.04	0.11	0.08	0.13	0.19	0.19
CaO	6.13	7.64	8.67	5.93	7.67	6.84	9.68	6.49	5.15
Na_2O	7.13	6.39	6.15	7.25	6.32	6.93	5.88	6.70	7.32
K_2O	1.20	0.86	0.70	1.40	0.89	1.12	0.66	1.17	1.67
P_2O_5	0.06	0.12	0.00	0.00	0.00	0.00	0.01	0.00	0.00
Cr_2O_3	0.09	0.00	0.01	0.00	0.00	0.08	0.00	0.01	0.01
NiO	0.00	0.06	0.00	0.00	0.00	0.00	0.05	0.04	0.00
Total	99.03	99.29	99.99	99.92	99.34	100.20	101.82	99.05	99.78
Formula on the basis of 32 oxygens									
Si	10.77	10.51	10.34	10.87	10.49	10.65	10.16	10.69	10.98
Ti	0.01	0.03	0.01	0.03	0.01	0.03	0.03	0.01	0.03
Al	5.09	5.36	5.55	5.04	5.46	5.25	5.72	5.22	4.83
Fe^{+2}	0.12	0.06	0.08	0.08	0.007	0.09	0.06	0.11	0.17
Mn	0.00	0.08	0.00	0.00	0.00	0.00	0.00	0.00	0.01
Mg	0.04	0.05	0.05	0.01	0.03	0.02	0.03	0.05	0.05
Ca	1.19	1.48	1.67	1.14	1.48	1.31	1.84	1.26	0.99
Na	2.50	2.24	2.15	2.52	2.21	2.41	2.02	2.35	2.55
K	0.28	0.20	0.16	0.32	0.20	0.25	0.15	0.27	0.38
P	0.00	0.02	0.00	0.00	0.00	0.01	0.00	0.00	0.00
Cr	0.01	0.00	0.00	0.00	0.00	0.00	0.00	0.00	0.00
Ni	0.00	0.01	0.00	0.00	0.00	0.00	0.01	0.00	0.00
Total	20.01	20.04	20.01	20.01	19.95	19.99	20.02	19.96	19.99
An	29.97	37.76	41.96	28.64	38.05	32.99	45.89	32.47	25.26
Ab	62.97	57.14	54.02	63.32	56.81	60.71	50.37	60.57	65.05
Or	7.06	5.10	4.02	8.04	5.14	6.30	3.74	6.96	9.69

FeO* is total iron as FeO.

Table 4.53. Representative analyses of clinopyroxenes in the benmoreites.

Sample No	MA-35	MA-35	MA-35	MA-35	MA-35	MA-35
	Pheno core	Pheno rim	Pheno	Groundmass	Pheno core	Micropheno
SiO_2	50.60	50.91	51.38	50.50	51.62	51.46
TiO_2	1.28	0.82	0.98	1.14	0.93	1.04
Al_2O_3	2.98	1.61	1.56	1.96	1.76	1.53
FeO*	12.63	12.03	12.22	13.09	11.96	11.75
MnO	0.44	0.45	0.40	0.55	0.50	0.37
MgO	12.72	13.51	14.16	13.48	14.02	14.12
CaO	17.51	18.96	19.24	18.54	19.45	19.85
Na_2O	1.12	0.40	0.57	0.47	0.31	0.56
K_2O	0.06	0.06	0.02	0.00	0.00	0.01
P_2O_5	0.05	0.09	0.07	0.08	0.04	0.04
Cr_2O_3	0.04	0.03	0.00	0.02	0.04	0.04
NiO	0.00	0.00	0.05	0.00	0.04	0.02
Total	99.43	98.87	100.65	99.83	100.67	100.79
Formula on the basis of 6 oxygens						
Si	1.90	1.93	1.91	1.90	1.92	1.91
Ti	0.04	0.02	0.03	0.03	0.03	0.03
Al	0.13	0.07	0.07	0.09	0.08	0.07
Fe^{+3}	0.07	0.03	0.09	0.06	0.03	0.09
Fe^{+2}	0.33	0.35	0.29	0.36	0.34	0.28
Mn	0.01	0.01	0.01	0.02	0.02	0.01
Mg	0.71	0.77	0.79	0.76	0.78	0.78
Ca	0.71	0.77	0.77	0.75	0.77	0.79
Na	0.08	0.03	0.04	0.03	0.02	0.04
K	0.01	0.00	0.00	0.00	0.00	0.00
P	0.00	0.00	0.00	0.01	0.00	0.00
Cr	0.00	0.00	0.00	0.00	0.00	0.00
Ni	0.00	0.00	0.00	0.00	0.00	0.00
Total	4.00	4.00	4.00	4.00	4.00	4.00
$Mg^{\#}$	0.64	0.67	0.68	0.64	0.69	0.68
Wo	38.57	39.92	39.44	38.68	39.95	40.55
En	38.95	39.56	40.36	39.10	40.06	40.12
Fs	22.48	20.52	20.15	22.22	19.99	19.33

Fe^{+3} is calculated by normalization according to Schumacher(1991).
$Mg^{\#} = Mg/(Mg+Fe^{+3}+Fe^{+2})$

Table 4.54. Representative analyses of Fe-Ti oxides in the benmoreites.

Sample	MA-35 Magnet. Mic.ph. core	MA-35 Magnet. Mic.ph. rim	MA-35 Magnet. Mic.ph	MA-35 Magnet. Mic.ph.	MA-35 Magnet. Pheno core	MA-35 Magnet Inclusi. in plag.	MA-35 Magnet. Inclusi. in cpx	MA-35 Magnet Pheno	MA-35 Ilm. Pheno
SiO_2	0.30	0.36	0.36	0.29	0.34	0.24	0.27	0.22	0.16
TiO_2	25.19	24.61	25.39	24.96	23.98	23.58	23.98	25.58	50.99
Al_2O_3	2.32	1.74	1.84	2.04	2.10	2.43	2.61	1.99	0.21
FeO*	68.69	66.66	69.27	67.24	68.52	65.96	68.81	69.48	44.16
MnO	0.72	0.71	0.83	0.84	0.74	0.67	0.70	0.82	0.80
MgO	2.65	1.81	2.06	2.07	2.55	3.25	2.78	2.28	3.04
CaO	0.00	0.04	0.05	0.08	0.05	0.00	0.05	0.02	0.03
Na_2O	0.34	0.00	0.41	0.05	0.55	0.34	0.02	0.37	0.03
K_2O	0.00	0.04	0.03	0.00	0.01	0.03	0.00	0.00	0.02
P_2O_5	0.08	0.00	0.00	0.09	0.03	0.00	0.05	0.00	0.00
Cr_2O_3	0.07	0.14	0.00	0.07	0.10	0.06	0.00	0.11	0.05
NiO	0.07	0.00	0.00	0.00	0.03	0.00	0.11	0.00	0.05
Total	100.43	96.11	100.24	97.73	99.00	96.56	99.38	100.87	99.49
Formula on the basis of 32 oxygens for magnetites and 6 oxygens for ilmenite									
Si	0.01	0.01	0.01	0.01	0.01	0.01	0.01	0.01	0.00
Ti	0.67	0.69	0.68	0.69	0.65	0.65	0.65	0.68	0.95
Al	0.10	0.08	0.08	0.09	0.09	0.10	0.11	0.08	0.01
Fe^{+3}	0.56	0.51	0.57	0.51	0.63	0.61	0.58	0.56	0.10
Fe^{+2}	1.48	1.58	1.50	1.57	1.42	1.41	1.48	1.49	0.82
Mn	0.02	0.02	0.02	0.03	0.02	0.02	0.02	0.02	0.02
Mg	0.14	0.10	0.11	0.11	0.14	0.18	0.15	0.12	0.11
Ca	0.00	0.00	0.00	0.00	0.00	0.00	0.00	0.00	0.00
Na	0.02	0.00	0.03	0.00	0.04	0.02	0.00	0.02	0.00
K	0.00	0.00	0.00	0.00	0.00	0.00	0.00	0.00	0.00
P	0.00	0.00	0.00	0.00	0.00	0.00	0.00	0.00	0.00
Cr	0.00	0.00	0.00	0.00	0.00	0.00	0.00	0.00	0.00
Ni	0.00	0.00	0.00	0.00	0.00	0.00	0.00	0.00	0.00
Total	3.00	3.00	3.00	3.00	3.00	3.00	3.00	3.00	2.00
Mn/Mg	0.14	0.20	0.18	0.27	0.14	0.11	0.13	0.17	0.14
sp	7.29	5.99	5.85	6.85	6.50	7.69	8.26	6.23	
mg-chr	0.16	0.31	0.00	0.16	0.20	0.12	0.00	0.23	
mg-fer	13.68	9.47	10.65	10.58	13.18	18.17	14.00	11.61	
trev	0.28	0.00	0.00	0.00	0.14	0.00	0.48	0.00	
mt	28.00	30.21	32.14	28.83	32.71	26.44	28.84	30.73	
usp	50.60	54.02	51.36	53.57	47.27	47.58	48.42	51.19	

Fe^{+3} is calculated by normalization according to Schumacher(1991).

4.8.6. TRACHYTE

4.8.6.1. PETROGRAPHY

Trachytes appear to be a homogeneous group, apart from variations in the presence of the phenocryst and microphenocryst minerals. They are holo- to slightly hypo-crystalline and porphyritic with 10-15 % of phenocrysts and a matrix texture varying from hypidiomorphic granular to pilotaxitic and trachytic. Phenocrysts include plagioclase, anorthoclase, amphibole, occasionally sanidine and clinopyroxene. The microphenocryst assemblage contains plagioclase, sanidine, augite, orthopyroxene, opaque oxides, altered amphibole and accessory apatite. There are also some microphenocrysts of resorbed and altered olivine(iddingsite). The groundmass is crystalline with a fluidal, trachytic texture comprised of sanidine, plagioclase laths, and opaque oxides. The modal composition of the rock is plagioclase(50-60%), anorthoclase(-5-10%), sanidine(3-5%), amphibole(5-7%), clinopyroxene(<5%), opaque oxides(3-5%), orthopyroxene (<3%), and olivine(1%).

Plagioclase pheno- and micropheno-crysts are subhedral, and show discontinuous, oscillatory or convolute zoning, and multiple twinning. They also form aggregates of fragmented crystals, and embayed crystals. They contain abundant inclusions of apatite needles and groundmass minerals. Some of the embayed or fragmented phenocrysts contain microlites of late stage crystallization within internal spaces. Plagioclase with sponge-like texture is also present.

Anorthoclase with fine lamellae or tartan twinning is common as subhedral phenocrysts, and has distinctive cores sieved with resorption hollows. They also have corroded rims, thin overgrowth rims and embayed cores. These cores contain abundant inclusions of the microphenocryst minerals, as well as apatite needles.

Brown to dark coloured amphiboles are common in the phenocryst phase. These amphiboles are generally subhedral and sometimes resorbed crystals. The amphiboles commonly have an iron-rich(partially opaque) rim varying in thickness, and are sometimes altered to a brownish semi-opaque material. They may show simple twinning and contain inclusions of apatite and feldspar. In some cases amphiboles which form aggregates with anorthoclase microphenocrysts do not have opaque rims at the contacts with anorthoclase. This implies that the opaque rims developed during a late magmatic event, probably after crystallisation of the rock.

Microphenocrysts of olivine are observed as iddingsite in reddish brown subhedral or euhedral crystals, sometimes with the original core preserved from alteration.

Phenocrysts and microphenocrysts of plagioclase, clinopyroxene, orthopyroxene and amphibole are set in a matrix of feldspar(varying from oligoclase An_{20} to anorthoclase), tiny clinopyroxene grains, magnetite and ilmenite, and occasional glass.

Groundmass is a mixture of sanidine, anorthoclase and plagioclase, rare opx and cpx. Alkali feldspars ,mainly sanidine are dominant. They exhibit an alignment together with plagioclase laths. The alignment indicates the movement of the crystal-liquid mush before final crystallization. Granules or prismatic crystals of opx and cpx are surrounded by feldspar laths. Generally, fine opaque granules accompany this texture.

In some vesicular types, secondary minerals like calcite occur in vesicles. In addition, some xenocrysts of quartz are observed.

4.8.6.2. MINERAL CHEMISTRY

4.8.6.2.1. OLIVINE

Olivines in the trachytes are largely altered to iddingsite with original compositions ranging from Fo_{59} to Fo_{41}(Figure 4.45). They are generally homogeneous and representative analyses are given in Table 4.55.

Olivine microphenocrysts are Fo_{59} to Fo_{56}. However, olivines in the groundmass are relatively Fe-rich with Fo_{48-41}. Generally, olivines have a high MnO content(about 1wt.%) which is relatively high, compared to other rock types of the association. Trace element(e.g., NiO and Cr_2O_3) contents are very low or insignificant.

4.8.6.2.2. FELDSPAR

The feldspars of the trachytes vary from andesine-oligoclase to anorthoclase and sanidine(Figure 4.65). Representative analyses are given in Table 4.56. When plotted on a feldspar diagram, the alkali feldspars tend to concentrate below the thermal minimum of Tuttle and Bowen(1958) at about Or_{37}(Figure 4.65).

Megacrysts are commonly andesine with a composition varying from An_{30} up to An_{43}. They show both reverse and normal zoning. The reversely zoned crystals have a composition An_{35-36} in the core varying to An_{39-40} in the rim, or An_{38} in the core varying to An_{42}. The normally zoned crystals show a compositional change from An_{43-41} in the core to An_{37-30} in the rim, or An_{33} in the core varying to An_{18}. Some megacrysts show oscillatory zoning patterns with sharp compositional changes. The An% changes are always smaller than 10% as is seen on zoning profiles from core to rim(Figure 4.66). The oscillatory zoning profiles reveal that the zoning may have been caused by combinations of magma mixing and disequilibrium crystallisation, as described by Stamatelopoulou-Seymour *et al.* (1990).

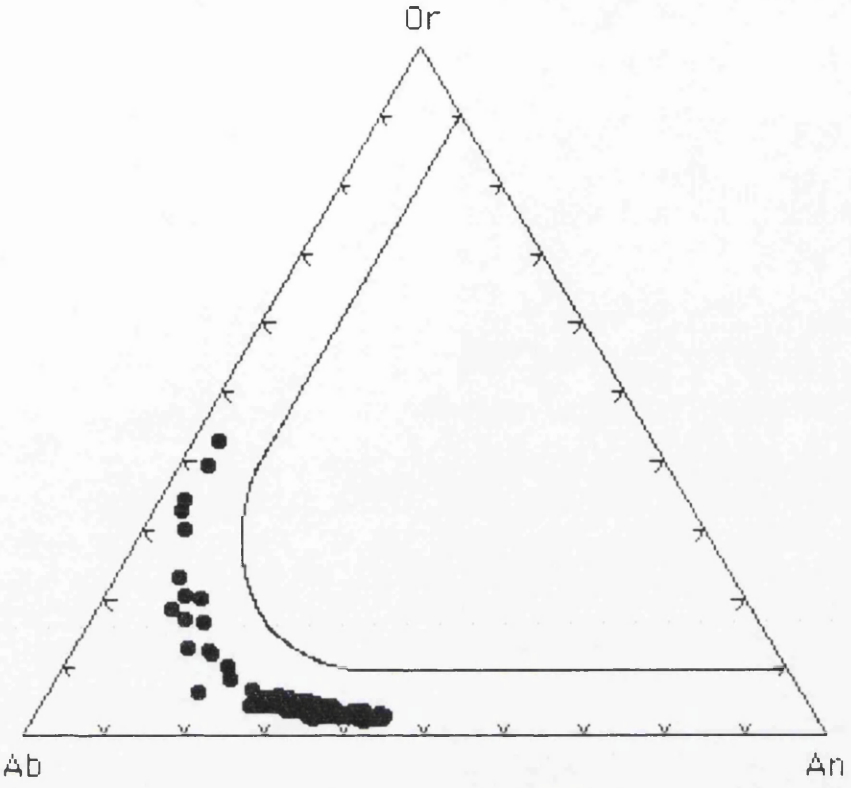

Figure 4.65. Or-Ab-An ternary diagram of feldspars in the trachytes.

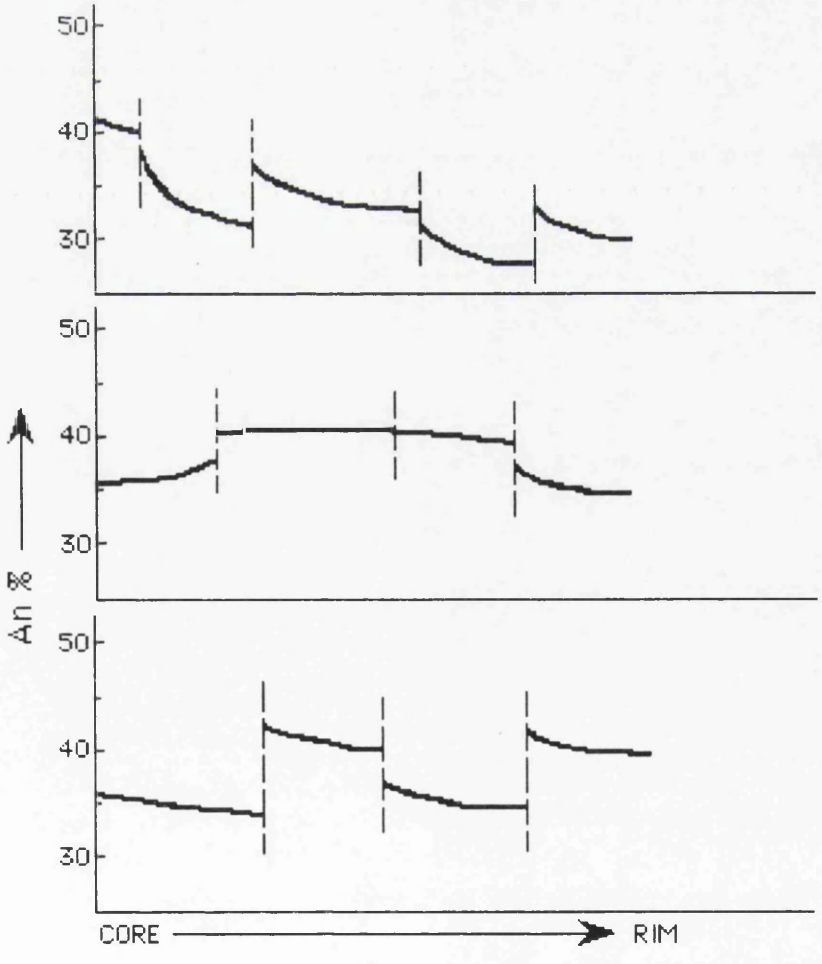

Figure 4.66. Schematic illustration of oscillatory zoning profiles for plagioclase megacrysts in the trachytes.

Phenocrysts and microphenocrysts of feldspar are generally oligoclase(An_{12-29}) and some andesine(An_{30-43}). Andesine phenocrysts show normal zoning with An_{33-35} in the core varying to more sodic rim(An_{21-26}). Some of them may also show reverse zoning from An_{36} in the core to An_{42} in the rim. Oligoclase phenocrysts are unzoned but some of them may have more potassic rims with Or_{19} than the cores.

Microlites contain commonly anorthoclase with a composition ranging from $An_{11}Ab_{71}Or_{18}$ to $An_3Ab_{63}Or_{34}$, and sanidine($An_3Ab_{57-53}Or_{40-44}$). In addition, some oligoclase and sparse andesine laths are present.

4.8.6.2.3. PYROXENE

The trachytes contain two pyroxenes, augite and orthopyroxene(Figure 4.67), according to the classification of Morrimoto *et al.* (1988). Representative analyses are given in Table 4.57.

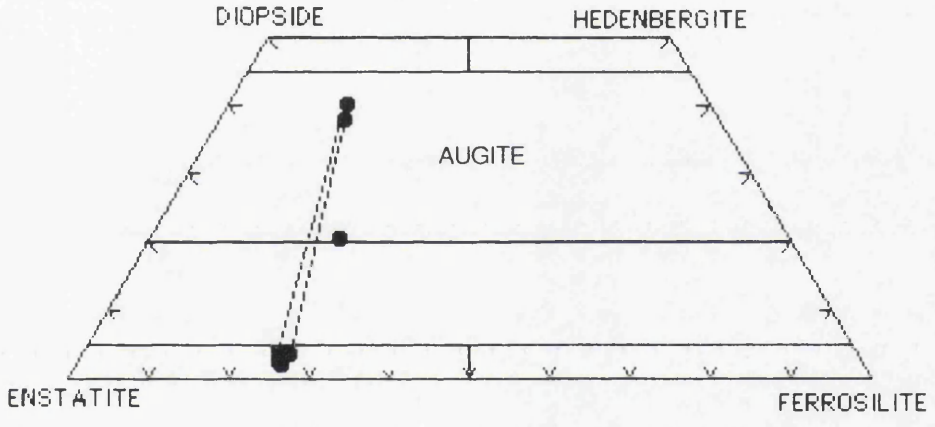

Figure 4.67. Pyroxene nomenclature of the trachytes(Morimoto *et al.*, 1988). Tie lines intersect Wo-En join at about Wo_{93-95}.

Augites have a composition of $Wo_{40-38}En_{46-47}Fs_{14-15}$, and $Mg/(Mg+Fe^{+3}+Fe^{+2})$ ratio 0.78-0.76. The augites are relatively low in Ti and Al, and high in Ca and Mg, compared to those of alkaline rocks(Kushiro, 1960; Le Bas, 1962). They have a TiO_2 between 0.72 and 0.62 wt.%, MnO 0.88 to 0.78 wt.%. Cr_2O_3 and NiO are very low or zero. In some rock samples, augites with low Ca content are present with a composition $Wo_{21}En_{56}Fs_{23}$ and a $Mg(Mg+Fe^{+3}+Fe^{+2})$ ratio 0.72. These augites have TiO_2(0.94 wt.%), MnO(0.75 wt.%) and high Na_2O content(3.8 wt.%) indicating the occurrence of aegirine molecule. Generally, Ti content of augites in the rock reveals a subalkaline host rock(Kushiro, 1960; Le Bas, 1962). Furthermore, Barberi *et al.* (1971) showed that the Al and Ti contents of clinopyroxene are a reflection of the crystallisation conditions so the crystallisation of plagioclase before pyroxene in the rock may result in Ti-poor pyroxenes containing small amounts of Al(Figure 4.68).

Orthopyroxenes with a composition $Wo_{4-2}En_{72-73}Fs_{24-25}$, and $Mg/(Mg+Fe^{+3}+Fe^{+2})$ ratio(0.75-0.77) occur commonly in the groundmass. They have TiO_2 0.25-0.46wt.%, relatively high MnO of 1.25-1.85wt.%. Cr_2O_3 and NiO are very low or zero. CaO varies from 1.14 to 2.08 wt.%. Ca is generally thought to be related to the temperature of crystallisation(Deer *et al.*, 1978). The orthopyroxene in the trachytes, which has a maximum Ca of 0.081 in the formula unit is consistent with about 1050°C and a pressure of 14 kbar(Boyd and England, 1965). Furthermore, the presence of orthopyroxene(not a stable low-pressure mineral in an alkali host magma; Green and Ringwood, 1967) suggests crystallisation of the trachyte at moderate pressure. This is also supported by the presence of kaersutite.

Generally, orthopyroxenes are enriched in Mg relative to augites and this relationship may indicate a disequilibrium conditions between two pyroxenes. Furthermore, the presence of subcalcic augite together with augite and orthopyroxene in the trachytes indicates a rather rapid rate of cooling. Orthopyroxene could occur as a result of alterations to the chemistry of the lavas by addition of a crustal component, causing the lavas to become subalkaline.

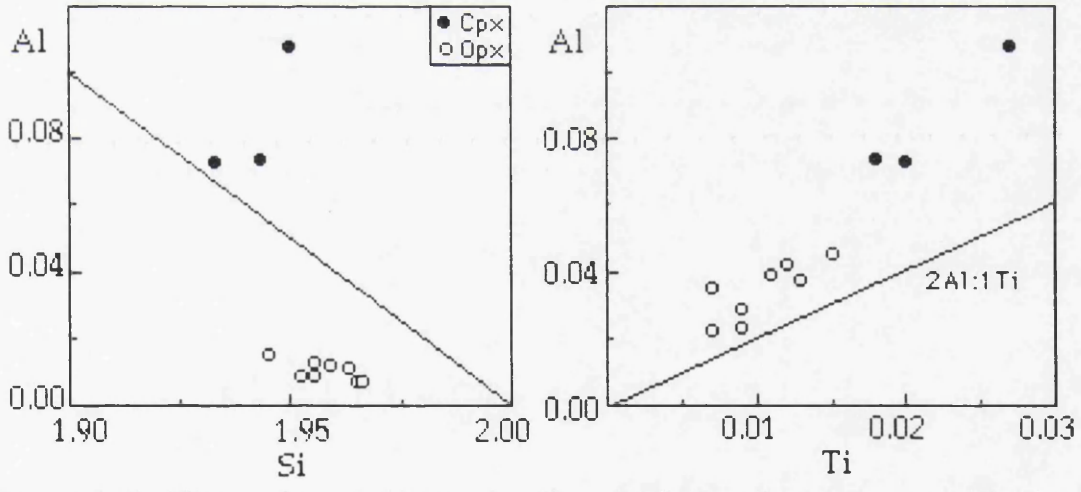

Figure 4.68. Plots of total Al versus Si and Ti for clinopyroxenes(Cpx) and orthopyroxenes(Opx) of the trachytes.

4.8.6.2.4. AMPHIBOLE

In the trachytes, calcic amphiboles occur(Table 4.58). They are dominantly kaersutite with Ti≥0.50 in the formula unit ranging down to Ti 0.47 in titanian magnesio-hastingsite(Figure 4.69), according to the classification of Leake(1978).

Kaersutites generally have small changes from core to rim for the major elements. TiO_2 and Al_2O_3 apparently decrease and MgO increases from core to rim. For Al, Ti ,Mg and Ca oxides the differences average about

0.65% with a maximum of 0.82 wt.% for TiO_2. Kaersutites have a TiO_2 content varying between 4.41 and 5.32 wt.%(0.50-0.58 per formula unit), $Mg/(Mg+Fe^{+2})$ ratio between 0.70 and 0.75, Al 1.79 to 1.93, Na 0.80 to 0.99, and Si varying from 6.07 to 6.22 per formula unit. TiO_2 in these kaersutites is at the lower end of the range of TiO_2(5-10 wt.%) in common kaersutites given by Deer *et al.* (1978).

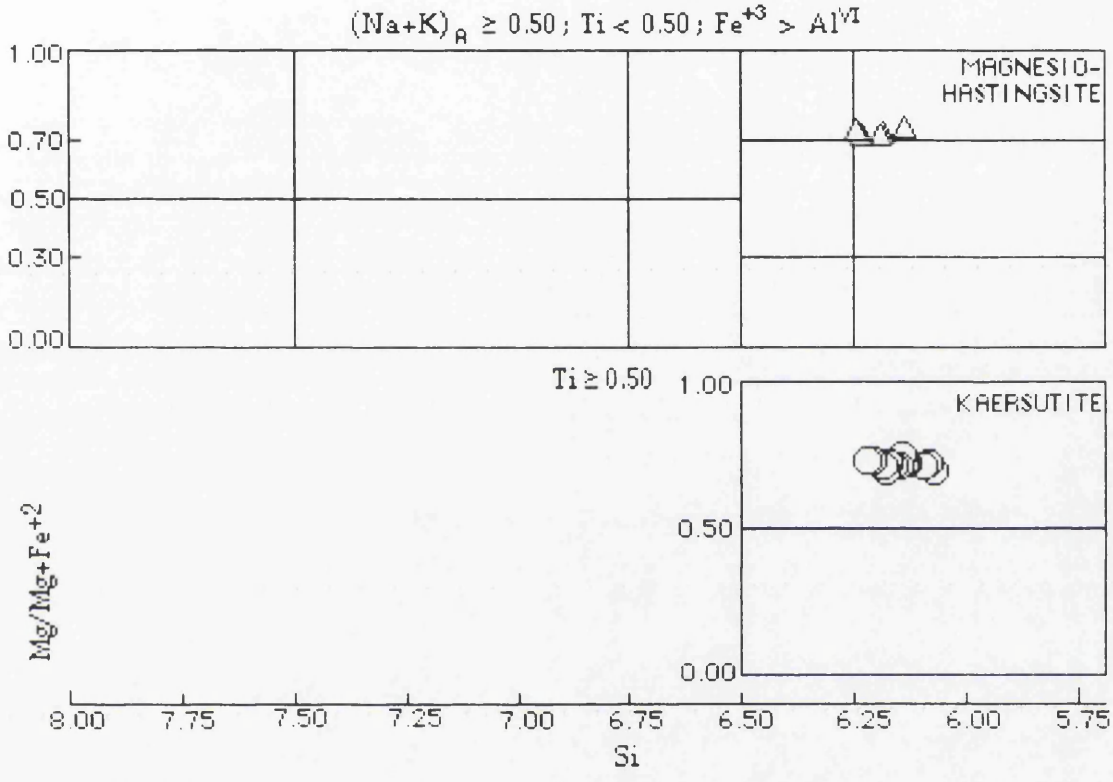

Figure 4.69. The classification and nomenclature of calcic amphiboles of the trachytes, according to Leake(1978).

Some of kaersutite phenocrysts exhibit slight compositional variations with decreasing Na and Fe/Mg from core to rim but very strong Fe/Mg enrichment in the opaque rims(Figure 4.70). These phenocrysts have a Fe/Mg of 0.47 in the core varying to 0.44 in the rim and 0.70-91 in the opaque rim(Figure 4.70). Opaque rims are resorbed in shape, indicating a reaction and resorption of kaersutite. O'Brien *et al.* (1988) described this type of resorption for clinopyroxene phenocrysts, caused by magma mixing. In addition, kaersutites are known as typical constituent of alkaline volcanic rocks. Kaersutite may represent crystallisation from magma at moderate depth e.g., 15-25 km(e.g., Green *et al.*, 1974; Irving, 1974).

Titanian magnesio-hastingsites have $Mg/(Mg+Fe^{+2})$ ratio ranging from 0.71 to 0.74. They have also a TiO_2 content varying from 0.47 to 0.49, Al content from 1.79 to 1.93, Na content from 0.85 to 0.93 per formula units(Figure 4.71). Si content ranges from 6.14 to 6.24 per formula units.

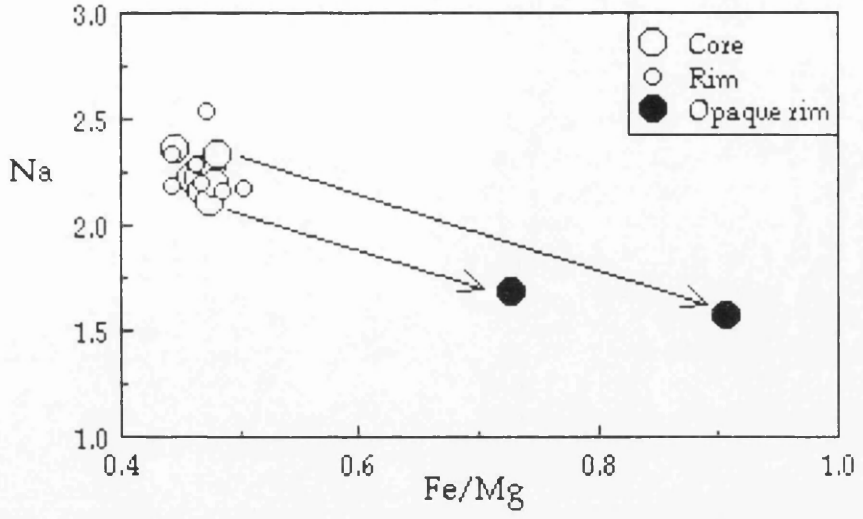

Figure 4.70. Amphibole analyses plotted in terms of Na content versus Fe/Mg ratios(Values are in per formula unit). The plot shows compositional variation from core to rim in the amphiboles of the trachytes.

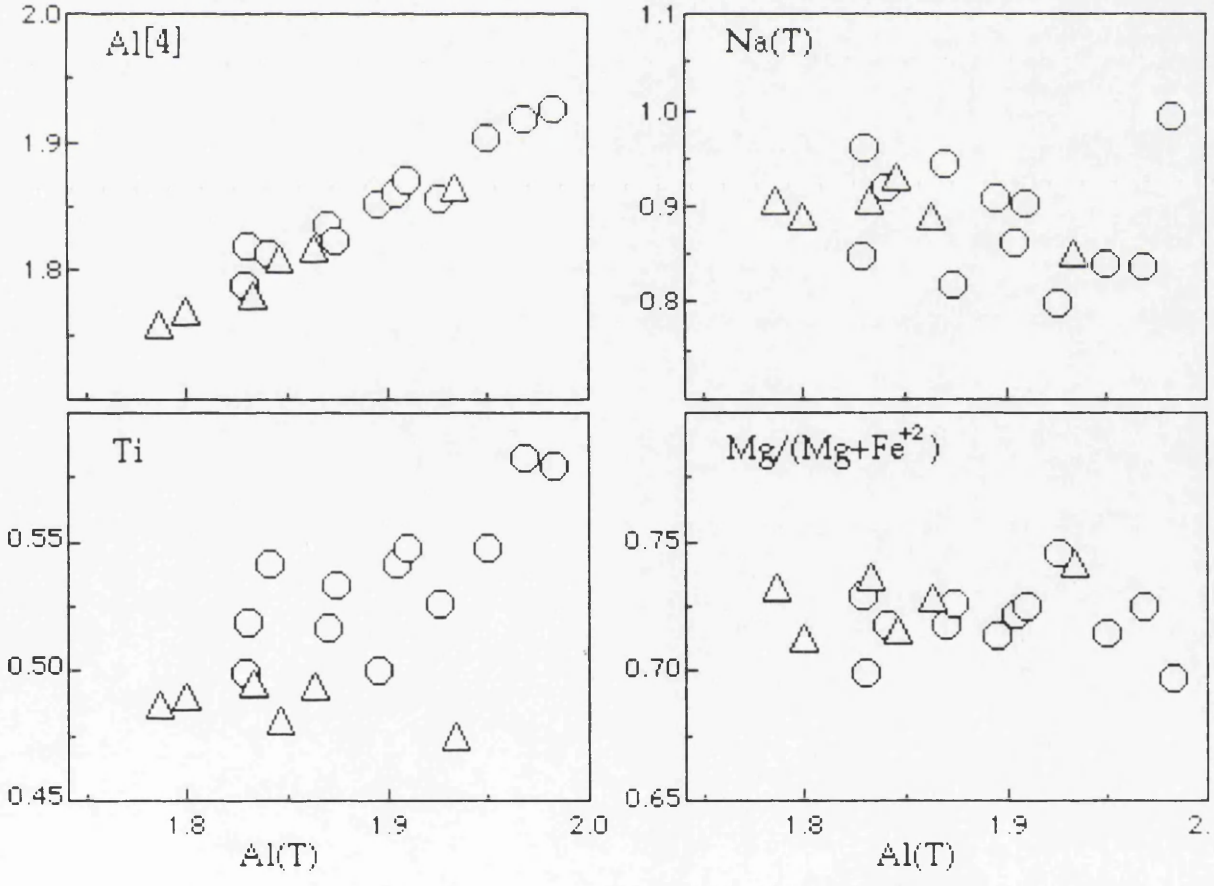

Figure 4.71. Plots of total Al(T) versus tetrahedral Al[4], Ti, Na and Mg/(Mg+Fe^{+2}) in the formula unit of amphiboles(○, kaersutite ; △, magnesio-hastingsite).

4.8.6.2.5. FE-TI OXIDES

In the trachytes, magnetite is the main oxide mineral, and some ilmenites are present(Figure 4.72; Table 4.59).

Magnetites are typically Ti-rich types with a TiO_2 content ranging from 5 to 16 wt.%. They have MgO(0.34-2.75 wt.%), MnO(0.48-1.68 wt.%) and Al_2O_3(0.55-2.67 wt.%). Generally, Ti-poor types have higher Al_2O_3 than Ti-rich types. With being enriched in Mg and Al, they show transition towards ulvospinel members(Usp9-30). Trace element contents in the magnetites are quite low, NiO(0-0.16 wt.%) and Cr_2O_3(0-0.12 wt.%). However, qualitative analyses indicate the presence of a significant amount of V in the composition.

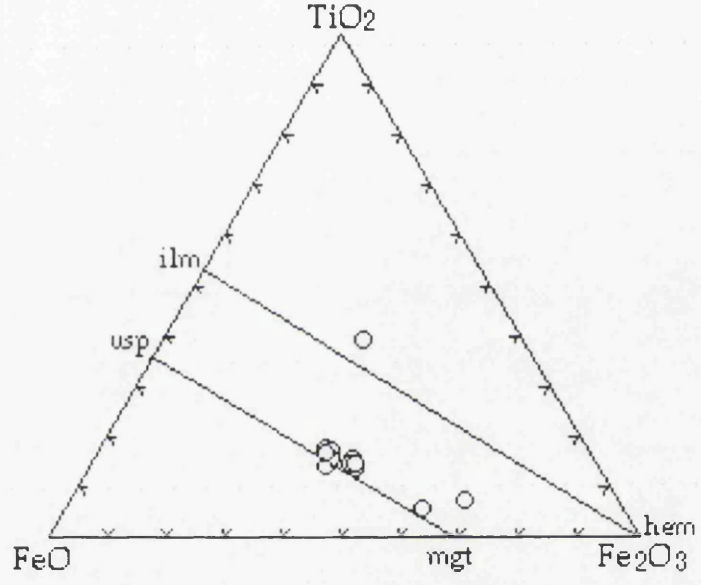

Figure 4.72. Compositions of iron-titanium oxide minerals in the trachytes.

As is usual ilmenites have relatively high MnO(3.78 wt.%), compared with magnetites. They have MgO and Al_2O_3 about 1.65 wt.%(Figure 4.73). The distribution of Mg and Mn between ilmenite and Ti-rich magnetite grains in the trachytes indicate an equilibrium between these phases so coexisting two oxide pairs can be used for geothermometry(Bacon and Hirschmann, 1988).

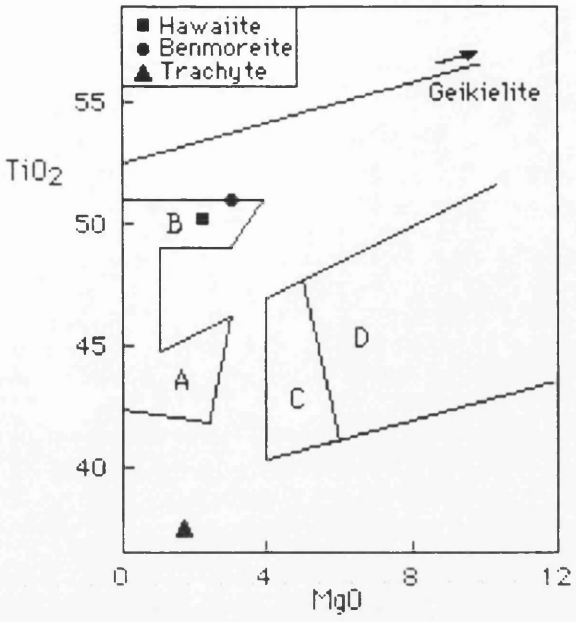

Figure 4.73. Plot of MgO versus TiO_2 for ilmenites in the Meydan alkaline association rocks. Typical fields of ilmenite compositions are from Haggerty(1976), A from felsic rocks; B from tholeiitic rocks; C from alkali basaltic rocks; D from kimberlites.

4.8.6.3. GEOTHERMOMETRY AND GEOBAROMETRY

Geothermometry and geobarometry calculations in the trachytes were made on the basis of two feldspar, two pyroxene and Fe-Ti oxide thermometers.

Feldspars of the trachytes is illustrated on a ternary plot(Figure 4.74), based on synthetic ternary feldspar compositions and thermodynamic data(Fuhrman and Lindsley, 1988). The plot indicates that sanidine is in equilibrium with anorthoclase and sodic plagioclase(oligoclase), and these feldspars reveal a solvi temperature about 825°C. However, more calcic plagioclase, mainly megacrysts, appear to be in disequilibrium with sanidine, which suggests a temperature below the solvus of 825°C(Figure 4.74). The disequilibrium in more calcic plagioclase is also confirmed with compositional oscillatory zoning.

Coexisting magnetite and ilmenite pairs were used as a geothermometer, following Anderson and Lindsley(1985). Fe-Ti oxide grains give a temperature between 1028 and 1056°C and a fO_2 between 1.38 and 1.28 relative to QFM buffer(Figure 4.75). Augites and orthopyroxene were also used as a two pyroxene thermometer, according to the method of Kretz(1982). Coexisting two pyroxene gave relatively high solvus temperatures between 1115 and 1156°C.

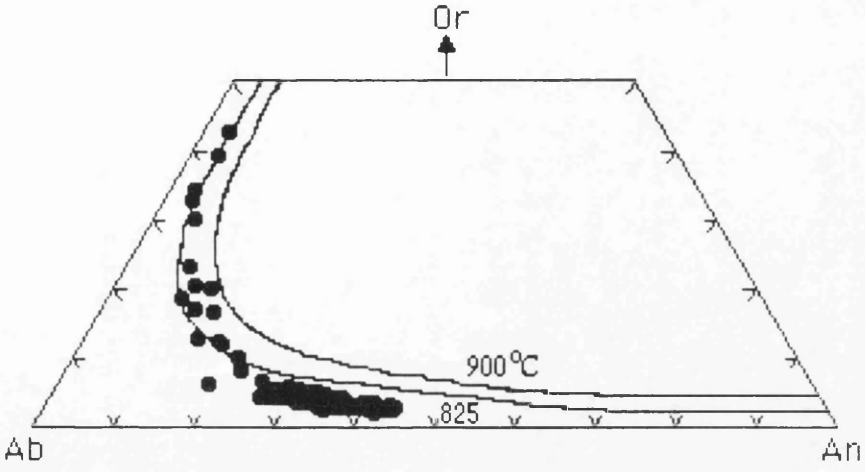

Figure 4.74. Ternary feldspar plot of the trachytes. Solvi are shown for 825°C at 1 kbar and 900°C at 0.5 kbar(Fuhrman and Lindsley, 1988).

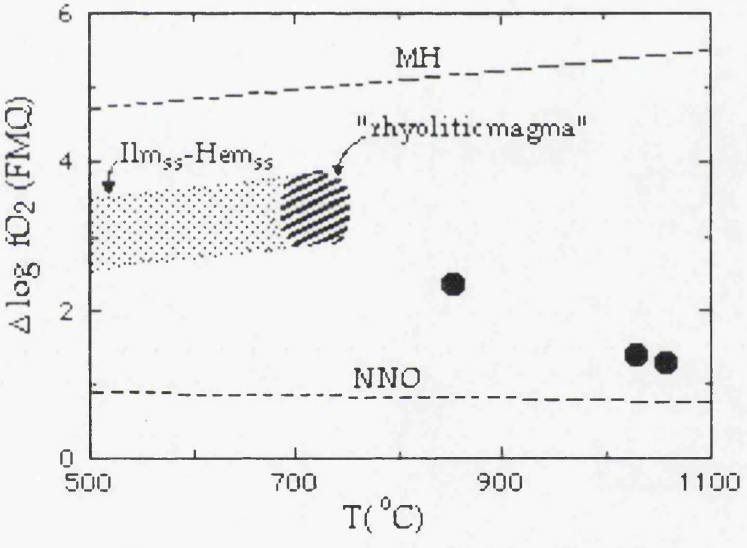

Figure 4.75. Oxygen fugacity relative to FMQ(Δlog fO_2) plotted against temperature for the trachytes. The field labelled Ilm_{ss}-Hem_{ss} represents the coexisting ilmenite and hematite solid solutions(Spencer and Lindsley, 1981).

Table 4.55. Representative analyses of olivines in the trachytes.

Sample	MA-1	MA-43	MA-43	MA-43	MA-1	MA-1
	Iddingsite	Iddingsite	Iddingsite	Iddingsite	Iddingsite	Iddingsite
SiO_2	32.38	32.85	33.56	33.62	30.25	33.45
TiO_2	0.08	0.40	0.16	0.17	0.16	0.15
Al_2O_3	0.76	0.42	0.62	0.51	1.08	0.55
FeO*	36.47	30.66	32.50	29.72	35.97	32.09
MnO	0.99	1.21	1.13	1.05	0.77	1.24
MgO	15.75	24.71	23.07	24.53	13.80	22.73
CaO	0.59	0.60	0.57	0.57	0.68	0.62
Na_2O	1.02	0.50	0.15	0.55	0.40	0.44
K_2O	0.14	0.19	0.09	0.21	0.14	0.05
P_2O_5	0.69	0.47	0.24	0.48	0.83	0.35
Cr_2O_3	0.04	0.00	0.02	0.00	0.00	0.03
NiO	0.00	0.04	0.00	0.00	0.08	0.00
Total	89.91	92.05	92.11	91.41	84.16	91.70
Formula on the basis of 4 oxygens						
Si	1.02	0.99	1.01	1.01	1.01	1.02
Ti	0.00	0.01	0.00	0.00	0.00	0.00
Al	0.03	0.02	0.02	0.02	0.04	0.02
Fe+2	0.99	0.77	0.82	0.75	1.04	0.81
Mn	0.03	0.03	0.03	0.03	0.02	0.03
Mg	0.77	1.11	1.04	1.10	0.71	1.03
Ca	0.02	0.02	0.02	0.02	0.03	0.02
Na	0.06	0.03	0.01	0.03	0.03	0.03
K	0.03	0.01	0.00	0.01	0.02	0.00
P	0.02	0.01	0.01	0.01	0.02	0.00
Cr	0.00	0.00	0.00	0.00	0.00	0.00
Ni	0.00	0.00	0.00	0.00	0.00	0.00
Total	2.97	2.99	2.97	2.98	2.92	2.96
Mg#	0.43	0.59	0.56	0.59	0.41	0.56
Fo	42.84	58.00	54.97	58.67	40.57	55.98
Fa	57.16	42.00	45.03	41.33	59.43	44.02

FeO* is total iron as FeO.

Table 4.56. Representative analyses of feldspars in the trachytes.

Sample	MA-18	MA-39	MA-39	MA-43	MA-1	MA-1	MA-18	MA-18	MA-39	MA-39	MA-43	MA-43
	Micro lite	Micro pheno	Micro lite	Micro lite	Micro lite	Micro lite	Micro pheno	Micro lite	Mega core	Mega rim	Pheno core	Pheno rim
	San.	San.	Anor.	Anor.	Anor.	Plag.	Plag.	Plag.	Plag.	Plag.	Plag.	Plag.
SiO_2	65.99	67.35	65.37	65.16	62.99	62.29	58.47	60.68	58.31	58.18	59.24	60.60
TiO_2	0.24	0.10	0.12	0.27	0.16	0.19	0.10	0.12	0.11	0.17	0.09	0.09
Al_2O_3	18.17	18.44	19.80	19.99	21.65	22.24	24.99	23.51	25.76	26.35	24.62	24.21
FeO*	0.52	0.80	0.59	0.52	0.58	0.60	0.49	0.68	0.46	0.46	0.47	0.45
MnO	0.02	0.00	0.08	0.01	0.01	0.00	0.06	0.02	0.01	0.02	0.00	0.00
MgO	0.03	0.00	0.05	0.00	0.01	0.11	0.11	0.03	0.17	0.13	0.05	0.09
CaO	0.68	0.53	1.01	1.56	3.46	4.05	7.05	5.44	7.63	8.48	6.82	5.33
Na_2O	6.46	5.90	7.33	7.76	8.09	7.76	6.94	7.85	7.13	6.59	7.16	7.80
K_2O	6.86	7.09	5.19	3.98	2.21	1.78	0.74	0.80	0.63	0.56	0.69	0.85
P_2O_5	0.11	0.00	0.00	0.02	0.00	0.04	0.01	0.00	0.00	0.00	0.00	0.01
Cr_2O_3	0.00	0.01	0.00	0.00	0.00	0.01	0.04	0.02	0.00	0.00	0.00	0.00
NiO	0.00	0.01	0.01	0.01	0.00	0.00	0.12	0.02	0.04	0.00	0.00	0.00
Total	99.08	100.23	99.55	99.28	99.16	99.07	99.12	99.17	100.25	100.94	99.14	99.43
Formula on the basis of 32 oxygens												
Si	11.90	12.21	11.74	11.64	11.31	11.22	10.56	10.68	10.47	10.34	10.67	10.97
Al	0.03	0.01	0.01	0.04	0.02	0.02	0.01	0.02	0.02	0.02	0.01	0.01
Ti	3.92	3.89	4.19	4.28	4.58	4.72	5.31	4.99	5.36	5.52	5.29	4.95
Fe+2	0.08	0.12	0.09	0.08	0.09	0.09	0.08	0.10	0.07	0.07	0.07	0.07
Mn	0.00	0.00	0.01	0.00	0.00	0.00	0.01	0.00	0.00	0.00	0.00	0.00
Mg	0.01	0.00	0.01	0.00	0.00	0.03	0.03	0.00	0.04	0.04	0.01	0.02
Ca	0.13	0.10	0.19	0.30	0.68	0.78	1.37	1.05	1.44	1.62	1.33	1.03
Na	2.29	2.05	2.55	2.73	2.82	2.71	2.43	2.74	2.44	2.27	2.53	2.74
K	1.60	1.62	1.19	0.92	0.51	0.41	0.17	0.18	0.14	0.13	0.16	0.20
P	0.02	0.00	0.00	0.00	0.00	0.01	0.00	0.00	0.00	0.00	0.00	0.00
Cr	0.00	0.00	0.00	0.00	0.00	0.00	0.00	0.00	0.00	0.00	0.00	0.00
Ni	0.00	0.00	0.00	0.00	0.00	0.00	0.01	0.00	0.00	0.00	0.00	0.00
Total	19.98	20.00	19.98	19.99	20.01	19.99	19.98	19.76	19.98	20.01	20.00	19.99
An	3.26	2.69	4.98	7.68	16.71	20.04	34.41	26.39	35.81	40.27	33.07	26.03
Ab	56.95	54.35	64.84	69.06	70.57	69.48	61.27	68.98	60.63	56.67	62.96	69.02
Or	39.79	42.96	30.18	23.26	16.72	10.48	4.32	46.33	3.56	3.36	3.97	4.95

FeO* is total iron as FeO.

Table 4.57. Representative analyses of pyroxenes in the trachytes.

Sample	MA-18	MA-1	MA-1	MA-1	MA-1	MA-43	MA-43	MA-43	MA-43	MA-43
	Cpx	Opx	Opx	Cpx	Opx	Opx	Opx	Opx	Cpx	Opx
SiO_2	50.57	53.87	53.39	51.22	53.60	52.91	52.70	53.44	51.20	53.55
TiO_2	0.94	0.43	0.33	0.72	0.25	0.41	0.54	0.26	0.62	0.46
Al_2O_3	2.38	0.98	0.53	1.63	0.82	0.89	1.04	0.51	1.65	0.87
FeO*	11.67	14.55	13.88	8.11	14.56	14.80	14.83	14.68	8.43	14.73
MnO	0.75	1.47	1.62	0.78	1.85	1.25	1.59	1.33	0.88	1.26
MgO	16.53	26.61	26.17	15.85	26.49	25.97	25.75	26.62	15.95	26.54
CaO	8.67	1.39	2.08	19.56	1.14	1.40	1.86	1.44	18.25	1.42
Na_2O	3.85	0.14	0.05	0.51	0.18	0.08	0.05	0.21	0.62	0.29
K_2O	0.09	0.08	0.04	0.02	0.00	0.00	0.01	0.03	0.03	0.01
P_2O_5	0.03	0.05	0.05	0.00	0.00	0.00	0.16	0.02	0.00	0.09
Cr_2O_3	0.00	0.00	0.00	0.00	0.00	0.01	0.00	0.00	0.00	0.05
NiO	0.04	0.02	0.00	0.04	0.00	0.00	0.00	0.00	0.09	0.04
Total	95.52	99.59	98.14	98.44	98.89	97.72	98.53	98.54	97.72	99.31
Formula on the basis of 6 oxygens										
Si	1.89	1.95	1.95	1.92	1.96	1.96	1.94	1.96	1.93	1.95
Ti	0.03	0.01	0.01	0.02	0.01	0.01	0.01	0.01	0.02	0.01
Al	0.10	0.04	0.02	0.07	0.04	0.04	0.05	0.02	0.07	0.04
Fe^{+3}	0.36	0.04	0.00	0.09	0.05	0.03	0.04	0.07	0.08	0.06
Fe^{+2}	0.00	0.40	0.42	0.17	0.39	0.43	0.42	0.38	0.19	0.39
Mn	0.02	0.05	0.05	0.02	0.06	0.04	0.05	0.04	0.03	0.04
Mg	0.92	1.44	1.43	0.88	1.44	1.43	1.41	1.45	0.90	1.44
Ca	0.35	0.05	0.08	0.78	0.04	9.06	0.07	0.06	0.74	0.06
Na	0.28	0.01	0.00	0.04	0.01	0.01	0.00	0.01	0.05	0.02
K	0.04	0.00	0.00	0.00	0.00	0.00	0.00	0.00	0.00	0.00
P	0.00	0.00	0.02	0.00	0.0	0.00	0.00	0.00	0.00	0.00
Cr	0.00	0.00	0.00	0.00	0.00	0.00	0.00	0.00	0.00	0.00
Ni	0.00	0.00	0.00	0.00	0.00	0.00	0.00	0.00	0.00	0.00
Total	4.00	4.00	4.00	4.00	4.00	4.00	4.00	4.00	4.00	4.00
$Mg^{\#}$	0.72	0.76	0.77	0.78	0.76	0.76	0.75	0.76	0.77	0.76
Wo	20.96	2.73	4.11	40.28	2.25	2.80	3.68	2.82	38.25	2.79
En	55.58	72.68	71.95	45.41	72.51	72.15	70.91	72.64	46.50	72.63
Fs	23.46	24.59	23.94	14.31	25.24	25.05	25.41	24.54	15.25	24.58

Fe^{+3} is calculated by normalization according to Schumacher(1991).
$Mg^{\#}=Mg/(Mg+Fe^{+3}+Fe^{+2})$

Table 4.58. Representative analyses of amphiboles in the trachytes.

Sample	MA-18 Kaer-sutite core	MA-18 Kaer-sutite rim	MA-18 Kaer-sutite core	MA-18 Has-tingsite core	MA-1 Kaer-sutite core	MA-39 Kaer-sutite core	MA-39 Kaer-sutite rim	MA-39 Kaer-sutite op. rim	MA-39 Kaer-sutite rim	MA-43 Has-tingsite Incl. in plag.
SiO_2	40.69	41.67	41.30	41.74	41.43	41.38	41.90	36.28	41.40	40.96
TiO_2	5.16	4.41	4.74	4.33	4.62	5.27	4.45	4.47	5.06	4.21
Al_2O_3	11.27	10.42	10.63	10.13	10.66	11.36	10.71	5.44	11.50	10.95
FeO*	11.19	10.95	11.46	10.72	11.35	11.40	11.46	19.07	12.12	11.70
MnO	0.37	0.53	0.44	0.44	0.45	0.38	0.62	1.48	0.42	0.35
MgO	13.28	13.90	13.58	14.35	14.02	13.67	13.83	14.71	14.01	13.73
CaO	11.06	10.72	10.62	10.77	10.61	10.95	10.91	7.77	11.24	10.47
Na_2O	3.43	3.13	2.82	3.12	3.27	2.94	3.11	1.99	3.01	2.93
K_2O	0.69	0.84	0.77	0.71	0.81	0.74	0.76	0.15	0.78	0.73
P_2O_5	0.07	0.00	0.00	0.04	0.00	0.11	0.01	0.13	0.00	0.01
Cr_2O_3	0.06	0.03	0.00	0.10	0.03	0.02	0.02	0.00	0.07	0.03
NiO	0.00	0.00	0.00	0.00	0.01	0.01	0.00	0.03	0.04	0.08
Total	97.27	96.60	96.36	96.45	97.26	98.23	97.78	91.52	99.65	96.15
Formula on the basis of 23 oxygens										
Si	6.07	6.22	6.18	6.24	6.16	6.08	6.18	5.78	6.09	6.13
$Al^{(4)}$	1.93	1.78	1.82	1.76	1.84	1.92	1.82	0.00	1.90	1.86
AlT	1.98	1.83	1.87	1.78	1.87	1.97	1.86	1.11	1.95	1.93
$Al^{(6)}$	0.06	0.05	0.05	0.03	0.03	0.05	0.05	0.00	0.04	0.07
Ti	0.58	0.49	0.53	0.49	0.52	0.58	0.49	0.58	0.55	0.47
Fe^{+3}	0.05	0.18	0.21	0.10	0.11	0.20	0.20	0.00	0.06	0.33
Mg	2.95	3.09	3.03	3.19	3.11	2.99	3.05	3.81	3.00	3.06
Fe^{+2}	1.34	1.19	1.22	1.24	1.29	1.20	1.21	2.65	1.42	1.14
Mn	0.05	0.07	0.06	0.06	0.06	0.05	0.08	0.22	0.05	0.04
FMT	13.03	13.07	13.09	13.11	13.13	13.06	13.08	14.29	13.10	13.12
Ca	1.77	1.71	1.70	1.73	1.69	1.72	1.72	1.45	1.73	1.68
NaM4	0.19	0.21	0.20	0.16	0.18	0.20	0.19	0.00	0.17	0.20
NaT	0.99	0.91	0.82	0.90	0.94	0.84	0.89	0.67	0.84	0.85
NaA	0.77	0.66	0.59	0.72	0.74	0.61	0.67	0.00	0.74	0.63
K	0.13	0.16	0.15	0.14	0.15	0.14	0.14	0.03	0.14	0.14
SumA	0.90	0.82	0.74	0.86	0.89	0.75	0.81	0.03	0.88	0.77
$Mg^{\#}$	0.70	0.74	0.73	0.73	0.72	0.73	0.73	0.58	0.71	0.74

Fe^{+3} is calculated by estimation according to Spear and Kimball(1984).
$Mg^{\#}=Mg/(Mg+Fe^{+2})$

Table 4.59. Representative analyses of Fe-Ti oxides in the trachytes.

Sample	MA-43	MA-43	MA-43	MA-39	MA-39	MA-1	MA-1	MA-1	MA-1	MA-18
	Magnt.	Magnt.	Magnt.	Magnt.	Magnt.	Magnt.	Magnt.	Magnt.	Magnt.	Ilmen.
SiO_2	0.30	0.20	0.27	0.32	0.27	0.28	0.24	0.29	0.32	0.26
TiO_2	16.74	16.41	14.52	12.91	5.96	14.76	15.81	13.69	13.59	35.69
Al_2O_3	1.42	1.19	1.97	1.81	2.67	0.72	0.56	2.55	2.56	1.66
FeO*	72.83	73.59	74.02	77.87	87.94	76.46	75.64	75.54	75.82	51.74
MnO	1.53	1.45	1.40	0.49	0.73	1.10	1.43	1.26	1.28	3.79
MgO	2.76	2.60	3.03	0.35	2.42	0.44	0.63	1.99	2.22	1.65
CaO	0.01	0.00	0.02	0.07	0.00	0.02	0.02	0.00	0.02	0.07
Na_2O	0.01	0.13	0.39	0.14	0.28	0.16	0.11	0.29	0.41	0.31
K_2O	0.17	0.00	0.04	0.00	0.04	0.04	0.02	0.01	0.02	0.02
P_2O_5	0.01	0.00	0.00	0.01	0.00	0.00	0.00	0.01	0.00	0.04
Cr_2O_3	0.04	0.05	0.12	0.06	0.00	0.00	0.08	0.05	0.12	0.01
NiO	0.13	0.02	0.02	0.00	0.00	0.03	0.17	0.12	0.16	0.08
Total	96.03	95.64	95.80	94.03	100.31	94.01	94.71	95.80	96.52	95.32
Formula on the basis of 32 oxygens for magnetites and 6 oxygens for ilmenite										
Si	0.01	0.01	0.01	0.01	0.01	0.01	0.01	0.01	0.01	0.01
Ti	0.46	0.46	0.40	0.37	0.17	0.43	0.45	0.38	0.37	0.68
Al	0.06	0.05	0.08	0.08	0.12	0.03	0.02	0.11	0.11	0.05
Fe^{+3}	0.99	1.03	1.22	1.16	1.55	1.11	1.05	1.12	1.15	0.59
Fe^{+2}	1.26	1.26	1.14	1.32	0.97	1.34	1.36	1.19	1.16	0.51
Mn	0.05	0.05	0.04	0.02	0.02	0.03	0.04	0.04	0.04	0.08
Mg	0.15	0.14	0.17	0.02	0.13	0.02	0.03	0.11	0.12	0.06
Ca	0.00	0.00	0.00	0.00	0.00	0.00	0.00	0.00	0.00	0.00
Na	0.00	0.01	0.03	0.01	0.02	0.01	0.01	0.02	0.03	0.02
K	0.01	0.00	0.00	0.00	0.00	0.00	0.00	0.00	0.00	0.00
P	0.00	0.00	0.00	0.00	0.00	0.00	0.00	0.00	0.00	0.00
Cr	0.00	0.00	0.00	0.00	0.00	0.00	0.00	0.00	0.00	0.00
Ni	0.00	0.00	0.00	0.01	0.00	0.00	0.01	0.00	0.00	0.00
Total	3.00	3.00	3.00	3.00	3.00	3.00	3.00	3.00	3.00	2.00
Mn/Mg	0.32	0.32	0.26	0.81	0.17	1.44	1.31	0.36	0.33	1.31
sp	4.07	3.37	5.27	2.43	6.41	2.07	1.62	6.84	6.72	
mg-chr	0.07	0.09	0.21	0.00	0.00	0.00	0.15	0.09	0.22	
mg-fer	15.81	15.24	15.03	0.00	8.23	1.12	2.89	6.57	7.79	
trev	0.52	0.08	0.06	0.00	0.00	0.11	0.67	0.43	0.57	
herc	0.00	0.00	0.00	2.61	0.00	0.00	0.00	0.00	0.00	
chr	0.00	0.00	0.00	0.12	0.00	0.00	0.00	0.00	0.00	
mt	48.98	51.45	54.64	71.89	76.26	69.50	65.16	62.69	61.93	
usp	30.55	29.77	24.79	22.95	9.11	27.20	29.50	23.38	22.77	

Fe^{+3} is calculated by normalization according to Schumacher(1991).

4.8.7. TEMPERATURE AND OXYGEN FUGACITY IN THE MEYDAN ALKALINE LAVAS

The liquidus temperatures of the Meydan lavas can be estimated by utilizing the olivine-liquid thermometer developed by Roeder and Emslie(1970) and Roeder(1974). Since all of these lavas generally contain less than 5% olivine phenocrysts only, core olivine compositions can be taken to represent the olivine in equilibrium with the bulk(whole-rock) composition. Such calculations yield temperatures of between 1142°C and 1248°C(±40) for alkali olivine basalt, and between 1025°C and 1141°C for hawaiite. The lowest temperatures are associated with more evolved rocks; between 1037°C and 1085°C for mugearite, and between 913°C and 964°C for benmoreite.

There are no rhombohedral oxides in the Meydan lavas except in a few samples, which prohibits the use of calibrated two-oxide oxygen barometers. Experimentally determined relations between oxygen fugacity, ferric-ferrous ratio, bulk composition, and temperature have been calibrated by Kress and Carmichael(1991). Utilizing measured values of the ferric-ferrous ratio, bulk composition, and arbitrary temperature of 1200°C, the fO_2 of the Meydan lavas has been calculated relative to the nickel-nickel oxide buffer(ΔNNO). Relative fO_2 is useful in that it is independent of temperature, because the ferric-ferrous ratio of a liquid remains nearly constant as it is equilibrated at various temperatures along an oxygen buffer curve(Kress and Carmichael, 1991).

4.9. THE ZILAN LAVA

4.9.1. PETROGRAPHY

The Zilan lava is generally hypocrystalline containing 5-7 % phenocrysts of mainly plagioclase and some pyroxene(cpx and opx). The mineral assemblage includes plagioclase(65%), anorthoclase(5%), orthopyroxene and clinopyroxene(7%), and opaque oxides(10%). Microphenocrysts are plagioclase, two pyroxenes and some equant opaque oxides. These phenocrysts and microphenocrysts are set in a microlitic and, or interstitial groundmass.

Plagioclase phenocrysts and microphenocrysts are subhedral laths showing multiple twinning, rare zoning, characteristic internal cracks and slight corrosion with resorption and embayment textures. In addition, they include opaque oxide and pyroxene grains, or apatite needles. Glomeroporhyritic clots of plagioclase and pyroxene enclosed in a fine grained interstitial groundmass also occur.

Subhedral pyroxene phenocrysts and microphenocrysts show simple twinning and internal cracks, and may form aggregates of microphenocrysts. They contain inclusions of opaque grains and apatite.

The groundmass is mainly fine laths of plagioclase, some anorthoclase and opaque oxide grains set in partly altered, brownish glass.

4.9.2. MINERAL CHEMISTRY

4.9.2.1. FELDSPAR

Feldspars in the Zilan lava range from andesine-oligoclase to anorthoclase(Figure 4.76). Representative compositions are given in Table 4.60.

Phenocrysts and microphenocrysts are generally andesine with a composition ranging from An_{30} to An_{38}. Some corroded phenocrysts are more calcic with a composition between An_{43} and An_{47}.

Microlites in the groundmass are mainly oligoclase with a composition varying from An_{24} to An_{30}. Anorthoclase microlites have a composition from $An_{16}Ab_{64}Or_{20}$ to $An_{22}Ab_{63}Or_{13}$. In addition, some andesine(An_{30-34}) is also present in the groundmass.

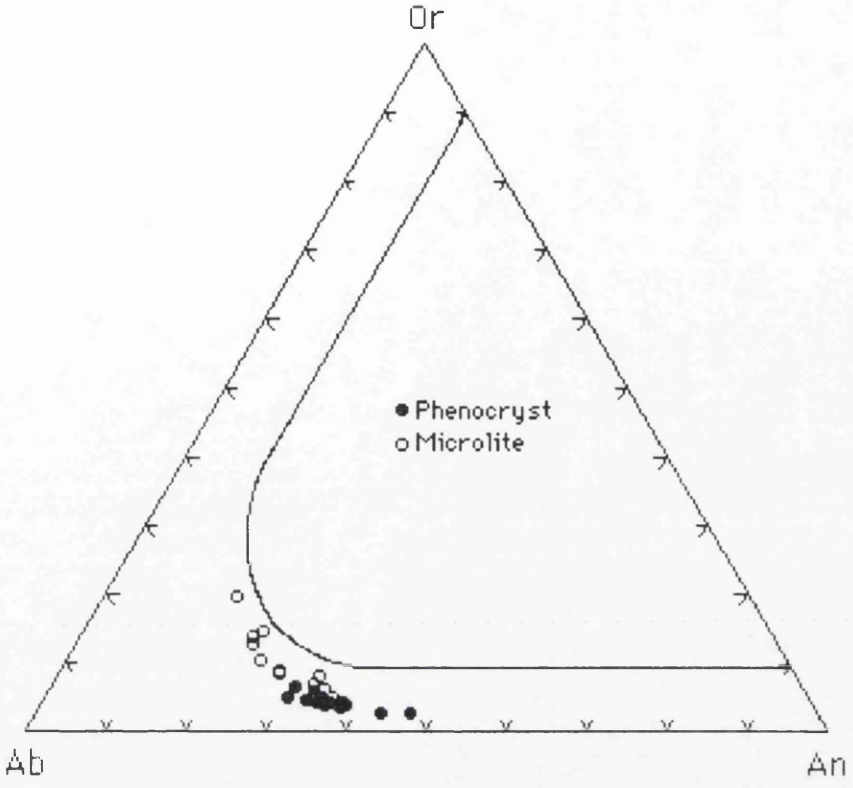

Figure 4.76. Ternary Or-Ab-An plot of feldspars in the Zilan lava.

4.9.2.2. PYROXENE

The pyroxene of the Zilan lava is mainly augite and some orthopyroxene(Figure 4.77), according to the classification of Morimoto *et al.* (1988). They are generally homogeneous compositions and the representative analyses are given in Table 4.61.

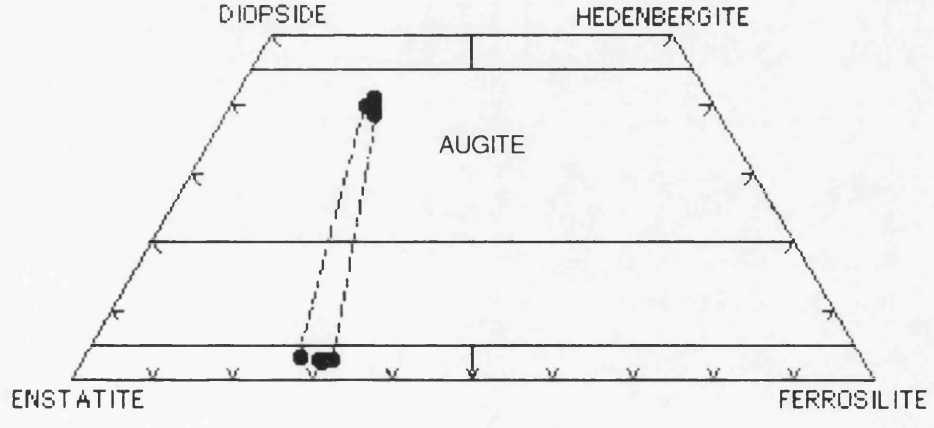

Figure 4.77. Pyroxene nomenclature of the Zilan lava on the ternary Wo-En-Fs plot. The tie lines intersect the Wo-En join at about between Wo_{95} and Wo_{99}.

Augites have a composition of $Wo_{39-41}En_{43-42}Fs_{18-17}$, and a $Mg/(Mg+Fe^{+3}+Fe^{+2})$ ratio from 0.71 to 0.76. Generally, they are Ti-poor types with a TiO_2 content below 1 wt.%(0.58-1 wt.%) which is characteristic for

subalkaline rocks(Figure 4.78)(Kushiro, 1960; Le Bas, 1962). Al_2O_3 content ranges from 1.79 to 3.05 wt.%. MnO content varies from 0.47 to 0.82 wt.%, and Na_2O content is between 0.59 and 0.99 wt.%. Trace element contents are quite low and insignificant.

Orthopyroxenes show a composition ranging from $Wo_3En_{67}Fs_{30}$ to $Wo_3En_{70}Fs_{27}$, and a $Mg/(Mg+Fe^{+3}+Fe^{+2})$ ratio from 0.70 to 0.73. They have a TiO_2 content(0.29-0.45 wt.%), Al_2O_3 content(1.04-1.31 wt.%)(Figure 4.79), MnO content(0.71-1.15 wt.%) and Na_2O content(0.17-0.37). Trace element contents are very low.

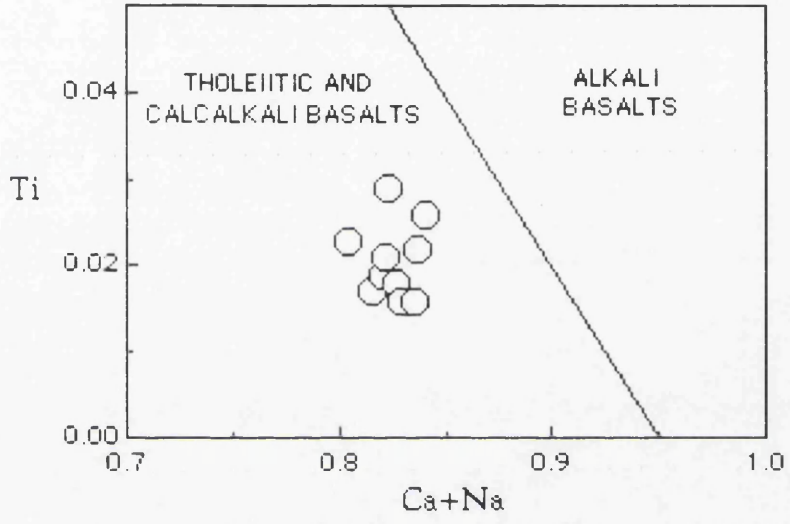

Figure 4.78. Plot of Ti versus Ca+Na per formula units for clinopyroxenes of the Zilan lava. The discrimination line for basaltic rocks is from Leterrier *et al.* (1982).

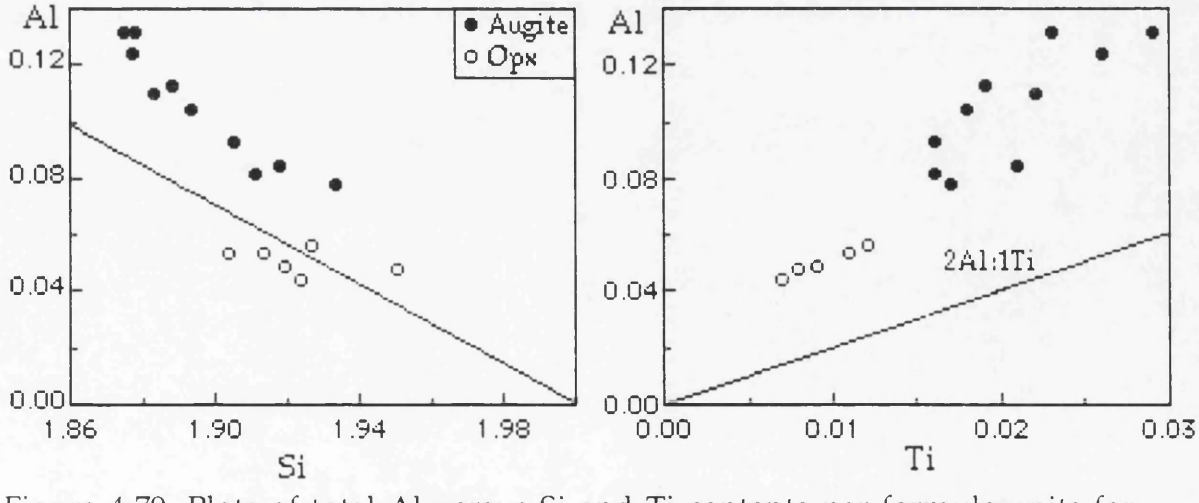

Figure 4.79. Plots of total Al versus Si and Ti contents per formula units for augites and orthopyroxenes of the Zilan lava.

4.9.2.3. FE-TI OXIDES

In the Zilan lava, the main oxide mineral is magnetite with lesser ilmenite (Figure 4.80). Generally, both have homogeneous compositions. Representative analyses are given in Table 4.62.

Magnetites are typically Ti-rich with 14 to 19 wt.% TiO_2. They have Al_2O_3 content varying from 1.9 up to 2.7 wt.%. MnO is between 0.8 and 1 wt.%. MgO ranges from 2.8 up to 3.1 wt.%. NiO and Cr_2O_3 are quite low.

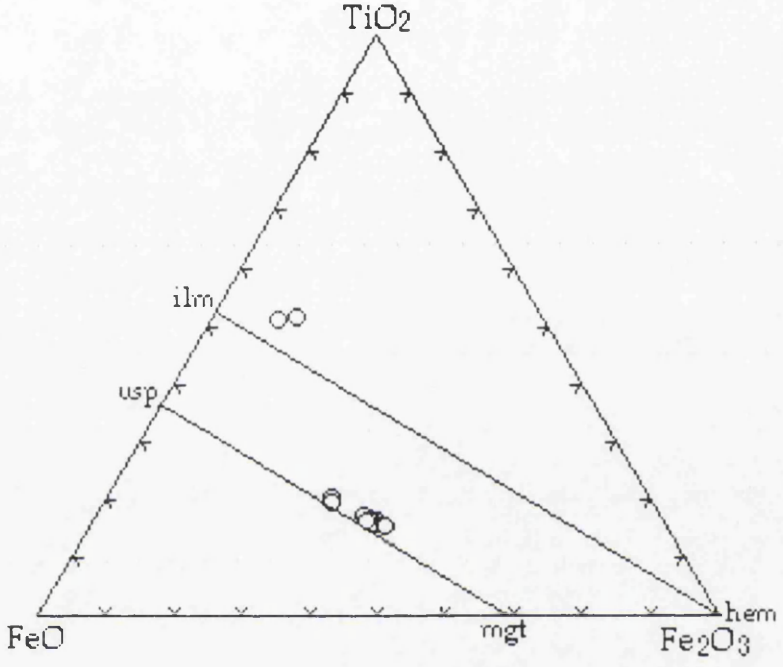

Figure 4.80. Compositions of iron-titanium oxides in the Zilan lava.

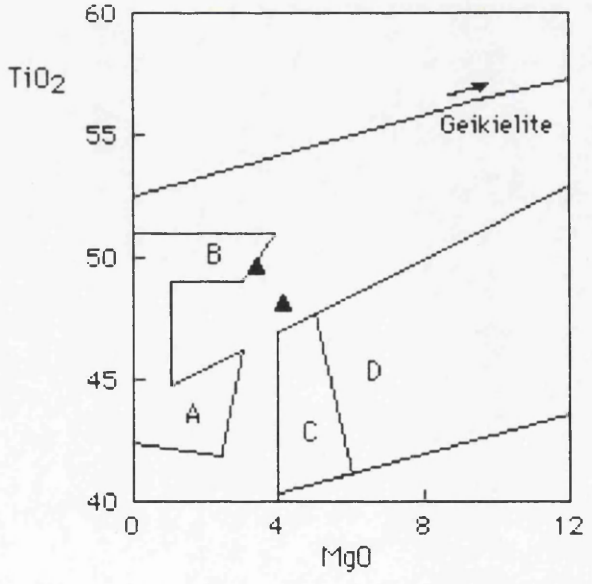

Figure 4.81. Plot of MgO versus TiO_2 for ilmenites in the Zilan lava. Typical fields of ilmenite compositions are from Haggerty(1976); A from felsic rocks; B from tholeiitic rocks; C from alkali basaltic rocks; D from kimberlites.

Ilmenites are almost stoichiometric with a Ti content between 0.8 and 0.9 in the formula units. MnO is about 1 wt.% and MgO is 3 to 4 wt.%(Figure 4.81). They are also poor in trace element contents. The distribution of Mn and Mg between ilmenite and Ti-rich magnetite in the Zilan lava shows equilibrium between these two phases, and is ideal for geothermometry(Bacon and Hirschmann, 1983).

4.9.3. GEOTHERMOMETRY AND GEOBAROMETRY

Geothermometry calculations in the Zilan lava were made on the basis of two pyroxenes and Fe-Ti oxides.

The feldspars of the Zilan lava are illustrated on a ternary plot in terms of equilibrium conditions of coexisting feldspars. The plot indicates that phenocrysts, which are dominantly andesine, appear to be in disequilibrium with groundmass oligoclase and anorthoclase(Figure 4.82). Furthermore, calcic plagioclase phenocrysts reveal a solvus temperature below 825°C whereas sodic plagioclase(microlites) fall generally on a solvus temperature between 825°C and 900°C. These results indicate that final equilibrium was not achieved and it is therefore unclear whether the temperatures obtained have any meaning.

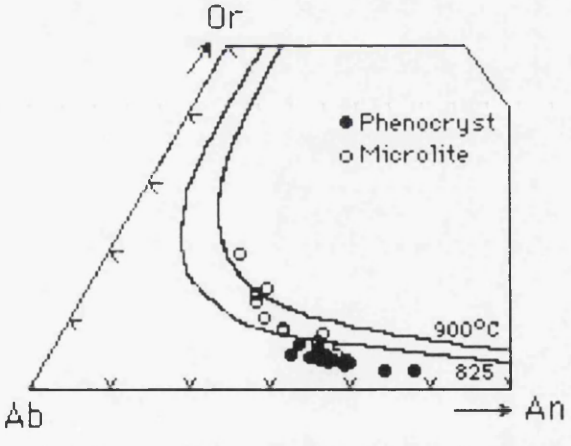

Figure 4.82. Ternary feldspar plot of the Zilan lava. Solvi for feldspars coexisting in equilibrium is shown for 825°C at 1 kbar and 900°C at 0.5 kbar(Fuhrman and Lindsley, 1988).

Augite and orthopyroxene phenocrysts were used as a geothermometer following the method of Kretz(1982). Coexisting two pyroxenes gave a solvus temperature between 1073°C and 1095°C(Table 4.63). These temperatures are consistent with typical basaltic crystallization and pyroxene equilibrium temperatures.

Following Anderson and Lindsley(1985), magnetite and ilmenite pairs gave a temperature between 841°C and 869°C, and a fO_2 between 0.30

and 0.54 relative to FMQ buffer. These temperatures are relatively low, compared to those obtained from the pyroxenes and presumably record subsolidus equilibrium.

Table 4.63. Coexisting two pyroxene compositions and calculated solvus temperatures, according to Kretz(1982).

	Opx	Cpx	Opx	Cpx	Opx	Cpx	Opx	Cpx	Opx	Cpx
Wo	0.027	0.398	0.028	0.409	0.030	0.405	0.031	0.395	0.032	0.406
En	0.683	0.435	0.690	0.444	0.681	0.440	0.673	0.431	0.678	0.427
Fs	0.271	0.167	0.254	0.146	0.269	0.155	0.264	0.173	0.270	0.166
T(°C)	1093		1080		1085		1095		1073	

Table 4.60. Representative analyses of feldspars in the Zilan lava.

Sample	MA-263	MA-263	MA-263	MA-263	MA-263	MA-263	MA-263	MA-263	MA-263
	Pheno	Pheno core	Pheno	Micro-lite	Micro-lite	Pheno	Micro-lite	Pheno	Micro-pheno
SiO_2	59.07	56.96	57.45	60.83	64.10	59.47	62.01	58.80	59.79
TiO_2	0.12	0.07	0.14	0.16	0.48	0.12	0.21	0.15	0.16
Al_2O_3	25.47	26.81	26.81	23.53	19.76	24.54	21.90	24.92	24.33
FeO*	0.44	0.31	0.47	0.54	1.06	0.35	0.76	0.38	0.69
MnO	0.06	0.00	0.00	0.00	0.05	0.02	0.05	0.08	0.06
MgO	0.14	0.06	0.22	0.02	0.17	0.05	0.27	0.14	0.07
CaO	7.45	9.73	8.91	5.48	3.22	6.75	4.39	7.13	6.36
Na_2O	6.85	5.84	6.26	7.05	6.91	7.08	7.19	7.12	7.34
K_2O	0.74	0.50	0.48	1.49	3.24	0.80	2.15	0.72	1.12
P_2O_5	0.06	0.00	0.00	0.00	0.12	0.00	0.00	0.18	0.06
Cr_2O_3	0.04	0.01	0.09	0.01	0.00	0.00	0.00	0.01	0.03
NiO	0.02	0.00	0.00	0.09	0.00	0.01	0.00	0.01	0.00
Total	100.46	100.29	100.83	99.20	99.11	99.19	98.93	99.64	100.01
Formula on the basis of 32 oxygens									
Si	10.54	10.13	10.26	10.95	11.55	10.72	11.19	10.58	10.72
Ti	0.02	0.01	0.02	0.02	0.07	0.02	0.03	0.02	0.02
Al	5.36	5.83	5.64	4.99	4.20	5.21	4.66	5.28	5.14
Fe^{+2}	0.06	0.05	0.07	0.08	0.16	0.05	0.11	0.06	0.10
Mn	0.01	0.00	0.00	0.00	0.01	0.00	0.01	0.01	0.01
Mg	0.04	0.02	0.06	0.00	0.04	0.01	0.07	0.04	0.02
Ca	1.42	1.85	1.70	1.06	0.62	1.30	0.85	1.37	1.22
Na	2.37	2.01	2.16	2.46	2.41	2.48	2.52	2.49	2.55
K	0.17	0.11	0.11	0.34	0.75	0.18	0.50	0.17	0.26
P	0.01	0.00	0.00	0.00	0.02	0.00	0.00	0.03	0.01
Cr	0.01	0.00	0.01	0.00	0.00	0.00	0.00	0.00	0.00
Ni	0.00	0.00	0.00	0.01	0.00	0.00	0.00	0.00	0.00
Total	20.01	20.01	20.03	19.90	19.83	19.99	19.95	20.05	20.07
An	35.85	46.59	42.82	27.46	16.40	32.82	21.96	33.99	30.27
Ab	59.85	50.62	54.41	63.73	63.76	62.63	65.12	61.79	63.28
Or	4.29	2.77	2.77	8.81	19.84	4.55	12.92	4.22	6.45

FeO* is total iron as FeO.

Table 4.61. Representative analyses of pyroxenes in the Zilan lava.

Sample	MA-263 Cpx	MA-263 Cpx	MA-263 Cpx	MA-263 Opx	MA-263 Opx	MA-263 Cpx	MA-263 Opx	MA-263 Opx	MA-263 Cpx
	micro-pheno	micro-pheno	pheno core	micro-pheno	pheno	pheno	micro-pheno	pheno	pheno
SiO_2	52.09	51.65	50.82	52.41	53.07	50.72	53.47	53.44	50.51
TiO_2	0.64	0.58	0.86	0.45	0.42	1.06	0.30	0.29	0.95
Al_2O_3	1.79	1.88	3.04	1.31	1.30	3.04	1.11	1.04	2.83
FeO*	10.11	9.78	10.51	17.60	18.80	10.07	18.13	18.90	9.98
MnO	0.66	0.66	0.61	1.00	0.93	0.47	1.15	0.99	0.53
MgO	14.77	15.08	14.77	24.58	25.09	14.60	23.42	25.01	14.38
CaO	19.49	19.41	18.56	1.46	1.60	19.30	1.53	1.68	19.69
Na_2O	0.56	0.84	0.99	0.28	0.45	0.82	0.37	0.17	0.78
K_2O	0.03	0.00	0.00	0.03	0.01	0.00	0.08	0.00	0.00
P_2O_5	0.02	0.13	0.12	0.12	0.03	0.08	0.11	0.05	0.23
Cr_2O_3	0.00	0.02	0.00	0.00	0.00	0.00	0.02	0.15	0.00
NiO	0.05	0.04	0.09	0.05	0.00	0.00	0.00	0.00	0.00
Total	100.21	100.07	100.37	99.29	101.70	100.16	99.69	101.72	99.88
Formula on the basis of 6 oxygens									
Si	1.93	1.91	1.88	1.92	1.90	1.88	1.95	1.92	1.88
Ti	0.02	0.02	0.02	0.01	0.01	0.03	0.01	0.01	0.03
Al	0.08	0.08	0.13	0.06	0.05	0.13	0.05	0.04	0.12
Fe^{+3}	0.06	0.11	0.13	0.07	0.14	0.10	0.05	0.09	0.10
Fe^{+2}	0.25	0.19	0.20	0.47	0.42	0.21	0.51	0.47	0.21
Mn	0.02	0.02	0.02	0.03	0.03	0.01	0.04	0.03	0.02
Mg	0.82	0.83	0.81	1.35	1.34	0.81	1.30	1.34	0.80
Ca	0.77	0.77	0.73	0.06	0.06	0.77	0.06	0.06	0.78
Na	0.04	0.06	0.07	0.02	0.03	0.06	0.03	0.01	0.06
K	0.00	0.00	0.00	0.00	0.00	0.00	0.00	0.00	0.00
P	0.00	0.00	0.00	0.00	0.00	0.00	0.00	0.00	0.01
Cr	0.00	0.00	0.00	0.00	0.00	0.00	0.00	0.00	0.00
Ni	0.00	0.00	0.00	0.0	0.00	0.00	0.00	0.00	0.00
Total	4.00	4.00	4.00	4.00	4.00	4.00	4.00	4.00	4.00
$Mg^{\#}$	0.73	0.73	0.71	0.71	0.71	0.72	0.70	0.71	0.72
Wo	40.23	40.00	38.83	2.90	3.08	40.34	3.10	3.23	41.11
En	42.41	43.20	42.99	68.14	67.23	42.46	66.26	66.89	41.75
Fs	17.36	16.80	18.18	28.96	29.69	17.20	30.64	29.88	17.14

Fe^{+3} is calculated by normalization according to Schumacher(1991).
$Mg^{\#}=Mg/(Mg+Fe^{+3}+Fe^{+2})$

Table 4.62. Representative analyses of Fe-Ti oxides in the Zilan lava.

Sample	MA-263	MA-263	MA-263	MA-263	MA-263	MA-263	MA-263	MA-263	MA-263
	Magnet.	Magnet.	Magnet. inclus.	Magnet. inclus.	Magnet.	Magnet.	Magnet.	Ilmenite	Ilmenite
	pheno	micro	in plag.	in px	micro	micro	micro	micro	micro
SiO_2	0.36	0.19	0.27	0.39	0.31	0.64	0.56	0.19	0.28
TiO_2	15.61	15.42	15.32	14.89	16.47	19.11	14.48	49.71	48.19
Al_2O_3	2.38	2.70	2.68	2.41	2.32	1.94	2.64	0.08	0.25
FeO*	74.83	75.95	76.05	72.62	74.22	71.11	75.31	45.70	44.28
MnO	0.97	0.82	0.91	0.83	0.97	0.99	0.90	1.23	0.97
MgO	2.88	3.10	3.14	3.03	3.03	2.92	2.91	3.38	4.14
CaO	0.05	0.09	0.00	0.30	0.00	0.02	0.22	0.07	0.00
Na_2O	0.33	0.26	0.16	0.11	0.31	0.20	0.49	0.08	0.26
K_2O	0.00	0.01	0.00	0.00	0.00	0.02	0.00	0.00	0.01
P_2O_5	0.00	0.00	0.00	0.20	0.08	0.00	0.00	0.00	0.00
Cr_2O_3	0.00	0.03	0.04	0.00	0.04	0.00	0.00	0.00	0.07
NiO	0.00	0.00	0.00	0.00	0.02	0.15	0.00	0.03	0.09
Total	97.41	98.57	98.57	94.78	97.77	97.10	97.51	100.47	98.54
Formula on the basis of 32 oxygens for magnetites and 6 oxygens for ilmenites.									
Si	0.01	0.01	0.01	0.01	0.01	0.02	0.02	0.01	0.01
Ti	0.423	0.41	0.41	0.41	0.44	0.52	0.39	0.91	0.89
Al	0.10	0.11	0.11	0.11	0.09	0.08	0.11	0.00	0.01
Fe^{+3}	1.05	1.07	1.06	1.03	1.00	0.84	1.10	0.18	0.21
Fe^{+2}	1.20	1.19	1.20	1.22	1.23	1.32	1.15	0.76	0.70
Mn	0.03	0.02	0.03	0.03	0.03	0.03	0.03	0.03	0.02
Mg	0.15	0.16	0.17	0.17	0.16	0.16	0.16	0.12	0.15
Ca	0.00	0.00	0.00	0.01	0.00	0.00	0.01	0.00	0.00
Na	0.02	0.02	0.01	0.01	0.02	0.01	0.03	0.00	0.01
K	0.00	0.00	0.00	0.00	0.00	0.00	0.00	0.00	0.00
P	0.00	0.00	0.00	0.01	0.00	0.00	0.00	0.00	0.00
Cr	0.00	0.00	0.00	0.00	0.00	0.00	0.00	0.00	0.00
Ni	0.00	0.00	0.00	0.00	0.00	0.00	0.00	0.00	0.00
Total	3.00	3.00	3.00	3.00	3.00	3.00	3.00	2.00	2.00
Mn/Mg	0.20	0.13	0.18	0.18	0.19	0.19	0.19	0.25	0.13
sp	6.43	7.10	7.10	6.81	6.35	5.75	6.95		
mg-chr	0.00	0.05	0.07	0.00	0.07	0.00	0.00		
mg-fer	13.21	13.47	13.90	14.79	14.55	16.12	12.39		
trev	0.00	0.00	0.00	0.00	0.07	0.59	0.00		
mt	53.50	53.52	53.03	51.59	50.22	41.40	56.35		
usp	26.87	25.86	25.90	26.82	28.75	36.15	24.30		

Fe^{+3} is calculated by normalization according to Schumacher(1991).

4.10. RHYOLITE DOME AND DYKES

4.10.1. PETROGRAPHY

Rhyolites vary from hyalo- to hypo-crystalline poorly vesicular to highly vesicular, porphyritic and sometimes perlitic rocks. They contain 10-25% phenocrysts of plagioclase, biotite and anorthoclase which may, or may not be associated with rounded quartz phenocrysts. Sanidine is also present both as phenocrysts and in the groundmass. In addition, brown amphibole, granular oxides, a few cpx, accessory zircon, apatite and a few titanites are present. Generally these crystals are set in microcrystalline to glassy matrix of mainly sanidine and plagioclase microlites. The modal composition of minerals is plagioclase(25-30%), anorthoclase and sanidine(10-25%), quartz(<3%), biotite(5-7%), amphibole(5-7%%), clinopyroxene(2%), oxides(3-5%), and accessories(<1%).

Phenocrysts and microphenocrysts of quartz occur as subhedral and anhedral crystals with irregular internal cracks.

Biotite and amphibole are subhedral and euhedral or rarely curved or branching crystals. They have a mottled appearance and are pseudomorphed by opaques. They include inclusions of apatite, opaques and rare zircon.

Feldspar phenocrysts are subhedral and may be glomeroporphyritic with quartz and biotite. Sanidines have carlsbad twinning while anorthoclase has albite or cross-hatched twinning, and contains inclusions of apatite, biotite and opaque oxides. Alkali feldspars also show overgrowth texture in which sanidine occurs over anorthoclase. Anorthoclase may be resorbed and sieve-like, especially around the rims. Some of these sieve-textured crystals are enclosed by fine quartz.

In the groundmass, glass is common and there are thin veins and vesicles filled by very fine tridymite crystals. These vesicles show sub-parallel arrangement caused by stress during emplacement of the dykes. In some rocks, the groundmass is perlitic and, or spherulitic textures. Spherulites are formed by alkali feldspar.

4.10.2. MINERAL CHEMISTRY

4.10.2.1. FELDSPAR

Feldspars in the rhyolite dome and dykes range from andesine-oligoclase to sanidine(Figure 4.83). Generally, they have similar compositions in both dome and dyke rocks. Representative analyses are given in Table 4.64.

Generally, megacrysts are andesine with a compositional range from An_{36} to An_{46}. They show normal zoning, changing in composition from

An_{46} in the core to more sodic rim(An_{19}), or An_{36} in the core varying to An_{21} in the rim. Some oligoclase megacrysts are also present in the same sample with a composition varying from An_{23} in the core to An_{19} in the rim. It is significant that some megacrysts display overgrowth texture in which oligoclase(An_{19}) is enclosed by sanidine(Or_{58}). The mantling of feldspar by feldspar is generally suggested to be related to a possible magma mixing in the evolution of volcanic rocks, as described by Pearce *et al.* (1987).

Phenocrysts and microphenocrysts of feldspar comprise both sodic plagioclase(oligoclase) and sanidine. Plagioclase crystals change in composition between An_{17} and An_{25}. They are slightly zoned from An_{25} in the core varying to An_{19} in the rim. Sanidines change in composition between Or_{55} and Or_{65}. In addition to these phases, sodic plagioclase(An_{16}) and sanidine microlites are present in lesser amount.

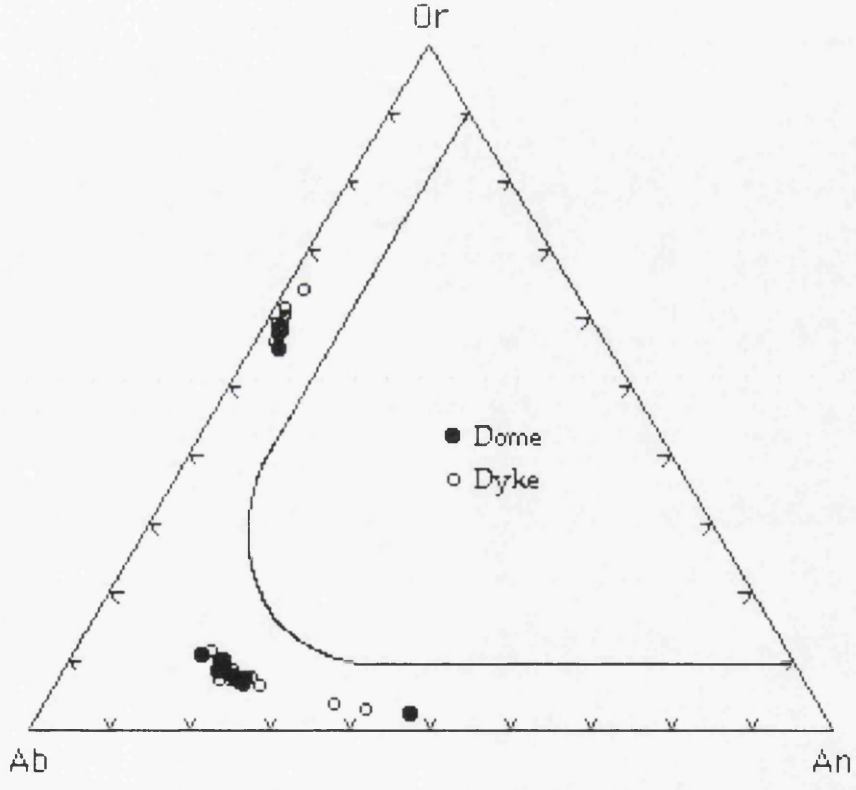

Figure 4.83. Or-Ab-An diagram of feldspars in rhyolite dome and dykes.

4.10.2.2. PYROXENE

The pyroxene of rhyolite dome and dykes is only augite(Figure 4.84), according to classification of Morimoto *et al.* (1988). Representative analyses are presented in Table 4.65.

Augites generally fall close to the augite-diopside dividing line on the plot(Figure 4.84) are $Wo_{44}En_{40}Fs_{16}$ with 0.13 to 0.28 wt.% TiO_2, 0.56 to 0.93 wt.% Al_2O_3(Figure 4.85), 0.84 to 1 wt.% MnO and Na_2O from 0.32 to 0.89 wt.%. Cr_2O_3 and NiO contents are very low or insignificant.

Some of the phenocrysts are slightly zoned, with a slightly more calcic rim. They show a compositional change from $Wo_{43}En_{41}Fs_{16}$ in the core to $Wo_{45}En_{40}Fs_{15}$ in the rim. Moreover, TiO_2 decreases from 0.28 wt.% in the core to 0.17 wt.% in the rim.

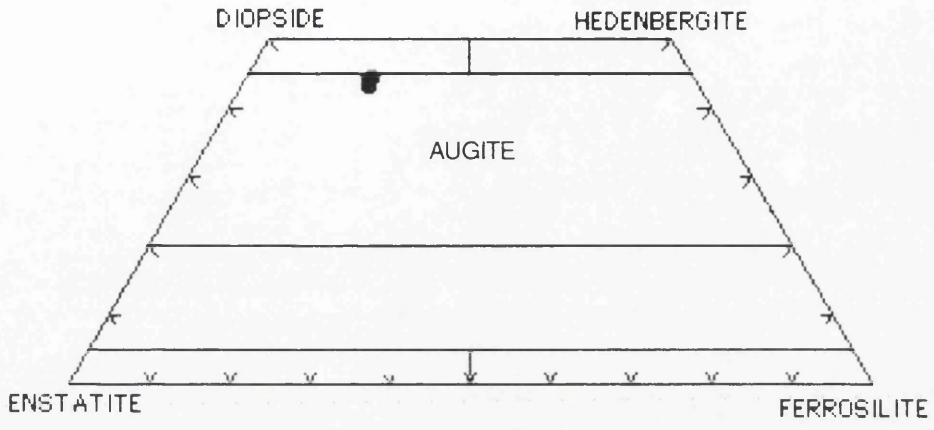

Figure 4.84. Pyroxene nomenclature of rhyolite dome and dykes on the Wo-En-Fs ternary plot(Morimoto *et al.*, 1988).

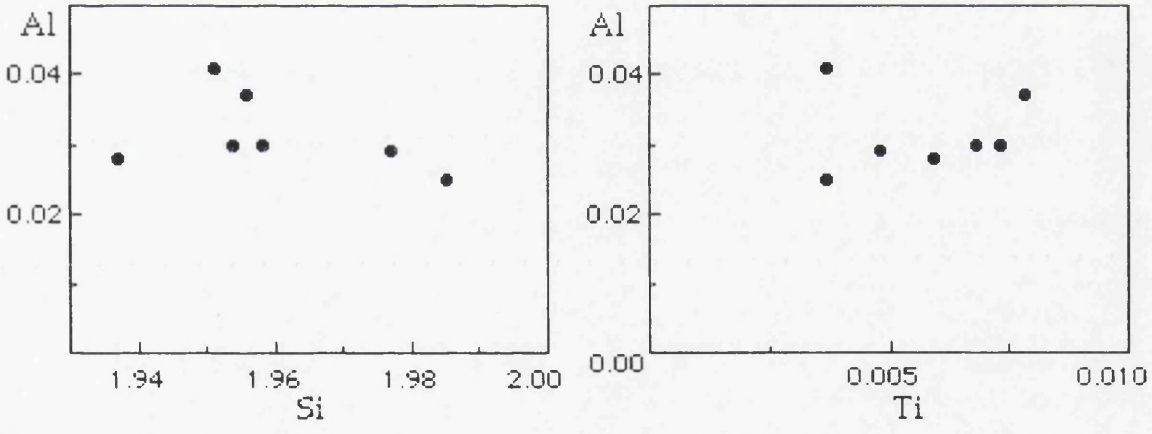

Figure 4.85. Plots of total Al versus Si and Ti per formula units of augites in the rhyolite dome.

4.10.2.3. AMPHIBOLE

In the rhyolite dykes, calcic amphiboles are present. They are magnesio-hornblende(Figure 4.86), according to the classification of Leake(1978). Generally, they have homogeneous compositions. The representative analyses are given in Table 4.66.

Magnesio-hornblendes of the dykes have a $Mg/(Mg+Fe^{+3}+Fe^{+2})$ ratio 0.71-0.72. TiO_2 content varies from 1.16 to 1.41 wt.%(0.13-0.15 per formula unit) and Al 0.82 to 0.97, Na 0.39 to 0.51 and Si from 7.09 to 7.23 per formula unit(Figure 4.87).

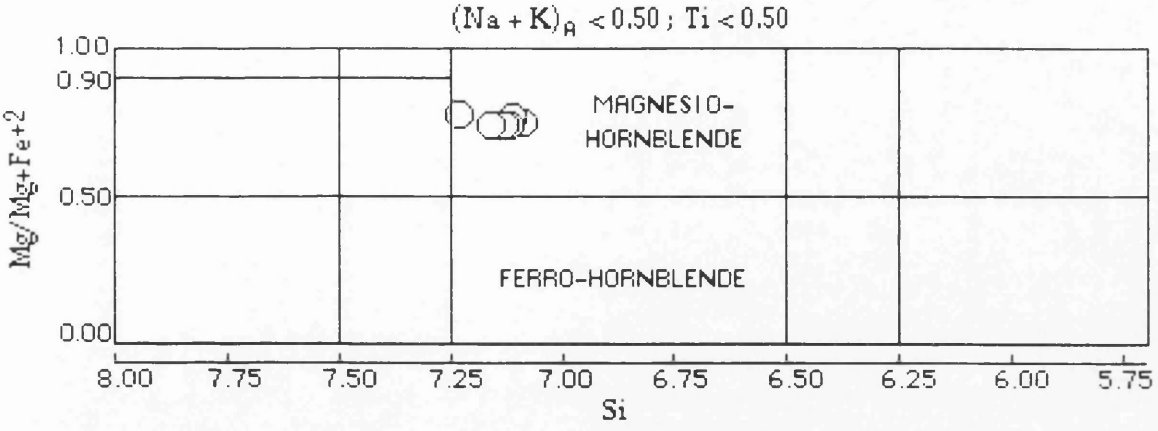

Figure 4.86. The classification and nomenclature of calcic amphiboles of the rhyolite dykes, according to Leake(1978).

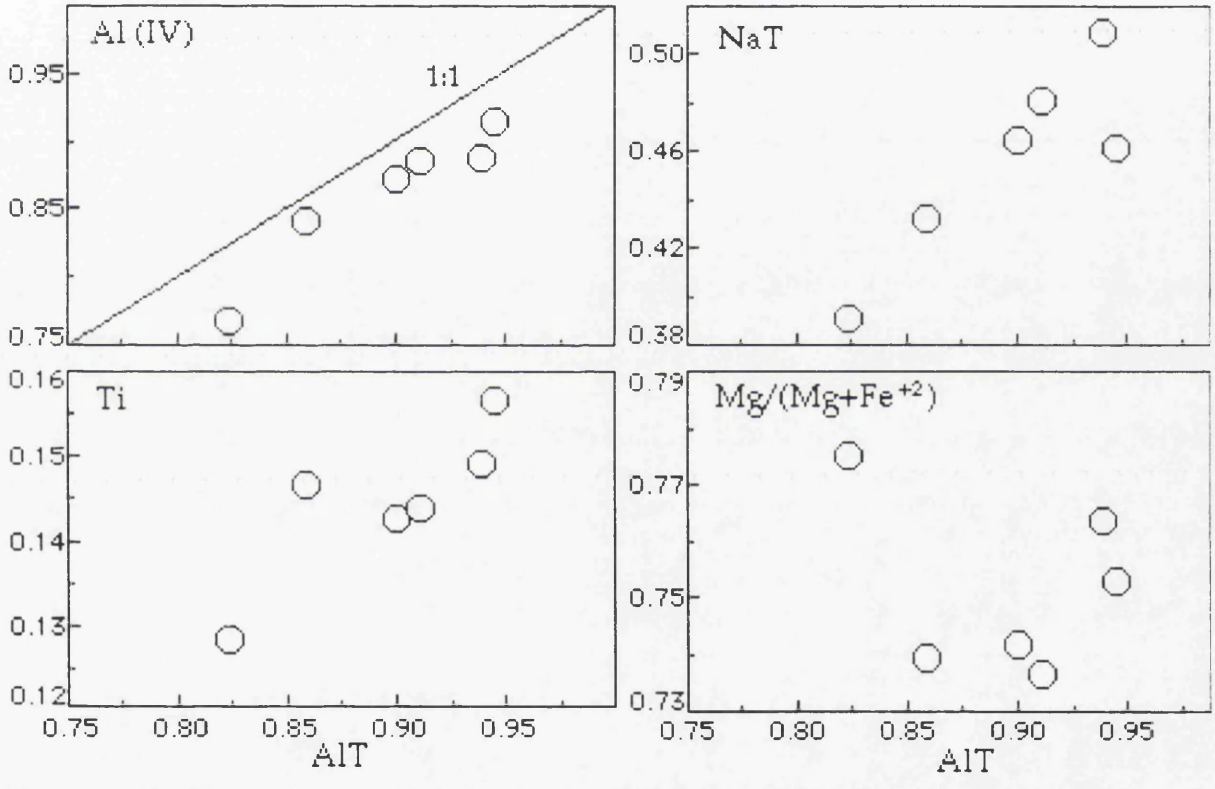

Figure 4.87. Plots of total AlT versus tetrahedral Al(IV), Ti, Na contents per formula units, and Mg/(Mg+Fe^{+2}) ratio of calcic amphiboles in the rhyolite dykes.

4.10.2.4. BIOTITE

Biotites in the rhyolite dome and dykes are phlogopite-annite rich types with a high Mg-content(Figure 4.88). They have end member compositions between phlogopite(51-60) and annite(20-24). Representative analyses are presented in Table 4.67.

The biotites in the rhyolite dome are effectively uniform with an Mg/(Mg+Fe^{+3}+Fe^{+2}) ratio of 0.67 to 0.68. Biotites in the dykes however have

range from 0.62 up to 0.71, and some of phenocrysts display slight zoning with a $Mg/(Mg+Fe^{+3}+Fe^{+2})$ ratio varying from 0.70 in the core to 0.67 in the rim. In addition, the Ti content of biotites in the dykes is 0.53 to 0.58 per formula units whereas those in the dome vary from 0.55 to 0.62 per formula unit.

Generally, biotites in both dykes and dome have Al varying from 2.17 to 2.47, Mn from 0.02 to 0.04, Mg from 3.09 to 3.57 and K from 1.59 to 1.71 per formula units.

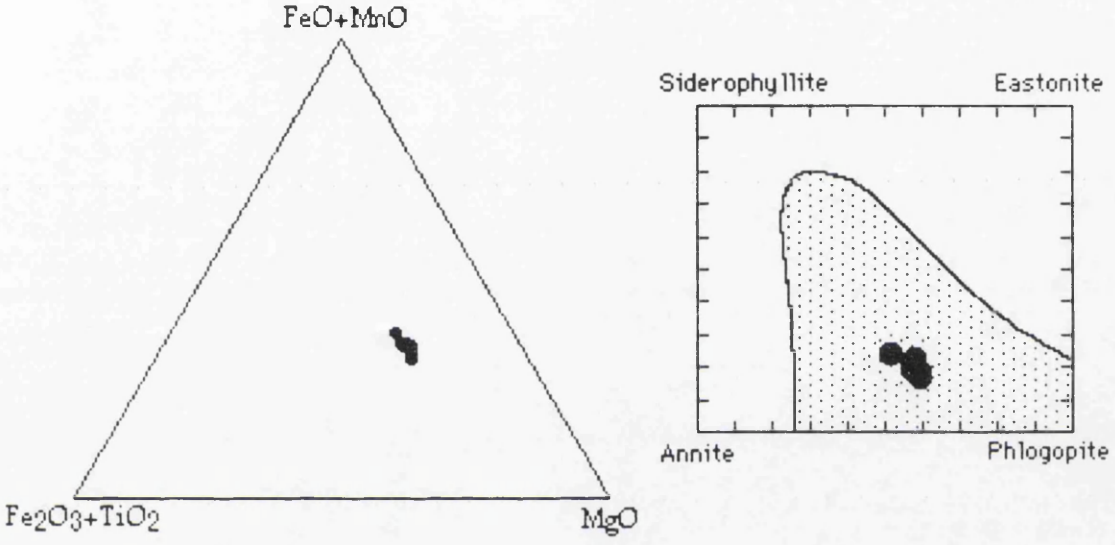

Figure 4.88. Compositional variations and the principal components of biotite compositions in the rhyolite dome and dykes. The shaded field in which most natural biotites lie is from Deer *et al.* (1992).

4.10.2.5. FE-TI OXIDES

In the rhyolite dome and dykes, ilmenite is the main oxide mineral, and some magnetite is also present, especially in the dome(Figure 4.89). Generally, they exhibit homogeneous compositions. Representative analyses are given in Table 4.68.

Ilmenites are almost stochiometric $FeTiO_3$, with a small solid solution towards $MgTiO_3$. They have TiO_2 from 38 to 40 wt.%, MnO 1.21 and 1.84 wt.%, and MgO between 1.27 and 2 wt.%(Figure 4.90).

Magnetites are slightly Ti-rich types with TiO_2 ranging from 6.35 to 6.39 wt.%, Al_2O_3 1.16 to 1.26 wt.%, MnO about 1wt.%, and MgO about 1.28 wt.%. Cr_2O_3 and NiO contents are insignificant. The distribution of Mg and Mn between magnetite and ilmenite indicates equilibrium between coexisting two phases(Bacon and Hirschmann, 1988), and these two phases can be used as a geothermometry.

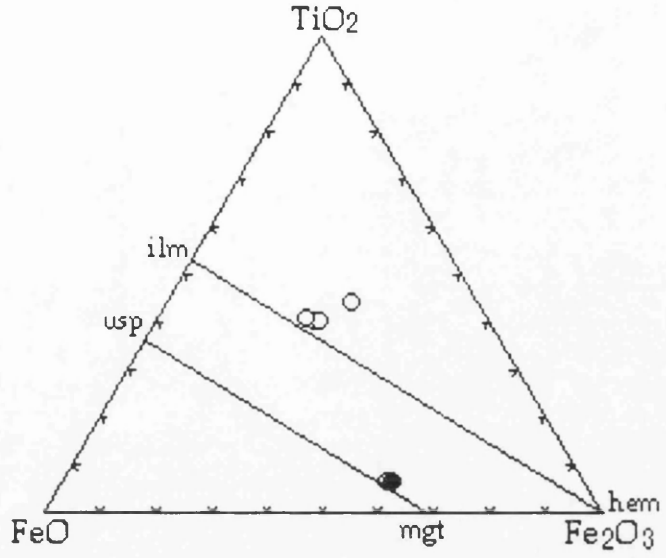

Figure 4.89. Compositions of iron-titanium oxides in the rhyolite dome(solid circle) and dykes(open circles).

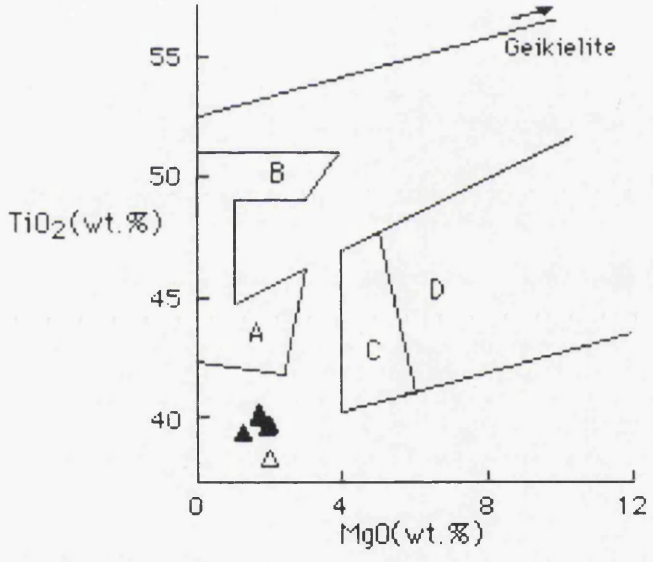

Figure 4.90. Plot of MgO versus TiO_2 for ilmenites in the rhyolite dome(open triangle) and dykes(solid triangles). Typical fields of ilmenite compositions are from Haggerty(1976), A from felsic rocks; B from tholeiitic rocks; C from alkali basaltic rocks; D from kimberlites.

4.10.3. GEOTHERMOMETRY AND GEOBAROMETRY

Geothermometry calculations in the rhyolite dome and dykes were made on the basis of two feldspars and Fe-Ti oxides.

The feldspars are shown on a ternary plot(Figure 4.91), based on thermodynamic data of Fuhrman and Lindsley(1988). On the plot, it is seen that sanidine is in equilibrium with some of the sodic plagioclase(oligoclase) which is mainly the rim composition of the phenocrysts. These feldspars in equilibrium reveal a solvi temperature at about 750°C. However, most of

the oligoclase and andesine which are megacrysts appear to be in disequilibrium with sanidine. In addition, these plagioclases in disequilibrium indicate a solvi temperature below 750°C(Figure 4.91). This disequilibrium feature, which is also exhibited by compositional zoning and overgrowth texture in megacrysts, confirms possible magma mixing in the genesis of these rocks.

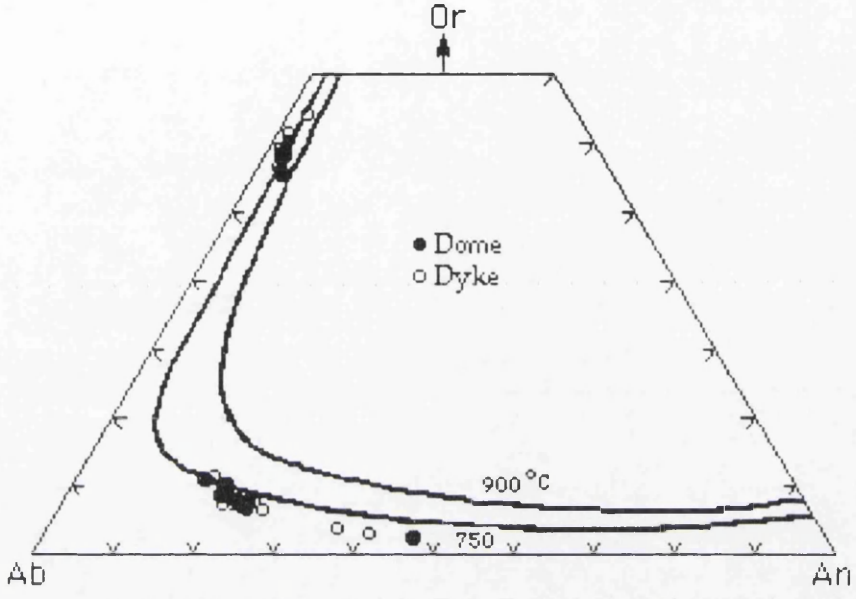

Figure 4.91. Ternary feldspar plot of the rhyolite dome and dykes. Solvi for coexisting in equilibrium is shown for 750°C at 1 kbar and 900°C at 0.5 kbar(Fuhrman and Lindsley, 1988).

Estimated temperatures of 645-655°C using the geothermometer of Blundy and Holland(1990) were obtained from a sodic plagioclase core and hornblende in the rhyolite dyke. Coexistence of ilmenite and magnetite gives information on temperature and fO_2 of the rhyolitic magma(Spencer and Lindsley, 1981; Burton, 1984). The fO_2 is approximately 1 log unit below the HM buffer and temperature is as low as 700°C(Figure 4.92). The rhyolitic magma is thought to have had stable hornblende, biotite, quartz, plagioclase, sanidine, titanite and Ti-rich magnetite, all of which are required to use the geobarometer based on the Al content of hornblende(Johnson and Rutherford, 1989). The estimated pressure ranges from 3.02 to 3.62 kbar.

Coexisting magnetite-ilmenite pairs which are in equilibrium were used as an oxide thermometer following the method of Anderson and Lindsley(1985). Fe-Ti oxide grains give a temperature range between 841°C and 850°C, and a fO_2 between 2.21 and 2.29 relative to FMQ buffer. It is significant that temperatures obtained from magnetite-ilmenite pairs are

relatively high, compared to those of feldspars in equilibrium and they presumably record different stages in the cooling history.

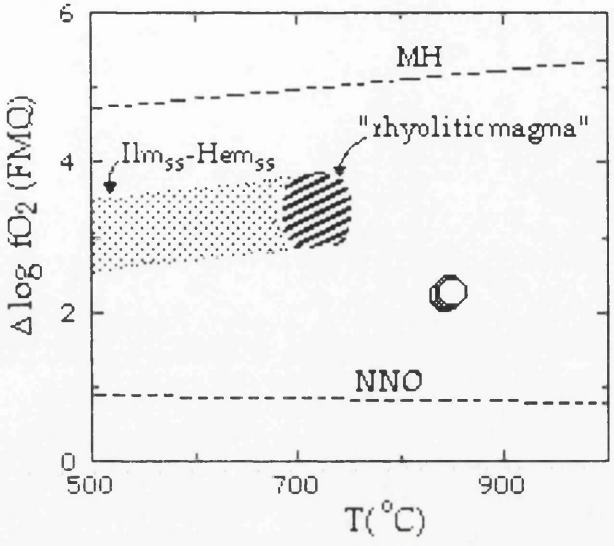

Figure 4.92. Oxygen fugacity relative to FMQ(Δlog fO_2) plotted against temperature for the rhyolite dykes. The field labelled Ilm_{ss}-Hem_{ss} represents the coexisting ilmenite and hematite solid solutions(Spencer and Lindsley, 1981).

Temperatures deduced from the compositions of Ti-rich magnetite and ilmenite in the rhyolite dykes are 841-850°C at an fO_2 of approximately 2 log units above the Ni-NiO buffer(Figure 4.92). These temperatures are higher than those estimated for the rhyolitic magma. Because the Fe-Ti oxide minerals are the most sensitive to physiochemical change(Bacon and Hirschmann, 1988), it is possible that the Ti-rich magnetite changed composition following magma mixing. Thus, those temperatures and fO_2 values may represent those of the mixed magmas.

It would be expected that heating of the rhyolitic magma during mixing with a mafic hot magma may cause rhyolitic melt to be oversaturated in H_2O, because H_2O solubility in silicate melts decreases with increasing temperature(Burnham and Jahns, 1962). As a result, the melt may have vesiculated and expanded during mixing and eruption.

Table 4.64. Representative analyses of feldspars in the rhyolite dome and dykes.

Sample	MA-38	MA-38	MA-38	MA-38	MA-38	MA-38	MA-31A	MA-31A	MA-31A	MA-62	MA-62
	Plag. mega core	San. mega rim	Plag. Pheno	San. Pheno	Plag mega core	Plag. mega rim	San. Pheno	Plag Pheno	Plag. micro -lite	Plag mega core	San. mega rim
SiO_2	62.05	64.53	62.03	65.49	55.24	61.75	65.16	57.09	61.79	61.43	64.91
TiO_2	0.00	0.16	0.02	0.11	0.10	0.02	0.02	0.07	0.03	0.00	0.19
Al_2O_3	22.26	18.74	22.86	19.03	27.40	23.02	18.73	26.37	23.08	22.98	19.28
FeO*	0.29	0.17	0.27	0.14	0.24	0.22	0.13	0.25	0.30	0.27	0.16
MnO	0.00	0.03	0.00	0.00	0.00	0.06	0.00	0.00	0.01	0.01	0.02
MgO	0.09	0.03	0.13	0.04	0.09	0.10	0.09	0.08	0.02	0.00	0.01
CaO	3.95	0.47	4.45	0.40	9.62	4.69	0.35	8.41	4.79	4.69	0.52
Na_2O	8.05	4.47	8.11	4.38	5.91	7.85	4.37	6.51	7.59	7.79	4.27
K_2O	1.63	9.93	1.40	10.07	0.44	1.31	10.19	0.51	1.29	1.08	9.83
P_2O_5	0.02	0.00	0.00	0.00	0.00	0.00	0.01	0.00	0.07	0.00	0.02
Cr_2O_3	0.06	0.00	0.01	0.04	0.00	0.00	0.01	0.00	0.00	0.07	0.00
NiO	0.08	0.01	0.00	0.00	0.00	0.00	0.00	0.01	0.00	0.03	0.00
Total	98.48	98.54	99.28	99.70	99.04	99.02	99.06	99.30	98.97	98.35	99.21
Formula on the basis of 32 oxygens											
Si	11.21	11.88	11.12	11.90	10.06	11.10	11.92	10.33	11.10	11.10	11.84
Ti	0.00	0.02	0.00	0.02	0.01	0.00	0.00	0.01	0.00	0.00	0.03
Al	4.74	4.07	4.83	4.07	5.88	4.87	4.04	5.62	4.89	4.90	4.15
Fe^{+2}	0.04	0.03	0.04	0.02	0.04	0.03	0.02	0.04	0.05	0.04	0.03
Mn	0.00	0.00	0.00	0.00	0.00	0.01	0.00	0.00	0.00	0.00	0.00
Mg	0.02	0.01	0.04	0.01	0.03	0.03	0.03	0.02	0.00	0.00	0.00
Ca	0.77	0.09	0.96	0.08	1.88	0.90	0.07	1.63	0.92	0.91	0.10
Na	2.83	1.59	2.82	1.54	2.09	2.73	1.55	2.28	2.64	2.73	1.51
K	0.38	2.33	0.32	2.33	0.10	0.30	2.38	0.12	0.30	0.25	2.29
P	0.00	0.00	0.00	0.00	0.00	0.00	0.00	0.00	0.01	0.00	0.00
Cr	0.01	0.00	0.00	0.01	0.00	0.00	0.00	0.00	0.00	0.00	0.00
Ni	0.00	0.00	0.00	0.00	0.00	0.00	0.00	0.00	0.00	0.01	0.00
Total	20.02	20.03	20.03	19.99	20.08	19.98	20.02	20.05	19.92	19.94	19.95
An	19.35	2.24	23.41	2.03	46.19	22.90	2.25	40.45	23.83	23.39	2.56
Ab	71.11	39.65	68.78	38.99	51.35	69.47	38.75	56.58	68.39	70.18	38.72
Or	9.54	58.11	7.81	58.98	2.46	7.63	59.50	2.97	7.78	6.43	58.72

FeO* is total iron as FeO.

Table 4.65. Representative analyses of clinopyroxenes in the rhyolite dykes.

Sample	MA-38B	MA-38B	MA-38B	MA-38B	MA-38B	MA-38B	MA-38B
	Pheno core	Pheno mid	Pheno rim	Pheno core	Pheno rim	Microphe.	Microphe.
SiO_2	52.20	52.28	52.55	51.87	51.87	52.37	51.41
TiO_2	0.28	0.26	0.17	0.13	0.24	0.21	0.13
Al_2O_3	0.84	0.70	0.67	0.56	0.68	0.64	0.93
FeO	8.71	8.52	8.41	8.46	8.34	8.61	8.21
MnO	0.97	0.90	1.04	0.96	0.96	0.84	1.00
MgO	14.29	14.18	13.89	13.69	14.26	13.87	13.91
CaO	21.00	21.59	21.56	21.33	21.51	21.56	21.00
Na_2O	0.69	0.78	0.56	0.32	0.50	0.58	0.89
K_2O	0.05	0.00	0.00	0.00	0.00	0.00	0.05
P_2O_5	0.00	0.00	0.00	0.04	0.03	0.00	0.00
Cr_2O_3	0.03	0.00	0.06	0.00	0.00	0.04	0.05
NiO	0.00	0.00	0.00	0.11	0.03	0.00	0.00
Total	99.06	99.21	98.91	97.47	98.42	98.72	97.58
Formula on the basis of 6 oxygens							
Si	1.96	1.95	1.98	1.99	1.96	1.97	1.95
Ti	0.01	0.01	0.00	0.00	0.01	0.01	0.00
Al	0.04	0.03	0.03	0.03	0.03	0.03	0.04
Fe^{+3}	0.09	0.10	0.05	0.02	0.07	0.05	0.11
Fe^{+2}	0.19	0.17	0.22	0.25	0.19	0.22	0.15
Mn	0.03	0.03	0.03	0.03	0.03	0.03	0.03
Mg	0.80	0.79	0.78	0.78	0.80	0.78	0.79
Ca	0.84	0.87	0.87	0.87	0.87	0.87	0.85
Na	0.05	0.06	0.04	0.02	0.04	0.04	0.07
K	0.00	0.00	0.00	0.00	0.00	0.00	0.00
P	0.00	0.00	0.00	0.00	0.01	0.00	0.00
Cr	0.00	0.00	0.00	0.00	0.00	0.00	0.00
Ni	0.00	0.00	0.00	0.00	0.01	0.00	0.00
Total	4.00	4.00	4.00	4.00	4.00	4.00	4.00
$Mg^{\#}$	0.74	0.75	0.74	0.74	0.75	0.74	0.75
Wo	43.35	44.36	44.67	44.69	44.25	44.70	44.17
En	41.03	40.52	40.03	39.89	40.80	39.99	40.69
Fs	15.62	15.12	15.30	15.42	14.95	15.31	15.14

Fe^{+3} is calculated by normalization acording to Schumacher(1991).
$Mg^{\#}=Mg/(Mg+Fe^{+3}+Fe^{+2})$

Table 4.66. Representative analyses of amphiboles in the rhyolite dykes.

Sample No	MA-62	MA-62	MA-62	MA-62	MA-62	MA-62
	Mag.-hornbl	Mag.-hornbl	Mag.-hornbl	Mag.-hornbl	Mag.-hornbl	Mag.-hornbl
	microphenо	microphenо	pheno core	pheno rim	microphenо	microphenо
SiO_2	48.45	49.12	48.76	47.94	48.45	47.95
TiO_2	1.29	1.16	1.36	1.41	1.32	1.29
Al_2O_3	5.19	4.74	5.46	5.54	4.93	5.21
FeO	11.55	10.84	11.27	11.55	11.43	11.57
MnO	0.62	0.63	0.53	0.49	0.56	0.60
MgO	15.98	15.96	15.98	15.65	16.08	15.79
CaO	11.25	11.24	11.18	11.06	11.24	11.20
Na_2O	1.63	1.37	1.80	1.61	1.51	1.67
K_2O	0.65	0.58	0.59	0.65	0.57	0.69
P_2O_5	0.00	0.06	0.09	0.00	0.00	0.12
Cr_2O_3	0.01	0.00	0.08	0.00	0.03	0.00
NiO	0.00	0.03	0.03	0.08	0.00	0.02
Total	96.59	95.73	97.13	95.98	96.12	96.11
Formula on the basis of 23 oxygens						
Si	7.13	7.23	7.11	7.09	7.16	7.11
Al4	0.87	0.77	0.89	0.91	0.84	0.89
AlT	0.90	0.82	0.94	0.97	0.86	0.91
Al6	0.03	0.06	0.05	0.05	0.02	0.03
Ti	0.14	0.13	0.15	0.16	0.15	0.14
Fe^{+3}	0.12	0.26	0.24	0.23	0.08	0.10
Mg	3.50	3.50	3.47	3.44	3.54	3.49
Fe^{+2}	1.30	1.07	1.13	1.19	1.33	1.33
Mn	0.08	0.08	0.07	0.06	0.07	0.08
FMT	13.17	13.10	13.12	13.14	13.19	13.17
Ca	1.77	1.77	1.75	1.75	1.78	1.78
NaM4	0.05	0.13	0.14	0.10	0.03	0.05
NaT	0.47	0.39	0.51	0.46	0.43	0.48
NaA	0.40	0.25	0.35	0.34	0.39	0.42
K	0.12	0.11	0.11	0.12	0.11	0.13
SumA	0.52	0.35	0.46	0.46	0.50	0.55
$Mg^{\#}$	0.71	0.72	0.72	0.71	0.71	0.71

Fe^{+3} is calculated by estimation according to Spear and Kimball(1984).
$Mg^{\#}=Mg/(Mg+Fe^{+3}+Fe^{+2})$

Table 4.67. Representative analyses of biotites in the rhyolite dome and dykes.

Sample	MA-31A Pheno core	MA-31A Pheno rim	MA-31A Pheno opaque	MA-31A Pheno core	MA-38B Micro	MA-38B Pheno core	MA-38B Pheno rim	MA-38B Micro	MA-38B Micro	MA-62 Pheno core
SiO_2	37.54	37.63	38.16	37.46	37.25	36.80	38.05	37.96	37.59	37.99
TiO_2	4.89	4.97	4.79	4.85	5.35	5.47	4.85	5.07	4.95	4.92
Al_2O_3	12.33	12.34	12.41	12.29	12.71	13.05	12.48	12.71	12.50	14.07
Fe_2O_3	2.12	2.21	2.19	2.19	2.26	2.28	2.21	2.28	2.56	2.29
FeO	10.79	11.26	11.18	11.16	11.51	11.62	11.26	11.65	11.51	11.69
MnO	0.25	0.26	0.27	0.21	0.27	0.29	0.25	0.27	0.21	0.32
MgO	15.84	15.29	15.97	15.86	15.55	15.46	16.08	16.30	16.06	13.86
CaO	0.20	0.26	0.13	0.12	0.00	0.04	0.00	0.03	0.04	0.04
Na_2O	1.16	1.14	0.78	1.06	1.02	0.66	0.78	0.94	0.72	0.62
K_2O	8.73	8.76	8.80	8.97	9.01	8.71	9.05	9.08	8.84	8.35
P_2O_5	0.00	0.00	0.00	0.09	0.00	0.02	0.00	0.00	0.00	0.00
Cr_2O_3	0.00	0.00	0.03	0.06	0.04	0.00	0.05	0.00	0.04	0.01
NiO	0.00	0.01	0.00	0.07	0.01	0.12	0.00	0.01	0.00	0.08
Total	93.85	94.13	94.71	94.39	94.98	94.52	95.06	96.30	95.02	94.24
Formula on the basis of 22 oxygens										
Si	5.64	5.65	5.68	5.62	5.56	5.51	5.65	5.58	5.61	5.66
Ti	0.55	0.56	0.54	0.55	0.60	0.62	0.54	0.56	0.56	0.55
Al	2.19	2.19	2.18	2.17	2.24	2.31	2.19	2.20	2.20	2.47
Fe^{+3}	0.24	0.25	0.25	0.25	0.25	0.26	0.25	0.25	0.25	0.26
Fe^{+2}	1.36	1.41	1.39	1.40	1.44	1.46	1.40	1.43	1.44	1.46
Mn	0.03	0.03	0.04	0.03	0.04	0.04	0.03	0.03	0.03	0.04
Mg	3.55	3.42	3.54	3.54	3.46	3.45	3.56	3.57	3.57	3.08
Ca	0.03	0.04	0.02	0.02	0.00	0.01	0.00	0.01	0.01	0.01
Na	0.34	0.33	0.23	0.31	0.29	0.19	0.22	0.27	0.21	0.18
K	1.67	1.68	1.67	1.72	1.72	1.67	1.71	1.71	1.68	1.59
P	0.00	0.00	0.00	0.01	0.00	0.00	0.00	0.00	0.00	0.00
Cr	0.00	0.00	0.00	0.01	0.01	0.00	0.01	0.00	0.00	0.00
Ni	0.00	0.00	0.00	0.01	0.00	0.01	0.00	0.00	0.00	0.01
Total	15.60	15.57	15.52	15.62	15.60	15.52	15.56	15.62	15.55	15.30
$Mg^{\#}$	0.69	0.67	0.68	0.68	0.67	0.67	0.68	0.68	0.68	0.64
Phlog.	59.13	57.05	59.02	59.05	57.67	57.55	59.32	59.52	59.53	51.30
Annite	22.60	23.57	23.18	23.32	23.95	24.27	23.32	23.87	23.93	24.28

Fe^{+3} is calculated by ratio according to Schumacher(1991).
$Mg^{\#}=Mg/(Mg+Fe+3+Fe+2)$

Table 4.68. Representative analyses of Fe-Ti oxides in the rhyolite dome and dykes.

Sample	MA-38B	MA-38B	MA-38B Inc. in bio	MA-31A	MA-31A	MA-31A	MA-62	MA-62
	Magnetite	Magnetite	Ilmenite	Ilmenite	Ilmenite	Ilmenite	Ilmenite	Ilmenite
SiO_2	0.31	0.21	0.24	0.26	0.13	0.28	0.16	0.30
TiO_2	6.39	6.36	38.29	39.61	39.40	39.72	40.02	40.23
Al_2O_3	1.16	1.26	0.14	0.25	0.11	0.20	0.13	0.16
FeO	84.27	83.72	54.77	54.50	54.77	55.15	54.40	54.66
MnO	0.90	0.97	1.23	1.21	1.83	1.26	1.31	1.26
MgO	1.28	1.28	2.00	1.88	1.27	1.97	1.76	1.70
CaO	0.03	0.02	0.04	0.03	0.08	0.00	0.01	0.03
Na_2O	0.24	0.34	0.07	0.35	0.25	0.32	0.02	0.16
K_2O	0.00	0.03	0.13	0.02	0.03	0.07	0.02	0.00
P_2O_5	0.01	0.03	0.00	0.00	0.01	0.00	0.00	0.00
Cr_2O_3	0.07	0.00	0.04	0.04	0.00	0.02	0.00	0.00
NiO	0.10	0.00	0.00	0.03	0.00	0.05	0.06	0.01
Total	94.76	94.22	96.95	98.18	97.88	99.04	97.89	98.51
Formula on the basis of 32 oxygens for magnetites and 6 oxygens for ilmenites								
Si	0.01	0.01	0.01	0.01	0.00	0.01	0.00	0.01
Ti	0.18	0.18	0.73	0.73	0.74	0.74	0.75	0.75
Al	0.05	0.06	0.00	0.01	0.00	0.01	0.00	0.00
Fe^{+3}	1.58	1.59	0.54	0.53	0.52	0.53	0.48	0.48
Fe^{+2}	1.05	1.03	0.61	0.61	0.63	0.61	0.66	0.65
Mn	0.03	0.03	0.03	0.03	0.04	0.03	0.03	0.03
Mg	0.07	0.07	0.08	0.07	0.05	0.07	0.07	0.06
Ca	0.00	0.00	0.00	0.00	0.00	0.00	0.00	0.00
Na	0.02	0.02	0.00	0.01	0.01	0.02	0.00	0.01
K	0.00	0.00	0.00	0.01	0.00	0.00	0.00	0.00
P	0.00	0.00	0.00	0.00	0.00	0.00	0.00	0.00
Cr	0.00	0.00	0.00	0.00	0.00	0.00	0.00	0.00
Ni	0.00	0.00	0.00	0.00	0.00	0.00	0.00	0.00
Total	3.00	3.00	2.00	2.00	2.00	2.00	2.00	2.00
Mn/Mg	0.43	0.43	0.38	0.43	0.80	0.43	0.43	0.50
sp	2.81	3.04						
mg-chr	0.11	0.00						
mg-fer	4.93	4.77						
trev	0.34	0.00						
mt	81.91	82.38						
usp	9.90	9.82						

Fe^{+3} is calculated by normalization according to Schumacher(1991).

4.11. PUMICE AND TUFF DEPOSITS

4.11.1. PETROGRAPHY

Pumice-tuff deposits range in thickness and distribution around Gurgurbaba. In general, the deposits thin and may disappear laterally within a few metres from the stream or paleostream channels, where they continue as thin beds mantling the topography(see chapter 3). The deposits consist of pale gray or cream pumice lapilli(80-90%), coarse ash and lithic clasts of volcanic rocks(10-20%). In general, the deposits are dominated by crystal-poor pumice clasts, and crystal-rich lithic clasts. Crystals in the pumice are predominantly plagioclase with some alkali feldspar, amphibole, biotite, pyroxene, ilmenite and magnetite. The deposit weathers yellowish and has up to 1 m of brown soil on top. In some places, small tuff surge deposits(fine-grained wavy or cross-bedded) occur at the upper stratigraphic level. Pumice beds drape underlying terrain and exhibit planar-beds and no flowage structures. All tephra units consist of poorly sorted lapilli and within the grain-size field of tephra-fall deposits as described by Walker(1971).

Pumice pyroclasts are equant to elongate and have sharp, angular surfaces. Most have 30% to 50% vesicles; vesicles are highly elongate. Rare pumice clasts are crowded with spherical vesicles. All pumices consist of aphyric glass and lack of phenocrysts(feldspar, biotite and pyroxene), indicating rapid rise of magma along fissures. Vesicle shapes range from spherical to highly elongate. Pumice pyroclasts may have parallel vesicles. Vesicles appear to have formed prior to eruption and were stretched during flow, parallel to fissure wall. Factors which controlled the pumice formation include (a) duration of magma explosion and cycles, (b) magma temperature, (c) gas content of magma, and (d) cooling duration.

4.11.2. GRAINSIZE DISTRIBUTION

Granulometric analyses were used as the main source of data to examine the grainsize variations in pumice-tuff deposits, following the method of Walker(1971). For this purpose, four samples from two localities were sieved.

From the raw grainsize data(Table 4.69), cumulative curves of the grainsize distribution were constructed(Figure 4.93), and the following determined(Table 4.70): Inman(1952) parameters of median diameter $Md\phi$; graphical standard deviation $G\phi$; which is a measure of sorting; and first order skewness $X\phi$; which is a measure of the assymetry of the distribution(Walker, 1971; Sparks, 1976; Cas and Wright, 1987).

On the gransize distribution plots(Figure 4.94), the samples show features of both pyroclastic fall(232A, 232B, 234A) and surge deposit(234B). The fall deposits are well to very well sorted($G\varnothing$ <2), and distinctively unimodal having a high proportion of pumice clasts. The surge deposit is also unimodal and very well sorted($G\varnothing$ <1), but the distribution has an extended coarse tail, or is negatively skewed(Figures 4.94 and 4.95).

Table 4.69. Details of sieve analyses of four samples from pumice-tuff deposits. The samples are as bottom and upper levels from two different localities. These data are used as a basis for the graphical analysis of the size distributions shown in Figures 4.93, 4.94 and 4.95.

Grain size		Unit- A				Unit- B			
		232B	(Bottom)	232A	(Upper)	234A	(Bottom)	234B	(Upper)
(mm)	(Ø)	wt.%	Cumul. wt.%	wt.%	Cumul. wt.%	wt.%	Cumul. wt.%	wt.%	Cumul. wt.%
>16	>-4	29.25	29.25			2.99	2.99		
>8	>-3	13.28	42.53	1.33	1.33	13.10	16.09		
>4	>-2	12.39	54.92	5.08	6.41	23.08	39.17		
>2	>-1	16.86	71.78	22.02	28.43	41.14	80.31	0.54	0.54
>1	> 0	10.04	81.82	31.48	59.91	15.36	95.67	1.34	1.88
>0.5	> 1	6.06	87.88	15.81	75.72	3.65	99.32	3.47	5.35
>0.25	> 2	3.88	91.76	8.68	84.40	0.04	99.36	23.25	28.60
>0.125	> 3	3.39	95.15	13.19	97.59	0.04	99.40	62.07	90.67
>0.0625	> 4	1.89	97.04	0.77	98.36	0.17	99.57	9.16	99.83
<0.0625	< 4	2.96	100.00	1.64	100.00	0.43	100.00	0.17	100.00

Table 4.70. Grainsize parameters for samples, derived graphically from the cumulative curves in Figure 4.93.

Inman parameter	232B	232A	234A	234B
MdØ	-2.40	-0.34	-1.78	2.29
GØ	0.15	1.72	1.10	0.61
XØ	17.93	0.48	-1.95	3.38

Note: $Md\emptyset(median\ diameter)=\emptyset_{50}$

$G\emptyset(graphical\ standard\ deviation)=(\emptyset_{84}-\emptyset_{16})/2$

$X\emptyset(first\ order\ skewness)=((\emptyset_{84}+\emptyset_{16})-Md\emptyset))/G\emptyset$

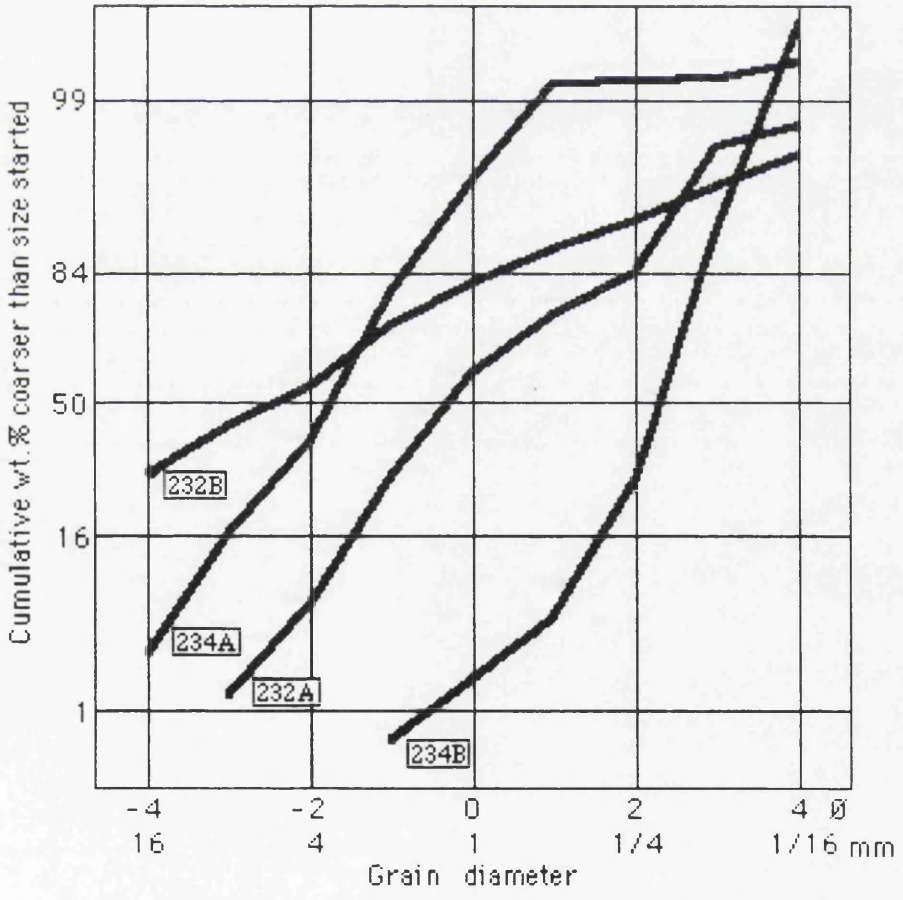

Figure 4.93. Graphical representation of grainsize analyses from samples of pumice-tuff deposits in Table 4.69. Cumulative plot on probability ordinate. The 16th, 50th and 84th percentiles are drawn, their intersection with the grain size distribution curves gives the grain diameters used to derive the Inman parameters in Table 4.70.

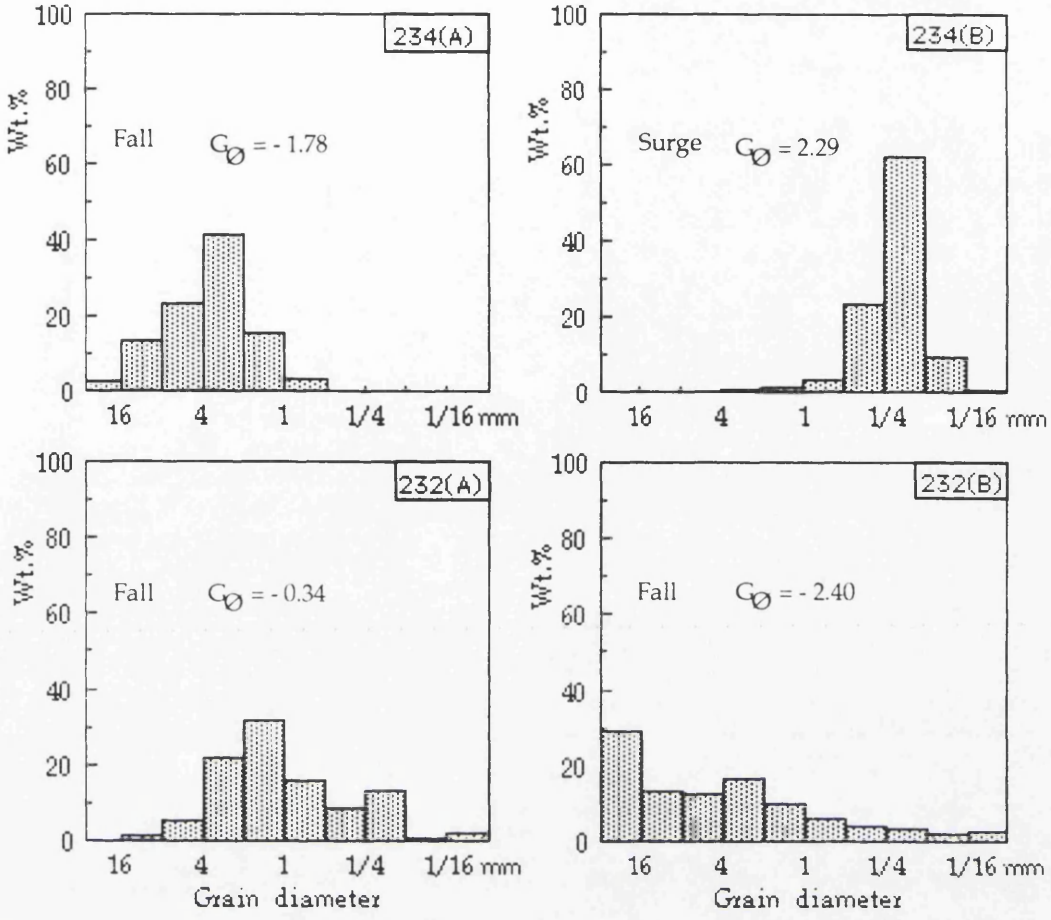

Figure 4.94. Histograms for grainsize distribution in pumice-tuff deposits. The deposits reflect both pyroclastic fall and surge features.

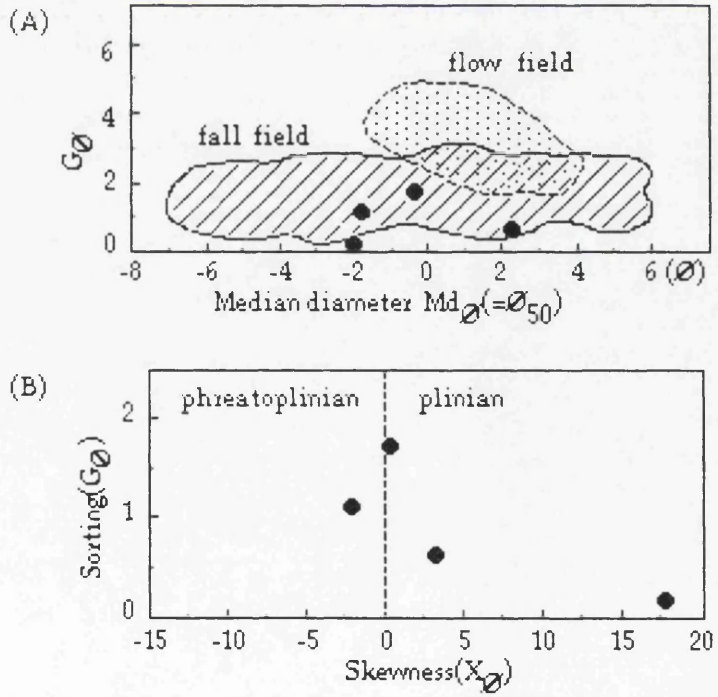

Figure 4.95. Grainsize characteristics of pumice-tuff deposits: (A), Mdø versus Gø plot. Pyroclastic fall and flow fields are from Walker(1971) and Walker *et al.* (1980); (B), plot of skewness(Xø) against sorting(Gø). Dividing line is from Sparks *et al.* (1981).

4.12. GURGURBABA LAVA

4.12.1. PETROGRAPHY

The Gurgurbaba lava is highly variable from grey-black to reddish brown obsidians-perlites, and from partially crystalline to hypocrystalline rocks. The more crystalline varieties are dense and poorly vesicular or perlitic.

Hypocrystalline varieties exhibit different texture and mineralogical compositions. They are generally porphyritic with about 15% phenocrysts and consist of sanidine, rare anorthoclase, plagioclase(labradorite to andesine), brown amphibole, biotite phenocrysts, and microphenocrysts of quartz, augite, orthopyroxene and opaque oxides. In addition, accessory iddingsite, zircon and apatite are present. Phenocrysts have regular crystal forms representing the slow and measured growth from slightly undercooled magma before it was finally emplaced. These pheno- and microphenocrysts are set in a partially glassy groundmass.

Hyalocrystalline types show different features of glassy rocks and their devitrification products. They exhibit spherulitic texture and continuous lamination of glassy bands. In some cases, they show well developed flow foliation consisting of alternating submillimetre scale bands of crystal-rich and crystal-free bands. The crystal rich bands contain quartz and feldspar crystals as well as numerous angular vesicles which are absent from the aphyric bands. The vesicles constitute up to 20% of the volume of the bands. Spherulites are most commonly less-densely packed and include mainly fibrous crystals of alkali feldspar and rarely quartz. In this texture, the crystalline material radiates outwards in all directions from a focus of nucleation as an aggregate of acicular branches. Two phases are evident in these aggregates. The outer ends of some coarse spherulitic growths consist of an extremely fine-grained pattern of interconnected quartz grains set in a single feldspar host, a fine-grained example of granophyric intergrowth. Spaces between large spherulites are filled by microcrystalline quartz.

Perlites show characteristic perlitic, or spongy-onion skin like textures with a glassy mass. They may also contain sanidine, plagioclase, biotite, amphibole and rare quartz crystals from 10% up to 40% within glassy matrix.

Alkali feldspars both sanidine and rare anorthoclase are subhedral and exhibit common alteration products such as sericite and clay. They contain inclusions of biotite. They also reveal corona texture but generally the original texture of the crystal is preserved. Some of the large crystals include quartz intergrowths with granophyric texture(e.g., Lofgren, 1971; Smith and Brown, 1988; Swanson *et al.*, 1989), and indicate rapid cooling

and freezing. The intergrowths appear as radiating or branching interconnected quartz grains. The quartz grains are angular or triangular in section.

Plagioclase phenocrysts are subhedral and commonly show sieve texture around rims or throughout entire crystals. They may also show normal zoning and albite twining. Some of them contain abundant glass inclusions giving the crystal a sponge-like texture. Some of the sieve textured crystals may have thin overgrown rims.

Quartz is present commonly as aggregates formed of fine grains and rarely as embayed crystals indicating a disequilibrium growth form or a solution effect due to decrease in pressure as magma rose to the surface. They also form clusters of interlocking fine grains as lenses or thin veins.

Pyroxenes both cpx and opx are subhedral and form aggregates with feldspars. Generally, opx is common.

Biotite forms subhedral elongated crystals. They are also present as crowded with opaque reaction products, mainly along the cleavages. Some phenocrysts of biotite have fine grained opaque oxides around the rim of the crystal. Brown amphibole is subhedral and coexists with a few biotites showing alteration into opaques. Accessory zircon is generally associated with biotite and, or opaque oxides.

In crystalline types, the groundmass contains mainly sanidine and plagioclase laths and acicular crystals in a glassy matrix. The groundmass occasionally shows hyalopolitic or fluidal texture.

4.12.2. ORIGIN OF DIFFERENT TEXTURES

Most silicic magma bodies are believed to be stratified with respect to volatiles(Kennedy, 1955; Smith, 1979; Hildreth, 1981; Blake, 1981; Sparks *et al.*, 1984). In addition, silicic lavas are characterized by a wide range of surface textures that vary in vesicularity, crystallinity, colour, and flow layering. The origin of these differences has generally been attributed to local chemical inhomogeneities, particularly with respect to volatile content.

Fink and Manley(1987) suggested three principal steps for the development of these textures in silicic lavas; (1) crystallization within the flow releases dissolved magmatic volatiles, (2) advance of the lava forms microcracks through which these gases can move upward, (3) cooling of the upper surface increases the yield strength and creates a nondeforming crust through which the rising gases are unable to migrate, and crystallization appears to be controlled by the ability of ions to migrate and this occurs preferentially in the central parts of flow where maintance of higher temperature and lower viscosites allows more rapid diffusion

4.12.3. MINERAL CHEMISTRY

4.12.3.1. FELDSPAR

The feldspar in the Gurgurbaba lava is mainly andesine An38-50, sanidine and minor labradorite An_{51-67}(Figure 4.96). Representative analyses are given in Table 4.71.

Phenocrysts of feldspar are generally andesine showing normal zoning. They have a composition from An_{45-46} in the core varying to An_{41-43} in the rim, or An_{50} in the core changing to An_{38} in the rim. Some phenocrysts of labradorite (An_{51}) are also present.

Microlites are labradorite with a composition from An_{62} up to An_{67}, and some andesine(An_{48-49}).

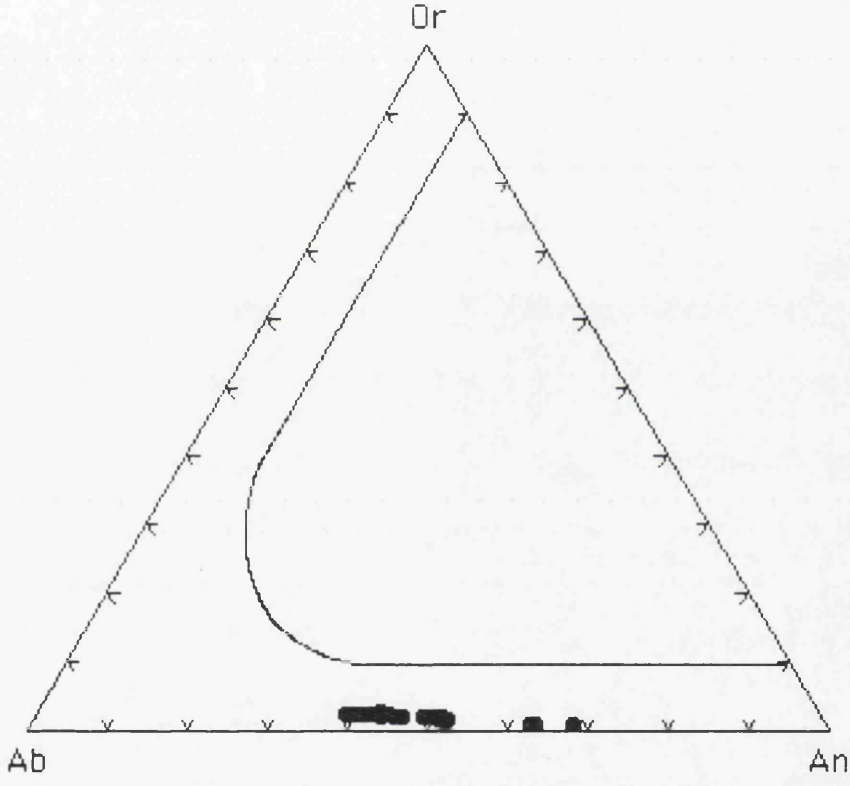

Figure 4.96. Or-Ab-An diagram of feldspars in the Gurgurbaba rhyolites.

4.12.3.2. PYROXENE

Pyroxenes in the Gurgurbaba lava are rare augite and common orthopyroxene(Figure 4.97), according to the classification of Morimoto *et al.* (1988). Both pyroxenes have homogeneous compositions. Representative compositions are presented in Table 4.72.

Augites show a composition ranging from $Wo_{36}En_{48}Fs_{16}$ to $Wo_{44}En_{44}Fs_{12}$, and a $Mg/(Mg+Fe^{+3}+Fe^{+2})$ ratio from 0.76 to 0.79. They are typically Ti-poor types with a TiO_2 content from 0.33 to 0.46 wt.% that is characteristic feature for subalkaline rocks(Kushiro, 1960; Le Bas, 1962). Al_2O_3 content ranges from 2.42 to 3.88 wt.%(0.11-0.17 per formula unit).

MnO is between 0.10 and 0.35 wt.%, and Na_2O is between 0.2 and 0.3 wt.%. Generally, Cr_2O_3 and NiO contents are very low but some of them are chromian augite(Cr_2O_3=0.30 wt.%).

Orthopyroxenes have a composition ranging from $Wo_1En_{77}Fs_{22}$ to $Wo_3En_{70}Fs_{27}$, and a $Mg/(Mg+Fe^{+3}+Fe^{+2})$ ratio from 0.73 up to 0.78. They have TiO_2 between 0.17 and 0.40 wt.%, Al_2O_3 between 1.23 and 4.45 wt.%(Figure 4.98), MnO between 0.28 and 0.62 wt.%, and Na_2O from 0.02 to 0.32 wt.%. Trace element contents are very low.

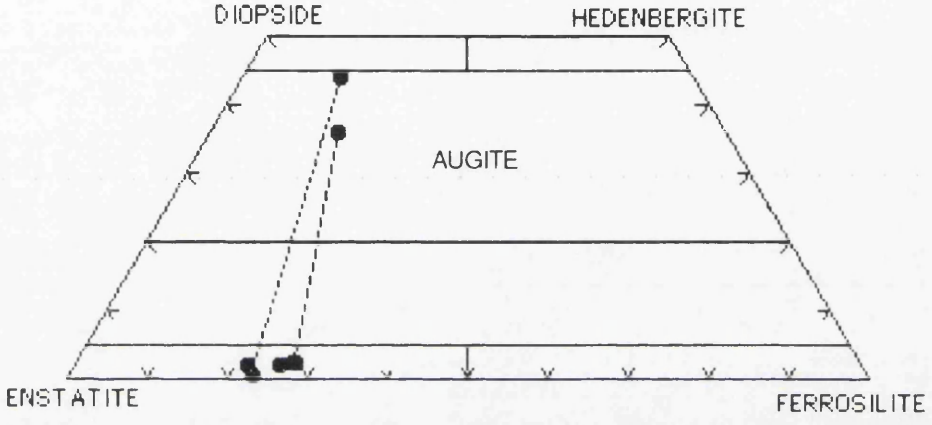

Figure 4.97. Pyroxene nomenclature of the Gurgurbaba lava on the Wo-En-Fs plot(Morimoto *et al.*, 1988). Tie lines intersect Wo-En join at about Wo_{92} and Wo_{98}.

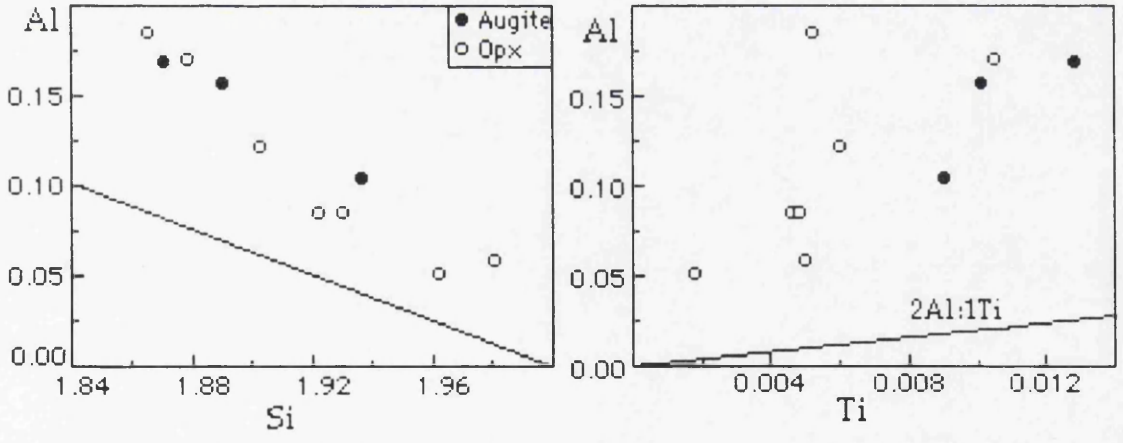

Figure 4.98. Plots of Al versus Si and Ti contents per formula unit of clinopyroxenes and orthopyroxenes in the Gurgurbaba lava.

4.12.3.3. AMPHIBOLE

Calcic amphiboles occur in the Gurgurbaba lava. They are magnesio-hastingsitic hornblende and magnesio-hornblende(Figure 4.99), according to the classification of Leake(1978). Representative analyses are given in Table 4.73.

Magnesio-hornblende has a $Mg/(Mg+Fe^{+3}+Fe^{+2})$ ratio 0.70 and a Ti content 0.24 per formula unit. It has a total Al content 1.39, Mn content 0.03, total Na content 0.49 in the formula units. Si content is 6.79 per formula unit.

Magnesio-hastingsitic hornblende has a $Mg/(Mg+Fe^{+3}+Fe^{+2})$ ratio 0.65, and a Ti content 0.25 per formula unit which reveals the mineral titanian. Al content is about 0.29, Mn content about 0.02 and Na content 0.73 per formula unit. Si content is 6.29 per formula unit.

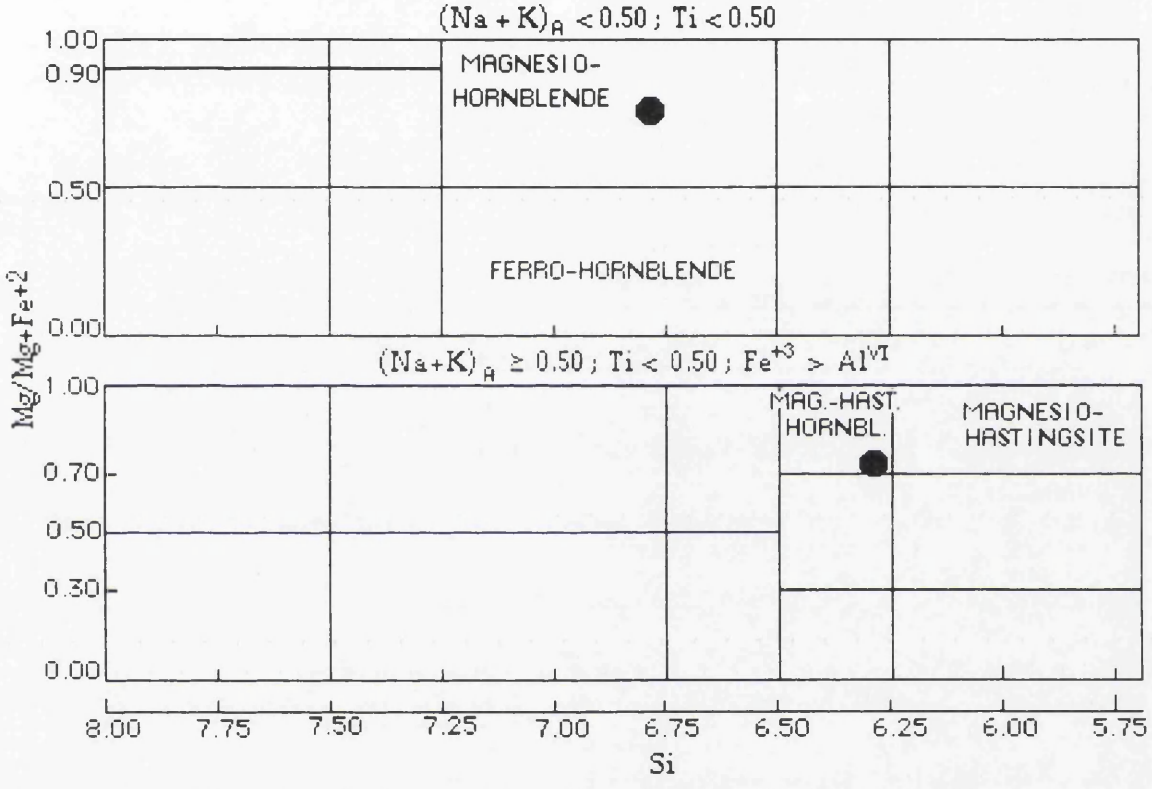

Figure 4.99. The classification and nomenclature of calcic amphiboles in the Gurgurbaba lava, according to Leake(1978).

4.12.3.4. BIOTITE

In the Gurgurbaba lava, phlogopite-annite rich types biotites are present(Figure 4.100), with an end member composition between phlogopite(49-56) and annite(30-18). Representative analyses are presented in Table 4.74.

Biotites have a $Mg/(Mg+Fe^{+3}+Fe^{+2})$ ratio ranging from 0.58 to 0.72. They are relatively Fe-rich, compared to those of the rhyolite dome and dykes. Biotites have also a TiO_2 content from 4.72 up to 6.84 wt.%, and 0.52 to 0.75 per formula units. They have MnO(0.20 to 0.30 wt.%), and Na_2O(0.51 up to 1 wt.%). Cr_2O_3 and NiO contents are insignificant.

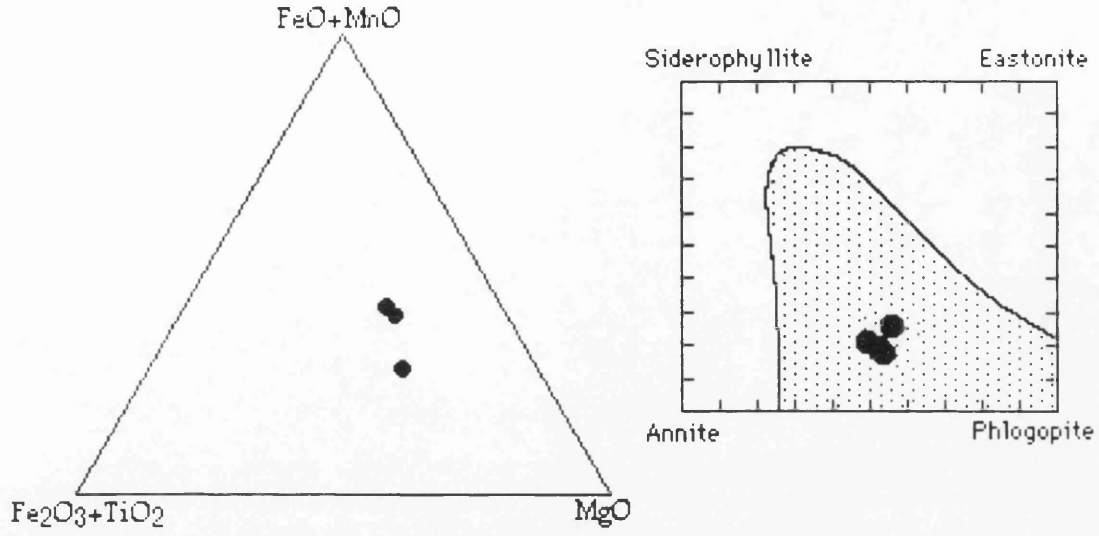

Figure 4.100. Compositional variations and the principal components of biotite compositions in the Gurgurbaba lava. The shaded area in which most natural biotites lie is from Deer *et al.* (1992).

4.12.3.5. FE-TI OXIDES

Magnetites are the main oxide minerals in the Gurgurbaba lava. They have homogeneous compositions. Representative analyses are given in Table 4.75.

Generally, magnetites are Ti-poor types with TiO_2 ranging from 4 up to 6 wt.%. They have a Al_2O_3 varying from 1.63 to 4.72 wt.%, MnO(0.35-0.45 wt.%), MgO(1.72-2.57 wt.%), and Na_2O(0.06-0.38 wt.%). Cr_2O_3 ranges between 0.15 and 0.25 wt.%, and NiO is zero to 0.18 wt.%.

4.12.4. GEOTHERMOMETRY

In the Gurgurbaba lava, coexisting augite and orthopyroxene provide a useful two pyroxene thermometer. Microphenocrysts of two pyroxenes were used according to method of Kretz(1982). Coexisting two pyroxenes gave a solvus temperature between 1032°C and 1196°C(Table 4.76).

Table 4.76. Coexisting pyroxene compositions and calculated solvus temperatures, according to the method of Kretz(1982).

	Opx	Augite	Opx	Augite	Opx	Augite	Opx	Augite
Wo	0.027	0.357	0.023	0.433	0.07	0.360	0.025	0.423
En	0.708	0.489	0.725	0.449	0.773	0.480	0.756	0.446
Fs	0.242	0.154	0.232	0.117	0.203	0.156	0.206	0.130
T(°C)	1196		1032		1180		1053	

Table 4.71. Representative analyses of feldspars in the Gurgurbaba lava.

Sample	MA-58A	MA-58A	MA-58A	MA-58A	MA-58A	MA-58A	MA-58A	MA-58A	MA-58A	MA-58A
	Micro-pheno	Micro-lite	Micro-pheno	Micro-lite	Pheno core	Pheno rim	Mega core	Mega rim	Pheno core	Pheno rim
SiO_2	54.89	50.96	58.32	56.00	56.31	57.82	57.05	57.34	55.45	58.46
TiO_2	0.00	0.00	0.03	0.10	0.06	0.01	0.03	0.04	0.00	0.01
Al_2O_3	28.08	30.74	26.44	27.06	26.90	26.77	27.32	26.69	28.30	26.04
FeO*	0.23	0.41	0.24	0.29	0.28	0.29	0.28	0.22	0.32	0.28
MnO	0.00	0.04	0.00	0.06	0.00	0.02	0.03	0.02	0.00	0.00
MgO	0.05	0.09	0.15	0.00	0.15	0.01	0.08	0.00	0.05	0.14
CaO	10.67	13.65	8.39	9.72	9.13	8.67	9.26	8.23	10.35	8.05
Na_2O	5.35	3.50	6.75	5.54	6.39	6.13	6.06	5.97	5.43	6.89
K_2O	0.35	0.21	0.51	0.42	0.44	0.51	0.44	0.47	0.34	0.48
P_2O_5	0.00	0.00	0.00	0.00	0.00	0.09	0.00	0.00	0.00	0.00
Cr_2O_3	0.00	0.01	0.00	0.08	0.05	0.00	0.00	0.00	0.00	0.00
NiO	0.00	0.00	0.00	0.00	0.00	0.00	0.00	0.01	0.03	0.00
Total	99.62	99.61	100.83	99.27	99.71	100.32	100.55	98.99	100.27	100.35
Formula on the basis of 32 oxygens										
Si	9.95	9.32	10.38	10.16	10.18	10.33	10.20	10.33	9.98	10.44
Ti	0.00	0.00	0.0	0.01	0.01	0.00	0.00	0.01	0.00	0.00
Al	5.99	6.27	5.55	5.79	5.73	5.64	5.76	5.67	6.00	5.48
Fe^{+2}	0.04	0.06	0.04	0.04	0.04	0.04	0.04	0.03	0.05	0.04
Mn	0.00	0.01	0.00	0.01	0.00	0.00	0.01	0.00	0.00	0.00
Mg	0.01	0.02	0.04	0.00	0.04	0.00	0.02	0.00	0.01	0.04
Ca	2.07	2.67	1.60	1.89	1.77	1.66	1.77	1.70	1.99	1.54
Na	1.88	1.24	2.33	1.95	2.24	2.13	2.10	2.09	1.90	2.39
K	0.08	0.05	0.12	0.10	0.10	0.12	0.10	0.11	0.08	0.11
P	0.00	0.00	0.00	0.00	0.00	0.01	0.00	0.00	0.00	0.00
Cr	0.00	0.00	0.00	0.01	0.01	0.00	0.00	0.00	0.00	0.00
Ni	0.00	0.00	0.00	0.00	0.00	0.00	0.00	0.00	0.01	0.00
Total	20.03	20.01	20.05	19.95	20.12	19.93	20.01	19.93	20.01	20.04
An	51.36	67.43	39.51	47.97	43.07	42.46	44.58	43.59	50.13	38.12
Ab	46.65	31.31	57.53	49.49	54.50	54.48	52.90	53.59	47.86	59.16
Or	1.99	1.26	2.96	2.54	2.43	3.06	2.52	2.82	2.01	2.72

FeO* is total iron as FeO.

Table 4.72. Representative analyses of pyroxenes in the Gurgurbaba lava.

Sample	MA-58A	MA-58A	MA-58A	MA-58A	MA-58A	MA-58A	MA-58A	MA-58A
	Opx	Opx-core	Opx	Cpx	Cpx	Cpx	Opx	Opx
SiO_2	53.27	53.64	54.01	52.63	51.34	50.46	52.98	54.56
TiO_2	0.17	0.18	0.23	0.33	0.37	0.46	0.40	0.19
Al_2O_3	2.01	2.02	2.95	2.42	3.66	3.88	4.07	1.39
FeO*	16.87	16.21	13.73	9.47	7.12	7.42	14.25	16.50
MnO	0.62	0.33	0.28	0.35	0.10	0.29	0.52	0.60
MgO	25.58	26.49	28.30	16.93	15.28	15.30	28.15	25.26
CaO	1.41	1.23	1.27	17.79	21.22	20.91	0.36	1.39
Na_2O	0.32	0.18	0.15	0.20	0.31	0.31	0.02	0.17
K_2O	0.03	0.00	0.00	0.00	0.06	0.03	0.00	0.01
P_2O_5	0.00	0.00	0.00	0.00	0.06	0.02	0.00	0.00
Cr_2O_3	0.17	0.00	0.40	0.09	0.53	0.29	0.00	0.00
NiO	0.00	0.03	0.03	0.00	0.02	0.00	0.00	0.10
Total	100.45	100.31	101.35	100.21	100.07	99.37	100.75	100.17
Formula on the basis of 6 oxygens								
Si	1.92	1.93	1.90	1.94	1.89	1.87	1.88	1.98
Ti	0.01	0.01	0.01	0.01	0.01	0.01	0.01	0.01
Al	0.09	0.09	0.12	0.11	0.16	0.17	0.17	0.06
Fe^{+3}	0.08	0.06	0.06	0.02	0.04	0.08	0.05	0.00
Fe^{+2}	0.43	0.43	0.35	0.28	0.18	0.15	0.37	0.50
Mn	0.02	0.01	0.01	0.01	0.00	0.01	0.02	0.02
Mg	1.38	1.42	1.49	0.93	0.84	0.85	1.49	1.37
Ca	0.05	0.05	0.05	0.70	0.84	0.83	0.01	0.05
Na	0.02	0.01	0.01	0.01	0.02	0.02	0.00	0.01
K	0.00	0.00	0.00	0.00	0.00	0.00	0.00	0.00
P	0.00	0.00	0.00	0.00	0.00	0.00	0.00	0.00
Cr	0.00	0.00	0.01	0.00	0.01	0.01	0.00	0.00
Ni	0.00	0.00	0.00	0.00	0.00	0.00	0.00	0.00
Total	4.00	4.00	4.00	4.00	4.00	4.00	4.00	4.00
$Mg^{\#}$	0.73	0.74	0.78	0.76	0.79	0.79	0.78	0.73
Wo	2.79	2.41	2.46	36.31	44.11	43.36	0.70	2.78
En	70.26	72.26	76.33	48.04	44.18	44.15	76.71	70.45
Fs	26.95	25.33	21.21	15.65	11.71	12.49	22.59	26.77

Fe^{+3} is calculated by normalization according to Schumacher(1991).
$Mg^{\#}=Mg/(Mg+Fe^{+3}+Fe^{+2})$

Table 4.73. Representative analyses of amphiboles in the Gurgurbaba lava.

Sample No	MA-58A Magnesio-hastingsitic hornblende	MA-58A Magnesio-hornblende
SiO_2	41.09	46.92
TiO_2	2.14	2.19
Al_2O_3	11.07	8.15
FeO*	12.33	11.57
MnO	0.19	0.21
MgO	13.11	15.11
CaO	10.55	11.35
Na_2O	2.47	1.75
K_2O	0.71	0.61
P_2O_5	0.00	0.06
Cr_2O_3	0.00	0.04
NiO	0.13	0.04
Total	93.74	98.00
Formula on the basis of 23 oxygens		
Si	6.29	6.79
Al4	1.71	1.21
AlT	1.99	1.39
Al6	0.29	0.18
Ti	0.25	0.24
Fe^{+3}	0.39	0.29
Mg	2.99	3.26
Fe^{+2}	1.18	1.11
Mn	0.02	0.03
FMT	13.13	13.10
Ca	1.73	1.76
NaM4	0.14	0.14
NaT	0.73	0.49
NaA	0.57	0.33
K	0.14	0.11
SumA	0.71	0.44
$Mg^{\#}$	0.73	0.76

Fe^{+3} is calculated by estimation according to Spear and Kimball(1984).
$Mg^{\#}=Mg/(Mg+Fe^{+2})$

Table 4.74. Representative analyses of biotites in the Gurgurbaba lava.

Sample No	MA-58A	MA-58A	MA-58A	MA-58A
	Microphenо	Microphenо	Microphenо	Microphenо
SiO_2	37.30	35.98	37.29	36.31
TiO_2	4.72	6.84	4.75	4.79
Al_2O_3	14.21	15.41	13.76	13.66
Fe_2O_3	2.81	1.87	2.69	2.69
FeO	14.35	9.55	13.71	13.71
MnO	0.30	0.02	0.20	0.27
MgO	14.35	16.28	14.13	14.35
CaO	0.05	0.00	0.00	0.01
Na_2O	0.51	1.30	0.69	0.71
K_2O	8.98	7.90	8.97	9.02
P_2O_5	0.00	0.00	0.00	0.00
Cr_2O_3	0.00	0.00	0.00	0.00
NiO	0.12	0.02	0.06	0.09
Total	97.70	95.17	96.25	95.52
Formula on the basis of 22 oxygens				
Si	5.26	5.27	5.53	5.45
Ti	0.53	0.75	0.53	0.54
Al	2.48	2.66	2.41	2.42
Fe^{+3}	0.31	0.21	0.30	0.30
Fe^{+2}	1.78	1.17	1.70	1.72
Mn	0.04	0.00	0.03	0.03
Mg	2.95	3.55	3.13	3.21
Ca	0.01	0.00	0.00	0.00
Na	0.15	0.37	0.20	0.21
K	1.70	1.48	1.70	1.73
P	0.00	0.00	0.00	0.00
Cr	0.00	0.00	0.00	0.00
Ni	0.01	0.00	0.01	0.01
Total	15.47	15.47	15.53	15.62
$Mg^{\#}$	0.59	0.72	0.61	0.61
Phlogopite	49.12	55.56	52.10	53.50
Annite	29.62	18.29	28.37	28.68

Fe^{+3} is calculated by ratio according to Schumacher(1991).
$Mg^{\#}=Mg/(Mg+Fe^{+3}+Fe^{+2})$

Table 4.75. Representative analyses of Fe-Ti oxides in the Gurgurbaba lava.

Sample No	MA-58A Magnetite	MA-58A Magnetite
SiO_2	0.31	0.50
TiO_2	6.01	4.48
Al_2O_3	1.64	4.72
FeO	80.65	79.01
MnO	0.35	0.45
MgO	1.72	2.57
CaO	0.12	0.00
Na_2O	0.38	0.06
K_2O	0.01	0.00
P_2O_5	0.00	0.04
Cr_2O_3	0.15	0.23
NiO	0.00	0.18
Total	91.34	92.24
Formula on the basis of 32 oxygens		
Si	0.01	0.02
Ti	0.17	0.13
Al	0.07	0.21
Fe^{+3}	1.58	1.50
Fe^{+2}	1.01	0.98
Mn	0.01	0.01
Mg	0.10	0.14
Ca	0.00	0.00
Na	0.03	0.00
K	0.00	0.00
P	0.00	0.00
Cr	0.01	0.01
Ni	0.00	0.01
Total	3.00	3.00
Mn/Mg	0.10	0.07
sp	4.05	11.34
mg-chr	0.26	0.38
mg-fer	6.45	3.89
trev	0.00	0.60
mt	79.77	76.93
usp	9.48	6.87

Fe^{+3} is calculated by normalization according to Schumacher(1991).

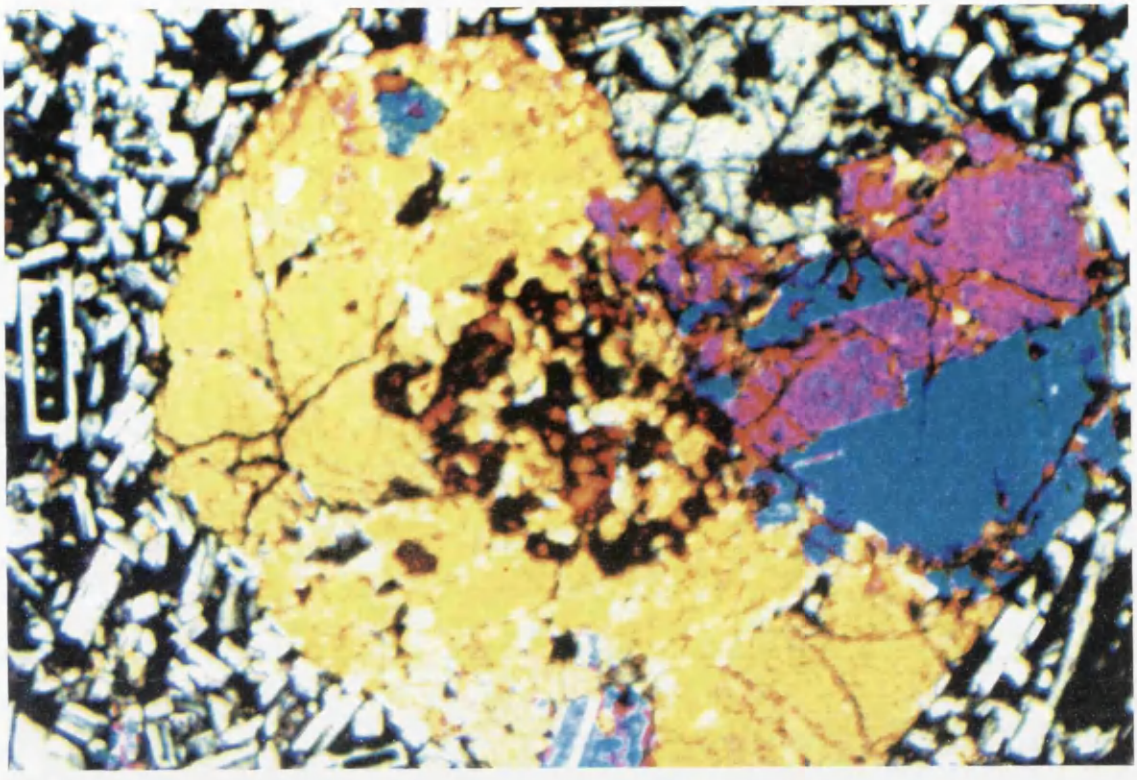

Photo 4.1. Sector twinning and fine olivine inclusions in augite in basaltic andesite from Kizildere lavas(MA-206). 40xC.N.

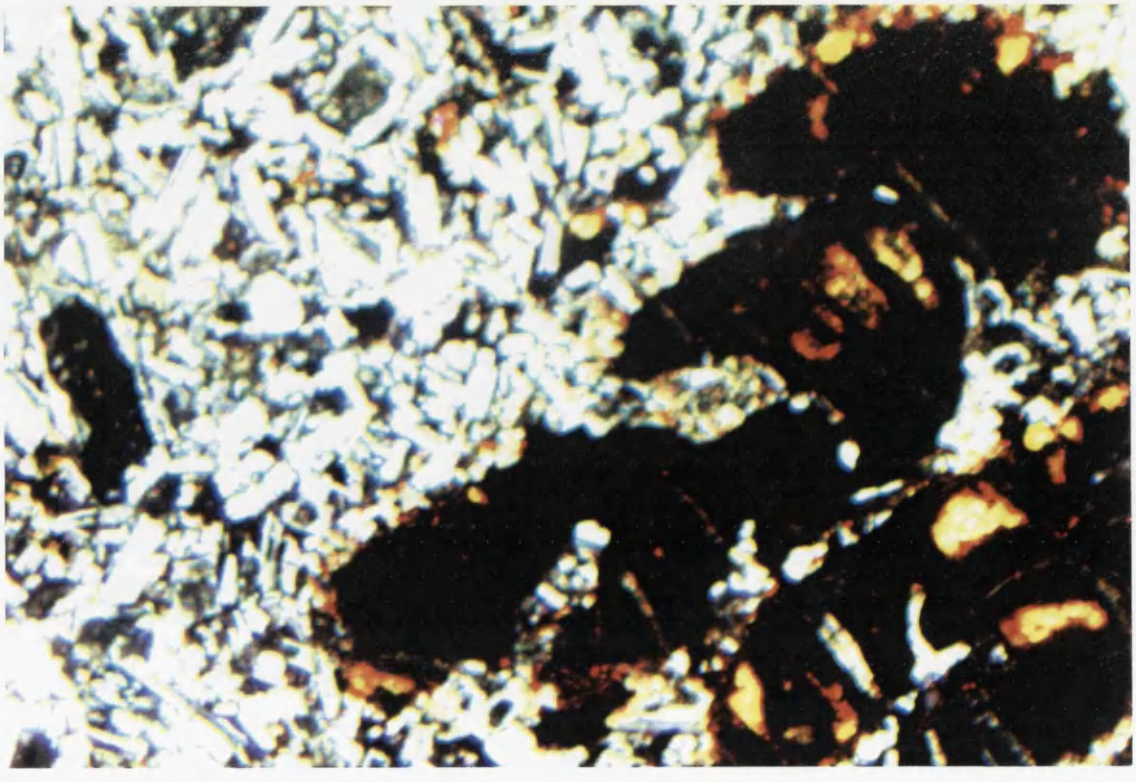

Photo 4.2. Skeletal and iddingsitized olivine phenocryst, and intersertal groundmass in basaltic andesite from Kizildere lavas(MA-206). 40xC.N.

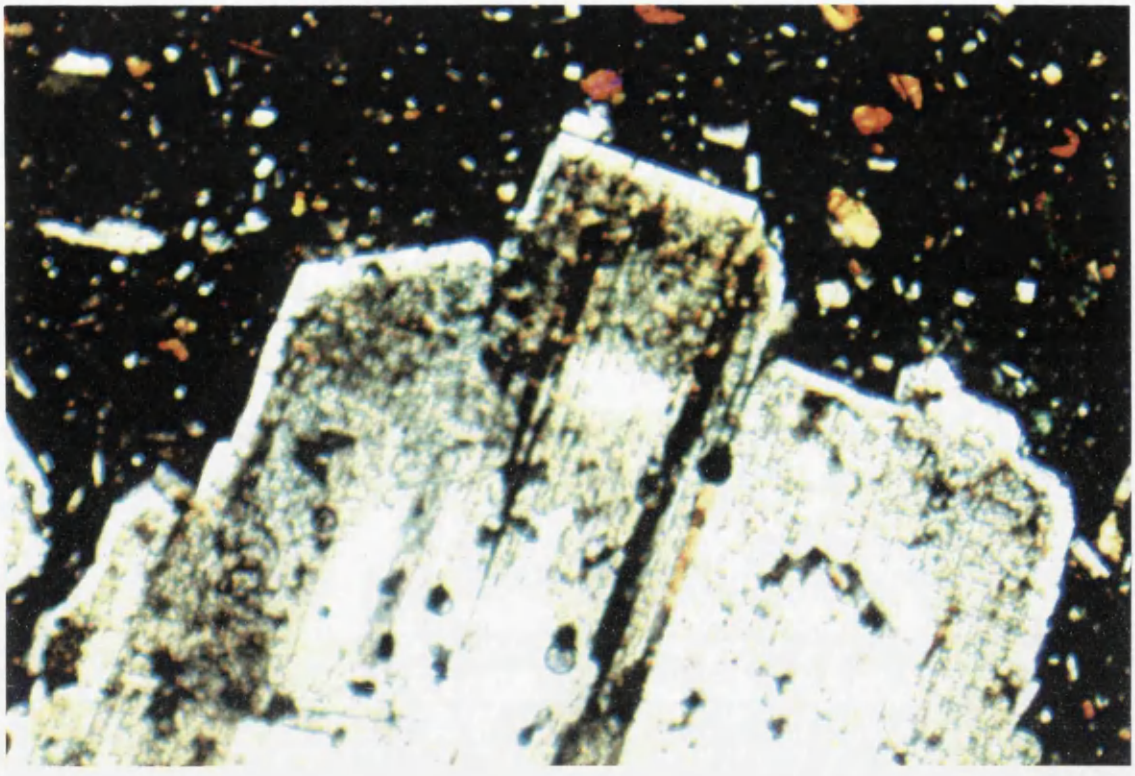

Photo 4.3. Sieve texture and thin overgrowth calcic rim in plagioclase phenocryst from andesite(MA-141A). 40xC.N.

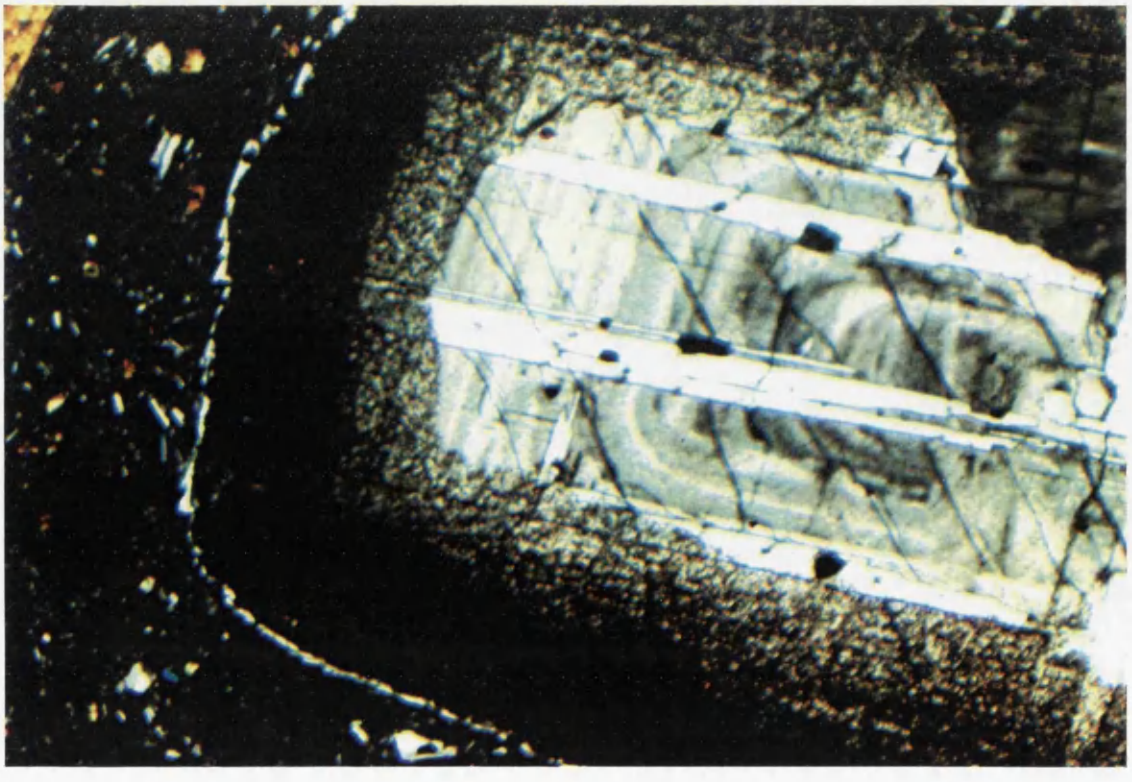

Photo 4.4. Sieve texture and zoning in plagioclase phenocryst from trachyandesite(MA-143). 40xC.N.

Photo 4.5. Embayed quartz phenocryst and fine-grained groundmass in dacite(MA-185). 40xC.N.

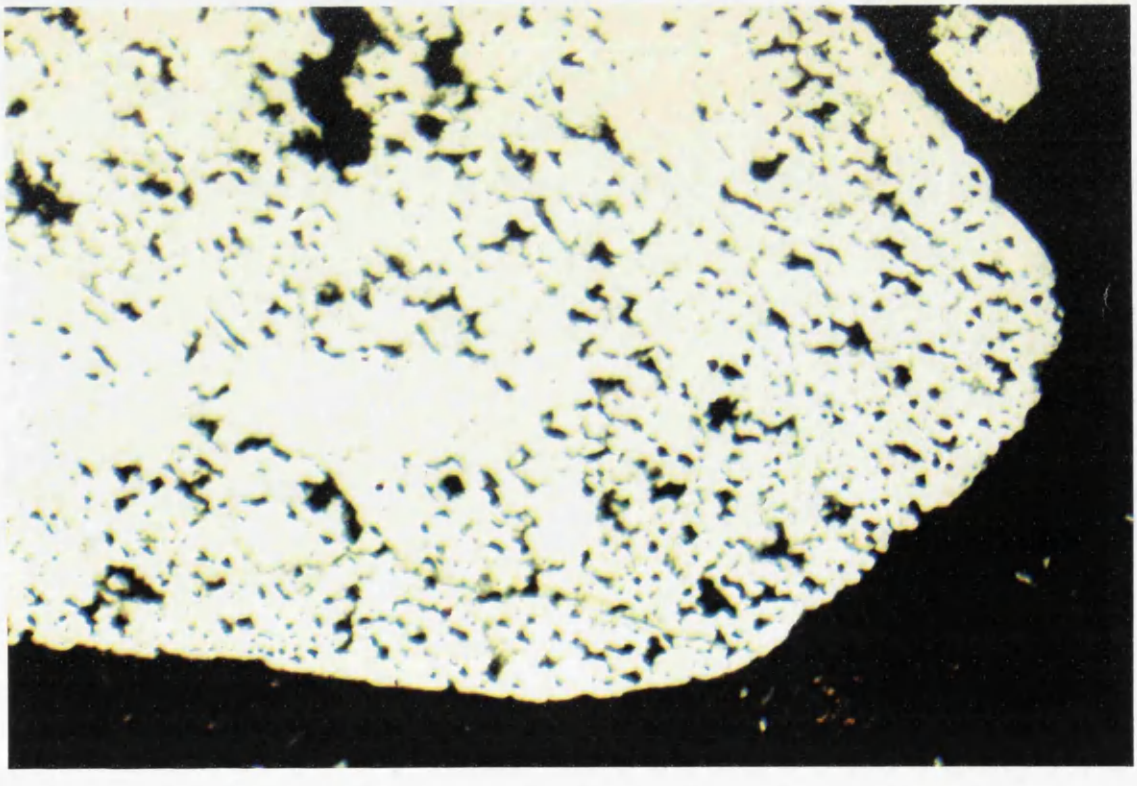

Photo 4.6. Plagioclase megacryst with sponge-like texture and partly corroded rim in Aladag lava(MA-55A). 40xC.N.

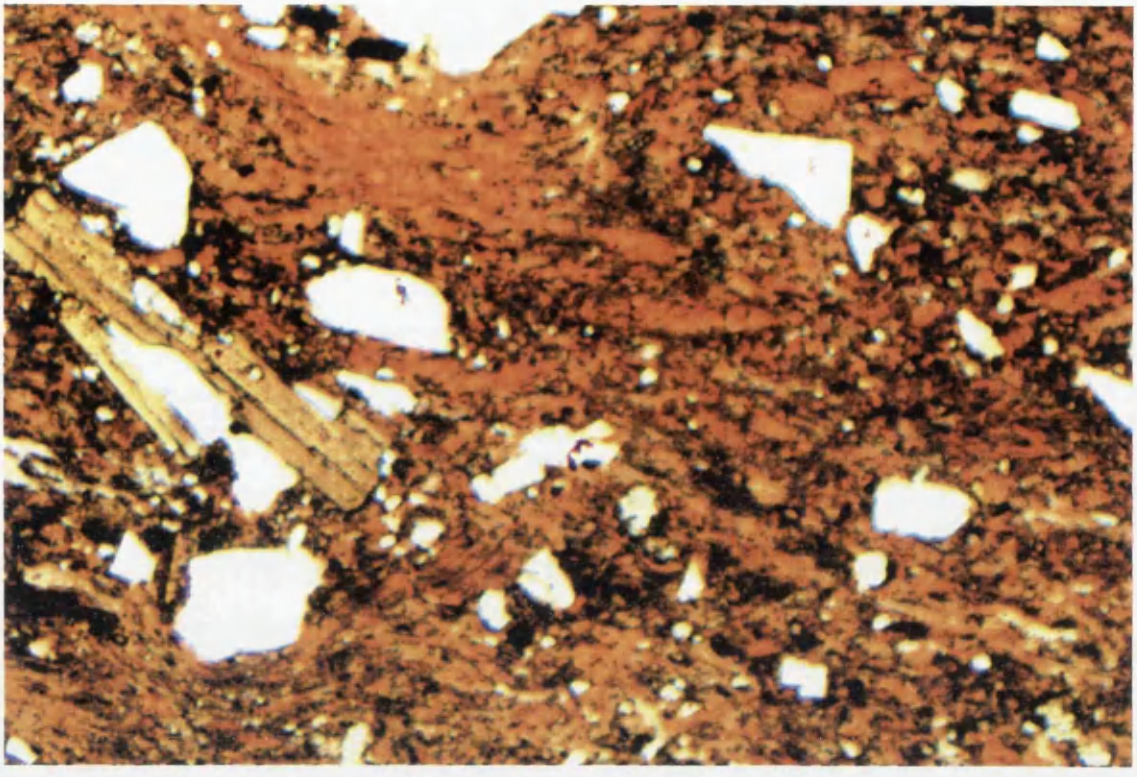

Photo 4.7. Eutaxitic texture and strong welding in ignimbrite(MA-75). 40xP.L.

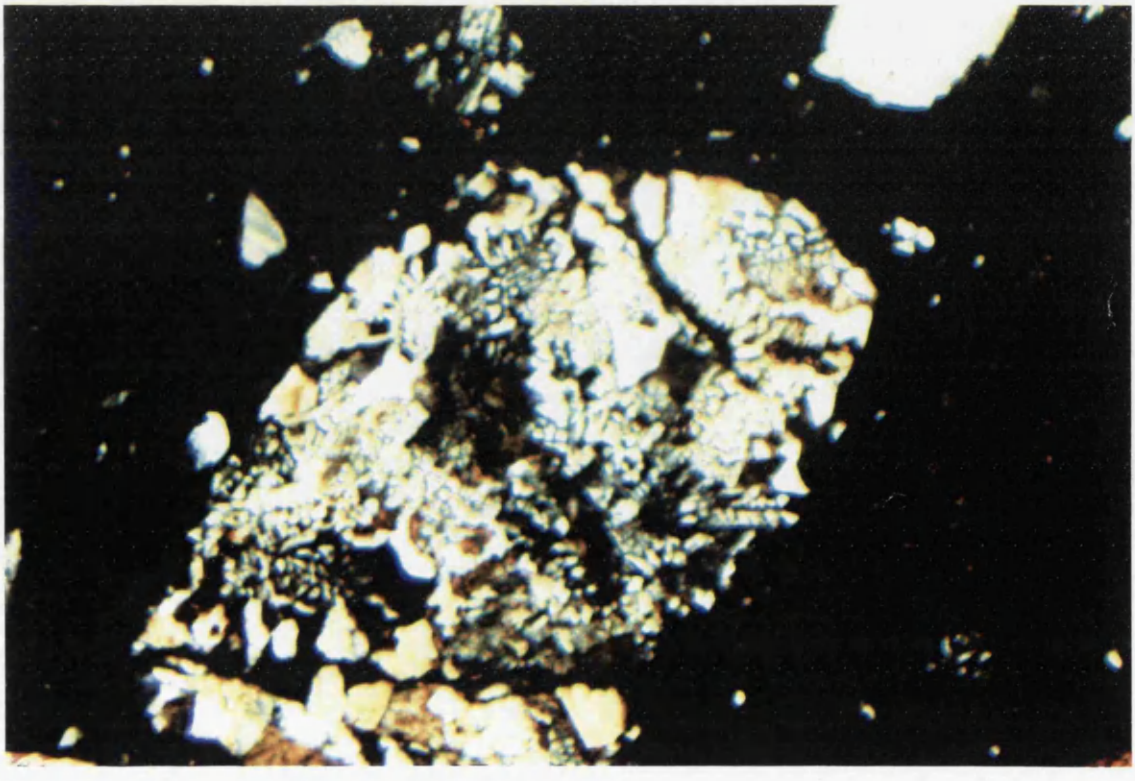

Photo 4.8. Granophyric textured granitoid fragment in ignimbrite(MA-74). 40xC.N.

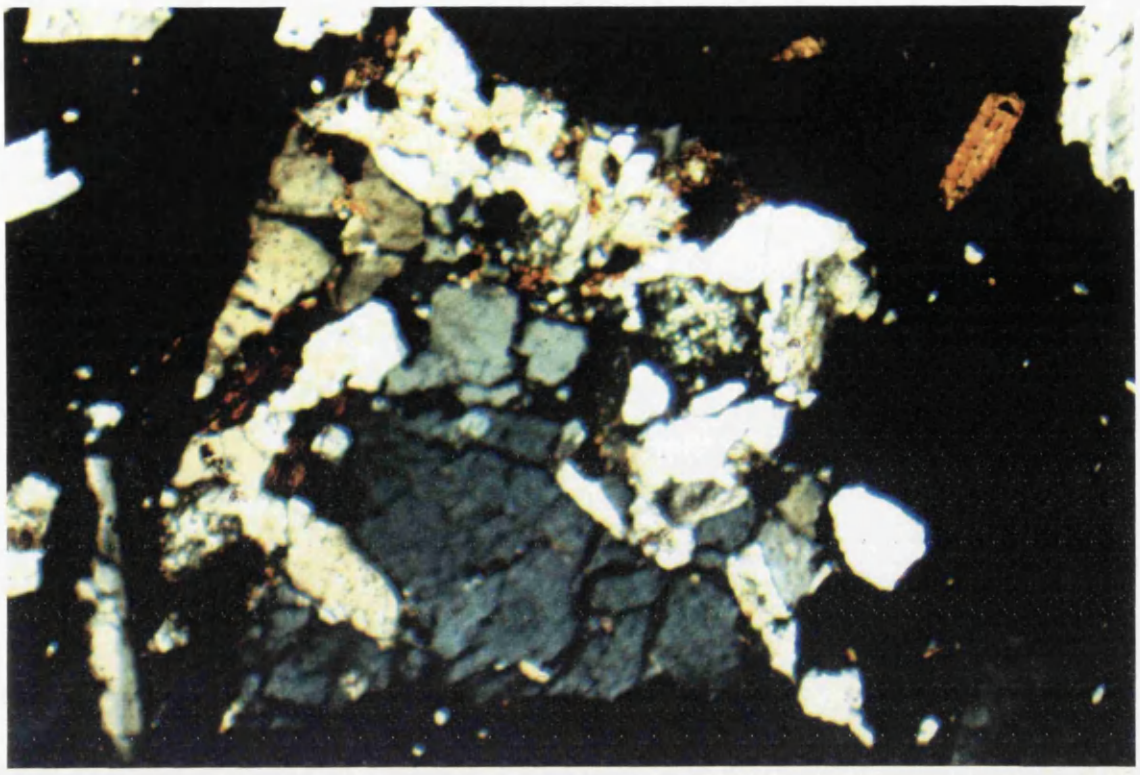

Photo 4.9. Granitoid fragment with equgranular texture in ignimbrite(MA-52). 40xC.N.

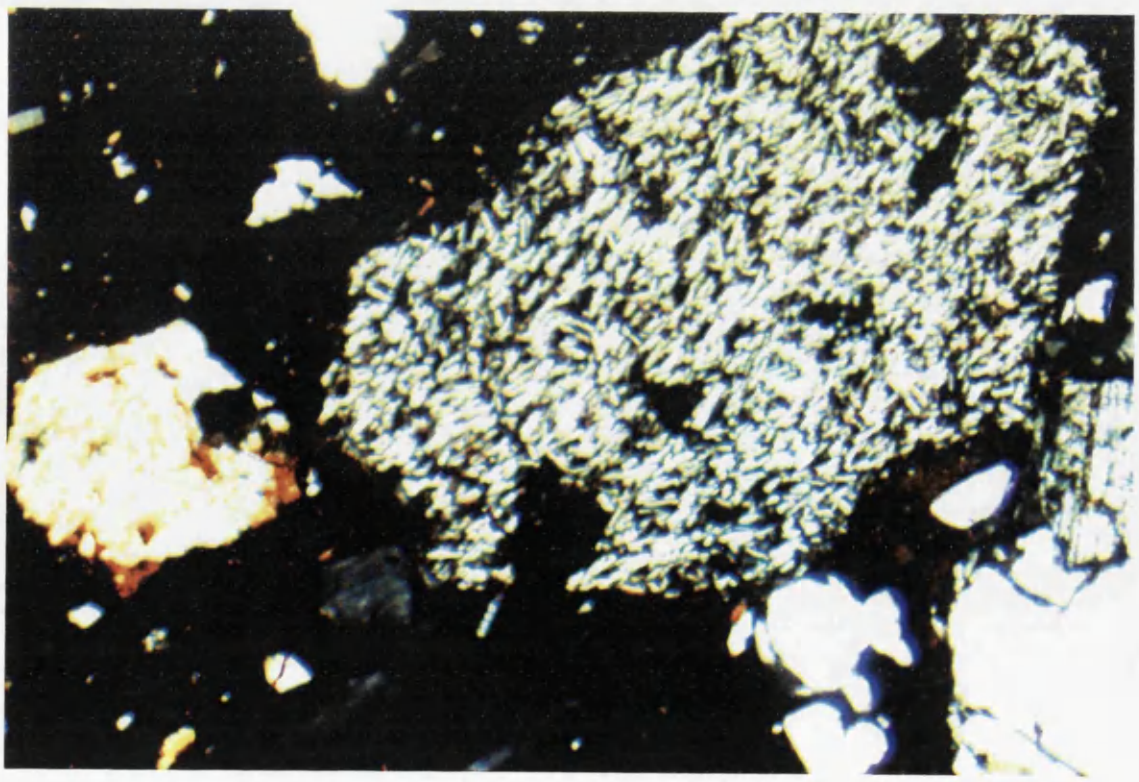

Photo 4.10. Trachyte and metasedimentary rock fragments in ignimbrite(MA-63). 40xC.N.

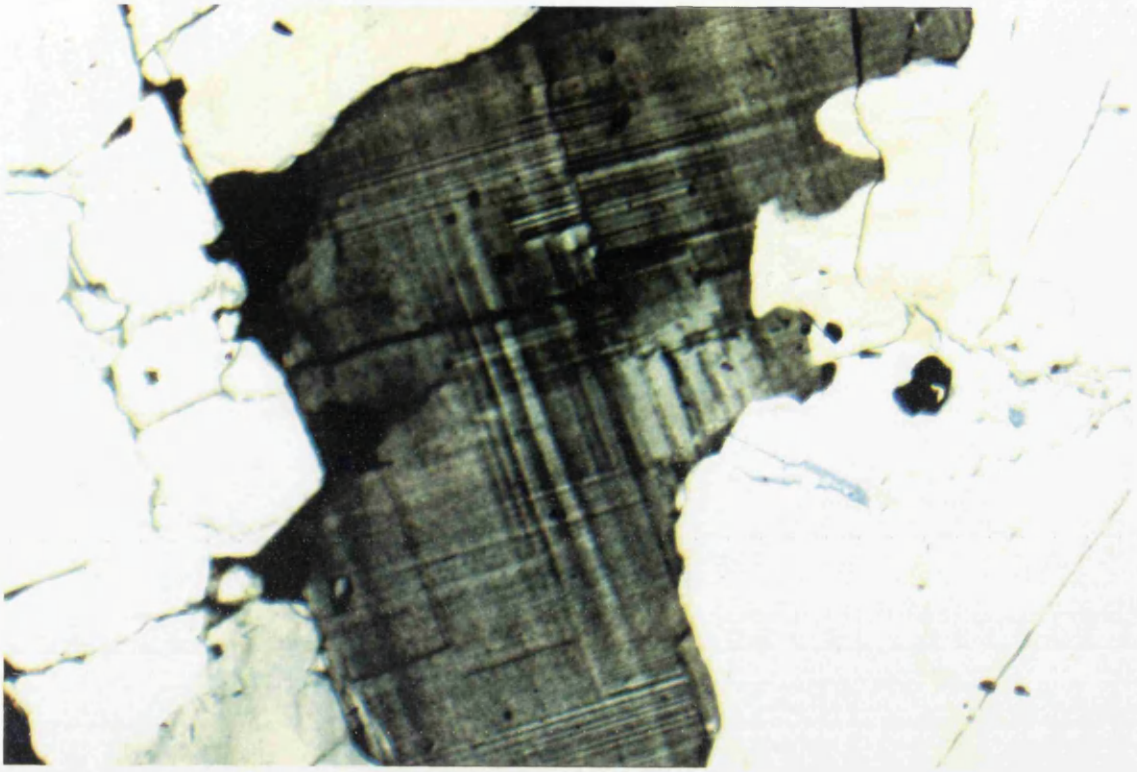

Photo 4.11. Anorthoclase phenocryst with cross-hatched twinning in ignimbrite(MA-57). 40xC.N.

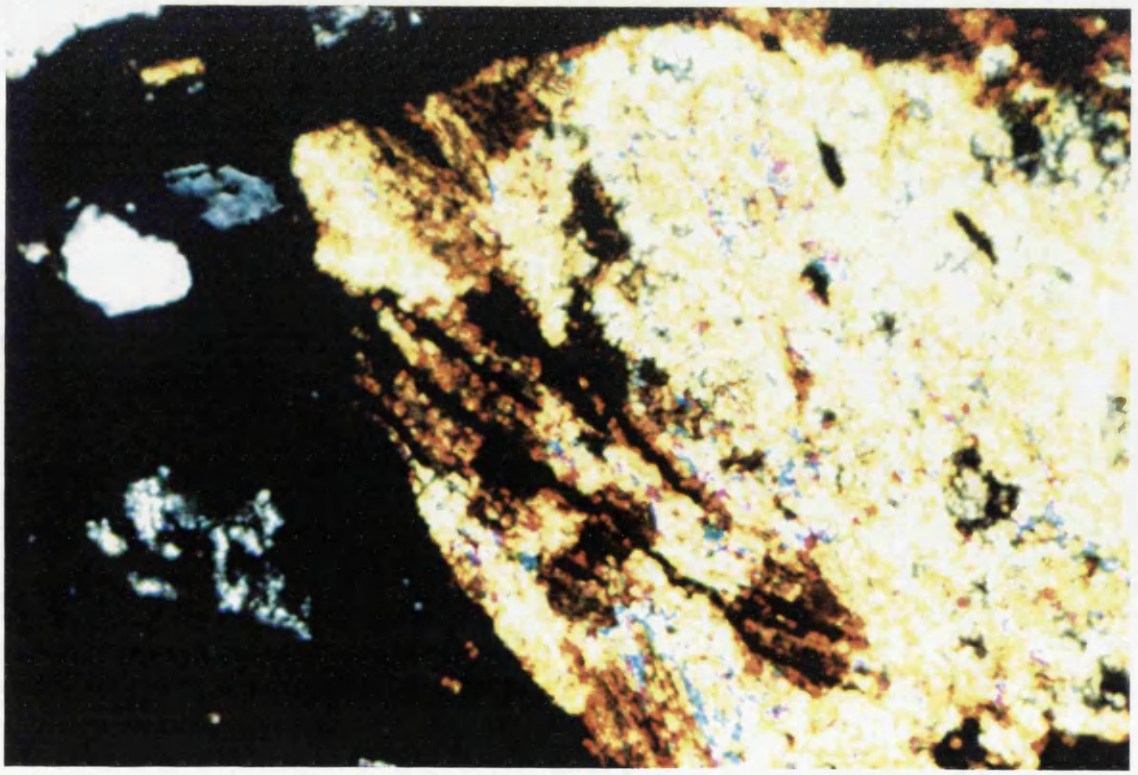

Photo 4.12. Metasedimentary rock fragment including biotite+chlorite+ quartz+muscovite from ignimbrite(MA-63). 100xC.N.

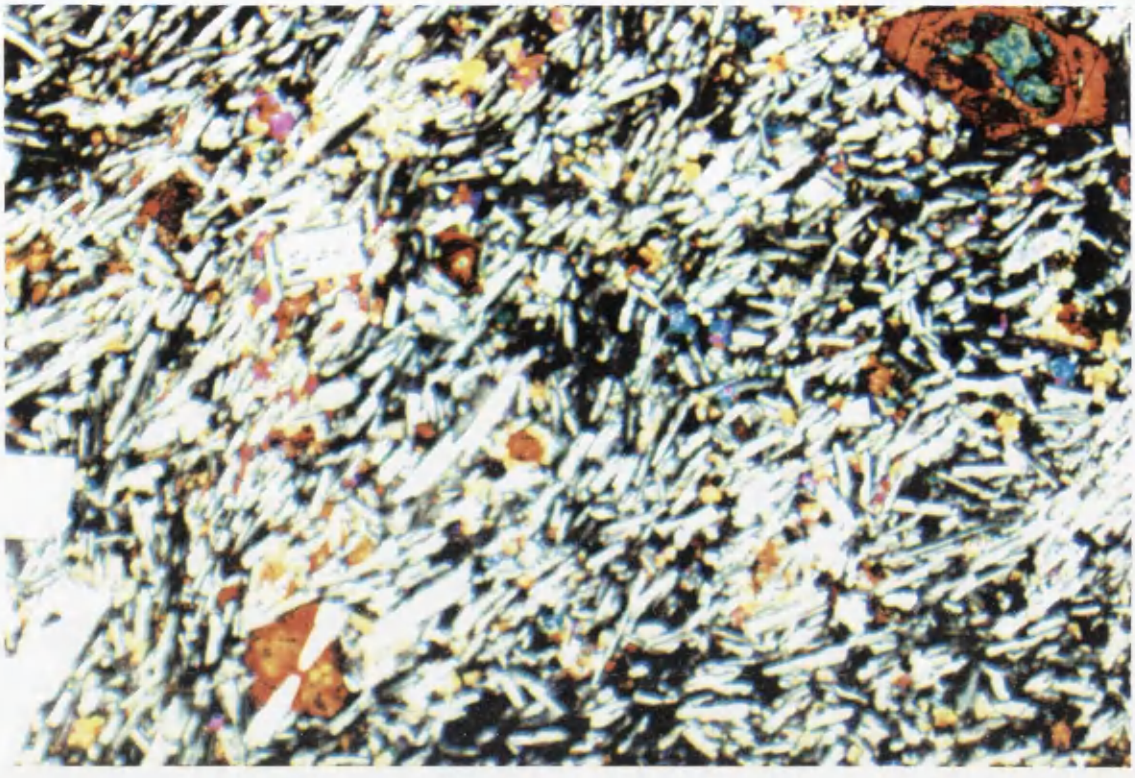

Photo 4.13. Intersertal texture in alkali olivine basalt(MA-22). 40xC.N.

Photo 4.14. Subophitic texture in alkali olivine basalt(MA-22). 40xC.N.

Photo 4.15. Resorption and arrangement of fine opaques around crystal rim in plagioclase from alkali olivine basalt(MA-9). 40xC.N.

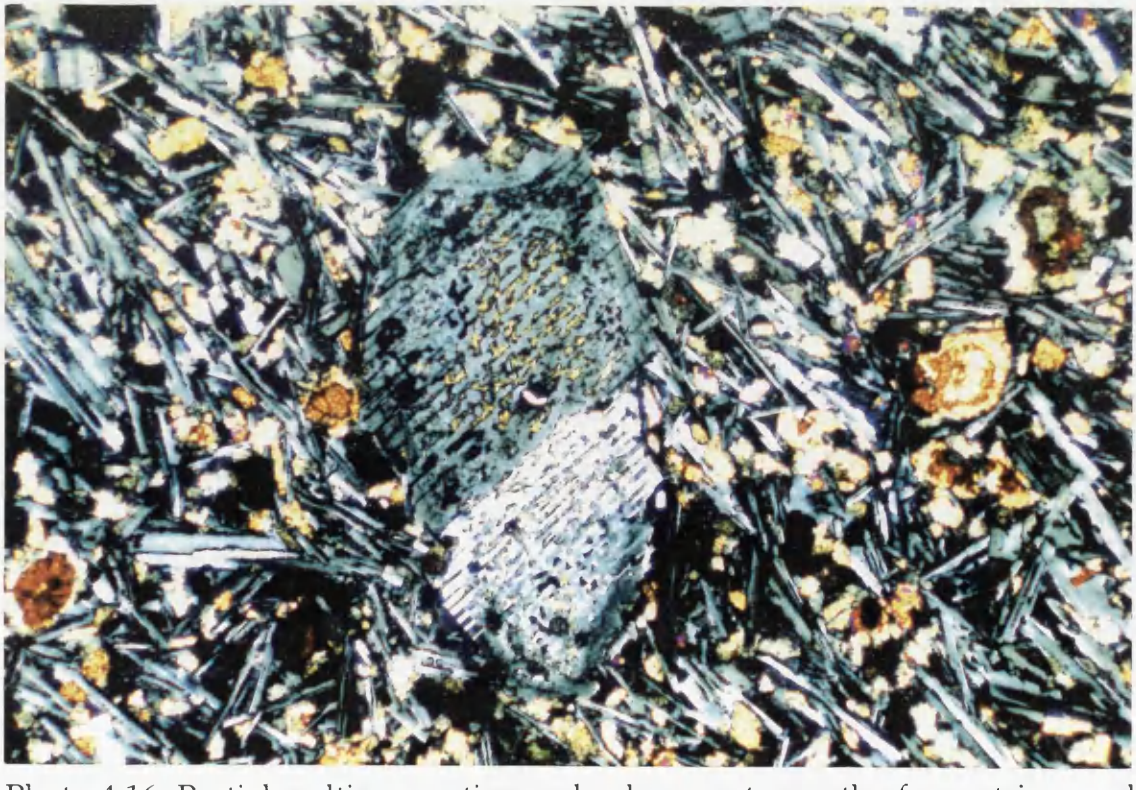

Photo 4.16. Partial melting reaction and subsequent growth of cpx strips and blobs in plagioclase phenocryst from alkali olivine basalt(MA-8). 40xC.N.

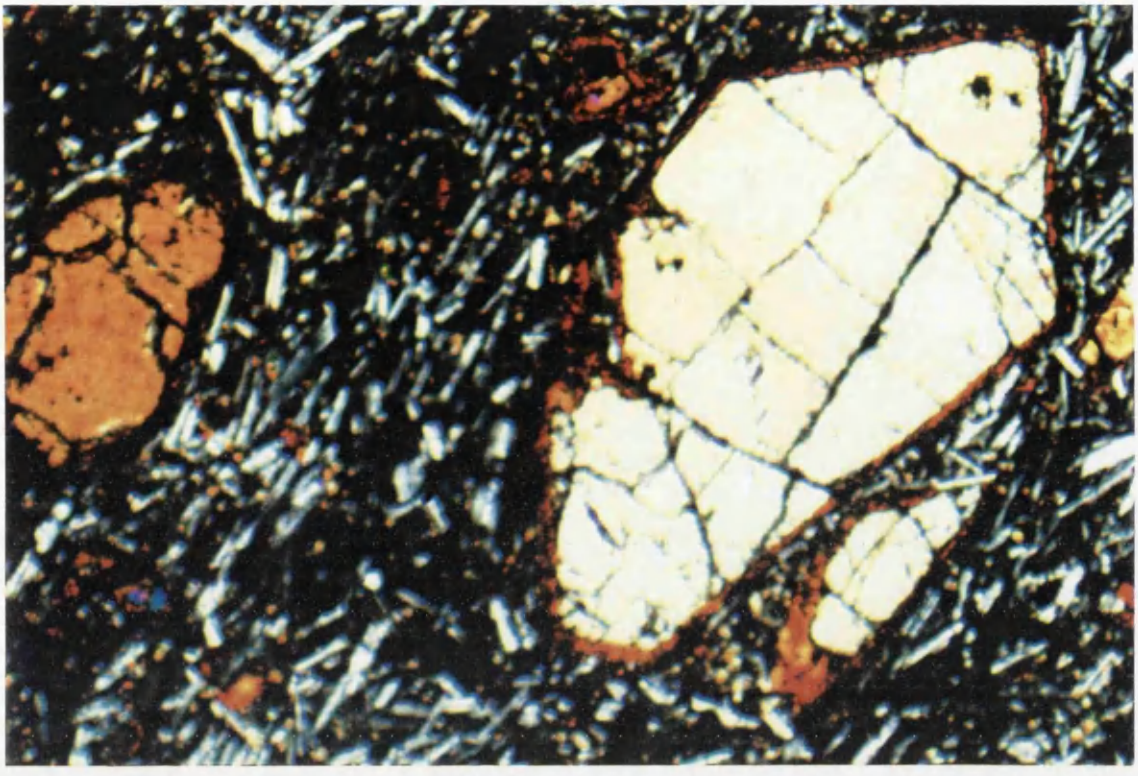

Photo 4.17. Olivine phenocryst with thin iddingsite rim in alkali olivine basalt(MA-25). 40xC.N.

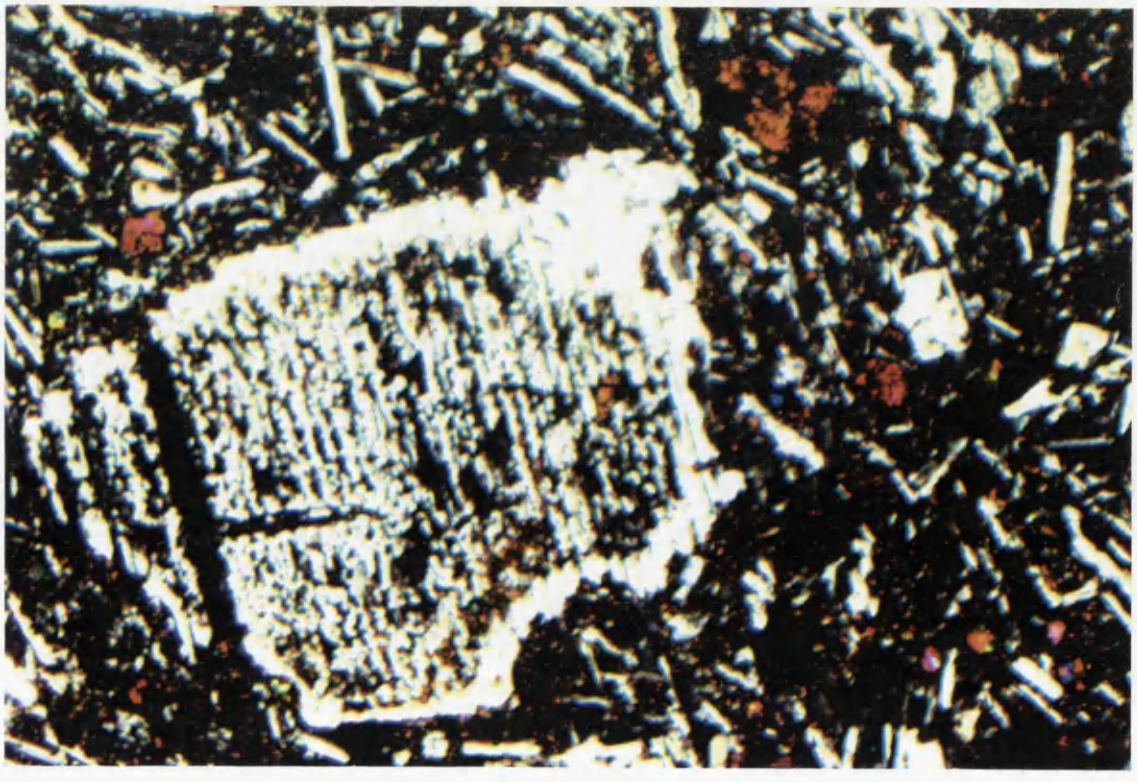

Photo 4.18. Sieve texture and fine-lamellae albite twinning in anorthoclase phenocryst from hawaiite(MA-5). 40xC.N.

Photo 4.19. Sieve textured and partially resorbed plagioclase phenocryst in hawaiite(MA-29). 40xC.N.

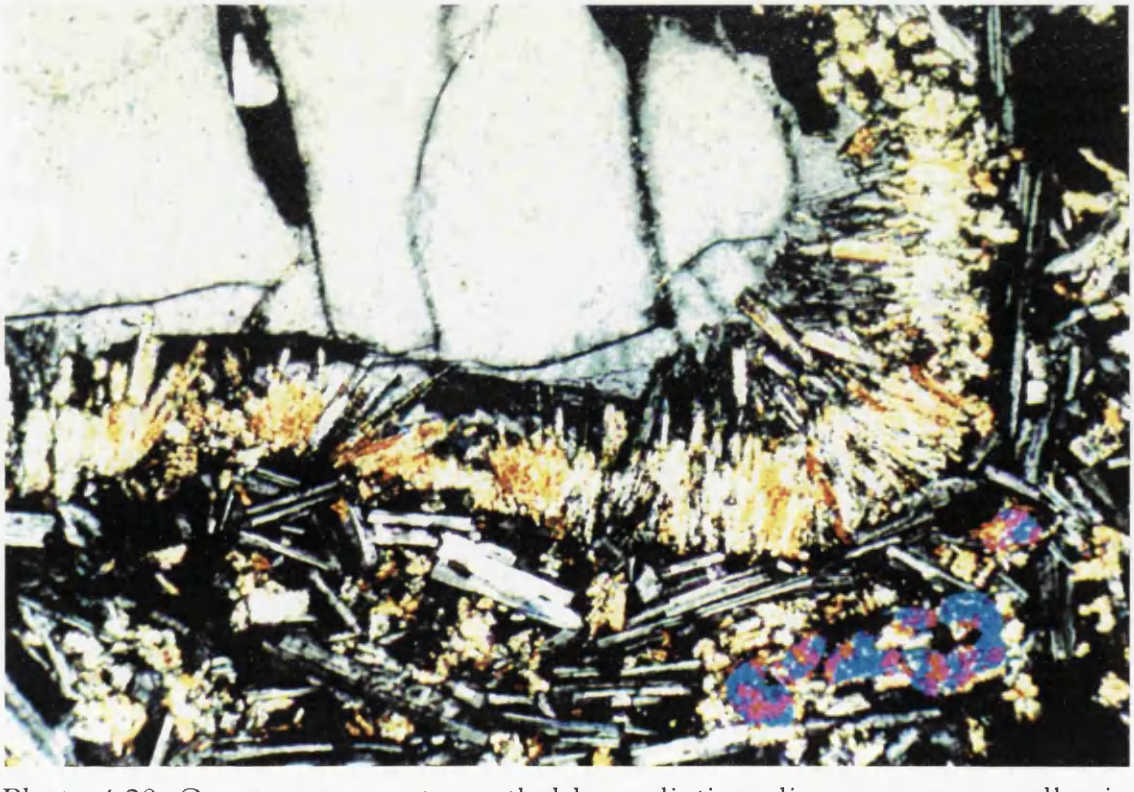

Photo 4.20. Quartz xenocryst mantled by radiating clinopyroxene needles in hawaiite(MA-29B). 100xC.N.

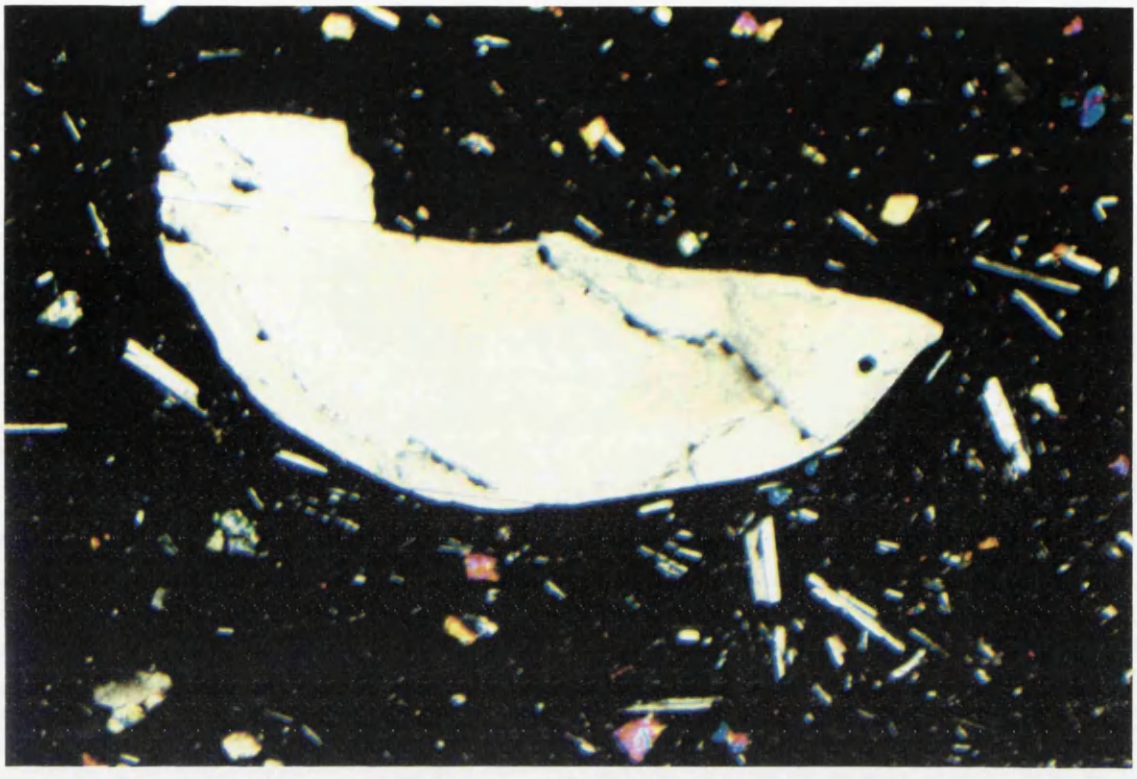

Photo 4.21. Partially resorbed plagioclase phenocryst in hawaiite(MA-33). 40xC.N.

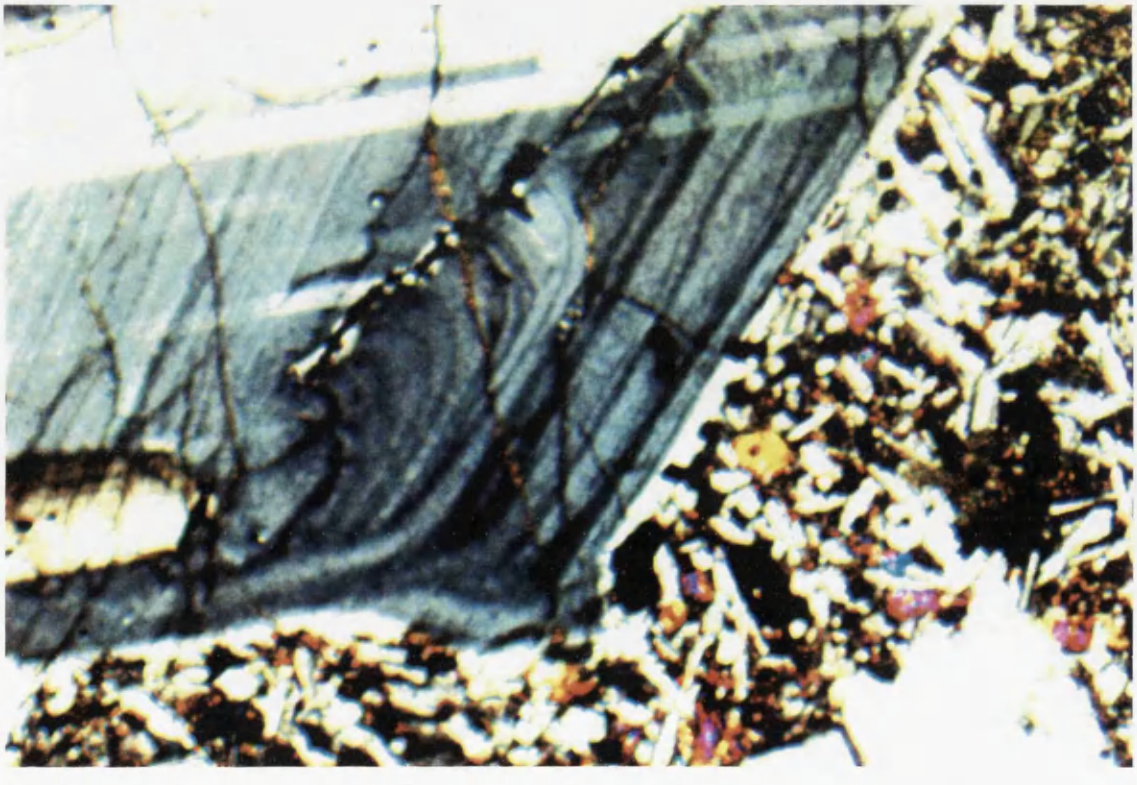

Photo 4.22. Oscillatory zoning in plagioclase megacryst from mugearite(MA-47). 40xC.N.

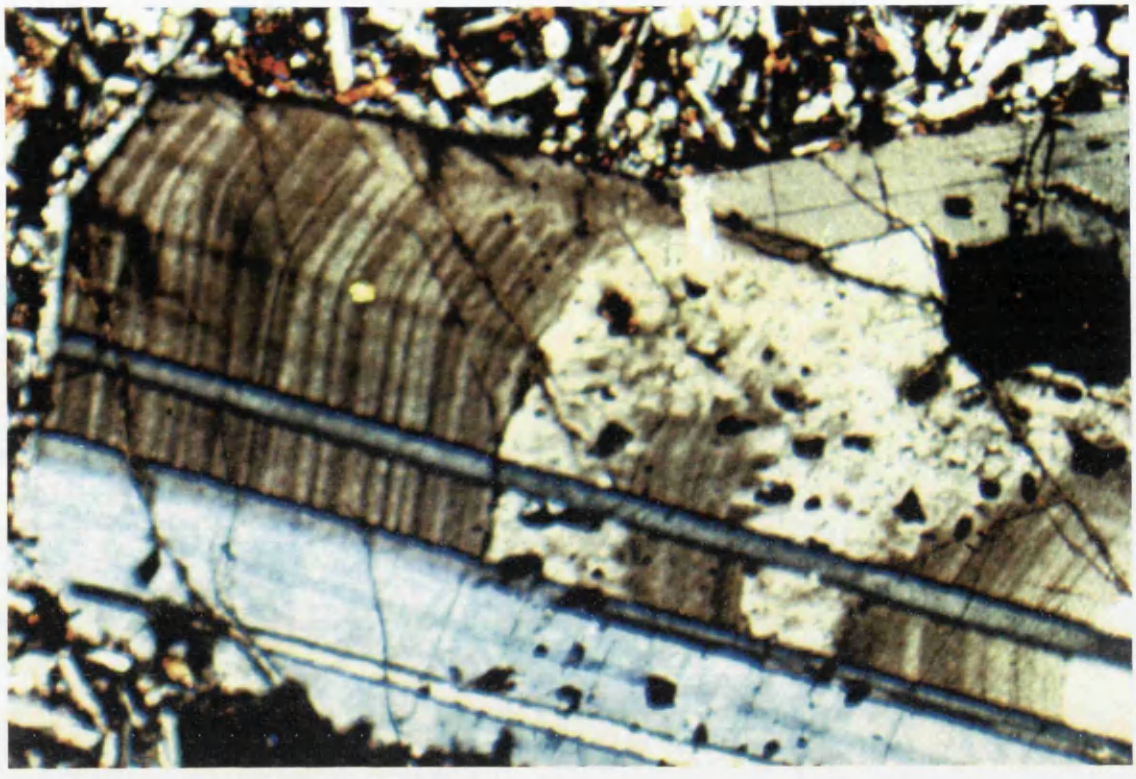

Photo 4.23. Oscillatory zoning and common twinning relationship in plagioclase megacryst in mugearite(MA-47). 40xC.N.

Photo 4.24. Overgrowth oscillatory zoning in plagioclase megacryst in mugearite(MA-7). 40xC.N.

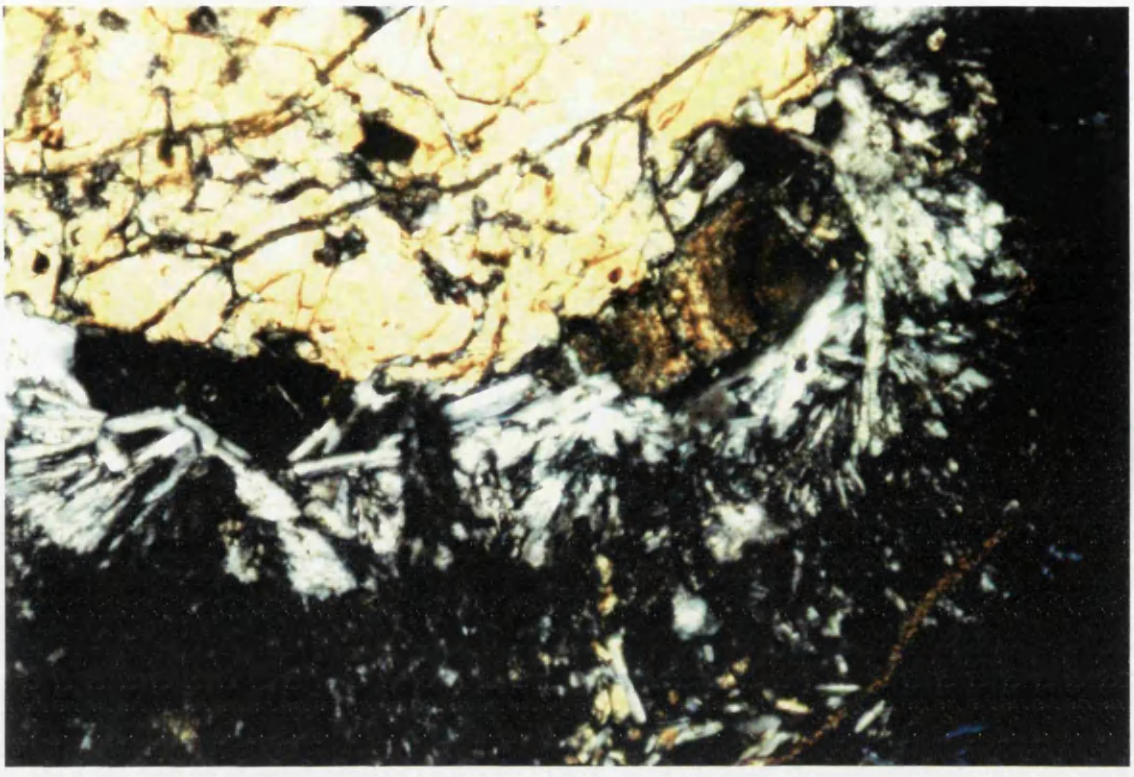

Photo 4.25. Augite phenocrysts enclosed by plagioclase needles from mugearite(MA-54). 160xC.N.

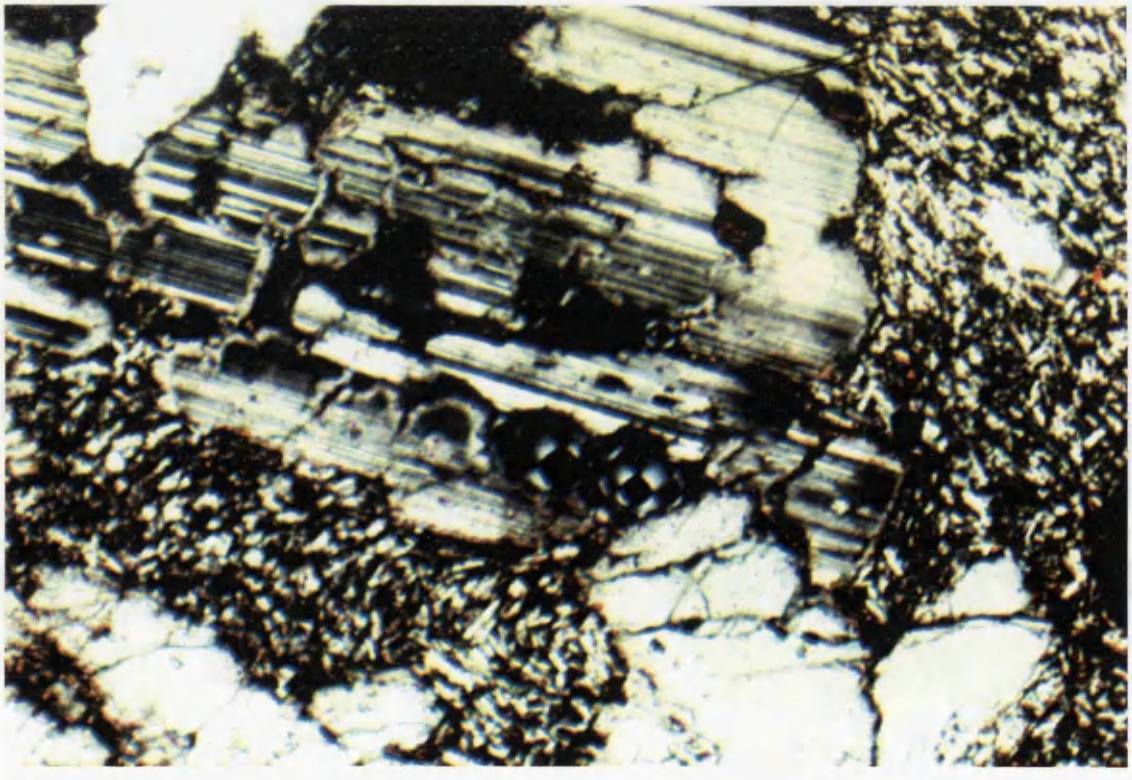

Photo 4.26. Embayment and fine-lamellae twinning in anorthoclase phenocryst in trachyte(MA-1). 40xC.N.

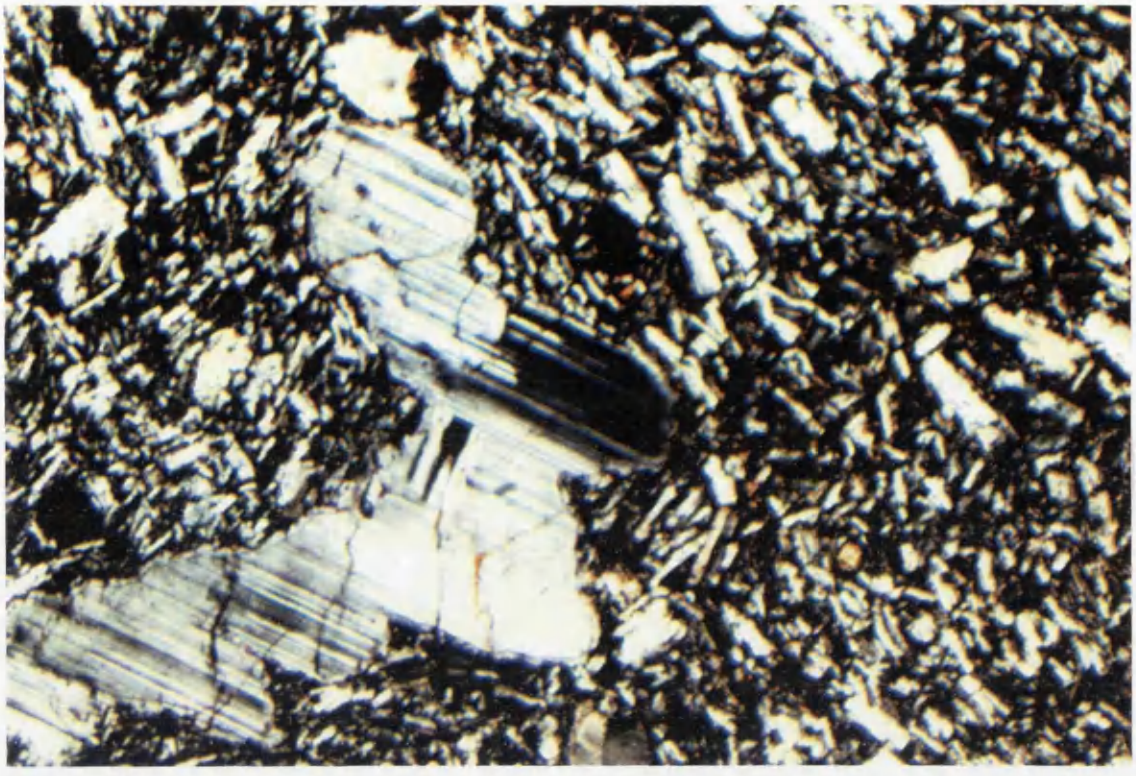

Photo 4.27. Trachytic texture and corroded anorthoclase megacryst with fine-lamellae twinning in trachyte(MA-14). 40xC.N.

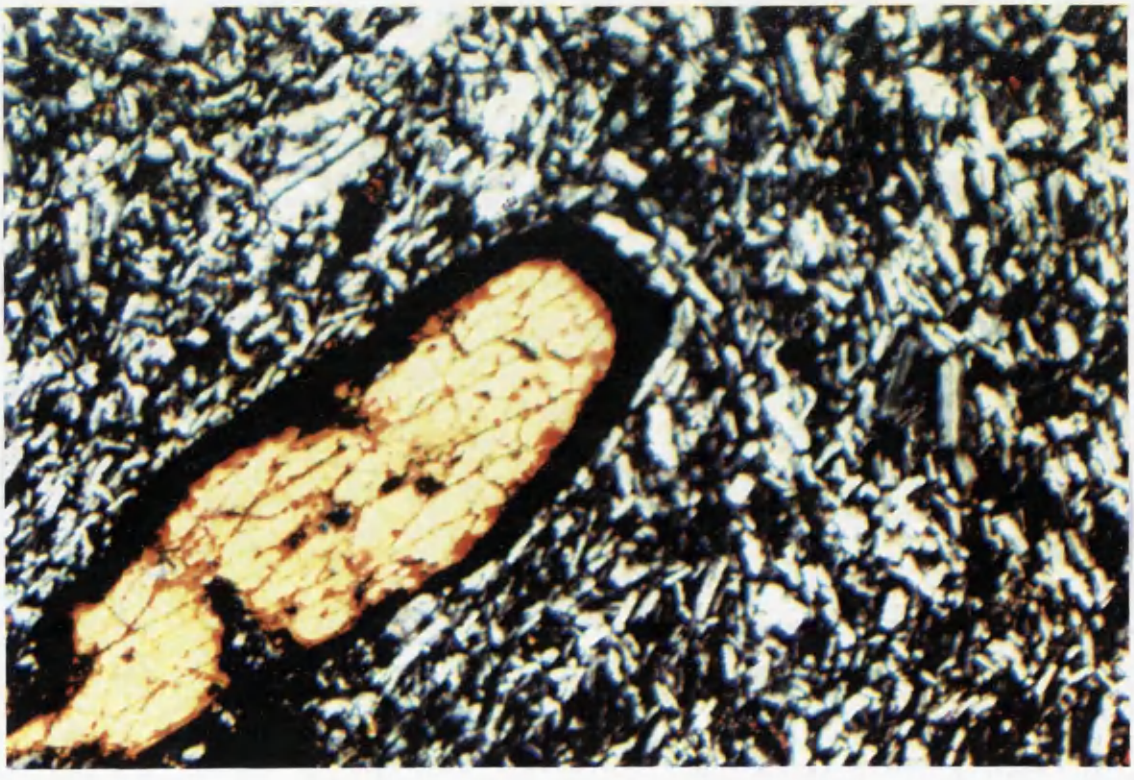

Photo 4.28. Kaersutite phenocryst with opaque rim in trachyte(MA-39). 40xC.N.

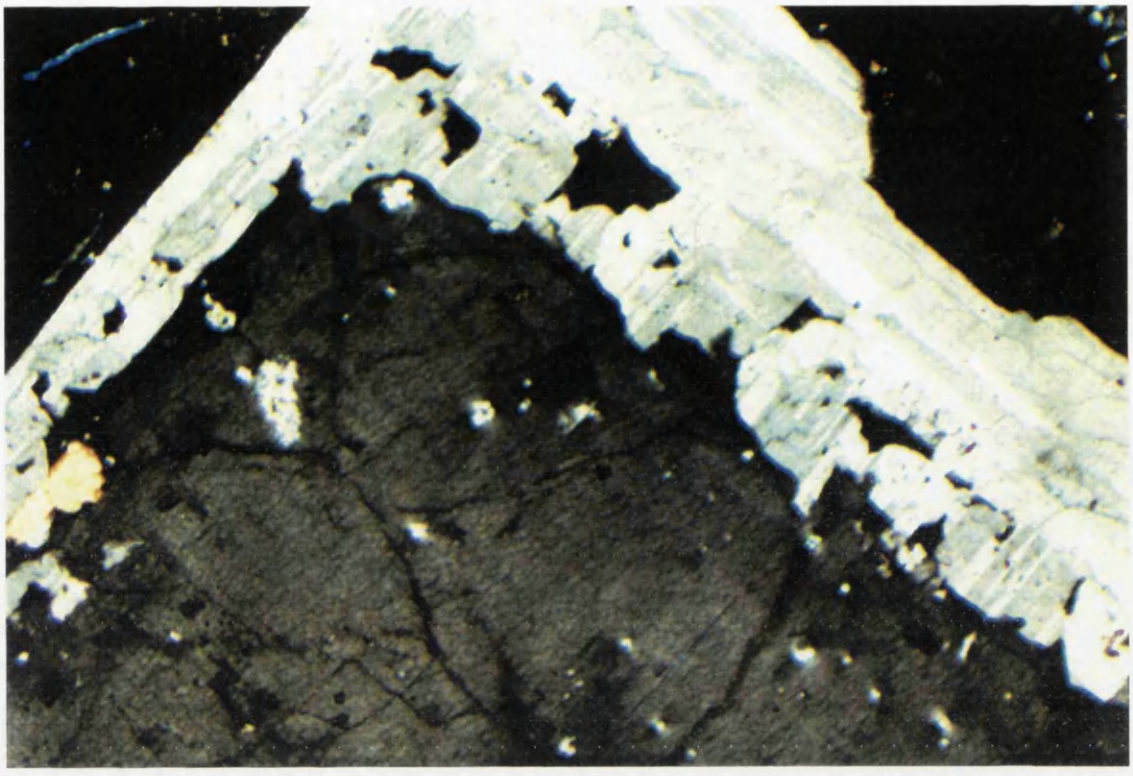

Photo 4.29. Plagioclase mantling on sanidine phenocryst in rhyolite dyke(MA-62). 40xC.N.

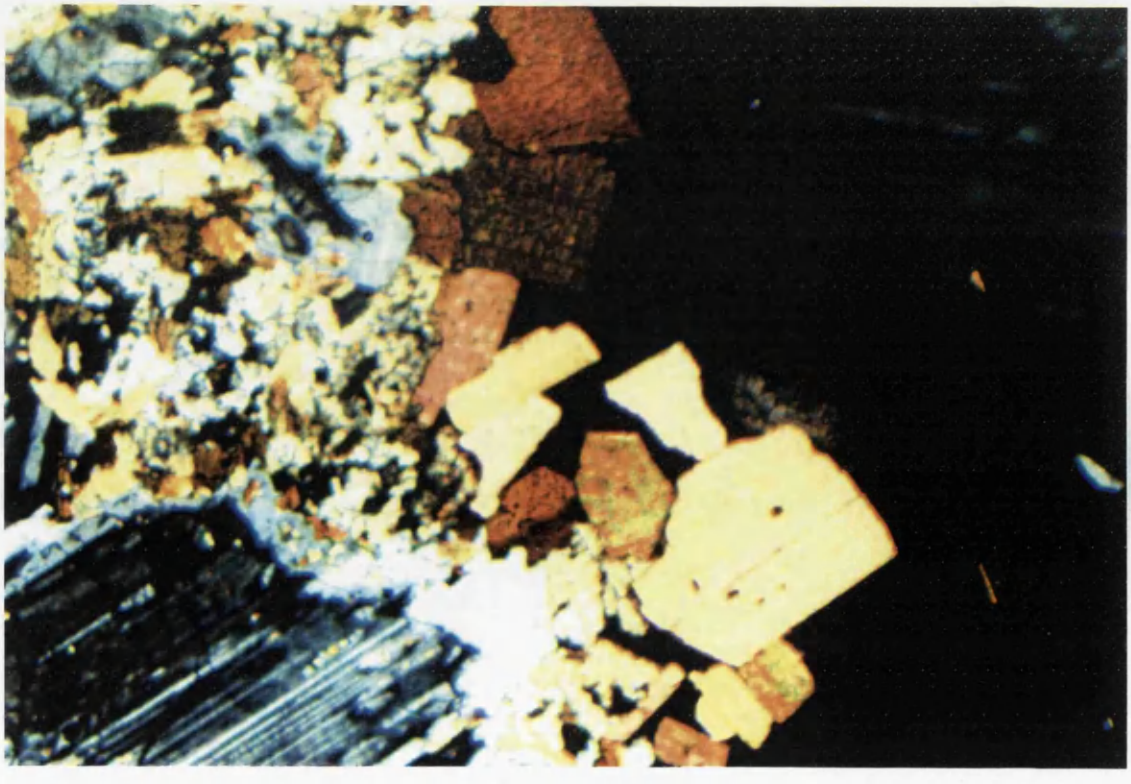

Photo 4.30. Glomeroporphyritic texture in rhyolite dome(MA-38B). 40xC.N.

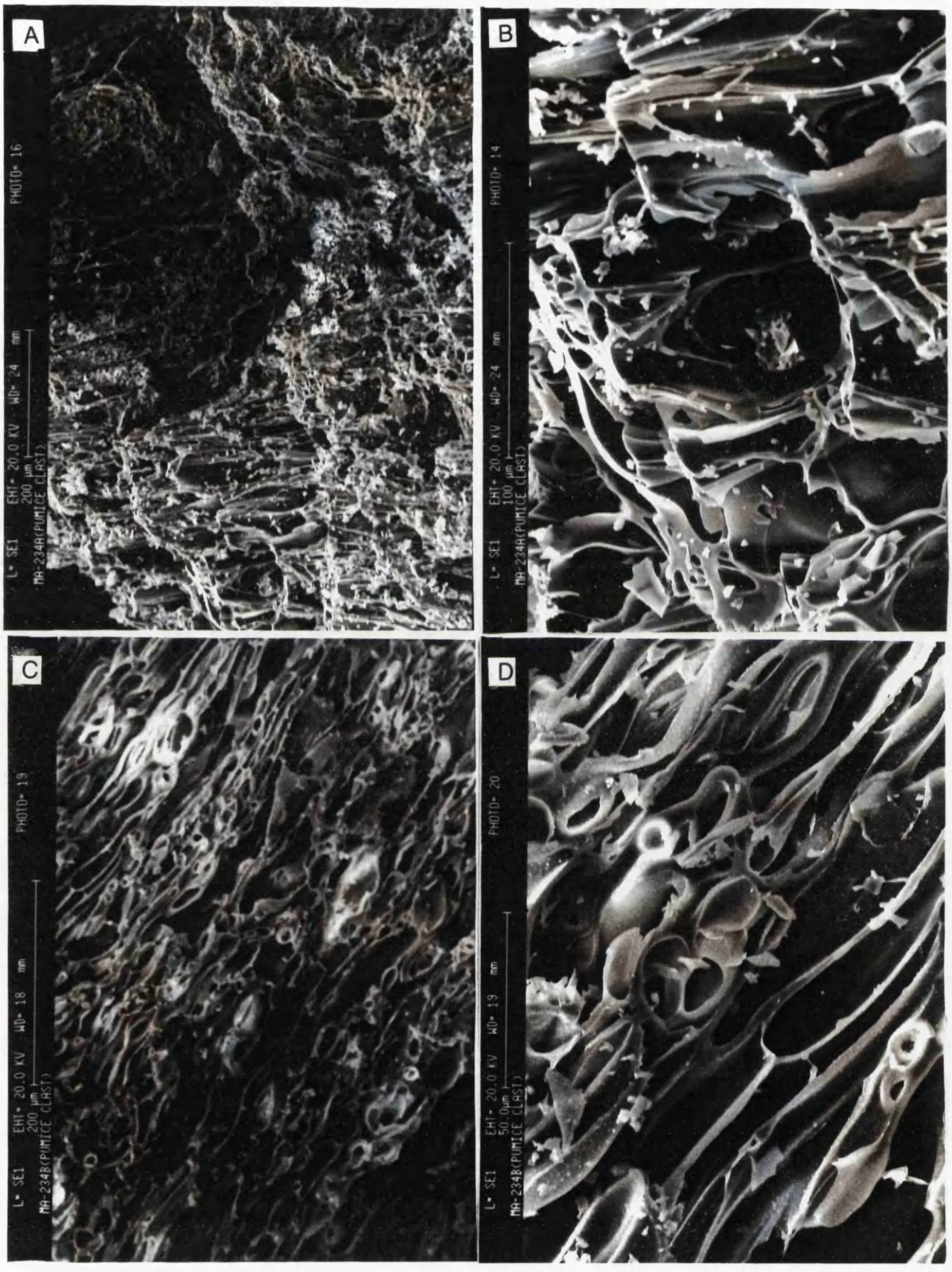

Photo 4.31. Scanning electron images of pumice pyroclasts from pumice deposits. A and C: Angular, subequant pumices which are all glass and contain no phenocrysts. Large cavities are composite and were formed by coalescence of adjacent vesicles. B and D: Details of A and C respectively, showing the variation in vesicle widths. Most vesicles are thin walled, and many exhibit some degree of coalescence.

CHAPTER 5. GEOCHEMISTRY

5.1. INTRODUCTION

This chapter is concerned with the general geochemical features of the rock types in terms of major, minor and rare earth elements. Sedimentary rocks are considered in terms of provenance and compositional changes in the volcanic rocks investigated in relation to magmatic processes involved in their formation.

For this purpose, fresh, unaltered samples were collected from 263 localities, chipped, and hand picked to yield the freshest material: 150 of those samples were analysed for major and trace elements, and 35 of them were also analysed for rare earth elements(Appendices 3 and 4).

The FeO contents of samples were determined by the method of titration with potassium dichromate as the X-ray Spectrometer gives total iron. Fe_2O_3 is calculated by subtracting FeO multiplied by 1.1114, from the total iron as Fe_2O_3. The amounts of H_2O and CO_2 were determined by a method of combustion, absorption and gravimetry(Riley, 1958). In most of the samples, volatile contents were determined by measuring loss on ignition.

Although, in most cases unaltered samples were selected from volcanic rocks, hydrothermal alteration may have affected the original rock composition by selectively mobilizing the constituent elements in some rocks, especially lavas in the Kizildere Formation. Flow differentiation and migration, and concentration of late-stage residual liquids during crystallization can also influence rock composition. Variations along strike in a single flow may reflect the changing composition of magma during the period of a single eruptive event(Lightfoot *et al.*, 1990a).

5.2. SEDIMENTARY GEOCHEMISTRY

5.2.1. CARBONATES

5.2.1.1. MAJOR AND TRACE ELEMENTS

As described in the petrography section, the carbonates vary from pure limestone to dolomitic carbonates with up to 25% clay, up to 5% detrital quartz, up to 3% detrital feldspar and up to 3% oxidized opaque grains. A geochemical study of the rocks was undertaken to understand the sedimentary and diagenetic processes involved in the rock formation.

Generally, SiO_2 variation is related to the abundance and silica content of the constituent silicates. Al is largely in the clay minerals and so positive correlation of other elements with Al will give an indication of which elements entered the sediment largely in clay minerals. Al_2O_3 versus major and trace element plots(Figures 5.1 and 5.2) indicate that:

(a) SiO_2, P_2O_5, TiO_2, $Fe^*_2O_3$, K_2O, Cr, Rb, Zr and Y show fair positive correlations with Al_2O_3. The scatter in the SiO_2 plot is caused by the presence of detrital quartz and feldspar.

(b)MgO, MnO and Th show a negative correlation with Al_2O_3 confirming their addition to the rock is largely in precipitated carbonate, not in detrital minerals.

(c) La, Cu, Co, Ba, Pb and Ce show no correlation with Al_2O_3. MnO is associated with carbonates and Ba with sulphates.

Calcite and dolomite selectively incorporate significant amounts of certain elements such as Mn and Sr. Furthermore, Graf(1962) and Weber(1964) and many others have shown that the trace elements in carbonate rocks mainly lie in the non-carbonate minerals, especially clay, detrital minerals, organic matter, phases formed during diagenesis and the elements absorbed upon all of these materials.

A S versus CaO plot does not reveal any significant correlation indicating that the amount of CaO combined with S in gypsum is generally very low and most of the Ca is in carbonates. Moreover, plots of S versus Sr, Ba and Ba+Sr(Figure 5.3) all show poor correlations.

Generally, Ba in the analysed samples is up to 77 ppm which is similar to marine limestones(<60ppm; Friedman,1969). Two samples have rather high values of Ba(114 ppm and 452 ppm), perhaps due to some hydrothermal fluid input.

The dolomitic carbonates have Sr between 33 ppm and 86 ppm. Veizer and Demovic(1974) indicated that the range of Sr in late diagenetic dolomites is 30-100 ppm but 100-600 ppm in early diagenetic dolomite. If these criteria hold generally, Sr contents in the studied samples are indicative of late diagenetic dolomite.

The chemistry of the original carbonates has been changed, in part at

least, as shown by the development of neomorphic and metasomatic fabrics(see Chapter 4). Generally, the contents of trace elements(except Sr, S and Ba) are assumed to be derived from the clay fraction as inferred from the good correlation between them and Al_2O_3 whereas MnO and Th seem related to the carbonates.

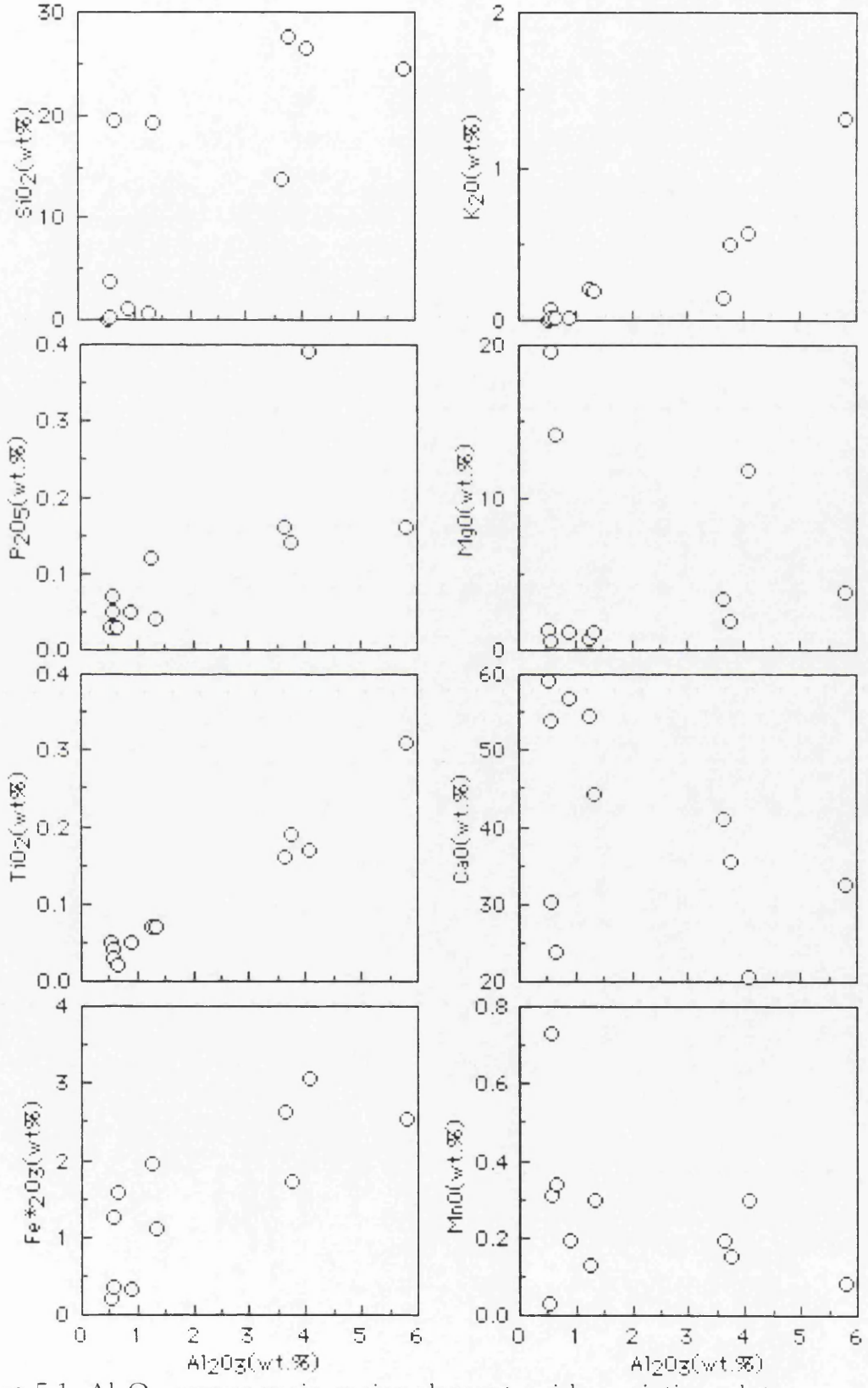

Figure 5.1. Al_2O_3 versus main major element oxide variation plots.

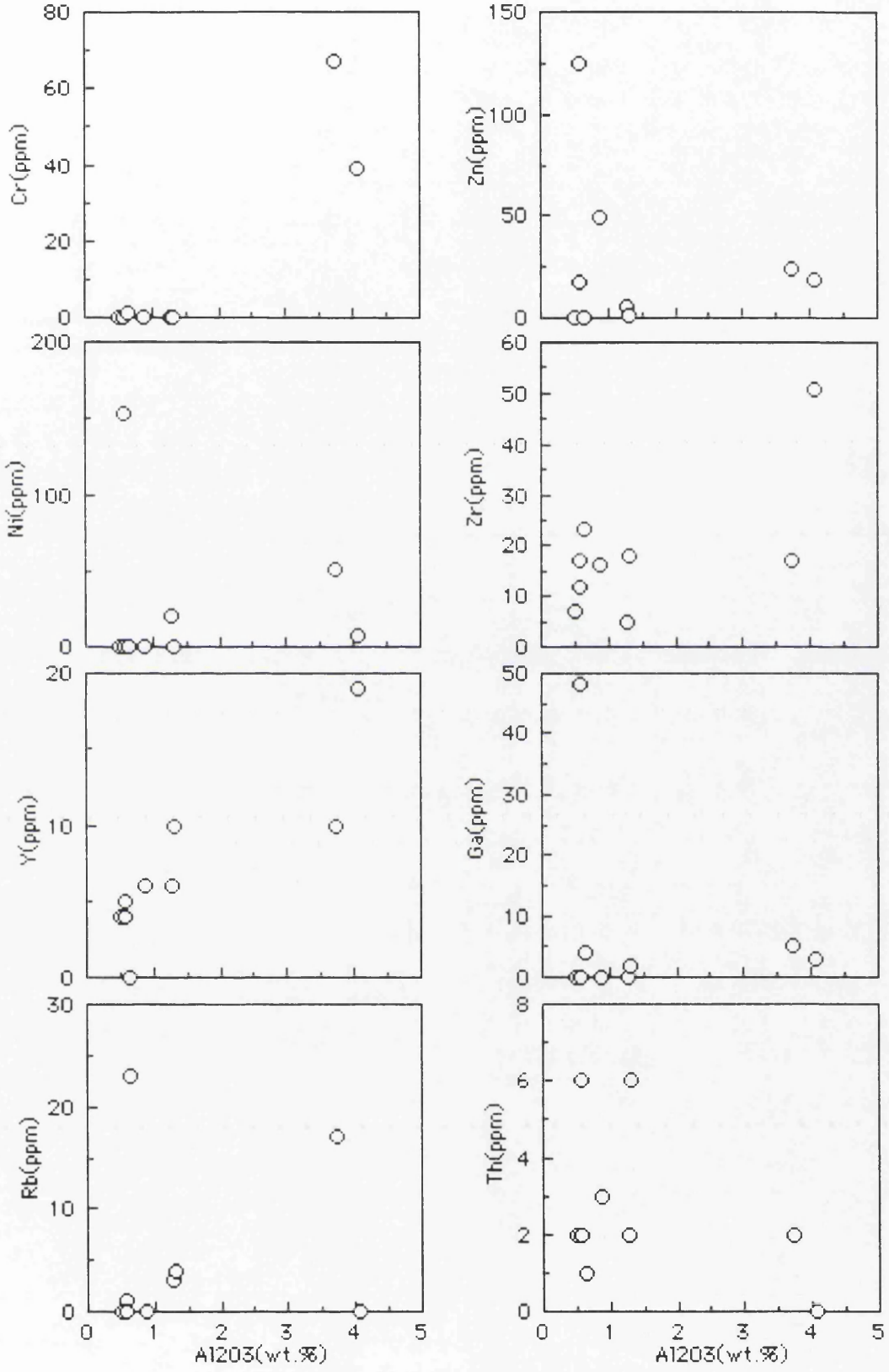

Figure 5.2. Al_2O_3 versus selected trace element variation plots.

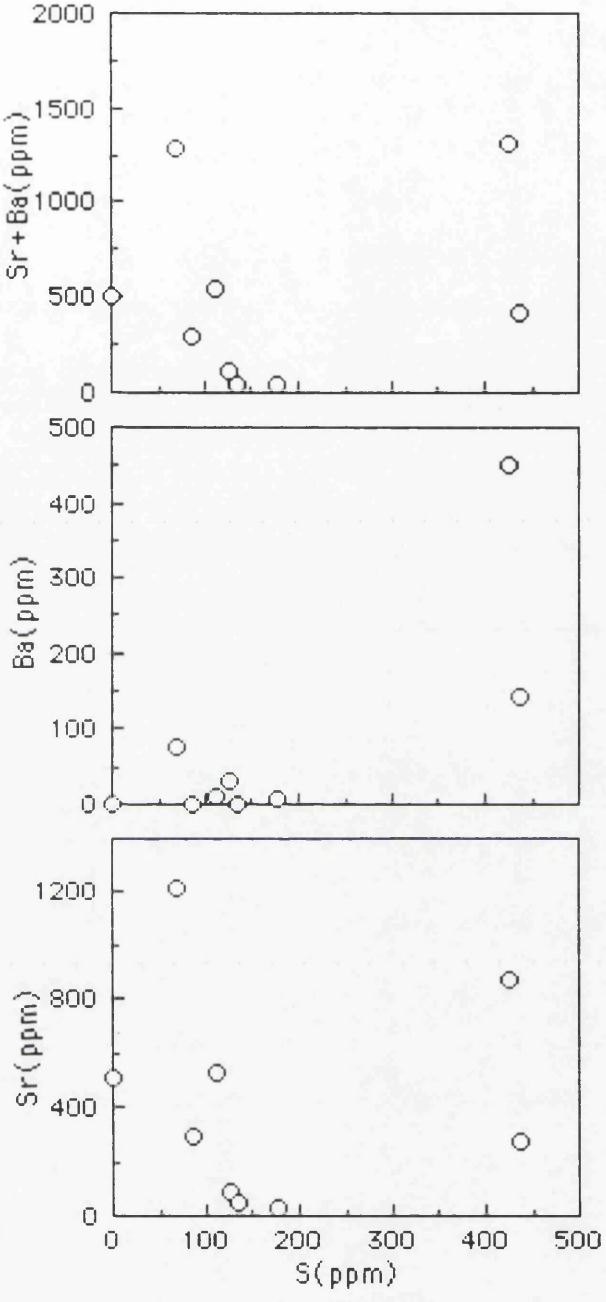

Figure 5.3. S versus Sr, Ba and Sr+Ba trace element plots.

5.2.2. SANDSTONES

5.2.2.1. CHEMICAL CLASSIFICATION

Blatt *et al.* (1980) devised a scheme for the chemical classification of sandstones using a ternary plot of Fe_2O_3+MgO, Na_2O and K_2O. The data from sandstones in the Kizildere Formation plot mainly within the field of greywacke(Figure 5.4) which is in agreement with petrographic descriptions.

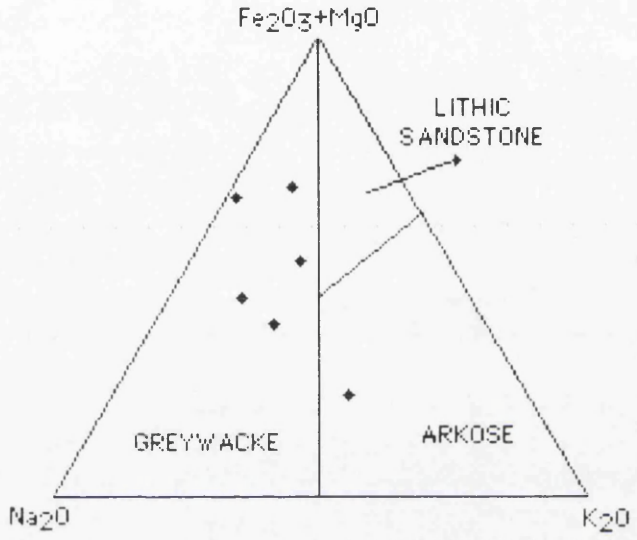

Figure 5.4. Major element chemical classification of sandstones from the Kizildere Formation, most of which fall within the greywacke field. Diagram is from Blatt *et al.* (1980).

Generally, the samples are SiO_2 poor sandstones with Na_2O/K_2O ratios about 0.5-1.4 and relatively low MgO, Ni and Cr that underline the low proportion of material derived from mafic sources. LIL elements exhibit generally low abundances relative to acid clast-dominated sandstones(e.g., Floyd and Leveridge, 1987; Floyd *et al.*, 1990) and with K/Rb ratios(238-435) higher than typical upper crust values(230; Shaw, 1968; Taylor and McLennan, 1985). The high loss on ignition(LOI), CaO and Sr contents of some samples reflects the presence of carbonate clasts.

Chemical classification of the rocks indicate that they are quartz-intermediate(Figure 5.5). Crook(1974) subdivided sandstones on the basis of SiO_2 content and the relative K_2O/Na_2O ratio into three classes and assigned each to a plate tectonic environment. According to these features, all of the sandstone samples from the study area may be classified as quartz-intermediate sediments(average 68-74% SiO_2, $K_2O/Na_2O<1$; Crook, 1974), which are indicative of Andean-type(Active continental) margins.

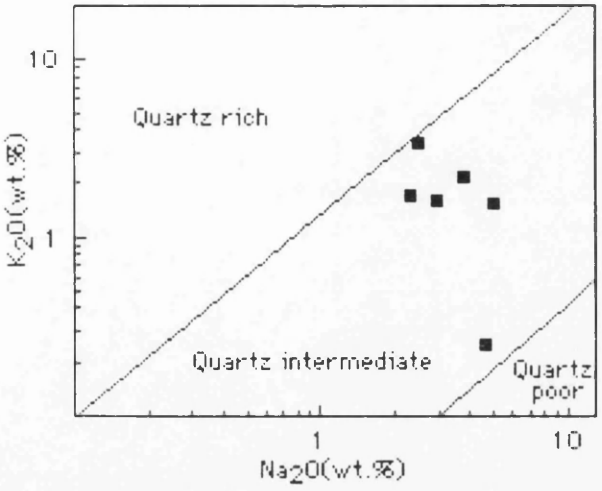

Figure 5.5. Analysis of quartz-richness of sandstones based on major element geochemistry(after Crook, 1974).

5.2.2.2. MAJOR AND TRACE ELEMENTS

The main aims of analysing the sediments are to determine their geochemical characteristics, to find out their geotectonic setting, and to characterize the provenance from which the sediments were derived. Chemical data for sandstones in the Kizildere Formation are listed in Appendices 3 and 4.

The sandstones have a SiO_2 range of 58.03-70.59 wt.%, high $Fe^*_2O_3$ and MgO contents of between 0.99 and 3.37 wt.%. On the major element variation plots(Figure 5.6), TiO_2 decreases as SiO_2 increases because Ti is mostly in clay minerals which decline with increasing quartz and feldspar content. SiO_2 shows positive correlation with K_2O, and suggests that the amount of K-feldspar increases as quartz increases. Similarly, SiO_2 shows a negative correlation with MgO, $Fe_2^*O_3$ and $Fe_2^*O_3$+MgO, indicating that quartz increased as clay minerals and mica declined. Al_2O_3 and SiO_2 correlation is not clear, suggesting that probably clay minerals and feldspars declined as SiO_2 increased. However, Na_2O and CaO show no correlation with increasing SiO_2(Figure 5.6). Generally, SiO_2 versus trace element plots are scattered(Figure 5.7). Rb and Ba exhibit fair positive correlation with SiO_2 due to increasing amount of K-feldspar. In addition, Ba and Rb show positive correlation with K_2O(Figure 5.8).

Generally, the compositional variation of the sandstones is quite scattered(Figures 5.6 and 5.7). Thus, the rocks can be considered as a mixture of clay, quartz, feldspar and carbonate with an end member Niggli c (3-45), mg (0-0.08), and k (0.15-0.45).

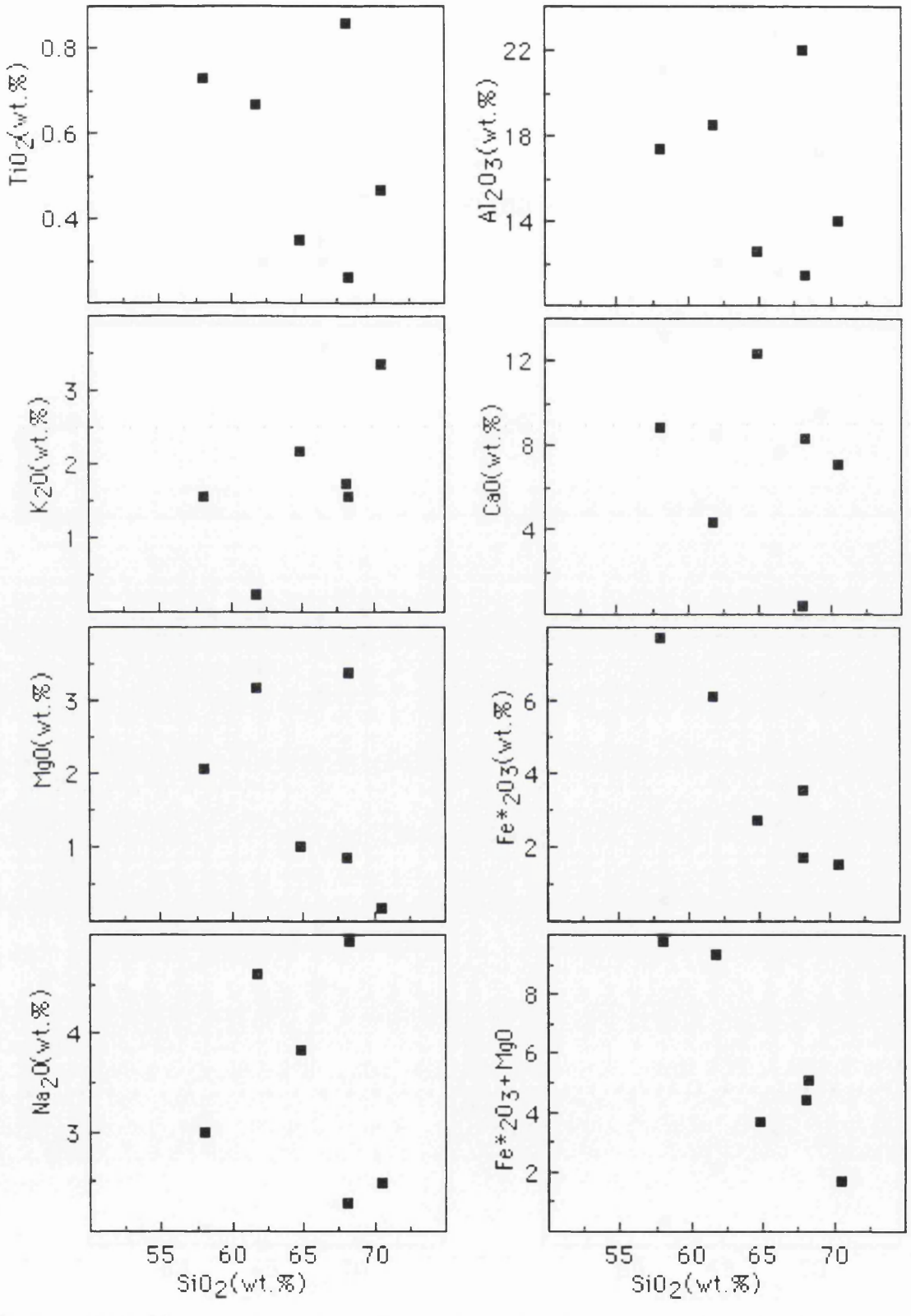

Figure 5.6. SiO_2 versus major element variation plots for sandstones in the Kizildere Formation.

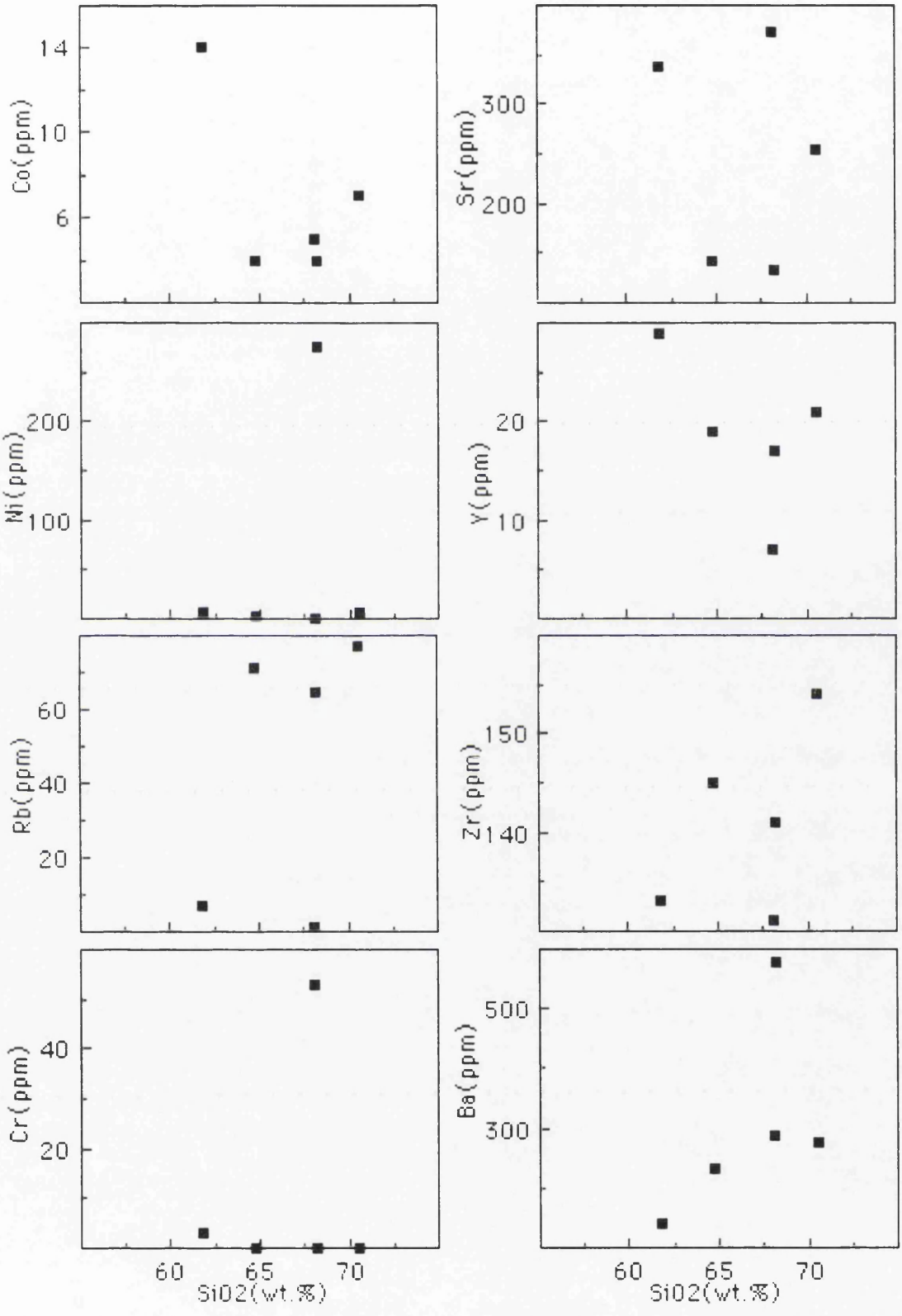

Figure 5.7. SiO_2 versus trace element variation plots for sandstones in Kizildere Formation.

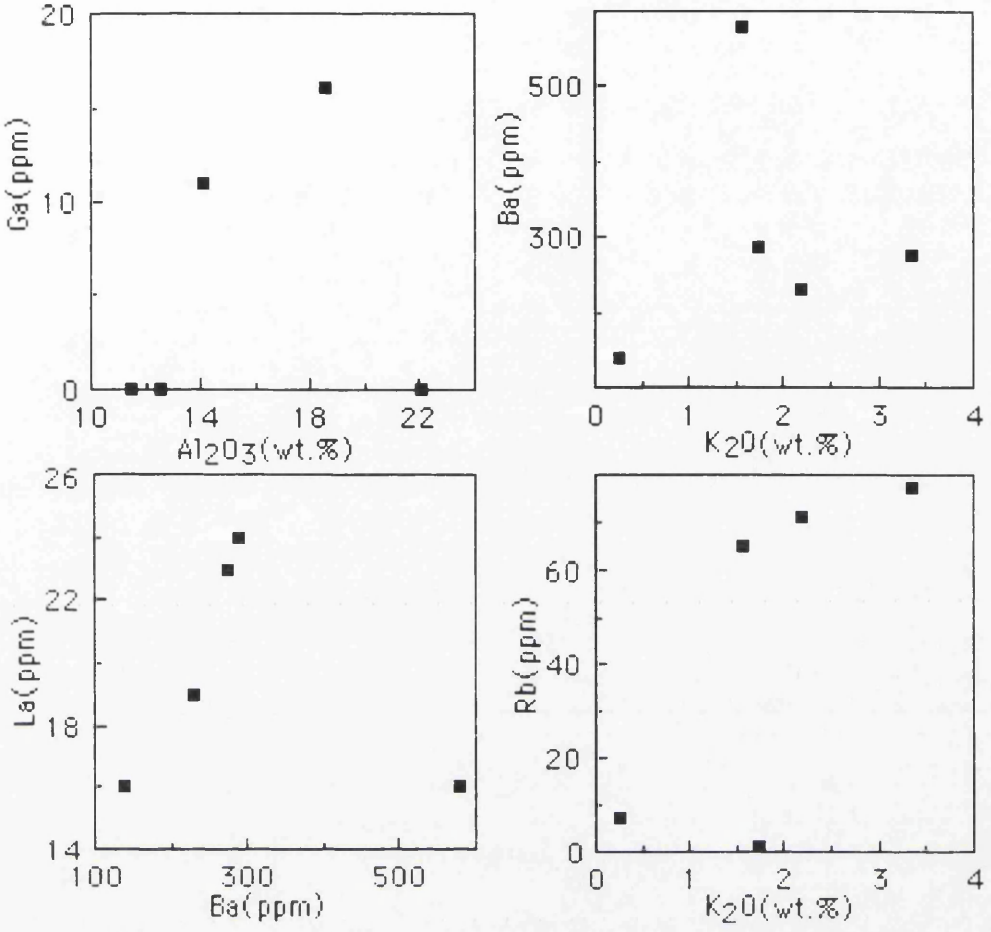

Figure 5.8. Ba versus La, Al_2O_3 versus Ga, and K_2O versus Rb and Ba variation plots for sandstones.

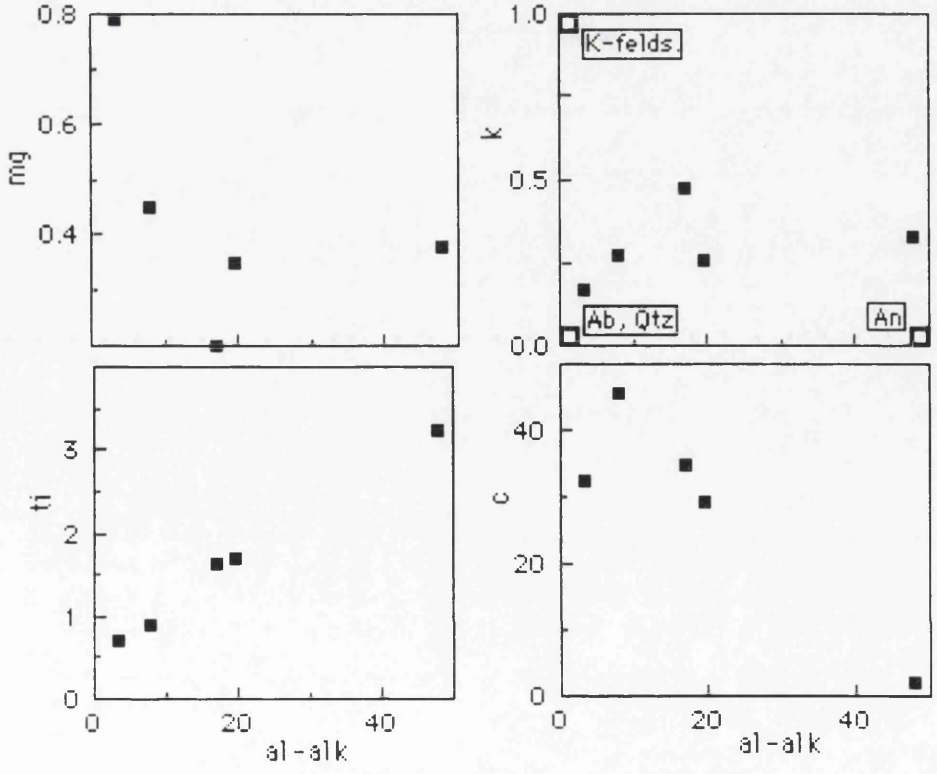

Figure 5.9. Niggli al-alk versus Niggli values variation plots for sandstones.

Niggli al-alk was used as an indicator of sheet mineral influence in the rocks because albite and K-feldspar each has al-alk=0, and the lack of a positive correlation of al-alk with Niggli c(=CaO)(Figure 5.9) suggests that calcic plagioclase is not a major influence on al-alk values. All of the analyzed samples(except one) are high in CaO(7-12wt.%) reflecting the presence of carbonate in the samples(Figure 5.10).

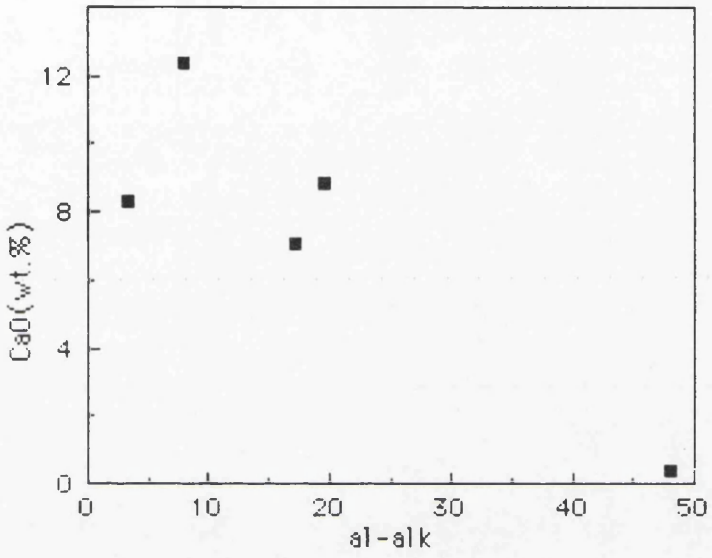

Figure 5.10. Niggli al-alk versus CaO(wt.%) plot for sandstones.

By using al-alk, the clay mineral and mica influence on the composition of the sandstones can be obtained(Senior and Leake, 1978). Therefore, Figures 5.11 and 5.12 suggest that K2O, $Fe^*_2O_3$(total), TiO_2, Rb, Zr and probably Ba, Ni and Zn were added in sheet silicate minerals such as mica and clay.

TiO_2 exhibits such a good positive correlation with al-alk that it might be useful in alkali metasomatized sediments where al-alk will be changed but not Ti(Senior and Leake, 1978). The elements suggested to be largely added to sediments in clay minerals are plotted against TiO_2(Figure 5.13) which generally displays better correlation than plotting against al-alk, presumably due to removal of the influence of variable amounts of feldspar. Likewise, Al_2O_3 shows a positive correlation with TiO_2, showing that much Al_2O_3 was added in clay minerals in addition to feldspar. Furthermore, Al_2O_3 also exhibits good positive correlation with al-alk(Figure 5.14), suggesting addition of Al_2O_3 mainly in clay minerals. SiO_2 does not show any correlation with al-alk due to the variable amounts of quartz in the samples.

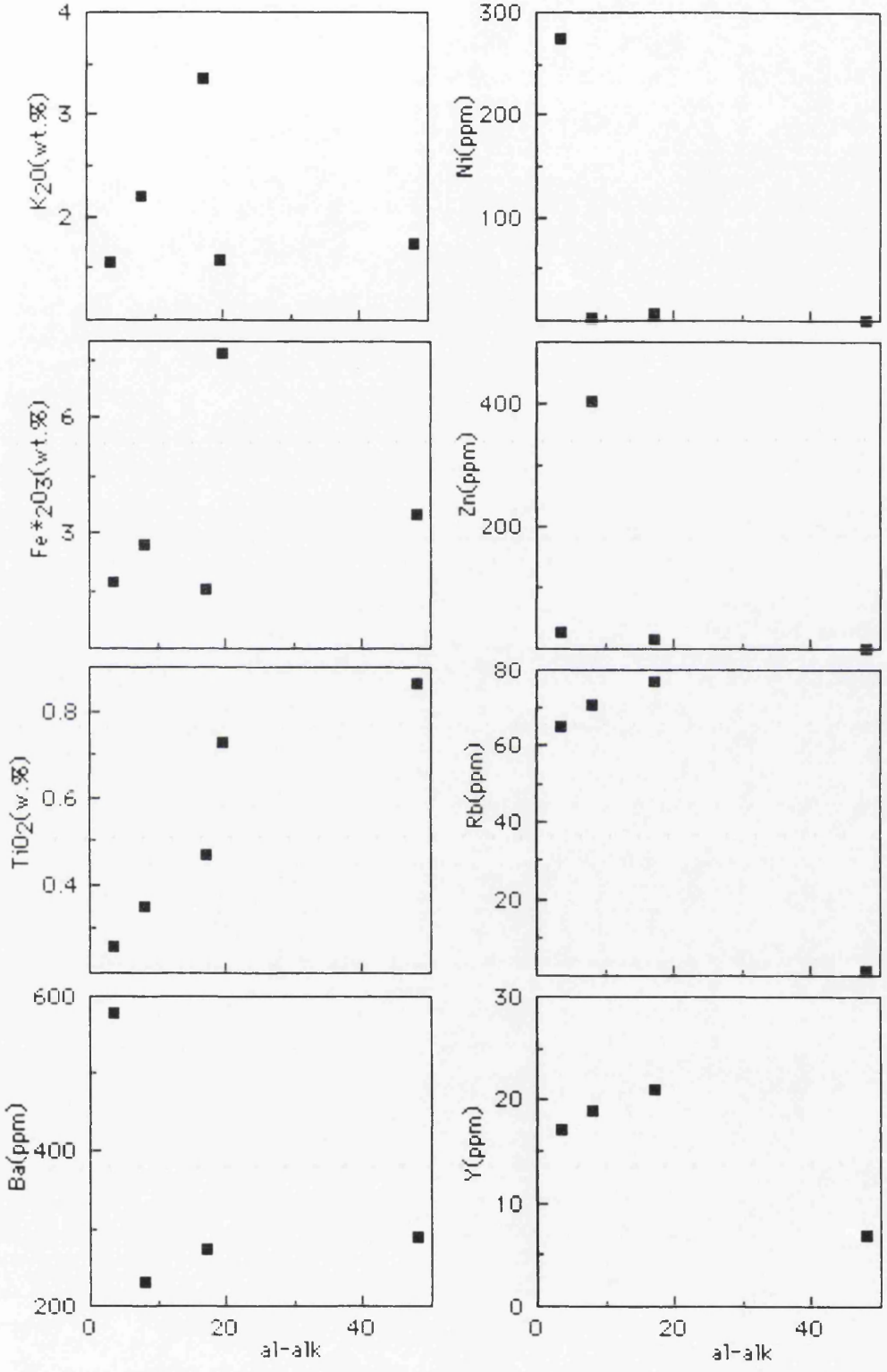

Figure 5.11. Niggli al-alk versus some major and trace elements.

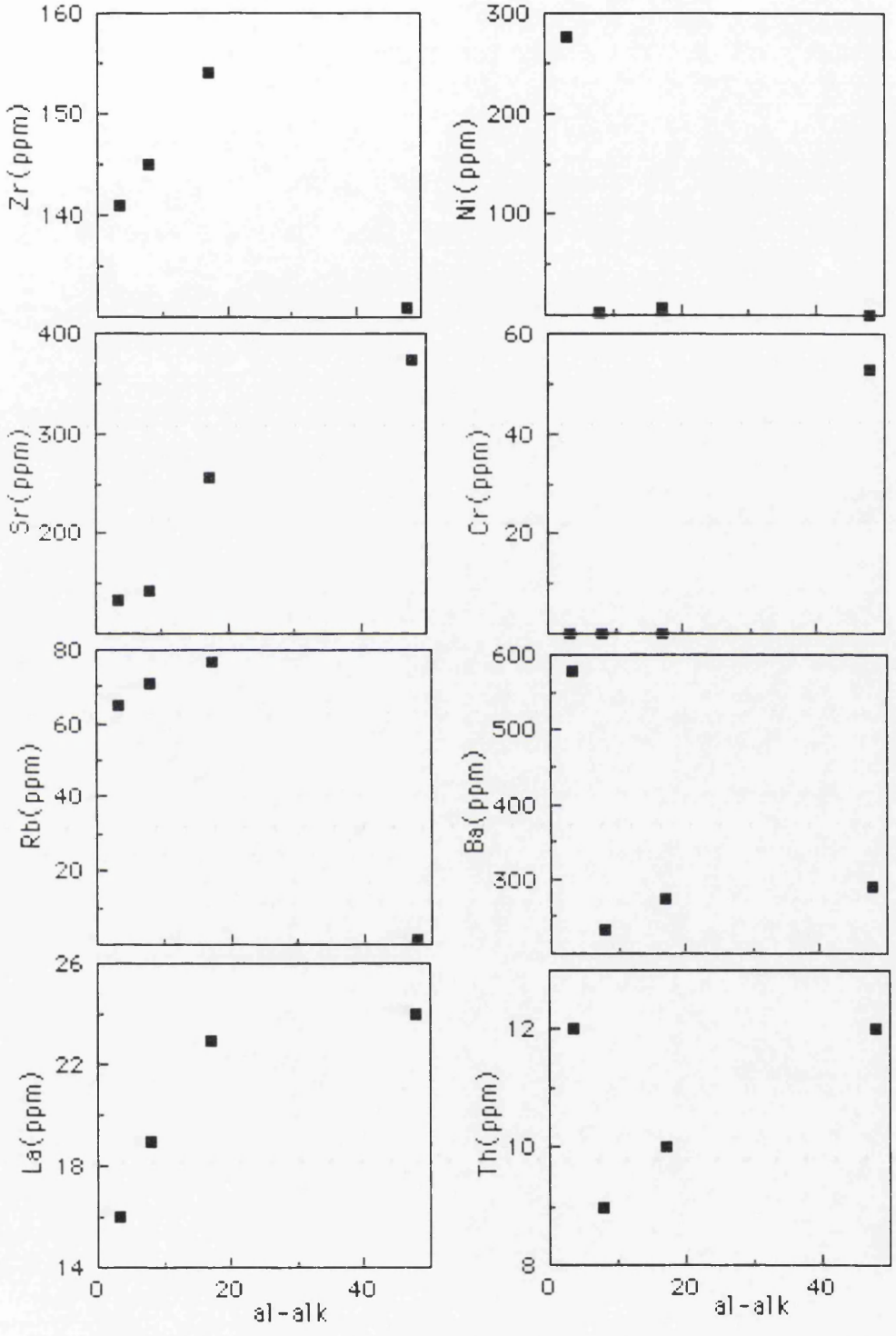

Figure 5.12. Niggli al-alk versus trace element variation plots for sandstones.

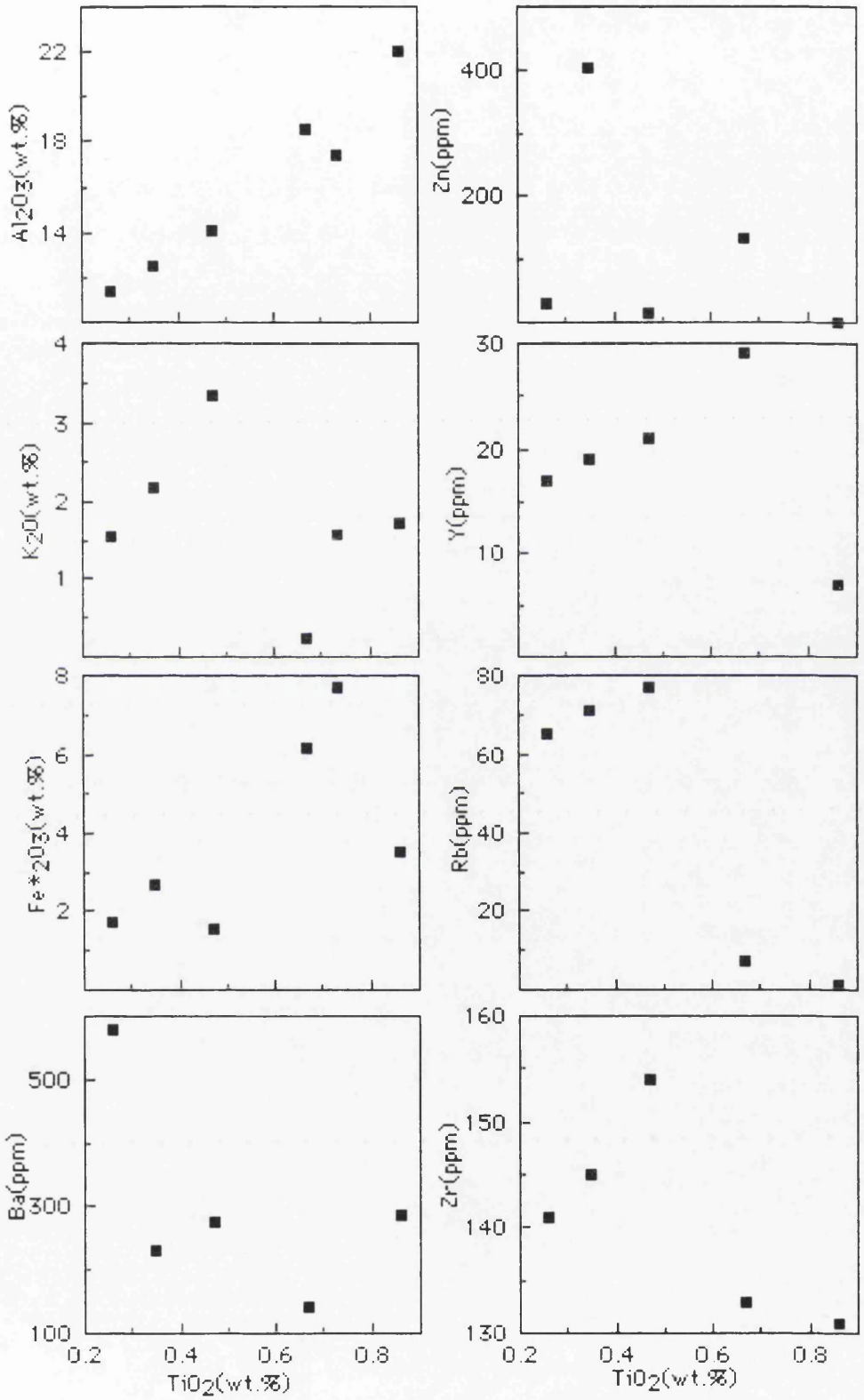

Figure 5.13. TiO_2 versus selected major and trace elements.

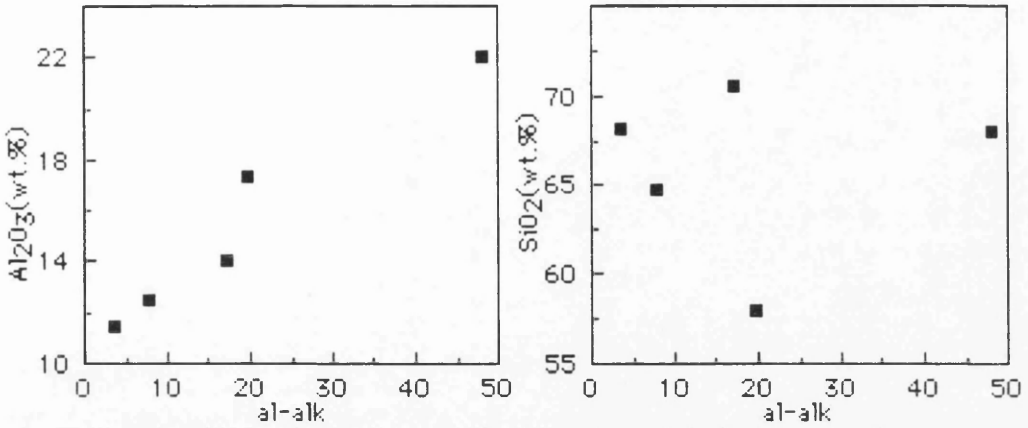

Figure 5.14. Niggli al-alk versus Al_2O_3(wt.%) and SiO_2(wt.%) plots.

CaO correlates with Sr in the sandstones and there is a negative correlation of c and al-alk(Figure 5.15), indicating that Ca and Sr were not originally added in the sheet silicates but probably with carbonate and/or feldspar. There is no clear correlation of K_2O and Sr(Figure 5.15).

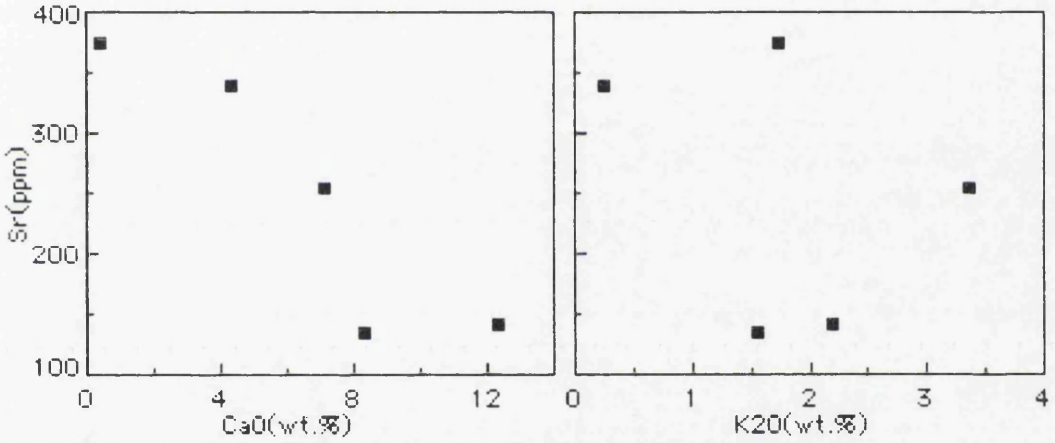

Figure 5.15. Sr(ppm) versus CaO(wt.%) and K_2O(wt.%) plots.

In general K_2O shows a positive correlation with Rb and Ba(Figure 5.16) which suggests that both Rb and Ba were substantially added to the sediments in clay, mica and feldspar.

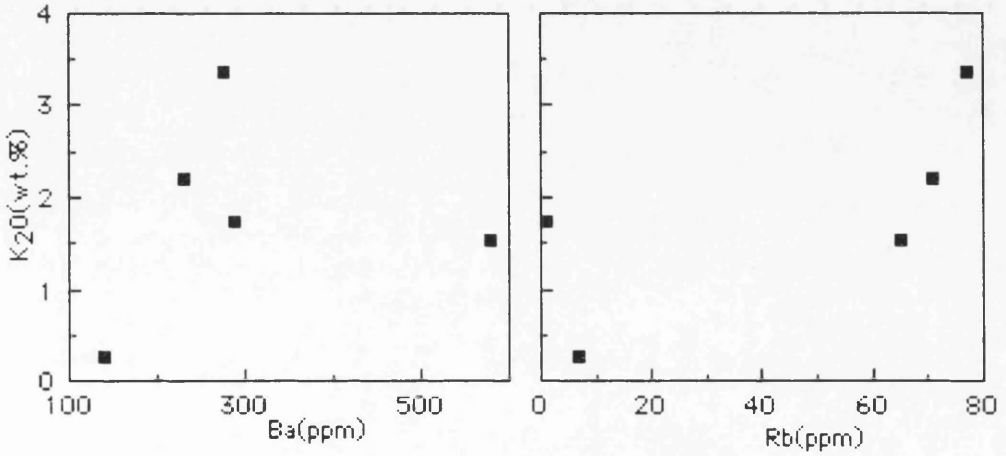

Figure 5.16. Ba(ppm) and Rb(ppm) versus K_2O(wt.%) plots.

Y shows little clear correlation with Zr, P_2O_5 and TiO_2(Figure 5.17) and al-alk which indicates that Y was probably added in apatite, zircon and partly in clay minerals and mica, i.e. a mixed source.

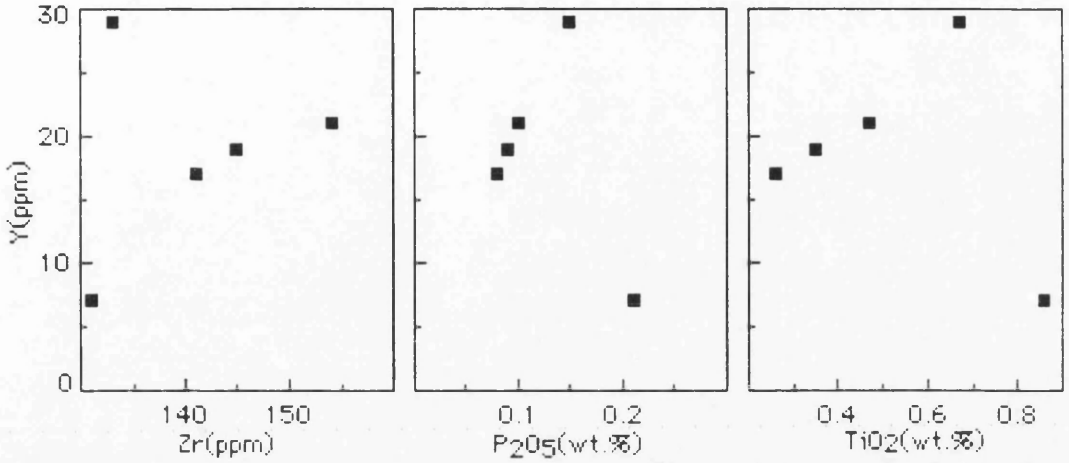

Figure 5.17. Y(ppm) versus Zr(ppm), P_2O_5(wt.%) and TiO_2(wt.%) plots.

Na_2O has a negative correlation with al-alk(Figure 5.18) suggesting the presence of sodic plagioclase in the sandstones.

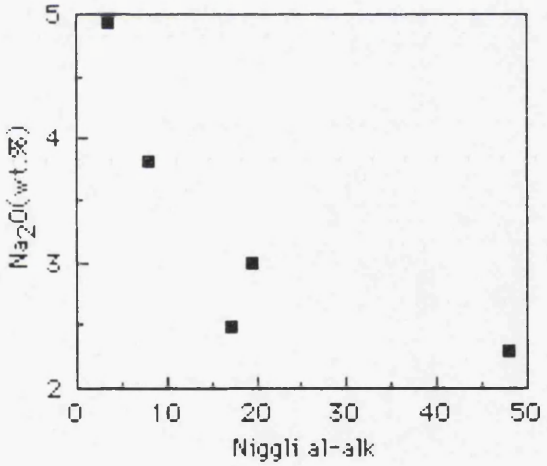

Figure 5.18. Niggli al-alk versus Na_2O(wt.%) plot.

The chemical composition of sandstones is influenced by features such as grain-size, degree of source weathering and diagenesis(Sawyer, 1986; Wronkiewicz and Condie, 1987). As the greywackes studied have relatively uniform grain-size, the grain-size is not considered a major variable controlling changes in the chemical composition of the rocks. Differential weathering at the source tends to mobilize and change the relative abundance of LIL elements(Nesbitt *et al.*, 1980). A measure of the degree of weathering in the source is provided by the chemical index of alteration(CIA)(Nesbitt and Young, 1982), where

$$CIA=mol\ [Al_2O_3/(Al_2O_3+CaO+Na_2O+K_2O)]x100$$

An average of CIA in the samples is 42 in the range of 30-54 respectively, excluding sample MA-102(CIA=77)(Figure 5.19). Generally, the average value is lower than average upper continental crust(CIA=50) and feldspar(CIA=50) (Nesbit and Young, 1982), suggesting low to moderately weathered sources for greywackes. However, sample MA-102(CIA=77) is comparable with illite and montmorillonite (CIA=75-85; Nesbit and Young, 1982), indicating that weathering effects have not proceeded to the stage where alkali and alkaline earth elements are substantially removed from clay minerals. Furthermore, it is suggested that diagenesis is another factor which mainly effect the LIL elements(Hower *et al.*, 1976), U(Colley *et al.*, 1984) and possibly the light REE(Van Weering and Klaver, 1985).

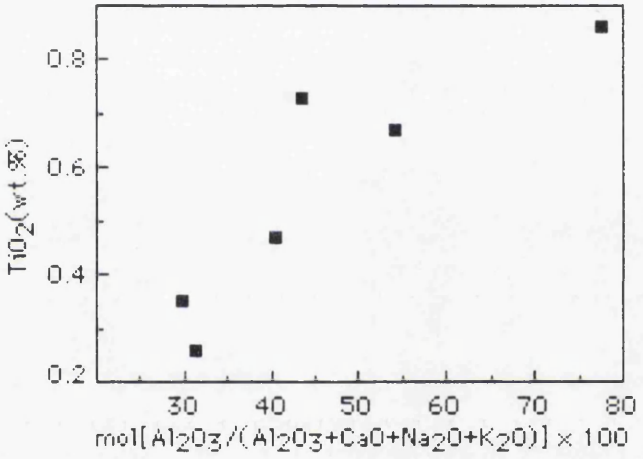

Figure 5.19. Chemical alteration index(CIA) versus TiO_2(wt.%) plot.

It has been suggested that the full range of elemental composition for greywackes in different tectonic environments can be more adequately compared utilizing upper continental crust normalized multi element patterns(Floyd *et al.*, 1991b). The elements are arranged from right to left in order of increasing ocean residence times and comprise a relatively stable group(Th-Nb) and a more mobile group(Ni-K). The patterns exhibited for greywackes(Figure 5.20) indicate a source composed largely of continental arc+active continental margin tectonic environments (e.g., Floyd *et al.*, 1991b).

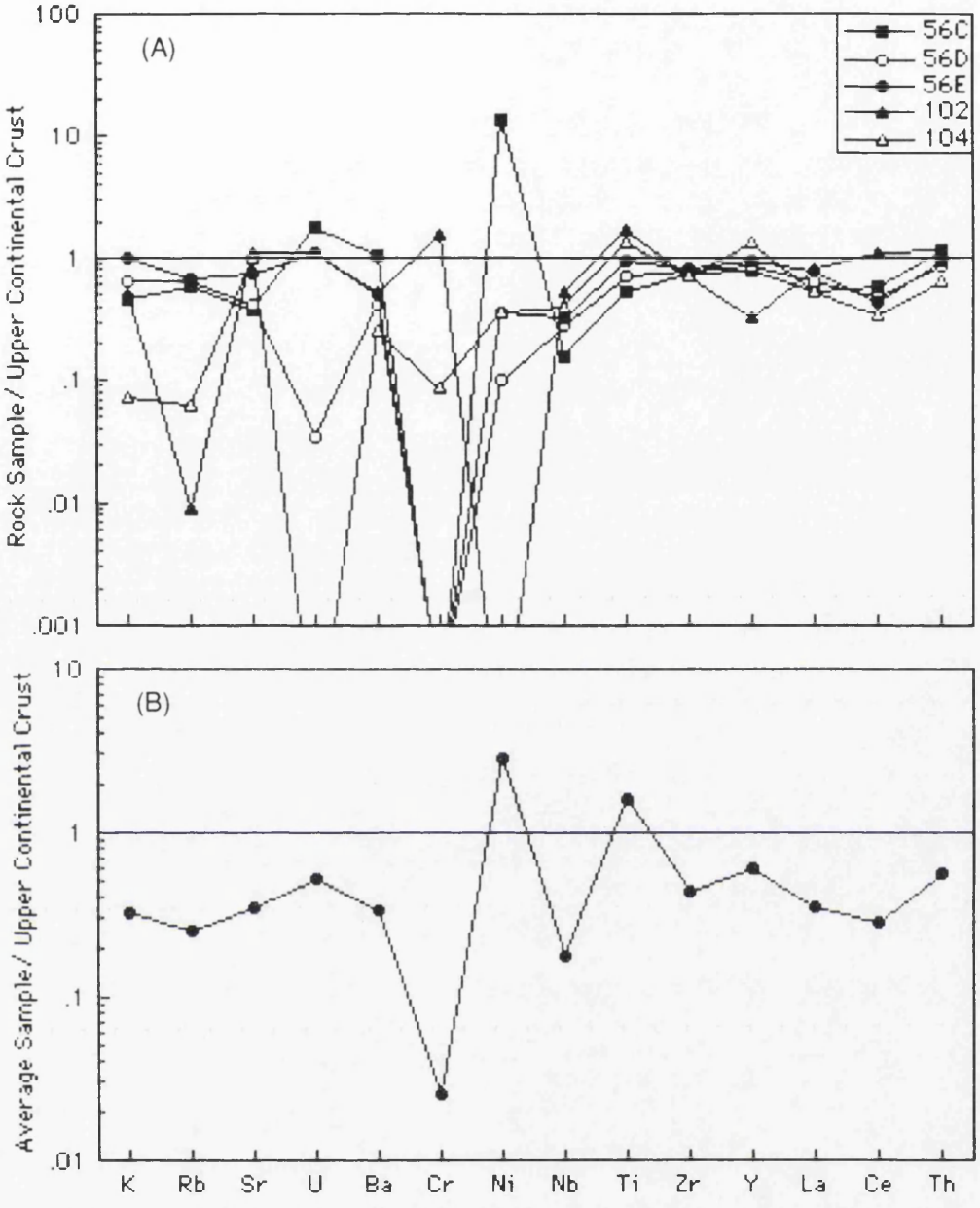

Figure 5.20. Normalized multi-element patterns for greywackes from the Kizildere formation(A), and for the average of five greywacke samples(B). Upper continental crust normalization values from Taylor and McLennan(1985).

5.2.2.3. TECTONIC SETTING OF GREYWACKES

The bulk chemistry of clastic sediments is mainly a reflection of the average composition of the source area, although other factors, such as degree of chemical weathering, mechanical sorting during sedimentation, and post-depositional mobilization, are important and can variably influence element distribution patterns(e.g., Bhatia, 1983; Taylor and McLennan, 1985; Sawyer, 1986: Wronkiewicz and Condie, 1987; Roser and Korsch, 1988).

A number of major oxide and trace element based diagrams

reportedly enable the determination of the tectonic environment of deposition of sediments(Bhatia, 1983 and 1985; Roser and Korsch, 1988), although the best discrimination is provided by ratios of stable trace elements in greywackes(Bhatia and Crook, 1986) that are quantitatively transferred from source to sink. Normalized REE patterns and ratios of transition and incompatible elements(e.g., La/Sc, La/Th, Th/Sc, Cr/V, Ti/Zr) in greywackes have been used to constrain provenance composition as these factors are generally considered to be quantitatively transferred from source to sink during sedimentation(McLennan *et al.*, 1980; Taylor and McLennan, 1985; Bhatia and Crook, 1986; McLennan, 1989). The above element groups are useful provenance discriminators as they are not strongly fractionated during weathering and sedimentary sorting(unlike many LIL elements), and also remain relatively immobile during any subsequent low-grade alteration.

Bhatia(1983) showed that the chemical composition and tectonic setting of sandstones was related with a progressive decrease in Fe_2O_3+MgO, TiO_2, Al_2O_3/SiO_2, and an increase in K_2O/Na_2O and $Al_2O_3/(CaO+Na_2O)$ in sandstones deposited in oceanic island arcs to continental island arcs to active continental margins to passive margins. The ratio Al_2O_3/SiO_2 gives an indication of the quartz enrichment in sandstones. The ratio K_2O/Na_2O is a measure of the K-feldspar and mica versus plagioclase content in the rock and the $Al_2O_3/(CaO+Na_2O)$ parameter is a ratio of the most immobile to the most mobile elements. Ti, Fe, and Mg are also relatively immobile. Bhatia(1983) developed discrimination diagrams based on these observations. Applying Bhatia's(1983) criteria to the chemical composition of the Kizildere Formation sandstones gave no clear tectonic setting(Figure 5.21; Table 5.1), probably because of the Ca-rich nature of the present samples which contrast with those used by Bhatia(1983).

Bhatia(1983) also developed some geochemical multi-element discrimination functions and used plots of them to identify the tectonic settings of sandstones. In this discrimination, continental arc setting that comprises sedimentary basins formed either on a well developed continental crust or on thin continental margins, and the oceanic island arc represent convergent plate margins. The active continental margin setting includes continental margins of Andean type and strike-slip types. Sediments are substantially derived from granite-gneisses and siliceous volcanics of the uplifted basement. The passive margin tectonic setting comprises rifted continental margins of the Atlantic type developed along the edges of continents. The Kizildere Formation sandstones are again scattered over several fields(Figure 5.22), but the small number of samples

studied means that any conclusion are necessarily tentative.

Table 5.1. Some compositional parameters of sandstones of various tectonic setting(after Bhatia, 1983) with the Kizildere sandstones.

Element (wt.%)	OIA	CIA	ACM	PM	MA-56C	MA-56D	MA-56E	MA-102	MA-104	MA-208
Fe_2O_3+MgO	11.73	6.79	4.63	2.89	5.10	3.68	1.72	4.38	9.32	9.76
Al_2O_3/SiO_2	0.29	0.20	0.18	0.10	0.17	0.19	0.20	0.32	0.30	0.30
K_2O/Na_2O	0.39	0.61	0.99	1.60	0.31	0.57	1.35	0.76	0.05	0.53
Al_2O_3 / ($CaO+Na_2O$)	1.72	2.42	2.56	4.15	0.86	0.78	1.46	8.24	2.00	1.47
TiO_2	1.06	0.64	0.46	0.49	0.26	0.35	0.47	0.86	0.67	0.73

Note: OIA=Oceanic island arc, CIA=Continental island arc, ACM=Active continental margin, PM=Passive margin.

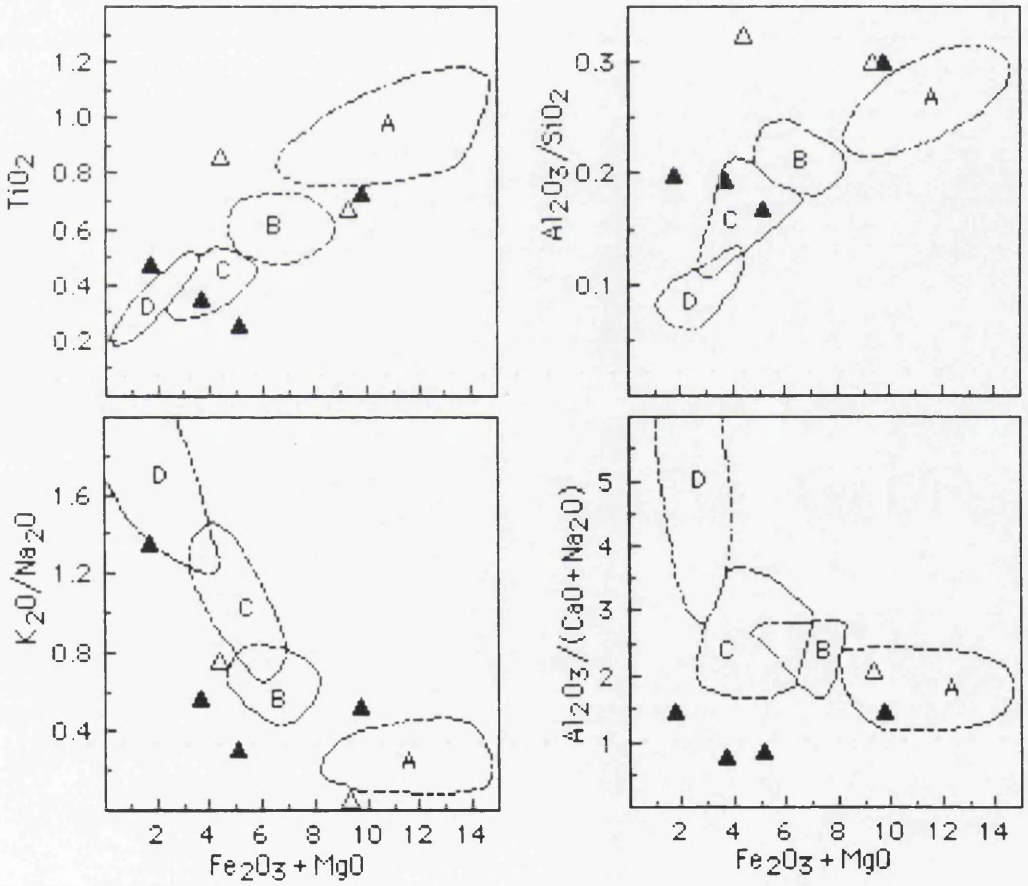

Figure 5.21. Major element composition plots of sandstones for tectonic setting discrimination. Plot of TiO_2, Al_2O_3/SiO_2, K_2O/Na_2O, and $Al_2O_3/(CaO+Na_2O)$ versus Fe_2O_3+MgO, (Fe_2O_3 represents total iron as Fe_2O_3). Open triangles represent samples with <5wt.%CaO, and closed triangles for samples with >5wt.% CaO. Fields are; A-Oceanic island arc, B-Continental island arc, C-Active continental margin, and D-Passive margin(Bhatia, 1983).

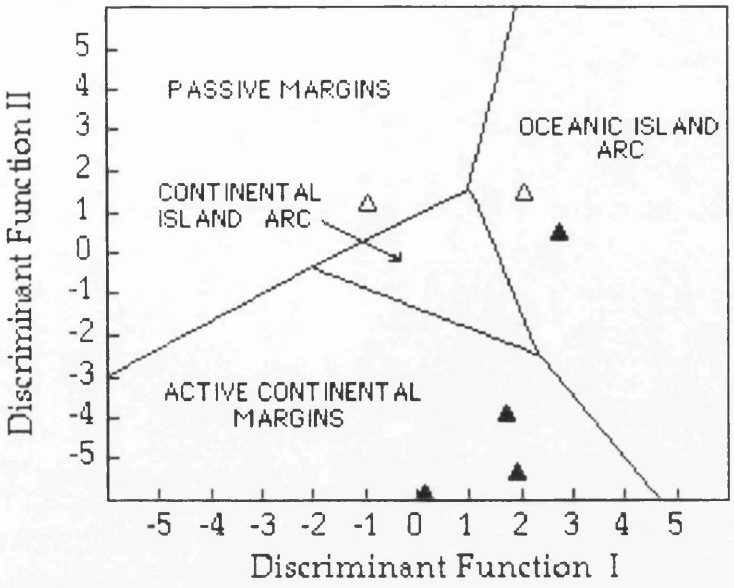

Figure 5.22. Plot of discriminant scores along Function I versus Function II, to discriminate sandstones(after Bhatia, 1983). Open triangles for samples with <5wt.% CaO and closed triangles for samples with >5wt.% CaO.

On the diagram of $K_2O/Na2O$ versus SiO_2(Figure 5.23), the Kizildere sandstones plot within the Active Continental Margin(ACM) field of Roser and Korsch(1986). This suggests that the presence of arc-derived material may be discounted. According to Roser and Korsch(1986) the location of data points on the diagram is primarily controlled by the nature of volcanism, the extent of plutonism and related erosional levels. The effect of mineralogical maturation through sediment recycling is of secondary consequence.

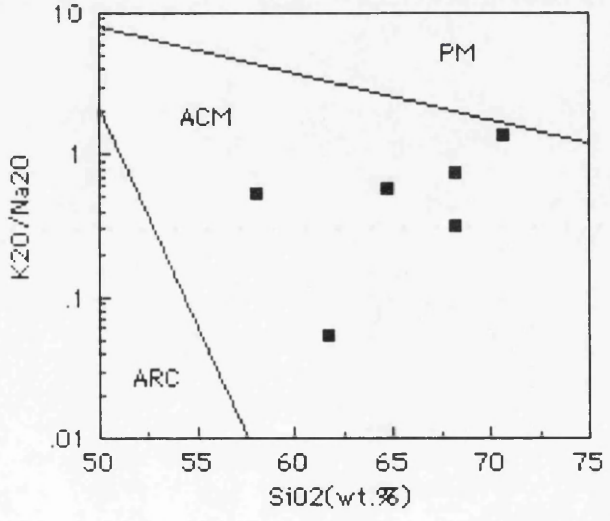

Figure 5.23. Tectonic discrimination diagram for Kizildere sandstones: PM, passive margin; ACM, active continental margin; ARC, arc(after Roser and Korsch, 1986).

Bhatia and Crook(1986) discriminated tectonic setting of greywackes, sandstones of wide mineralogical range, by using plots of trace elements such as La, Ce, Th, Zr and Co, which are immobile due to their relatively low mobility during sedimentary processes and their low residence times in sea water(Holland, 1978). In Figure 5.24, the greywackes fall within the active continental margin and continental island arc fields of Bhatia and Crook(1986).

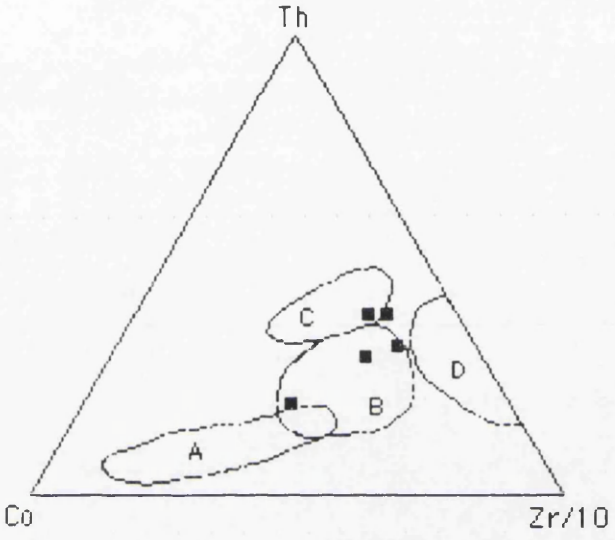

Figure 5.24. Th-Co-Zr/10 plot for tectonic setting of the greywackes studied. Discrimination fields are A-Oceanic island arc; B-Continental island arc; C-Active continental margin; D-Passive margin(from Bhatia and Crook, 1986).

5.2.2.4. CHEMICAL DISCRIMINATION OF PROVENANCE

Trace elements including the REE, Zr, Ti, Y, Hf and U are useful in determining the source of sediments as they have intermediate ionic potential and low ocean residence times(Holland, 1978; Henderson, 1982). These elements are readily incorporated into sediments and also give some indication about the source composition(Taylor and McLennan, 1985).

A K versus Rb plot may be used to distinguish those sediments derived from rocks of acid and intermediate compositions from those derived from rocks of basic compositions(e.g., Floyd and Leveridge, 1987; Floyd *et al.*, 1990). The relatively high K/Rb ratios of the Kizildere sediments are indicative of derivation from acid and intermediate source rocks with some input from basic sources(Figure 5.25). In Figure 5.25, greywackes lie above a K/Rb ratio of 230, except one sample, and suggest that greywackes were derived from mainly acidic to intermediate compositions. In addition, Figure 5.26 confirms an acidic source for greywackes.

The levels of Cr and Ni have been used to indicate a mafic input to sediments(e.g., Hiscott, 1984; Haughton, 1988; Wrafter and Graham, 1989). The low levels of Cr and Ni found in the Kizildere sandstones again indicate little basic input into the system. The Ni/Co ratio is generally lower than 1 but sample MA-56C has 68.75, either due to weathering in the source rock that selectively enriched Ni or to a Ni-rich source rock. In addition, Th/U ratio in the rocks is lower than 4(upper continental crust Th/U=3.8; Taylor and McLennan, 1985), suggesting that they are mainly derived from acid and intermediate source.

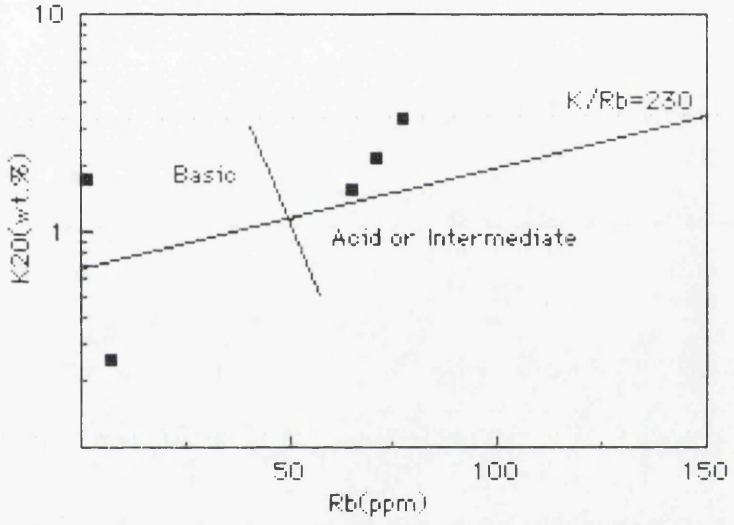

Figure 5.25. Distribution of K(log wt.%) and Rb(ppm) in greywackes relative to a K/Rb ratio of 230(main trend of Shaw, 1968). Boundary line between acid or intermediate and basic compositions after Floyd and Leveridge(1987).

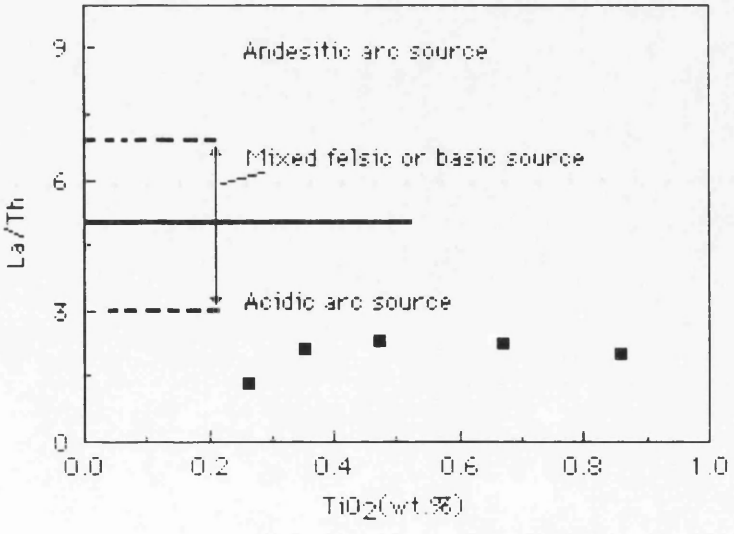

Figure 5.26. Plot of TiO_2(wt.%) versus La/Th ratio indicating the source of greywackes(source fields from Bhatia and Taylor, 1981; McLennan *et al.*, 1984; Taylor and McLennan, 1985).

5.2.2.5. RARE EARTH ELEMENTS

Rare earth elements in sediments are generally considered to reflect the nature of the source area undergoing denudation(e.g., McLennan *et al.*, 1980; Taylor and McLennan, 1981; Sawyer, 1986). Two representative samples of greywackes from Kizildere formation were analysed to determine their REE content. The REE patterns are given in Figure 5.27. Generally, greywackes are characterised by moderate LREE enrichment(La_N/Lu_N=8-11) and less fractionated HREE(Gd_N/Yb_N=0.80-0.85). Low Gd content is presumably due to analytical uncertainties. Both samples show slight positive Eu anomaly(Eu_N/Eu^*=1.35-1.53). This positive Eu anomaly can be interpreted to be result of plagioclase enrichment during sedimentary sorting. Such phenomenon has only been recognized in volcanogenic sediments where weathering effects are minor and plagioclase an abundant constituent(McLennan, 1989). Generally, low REE abundance and particularly $Gd_N/Yb_N<1$ may have resulted from modest amounts of zircon. Compared to typical, well-mixed, fine-grained materials derived from the continental crust (such as NASC; Figure 5.27), the greywackes show a closer degree of LREE enrichment but a lower degree of HREE enrichment.

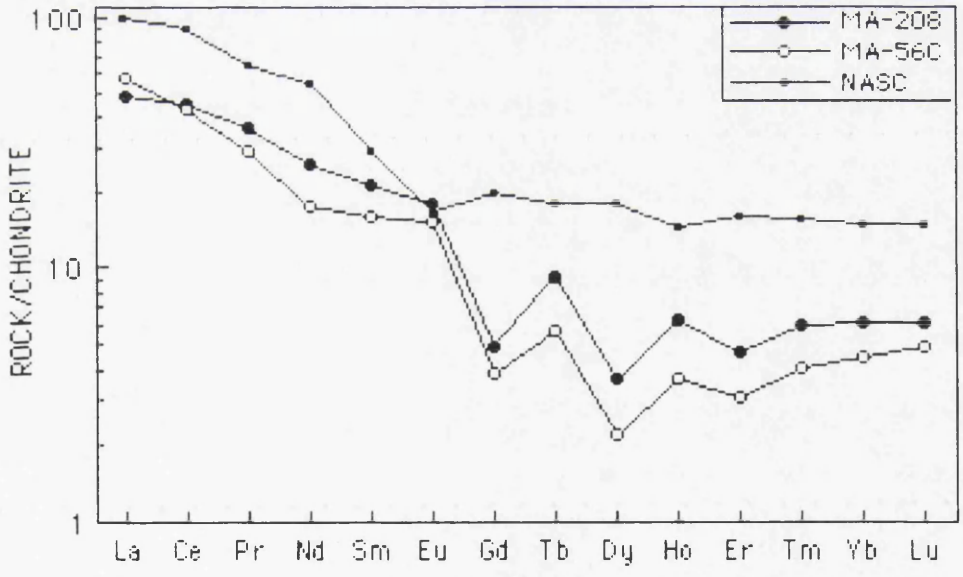

Figure 5.27. Chondrite-normalized(Boynton, 1984) REE patterns of greywackes. North American Shale Composite, NASC(Henderson, 1984) is also shown for comparison.

It is a common assertion that sedimentary rocks deposited at active continental margins, such as island arcs or continental arcs, will have REE characteristics similar to undifferentiated volcanic rocks of the arc itself(i.e., similar to andesites) with lower REE abundances, La/Sm and La/Yb ratios

and without negative Eu anomalies(e.g., Gromet *et al.*, 1984; Gibbs *et al.*, 1986). However, sediments deposited at active continental margins generally show REE patterns intermediate between a 'typical andesite pattern' and PAAS(Post-Archean Australian Shale)(McLennan *et al.*, 1990).

On the basis of petrographic, geochemical, and isotopic data, several major source components for sediments deposited at active continental margins were suggested(e.g., McLennan *et al.*, 1989, 1990). One source is old upper crust which is made up of either old igneous and metamorphic terranes or old, recycled sedimentary rocks. Such sources are likely to have flat HREE patterns which is probably characteristic for average, or typical upper continental crust. A second major source is a young component derived from island arc or continental arc material. At shallow depth(e.g., within the field of plagioclase stability) igneous material which has not undergone significant crystal fractionation will show less fractionated REE patterns with no Eu anomalies. A third possible source is fractionated felsic plutonic rocks which might be incorporated into sediments during explosive volcanism, or more likely when the arc is maturated and dissected to expose plutonic root zones. They are likely to exhibit different REE patterns but in general will have negative Eu anomalies as plagioclase was removed or retained in the parental source during their igneous history(McLennan *et al.*, 1990).

The REE patterns of greywackes from the Kizildere formation which has less fractionated LREE and depleted HREE than the North American Shale Composite(NASC), with slightly positive Eu anomalies probably represents the source rocks of young components derived from continental arc material. HREE depletion is probably the signature of either garnet fractionation(Taylor and McLennan, 1985), or a reflection of the mantle source REE pattern(Stern *et al.*, 1989).

5.3. VOLCANIC GEOCHEMISTRY

5.3.1. NOMENCLATURE AND DESCRIPTIVE GEOCHEMISTRY OF VOLCANIC ROCKS

The modified total alkali versus silica(TAS) diagram recommended by the international Union of Geological Sciences(IUGS) for the classification of volcanic rocks(Zanettin, 1984; Le Bas *et al.*, 1986) was used to name rock types(Figure 5.28). In addition, descriptive rock names were also used on other volcanic rock classification plots given by Cox *et al.* (1979), Middlemost(1980), and Krementskiy *et al.* (1980).

The TAS is subdivided into alkaline and subalkaline rocks, according to Irvine and Baragar(1971), and MacDonald and Katsura(1964). Rock classification is also based on normative minerals, and this classification shows the silica saturation of rocks in each rock association. For this purpose, using a Fe^{+2}/Fe^{+3} ratio of 9:1(Ringwood, 1975), the CIPW normative mineralogy and Niggli values were calculated for each sample(Appendix 3).

Moreover, to distinguish lava suites, two main criteria are also considered; (1) the concentration of selected major element oxides(e.g., Al_2O_3) and the ratio of MgO to FeO[Mg number= mol% $Mg/(Mg+Fe^{+2})$] assuming 15% of the Fe is Fe_2O_3 to reduce oxidation influence on the rocks), (2) the ratios of selected incompatible trace elements(La/Sm and Gd/Yb which reflect the slopes of the LREE, MREE and HREE portions of the chondrite-normalized REE plots), and ratios reflecting the range in large-ion lithophile to high field strength elements(LILE/HFSE; such as Th/Nb, Th/Yb and Ce/Yb) and the HFSE ratios(such as Zr/Nb and Ti/Y).

The TAS diagram reveals that the Meydan lavas lie along a trend of mildly alkalic differentiation(Figure 5.28). The samples plot as a group in the basalt and trachybasalt(hawaiite) fields; differentiated rocks form a trend line from mugearite to benmoreite to trachyte. A few samples lie on, or slightly beyond the field boundary which separates the hawaiite field from the low SiO_2 - high alkali tephrite field of Le Bas *et al.* (1986); these samples are considered to be hawaiites(Figure 5.28).

In the alkaline suite, alkali olivine basalts and hawaiite samples are generally ol, ne and di normative. However, mugearites are ne and di normative. Silica over saturated rocks of the alkaline suite, benmoreite and trachytes, are q, hy and di normative. The Aladag and Zilan lavas are q, hy and di normative, and their chemistry shows a transitional character between alkaline and subalkaline. In the subalkaline rocks, the Kizildere lavas, andesite, trachyandesite, ignimbrite, rhyolite dome-dykes and the Gurgurbaba lava are q, hy and di normative whereas agglomerate clasts and

dacite are q and hy normative.

As seen on different classification plots, there are small differences in the transition areas. In addition to the above criteria, the Irvine and Baragar(1971) classification on the basis of normative mineralogy is used to define sodic and potassic groups. Generally, the Meydan alkaline lavas and the Aladag lava are sodic in composition but a few samples fall on the dividing line between sodic and potassic groups(Figure 5.30). On the discrimination diagram for sodic-potassic types, the rhyolite dome-dykes and the Gurgurbaba lava are in the field of normal rock types but the ignimbrites show slightly sodic enrichment(Figure 5.31). Furthermore, subalkaline rocks generally fall within the medium-K field but ignimbrites, rhyolite dome-dykes and the Gurgurbaba lavas fall within the high-K field of Peccerillo and Taylor(1976)(Figure 5.29). Nomenclature of these rocks both alkaline and subalkaline are also shown on the plot of normative plagioclase composition(NPC=Anx100/[An+Ab+5/3Ne]) versus normative colour index(NCI=Ol+Px+Mt+Ilm)(Figures 5.32 and 5.33).

Subalkaline rocks(Figure 5.34) were subdivided into calcalkaline and tholeiitic types on plots of FeO*/MgO versus SiO_2(Miyashiro, 1974) and normative plagioclase composition versus Al_2O_3 composition(Irvine and Baragar, 1971). Generally, subalkaline rocks fall in the calcalkaline field, containing above 13 wt.% Al_2O_3 with some in the tholeiitic field(Figures 5.35 and 5.36). Since FeO* would be increased by oxidation, normative plagioclase composition versus Al_2O_3 plot gives much the most reliable discrimination for subalkaline rocks(Figure 5.36).

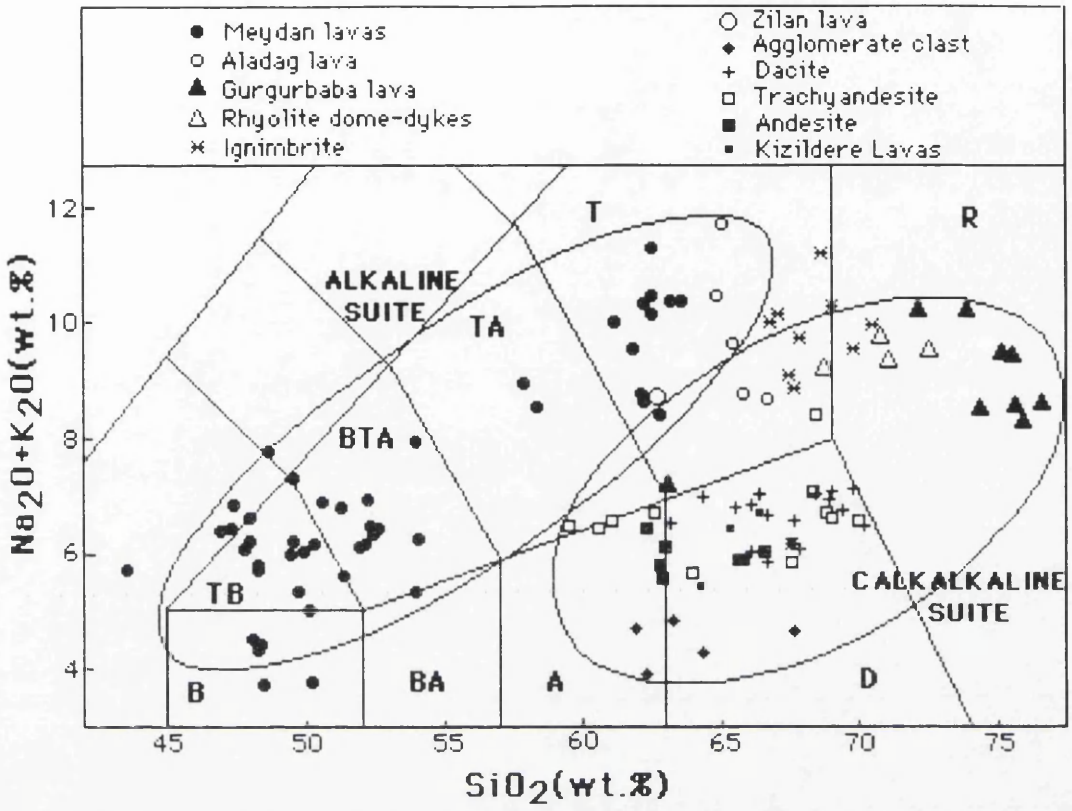

Figure 5.28. Total alkali versus silica(TAS) diagram and classification of volcanic rocks of the study area. Fields are B-Basalt, BA-Basaltic andesite, TB-Trachybasalt, BTA-Basaltic trachyandesite, A-Andesite, TA-Trachyandesite, T-Trachyte, D-Dacite and R-Rhyolite(Zanettin, 1984; Le Bas *et al.*, 1986).

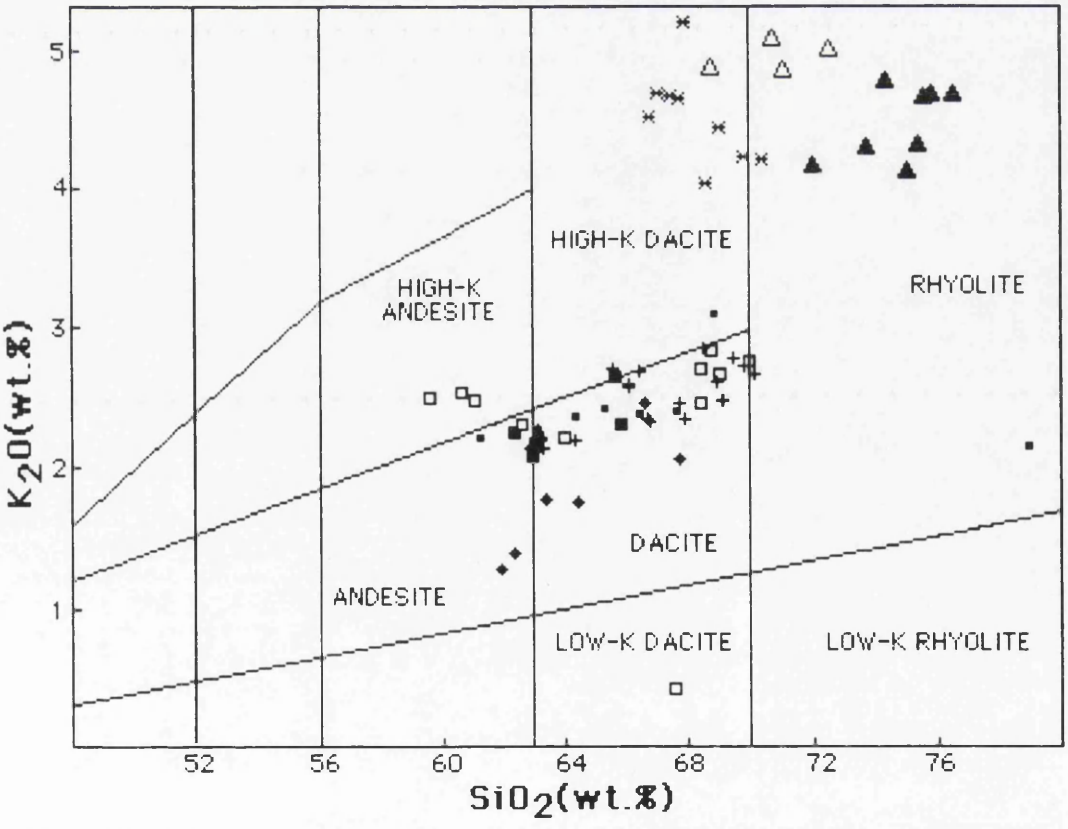

Figure 5.29. SiO_2 versus K_2O plot of subalkaline volcanic rocks of intermediate and acid composition. Dividing lines indicate boundaries given by Peccerillo and Taylor(1976).

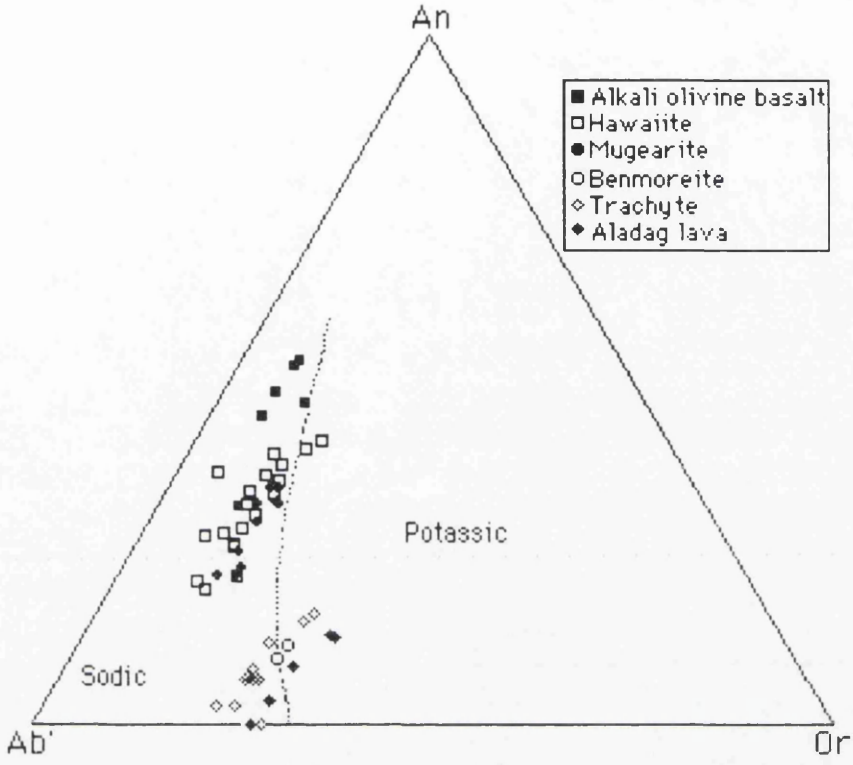

Figure 5.30. An-Ab'-Or projection of alkaline rocks, showing sodic and potassic rock types(Irvine and Baragar, 1971).

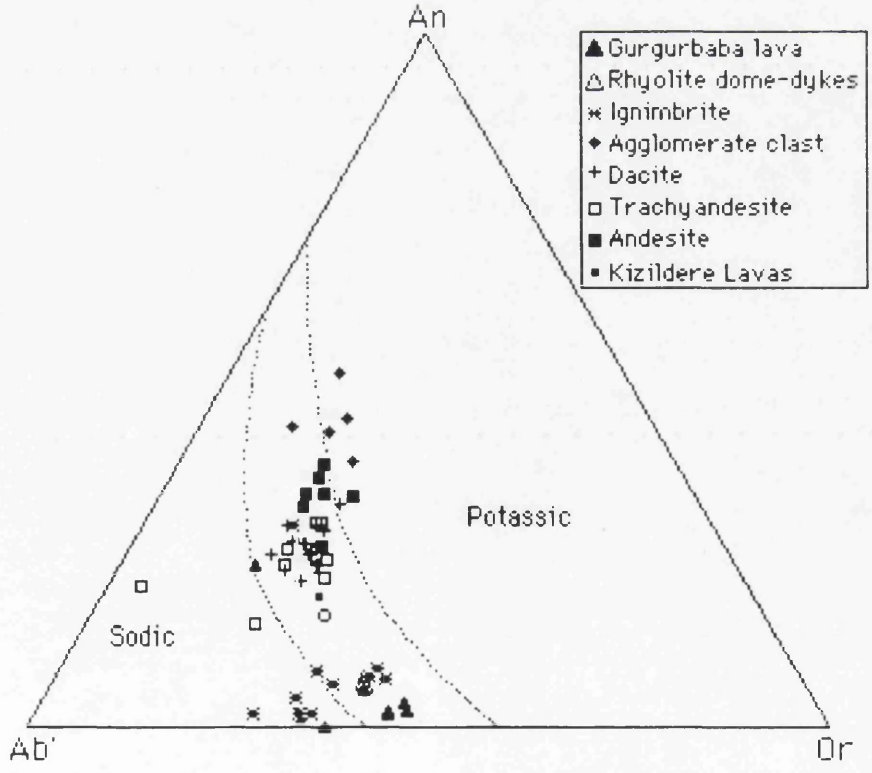

Figure 5.31. An-Ab'-Or projection of subalkaline rocks, showing sodic and potassic rock types(Irvine and Baragar, 1971).

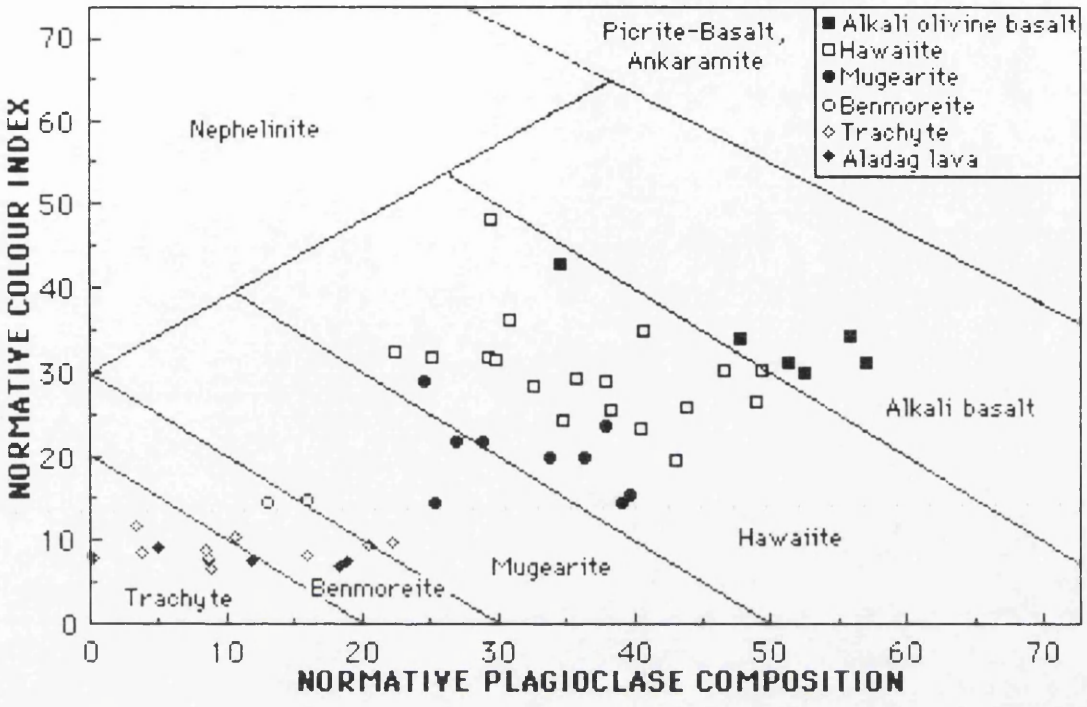

Figure 5.32. Plot of normative colour index versus normative plagioclase composition for alkaline rock(after Irvine and Baragar, 1971).

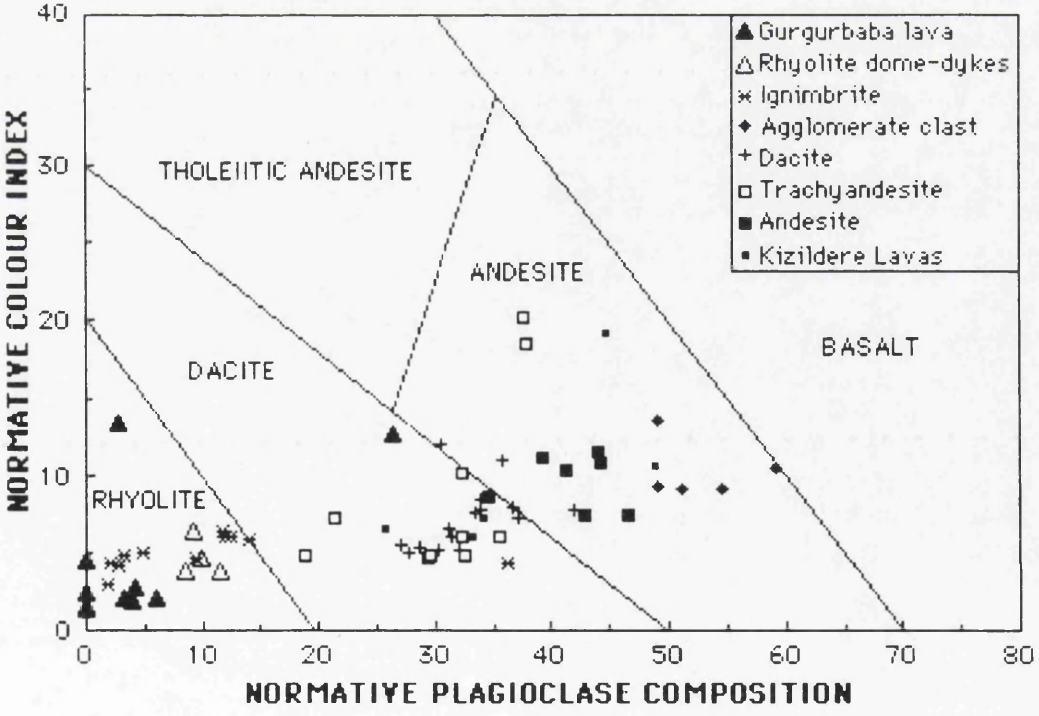

Figure 5.33. Plot of normative colour index versus normative plagioclase composition for subalkaline rock(after Irvine and Baragar, 1971).

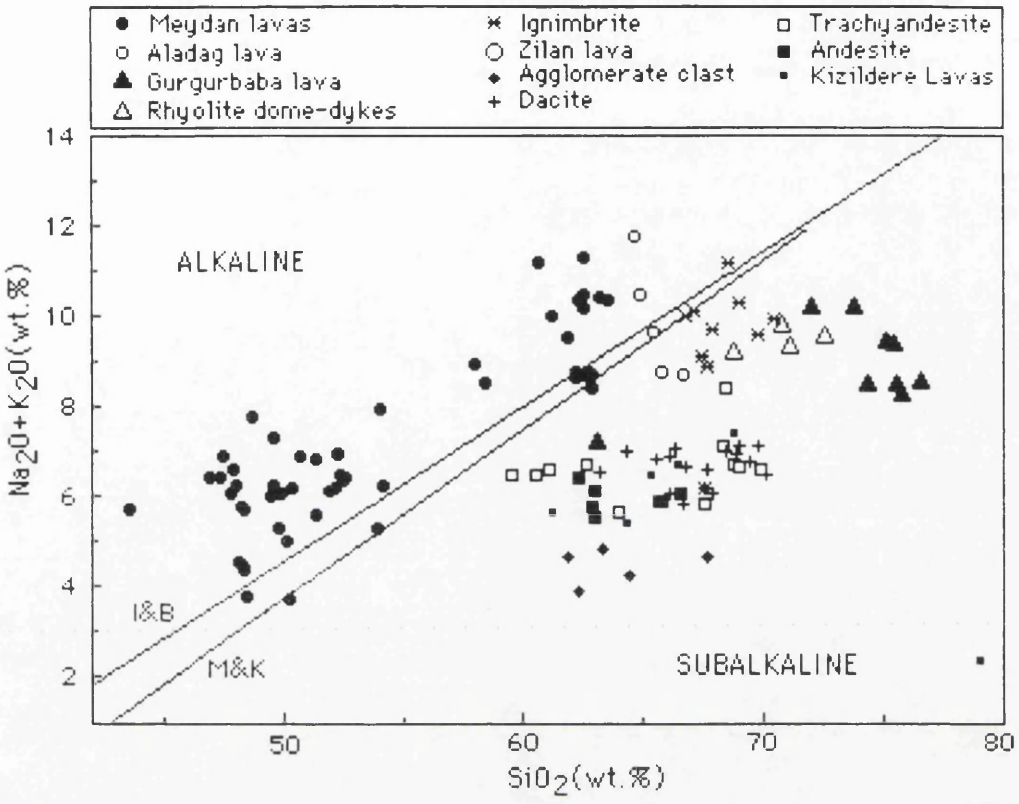

Figure 5.34. Total alkalies versus SiO_2 plot for volcanic rocks of the studied area. The boundary lines between alkaline and subalkaline fields are from I&B; Irvine and Baragar(1971), and M&K; MacDonald and Katsura(1964).

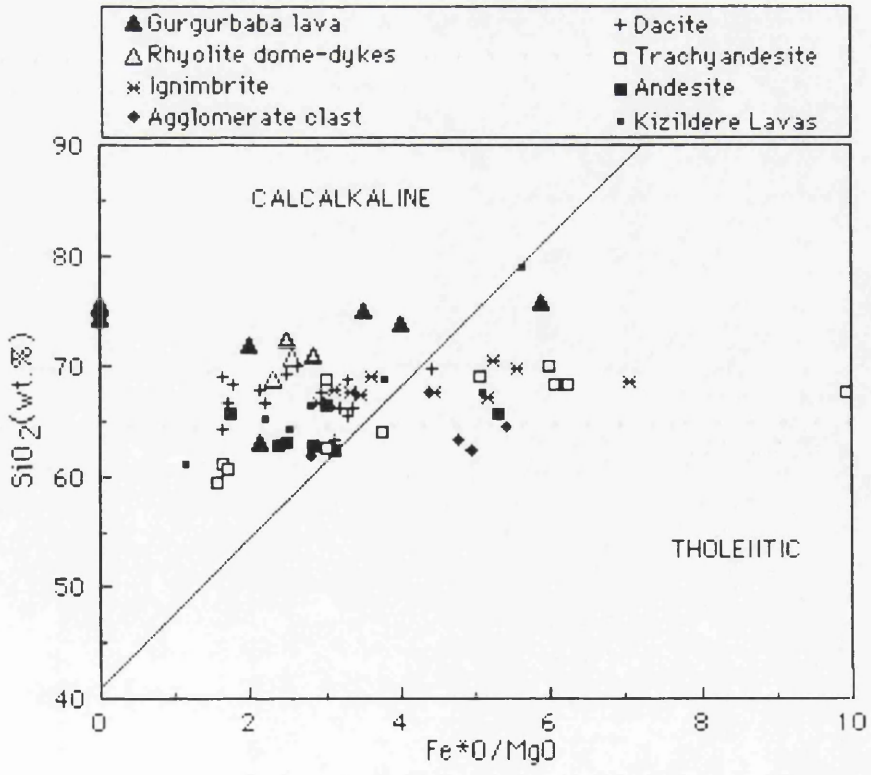

Figure 5.35. SiO_2 versus Fe*O/MgO plot for subalkaline volcanic rocks. Dividing line is from Miyashiro(1974).

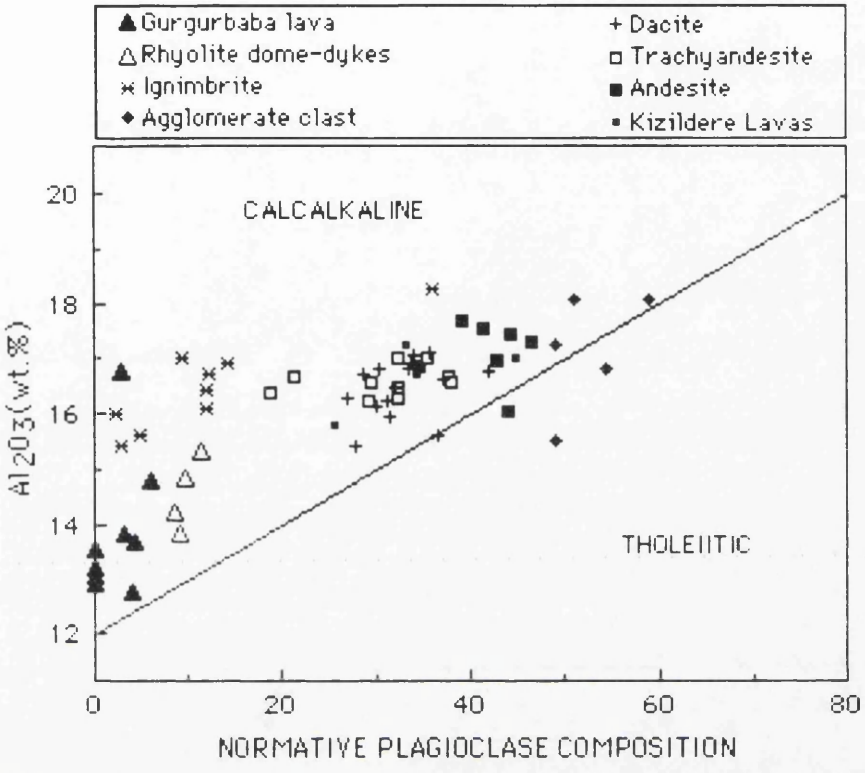

Figure 5.36. Al_2O_3 versus normative plagioclase composition plot for subalkaline rocks, discriminating calkalkaline and tholeiitic rock types(Irvine and Baragar, 1971).

5.3.2. THE MEYDAN ALKALINE ASSOCIATION

5.3.2.1. MAJOR AND TRACE ELEMENTS

Selected major and trace elements variation diagrams show a progressive stratigraphic and temporal change from early products to more evolved rock types in the alkaline association. Generally, compared with other rocks of the alkaline suite, alkali olivine basalts(AOB) are enriched in MgO and CaO. Compared with hawaiites, AOB is enriched in MgO, CaO, Al_2O_3 and depleted in TiO_2, Na_2O, K_2O, P_2O_5 and $Fe^*_2O_3$(total iron). Compared with mugearites, AOB is enriched in MgO, CaO and depleted in TiO_2, Al_2O_3, Na_2O, K_2O, P_2O_5, and $Fe^*_2O_3$. Compared with more evolved rocks(benmoreites and trachytes), AOB is enriched in Al_2O_3, MgO, CaO, and $Fe^*_2O_3$(Figure 5.37).

Selected MgO variation diagrams show a large chemical variation for the Meydan alkaline rocks(Figure 5.38). All major element oxides show consistent trends. The AOB analyses have MgO values between 6 wt.% and 10.5 wt.%. Hawaiites have MgO values between 4 wt.% and 6.5 wt.% but one of them with a MgO value of about 9.5 wt.% shows petrographic evidence of olivine accumulation. Progressive decrease in MgO corresponds to a general decrease in the compatible elements (for example Ni, Ca) and a general increase in the incompatible elements such as Zr, P, Ba, and K(Figures 5.38, 5.39 and 5.40). With decreasing MgO, the enrichment trends of TiO_2 and P_2O_5(especially in AOB, hawaiite and mugearite) reflect the incompatibility of Ti and P in the basaltic magmas. However, it is also seen that there is a significant decrease of TiO_2 and P_2O_5 in more evolved rocks, trachytes(Figure 5.38). Ti ceases to be incompatible at a MgO content of between 5 % and 6 %, but P ceases to be incompatible at about 3.5 % as seen in the figures. A comparison of incompatible element ratios is given in Table 5.2.

For the Meydan alkaline rocks, Niggli value variation diagrams for selected major and trace elements are given in Figures 5.41, 5.42 and 5.43. These diagrams support the presence of consistent compositional trends in the alkaline suite of Meydan.

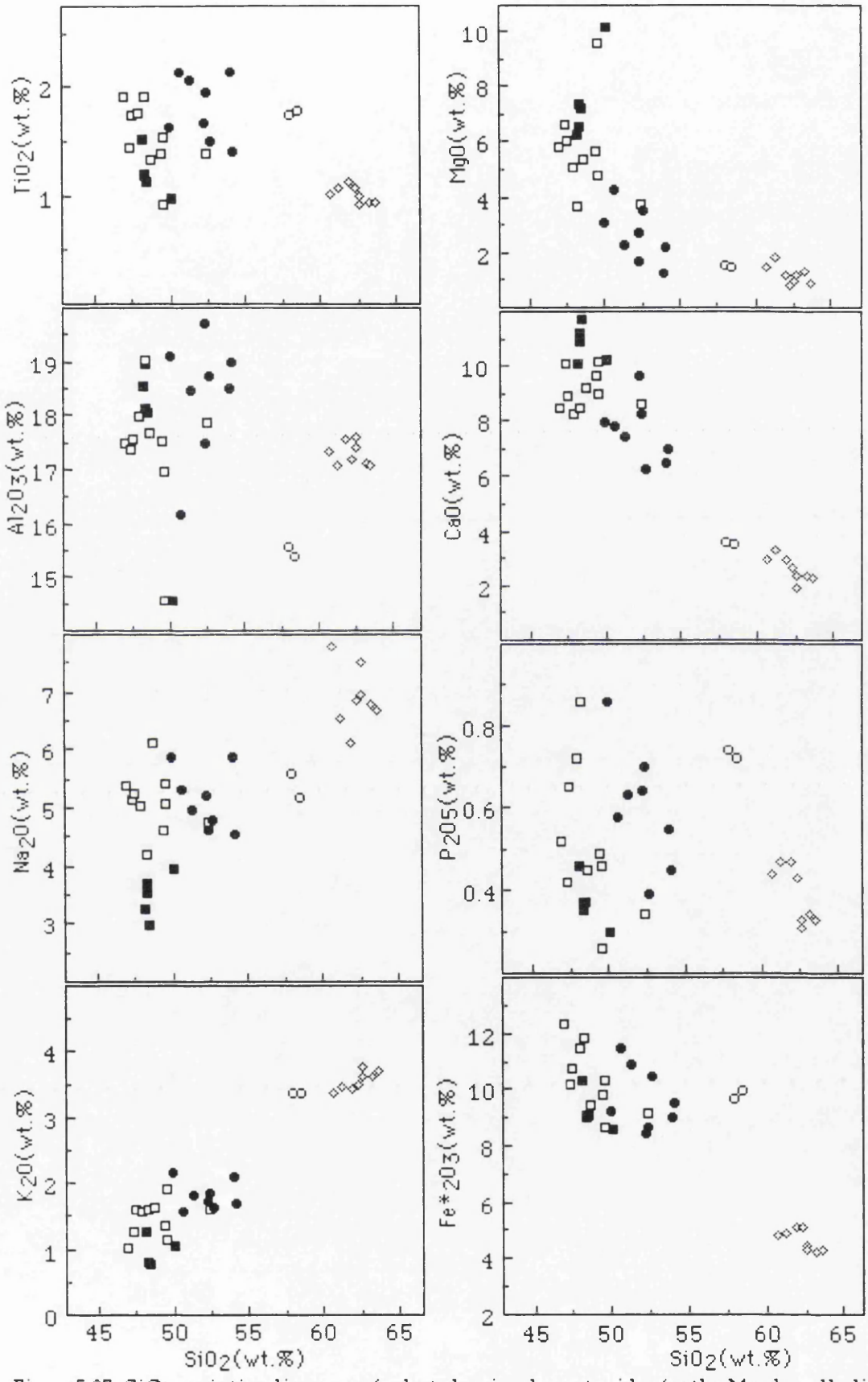

Figure 5.37. SiO_2 variation diagrams of selected major element oxides for the Meydan alkaline association. The symbols for rock types are ■, alkali olivine basalt; □, hawaiite; ●, mugearite; ○, benmoreite; ◇, trachyte.

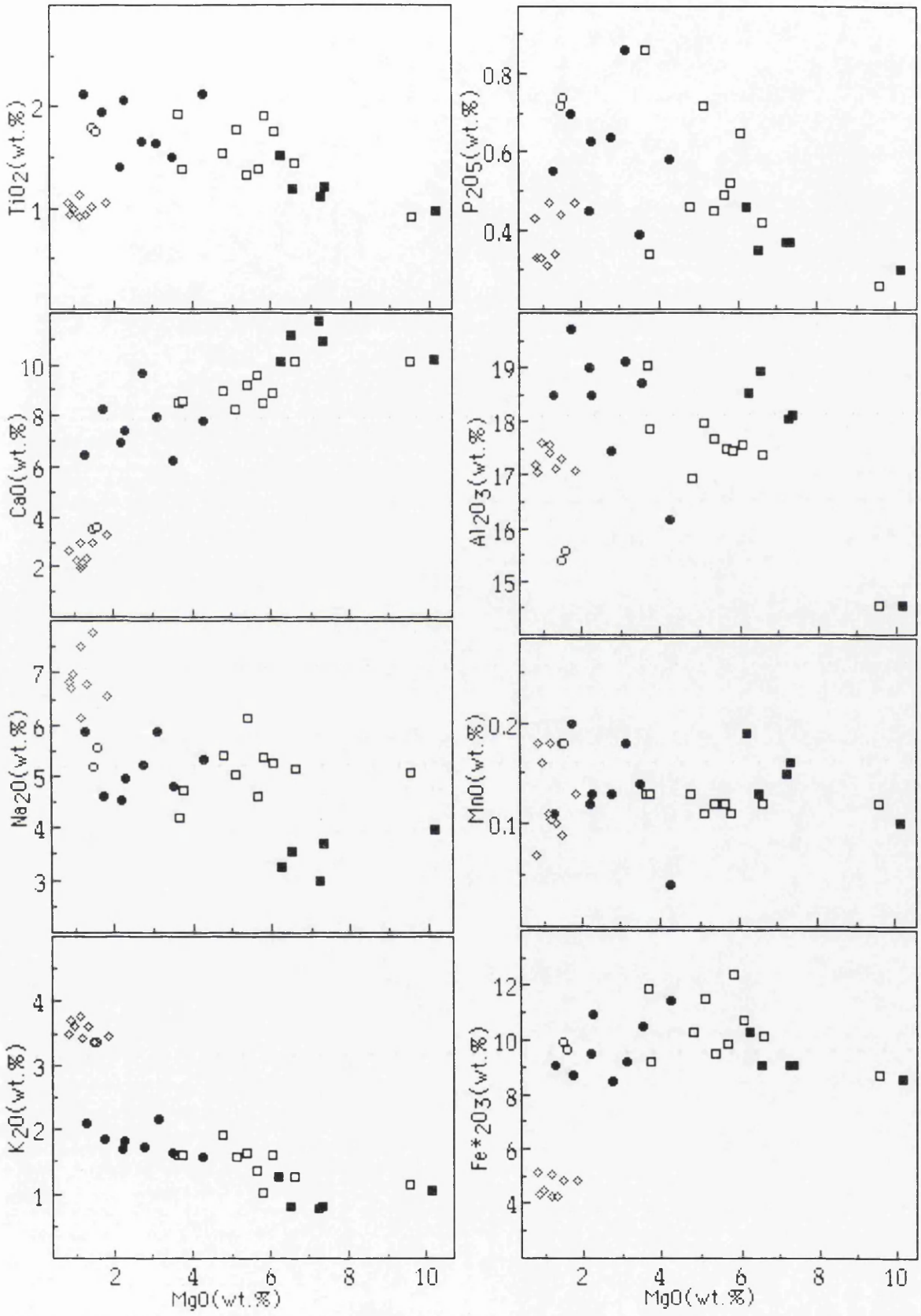

Figure 5.38. MgO variation diagrams of major oxides for the Meydan alkaline association. The symbols for rock types are ■, alkali olivine basalt; □, hawaiite; ●, mugearite; ○, benmoreite; ◇, trachyte.

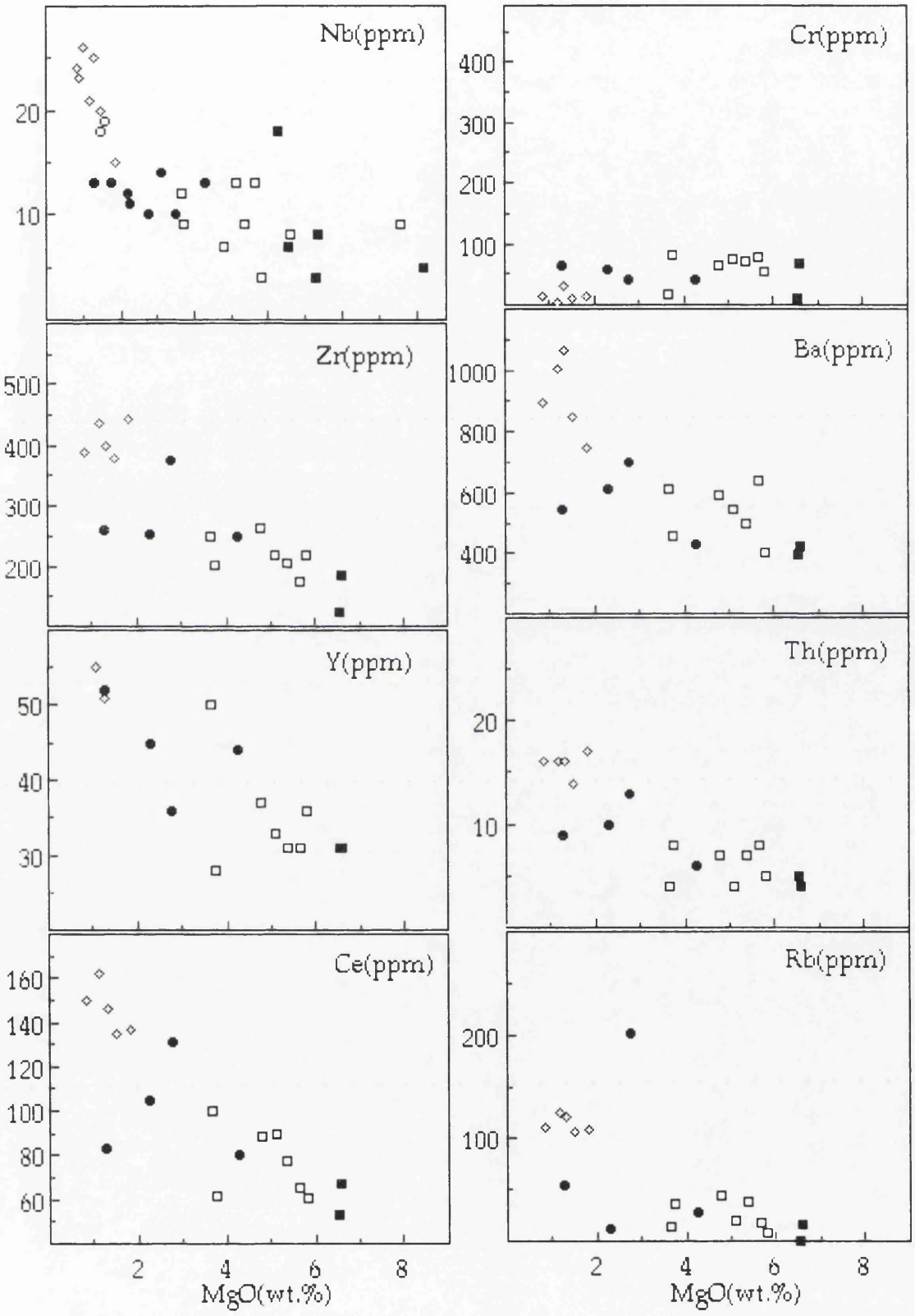

Figure 5.39.MgO variation diagrams of trace elements for the Meydan alkaline association. The symbols are ■, alkali olivine basalt; □, hawaiite; ●, mugearite; ○, benmoreite; ◇, trachyte.

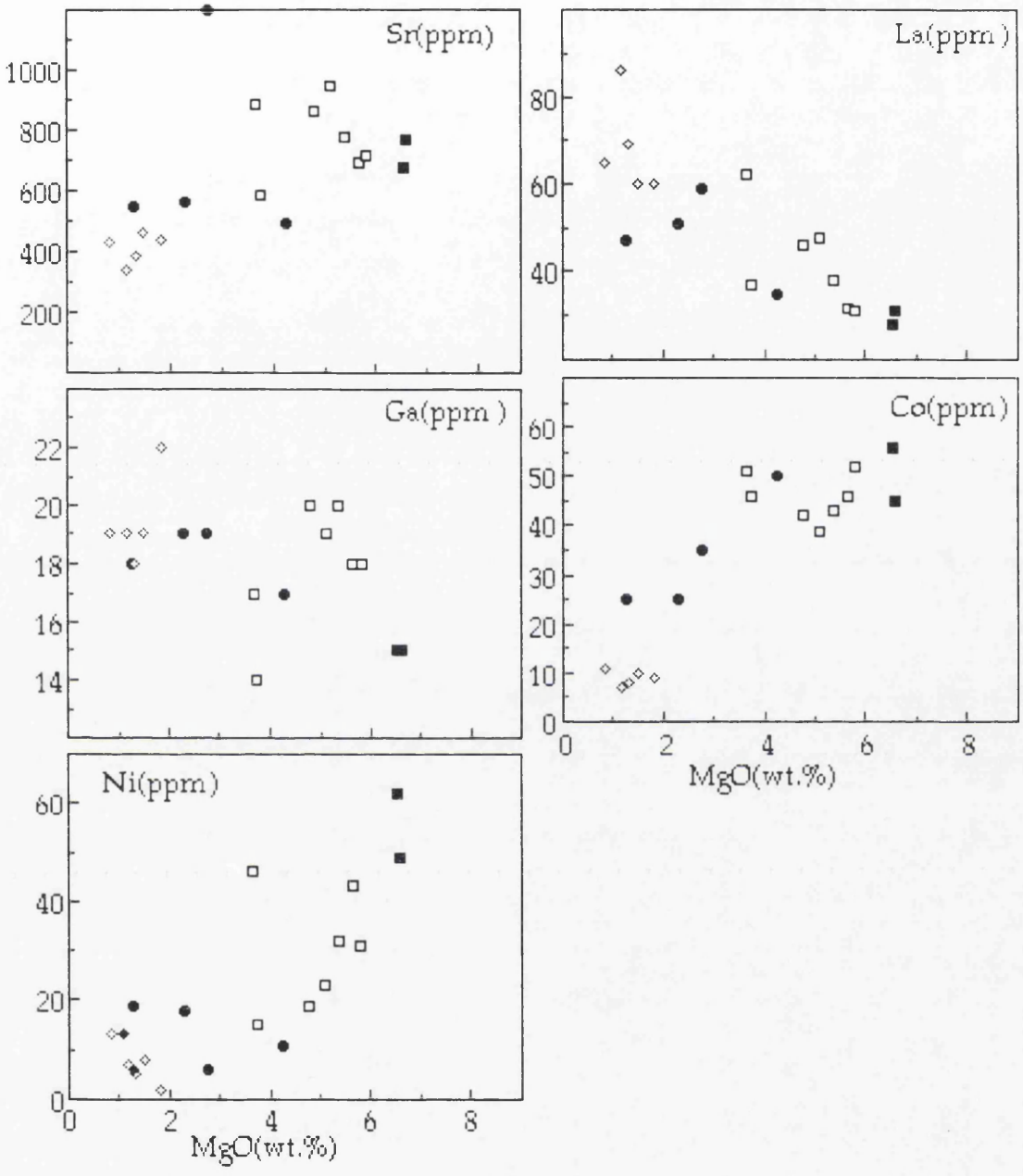

Figure 5.40. MgO variation diagrams of trace elements for the Meydan alkaline association. Symbols are as the same as previous plots.

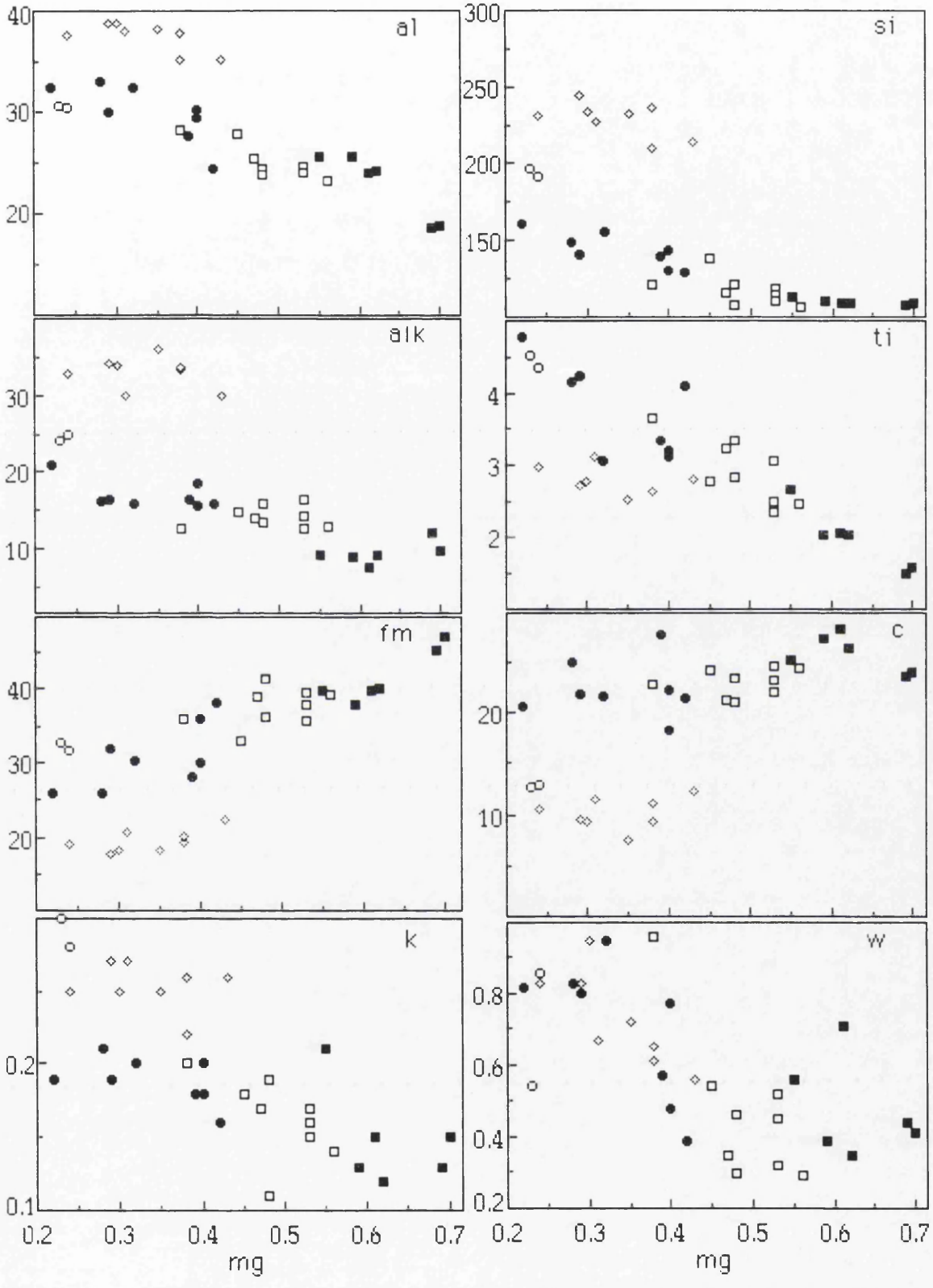

Figure 5.41. Plots of Niggli values variation diagrams for the Meydan alkaline association. The symbols represent ■, alkali olivine basalt; □, hawaiite; ●, mugearite; ○, benmoreite; ◇, trachyte.

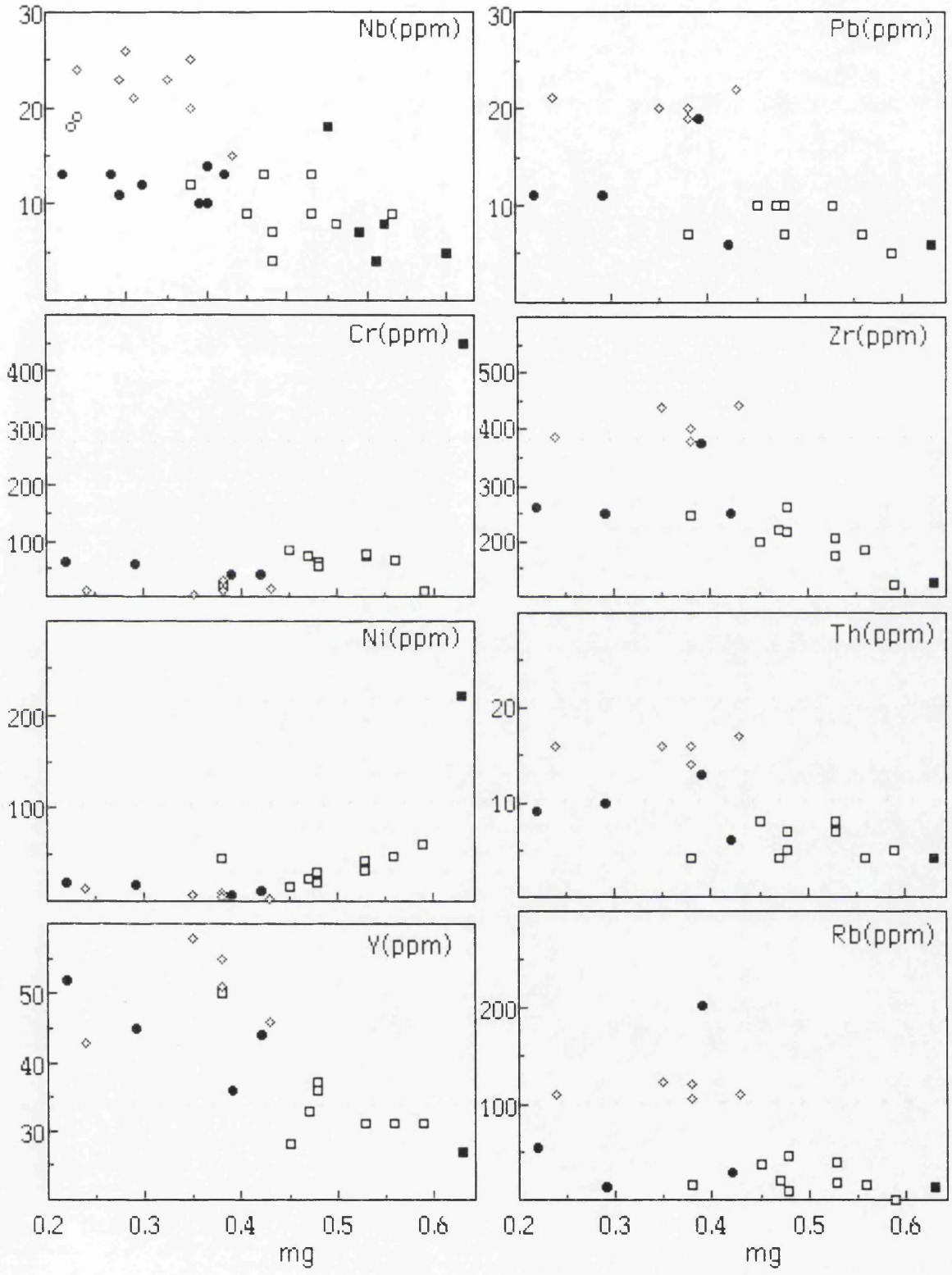

Figure 5.42. Niggli value mg versus trace element variation diagrams for the Meydan alkaline association. The symbols for rock types represent ■, alkali olivine basalt; □, hawaiite; ●, mugearite; ○, benmoreite; ◇, trachyte.

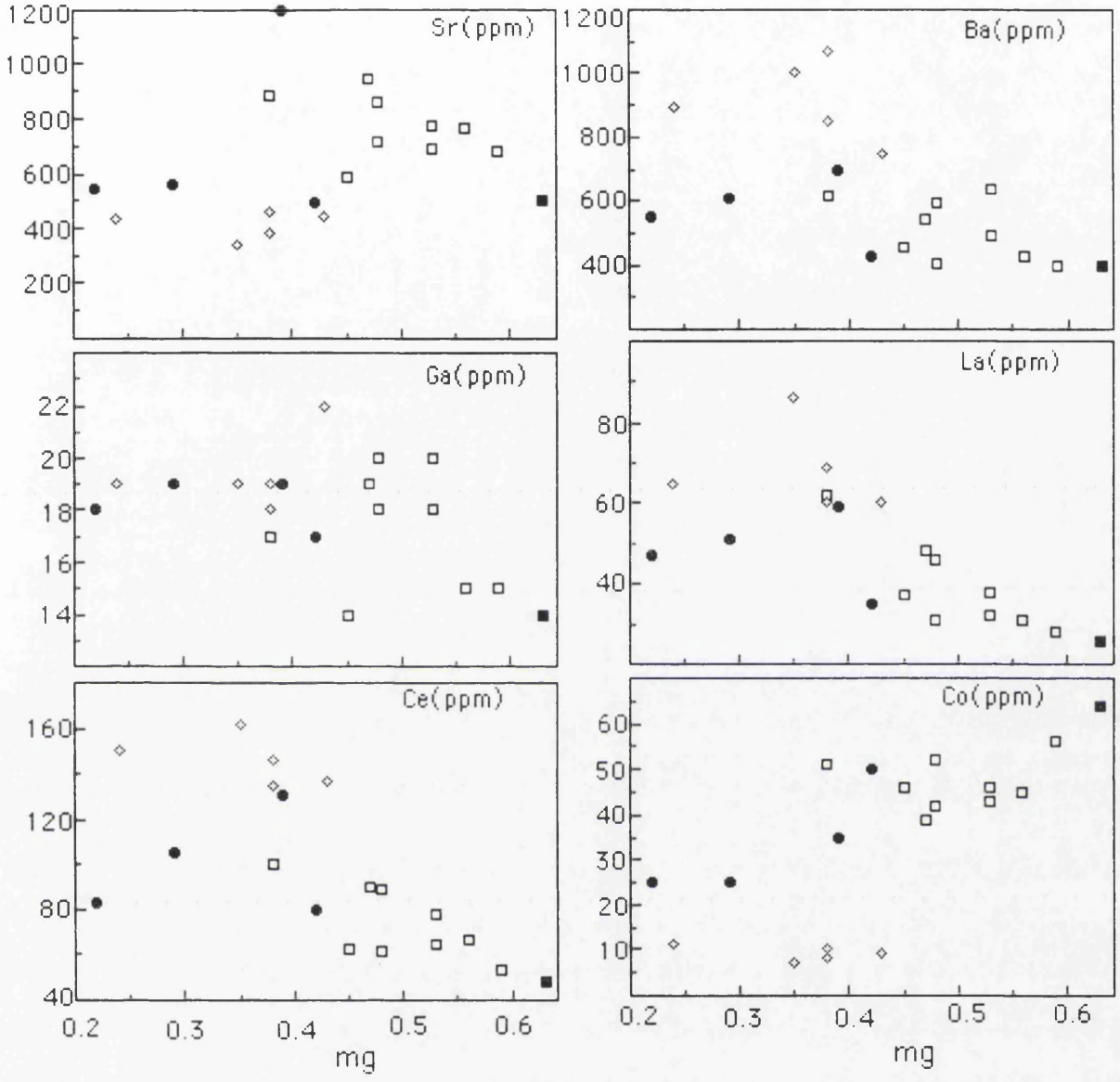

Figure 5.43. Niggli value mg versus trace element variation diagrams for the Meydan alkaline association. Symbols are as the same as previous plots.

An AFM plot of the Meydan alkaline association shows weaker iron enrichment than the alkaline fractionation trend of Hawaiian volcanic rocks(Figure 5.44), presumably due to presence of abundant iron-oxides, especially Ti-rich magnetite in the rocks. The FeO content of the suite is particularly low and the CaO content rather high relative to other alkalic suites and the Hawaiian suite. The high CaO content may indicate a high proportion of normative diopside in the parental magma, while the low FeO content may hint at a residual phase with a high FeO content. By comparing the FeO contents of mantle minerals it is evident that the presence of spinel in a residum could account for a low FeO content in a magma produced at low degrees of partial melting. As seen on the AFM plot, more evolved rocks, particularly trachytes, show significant alkali enrichment, by forming a gap from mugearites and benmoreites.

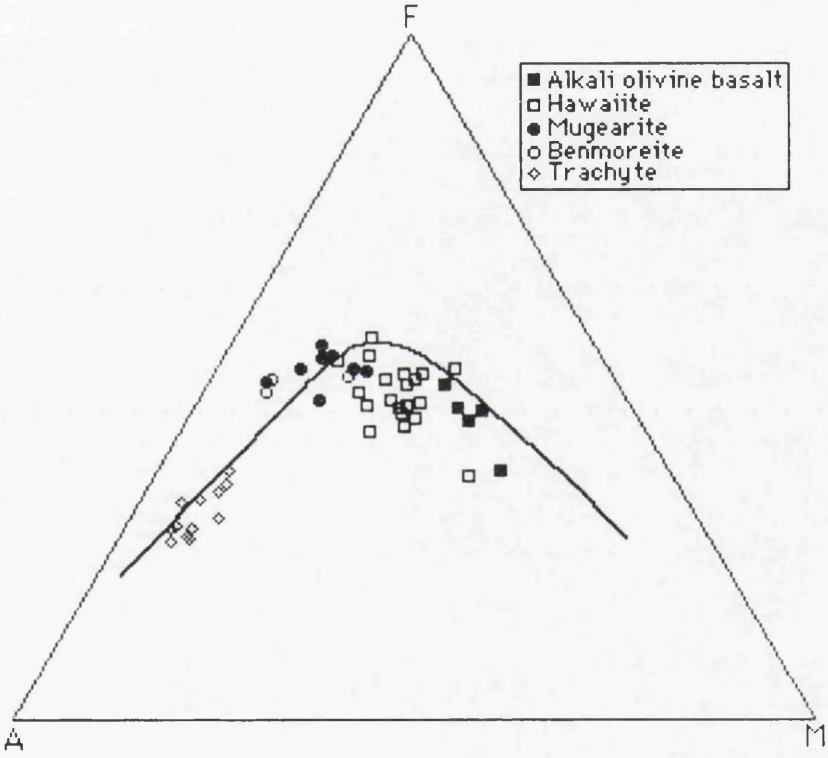

Figure 5.44. AFM plot of the Meydan alkaline rocks. Solid line represents Hawaiian alkali trend.

If the Fe*O/MgO ratio is considered as a fractionation index, some important points may be obtained. The increasing Na_2O content from alkali olivine basalt to benmoreite is very clear with increasing Fe*O/MgO, but after evolution of benmoreite the Fe*O/MgO ratio begins to decrease with increasing Na_2O in trachyte(Figure 5.45). Similarly, the decreasing content of CaO is more significant, especially in the initial evolution stages with increasing Fe*O/MgO ratio. However, after evolution of benmoreites, CaO

shows a particularly constant range with decreasing Fe*O/MgO ratio in trachytes(Figure 5.45). In the light of these facts, there are two possible petrogenetic models; (1) all the products were derived from the same parent magma, evolving under different conditions(shallow fractionation of a saturated olivine basalt parental magma). Thus, Green and Ringwood(1967) showed that shallow fractionation of a saturated olivine basalt magma could generate evolutionary trends towards more and more oversaturated rocks whereas the fractionation of the same magma at increasing depth may produce more and more undersaturated residual melts; (2) the various products may proceed from different parental magmas, obtained by variable proportions of partial melting of a common source.

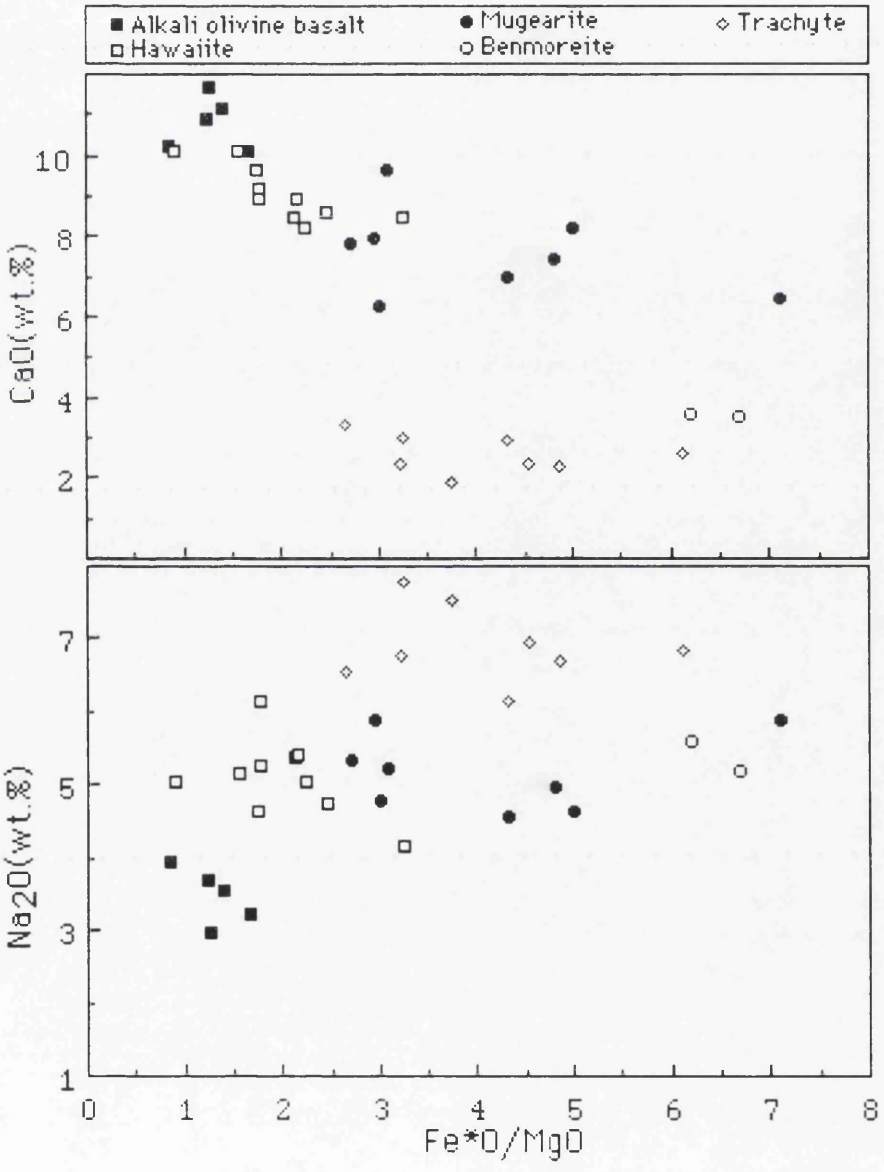

Figure 5.45. Fe*O/MgO versus Na_2O and CaO plots for the Meydan alkaline association.

Perhaps the most significant evidence that the alkaline rocks were produced predominantly by fractional crystallization with other processes such as contamination or mixing being of lesser importance, is found in the behaviour of some of the trace elements. Residual element relationships show in general a good positive correlation where Nb and Ba are plotted versus La+Ce(Figure 5.46). The correlation straight lines for these elements intersect the origin, suggesting a common source for the Meydan alkaline rocks. Only a fractional crystallization process can maintain unchanged the ratio of residual elements. Similar behaviour has also been noted by Innocenti *et al.* (1980).

The Nb/Y ratio versus Nb plot is given in Figure 5.46, showing a variation range for Nb/Y between 0.11 and 0.55. There would be a constant Nb/Y ratio, if the evolution of rocks proceed from a fractional crystallization process controlled by the Rayleigh law. However, Nb/Y variability is characteristic for a partial melting trend. Zr and Nb show very small increases with SiO_2, and are poorly correlated with each other(Figure 5.46). As distribution coefficents for these elements are closely similar it is very difficult to change the Zr/Nb ratio by limited fractional crystallization(Pearce and Norry, 1979). P_2O_5 is also poorly correlated with SiO_2. This variation in incompatible elements requires the high-P phase assemblage to include accessory minerals such as apatite.

As a result, it can be said that different melts proceeded from a common source partial melting with further differentiation by fractional crystallization. This suggestion is also stressed by the variation of some other element ratios, where linear correlations pass through the origin(Figure 5.47).

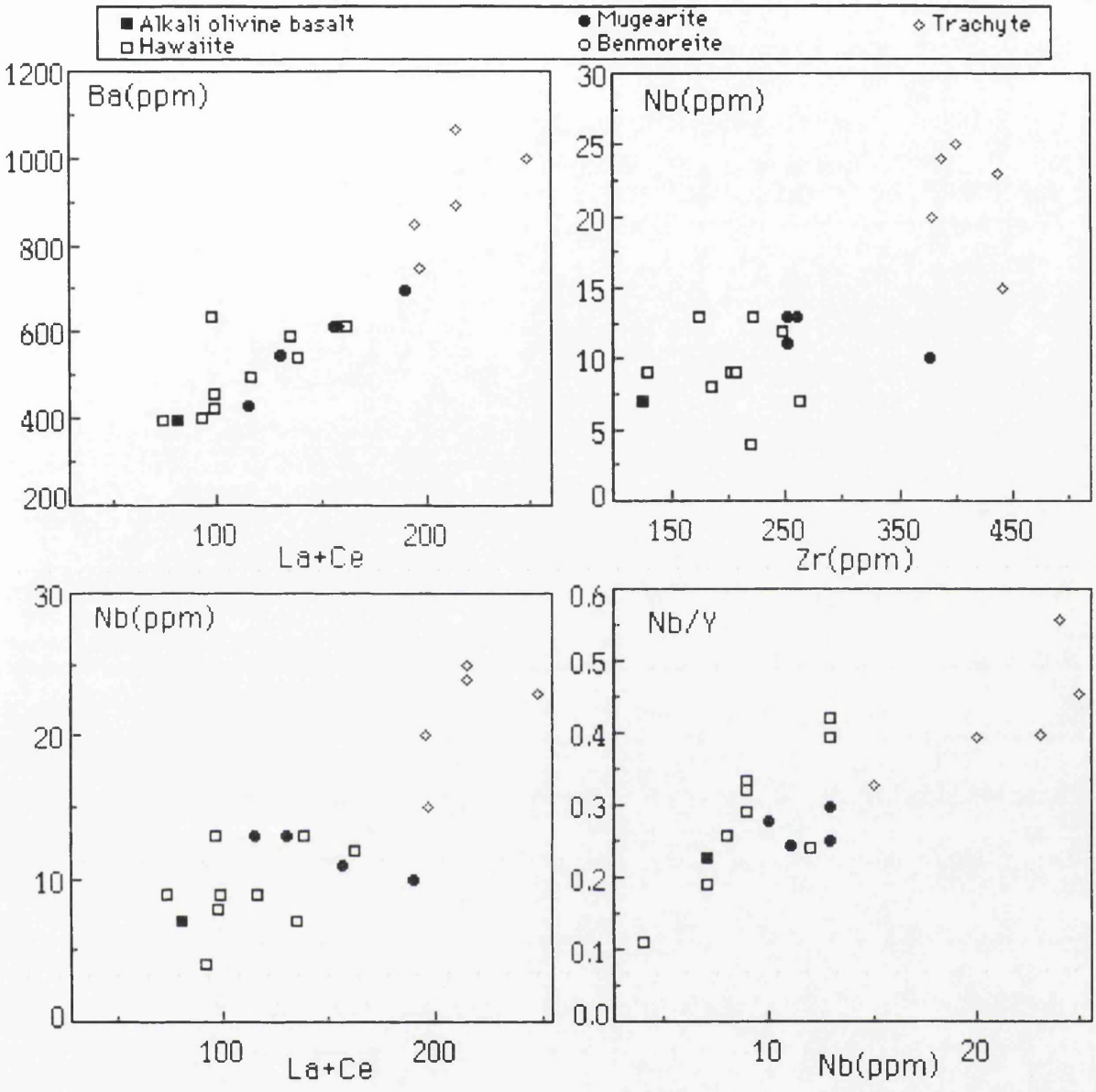

Figure 5.46. Ba and Nb versus La+Ce, Zr and Nb/Y versus Nb plots for the Meydan alkaline rocks.

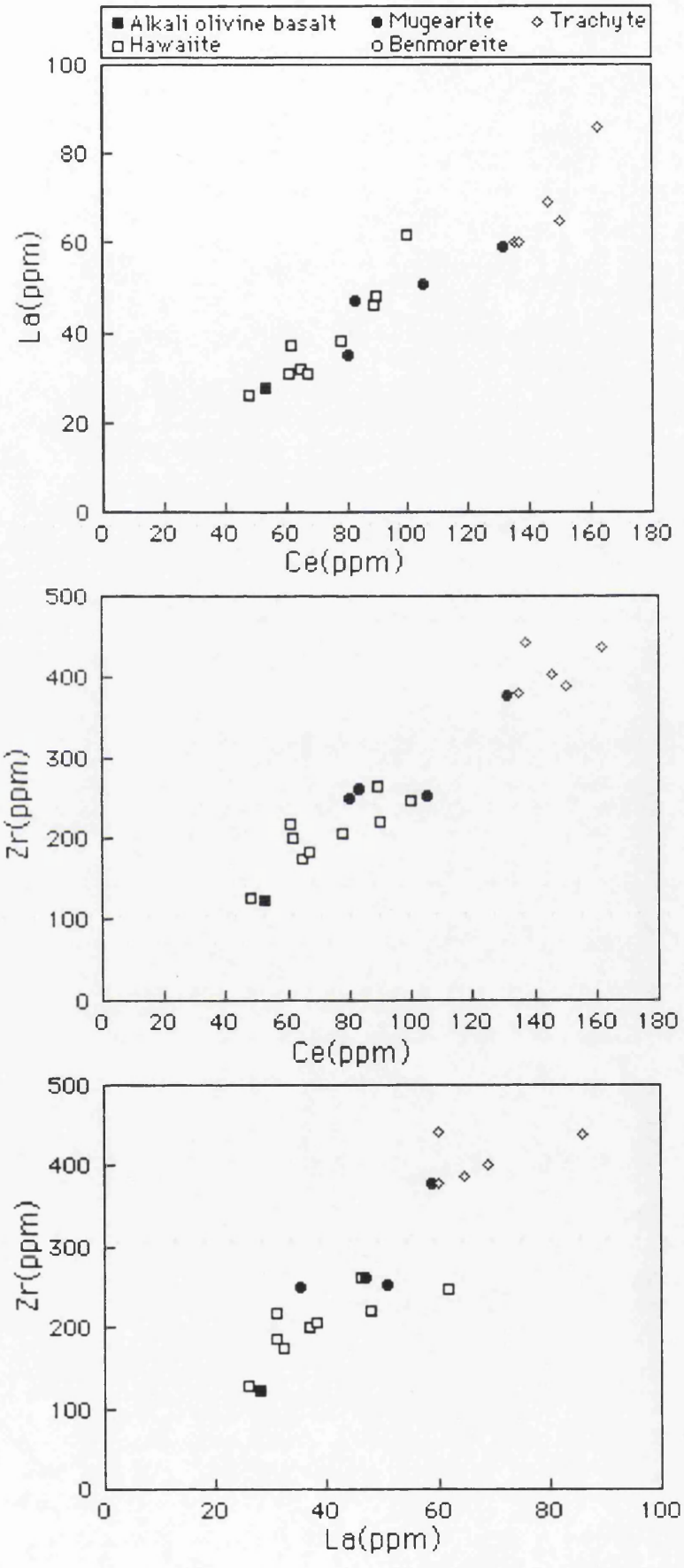

Figure 5.47. Linear correlation between pairs of residual elements in the Meydan alkaline volcanic rocks.

The relative effects of fractional crystallization and partial melting on magma composition may be investigated by comparing the behaviour of a highly refractory element against a highly incompatible element(Maaloe, 1985). If partial melting were the major control, then concentration of Ni should be virtually constant, while that of Nb should vary. With fractional crystallization the Ni content should decrease rapidly while the Nb content should increase slightly. The slope of the Ni/Nb correlation in the Meydan alkaline association thus clearly indicates fractionation(Figure 5.48).

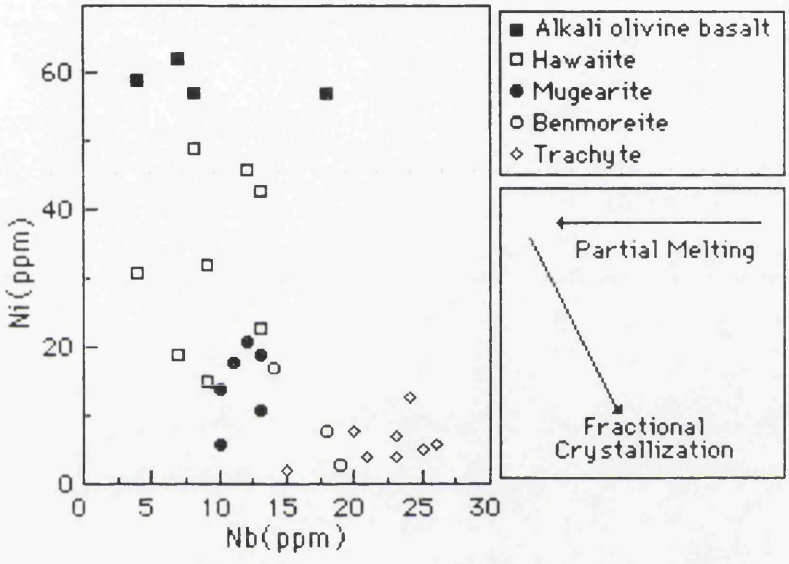

Figure 5.48. Nb versus Ni plot indicating that the variation in concentrations is caused by fractional crystallization.

Trace element data show high concentrations of incompatible elements such as Rb, Sr, Ba and Nb. This feature is characteristic for alkali basaltic rocks as pointed out by Gast(1968). The concentration in each of the incompatible elements varies from sample to sample, in particular differentiated rocks show very distinctive Sr, Rb, Ba, Zr which can be explained by fractional crystallization(Table 5.2). Furthermore, Nb, La, Ce, P, Ti, Y are highly incompatible during fractionation of olivine, pyroxene and plagioclase(Cox *et al.*, 1979). However, the contents in trace elements are almost constant within more primitive lavas but the compatible elements(Co, Cr and Ni) show more scatter as result of the influence of fractionating ferromagnesian minerals, even if the general tendency is to have lower abundances when MgO decreases.

CaO/Al_2O_3 ratios decrease with increasing $Fe_2{}^*O_3/MgO$ ratio for the Meydan lavas indicating the strong influence of cpx and olivine fractionation(Figure 5.49A). The high CaO/Al_2O_3 and low $Fe_2{}^*O_3/MgO$ ratios of alkali olivine basalts and some hawaiites may be in part due to cpx

accumulation. In addition, trachytes show deviation with low CaO/Al_2O_3 and $Fe_2{}^*O_3/MgO$ ratios, suggesting involvement of other magmatic processes(magma mixing±contamination) including fractionation. Alkali olivine basalt and hawaiite increase in Al_2O_3 with increasing silica indicating that initially plagioclase was probably not an important liquidus phase. CaO/Na_2O versus Al_2O_3 plot shows that alkali olivine basalt and hawaiite lie along a trend consistent with plagioclase fractionation and, or, accumulation(Figure 5.49B).

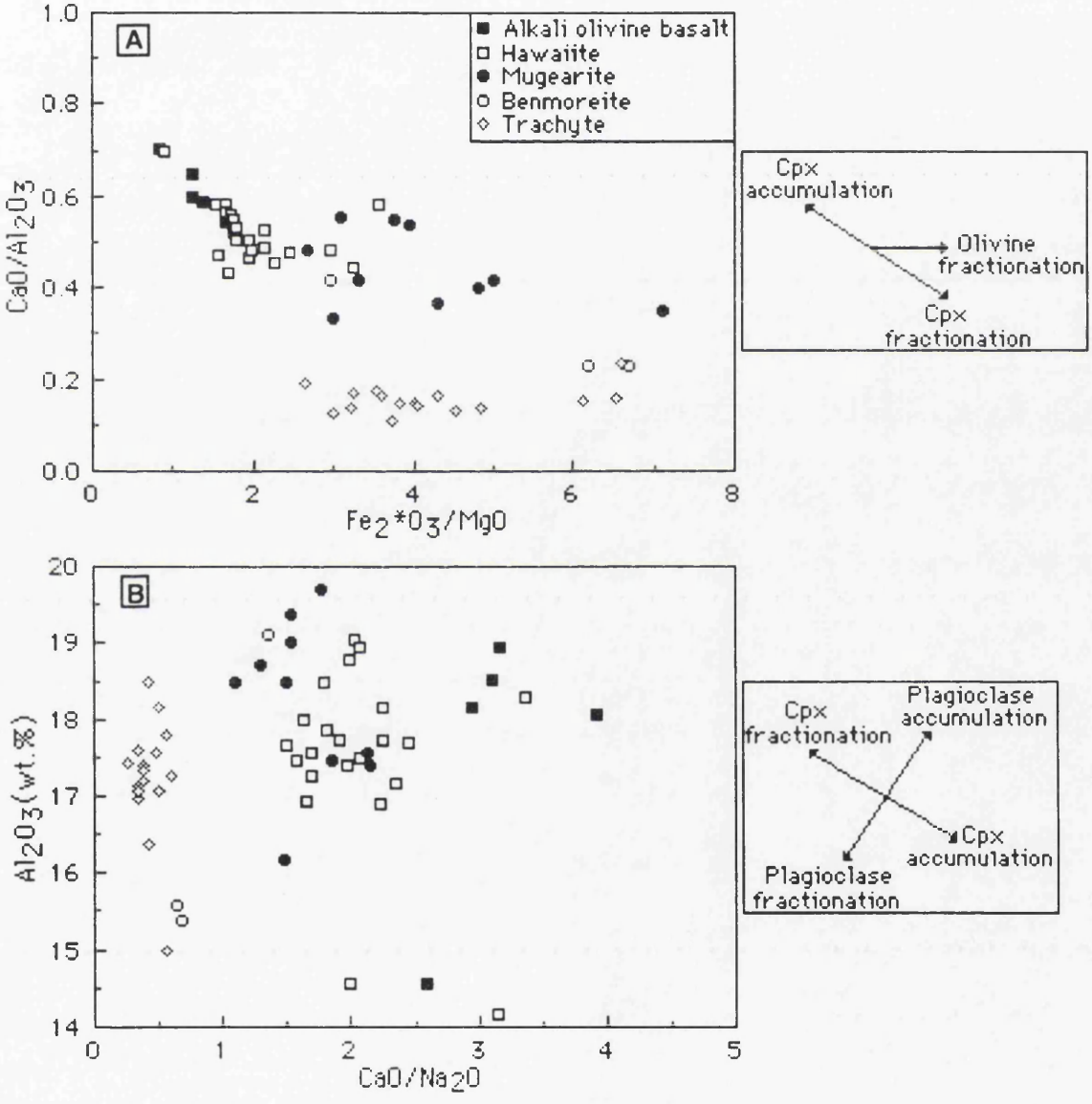

Figure 5.49. $Fe_2{}^*O_3/MgO$ versus CaO/Al_2O_3 ratio plot(A), and CaO/Na_2O versus Al_2O_3(wt.%) plot(B), indicating influence of fractionating mineral phases in the Meydan alkaline association.

Table 5.2. Incompatible element ratios for average rock compositions of the Meydan alkaline association.

	ALKALI OLIVINE BASALT	HAWAIITE	MUGEARITE	BENMOREITE	TRACHYTE
K/Rb	9360	589.60	246.20	321.50	311.40
K/Ba	23.57	28.29	31.85	38.08	38.92
K/Nb	1337.10	1637.7	1518.30	1728.12	1613.60
K/Zr	76.09	68.80	63.90	84.04	86.58
Ba/Rb	397	20.80	7.70	8.44	8.00
Ba/Zr	3.20	2.43	2.00	2.20	2.20
Rb/Zr	0.01	0.11	0.26	0.26	0.27
Zr/Nb	17.5	23.70	23.70	20.56	18.60
P/Ce	69.80	66.80	59.60	48.37	26.70
La/Ce	0.52	0.55	0.48	0.47	0.43

The elements Ba, La, Ce and P are highly incompatible during melting of a source containing olivine, pyroxene and plagioclase. Thus the abundance ratios of these elements in the Meydan basalts may reflect their values in the mantle source. The Meydan basalts have Ba/La values close to the inferred primitive mantle ratio of 9.9(Sun and McDonough, 1989). Basalts have P/Ce values ~70, comparable with the 75±15 common to MORB and ocean island basalts(Sun and McDonough, 1989). Using two-element plots(Figure 5.50), the relative enrichment of the trace elements can be examined by comparison to the mantle(e.g., Chauvel and Jahn, 1984). By combining a number of plots, a relative enrichment order for the trace elements can be identified $Y<TiO_2<Zr=Nb<Sr<P_2O_5<Rb=Ba$. This is quite comparable to the order established for alkaline rocks by Dawson(1967), Kable *et al.* (1975), Janh *et al.* (1979), Chauvel and Jahn(1984). Furthermore, it is also possible to evaluate the absolute enrichment of the elements and compare it with the REE enrichment as already proposed by Sun *et al.* (1979). Such an example is shown in Figure 5.51 for the sample MA-27. This sample which is the most primitive lava of the Meydan alkaline association, shows a very fractionated pattern(Figure 5.51) in which the non-REE elements, except Nb behave consistently with the REE elements. The strong enrichments in LREE, Rb, Ba relative to the HREE suggest the mantle source was enriched in a comparable manner and, or, that the melting process which created such an enrichment affected the non-REE elements as well as the REE elements. Mantle heterogeneites are assumed to affect Rb and Nb equally but Y scarcely at all(e.g., Wood, 1979; Sun and Nesbitt, 1977; Pearce, 1982).

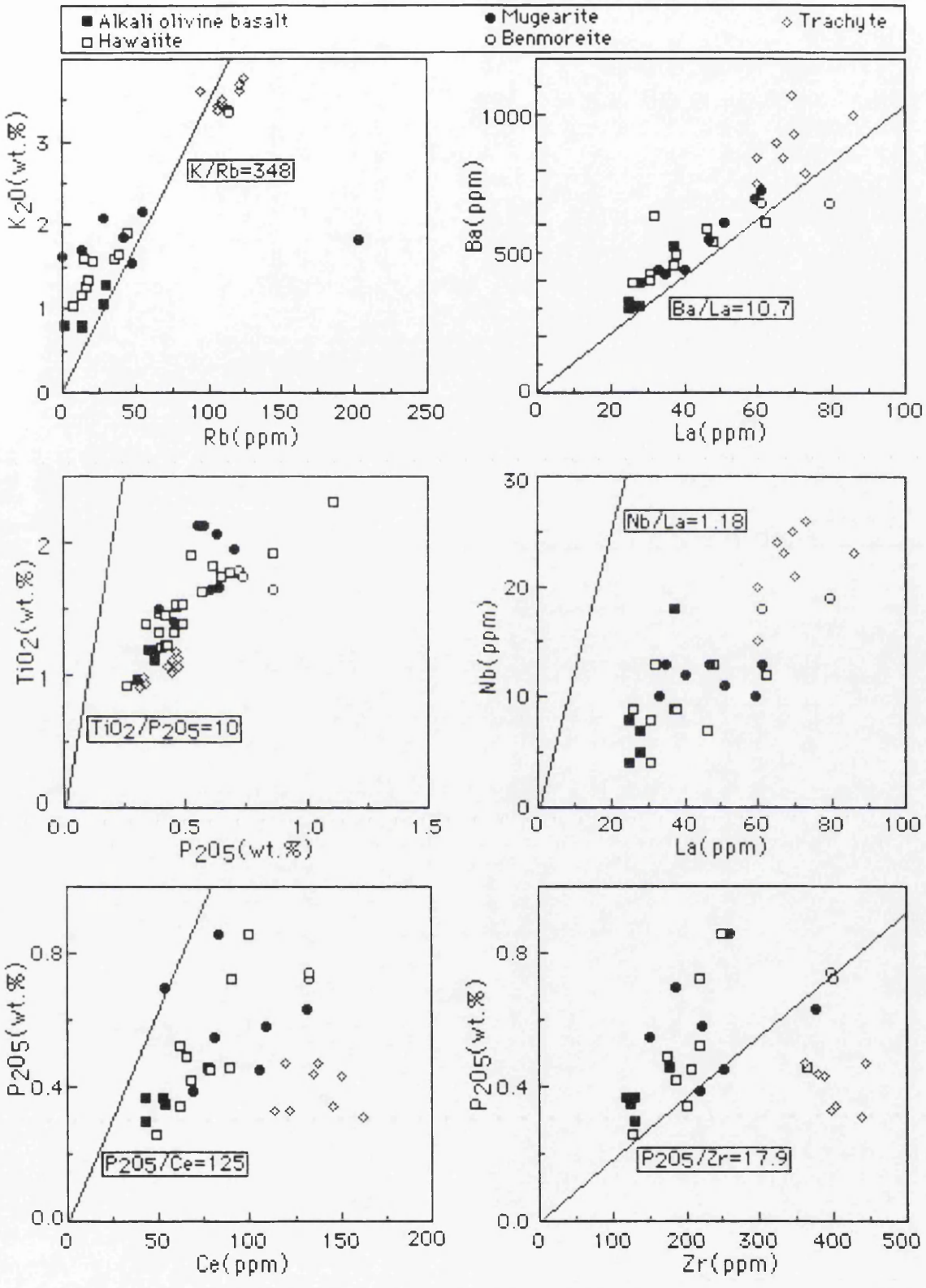

Figure 5.50. Two-element plots. Mantle values are presented for comparison and shown both as a line and as a given ratio. These plots allow us to determine the enrichment order among trace elements. The mantle values are from Sun and Nesbitt(1977), Sun *et al.* (1979), and Sun(1982).

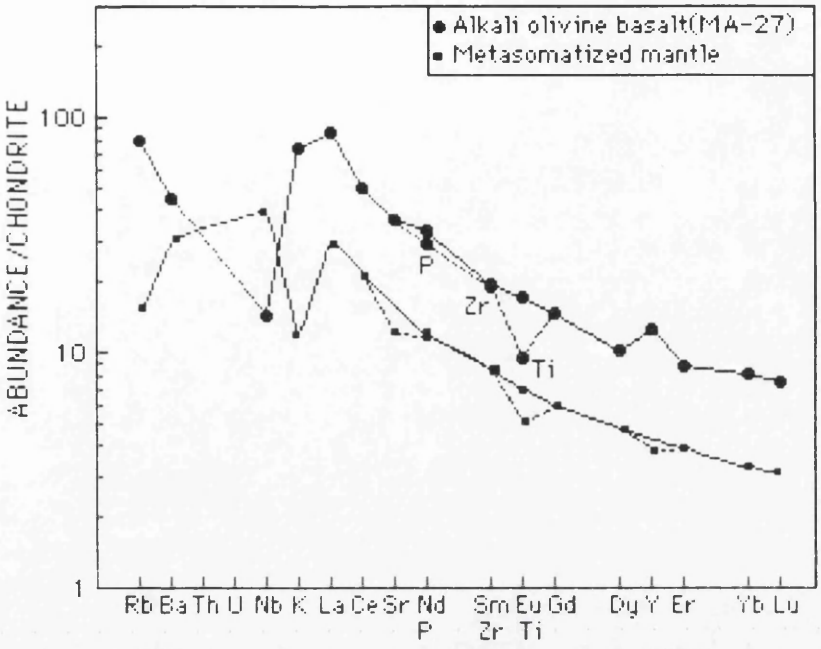

Figure 5.51. Enlarged REE diagram as proposed by Sun *et al.* (1979). One sample(MA-27, alkali olivine basalt) and a hypothetical metasomatized source(after Chavuel and Jahn, 1984) are presented. Values concerning the non-REE in the metasomatized source have been interpolated from the REE pattern. Normalization values are from Thompson(1982) and Boynton(1984).

5.3.2.2. INCOMPATIBLE ELEMENTS

The principal features of the immobile element abundances, depicted in terms of Mid-Ocean Ridge Basalt(MORB) and primordial mantle-normalized patterns for the Meydan alkaline association, are given in Figures 5.52 and 5.53. Following Pearce(1983), the elements are ordered, in the figures, on the basis of their mobility in aqueous fluids and their incompatibility in small degree partial melts. The elements placed on the left(Sr, K, Rb, Ba) are mobile and those on the right are immobile; the incompatibility of both the mobile and immobile elements increases from outside to the centre of the pattern. In this pattern, the order of incompatibilty during lherzolite melting increases from Y to Th and Sr to Th.

Comparison of a number of basalt patterns has suggested that melting of plume asthenosphere produces "humped" patterns with Ba, Th and Nb the most enriched elements and the degree of enrichment directly related to the degree of incompatibility. By contrast, basalts derived from mantle enriched by a subduction component exhibit selective enrichment mainly in the large lithophile(LIL) elements, Sr, K, Rb, Ba, Th and the LREE(Pearce, 1983). These patterns best highlight source enrichment processes when pyroxene, plagioclase and oxides are the only crystallizing phases. Crustal assimilation can have the same, but less pronounced, effect as the subduction component, leading to LIL element enrichment(e.g., Pearce *et al.*, 1990).

It appears from the figures that all the alkaline rocks show quite similar patterns. In general, the Meydan volcanic rocks from alkali olivine basalt to trachyte are characterized by enrichment in all elements from Sr to Y(Figure 5.52). A general change from primitive to more evolved compositions is accompanied by an increase in incompatible element enrichments. However, in some elements(P only in trachyte, Ti in all rock types), a negative anomaly is seen and the low Rb ratio of AOB is significant on the pattern. Furthermore, the rocks have characteristic Nb patterns, negative and progressively increasing anomalies similar to continental tholeiites(Dupuy and Dostal, 1984) and subduction related basalts(Pearce, 1983). Therefore, the depletion of Nb relative to the adjacent LIL elements in the Meydan lavas characterizes a small subduction component in the mantle source or assimilation of crust by the basic magma prior to eruption.

The MORB-normalized patterns of some volcanic rocks from the literature are compared with the Meydan alkaline volcanic rocks. Patterns of the rocks studied closely resemble the patterns of the Ethiopian and Central Chile volcanic rocks(Pearce, 1982 and 1983). However, the enrichment levels of almost all elements are considerably higher in the rocks of the Meydan association. The relatively strong incompatible element enrichments in these rocks could be due to factors such as an enriched source, degree of partial melting, or the level of crustal contamination, or degree of fractionation.

The usual spidergram masks variation in source and the subtle ratio variations and is dominated by concentration variations due to fractional crystallization which results in a spread of data. Also, the absolute concentrations of Zr, Ti and Y are so similar in most samples that the curves overlap. By normalizing these curves to Nb in each rock, the curves are effectively spread and subtle differences such as the progressive change in the Ti/Y ratio can be clearly seen on such a spidergram(Myers and Breitkopf, 1989). The ratio spidergram provides a simple, yet powerful tool for identification of incompatible element ratio variations which may reflect source heterogeneity and, or, other non-differentiation related process active within a volcanic province(Myers and Breitkopf, 1989). The Meydan alkaline volcanic rocks have generally similar patterns(Figure 5.54), suggesting that they were derived from a homogeneous melt and that compositional variations are due primarily to differentiation. However, trachyte and benmoreite have slightly different patterns. These differences can be result of other magmatic processes(e.g., contamination±magma mixing) involving differentiation.

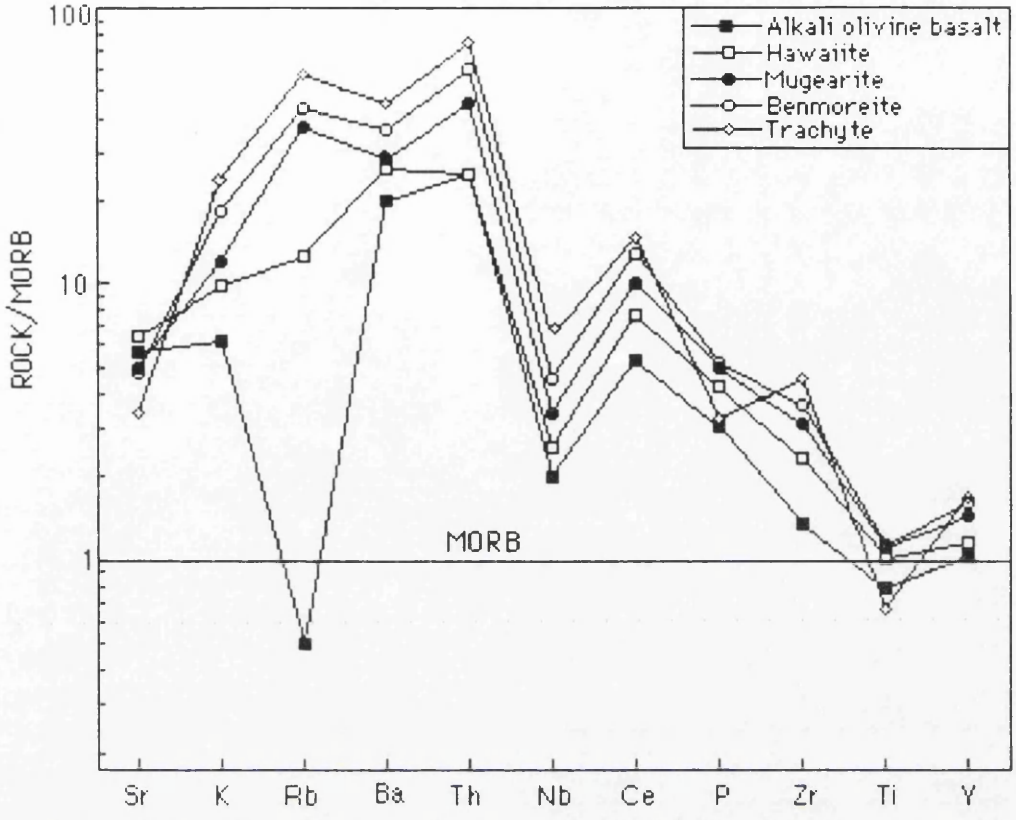

Figure 5.52. Normalized trace element patterns of average rocks of the Meydan alkaline association(MORB normalizing values are from Pearce, 1983).

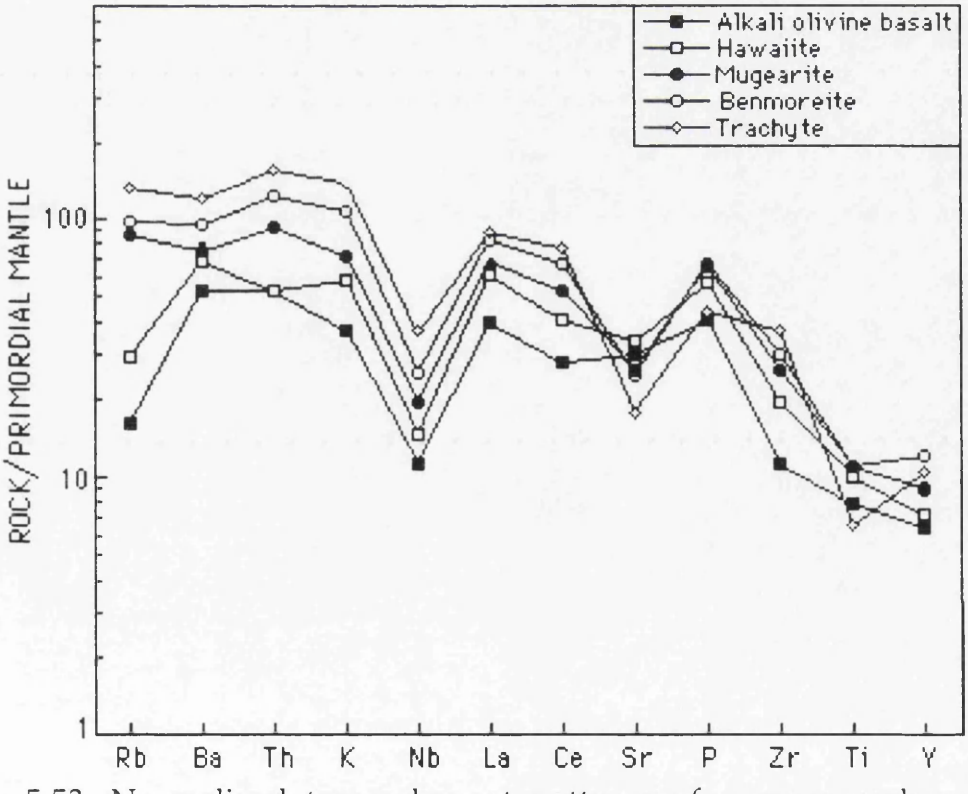

Figure 5.53. Normalized trace element patterns of average rocks of the Meydan alkaline association. Normalizing primordial mantle values are from Wood *et al.* (1979a).

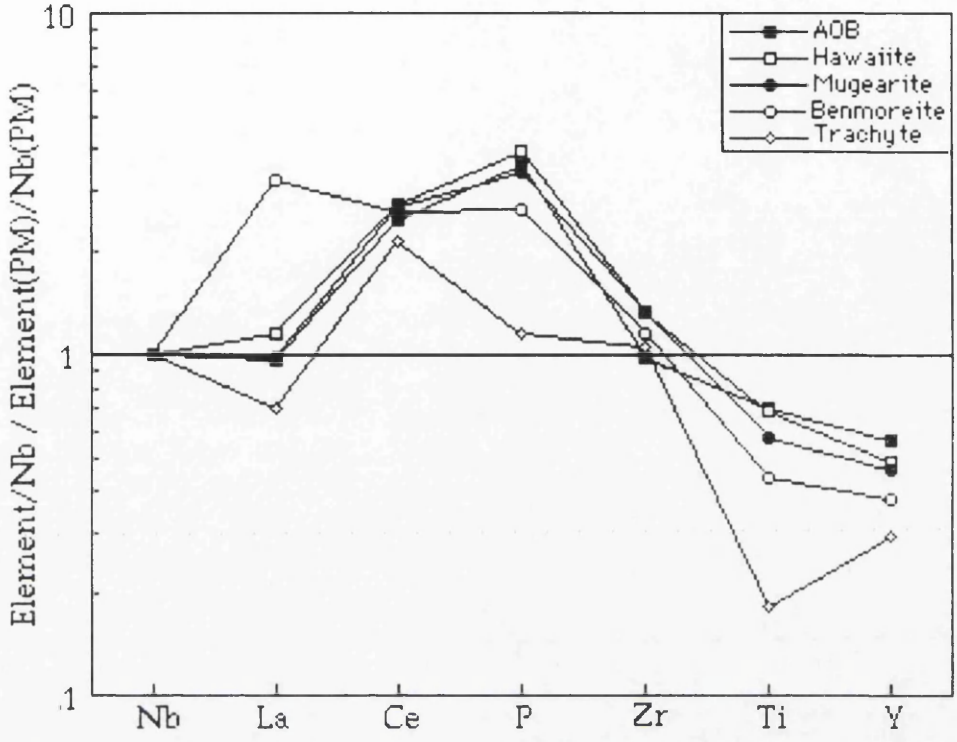

Figure 5.54. Nb-normalized spidergram of average rock types of the Meydan alkaline association. Primordial mantle(PM) values are from Wood *et al.* (1979).

To investigate the relationship between the large ion lithophile elements(LILE) and the high field strength elements(HFSE) in the Meydan lavas, they are plotted on Rb/Y versus Nb/Y plot(Figure 5.55). Generally, the Meydan lavas define within-plate enrichment style with a gradient close to unity. In addition, they show a component of subduction-related enrichment, having elevated Rb/Nb relative to primordial mantle value, and a significant component of HFSE enrichment is represented by elevated Nb/Y. Such an enrichment in the HFSE is inconsistent with the generally accepted view of the subduction component enrichment(e.g., Pearce, 1983). Given the conventional view that HFSE are not enriched by subduction component, it is possible to explore the variations between lavas that are not due to subduction component by considering only HFSE. In Zr/Nb versus Y/Nb plot(Figure 5.56), the Meydan lavas are scattered between normal(N-type) and transitional(T-type) MORB, and show relatively high Zr/Nb ratios. This implies that subduction component played a minor role in the genesis of the Meydan lavas.

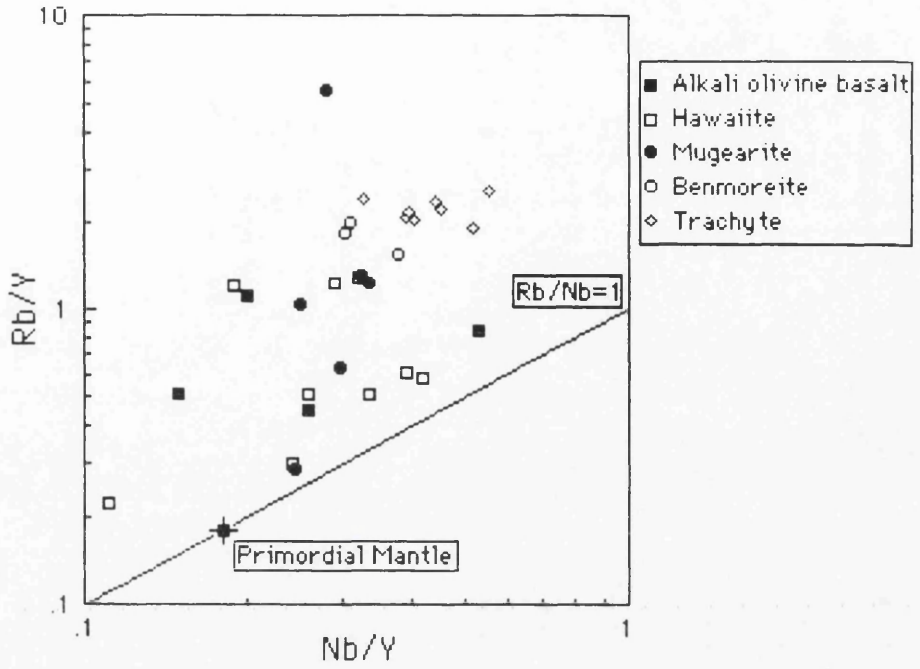

Figure 5.55. Rb/Y versus Nb/Y plot of the Meydan alkaline association.

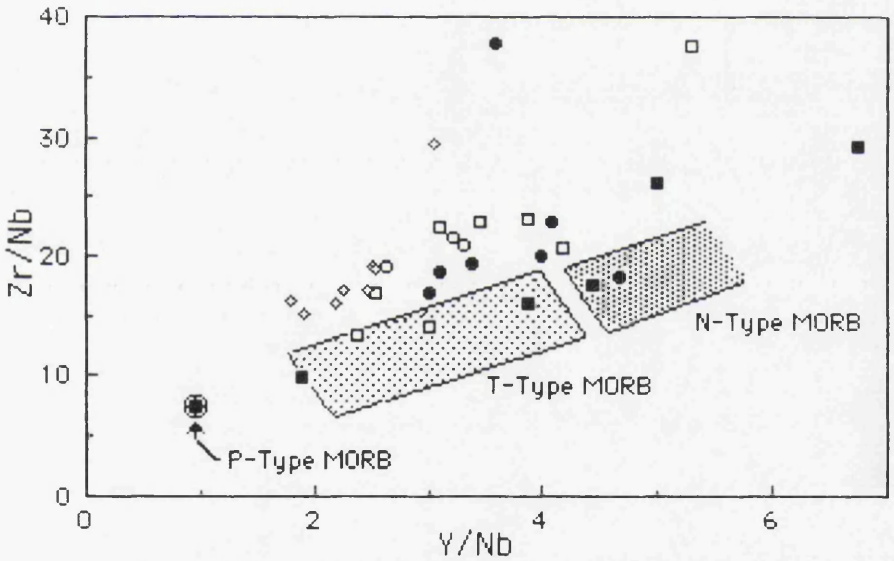

Figure 5.56. Zr/Nb versus Y/Nb plot of the Meydan alkaline association. MORB fields are from Le Roex *et al.* (1983).

5.3.2.3. CHEMICAL VARIATION BY FRACTIONATION

The chemical variations occurring in a natural sequence of rocks are commonly illustrated by referring to variation diagrams. For a rock series supposed to have been derived by a process of fractional crystallization, the best parameter for a variation would be the fractionation of the initial composition as expressed in a series of residual liquids(Treuil and Varet, 1973; Barberi *et al.*, 1975).

A better approximation can be obtained by referring to trace elements with a residual behaviour(incompatible element; Treuil and

Varet, 1973). In fact C_r(concentration of a residual element) is a simple function of the fraction f of residual liquid($C_r = C^o \times 1/f$) where C^o is the initial concentration in the magma of the residual element. It is necessary to know the initial composition of the melt C^o at upper crustal levels. This composition can be estimated in the light of the distribution curve of elements with high values of the partition coefficient D at the beginning of fractionation, such as Ni and Cr. These curves are in fact practically vertical in a restricted range corresponding to the most basic part of the series and the composition of the parent magma can be assumed by extrapolation(Figure 5.57). Therefore, e.g. Ce content of the parent magma was taken as 40 ppm relative to the most primitive composition(alkali olivine basalt).

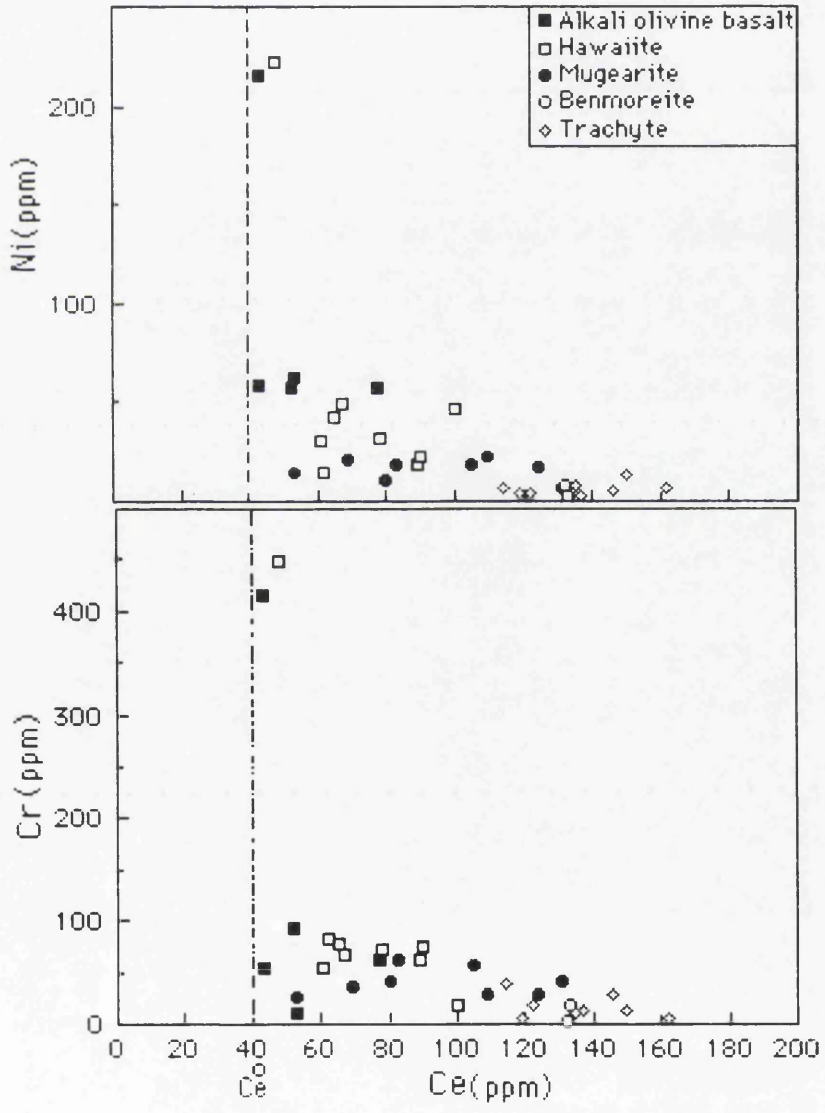

Figure 5.57. Estimation of Ce content($Ce^o \cong 40$ ppm) in the parent magma by extrapolation of Ni and Cr distribution in the Meydan alkaline volcanic association.

The f-values (fraction corresponding to the residual liquid) has been calculated for Meydan rocks using Ce. In Figures 5.58 and 5.59 the major and some trace elements are plotted as a function of $f=C^{o}_{ce}/C_{ce}$. Elements with a residual behaviour exhibit a regular enrichment whereas the distribution of non residual elements is characterized by discontinuities. These discontinuities reflect change in the solid/liquid partition coefficients, which are related to modifications of the equilibrium conditions of the fractionation process. Such modifications can be due either to changes in the crystallizing phases or to variations in the physico-chemical parameters such as oxygen fugacity. The study of such discontinuities can therefore be used as a guide in reconstructing the fractionation process(Barberi *et al.*, 1975).

The main variations occurring within the Meydan alkaline rocks can be clearly observed in the variation diagrams(Figures 5.58 and 5.59). The first stage of the differentiation(f=1-0.4) corresponds to transition from AOB to hawaiites. The solid phases involved in the differentiation are olivine, plagioclase and clinopyroxene. The fractionation is at first(f=1-0.5) mainly controlled by olivine and than dominantly by plagioclase and clinopyroxene. The second stage of differentiation(f=0.5) marks the transition from hawaiites to mugearites and benmoreites and finally to oversaturated trachytes. The third stage begins at f=0.3 with a discontinuity marked by the reversal of $Fe^{*}_{2}O_3$(total iron), TiO_2 and Cu trends, these elements showing a sudden and progressive decrease in concentration. Simultaneously Al_2O_3 progressively decreases, showing a discontinuity of opposite direction from benmoreites to trachytes. Near to f=0.45 there is a marked decrease of CaO, MgO, Co. Variations of this type are rather frequent in volcanic series characterized by an Fe-Ti enrichment in the initial and intermediate stages of fractionation. Such a trend is usually considered typical of series produced by fractionation(Barberi *et al.*, 1975). The discontinuity at f=0.4 corresponds to the intervention of new solid phase in the fractionation, namely Fe-Ti oxides. In addition, the crystallization of iron-rich cpx also plays an important role in fractionation.

Groups of trace elements characterized by different behaviour during differentiation are easily recognized by means of variation diagrams as a function of residual fraction: (1) incompatible elements(La, Ce, Zr, Nb, Th) throughout the range of differentiation; (2) transition elements are strongly partionated in the first crystallizing minerals, for example Cr and Ni in olivines(Curtis, 1964; Treuil *et al.*, 1971). In Figure 5.60 from which the linear relationships exist between pairs of REE such as La vs. Sm, Lu vs. Dy. The concentration ratio between each pairs of these elements is therefore

kept constant during the differentiation; this means that the rate of increase of each element relative to the other depends only on the initial concentration ratio in the parent magma. The La/Sm ratio is greater than 1 in alkali olivine basalts which is typical for alkali basalts and tholeiites from continental settings(Schilling, 1971; Treuil and Varet, 1973). If a linear correlation between La and Sm is maintained during differentiation, the La/Sm ratio in basalts is determined by variation in the shape of REE distribution curves(e.g., Barberi *et al.*, 1975).

The most primitive lavas in the Meydan association have concentrations of Cr and Ni which indicate that they have not evolved significantly from possible primary mantle-derived liquids. The transition elements Cr, Ni and to a lesser extent Co show a trend of depletion as lavas decrease in CaO. Nb and Th are incompatible throughout the suite, whereas the behaviour of Rb, Sr, Y, Ba and REE is more complex and can be related to one or more of the crystallizing phases.

The geochemical variation within the Meydan suite can be qualitatively explained by fractional crystallization of the observed phenocryst phases. In the interval ~12 to ~8 wt.% CaO, cpx±ol are the fractionating phases. Ni and Co are incorporated into olivine and the depletion of lavas in Cr is mainly caused by cpx. At about 8 wt.% CaO plagioclase and magnetite start to fractionate. Magnetite fractionation causes the contents of Fe and Ti to decrease.

Contrary to this, plagioclase does not affect the trend of Sr notably. Either plagioclase did not fractionate because of the small difference in density of melt and plagioclase(Drake and Weill, 1975), or the Sr trend was caused by combined effects of several phases with different Sr concentrations. It should also be noted that there is no significant Eu anomaly in REE patterns. However, this may be caused by a high oxygen fugacity of the magma and thus by the oxidation state of Eu(Drake, 1975), which will not enter plagioclase as Eu^{+3}. The fractionation of cpx may also explain the Eu concentrations. Concominant fractionation of cpx and plagioclase might thus balance one another's effect on Eu.

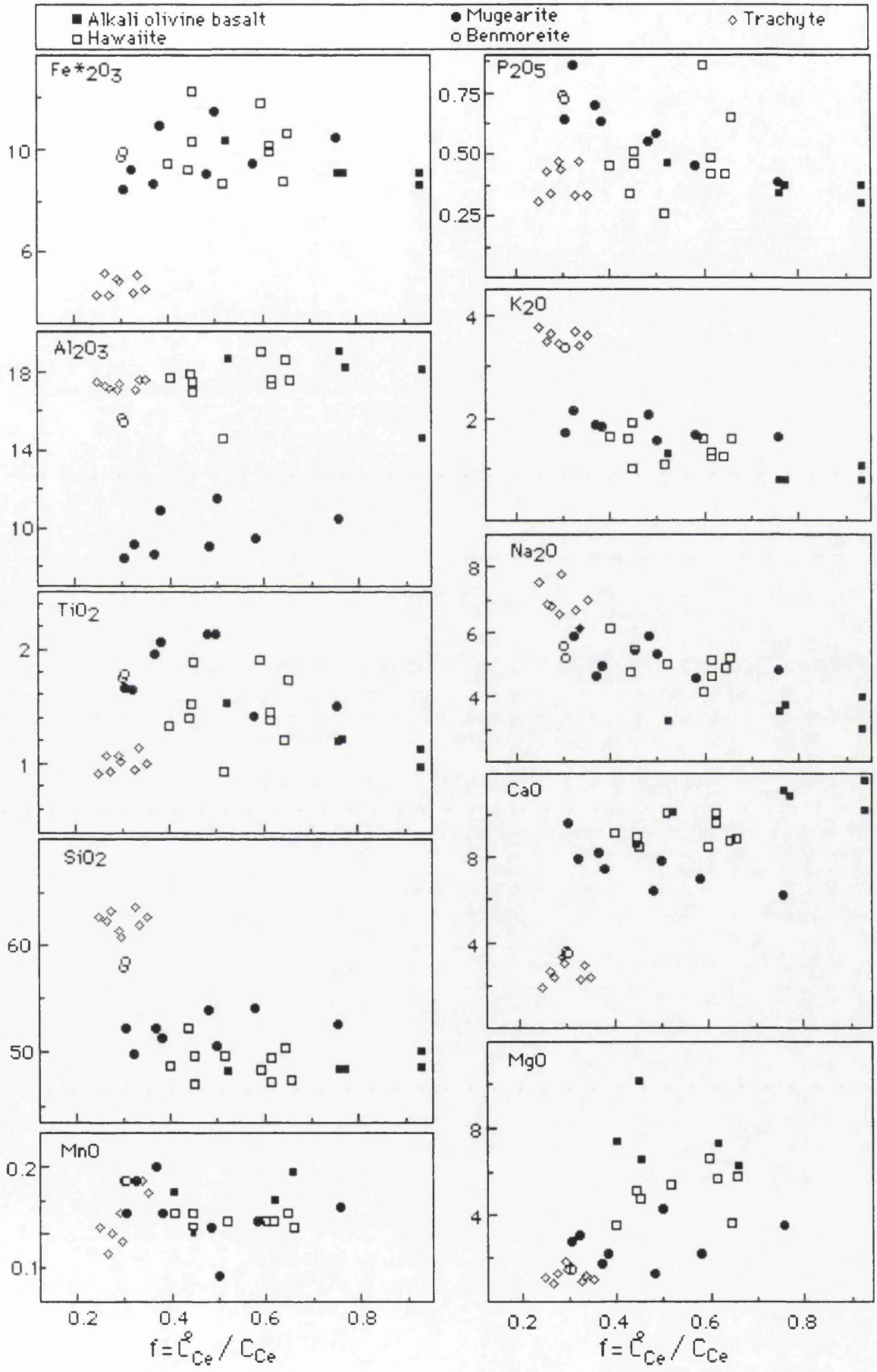

Figure 5.58. Major element(wt.%) variation plots as a function of the residual liquid fraction f.

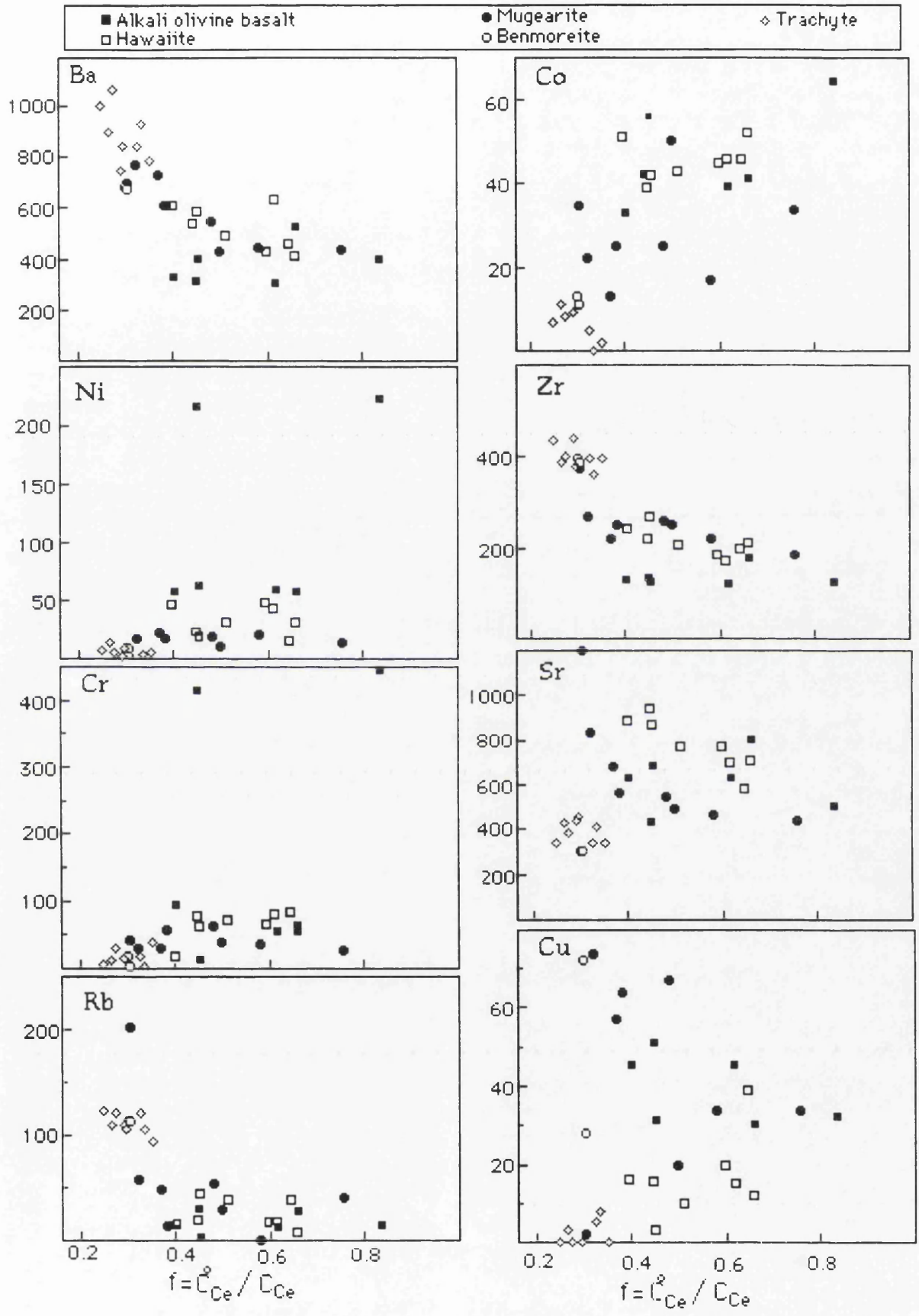

Figure 5.59. Trace elements(ppm) variation plots as a function of the residual liquid fraction($f=C^{\circ}_{Ce}/C_{Ce}$).

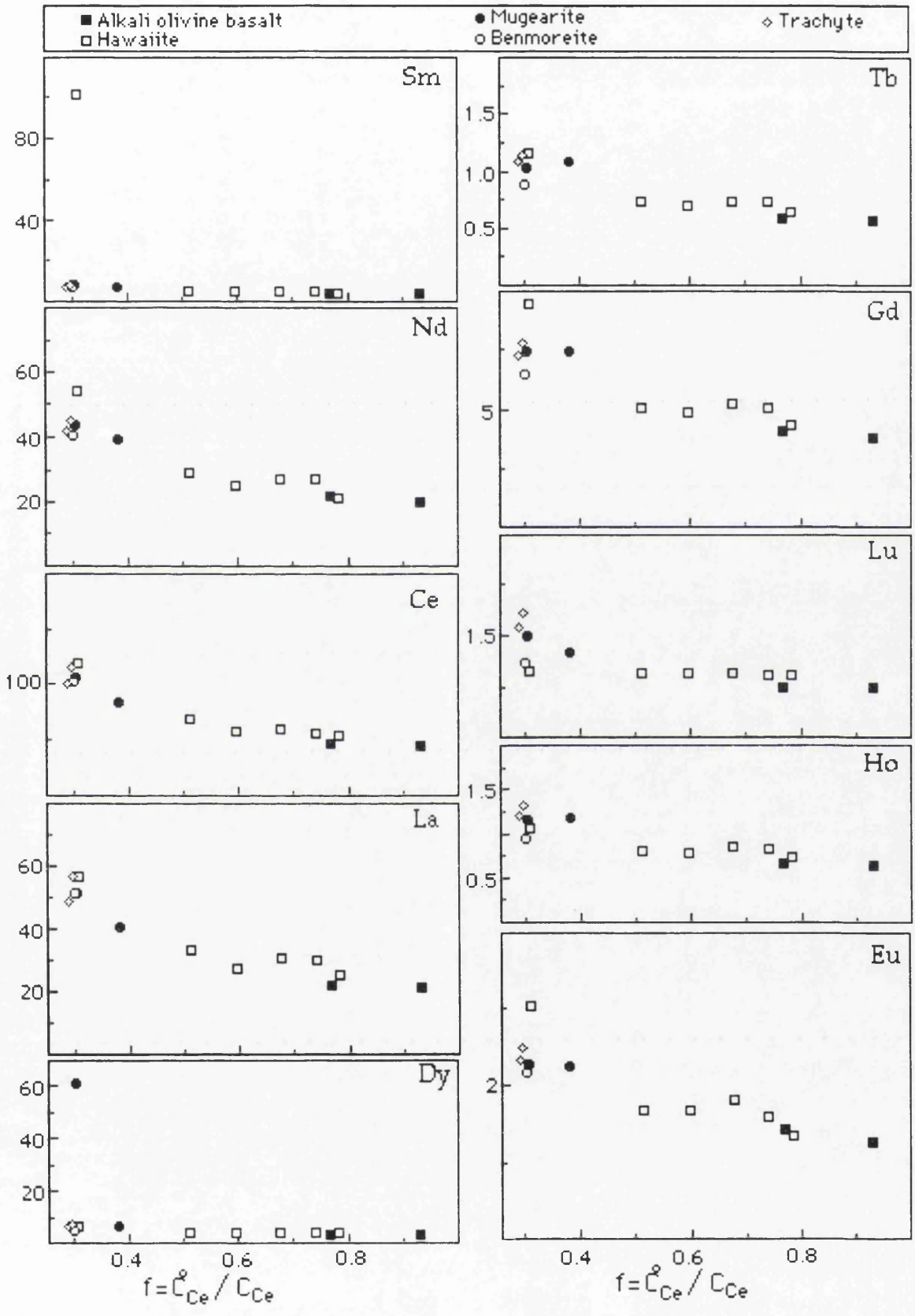

Figure 5.60. REE distribution(in ppm) plots in the Meydan alkaline association as a function of the residual liquid fraction($f=C^{\circ}_{Ce}/C_{Ce}$).

5.3.2.4. RARE EARTH ELEMENTS

In the Meydan alkaline association, all lavas are enriched in REE contents relative to chondrites. Generally, they have fractionated, slightly concave-upward REE patterns.

Basaltic rocks including alkali olivine basalt, hawaiites and mugearites(collectively termed basaltic rocks below) show highly fractionated REE patterns(Figure 5.61), with chondrite-normalized$(La/Lu)_N$= 9 to 11(Table 5.3). It has been suggested that alkaline rocks are characterized by a large enrichment of total REE and LREE relative to chondrites(Cullers and Graf, 1984). The heavy REE contents of basaltic rocks are rather uniform, with$(Lu)_N$=7.4-15.4, but the light REE show a little variation with$(La)_N$=71.9-164.9. There is no clear positive correlation between$(La/Yb)_N$, a measure of the degree of REE fractionation, and normative ne values as observed in oceanic alkali basalts of the Honolulu volcanic series of Oahu(Clague and Frey, 1982). It has been shown that large Eu anomalies are absent in alkaline volcanic rocks(e.g., Kay and Gast, 1973; Sun and Hanson, 1975a, b; Shimizu and Arculus, 1975). However, basaltic rocks show slight positive Eu anomalies. Differentiated rocks, benmoreites and trachytes show similar REE patterns to basaltic rocks but they show greater REE fractionation from basaltic rocks with $(Lu)_N$=11.3-18.9, $(La)_N$=156.3-182.4 and $(La/Lu)_N$=8.8-13.1(Table 5.3 and Figure 5.62). In more evolved rocks(benmoreite and trachyte), there are very slight negative Eu anomalies(Eu/Eu*<1; Ragland, 1989).

In general, there is no Eu anomaly in the Meydan alkaline rocks. It has been shown that rocks derived from the mantle, especially alkaline rocks, are not characterized by Eu anomalies of any sort whereas those with a Eu anomaly are usually attributed to late stage addition or removal of feldspar(Cullers and Graf, 1984). In addition, lack of any significant Eu anomaly in the Meydan rocks may indicate quite oxidizing conditions(Ragland, 1989).

Figure 5.63 highlights the progressive enrichment of REE elements from alkali olivine basalt to trachyte with almost parallel REE patterns. Normalizing the REE abundances of each rock sample to sample(MA-27), which has the lowest REE abundances and is supposed to be the most primitive one, allows a more magnified view of the variations from rock to rock than on a chondrite normalized plot(Hanson, 1980 and 1989). In this plot(Figure 5.64), patterns for samples of alkali olivine basalt and hawaiite are almost flat and parallel each other. All other rock samples are slightly concave upward with slight negative Eu anomalies, especially mugearite

which has a distinctive negative Eu anomaly. These characteristics suggest that mugearite, benmoreite and trachyte might have undergone removal of plagioclase and cpx relative to alkali olivine basalt and hawaiite.

Table 5.3. Selected REE ratio and variation in the Meydan alkaline association.

Rock	Sample	$(La)_N$	$(Lu)_N$	$(La/Lu)_N$	$(La/Yb)_N$	$(Eu)_N$	$(Eu/Eu^*)_N$
Alkali olivine basalt	MA-23	71.94	7.67	9.37	8.55	18.44	1.05
	MA-27	69.38	7.44	9.32	8.59	17.15	1.01
	MA-29B	88.84	9.78	9.07	8.49	21.95	1.03
Hawaiite	MA-40	107.34	9.96	10.77	9.80	22.95	0.99
	MA-166	96.84	9.41	10.29	9.27	21.66	0.95
	MA-175	99.59	9.95	10.00	9.11	23.36	1.05
Mugearite	MA-53	132.24	12.93	10.22	9.16	33.24	0.92
	MA-54	164.89	15.39	10.71	10.03	34.14	0.91
Benmoreite	MA-34A	165.27	11.30	14.62	13.12	29.99	0.98
Trachyte	MA-10	182.38	18.94	9.62	9.38	35.71	0.95
	MA-43	156.34	16.67	9.37	8.88	33.49	0.94

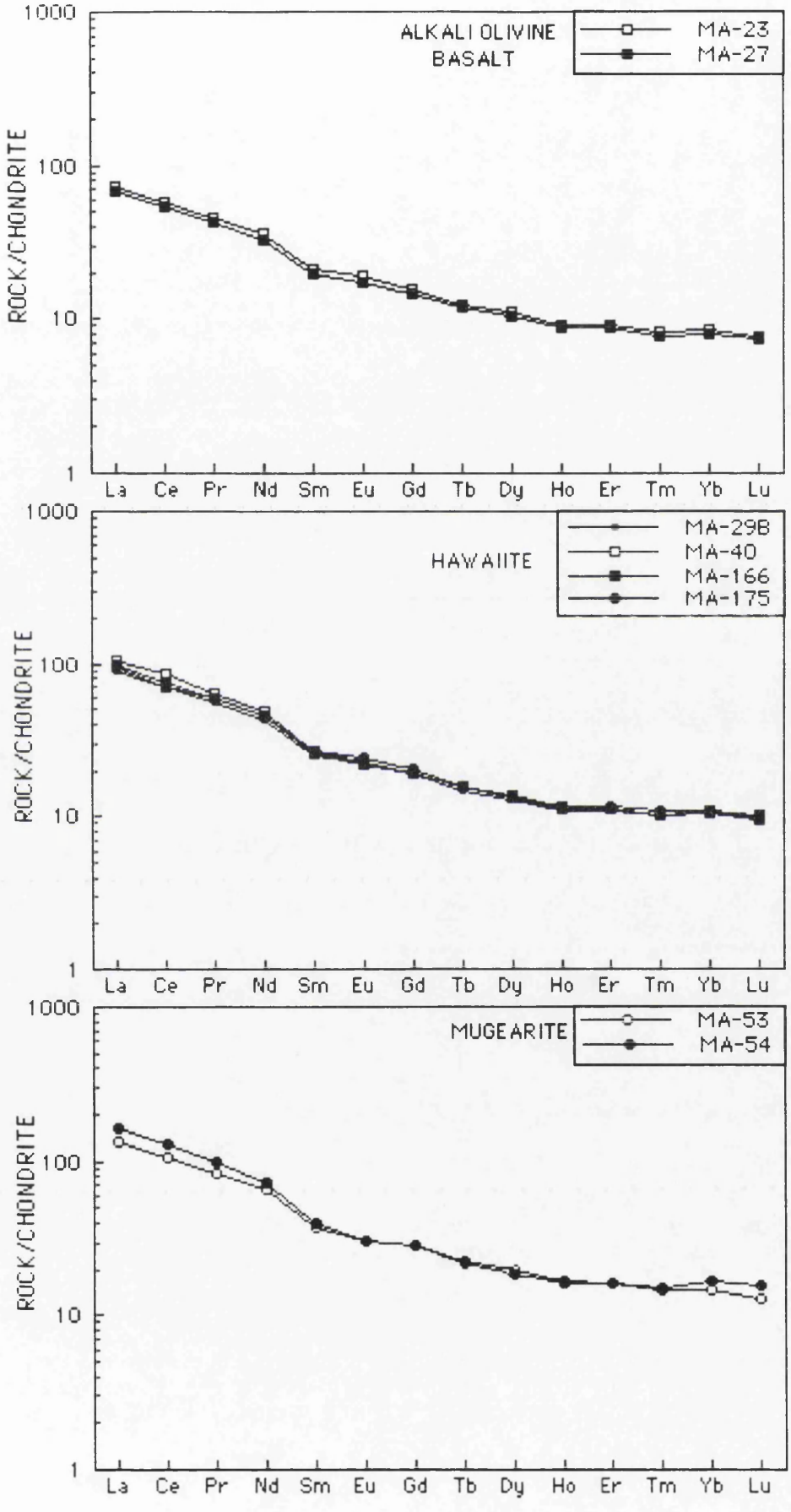

Figure 5.61. Chondrite-normalized REE patterns of basaltic rocks of the Meydan alkaline association. Chondritic values are from Boynton(1984).

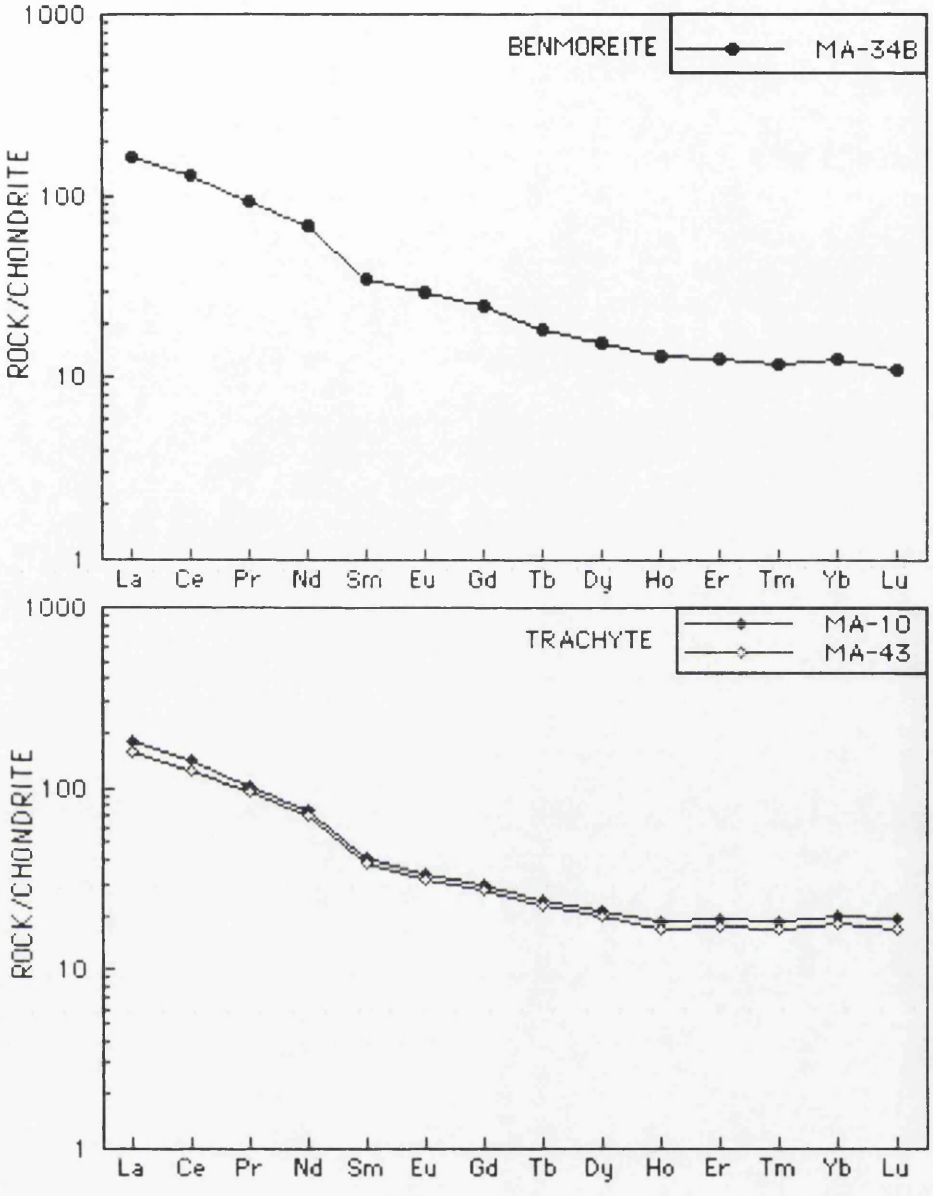

Figure 5.62. Chondrite-normalized REE patterns of more evolved rocks of the Meydan alkaline association. Chondritic values are from Boynton(1984).

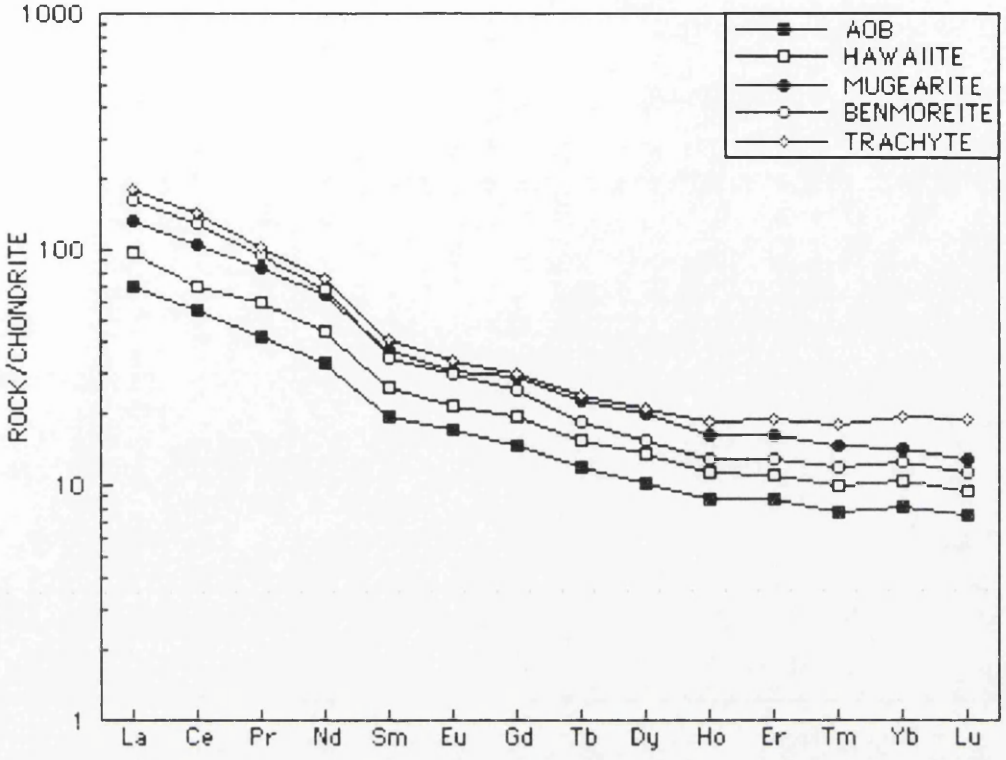

Figure 5.63. Rare earth element patterns showing enrichment of element contents from alkali olivine basalt to the most evolved rocks, the trachytes in the Meydan alkaline association.

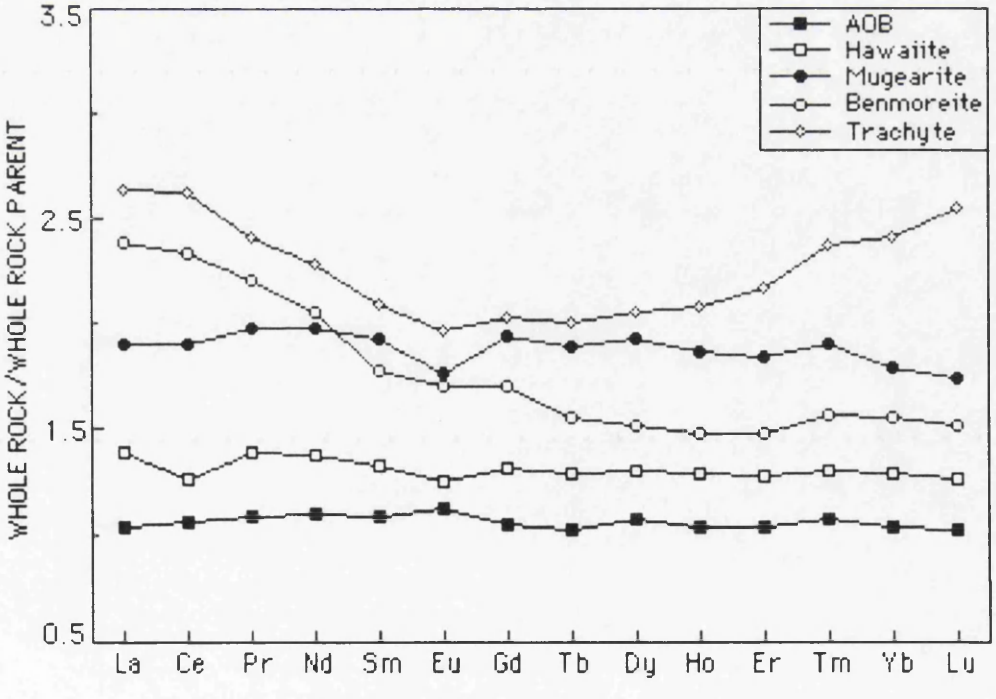

Figure 5.64. Normalized REE contents of the Meydan alkaline rocks to the most primitive sample(MA-27), highlighting relative abundances of REE in each rock type.

The REE pattern for a parental type alkali olivine basalt sample(10.25 wt.% MgO) and a hawaiite sample are shown in Figure 5.65, where it can be compared with an average estimated for the sodic alkalic suite(Schilling and Winchester, 1969). The slope of the curves is similar and apparently there is no systematic difference in the REE patterns between the alkalic suite average and alkali olivine basalt. However, both alkali olivine basalt and hawaiite show slight depletion in MREE relative to alkalic suite average(Figure 5.65).

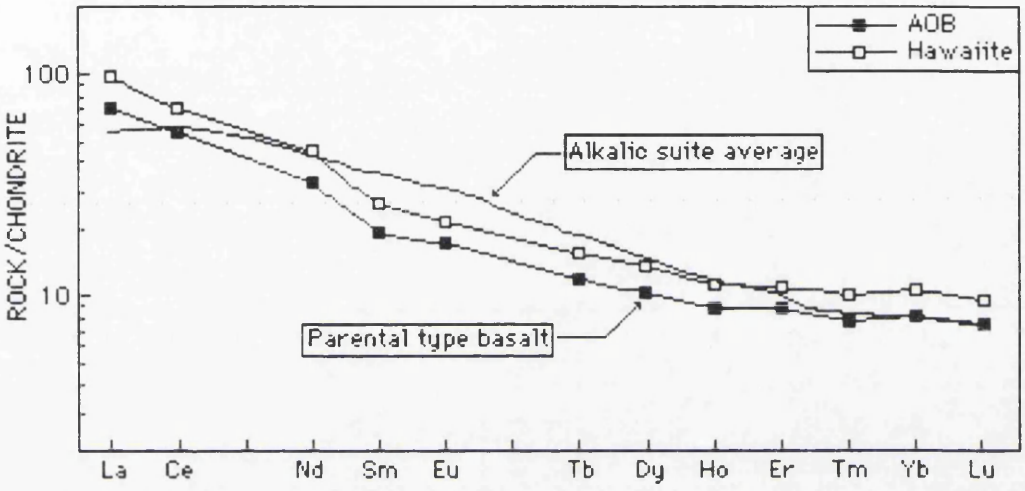

Figure 5.65. The REE average pattern for the alkalic suites estimated by Schilling and Whinchester(1969). The REE pattern for the parental type alkali olivine basalt(MA-27) is also shown for comparison.

The Meydan lavas exhibit a variation in LREE contents that closely resembles the expected distribution in lavas related by fractional crystallization(Figure 5.66). Therefore, their REE patterns do not represent primary liquids and do not provide information concerning melting processes.

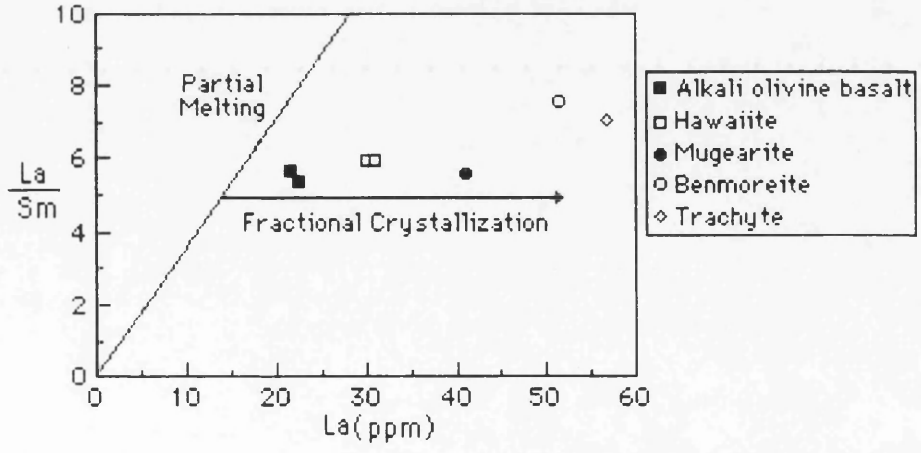

Figure 5.66. La/Sm versus La plot. The trend has been considered to indicate that a suite of lavas are related by different degrees of partial melting and fractional crystallization(Minster and Allegre, 1978).

When LREE abundances in the Meydan lavas are plotted on La-Ce, Nd-Ce, and Sm-Ce diagrams, the La-Ce trend passes near the origin, but the Nd-Ce and Sm-Ce trends do not(Figure 5.67). These trends imply that, although La and Ce have behaved as strongly incompatible or hydromagmatophile elements, Nd and Sm have behaved as moderately incompatible or magmatophile elements during fractionation(Sun and Hanson, 1975a, b; Allegre and Minster, 1978). The general lack of correlations between REE and P_2O_5, TiO_2, Sr, Nb and Zr indicates that accessory phases did not control REE distributions. Nd-Ce trend can be qualitatively matched to a fractional crystallization trend. However, more evolved rocks, especially benmoreite and trachyte, show a slight departure from linearity in the REE correlation. Accordingly, it is reasonable to conclude that the REE contents of the lavas have been modified by complex processes involving crystal fractionation, contamination and, or, magma mixing. If La and Ce showed hydromagmatophile behaviour during crystal fractionation, the concentration of these elements would be a simple function of the fraction of residual liquid(Ferrara and Treuil, 1974).

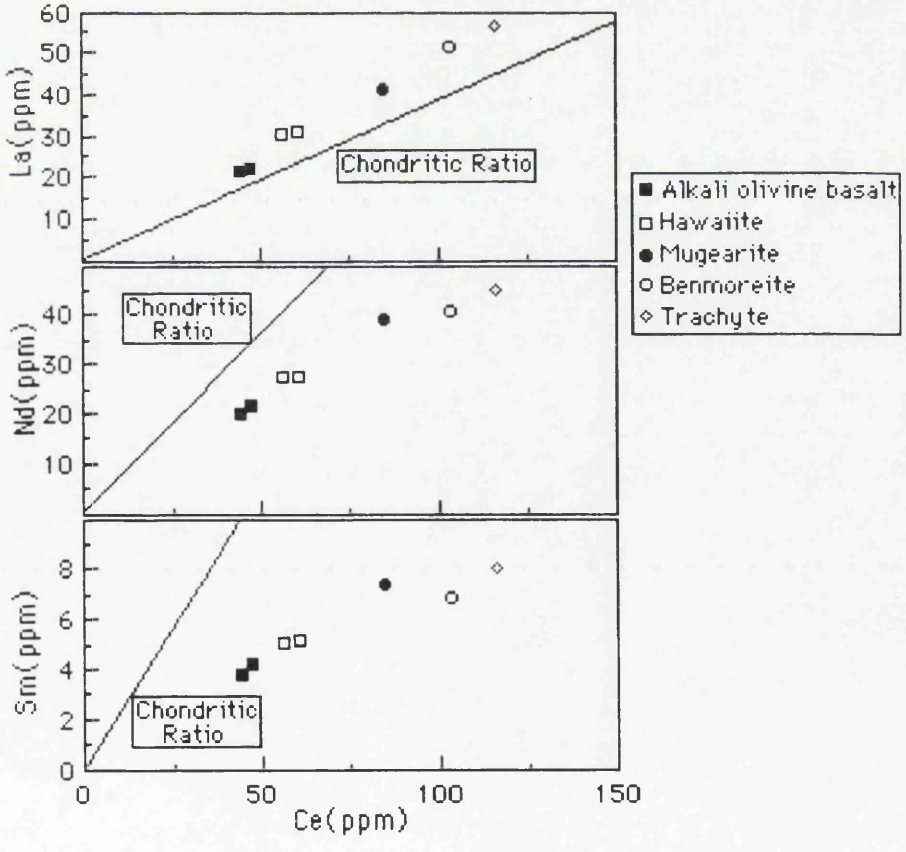

Figure 5.67. Ce versus La, Nd and Sm plots showing LREE interrelation.

5.3.2.5. SOURCE CHARACTERISTICS OF THE MEYDAN LAVAS

The major element composition of the alkaline lavas of the Meydan association is distinct in four ways from the calcalkaline lavas in the region. FeO and TiO_2 are more abundant and Al_2O_3 lower in the alkaline rocks which also plot consistently in the alkaline fields of MacDonald and Katsura(1964), and Irvine and Baragar(1971).

A nearly universal characteristic of subduction-related lavas is their enrichment of alkali(K, Rb) and alkaline earth elements(Ba, Sr) relative to high-field-strength(HFS) elements(Ti, Nb, Zr) and LREE(Perfit *et al.*, 1980; Gill, 1981; Arculus and Johnson, 1981; Hickey *et al.*, 1986a, b; Hildreth and Moorbath, 1988). One index of this enrichment is the Ba/TiO_2 ratio, which is plotted against MgO (Figure 5.68). The Meydan lavas have Ba/TiO_2 ratios lower than the subduction-related lavas, but higher than the Hawaiian suite of lavas(Basaltic Volcanism Study Project, 1981).

The more evolved rocks, benmoreite and trachyte, have elevated Nb abundances relative to the primitive alkali olivine basalt and hawaiite lavas, and calcalkaline lavas(<15ppm). Low Ba/Nb, Sr/Zr, Ba/La, La/Nb(Figure 5.68) and La/Zr ratios demonstrate that alkali olivine basalt and hawaiites are similar in composition to oceanic island basalts, and that slab-derived material played a minor role in the genesis of these lavas(Gill, 1981).

It has been shown that intraplate basaltic rocks have geochemical characteristics with no Nb and Ta anomalies(Sun and McDonough, 1989) and include a range of alkalic lavas with primary melt characteristics(Frey *et al.*, 1978). Compared with these intraplate basaltic rocks, alkali olivine basalt and hawaiite from the Meydan alkaline association exhibit significant Nb anomalies. The geochemical compositions of the Meydan basalts indicate they were derived from an enriched mantle source, but the enrichment process was not related to the processes which generated the convergent margin magmas. This is shown by the low Ba/La(11) and Ba/Nb(10) ratios for basalts versus high Ba/La and Ba/Nb ratios in the convergent margin lavas, which are typical of magmas related to a subduction zone(Sun, 1980). These data suggest that the Meydan alkalic magmas were generated in the mantle, possibly within the underlying continental lithospheric mantle at a depth >20kbar.

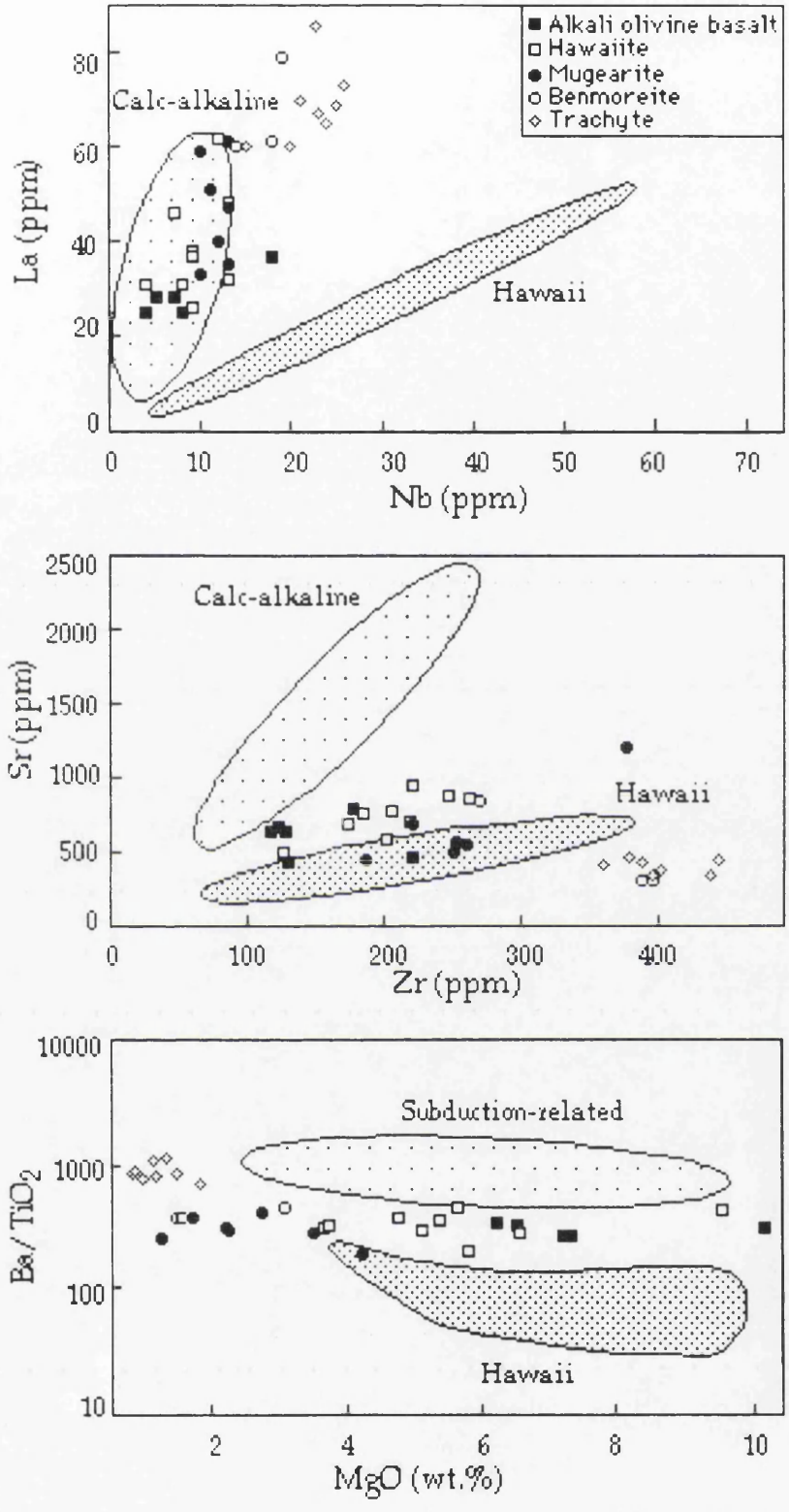

Figure 5.68. Trace element variation plots for the Meydan alkaline volcanic rocks. Hawaiian samples are from Basaltic Volcanism Study Project(BVSP, 1981). The calcalkaline lavas are from Righter and Carmichael(1992), and Lange and Carmichael(1990). The subduction related lavas include these calcalkaline lavas as well as alkaline lavas from Wallace and Carmichael(1989), Allan and Carmichael(1984), and Luhr and Carmichael(1981).

5.3.3. CALCALKALINE ASSOCIATION

5.3.3.1. KIZILDERE LAVAS

5.3.3.1.1. MAJOR AND TRACE ELEMENTS

Kizildere lavas are basaltic andesite, andesite and rhyolite with SiO_2 content ranging from 55 to 79 wt.%. They have chemical compositions typical of medium-K suites(Peccerillo and Taylor, 1976; Gill, 1981). In plots of SiO_2 versus FeO*/MgO(Miyashiro, 1974) and Al_2O_3 versus normative plagioclase composition(Irvine and Baragar, 1971), the lavas are classified as calcalkaline. In addition, they show little iron enrichment and plot in the calcalkaline field on an AFM diagram(Figure 5.72). The geochemical characteristics of the lavas are also comparable with those of calcalkaline suites erupted at convergent plate margins(Pearce, 1982).

Basaltic andesite and andesitic lavas are aluminous(15.5-17.5 wt.% Al_2O_3), and MgO varies between 0.5 and 5 wt.%(Mg-number=15-60). They have high Ni, Co, Ba, Rb, Th and Sr abundances relative to the rhyolite. Furthermore, they are characterized chemically by low TiO_2, low Na_2O/K_2O and K/Rb, high Rb, Sr, Ba, Th and high La/Yb, Rb/Sr, Ba/Nb, Ba/La and La/Zr. Therefore, the lavas display orogenic imprint as suggested by high Ba/La, Ba, Nb, K/Nb, Th/La, Pb/La(Hickey *et al.*, 1986a, b), and low Zr/TiO_2(Winchester and Floyd, 1977). However, the lavas are enriched in most compatible elements compared to calcalkaline andesites of typical orogenic environments(Gill, 1981).

In the Kizildere lavas, some of the major and trace elements show correlation with SiO2(Figures 5.69, 5.70 and 5.71). TiO_2, Al_2O_3, MgO, CaO, P_2O_5, MnO and FeO* decrease, whereas K_2O increases, with increasing SiO_2. Although the data are scattered, with increasing SiO_2 there is an overall increase in incompatible elements(Nb) and depletion in compatible elements(Ni, Cr, Co) which may be explained by fractional crystallization processes from basaltic andesite to andesitic and rhyolite lavas. Zr and Rb show well-defined increases with increasing SiO_2 but other incompatible elements, Th and Nb, have lower enrichment. The overall chemical trends seen, of progressive increase in SiO_2, K_2O and incompatible elements(e.g., Zr, Rb, Nb) with decrease in MgO, FeO*, Na_2O, CaO and compatible elements(e.g., Ni, Cr, Co) suggests qualitatively that these lavas may have developed mainly by fractional crystallization. If a suite of rocks is generally related by fractional crystallization process, then the parent and derivative lavas should have similar incompatible element ratios(e.g., K/Rb, Ba/Rb, Ba/La).

Cr, Ni, MgO and CaO show decreasing compatible behaviour in basaltic to andesitic compositions reflecting significant olivine in basaltic andesite and cpx precipitation in both basaltic andesite and andesite. The greater

compatibility of CaO, Sr and Eu in siliceous liquids reflects an increased weight fraction of plagioclase in the solid removed and an increase in the values of $D_{Sr}^{plag/liq}$ with increasing content and decreasing temperature of the melt(Drake and Weill, 1975). Major magnetite crystallization in andesitic liquids is marked by the compatibility of FeO* and TiO_2. Apatite precipitation is marked by the compatible behaviour of P. Local concentrations of P in the liquid may cause local crystallization of apatite as minute crystals that may be included in rapidly growing phenocrysts, preventing the enrichment of P in liquid expected on the separation of P_2O_5-poor phases(Green and Watson, 1982).

The alkali elements, K and Rb, are very sensitive indicators of fractionation processes(Taylor and McLennan, 1988). K/Rb ratios appear to increase with increasing K_2O, and Rb shows negative correlation with Sr(Figure 5.73). In addition, Zr has a negative correlation with Y, Cr and Co(Figure 5.74), indicating that clinopyroxene and some magnetite fractionation played a role in the evolution of the andesitic lavas, with significant clinopyroxene fractionation because Y is more compatible in clinopyroxene with increasing silicic liquid compositions(Pearce and Norry, 1979).

The distribution of K/Rb versus Zr/Y(Figure 5.75) is a useful fractionation measure. Although some andesite samples lie on a linear trend representing crystal fractionation, others are scattered indicating possible mixing. Moreover, a nearly linear trend on a Y/Rb versus K/Rb plot suggests magma mixing(Figure 5.75).

The Kizildere lavas have generally high La/Y and low Nb/Y ratios(Figure 5.76). On a CaO versus Y plot, the lavas plot mainly on the Y depleted side of the standard calcalkali trend of Lambert and Holland(1974), and define a J-type trend from basaltic andesite to andesites and then an L-type trend from andesites to rhyolite(Figure 5.76). The trends suggest that hornblende+cpx was an early fractionation phase in the evolution of andesites and followed by plagioclase in the generation of rhyolite.

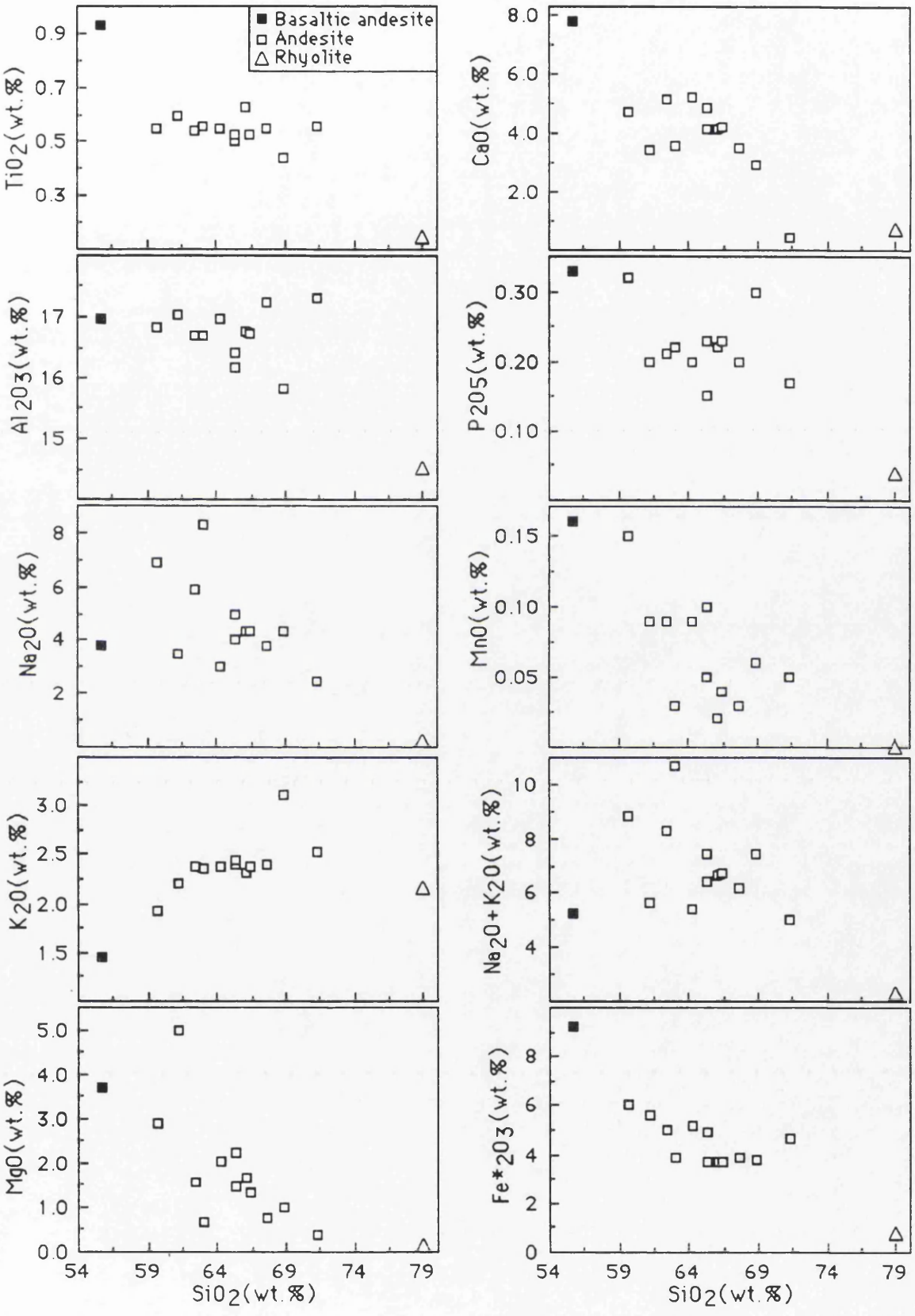

Figure 5.69. SiO_2(wt.%) versus major element plots for the Kizildere lavas.

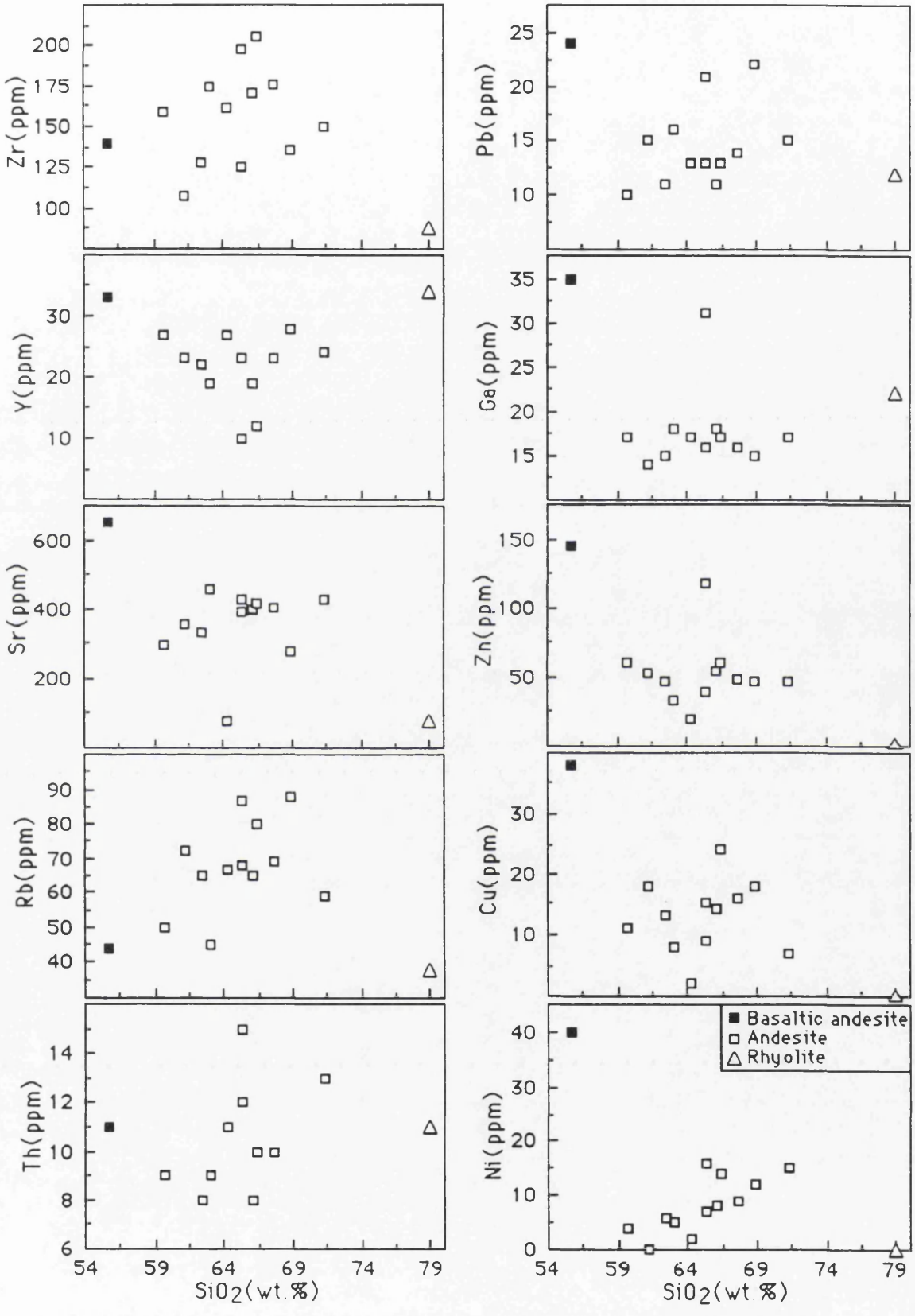

Figure 5.70. SiO_2(wt.%) versus trace element plots for the Kizildere lavas.

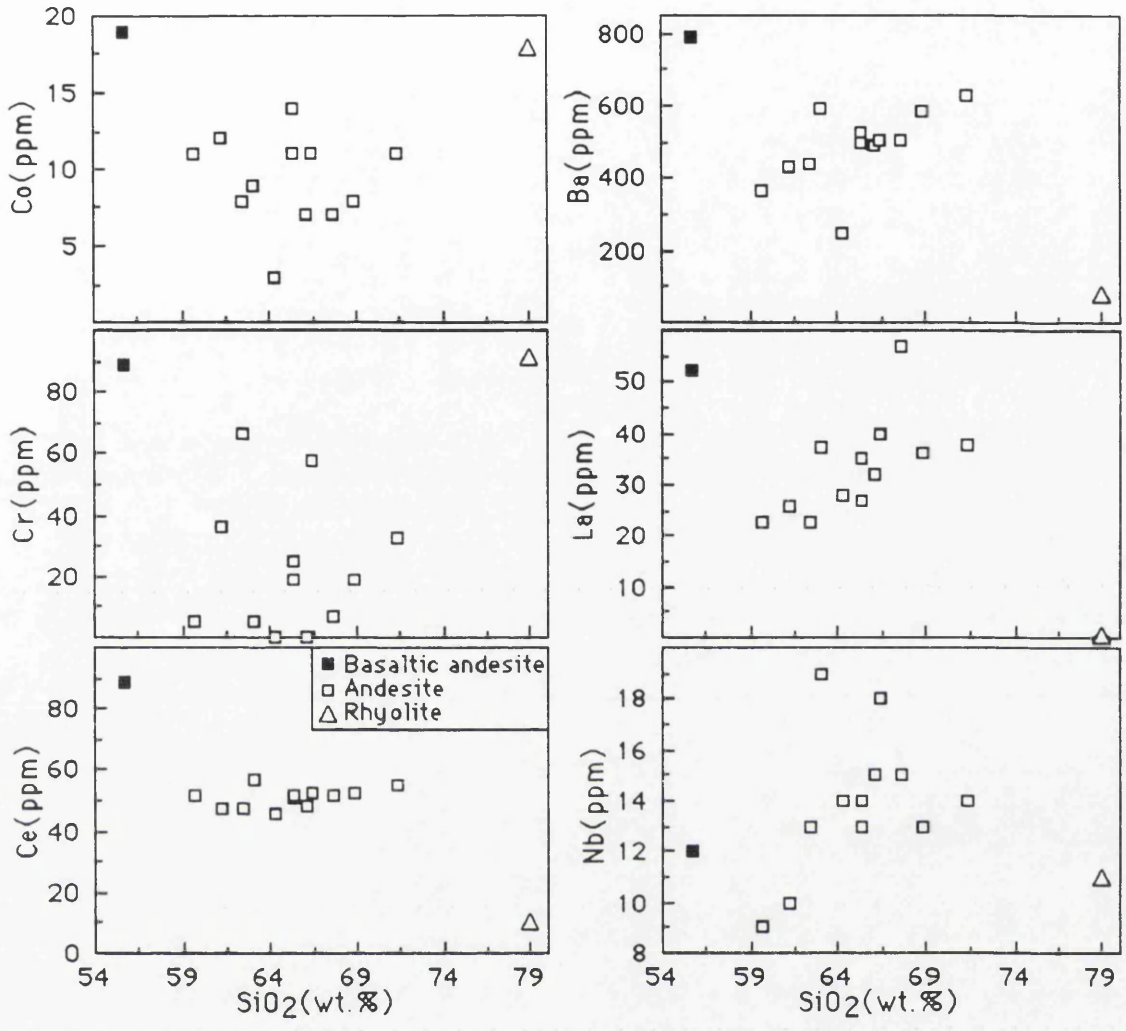

Figure 5.71. SiO_2(wt.%) versus trace element plots for the Kizildere lavas.

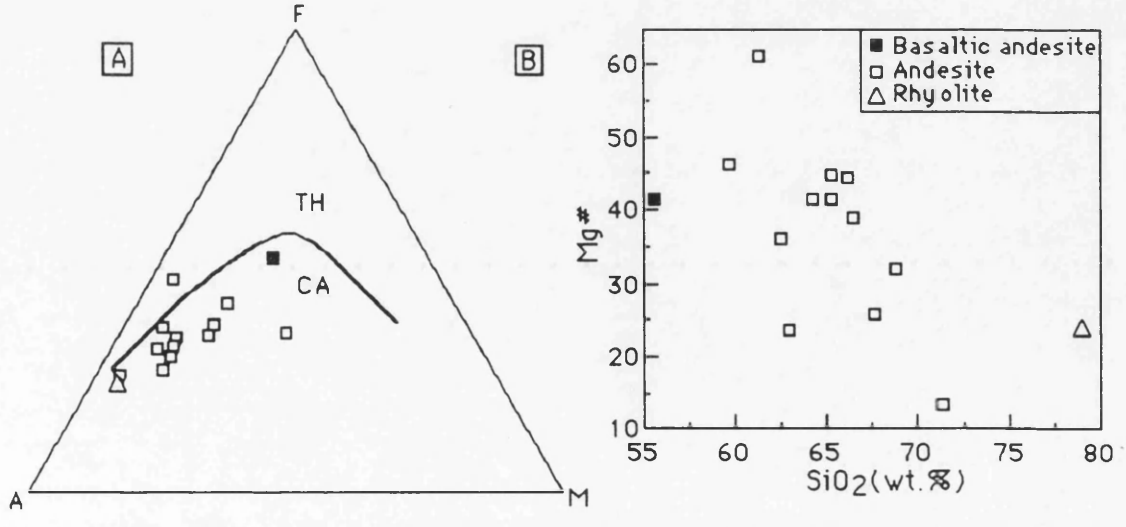

Figure 5.72. AFM plot showing the composition of the Kizildere lavas(A). The thick line separates tholeiitic(TH) and calcalkaline(CA) compositions(Irvine and Baragar, 1971). Mg-number($Mg^{\#}$=100xMg/Mg+Fe^{+2}) versus SiO_2(wt.%) plot(B).

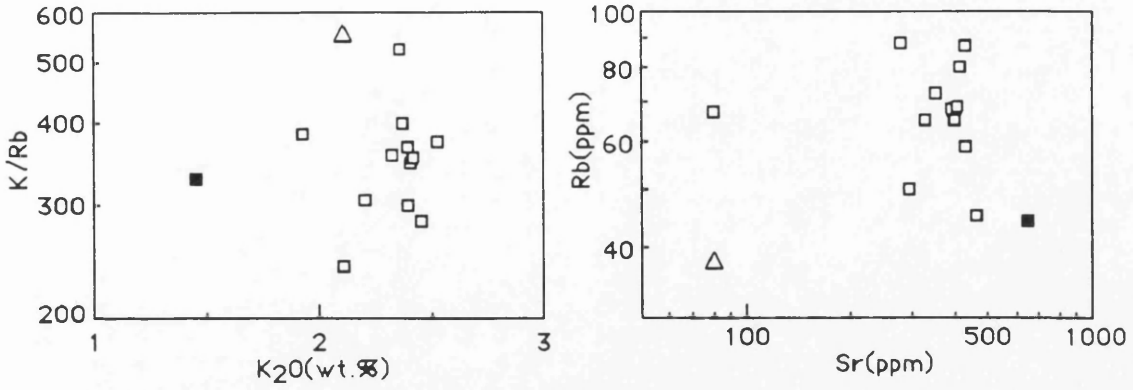

Figure 5.73. Log K/Rb versus K_2O(wt.%) and log Rb(ppm) versus log Sr(ppm) plots. The symbols are ■, basaltic andesite; □, andesite; △, rhyolite.

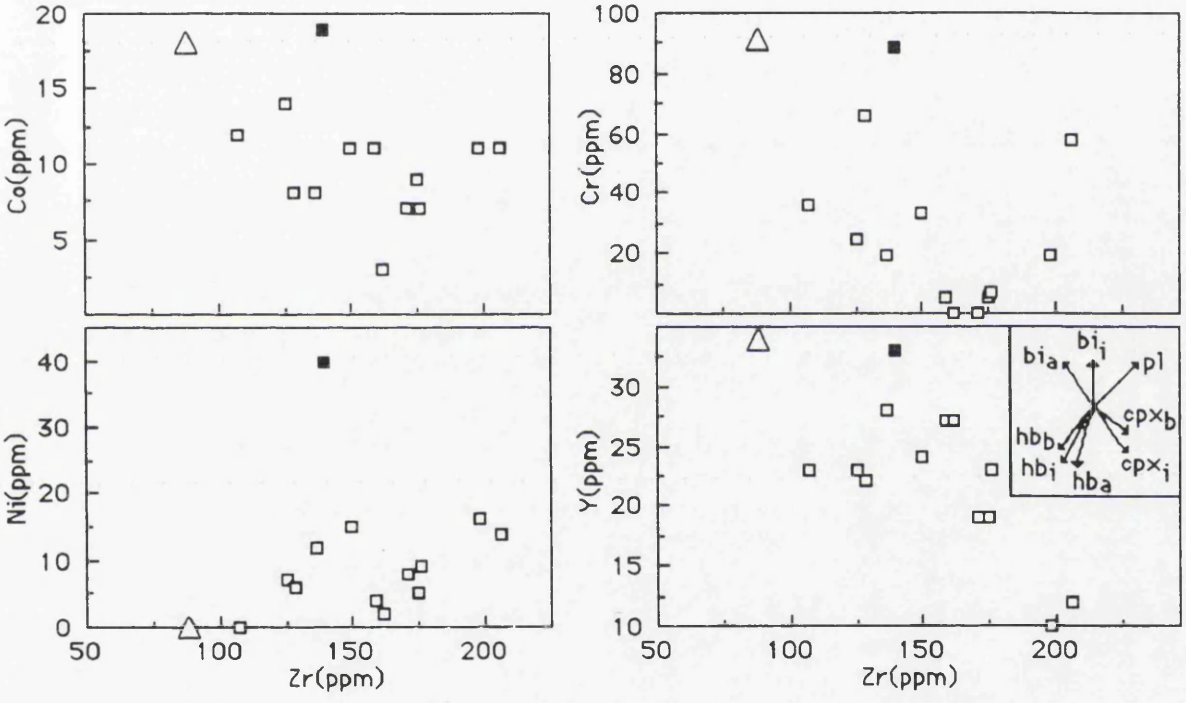

Figure 5.74. Zr(as a fractionation index) versus Co, Ni, Cr and Y plots for the Kizildere lavas. The symbols are ■, basaltic andesite; □, andesite; △, rhyolite.

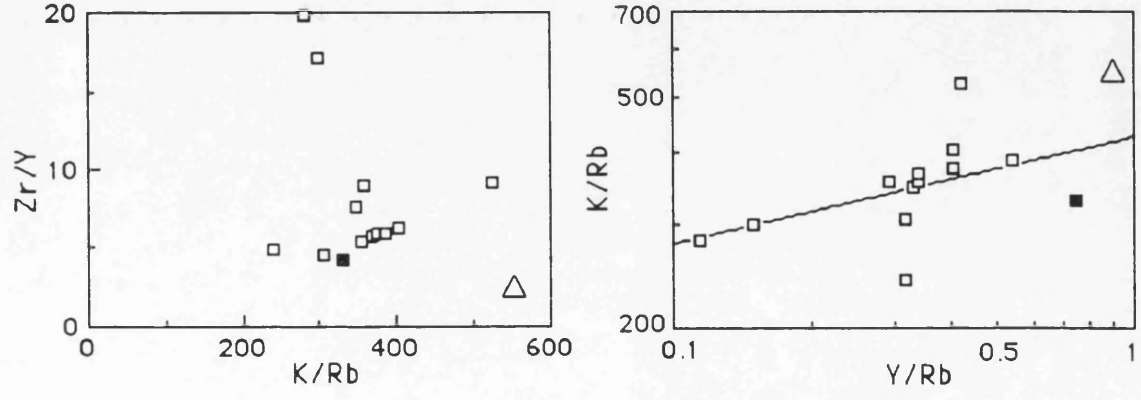

Figure 5.75. K/Rb versus Zr/Y and log Y/Rb versus log K/Rb plots for the Kizildere lavas. The symbols are ■, basaltic andesite; □, andesite; △, rhyolite.

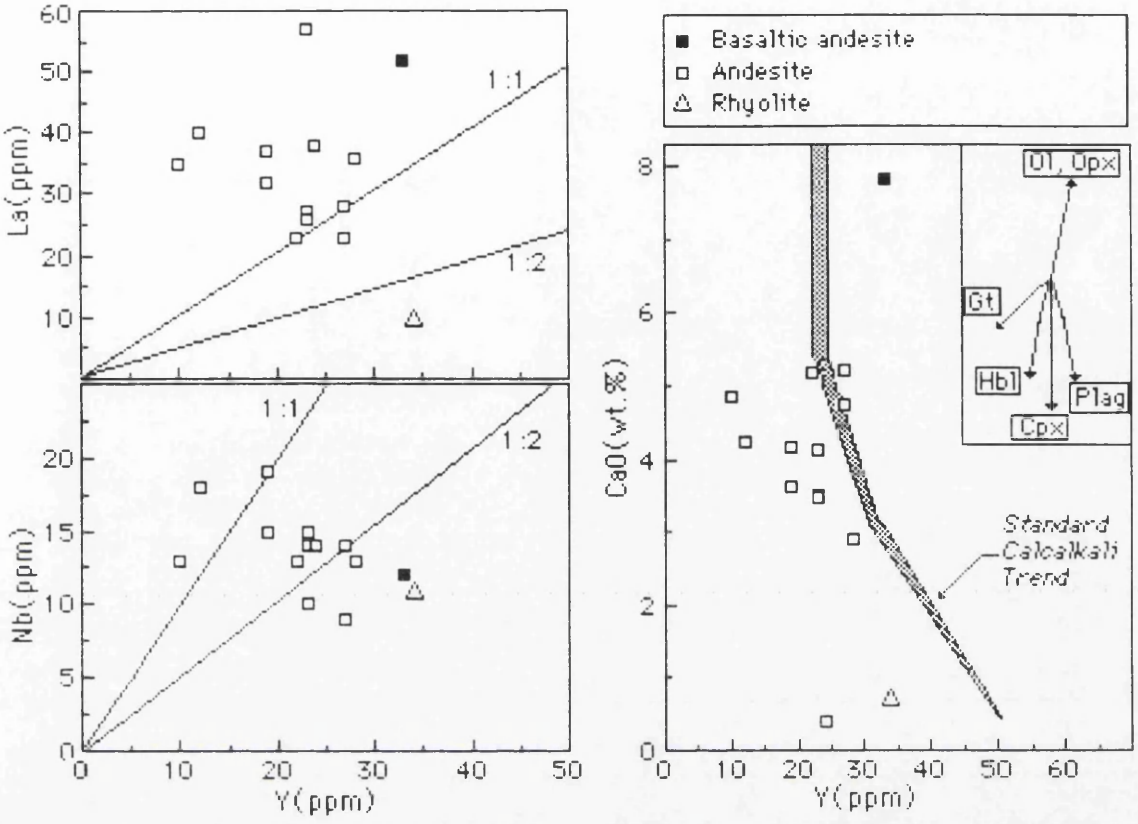

Figure 5.76. Y(ppm) versus Nb(ppm), La(ppm) and CaO(wt.%) plots for Kizildere lavas. Shaded area represents the "standard" calcalkaline trend of Lambert and Holland(1974). The vectors show qualitative trends of the effect of fractional crystallization of common silicates.

5.3.3.1.2. INCOMPATIBLE ELEMENTS

The Mid-Ocean Ridge Basalt(MORB) and Primordial Mantle(PM)-normalized trace element patterns of the lavas are shown in Figures 5.77 and 5.78. Generally, the andesitic rocks exhibit similar patterns to the rhyolite. All samples have a characteristic negative Nb anomaly being more akin to subduction values.

In MORB-normalized patterns(Figure 5.77), LILE enrichment, especially in Th, is most pronounced. The rocks also show progressively decreasing negative Ba, Sr, P and Ti anomalies, presumably suggesting fractional crystallization of plagioclase, magnetite and apatite. In the mantle normalized patterns(Figure 5.78), they show enrichment in hydrophile elements(K, Rb, Th) relative to REE and HFSE(Zr, Ti). The relatively varying Sr/Zr ratios and Zr implies that this may be the result of plagioclase fractionation. Y is less incompatible reflecting its preferential removal by cpx(Pearce and Norry, 1979). In addition, the less incompatible behaviour of Zr, reflected in increase in Zr with fractionation, may also reflect cpx crystallization(Villemant *et al.*, 1981).

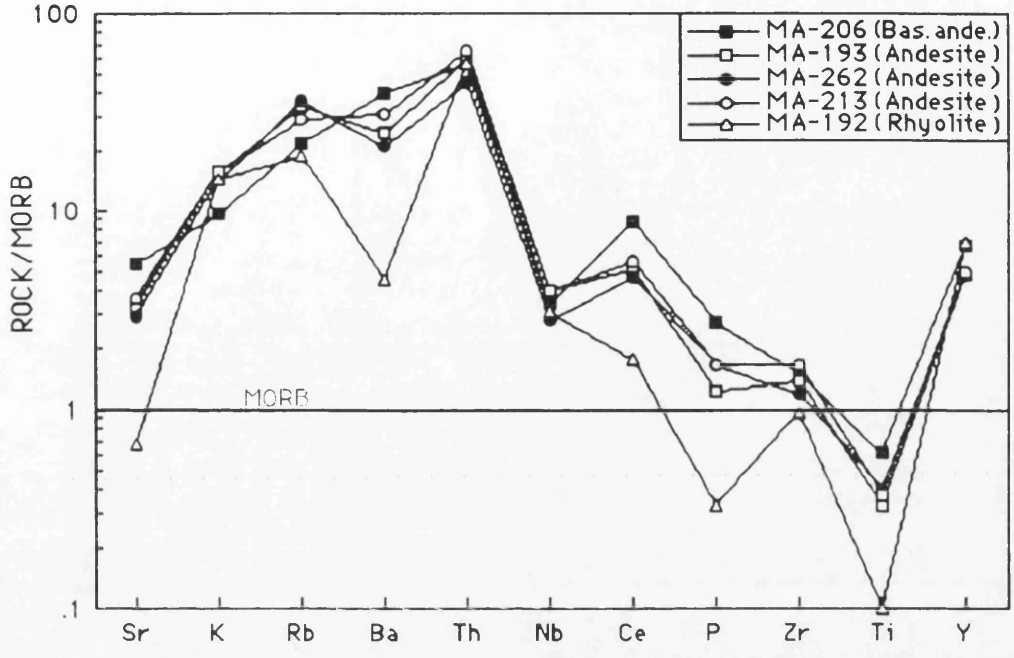

Figure 5.77. MORB-normalized trace element patterns of the Kizildere lavas(MORB normalizing values are from Pearce, 1983).

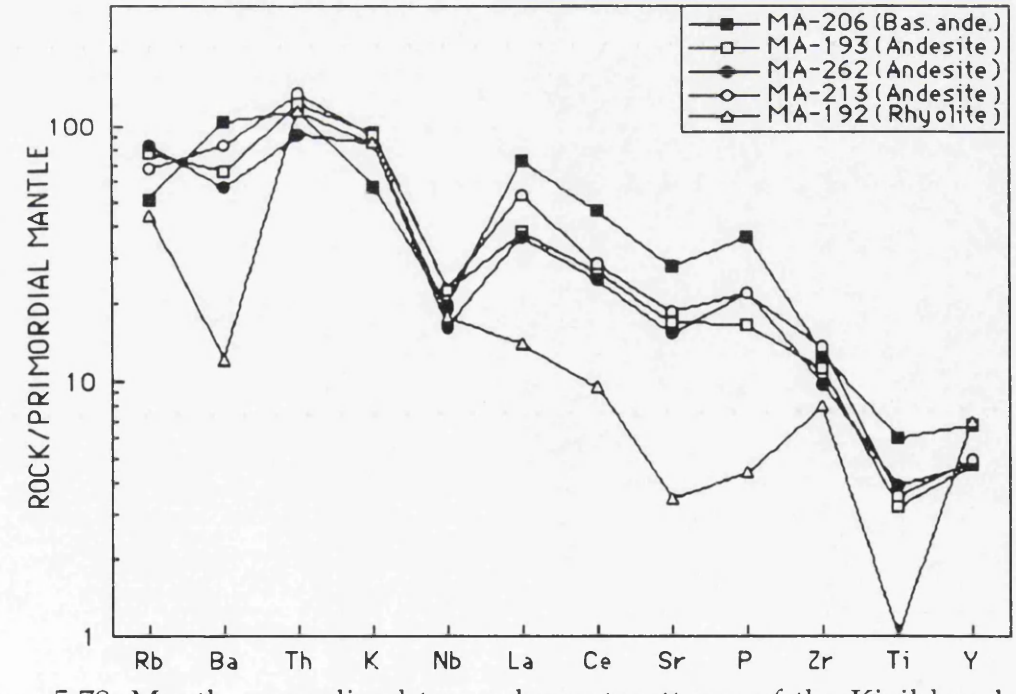

Figure 5.78. Mantle-normalized trace element patterns of the Kizildere lavas. Normalizing primordial mantle values are from Wood *et al.* (1979a).

5.3.3.1.3. RARE EARTH ELEMENTS

The REE patterns of Kizildere lavas are comparable with typical medium-K suites(Gill, 1981). They show highly fractionated patterns(Figure 5.79) with steep slopes and $(La/Lu)_N$=13.35-27.77 . HREE patterns are relatively flat and parallel to each other. They do not have characteristic Eu anomalies. Sample MA-193 has a slightly negative Eu anomaly with $(Eu/Eu^*)_N$=0.89 and samples MA-199 and MA-213 have slightly positive anomalies with $(Eu/Eu^*)_N$=1.30 and 1.39 respectively. The positive Eu anomaly may result from the presence in the melt of hornblende, clinopyroxene and apatite(Hanson, 1980).

The lavas are characterized by LREE enrichment and HREE depletion compared with medium-K suites. Relatively low Y and Yb contents and presence of strongly fractionated REE patterns, reflected in high $(La/Lu)_N$ ratios, in the Kizildere lavas may indicate that garnet did not play a significant role as a fractionating or residual phase in their generation(Hanson, 1980). On the contrary, the relatively concave-up REE patterns and near constant Y contents suggest significant amphibole participation in the andesitic lavas.

The inverse REE distribution patterns(1/D, for D values for andesitic rocks: Arth, 1976; Henderson, 1982) for plagioclase, clinopyroxene and hornblende have been compared in REE patterns. The REE suggests that clinopyroxene and hornblende are major controlling phases for the Kizildere lavas. It is possible that different levels of HREE enrichment reflect, in part, higher K_D^{HREE}'s of hornblende relative to cpx(Nicholls and Harris, 1980), as well as different proportions of these minerals fractionated. Alternatively differences in REE patterns of andesitic rocks may reflect, in part contamination by different crustal sources, but data are not diagnostic enough to allow any specific model to be favoured. The LREE-enriched patterns of the andesites might indicate crustal assimilation or crystal fractionation. The local presence of cognate xenoliths suggests that both processes operated within a high level magma chamber.

One sample(MA-199) exhibits a negative Ce anomaly. Negative Ce anomalies have been attributed to involvement of Ce-depleted oceanic sediments or altered basaltic crust or to slab dehydration and production of Ce^{+4}(Heming and Rankin, 1979; Hole *et al.*, 1984; White and Patchett, 1984). However, the Ce anomaly in the lavas is not consistent and may be caused by post-eruptive weathering or alteration under oxidizing conditions(Hanson, 1980; Nagashima *et al.*, 1986). Moreover, Ludden and Thompson(1979) note that LREE, particularly Ce, shows considerable mobility during low-temperature weathering processes(e.g., thermal alteration).

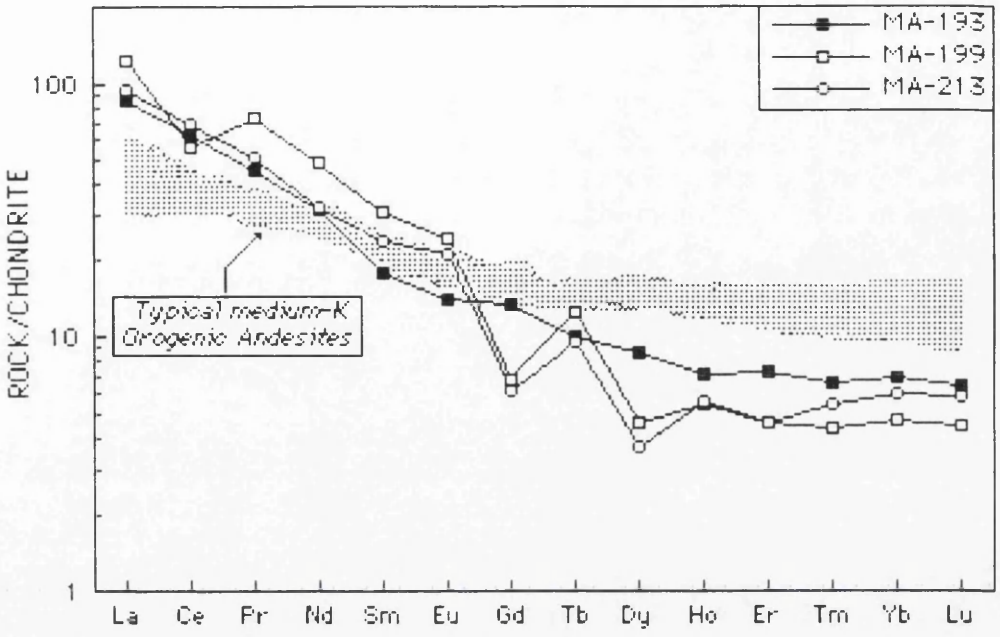

Figure 5.79. Chondrite-normalized REE patterns of the Kizildere andesite lavas. Normalizing values are from Boynton(1984). Typical medium-K orogenic andesites(Gill, 1981) are shown for comparison.

5.3.3.2. TUFF

5.3.3.2.1. MAJOR AND TRACE ELEMENTS

Studies of volcanic successions have illustrated that chemical analyses can be an important in correlation(e.g., Hildreth and Mahood, 1985; Sarna-Wojcick *et al.*, 1987; de Silva and Francis, 1989). Microprobe analysis of individual glass shards or phenocrysts has emerged as one of the most powerful tools in tephrachronology because of the number of elements which can be determined and the great precision obtained by determining variability between pyroclasts(Sarna-Wojcick *et al.*, 1987). In addition, analysis of pumice clasts or fiamme has also proved useful(Hildreth and Mahood, 1985).

Application of above techniques to tuffs from Kizildere formation is rarely possible for several reasons. Devitrification, hydration and recrystallization of glass shards, in connection with diagenesis and hydrothermal alteration precludes disaggregation of the pyroclastic material into individual components or obscures recognition of these pyroclasts. These factors mean that in general terms, whole-rock chemical analysis is the only approach that can be applied in tephrachronological studies(e.g., Orton, 1992).

Considerably less is known about the effects of post-depositional changes on the mobilization of either major or trace elements in rhyolitic rocks, particularly in thin beds of volcanic ash(cf. Zielinski 1982; Yamamoto *et al.*, 1986). In this study, due to uncertainty regarding to the nature and mobility of

elements during chemical alteration, the major and trace elements determined have been taken as representing the original chemical compositions.

Analysed samples range in composition from 71 to 80 wt.% SiO_2 and 0.13 to 0.95 wt.% TiO_2. They are characterized by low and restricted abundances of many stable incompatible elements relative to Zr, a feature typical of calcalkaline intermediate-acidic rocks, rather than tholeiitic series acidic differentiates(Winchester and Floyd, 1977). It is suggested that Zr, Nb, Y, Cr and Cu are immobile during chemical alteration(e.g., Pearce and Cann, 1973; Floyd and Winchester, 1975). Thus, the discrimination of different tuffs should be based on these elements. The vitric tuffs have a subalkaline rhyolite bulk composition(Figure 5.80) in terms of immobile trace element ratios. Lithic samples of tuff contain anomalously high levels of MgO(~4 wt.%) for intermediate and felsic rocks, probably reflecting the incorporation of clastic material. Thus, they plot in the alkaline field(Figure 5.80). All samples have poor iron enrichment and plot in calcalkaline field on an AFM plot(Figure 5.80).

Zr displays a fair correlation with most of the major and trace elements. SiO_2, MnO, Y, Ce, La and Nb correlate positively whereas Al_2O_3, MgO, Na_2O, P_2O_5, Sr, Pb, Ga, Cr and Ba show negative correlation with increasing Zr. TiO_2, CaO, K_2O and Rb exhibit no correlation with Zr(Figures 5.81 and 5.82). Decrease in Al_2O_3, Na_2O, MgO and compatible element(Cr), and increase in SiO_2 and incompatible elements(Y, Ce, La) with increasing Zr as a fractionation index may be explained by plagioclase, Fe-Ti oxides and cpx fractionation in the evolution of the bulk rhyolitic magma.

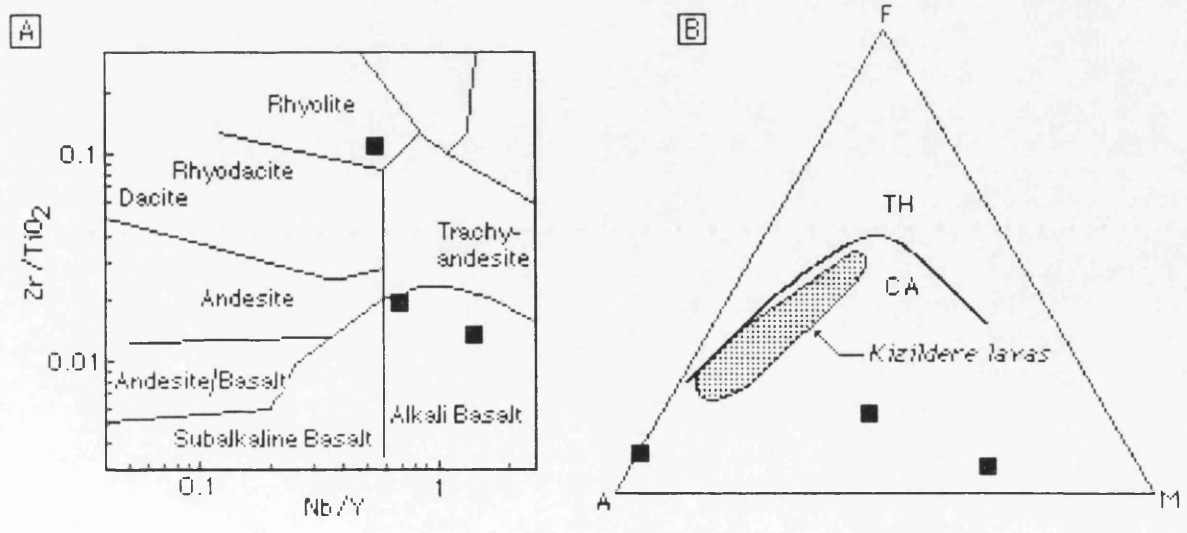

Figure 5.80. (A), Chemical classification of tuffs from the Kizildere formation. Diagram is from Winchester and Floyd(1977). (B), The AFM plot for tuffs. The field of the Kizildere lavas is superimposed for comparison.

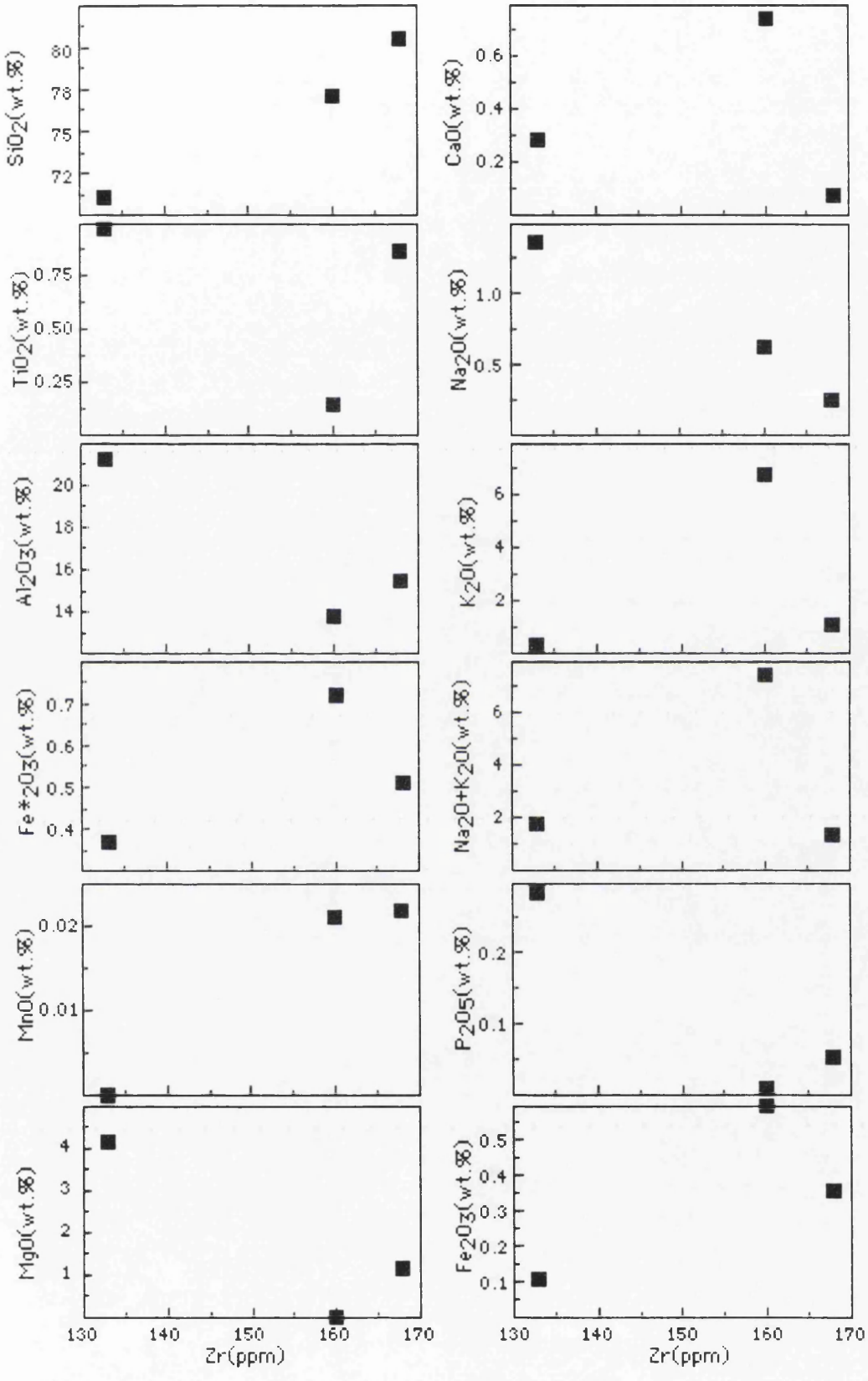

Figure 5.81. Zr(ppm) versus major element plots of tuffs.

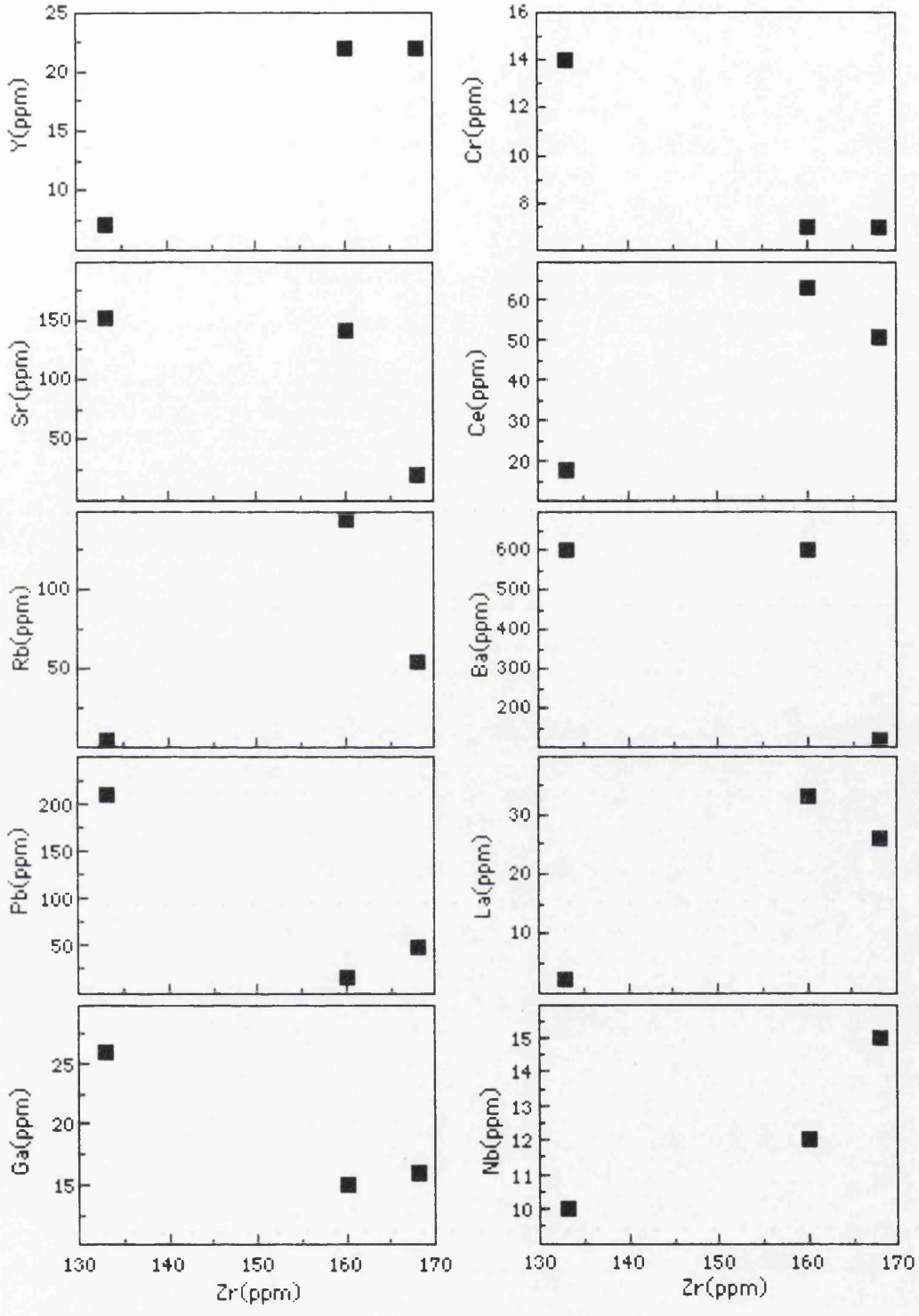

Figure 5.82. Zr(ppm) versus trace element plots of tuffs.

In terms of the chemical discrimination of tectonic environment, the tuffs display similar characteristics to those of volcanic arcs(Figure 5.83) with low TiO_2(<1 wt.%), Nb(10-15 ppm), Y(7-22 ppm) and Zr/Nb(11.20-13.33) ratios(Pearce *et al.*, 1984; Harris *et al.*, 1986; Leat *et al.*, 1986). Thus, it is suggested that the tuffs are the products of calcalkaline volcanic activity and are associated with an active continental margin.

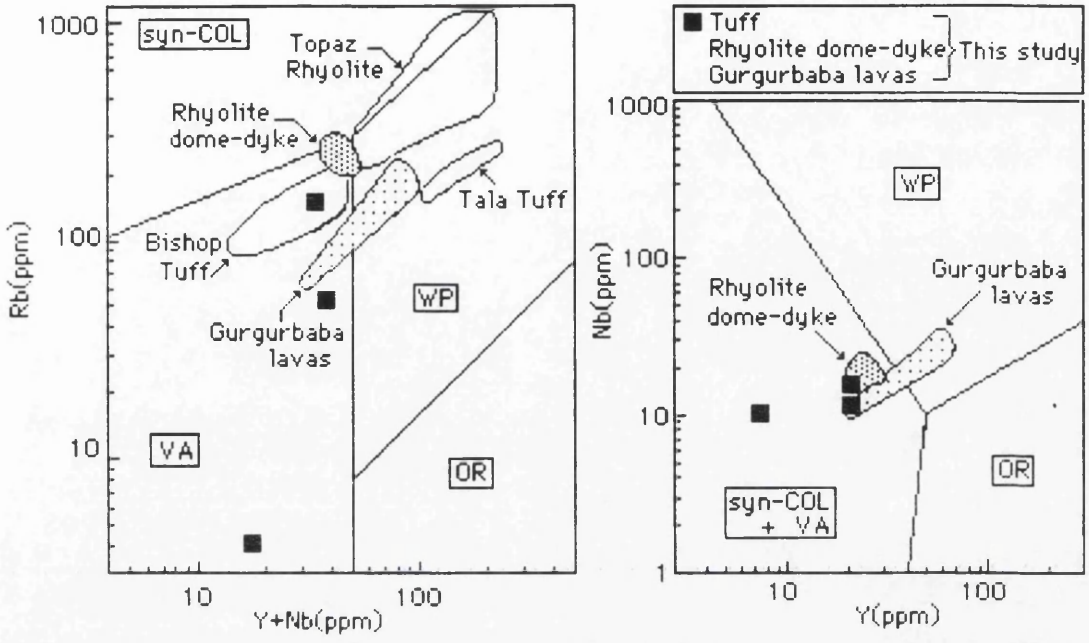

Figure 5.83. Chemical discrimination of the tectonic environment for tuffs from the Kizildere formation. The Gurgurbaba lavas and the rhyolite dome and dykes from this study, the Bishop Tuff(Hildreth, 1977), the Tala Tuff(Mahood, 1981) and topaz rhyolites(Christiansen *et al.*, 1986) from the United States. Diagrams are from Pearce *et al.* (1984): VA=volcanic arc; syn-COL=syn-collision; WP=within plate ; and OR=ocean ridge.

5.3.3.3. ANDESITES

5.3.3.3.1. MAJOR AND TRACE ELEMENTS

Andesites have 59-66 wt.% SiO_2 and medium-K_2O contents(1.6-2.8 wt.%) which project into medium-K fields(Peccerillo and Taylor, 1976; Gill, 1981). The rocks fall into the subalkaline field of Irvine and Baragar(1971) based on the Na_2O+K_2O versus SiO_2 plot. In a plot of SiO_2 versus FeO*/MgO(Miyashiro, 1974) all lavas are classified as calcalkaline. Although the lavas straddle the tholeiitic-calcalkaline boundary in the Al_2O_3 versus normative plagioclase composition diagram of Irvine and Baragar(1971), they show little iron enrichment and plot in the calcalkaline field on an AFM diagram(Figure 5.87).

Generally, the andesites have 15.5-18.0 wt.% Al_2O_3, MgO between ~1 and 3.5 wt.%(Mg-number=34-52) and they contain low Ni, Cr, Co and high Ba, Rb, Th, Sr and Zr(Figures 5.84, 5.85 and 5.86). They have trace element abundances and incompatible element ratios which are similar to and comparable with those of calcalkaline rocks erupted at convergent plate margins(Jakes and Gill, 1970; Gill, 1981; Ewart, 1976, 1982; Pearce, 1982). They are characterized chemically by wide variation in SiO_2 and Al_2O_3, low TiO_2, low Na_2O/K_2O and K/Rb, high Rb, Sr, Ba, Th and high La/Yb, Rb/Sr, Ba/Nb, Ba/La and La/Zr. Low TiO_2 content(<1 wt.%) suggests that andesites are orogenic lavas(Gill, 1981; Pearce and Cann, 1973). The rocks display an orogenic imprint as suggested by high Ba/La, Ba/Nb, K/Nb, Th/La, Pb/La(Hickey *et al.*, 1986a, b), low Zr/TiO_2(Winchester and Floyd, 1977), low TiO_2, absence of iron enrichment in the AFM plot. The rocks have also low Co, Cr, Ni and nearly constant FeO*/MgO ratios. The K/Rb ratio is low to moderate(250-450). Compared to calcalkaline andesites typical of orogenic environments(Gill, 1981), the rocks are enriched in most incompatible elements, but trace element ratios are similar. Relatively high La/Nb ratios reflect relative Nb depletions similar to those of destructive margin magmas(Brique *et al.*, 1984).

In general, fractionation of phenocryst phases adequately explains major and trace element variations within andesites. Dominant cations of all phenocryst phases show compatible behaviour(i.e. abundances of these elements decrease as silica increases), hence fractionation of plagioclase and pyroxene can explain the decrease of CaO and MgO with increasing SiO_2. Moreover, the observed slightly negative Eu anomalies and decrease of Eu with increasing SiO_2 may show plagioclase fractionation(at the oxygen fugacities typical of andesites, Eu is divalent; Gill, 1981). The fractionation of magnetite is shown by compatible behaviour of bulk Fe_2O_3 and TiO_2 and relative depletion of Ti. Apatite fractionation is shown by the compatible behaviour of P_2O_5 and small relative depletions in the silicic samples.

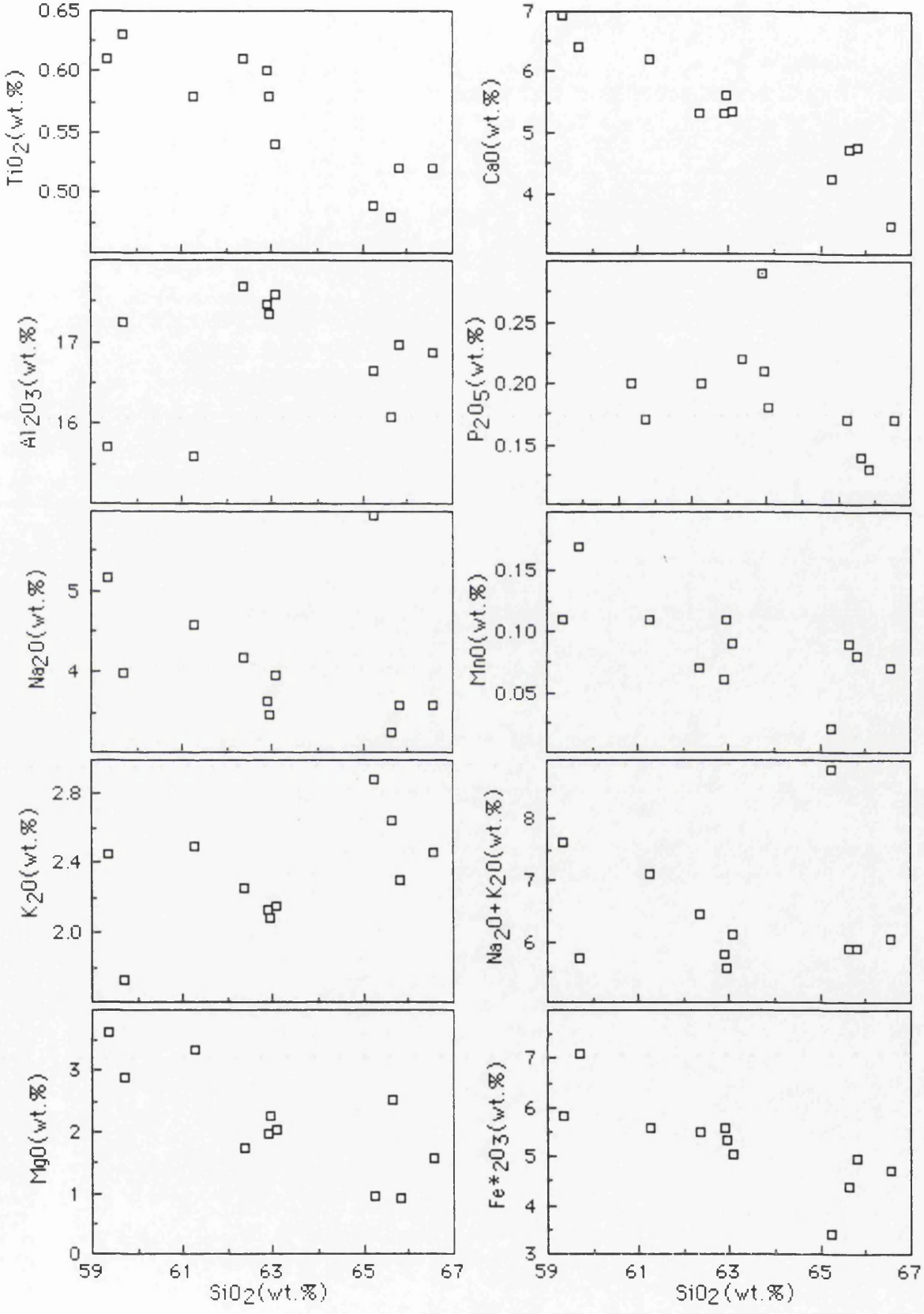

Figure 5.84. SiO_2(wt.%) versus major element plots for the andesites.

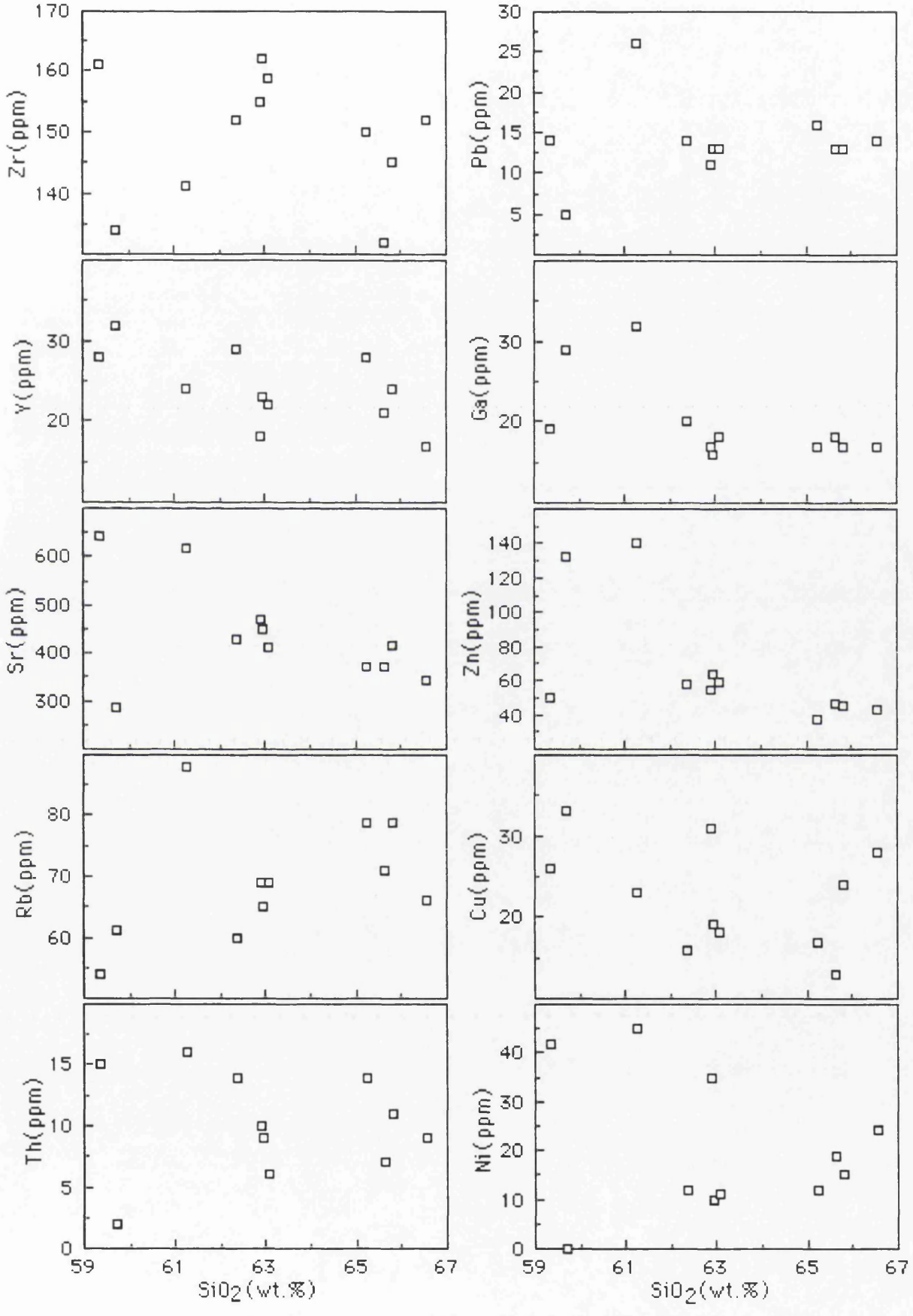

Figure 5.85. SiO_2(wt.%) versus trace element plots for the andesites.

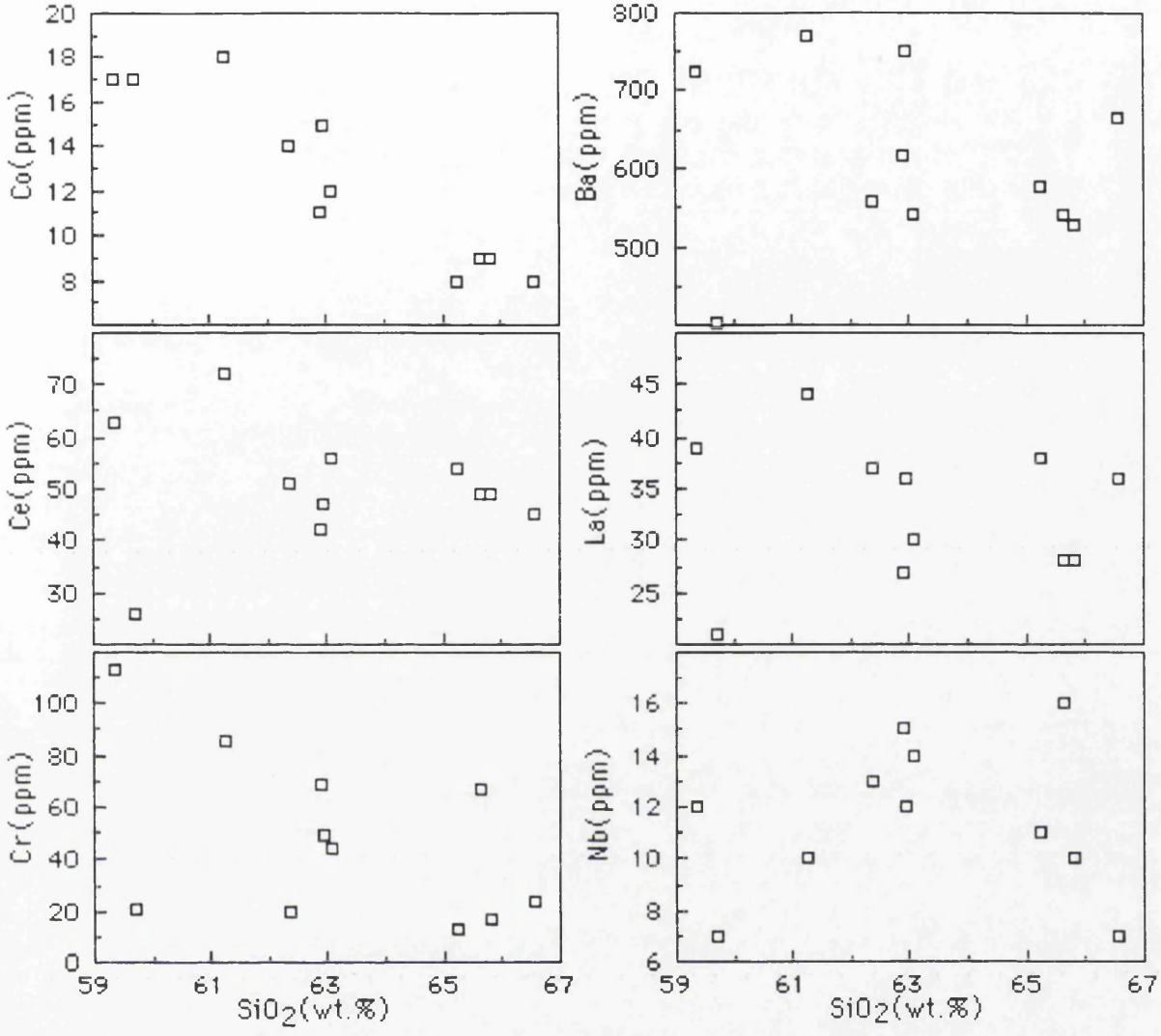

Figure 5.86. SiO_2(wt.%) versus trace element plots for the andesites.

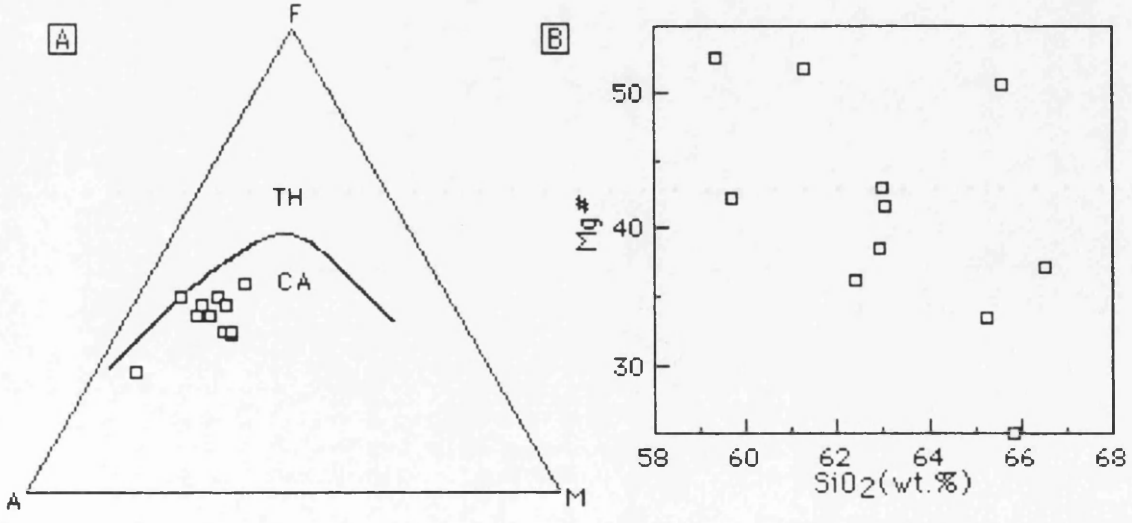

Figure 5.87. (A), AFM plot showing the composition of andesites. The thick line separates tholeiitic(TH) and calcalkaline(CA) compositions(Irvine and Baragar, 1971). (B), Mg-number($Mg^{\#}$= 100xMg/Mg+Fe^{+2}) versus SiO_2(wt.%) plot.

Most of the major and trace elements show correlations with SiO_2. Concentrations of TiO_2, FeO*, MgO, CaO, Na_2O, MnO and P_2O_5 decrease whereas Al_2O_3 and K_2O increase with increasing SiO_2. Although the data are scattered, with increasing SiO_2 there is an overall increase in abundance of incompatible elements(e.g., Zr, Rb,) and depletion in compatible trace elements(e.g., Ni, Cr, Co) which may be explained by crystal fractionation processes. Ba and Th concentrations show well-defined increases with increasing SiO_2, but other typically incompatible elements like Ce, Nb and Zr have lower enrichment factors. The overall chemical trends seen, of progressive increase in SiO_2, K_2O and incompatible trace elements(e.g., Zr, Rb) with decrease in MgO, FeO*, Na_2O, CaO and compatible trace elements(e.g., Ni, Cr, Co) suggests qualitatively that these lavas developed by fractional crystallization of a parent magma. Cr, Ni, MgO and CaO show decreasing compatible behaviour in the andesites reflecting significant crystallization of cpx crystallization. Major magnetite crystallization is marked by the compatibility of FeO* and TiO_2. Apatite precipation is marked by the compatible behaviour of P_2O_5. If a suite of rocks is generally related by fractional crystallization process, than the parent and derivative lavas should have similar incompatible element ratios(e.g., K/Rb, Ba/Rb, Ba/La).

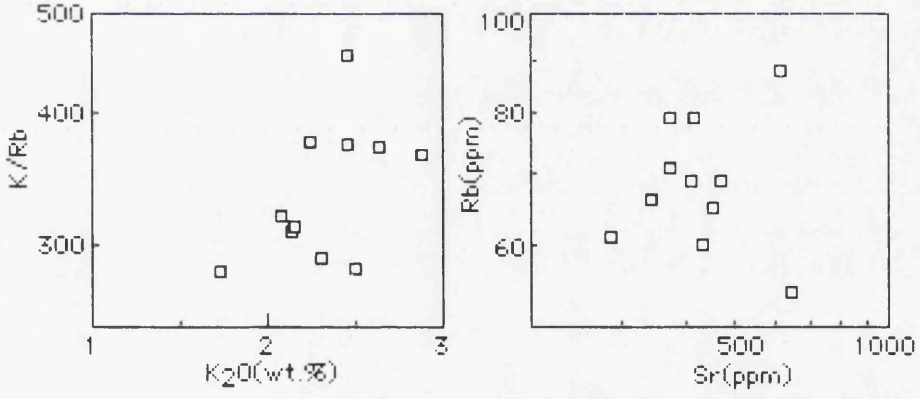

Figure 5.88. Log K/Rb versus K_2O(wt.%), and log Rb(ppm) versus log Sr(ppm) plots.

K/Rb ratios appear to decrease with increasing K_2O, and Rb shows positive correlation with Sr(Figure 5.88). Zr(as a fractionation index) versus Ni, Cr and Co correlations are poor(Figure 5.89), expressing that cpx and magnetite fractionation played a minor role in the evolution. Furthermore, Zr versus Y trend appears to decrease because Y becomes more compatible in cpx with increasing silicic liquid compositions($D_Y^{cpx/liq}$=0.5-0.4: basic-acid; Pearce and Norry, 1979). The distribution of the rocks on the incompatible element ratio plot K/Rb versus Zr/Y(Figure 5.90) displays no clear linear trend, suggesting that crystal fractionation was not the predominant process. Moreover, the

nearly linear trend on a Y/Rb versus K/Rb plot(Figure 5.90) depicts magma mixing. A Zr versus Nb plot shows a positive correlation reflecting the incompatibility of Nb(Figure 5.91).

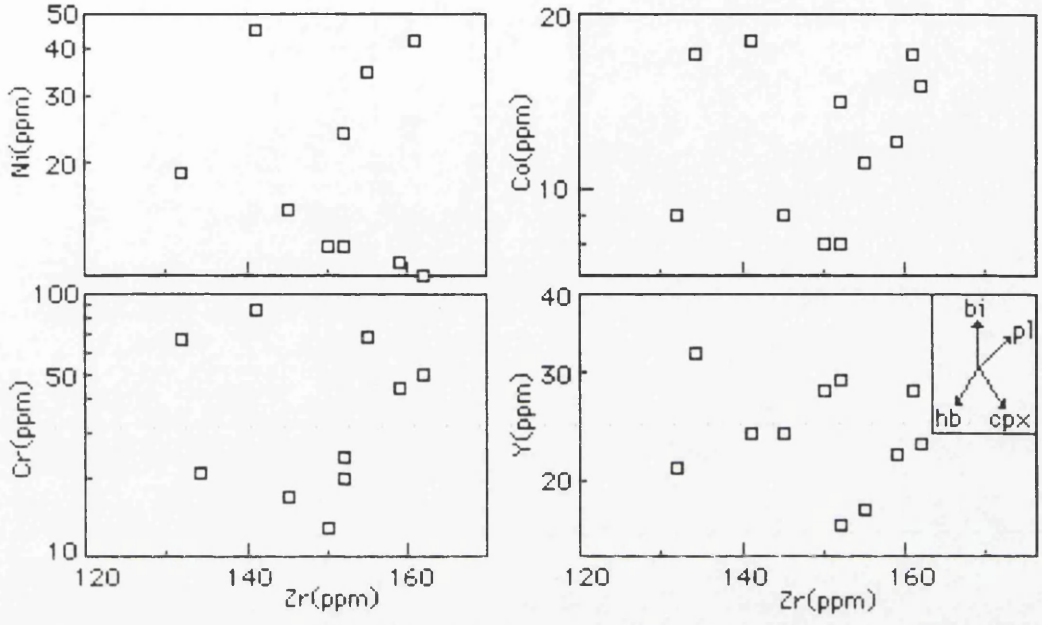

Figure 5.89. Zr(ppm) versus log Ni(ppm), Co(ppm), Cr(ppm) and Y(ppm) plots.

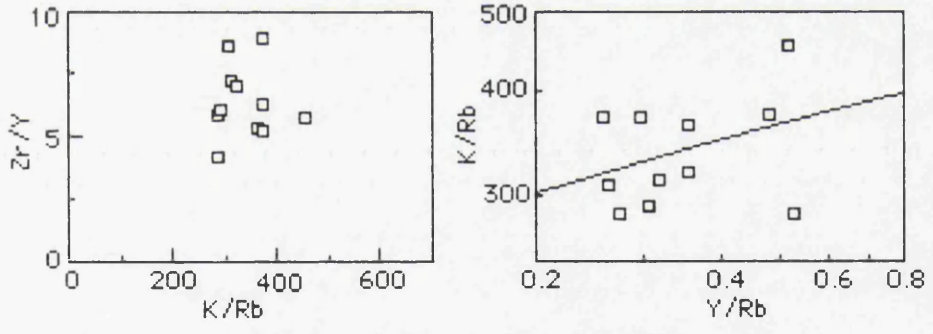

Figure 5.90. Zr/Y versus K/Rb, and log K/Rb versus log Y/Rb plots.

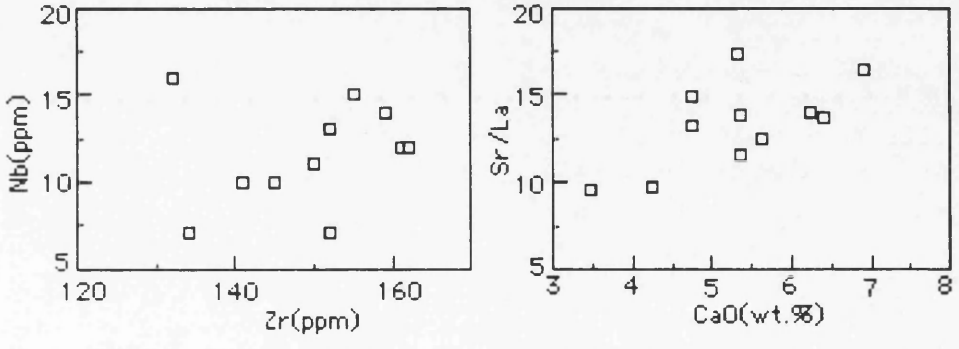

Figure 5.91. Zr(ppm) versus Nb(ppm) and CaO(wt.%) versus Sr/La plots.

The relative decrease in Cr, Co(transition elements) with increasing Th considered as an differention index(Allegre *et al.*, 1977) shows that fractional crystallization involving clinopyroxene is the main petrogenetic process(Figure

5.92). Hornblende and magnetite have been suggested as providing the silica enrichment in calcalkaline suites(Osborn, 1962; Cawthorn and O'Hara, 1976). Moreover, amphibole can be an important fractionating phase in producing calcalkaline lavas(Arculus, 1976; Cawthorn and O'Hara, 1976).

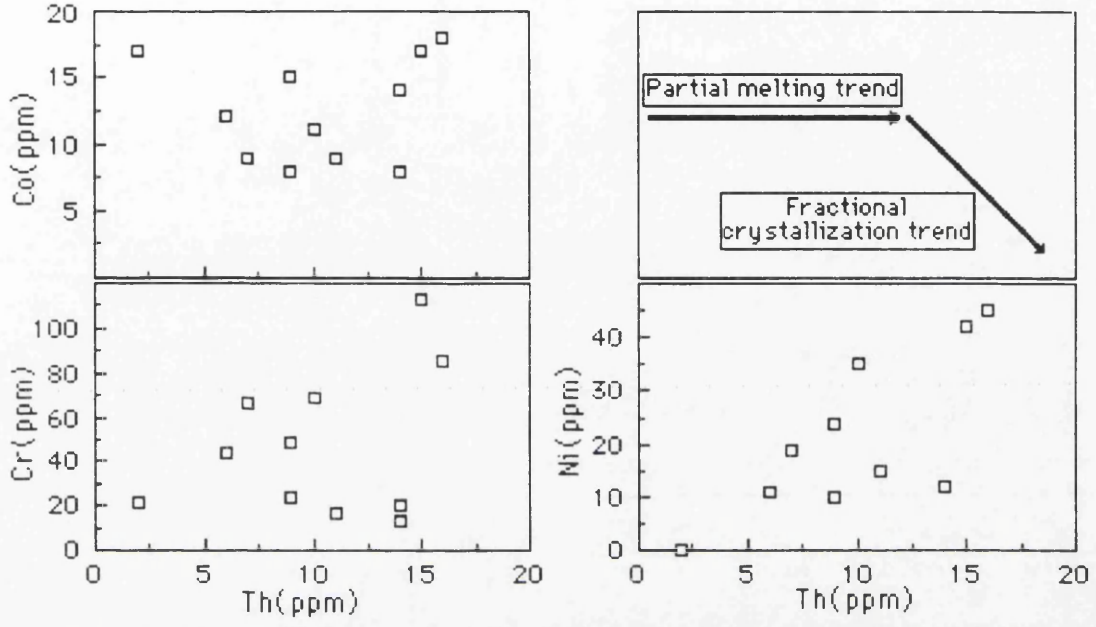

Figure 5.92. Process identification plots based on the relative concentrations of incompatible(Th) and compatible (Co, Cr, Ni) elements.

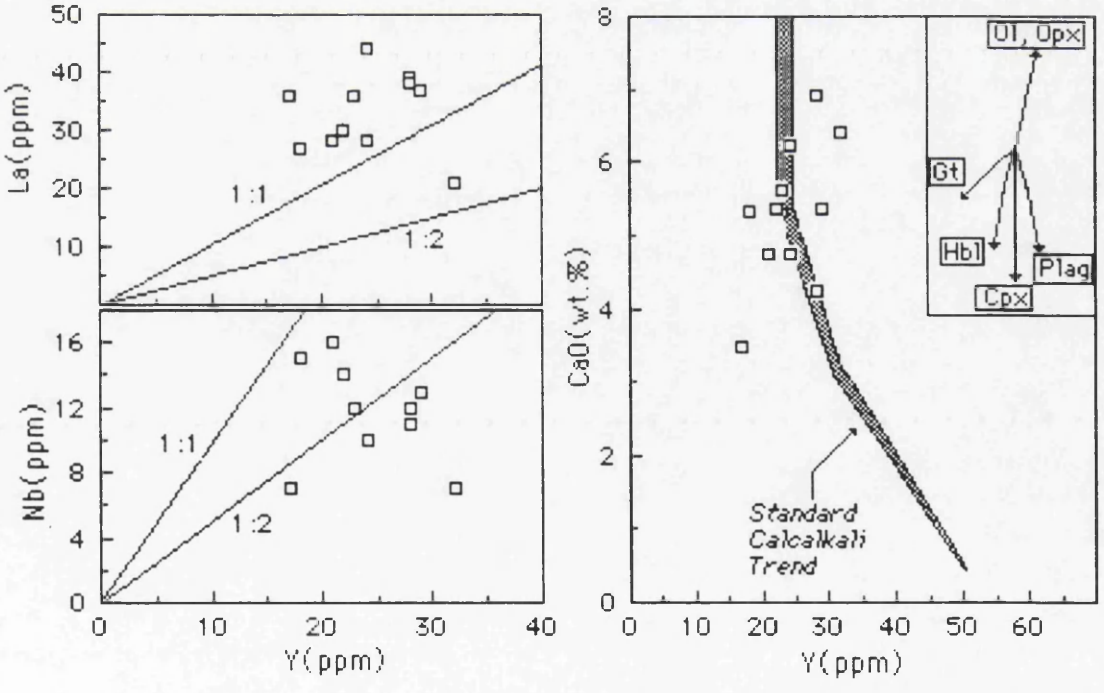

Figure 5.93. Y(ppm) versus Nb(ppm), La(ppm) and CaO(wt.%) plots for andesites. Shaded area represents the "standard" calcalkaline trend of Lambert and Holland(1974). The vectors show qualitative trends of the effect of fractional crystallization of common silicates.

Andesites have high La/Y and low Nb/Y ratios(Figure 5.93). In calcalkaline suites, Lambert and Holland(1974) used CaO versus Y to define J and L type trends, which lead respectively to depletion and enrichment in Y relative to a calcalkaline series standard. The J and L trends have been termed hornblende-(±garnet) and pyroxene controlled differentiation trends respectively, as these minerals can be critical in determining trend direction. In the Y versus CaOplot(Figure 5.93), andesite samples plot on both the Y depleted and Y enriched side of the standard calcalkaline trend as obtained by pyroxene and plagioclase dominated fractionation(Lambert and Holland, 1974). They show generally Y depletion relative to the standard calcalkali trend, and define J type trend(Figure 5.93), indicating hornblende and pyroxene controlled fractionation.

Gill(1978) suggested that significant hornblende fractionation ought to be detected by a marked decrease of K/Rb, Ba/Rb and Ba/La and an increase in Cr/V in derivative andesites, and that HREE and Y remain constant or decrease during fractionation. Some samples have high Ba and Sr, and low Rb and high K/Rb and Ba/Rb ratios and these have probably suffered crustal contamination during ascent. High Ba/La(29) and Ba/Nb(>34) ratios in the andesites are similar to those of convergent margin lavas related to a subduction zone(Sun, 1980). K_2O and Rb enrichment could be explained by a number of factors e.g. assimilation of a K_2O and Rb-rich crustal component or combined assimilation simultaneously with fractional crystallization(AFC)(De Paolo, 1981; Grove *et al.*, 1982); plagioclase controlled melting in the mantle above subducted slab(Rogers *et al.*, 1985); zone melting or zone refining or volatile transfer(McBirney, 1984).

5.3.3.3.2. INCOMPATIBLE ELEMENTS

In MORB normalized spidergrams(Figure 5.94), the andesites have a significant Nb anomaly being more akin to "normal" subduction values. LIL enrichment particularly in Th is very high. The negative anomalies shown by Ti and P may reflect Fe-Ti oxide and apatite fractionation during differentiation. The high LILE contents in the andesites may result from crustal contamination.

On the mantle normalized pattern(Figure 5.95), the rocks show enrichment in hydrophile elements(K, Rb, Ba) relative to REE and HFSE(Zr, Nb, Ti). The relatively constant Sr/Zr through a wide range of SiO_2 and Zr implies that plagioclase fractionation was not important. The rocks are strongly enriched in K, Rb, and also Ba, Pb relative to Sr and HFSE whereas they are strongly depleted in Ti, Y and HREE.

M-HREE and Y elements are less incompatible reflecting their preferential removal by cpx($D_Y^{cpx/liq}$=0.5-0.4: basic-acid; Pearce and Norry,

1979). The less incompatible behaviour of Zr, reflected in a slight increase in the Zr with fractionation may also reflect cpx crystallization($D_{Zr}^{cpx/liq}$=0.27±0.15; Villemant *et al.*, 1981).

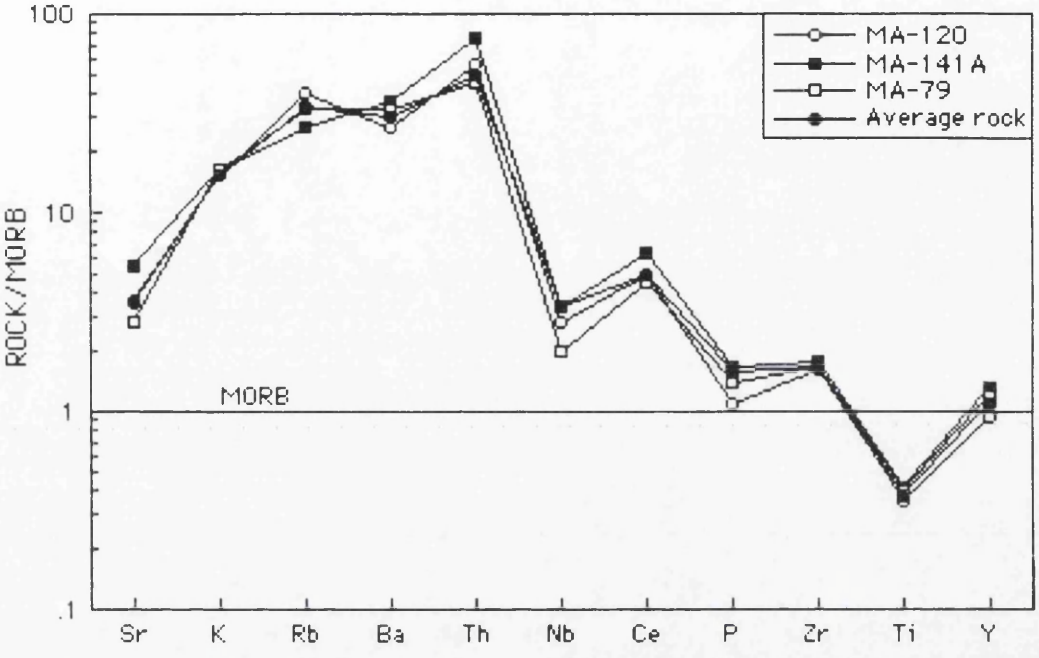

Figure 5.94. MORB-normalized trace element patterns of andesites(MORB normalizing values are from Pearce, 1983).

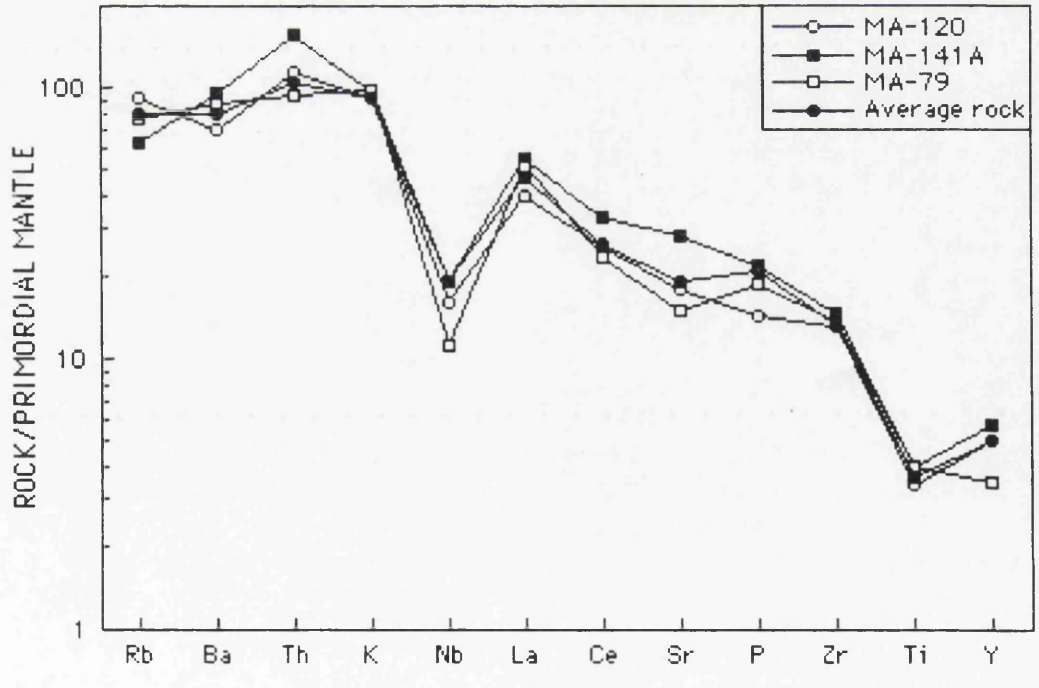

Figure 5.95. Mantle-normalized trace element patterns of andesites. Normalizing primordial mantle values are from Wood *et al.* (1979a).

5.3.3.3.3. RARE EARTH ELEMENTS

The REE patterns for representative lavas are shown in Figure 5.96. Generally, the andesites have significant LREE enrichment and relatively flat HREE patterns which are subparallel to each other. The REE patterns are typical of medium-K suites(Gill, 1981). However, the andesites show highly fractionated patterns with $(La/Lu)_N$=13.82-17.36 patterns illustrated by LREE enrichment and HREE depletion relative to medium-K andesites(Figure 5.96). They do not show a significant Eu anomaly with $(Eu/Eu^*)_N$=0.88-0.95 and 1.43 in one sample(MA-121), suggesting the absence of plagioclase as a crystallizing phase during the early crystal fractionation.

Relatively low Y and Yb contents and the presence of strongly fractionated REE patterns (reflected in high La/Lu ratios) in lavas suggests that garnet did not play a significant role as a fractionating or residual phase in their generation. Amphibole is an observed phase in lavas and the rocks show chemical features expected from significant amphibole participation in their generation i. e. near constant and decreasing Y contents($D_Y^{am/liq}$=1.6-6: basic-acid; Pearce and Norry, 1979) and HREE contents generating V-shaped REE patterns with minima at Dy-Ho(Nicholls and Harris, 1980). To be an effective influence on REE behaviour, therefore, hornblende fractionation is to be a deep-crustal process for which petrographic evidence is mainly lost during magma ascent.

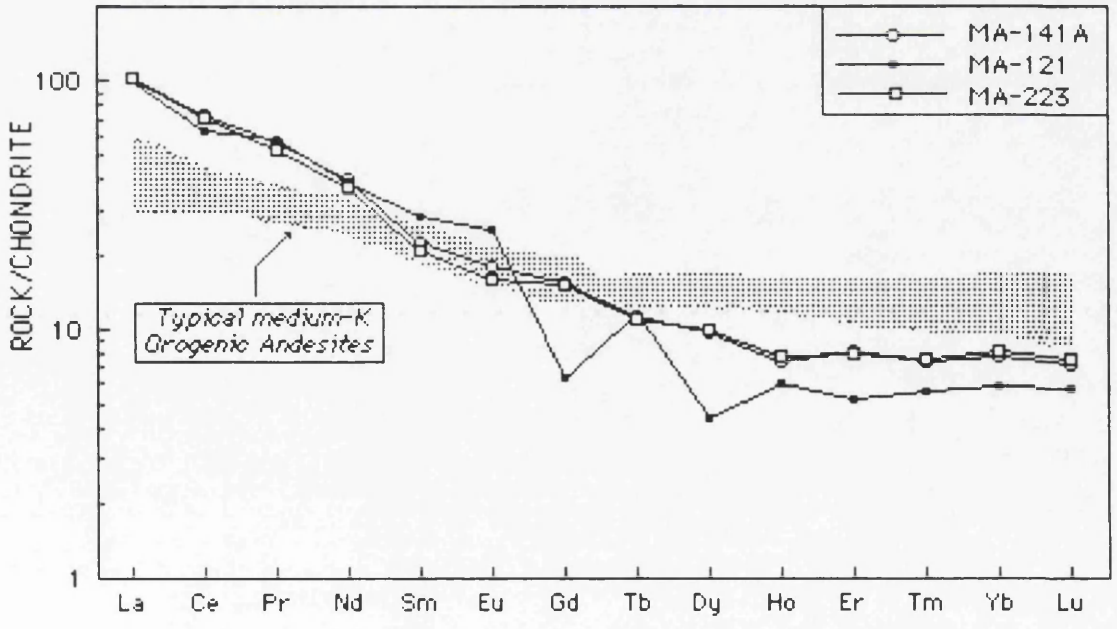

Figure 5.96. Chondrite-normalized REE patterns of andesites. Normalizing values are from Boynton(1984). Typical medium-K orogenic andesites(Gill, 1981) have abundances within shaded area.

5.3.3.3.4. SOURCE CHARACTERISTICS

The andesites have geochemical characteristics typical of convergent margin lavas related to a subduction zone(Saunders *et al.*, 1980; Gill, 1981; Ewart, 1982; Pearce, 1983; Thompson *et al.*, 1984; White and Patchett, 1984). These include low Na_2O/K_2O ratios, low Nb and TiO_2 abundances and high ratios of LIL elements to LREE and HFSE. There are notable increases in LIL element content and the degree of LREE-enrichment in the andesites.

Strong depletions in Nb, and to a lesser extent in TiO_2, are often attributed to an accessory residual phase during melting under hydrous conditions(e.g., Saunders *et al.*, 1980), although this signature may be due to the insolubility and high ionic potential of these elements in leaching aqueous fluids derived from a dehydrating, subducted slab(Woodhead, 1989). The marked enrichments in LREE and LILE can be attributed to dehydration of a subduction component and, or, subducted sediment(Pearce, 1983; Thompson *et al.*, 1984; White and Patchett, 1984; White and Dupre, 1986; Davidson *et al.*, 1987). Thus, the source composition of the andesite lavas is controlled by subducted slab-mantle interactions. The mantle source of the andesites most probably contains three components, two derived from subducted matter(oceanic crust and sediments) and one from the overlying mantle wedge. The overlying mantle may either be asthenosphere or lithosphere.

The small Mg-numbers, low Cr and Ni contents and relatively negative slopes in Cr-Zr and Ni-Zr plots of the andesites indicate that the rocks cannot be derived by progressive partial melting of a peridotitic source. Therefore, the andesites do not represent primary partial melts of eclogite or garnet peridotite or any mantle peridotite source. Andesites are frequently viewed as a part of a differentiation series from basalt to more felsic compositions(e.g., Gill, 1981; Grove and Kinzler, 1986). The presence of good correlations between major and trace elements suggests the descent of the andesites from a common parental magma(e.g., basaltic magma) through fractional crystallization(±magma mixing). Several geological lines of evidence also suggest that crystal fractionation of a parental magma is a reasonable mechanism in generating andesites.

5.3.3.4. TRACHYANDESITES

5.3.3.4.1. MAJOR AND TRACE ELEMENTS

The trachyandesites are calcalkaline, medium-K andesites(Peccerillo and Taylor, 1976; Gill, 1981). They have chemical compositions transitional between andesites and dacites with high SiO_2 contents. On an AFM plot(Figure 5.100), the trachyandesites show little iron enrichment and plot in the calcalkaline field(Irvine and Baragar, 1971).

Most of the major and trace elements in the lavas vary linearly with SiO_2(Figures 5.97, 5.98 and 5.99). Concentrations of TiO_2, FeO*, CaO, MnO and MgO decrease whereas Al_2O_3, Na_2O and K_2O increase with increasing SiO_2.

P_2O_5, Ba, Sr, Zr, Ce, Th, Nb and Y which are typically incompatible in basaltic systems(i.e., they partition preferentially into melt rather than equilibrium mineral phases) increase in abundance with increasing SiO_2. Cr and Ni are usually strongly compatible elements during crystallization but the concentrations of these elements are nearly constant in the trachyandesites. Ba and Th show well-defined increases with increasing SiO_2 but other typically incompatible elements like Nb and Zr have lower enrichment trends. Generally, trace element contents of the trachyandesites are similar to the andesites but with a greater range for some elements.

The petrographic appearence of magnetite as a phenocrystal or microphenocrystal phase within the lavas indicates that the residual magma will have decreasing FeO*, TiO_2, Cr, Co and Ni contents in the rocks. Limited apatite precipitation is indicated by the generally constant P_2O_5 abundances. Gill(1981) indicated that P_2O_5 contents in calcalkaline suites usually remain constant throughout a range of SiO_2. Al_2O_3 and CaO correlate positively and significantly, indicating plagioclase accumulation(Ewart, 1976a). Plagioclase removal is indicated by the decrease in Al_2O_3 and decrease in the slope of the Na_2O-SiO_2 trend for more silicic compositions. A continuing decrease in MgO is probably related to removal of orthopyroxene.

The gentle decrease in Rb and Ba in low SiO_2 samples suggests amphibole fractionation from a parent magma. Since Rb and Ba have large ionic radii, these elements tend to concentrate in amphibole. In silicic samples, Rb shows a positive correlation with increasing SiO_2. Mixing with more Rb-rich magma such as dacite is capable of producing such Rb enrichments. Generally, Sr is strongly concentrated into plagioclase, and the partition coefficient for Sr increases with decreasing An%(D_{Sr}>1 in anorthite, and >30 in oligoclase; Jensen, 1973). The negative trend of Sr against SiO_2 in the lavas therefore suggests plagioclase fractionation.

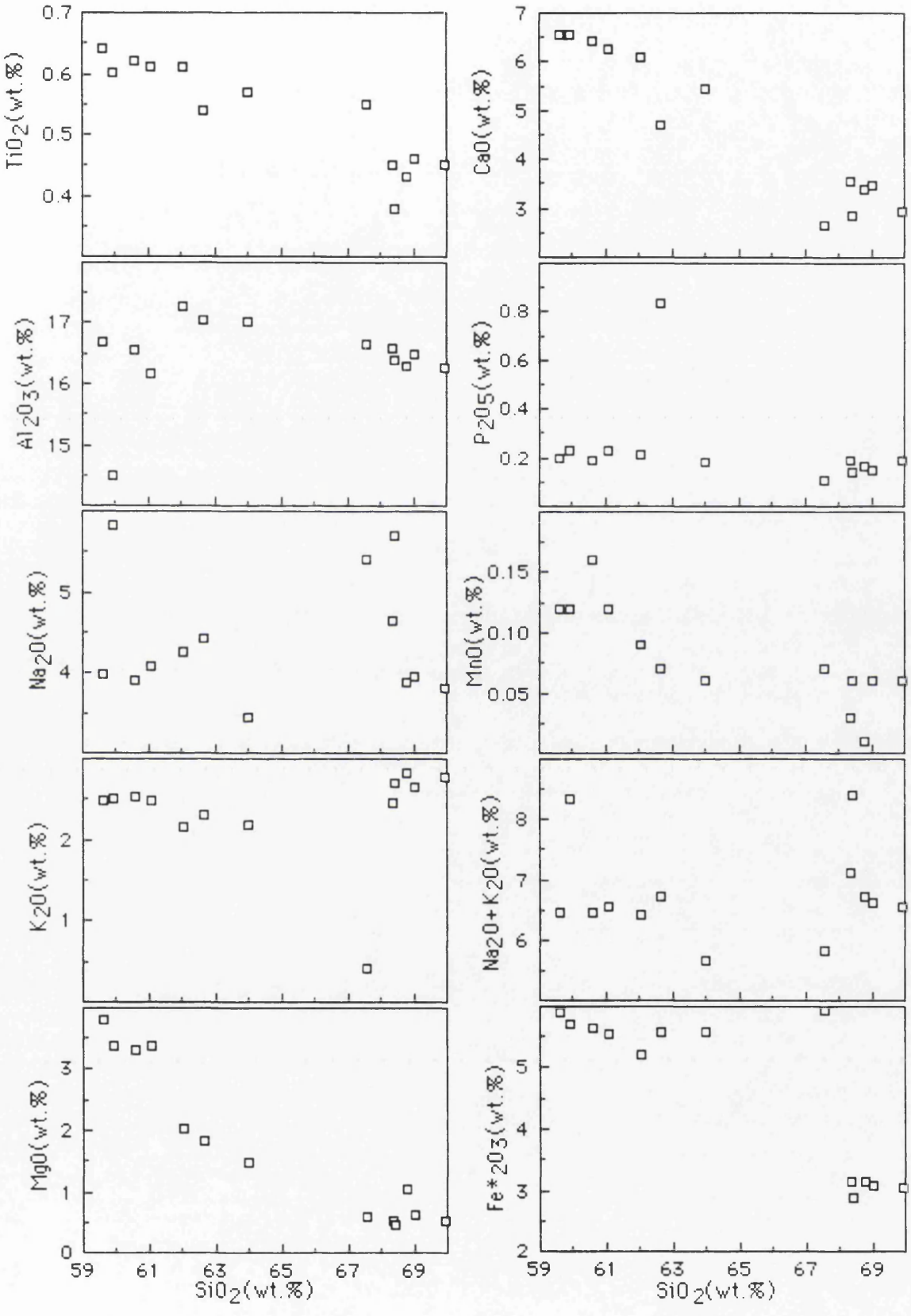

Figure 5.97. SiO_2(wt.%) versus major element plots for the trachyandesites.

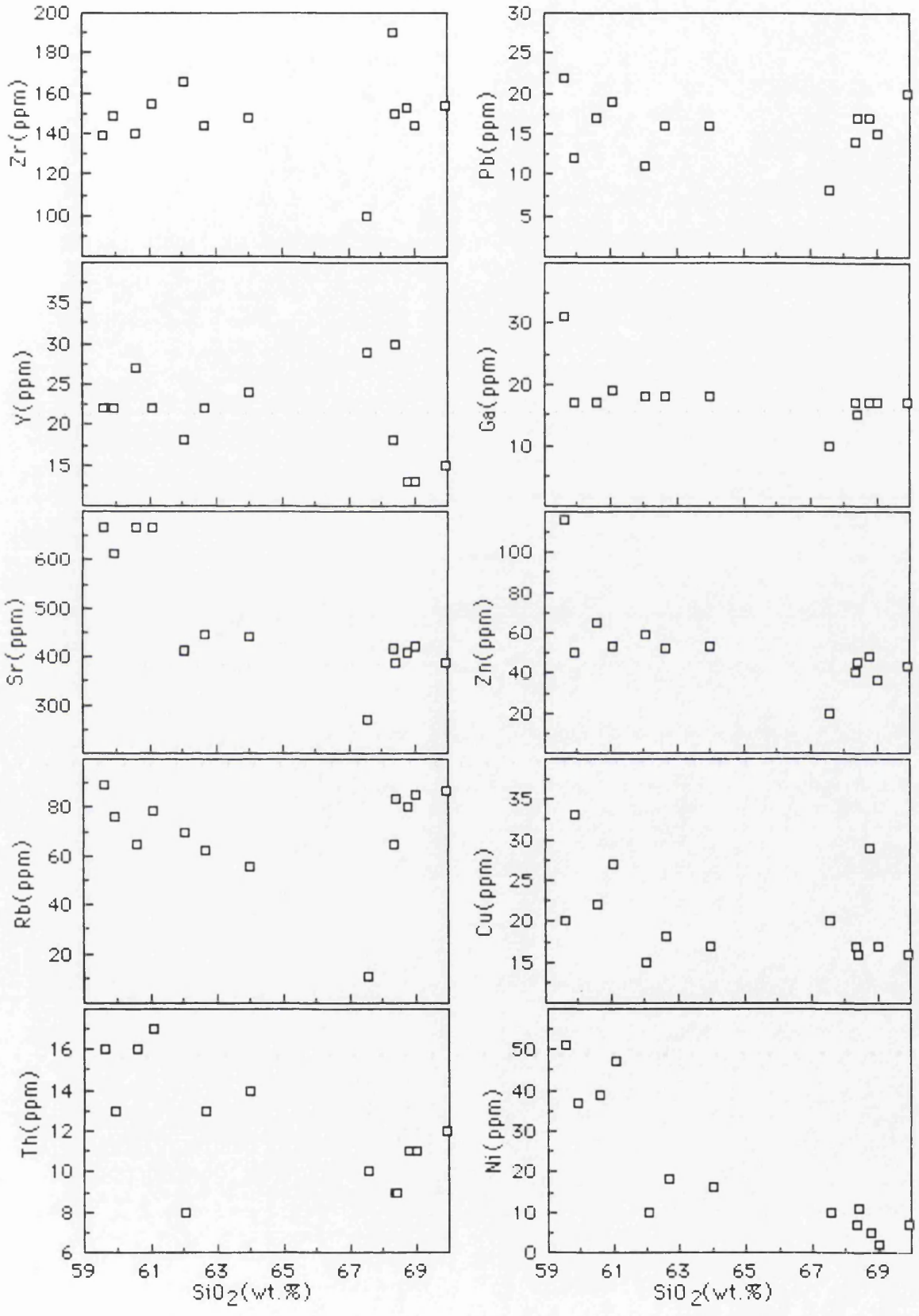

Figure 5.98. SiO_2(wt.%) versus trace elements plots for the trachyandesites.

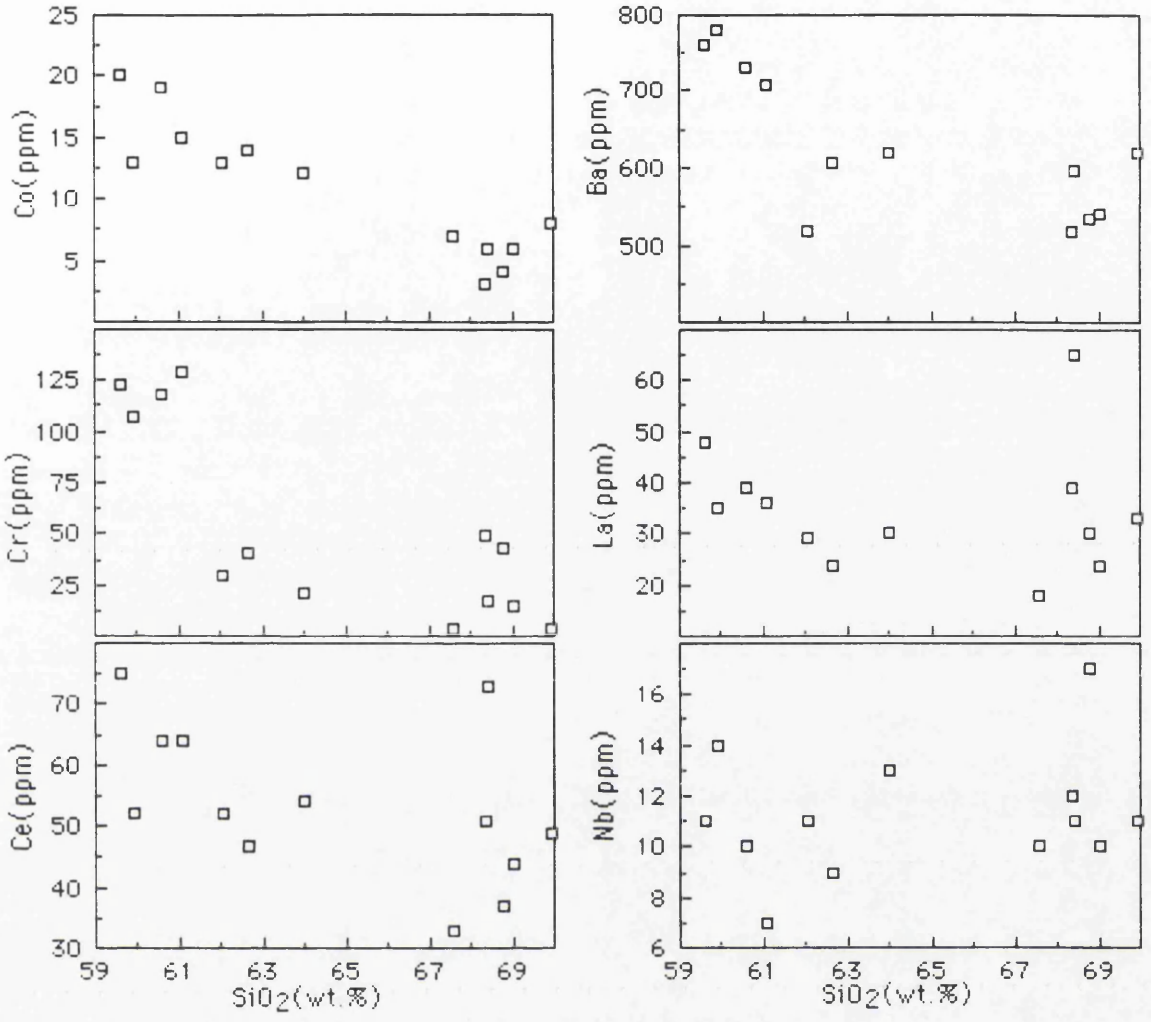

Figure 5.99. SiO_2(wt.%) versus trace elements plots for the trachyandesites.

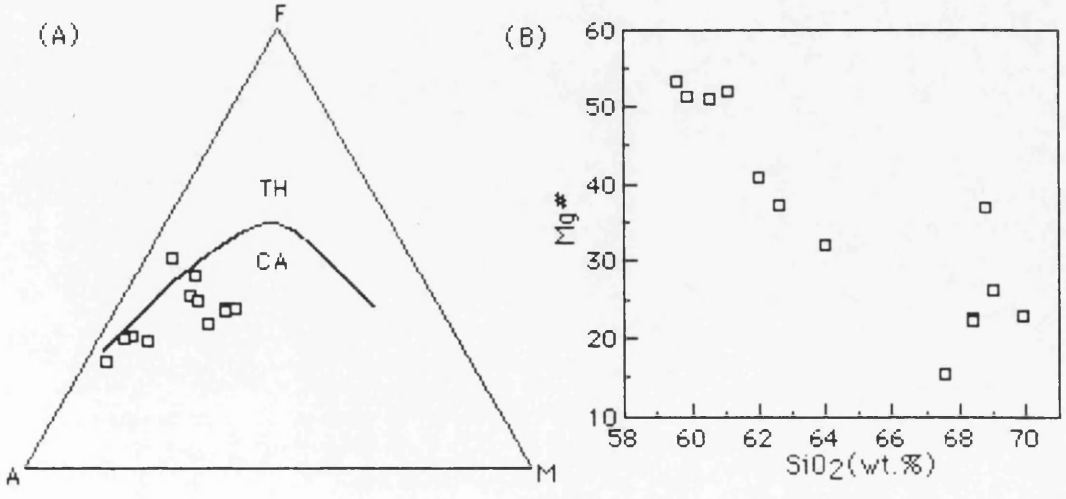

Figure 5.100. (A), AFM plot showing the composition of trachyandesites. The thick line separates tholeiitic(TH) and calcalkaline(CA) compositions(Irvine and Baragar, 1971). (B), Mg-number($Mg^{\#}$= 100xMg/(Mg+Fe^{+2})) versus SiO_2(wt.%) plot.

K/Rb ratios decrease with increasing K_2O, and Rb shows no correlation with Sr(Figure 5.101). Zr versus Ni, Cr and Co correlations(Figure 5.102) are relatively good indicating that cpx and magnetite fractionation were important. Y versus Zr trend seems to flatten out in silicic samples because in silicic compositions Y is more compatible in cpx(Pearce and Norry, 1979). The distribution of the lavas on an incompatible element ratio plot , K/Rb versus Zr/Y(Figure 5.103), may be arcuate with decreasing Zr/Y which would indicate mixing. In addition, the nearly linear trend on the Y/Rb versus K/Rb plot reflects magma mixing(Figure 5.103).

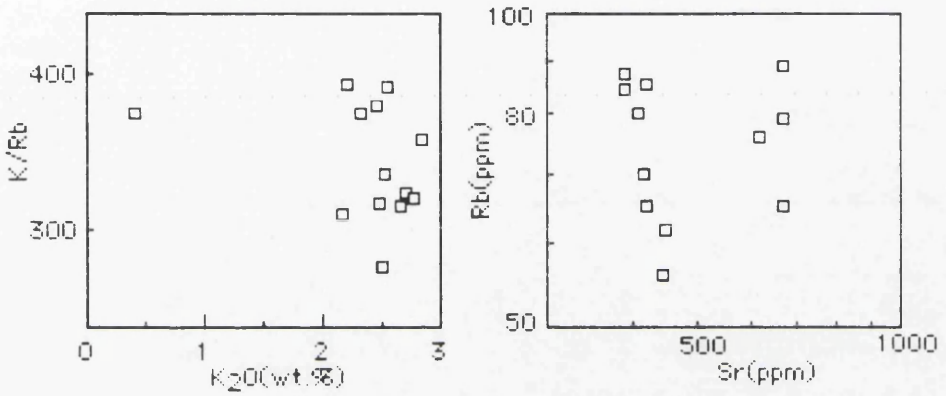

Figure 5.101. Log K/Rb versus K_2O(wt.%) and log Rb versus log Sr plots.

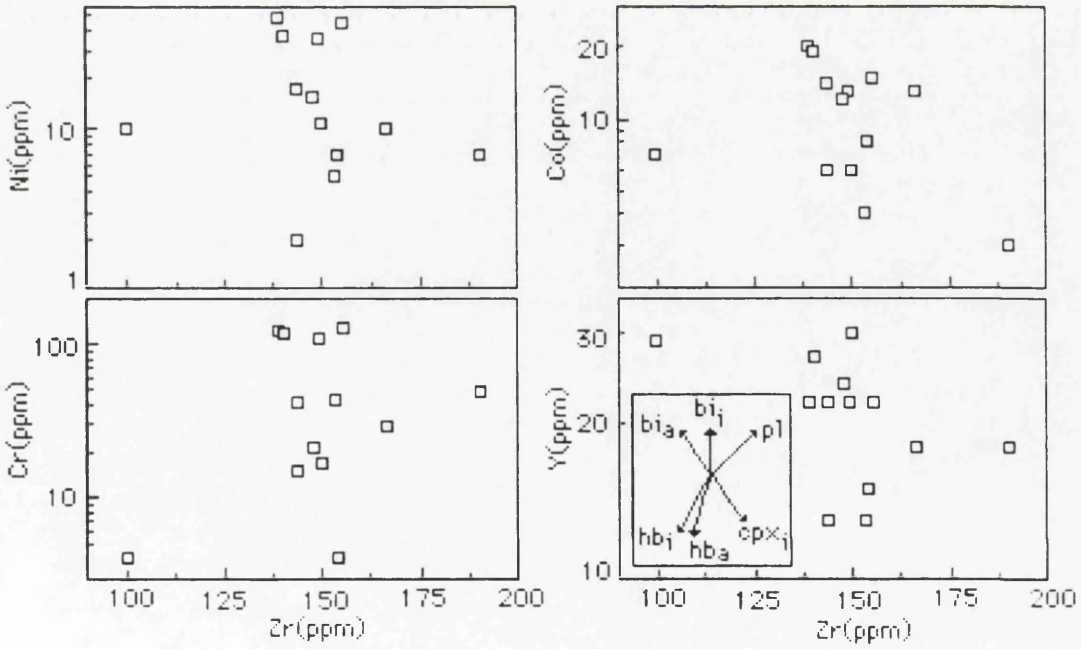

Figure 5.102. Zr(ppm) versus log Ni(ppm), Co(ppm), Cr(ppm) and Y(ppm) plots.

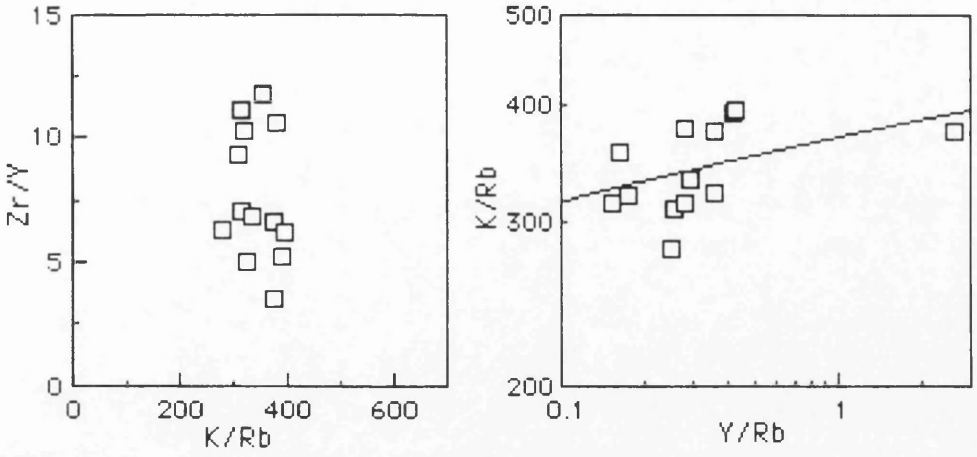

Figure 5.103. Zr/Y versus K/Rb and log K/Rb versus log Y/Rb plots.

The trachyandesites have high La/Y and low La/Y ratios(Figure 5.104), similar to the andesites. Generally, the rocks show depletion in Y relative to most calcalkali series(Lambert and Holland, 1974). In a Y versus CaO plot(Figure 5.104), they define a J-type trend indicating hornblende and cpx-controlled fractionation. Hornblende is an observed phase in the rocks. Thus, the chemical features can be expected to result from a significant hornblende fractionation i.e. near constant or decreasing Y contents($D_Y^{amp/liq}$=1.6-6: basic-acid; Pearce and Norry, 1979).

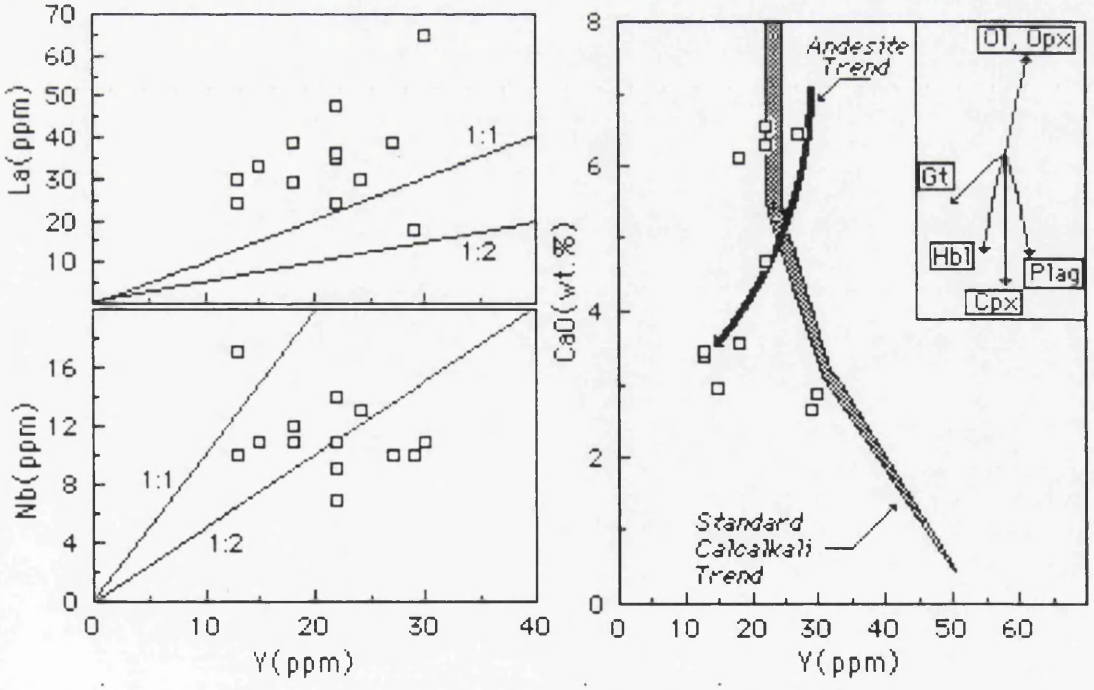

Figure 5.104. Y(ppm) versus Nb(ppm), La(ppm) and CaO(wt.%) plots for the trachyandesites. The thick line represents the trend of the andesites, and the shaded area is the "standard" calcalkaline trend of Lambert and Holland(1974). The vectors show qualitatively the effects of fractional crystallization of common silicates.

The effects of amphibole fractionation on major and trace element abundances are poorly understood, and distribution coefficients vary widely depending on the composition of the melt and amphibole(Cawthorn and O'Hara, 1976; Irving, 1978). However, amphibole fractionation would require high pressures and high water contents(>8 kbar and 3 wt.% H_2O; Eggler and Burnham, 1973). By comparison with experimental data on similar bulk compositions(Eggler, 1972a; Green, 1972; Allen *et al.*, 1975; Cawthorn and O'Hara, 1976; Allen and Boettcher, 1978), the abundance of hornblende and the relative scarcity of plagioclase phenocrysts in the rocks suggests that these lavas had relatively high water contents prior to eruption(>2% H_2O in the melt) and probably evolved in lower- to mid crustal magma chambers(P=3-15 kbar).

5.3.3.4.2. INCOMPATIBLE ELEMENTS

The trachyandesites are plotted on Mid-Ocean Ridge Basalt(MORB) and Primordial mantle(PM)-normalized patterns(Figures 5.105 and 5.106). Generally, they are characterized by LILE enrichment and HFSE depletions which is similar to those of andesites. On the MORB-normalized pattern(Figure 5.105), LILE enrichment, particularly in Th, is very significant. The rocks display negative Nb and Ti anomalies. Negative Nb reflects a subduction component in their genesis, and Ti anomaly may reflect Fe-Ti oxide fractionation during their evolution.

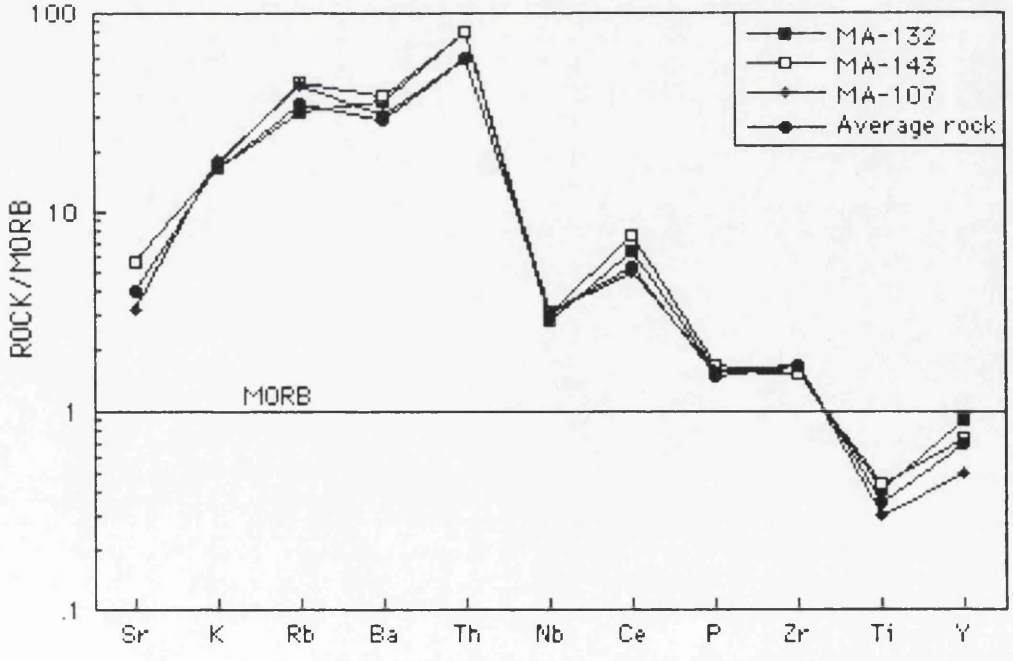

Figure 5.105. MORB-normalized trace element patterns of trachyandesites(MORB- normalizing values are from Pearce, 1983).

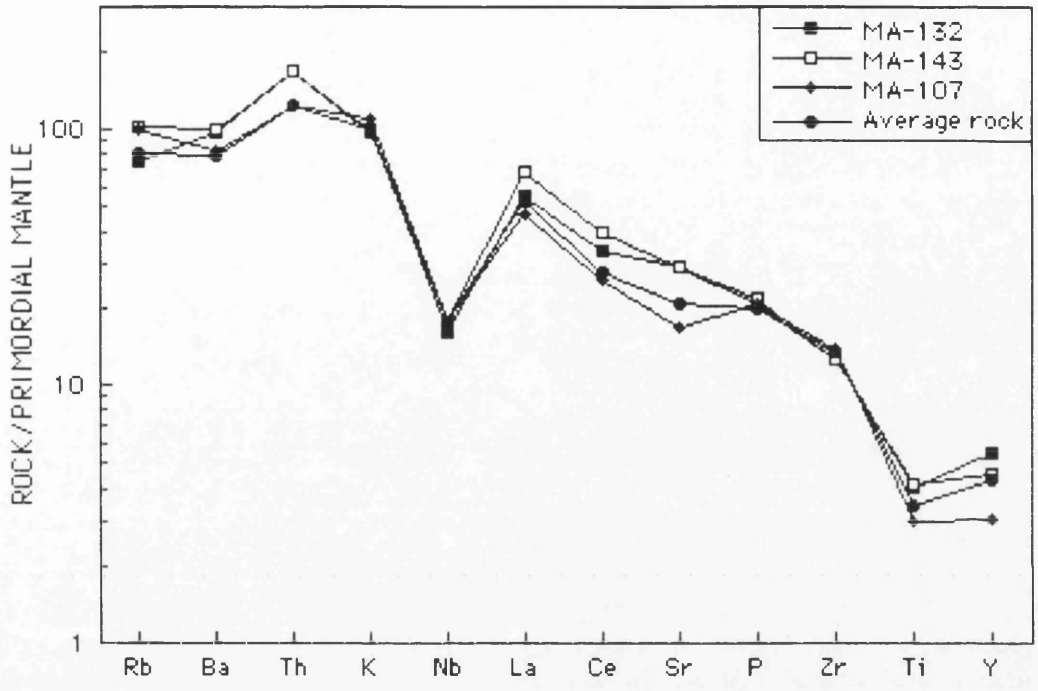

Figure 5.106. Mantle-normalized trace element patterns of trachyandesites. Normalizing primordial mantle values are from Wood *et al.* (1979a).

5.3.3.4.3. RARE EARTH ELEMENTS

The trachyandesites show highly fractionated REE patterns(Figure 5.107) with $(La/Lu)_N$=17.23-21.24 which is more fractionated than the andesites(La/Lu=13-82-17.36). The REE patterns are similar to those of medium-K suites(Gill, 1981) but are LREE enriched and HREE depleted relative to medium-K suites. They do not exhibit any significant Eu anomaly with $(Eu/Eu^*)_N$=0.97 suggesting that plagioclase was not a significant fractionating phase. However, sample MA-132 has a slight positive Eu anomaly with $(Eu/Eu^*)_N$=1.33, probably suggesting plagioclase accumulation, similar to that found in continental margin andesitic rocks(e.g., Noble *et al.*, 1975; Dostal *et al.*, 1977). However, it is suggested that Eu anomalies are uncommon in orogenic andesites despite evidence of plagioclase accumulation and fractionation due to high Eu^{+3}/Eu^{+2} and Fe^{+3}/Fe^{+2} ratios(Gill, 1981).

The relative constancy of HREE despite LREE enrichment can in principle be explained by fractionation of a phenocryst assemblage in which hornblende plays an important role. Fractionation of the plagioclase+pyroxene±titanomagnetite is less significant. However, the general concave-up REE patterns are all features more likely to reflect the influence of hornblende(Nicholls and Harris, 1980). As amphibole-melt partition coefficients for HREE in most andesitic rocks fall between 0.5 and 2(Gill, 1981), hornblende fractionation is seemingly a feasible HREE suppressant, but were

this the dominant process, the still larger preference of amphibole for MREE(Gd to Er) would yield dish-shaped REE patterns. Interaction of andesites with hornblende-rich lower crustal rocks, either by assimilation and reaction with enclosing wall rocks or by mixing with silicic partial melts therefore might provide an alternative means of HREE suppresion.

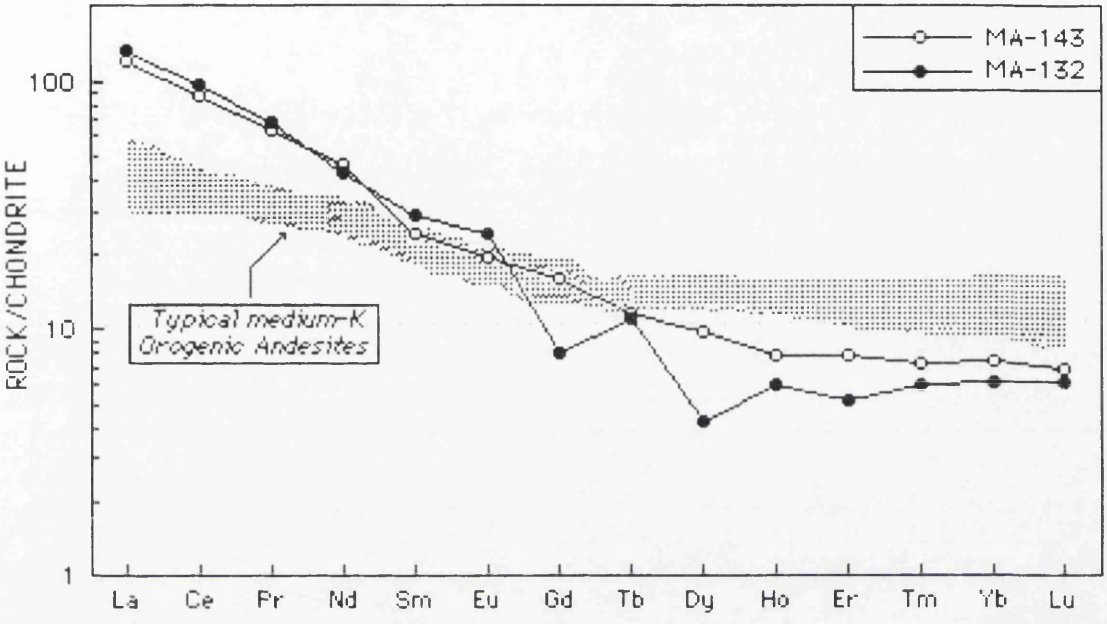

Figure 5.107. Chondrite-normalized REE patterns of trachyandesites. Normalizing values are from Boynton(1984). The REE pattern of medium-K orogenic andesites(Gill, 1981) is also shown for comparison.

5.3.3.5. DACITES

5.3.3.5.1. MAJOR AND TRACE ELEMENTS

Dacites range in SiO_2 from 63 to 70 wt.%(Appendix 3; Figures 5.108 and 5.109). All samples are quartz and hypersthene normative. In the classification scheme of Peccerillo and Taylor(1976), they fall in the field of medium-K dacites. All the samples exhibit calcalkaline characteristics and fall within calcalkaline fields on most discrimination plots, and display high ratios of large ion lithophile elements(LILE) to HFSE, and low TiO_2 concentrations. A calcalkaline affinity is denoted by an enrichment in the LFS element concentrations(Pearce, 1982; Gill, 1981). As typical of calcalkaline volcanics(Gill, 1981), abundances of TiO_2, Al_2O_3, FeO, MnO, MgO, CaO and P_2O_5 decrease, Mg/(Mg+Fe) decreases, and Na_2O and K_2O increase with increasing SiO_2 content(Figures 5.109 and 5.110). Dacites show chemical characters that are comparable with those reported for products from continental margins(Ewart, 1976a, 1982), and have similar concentrations of K and the related elements Rb, Sr, Ba, Zr, Th(Baker, 1982). They have generally high Fe/Mg ratios which is similar to continental margin calcalkaline rocks(Jakes and White, 1972).

The compatible trace elements(Ni, Co, Cu) show a wide range in abundances and negative correlation with SiO_2(Figures 5.111 and 5.112), and positive correlation with total iron, MgO and CaO. Dacites are characterized by relatively high Rb abundances, consistent with their high K_2O values. Using SiO_2 as a differentiation index, there is a marked progressive increase in Rb and Ba abundance with increasing SiO_2 content, Zr shows a slight increase, and Sr is variable but shows an overall slight decrease in concentration(Figure 5.111).

The general trends of progressive increase in SiO_2, K_2O and incompatible elements(e.g., Rb, Ba, Th, REE) with decrease in MgO, total Fe, CaO, TiO_2 and compatible trace elements, suggest qualitatively that the evolution of dacites was mainly by fractional crystallization of a parent magma with lesser other magmatic processes(Figure 5.113).

The decreases in MgO, FeO_t, CaO, Al_2O_3 and MnO with SiO_2 reflect crystallization of cpx±opx and plagioclase whereas the decrease in TiO_2 reflects crystallization of titaniferous magnetite. The slight increase in Na_2O indicates that plagioclase was the dominant crystalline phase, according to petrographic observations, and the generally accepted incompatible behaviour of K_2O explains the positive correlation of this oxide with SiO_2. There is considerable scatter on the P_2O_5-SiO_2 plot but the data fit best with an overall decrease in P_2O_5 as SiO_2 increases. CaO, FeO_t, MgO, TiO_2 and P_2O_5 correlate negatively with incompatible elements. Their decreasing concentrations can be shown to relate to the fractionation of modal proportions of plagioclase, biotite,

Fe-Ti oxide and apatite. High abundance of Al_2O_3 and CaO correspond to the abundant calcic plagioclase phenocrysts.

Variation diagrams for trace elements also show considerable scatter which in part reflects analytical uncertainties. However, the systematic trends shown by most elements are broadly consistent with crystallization of the observed phenocryst phases. The incompatible elements Rb, Ba, Zr increase with increasing SiO_2 whereas the concentrations of the compatible elements Sr, Zn, Cr decrease. Nb and Y show a slight positive correlation with SiO_2. The abundance of Ni is very close to the detection limits of analytical techniques.

Figure 5.108 shows a plot of Fe_2O_3/FeO versus LOI(loss on ignition) for all analysed dacite samples. Dacites are very oxidized but are not extensively hydrated. Generally, for the most of samples Fe_2O_3/FeO is higher than 3, and LOI is smaller than 2 wt.%(Figure 5.108).

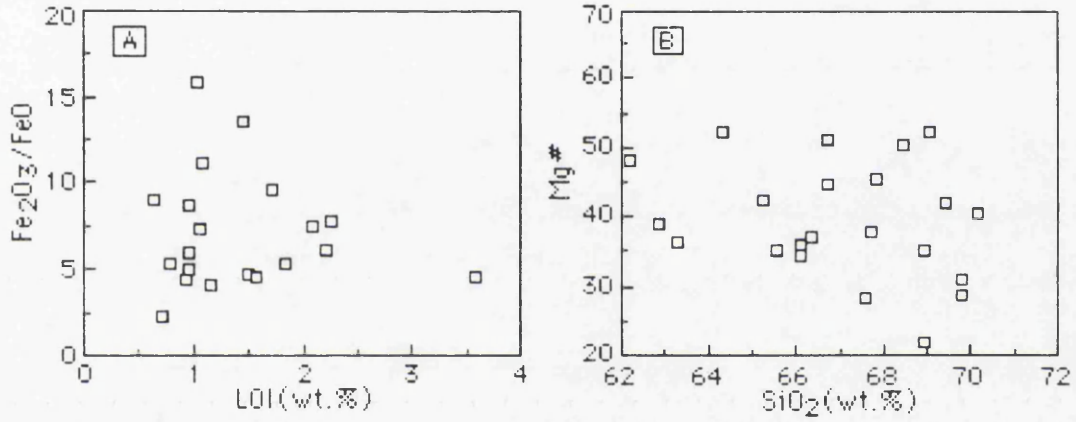

Figure 5.108. LOI versus Fe_2O_3/FeO plot showing oxidation and hydration(A), and $Mg^{\#}$ number[$Mg^{\#}=Mg/(Mg+Fe^{+2})$] versus SiO_2(wt.%) plot of dacites(B).

In Figure 5.114A, total iron as FeO_t is plotted against MgO. The samples cluster around the trend of experimentally produced melt at 5 kb H_2O, from olivine tholeiite at the FMQ buffer(Helz, 1976). In addition, most of the data falls within the trends of hybrid calcalkaline rocks from Oraefajokull(Prestvik, 1980) and Askja(Sigurdsson and Sparks, 1981). Figure 5.114B is a plot of FeO_t versus CaO. Rocks plotting to the lower right of the line usually crystallize biotite and, or, hornblende, have higher Fe^{+3}/Fe^{+2} ratios than the high-Fe types, and are usually calcalkaline and metaluminous to peraluminous. Rocks plotting close this line usually crystallize orthopyroxene±biotite and hornblende, and are usually metaluminous. Rocks having still high-Fe usually crystallize fayalite and are peralkaline or subaluminous(Warshaw and Smith, 1988). Generally, the dacites studied plot as low-Fe, calcalkaline and metaluminous types(Figure 5.114B). This is in accordance with calculated fO_2 and observed phenocryst types in these rock.

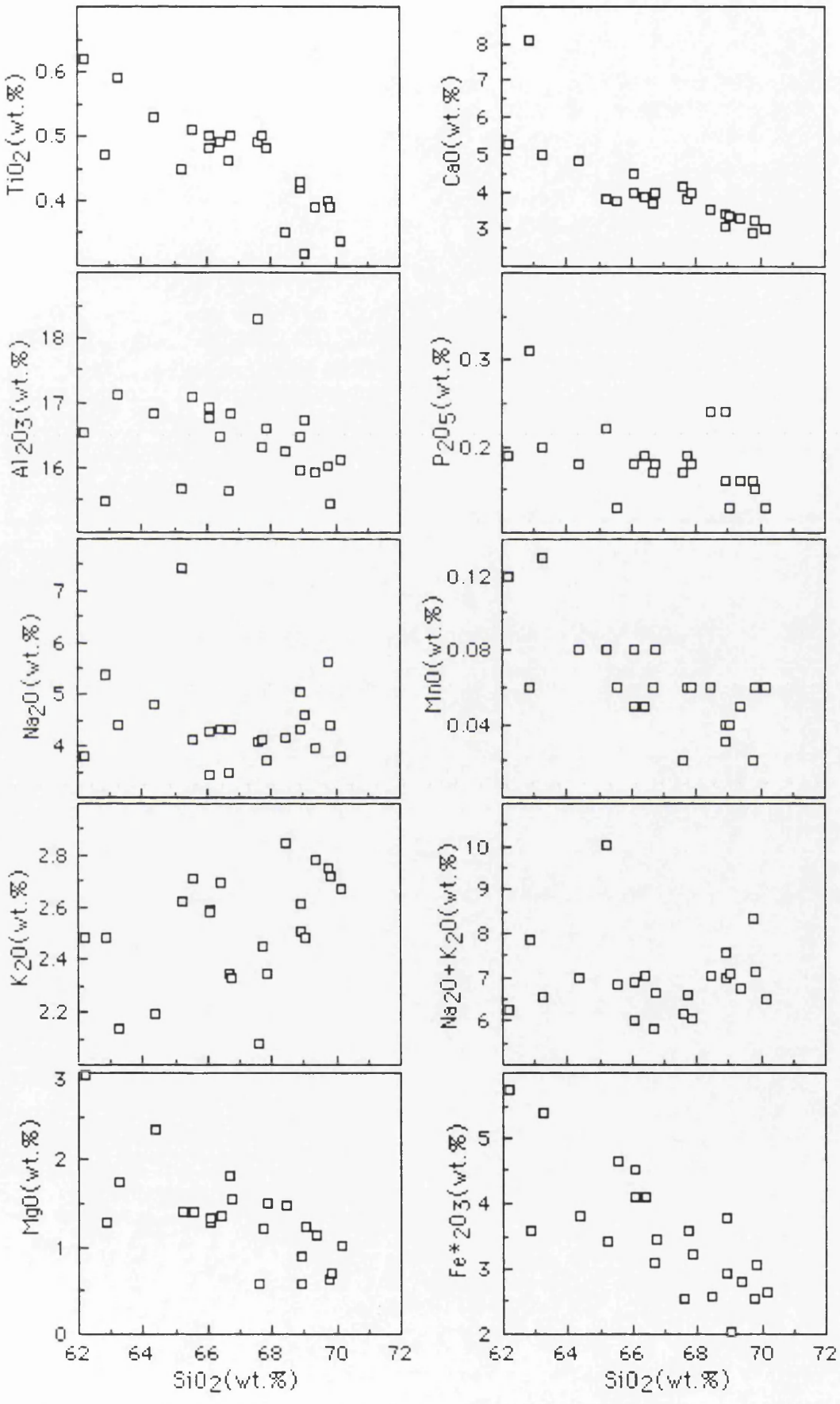

Figure 5.109. SiO_2(wt.%) versus major element plots for dacites.

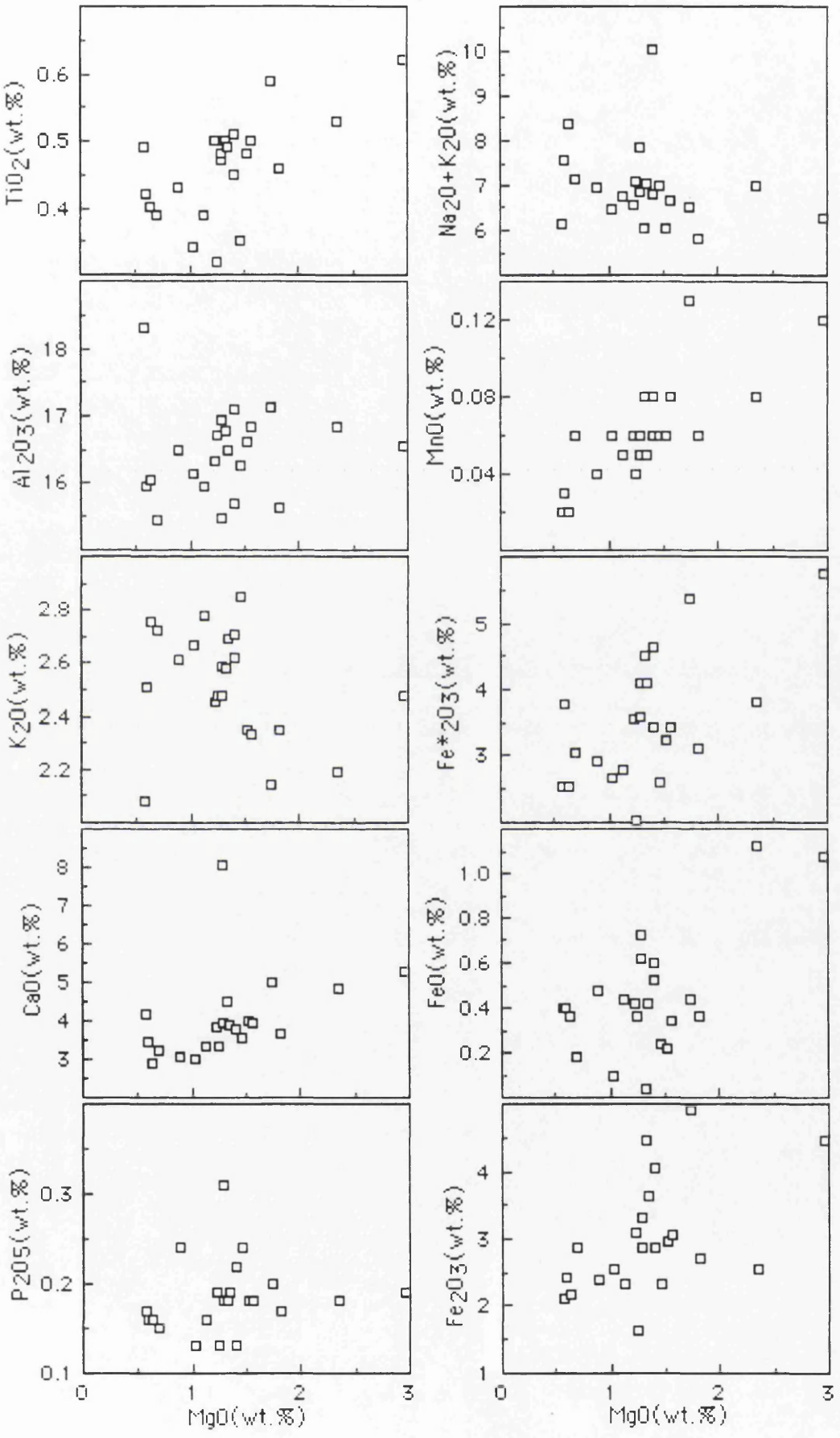

Figure 5.110. MgO(wt.%) versus major element plots of dacites.

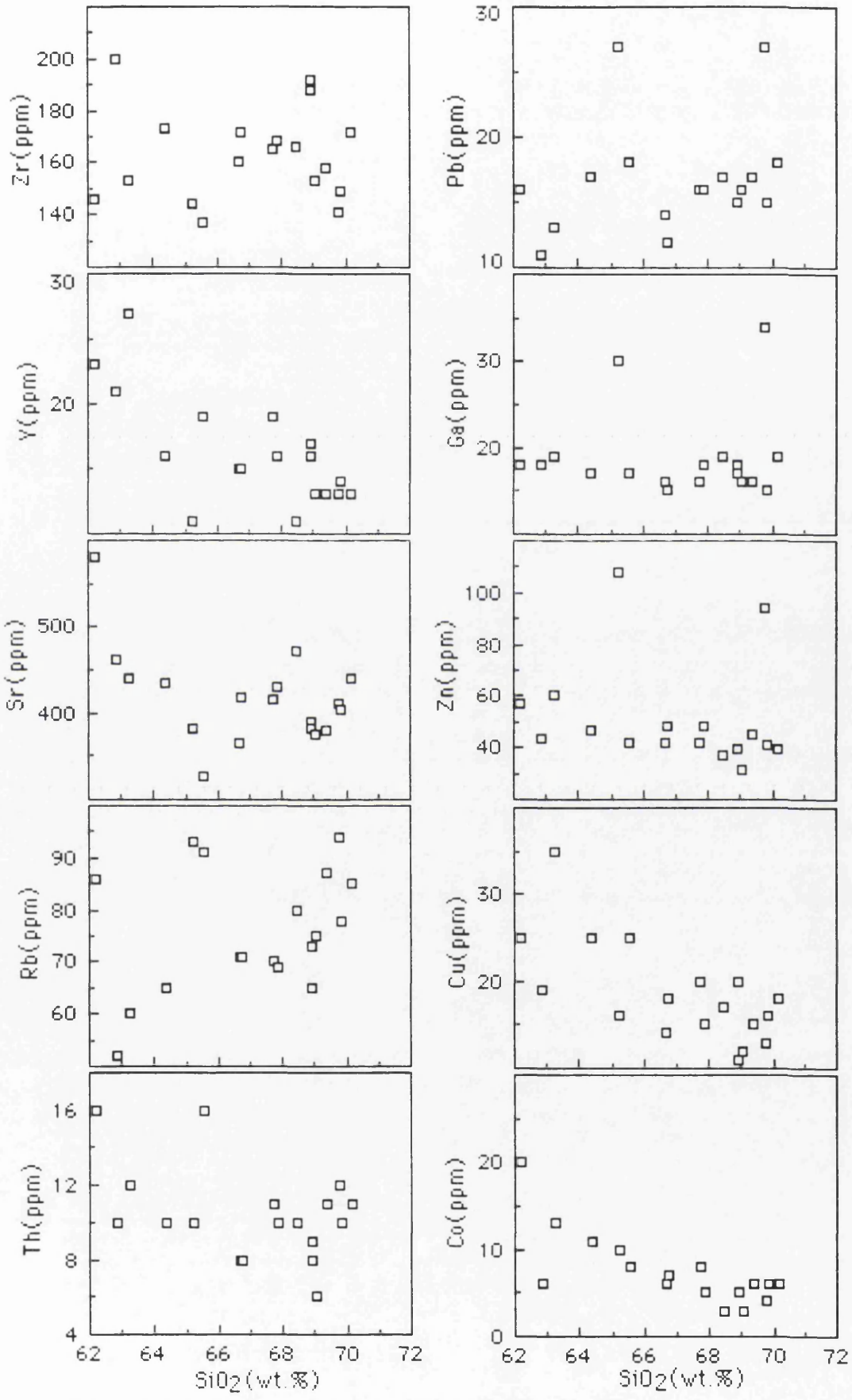

Figure 5.111. SiO_2(wt.%) versus trace element plots for dacites.

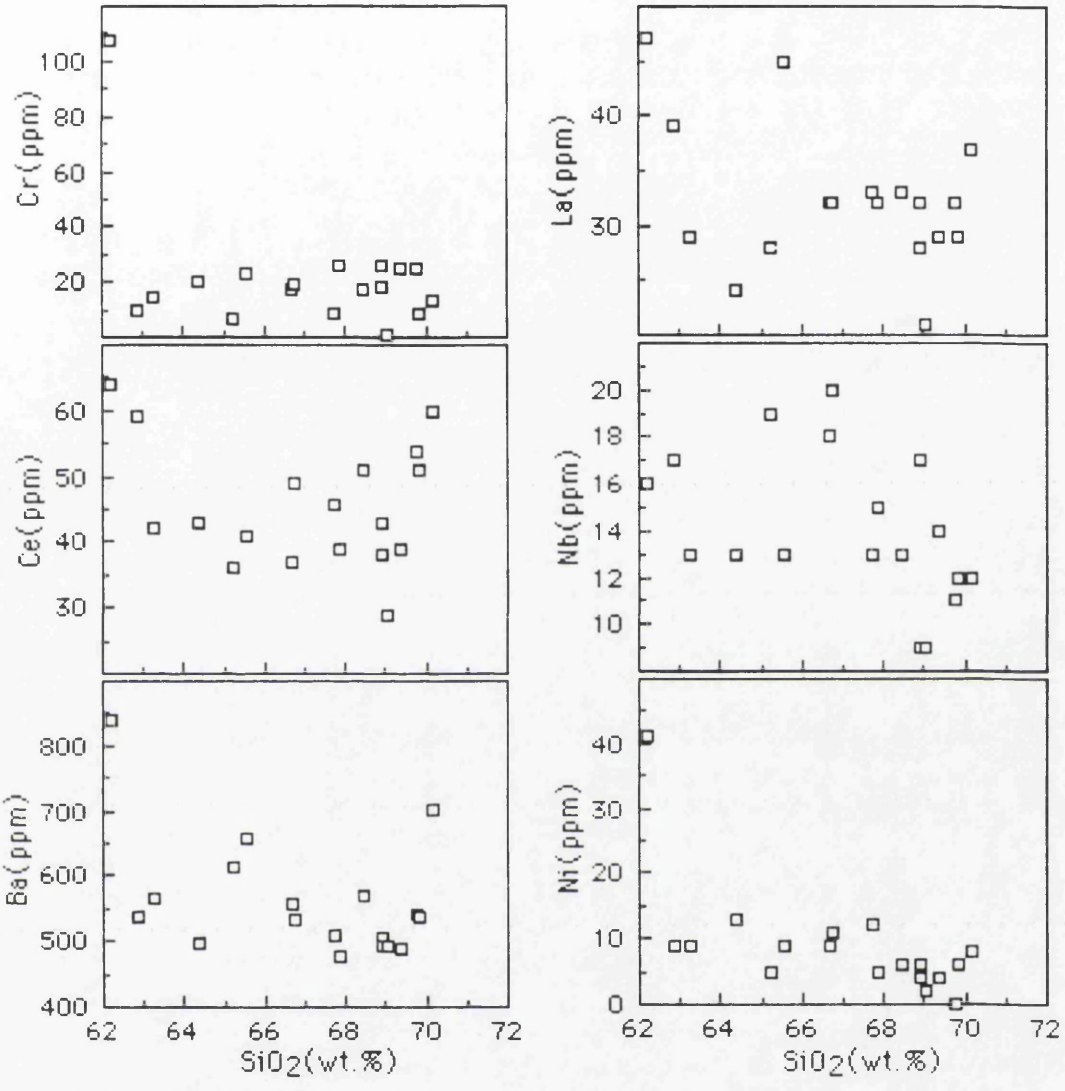

Figure 5.112. SiO_2(wt.%) versus trace element plots continued.

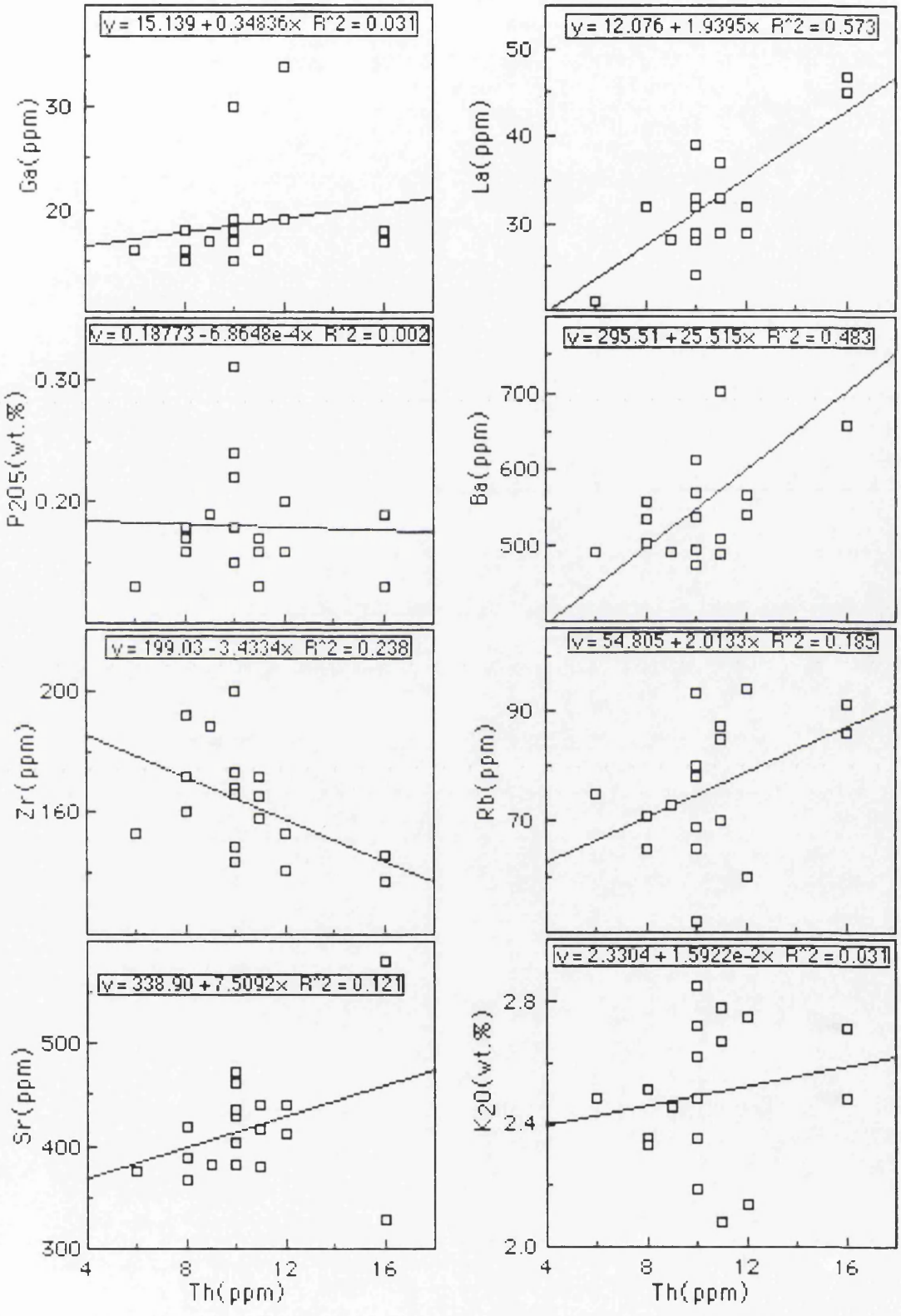

Figure 5.113. Th(as a differentiation index) versus incompatible element plots.

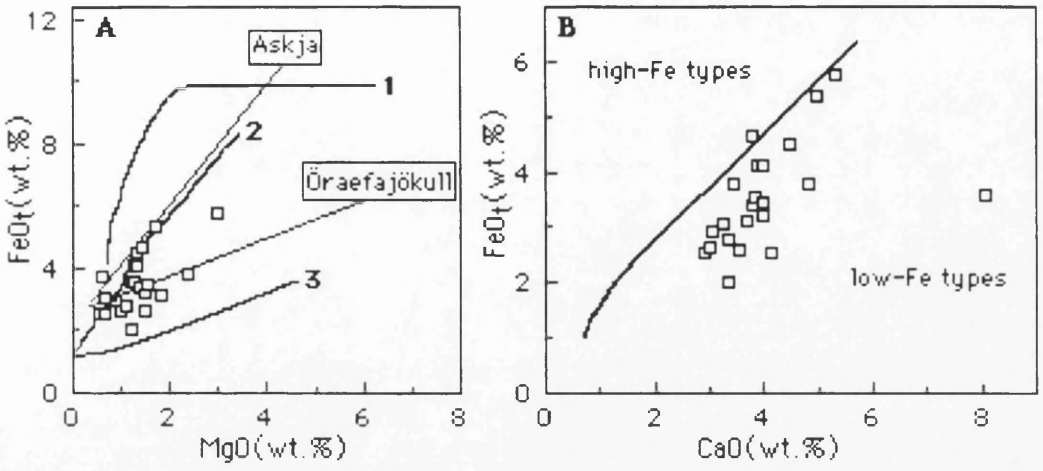

Figure 5.114. (A), total FeO_t versus MgO for dacites. The trends of experimentally produced melts at 1kb(fH_2O=0.67, G-CH buffer) from a Kilauea basalt(Spulger and Rutherford, 1983) and at 5 kb H_2O from an olivine tholeiite at the FMQ and HM buffers(Helz, 1976) are shown for comparison(nos, 1, 2, 3 respectively); (B), total FeO_t versus CaO plot. Thick line separates high-Fe types from low-Fe ones(Warshaw and Smith, 1988).

The dacites have high Al_2O_3 content(15.5 to 18 wt.%) reflecting the increased proportion of feldspar component. The rocks also have high concentrations of alkalis ranging between 6 and 10 wt.% Na_2O+K_2O. Generally, K_2O/Na_2O ratios are lower than 1. The molar ratio of Al_2O_3 to Na_2O+K_2O+CaO(A/CNK) is less than 1.1 but mainly about 1.0. Therefore the dacites are considered as metaluminous in composition(Figure 5.115), according to the definition of Shand(1947).

The calcalkaline chemistry of the dacites is well illustrated in an AFM plot(Figure 5.116). They are characterized by low Fe/Mg ratios and alkalies, and high CaO and Al_2O_3.

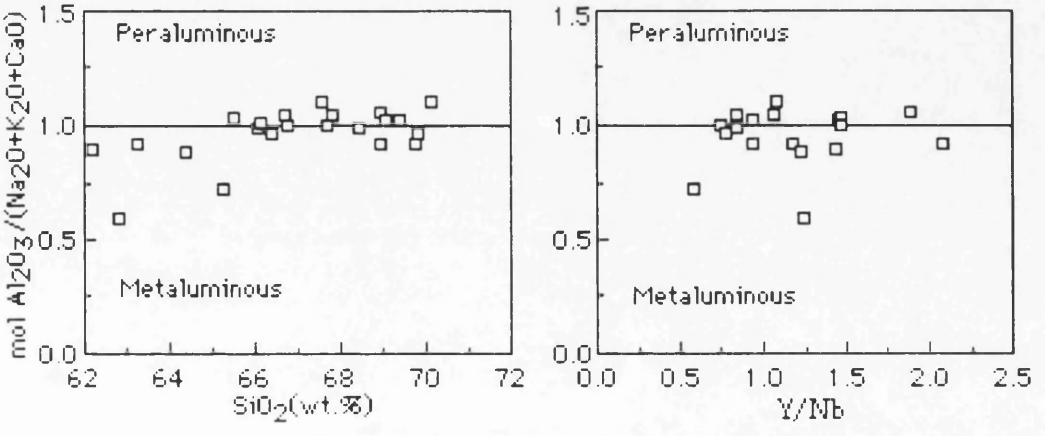

Figure 5.115. Mol $Al_2O_3/(Na_2O+K_2O+CaO)$ versus SiO_2 and Y/Nb plots.

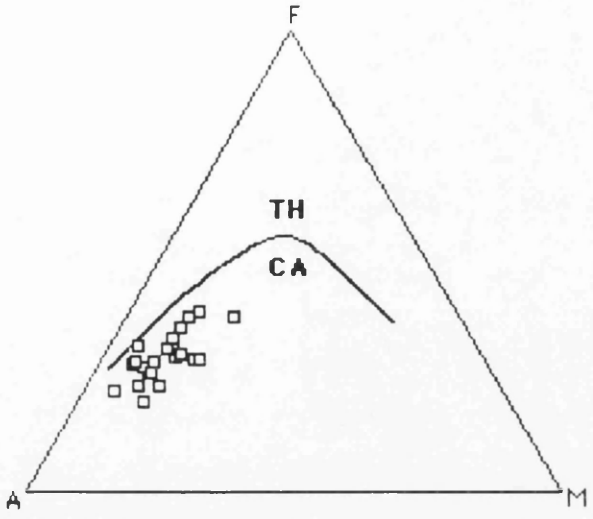

Figure 5.116. AFM plot showing the composition of dacites. The thick line separates tholeiitic(TH) and calcalkaline(CA) compositions(Irvine and Baragar, 1971).

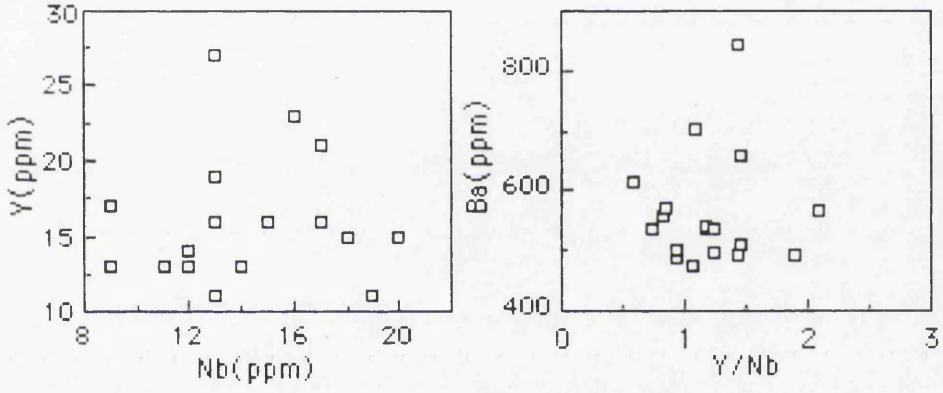

Figure 5.117. Y versusNb and Ba versus Y/Nb plots for dacites.

Dacites have high La/Y and Nb/Y ratios compared with the Gurgurbaba lavas(Figures 5.117 and 5.118). Lambert and Holland(1974) used CaO versus Y to define J and L type trends, which lead respectively to depletion and enrichment in Y relative to a calcalkaline series standard. The J and L trends have been termed hornblende-(±garnet) and pyroxene controlled differentiation trends respectively, as these minerals can be critical in determining trend direction. In the Y versus CaOplot(Figure 5.118), dacite samples generally plot on the Y depleted side of the standard calcalkaline trend as obtained by pyroxene and plagioclase dominated fractionation(Lambert and Holland, 1974). They are slightly Y depleted relative to the standard calcalkali trend, and define a J-type trend(Figure 5.118), indicating hornblende controlled fractionation.

Figure 5.119(TiO2 versus Zr plot; Pearce and Norry, 1979) shows the fractionation trends followed by dacites. The fractionation vectors suggest that the crystallization of magnetite and amphibole and possibly biotite was most

important in causing Ti to decrease relative to Zr during fractionation(Figure 5.119). Pearce(1982) emphasized that because of the early crystallization of magnetite, volcanic arc lavas never reach the higher Ti contents of within plate lavas, for any given Zr concentration.

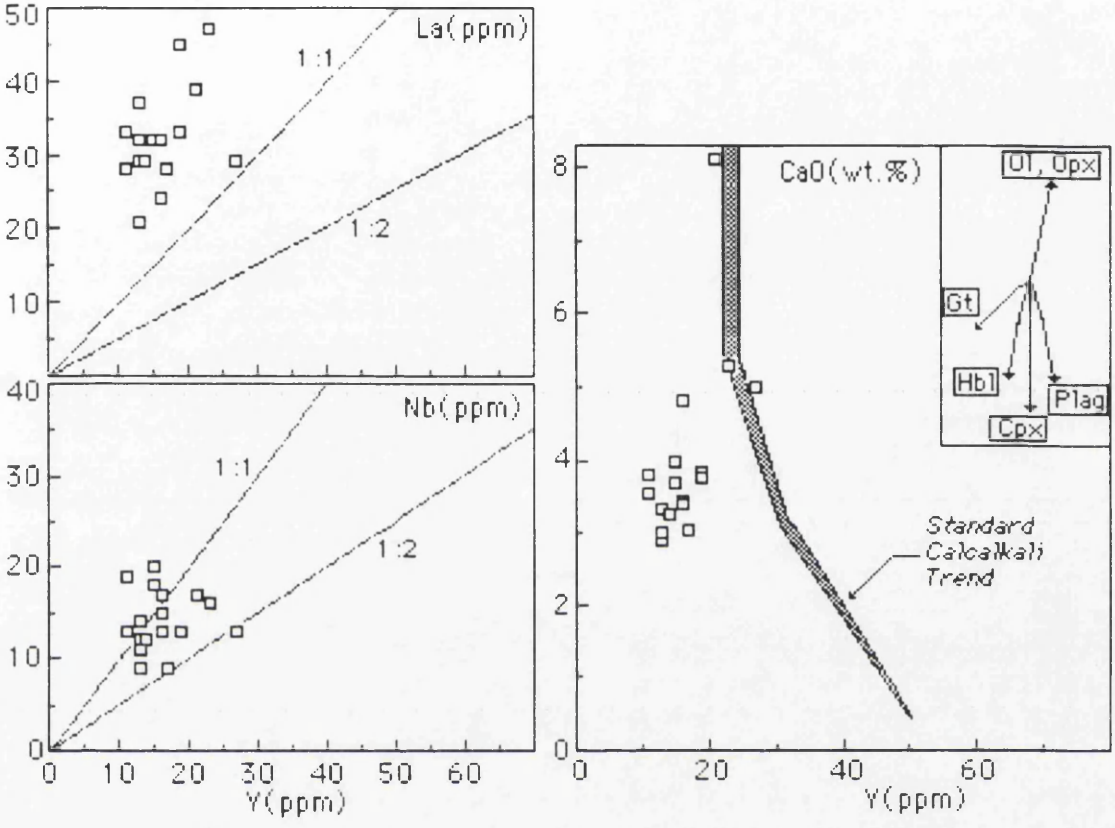

Figure 5.118. Y(ppm) versus Nb(ppm), La(ppm) and CaO(wt.%) plots for dacites. Shaded area represents the "standard" calcalkaline trend of Lambert and Holland(1974). The vectors show qualitative trends of the effect of fractional crystallization of common silicates.

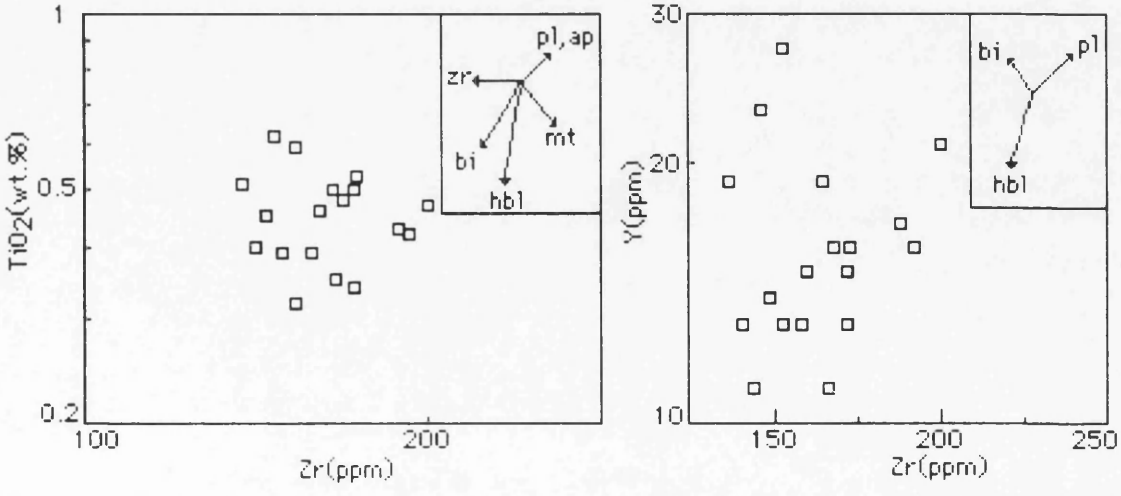

Figure 5.119. Zr(ppm) versus TiO_2(wt.%) and Y(ppm) plots showing the fractionation trends in dacites. Modelled fractionation vectors are from Pearce and Norry(1979).

Using trace element compositions, Pearce *et al.* (1984) have attempted to interpret the tectonic settings of granitic rocks. In this classification(Figure 5.120), the dacites fall clearly within VAG(Volcanic Arc Granites). Although this discrimination points to a certain setting, it is unlikely that simple diagrams will provide a unique definition because of wide variety of crustal components may have involved in the genesis of dacites. Furthermore, rather than the tectonic setting existing when granitic magma was actually produced, these plots seem to diagnose the setting in which the protolith was formed(Arculus, 1987; Twist and Harmer, 1987).

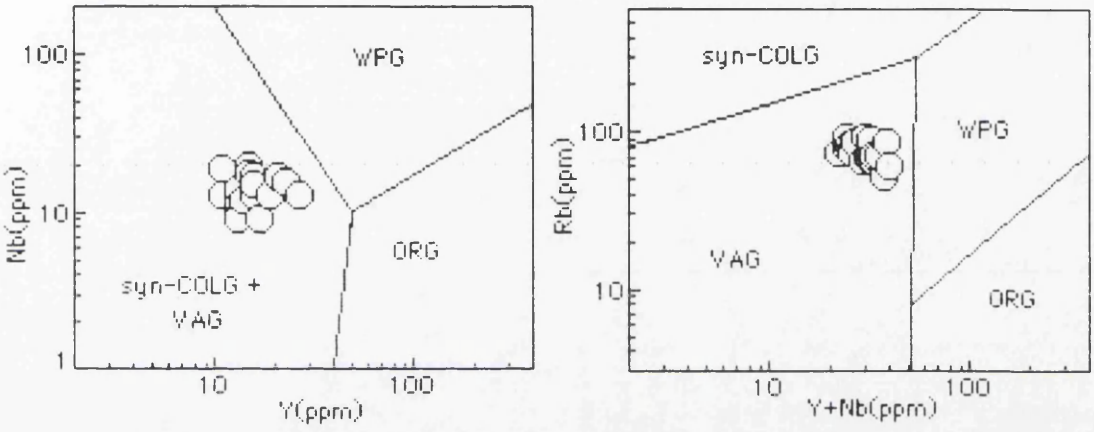

Figure 5.120. Trace element discriminant diagrams for granitic rocks(Pearce *et al.*, 1984) showing the compositions of dacites. VAG=volcanic arc granites; syn-COLG=syn-collision granites; WPG=within plate granites; and ORG=ocean ridge granites.

The A'FK and ACF plots(Figure 5.121) show that the dacites are more peraluminous than other peralumious volcanic series given in the plot. In the A'FK plot(Figure 5.121), most of the samples plot below the K-feldspar-cordierite tie line, thus necessitating the participation of a strongly peralumious phase(either melt, sillimanite or andalusite, muscovite or tourmaline). The other point emphasized by the A'KF plot is the felsic nature of the dacites. The dacites have compositions closer to the minimum melt and correspond to a much felsic peraluminous series. In figures, the major element data for the dacites are also compared with experimentally produced melt compositions. The experiments of Green(1976), Clemens and Walls(1981) and Vielzeuf and Holloway(1988) are appropriate to discussion of the compositions of peraluminous granitic liquids generated at high temperatures by fluid-absent melting of biotite. Liquid compositions obtained at lower temperatures in H_2O-saturated experiments on a tourmaline leucogranite(Benard *et al.*, 1985) are also shown for comparison(Figure 5.121). The dacites do not plot in the fields for high temperature liquid compositions, they are more mafic and calcic, depleted in K than liquids generated by fluid-absent melting of biotite.

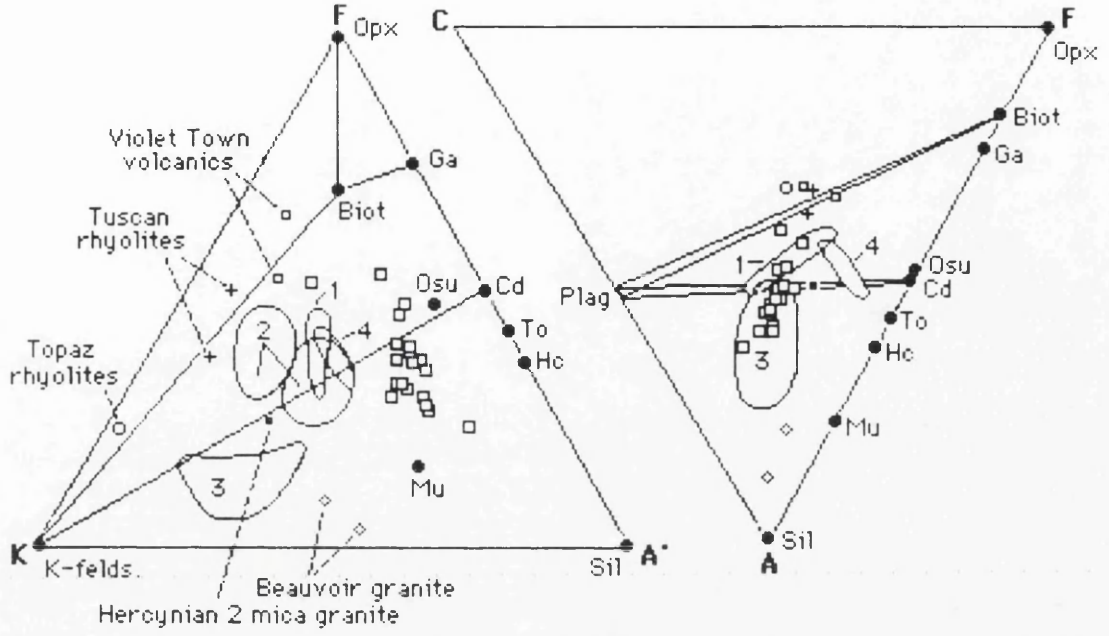

Figure 5.121. A' (Al_2O_3-Na_2O-K_2O-CaO) K(K_2O) F(FeO_t+MgO) and A(Al_2O_3-Na_2O-K_2O) C(CaO) F(FeO_t+MgO) plots for dacites(open squares), for various examples of crustal anatectic series and for experimental glass compositions in peraluminous systems(1, Green, 1976; 2, Clemens and Wall, 1981; 3, Benard *et al.*, 1985; 4, Vielzeuf and Holloway, 1988). Source of data: Tuscan rhyolites(Dupuy, 1970); Violet Town volcanics(Clemens and Wall, 1984); topaz rhyolites(Christiansen *et al.*, 1983); Beauvoir granite(Pichavant *et al.*, 1987b) and Hercynian two-mica granites (La Roche *et al.*, 1980). Biotite(Biot), muscovite(Mu), tourmaline(To) and hercynite(Hc) compositions taken from Pichavant *et al.* (1988). For other phases, orthopyroxene(Opx), Fe-Mg garnet(Ga), cordierite(Cd), osumilite(Osu), sillimanite and andalusite(Sill), end-member compositions have been plotted.

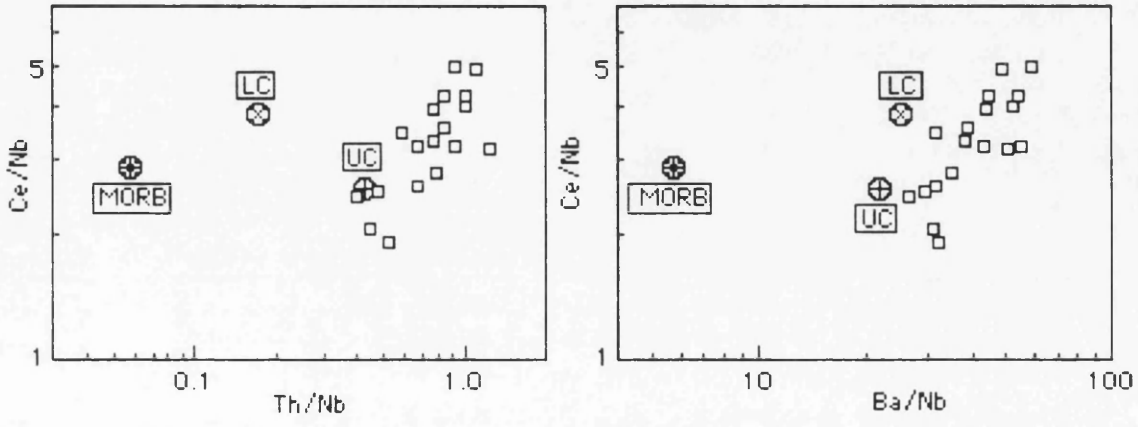

Figure 5.122. Comparison of Ce/Nb, Th/Nb and Ba/Nb ratios of dacites with mid-ocean ridge basalt(MORB)(Pearce, 1983), lower continental crust(LC) and upper continental crust(UC)(Taylor and McLennan, 1985) values.

Ce/Nb versus Th/Nb(Figure 5.122) and Ce/Nb versus Ba/Nb plots for dacites emphasize their close similarity, significantly to the average composition for the upper continental crust. These plots also demonstrate that the dacites do not lie on a mixing line between MORB and crustal composition, and therefore could have not been formed by contamination of MORB magmas by upper or lower crustal material.

Recent experimental results emphasize the enrichment of Na relative to Ca and K during dehydration melting of amphibolite at various pressures(Rapp *et al.*, 1991). Many Archean trondjemites and tonalites, believed to have been derived from metamorphosed basaltic sources, show a Na enrichment(trondhjemitic trend)(Barker *et al.*, 1981). This is in strong contrast to the typical calcalkalic differentiation trend characteristic of most arc volcanic suites(Figure 5.123). Dacites from this study show Na enrichment(Figure 5.123), suggesting geochemical signature of slab-derived material (Drummond and Defant, 1990; Defant and Drummond, 1990).

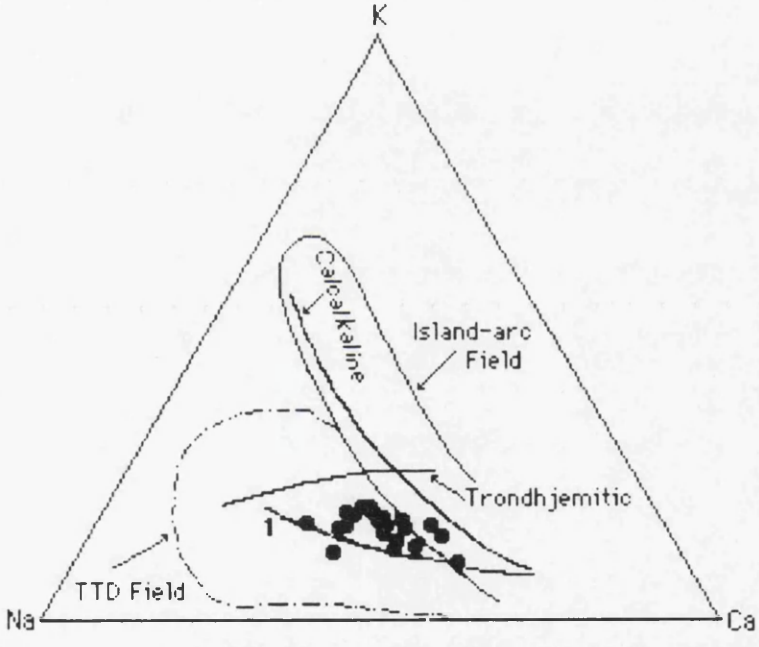

Figure 5.123. Ternary plot of Ca, Na, and K with calcalkaline(Nockholds and Allen, 1953) and trondhjemitic(Barker *et al.*, 1981) trends superimposed. Trondhjemite, tonalite, and dacite(TTD) field encompasses all Archean trondhjemites, tonalites, and dacites believed to be derived from partial melting of metamorphosed basalt(Drummond and Defant, 1990). Curve 1 represents trend trough Archean TTD believed to be generated from partial melting of subducted oceanic crust(Defant and Drummond, 1993).

The geochemical signatures of dacites are similar to Archean high-Al trondhjemites-tonalites-dacites that are thought to be derived from a basaltic source. A plot of Sr/Y versus Y(Figure 5.124) indicates that dacites are mainly

within the adakite and Archean high-Al trondhjemite-tonalite-dacite field. Defant and Drummond(1990) have shown that partial melting of metamorphosed basalt will generate dacitic melts with high Sr/Y and low Y. Moreover, partial melting of an amphibolite-eclogite source would generate melting curves that pass through the adakite field toward high Sr/Y and low Y whereas basalt genesis via partial melting of mantle wedge and subsequent closed- or open-system differentiation toward andesites, dacites, and rhyolites drives magmas in the opposite direction(i.e, toward low Sr/Y and high Y)(Defant and Drummond, 1993).

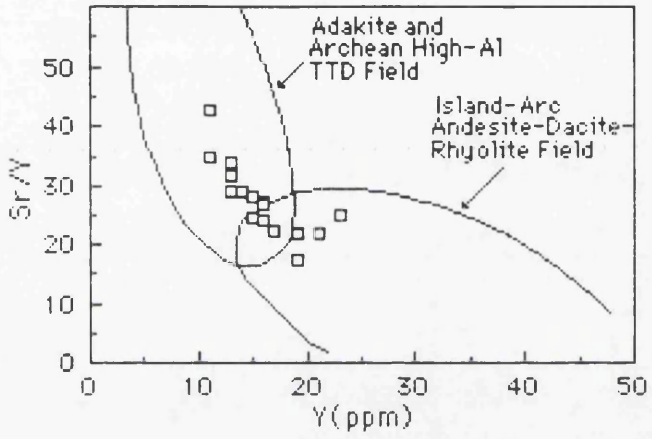

Figure 5.124. Plot of Sr/Y versus Y for the dacites. Adakite and Archean high-Al trondhjemite-tonalite-dacite(TTD), island-arc andesites, dacites, and rhyolites fields(Defant and Drummond, 1990) are superimposed for comparison.

5.3.3.5.2. INCOMPATIBLE ELEMENTS

The highly incompatible element ratios such as K/Rb and La/Ce show negative correlation, but Zr/Nb has positive correlation, with increasing SiO_2(Figure 5.125). In addition, the dacites with high Ba/La(>15) and Ba/Nb ratios(Figure 5.126) are similar to those of magmas related to a subduction zone(Sun, 1980). In general, concentrations of the large ion lithophile(LIL) incompatible elements(e.g., K, Rb, Ba and to a lesser extent Sr) vary as a function of the fractionation. However, as biotite and hornblende are not residual, the ratios of LIL incompatible elements K/Rb, K/Ba change little during moderate degrees of fractionation.

The rocks have similar MORB and PM-normalized patterns(Figures 5.127 and 5.128), showing enrichment in all elements. In a MORB-normalized spidergram(Figure 5.127), the dacites have a negative Nb anomaly being more akin to "normal" subduction values. LIL enrichment, particularly Th, is significant. The negative anomalies shown by Ti and P may reflect Fe-Ti oxide

and apatite fractionation during differentiation. Using the method of Pearce(1983), the trace element pattern of dacites is closely similar to that of calcalkaline dacites and may be interpreted in terms of derivation from a mantle source containing a subduction component(with low Nb and high LIL elements) and a within plate component with high LIL and HFS elements.

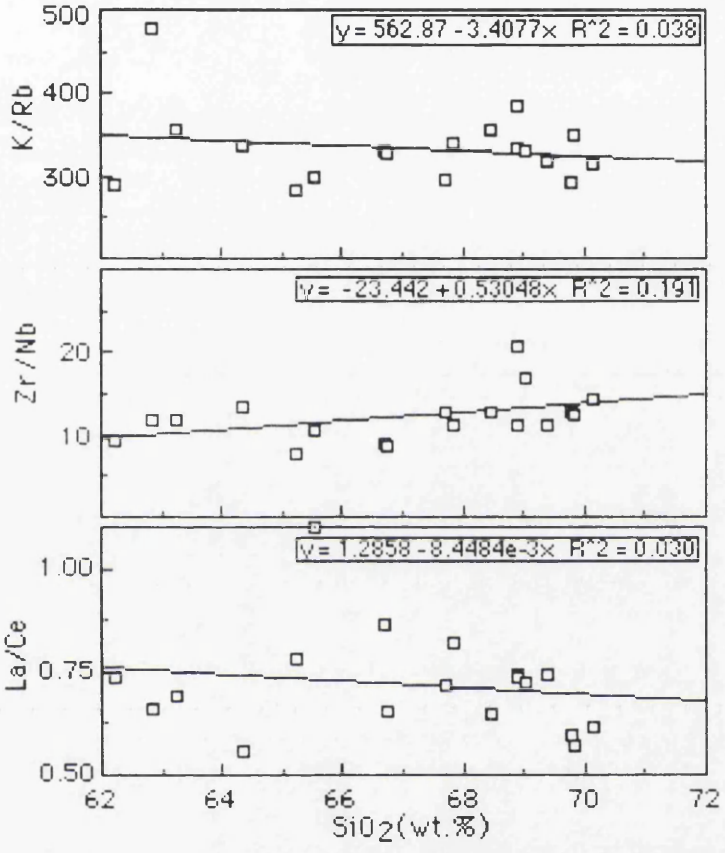

Figure 5.125. Variations in ratios of highly incompatible elements as a function of SiO_2 content.

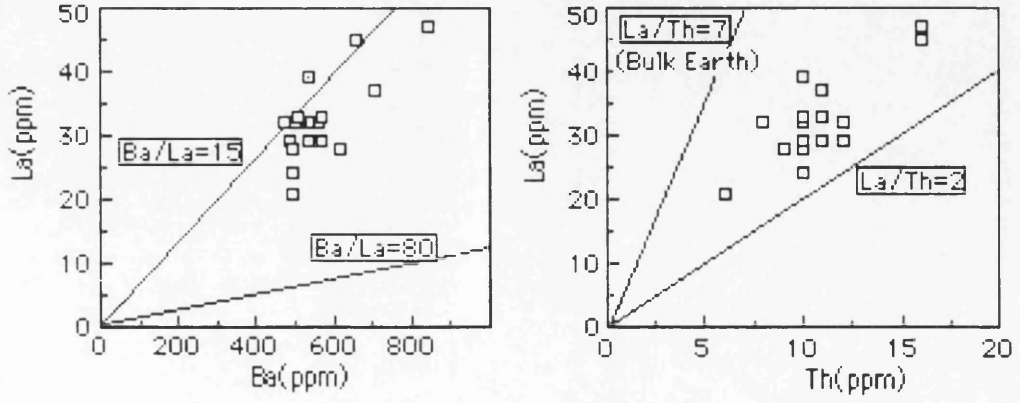

Figure 5.126. La versus Ba and Th incompatible element plots for dacites.

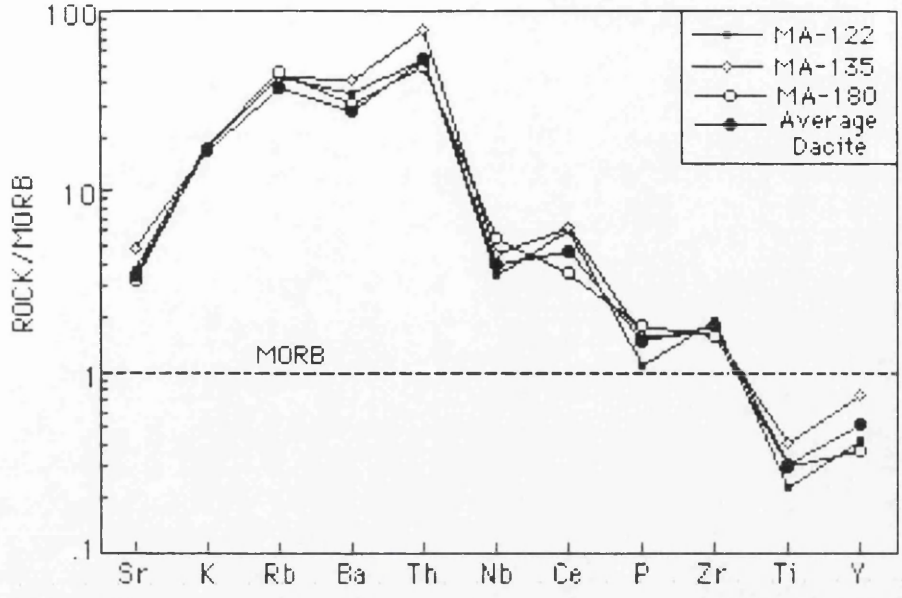

Figure 5.127. MORB-normalized trace element patterns of dacites. MORB normalizing values are from Pearce(1983).

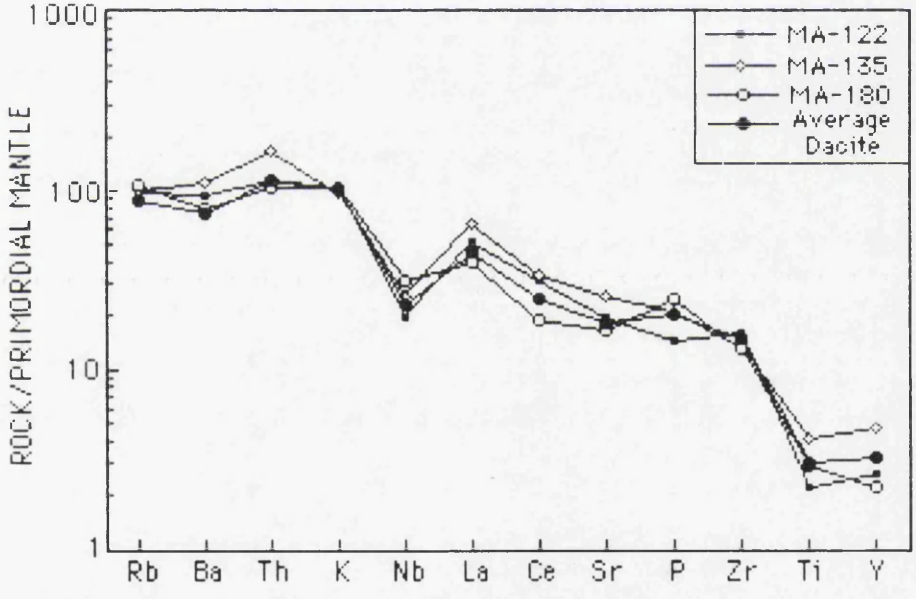

Figure 5.128. Mantle-normalized trace element patterns of dacites. Normalizing primordial mantle values are from Wood *et al.* (1979a).

The trace element characteristics of dacites are shown in the spider diagram in Figure 5.129, normalized to ORG(Ocean Ridge Granite) composition(Pearce *et al.*, 1984). The dacites have similar concentrations and patterns for the large ion lithophile elements(LILE), but the high field strength elements(HFSE) and the REE give a slightly different picture. Generally, the dacites have significantly low concentrations of HFSE and the REE are depleted relative to ORG. This is most pronounced in the case of Zr, Sm, Y and Yb. These patterns show similarities with the pattern of volcanic arc granites which are

characterized by enrichments in K, Rb, Ba, Th relative to Nb, Ce, Zr, Y, Sm and Yb(Pearce *et al.*, 1984).

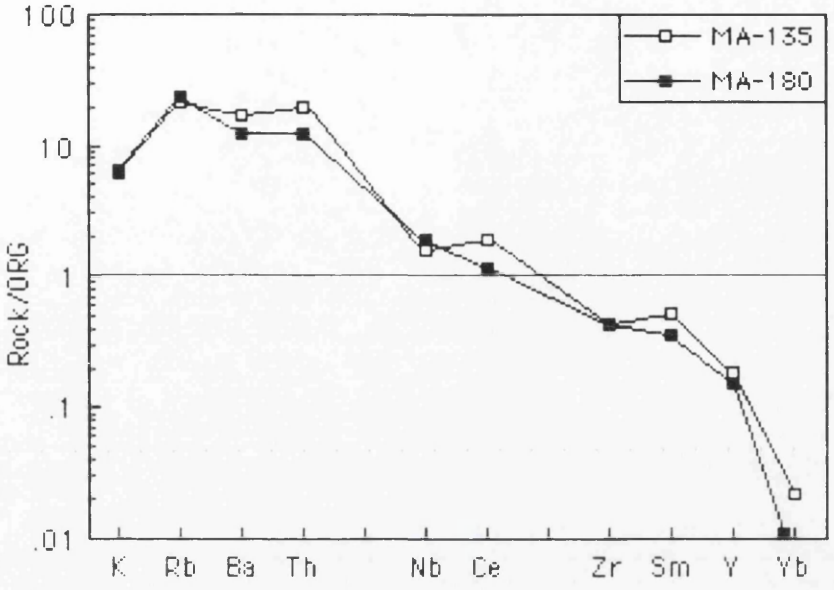

Figure 5.129. Geochemical patterns of dacites normalized to Ocean Ridge Granite(ORG; Pearce *et al.*, 1984) composition.

5.3.3.5.3. RARE EARTH ELEMENTS

The REE patterns are highly fractionated, exhibiting moderately steep slopes with $(La/Lu)_N$ ratios from 15 to 30, and all patterns are slightly concave upward(Figure 5.130). They are all more strongly enriched in LREE than HREE. There is also progressive enrichment in all REE and a slight negative Eu anomaly with $(Eu/Eu^*)_N$=0.91-0.98, except one sample $(Eu/Eu^*)_N$=1.47(Table 5.4). The dacites are characterized by LREE enrichment relative to HREE. The strong LREE enrichment and a negative Eu anomaly are similar to typical of calcalkaline acid rocks found at convergent plate margins.

Table 5.4. Selected REE content and ratios of the dacites.

Sample	$(La)_N$	$(Lu)_N$	$(Eu)_N$	$(Eu^*)_N$	$(La/Lu)_N$	$(La/Ce)_N$	$(La/Yb)_N$	$(Eu/Eu^*)_N$
MA-84	89.91	4.93	14.30	15.37	18.25	1.39	16.39	0.93
MA-94	62.02	2.83	11.19	11.39	21.95	1.42	18.92	0.98
MA-122	87.54	2.84	12.28	12.99	30.86	1.31	26.72	0.95
MA-135	118.08	7.93	18.84	20.60	14.88	1.45	14.17	0.91
MA-180	58.44	2.64	15.58	10.55	22.13	1.19	23.04	1.47

The REE behave as incompatible elements as do the HREE although to a lesser extent. The rocks are moderately LREE enriched and have a wide and depleted range of HREE abundances. With increasing La, REE patterns become HREE depleted. However, the patterns are generally LREE enriched with relatively flat HREE patterns which are subparallel to each other, though at increasing absolute REE abundance levels from sample MA-180 to MA-84.

A slightly concave and LREE enriched patterns of the rocks are consistent with amphibole fractionation(Green and Pearson, 1985; Romick, 1987). However, the flat HREE patterns of dacites are not consistent with the presence of garnet or amphibole in the source rock(Hanson, 1980). In addition, lack of any significant Eu anomalies in the rocks may indicate that plagioclase was not stable in the source and, or, did not extensively fractionate during magma ascent.

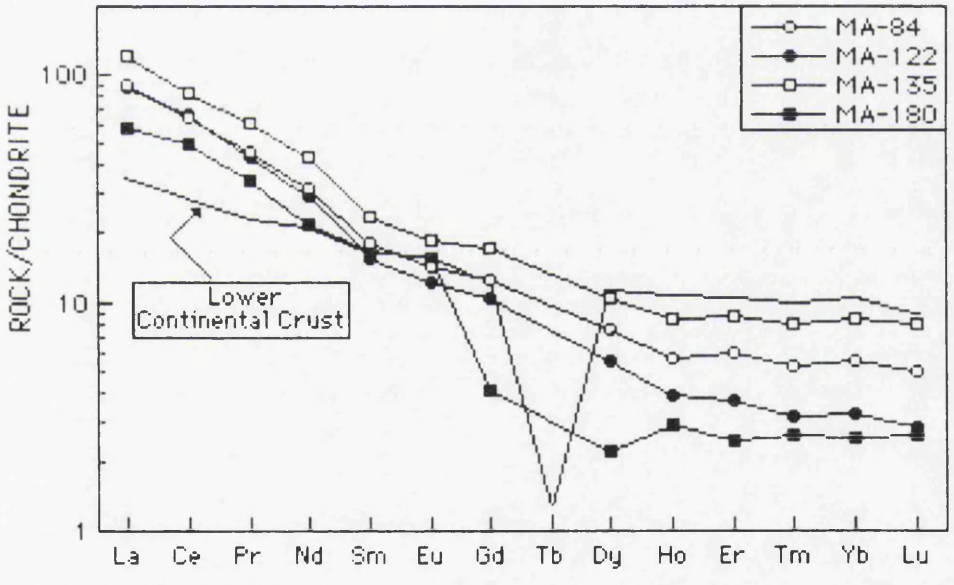

Figure 5.130. Chondrite-normalized REE patterns of dacites. Normalizing values are from Boynton(1984) and Lower Continental Crust vaues from Taylor and McLennan(1985).

5.3.3.6. AGGLOMERATE

5.3.3.6.1. MAJOR AND TRACE ELEMENTS

The agglomerate clasts were analysed to determine the chemical composition of the host magma and the role of magmatic processes in the evolution of the rock. The clasts are mainly andesites and rare dacites with SiO_2 varying between 62 and 68 wt.%. In plots of SiO_2 versus FeO*/MgO(Miyashiro, 1974) and Al_2O_3 versus normative plagioclase composition(Irvine and Baragar, 1971), the clasts tend to straddle the tholeiitic-calcalkaline boundary. In addition, they show moderate iron enrichment and plot in the tholeiitic field on an AFM diagram(Figure 5.134). Thus, the clasts show geochemical variation from calcalkaline to tholeiitic composition. Generally, the geochemical characteristics are comparable with those of medium K-suites which is confirmed by the plotting of the samples in the medium-K field(Peccerillo and Taylor, 1976; Gill, 1981).

The clasts have typically 15 to 18 wt.% Al_2O_3. MgO varies from 1.20 to 2.75 wt.%(Mg-number = 24 to 38). They also have low abundances of Ni, Cr, Co, Rb, and Th relative to other andesitic rocks studied. Moreover, they are characterized by low TiO_2(<1 wt.%), Na_2O/K_2O and K/Rb, and high Sr, Ba, Ba/Nb and La/Zr ratios. The rocks are generally enriched in most compatible elements relative to typical calcalkaline andesites from orogenic environments(Gill, 1981).

Variation diagrams indicate that most of the major and trace elements show fair correlations with SiO_2(Figures 5.131, 5.132 and 5.133). Al_2O_3, MgO, CaO and MnO decrease whereas K_2O increases with increasing SiO_2. P_2O_5 exhibits inflection due to apatite accumulation at early stages and then decreases in more silicic compositions. Although there is scatter for some trace elements, Zr, Sr, Cu, Ni, Co, Cr and La decrease whereas Pb, Zn, Ba and Ce increase with increasing SiO_2. Rb is relatively constant, excluding one sample. Nb increases in intermediate stages and then shows negative correlation in more silicic compositions. Generally, the enrichment in incompatible elements(Ba and Ce) and depletion in compatible elements(Co, Cr, Ni), MgO and CaO may be explained by crystal fractionation processes.

Major magnetite crystallization is marked by decreasing concentrations of FeO* and TiO_2. Negative correlations of Cr, Ni, MgO and CaO with SiO_2 may reflect significant cpx fractionation. The great compatibility of CaO and Sr in silicic compositions indicates plagioclase fractionation. In addition, inflection in P_2O_5 reflects apatite accumulation and fractionation.

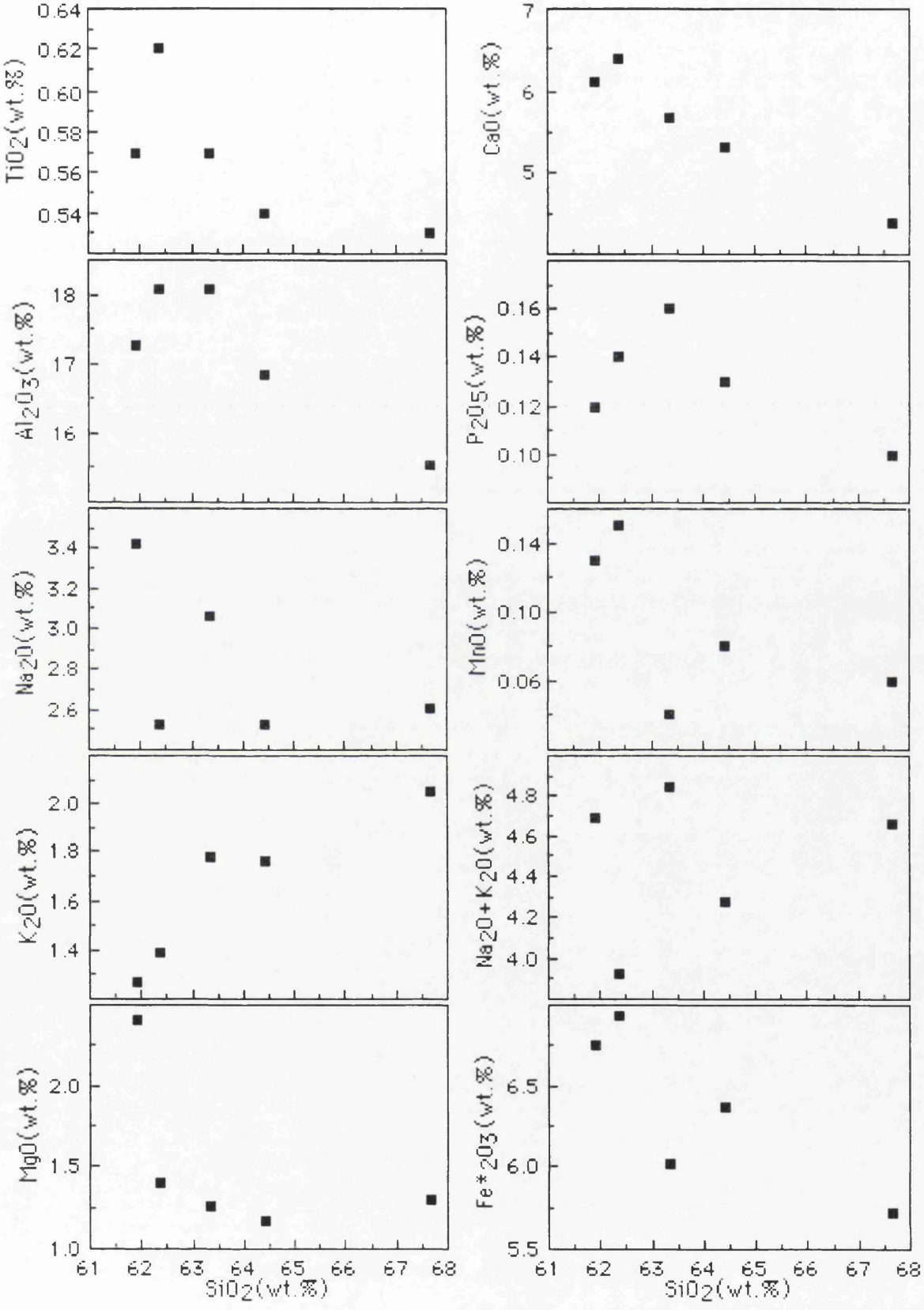

Figure 5.131. SiO_2(wt.%) versus major element plots for the agglomerate clasts.

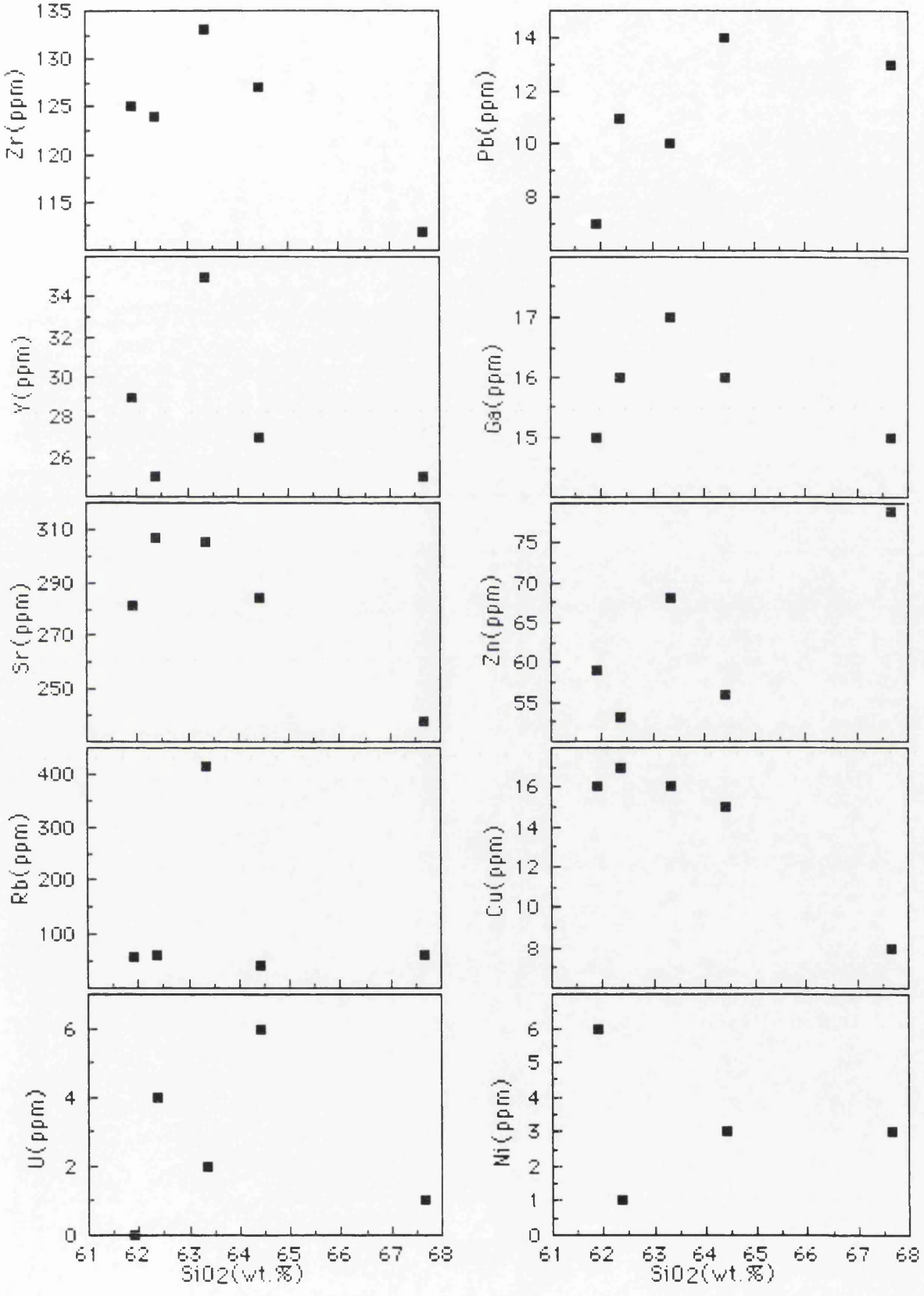

Figure 5.132. SiO_2(wt.%) versus trace element plots for the agglomerate clasts.

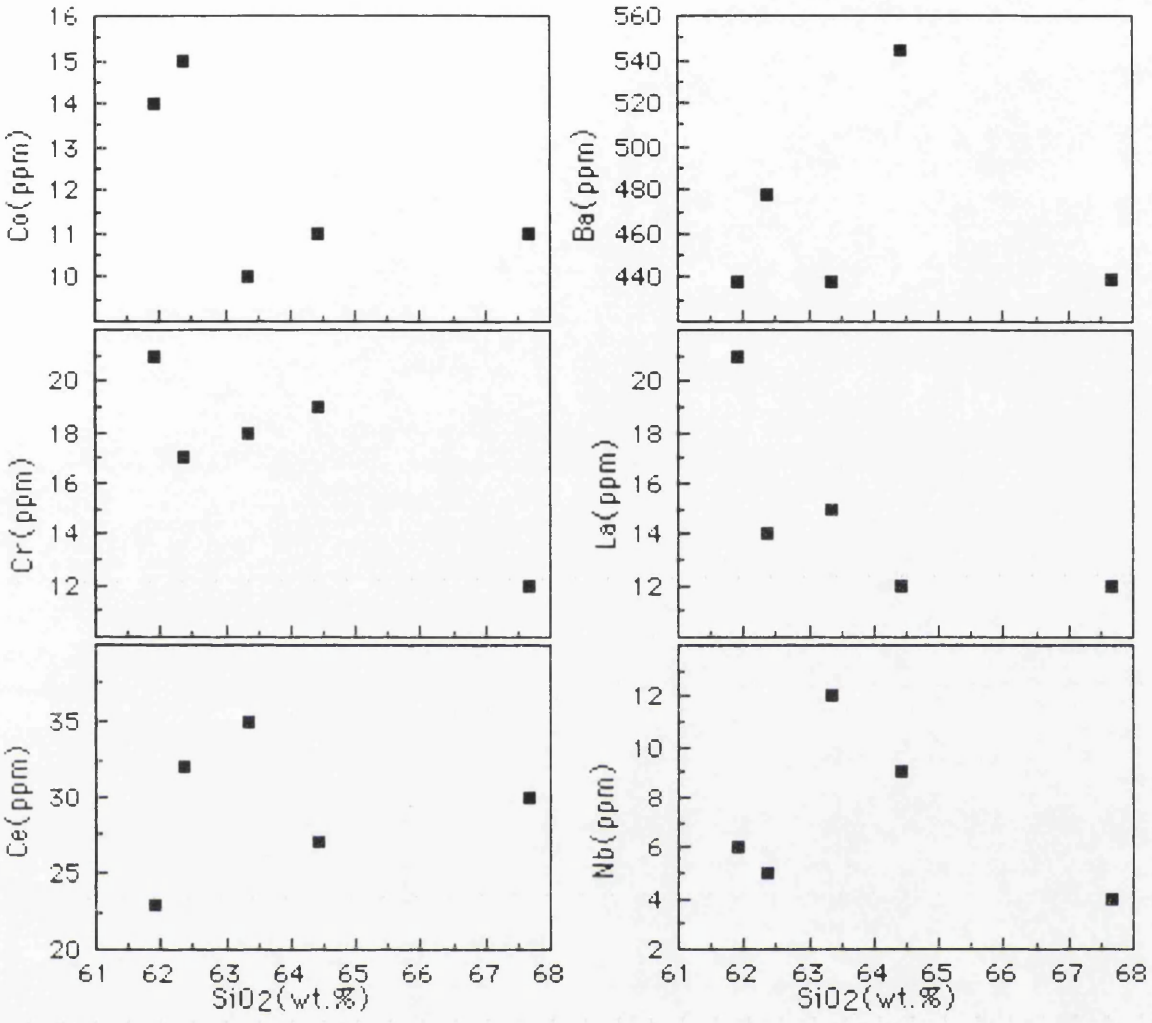

Figure 5.133. SiO_2(wt.%) versus trace element plots for the agglomerate clasts.

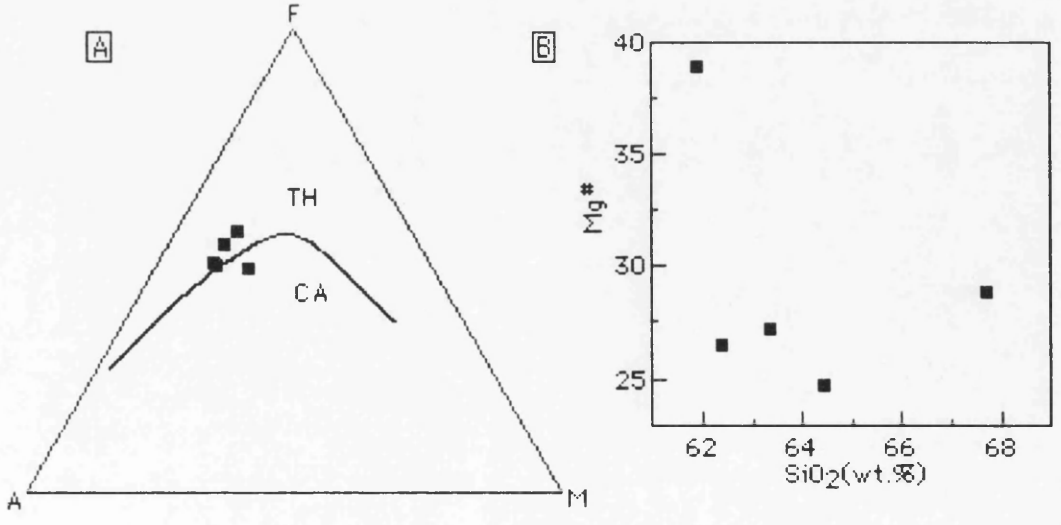

Figure 5.134. AFM plot showing the composition of the agglomerate clasts(A). The thick line separates tholeiitic(TH) and calcalkaline(CA) compositions(Irvine and Baragar, 1971). Mg-number($Mg^{\#}$=100xMg/Mg+Fe^{+2}) versus SiO_2(wt.%) plot(B).

The agglomerate clasts have low La/Y and low Nb/Y ratios compared with andesitic rocks and the Kizildere lavas(Figure 5.135). In a CaO versus Y plot(Figure 5.135), they plot on the Y-depleted side of the standard calcalkali trend of Lambert and Holland(1974). Thus, they define J-type fractionation trend that is similar to the Kizildere andesite lavas(Figure 5.135), suggesting clinopyroxene±hornblende dominated fractionation in their evolution.

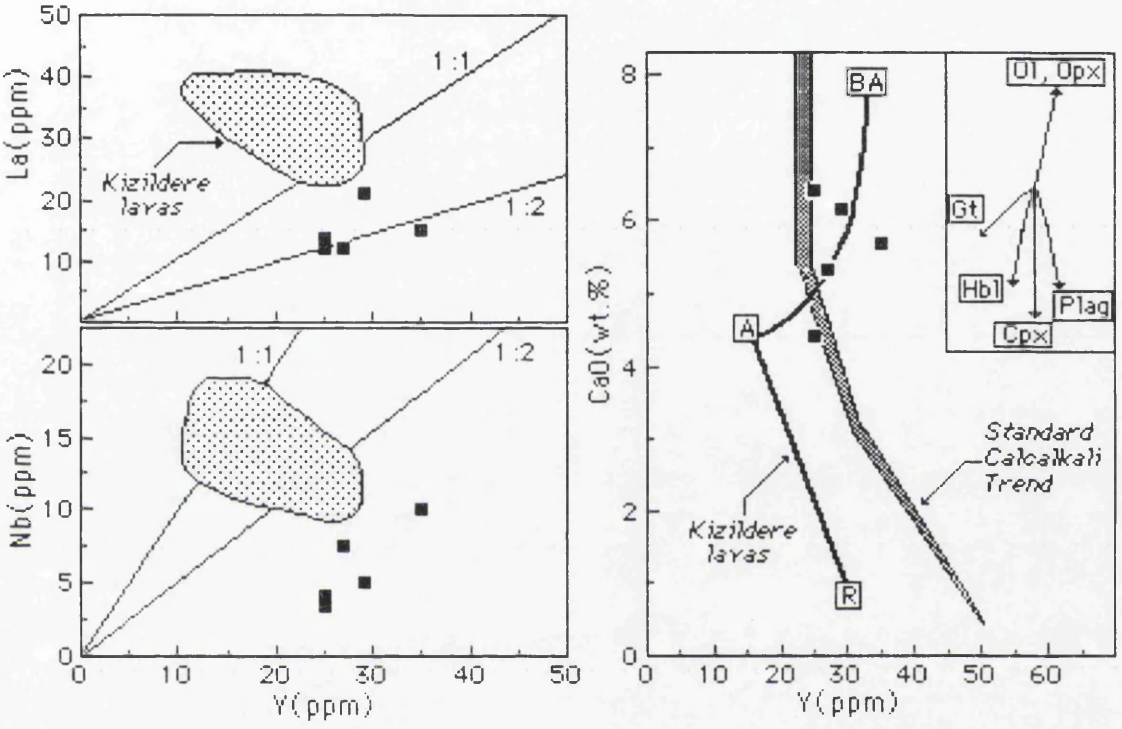

Figure 5.135. Y(ppm) versus Nb(ppm), La(ppm) and CaO(wt.%) plots for the agglomerate clasts. Shaded area represents the "standard" calcalkaline trend of Lambert and Holland(1974). The trend of the Kizildere lavas is superimposed; BA-basaltic andesite; A-andesite and R-rhyolite. The vectors show qualitative trends of the effect of fractional crystallization of common silicates.

5.3.3.6.2. INCOMPATIBLE ELEMENTS

The mid-ocean ridge basalt(MORB) and primordial mantle(PM) normalized patterns of the clasts are shown in Figures 5.136 and 5.137. Generally, the patterns are similar to each other with LILE enrichment and relatively HFSE depletion. In MORB-normalized patterns(Figure 5.136), they show characteristic negative Nb anomalies. In addition, P, Ti and slight Ba anomalies are present, presumably resulting from apatite, magnetite and plagioclase fractionation. In PM-normalized patterns(Figure 5.137), the enrichment in hydrophile elements, K, Rb and Th, relative to HFSE(Zr, Ti and Y) is well pronounced. Compared with the other andesitic rocks studied, the

agglomerate clasts display quite similar MORB- and PM-normalized patterns with enrichment in LILE and depletion in HFSE.

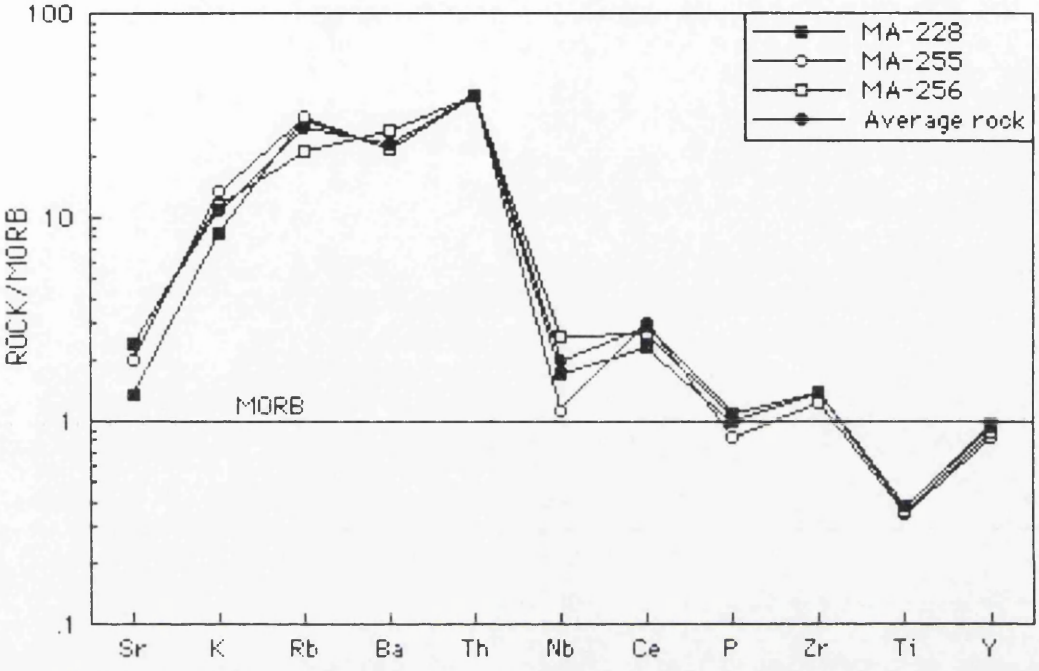

Figure 5.136. MORB-normalized trace element patterns of the agglomerate clasts(MORB normalizing values are from Pearce, 1983).

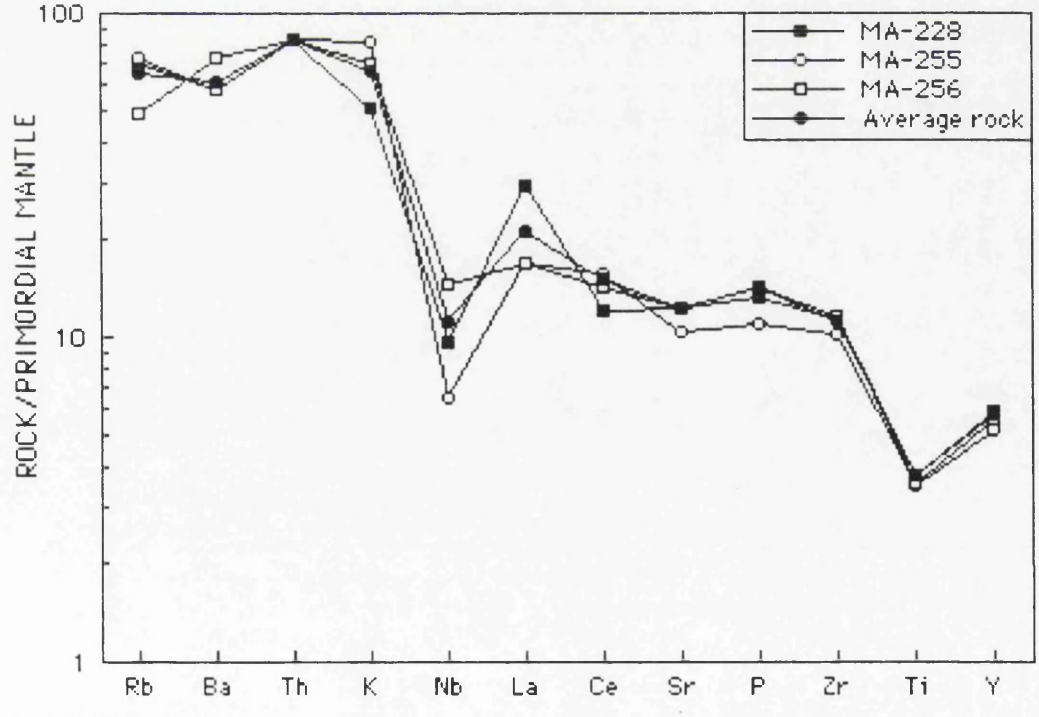

Figure 5.137. Mantle-normalized trace element patterns of the agglomerate clasts. Normalizing primordial mantle values are from Wood *et al.* (1979a).

5.3.3.6.3. RARE EARTH ELEMENTS

The REE contents of two agglomerate clasts were determined and shown in Figure 5.138. They have moderately fractionated REE patterns with $(La/Lu)_N$=5.27-6.04 and LREE enrichment and relatively flat REE patterns. The samples do not exhibit significant Eu anomalies. Sample MA-228 has a slightly negative Eu anomaly with $(Eu/Eu^*)_N$=0.94 whereas MA-256 shows a positive Eu anomaly with $(Eu/Eu^*)_N$=1.46.

In general, both samples have similar patterns but sample MA-256 displays relative depletion in MREE(Gd to Er). These REE patterns are comparable with medium-K suites(Gill, 1981). Compared with the other andesitic lavas studied, the agglomerate clasts have relatively low LREE and high HREE contents reflected by less fractionated REE patterns. The concave-up and flat HREE patterns imply important amphibole participation in the generation of the rocks. Furthermore, the flat distribution of the HREE indicates that the primary melt was not in equilibrium with a major garnet bearing-residum.

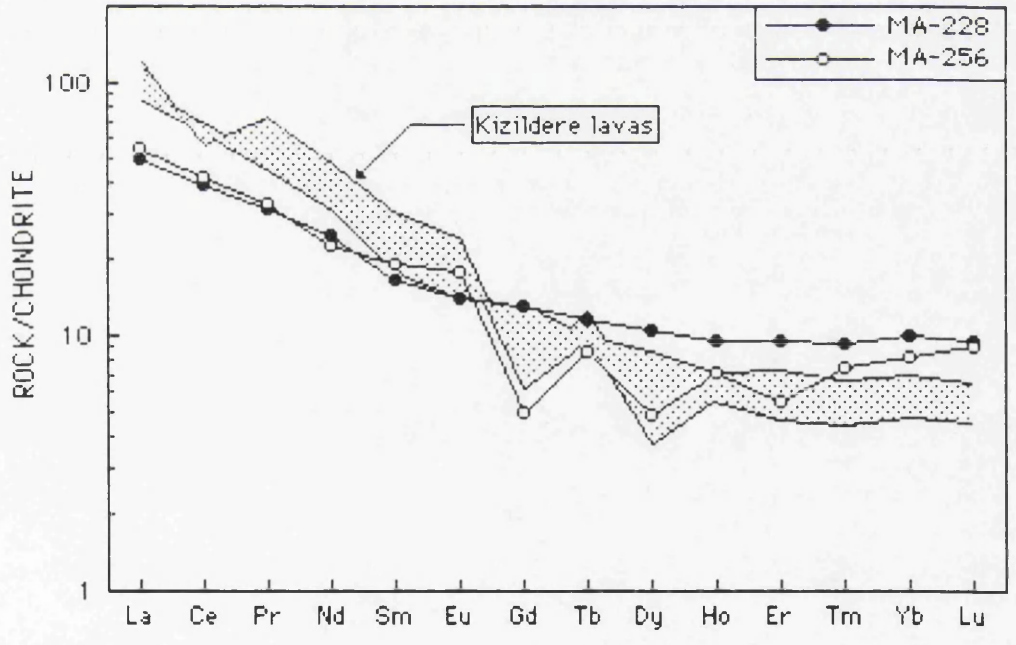

Figure 5.138. Chondrite-normalized REE patterns of the agglomerate clasts. Normalizing values are from Boynton(1984). Shaded area represents the Kizildere andesite lavas.

5.3.3.7. IGNIMBRITES

5.3.3.7.1. MAJOR AND TRACE ELEMENTS

The ignimbrites are rhyolitic to trachytic in chemical composition with 66-70 wt.% SiO_2 and normative corundum. They are high-K types according to the classification of Peccerillo and Taylor(1976) and Gill(1981). The rocks are peraluminous with high K/(K+Na+Ca) ratios. Mg-number [$Mg^{\#}=100xMg/(Mg+Fe^{+2})$] ranges from 20 to 40 and shows a negative correlation with SiO_2 content(Figure 5.139).

On variation plots(Figures 5.140, 5.141 and 5.142), Al_2O_3, MgO, CaO, P_2O_5, $Fe^*{}_2O_3$, Sr, Cu and Co decrease whereas Na_2O, Na_2O+K_2O, Zr, Y and La increase with increasing SiO_2 content. On AFM plot(Figure 5.139), the ignimbrites plot in the calcalkaline field(Irvine and Baragar, 1971) being relatively evolved and lacking of any iron enrichment.

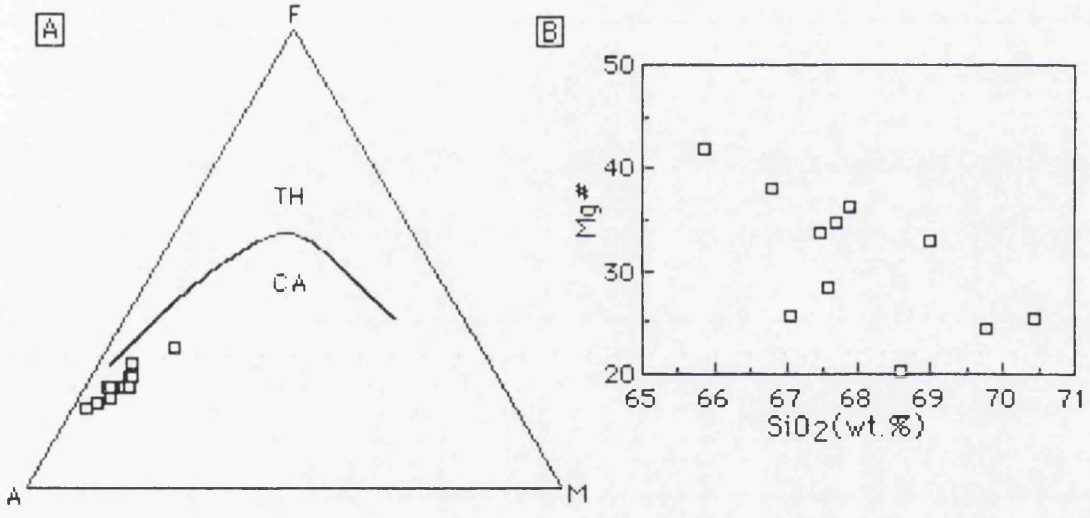

Figure 5.139. (A), AFM plot showing the composition of ignimbrites. The thick line separates tholeiitic(TH) and calcalkaline(CA) compositions(Irvine and Baragar, 1971). (B), SiO_2 versus $Mg^{\#}$(Mg-number=100xMg/Mg+Fe^{+2}) for ignimbrites.

The ignimbrites have Al_2O_3 varying from 15 to 18 wt.% reflecting the increasing proportion of feldspar components. The rocks have also high concentrations of alkalies with 6 to 11 wt.% Na_2O+K_2O. Generally, K_2O/Na_2O ratios are lower than 1. The molar ratio of Al_2O_3 to Na_2O+K_2O+CaO(A/CNK) is less than 1.2 but is also equal to or larger than 1.0. Therefore the ignimbrites are peraluminous to slightly metaluminous in composition(Figure 5.143), according to the definition of Shand(1947). In general, the rocks are not strongly peraluminous indicating that they are not the eruptive equivalents of S-type granites(e.g., White and Chapell, 1983).

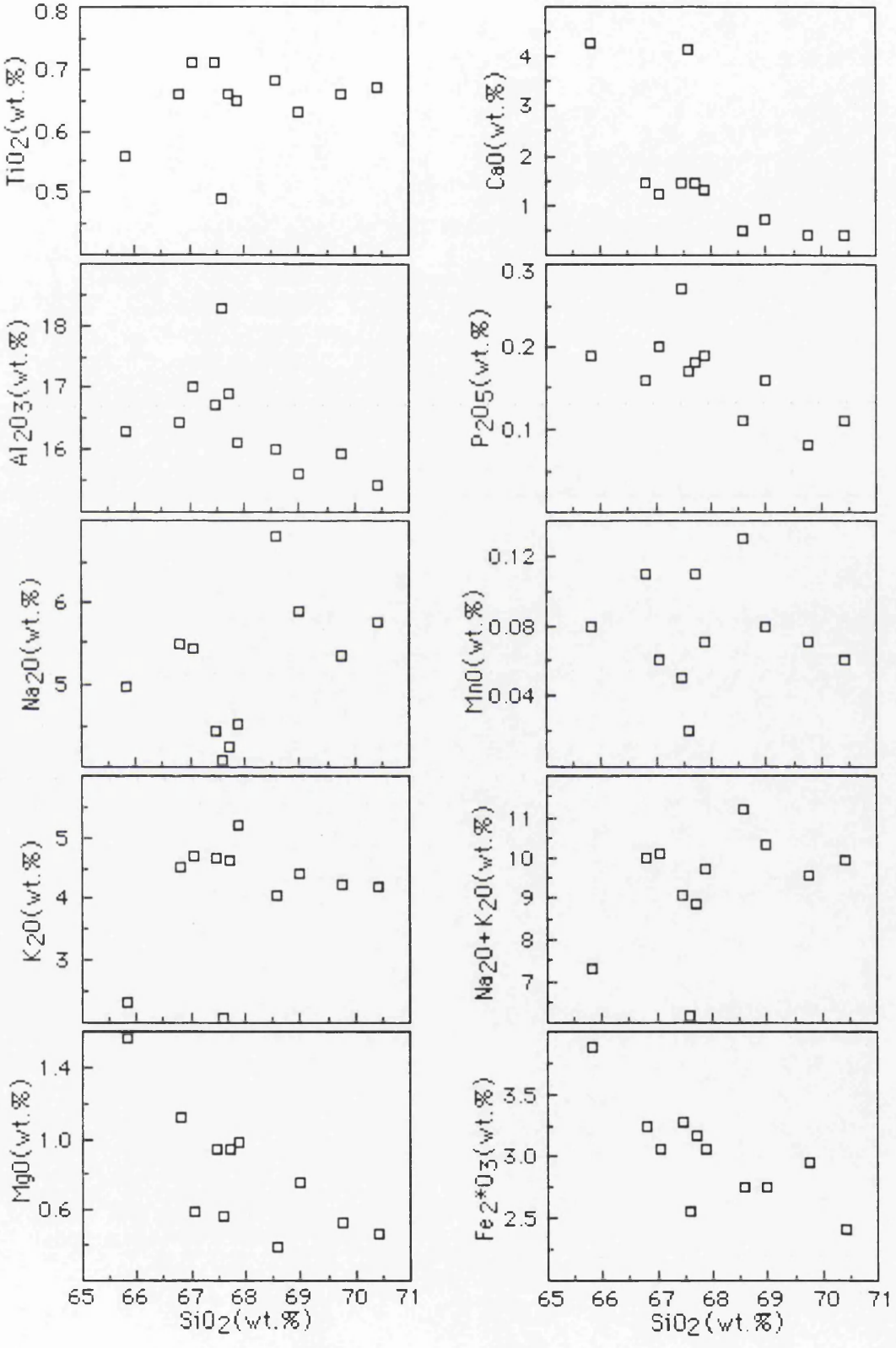

Figure 5.140. SiO_2 versus major element plots for ignimbrites.

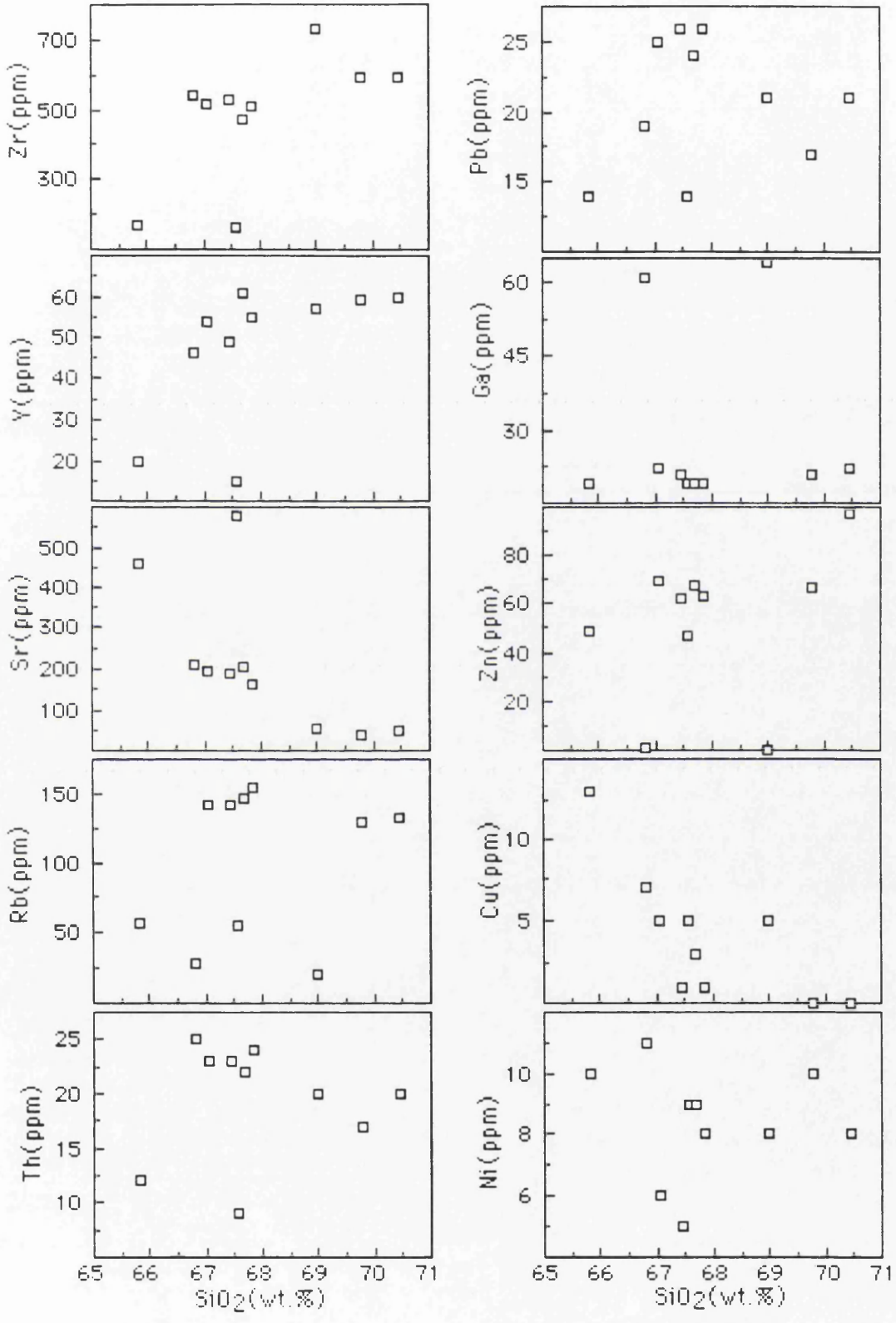

Figure 5.141. SiO_2 versus trace element plots for ignimbrites.

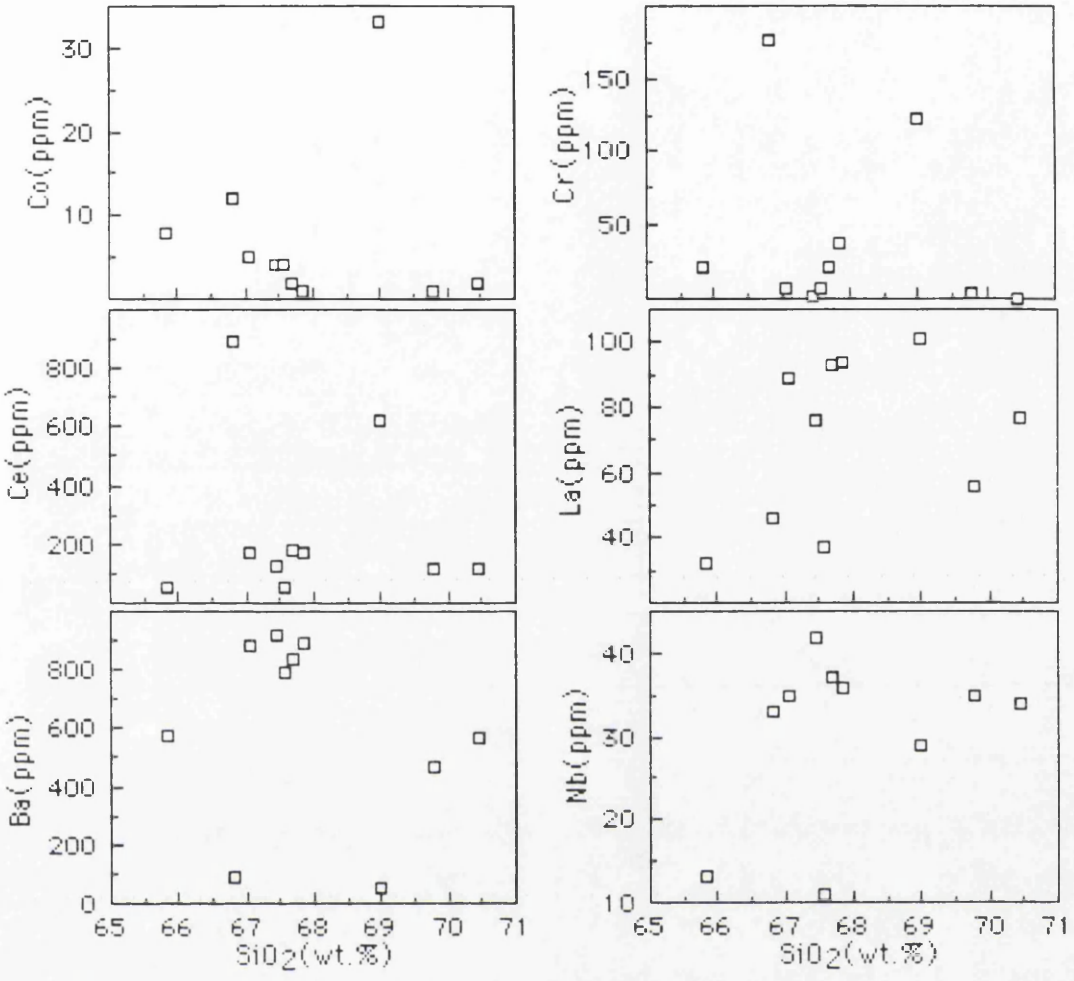

Figure 5.142. SiO_2 versus trace element plots for ignimbrites.

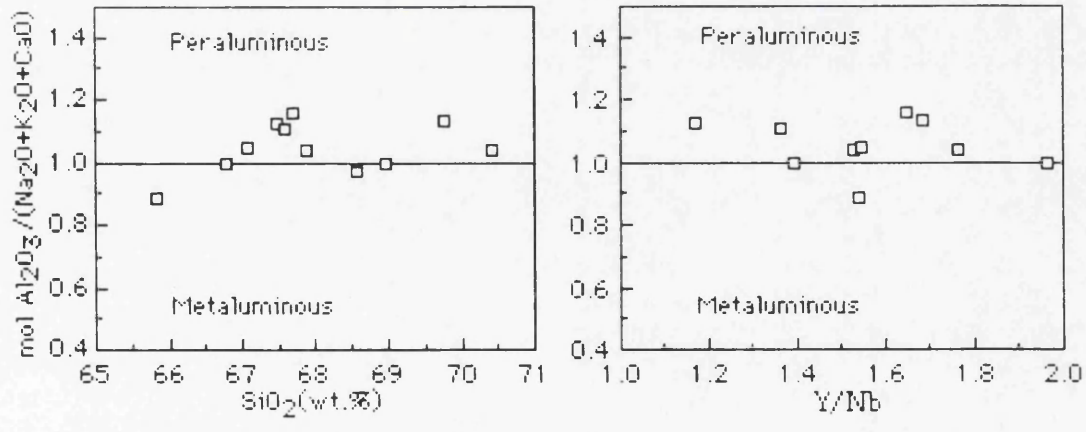

Figure 5.143. Mol $Al_2O_3/(Na_2O+K_2O+CaO)$ versus SiO_2 and Y/Nb plots.

The ignimbrites show significantly higher La/Y and Nb/Y ratios than the Gurgurbaba lavas and rhyolite dome-dykes. Lambert and Holland(1974) used CaO versus Y to define J and L type trends, which lead respectively to depletion and enrichment in Y relative to the calcalkaline series standard. In the Y versus CaO plot(Figure 5.144), the ignimbrite samples generally plot on the Y

enriched side of the standard calcalkaline trend, and suggest plagioclase controlled fractionation.

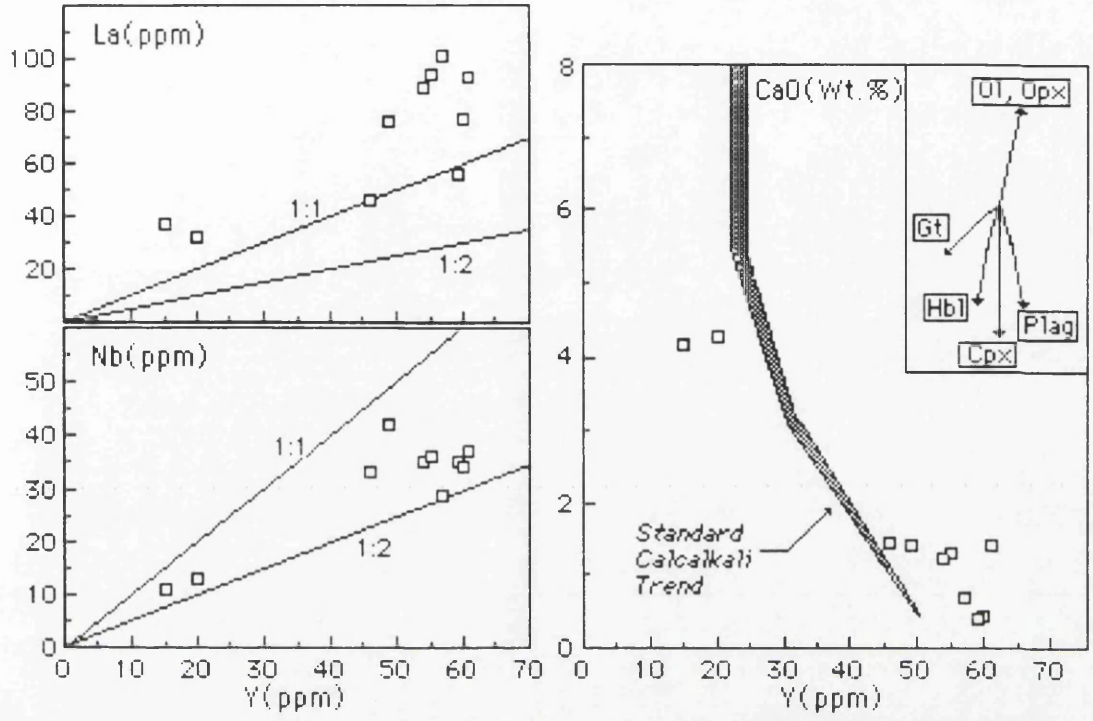

Figure 5.144. Y(ppm) versus Nb(ppm), La(ppm) and CaO(wt.%) plots for dacites. Shaded area represents the "standard" calcalkaline trend of Lambert and Holland(1974). The vectors show qualitative trends of the effect of fractional crystallization of common silicates.

Using trace element compositions, Pearce *et al.* (1984) have attempted to interpret the tectonic settings of granitic rocks. In this classification(Figure 5.145), the ignimbrites mainly plot in the WPG(within plate granites) but two samples in the field of VAG(volcanic arc granites). Although this discrimination points a certain setting, it is unlikely that these plots will provide a unique definition for the ignimbrites. Furthermore, rather than the tectonic setting existing when granitic magma was actually produced, these plots seem to diagnose the setting in which the protolith was formed(Arculus, 1987; Twist and Harmer, 1987).

The compositions of the ignimbrites are generally uniform but there is some compositional variations from early to late products. The trace elements are comparable to the Bishop Tuff(Hildreth, 1979, 1981) with generally high and covarying concentrations of Mn, Tb, Yb, Lu and Th. On the enrichment factor diagram(Figure 5.146), the ignimbrites display similar enrichment of Na, Mg, Al, P, Ca, Mn, Sr, Sm, Tb, Yb, Lu, Th to that in the Bishop Tuff but are different in respect of Si, K, Ti, Fe, Co, Rb, La, Ce, Nd, Sm, Eu. The enrichment in REE is more marked than in the Bishop Tuff.

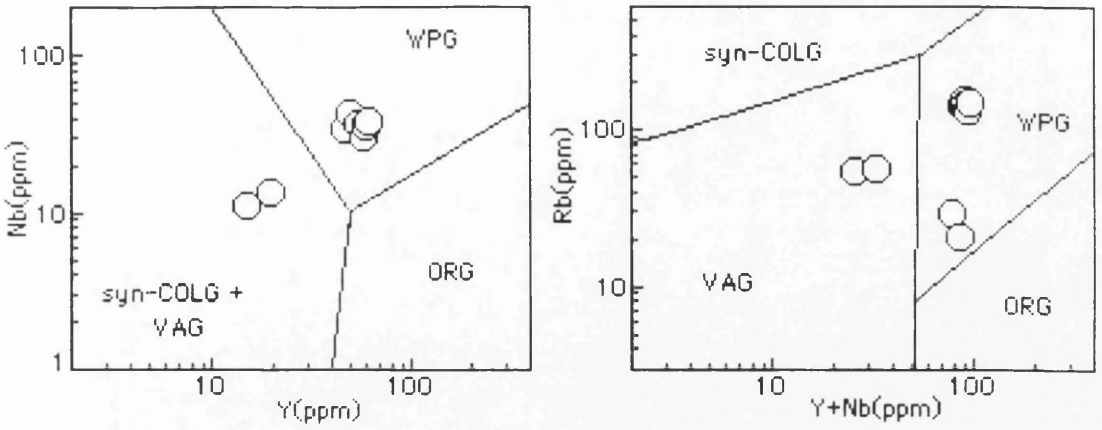

Figure 5.145. Trace element discriminant diagrams for granitic rocks(Pearce *et al.*, 1984) showing the compositions of ignimbrites. VAG=volcanic arc granites; syn-COLG=syn-collision granites; WPG=within plate granites; and ORG=ocean ridge granites.

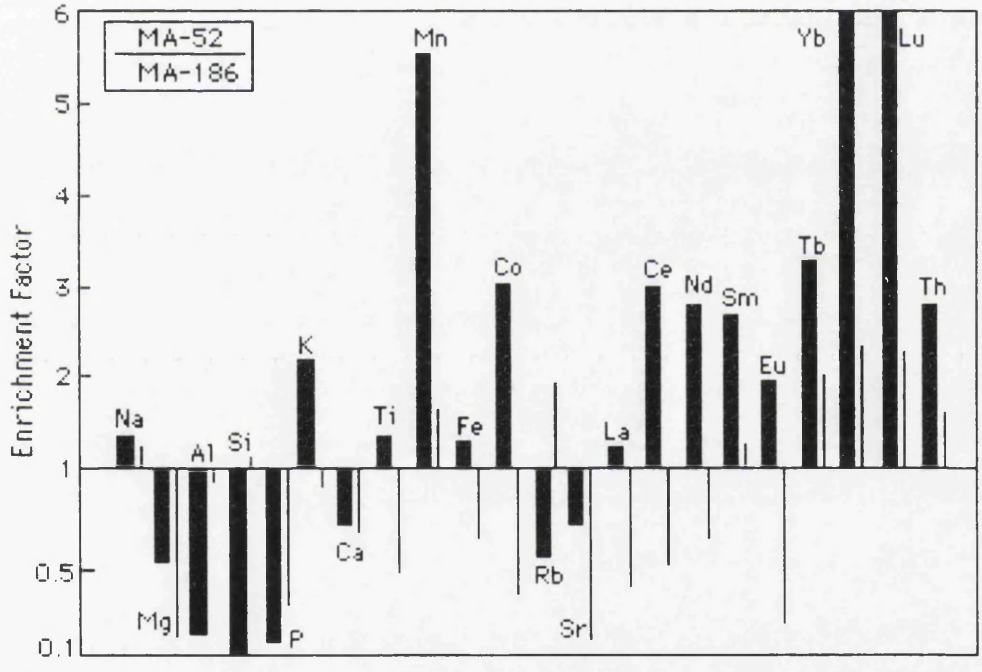

Figure 5.146. Enrichment factor diagram showing evolutionary trends in the ignimbrites, (thick lines) derived by comparing an incompatible element-rich and an incompatible element-poor sample(MA-52/MA-186). Enrichment factors for the Bishop Tuff(Hildreth, 1979, 1981) are also shown(thin lines) for comparison.

Ba, Sr and Zr show non-linear negative correlations with SiO_2 content, suggesting progressive removal of plagioclase and zircon during differentiation. K/Rb is positively correlated with SiO_2, suggesting biotite fractionation. It seems that biotite-rich samples show high Rb, and low Sr and Zr contents. Rb/Sr varies little with SiO_2 up to about 68 % SiO_2 then increases

exponentially to the high silica types(Figure 5.147). The TiO_2 versus Zr plot also exhibits a non-linear trend but the positive correlation between these elements(Figure 5.147) shows that biotite, ilmenite and zircon all behaved similarly, suggesting fractionation of biotite with zircon and ilmenite. The biotite-rich samples have high TiO_2, suggesting concentration of ilmenite as a free phase as well. Since Rb partitions strongly into mica relative to alkali feldspar or silicate melt(Arth, 1976; Long, 1978) the low K/Rb ratio of the biotite rich samples(a biotite plagioclase accumulation) is expected.

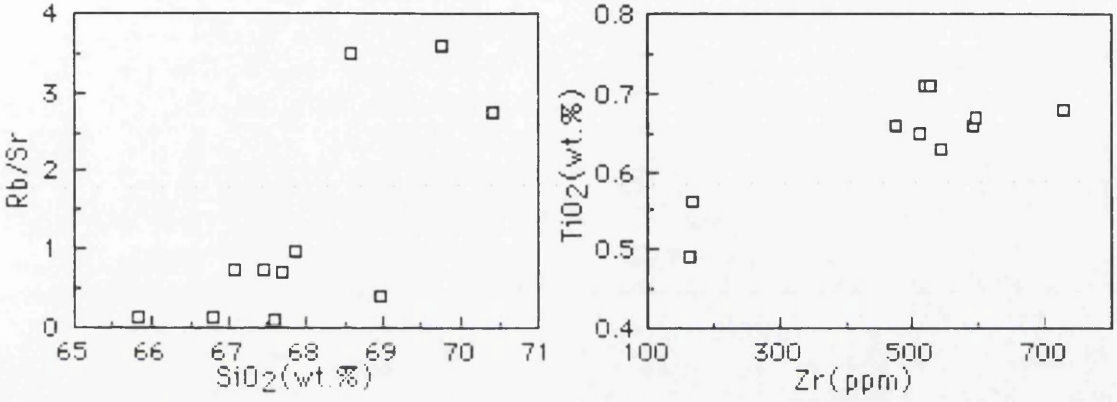

Figure 5.147. SiO_2 versus Rb/Sr, and Zr versus TiO_2 variation plots. Note the markedly non-linear variations that contrast with the linear trends described for granitoid suites(e.g., Chappell, 1978).

5.3.3.7.2. INCOMPATIBLE ELEMENTS

The ignimbrites show similar MORB and PM-normalized patterns(Figures 5.148 and 5.149). They are characterized by enrichment in all elements from Sr to Y(Figure 5.148). In some elements(e.g., Sr, Ba, P, Ti) a negative anomaly is seen and the low Rb and Sr ratio of sample MA-57 is marked on the patterns. The negative anomalies shown by Ti and P may reflect Fe-Ti oxide and apatite fractionation. In addition, the rocks have characteristic Nb patterns, negative and progressively increasing anomalies similar to subduction related lavas(Pearce, 1983). Therefore, the depletion of Nb relative to the adjacent LIL elements suggests a minor subduction component in the source of the rocks.

The trace element characteristics of two ignimbrite samples are also shown in the spider diagram in Figure 5.150, normalized to ORG(Ocean-Ridge Granite) composition(Pearce *et al.*, 1984). The samples have similar patterns and progressively enriched concentrations for HFSE and the REE but LILE give slightly different pattern. Generally, the samples have low concentrations of HFSE and the REE being depleted relative to ORG. This is the most pronounced in the case of Sm, Y and Yb.

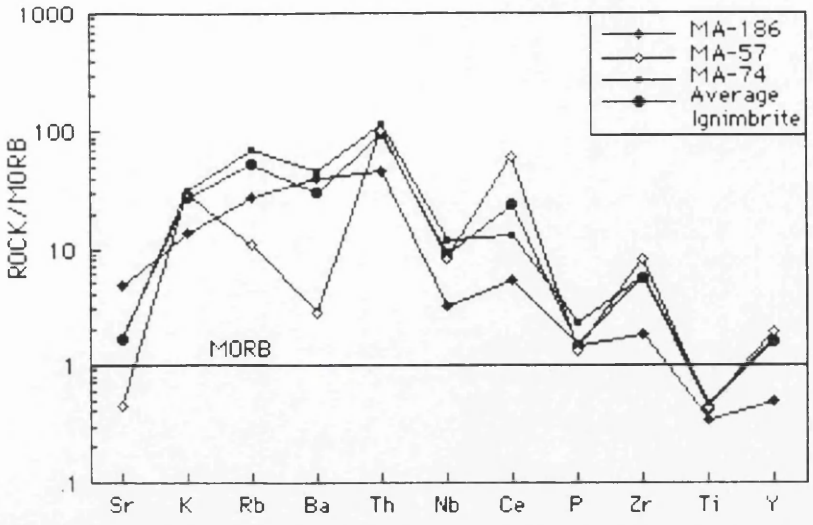

Figure 5.148. MORB-normalized trace element patterns of ignimbrites(MORB normalizing values are from Pearce, 1983).

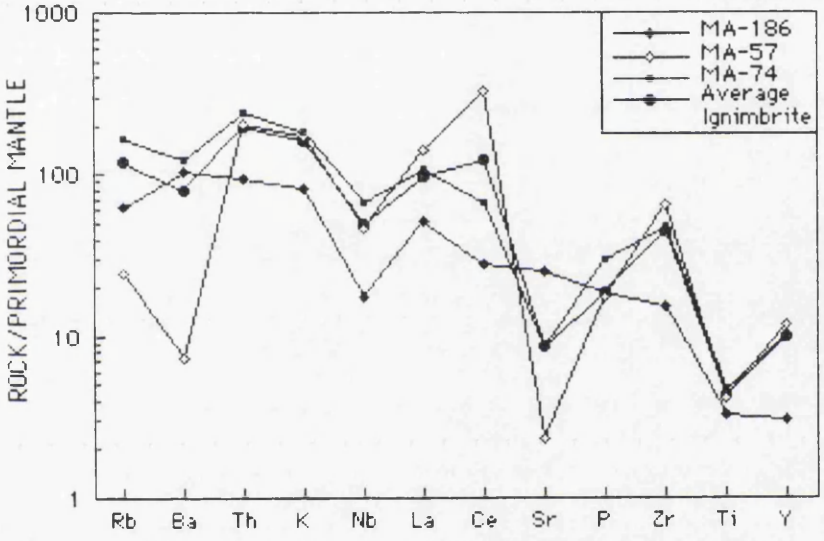

Figure 5.149. Mantle-normalized trace element patterns of ignimbrites. Normalizing primordial mantle values are from Wood *et al.* (1979a).

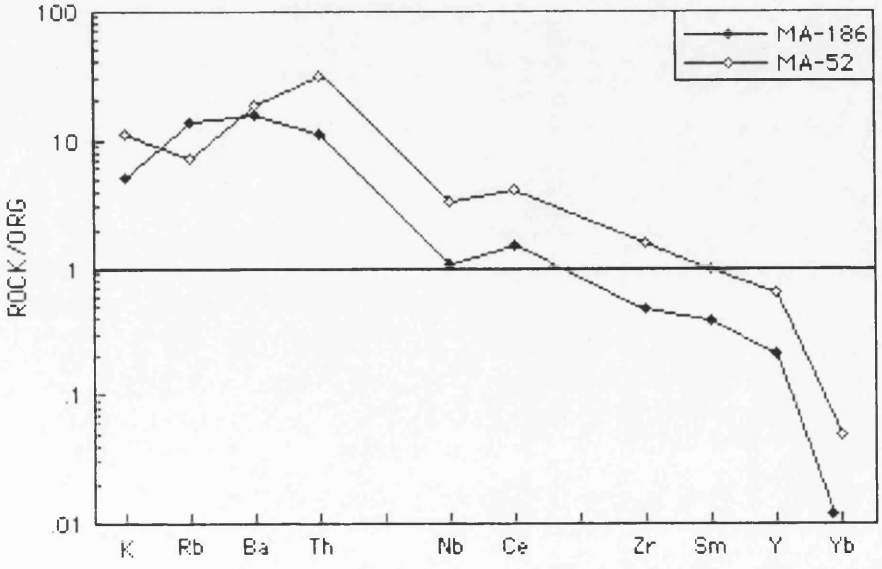

Figure 5.150. Geochemical patterns of ignimbrites normalized to Ocean Ridge Granite(ORG; Pearce *et al.*, 1984) composition.

5.3.3.7.3. RARE EARTH ELEMENTS

The REE patterns of the ignimbrites are shown in Figure 5.151. The rocks generally display LREE enriched and relatively flat HREE patterns with $(La/Lu)_N$=13.73-35.46. LREE concentrations are between 200 and 100 times chondrite values. They show progressive enrichment of all REE with increasing SiO_2 content. Sample MA-186(SiO_2=66wt.%) exhibits slightly steep pattern with $(La/Lu)_N$=35.46 and low LREE enrichment relative to the other samples. All samples, except sample MA-186, have slight negative Eu anomalies with $(Eu/Eu^*)_N$=0.77-0.79, indicating minor plagioclase control in the fractionation. The presence and absence of the Eu anomalies in the granitic rocks usually are related to the amount of equilibration of the magma with plagioclase(Cullers and Graf, 1984).

The REE contents of the ignimbrites are compared with Lower and Upper Continental Crust(Taylor and McLennan, 1985). Compared with Lower Continental Crust, ignimbrites display high LREE enrichment and moderate HREE enrichment. They have REE contents close to Upper continental crust values, suggesting that they are more likely derived from upper continental crust.

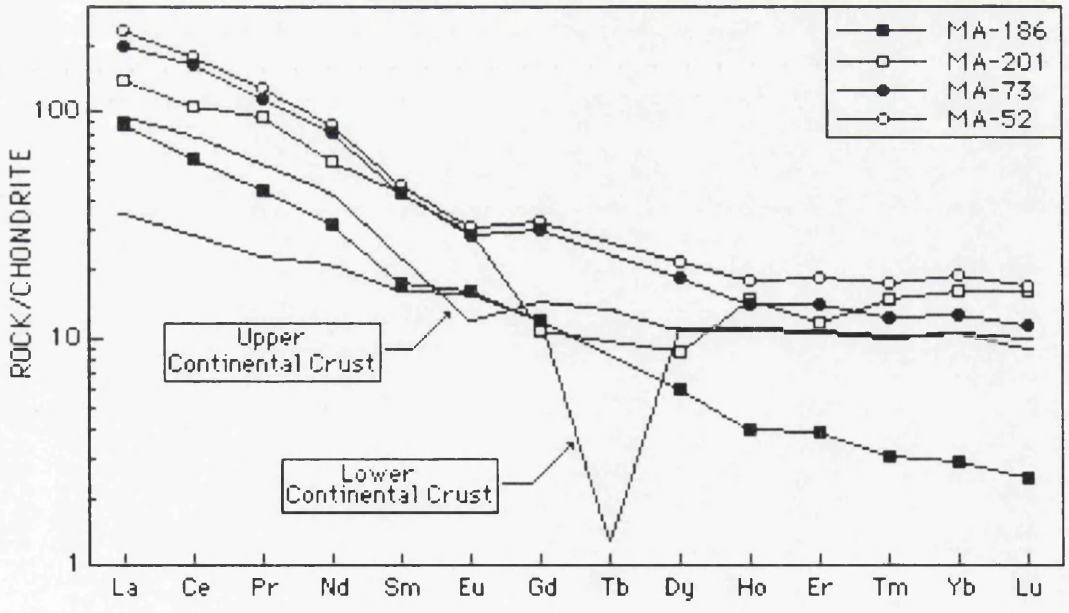

Figure 5.151. Chondrite-normalized REE patterns of ignimbrites. Normalizing values are from Boynton(1984) and Lower and Upper Continental Crust from(Taylor and McLennan, 1985).

5.3.3.8. RHYOLITE DOME AND DYKES

5.3.3.8.1. MAJOR AND TRACE ELEMENTS

The dome and dykes are low silica rhyolites(68.5 to 72.5 wt.% SiO_2) with Mg-numbers from 38.60 to 43.46(Figure 5.152), and characterized by a narrow range of major and trace element contents. They are typically high-K rhyolites according to the classification of Peccerillo and Taylor(1976) and Gill(1981). Generally, they have also high Al_2O_3 and alkalies and low FeO*, MgO, CaO and TiO_2. These characteristics are similar to those of the Gurgurbaba lava, and rhyolites of continental arcs(e.g., Ewart, 1979; Hildreth and Moorbath, 1988). The chemical composition of the dome and dykes lie within the low silica samples of the Gurgurbaba lavas, implying that are related to each other. The rocks do not show any iron enrichment and plot in the calcalkaline field on AFM plot(Figure 5.152).

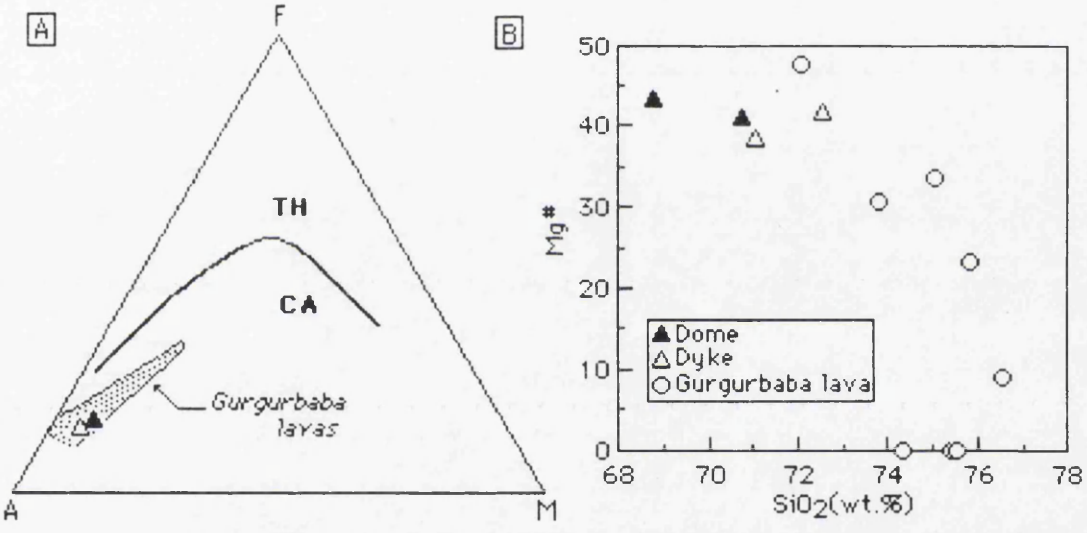

Figure 5.152. (A), AFM plot showing the composition of dome and dykes. Gurgurbaba lavas(shaded area) are also shown for comparison. The thick line separates tholeiitic(TH) and calcalkaline(CA) compositions(Irvine and Baragar, 1971). (B), Mg-number($Mg^{\#}$=mol 100xMg/(Mg+Fe^{+2})) versus SiO_2 variation plot.

The rocks are generally not oxidized(Fe_2O_3/FeO<2) and not extensively hydrated(LOI<2.65 wt.%). The concentrations of CaO(<2 wt.%), FeO*(<2.1 wt.%), MgO(<0.90 wt.%), TiO_2(<0.42 wt.%) and P_2O_5(<0.10 wt.%) in the rocks are relatively low, similar to those of low silica rhyolites. Although the data are limited, variation plots for both the rhyolite dome and dykes show fair correlations with some of major and trace elements. In the rhyolite dome, TiO_2, Al_2O_3, Na_2O, K_2O, P_2O_5, FeO*, Zr, Y, Rb, Th, Pb, Ga, Ce, La and Nb increase whereas CaO, MnO, MgO, Sr, Co, Cr and Ba decrease, and Rb, Zn and Ni are relatively constant with increasing SiO_2(Figure 5.153, 5.154 and 5.155).

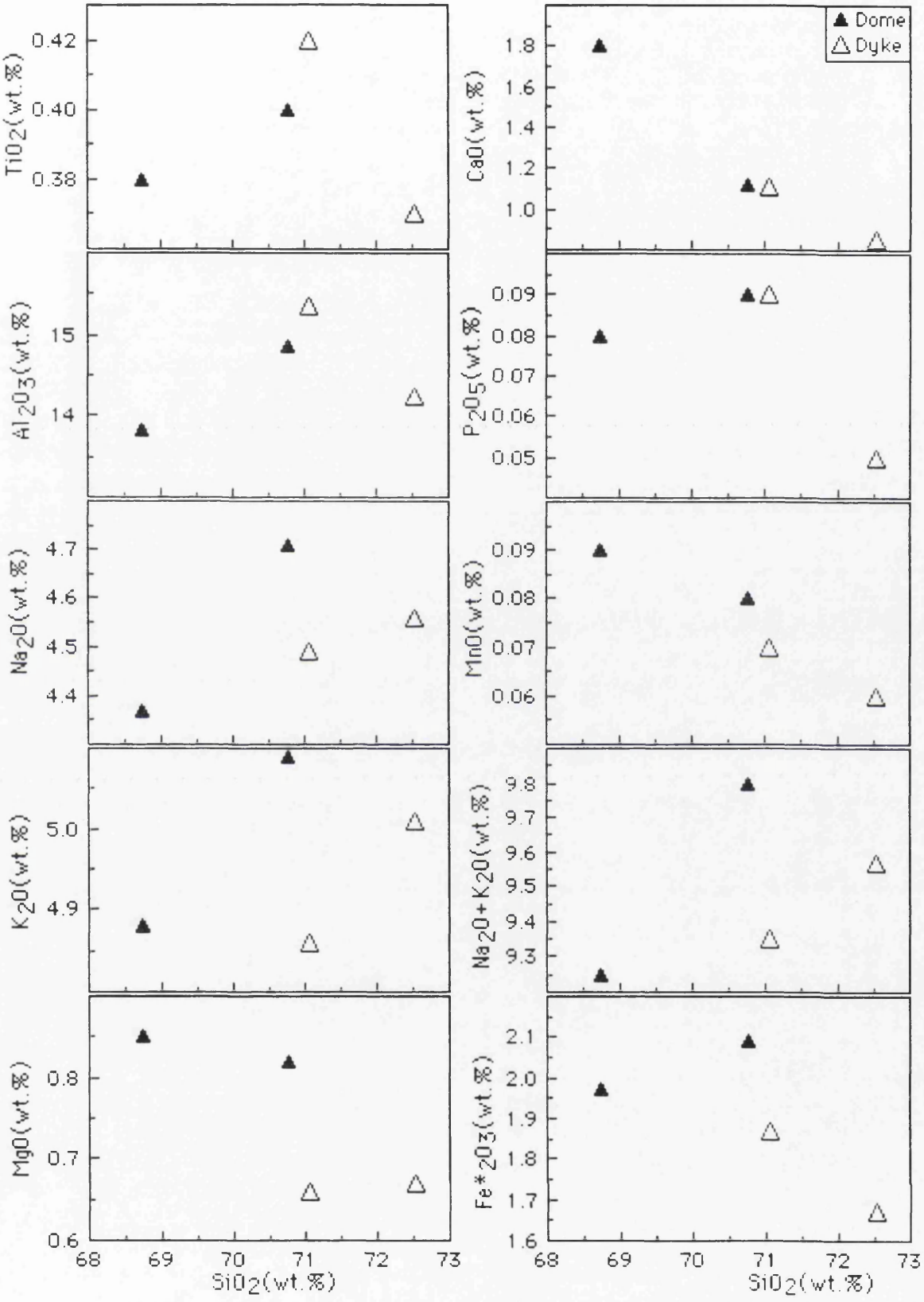

Figure 5.153. SiO_2(wt.%) versus major element plots for the rhyolite dome and dykes.

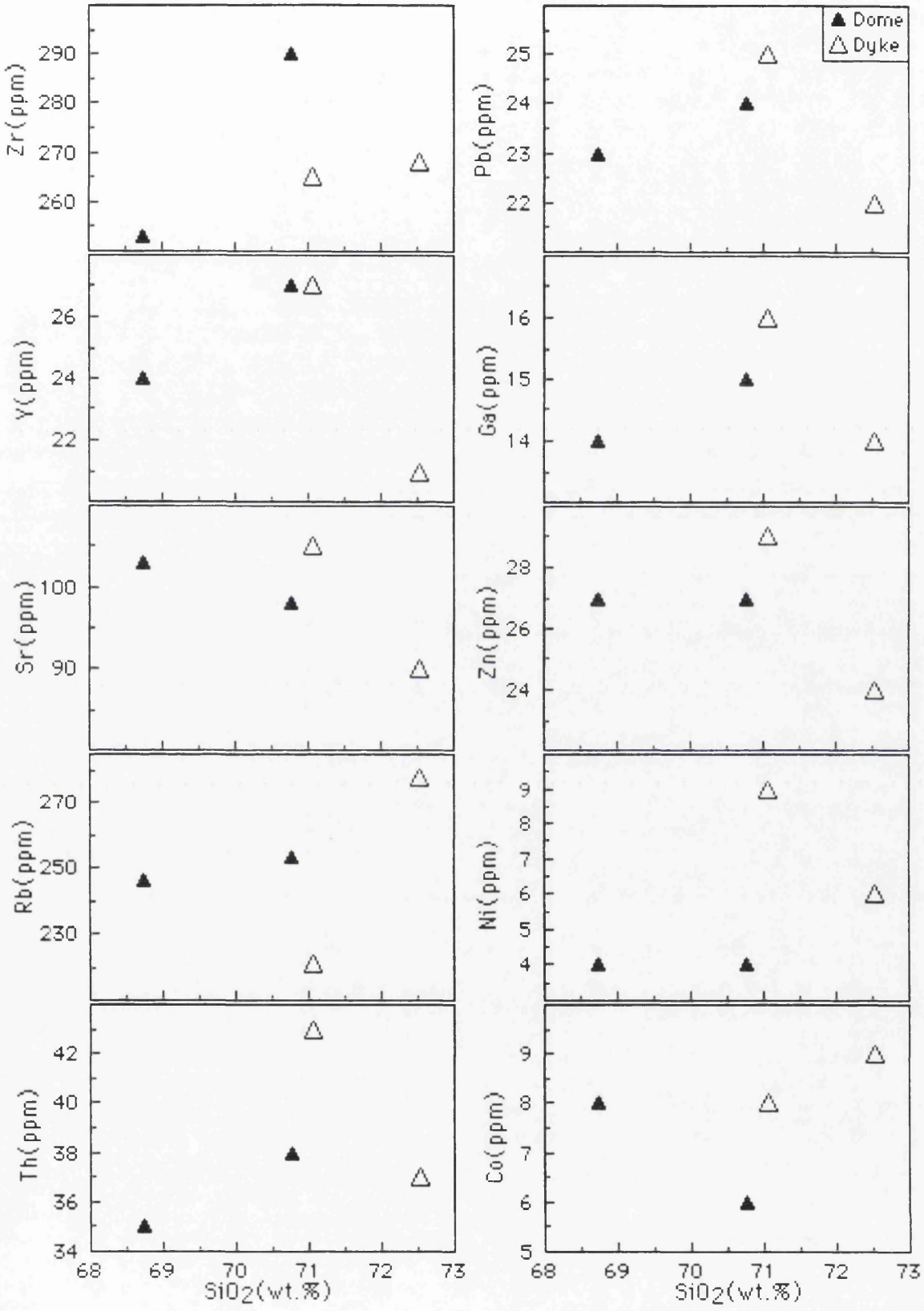

Figure 5.154. SiO_2(wt.%) versus trace elements plots for the rhyolite dome and dykes.

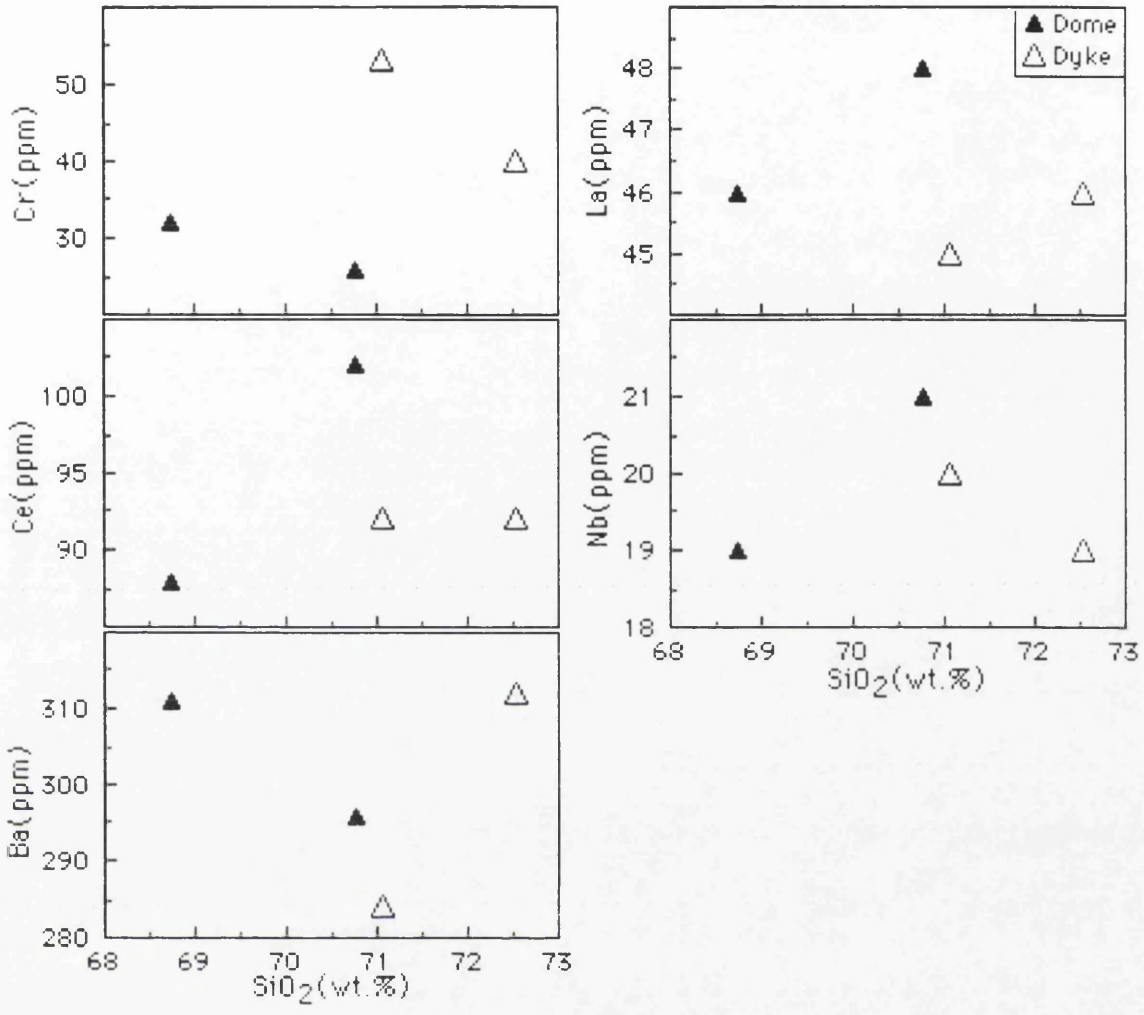

Figure 5.155. SiO_2(wt.%) versus trace elements plots for the rhyolite dome and dykes.

However, Na_2O, K_2O, Zr, Rb, Co, Ba and La increase whereas TiO_2, Al_2O_3, CaO, P_2O_5, MnO, FeO*, Y, Sr, Th, Pb, Ga, Zn, Ni, Cr and Nb decrease with increasing SiO_2 in the rhyolite dykes(Figure 5.153, 5.154 and 5.155). These compositional variations can be explained by fractionation of plagioclase, hornblende, Fe-Ti oxides and apatite. The trend toward low-Ti composition in the dykes may result from accumulation of phenocrysts assemblages without Fe-Ti oxides, whereas the trend to high-Ti composition in the dome probably result from accumulation of assemblages including Fe-Ti oxides, in general precipitated from more fractionated magma(Pearce and Norry, 1979).

The rhyolite dome and dykes have generally low Fe/Mg ratios(Figure 5.156). On a CaO versus FeO_t plot(Figure 5.156), they fall close to the boundary line which separates high-Fe types from low-Fe ones(Warshaw and Smith, 1988). It is suggested that rocks plotting close this line usually crystallize orthopyroxene±biotite and hornblende, and are usually metaluminous(Warshaw and Smith, 1988).

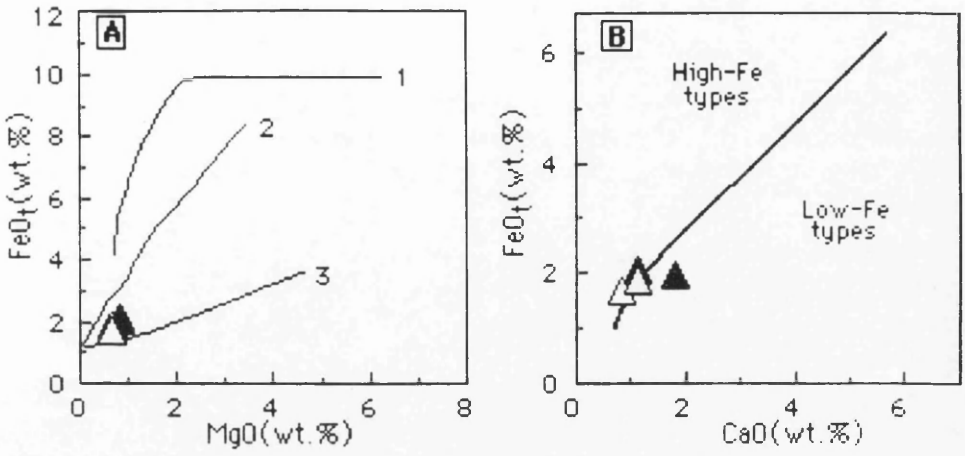

Figure 5.156. (A), FeO_t(total iron as Fe_2O_3) versus MgO for the rhyolite dome(solid triangles) and dykes(open triangles). The trends of experimentally produced melts at 1kb(fH_2O=0.67, G-CH buffer) from a Kilauea basalt(Spulger and Rutherford, 1983) and at 5 kb H_2O from an olivine tholeiite at the FMQ and HM buffers(Helz, 1976) are shown for comparison(nos, 1, 2, 3 respectively); (B), total iron(as Fe_2O_3) versus CaO plot. Thick line separates high-Fe types from low-Fe ones(Warshaw and Smith, 1988).

The dome and dykes have high La/Y and Nb/Y ratios relative to the Gurgurbaba lavas(Figure 5.157). In the Y versus CaO plot(Figure 5.157), they plot clearly on the Y depleted side of the standard calcalkaline trend defined by Lambert and Holland(1974). They are depleted in Y relative to the Gurgurbaba lava, and tend to define a J-type trend, suggesting hornblende controlled fractionation.

Zr can be used as a useful fractionation index because of its highly residual behaviour in silicic melts(Barberi *et al.*, 1975; Baker *et al.*, 1977). Zr versus compatible element(Co, Cr and Ni) and incompatible element(Y) plots suggest that the dome and dykes followed fractionation paths similar to the Gurgurbaba lava(Figure 5.158). However, the Zr versus Y plot implies that hornblende±cpx played a significant role in the evolution of the dome and dykes, relative to the Gurgurbaba lava.

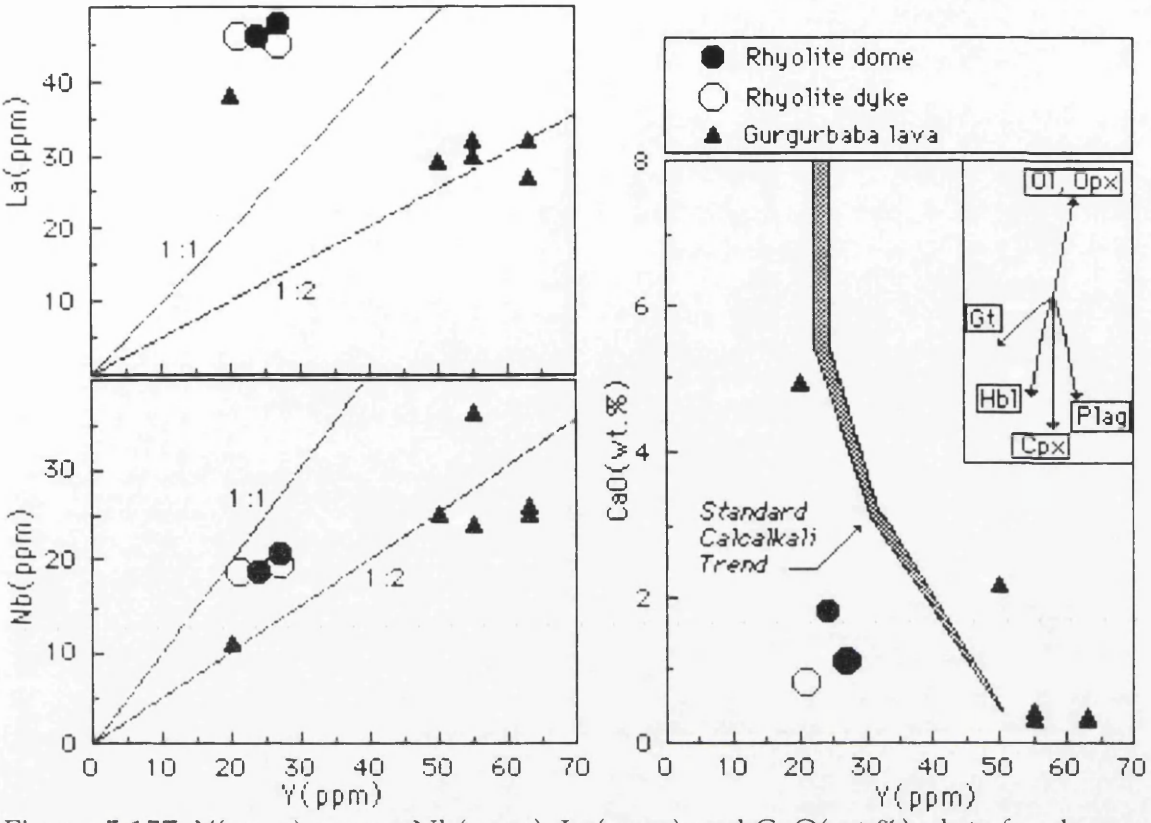

Figure 5.157. Y(ppm) versus Nb(ppm), La(ppm) and CaO(wt.%) plots for dome and dykes. Shaded area represents the "standard" calcalkaline trend of Lambert and Holland(1974). The Gurgurbaba lavas are also shown for comparison. The vectors show qualitative trends of the effect of fractional crystallization of common silicates.

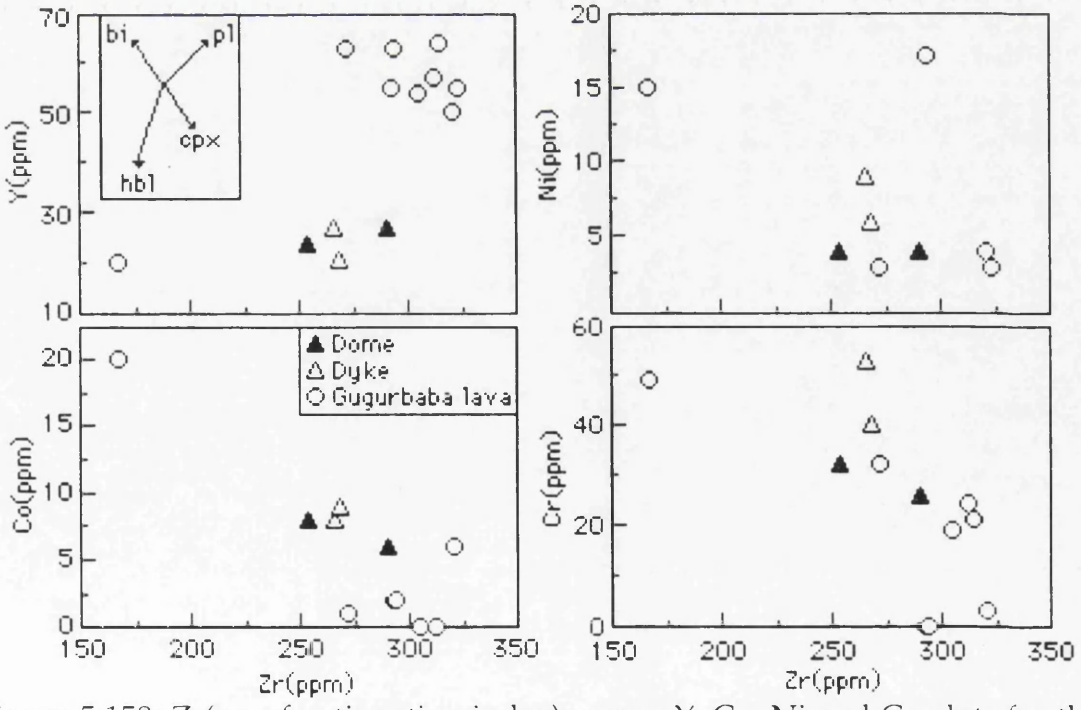

Figure 5.158. Zr(as a fractionation index) versus Y, Co, Ni and Cr plots for the rhyolite dome and dykes. The Gurgurbaba lavas are superimposed for comparison. The fractionation vectors were calculated from K_D values of Pearce and Norry(1979).

Generally, the major element composition of the rocks is quite restricted. Silica contents vary little with fractionation trend. As a result silica concentrations are a poor indicator of the chemical variability of the rocks. The low silica content may be interpreted as the result of crystallization near the minimum in the granite system(e.g., Christiansen *et al.*, 1984). In addition, Manning(1981) showed that the stability field for quartz expands with increasing fluorine content in a water-saturated haplogranite system at 1 kb pressure. Therefore, it is possible that enchanced quartz fractionation could lead to a reversal of normal SiO_2 enrichment during fractional crystallization of a fluorine-rich rhyolite(Christiansen *et al.*, 1986). The great variability among the felsic rocks can best be illustrated in a triangular diagram showing the normative constituents Q, Ab and Or. As seen on the plot(Figure 5.159), the rocks are relatively poor in normative quartz and contain normative albite and orthoclase, and plot close to a possible path of fractionation determined at 2 kb(Tuttle and Bowen, 1958; Luth *et al.*, 1964; Whitney, 1975). Such Ab-rich compositions may reflect the combined effects of Al, Fe, Li, B and H_2O on phase relations and compositions of residual liquids in the Q-Or-Ab system(Pichavant *et al.*, 1987a).

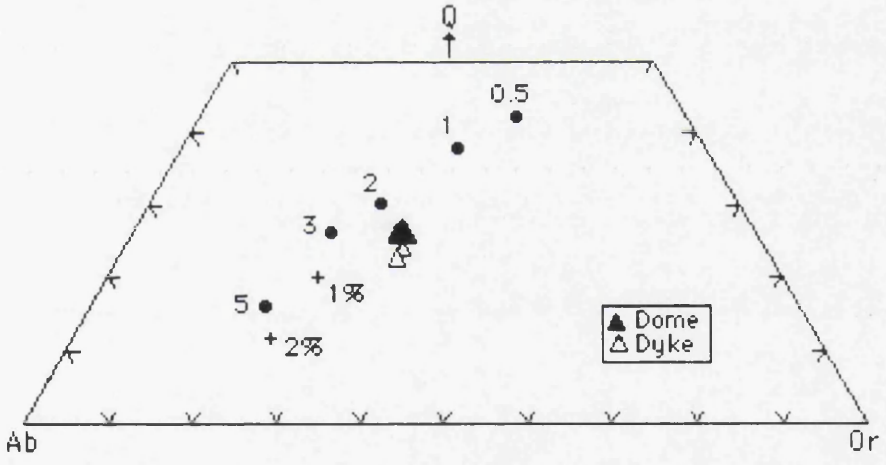

Figure 5.159. Normative composition of rhyolite dome and dykes in terms of quartz(Q), albite(Ab), and orthoclase(Or) compared to experimentally determined ternary minima in: 1) the hydrous granite system at pressures given in kb(P_{H_2O}) next to the filled circles(Tuttle and Bowen, 1958; Luth *et al.*, 1964; and Whitney, 1975); and 2) the F-bearing granite system at 1 kb(Manning, 1981). The numbers next to the crosses indicate weight % F in the water-saturated system at 1 kb.

The rocks have relatively high Al_2O_3 contents(13.75-15.50 wt.%). Such high Al_2O_3 is found in low silica rhyolites, reflecting the increased feldspar proportion. The molar ratio of Al_2O_3 to $CaO+Na_2O+K_2O$(A/CNK) is less than 1.1 but generally close to 1.0. Therefore the dome and dykes are metaluminous

in composition(Figure 5.160), implying that they are not the eruptive equivalents of S-type granites(e.g., White and Chappell, 1983). In addition, the agpaiitic index(AI=mol Na+K/Al) is less than 1 for both dome(AI=0.89-0.91) and dykes(AI=0.82-0.91), showing that they are not peralkaline or alkaline rhyolites(e.g., Streckeisen, 1979). The rocks are similar to that of I-type granitic rocks which are free of normative corundum and are in theory derived by fractional crystallization or remelting of basaltic parents(Chappell and White, 1974). I-type granitic rocks also have A/CNK ratios less than 1.1(Chappell and White, 1992). Barbarin(1990) suggested that granitic rocks with A/CNK generally less than 1.1 and FeO*/(FeO+MgO) less than 0.8 represent petrogenetically "hybrid continental groups". Accordingly, the rhyolite dome and dyke may have been derived as a hybrid of the mantle and crustal sources, a topic later investigated with Sr isotopes.

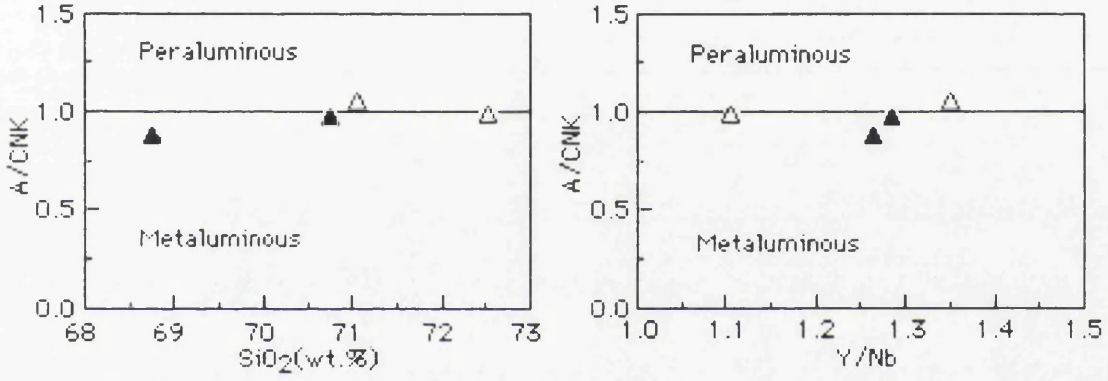

Figure 5.160. A/CNK(=mol $Al_2O_3/CaO+Na_2O+K_2O$) versus SiO_2 and Y/Nb plots of the dome(solid triangle) and dykes(open triangle) indicating the metaluminous character of rhyolite dome and dykes.

Rb abundances in the rhyolite dome and dykes are between 220 and 280 ppm which are slightly low compared with those of silicic magmas thought to have formed by crustal partial melting(Vidal *et al.*, 1982; Pichavant and Montel, 1988). Partial melting of most crustal rocks would be rhyolitic to dacitic in composition(Wyllie, 1977). Green and Pearson(1986a) showed that most crustal melting would be buffered at low TiO_2 contents by refractory Ti-rich phases, producing partial melts having ~1 wt.% TiO_2 at 60 wt.% SiO_2, or perhaps more important, <0.5 wt.% TiO_2 in rhyolitic extracts. Furthermore, rutile, ilmenite, sphene, titanomagnetite and Ti-bearing amphibole and garnet could all provide Ti-Nb-Ta sinks during partial melting of heterogeneous lower crustal rocks.

The trace element data for the rhyolite dome and dykes are plotted on the discrimination diagrams for granitic rocks developed by Pearce *et al.* (1984). On the Y versus Nb plot(Figure 5.161), the rhyolite dome and dykes fall in the syn-COLG(syn-collisional granite)+VAG(volcanic arc granite) field. In the

Y+Nb versus Rb plot(Figure 5.161), however, they straddle the boundaries of the VAG, syn-COLG and WPG fields. Therefore, it is unlikely that these diagrams will provide a unique definition for these rhyolites because of the wide variety of crustal components which may have been involved in their genesis. Furthermore, rather than the tectonic setting existing when granitic magma was actually produced, these plots seem to diagnose the setting in which the protolith was formed(Arculus, 1987; Twist and Harmer, 1987).

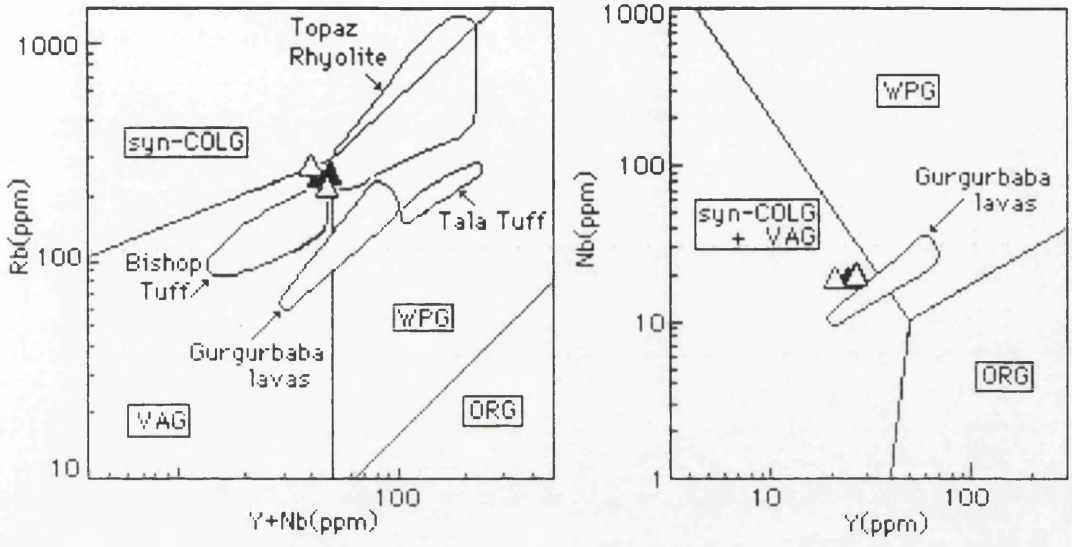

Figure 5.161. Trace element discriminant diagram for granitic rocks(Pearce *et al.*, 1984) showing the composition of rhyolite dome(solid triangles) and dykes(open triangles), and compared with the Gurgurbaba rhyolite(this study), the Bishop Tuff(Hildreth, 1977), the Tala Tuff(Mahood, 1981) and topaz rhyolites(Christiansen *et al.*, 1986) from the United States. VAG=volcanic arc granites; syn-COLG=syn-collision granites; WPG=within plate granites; and ORG=ocean ridge granites.

5.3.3.8.2. INCOMPATIBLE ELEMENTS

The MORB and PM-normalized patterns of the average rhyolite dome and dyke samples are shown in the form of geochemical features(Pearce, 1982) in Figures 5.162 and 5.163. Both dome and dyke have quite similar patterns matching each other. On the MORB-normalized patterns, they are characterized LILE(especially Rb, Ba and Th) enrichments relative to HFSE and REE. They have strong negative P and Ti anomalies which are below MORB, presumably due to removal of these elements in fractionating phases such as Fe-Ti oxides and apatite. The content of HFSE, Nb and Zr, is greater than that of MORB. On the PM-normalized patterns(Figure 5.162), they display significant negative Ba, Sr, P and Ti anomalies. In addition, there is slight

negative Nb anomaly in both patterns. All of these features are similar to the Gurgurbaba lavas.

The dome and dykes are characterized by low Ba/La and low La/Th ratios which is similar to the Gurgurbaba lavas(Figure 5.164). This suggests that they are typically related to the intraplate magmas rather than convergent plate magmas.

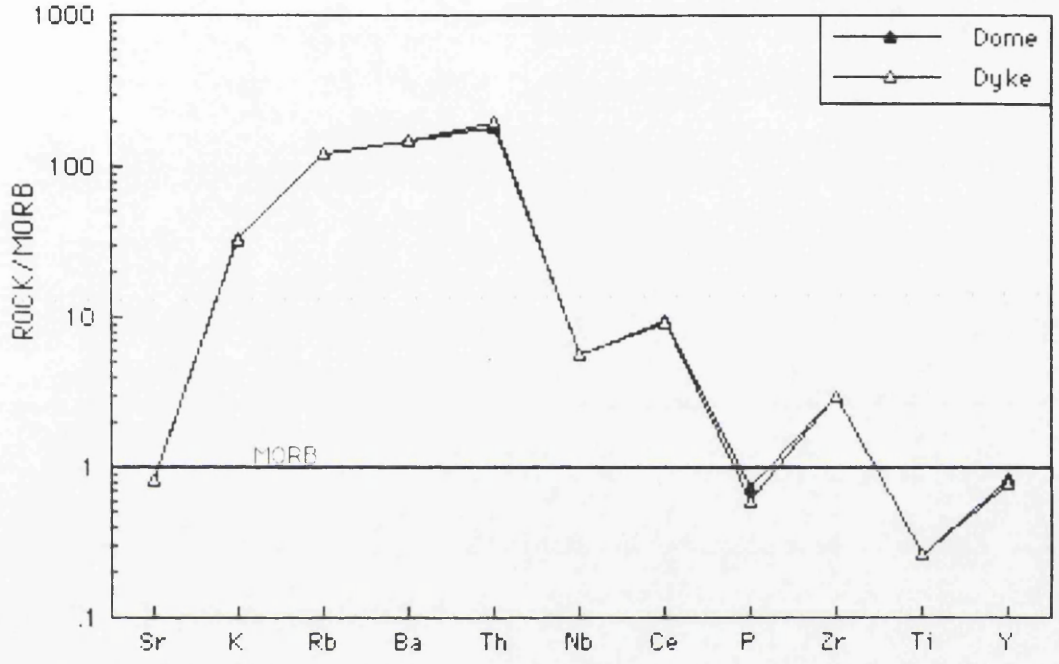

Figure 5.162. MORB-normalized trace element patterns of the rhyolite dome and dyke(MORB normalizing values are from Pearce, 1983).

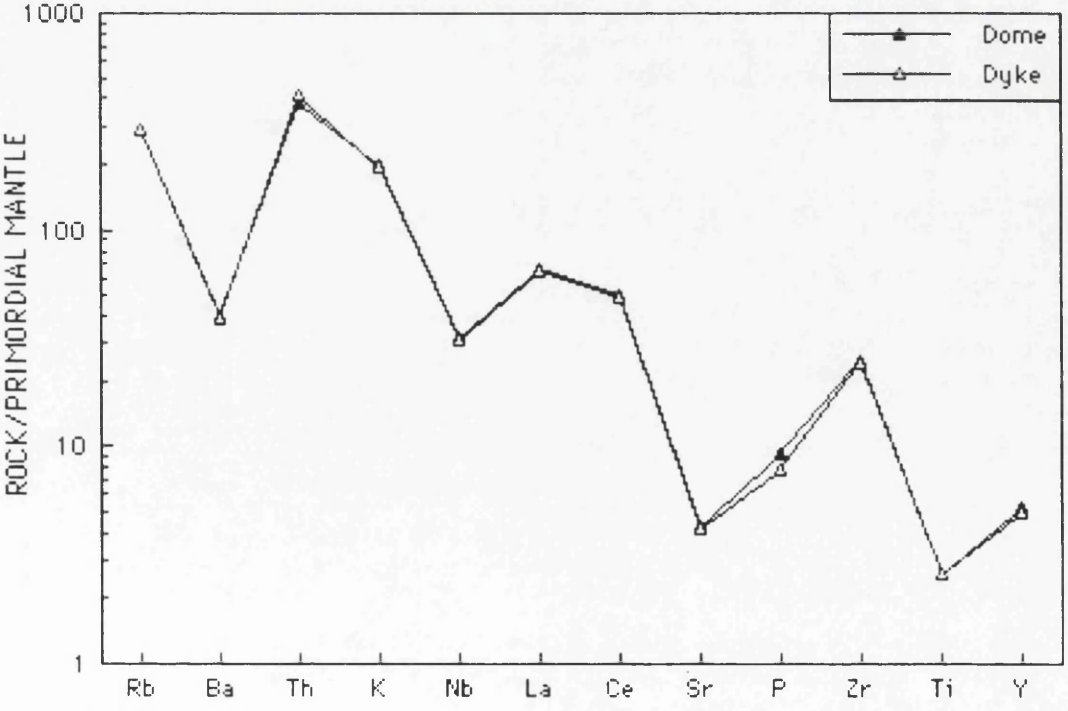

Figure 5.163. Mantle-normalized trace element patterns of the rhyolite dome and dyke. Normalizing primordial mantle values are from Wood *et al.* (1979a).

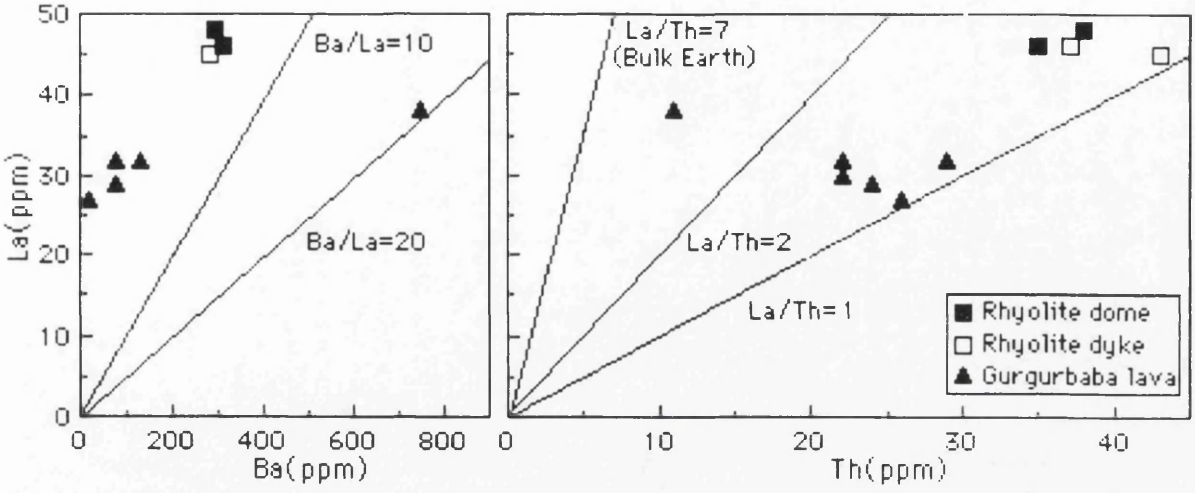

Figure 5.164. Incompatible trace element variation plots for rhyolite dome and dykes compared with the Gurgurbaba rhyolite lavas.

5.3.3.8.3. RARE EARTH ELEMENTS

The rhyolite dome and dykes are characterized by LREE-enriched and relatively HREE-depleted patterns(Figure 5.165). They have moderately fractionated REE patterns with $(La/Lu)_N$=9.77-12.17. In addition, they have strong negative Eu anomalies with $(Eu/Eu^*)_N$=0.47-0.53, suggesting significant plagioclase fractionation in the rocks. LREE enrichment is nearly 100 times chondrite values and represented by a steeper slop from La to Gd. HREE patterns are nearly flat from Dy to Lu. The relatively concave-up REE patterns and near constant Y contents may suggest significant amphibole participation. The enrichment of HREE is probably related to the abundance of zircon(Nagasawa, 1970; Puchelt and Emmermann, 1976).

The REE contents of the rocks are compared with Lower and Upper Continental crust values(Taylor and McLennan, 1985). They typically display REE patterns similar to upper continental crust. Therefore it is suggested that the rhyolite dome and dykes may have been derived from melted upper continental crust.

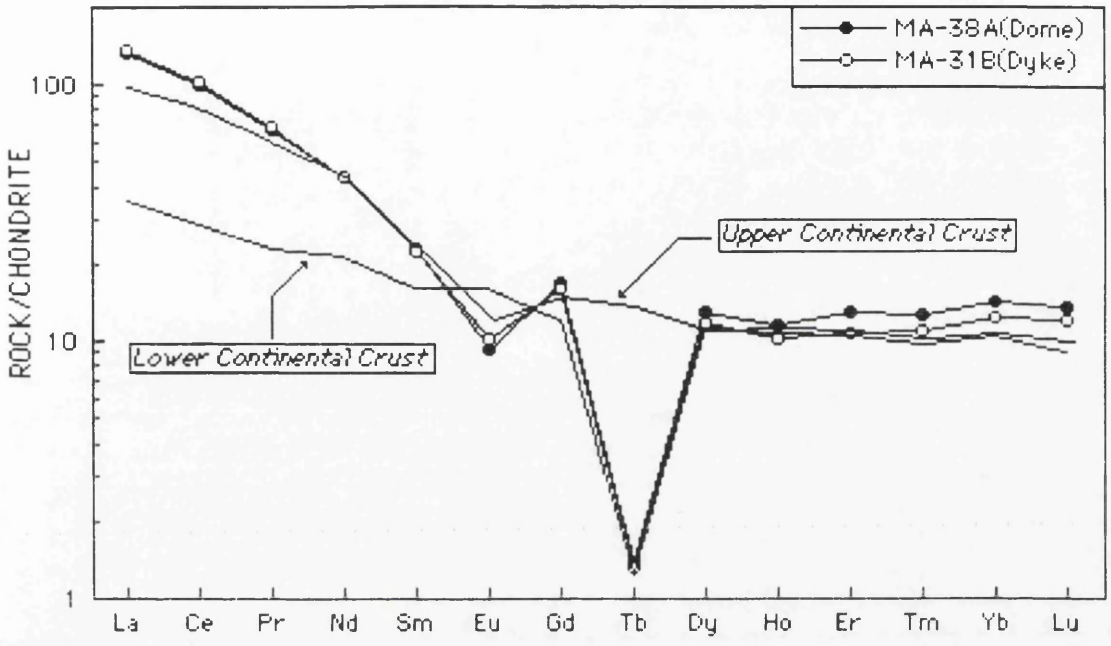

Figure 5.165. Chondrite-normalized REE patterns of dome and dyke. Normalizing values are from Boynton(1984). Lower and Upper Continental Crust values are from Taylor and McLennan(1985).

5.3.3.9. PUMICE

5.3.3.9.1. MAJOR AND TRACE ELEMENTS

Geochemical studies of tephra are complicated by their transportation through the air which sorts particles by both size and density. Sarna-Wojcick *et al.* (1981) demonstrated that wind sorting produces deposits which do not retain the geochemical characteristics of the bulk magma. Pumice-sized tephra(1-10 cm) are sufficiently larger than the average phenocrysts that they may reflect the bulk composition of the magma, since the minerals have not had the opportunity to segregate from the melt. For this reason, geochemical modelling was restricted to samples containing pumice-sized tephra. It is assumed that they represent liquid compositions and that their trace element characteristics are representative of magma(e.g., Romick *et al.*, 1992).

In the pumice tephra, two magma types, rhyolite and trachybasalt, are recognized on the basis of chemical composition. The two magma types are pumice clasts(rhyolite, 74-75 wt.% SiO_2) and lithic clasts(trachybasalt, 47-51 wt.% SiO_2). Two chemical analyses of pumice and lithic clasts collected from the deposits are shown in the chemical variation plots(Figures 5.167, 5.168 and 5.169). In most of the variation plots, pumice and lithic clasts show almost linear arrays. However, lithic fragments are separated from rhyolitic pumice clasts by a silica gap of about 20%.

The clasts are also classified in terms of their primary petrochemical compositions on the Nb/Y versus Zr/TiO_2 diagram(Figure 5.166; Winchester and Floyd, 1977). Interpretation of this diagram must be with care because clasts may have suffered considerable modification from primary igneous compositions. In terms of the Nb/Y ratio as an index of original alkalinity the clasts are clearly subalkaline. The AFM plot is based on major elements susceptible to mobility during alteration and cannot be interpreted with the same degree of confidence as diagrams based on immobile trace elements. However, pumice clasts show a lack of iron enrichment and plot in the calcalkaline field, similar to the Gurgurbaba lavas. Lithic clasts show clear iron enrichment and plot close to the tholeiitic-calcalkaline boundary(Figure 5.166).

The lithic clasts represent a basaltic magma thought to most closely represent the end-member basalt composition. This composition is that of an alkaline trachybasalt(Le Bas *et al.*, 1986) which is similar to those of the Meydan lavas. The pumice clasts represent a rhyolite magma. The lithic clasts have FeO/MgO ratios 2.12-2.65 and TiO_2 contents of higher than 1.5 wt.% whereas the pumice clasts have FeO/MgO ratio of 4.25-4.78 and TiO_2 contents of less than 0.5 wt.%. The slightly silicic composition of the pumice clasts may simply reflect a lower percentage of phenocrysts in the magma. Because of secondary

hydration of the glass, the major element analyses of the pumice clasts have been recalculated anhydrous.

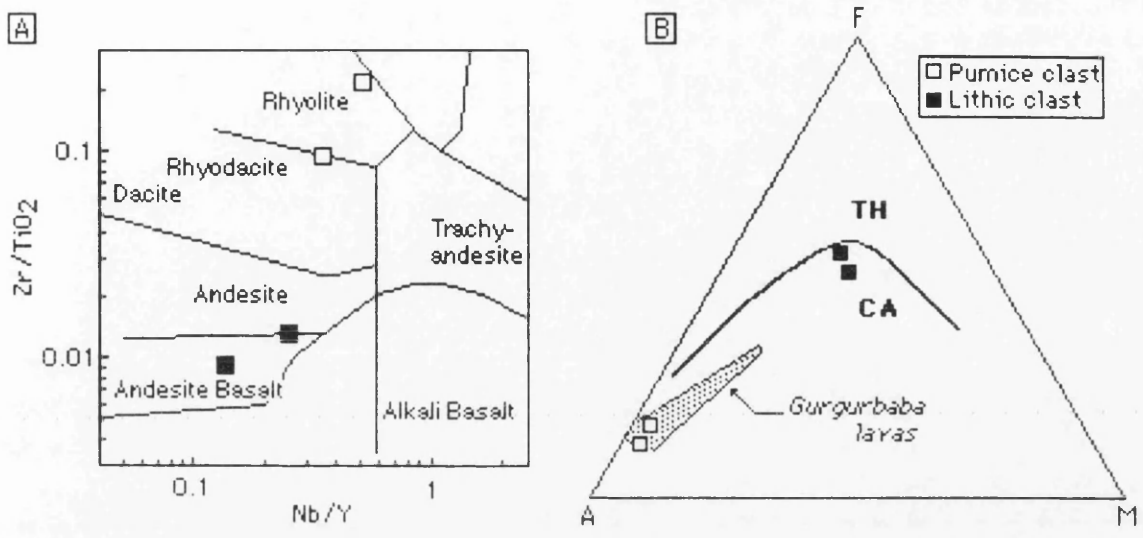

Figure 5.166. (A), Nb/Y versus Zr/TiO_2 showing chemical composition of the lithic and pumice clasts. Field boundaries are from Winchester and Floyd(1977). (B), AFM plot of pumice and lithic clasts. The Gurgurbaba lavas(shaded area) are also shown for comparison. The thick line separates tholeiitic(TH) and calcalkaline(CA) compositions(Irvine and Baragar, 1971).

Zr was chosen as an index of fractionation because of its incompatibilty in the crystallizing minerals(Figure 5.170). Ba, Th, Zr and Rb behave incompatibly in the pumice tephra. Transition elements(Ni, Cr and Co) are in low abundance due to their extraction from precursor liquids possibly by hornblende and clinopyroxene fractionation. The pumice clasts are relatively rich in Yb and Th and relatively poor in La.

Large ranges in the abundances of some elements in the two pumice clasts analysed may reflect the complexing, or speciation, of certain trace elements and vapour during the vesiculation of magmas. This possibly, however cannot be confirmed by the data because whole pumice clast analyses typically do not reflect the abundances of magmatic volatiles such as H_2O, CO_2, F, Cl and S, all of which are readily lost during explosive eruptions(Webster and Duffield, 1991).

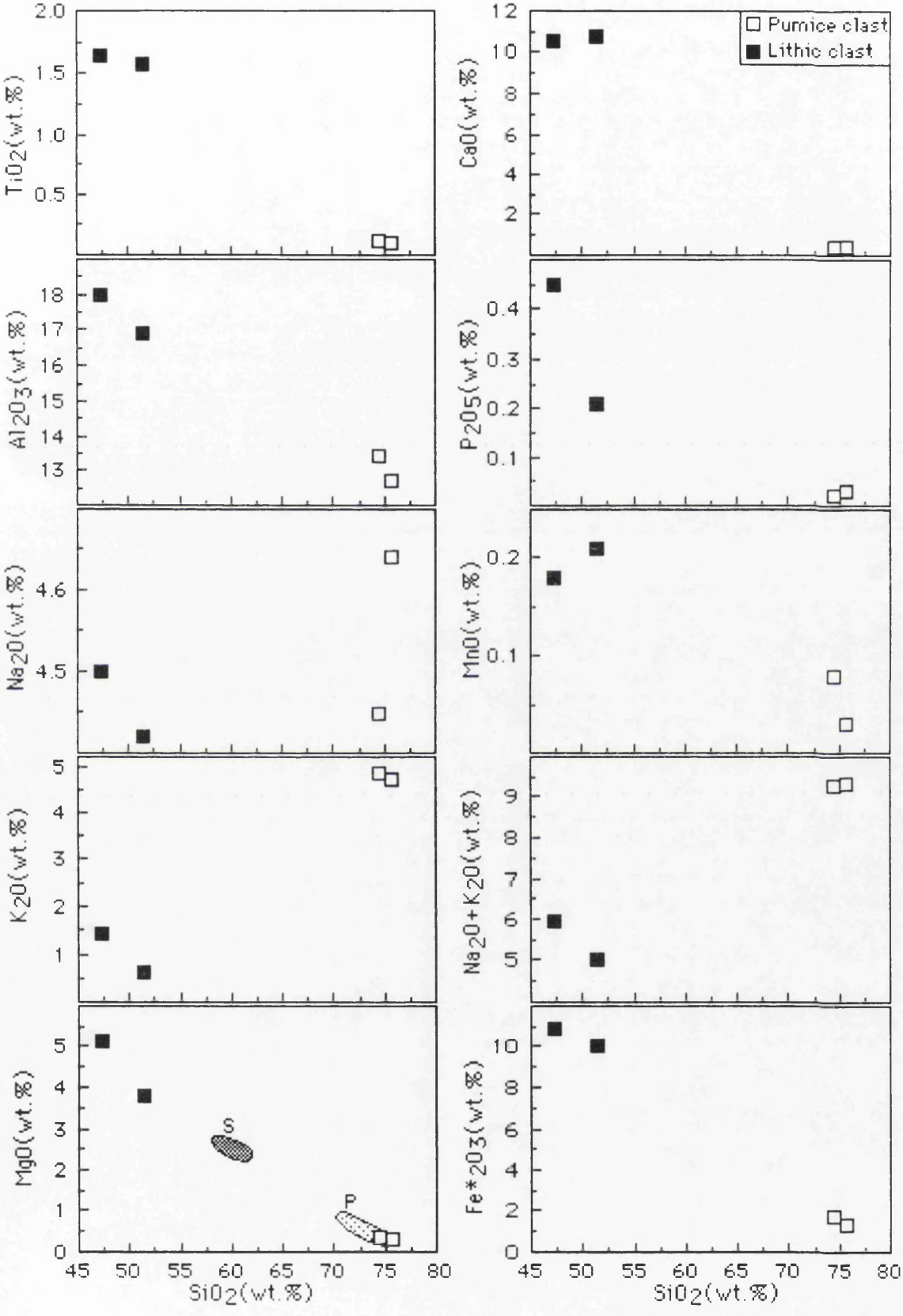

Figure 5.167. SiO_2(wt.%) versus major element plots for pumice and lithic clasts. Fields on the SiO_2 against MgO plot represent rhyolite-rhyodacite pumices(P) and andesite scoria(S) from mixed magma eruption of Taupo volcano(Blake *et al.*, 1992).

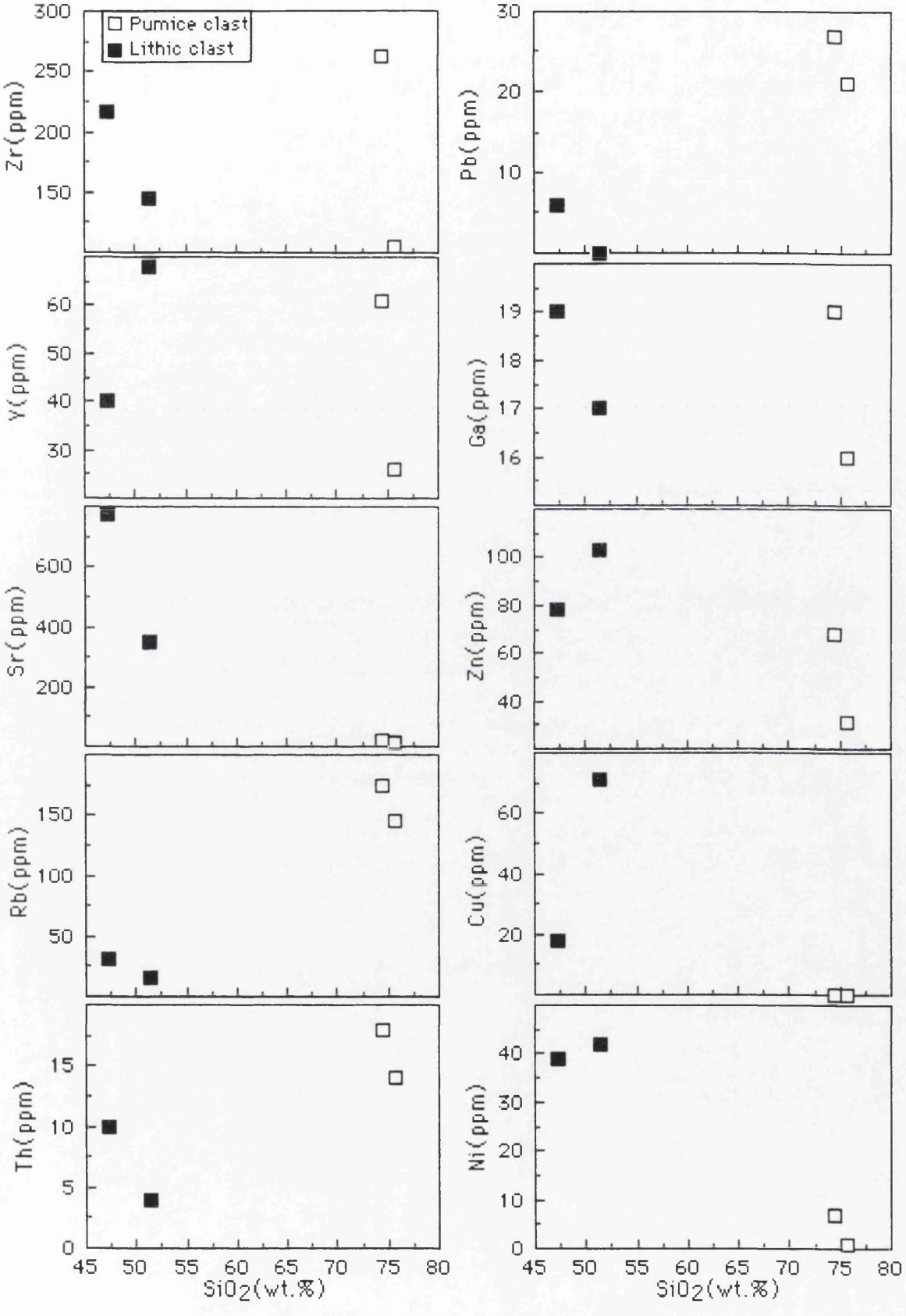

Figure 5.168. SiO_2(wt.%) versus trace element plots for pumice and lithic clasts.

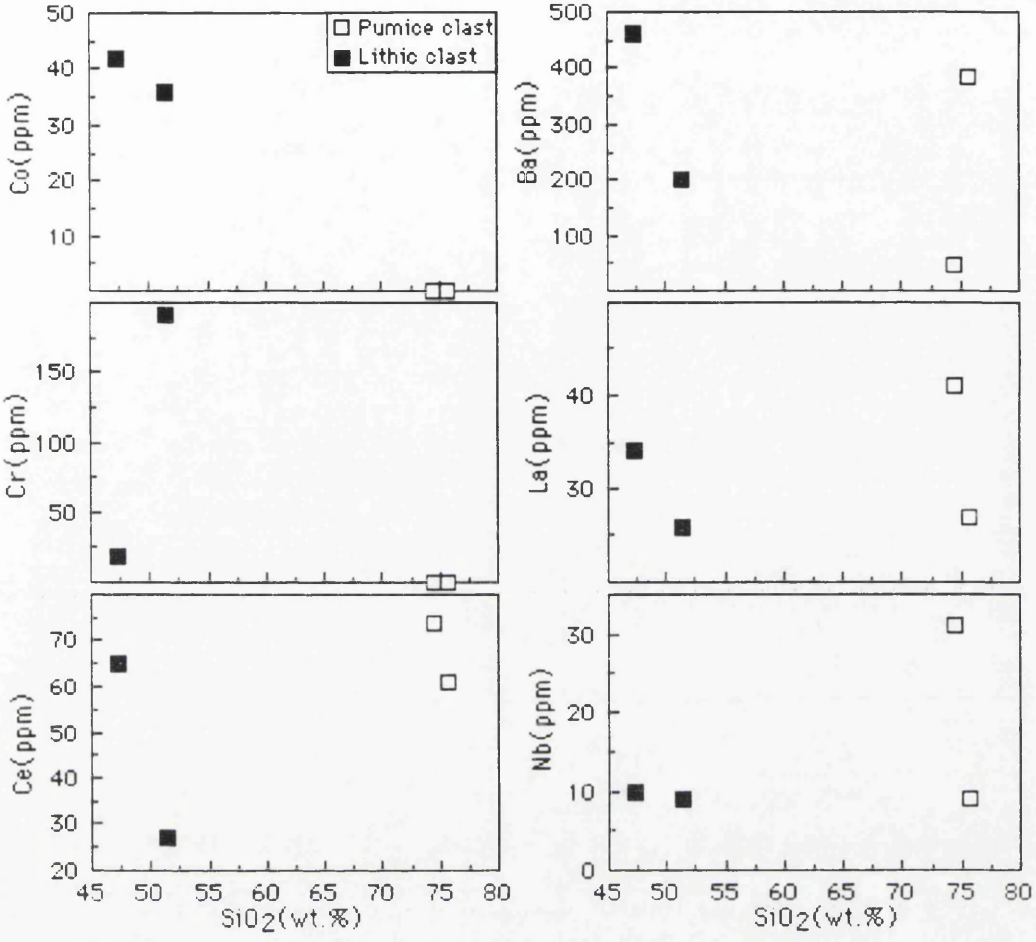

Figure 5.169. SiO_2(wt.%) versus trace element plots for pumice and lithic clasts.

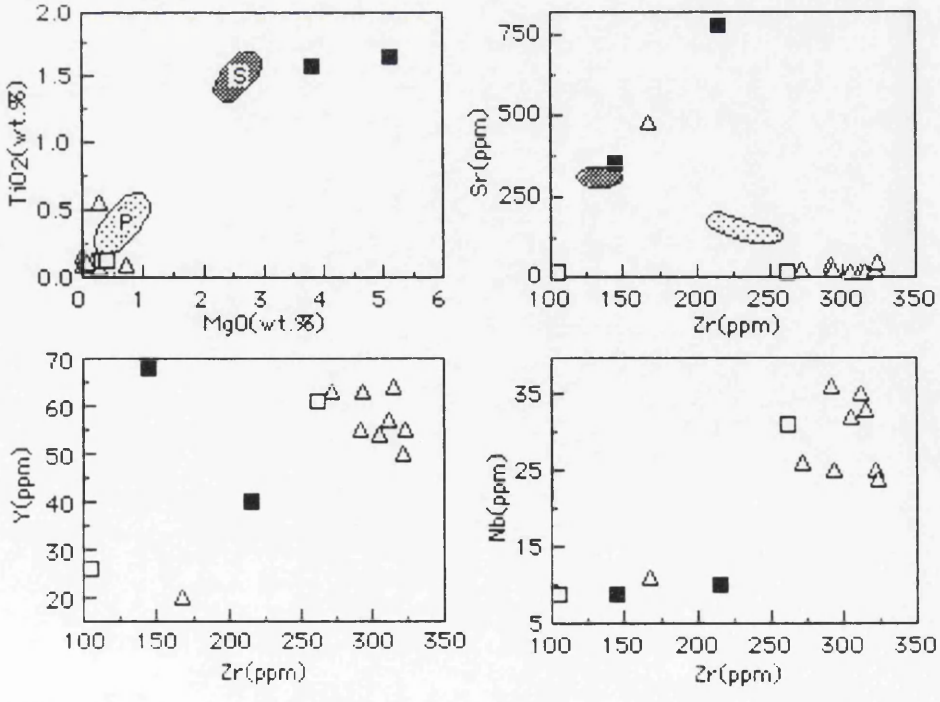

Figure 5.170. MgO versus TiO_2, and Zr(as a fractionation index) versus Sr, Y and Nb variation plots of the pumice(□) and lithic(■) clasts. The Gurgurbaba lavas(△) are shown for comparison. Fields represent rhyolite-rhyodacite pumices(P) and andesite scoria(S) from mixed magma eruption of Taupo volcano(Blake *et al.*, 1992).

Both pumice and lithic clasts have low La/Y and Nb/Y ratios(Figure 5.71). Pumice clasts typically plot within range of the Gurgurbaba lavas. Furthermore, in CaO versus Y plot(Figure 5.71), the pumice clasts lie on the same trend of the Gurgurbaba lavas whereas the lithic clasts plot completely away from this trend. This suggests that the pumice composition defines end product of the Gurgurbaba lavas with a plagioclase-dominated fractionation in their evolution.

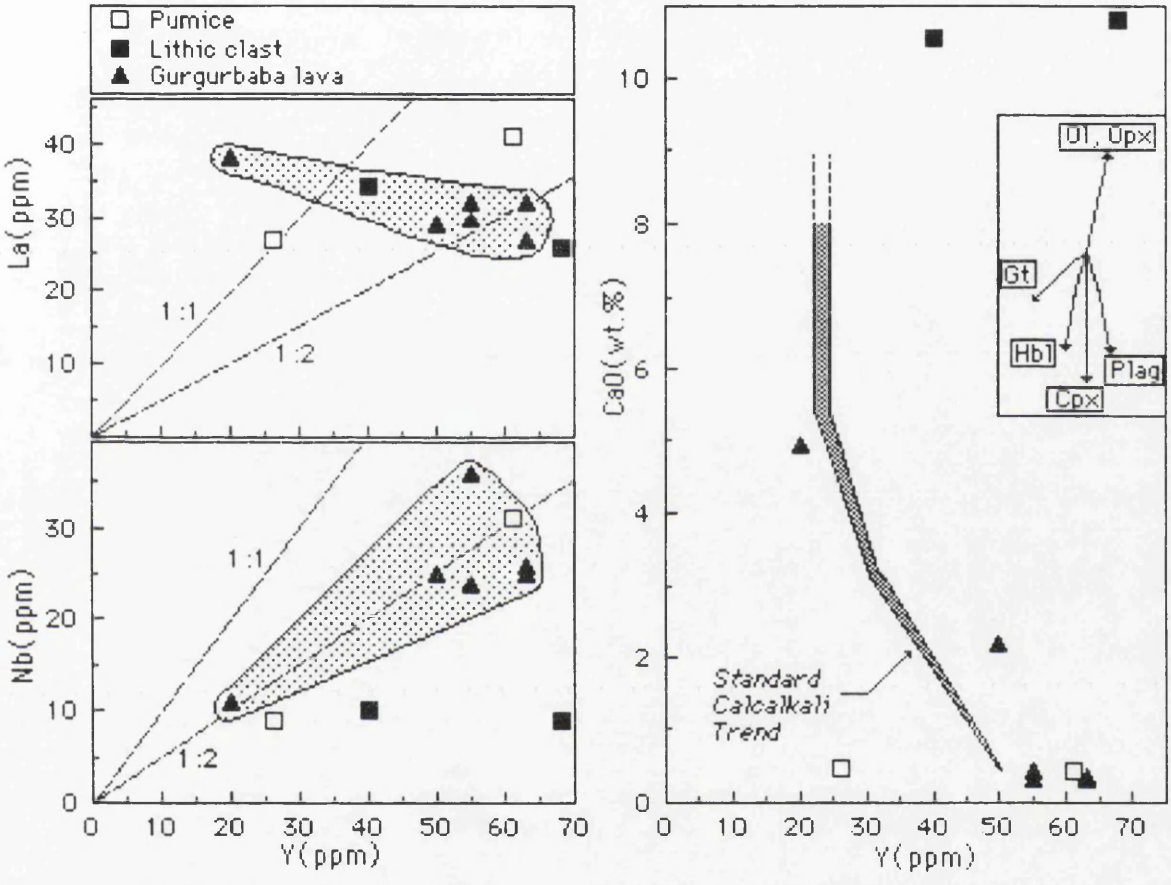

Figure 5.71. Y(ppm) versus Nb(ppm), La(ppm) and CaO(wt.%) plots for pumice and lithic clasts. Shaded area represents the "standard" calcalkaline trend of Lambert and Holland(1974). The Gurgurbaba lavas are superimposed for comparison. The vectors show qualitative trends of the effect of fractional crystallization of common silicates.

5.3.3.9.2. INCOMPATIBLE ELEMENTS

The mid-ocean ridge basalt(MORB) and primordial mantle(PM)-normalized patterns of pumice and lithic clasts are shown in Figures 5.172 and 5.173. The patterns display very distinctive features for pumice and lithic clasts. However, the patterns are quite similar within each clast type.

On MORB-normalized patterns(Figure 5.172), pumice clasts show significant LILE(K, Rb and Th) enrichment relative to HFSE and Sr. They also exhibit strong negative Ba, P and Ti and slight Nb anomalies. Depletions of Ba,

P and Ti, are presumably due to removal of these elements in fractionating phases such as plagioclase, apatite and Fe-Ti oxides. Lithic clasts show moderate LILE enrichment, especially in Th, relative to HFSE. Lithic clasts display slight negative Nb and Ti anomalies. On PM-normalized patterns(Figure 5.173), the distinctive features of both clasts are again illustrated. Pumice clasts have negative Ba, Nb, Sr and Ti anomalies. The lithic clasts exhibit moderate enrichment of LILE with a gentle slope from Sr to Th and Ce to Y and a slight depletion in Nb and Ti.

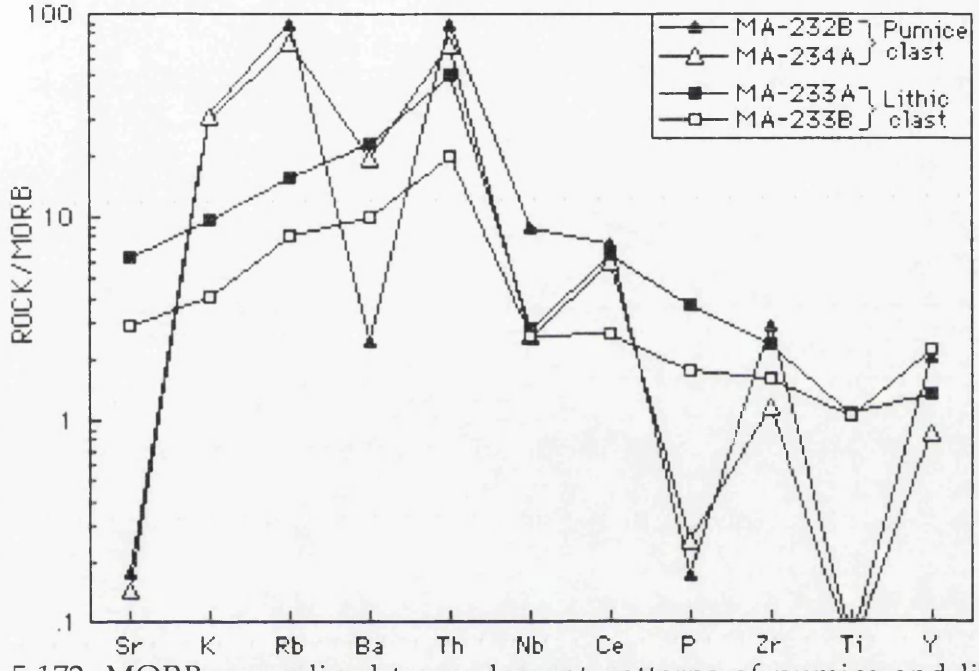

Figure 5.172. MORB-normalized trace element patterns of pumice and lithic clasts(MORB normalizing values are from Pearce, 1983).

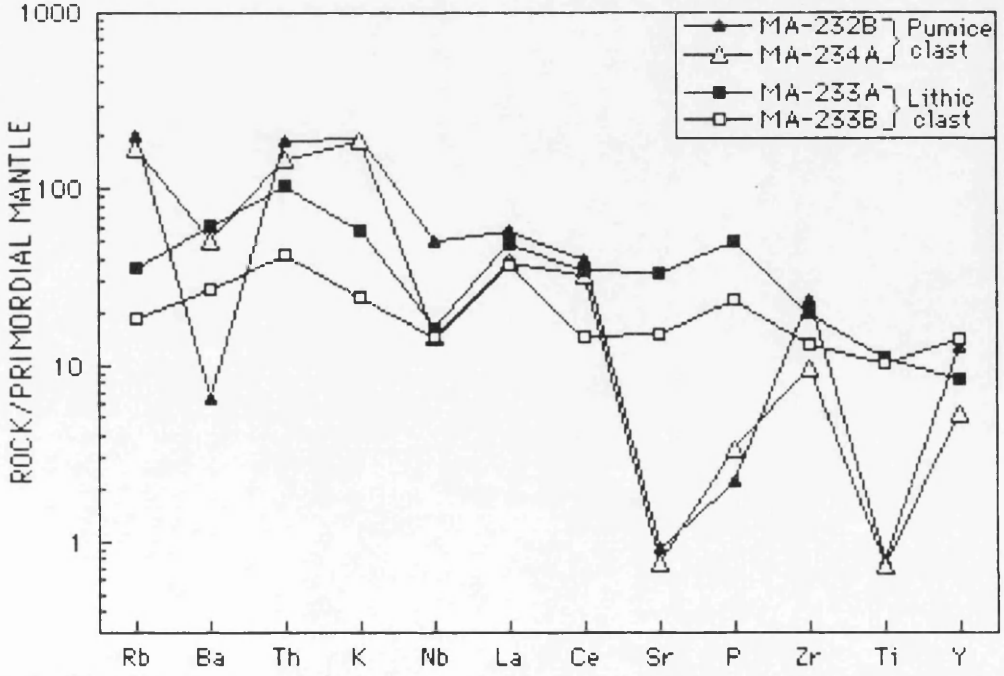

Figure 5.173. Mantle-normalized trace element patterns of pumice and lithic clasts. Normalizing primordial mantle values are from Wood *et al.* (1979a).

The distinctive patterns of lithic clasts suggest that they are not cogenetic with pumice clasts which represent bulk magma composition. In addition, the pumice clasts show similar patterns to the Gurgurbaba lavas, indicating that they are cogenetic and presumably derived from the same parental magma composition.

5.3.3.9.3. RARE EARTH ELEMENTS

The pumice clasts have moderately fractionated REE patterns(Figure 5.174) with $(La/Lu)_N$=2.32-3.68 and $(Eu/Eu^*)_N$=0.36-0.94. REE concentrations increase with increasing SiO_2. In addition, there is less MREE enrichment than LREE and HREE with concave upward shapes. Hornblende has significantly larger distribution coefficients for MREE and HREE than LREE. Therefore, hornblende fractionation would result in an increase in the LREE concentrations and the La/Yb ratio, but only slight enrichment or even depletion in MREE and HREE of the residual melt. The negative Eu anomalies imply that they may represent derivative liquids after plagioclase fractionation.

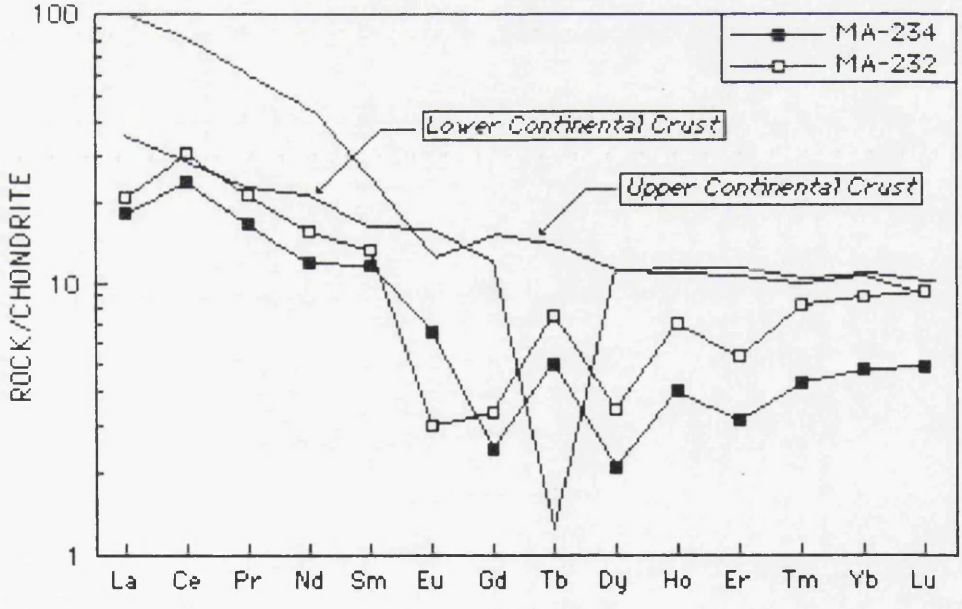

Figure 5.174. Chondrite-normalized REE patterns of the pumice clasts. Normalizing values are from Boynton(1984). Lower and Upper continental crust(Taylor and McLennan, 1985) are shown for comparison.

The REE patterns of the pumice clasts have been compared with Lower and Upper continental crust values(Taylor and McLennan, 1985). Generally, the patterns show a major depletion in all REE relative to both Lower and Upper Continental Crust. This is much pronounced in MREE from Sm to Er. The

anomalous variation in MREE may result from significant vapour phase alteration(Christiansen *et al.*, 1986). These REE characteristics are similar to those of the Gurgurbaba lavas. However, the Eu anomaly in pumice clast are significantly larger and more negative than the Gurgurbaba lavas, suggesting plagioclase dominated fractionation.

5.3.3.9.4. SOURCE CHARACTERISTICS AND IMPLICATIONS FOR MAGMATIC EVOLUTION

On the basis of the geochemical data, the pumice tephra are considered to be comagmatic in the sense that they were derived from the high-level magma chamber, shared a common parent with the Gurgurbaba lavas underlain by pumice deposits, and followed closely similar crystallization paths. Lithic clasts are genetically not related to pumices, and presumably represent wall-rock fragments.

Although the grain size is small for them to be used to reliably characterize the bulk composition of their respective magmas, their major and trace element compositions, and their mineral chemistry, suggest that they were derived from eruptions involving rhyolitic magmas. Silicic magmas containing sufficient water for amphibole to be stable(>~4 wt.%: Eggler and Burnham, 1973; Rutherford *et al.*, 1985; Rutherford and Devine, 1988) may preferentially erupt as pyroclastic air fall deposits(tephra) rather than lava flows.

The geochemical data implies the presence of compositional and thermal gradients between the pumices and the Gurgurbaba lava. An eruption that taps such a stratified chamber from its roof will preferentially tap the layer of lowest density which will normally be at the top, denser layers being tapped later depending on the thickness of top layer and the withdrawal rate(e.g., Blake *et al.*, 1992). A thick capping layer and low discharge rate favour selective withdrawal of the uppermost layer, whilst a thin cap and high discharge rate favour the lower layer being tapped(Blake and Ivey, 1986). During the pumice eruption, a uniform eruption rate is implied by the patterns of clast dispersal and the lack of vertical size grading that reflects a constant rate of magma removal from the magma chamber.

The lower part of the unit contains a greater proportion of lithic clasts than upper parts. One possible explanation is that the opening phase involved a higher evacuation rate than the closing phase. The grain size characteristics of the upper and lower parts are different implying significant differences in discharge rate. However, the fragmentation levels in the conduit may migrate up or down to accommodate imbalances in the rate of entry to, and exit from, the conduit.

Laboratory experiments of withdrawal from two-layer chambers(Jirka and Katavola, 1979; Blake and Ivey, 1986) show that the composition of the effluent at very low concentrations of the lower layer is very sensitive to the size of diffusive density gradient at the interface. Generally, the proportion of lower layer is increased by increasing the discharge rate or thinning of the upper layer(Jirka and Katavola, 1979; Blake and Ivey, 1986; Blake *et al.*, 1992). Convection in the chamber would have been controlled by cooling at the roof more than by convective fractionation induced by side wall crystallization. The rhyolitic magma will tend to be kept homogenized by turbulent convection rather than become zoned by convective fractionation(de Silva, 1991). This may provide an explanation for the mineralogical and compositional similarity of the pumice and the Gurgurbaba lava.

5.3.3.10. GURGURBABA LAVA

5.3.3.10.1. MAJOR AND TRACE ELEMENTS

The Gurgurbaba lavas are high-K rhyolites and have major element compositions characterized by a narrow range of SiO_2, high Al_2O_3, high alkalies and low FeO_t, MgO, CaO, TiO_2. Hypocrystalline types are enriched in Na_2O and depleted in TiO_2, Al_2O_3, K_2O, P_2O_5, $Fe_2{}^*O_3$. One sample(MA-58A) from the lower part of Gurgurbaba lavas exhibits an unusual composition with only 63 wt.% SiO_2. Obsidian glasses are depleted in K_2O, CaO, MgO, FeO_t and TiO_2, and enriched in Na_2O relative to the crystalline types. Generally, the Gurgurbaba lavas show a composition range which includes the composition of the rhyolite dome and dykes. It suggests that these dykes and dome are genetically related to the Gurgurbaba lavas. The Gurgurbaba lavas show a progressive decrease of TiO_2 and an increase of SiO_2, as a function of increasing FeO*/MgO ratio.

Figure 5.175A shows a plot of Fe_2O_3/FeO versus LOI(loss on ignition) for the Gurgurbaba lavas. Although these two variables are correlated the plot shows that the rocks are not oxidized($Fe_2O_3/FeO<2$, except one sample, MA-58A=6.5) and not extensively hydrated(LOI<2, except perlitic samples). Furthermore, $Mg/(Mg+Fe^{+2})$ ratio decreases with increasing SiO_2(Figure 5.175B).

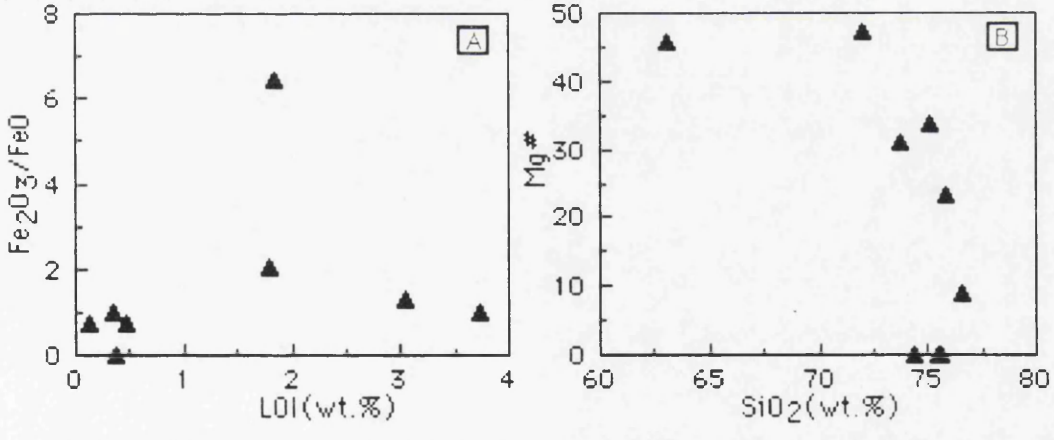

Figure 5.175. LOI versus Fe_2O_3/FeO plot showing oxidation and hydration(A), and $Mg^{\#}$ number[$Mg/(Mg+Fe^{+2})$] versus SiO_2 plot(B) of the Gurgurbaba lavas.

The concentrations of CaO(<2 wt.%, one sample 4 wt.%), $Fe^*{}_2O_3$(<1.5 wt.%, one sample 4.83 wt.%), MgO(<0.70 wt.%, one sample 2 wt.%), TiO_2(<0.55wt.%) and P_2O_5(<0.20wt.%) in the Gurgurbaba lavas are relatively low and similar to those found in high-silica rhyolites. All of these elements

correlate negatively with incompatible elements. Their decreasing concentrations can be shown to relate to the fractionation of modal proportions of plagioclase, biotite, Fe-Ti oxides and apatite. Manganese concentrations are also low, less than 0.14 wt.% MnO but in general Mn appears to behave as an incompatible element. MnO decreases with differentiation from 0.14 to 0.07 wt.%. In SiO_2 variation plots(Figures 5.176, 5.177 and 5.178), Al_2O_3, CaO, TiO_2, MgO, Fe_2O_3, P_2O_5, Ba and Ga increase whereas K_2O, Th, Y and Rb decrease with decreasing SiO_2, suggesting fractionation of plagioclase, hornblende and apatite. On the AFM plot(Figure 5.179), the Gurgurbaba lavas are relatively evolved and plot in the calcalkaline field and show a typical trend lacking any iron enrichment.

In Figure 5.180A, total iron is plotted against MgO. Generally, the rocks have low Fe/Mg ratios. Figure 5.180B shows a plot of total iron(as Fe_2O_3) versus CaO for the Gurgurbaba lavas. The thick line separates higher-Fe types from lower-Fe ones(Warshaw and Smith, 1988). Rocks plotting to the right of this line usually crystallize biotite and, or, hornblende, have higher Fe^{+3}/Fe^{+2} ratios than the higher-Fe types, and are usually metaluminous to peraluminous. Rocks plotting close to this line usually crystallize orthopyroxene±biotite and hornblende, and are usually metaluminous(Warshaw and Smith, 1988).

Gurgurbaba rhyolite lavas show significantly lower La/Y and Nb/Y ratios, when compared with ignimbrites and the rhyolite dome and dykes. Lambert and Holland(1974) used CaO versus Y to define J and L type trends, which lead respectively to depletion and enrichment in Y relative to a calcalkaline series standard. The J and L trends have been termed hornblende-(±garnet) and pyroxene controlled differentiation trends respectively, as these minerals can be critical in determining trend direction. In the Y versus CaOplot(Figure 5.181), the Gurgurbaba samples generally plot on the Y enriched side of the standard calcalkaline trend. They are slightly Y enriched relative to the standard calcalkali trend, and define an L type trend(Figure 5.181), and apparently follow the standard calcalkaline trend suggesting plagioclase controlled fractionation.

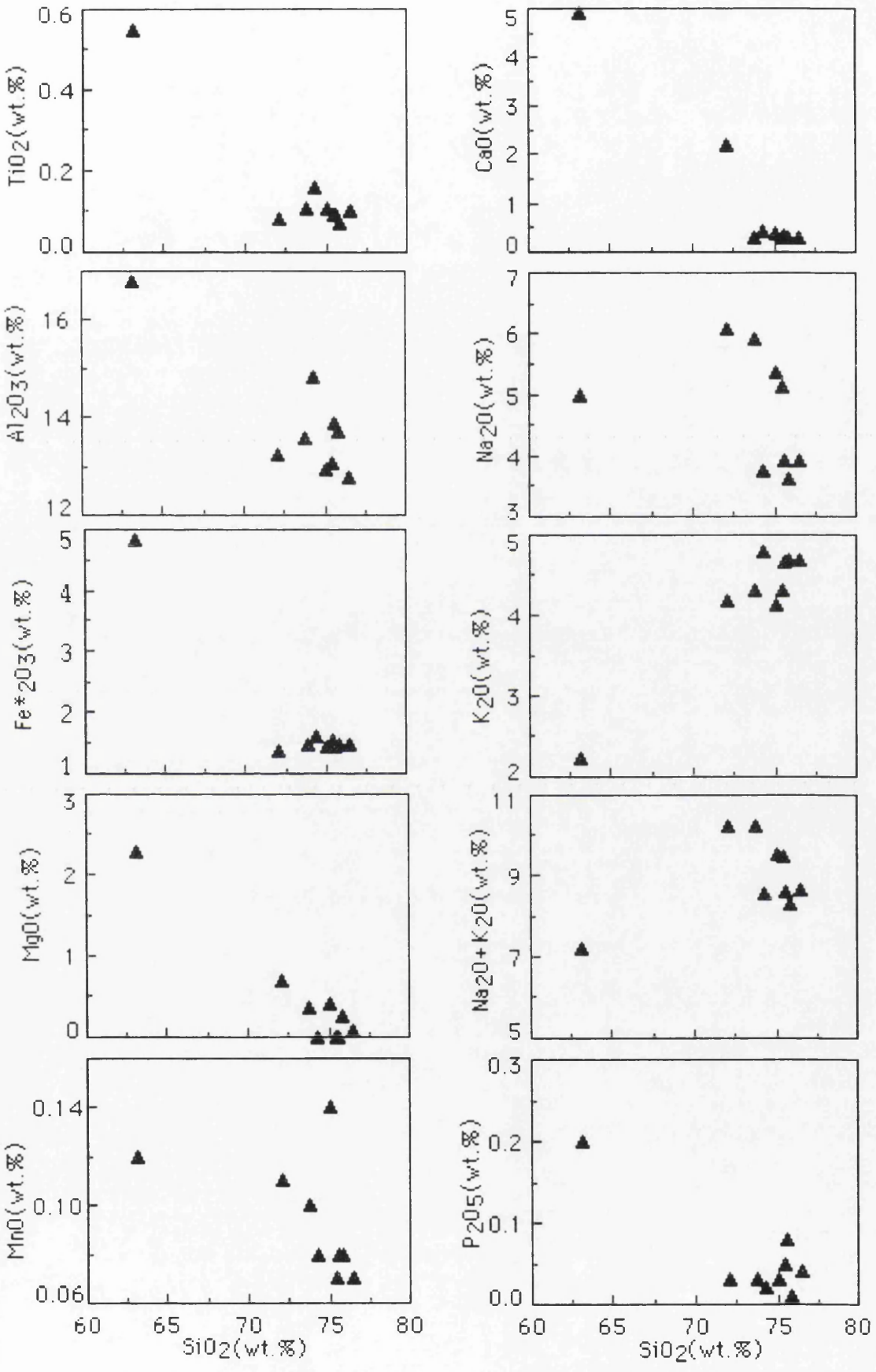

Figure 5.176. SiO_2 variation diagrams of major elements for the Gurgurbaba rhyolite lavas.

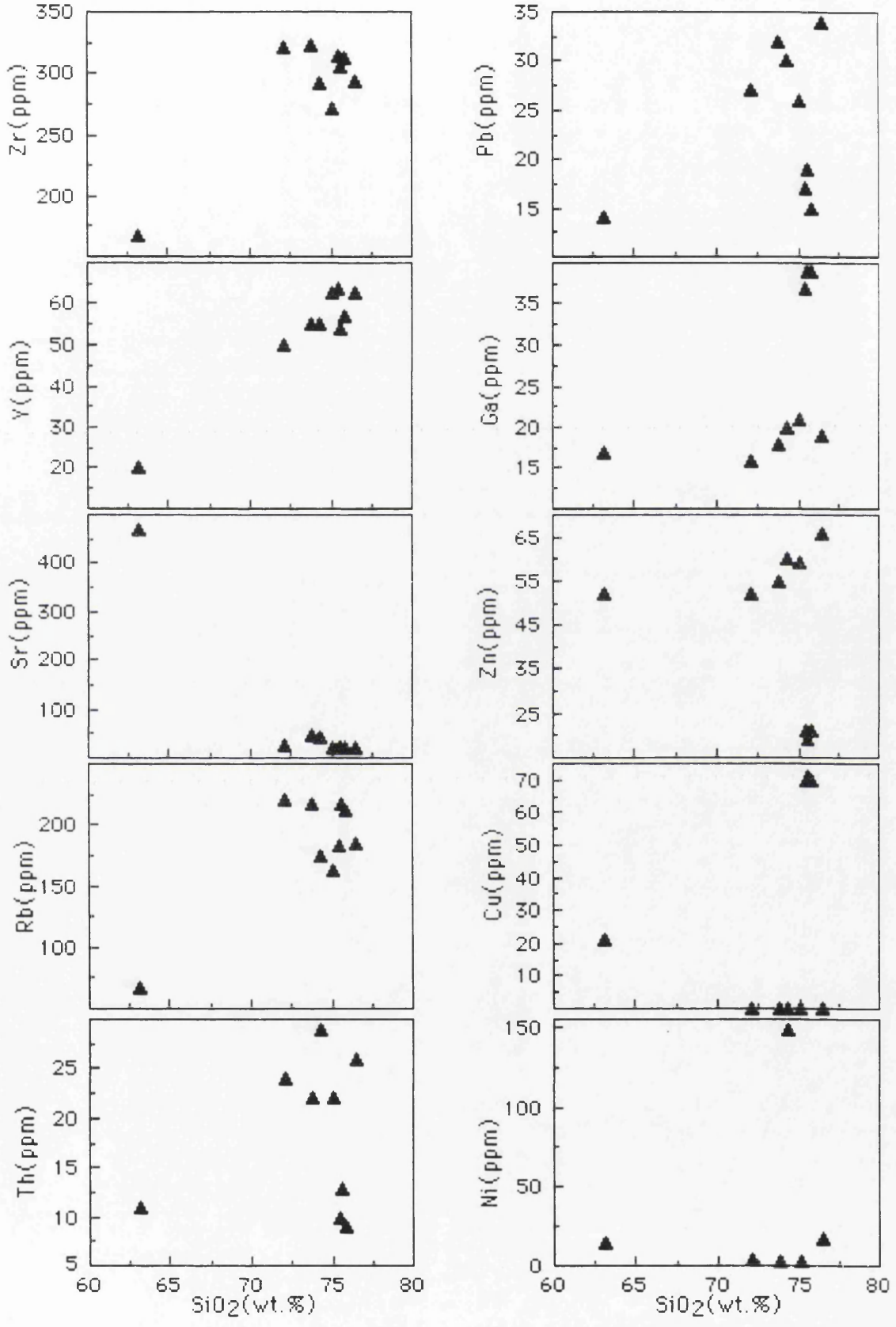

Figure 5.177. SiO_2 variation diagrams of trace elements for the Gurgurbaba rhyolite lavas.

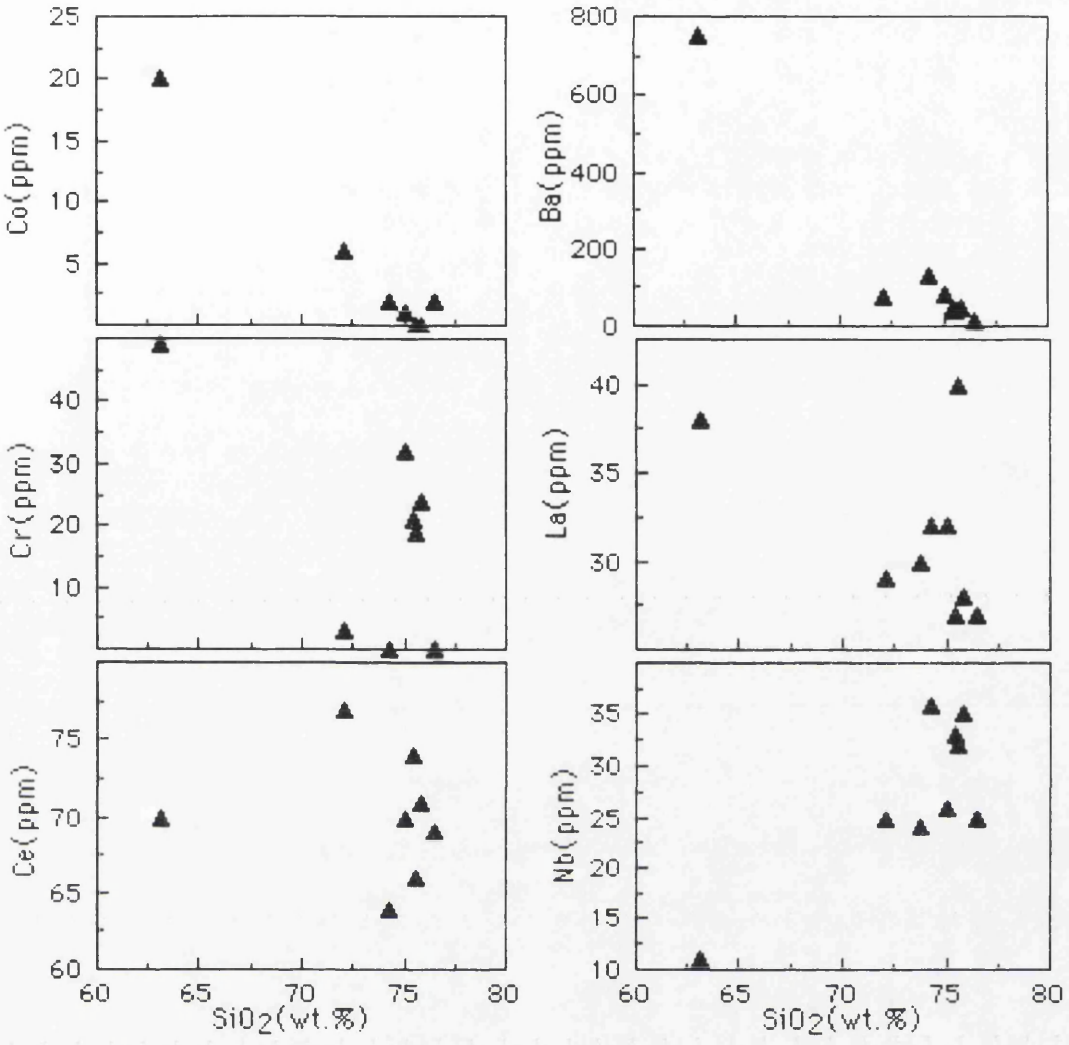

Figure 5.178. SiO_2 variation diagrams of trace elements for the Gurgurbaba rhyolite lavas.

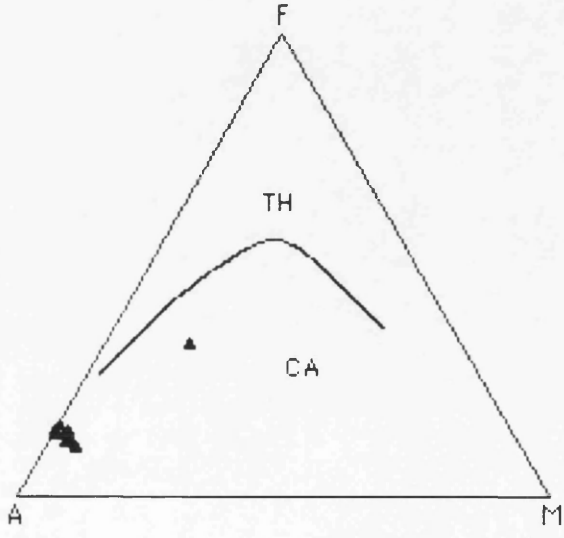

Figure 5.179. AFM plot of the Gurgurbaba lavas. The thick line separates tholeiitic(TH) and calcalkaline compositions(Irvine and Baragar, 1971).

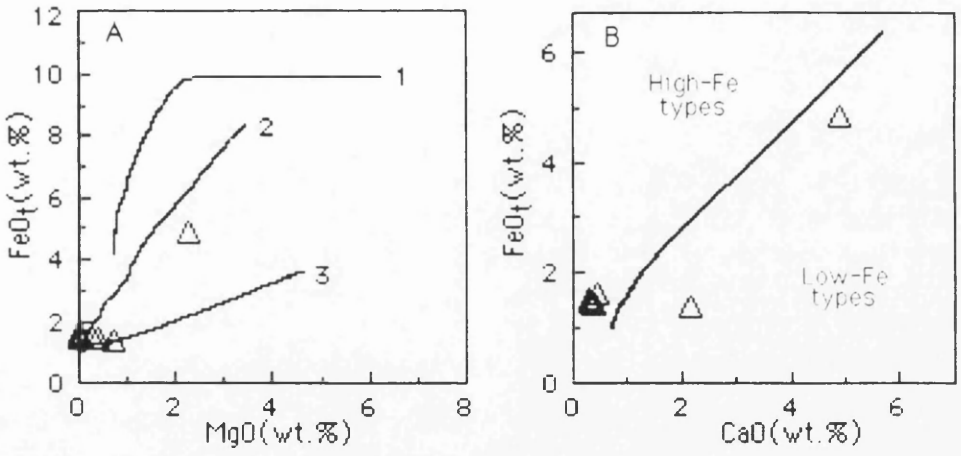

Figure 5.180. (A), total iron(as Fe_2O_3) versus MgO for the Gurgurbaba lavas. The trends of experimentally produced melts at 1kb(fH_2O=0.67, G-CH buffer) from a Kilauea basalt(Spulger and Rutherford, 1983) and at 5 kb H_2O from an olivine tholeiite at the FMQ and HM buffers(Helz, 1976) are shown for comparison(nos, 1, 2, 3 respectively); (B), total iron(as Fe_2O_3) versus CaO plot. Thick line separates high-Fe types from low-Fe ones(Warshaw and Smith, 1988).

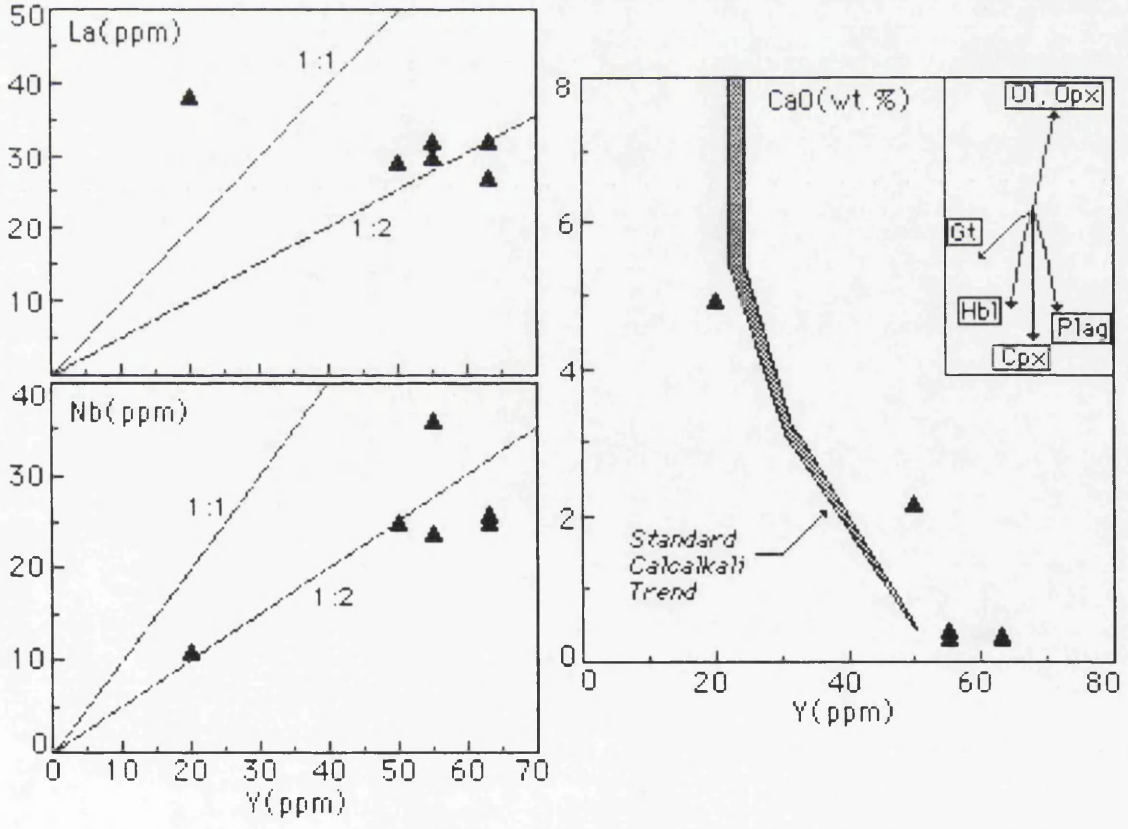

Figure 5.181. Y(ppm) versus Nb(ppm), La(ppm) and CaO(wt.%) plots for the Gurgurbaba lavas. Shaded area represents the "standard" calcalkaline trend of Lambert and Holland(1974). The vectors show qualitative trends for the effect of fractionation of the common silicates.

Generally, the major element composition of the Gurgurbaba lavas is fairly restricted. All samples, except(MA-58A) are high-silica rhyolites with high Na, K and low Fe/Mg, Ti, Ca and P. All rhyolites have SiO_2 concentrations greater than 72wt.% except MA-58A with 63 wt.%. Generally, silica contents vary little with differentiation trend. As a result silica concentrations are poor indicator of the chemical variability of the Gurgurbaba lava. The low silica content may be interpreted as the result of crystallization near the minimum in the granite system(e.g., Christiansen *et al.*, 1984). Furthermore, Manning(1981) showed that the stability field for quartz expands with increasing fluorine content in a water-saturated haplogranite at 1 kb pressure(Figure 5.182). Therefore, it is possible that enchanced quartz fractionation could lead to a reversal of normal SiO_2-enrichment during fractional crystallization of a fluorine-rich rhyolite(Christiansen *et al.*, 1986). Hypocrystalline types and obsidian glasses plot in separate fields in the Q-Or-Ab diagram(Figure 5.182). Hypocrystalline types cluster near and below the low pressure H_2O-saturated minima. In contrast, obsidian glasses are shifted towards higher normative Ab. Such Ab-rich compositions may reflect the combined effects of Al, F, Li, B and H_2O on phase relations and compositions of residual liquids in the Q-Or-Ab system(Pichavant *et al.*, 1987a).

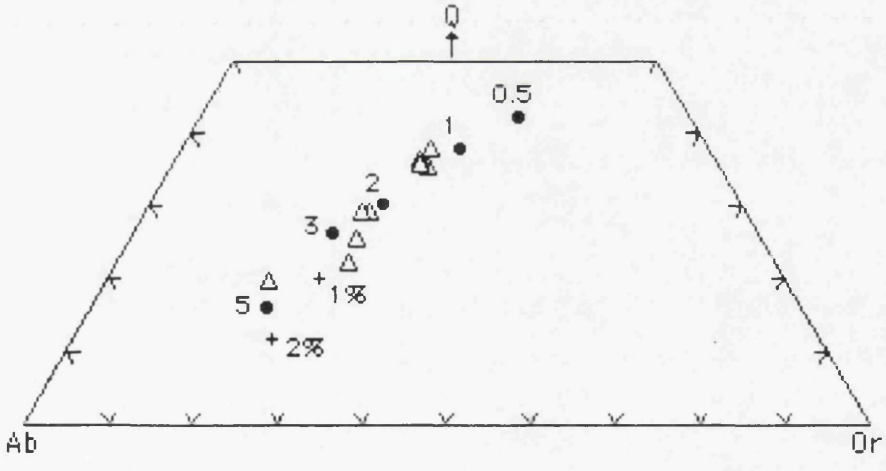

Figure 5.182. Normative composition of the Gurgurbaba rhyolites in terms of quartz(Q), albite(Ab), and orthoclase(Or) compared to experimentally determined ternary minima in: 1) the hydrous granite system at pressures given in kb(P_{H_2O}) next to the filled circles(Tuttle and Bowen, 1958; Luth *et al.*, 1964; and Whitney, 1975); and 2) the F-bearing granite system at 1 kb(Manning, 1981). The numbers next to the crosses indicate weight % F in the water-saturated system at 1 kb.

The Gurgurbaba lavas contain 12wt.% to 16wt.% Al_2O_3. High Al_2O_3 contents are found in the low silica rhyolites, reflecting the increased proportion of feldspar components. The lavas have high concentrations of alkalies ranging between 7 wt.% and 10 wt.% Na_2O+K_2O. In general, K_2O/Na_2O ratios are lower than one(0.45 to 1.29). Because a few obsidians have been analysed from the rhyolites, it remains to be demonstrated that these high ratios are magmatic and not the result of alkali-metasomatism during subaerial crystallization. Generally, K decreases with increasing incompatible elements and Na, presumably a result of the combined fractionation of potassic sanidine and biotite. In spite of high alkali concentrations, the rhyolites are not peralkaline or alkali rhyolite(e.g., Streckeisen, 1979). The Gurgurbaba lavas are slightly peraluminous, probably as result of the loss of alkalies during crystallization. The molar ratio of Al_2O_3 to Na_2O+K_2O+CaO(A/CNK) is less than 1.1 but also equal to or larger than 1.0 therefore, the Gurgurbaba lavas are metaluminous to slightly peraluminous in composition(Figure 5.183) according to the definition of Shand(1947). In general, the lavas are not strongly peralumious indicating that they are not the eruptive equivalents of S-type granites(e.g., White and Chappell, 1983).

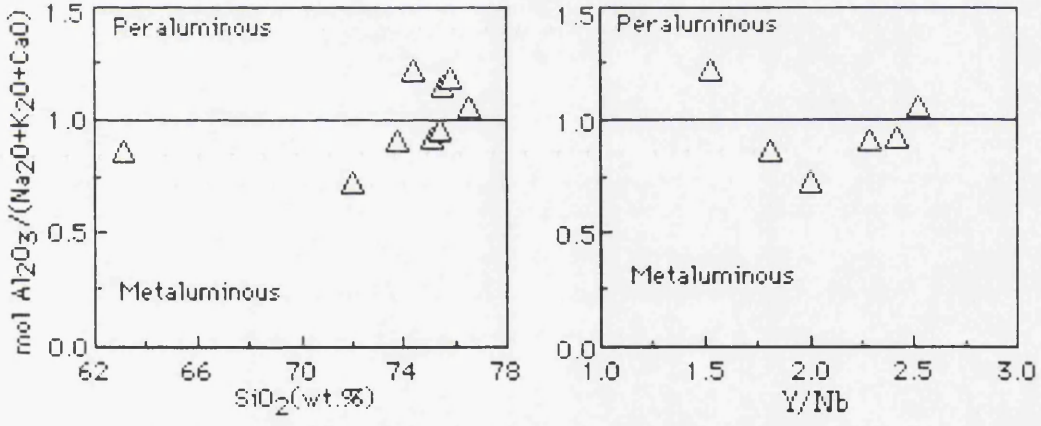

Figure 5.183. Mol $Al_2O_3/(Na_2O+K_2O+CaO)$ versus SiO_2 and Y/Nb plots indicating the metaluminous to peraluminous character of the Gurgurbaba lavas.

Granitic rocks are classified into two major groups according to their source by Chappell and White(1974). I-types are free of normative corundum and are in theory derived by fractional crystallization or remelting of basaltic parents while S-types have normative corundum and a metasedimentary source and contain modal cordierite and biotite±garnet, Al-silicate polymorphs and muscovite. The Gurgurbaba rhyolites are similar to that of I-type granitic rocks. Their slightly peraluminous character is not unusual since almost one

half of the I-type granitic rocks are weakly peraluminous with A/CNK ratio less than 1.1(Chappell and White, 1992). Barbarin(1990) compared the main petrogenetic classifications of granitic rocks with each other and proposed a classification based on whether they were derived from the mantle , the crust or were a hybrid of both. Granitic rocks with A/CNK generally less than 1.1 and $FeO_t/(FeO_t+MgO)$ less than 0.8 are termed "hybrid continental groups".

The A'KF and ACF plots(Figure 5.184) show that the Gurgurbaba rhyolites are more peraluminous than topaz rhyolites and other peraluminous volcanic series such as the Violet Town volcanics(Clemens and Wall, 1981) or the Tuscan rhyolites(Dupuy, 1970). In the A'KF plot(Figure 5.184), most of the samples plot below the K-feldspar-cordierite tie line, thus necessitating the participation of a strongly peraluminous phase(either melt, sillimanite or andalusite, muscovite or tourmaline). The other point emphasized by the A'KF plot is the felsic nature of the Gurgurbaba lavas, particularly glassy types. The Gurgurbaba lavas have compositions closer the minimum melt and correspond to a more felsic peraluminous series. Examples of felsic peraluminous granites plotted for comparison(Figure 5.184) include the Hercynian two-mica granites(La Roche *et al.*, 1980) and the Beauvoir granite(Cuney *et al.*, 1986). Generally, the Gurgurbaba lavas fall between the Hercynian two-mica granites and the Beauvoir granite and therefore it can be concluded that the rhyolites are the chemical equivalent of these leucogranites, in terms of major element chemistry. The obsidian glasses presumably represent fractionation products of these felsic peraluminous magmas. In Figure 5.184 the major element data for the Gurgurbaba lavas are compared with the relevant experimentally produced melt compositions. The experiments of Green(1976), Clemens and Wall(1981) and Vielzeuf and Holloway(1988) are appropriate for discussion of the compositions of peraluminous granitic liquids generated at high temperatures by fluid-absent melting of biotite. Liquid compositions obtained at lower temperatures in H_2O-saturated experiments on a tourmaline leucogranite(Benard *et al.*, 1985) are shown for comparison(Figure 5.184). The Gurgurbaba lavas do not plot in the fields for high temperature liquid compositions, and they are less mafic and calcic, enriched in K and more peraluminous than liquids generated by the fluid-absent melting of biotite(Figure 5.184).

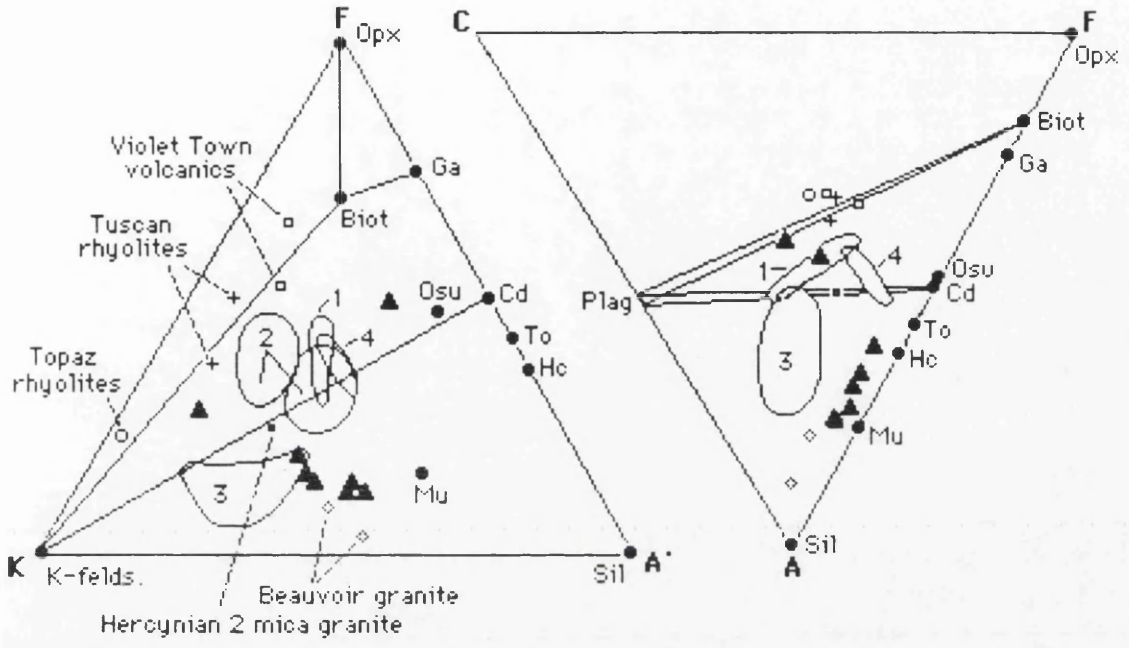

Figure 5.184. A' (Al_2O_3-Na_2O-K_2O-CaO) K(K_2O) F(FeO_t+MgO) and A(Al_2O3-Na_2O-K_2O) C(CaO) F(FeO_t+MgO) plots for the Gurgurbaba lavas(solid triangles), for various examples of crustal anatectic series and for experimental glass compositions in peraluminous systems(1, Green, 1976; 2, Clemens and Wall, 1981; 3, Benard *et al.*, 1985; 4, Vielzeuf and Holloway, 1988). Source of data: Tuscan rhyolites(Dupuy, 1970); Violet Town volcanics(Clemens and Wall, 1984); topaz rhyolites(Christiansen *et al.*, 1983); Beauvoir granite(Pichavant *et al.*, 1987b) and Hercynian two-mica granites (La Roche *et al.*, 1980). Biotite(Biot), muscovite(Mu), tourmaline(To) and hercynite(Hc) compositions taken from Pichavant *et al.* (1988). For other phases, orthopyroxene(Opx), Fe-Mg garnet(Ga), cordierite(Cd), osumilite(Osu), sillimanite and andalusite(Sill), end-member compositions have been plotted.

The compositions of rhyolites are generally similar but glassy types have higher K/Na ratios than hypocrystalline types. The analyses show high Si, K and Na, and low Ti, Mg, Ca, and P in glassy types. Most of the lavas are diopside normative. Trace element geochemistry of the lavas is typical of the Bishop Tuff(Hildreth, 1979) with generally high and covarying concentrations of Th and Rb(Figure 5.185). On the enrichment factor diagram(Figure 5.185), these rhyolite lavas display similar enrichment in magnitude and direction(except for K, Mn, Ce, Nd and Yb) to those of the Bishop Tuff.

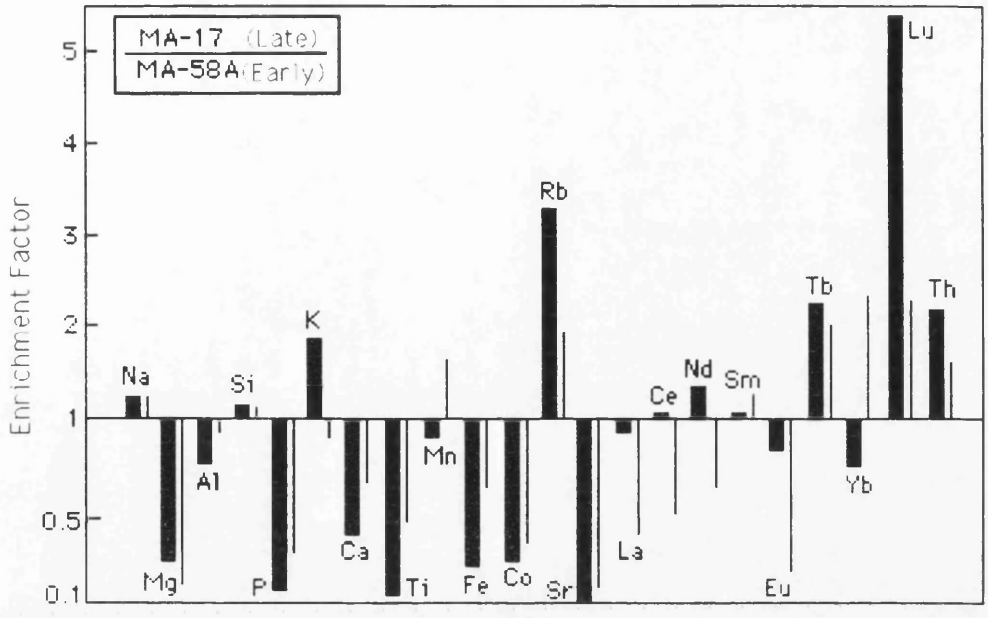

Figure 5.185. Enrichment factor diagram showing evolutionary trends in the Gurgurbaba rhyolite lava, (thick line) derived by comparing an incompatible element-rich and an incompatible element-poor sample(MA-17/MA-58A). Enrichment factors for the Bishop Tuff(early/late; Hildreth, 1979, 1981) are also shown with thin lines for comparison.

Compared to the major elements, the ranges of variation observed for the trace elements are much greater. Rhyolites are variably enriched in incompatible elements(Rb, Th, Y, Nb, Ga and HREE) and depleted in feldspar-compatible elements(Ba, Eu and Sr). Zr is generally low as well, consistent with its compatibility in fractionating zircon. The concentrations of many elements that are taken up by mafic silicates are extremely low, but as they lie near detection limits for the analytical methods and their concentrations are not well known. Generally, the rocks are enriched in elements(such as Na, Mn, Zn, Rb, Sm, HREE, Th) that tend to be concentrated roofward in silicic magma chambers, and depleted in elements(such as Mg, P, K, Ca, Ti, Cr, Fe, Co, Zr, Sr, Ba, La, Ce, Nd and Eu) that tend to be concentrated downward(Hildreth, 1979, 1981; Smith, 1979). The observed variations demonstrate the existence of compositional changes between the erupted magmas. The last erupted magmas are less fractionated relative to the first erupted. The compositional changes reflect different amounts of shallow level fractionation and, or, differences in conditions of partial melting between erupted magmas.

Using trace element compositions, Pearce *et al.* (1984) have attempted to interpret the tectonic settings of granitic rocks. In this classification(Figure 5.186), Gurgurbaba lavas consistently fall in the field of WPG(within plate granites) similar to Tala Tuff(Mahood, 1981) but one sample(MA-58A) falls clearly in the field of VAG(volcanic arc granites) similar to Bishop

Tuff(Hildreth, 1977). Although this discrimination points to a certain setting, it is unlikely that simple diagrams will provide a unique definition for these rhyolites because of the wide variety of crustal components may have involved in their genesis. Furthermore, rather than the tectonic setting existing when granitic magma was actually produced, these plots seem to diagnose the setting in which the protolith was formed(Arculus, 1987; Twist and Harmer, 1987). Therefore, trace element data reflect the nature of the source materials perhaps more strongly than the tectonic processes acting upon them(Roberts and Clemens, 1993).

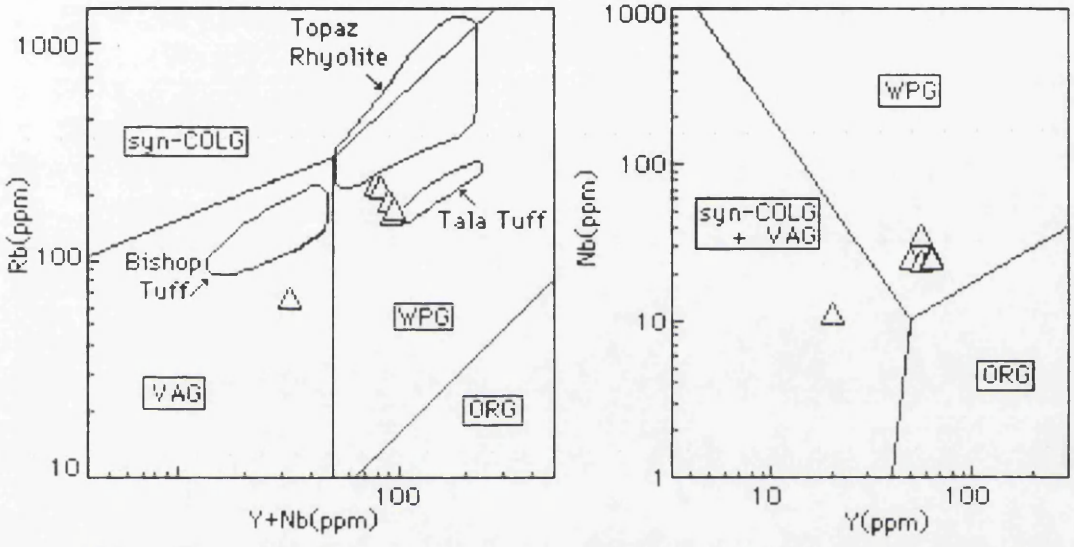

Figure 5.186. Trace element discriminant diagram for granitic rocks(Pearce *et al.*, 1984) showing the compositions of the Gurgurbaba rhyolites, the Bishop Tuff(Hildreth, 1977), the Tala Tuff(Mahood, 1981) and topaz rhyolites(Christiansen *et al.*, 1986) from the United States. VAG=volcanic arc granites; syn-COLG=syn-collision granites; WPG=within plate granites; and ORG=ocean ridge granites.

5.3.3.10.2. INCOMPATIBLE ELEMENTS

The Gurgurbaba lavas show a similar mid ocean ridge basalt(MORB) and primordial mantle(PM) normalized patterns. However, sample(MA-58A) is represented by a pattern, having lower Rb,Th, K, Nb and higher Sr ratio than other sample(Figures 5.187 and 5.188). The behaviour of compatible elements such as Ba and Sr may serve to discriminate between partial melting and crystal fractionation(e.g., Christiansen *et al.*, 1984). The use of incompatible elements(Rb) to approximate the melt fraction may lead to errors as these elements are particularly mobile during post-emplacement alteration(Pichavant *et al.*, 1988). Furthermore, devitrification mobilizes a number of trace

elements(U, F, Cl, Li, Be), but it has not been demonstrated that devitrification without significant vapor phase alteration significantly changes concentrations of many other trace elements, including the petrogenetically important elements like Rb, Sr, Ba, Y, Zr, Hf, Nb, Ta, REE, Sc and Ga(Christiansen *et al.*, 1986). In addition, hydration may involve significant addition of Sr, Ca and other elements(Hargrove, 1982).

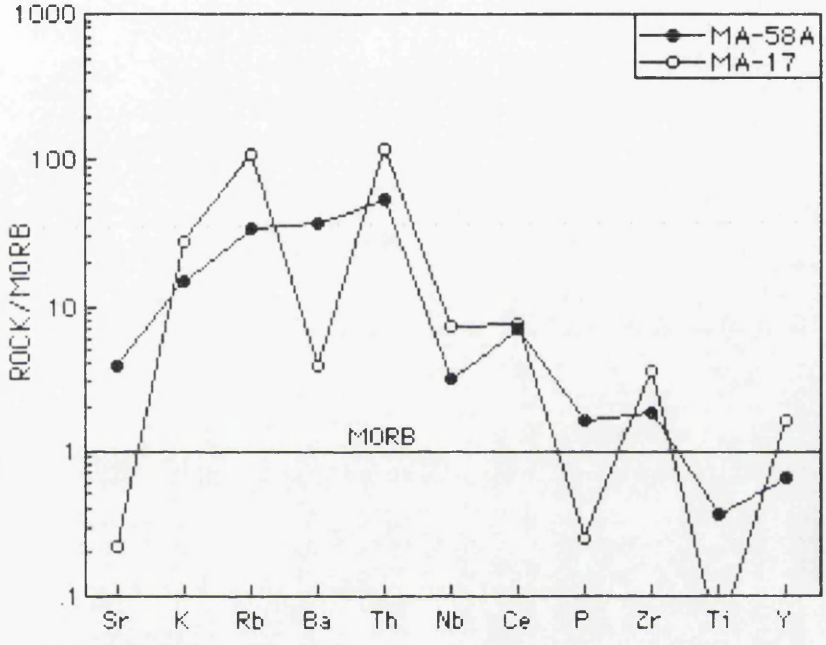

Figure 5.187. MORB-normalized trace element patterns of the Gurgurbaba rhyolites(MORB normalizing values are from Pearce, 1983).

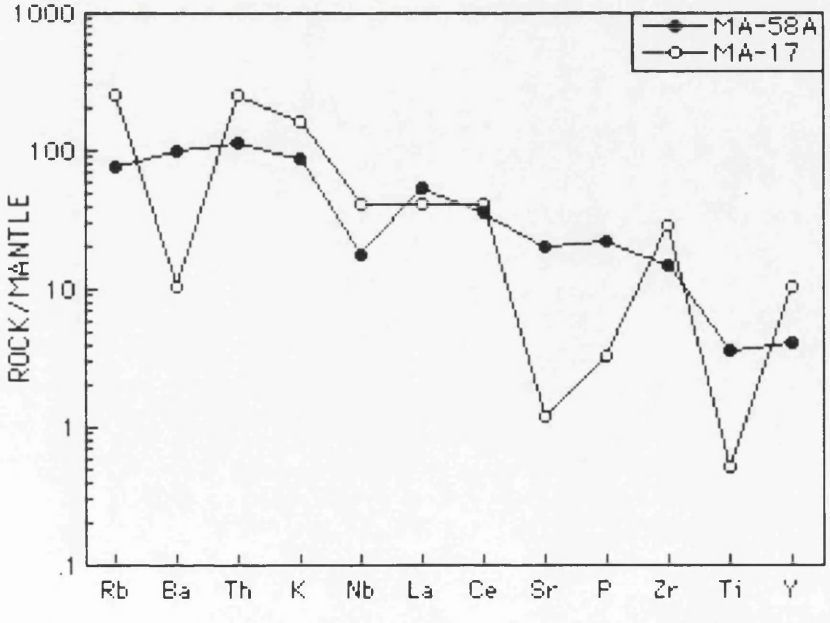

Figure 5.188. Mantle-normalized trace element patterns of the Gurgurbaba rhyolites. Normalizing primordial mantle values are from Wood *et al.* (1979a).

The trace element characteristics of two samples of the Gurgurbaba rhyolites are shown in the spider diagram in Figure 5.189, normalized to ORG(Ocean Ridge Granite) composition(Pearce *et al.*, 1984). The samples have similar concentrations and patterns for the large ion lithophile elements(LILE) except Ba, but the high field strength elements(HFSE) and the REE give slightly different picture. Generally, the samples have low concentrations of HFSE and the REE being depleted relative to ORG. This is most pronounced in the case of Zr, Sm, Y and Yb.

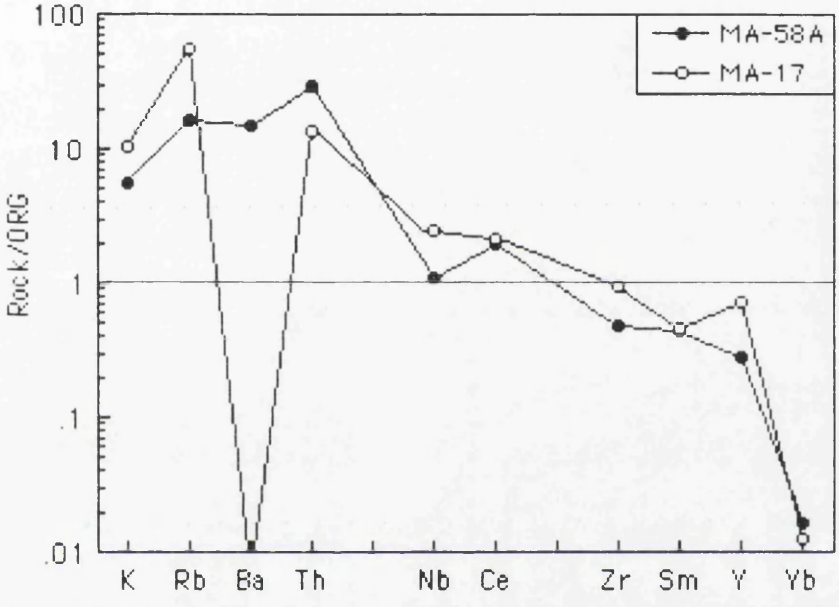

Figure 5.189. Geochemical patterns of the Gurgurbaba rhyolites normalized to Ocean Ridge Granite(ORG; Pearce *et al.*, 1984) composition.

Generally, low Ba/La, Ba/Nb and La/Th(Figure 5.190) ratios for Gurgurbaba lavas indicate that they are not related to the convergent margin magmas, but to intraplate magmas.

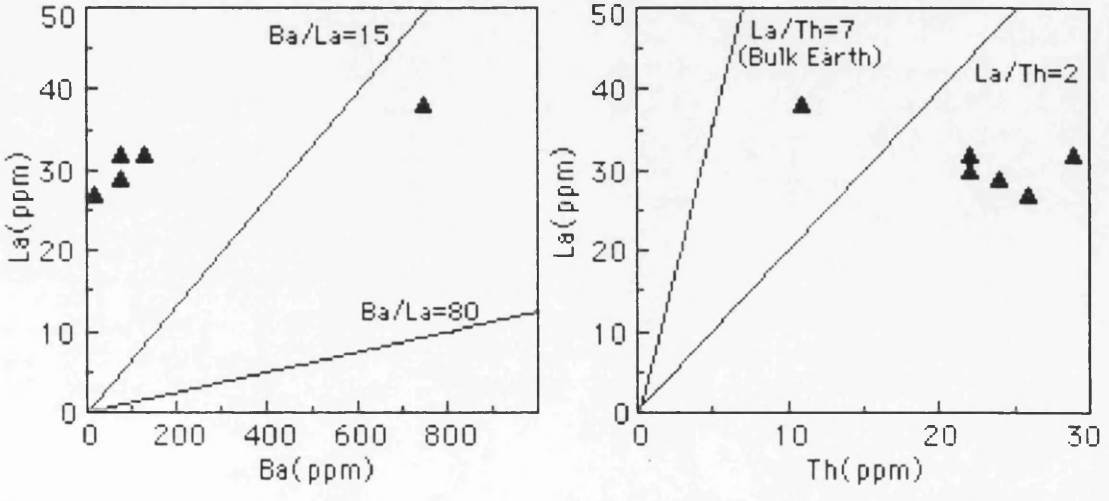

Figure 5.190. Incompatible trace element variation plots for the Gurgurbaba rhyolite lavas.

5.3.3.10.3. RARE EARTH ELEMENTS

The REE patterns of the Gurgurbaba lavas are shown in Figure 5.191. The patterns show some variability with $(La/Lu)_N$=3.19-17.99, perhaps due to different differentiation histories but they generally display low $(La/Ce)_N$=1.33-1.43, $(La/Yb)_N$=16.54-20.52, and $(Eu/Eu^*)_N$=0.96-1.01. LREE concentrations generally do not exceed 200 times chondrite values and more typically are near or less than 100 times chondrite. The presence of apatite, together with general increase in D_{REE} with increasing magmatic SiO_2, can explain the lower REE concentrations and the stronger relative depletion in Gd and Dy. The amount of zircon removed is insufficent to give rise to HREE depletion(even with D_{Yb}^{zircon}=300, Nagasawa, 1970).

The Gurgurbaba lavas are comparable with Upper Continental Crust(Taylor and McLennan, 1985), in terms of REE contents. This therefore suggests that the Gurgurbaba rhyolite might be derived from upper continental crust.

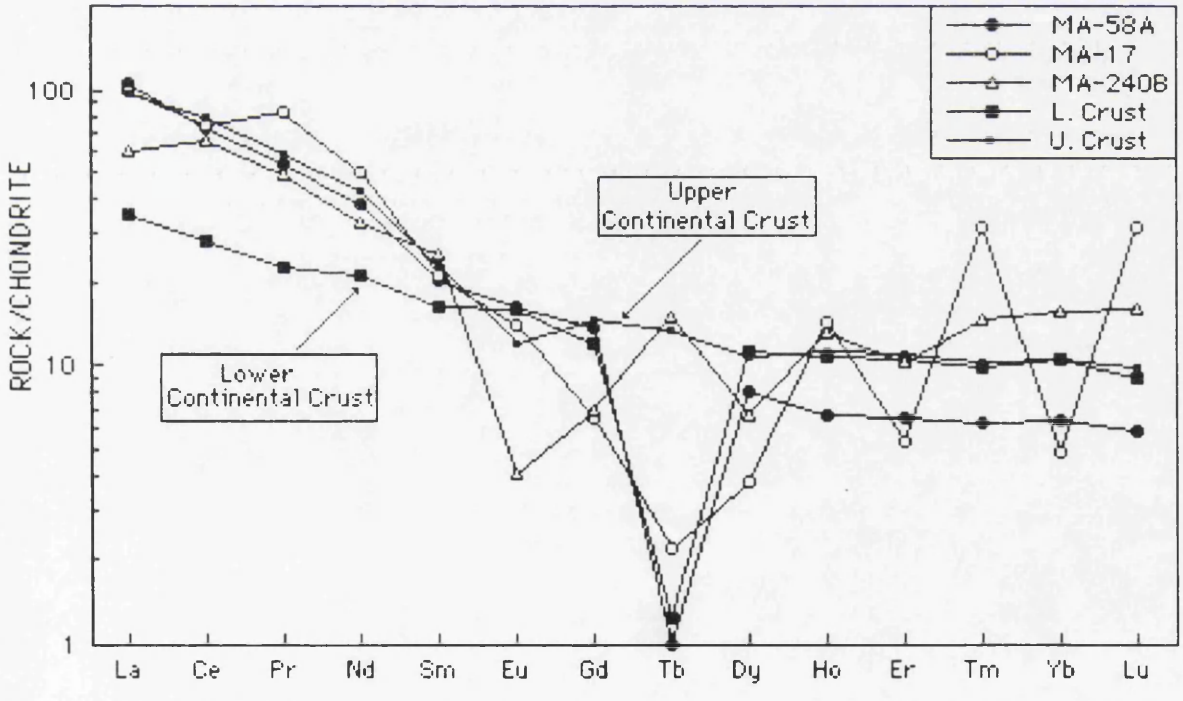

Figure 5.191. Chondrite-normalized REE patterns of the Gurgurbaba lavas(MA-58A and 17, hypocrystaline types; MA-240B, obsidian glass). Normalizing values are from Boynton(1984), Lower and Upper Continental Crust from Taylor and McLennan(1985).

5.3.3.10.4. SOURCE CHARACTERISTICS

Granitic rocks are the most abundant rocks in the crust(Clarke, 1992) and can be produced from various sources by partial melting processes(e.g., Tuttle and Bowen, 1958; Helz, 1976; Wyllie, 1983; Ellis and Thompson, 1986; Conrad *et al.*, 1988; Vielzeuf and Halloway, 1988). The amount of melt produced by this process is dependent on P-T fluid conditions at, and the composition of the source region. Granitic magmas must originally contain restite at their source and many of them never completely rid themselves of that component(Chappell and White, 1992). The proportion of the melt and restite varies from granitic rocks that are pure magma to those that contain abundant restite. Melt-dominated granitic rocks can be identified from restite- dominated ones by decreasing K/Rb with increasing SiO_2(Wyborn *et al.*, 1992). Accordingly, the Gurgurbaba rhyolites are comparable with melt-dominated granitic rocks(Figure 5.192A). Generally, the origin of silicic magmas has been ascribed to partial melting of crustal rocks, with basalt supplying the critical heat source(Hildreth, 1981; Huppert and Sparks, 1988).

Y/Nb ratio is generally unchanged by crustal assimilation(Eby, 1990), therefore varying Y/Nb ratios(Figure 5.192B) in the Gurgurbaba rhyolites at similar stages of their magmatic evolutions might have originated from heteregenous source material(Sewell *et al.*, 1992).

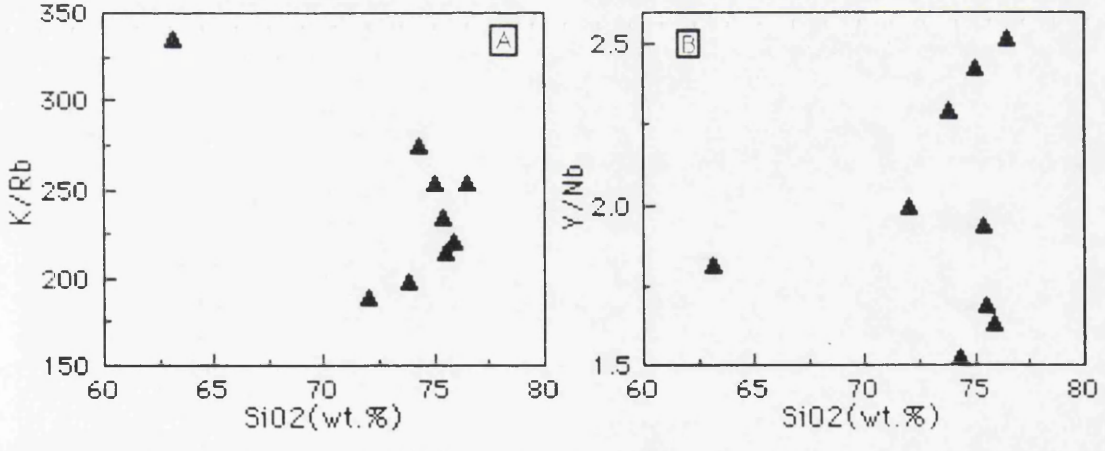

Figure 5.192. SiO_2 versus K/Rb ratio plot(A) and Y/Nb ratio plot(B) of the Gurgurbaba lavas.

5.4. TRANSITIONAL ASSOCIATION

5.4.1. THE ALADAG LAVA

5.4.1.1. MAJOR AND TRACE ELEMENTS

The Aladag lava is trachytic in composition and saturated with silica. Generally, it is silica-rich metalumious rocks. Agpaitic index (Na+K)/Al is less than 1 and normative quartz moderate(4-7.5%), in accordance with a relatively wide range of SiO_2 content. The significant aspects of major and trace element variations within rocks are represented in Figures 5.193, 5.194, 5.195 and 5.196. Generally, the rocks are a chemically coherent set of samples whose data define a smooth major element trends relative to SiO_2. $Fe^*_2O_3$(total), and Na_2O+K_2O contents decrease whereas CaO, TiO_2, and Al_2O_3 increase with increasing SiO_2(Figure 5.193). Trace elements also define smooth trends. Zr, Rb, Th, Ni, Co and Cr decrease whereas Y, Ga, Zn and La increase with increasing SiO_2(Figures 5.194 and 5.195). Depletion in MgO, P_2O_5, Rb, Co, Ni and enrichment in Y, La, Ga, CaO and high Ba/Sr ratios represents the rocks derived by crystal fractionation from less evolved rocks.

Crystal-liquid fractionation as an operative differentiation tool in silicic magmas has been seriously critized(e.g., Hildreth, 1981); however it is still the most important way of deriving intermediate and felsic rocks from basaltic magmas, although more efficient mechanisms than simple crystal settling have been proposed(McBirney *et al.*, 1985). Quantitative modelling of trace elements is subject to considerable uncertainty because the mode involves large amounts of feldspar. Drake and Weill(1975) have demonstrated that plagioclase/melt distribution coefficients are temperature and melt-composition dependent. The Aladag lavas show major and trace element variation that is consistent with crystal fractionation controlled by clinopyroxene, magnetite and plagioclase(Figure 5.197).

A two feldspar occurrence is suggestive of near water-saturated conditions. Fractionation of an anhydrous assemblage dominated by sanidine, with small amounts of cpx, Fe-Ti oxides, apatite and zircon, could have led to a progressive H_2O enrichment culminated with a renewed coprecipitation of two-feldspar assemblage in the magma. Nevertheless, the following chemical data argue against this hypothesis; (a) high Ba and Sr abundances with the expected depletion produced by alkali feldspar separation, (b) the considerable Th enrichment is not consistent with zircon fractionation($D_{Th}^{(zircon/melt)}$=61-92, Mahood and Hildreth, 1983).

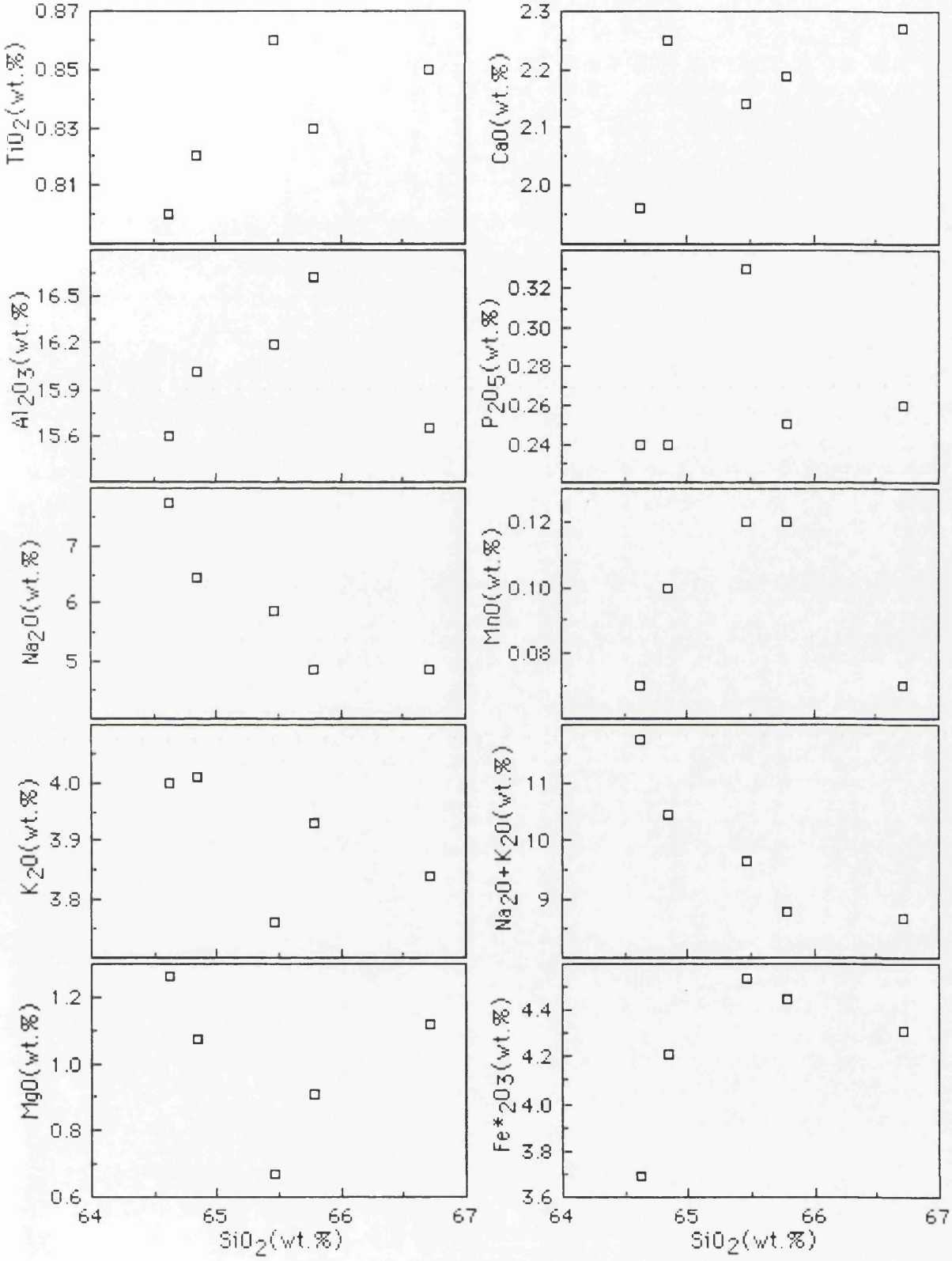

Figure 5.193. SiO_2 versus major element plots for the Aladag lavas.

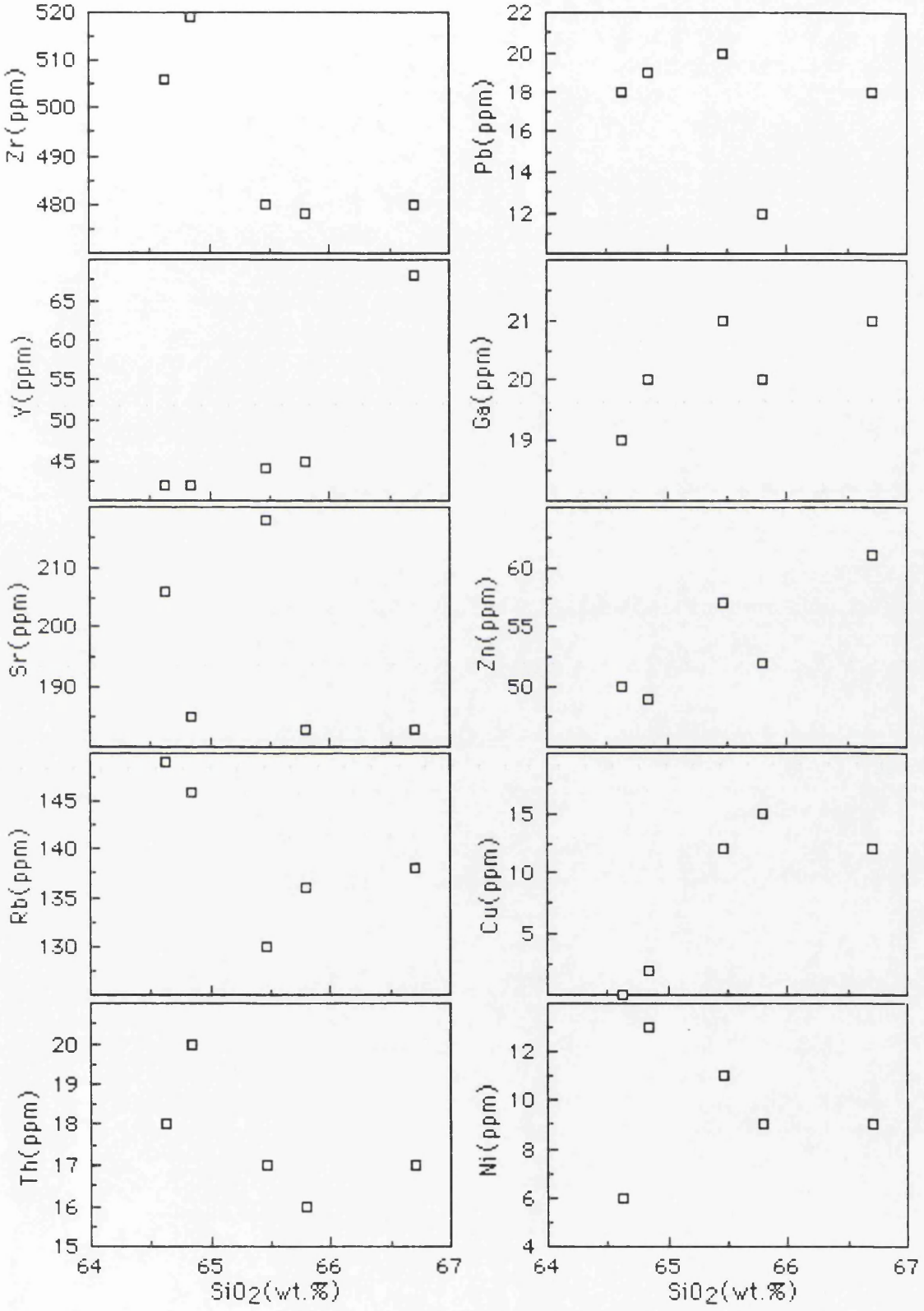

Figure 5.194. SiO_2 versus trace element plots for the Aladag lavas.

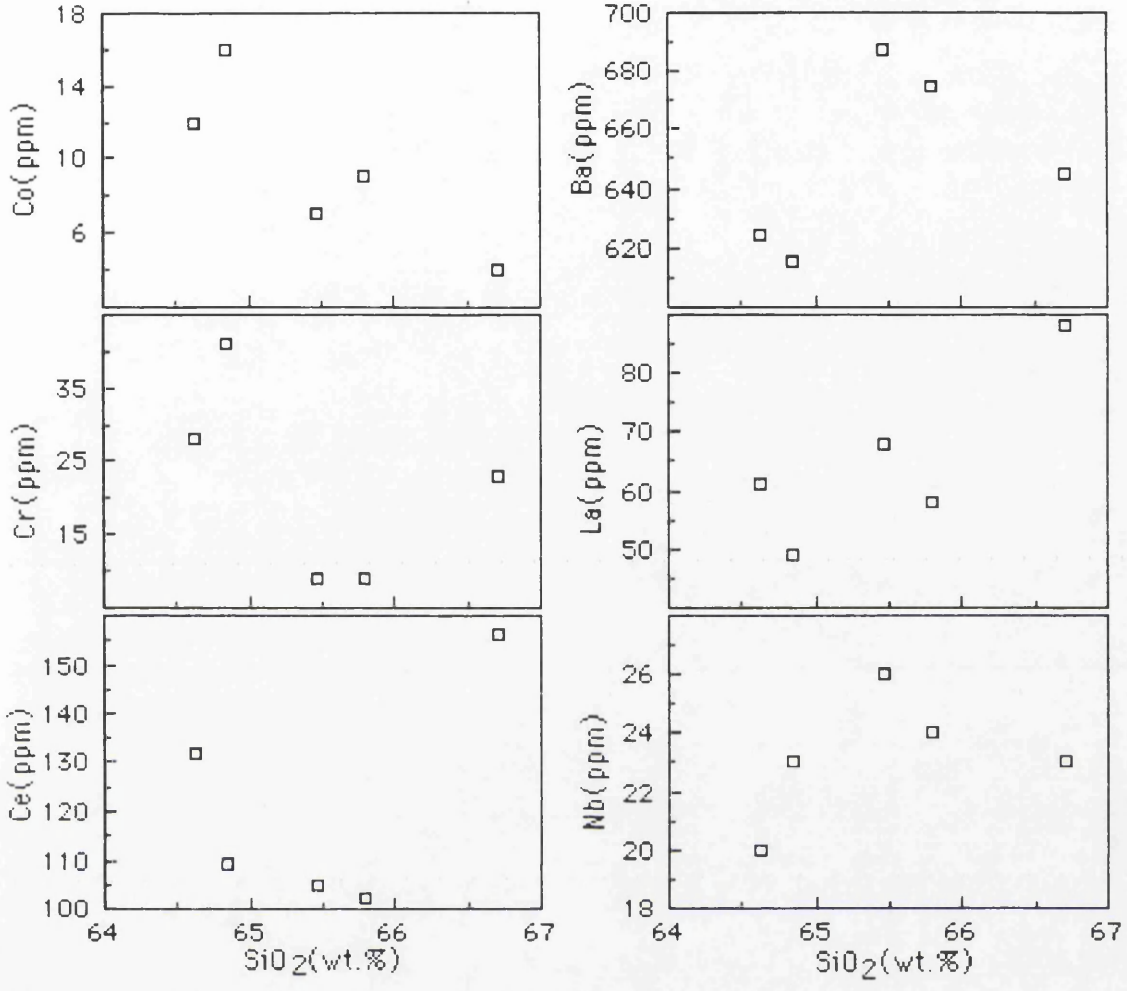

Figure 5.195. SiO_2 versus trace element plots for the Aladag lavas.

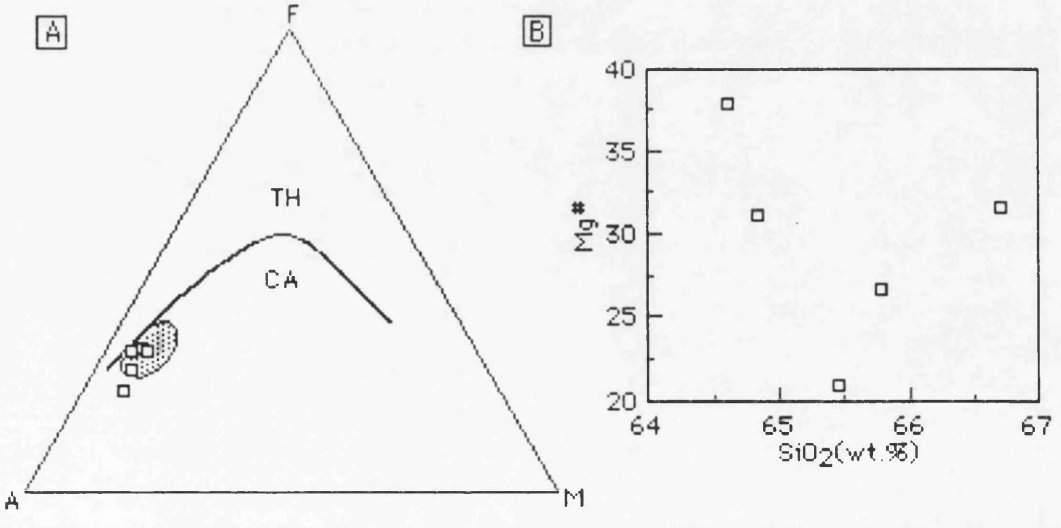

Figure 5.196. (A), AFM plot showing the composition of the Aladag lava. The trachytes of the Meydan alkaline association(shaded area) are shown for comparison. The thick line separates tholeiitic(TH) and calcalkaline(CA) compositions(Irvine and Baragar, 1971). (B), Mg-number [$Mg^{\#}$=100xMg/(Mg+Fe^{+2})] versus SiO_2(wt.%) plot.

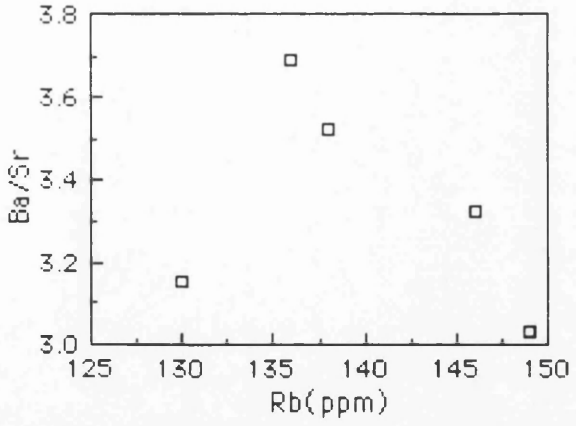

Figure 5.197. Rb versus Ba/Sr ratio reflecting crystal fractionation for the Aladag lava.

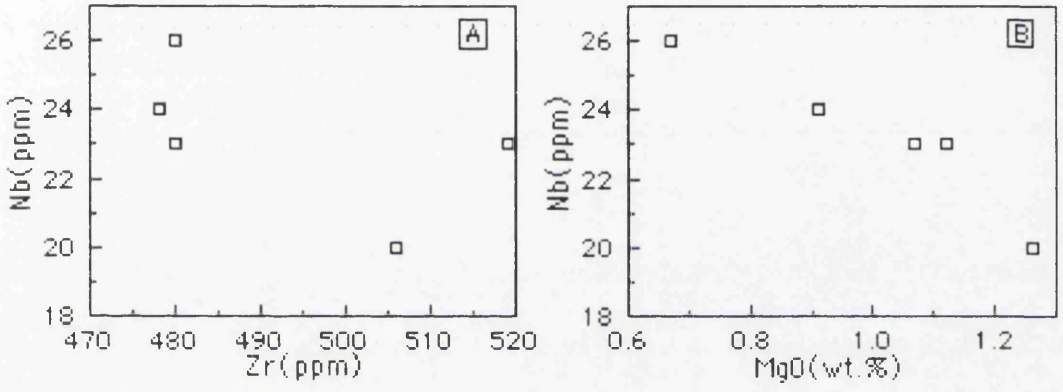

Figure 5.198. Zr versus Nb plot(A) showing the effect of zircon fractionation, and MgO versus Nb plot(B).

With increasing differentiation, the trachytic melts also become richer in SiO_2, MgO, K_2O and TiO_2 and poorer in Al_2O_3, CaO, P_2O_5 and Zr. These variations are consistent with fractionation of anorthoclase and small amounts of apatite and zircon. FeO(total) decreases which is consistent with fractionation of magnetite.

In general terms, Zr, Nb and Rb all behave as incompatible elements with variable but fairly uniform enrichment(Figure 5.198). Ba and Sr show a marked decrease while Y variations are scattered, a feature taken to reflect abundant apatite in the rocks(D_{ap}^{Y}=15-40; Pearce and Norry, 1979).

5.4.1.2. INCOMPATIBLE ELEMENTS

The incompatible element abundances of the Aladag lava have been normalized to mid-ocean ridge basalt(MORB) and primordial mantle(PM) values and given in Figures 5.199 and 5.200. Generally, samples show similar patterns having enrichment mainly in the large ion lithophile(LIL) elements, K,

Rb, Ba, Th and LREE. These patterns highlight a source enrichment process when pyroxene, plagioclase and oxide are the only crystallizing phase.

The rocks have less pronounced Nb anomalies reflecting small proportion of subduction component in the genesis of the lavas. In addition, they display significant negative Ba, P and Ti anomalies, presumably indicating the fractionation of plagioclase, apatite and Fe-Ti oxides.

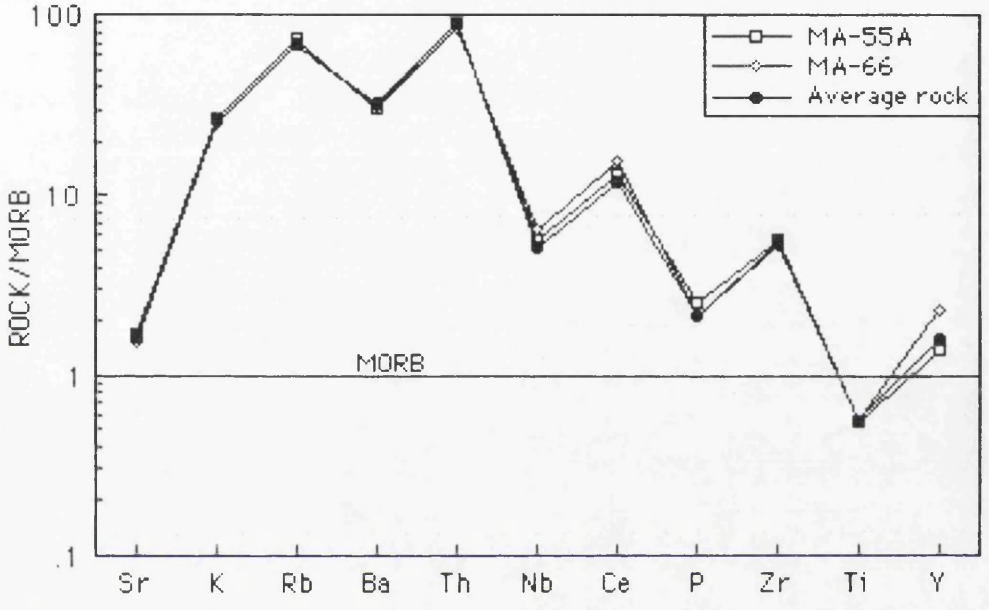

Figure 5.199. MORB-normalized trace element patterns of the Aladag lava(MORB normalizing values are from Pearce, 1983).

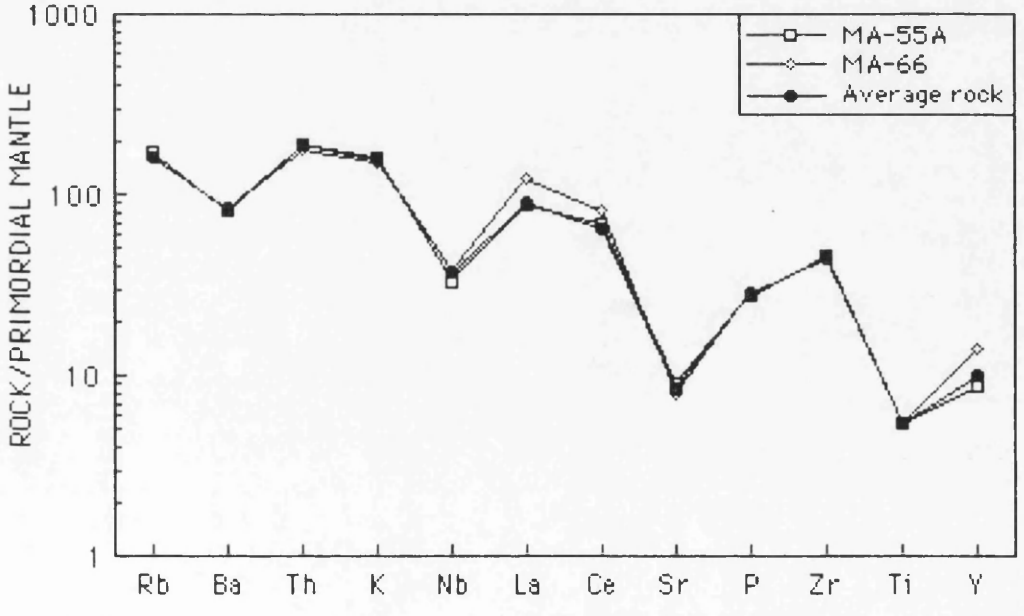

Figure 5.200. Mantle-normalized trace element patterns of the Aladag lava. Normalizing primordial mantle values are from Wood *et al.* (1979a).

5.4.2.3. RARE EARTH ELEMENTS

The Aladag lava has high total REE contents and characterized by a moderate negative Eu anomaly. The rock is clearly REE enriched and La abundance is about 200 times chondrite. The rock has moderately fractionated REE patten with $(La/Lu)_N$=10 and $(Eu/Eu^*)_N$=0.78. HREE contents show rather a flat pattern(Figure 5.201). Clearly the LREE are not behaving as incompatible elements in the rock. Apatite fractionation will contribute to the apparent compatible behaviour of the LREE(D_{ap}^{LREE}=10-80; Nagasawa, 1970; Watson and Green, 1981). The non-incompatible behaviour of the LREE in felsic liquids has been emphasized by Miller and Mittlefehldt(1982).

Although the behaviour of the REE in felsic magma is not well understood(e.g., Miller and Mittlefehldt, 1982), in the absence of zircon fractionation and within the known distribution coefficients of trachytic lavas(Berling and Henderson, 1969; Korringa and Noble, 1971; Long, 1978; Pearce and Norry, 1979). The uniform REE patterns(Figure 5.201) and the inter-element variation may suggest a simple genetic relationship between the Aladag lava and Meydan trachyte. However, the Meydan trachytes do not exhibit a characteristic Eu anomaly whereas the Aladag lava does. Zircon does occur as a groundmass phase in the Aladag lava but its extremely small size suggests that it would be unlikely to fractionate by gravitational settling.

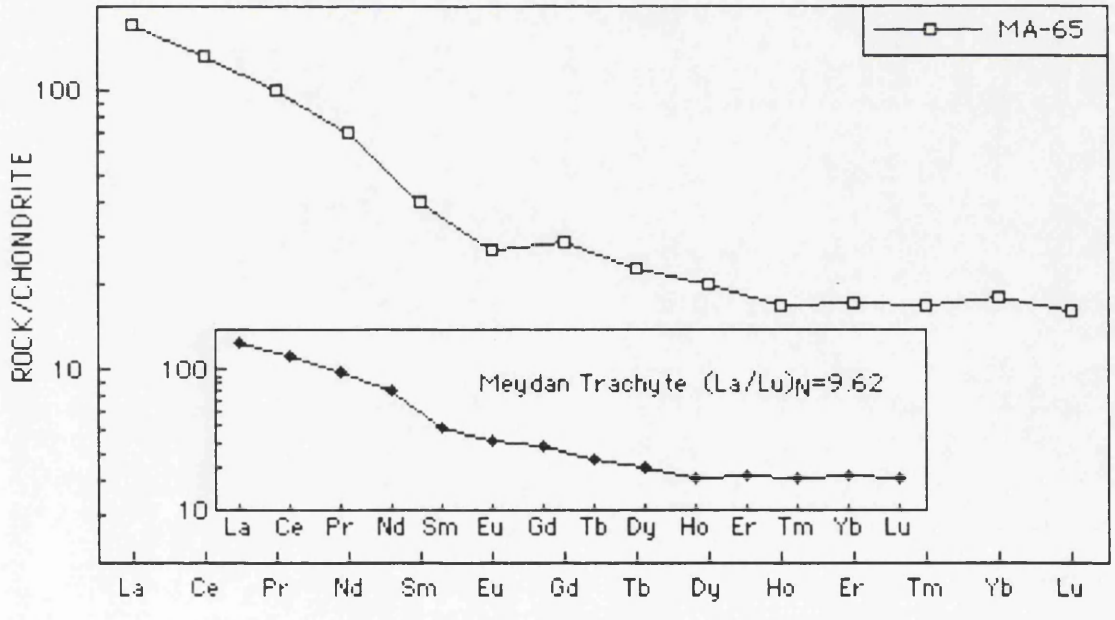

Figure 5.201. Chondrite-normalized REE patterns of the Aladag trachyte lava. Meydan trachyte is also shown for comparison. Normalizing values are from Boynton(1984).

5.4.2. THE ZILAN LAVA

5.4.2.1. MAJOR AND TRACE ELEMENTS

The Zilan lava is trachytic in composition with an SiO_2 range of 62-64 and Mg-number 27-54. Although they plot in the mildly alkaline field in a SiO_2 versus total alkalis diagram(Le Bas *et al.*, 1986), they do not reflect chemical features of alkaline volcanic rocks. Furthermore, they show transition between subalkaline and alkaline character with Nb/Y ratio 0.53-0.61 and Zr/TiO_2 ratio 002-0.04 if the Nb/Y ratio is considered as a index of alkalinity(Winchester and Floyd, 1977). They show no iron enrichment on the AFM plot(Figure 5.202).

Variation in the major and trace element composition is important despite the limited analysed samples. They have TiO_2(1.12-1.31 wt. %), Al_2O_3(16.10-17.83 wt.%), MgO(1.11-3.19 wt.%), CaO(3.94-4.92 wt.%) and FeO*/MgO ratio 4.70-1.53. Trace elements, Zr, Y, Rb, Ce, Ba, also display important variations. These major and trace element compositional variations can be explained by crystal fractionation. Moreover, Ba/Sr ratio increases with increasing Rb content, emphasising that the rock evolved by crystal fractionation.

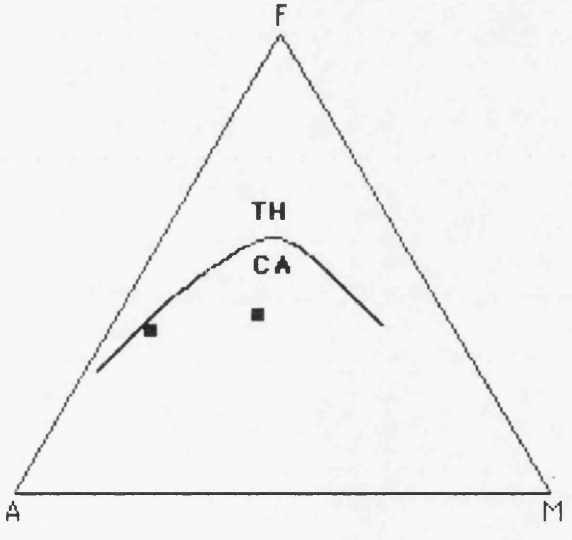

Figure 5.202. AFM plot showing the composition of Zilan lava. The thick line separates tholeiitic(TH) and calcalkaline(CA) compositions(Irvine and Baragar, 1971).

SiO_2 is poor indicator of fractionation due to the narrow range in the rock. Zr, Nb, Rb, Ba and Y all behave as incompatible elements with a significant enrichment. The major and trace elements have been plotted against Zr. Since Zr is incompatible and shows a wide range in the samples, and is considered to partition strongly in favour of the melt it has been chosen as a

fractionation index. TiO_2, CaO, Al_2O_3, P_2O_5, MnO and MgO display positive correlation whereas Na_2O, K_2O and FeO* show negative correlation with Zr(Figure 5.203). In addition, trace elements(Y, Rb, Nb, Ce, Ba, Ga, La, and Zn) correlate positively whereas Co, Cr and Cr exhibit negative correlation with Zr(Figure 5.204).

It can be assumed to a first approximation that trace and major element trends are dependent on the crystal fractionation processes. The trends in Figure 5.203 and 5.204 indicate that crystal fractionation is the main mechanism in element variation between samples. This is clear from a mutual increase in the incompatible elements Nb, Y, Zr, Rb, La and Ce. The increase in CaO, MgO, TiO_2 with Al_2O_3 all show that plagioclase, cpx and Fe-Ti oxide did not crystallize simultaneously. The decrease of K_2O may be explained by crystallization of anorthoclase. The positive correlation of TiO_2 and P_2O_5 with Zr emphasises the significance of apatite and Fe-Ti oxide fractionation. The positive correlation of Zr with incompatible elements, Nb, Rb and Ba, indicates the lack of zircon fractionation. The ratios of HFSE are variable between two samples(e.g., Nb/Zr=0.06-0.11). There is also significant variation in the range of LILE/HFSE(e.g., Rb/Zr=0.22-0.44). LILE/HFSE ratios which decrease with increasing Zr content, suggest the fractionation of anorthoclase. In addition, decreasing Sr/Zr with increasing Zr implies plagioclase+cpx fractionation.

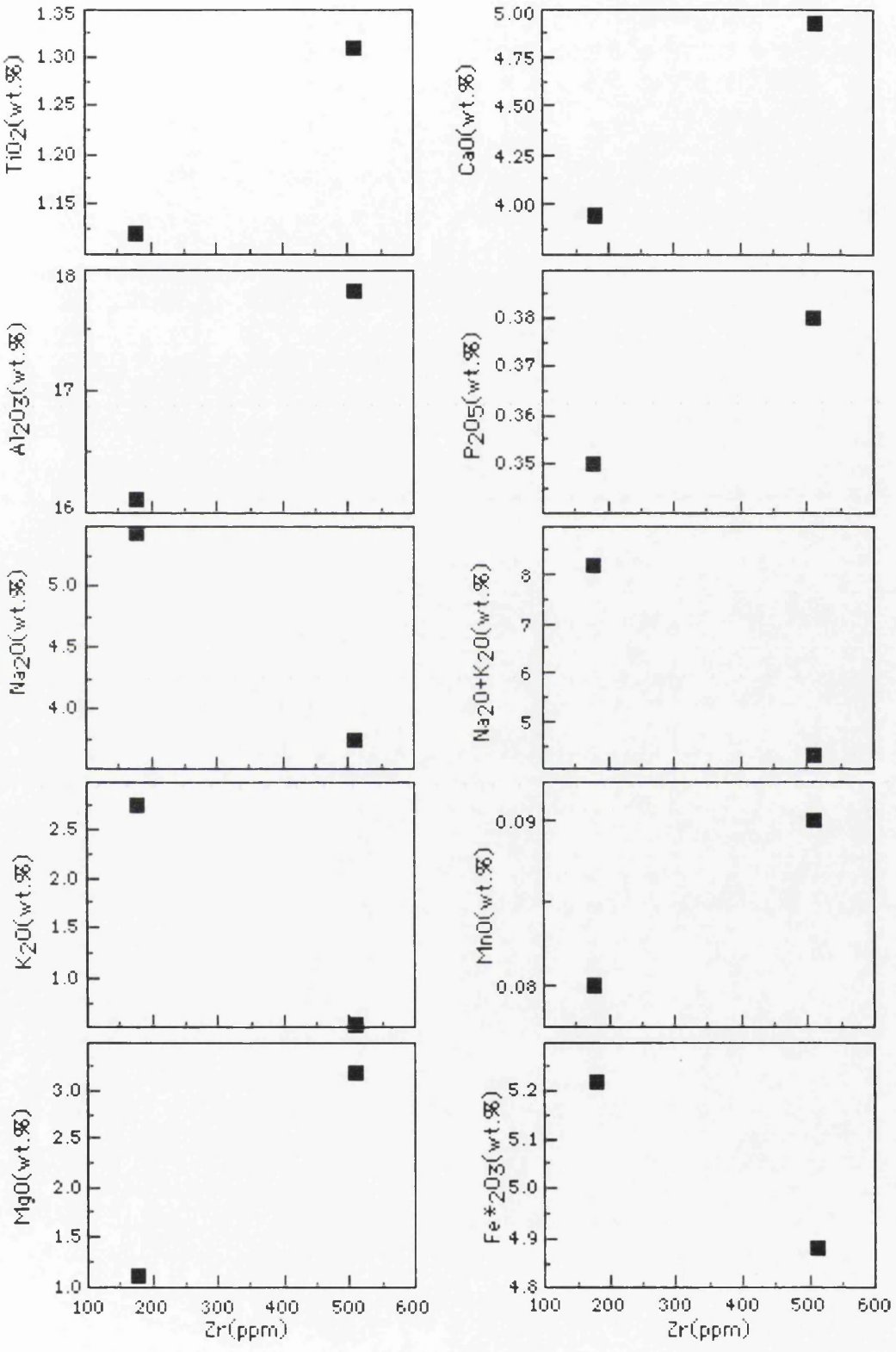

Figure 5.203. Zr (ppm) versus major element plots for the Zilan lava.

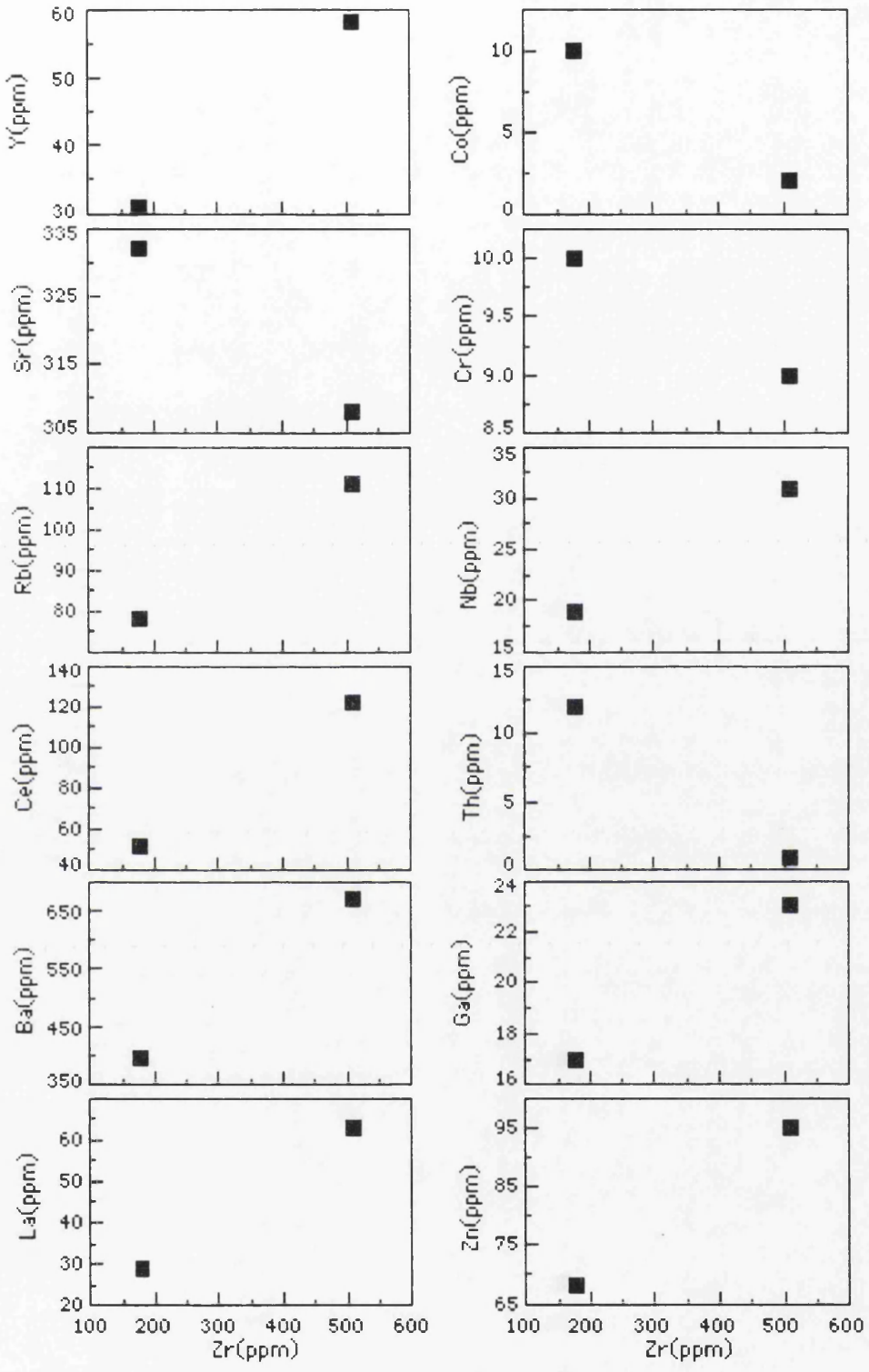

Figure 5.204. Zr(ppm) versus trace element plots for the Zilan lava.

5.4.2.2. INCOMPATIBLE ELEMENTS

The MORB- and PM-normalized incompatible element patterns of two samples are shown in Figures 5.205 and 5.206. In general, both samples display similar patterns marked by enrichments in all elements from Sr to Y(Figure 5.205). However, a general change from sample 226A to MA-263 is characterized by increase in incompatible elements, except K and Th. This

relative incompatible element enrichment between two samples could be due to degree of fractionation. On MORB-normalized patterns(Figure 5.205), they show marked negative Ba, P, Ti and slight Nb anomalies. Similarly, negative Ba, Sr, P, Ti and Nb anomalies are pronounced in PM-normalized patterns. These negative anomalies may result from fractionating phases such as plagioclase, apatite and Fe-Ti oxides.

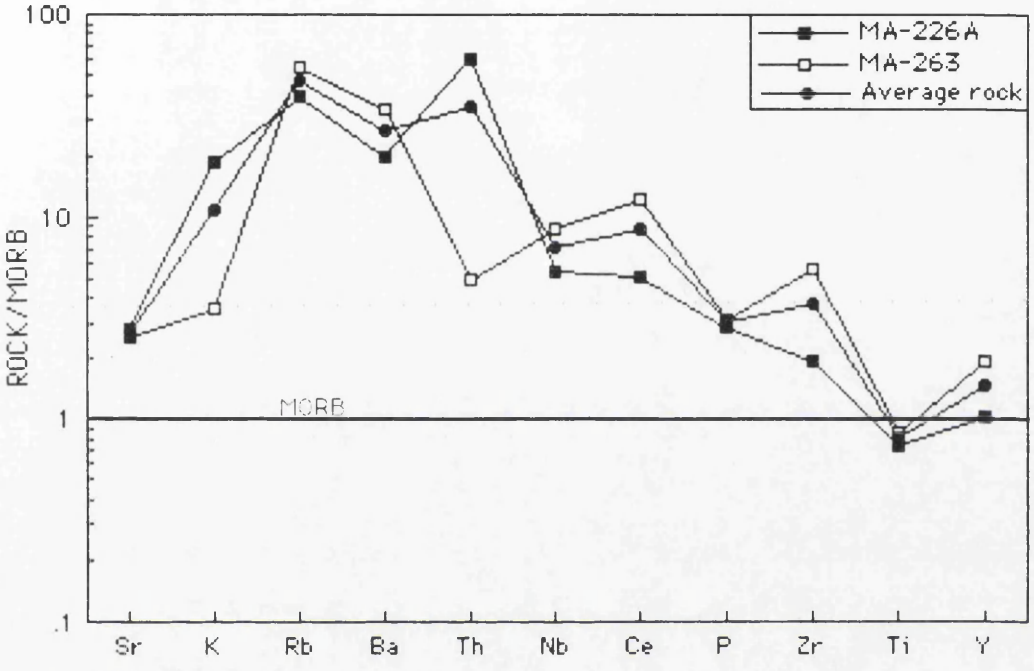

Figure 5.205. MORB-normalized trace element patterns of the Zilan lava(MORB normalizing values are from Pearce, 1983).

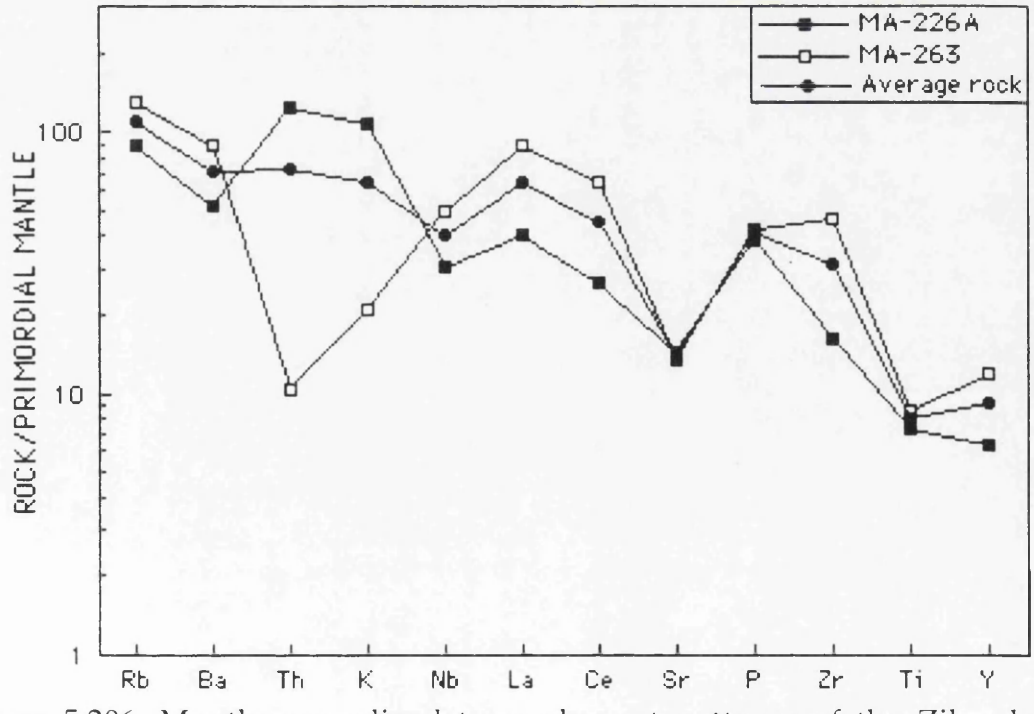

Figure 5.206. Mantle-normalized trace element patterns of the Zilan lava. Normalizing primordial mantle values are from Wood *et al.* (1979a).

5.4.2.3. RARE EARTH ELEMENTS

The REE patterns of two samples from the Zilan lava are shown in Figure 5.207. Although they have different REE contents, both samples have similar patterns represented by LREE enrichment and relatively flat HREE. Generally, the patterns are moderately fractionated with $(La/Lu)_N$=8.06-8.66. The high total REE enrichment in sample MA-263 relative to sample 226A is probably due to extensive crystal fractionation(Zr/Nb=9.37-16.45). Both samples lack significant Eu anomalies with $(Eu/Eu^*)_N$=0.95-1.25, implying that plagioclase was not an important fractionating phase in the evolution of the rocks. In general, the LREE appear to be incompatible. Apatite fractionation will contribute to the compatible behaviour of the REE(D_{ap}^{LREE}=10-80; Nagasawa, 1970; Watson and Green, 1981). HREE fractionation as indicated by the Tb/Yb ratio is nearly the same in both samples$(Tb/Yb)_N$=1.35-1.36.

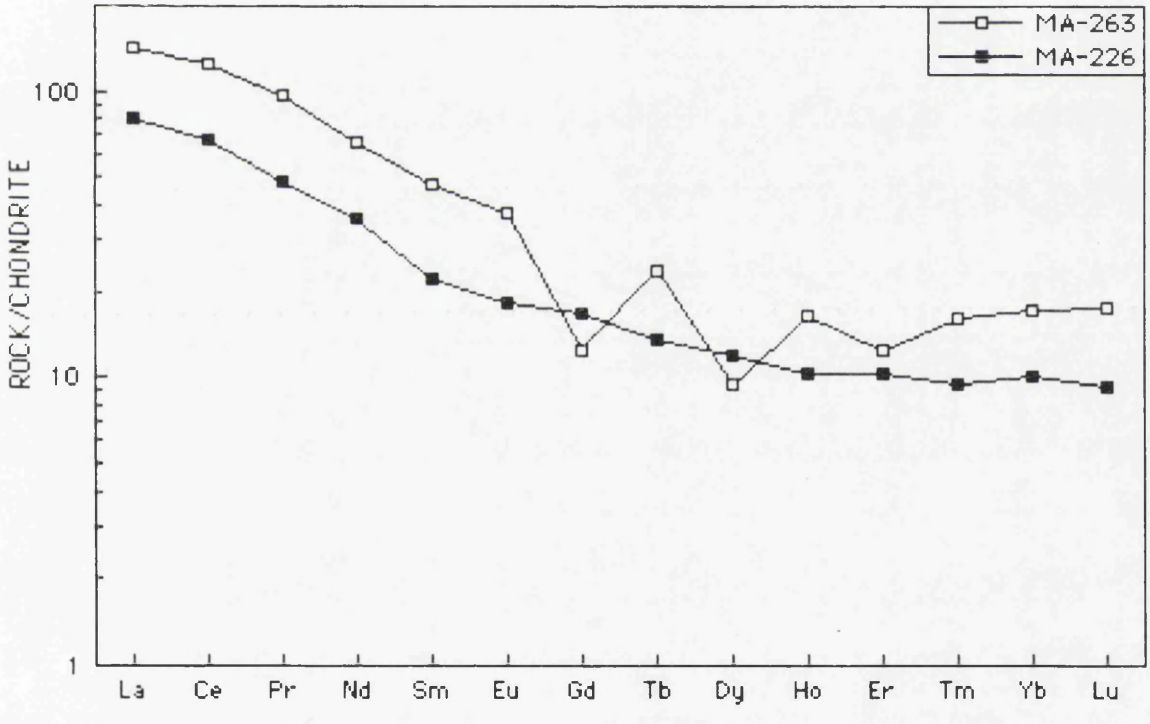

Figure 5.207. Chondrite-normalized REE patterns of the Zilan lava. Normalizing values are from Boynton(1984).

CHAPTER 6. OXYGEN AND STRONTIUM ISOTOPE GEOCHEMISTRY

6.1. INTRODUCTION

This chapter describes the O and Sr isotope variations found in the alkaline and calcalkaline volcanic rocks of the Meydan-Zilan area. Generally, the calcalkaline rocks are more evolved than the alkaline lavas that include primitive basaltic magmas. Various models have been proposed to interpret the genesis of the Eastern Anatolian volcanic rocks(e.g., Innocenti *et al.*, 1980, 1982a; Ercan *et al.*, 1990; Pearce *et al.*, 1990). O and Sr isotopes will be used to examine and extend hypotheses developed in the previous studies, and to develop models based upon isotope and trace element data.

O and Sr isotopes should be good indicators of crustal contamination or assimilation because crustal rocks are enriched in ^{18}O and ^{87}Sr compared with primary mantle-derived magmas(Taylor, 1980; James, 1981). Many authors have suggested that the $^{87}Sr/^{86}Sr$ ratios of primary calcalkaline magmas in continental settings have been modified by mixing with ^{87}Sr-rich crustal material(e.g., Leeman and Manton, 1971; Francis *et al.*, 1980; Briqueu and Lancelot, 1979; Leeman, 1981).

6.2. THE APPROACH OF ISOTOPE STUDY

It has increasingly been demonstrated(e.g., Dosso and Murthy, 1980; Menzies and Murthy, 1980a, b; Hawkesworth *et al.*, 1984) that the low ε_{Nd}, high ε_{Sr} signatures that typify upper continental crust can also be found in wholly mantle-derived samples. It is now accepted that some portions of the upper mantle, particularly the sub-continental lithospheric mantle, preserve a record of long-lived heterogeneity with, amongst other characteristics, elevated Rb/Sr and low Sm/Nd; with time, these generate high $^{87}Sr/^{86}Sr$ and low $^{143}Nd/^{144}Nd$ so that radiogenic isotopes are no longer thought to provide unequivocal discrimination between crust and mantle sources(Ellam and Harmon, 1990).

As a consequence, the recognition of interaction between mantle-derived magmas and continental crust remains problematical, especially at destructive plate margins. In this setting, not only is there potential for assimilation of continental materials as magmas pass through the continental crust(e.g., Harmon *et al.*, 1981; Hildreth and Moorbath, 1988; Davidson and Harmon, 1989), i.e. crustal contamination, but, there is also the possibility that crustal materials are injected into the mantle by subduction resulting in mantle source

contamination(e.g., Kay, 1977; Rogers *et al.*, 1985, 1987; Tera *et al.*, 1986; Woodhead *et al.*, 1987; Ellam and Harmon, 1990).

Several studies have sought to refine crust-mantle discrimination by combining radiogenic isotope variations with major and trace element data(e.g., Davidson, 1986; Hickey *et al.*, 1986a, b; Ellam *et al.*, 1988, 1989; Rogers and Hawkesworth, 1989). Distinctive isotope-trace element trends that are thought to distinguish crust and mantle processes have emerged. In these, a key factor has been the behaviour of Sr, which is compatible with plagioclase in the upper crust but incompatible in the mantle and, perhaps, also in lower crust that is plagioclase-free(e.g., Hawkesworth and Vollmer, 1979; Cox and Hawkesworth, 1985). Thus, although progress has been made towards the distinction of mantle and crustal processes by combining the information available from both radiogenic isotope ratios and elemental abundance data, additional independent constraints are needed.

Oxygen isotope data provide a means of testing the proposed crust-mantle discrimination techniques because $^{18}O/^{16}O$ ratios are sensitive indicators of crustal involvement in magmatism. A large body of data on upper mantle peridotite xenoliths, mid-ocean ridge basalts, oceanic basalts and intra-oceanic island arc basalts indicate that the extent of ^{18}O heterogeneity within the mantle is small, the upper mantle having an average $\delta^{18}O$ value of about +5.8±0.8‰(e.g., Taylor, 1968; Muehlenbachs and Clayton, 1972; Pineau *et al.*, 1976; Kyser *et al.*, 1982; Harmon and Hoefs, 1984; Ito *et al.*, 1984; Harmon *et al.*, 1986; Kempton *et al.*, 1988). In contrast, the continental crust and oceanic crust display much more variation in O-isotope composition, because oxygen isotope fractionation occurs most readily in silica-rich systems at low temperature. In general, high $\delta^{18}O$ values are found in rocks that have experienced a cycle of crustal residence and weathering, or were formed at low temperature in the presence of marine or meteoric water. Contamination of mantle-derived magmas with such rocks in the continental crust will introduce a high ^{18}O signature to the lavas which is diagnostic of crustal involvement.

In this study, alkaline and calcalkaline volcanic rocks from the Meydan-Zilan area, where continental type crust is well developed, were analyzed for O and Sr isotopes. The results will be discussed in the light of the above points and in view of O-Sr isotopic variations that are considered diagnostic of particular petrogenetic processes.

6.3. OXYGEN AND STRONTIUM ISOTOPE RESULTS

Oxygen isotopic results from mineral separates and whole-rock $^{87}Sr/^{86}Sr$ isotopic results are presented in Tables 6.1 and 6.2 together with SiO_2, K, Rb and Sr concentrations. The total range of plagioclase $\delta^{18}O$ values and whole-rock $^{87}Sr/^{86}Sr$ ratios are +7 to +9‰ and 0.704819 to 0.706369, respectively. Sr contents range from 183 to 837 ppm with the exception of a few samples with lower values. K/Rb ratios are mostly in the range ~100 to 1500. Rb/Sr ratios vary from 0.02 to 0.74 with exception of two samples(Rb/Sr=2.5-3).

Basaltic rocks, alkali olivine basalt and hawaiite, from the Meydan alkaline suite have plagioclase $\delta^{18}O$ values about +7‰ which is comparable with mantle derived magmas(Kyser, 1986). However, the evolved rocks of the suite have higher $\delta^{18}O$ values of +8‰ to +9.5‰. Silicic rocks have variable $\delta^{18}O$ values ranging from +7‰ to +9‰. The $\delta^{18}O$ values of the calcalkaline rocks are in the same range as the Meydan alkaline rocks. Different minerals are variably susceptible to oxygen isotope exchange, feldspars being more readily affected than quartz or ferromagnesian minerals(Taylor, 1987). Thus, differences in $\delta^{18}O$ may be due to either changes in the $\delta^{18}O$ value of meteoric fluids with time, or reflect variations in water/rock ratios.

At magmatic temperatures the fractionation of O-isotopes between plagioclase and silicate melts is generally less than 0.3‰. Plagioclase in equilibrium with basaltic liquids typically has $\delta^{18}O$ values slightly higher than the magma from which it crystallized(Muehlenbachs and Kushiro, 1974; Kyser *et al.*, 1981) whereas in more evolved magmas the sense of fractionation is reversed, producing plagioclase with slightly lower $\delta^{18}O$(Taylor and Sheppard, 1986). In the Meydan basaltic rocks, the plagioclase probably has a $\delta^{18}O$ value close to that of the original magma. Consequently the +5.6‰ $\delta^{18}O$ value represent the best estimate for the original $\delta^{18}O$ of the Meydan magma, well within the range of $\delta^{18}O$ described for mantle-derived basalts(Kyser, 1986).

Table 6.1. $\delta^{18}O$ isotope compositions of mineral separates from Meydan-Zilan area volcanic rocks.

	Rock Type	Sample No	Mineral Separates	$\delta^{18}O(\pm\sigma)$(SMOW)
Meydan Alkaline Suite	Alkali olivine basalt	MA-236	Plagioclase	+7.18 ± 0.1
			Augite	+6.84 ± 0.1
	Hawaiite	MA-235	Plagioclase	+6.96 ± 0.1
	Mugearite	MA-53	Plagioclase(phenocryst)	+7.85 ± 0.1
			Plagioclase(groundmass)	+7.29 ± 0.1
			Augite	+5.31 ± 0.1
			Magnetite	+5.39 ± 0.1
	Benmoreite	MA-35	Plagioclase	+8.25 ± 0.1
			Augite	+7.14 ± 0.1
			Magnetite	+6.17 ± 0.1
	Trachyte	MA-238	Plagioclase	+9.96 ± 0.1
			Kaersutite	+8.11 ± 0.1
			Magnetite	+6.03 ± 0.1
Transitional Suite	Aladag lava	MA-55	Plagioclase	+8.27 ± 0.1
			Magnetite	+4.55 ± 0.1
	Zilan lava	MA-263	Plagioclase	+8.33 ± 0.1
			Magnetite	+5.70 ± 0.1
Medium-K Suite	Andesite	MA-131	Plagioclase	+8.79 ± 0.1
		MA-223	Plagioclase	+8.35 ± 0.1
	Trachyandesite	MA-143	Plagioclase	+8.25 ± 0.1
	Dacite	MA-122	Plagioclase	+8.26 ± 0.1
		MA-187	Plagioclase	+8.36 ± 0.1
High-K Suite	Ignimbrite	MA-45	Plagioclase	+7.63 ± 0.1
		MA-57	Plagioclase	+7.25 ± 0.1
		MA-186	Plagioclase	+7.13 ± 0.1
		MA-186	Biotite	+7.99± 0.1
	Rhyolite dome	MA-251	Plagioclase	+8.53 ± 0.1
			Biotite	+8.05 ± 0.1
	Rhyolite dyke	MA-31A	Plagioclase	+6.89 ± 0.1
			Biotite	+7.68 ± 0.1
			Magnetite	+3.93 ± 0.1
	Pumice tephra	MA-232A	Plagioclase	+9.02 ± 0.1
		MA-234A	Plagioclase	+8.09 ± 0.1
		MA-234B	Plagioclase	+8.87 ± 0.1

Table 6.2. $^{87}Sr/^{86}Sr$ isotope ratios and some element variations in the Meydan-Zilan area volcanic rocks.

	Rock Type	Sample No	$^{87}Sr/^{86}Sr(\pm 2\sigma)$	SiO_2 (wt.%)	K_2O (wt.%)	Sr (ppm)	Rb (ppm)	Rb/Sr	1/Sr
Meydan Alkaline Suite	Alk. oliv. basalt	MA-23	0.704819 ± 16	48.00	0.78	630	14	0.022	0.0016
		MA-27	0.705580 ± 18	51.28	1.08	429	28	0.065	0.0023
	Hawaiite	MA-175	0.705607 ± 18	48.96	1.32	705	40	0.057	0.0014
		MA-166	0.705335 ± 17	51.35	1.32	618	40	0.065	0.0016
	Mugearite	MA-53	0.705104 ± 17	52.50	1.87	565	13	0.023	0.0018
		MA-176	0.705134 ± 14	50.08	1.33	459	26	0.057	0.0022
	Benmoreite	MA-34A	0.705394 ± 18	49.73	2.16	837	57	0.068	0.0012
	Trachyte	MA-10	0.705394 ± 17	60.68	3.37	460	106	0.230	0.0023
Medium-K Transitional Suite	Aladag lava	MA-65	0.705536 ± 16	65.79	3.93	183	136	0.743	0.0055
		MA-55A	0.705551 ± 18	64.62	4.00	206	149	0.723	0.0049
	Zilan lava	MA-263	0.705591 ± 18	62.42	0.53	308	111	0.360	0.0033
	Andesite	MA-131	0.706369 ± 18	60.34	2.47	618	88	0.142	0.0016
	Dacite	MA-122	0.705580 ± 17	70.15	2.67	441	85	0.193	0.0023
High-K Suite	Ignimbrite	MA-186	0.705588 ± 16	67.57	2.08	580	55	0.095	0.0017
		MA-57	0.706089 ± 21	68.98	4.43	53	133	2.509	0.0188
	Rhyolite dyke	MA-31B	0.706089 ± 17	72.52	5.01	90	278	3.088	0.0111
	Gurgurbaba lava	MA-58A	0.705746 ± 16	63.11	2.24	472	67	0.142	0.0021

6.3.1. RESULTS AND POST-ERUPTIVE ALTERATION

Fine-grained and glassy volcanic rocks are susceptible to post-eruptive hydrothermal or deuteric alteration and low-temperature weathering and hydration processes which can result in a significant increase in ^{18}O contents. Such ^{18}O enrichment results from the secondary uptake of water as a result of either low temperature hydrothermal or deuteric processes or through weathering or hydration reactions(Taylor, 1968; Muehlenbachs and Clayton, 1972; Cerling *et al.*, 1985). Indeed, O-isotope compositions of volcanic rocks are a sensitive monitor of the extent of secondary alteration, with increases in $\delta^{18}O$ values directly related to the extent of water uptake, and with significant ^{18}O enrichments occurring without noticeable changes in bulk chemical composition(Muehlenbachs and Clayton, 1972; Cerling *et al.*, 1985; Dobson and O'Neil, 1987).

Increases in $\delta^{18}O$ due to exchange during hydration have been demonstrated for a number of suites of siliceous glasses(Taylor, 1968; Garlick and Dymond, 1970; Stuckless and O'Neil, 1973; Cerling *et al.*, 1985) and are also common during low-temperature alteration of mafic-intermediate volcanic rocks(Matsuhisa and Kurasawa, 1983; Muehlenbachs, 1986; O'Neill, 1986; Harmon *et al.*, 1987; Harris *et al.*, 1989, 1990; Iacumin *et al.*, 1991).

In this study, although care was taken to analyse the freshest possible samples, the rocks analyzed may show alteration, and these tend to have rather high loss on ignition(LOI) values. Before considering isotopic variation in magmas it is necessary to examine the possible effects of weathering processes on isotopic composition. The lavas have LOI contents lower than 2.5 wt.% with no correlation with $\delta^{18}O$ values, showing no evidence of alteration by weathering(Figure 6.1). Generally, there appears to be no correlation between $\delta^{18}O$ and loss on ignition(LOI) in the silicic rocks, suggesting that secondary alteration has not raised the $\delta^{18}O$ values. However, pumice samples with high $\delta^{18}O$ values have LOI contents of 3.5-5.0 wt.%. Therefore, it is inferred that subsequent post-eruptive hydration of pumice may have induced a change in the $\delta^{18}O$ values. Thus, the oxygen isotopic data of pumice samples will not be included in mixing models.

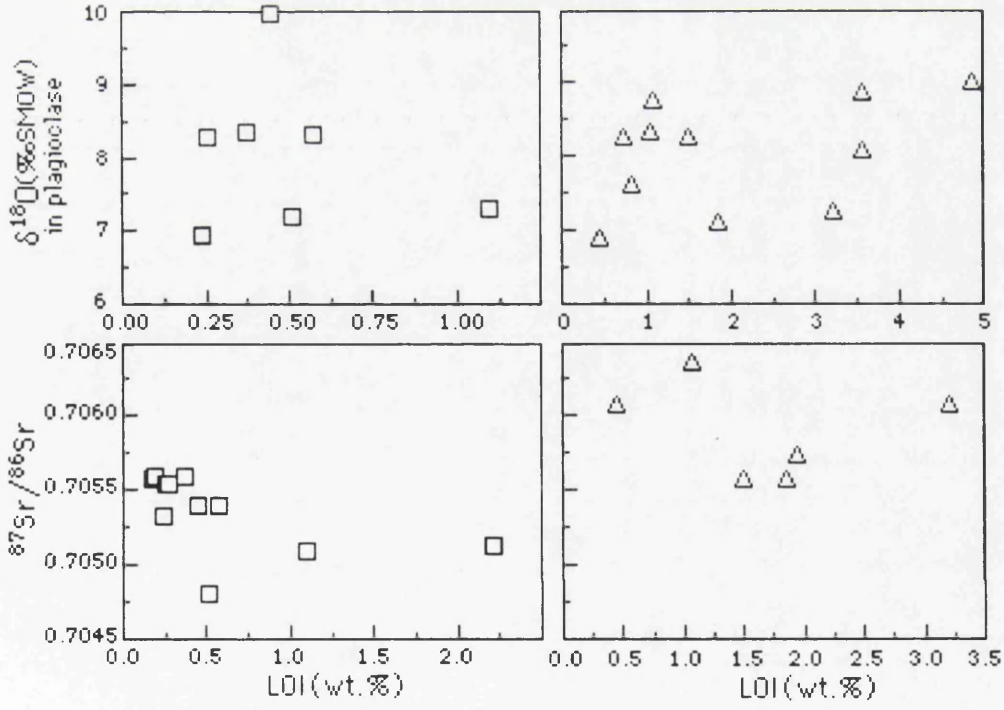

Figure 6.1. $\delta^{18}O$ in plagioclase and whole-rock $^{87}Sr/^{86}Sr$ versus loss on ignition(LOI wt.%, total volatile content) plots for alkaline and transitional(squares) and calcalkaline(triangles) rocks studied. A LOI of 0.5 wt.% is considered to be a plausible primary volatile content for lavas erupted at the surface.

6.3.2. OXYGEN ISOTOPE VARIATIONS

The volcanic rocks studied display a large range in $\delta^{18}O$ values. Indeed, even within individual fractionation series(e.g., the Meydan alkaline suite) there are substantial $\delta^{18}O$ variations. Closed system crystal fractionation is known to modify $^{18}O/^{16}O$ ratios, but the effect is very small at magmatic temperatures(Taylor, 1968; Anderson *et al.*, 1971; Muehlenbachs and Kushiro, 1974). Modelling of fractional crystallization from parental basalt to rhyolitic differentiate(Matsuhisa, 1979; Sheppard and Harris, 1985; Woodhead *et al.*, 1987) suggests an increase in $^{18}O/^{16}O$ ratio of only 0.5 to 1.0‰. In the lavas studied, while major element variations appear to be consistent with evolution of the various lava series by fractional crystallization of plagioclase, pyroxene and olivine, $\delta^{18}O$ values vary much more than expected for closed system fractional crystallization, suggesting a role for ^{18}O-rich continental crust in the petrogenesis of these lavas.

Since the calcalkaline rocks studied are more or less porphyritic, isotopic and chemical compositions of whole rocks do not necessarily represent magma compositions. Each variation trend could represent a suite of rocks which have variable amounts of phenocrysts with similar composition of melt(matrix), or rocks derived from a common source by fractional crystallization. Variable degrees of crustal assimilation or variable $\delta^{18}O$ values of assimilated material seemingly produced the $\delta^{18}O$ variation.

In the Meydan suite, if magmatic processes controlled by fractional crystallization or melting of a homogeneous reservoir were dominant, a smooth increase in ^{18}O(up to 1‰) would be expected at least within a single stage of volcanic activity(Taylor, 1968; Matsuhisa, 1979; Muehlenbachs and Byerly, 1982). There is a slight enrichment of $\delta^{18}O$ during extreme fractional crystallization, but it is very small for such high-temperature magmas. Such magmatic process also produce little isotopic fractionation of Sr, so that $^{87}Sr/^{86}Sr$ ratios would be virtually constant throughout a rock suite derived from a common magma. Assimilation of ^{18}O-rich or ^{87}Sr-rich material into magma will be demonstrated in a $\delta^{18}O$ versus SiO_2 plot and in a $^{87}Sr/^{86}Sr$ versus Sr plot.

Generally, O-isotope against element plots are quite scattered for the calcalkaline rocks(Figures 6.2 and 6.3). However, the Meydan alkaline suite displays a fair correlation. With increasing $\delta^{18}O$, SiO_2, Na_2O, K_2O, Zr, Y, Rb, Th, Ba, Ce, La and Nb show slight enrichment whereas TiO_2, Al_2O_3, FeO*(total), MgO, CaO, Sr, Co, Cr and Ni exhibit negative correlation in the Meydan suite(Figures 6.2 and 6.3).

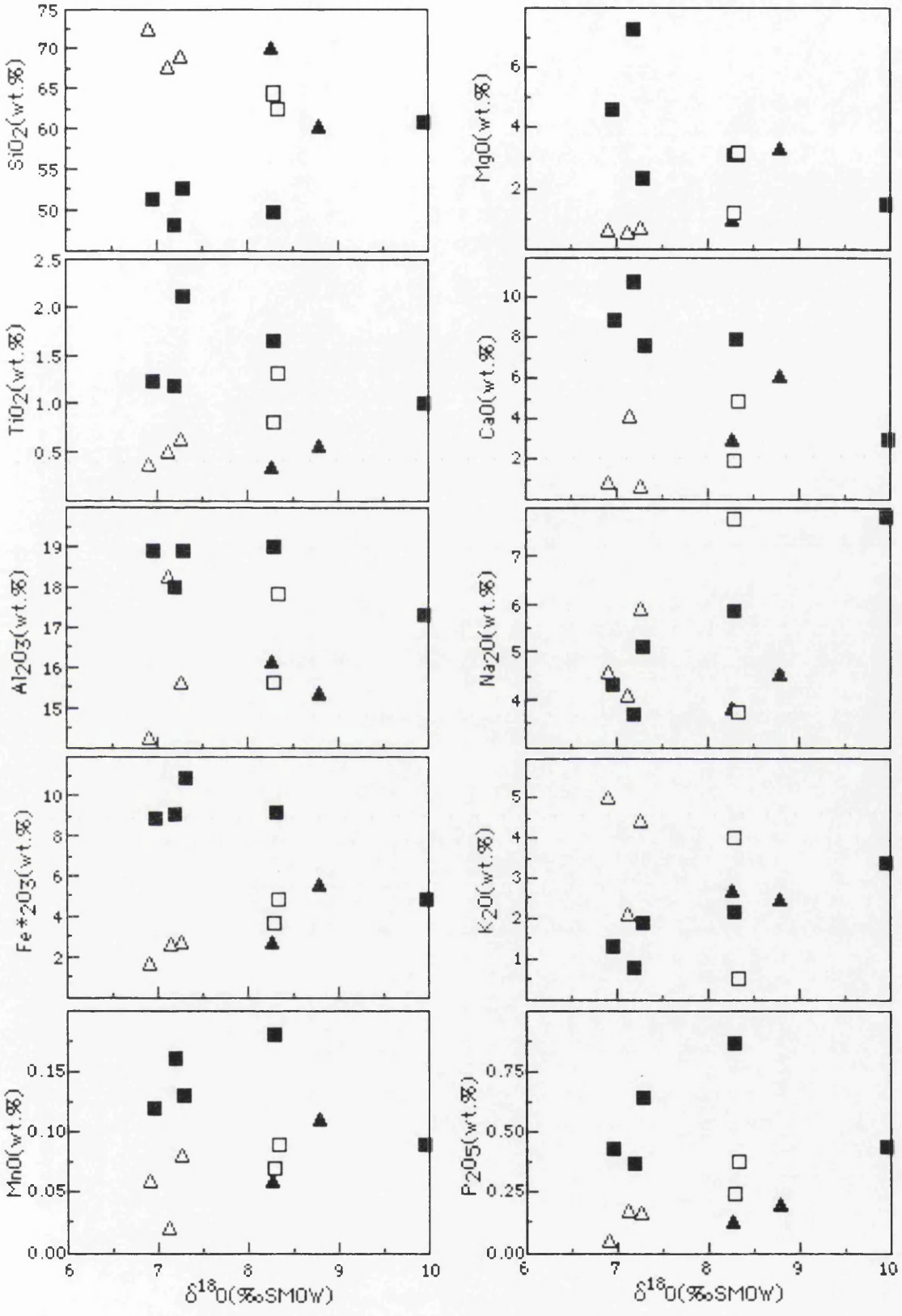

Figure 6.2. $\delta^{18}O$(‰ SMOW) versus major element plots for the Meydan alkaline suite(closed squares), the Aladag and Zilan lavas(open squares), medium-K suite (closed triangles) and high-K suite(open triangles) volcanic rocks of the Meydan-Zilan area.

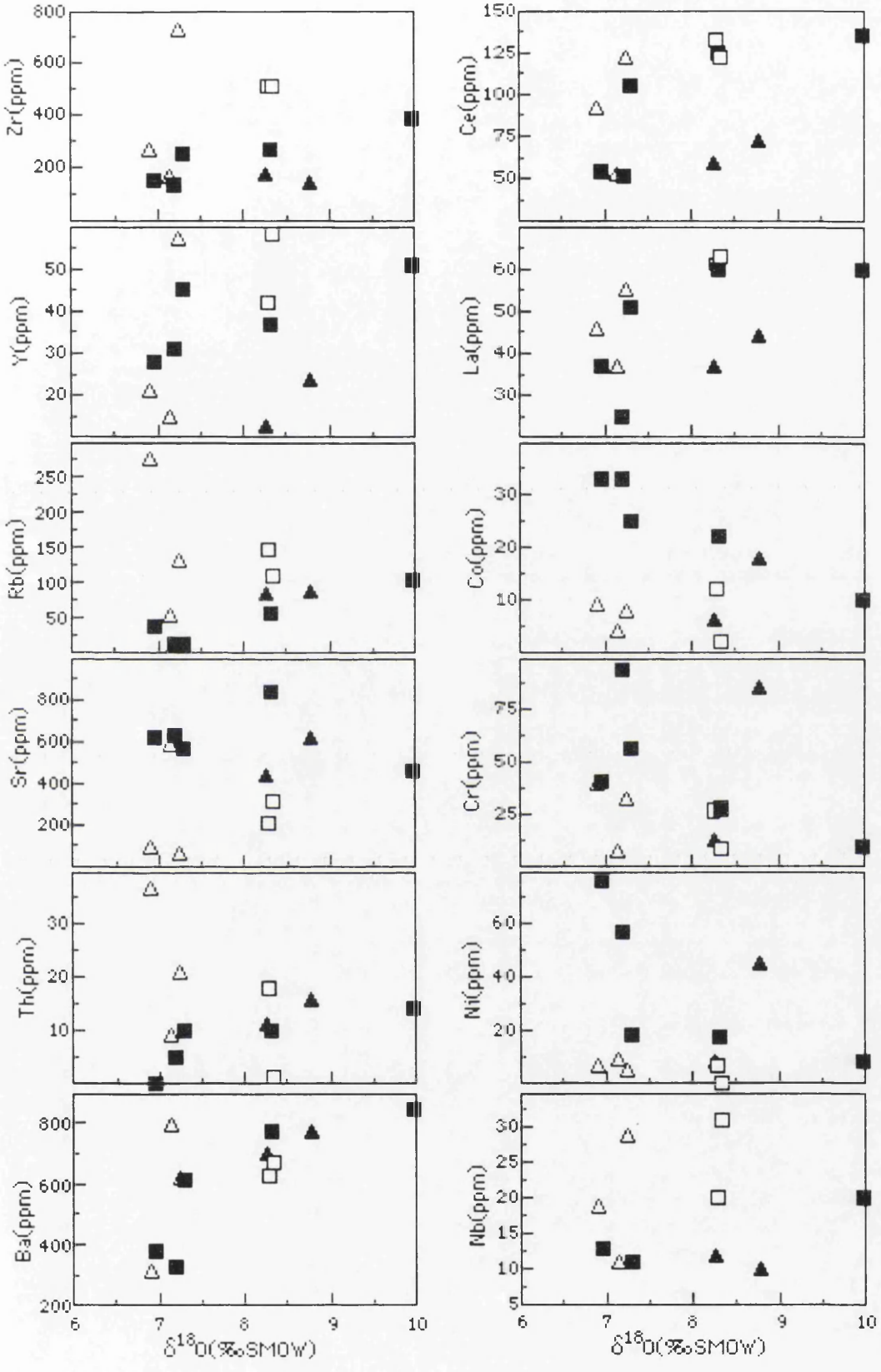

Figure 6.3. $\delta^{18}O$(‰ SMOW) versus trace element plots for the Meydan alkaline suite(closed squares), the Aladag and Zilan lavas(open squares), medium-K suite (closed triangles) and high-K suite(open triangles) volcanic rocks of the Meydan-Zilan area.

In the $\delta^{18}O$ versus SiO_2 plot(Figure 6.4), the predicted effects of closed system evolution are illustrated and compared with data. The primitive samples have relatively low $\delta^{18}O$ values, and it is clear that virtually none of the evolved rocks could have formed from these primitive rocks by a simple, closed-system process. The data are most readily explained by contamination with ^{18}O-rich crust during intracrustal differentiation. The most highly differentiated rocks display the highest $\delta^{18}O$ values, suggesting either a process of combined assimilation-fractional crystallization(Taylor, 1980) and, or a process of mixing of high-$\delta^{18}O$ anatectic magmas with undersaturated magmas. Notably, the degree of contamination in the Meydan lavas is greatest for the evolved rocks, a feature that may suggest a coupled assimilation-fractional crystallization(AFC) process.

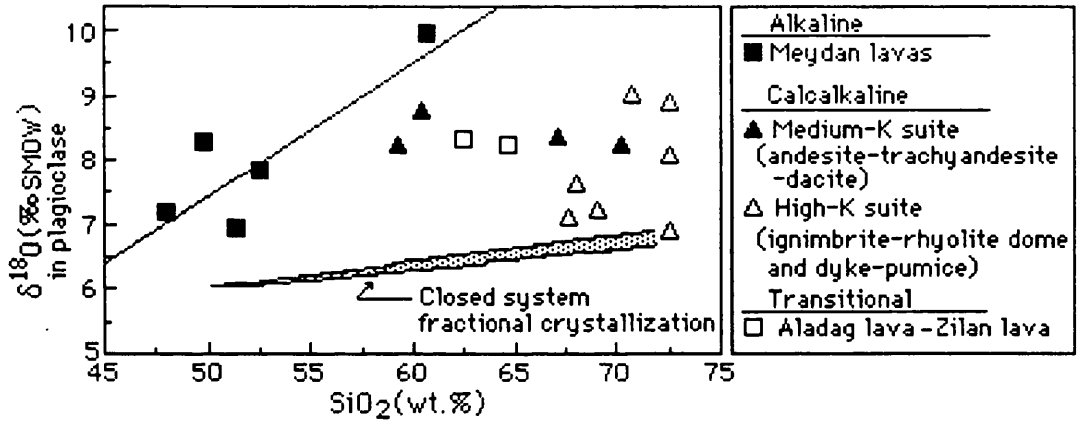

Figure 6.4. Plot of $\delta^{18}O$ versus SiO_2 for the lavas, with least-squares linear regression line for the alkaline rock suites. Shaded area indicates predicted variation due to closed system fractional crystallization of a parental basaltic melt with 50 wt.% SiO_2 and $\delta^{18}O$=6‰, for average solid-melt fractionations between 0.99980 and 0.99965.

6.3.3. STRONTIUM ISOTOPE VARIATIONS

Generally, there is little Sr-isotope difference between the alkaline and calcalkaline suites of the Meydan-Zilan volcanic rocks, suggesting that both may have originated from similar sources and by similar processes, even if these sources and processes can generate large variations in Sr isotope signature. Generally, the high Sr-isotope values of the rocks cannot be explained by closed system fractional crystallization.

The large variation in $^{87}Sr/^{86}Sr$ observed in the Meydan suite is evidence of open system processes. The association of radiogenic Sr isotopes with a large relative Sr contribution from the within-plate component implies that this component has elevated $^{87}Sr/^{86}Sr$ in contrast with the low $^{87}Sr/^{86}Sr$ subduction component. This is possibly evidence to link the within-plate component with an enriched mantle source. The AFC(assimilation-fractional crystallization) that may be proposed as the main mechanism of the evolution for the saturated series would account for the rise in $^{87}Sr/^{86}Sr$ with SiO_2. The isotopic contrasts between basaltic parents and those magmas which have evolved by AFC are useful in that they allow tests of mixing hypothesises involving these two magma types.

Generally, Sr-isotopic ratio versus element plots are quite scattered(Figures 6.5 and 6.6). However, in the Meydan suite, SiO_2, Na_2O, K_2O, Zr, Rb, Th, Ba, Ce and La display fair positive correlation, and TiO_2, FeO*(total), CaO and Cr show negative correlation with Sr-isotopic ratio(Figures 6.5 and 6.6).

In a $^{87}Sr/^{86}Sr$ versus 1/Sr plot, a simple mixing process should give a straight line(Langmuir *et al.*, 1978) provided that mixing is the only process involved and that the end members are compositionally homogeneous. The correlation between major and trace elements and isotopes reflects only the heterogeneity in the analysed samples and does not answer the question whether magma mixing can produce homogeneous lavas or not.

The high $^{87}Sr/^{86}Sr$ ratio, SiO_2, Al_2O_3 and K_2O of the basic magma suggest that it may have already undergone interaction with the crust prior to its emplacement into a magma chamber before the eruption. The interaction was possibly with the lower crust by a MASH process(melting-assimilation-storage-homogenisation) of Hildreth and Moorbath(1988).

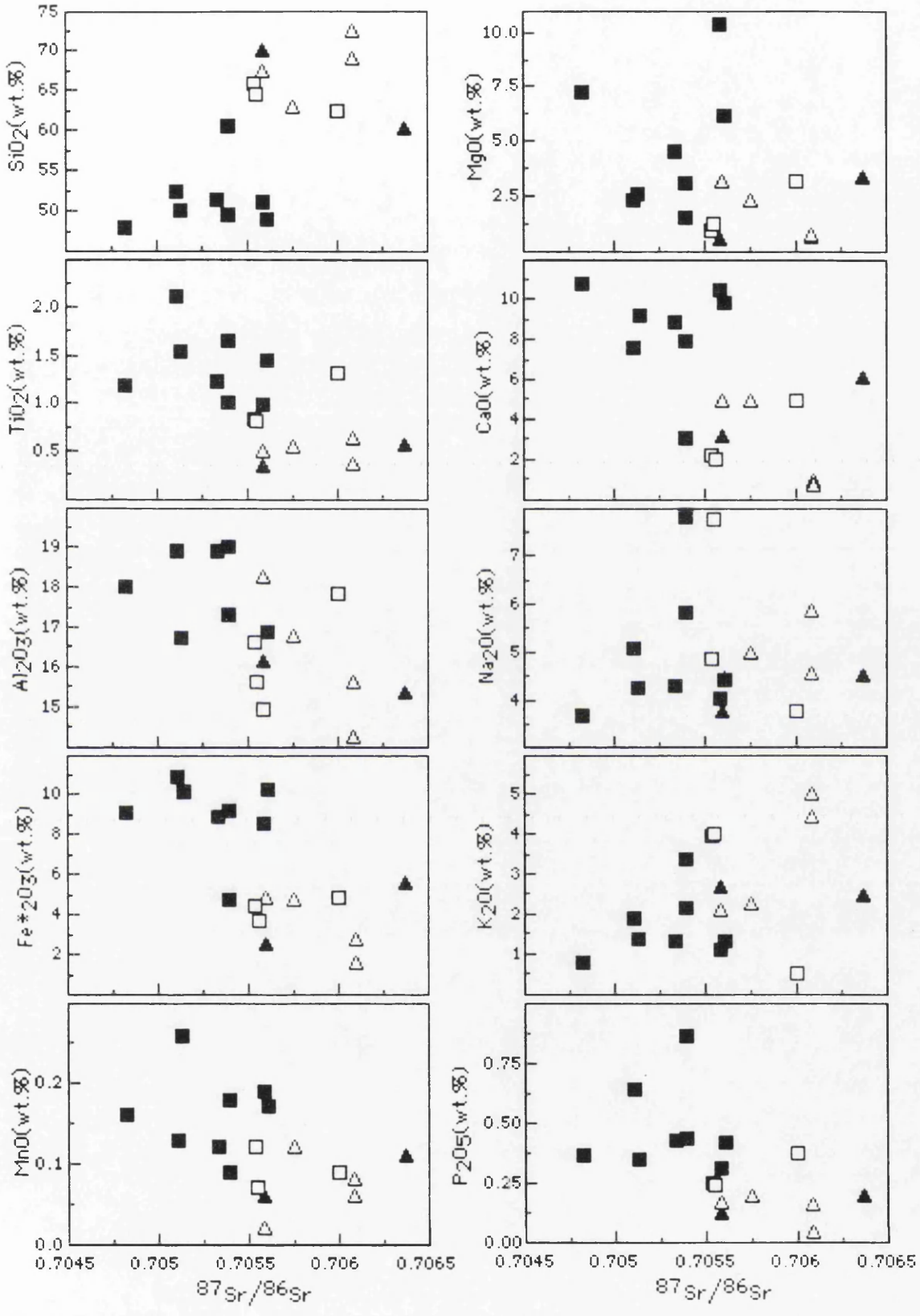

Figure 6.5. $^{87}Sr/^{86}Sr$-isotopic ratio versus major element plots for the Meydan alkaline suite(closed squares), the Aladag and Zilan lavas(open squares), medium-K suite (closed triangles) and high-K suite(open triangles) volcanic rocks of the Meydan-Zilan area.

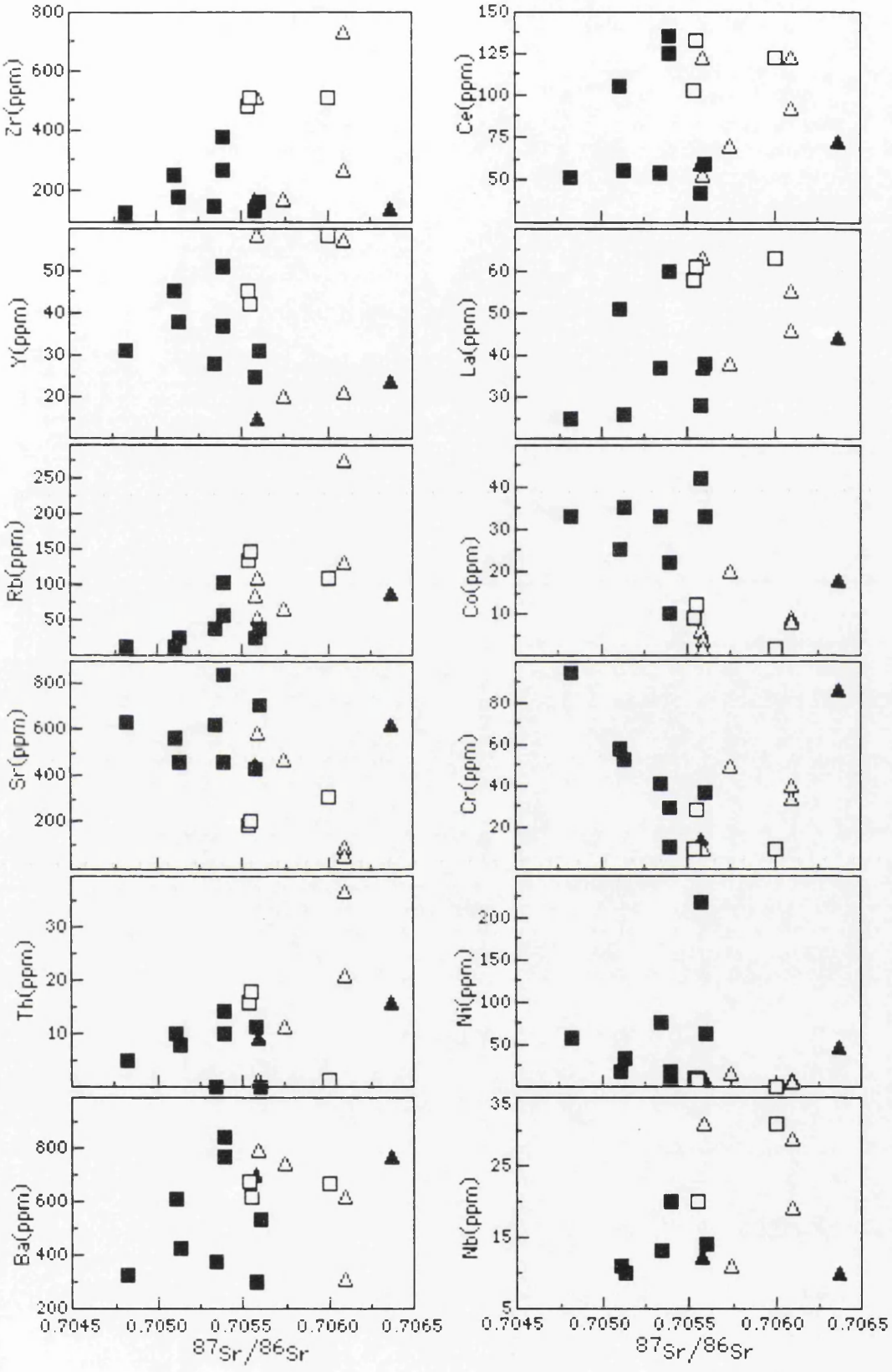

Figure 6.6. $^{87}Sr/^{86}Sr$-isotopic ratio versus trace element plots for the Meydan alkaline suite(closed squares), the Aladag and Zilan lavas(open squares), medium-K suite (closed triangles) and high-K suite(open triangles) volcanic rocks of the Meydan-Zilan area.

6.4. IMPLICATIONS FOR CRUSTAL INVOLVEMENT

Carlson *et al.* (1981) and Mahoney *et al.* (1982) have suggested that some continental basalts with greater than 5 wt.% MgO have been contaminated by continental crust. Others have argued that the observed chemical and isotopic variations found in continental intraplate basalts may reflect heterogenities in the mantle or varying amounts of mixing between two or more mantle components, and there is no need to call upon crustal contamination(e.g., De Paolo, 1983; Menzies *et al.*, 1984). In spite of the obvious compositional differences between crust and mantle, which should render crustal contamination of mantle magmas readily identifiable, crustal contamination has been under-emphasised in the study of many basaltic suites(Patchett, 1991). In some cases, crustal contamination is isotopically indistinguishable from the geochemical effects on a basaltic magma derived from a depleted mantle source and contaminated by melt from ancient subcontinental lithosphere(Glazner and Farmer, 1992).

If crustal rocks are assimilated by a magma during fractionation, correlations exist between indices of fractionation(MgO, SiO_2) and indices of contamination($^{87}Sr/^{86}Sr$). The elements shown in Figure 6.7 were chosen for several reasons; (1) Sr is normally depleted in the crust, (2) Rb, Pb, Th and Ba are normally enriched in the continental crust, (3) Zr is concentrated in small volume melts, (4) Ni and SiO_2 are rough indices of fractionation(e.g., Menzies and Kyle, 1990). Moreover, it would be expected that the more contaminated rocks would have high $\delta^{18}O$ values(e.g., Taylor, 1980; James, 1982).

In variation plots(Figure 6.7), an increase in the $^{87}Sr/^{86}Sr$ ratio is accompanied by a decrease in the content of Sr, and an increase in Rb, Th, Ba, Zr and SiO_2 contents. The gradual increase in Sr-isotopic ratio with increasing silica is compatible with assimilation of crust rich in ^{87}Sr and fractional crystallization changes to the SiO_2 content.

Sr-isotopic data are plotted on a $^{87}Sr/^{86}Sr$ versus Sr diagram(Figure 6.8) and the array defined by the volcanic rocks studied is similar that given by crustal contamination(cf. British Tertiary Volcanic province).

The involvement of crustal material in the genesis of volcanic rocks can also be monitored by use of the Th/Ta ratio since Th is concentrated in crustal rocks and Ta is generally depleted(Pearce, 1983). This diagram does not, however, distinguish between crustal material added to a source region during accretion of lithospheric mantle or addition of crustal material during stoping of wall rock(Menzies and Kyle, 1990).

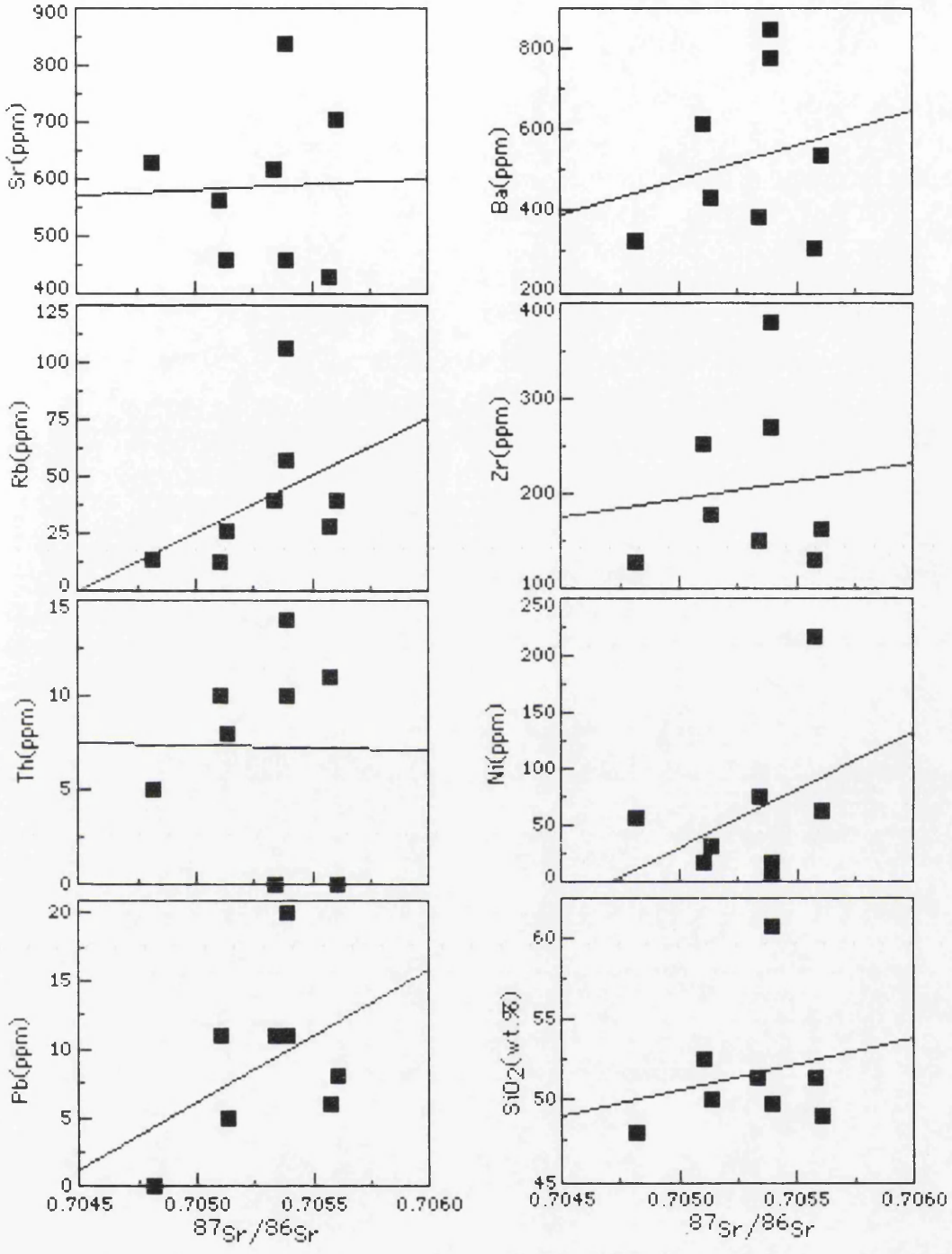

Figure 6.7. Element-isotope variation plots utilizing elements commonly depleted in the crust(Sr), enriched in the crust(Rb, Pb, Th), and an index of fractionation(SiO_2) for the Meydan alkaline suite, with linear regression lines.

The lack of any marked enrichment in Th makes it rather unlikely that high-level crustal contamination has been a dominant process. One could use the data to argue against supra-subduction enrichment processes as a major contributor to alkaline basaltic volcanism. Furthermore, the high Zr/Ba(low La/Nb) ratios of basalts are not compatible with supra-subduction enrichment processes(e.g., Ormerod *et al.*, 1988). The only evidence of possible supra-subduction process(or crustal contamination) is the observation that the highest

La/Nb ratios are in the rocks with the highest $^{87}Sr/^{86}Sr$. This could be explained by addition of a minor amount of crustal material during eruption or involvement of subduction modified-lithosphere. It is important to stress, however that the dominant control on the geochemistry of the Meydan lavas does not appear to be processes associated with contamination by crustal rocks or melting of accreted subcrustal lithosphere.

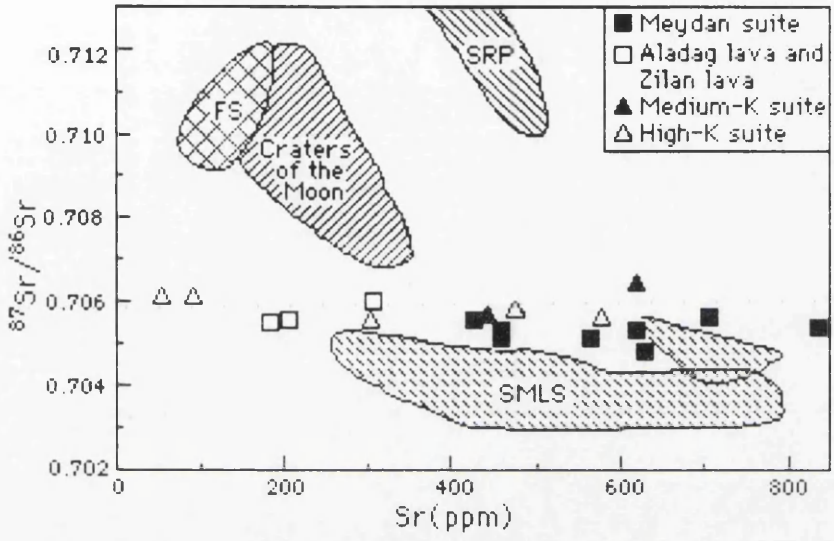

Figure 6.8. Element-isotope variation diagram as a measure of crustal contamination in the alkaline(open squares) and calcalkaline(triangles) volcanic rocks studied. Crustal contamination of a magma containing low $^{87}Sr/^{86}Sr$ and high Sr with crustal rocks containing high $^{87}Sr/^{86}Sr$ and low Sr produces a negative correlation on this diagram(Menzies and Kyle, 1990). Note the negative correlation of the Snake River Plateau(SRP) and the Syke Main Lava Series(SMLS) data and the positive correlation of the Ferrar Supergroup flood basalts(FS)(Moorbath and Thompson, 1980; Mensing *et al.*, 1984; Menzies and Kyle, 1990).

K_2O/TiO_2 is a strong indicator of crustal contamination because K_2O is strongly enriched in the crust relative to mantle-derived magmas(Hart and Carlson, 1987). In the Meydan suite, K_2O/TiO_2 increases with increasing $^{87}Sr/^{86}Sr$(Figure 6.9). This isotopic correlation supports crustal involvement but the isotopic composition of the evolved basaltic rocks, hawaiites, is not distinctive from the primary basalts in the Meydan suite, implying crustal contamination is not significant. Notwithstanding the argument of De Paolo(1981) that contamination does not always produce well-defined geochemical trends, there is no compelling evidence for crustal contamination for most of the basaltic rocks. Indeed, the aphyric nature of the basaltic rocks(alkali olivine basalt and hawaiite) argues against a significant residence time for the basalts in a crustal magma chamber.

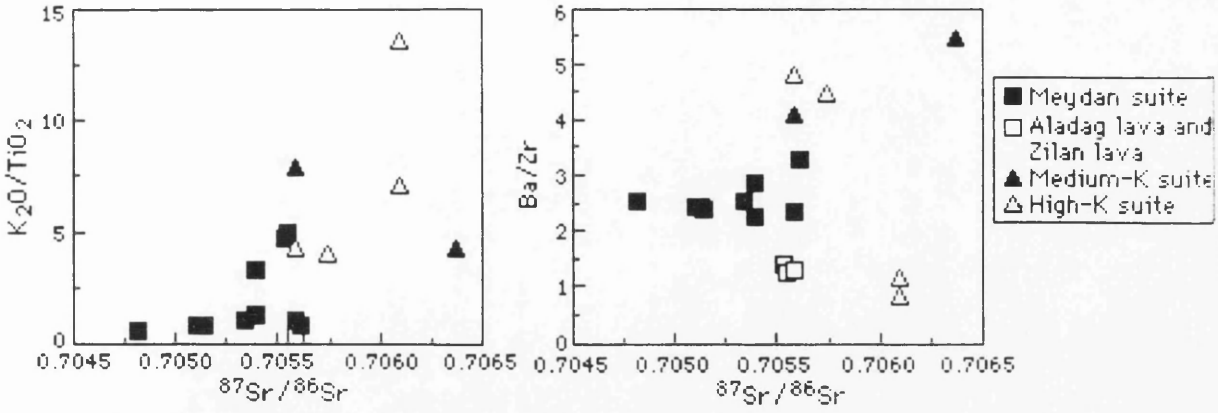

Figure 6.9. $^{87}Sr/^{86}Sr$ versus K_2O/TiO_2 and Ba/Zr plots for the Meydan-Zilan volcanic rocks.

6.5. THE ROLE OF CRUSTAL CONTAMINATION

Crustal contamination tends to increase $^{87}Sr/^{86}Sr$, as many crustal rocks have very radiogenic Sr isotope ratios. High $^{87}Sr/^{86}Sr$ ratios in many continental volcanic rocks indicate that crustal contamination has occurred. Many authors have suggested that since the majority of mantle-derived rocks plot on a single negative correlation between $^{143}Nd/^{144}Nd$ and $^{87}Sr/^{86}Sr$, then rocks which plot off that trend do so because they have been contaminated with continental crust(e.g., DePaolo and Wasserburg, 1979a, b; Menzies and Murthy, 1980b). Stable isotopes, and $\delta^{18}O$ in particular, remain the best indication as to whether contamination has taken place(Taylor, 1980) and ^{87}Sr is often more sensitive than ^{143}Nd.

For suites of related magmatic rocks, plots of $^{87}Sr/^{86}Sr$(or $\delta^{18}O$) against a differentiation index such as SiO_2 provide a reasonable method of assessing whether significant contamination with crustal material has taken place(Hawkesworth, 1982). Taylor(1980) has argued that similar tests may be applied using diagrams of $\delta^{18}O$ versus $^{87}Sr/^{86}Sr$. Generally, crustal contamination of continental magmatic rocks does take place and tends to be accompanied by increasing differentiation(Hawkesworth and van Calsteren, 1984).

The increase of $\delta^{18}O$ with increasing SiO_2 is greater than that which might be due to fractional crystallization(Anderson *et al.*, 1971; Matsuhisa, 1979). This suggests that the relatively high $^{87}Sr/^{86}Sr$ ratios in the basaltic rocks do not reflect crustal contamination.

There is no significant correlation between $^{87}Sr/^{86}Sr$ and SiO_2(Figure 6.5) ruling out any simple mixing model between magmas and crustal materials. However, the rocks clearly form part of a broad hyperbolic curve, characteristic of Sr contamination of magmas with primary $^{87}Sr/^{86}Sr$ and variable Sr contents at the time of interaction with the high-^{87}Sr source.

Derivative lavas had already reached their final magmatic Sr contents before exposure to the ^{87}Sr-rich contaminant;

(a) Many lavas of high $^{87}Sr/^{86}Sr$ are SiO_2 undersaturated which suggests that they have not assimilated much continental crust.

(b) Magmas presumably derived by anatexis of continental crust typically have high $^{87}Sr/^{86}Sr$ ratios and low Sr contents.

The Meydan alkaline rocks from this study display only a very narrow range in $^{87}Sr/^{86}Sr$. This would usually be interpreted as reflecting a negligible role for contamination. However basic lavas from this suite have very high Sr contents(>500 ppm), compared with the likely composition of a crustal component(<500 ppm). It may be possible that the isotopic effects of contamination are hidden by the high Sr contents of the basic lavas of this suite, until the later stages of crystallization when the Sr content of the liquid has been reduced by fractional crystallization of feldspar. The effect on the major elements of adding small quantities of crust to a magma is likely to be significant and may be sufficient to invalidate the least squares modelling of fractional crystallization. Evidently, the SiO_2 content of a magma is also altered quite significantly by small amounts of crustal contamination.

The continental crust is a major reservoir of radiogenic Sr. Lavas with enriched Sr isotope ratios have often been assumed to have interacted with the continental crust(e.g., Allegre *et al.*, 1981). However the discovery of similar isotopic signatures in oceanic basalts(e.g., Dosso and Murthy, 1980) and mantle xenoliths(e.g., Menzies and Murthy, 1980a), has illustrated that the continental crust is not a unique source of high $^{87}Sr/^{86}Sr$. It is believed that such features represent mantle processes such as partial melting and fluid or melt migration which fractionate parent and daughter elements. In areas of the mantle which remain isolated from the main convective circulation for long periods of time, notably the sub-continental lithosphere, these elemental fractionations lead to the generation of anomalous isotope ratios.

Therefore elevated $^{87}Sr/^{86}Sr$ may not be interpreted as unambiguous evidence of crustal involvement in the rocks studied. However consideration of the elemental variations which accompany isotopic enrichment may allow the role of continental crust to be assessed. Two potential processes of continental crustal involvement can be considered:

(a) Crust may be recycled into mantle as a terrigenous sedimentary component from the subducted slab. This type of continental incorporation will be dealt with as a subduction component.

(b) Continental crust may be incorporated into ascending magmas during their passage through the crust. This is the process implied here by the phrase "crustal contamination".

The Meydan-Zilan volcanic rocks sit upon continental crust, which is composed of a complex mixture of rock types. Crustal xenoliths from the ignimbrite unit reveal a wide range of crustal lithologies such as acidic igneous, sedimentary and metamorphic rocks. Most of these xenoliths are small(<2 cm), partly rounded and highly altered by weathering and hydrothermal processes, so their chemistry has been changed by alteration which limits their use as representatives of potential crustal contaminants. Nevertheless, the existence of small rounded xenoliths is evidence of some contamination.

6.6. ASSIMILATION AND FRACTIONAL CRYSTALLIZATION

A variant of the contamination hypothesis is combined assimilation-fractional crystallization(Taylor, 1980; De Paolo, 1981) which is perhaps the most commonly demonstrated contamination process. Assimilation of crust is accompanied by, and indeed promoted by the latent heat of crystallization. Under certain conditions it may be possible to produce a significant shift in $^{87}Sr/^{86}Sr$ and a small shift in $\delta^{18}O$ by AFC processes. Such conditions include high-level emplacement, where the proportion of cumulate to assimilated material is high, and where the cumulate has a preference for Sr. Plagioclase is the only candidate capable of fulfilling these conditions. The lack of Eu anomalies, however, preclude such extensive involvement of this phase.

Such contamination models require significant interaction of basaltic magma with more silicic crust either by underplating of, emplacement in, or traversing through the crust by basaltic magma. If such extensive interaction is postulated, silicic lavas would be produced by crustal melting.

In AFC systems a positive relationship is produced between indices of contamination(e.g., $^{87}Sr/^{86}Sr$) and differentiation(e.g., SiO_2), as fractional crystallization is accompanied by addition of radiogenic Sr to the remaining liquid. It seems likely that small isotopic variations observed in the Meydan suite are the result of AFC(Figure 6.10). Oxygen isotopes are also commonly used to confirm that assimilation-fractional crystallization has taken place and to constrain models. Oxygen isotopes are, in theory, a better constraint for such calculations than Sr-isotopes because the absolute concentration of oxygen in magma and contaminant can be assumed to be equal(Taylor, 1980) and the $\delta^{18}O$ of the contaminant is not likely to be greater than +15‰ to +20‰.

Pearce *et al.* (1990) showed that combined assimilation and fractional crystallization(AFC) was an important process in the origin of alkaline volcanic rocks(Mus, Nemrut and Tendurek) from the area of thickened crust in the Eastern Anatolian Collision Zone. However, calcalkaline rocks(Kars and Ararat) follow a line of constant Sr isotope ratio from basaltic andesite to dacite composition, probably indicating a fractionation-dominated history, or that the

magmas assimilated young crust of similar Sr isotope ratio(Figure 6.10; Pearce *et al.*, 1990). Pearce *et al.* (1990) also pointed out that in terms of processes, there may be strong similarities between Eastern Anatolia and the Central Chilean Andes for which Hildreth and Moorbath(1988) proposed a blending of subcrustal and deep crustal magmas in zones of melting, assimilation, storage and homogenization(MASH) of the mantle-crust transition.

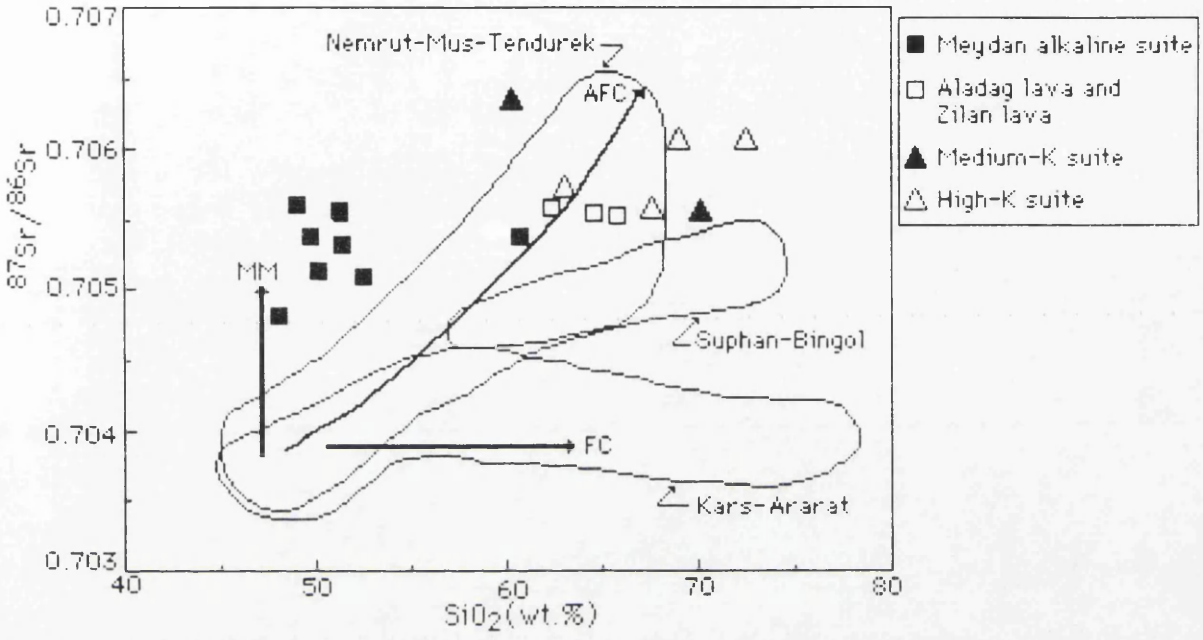

Figure 6.10. $^{87}Sr/^{86}Sr$ versus SiO_2(wt.%) plot of the Meydan-Zilan volcanic rocks studied. Assimilation fractional crystallization(AFC), mantle metasomatism(MM) and fractional crystallization(FC) trends and fields for the Nemrut-Mus-Tendurek, Suphan-Bingol and Kars-Ararat volcanic rocks of the eastern Anatolian volcanic province(Pearce *et al.*, 1990) are also superimposed for comparison.

To further illustrate AFC processes in the evolution of the Meydan lavas, several elements have been chosen as shown in the previous section. These elements would tend to be sensitive to the addition of crustal rocks(e.g., Sr, Rb, Pb, Th) and SiO_2 as an index of fractionation(e.g., Menzies and Kyle, 1990). Sr, Pb, Th and SiO_2 increase with increasing $^{87}Sr/^{86}Sr$ ratio and Rb shows considerable scatter. If the basaltic rocks underwent closed-system fractional crystallization, all fractionated derivatives should have $^{87}Sr/^{86}Sr$ ratios identical to the least fractionated rock type. This is not the case in the Meydan alkaline suite. The element-isotope correlation suggests that whilst fractionation proceeded it was associated with assimilation of crustal rocks rich in Pb and Th.

The decrease in Sr content with increasing $^{87}Sr/^{86}Sr$ is normally attributed to crustal contamination. The negative correlation indicates that the

Sr content of the residual magma decreased presumably by plagioclase fractionation as assimilation proceeded. Furthermore, plagioclase had already fractionated and the observed correlation indicates that contamination had already started after plagioclase fractionation. Further evidence for crustal contamination in the genesis of the Meydan rocks may be found in the following features.

(1) Selective diffusion of K into a magma during AFC has been demonstrated in experimental runs(Watson, 1982; Watson and Jurewicz, 1985), a factor that may explain the apparent poor fractionation mass balance solutions for K_2O.

(2) Late-stage exchange of oxygen isotopes with upper crustal material is clearly indicated by the elevated oxygen isotopic values.

(3) The high Th/Nb ratio indicates either addition of Th during recycling processes in the mantle source or high-level crustal contamination.

The isotopic data of the Meydan suite are quite similar to that of volcanic rocks from the Andes, a feature consistent with the depletion in Nb observed in the MORB-normalized patterns.

6.7. MIXING WITH A CRUSTAL COMPONENT

Crustal contamination of magmas may be due to (1) addition of fluids coming from the continental crust or to (2) melting of continental crust material.

Aqueous fluids leaching the continental crust cannot have high concentration of contaminant Sr since feldspars are stable phases in the continental crust at high temperature. Moreover, fluids released by the breakdown of mica, although potentially high in $^{87}Sr/^{86}Sr$ ratio, are expected to be very low in strontium. Thus, if this mechanism of crustal contamination only is allowed, the $^{87}Sr/^{86}Sr$ ratio of basic-intermediate magmas might be significantly increased only through the passage of very high quantities of fluids(Toscani *et al.*, 1990). The petrographic features of the calcalkaline rocks support an important role for aqueous fluids: amphibole and biotite are present in most of the samples.

Contamination can often be simply represented by mixing in various proportions of two homogeneous sources. Such a model should cause the data to cluster along a straight line between the compositions of the two sources in a simple variation diagram. In a $^{87}Sr/^{86}Sr$ versus 1/Sr diagram, which should show a good positive trend if simple two end-member mixing took place(Faure, 1986), the trend is not well defined(Figure 6.11). An alternative method of crustal contamination may be considered in which assimilation is not necessarily accompanied by fractional crystallization, but the crust is

simply melted by hot uprising magmas. In this case higher temperature basaltic magmas are more likely to become contaminated than cooler more differentiated magmas. An elemental test for such a process is available in the form of the diagram $^{87}Sr/^{86}Sr$ versus 1/Sr(Figure 6.11). In this plot fractional crystallization will change 1/Sr but not $^{87}Sr/^{86}Sr$ producing horizontal trends. Crustal contamination by bulk assimilation, on the other hand, would produce a mixing trend between uncontaminated(low $^{87}Sr/^{86}Sr$) lavas and crust(high $^{87}Sr/^{86}Sr$, high $1/Sr \geq 0.002$ i.e. $Sr \leq 500ppm$). Within individual fractionation trends, as defined by the K_2O versus SiO_2 plot, some small scale contamination may be inferred.

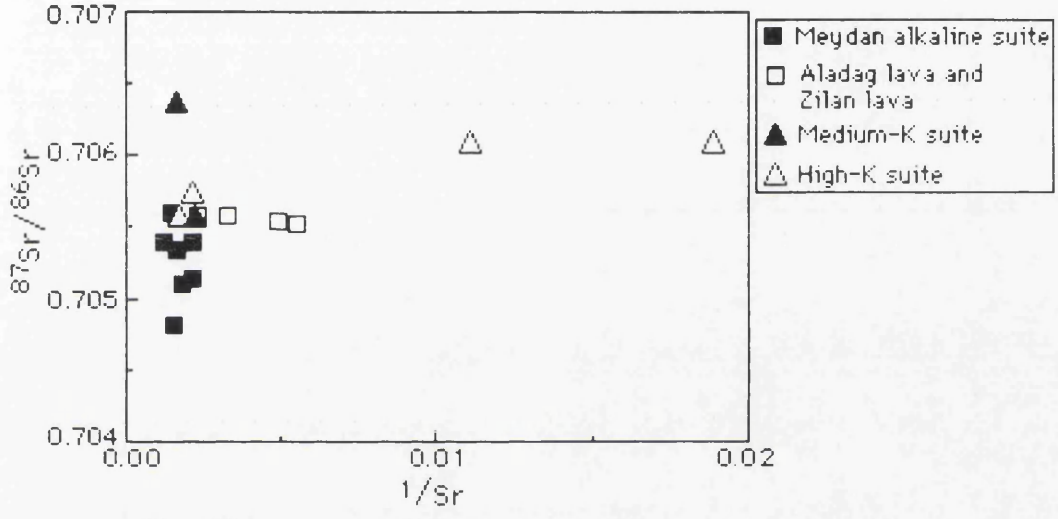

Figure 6.11. $^{87}Sr/^{86}Sr$ versus 1/Sr plot for the Meydan-Zilan volcanic rocks.

Although melting of the crust has been rarely invoked since it needs a large quantity of heat(Hawkesworth *et al.*, 1979a, b), it might have been effective, especially in the evolution of the calcalkaline rhyolitic rocks(see Chapter 5).

Diagrams of Sr-isotopic ratios versus trace element ratios(e.g, 1/Sr, Rb/Sr) are frequently used to evaluate the contribution of two different components which mix together(e.g., Pushkar *et al.*, 1972; DePaolo, 1981; Powell, 1984; Faure, 1986) and of fractional crystallization. Rb/Sr ratios could have been fractionated during a contamination event as a result of feldspar fractionation and, or, as a result of the magma being contaminated by a partial melt of country rock. The fractionation of Rb/Sr may be modelled by feldspar fractionation.

Considering only the $^{87}Sr/^{86}Sr$ and Rb/Sr ratios(Figure 6.12), the distribution of samples in the plot might be explained through the combination of (1) involvement of crustal material with a less radiogenic, basic parental magma(a process which produces increase of both Sr-isotope and Rb/Sr ratios) and (2) fractional crystallization with variable D_{Sr} depending on the

plagioclase/(Fe-Mg) minerals ratio(which may be responsible for the high degree of scattering of the data).

The Rb/Nb ratio has been chosen as an index of assimilation for the Meydan suite because plagioclase-olivine-augite-magnetite(POAM) fractionation would not fractionate this ratio significantly whereas crustal assimilation would cause the Rb/Nb ratio to increase(e.g., Pearce *et al.*, 1990). Increasing Rb at a constant Rb/Nb ratio can be explained by fractional crystallization. Rb/Nb ratio versus $^{87}Sr/^{86}Sr$ isotopic ratio plot supports the model of crustal assimilation(Figure 6.13).

Moreover, the relationship between $^{87}Sr/^{86}Sr$ and Rb/K(Figure 6.14) for the Meydan rocks indicates a systematic increase in the Sr-isotope ratio with increasing Rb/K revealing that source heterogeneity or source mixing(Galer and O'Nions, 1986) best explains the trace element and isotopic characteristics of the data and that crustal influence was minimal.

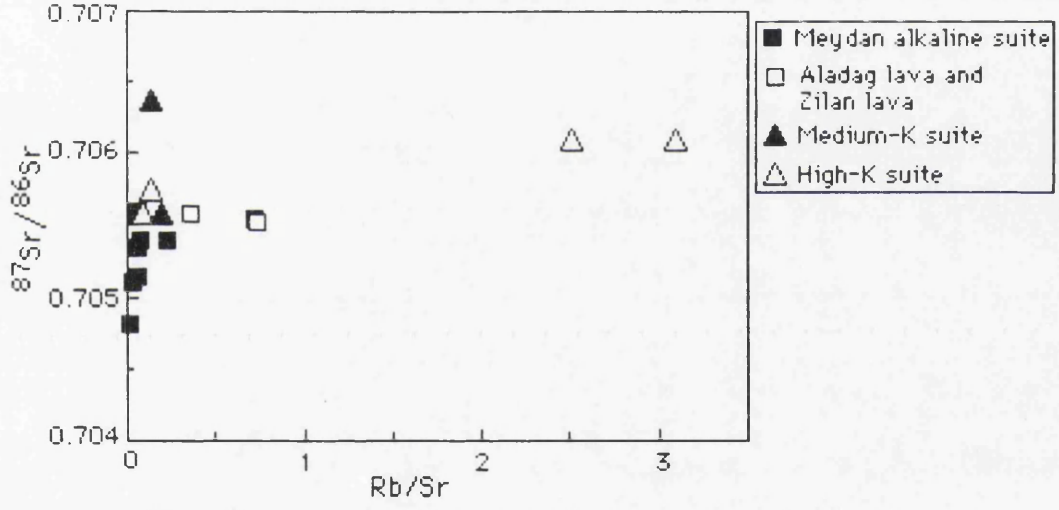

Figure 6.12. $^{87}Sr/^{86}Sr$ versus Rb/Sr plot for the volcanic rocks.

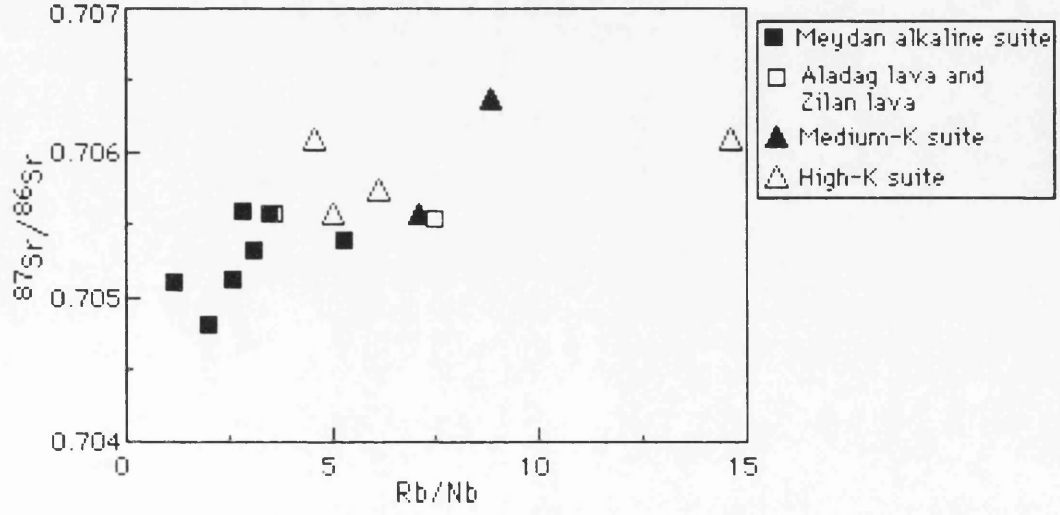

Figure 6.13. Plot of $^{87}Sr/^{86}Sr$ versus Rb/Nb for the volcanic rocks.

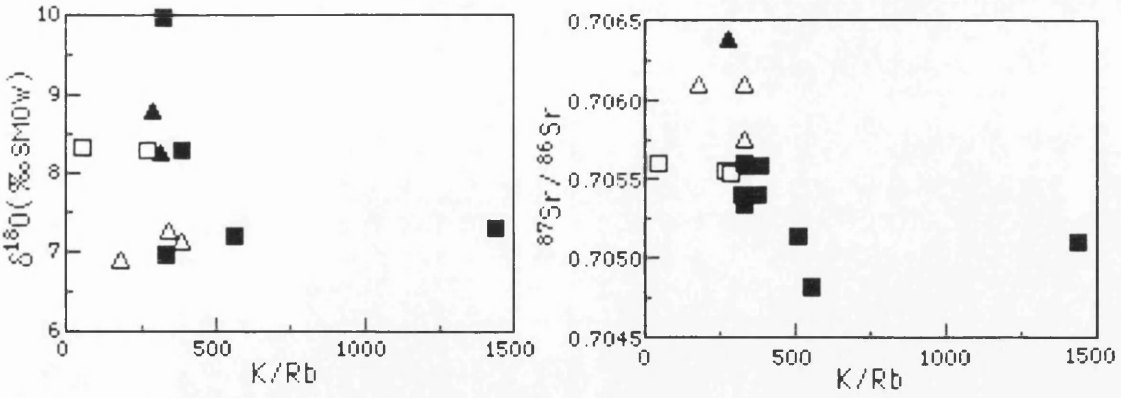

Figure 6.14. K/Rb versus $\delta^{18}O$ and $^{87}Sr/^{86}Sr$ plots for the volcanic rocks.

In the calcalkaline suite, a negative correlation between $^{87}Sr/^{86}Sr$ and 1/Sr for the medium-K suite, and slightly positive for the high-K suite is not consistent with an AFC process. However, there are important constraints on such a model which are unlikely to be satisfied by these lavas.

(a) Sr must behave highly incompatibly, therefore plagioclase is unlikely to be part of the fractionating assemblage. Its ubiquitous presence in the lavas suggests that plagioclase does fractionate and this is supported by major element modelling.

(b) If Sr were to behave highly incompatibly, this would tend to reduce the amount of isotopic variation produced by assimilation of low Sr, high $^{87}Sr/^{86}Sr$ crust. For a given assimilant, a play-off exists between Sr content enrichment due to fractional crystallization and $^{87}Sr/^{86}Sr$ enrichment by assimilation. Only by assimilation of very $^{87}Sr/^{86}Sr$ rich crust are both high Sr content and high $^{87}Sr/^{86}Sr$ attainable.

(c) The crystallization-dominated system required to enrich Sr to an extent greater than the dilutant effect of assimilation is highly favourable to the development of a positive relationship between differentiation and contamination indices(e.g., SiO_2 and $^{87}Sr/^{86}Sr$).

It therefore appears that crustal contamination during magma ascent is not a suitable process by which to generate the isotopic variation in the calcalkaline suite. It is however possible that minor amounts of contamination have occurred in the more differentiated rocks. Furthermore, since the Meydan alkaline rocks have $^{87}Sr/^{86}Sr$ ratios which are lower than 0.706, it is postulated that they were generated by a magma less rich in radiogenic Sr than 0.706. It is to be noted that low $^{87}Sr/^{86}Sr$ values are closer to those characterizing an " enriched" mantle.

Finally, the volcanological model which emerges from the results obtained is that of open-system magma chambers. The different compositions of the products are explained as being magmas which originated at different depths in the magma chambers.

6.8. CRUSTAL CONTAMINATION VERSUS SOURCE CONTAMINATION

The lavas from the Meydan suite are enriched in radiogenic Sr, yet their plagioclase components have mantle-like $\delta^{18}O$ values. This pattern of Sr and O isotopic variation is similar to that described for basalts which have been derived from a contaminated mantle source region(Taylor, 1980; James, 1981). In such a source, the trace element and Sr-isotope compositions of partial melts are dominated by the composition of the contaminant, whereas the O isotope composition of the melt is controlled by the composition of mantle. They may represent highly fractionated magmas that have assimilated little or no crustal material on their way to the surface(Figure 6.15).

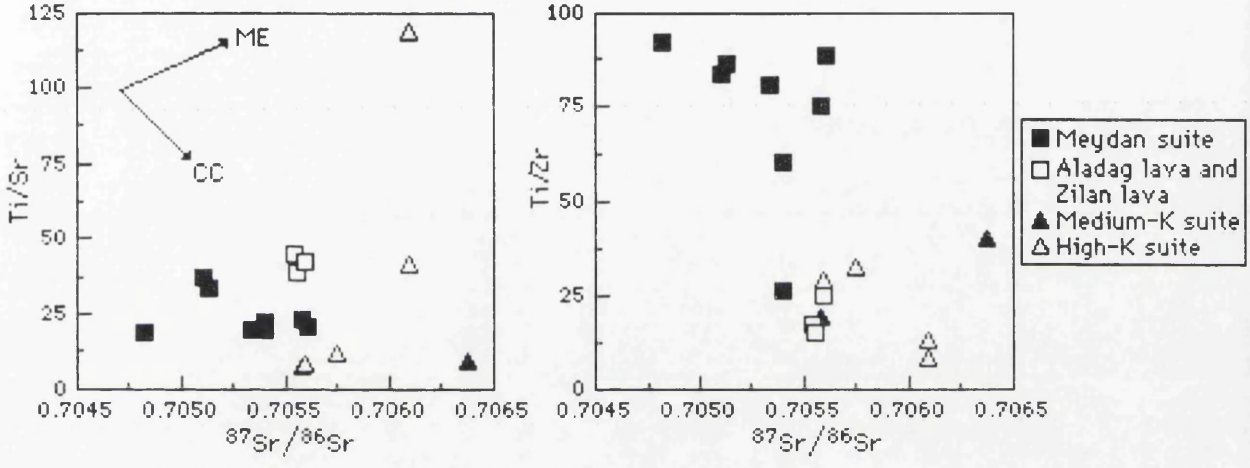

Figure 6.15. $^{87}Sr/^{86}Sr$ versus Ti/Sr and Ti/Zr plots. Vectors show possible trends of mantle enrichment(ME) and crustal contamination(CC).

In contrast to the well developed oxygen isotope-major element variations, the $\delta^{18}O$ versus $^{87}Sr/^{86}Sr$ trend is less impressive. There is a broad tendency for $\delta^{18}O$ values to increase with increasing $^{87}Sr/^{86}Sr$(Figure 6.16).

Two main conclusions emerge from the oxygen and strontium isotope variations displayed in Figure 6.16. First, there is strong evidence that fractional crystallization was accompanied by crustal contamination in the magma. This is best exemplified by the strong relationships between $\delta^{18}O$ values and bulk composition and is also indicated by the oxygen and radiogenic isotope variations. Secondly, it is also clear that such contamination was not solely responsible for the full extent of Sr isotope variation in the lavas.

Oxygen isotope data indicate that crustal contamination is likely to be the cause of the somewhat smaller radiogenic isotope shifts that are accompanied by large ^{18}O enrichments within individual fractional crystallization series. Thus, in the lavas at least Sr isotope ratios are surprisingly insensitive to crustal contamination, whereas O-isotope ratios are extremely sensitive indicator of open system evolution within the continental crust(e.g., Ellam and Harmon, 1990).

Because the oxygen contents of silicate rocks are more or less identical regardless of rock types(45 to 50 wt.%), changes in $\delta^{18}O$ by mixing of rocks and magmas would be proportional to the mixing ratio of the end-members. In contrast, the magnitude of change in $^{87}Sr/^{86}Sr$ by mixing strongly depends on the Sr contents of the end-members which vary widely in different rock types.

Reasonable $\delta^{18}O$ values for crustal materials could range from about +10‰ to in excess of +20‰ within sub-arc basement. However, a generalized petrogenetic scheme is illustrated. The main theme is the two stage process of (1) source contamination controlled by the extent of hydrous flux from the subducted slab which gives rise to a large range of Sr isotopes, but only minor $\delta^{18}O$ variations followed by (2) crustal assimilation and fractional crystallization which produces intermediate to acid lavas lying on steep O-Sr arrays(Figure 6.16).

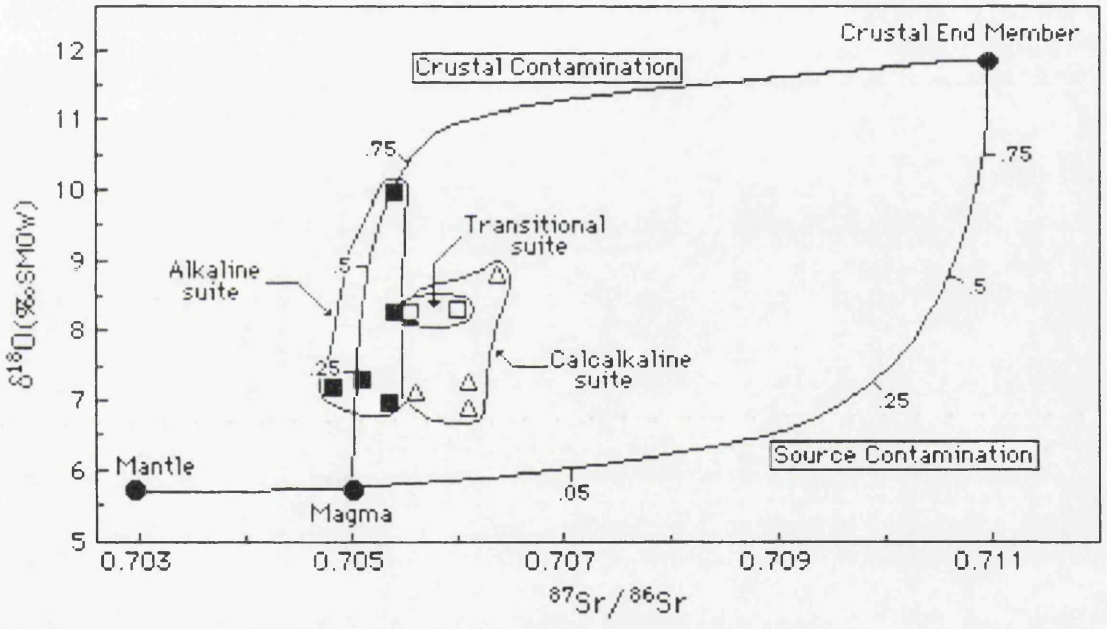

Figure 6.16. Plot of $\delta^{18}O$ versus $^{87}Sr/^{86}Sr$ for the volcanic rocks studied, with simple mixing lines to illustrate the proposed two stage petrogenetic model. Addition of subducted slab to the mantle(i.e., source contamination) results in relatively minor $\delta^{18}O$ variation within the $^{87}Sr/^{86}Sr$ range. In contrast, subsequent crustal contamination of magmas derived from the hybrid mantle-slab source results in large ^{18}O enrichment, even, for quite small $^{87}Sr/^{86}Sr$ variations. Mixing trajectories are highly sensitive to the Sr/O ratios of the end members, and the major difference between source contamination and crustal contamination models reflects the high Sr content of mafic magmas compared with that of their mantle source(James, 1981). For illustrative purposes, the following Sr/O ratios were chosen: mantle=1, crustal contamination=20, and mafic magma=60, which may, assuming constant O abundance, be taken to imply Sr content of 10, 200 and 600 ppm respectively(Ellam and Harmon, 1990).

CHAPTER 7. PETROGENESIS

7.1. INTRODUCTION

So far, the volcanic rock types and suites in the studied area were described in terms of petrography, major and trace element geochemistry, and isotope geochemistry. Three main volcanic suites were recognized; alkaline, calcalkaline(medium- and high-K suites) and transitional suites, all of which have characteristic petrographic and geochemical features. The genetic and, or magmatic processes involved in the evolution of these suites were examined using petrographic and geochemical evidence. In this chapter, the petrogenesis is deduced.

7.2. A REVIEW OF PETROGENETIC MODELS IN THE EASTERN ANATOLIA VOLCANIC PROVINCE

Lambert *et al.* (1974) suggested that the Mount Ararat volcanic rocks resulted from crustal shearing, and are not related to a subduction zone whereas Innocenti *et al.* (1975, 1976 and 1980) regarded the volcanic rocks of the Lake Van area as related to ***subduction of the Arabian plate*** underneath the Anatolian-Iranian plate during the Neogene. In contrast, Bas(1979 and 1981) suggested that the young volcanics of the Erzincan area are the result of ***partial melting of thickened continental crust*** rather than subduction. Sengor and Kidd(1979), Saroglu *et al.* (1980), Savci(1980), Yilmaz(1984), Saroglu and Yilmaz(1984) also suggested that the volcanism in Eastern Anatolia is ***the result of partial melting of thickened continental crust,*** and uprising along extensional fractures related to a compressional regime continuing since the middle Miocene. Tokel(1979, 1980a and b, 1984) also emphasized that the Neogene volcanic rocks of the Kars and Erzurum regions did not originate from subduction but their explanation was ***rifting and related mantle upwelling.***

Yilmaz(1984) pointed out that the young volcanic rocks of Eastern Anatolia could be divided into three stages: In the first stage, mildly alkaline volcanism erupted by ***partial melting in shallow mantle.*** In the second stage, calcalkaline volcanism ***derived from subcrustal material*** took place. In the third stage, an efficient Tibet-type volcanism and alkaline volcanism started as ***the result of partial melting of continental crust.*** It is therefore clear that widely differing views of the source and cause of the magmatism in Eastern Anatolia have been proposed.

Ercan *et al.* (1990) queried the derivation of the tholeiitic lavas of Mount Ararat, Eleskirt-Tutak, Kars-Sarikamis and Erzurum from continental crust as they exhibit similar features to tholeiites generated from

depleted mantle(Tokel, 1984). The derivation of tholeiitic lavas from continental crust seems unlikely because of their basaltic composition. More likely it is magma generation by crustal thickening between colliding plates which generate lithospheric thinning by extension, and ***partial melting in shallow mantle*** (Ercan *et al.*, 1990).

Stress conditions due to continental crust thickening have been investigated by many workers(Artyuskhov, 1973 and 1981; Turcotte and Emerman, 1983; Turcotte, 1983). They concluded that crustal thickening will cause thinning of the mantle lithosphere beneath the crust. As a result of this, magma uprising will begin due to isostasy, and will create horizontal extensional stresses. Eventually, these large horizontal stresses will overcome regional compression. However, volcanic rocks showing different characteristics on the thickened Anatolian plate should have formed after collision, and the alkaline Karacalidag volcano located on a much thinned Arabian plate should have formed by ***an impactogene-type rifting*** of the Arabian plate due to related stress balancing after continent-continent collision. Furthermore, the magmas produced have chemical characteristics different from other volcanic rocks in being less contaminated and chemically close to their mantle parent(Ercan *et al.*, 1990).

Recently, Pearce *et al.* (1990) suggested that because of the thermal constraints in melting convecting upper mantle and the weight of evidence against a mantle plume origin, volcanism across the Eastern Anatolian Collision Zone could have been caused by ***thermal perturbation of metasomatized subcontinental lithosphere***(Figure 7.1). They pointed out that the degree of partial melting was lower in the unthickened lithosphere of the foreland than in the lithosphere of the thickened zone. In the Arabian foreland, the mantle lithosphere may have experienced a time-integrated metasomatism, by low-degree partial melts from the asthenosphere. A similar source is required by the Mus-Nemrut and Tendurek regions of the thickened zone. By contrast, in the Kars-Ararat province, which is north of thickened zone, the lithosphere was enriched by fluids and melts during the late Cretaceous-Eocene Pontide subduction event. Ararat thus has a volcanic arc chemistry but not an arc setting. The Suphan-Bingol province may also be related to a short-lived Eocene-Miocene subduction event. The Eastern Anatolia region is characterised by a set of mantle domains running parallel to the collision zone, each of which has yielded magmas of a particular composition since the start of magmatism in the region. Kars and Ararat, in particular, show polybaric crystallization. Isotope-trace element systematics indicate that combined assimilation-fractional crystallization is an important process in the thickened crust, south of Ararat(Pearce *et al.*, 1990).

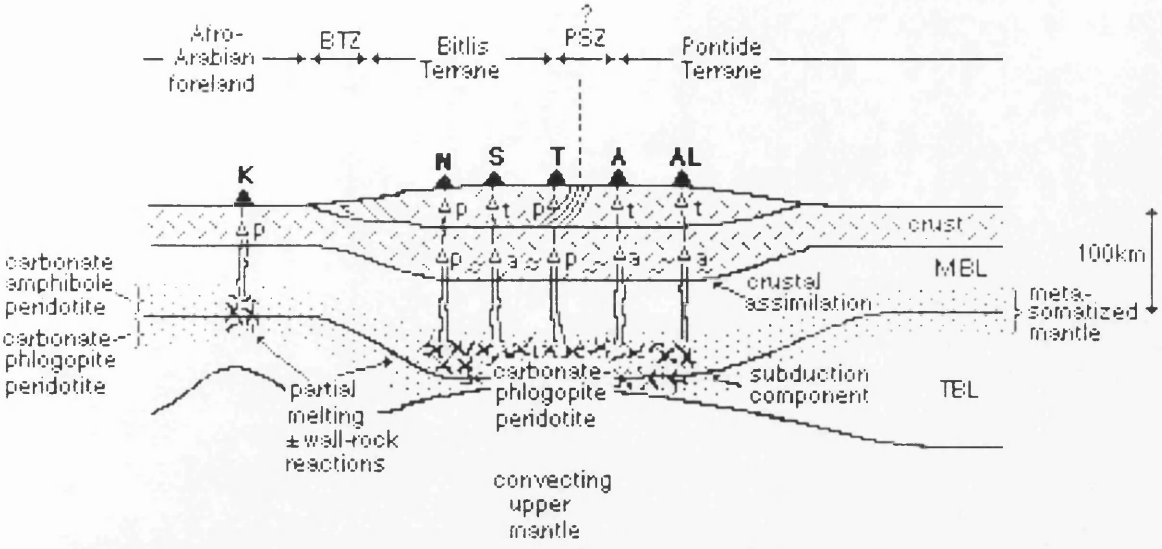

Figure 7.1. Schematic petrogenetic model across the Eastern Anatolian volcanic province(after Pearce *et al.*, 1990). Symbols are PSZ-Pontide Suture Zone; TBL-Thermal boundary layer; MBL-Mechanical boundary layer; K-Karacalidag; N-Nemrut; S-Suphan; T-Tendurek; A-Ararat; AL-Aladag; p-POAM fractionation; t-two pyroxene and plagioclase-dominated fractionation; a-amphibole±garnet-dominated fractionation.

7.3. THE MEYDAN ALKALINE SUITE

Magma petrogenesis is best unravelled through isotopic studies, and the distribution of compatible elements(e.g., Mg, Fe, Ni, Cr) and incompatible elements(e.g., K, Rb, REE). Isotopic studies are insensitive to crystal fractionation, and also the degree of partial melting. Variation in compatible elements is normally a measure of fractionation and, or degree of melting.

7.3.1. OPEN-SYSTEM FRACTIONATION

The Meydan alkali olivine basalt, hawaiite and more evolved rocks had a related origin because they were discharged from the same vent, have similar incompatible element patterns, a characteristic progressively increasing negative Nb anomaly and the alkali olivine basalt and hawaiites are chemically transitional.

To identify these magmatic processes, the process identification diagrams developed by Minster and Allegre(1978), Allegre and Minster(1978) are used. These diagrams rely on the relative behaviour of moderately incompatible and strongly incompatible elements. In Figure 7.2, the concentrations of these are labelled C^M and C^H. During closed system

fractional crystallization C^H/C^M will remain constant or increase very slightly; however, during batch partial melting, C^H/C^M will decrease as the degree of melting increases.

In Figure 7.2, the alkali olivine basalt and hawaiites lie along linear trends that pass nearly through the origin(except the Ba/Zr versus Ba plot), but the mugearites, benmoreites and trachytes plot in a distinctly different manner. These relationships suggest that in the alkali olivine basalt and hawaiites, partial melting played an important role whereas the mugearites, benmoreites and trachytes are less controlled by small degrees of partial melting than by fractionation. Decreasing degrees of partial melting yield alkaline magmas more enriched in incompatible elements (Mysen and Kushiro, 1977; Presnall *et al.*, 1978).

The derivation of the mugearites, benmoreites and trachytes by fractional crystallization of an alkali olivine basalt parental magma may account for their relative enrichment in incompatible elements. This enrichment is clear in trace element patterns. Furthermore, the following observations stress the fractionation; (a) the decreasing of MgO from alkali olivine basalt through to trachytes, and (b) mugearites, benmoreites and trachytes, as more evolved rocks, have common megacrysts whereas the alkali olivine basalt and hawaiites are fine grained.

Enrichment of mugearites, benmoreites and trachytes in incompatible elements may also come from crustal contamination, or from magma mixing with more differentiated magma. O'Hara(1977) and O'Hara and Mathews(1981) have shown that significant changes can occur in the ratio of highly incompatible and moderately incompatible elements in an open-system magma chamber. In an open system, this ratio is no longer dependent only on the rate of crystallization, but also on the rates of magma replenishment and magma escape. Pankhurst(1977) has shown that curves of open-system fractionation plotted on process identification diagrams can vary anywhere over the area between the curves for batch partial melting and closed-system fractionation. The mugearite, benmoreite and trachyte magmas were modified by open-system fractionation and replenishment with increasing fractional crystallization as result of a long residence period in a magma chamber.

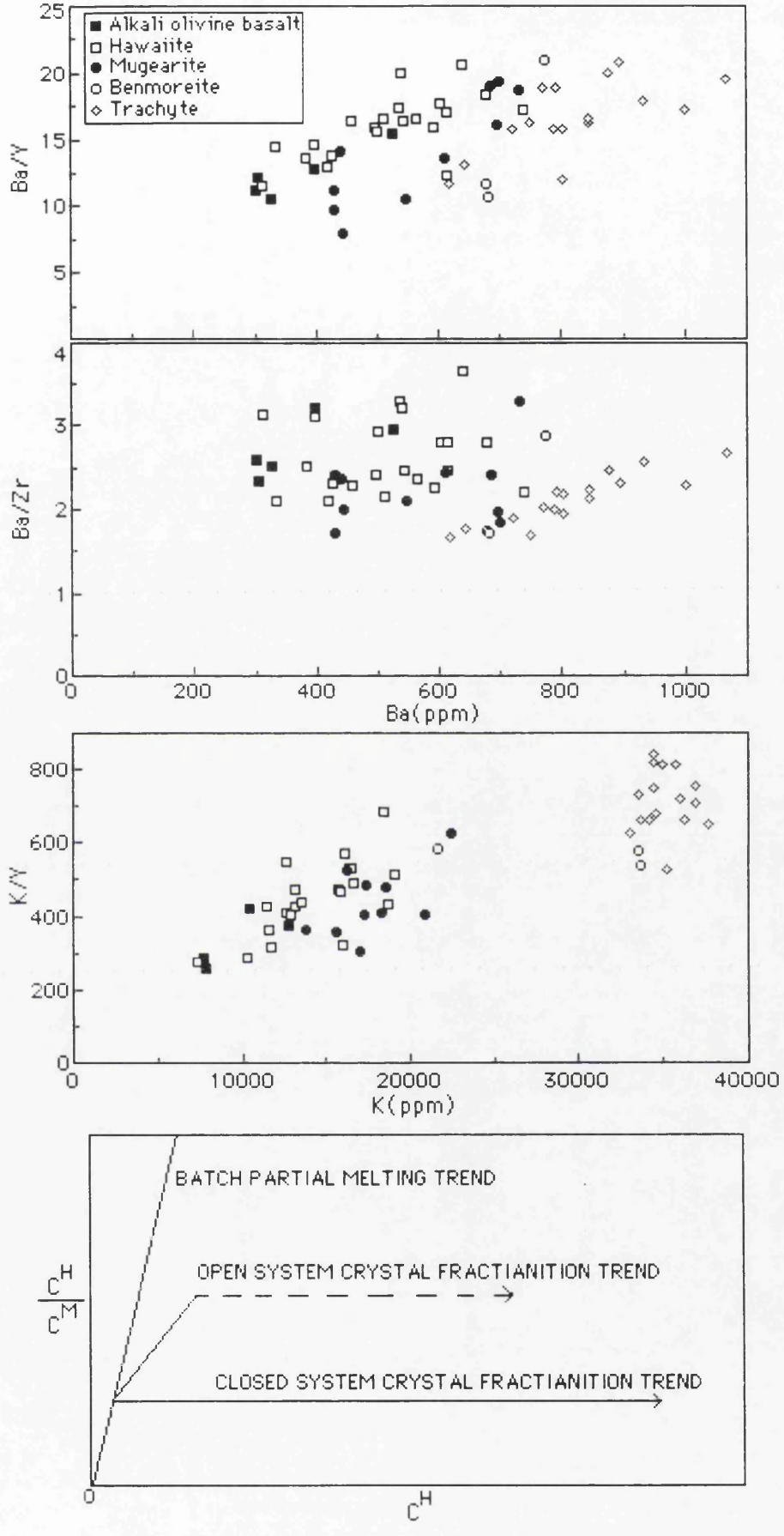

Figure 7.2. Process identification diagrams for the Meydan alkaline suite, based on the relative concentration of moderate incompatible(C^M) and highly incompatible(C^H) elements.

The direction and extent of differentiation in the Meydan alkaline suite can also be demonstrated by the variation of a highly compatible element(Ni) and a highly incompatible element(K_2O)(Figure 7.3). The data points for the suite preclude the possibility that they evolved by simple closed-system fractional crystallization. The distribution of data from alkali olivine basalt to trachyte reflects open-system fractional crystallization from a single batch of primary magma, involving contamination and or mixing.

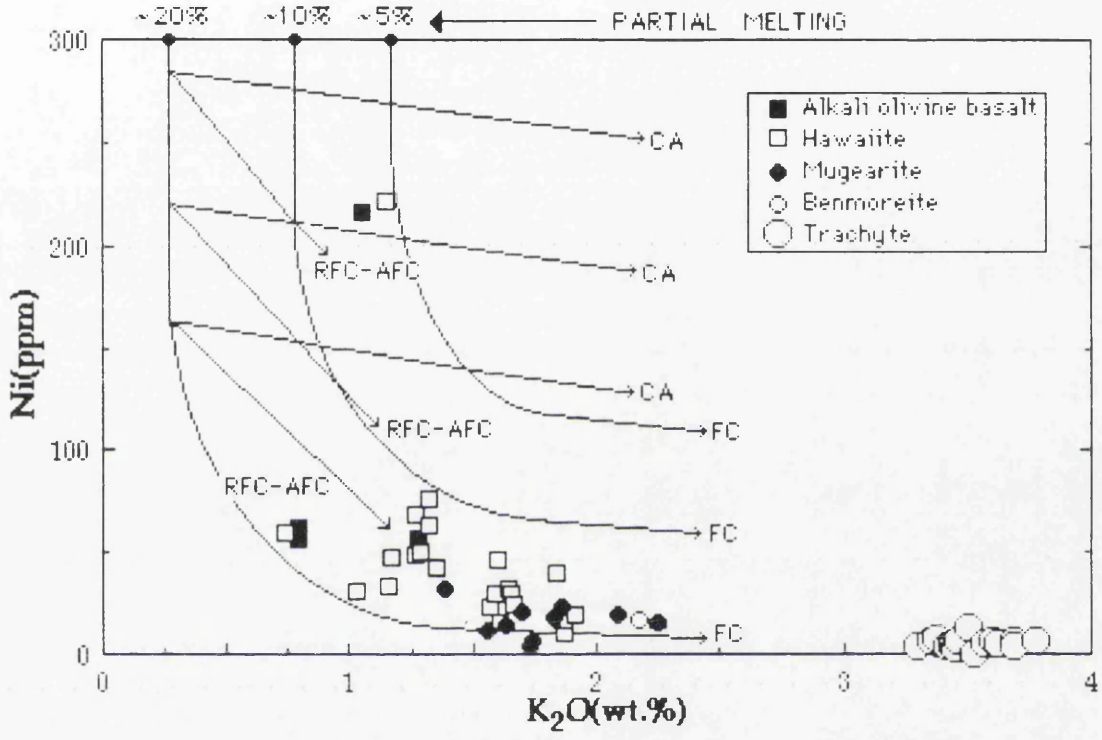

Figure 7.3. Ni(ppm) versus K_2O(wt.%) plot showing possible path of differentiation for the Meydan alkaline association. Lines marked FC are differentiation paths of closed-system fractionation from hypothetical primary magmas approximating 20%, 10% and 5% partial melt fractions of mantle peridotite. Lines marked RFC-AFC are approximate differentiation paths of open-system fractional crystallization, in which fractionation is contemporaneous with magma recharge(RFC) and, or assimilation(AFC). Open-system processes result in derivative magmas that are enriched in incompatible elements at a greater rate than are the closed-system derivatives(O'Hara and Mathews, 1981; DePaolo, 1981). Crustal assimilation without contemporaneous fractional crystallization results in differentiation along the paths marked CA, in which the derivative magmas are not only enriched in incompatible elements but also maintain high levels of compatible elements(Huppert and Sparks, 1985).

7.3.2. IMPORTANCE OF CRYSTAL FRACTIONATION

Although the genesis of the Meydan lavas appears to have involved variations in an open-system with crystal fractionation as the main factor controlling the variations in bulk composition. The evolved rocks have low concentrations of P_2O_5, Sr and TiO_2 and high Rb and Zr contents compared to the basaltic rocks. The REE patterns of trachytes are also slightly different from those of the basaltic rocks. These features were interpreted as a consequence of the fractionation of apatite, plagioclase and Fe-Ti oxides as shown by drastic decrease of the Ti/Zr ratio in these lavas compared to the basaltic rocks.

Concerning the less evolved liquids, alkali olivine basalts and hawaiites, the effects of crystal fractionation cannot be totally ignored but they are thought to be minor and to have had no important consequence for the REE because only olivine and clinopyroxene would be involved in the first steps of fractionation.

7.3.3. POSSIBLE FRACTIONATION PATHS

Incompatible element versus Sr plots show plagioclase fractionation by progressive depletion in Sr from hawaiites through mugearite and more evolved trachytes(Figure 7.4). Microscopic investigations show that the mugearite and trachytes have a large volume of feldspar megacrysts. These megacrysts become more sodic(andesine-oligoclase) and culminate in anorthoclase rims in some trachytes.

The fact that the hawaiites have higher Sr/Zr ratios than the alkali olivine basalt rules out their derivation from alkali olivine basalt by low-pressure fractionation. The hawaiites may have been derived, however, from an alkali olivine basalt parent by fractionation of a cpx-dominated assemblage at high pressures(e.g., Frey *et al.*, 1990). The trace element distribution coefficients for cpx in alkaline magmas range from 0.11 to 0.16 for Sr(Irving, 1978; Villemant *et al.*, 1981) and from 0.12 to 0.27 for Zr(Villemant *et al.*, 1981; Nelson *et al.*, 1987a), and in the absence of plagioclase in the fractionating assemblage at elevated pressures there would be no significant fractionation between Sr and Zr(Figure 7.4A). The appearance of plagioclase in the fractionating assemblage might explain the decrease in the Sr/Zr ratio across hawaiitic composition.

Olivine and possibly titanomagnetite fractionation is evident in the significant variation of Cr and Ni. The depletion of Mg by forsteritic olivine fractionation in the alkali olivine basalt and hawaiites resulted in the crystallization of fayalitic olivine microphenocrysts in mugearites and trachytes(Figure 7.4B).

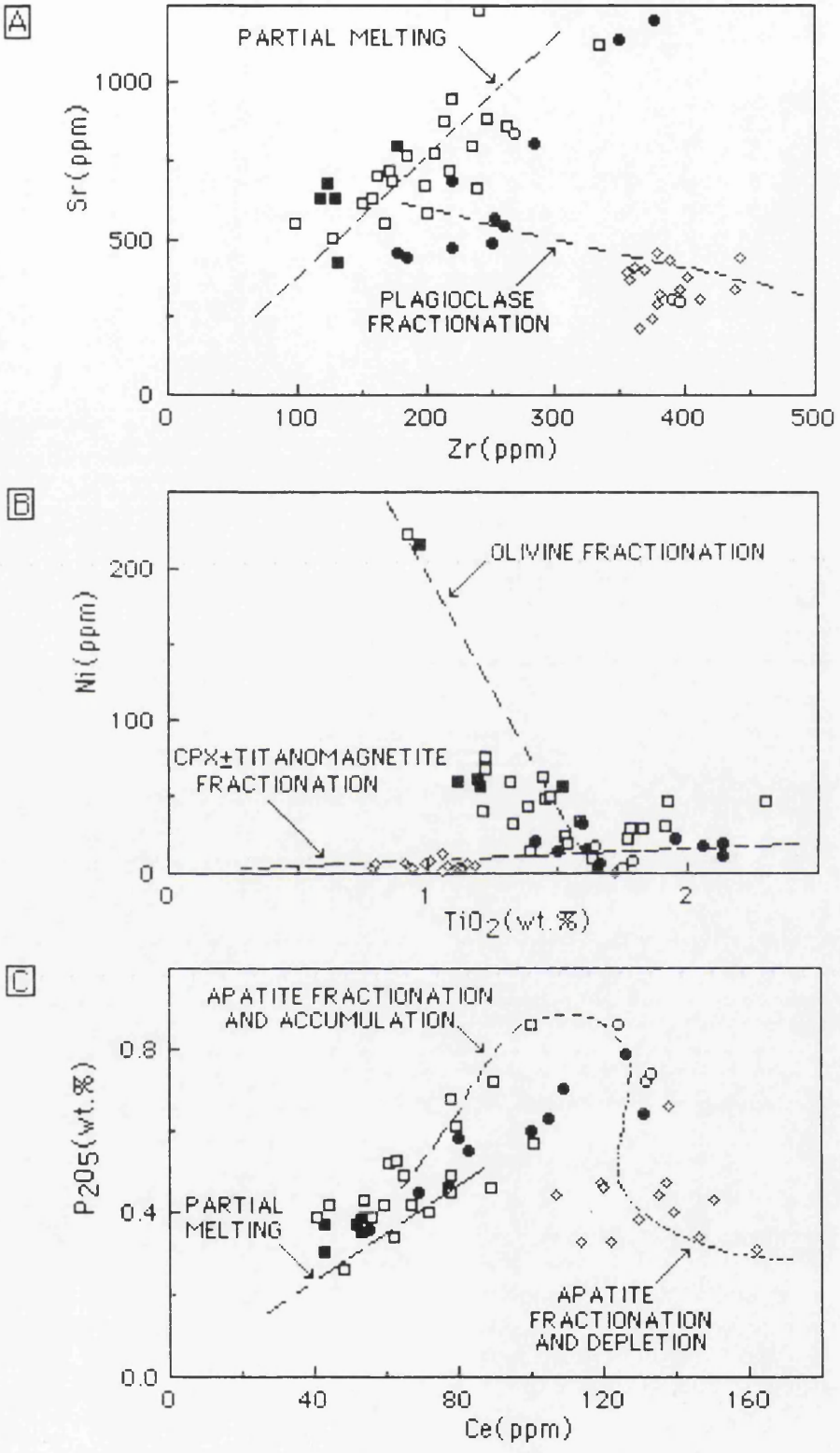

Figure 7.4. Trace element plots of the Meydan alkaline suite showing possible fractionation paths for (A), plagioclase; (B), olivine and titanomagnetite±clinopyroxene and (C), apatite. The symbols are ■, alkali olivine basalt; □, hawaiite; ●, mugearite; ○, benmoreite; ◇, trachyte.

An incompatible element versus P_2O_5 plot(Figure 7.4C) shows that the alkali olivine basalt and some of the hawaiites lie along positive linear trends which pass through the origin; this trend represents the incompatibility of these elements during partial melting. There are also two trends which do not pass through the origin. One includes the hawaiites and some mugearites that have been affected by apatite accumulation. The other trend, which includes all of the differentiated rocks, peaks and then declines as apatite removes P from the magma(Figure 7.4C).

7.3.4. QUANTITATIVE MODELLING OF FRACTIONAL CRYSTALLIZATION

The importance of fractional crystallization in the evolution of the Meydan suite was evaluated quantitatively by the mass balance mixing calculations of Stormer and Nicholls(1978) which can test fractional crystallization(by subtraction, or addition, of chemically-analysed phenocrysts or cumulate minerals), assimilation(by addition of chemically-analysed country rocks or xenoliths), fractional melting(by subtraction of xenocrysts or refractory residual rocks from an assumed parental material) and magma mixing.

Mass balance mixing programs are able to produce a number of arithmetical models; however, before accepting the model with the best fit(that is the lowest sum of the residuals squared), this model should be petrologically and geochemically plausible. The method requires the system being modelled to have fewer mineral phases than chemical components(Middlemost, 1988). The first criterion for selecting reasonable solutions to major element mass balance calculations is that ideally the sums of the residuals squared(Σr^2) should be less than 1.25(e.g., Kempton *et al.*, 1987) or 1.5(e.g., Luhr and Carmichael, 1980). Furthermore, Kempton *et al.* (1987) recommended three criteria in selecting a single model from among several numerically acceptable models; (1) the match between trace element concentrations calculated using assemblage and percentage of fractionation determined by mass balance and trace element concentrations in the actual lavas; (2) the plausibility of the assemblage, that is, whether the relative abundance of fractionated phases prescribed by the model compared well with observed phenocrysts or xenocryst model abundances; (3) when 1 and 2 failed to discriminate between models, the assemblage accepted was the one with the least number of phases.

The genetic relationship between alkali basalt and trachytic magmas via fractional crystallization has been well established. Fractionation trends of mafic magmas can follow different evolutionary paths depending on pressure, water content and oxygen fugacity, but the resulting liquid compositions are largely dependent on the starting basaltic compositions(Kuno, 1968; Coombs and Wilkinson, 1969). Trachytic magmas probably evolved at low pressures by fractional crystallization of alkali basaltic magmas, and the degree of silica saturation found in trachytic rocks is controlled by the silica saturation of the parental magma(Middlemost, 1988).

Potential fractionating phases in the Meydan alkaline association include phenocrysts, megacrysts, and mineral phases of plagioclase, olivine, augite and magnetite(Table 7.1). Anorthoclase is present in more evolved rocks, but it is not a significant fractionating phase.

Mass balance calculations(Bryan *et al.*, 1969) were also made for trace elements. Selected trace element modelling results based on these calculations are given in Table 7.2, using mineral-partition coefficients from the literature and F values(=fractions from the major element mass balance modelling). The trace element modelling of crystal fractionation for evolved rocks gives poor solutions. Thus, variations in incompatible elements that are insensitive to crystal fractionation processes may be due to processes such as contamination and, or magma mixing which have disturbed crystal fractionation.

Table 7.1. Testing the feasibility of fractionation in the Meydan alkaline suite, utilizing mass balance mixing calculations(Stormer and Nicholls, 1978).

A) Testing the feasibility of fractionation **from alkali olivine basalt to hawaiite,** using phases; plagioclase($An_{75}Ab_{24}Or_1$), olivine($Fo_{84}Fa_{16}$), augite($Wo_{45}En_{38}Fs_{17}$) and magnetite.

	Bulk comp. of added or subtr. matl. (%)	*Obs. diff. between magmas*	*Calc. diff. between magmas*	*Obs.-calc. (residuals)*
SiO_2	47.90	-0.492	-0.215	-0.276
TiO_2	0.68	0.573	0.410	0.163
Al_2O_3	20.04	-1.000	-0.883	-0.123
Fe_2O_3*	4.94	2.688	2.962	-0.275
MnO	0.11	-0.021	-0.001	-0.020
MgO	8.62	-1.423	-1.379	-0.044
CaO	15.70	-2.931	-2.919	-0.012
Na_2O	1.90	1.474	1.186	0.200
K_2O	0.07	0.774	0.569	0.205
P_2O_5	0.02	0.363	0.268	0.094

Sum of the squares of the residuals = 0.3296

Phase name	*Amount as wt.% of init. magma*	*Amount as wt.% of all phases*	*Amount as wt.% of added phases*	*Amount as wt.% of subtrd. phases*
Olivine	-3.93	10.12	0.00	10.15
Magnetite	0.15	0.37	100.00	0.00
Augite	-11.88	30.57	0.00	30.68
Plagioclase	-22.91	58.94	0.00	59.16
Total relative to initial magma			0.15	38.72

B) Testing the feasibility of fractionation **from hawaiite to mugearite,** using phases; plagioclase($An_{63}Ab_{35}Or_2$), olivine($Fo_{65}Fa_{35}$), augite($Wo_{47}En_{39}Fs_{14}$) and magnetite.

	Bulk comp. of added or subdr. matl.	*Obs. diff. between magmas*	*Calc. diff. between magmas*	*Obs.-calc. (residuals)*
SiO_2	43.25	3.338	2.623	0.715
TiO_2	1.11	0.287	0.327	-0.039
Al_2O_3	17.54	0.501	0.252	0.249
Fe_2O_3*	15.38	-0.047	-1.202	0.555
MnO	0.24	0.020	-0.039	0.059
MgO	10.14	-2.804	-2.788	-0.016
CaO	9.92	-0.797	-0.910	0.113
Na_2O	2.25	-0.067	0.937	-1.005
K_2O	0.16	0.257	0.583	0.325
P_2O_5	0.01	-0.089	0.217	-0.306

Sum of the squares of the residuals = 2.1090

Phase name	*Amount as wt.% of init. magma*	*Amount as wt% of all phases*	*Amount as wt.% of added phases*	*Amount as wt.% of subtrd. phases*
Olivine	-9.13	25.87	0.00	25.87
Augite	-4.58	12.98	0.00	12.98
Magnetite	-2.56	7.24	0.00	7.24
Plagioclase	-19.03	53.91	0.00	53.91
Totals relative to initial magma =			0.00	35.30

C) Testing feasibility of fractionation **from mugearite to benmoreite**, using the phases; plagioclase($An_{53}Ab_{44}Or_3$), olivine($Fo_{48}Fa_{52}$), augite($Wo_{45}En_{35}Fs_{20}$) and magnetite.

	Bulk comp. of added or subract. matl.	*Obs. diff. between magmas*	*Calc. diff. between magmas*	*Obs.-calc. (residuals)*
SiO_2	47.89	6.580	6.409	0.171
TiO_2	2.71	-0.141	-0.557	0.416
Al_2O_3	22.33	4.120	4.224	0.104
Fe_2O_3*	9.23	0.424	0.438	-0.015
MnO	0.14	-0.018	0.023	-0.041
MgO	2.29	-0.223	-0.488	0.265
CaO	10.97	-4.651	-4.547	-0.104
Na_2O	4.01	0.605	0.721	-0.116
K_2O	0.40	1.519	1.803	-0.284
P_2O_5	0.03	0.027	0.422	-0.395

Sum of the squares of residuals = 0.5464

Phase name	*Amount as wt.% of init. magma*	*Amount as wt.% of all phases*	*Amount as wt.% of added phases*	*Amount as wt.% of subtrd. phases*
Plagioclase	46.95	77.00	0.00	77.00
Augite	-6.93	11.38	0.00	11.38
Magnetite	-5.35	8.78	0.00	8.78
Olivine	-1.68	2.75	0.00	2.75
Total relative to initial magma =			0.00	60.91

D)Testing the feasibility of fractionation **from benmoreite to trachyte**, using the phases; plagioclase, olivine, augite and magnetite.

	Bulk comp. of added or subtrd. matl.	*Obs. diff. between magmas*	*Calc. diff. between magmas*	*Obs.-calc. (residuals)*
SiO_2	28.51	5.158	5.433	-0.275
TiO_2	11.09	-0.851	-1.573	0.722
Al_2O_3	5.29	1.673	1.824	-0.151
Fe_2O_3*	37.19	-5.626	-5.091	-0.535
MnO	0.52	0.000	-0.053	0.053
MgO	7.66	-0.601	-1.049	0.448
CaO	8.30	-1.193	-0.928	-0.264
Na_2O	1.28	1.494	0.837	0.657
K_2O	0.11	0.336	0.556	-0.220
P_2O_5	0.04	-0.390	0.045	-0.435

Sum of the squares of the residuals = 1.8482

Phase name	*Amount as wt.% of init. magma*	*Amount as wt.% of all phases*	*Amount as wt.% of added phases*	*Amount as wt.% of subtrd. phases*
Plagioclase	-2.18	14.08	0.00	14.08
Augite	-5.61	36.20	0.00	36.20
Magnetite	-6.84	44.17	0.00	44.17
Olivine	-0.86	5.54	0.00	5.54
Totals relative to initial magma =			0.00	15.49

Table 7.2. Trace element modelling of fractionation in the Meydan suite, using distribution coefficients for basaltic and basaltic andesite liquids(Arth, 1976; Pearce and Norry, 1979; Green *et al.*, 1989; Schock, 1979; Fujimaki *et al.*, 1984; Dostal *et al.*, 1983; Leeman and Lindstrom, 1978; Lindstrom and Weill, 1978; Henderson, 1982; Green and Pearson, 1987).

A) Fractionation **from alkali olivine basalt to hawaiite.**

	Parent composition	*Daughter composition*	*Daughter calculated*	*Residuals*	*Bulk K_Ds*
Rb	10	20	16.68	3.32	0.000
Sr	679	947	-178.49	-185.23	0.000
Ba	397	542	6.64	-120.00	0.000
Y	31	33	44.63	-11.63	0.287
Zr	123	220	205.1	14.90	0.000
Nb	11	10	18.34	-8.34	0.000
Ni	62	23	103.39	-80.39	0.000
Co	56	39	93.38	-54.38	0.000
Cr	11	74	18.34	55.66	0.000

B) Fractionation **from hawaiite to mugearite.**

	Parent composition	*Daughter composition*	*Daughter calculated*	*Residuals*	*Bulk K_Ds*
Rb	20	13	27.84	-14.84	0.044
Sr	947	565	294.66	270.34	0.991
Ba	542	612	77.27	-120.63	0.129
Y	33	45	44.50	0.50	0.136
Zr	220	252	305.98	-53.98	0.047
Nb	10	11	13.98	-2.98	0.032
Ni	23	18	9.52	8.48	3.549
Co	39	25	24.04	0.96	2.398
Cr	74	57	1.19	55.81	12.942

C) Fractionation **from mugearite to benmoreite.**

	Parent composition	*Daughter composition*	*Daughter calculated*	*Residuals*	*Bulk K_Ds*
Rb	48	114	113.40	0.60	0.059
Sr	685	306	-191.80	-157.56	1.427
Ba	731	679	232.94	-209.30	0.182
Y	39	58	85.31	-27.31	0.143
Zr	221	389	-132.69	-133.67	0.058
Nb	25	18	59.88	-41.88	0.044
Ni	23	8	4.21	3.79	2.858
Co	13	11	14.81	-3.81	0.857
Cr	29	3	0.00	3.00	17.350

D) Fractionation **from benmoreite to trachyte**.

	Parent composition	*Daughter composition*	*Daughter calculated*	*Residuals*	*Bulk K_Ds*
Rb	114	122	135.42	-13.42	0.022
Sr	306	339	-308.33	-8.03	0.285
Ba	679	845	148.25	41.39	0.043
Y	58	52	64.18	-12.18	0.425
Zr	389	396	-198.67	-60.69	0.089
Nb	18	23	20.79	2.21	0.182
Ni	8	4	0.85	3.15	13.751
Co	11	5	6.76	-1.76	3.767
Cr	3	18	0.00	18.00	15.320

7.3.5. CRUSTAL CONTAMINATION

The evidence for open system crustal magma chambers raises the possibility that Meydan lavas may have been modified by assimilation of the chamber walls(DePaolo, 1981). Open-system fractionation of basaltic magma during passage through the crust has been advocated to explain the chemical variability of the Meydan alkaline suite. Because of complexities in open-system fractionation, evolved magmas can result from a wide range of conditions which may have produced the scatter observed in some of the variation diagrams. More evolved rocks contain high Sr-isotope ratios that have been attributed to crustal contamination. Crustal contamination could account for the increased K_2O/Na_2O ratios in the evolved rocks(Watson, 1982), as well as their relative enrichment in many trace elements. However, these enrichments can also be produced by fractional crystallization processes.

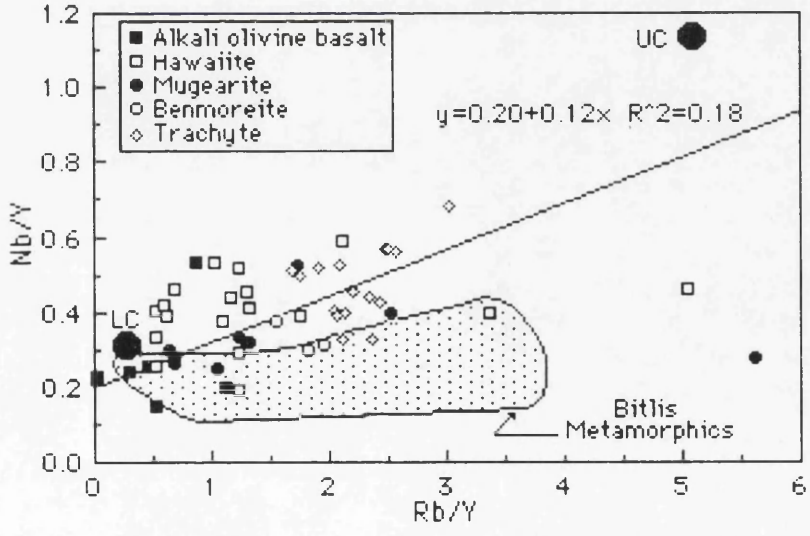

Figure 7.5. Nb/Y versus Rb/Y plot for the Meydan alkaline suite. Data sources for crustal rocks are Lower(LC) and Upper Continental Crust (UC) values(Taylor and McLennan, 1985), and basement rocks(Bitlis metamorphics; Genc, 1990).

To test the influence of crustal contamination on the petrogenesis of the Meydan rocks, the Nb/Y versus Rb/Y plot devised by Leeman and Hawkesworth(1986) was also used(Figure 7.5). The usefulness of this plot stems from the fact that mafic alkali rocks and their derivatives have high Nb contents and low Rb/Nb ratios compared to crustal rocks. Contaminated lavas, therefore, should lie along mixing paths, intermediate between uncontaminated lavas and crustal rocks having high Rb/Y and low but, fairly constant, Nb/Y ratios. The Meydan alkaline rocks lie almost on a linear trend, suggesting that crustal contamination was not very important.

7.3.6. MAGMA MIXING

The periodic replenishment of crustal magma chambers is supported by petrographic evidence for magma mixing in the mugearites and possibly trachytes. Mugearites contain plagioclase megacrysts with oscillatory zoning, all of which zoning profiles suggested a combination of magma mixing and disequilibrium crystallization. Trachytes have resorbed and dark rimmed kaersutites, and both normal and reversely zoned plagioclase phenocrysts. These features are consistent with chemical and isotopic evidence that they evolved in a crustal magma chamber. However, there is little petrographic evidence for magma mixing in the alkali olivine basalt and hawaiites.

7.3.7. PARTIAL MELTING

Primary basalts equilibrated with mantle olivine should have Mg-numbers greater than 68(Irving, 1978) and Ni contents of about 300 ppm(Sun and Hanson, 1975; Frey *et al.*, 1978). Generally, alkali olivine basalts from the Meydan suite have Mg-numbers and Ni contents lower than primary basalts. However, two samples(MA-27 and 64) are close to a primary basaltic composition.

The degree of partial melting required to produce these two compositions can be estimated using the Rayleigh law. Following the Rayleigh distribution law calculated from trace element data, batch partial melting depends largely on the mineral-melt distribution coefficient for any particular element(Shaw, 1970). The equation for batch partial melting can be written as $C_i/C_o=1/F$, where C_i is the trace element concentration in the liquid, C_o is the trace element concentration in the mantle source, and F is the degree of partial melting(Shaw, 1970). Using a mantle source concentration of 2.5 times chondritic values for Zr(15.5 ppm) and a Rb mantle source concentration of 1 ppm(Frey *et al.*, 1978), the degree of partial melting calculated is ~4%-12% for the near primary basalt samples.

The lack of primitive magmas in the suite suggests that basaltic rocks represent fractionated liquids derived from reservoirs at deep crustal or

upper mantle levels. Moreover, if, as suggested above, the alkali olivine basalt was modified by open-system fractionation, then the calculated extent of partial melting is not likely to be correct.

A partial melting diagram can be used to help better understand the intraplate process and to define the composition of a possible reservoir. On such a diagram(Figure 7.6), small degrees of melting have high Zr/Y and low Zr/Nb for the melts whereas large degrees of melting have high Zr/Nb and low Zr/Y magmas(Menzies and Kyle, 1990). In Figure 7.6, the variation in Zr/Y versus Zr/Nb is plotted for Meydan volcanic rocks and variation is compared with plume-type, transitional-type and normal-type MORB(LeRoex, 1987). In Figure 7.6, the oceanic samples define a mixing hyperbola between a magma produced by a large degree melting such as MORB($^{87}Sr/^{86}Sr<0.703$) and a small degree melting such as an enriched mantle plume($^{87}Sr/^{86}Sr>0.703$). The samples from the Meydan lavas indicate a large degree of melting of an enriched mantle source($^{87}Sr/^{86}Sr\geq0.705$). Thus, the basaltic rocks from the Meydan area can be interpreted as large degree partial melts of a isotopically enriched mantle source, on the basis of low $(La/Yb)_N$, low Zr/Y and high Zr/Nb ratios. Moreover, since crustal processes have not dominated the geochemistry of the basaltic rocks, it can be deduced that the source was in the mantle being enriched in LILE and LREE and with a radiogenic $^{87}Sr/^{86}Sr$ ratio. The REE pattern have gentle slopes, primarily caused by large degrees of melting.

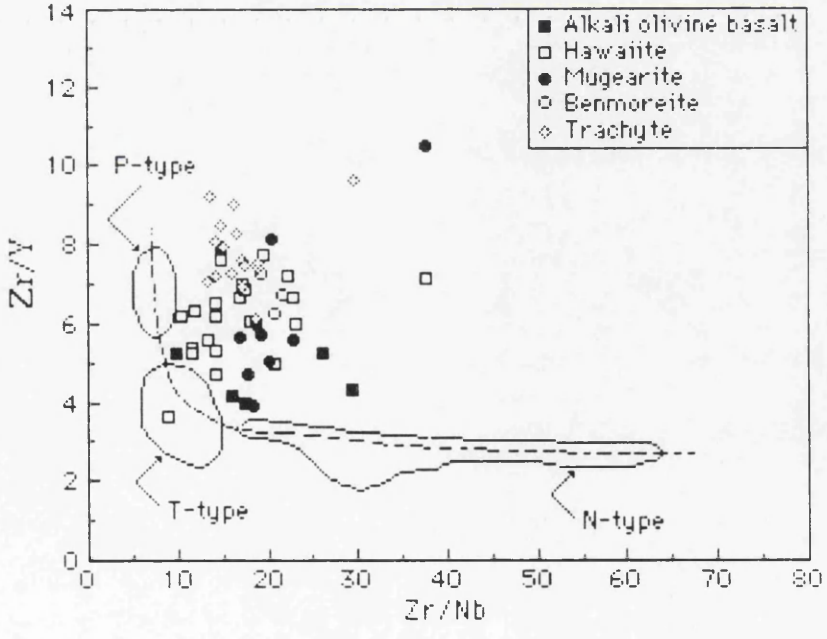

Figure 7.6. Zr/Y versus Zr/Nb plot as a measure of the amount of partial melting involved in the genesis of the Meydan volcanic rocks. The fields of N-, T-, P-type MORBs are shown as a classic demonstration of mantle source mixing between a plume and MORB mantle(after Menzies and Kyle, 1990).

7.3.8. PETROGENETIC MODEL AND PARENTAL MAGMA SOURCE

Consideration of the Di-Ol-Neph and Di-Ol-Sil projections of Sack *et al.* (1987) indicates that the benmoreites and trachytes, which contain augite, in addition to olivine and plagioclase phenocrysts, fall along a low pressure cotectic, although the other lavas(alkali olivine basalt, hawaiite and mugearite) plot generally between the 8-10 kbar and 1 bar olivine-augite-plagioclase cotectics(Figure 7.7). If fractionation of olivine, augite and plagioclase occurred, as suggested by fractionation calculations, then complete separation of augite and plagioclase from the parent magma in the case of the hawaiite and the mugearite must have occurred. Consequently, the parent magma may have undergone medium- to high-pressure fractionation of olivine, augite and plagioclase, which was later followed by low-pressure olivine, augite and plagioclase fractionation.

So far the evidence has already been outlined for high to low pressure fractionation of silicate phases and contamination with crust during the evolution of the Meydan suite. Furthermore, correlations between incompatible trace elements, major elements and isotopes support a model where the chemical variability of the rocks is controlled by open system fractionation and crustal contamination±magma mixing. However, whether the magma that underwent fractional crystallization and contamination came from the lithosphere or the asthenosphere remains a contentious issue. It is apparent from the isotope-element plots that the lowest $^{87}Sr/^{86}Sr$ end of any plot is characterized by an $^{87}Sr/^{86}Sr \leq 0.705$, similar to mantle-derived magmas. The uniform Sr-isotope data of the basaltic rocks are indicative of an initial magma derived from a source enriched in Rb and REE.

A large negative Nb anomaly cannot be accounted for in the alkali olivine basalts by crustal contamination without significant enrichment of those trace elements which have large abundance in the crust. The enrichments and depletions are characteristic of a mantle source. Enrichments in Ba and depletions in Nb are characteristic of subduction-related magmas and are most likely the result of fluid metasomatism of the mantle (Hawkesworth *et al.*, 1979; Tatsumi *et al.*, 1986; Brandon and Goles, 1988).

Variable and small degrees of melting(0-5%) in the source can cause variability in the abundances of strongly incompatible elements whereas larger degrees of melting produce very little change(Hanson, 1978). Large degrees of melting will not greatly effect the incompatible element ratios Rb/Sr and Ba/Zr, because their bulk partition coefficients are similar in a

lherzolite system(Pearce, 1983), and cannot therefore account for the increase in these ratios with decreasing Mg-number. These factors make it unlikely that the compositional variability can be completely produced by varying the range of melting of the mantle source.

The parental magma of the Meydan suite is not believed to be derived from depleted asthenosphere and must therefore originate in the lithosphere or deeper mantle. The most primitive samples have $^{87}Sr/^{86}Sr$=0.7045-0.7050 and Sr=100-150ppm. These chemical characteristics are similar to melts produced in source regions that comprise a mix of enriched mantle and recycled components. The LIL enrichment and relatively high $^{87}Sr/^{86}Sr$ of basaltic lavas in general cannot be accounted for by partial melting of unmodified mantle peridotite and are generally attributed to models involving melting of upper mantle sources which themselves were enriched in fluids released by partial melting or dehydration of the subducted slab(Saunders *et al.*, 1980).

Another possibility is that after extraction, the melts passed through a subcontinental lithosphere with a different isotopic composition and were contaminated by the surrounding rocks. When the melts migrate through the subcontinental lithosphere, they react with the surrounding peridotite, dissolving pyroxene and crystallizing olivine and spinel(Kelemen *et al.*, 1990, 1992). This process can develop enrichment in Ba, K, La, Ce combined with Ti, Zr and Nb depletion(Kelemen *et al.*, 1990) as observed in the evolved rocks. Furthermore, studies of mantle-derived volcanic rocks and xenoliths have showed the enrichment of incompatible elements within the subcontinental lithosphere by interaction of mantle peridotite with uprising fluids or magmas(Menzies and Murthy, 1980a, b; Hawkesworth *et al.*, 1984; Worner *et al.*, 1986).

Finally, the chemical and isotopic variation of the basalt may reflect derivation from a variably enriched subcontinental lithosphere. If mantle metasomatism is largely a product of the fluids or melts that are released from the subducted slab, any later melts are likely to be characterized by high LILE/HFSE ratios, possibly as a consequence of HFSE-rich residual phases being left in the slab during melting. A large variety of subducted material might be involved in metasomatism in the upper mantle(Schreyer *et al.*, 1987).

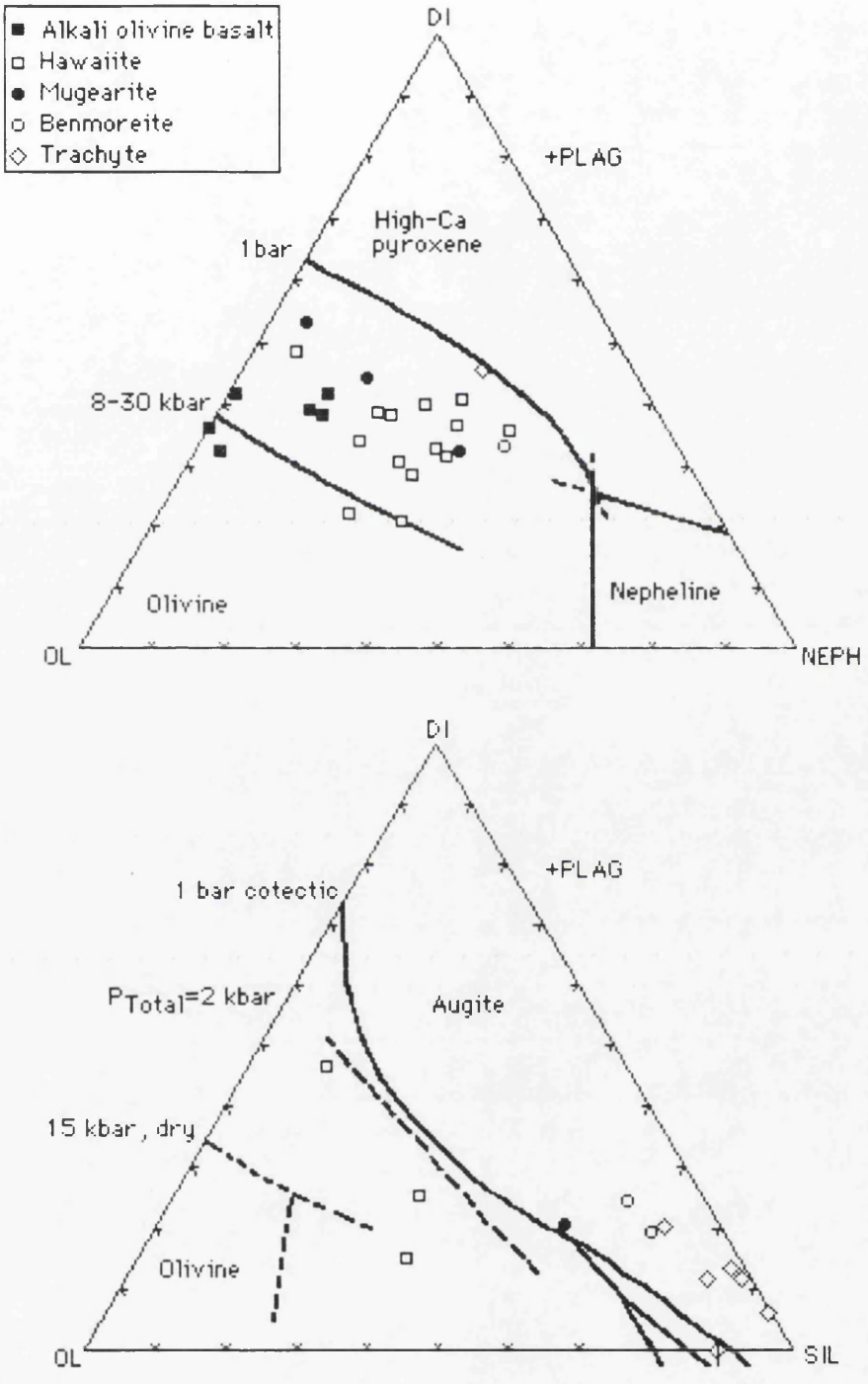

Figure 7.7. Di-Ol-Neph and Di-Ol-Sil projections of Sack *et al.* (1987) showing 1 bar cotectic defined by the experiments of Walker *et al.* (1979) and Grove *et al.* (1982), a schematic 2 kbar cotectic defined by Spulger and Rutherford(1983), and a 15 kbar cotectic taken from Stolper(1980).

7.4. CALCALKALINE SUITE

A recently proposed geochemical discrimination diagram La-Nb(Ta)-Y(Tb)(Cabanis and Lecolle, 1989) is presented in Figure 7.8 as the basis for the tectonic interpretation. Different La/Nb(or Th/Ta) ratios separate an orogenic domain from a non-orogenic domain(Treuil and Varet, 1973; Joron and Treuil, 1977). The Y/Nb(or Tb/Ta) ratio corresponds to an alkalinity index(Floyd and Winchester, 1975). The location of the average upper continental crust value in the diagram(Taylor and McLennan, 1985) permits a suitable discrimination of the continental crust component.

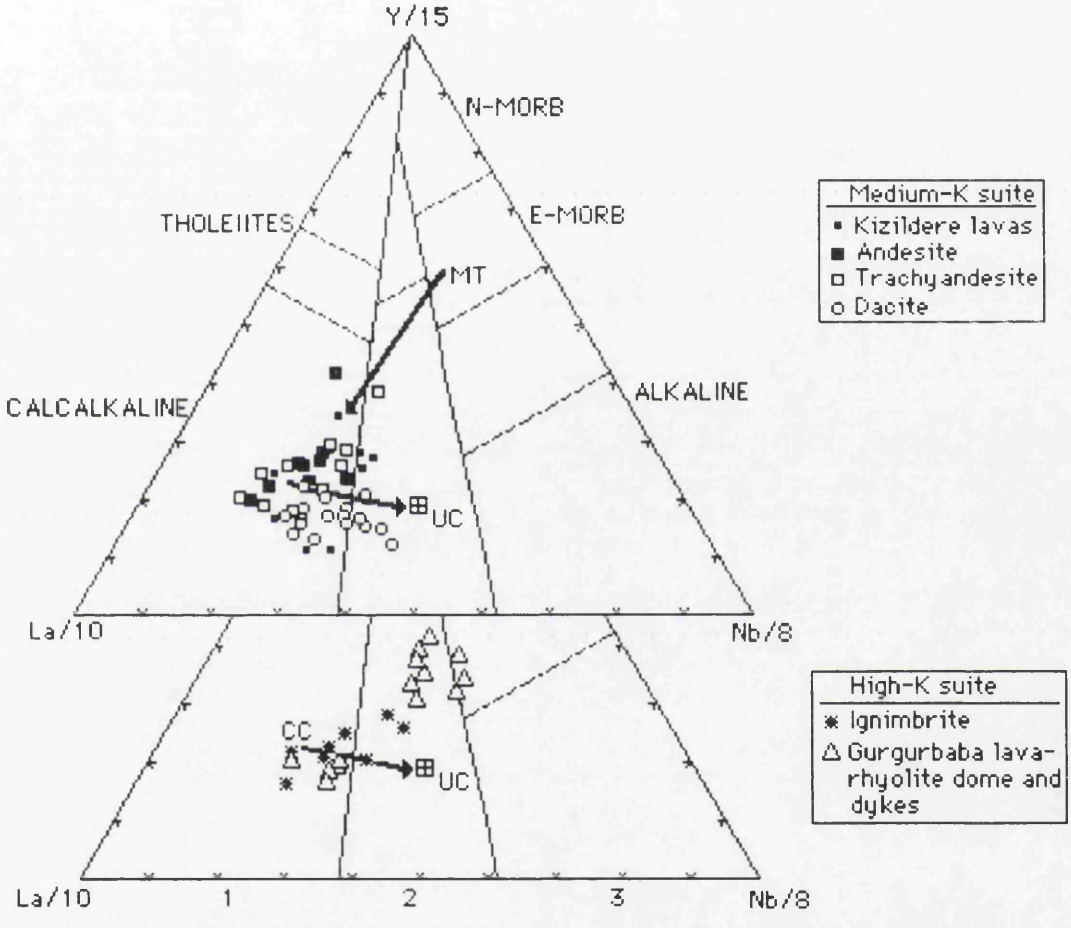

Figure 7.8. Y-La-Nb triangular plot for the calcalkaline rocks of the Meydan-Zilan area. Fields are 1-orogenic domain; 2-late to post-orogenic domain with continental crust influences; 3-non orogenic domain(after Cabanis and Lecolle, 1989). Arrows represent MT-mixing line between an OIB-component and a subduction component; CC-upper crustal mixing line between a subduction component and the upper crustal component(UC).

The Meydan-Zilan calcalkaline volcanic rocks plot into four distinctive areas(Figure 7.8). (1) Kizildere lavas, andesites and trachyandesites fall into the calcalkaline orogenic domain(field 1); (2) dacites and ignimbrite show

transition from the orogenic domain(field 1) to an intermediate domain(field 2); (3) the rhyolite dome and dykes fall into the orogenic domain(field 1); (4) The last magmatic episode, the Gurgurbaba lavas, plot in an intermediate orogenic domain(field 2). The changing characteristics of the magmatic sources and their derived volcanic products are believed to be related to a collision tectonic environment.

7.4.1. MEDIUM-K SUITE

The medium-K suite lavas(andesite, trachyandesite and dacite) are regarded as largely cogenetic and related to one another by processes thought to be important during the evolution of the crustal magma chambers i.e., crystal fractionation, assimilation and mixing. K/Rb ratios of the rocks are typically between ~500-250, and do not vary systematically with Mg-number which suggests open system crystallization, in part. Because Rb is preferentially excluded from amphibole as compared to K, the melts from which the minerals crystallized would have had even lower K/Rb than the crystals. Moreover, recent studies have shown that a diversity of open-system processes may affect magmatic compositions during melting, crystallization and eruption(McBirney, 1980; Dungan *et al.*, 1986; Leeman and Hawkesworth, 1986; Reagan *et al.*, 1987; Norman and Leeman, 1990).

7.4.1.1. IMPLICATIONS OF MAJOR ELEMENT MODELLING

The results of major element modelling may be compared with relationships established by experimental petrology to evaluate the model and help constrain some of physical conditions of the magma evolution. Many experimental studies on calcalkaline rocks have focused on the nature of andesite genesis, and the likelihood of generating andesites as primary melts(e.g., Eggler and Burnham, 1973). However, the Meydan-Zilan andesites are not primary but are differentiates of a basaltic parent.

Grove and Baker(1984) studied the evolution of tholeiitic and calcalkaline lava series in terms of the system clinopyroxene-olivine-quartz-plagioclase. The medium-K suite lavas are plotted in the plagioclase-saturated pseudoternary projection of this system(Figure 7.9). The compositional continuity and range of variation in the medium-K suite rocks are consistent with fractional crystallization as the origin of the calcalkaline trend. Differences in the relative amounts of plagioclase-clinopyroxene fractionation can be seen in pseudo-quaternary, CMAS projections.

Grove and Baker(1984) defined the 1 atm phase boundaries for subalkaline rocks. Low pressure is the likely cause of the apparent shrinkage of the cpx field and growth of the olivine field(O'Hara, 1968; Baker and Eggler, 1983). Generally, the medium-K suite appears to define an opx-cpx cotectic that

parallels the 1 bar line but is shifted toward the quartz corner(Figure 7.9). Liquids derived under conditions of moderate pressure and water undersaturation in the middle to upper crust evolve to andesites and dacites by continued crystallization involving plagioclase, augite and magnetite(Grove and Baker, 1984). Earlier crystallization of pyroxenes(and later crystallization of plagioclase) is expected at high pressures(e.g., Stolper, 1980) affecting primarily Fe and Al during fractionation.

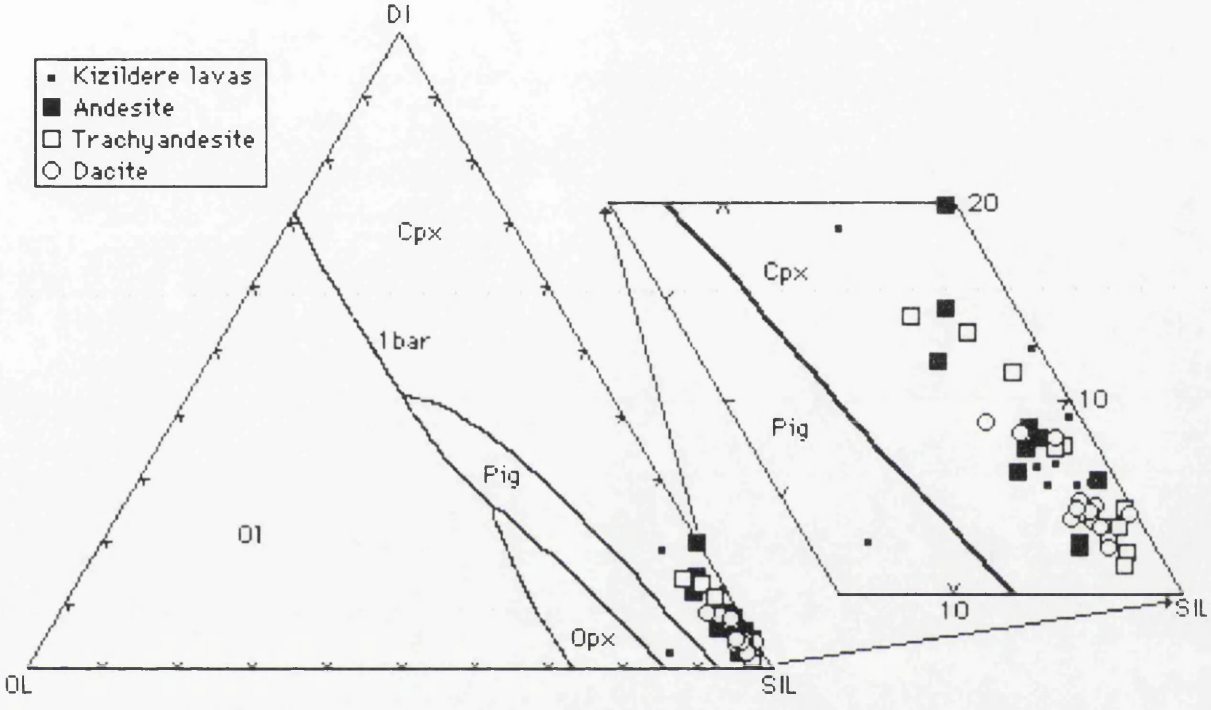

Figure 7.9. Di-Ol-Sil projection of Grove and Baker(1984) for the medium-K calcalkaline suite of the Meydan-Zilan volcanic rocks.

7.4.1.2 CRYSTALLIZATION CONDITIONS INFERRED FROM MAJOR ELEMENTS

Plagioclase and cpx are important crystallizing phases when basaltic magma cools within the crust. As the pressure of crystallization decreases, the cpx/plagioclase ratio decreases(Gust and Perfit, 1987). Increasing the water content of the magma decreases the proportion of plagioclase(e.g., Eggler, 1972b; Presnall *et al.*, 1978; Baker and Eggler, 1983). Abundances of Al_2O_3, CaO and Sr are sensitive indicators of the petrogenetic role of plagioclase and cpx. Fractionation of cpx decreases CaO in the residual liquids, and fractionation of plagioclase decreases Al_2O_3 and Sr in the residual liquids.

Because plagioclase-rich fractionating assemblages appear to be stable only at low pressures and water contents(Eggler, 1972b; Presnall *et al.*, 1978),

production of dacites occurs in the shallow crust. In addition, the amphibole phenocrysts in dacites imply high water contents; therefore plagioclase proportions in crystallizing assemblages are an unreliable barometer.

The transition from basaltic parent to andesites may have occurred at relatively deep crustal levels. The contrasting crystallization conditions and by implication contrasting depths of crystallization, provide a framework to interpret trace element and isotopic variations resulting from contamination with upper and lower crust. Geochemical variations from andesite to trachyandesite reflect processes(fractional crystallization and contamination±mixing) occurring within the mid to lower crust. However, geochemical variations from trachyandesite to dacite result from upper crustal processes. During the formation of the dacites, it is presumed that the process involves assimilation of a shallow crustal contaminant that is relatively enriched in alkali elements and Th(e.g., McMillan *et al.*, 1989).

In summary, fractional crystallization was the dominant process creating the compositional variation in the medium-K suite. Lower crustal assimilation was significant in the compositional range from the basaltic parent to andesite, and upper crustal assimilation was significant in the compositional range from trachyandesite to dacite.

7.4.1.3. CRYSTAL FRACTIONATION

The medium-K suite falls along the hypothetical low-pressure cotectic of Grove and Kinzler(1986) on their pseudo-ternary diagram and displays fair correlations on variation plots. These observations suggests that crystal fractionation may be an extremely important process during the evolution of the magma chambers. Fractional crystallization of ferromagnesian silicates, oxides and of plagioclase is suggested respectively by the low contents of Ni, Co and Cr, and by Eu anomalies in the suite.

Assuming one of the more mafic andesites as a starting composition, most of the major and trace element variability of the rocks can be accounted for by fractional crystallization from andesite via trachyandesite to trachyte. Mass balance least squares mixing models(Stormer and Nicholls, 1978) show that the range of the trachyandesite major element compositions can be closely reproduced by plausible fractionation models. Two models can fit the major element data; one dominated by hornblende, the other by plagioclase with other anhydrous phases. Gill(1981) discussed the difficulty in distinguishing between these two models because, mathematically, hornblende compositions can be approximated by mixtures of plagioclase, augite and magnetite. However, the hornblende model is favoured for the following reasons:

(1) Hornblende is a common phenocryst phase in andesites. Virtually all of the lavas carry phenocrystic pseudomorphs after hornblende and fresh cores of brown hornblende are preserved in some samples; (2) One cognate xenolith found comprises several euhedral grains of hornblende in a continuous matrix of plagioclase; (3) Phenocrysts of plagioclase are rare; (4) Trace element variations indicate significant hornblende fractionation(see Chapter 5).

Mass balance calculations using hornblende tend to yield better fits than models which exclude it from the crystallizing assemblage. The combination of hornblende and magnetite can produce an acceptable mass balance fit. Augite also occurs as phenocrysts in andesites but it does not emerge as a major component an any of the hornblende-bearing models.

Major element mass-balance calculations(Stormer and Nicholls, 1978) are given in Table 7.3. Several authors have arbitrarily chosen the sum of the squares of the residual(Σr^2) values below 1.5(Luhr and Carmichael, 1980) or 1.2(Wyers and Barton, 1986) to be indicative of crystal fractionation. Σr^2 values much greater than ~0.1, however, suggest that other processes(e.g., assimilation and magma mixing) in addition to crystal fractionation occurred during the evolution of the magmatic system if the samples are related petrogenetically(e.g., Defant and Nielsen, 1990).

Mass-balance calculations(Bryan *et al.*, 1969) were also made for trace element modelling using mineral partition coefficients and F values from the mass-balance calculations. Selected trace element modelling results based on these calculations are given in Table 7.4. The trace element modelling of crystal fractionation for the medium-K suite through mass-balance calculations gives poor solutions in part due to incompatible elements that are insensitive to crystal fractionation processes but influenced by contamination and, or magma mixing which may have disturbed the crystal fractionation systematics.

Table 7.3. Testing the feasibility of fractionation in the medium-K suite, using mass balance mixing models(Stormer and Nicholls, 1978).

A) Testing the feasibility of fractionation **from andesite to trachyandesite,** using phases; plagioclase, hornblende and magnetite.

	Composition of initial magma	*Composition of final magma*	*Bulk comp. of added or subtr. matl.*	*Obs. diff. between magmas*	*Calc. diff. between magmas*	*Obs.-calc. (residuals)*
SiO_2	58.45	62.04	40.74	3.593	3.563	0.030
TiO_2	0.65	0.61	1.40	-0.039	0.132	0.093
Al_2O_3	17.78	17.29	19.01	-0.482	-0.288	-0.194
Fe_2O_3*	7.30	5.21	17.75	-2.089	-2.097	0.008
MnO	0.18	0.09	0.16	-0.085	-0.012	-0.074
MgO	2.99	2.02	6.67	-0.970	-0.777	-0.192
CaO	6.60	6.11	11.07	-0.487	-0.829	0.342
Na_2O	4.10	4.25	2.80	0.147	0.242	-0.095
K_2O	1.78	2.16	0.37	0.377	0.299	0.078
P_2O_5	0.18	0.21	0.02	0.035	0.031	0.004

Sum of the squares of the residuals = 0.2216

Phase name	*Amount as wt.% of init. magma*	*Amount as wt.% of all phases*	*Amount as wt.% of added phases*	*Amount as wt.% of subtrd. phases*
Plagioclase	-7.39	44.18	0.00	44.18
Hornblende	-7.02	41.95	0.00	41.95
Magnetite	-2.32	13.86	0.00	13.86
Total relative to initial magma			0.00	16.73

B) Testing the feasibility of fractionation **from trachyandesite to dacite,** using phases; plagioclase, augite, hornblende and magnetite.

	Composition of initial magma	*Composition of final magma*	*Bulk comp. of added or subtr. matl.*	*Obs. diff. between magmas*	*Calc. diff. between magmas*	*Obs.-calc. (residuals)*
SiO_2	62.04	70.17	49.98	8.129	7.915	0.214
TiO_2	0.61	0.34	0.69	-0.270	-0.137	-0.133
Al_2O_3	17.29	16.14	19.84	-1.149	-1.450	0.302
Fe_2O_3*	5.21	2.66	9.63	-2.550	-2.733	0.183
MnO	0.09	0.06	0.10	-0.030	-0.014	-0.016
MgO	2.02	1.02	4.37	-1.000	-1.313	0.313
CaO	6.11	2.99	11.00	-3.120	-3.138	0.018
Na_2O	4.25	3.81	3.95	-0.440	-0.056	-0.383
K_2O	2.16	2.67	0.43	0.510	0.878	-0.368
P_2O_5	0.21	0.13	0.01	-0.080	0.049	-0.129

Sum of the squares of the residuals = 0.5851

Phase name	*Amount as wt.% of init. magma*	*Amount as wt.% of all phases*	*Amount as wt.% of added phases*	*Amount as wt.% of subtrd. phases*
Plagioclase	-25.83	65.89	0.00	65.89
Augite	-6.95	17.72	0.00	17.72
Hornblende	-2.64	6.74	0.00	6.74
Magnetite	-3.79	9.65	0.00	9.65
Total relative to initial magma			0.00	39.21

Table 7.4. Selected trace element modelling based on least squares mass-balance calculations(Bryan *et al.*, 1969), using mineral-distribution coefficients(Pearce and Norry, 1979; Gill, 1981; Philpotts and Schetzler, 1970; Schetzler and Philpotts, 1970; Green and Pearson, 1983; Watson and Ryerson, 1986).

A) Fractionation from **andesite to trachyandesite.**

	Parent composition	*Daughter composition*	*Daughter calculated*	*Residuals*	*Bulk K_Ds*
Rb	61	70	72.51	-2.51	0.049
Sr	288	415	294.29	120.71	0.881
Ba	403	518	-181.95	44.59	0.114
Y	32	18	31.18	-13.18	1.143
Zr	134	166	143.59	22.41	0.620
Nb	7	11	7.40	3.60	0.694
Ni	40	10	17.39	-7.39	5.583
Co	17	13	6.19	6.81	6.561
Cr	21	29	1.14	27.86	17.017

B) Fractionation from **trachyandesite to dacite.**

	Parent composition	*Daughter composition*	*Daughter calculated*	*Residuals*	*Bulk K_Ds*
Rb	70	85	109.10	-24.10	0.052
Sr	415	441	-268.93	54.57	1.152
Ba	518	703	128.57	-80.93	0.115
Y	18	13	21.31	-8.31	0.639
Zr	166	172	239.19	-67.19	0.220
Nb	11	12	15.19	-3.19	0.310
Ni	10	8	3.70	4.30	3.122
Co	13	6	2.65	0.35	2.779
Cr	29	13	0.20	12.80	11.620

7.4.1.4. IMPORTANCE OF AMPHIBOLE FRACTIONATION IN THE MEDIUM-K SUITE

The extent to which amphibole fractionation influences the trace element chemistry of calcalkaline magmas depends strongly upon the timing and amount of amphibole crystallization. Hornblende distribution coefficients for the REE are highly dependent upon melt composition, temperature and pressure(Arth, 1976; Schnetzler and Philpots, 1970; Fujimaki et al, 1984; Green and Pearson, 1985). At a constant pressure distribution coefficients increase with decreasing temperature and increasing silica content of the melt. In addition, the degree to which hornblende preferentially extracts the M-HREE, relative to the LREE, increases between andesite and dacite(Green and Pearson, 1985). In andesite melts, amphibole fractionation increases the La/Yb ratio of the residual melt but the REE pattern does not develop a strongly concave shape. If little amphibole fractionation occurs before eruption the effect on the

REE chemistry of the magma would be minimal. As the magma evolves to dacitic compositions, hornblende REE distribution coefficients increase and hornblende fractionation becomes the dominant influence on the REE concentrations.

At shallow levels within the crust, hornblende crystallization may cease and be replaced by pyroxenes in andesitic magmas. Pyroxene with plagioclase fractionation has a similar bulk distribution coefficients for REE to hornblende fractionation. During the fractionation of the REE by pyroxene with plagioclase the high La/Yb and concave REE patterns derived from the earlier fractionation of hornblende will not be seriously changed. The result will be a more evolved magma, but a similar REE pattern. Furthermore, open-system behaviour will result in residual melts with higher La/Yb ratios and higher incompatible element concentrations than in closed-system fractionation case, but the characteristic shape of the hornblende-influenced REE pattern will remain.

7.4.1.5. POTENTIAL ROLE OF CRUSTAL MATERIAL

The possible interaction of parental magmas with crustal material is suggested by the following geological and geochemical considerations: (a) andesites may contain xenocrystic quartz, (b) the rocks have high $^{87}Sr/^{86}Sr$ ratios(0.706). Furthermore, since the rocks display high SiO_2 and LILE concentrations, it is inferred that crustal differentiation controls their eruptive compositions(e.g., James, 1982; Thorpe *et al.*, 1984b; Harmon and Hoefs, 1984; Harmon *et al.*, 1984).

The extent of assimilation appears to be limited because the $^{87}Sr/^{86}Sr$ ratios are not greatly increased over mantle values. Alternatively, young crust of similar isotopic composition could be assimilated. Hildreth and Moorbath(1988) described how upper crustal assimilation plus fractional crystallization is much more effective in lowering K/Rb and raising Rb concentrations than fractional crystallization alone, whether hornblende-dominated or not. The high La/Yb ratios indicate an added element to pervasive crystal contamination. Hildreth and Moorbath(1988) suggest garnet involvement in the production of normalized increases in LREE abundances and LREE/HREE ratios. Increasing garnet control likely correlates with increasing crustal thickness(Kay *et al.*, 1988; Hildreth and Moorbath, 1988). Therefore, both Kay *et al.* (1988), and Hildreth and Moorbath(1988) conclude that a garnet signature suggests partial melting of garnet-bearing country rocks stabilized in areas of thickened crust(~55km). Crustal thickening necessitates that contamination involves incorporation of partial melts of wall rock, rather than bulk ingestion of wall rock. Such a contamination process may produce

selective enrichments in certain incompatible elements, such as K(Maury and Bizouard, 1974; Watson, 1982; Tindle and Pearce, 1983).

7.4.1.6. MAGMA MIXING

Magma mixing processes have often been proposed to account for the genesis of calcalkaline andesitic lavas(e.g., Eichelberger, 1978; Gerlach and Grove, 1982). One model for chemical variation in intermediate rocks involves mixing of mafic and silicic magmas(e.g., Anderson, 1976; Eichelberger, 1981). In this model the mafic end member may represent additions from the mantle, whereas the silicic end member may be derived through crustal contamination and, or fractional crystallization(e.g., Grove and Donelly-Nolan, 1986). Magma mixing has also been demonstrated in many other silicic systems(e.g., Reid *et al.*, 1983; Cantagrel *et al.*, 1984; Vogel *et al.*, 1984; Bacon, 1986)

A variety of data suggest that disequilibrium has existed in the rocks e.g. oscillatory zoning in plagioclase phenocrysts may be related to rapid crystal growth(Hollister and Gancarz, 1971; Nakamura, 1973). Sieve textures, resorption and embayment in plagioclase appear to be associated with either magma mixing or assimilation according the experimental work of Tsuchiyama(1985).

The mineralogical and petrographical disequilibrium characteristics could be due to involvement of complex processes such as assimilation, magma mixing. This is supported by the $>0.1\Sigma r^2$ values from the mass-balance modelling and the large variations in the incompatible element ratios. It is difficult to constrain the extent of the processes because of the lack of knowledge of the compositions of the primary melts and of likely material which could be assimilated.

7.4.1.7. PETROGENETIC MODEL AND PARENTAL MAGMA SOURCE

The correlation between major and trace elements may suggest the descent of the andesites from a common parent through fractional crystallization. The geochemical features also suggest that magmas behaved as open systems in the evolution of trachyandesites and dacites.

Trace element and isotopic data indicate that lower crustal contamination occurs during the evolution of primary magma to andesite. A very thick crust and the resultant high temperature of the lower crust may induce large scale lower crustal melting and contamination of mantle-derived magmas(MASH zone of Hildreth and Moorbath, 1988). The lower crustal contribution to magmas is probably a partial melt of a subducted slab-derived

materials, and it causes enhanced Rb and Th contents plus increased La/Yb in the evolving magmas. Thus, partial melting of the lower crust produces incompatible element-rich contaminants that are incorporated into the evolving magmas, and are transported to higher crustal levels, thereby enhancing the compositional stratification of the continental crust. Trachyandesites and dacites in the suite form by low pressure fractional crystallization and mixing(especially for trachyandesites). The upper crust behaves as a leaky crucible during this differentiation to dacite, with upper crustal contaminants causing significant enrichments of Rb and Th in the evolving magmas.

The geochemical evidence in the andesites is inconsistent with a parental magma forming high degrees of melting of a garnet lherzolite mantle source. Degrees of melting may result from greater fluxing of mantle by slab-derived fluids. The composition of this parental magma has been subsequently affected by crustal processes. The parental magma rising through thick crust, has a more protracted history of high pressure, cpx-dominated fractionation.

Fluids or melts coming from the subducted slab possibly invaded and metasomatized portions of overlying mantle. Although the mechanisms are not known in detail(Arculus and Powell, 1986), the process is commonly invoked to explain the geochemical imprint of the "orogenic" magmas(e.g., Toscani *et al.*, 1990). Two extreme agents may cause metasomatism; aqueous fluids and silicate melts. Aqueous fluids coming from the subducted slab material are enriched in many elements(alkalis, alkaline earth, REE, HFSE in decreasing order). Reactions of these fluids with mantle material produce hydrated minerals such as amphibole. Amphibole retains abundant strontium, which if highly radiogenic, may significantly change the Sr-isotope ratio of the whole system. Involvement of salic melts generated by partial melting of a highly radiogenic subducted slab would lead to comparable results.

7.4.2. HIGH-K SUITE

Chemical variations in the high-K suite(ignimbrite, the rhyolite dome and dykes, pumice and the Gurgurbaba lava) could involve fractional crystallization, magma mixing, crustal melting, and the complexing of volatiles and incompatible elements during magmatic degassing. However, the primary question is whether the parental rhyolite magmas were melted from the crust or were derived from a basaltic precursor by fractional crystallization. It is highly unlikely that the rhyolitic rocks were derived by direct melting of crust. On the other hand, the rhyolites cannot have been derived by closed-system fractional crystallization of a basaltic precursor because the rhyolites have higher $^{87}Sr/^{86}Sr$ ratios than the basaltic rocks.

Consequently, the geochemical data point to an origin of the silicic rocks by fractional crystallization of a hybrid magma with mantle and crustal components. One end member scenario is that the basalt provides the heat that causes melting of the crust, and thus forms a separate silicic magma with its own crustal origin.

In the feldspar ternary system(Figure 7.10; projection method of Sack *et al.*, 1987) the rocks are shifted to the albite corner, plotting away from the two-feldspar cotectic of Carmichael *et al.* (1974). These trends are consistent with the observed modal mineral assemblages in the rocks, suggesting that the rocks are non-minimum melts.

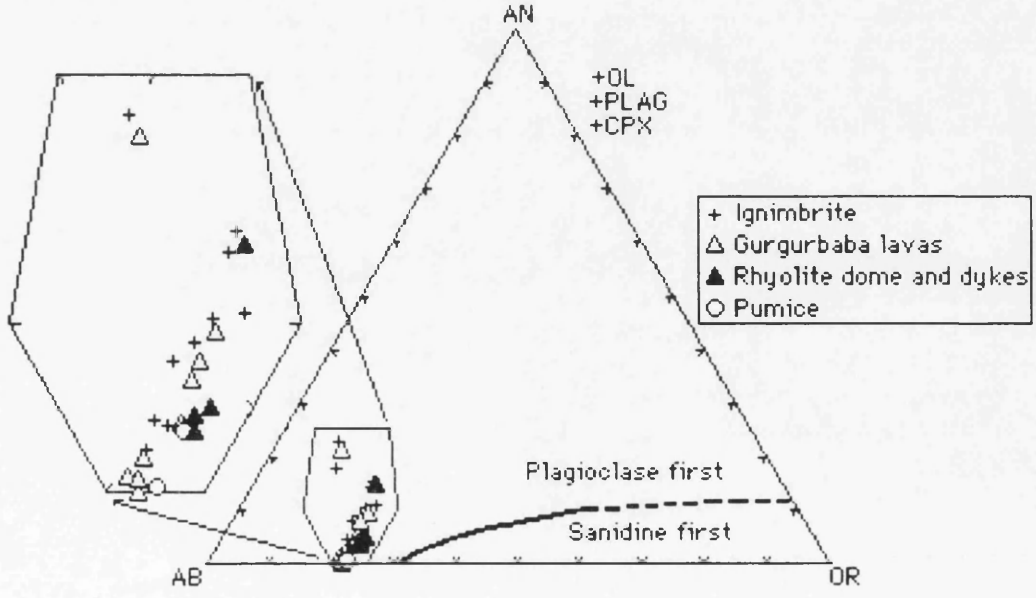

Figure 7.10. High-K suite rocks projected on to the normative join An-Ab-Or by the projection scheme of Sack *et al.* (1987) and two-feldspar liquidus of Carmichael *et al.* (1974).

7.4.2.1. FRACTIONAL CRYSTALLIZATION

The composition of the medium-K suite indicates that the silica-saturated liquids were produced as result of the fractionation of solids, liquids and possibly, by alkali-halogen bearing vapour phases. The less evolved magmas may have acted as heat sources to induce partial melting of the upper crust. At least three fractionating mineral assemblages are predicted from major and trace element variations. Differentiation of liquids would have been sensitive to fractionation of biotite, amphibole, plagioclase±alkali feldspar and Fe-Ti oxides. The evolved pumices represent the most fractionated liquids, and their low Sr and Ba contents imply extensive fractionation of plagioclase and sanidine, respectively.

Mass-balance calculations(Stormer and Nicholls, 1978) were made to test the effects of crystal fractionation. In the model, the least evolved sample(MA-58A) from the Gurgurbaba lavas was taken as the parent of the evolved rhyolites and pumice. Using the model, fractional crystallization gives acceptable solutions for the major elements(Table 7.5). Selected trace element modelling based on these calculations is also given in Table 7.6, using mineral-partition coefficients and F values from the mass balance calculations. The trace element calculation gives relatively poor solutions for trace elements, presumably due to the involvement of accessory phases(zircon and apatite) in the fractionating assemblage. It is reasonable, therefore, to assume that the bulk distribution coefficients for many incompatible elements changed abruptly with the crystallization of accessory minerals during fractionation.

Major crystal fractionation within high-silica magma chambers has been regarded as unimportant(Hildreth, 1979, 1981), on the basis that crystal settling rates are too slow in viscous polymerized melts to allow significant gravitational separation of crystals. However, gravitational settling of crystals need not occur in order for fractional crystallization to proceed(McBirney, 1980). The relatively cold walls of magma chambers are the most likely place for crystallization to occur. Crystallization on the walls may create a boundary layer of more siliceous, less dense magma. The buoyant boundary layer can then rise along the edges of the magma chamber, and collect at the top to form a high silica cap. Throughout the process, fractionated rhyolitic magma is close to wallrock, from which it could become slightly contaminated(e.g., Musselwhite *et al.*, 1989).

Table 7.5. Testing crystal fractionation in the medium-K suite, using the least squares mass-balance mixing calculations(Stormer and Nicholls, 1978).

A) Testing the feasibility of fractionation **from low silica rhyolite(MA-58A) to high silica rhyolite(MA-17)** in the Gurgurbaba lavas.

	Composition of initial magma	*Composition of final magma*	*Bulk comp. of added or subtr. matl.*	*Obs. diff. between magmas*	*Calc. diff. between magmas*	*Obs.-calc. (residuals)*
SiO_2	63.52	72.17	48.17	8.947	8.897	-0.250
TiO_2	0.55	0.08	1.15	-0.472	-0.397	-0.076
Al_2O_3	16.88	13.25	23.88	-3.635	-3.939	0.304
Fe_2O_3*	4.21	1.22	9.01	-2.984	-2.887	-0.097
MnO	0.13	0.11	0.08	-0.017	0.010	-0.027
MgO	2.29	0.70	2.80	-1.592	-0.779	-0.813
CaO	4.95	2.18	7.93	-2.773	-2.131	-0.641
Na_2O	5.01	6.08	4.21	1.073	0.694	0.379
K_2O	2.25	4.18	1.73	1.927	0.909	1.017
P_2O_5	0.20	0.03	1.05	-0.174	-0.378	0.204

Sum of the squares of the residuals = 2.4642

Phase name	*Amount as wt.% of init. magma*	*Amount as wt.% of all phases*	*Amount as wt.% of added phases*	*Amount as wt.% of subtrd. phases*
Plagioclase	-27.80	75.00	0.00	75.00
Hornblende	-0.97	2.62	0.00	2.62
Biotite	-5.73	15.46	0.00	15.46
Magnetite	-2.56	6.92	0.00	6.92
Total relative to initial magma			0.00	37.07

B) Testing the feasibility of fractionation **from low silica rhyolite(MA-58A) to high silica rhyolite(MA-17)** in the Gurgurbaba lavas, with sanidine (addition model).

	Composition of initial magma	*Composition of final magma*	*Bulk comp. of added or subtr. matl.*	*Obs. diff. between magmas*	*Calc. diff. between magmas*	*Obs.-calc. (residuals)*
SiO_2	63.52	72.17	35.39	8.647	8.803	-0.156
TiO_2	0.55	0.08	2.44	-0.472	-0.565	0.092
Al_2O_3	16.88	13.25	28.01	-3.635	-3.532	-0.103
Fe_2O_3*	4.21	1.22	13.24	-2.984	-2.876	-0.108
MnO	0.13	0.11	0.16	-0.017	-0.012	-0.006
MgO	2.29	0.70	6.93	-1.592	-1.491	-0.101
CaO	4.95	2.18	13.35	-2.773	-2.673	-0.099
Na_2O	5.01	6.08	3.83	1.073	0.539	0.534
K_2O	2.25	4.18	-3.78	1.927	1.905	0.022
P_2O_5	0.20	0.03	0.44	-0.174	-0.098	-0.075

Sum of the squares of the residuals = 0.3662

Phase name	*Amount as wt.% of init. magma*	*Amount as wt.% of all phases*	*Amount as wt.% of added phases*	*Amount as wt.% of subtrd. phases*
Plagioclase	-31.53	49.50	0.00	71.96
Hornblende	-0.26	0.41	0.00	0.60
Biotite	-10.53	16.54	0.00	24.04
Magnetite	-1.49	2.34	0.00	3.41
Sanidine	19.88	31.21	100.00	0.00
Total relative to initial magma			19.88	43.81

C) Testing the feasibility of fractionation **from low silica rhyolite(MA-58A) to rhyolitic pumice(MA-234A).**

	Composition of initial magma	*Composition of final magma*	*Bulk comp. of added or subtr. matl.*	*Obs. diff. between magmas*	*Calc. diff. between magmas*	*Obs.-calc. (residuals)*
SiO_2	63.52	75.62	50.72	12.094	11.903	0.191
TiO_2	0.55	0.11	0.40	-0.441	-0.141	-0.300
Al_2O_3	16.88	12.74	21.49	-4.148	-4.187	0.039
Fe_2O_3*	4.21	1.36	7.71	- 2.846	-3.033	0.187
MnO	0.13	0.03	0.10	-0.096	-0.033	-0.063
MgO	2.29	0.32	3.53	-1.972	-1.534	-0.437
CaO	4.95	0.46	10.96	-4.491	-5.021	0.530
Na_2O	5.01	4.64	4.02	-0.367	0.298	-0.665
K_2O	2.25	4.69	0.26	2.439	2.121	0.318
P_2O_5	0.20	0.03	0.81	-0.173	-0.374	0.201

Sum of the squares of the residuals = 1.2231

Phase name	*Amount as wt.% of init. magma*	*Amount as wt.% of all phases*	*Amount as wt.% of added phases*	*Amount as wt.% of subtrd. phases*
Plagioclase	-34.90	73.01	0.00	73.01
Augite	-8.83	18.47	0.00	18.47
Hornblende	-0.97	2.03	0.00	2.03
Magnetite	-3.10	6.49	0.00	6.49
Total relative to initial magma			0.00	47.80

D) Testing the feasibility of fractionation **from low silica rhyolite(MA-58A) to rhyolite dome(MA-38B)** , with sanidine(addition model).

	Composition of initial magma	*Composition of final magma*	*Bulk comp. of added or subtr. matl.*	*Obs. diff. between magmas*	*Calc. diff. between magmas*	*Obs.-calc. (residuals)*
SiO_2	63.52	71.01	0.78	7.484	7.375	0.110
TiO_2	0.55	0.39	4.61	-0.159	-0.443	0.284
Al_2O_3	16.88	14.29	40.71	-2.590	-2.774	0.184
Fe_2O_3*	4.21	1.84	24.98	-2.368	-2.431	0.063
MnO	0.13	0.09	0.31	-0.033	-0.022	-0.010
MgO	2.29	0.88	13.89	-1.414	-1.366	-0.048
CaO	4.95	1.86	30.83	-3.092	-3.043	-0.049
Na_2O	5.01	4.51	3.72	-0.496	0.084	-0.579
K_2O	2.25	5.04	-22.05	2.787	2.845	-0.057
P_2O_5	0.20	0.08	2.22	-0.120	-0.224	0.104

Sum of the squares of the residuals = 0.4854

Phase name	*Amount as wt.% of init. magma*	*Amount as wt.% of all phases*	*Amount as wt.% of added phases*	*Amount as wt.% of subtrd. phases*
Plagioclase	-32.22	42.63	0.00	74.87
Hornblende	-0.58	0.77	0.00	1.35
Biotite	-9.10	12.04	0.00	21.15
Magnetite	-1.13	1.50	0.00	2.63
Sanidine	32.54	43.05	100.00	0.00
Total relative to initial magma			32.54	43.04

Table 7.6. Selected trace element modelling based on the least squares mass-balance mixing calculations(Bryan *et al.*, 1969), using mineral distribution coefficients for acidic melts(Arth, 1976; Pearce and Norry, 1979; Nash and Crecraft, 1985; Mahood and Hildreth, 1983).

A) Fractionation from **low silica rhyolite(MA-58A) to high silica rhyolite(MA-17)** in the Gurgurbaba lavas.

	Parent composition	*Daughter composition*	*Daughter calculated*	*Residuals*	*Bulk K_Ds*
Rb	67	221	103.91	117.06	0.160
Sr	472	27	3.16	23.84	10.575
Ba	749	78	-127.02	205.02	1.668
Y	20	50	14.08	35.92	1.671
Zr	167	321	156.40	164.60	1.125
Nb	11	25	9.33	15.67	1.314
Ni	15	4	25.30	-21.30	0.000
Co	20	6	9.68	-3.68	2.389
Cr	49	3	62.67	-59.67	0.529

B) Fractionation from **low silica rhyolite(MA-58A) to high silica rhyolite(MA-17)** in the Gurgurbaba lavas, with sanidine(addition model).

	Parent composition	*Daughter composition*	*Daughter calculated*	*Residuals*	*Bulk K_Ds*
Rb	67	221	89.13	131.87	0.124
Sr	472	27	5.93	21.07	14.427
Ba	749	78	-207.79	285.79	2.580
Y	20	50	18.71	31.29	1.205
Zr	167	321	170.82	150.18	0.931
Nb	11	25	6.43	18.57	2.647
Ni	15	4	20.78	-16.78	0.000
Co	20	6	0.00	6.00	28.732
Cr	49	3	8.43	-5.43	6.399

C) Fractionation from **low silica rhyolite(MA-58A) to rhyolite pumice(MA-234A).**

	Parent composition	*Daughter composition*	*Daughter calculated*	*Residuals*	*Bulk K_Ds*
Rb	67	146	121.35	24.65	0.073
Sr	472	17	1.09	15.91	10.463
Ba	749	3846	82.23	301.77	1.024
Y	20	26	10.52	15.48	2.002
Zr	167	105	124.72	-19.72	1.455
Nb	11	9	8.16	0.84	1.466
Ni	15	1	28.48	-27.48	0.000
Co	20	0			
Cr	49	0			

D) Fractionation from **low silica rhyolite(MA-58A) to rhyolite dome(MA-38B).**

	Parent composition	*Daughter composition*	*Daughter calculated*	*Residuals*	*Bulk K_Ds*
Rb	67	246	100.47	145.53	-2.374
Sr	472	103	15.85	87.15	29.265
Ba	749	311	116.62	194.38	-11.582
Y	20	24	17.06	6.94	2.326
Zr	167	253	151.99	101.01	1.784
Nb	11	19	6.69	12.31	5.140
Ni	15	4	16.91	-12.91	0.000
Co	20	8	0.03	7.97	-9.666
Cr	49	32	12.28	19.72	12.525

7.4.2.2. CONVECTIVE FRACTIONATION AND COMPOSITIONAL ZONATION

The more evolved compositions may exhibit large ranges in trace elements for relatively small variations in major elements(e.g., Storey, 1981; Marsh, 1987) and most incompatible elements may vary markedly in abundance toward the top of the magma chamber(e.g., Leat *et al.*, 1984). The differences in trace elements between the pumice and the Gurgurbaba lavas indicate that large changes in liquid compositions occurred in the crystallized parts of the magma chamber where the accessory minerals were not strongly concentrated.

Fluid dynamic modelling of magmas has shown that zonation of reservoir liquids can develop by thermal and compositional convection of fractionated boundary layers at the magma chamber margins(Turner and Gufstafson, 1981; Huppert and Sparks, 1984). Some workers(e.g., McBirney *et al.*, 1985; Tait *et al.*, 1989) have argued that fractionated liquids rise as diffusion-limited chemical boundary layers alongside the chamber margins. Turner and Gufstafson(1981) proposed that the felsic capping layer produced by this mechanism may split into thin layers with slightly different densities, so that a fine-scale zonation develops independently of that in the less evolved, bulk-magma reservoir. Trial and Spera(1990), in contrast, proposed that convecting liquids must percolate along the entire length of the side wall cumulate zone before fractionated liquids will reach the top of the magma reservoir. Their treatment considered two extremes in diffusive species(SiO_2 and H_2O) that widely bracket the behaviour of most incompatible elements in evolved magmas(Allegre and Minster, 1978; Tait *et al.*, 1989).

Thick pumice fall-out deposits are likely to reflect the compositional gradients in subvolcanic magma chambers(Wolff and Storey, 1984; Luhr and

Giannetti, 1987) but systematic variations are rare in the pumice deposits studied. Several lines of evidence, however, indicate that the bulk of the magmas were compositionally stratified. The stratigraphy implies an overall compositional progression of erupted magmas with time from rhyolitic pumice to the Gurgurbaba lavas(crystal poor). The compatible and incompatible elements(e.g., Ba and Th) show the type variation with stratigraphy that is commonly observed in zoned felsic rocks(McBirney *et al.*, 1985; Wolff *et al.*, 1990).

The model envisaged for the magma chamber shows a capping layer of crystal-poor rhyolitic magma(the Gurgurbaba lava) that overlies relatively crystal rich-rhyolitic liquids with high Ba and Sr contents.

7.4.2.3. MAGMA MIXING

Efficient magma mixing can greatly modify liquid compositions in the resulting hybrids(Storey *et al.*, 1989) and will change relationships between crystals and the matrix glass in the erupted rocks. Small volume magma chambers are especially susceptible to rapid mixing of magmas and their crystal populations(Blake, 1981; Wolff and Storey, 1984). Crystals can be redistributed by convecting boundary layers or plumes, by crystal settling, by collapse of wall cumulates and masses(Storey *et al.*, 1989), by transport in the boundary layer flow along the chamber roof and walls(Huppert and Sparks, 1984; Tait *et al.*, 1989) and by convective mixing(Anderson, 1976; McBirney, 1980). The net effect of these processes is to provide efficient mechanisms for crystal fractionation that otherwise would not operate in magmas with high viscosities(McBirney *et al.*, 1985). Furthermore, the fluid dynamic limits on the efficiency of mixing between mafic and felsic magmas appear to preclude the generation of high-K, I-type granitic rocks by this mechanism(Sparks and Marshall, 1986).

Models that test the chemical signatures of combined magma mixing and crystal fractionation in the magmas demonstrate that replenishment by less evolved magmas would have had the net effect of buffering the system in both compatible and incompatible elements(e.g., O'Hara and Mathews, 1981).

Pumice clasts do not exhibit the features that typically indicate mixing of mafic and evolved magmas, such as banded clasts(e.g., Worner and Wright, 1984; Wolff, 1985). Magma mixing may have triggered the explosive eruption of pumice deposits(Sparks *et al.*, 1977). Furthermore, sudden fluctuations in the volatile and chemical budget during explosive eruptions might have promoted brief periods of rapid crystallization along the chamber walls(e.g., Leat *et al.*, 1984; Brandeis and Jaupart, 1986).

7.4.2.4. CRUSTAL MELTING

The high-K suite is generally enriched in incompatible elements(e.g., Th, Rb and REE) compared to the medium-K suite. These geochemical features suggest the importance of crustal rocks in the magma source.

Huppert and Sparks(1988) predict that anatexis leading to the formation of acid magmas is to be expected when basaltic magmas are emplaced into continental crust. Melting of the roof rock may result in large quantities of silicic magma being formed, thus impeding the further passage of basaltic liquids to the surface. Their model requires crustal country-rock temperatures in excess of 500°C. Generation of rhyolitic magma by crustal melting may occur either by bulk melting, or partial melting(leaving a non-erupted refractory residue). These processes would generate rhyolites with contrasting trace element relationships to the crustal protoliths.

The most important heat-producing elements in sialic crust are Th and U. Th/U values for calcalkaline crustal rocks are typically 3-5, rarely exceeding 7(Thompson *et al.*, 1984; Taylor and McLennan, 1985). The high-K suite rocks(Th=10-40 ppm) do not have Th values similar to upper crustal composition(Th=10.7 ppm; Taylor and McLennan, 1985), suggesting that they were not generated by bulk melting of crust.

The explanation that the low Th contents of silicic melts formed by partial melting of sialic crust(Noble *et al.*, 1984; Pichavant and Montel, 1988; Vidal *et al.*, 1982; France-Lanord and Le Fort, 1988) has some support from experimental studies which indicate that Th is retained in the refractory residue relative to some other trace elements, possibly including Ta, during partial melting of crust(Harrison *et al.*, 1986).

Finally, the high Th abundances(>10 ppm) in the medium K suite therefore do not support the hypothesis that they represent partial melts of sialic crust. The rocks may represent melts of local sialic crust which is further supported by Sr-isotopic data indicating involvement of young sialic crust.

7.4.2.5. PETROGENETIC MODEL AND PARENTAL MAGMA SOURCE

The model for the origin of high-K, I-type granitic rocks places them in a postcollisional setting, where melting of the source rocks occurs as a consequence of decompression following crustal thickening. Thickening of the crust would lead to telescoping and metamorphism of a pile of sedimentary and volcanic detritus as well as any underlying old crust. Extension following thickening would then allow mantle upwelling and underplating of the lower crust by mafic magmas. The input of this extra heat into an already hot crust would cause wide-spread partial melting in the crustal pile, and the melts

could potentially ascend to shallower levels(Sonder *et al.*, 1987; Dewey, 1984; Windley, 1991).

Roberts and Clemens(1993) suggested that high-K granitic rocks involve fluid-absent partial melting of fertile metaluminous protoliths(mostly metamorphosed igneous rocks in the lower crust) heated by under plated or intraplated mafic magma. Huppert and Sparks(1988) modelled the thermal effects of intrusion of basaltic magma into continental crust. Temperatures in the range of 900-950°C can be expected. These temperatures are much higher than can be achieved in simple crustal thickening(England and Thompson, 1984). Melting reactions are likely to be similar to the following(Clemens and Vielzeuf, 1987): Bt+Qtz+Pl=(Opx/Cpx)+Kfs+melt, and Hbl=Pl+Qtz+Opx+Cpx+melt. Lower crustal melting at granulite facies conditions occurs mostly under fluid-absent conditions(e.g., Clemens, 1990). In these conditions H_2O for hydrous water-undersaturated magmas is derived solely from the breakdown of micas and amphiboles.

For fluid-absent source materials of mafic to intermediate composition, with H_2O contents between 0.7 and 1.6 wt.%, the predicted amounts of partial melts are between 30% and 60%(T=900-950°C, P=5-10 kbar) of the source material. The parental magmas of the high-K suite rocks may be derived as partial melts of intermediate to transitional, high-K calcalkaline, meta-igneous rocks in the continental crust. These source materials could be derived from enriched subcontinental lithospheric mantle. Therefore, the chemistry of the rhyolites depends on the nature of the protoliths rather than the processes involved in their generation(e.g., Roberts and Clemens, 1993).

7.4.2.6. EVOLUTION MODEL FOR PUMICE DEPOSITS AND THE GURGURBABA DOME

Most phases of silicic dome growth have some associated explosive activity. Explosive activity associated with volcanic dome growth has been analysed by Newhall and Melson(1983), Heiken and Wohletz(1987) with regard to history, rate of growth, and petrologic controls of explosions.

Water plays an important role in all explosive activity associated with dome growth and destruction. Estimates of pressures in volcanic explosions(Sparks, 1978; Wilson, 1980; Wilson *et al.*, 1980) indicate that magma containing a few percent of dissolved volatiles can generate pressures of several tens of bars at a stage when the magma foam has the same vesicularity as typical pumice. Dome emplacement is commonly preceded by explosive Plinian and phreatomagmatic eruptions, each with both magmatic and meteoric water as a main volatile component and driving medium(Heiken and Wohletz, 1987). Heiken and Wohletz(1987) proposed four eruptive types of

tephra deposits: (1) Plinian and phreatomagmatic tephra eruptions preceding dome emplacement; (2) Vulcanian tephra related to periodic and continuing dome growth; (3) Pelean and Merapian tephra associated with dome destruction; and (4) phreatic tephra(from explosively active hydrothermal systems).

The pumice-tuff units in the study area were probably deposited during one eruptive event. The basal layer of the units show features typical of proximal deposition by fall-out from a plinian eruption plume(Walker, 1973, 1980; Wright *et al.*, 1980; Fisher and Schmincke, 1984). A fine-grained upper layer mantles topography but thickens in valleys, which is commonly seen in surges(Fisher, 1979; Wohletz and Sheridan, 1979; Wright *et al.*, 1980; Walker and McBroom, 1983; Fisher and Schincke, 1984). The clast morphology also suggests deposition from surge clouds(e.g., Sheridan and Marshall, 1983; Wohletz, 1983). These fine beds are transitional to even finer, cross-bedded layers in distal regions, which show typical sedimentary structures of a surge sequence. Fine proximal deposits are similar to the planar bedded surge facies of Wohletz and Sheridan(1979), which is a lower energy depositional regime. The proximal to distal transition in the deposits may result from cooling of hot, "dry steam" propelled surges with condensation of water in the more distal zones. Water condensation caused the formation of accretionary lapilli and accelerated rates of deposition of fines. These bed form changes result from progressive energy loss and cooling as the surge travels and deflates(Wohletz and Sheridan, 1979).

The unit eruption started with a Plinian eruption column and resulting pumice fall. The column height is related to the thermal flux, which is related to the magma discharge rate(Wilson *et al.*, 1978).

Bimodal size distribution in distal plinian ash deposits are generally related to premature removal of ultra-fines through aggregate formation and settling(e.g., Brazier *et al.*, 1983).

Experiments with particle-laden convective plumes show that entrainment of falling clasts into the column can lead to marginal column collapse during the progress of an eruption(Carey *et al.*, 1988). Gravity-driven flows resulting from marginal column collapse would tend to follow topographic depressions. Dilute, hot clouds that escape from surges elutriate glass shards and loose crystals from the surges, comparable to ignimbrite ash clouds(Sparks *et al.*, 1973; Fisher, 1979; Wohletz and Sheridan, 1979; Wright *et al.*, 1980; Wilson and Walker, 1982; Walker, 1983). Such clouds add crystals to the accumulating plinian fall deposits.

The eruptive regime changed from predominantly fall to surge. This led to emplacement of cross-beds close to the vent, where the surges were too hot

for water condensation; further away steam condensation led to the deposition of fine-grained deposits.

The lithic clasts in the plinian deposits indicate that vent erosion initially occurred predominantly in the upper part of the volcanic edifice. No lithics from deeper zones were found in the fall layer, and it was assumed that the deeper section of the vent kept its original diameter. Reaming of only the upper part of the vent will not lead to as large an increase in magma discharge rate as widening of the whole vent(Wilson *et al.*, 1980). The lack of reversed size grading of the pumice clasts suggests that no major increase in magma discharge rate occurred during the course of the plinian eruption. The switch from a plinian column with fall out to a surge regime is therefore not primarily the result of column collapse due to an increased magma discharge rate as a result of vent-widening during the plinian phase(e.g., Sparks and Wilson, 1976). On the contrary, the relatively small volume of surge beds suggests low magma discharge rates during surge phase.

The different lithic contents of the pumice unit may have resulted from a shift from a vent to a fracture system, whereby magma traversed a sequence of country rocks. Fine-grained surge units probably resulted from extensive water-magma interactions.

Estimates of explosion pressures in volcanic eruptions(Sparks, 1978; Wilson, 1980; Wilson *et al.*, 1980) indicate that magma containing a few percent of dissolved volatiles can generate pressures of several tens of bars at a stage when magma foam has the same vesicularity as typical pumice. Pumice can float for thousands of kilometers(Frick and Kont, 1984). Pumice fall deposits have pumice with a density less than 1.0 g/cm^3(Whitham and Sparks, 1986).

For pumice deposits and the related Gurgurbaba rhyolite-obsidian dome in this research, a Plinian and phreatomagmatic eruptive model is proposed(Figure 7.11). Emplacement of the dome was preceded by a Plinian eruption. Most silicic domes are extruded at the end of an eruption cycle that begins with highly energetic, gas-rich eruptions that produce Plinian pumice deposits and associated pyroclastic flows. If there is ample ground or surface water close to the vent, phreatomagmatic activity can produce fine-grained silicic tephra that are present both as widespread deposits and a proximal tuff ring through which the dome is later extruded. Examples include Plinian pumice deposits in the Medicine Lake Highland(Fink, 1983), Chaos Crags(Heiken and Eichelberger, 1980), and Panum Crater(Sieh, 1983), California. These deposits have small volumes(<0.5 km^3), are associated with fissure eruptions of silicic magma, and are overlain by silicic domes.

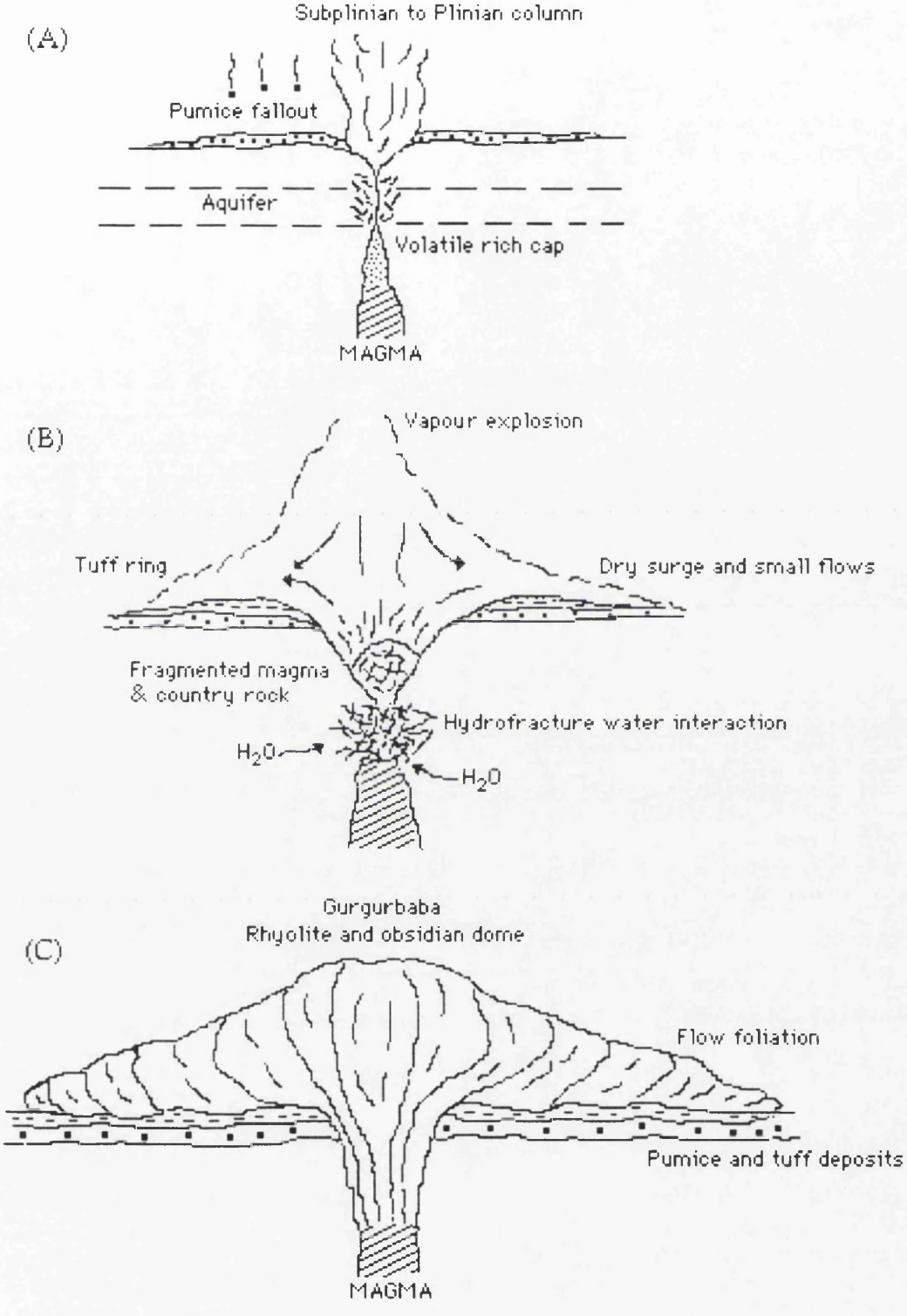

Figure 7.11. Schematic illustration of pumice production preceding the formation of the Gurgurbaba dome with a Plinian stage(A), followed by phreatomagmatic explosions(B), and final stage of dome formation(C).

CHAPTER 8. CONCLUSIONS

A petrographical, geochemical and petrological study of volcanic rocks from the Meydan-Zilan area has revealed a number of conclusions of both local and regional significance for the eastern Anatolian volcanic zone. Thus, future work in the region should be based on the following conclusions.

8.1. GEOLOGY AND STRATIGRAPHY

1) **The volcanism in eastern Anatolia** shows wide variation in space, time and eruptive products. Collision volcanism started in the late Miocene(Innocenti *et al.*, 1976). Eastern Anatolia has thick(50 km) continental crust(Pearce *et al.*, 1990). The minimum proposed age of collision is 12 Ma(Sengor and Kidd, 1979; Sengor and Yilmaz, 1981) and the maximum is late Eocene(Robertson and Aktas, 1984; Michard *et al.*, 1984).

2) **The volcanic activity** in the studied area probably started in post late Burdigalien(Innocenti *et al.*, 1980). The stratigraphy starts with a volcanosedimentary sequence consisting of limestone, sandstone, lava flows, tuff and tuffite. Carbonates of this formation contain shallow marine microfossils giving an age of Burdigalien-Middle Miocene.

8.2. PETROGRAPHY

1) **Carbonates** are biomicrite, biomicrosparite and biosparite with pure carbonate to high terrigenous content. They have undergone differential diagenesis, resulting in new fabrics. There were at least three stages in the formation of carbonates, involving neomorphism, silicification and dolomitization. Volcanic activity also provided material and thermal heat. Sandstones are immature feldspar and lithic greywackes deposited close to a source area with little physical and chemical alteration. Tuffs are crystal to lithic with argillization and silicification. Lavas are hyalorhyolite, basaltic andesite and andesite with common alteration into calcite, sericite, epidote, chlorite and clay.

2) **Andesite** contains sieve textured and calcic overgrown plagioclase phenocrysts, hornblende and biotite with breakdown products, quartz with embayments. Augite+opx and magnetite+ilmenite suggest equilibrium crystallization. Two pyroxenes gave solvi temperatures 1013-1074°C. Fe-Ti oxides gave temperatures 786-834°C and fO_2=1.56-1.98 relative to FMQ.

3) **Trachyandesite** contains plagioclase phenocrysts with sieve texture and thin overgrown rims, quartz with embayments caused by dissolution, hornblende with breakdown products, all of which reflect

disequilibrium conditions interpreted as the result of magma mixing, or basic and acidic magma interaction. Magnetite and ilmenite suggest disequilibrium. Two pyroxenes gave solvi temperature 1015-1089°C.

4) **Dacite** displays a variety of disequilibrium textures. Plagioclase exhibits abrupt shifts to a more calcic composition, and sieve texture with a thin calcic overgrowth. Quartz is rounded and embayed, hornblende or rare biotite is rimmed or replaced by fine-grain opaques and silicates, suggesting a large degree of thermal and chemical disequilibrium induced by magma mixing. Magnetite and ilmenite gave temperatures of 822-828°C and fO_2=1.71-1.76 relative to FMQ. Plagioclase and hornblende gave temperatures of 724-793(±75)°C, and the hornblende barometer yielded 5.08-8.90(±0.5) kbar.

5) **The Aladag lava** has sponge-like plagioclase megacrysts, and Ti-poor augites reflecting crystallization under low and falling oxygen fugacity. Opx and augite may indicate disequilibrium whereas magnetite and ilmenite suggest equilibrium giving a temperature 869-1017°C. Sanidine and sodic plagioclase in equilibrium indicate solvus a temperature of 825-800°C.

6) **Ignimbrites** show moderate to strong welding indicating high temperature emplacement. They contain volcanic, granitoid and rock fragments, representing restite or readjusted restite material, and country rock xenoliths. The rocks contain Ti-rich(5.5-6.7 wt.%) biotites showing Ti+a vacancy substitution and a very high temperature of crystallization. Magnetite and ilmenite indicate equilibrium giving temperatures of 846-921°C and fO_2=1.42-2.29 relative to FMQ. Alkali feldspar and sodic plagioclase in equilibrium indicate 750-900°C. Metamorphic rock assemblages reveal a maximum 6.5 kbar and 725°C.

7) **The Meydan alkaline** association displays evolution from alkali olivine basalt to trachyte. One hawaiite sample contains a gabbroic xenolith with cognate crystals of olivine and plagioclase.

8) In **the alkali olivine basalt**, plagioclase phenocrysts are present with strips and blobs of cpx implying melt reaction. This is interpreted as partial melting solution of plagioclase, and subsequent growth of cpx in the holes. Corroded grains of plagioclase(An_{26-38}) are also found in reaction with the surrounding matrix.

9) In **the hawaiite**, some plagioclase phenocrysts may show sieve texture and corroded rims. Some cpx are enclosed by fine opaque grains, indicating a melt reaction or disequilibrium growth. Rare xenocrysts of quartz occur with rounded shape and surrounded by cpx indicating a reaction rim.

10) **The Mugearite** is highly porphyritic with plagioclase

megacrysts(up to 1 cm) showing oscillatory zoning and containing abundant glass inclusions. Plagioclase megacrysts show complex oscillatory zoning and have abrupt increases or decreases of An%. Zoning profiles of these megacrysts suggest a combination of magma mixing and disequilibrium crystallization.

11) In **the benmoreite**, some anorthoclase phenocrysts exhibit corroded texture and, or reaction rims with opaque grains. Magnetite and ilmenite indicate equilibrium and gave temperatures of 890-1017°C and fO_2= -0.96 and -1.01 relative to FMQ buffer.

12) In **the trachyte**, plagioclase megacrysts with oscillatory and convolute zoning reveal combinations of magma mixing and disequilibrium crystallization. The rock contains kaersutitic amphibole with a resorbed shape and an iron-rich(opaque) rim, indicating a reaction caused by magma mixing. Kaersutite may represent crystallization from magma at moderate depth(15-25 km). Coexisting Ti-poor augite and orthopyroxene may indicate disequilibrium. Magnetite and ilmenite show equilibrium and gave temperatures of 1028-1056°C and fO_2=1.38-1.28 relative to FMQ buffer. Alkali feldspar and sodic plagioclase reveal a solvi temperature of about 825°C whereas calcic plagioclase is below 825°C.

13) In **the Meydan alkaline lavas**, olivine-liquid thermometers yield 1142-1248(±40)°C for the alkali olivine basalt; 1025-1141(±40)°C for the hawaiite; 1037-1085(±40)°C for the mugearite and 913-964(±40) for the benmoreite.

14) **The Zilan lava** contains Ti-poor augite and opx giving a solvus temperature of 1073-1095°C. Sodic plagioclases reveal a solvus temperature between 825-900°C but calcic plagioclase below 825°C. Magnetite and ilmenite show equilibrium, and gave temperatures of 841-869°C and fO_2=0.30-0.54 relative to FMQ, presumably recording subsolidus equilibrium.

15) In **the rhyolite dome and dykes**, sanidine is mantled by plagioclase, indicating magma mixing. Magnetite and ilmenite show equilibrium and yielded temperatures of 841-850°C and fO_2=2.21-2.29 relative to FMQ. These temperatures may record different stages of cooling history. It is possible that Ti-rich magnetite changed composition following magma mixing. Sodic plagioclases in equilibrium with sanidine indicate a solvi temperature of about 750°C whereas calcic plagioclases in disequilibrium show a solvi temperature below 750°C. Sodic plagioclase core and hornblende in a dyke gave 645-655°C. Hornblende-Al content barometer yielded 3.02-3.62 kbar.

16) **Pumices** are highly vesiculated aphyric glass, indicating rapid rise of magma along fissures. Factors, which controlled the pumice

formation, are (a) duration of magma explosion and cycles, (b) temperature and gas content of magma, and (c) cooling duration. On the basis of grain-size distribution analysis, pumice tephra show features of pyroclastic fall and surge, representing products of mainly plinian and rare phreatoplinian type explosions.

17) **The Gurgurbaba lava** varies from hypocrystalline to glassy and perlitic rocks, and also shows variations in vesicularity, colour and flow layering all of which have been attributed to local chemical inhomogeneities, particularly volatile content. In the hypocrystalline type, augite and opx gave solvus temperatures of 1032-1196°C.

8.3. GEOCHEMISTRY

1) In **the carbonates,** Al is largely added in clay minerals. The scatter in SiO_2 content is caused by the presence of detrital quartz and feldspar. The trace elements(except Sr, Ba and S) are assumed to be derived from clay mineral fractions. The Sr content in dolomitic carbonate is indicative of late diagenetic formation for the dolomite.

2) **Sandstones** are quartz-intermediate greywackes with low proportion of material derived from mafic sources, and indicative of Andean-type margins. K/Rb ratios are higher than the average upper continental crust. Ti is mostly in clay minerals. The compositional variation is quite scattered and considered as a mixture of clay, quartz feldspar and carbonate; calcic plagioclase is not major influence on composition. K, Fe, Ti, Rb, Zr and probably Ba, Ni and Zn were added in sheet silicates(mica and clay). Al was added in clay as well as feldspar. Rb and Ba were substantially added in clay, mica and feldspar. Y was added in apatite, zircon and partly in clay and mica. Sandstones reveal low to moderately weathered sources. Trace element patterns indicate a source composed largely of continental arc+active continental margin environments. The rocks gave no clear tectonic discrimination based on major and trace elements because of the Ca-rich nature of the samples. High K/Rb and Th/U ratios are indicative of derivation from acid and intermediate source rocks with some input from basic sources. The rocks show less fractionated LREE and depleted HREE patterns than NASC, representing the source rocks of young components, possibly derived from continental arc material.

3) **Volcanic rocks** are divided into two main groups; alkaline and calcalkaline. Meydan lavas from alkali olivine basalts to trachyte lie along a trend of mildly alkaline differentiation. The Aladag and Zilan lavas(q, hy, di normative) show a transitional character. Kizildere lavas, andesite, trachyandesite, dacite and agglomerate are medium-K calcalkaline.

Ignimbrite, rhyolite dome and dykes, pumice and the Gurgurbaba lava are high-K calcalkaline.

4) In **the Meydan alkaline suite**(alkali olivine basalt, hawaiite, mugearite, benmoreite and trachyte), major and trace element variations suggest presence of a consistent compositional trend with weak iron enrichment and alkali enrichment(especially in evolved rocks). The rocks were produced predominantly by fractional crystallization(±contamination and magma mixing). They came from a common source. Melts proceeded from a common source partial melting with further differentiation by fractional crystallization. The geochemical variation within the suite can be explained by fractional crystallization of the observed phenocryst phases, olivine, augite, plagioclase and magnetite. Fractionation was at first mainly controlled by olivine and then augite and plagioclase. Evolved rocks, benmoreites and trachytes, show deviation from the main fractionation trend suggesting involvement of other magmatic processes(magma mixing±contamination).

The strong enrichment in LREE, Rb, and Ba relative to HREE suggest the mantle source was enriched. MORB and PM-normalized incompatible trace element patterns are characterized by enrichment in all elements. They have also characteristic Nb patterns, negative and progressively increasing similar to continental tholeiites and subduction related magmas, presumably indicating a subduction component in the mantle source. Nb-normalized trace element spidergrams suggest that they were derived from a homogeneous melt and compositional variations are primarily due to differentiation. However, evolved rocks also involved contamination±magma mixing. The lavas define within-plate enrichment style and a subduction component played a minor role in the genesis of lavas.

The suite has moderately fractionated REE patterns. There is no significant Eu anomaly, presumably due to high oxygen fugacity and oxidizing conditions. REE patterns suggest that mugearite, benmoreite and trachyte have gone removal of augite and plagioclase relative to alkali olivine basalt and hawaiite. Accessory phases did not control REE distributions. REE contents of the rocks have been modified by complex processes involving crystal fractionation, contamination±mixing.

The Meydan lavas have Ba/TiO_2 ratios lower than subduction-related lavas, similar to Hawaiian lavas. Compared with intraplate lavas, the rocks exhibit Nb anomaly. Therefore, they were derived from an enriched mantle source, but the enrichment process was not related to the processes which generate convergent margin magmas. Meydan alkalic

magmas were generated in the mantle, possibly within the underlying continental lithospheric mantle at a depth >20 kbar.

5) **Kizildere lavas**(basaltic andesite, andesite and rhyolite are medium-K with little iron enrichment. The lavas display orogenic imprint and are enriched in most incompatible elements compared to typical orogenic lavas. Major and trace element variation can be explained by mainly fractional crystallization from basaltic andesite to andesite and rhyolite. Cpx and magnetite fractionation were important in the evolution of andesitic lavas, involving magma mixing. Hornblende and cpx were early fractionating phases in the evolution of andesites and were followed by plagioclase in rhyolite. MORB- and PM-normalized incompatible element patterns display negative Nb anomalies, and suggest fractionation of plagioclase, magnetite and apatite. They have fractionated REE patterns, suggesting that garnet did not play a significant role as a fractionating or residual phase in their generation. However, cpx and hornblende are the major controlling phases on REE distribution.

6) **Tuffs** show calcalkaline, intermediate-acidic rock characteristics with mainly rhyolitic bulk composition. Plagioclase, Fe-Ti oxides and cpx fractionation were important in the evolution of the bulk rhyolitic magma. They have features similar to volcanic arc rocks in terms of geochemical discrimination of tectonic environment. Thus, they are the product of calcalkaline volcanic activity associated with an active continental margin.

7) **Andesites** are medium-K with little iron enrichment, and are enriched in most incompatible elements relative to typical orogenic lavas. Chemical variation suggests that the lavas developed by fractional crystallization of a parent magma. Fractionation of plagioclase, cpx, magnetite and apatite explains major and trace element variations. Cpx, plagioclase and magnetite fractionation played a minor role. However, the rocks define hornblende±cpx controlled fractionation. Crystal fractionation was not the dominant process, and magma mixing may have taken place in the evolution of rocks. MORB- and PM-normalized incompatible element patterns display negative Nb anomalies. The rocks have fractionated LREE and relatively flat HREE patterns, suggesting that garnet did not play a significant role as a fractionating or residual phase in their generation. However, REE patterns reflect significant hornblende fractionation which has to be a deep-crustal process. The marked enrichments in LREE and LILE can be attributed to dehydration of a subduction component. Thus, the source composition of the andesites is controlled by subducted slab-mantle interactions.

8) **Trachyandesites** have trace element contents similar to the

andesites. Geochemical variations suggest that hornblende, plagioclase, cpx and magnetite fractionation have taken place. Fractionation of plagioclase+cpx±magnetite is less significant. However, hornblende±cpx controlled fractionation and magma mixing were important in the evolution of the rocks. The rocks evolved in lower to mid-crustal magma chambers(P=3-15 kbar). MORB- and PM-normalized incompatible element patterns exhibit LILE enrichment and relatively HFSE depletions with negative Nb anomalies. The rocks have highly fractionated REE patterns with no significant Eu anomalies. The REE patterns reflect the influence of hornblende fractionation.

9) **Dacites** are medium-K, low-Fe, metaluminous, and show hybrid calcalkaline rock features. Fractionation of plagioclase, hornblende, biotite, Fe-Ti oxide and apatite were important in the evolution of the rocks. However, the rocks show hornblende-dominated fractionation. They show compositions close to the minimum melt but do plot in the fields of high temperature liquid compositions. They are more mafic and calcic than liquids generated by fluid-absent melting of biotite. The rocks also show similar trace element compositions to the upper continental crust. They display Na-enrichment, indicating a geochemical signature of slab-derived material. MORB- and PM-normalized incompatible element patterns exhibit enrichment in all elements with negative Nb anomalies. They have highly fractionated REE patterns with no significant Eu anomaly and reflecting significant hornblende fractionation. Flat HREE pattern is not consistent with presence of garnet in the source rock.

10) **Agglomerate** clasts are mainly andesites and rare dacites. Major and trace element variations can be explained by fractionation of cpx, hornblende, plagioclase, magnetite and apatite. They define a hornblende±cpx-dominated fractionation trend in their evolution, similar to the Kizildere andesite lavas. MORB- and PM-normalized incompatible element patterns show LILE enrichment and relative HFSE depletion with negative Nb anomalies. They have moderately fractionated REE patterns with relatively flat HREE and no Eu anomaly. The REE patterns reflect hornblende participation in their generation, and suggest that the primary melt was not in equilibrium with a garnet-bearing residuum.

11) **Ignimbrites** are high-K, lack iron enrichment, and are peraluminous to slightly metaluminous. They are not eruptive equivalents of S-type granites. Major and trace element variation suggest plagioclase, biotite, Fe-Ti oxide and zircon fractionation in their evolution. However, they define a plagioclase-dominated fractionation trend and show some compositional variations from early to late products. MORB- and PM-

normalized incompatible trace element patterns display enrichment in all elements with slightly negative Nb anomalies. The rocks have LREE enriched and relatively flat HREE patterns with negative Eu anomalies, reflecting significant plagioclase fractionation. Generally, they have REE contents close to upper continental crust values.

12) **The rhyolite dome and dykes** are high-K, metaluminous and lack iron enrichment. Geochemical variations can be explained by fractionation of plagioclase, hornblende, Fe-Ti oxide and apatite. The rocks followed fractionation paths similar to the Gurgurbaba lava but hornblende±cpx played an important role in their evolution relative to the Gurgurbaba lava. The rocks plot close to a possible path of fractionation determined at 2 kbar. The rocks are equivalent of I-type granitic rocks, and may represent petrogenetically "hybrid continental groups" derived as a hybrid of mantle and crustal sources. On MORB- and PM-normalized incompatible trace element patterns, they are characterized with LILE element enrichment relative to HFSE and REE with negative Nb anomalies. Trace element contents suggest that the rocks are related to intraplate magmas. The rocks display moderately fractionated REE patterns with strong negative Eu anomalies. The REE patterns reflect significant plagioclase and hornblende fractionation. Generally, REE contents are close to upper continental crust values.

13) In **the pumice deposits**, pumice clasts are rhyolitic whereas lithic clasts are trachybasaltic in composition. Pumice clasts lack iron enrichment but lithic clasts show moderate iron enrichment. Pumice composition defines the end product of the Gurgurbaba lavas with a plagioclase-dominated fractionation in their evolution. Pumice shows significant LILE enrichment relative to HFSE with depletions in some elements, reflecting plagioclase, apatite and Fe-Ti oxide fractionation. However, lithic clasts show moderate enrichment in LILE, relative to HFSE. Pumice and lithic clasts have distinctive incompatible trace element patterns, suggesting that they are not cogenetic. Lithic clasts represent wall-rock fragments. Pumice displays moderately fractionated REE patterns with negative Eu anomalies. REE patterns reflect significant plagioclase and hornblende fractionation, similar to the Gurgurbaba lava. Geochemical data suggest that pumice tephra is cogenetic to the Gurgurbaba lava in the sense that they were derived from the high-level magma chamber, and shared a common parent with the Gurgurbaba lava. The data also implies the presence of compositional and thermal gradients between pumice and the Gurgurbaba lava, and a constant rate of magma removal from the magma chamber.

14) **The Gurgurbaba lavas** are high-K, lack iron enrichment and are metaluminous to slightly peraluminous. Chemical variation suggests shallow level fractionation of plagioclase, alkali feldspar, biotite, hornblende, Fe-Ti oxide and apatite. However, the rocks define plagioclase controlled fractionation in their evolution. They are eruptive equivalents of I-type granitic rocks(leucogranites) and comparable with melt-dominated granitic rocks, and may represent hybrid continental groups. On an element enrichment factor diagram, they display similar enrichment in magnitude and direction to that of the Bishop Tuff. Incompatible element ratios suggest that the rocks are related to intraplate magmas. They have fractionated REE patterns with slightly negative Eu anomalies. The REE contents are comparable with upper continental crust values.

15) **The Aladag lava** is trachytic and transitional in composition. Major and trace element variations indicate fractionation of cpx, anorthoclase, plagioclase, and small amounts of Fe-Ti oxide, apatite and zircon in the evolution of the rock. Two feldspar occurrence in the rock is suggestive of near water-saturated conditions. The rock shows enrichment in LILE and LREE elements, highlighting source enrichment. The rock also displays a weak negative Nb anomaly. REE patterns are moderately fractionated with relatively flat HREE patterns and negative Eu anomalies. The REE pattern is similar to trachyte of the Meydan lavas, suggesting genetic relationship between two lavas.

16) **The Zilan lava** is trachytic and transitional in composition with no iron enrichment. Major and trace element variations can be explained by fractionation of plagioclase, cpx, Fe-Ti oxide and apatite. There is a lack of zircon and anorthoclase fractionation. Incompatible trace element patterns display slightly negative Nb anomalies. The rock shows moderately fractionated REE patterns with LREE enriched and relatively flat HREE patterns.

8.4. O- AND Sr-ISOTOPE GEOCHEMISTRY

1) **Oxygen and Sr-isotopic results** range +7‰ to +9‰, and 0.7048 to 0.7063 respectively in the volcanic rocks studied. Alkali olivine basalts and hawaiite have plagioclase $\delta^{18}O$ about +7‰, comparable with mantle derived magmas. An estimate of +5.6‰ $\delta^{18}O$ may represent the original $\delta^{18}O$ of the Meydan magma. Secondary alteration has not raised the $\delta^{18}O$ values. However, post-eruptive hydration of pumice may have induced a change in the $\delta^{18}O$ values. $\delta^{18}O$ values in the Meydan suite vary much more than expected for closed system fractional crystallization, suggesting the involvement of ^{18}O-rich continental crust in the petrogenesis of the

rocks. In the calcalkaline suite, variable degrees of crustal assimilation or variable $\delta^{18}O$ values of assimilated material seemingly produced the $\delta^{18}O$ variation.

2) **O-isotope versus element plots** are quite scattered for the calcalkaline suite. The trends of data in the Meydan suite are explained by contamination with ^{18}O-rich crust during infracrustal differentiation, and the degree of contamination is large for evolved rocks. Generally, alkaline and calcalkaline suites have similar Sr-isotope ratios suggesting that both may have originated from similar sources and, or by similar processes. Sr-isotope ratio versus element plots are quite scattered. In the Meydan suite, the relatively high $^{87}Sr/^{86}Sr$ ratio of the basic magma suggests that it may have already gone interaction with crust prior to its emplacement into a magma chamber before eruption, possibly in the lower crust by a MASH process. In the Meydan suite, $^{87}Sr/^{86}Sr$ values are closer to those characterizing an "enriched" mantle. High level crustal contamination has not been a dominant process. In the Meydan suite, the element-isotope correlation implies that fractionation proceeded with assimilation of crustal rocks in the evolved rocks. In the calcalkaline suite, data are not consistent with an AFC process. Therefore, crustal contamination during magma ascent is not a process by which to generate the isotopic variations in the calcalkaline suite. However, minor amounts of contamination have occurred in the differentiated rocks.

3) **The pattern of Sr and O isotopic variation** in Meydan suite is similar to rocks derived from a contaminated mantle source region. Sr-isotope compositions of partial melts are dominated by composition of the contaminant, whereas the O-isotope composition of the melt is controlled by composition of the mantle source. The two stage process of (a) source contamination controlled by the extent of hydrous flux from the subducted slab which gives rise to a large range of Sr-isotopes followed by (b) crustal contamination and fractional crystallization.

8.5. PETROGENESIS

1) In **the Meydan alkaline suite**, partial melting played an important role in the evolution of the alkali olivine basalt and hawaiite, whereas the evolved rocks(mugearite, benmoreite and trachyte) are controlled mainly by fractional crystallization. Mugearite, benmoreite and trachyte magmas were modified by open-system fractionation and replenishment with increasing fractional crystallization involving contamination±magma mixing as result of a long residence period in a magma chamber. Crystal fractionation was the main factor controlling the

chemical variations in bulk magma composition. Hawaiite has been derived from alkali olivine basalt parent by fractionation of a cpx-dominated assemblage at high pressures. Olivine and titanomagnetite fractionation is also evident. Plagioclase and apatite fractionation were significant in the evolution of benmoreite and trachyte. Generally, the lavas were not affected dominantly by crustal contamination. Mugearite and trachyte evolved in a crustal magma chamber, involving magma mixing. However, alkali olivine basalt and hawaiite did not evolve in open-system crustal magma chambers.

2) In the Meydan alkaline suite, **the degree of partial melting** calculated for the near primary basalt samples is between 4% and 12%. Generally, basaltic rocks represent fractionated liquids derived from an enriched upper mantle source. Thus, the basaltic rocks of the Meydan suite are interpreted as large degree melts of an isotopically enriched mantle source. The mantle source was enriched in LILE, LREE and radiogenic $^{87}Sr/^{86}Sr$. Benmoreite and trachyte fall along a low pressure cotectic whereas alkali olivine basalt, hawaiite and mugearite plot between 8-10 kbar and 1 kbar cotectics. The parental magma may have undergone medium to high pressure fractionation of olivine, augite and plagioclase, which was later followed by low pressure olivine, augite and plagioclase fractionation.

3) In the Meydan alkaline suite, **incompatible trace elements,** major elements and isotopes support a model where the chemical variability of the rocks is controlled by open-system fractionation and crustal contamination±magma mixing. The initial magma was derived from a source enriched in Rb and REE. The enrichments in Ba and depletions in Nb are most likely the result of fluid metasomatism of mantle. Furthermore, the chemical characteristics are similar to melts produced in source regions that comprise a mix of enriched mantle and recycled components. Finally, the chemical and isotopic variation of the suite may reflect derivation from a variably enriched subcontinental lithospheric mantle. If mantle metasomatism is largely a product of the fluids or melts that are released from the subducted slab, any later melts are likely to be characterized by high LILE/HFSE ratios, possibly as result of HFSE-rich residual phases being left in the slab during melting.

4) **The medium-K suite rocks**(andesite, trachyandesite and dacite) are cogenetic and related to each other by fractional crystallization and assimilation±mixing during the evolution of crustal magma chambers. The compositional continuity and range of variation in the suite are consistent with fractional crystallization as the origin of the calcalkaline trend. The suite defines a opx-cpx cotectic that parallels the 1 bar line but is shifted towards the quartz corner. Liquids derived under conditions of moderate

pressure and water saturation in the mid- to upper crustal levels evolved to andesites. Assimilation of the lower crust was significant in the compositional range from parental magma to andesite. Production of dacites occured in the shallow crust and at high water contents. Transition from the parent magma to the andesites may have occurred at relatively deep crustal levels. Geochemical variations from andesite to trachyandesite reflect fractional crystallization and contamination±mixing occurring within the mid- to lower crust. However, variations from trachyandesite to dacite result from upper crustal processes involving assimilation of a shallow crustal contaminant that is relatively enriched in alkali elements.

5) In **the medium-K suite rocks**, crustal differentiation controls their eruptive compositions but the extent of assimilation is limited. Contamination involves incorporation of partial melts of wall rock, producing selective enrichments in certain incompatible elements. The mineralogical and petrochemical disequilibrium characteristics are due to involvement of assimilation±mixing which is also supported by mass-balance mixing calculations with large variations in the incompatible elements.

6) **The geochemical features** in the medium-K suite suggest that the magmas were open-system in the evolution of trachyandesite and dacite. Trace element and isotopic data indicate that contamination with lower crustal matter occured during the evolution of primary magma to andesite; the lower crustal contribution to the magma was probably a partial melt of a subducted slab-derived material. Trachyandesite and dacite formed by low pressure fractional crystallization and mixing. Upper crustal contaminants caused significant enrichments of Rb and Th in the evolved magmas. The parental magma for the suite may have resulted from fluxing of the mantle by slab-derived fluids, and the composition of this parental magma has been subsequently affected by crustal processes.

7) **The high-K suite rocks**(ignimbrite, rhyolite dome and dykes, pumice and the Gurgurbaba lava) involve fractional crystallization, magma mixing, crustal melting, and the complexing of volatiles and incompatible elements during magmatic degassing. The geochemical data points to an origin of the rocks by fractional crystallization of a hybrid magma(mantle and crustal components). The rocks are non-minimum melts. Differentiation of liquids involve biotite, hornblende, plagioclase±K-feldspar, and Fe-Ti oxide.

8) The differences in trace elements between **pumice and the Gurgurbaba lava** indicate that large changes in liquid compositions occurred in the crystallized parts of magma chamber. Most of the magmas were

compositionaly stratified. The magma chamber had a capping layer of crystal-poor rhyolitic magma overlying relatively crystal-rich liquids.

9) **Pumice** does not exhibit the features of mixed mafic and evolved magmas. Sudden fluctuations in the volatile and chemical budget during explosive eruptions have promoted brief periods of rapid crystallization along the magma chamber walls.

10) **The geochemical features** in the high-K suite suggest the importance of crustal rocks in the primary magma source. The rocks were not generated by bulk melting of crust but may represent melts of local sialic crust. The parental magmas of the suite may have been derived as partial melts of intermediate to transitional, high-K calcalkaline, meta-igneous rocks in the continental crust. Furthermore, these source materials could have been derived from enriched subcontinental lithospheric mantle.

11) **Pumice tephra** were probably deposited during one eruptive event. The eruption regime changed from predominantly pyroclastic fall to surge. There was no major increase in magma discharge rate during the eruption. A plinian and phreatomagmatic eruptive model is proposed for pumice deposits and the Gurgurbaba rhyolite dome; (a) a plinian stage, (b) followed by phreatomagmatic explosions, and (c) dome formation.

REFERENCES

Abrecht, J. & Hewitt, D.A. 1988. Experimental evidence on the substitution of Ti in biotite. *Am. Min. 73, 1275-1284.*

Agrali, B. 1966. Ercis-Zilan bolgesinin jeolojisi ve linyit imkanlari. *M.T.A. Rap. No, 3766.*

Aktimur, S. 1986. Van-Ercis yoresinin landsat-4 TM goruntuleri yardimiyla jeoloji ve tektonik yapisinin incelenmesi. *M.T.A. Rap. No, 8086.*

Allan, J.F. & Carmichael, I.S.E. 1984. Lamprophyric lavas in the Colima graben, SW Mexico. *Cont. Min. Petrol. , 88, 203-216.*

Allegre, C.J., Dupre, B., Lambert, B. & Richard, P. 1981. The sub-continental versus sub-oceanic debate. I: Lead-neodymium-strontium isotopes in primitive alkali basalts from a shield area: the Ahaggar volcanic suite. *Earth Planet. Sci. Lett., 52, 85-92.*

Allegre, C.J. & Minster, J.F. 1978. Quantitative models of trace element behaviour in magmatic processes. *Earth Planet. Sci. Lett., 38, 1-25.*

Allegre, G.J., Treuile, M., Minster, J.F., Minster, B. & Albarede, F. 1977. Systematic use of trace element in igneous process part I: Fractional crystallization process in volcanic suites. *Cont. Min. Petrol., 60, 57-75.*

Allen, J.C., Boettcher, A.L. & Marland, G. 1975. Amphiboles in andesite and basalt: I. Stability as a function of P-T-fO_2. *Am. Min. ,60, 1069-1085.*

Allen, J.G. & Boettcher, A.L. 1978. Amphiboles in andesites and basalt: II. Stability as a function of P-T-fH_2O-fO_2. *Am. Min. , 63, 1047-1087.*

Altinli, I.E. 1966. Dogu ve Guneydogu Anadolu'nun Jeolojisi. *M.T.A. Dergisi, 66.*

Ambraseys, N.N. 1970. Some characteristic features of the North Anatolian Fault Zone. *Tectonophysics, 9, 143-165.*

Anderson, A.T., Clayton, R.N. & Mayeda, T.K. 1971. Oxygen isotope thermometry of mafic igneous rocks. *J. Geol., 79, 715-729.*

Anderson, A.T.J. 1976. Magma mixing: Petrologic process and volcanological tool. *J.Volcanol. Geotherm. Res., 1, 3-33.*

Anderson, A.T.J. 1984. Probable relations between plagioclase zoning and magma dynamics, Fuego Volcano, Guatemala. *Am. Min., 69, 660-676.*

Anderson, D.J. & Lindsley, D.H. 1985. New(and final) models for the Ti-rich magnetite/ilmenite geothermometer and oxygen barometer. *Trans. Am. Geophys. Un.(EOS), 66, 416.*

Arculus, R.J. 1976. Geology and geochemistry of the alkali basalt-andesite association of Grenada, Lesser Antilles island arc. *Geol. Soc. Am. Bull., 87, 612-624.*

Arculus, R.J. 1987. The significance of source versus process in the tectonic controls of magma genesis. *J. Volcanol. Geotherm. Res., 32, 1-12.*

Arculus, R.J. & Johnson, R.W. 1981. Island-arc magma sources: A geochemical assessment of the roles of slab-derived components and crustal contamination. *Geochem. Journal,15, 109-133.*

Arculus, R.J. & Powell, R. 1986. Source component mixing in the regions of arc magma generation. *J. Geophys. Res., 91, 5913-5926.*

Arth, J.G. 1976. Behaviour of trace elements during magmatic processes-a summary of theoretical models and their application.*U.S. Geol. Surv. J. Res. ,4, 41-48.*

Artyuskhov, E.V. 1973. Stress in the lithosphere caused by crustal thickness inhomogeneities. *J. Geophys. Res., 78, 7675-7708.*

Artyuskhov, E.V. 1981. Mechanism of continental riftogenesis. *Tectonophysics,73, 9-14.*

Atlas, L. 1952. The polymorphism of $MgSiO_3$ and solid state equilibria in the system $MgSiO_3$-$CaMgSi_2O_6$. *J. Geol., 60, 125-147.*

Bacon, C.R. 1986. Magmatic inclusions in silicic and intermediate volcanic rocks. *J. Geophys. Res., 91, 6091-6112.*

Bacon, C.R. & Hirschmann, M.M. 1988. Mg/Mn partitioning as a test for equilibrium between coexisting Fe-Ti oxides. *Am. Min., 73, 57-61.*

Baker, B.H., Goles, G.G., Leeman, W.P. & Lindstrom, M.M. 1977. Geochemistry and petrogenesis of a basalt-benmoreite-trachyte suite from the southern part of the Gregory rift, Kenya. *Cont. Min. Petrol., 64, 303-332.*

Baker, D.R. & Eggler, D.H. 1983. Fractionation paths of Atka(Aleutians) high-alumina basalts: constraints from phase relations. *J. Volcanol. Geotherm. Res.,18, 387-404.*

Baker, P.L. 1982. Evolution and classification of orogenic volcanic rocks. *In:* Thorpe, R.S. (eds) *Andesites: Orogenic Andesites and Related Rocks. John Wiley, 11-23.*

Barbarin, B. 1990. Plagioclase xenocrysts and mafic magmatic enclaves in some granitoids of Sierra Nevada Batholith, California. *J. Geophys. Res., 95, 17747-17756.*

Barberi, F., Bizouard, H. & Varet, J. 1971. Nature of the clinopyroxene and iron enrichment in alkalic and transitional basaltic magmas. *Cont. Min. Petrol., 33, 93-107.*

Barberi, F., Ferrara, G., Santacroce, R., Treuil, M. & Varet, J. 1975. A transitional basalt-pantellerite sequence of fractional crystallization the Boina Centre(Afar Rift, Ethiopia). *J. Petrol., 16, 22-56.*

Barker, F., Arth, J.G. & Hudson, T. 1981. Tonalites in crustal evolution. *Phil. Trans. R. Soc. London, A301, 293-303.*

Bas, H. 1979. Petrologische und geochemische untersuchungen an subrezenten volcaniten der nordanatolischen storungszone(Abschnitt: Erzincan-Niksar), Turkei. *Ph.D thesis, Hamburg University, 116p.*

Bas, H. 1981. Erzincan ve Resadiye-Niksar yorelerindeki genc volkanitlerin jeokimyasi ve petrolojisi. *Turkiye Jeol. Kur. 35.Bilimsel ve Teknik Kurultayi Bildiri Ozetleri Kitabi, 27.*

Basaltic Volcanism Study Project. 1981. *Basaltic Volcanism on The Terrestrial Planets. Pergamon Press, New York, 1286p.*

Benard, F., Moutou, P. & Pichavant, M. 1985. Phase relations of tourmaline leucogranites and the significance of tourmaline in silicic magmas. *J. Geol., 93, 271-291.*

Berling, R. & Henderson, C.M.B. 1969. The distribution of Sr and Ba between the alkali feldspar, plagioclase and groundmass phases of porphyritic trachytes and phonolites. *Geochim. Cosmochim. Acta, 33, 247-255.*

Bhatia, M.R. 1983. Plate tectonics and geochemical composition of sandstones. *J. Geol., 91, 611-627.*

Bhatia, M.R. 1985. Composition and classification of Palaeozoic flysch mud rocks of eastern Australia: implications in provenance and tectonic setting interpretation. *Sed. Geol., 41, 249-268.*

Bhatia, M.R. & Crook, K.A.W. 1986. Trace element characteristics of greywackes and tectonic setting discrimination of sedimentary basins. *Cont. Min. Petrol., 92, 181-193.*

Bhatia, M.R. & Taylor, S.R. 1981. Trace element geochemistry and sedimentary provinces: a study from the Tasman geosynclines, Australia. *Chem. Geol., 33, 115-125.*

Blake, S. 1981. Eruptions from zoned magma chambers. *J. Geol. Soc. London, 138, 281-287.*

Blake, S. 1984. Volatile oversaturation during the evolution of silicic magma chambers as an eruption trigger. *J. Geophys. Res., 89, 8237-8244.*

Blake, S. & Ivey, G.N. 1986. The dynamics of magma mixing during flow in volcanic conduits. *Cont. Min. Petrol., 94, 72-81.*

Blake, S., Wilson, C.J.N., Smith, I.E.M. & Walker, G.P.L. 1992. Petrology and dynamics of the Waimihia mixed magma eruption, Taupo Volcano, New Zealand. *J. Geol. Soc. London, 149, 193-207.*

Blatt, H., Middleton, G. & Murray, K. 1980. *Origin of Sedimentary Rocks. Prentice-Hall, New Jersey, 634p.*

Blumenthal, B. 1958. Der volcan Ararat und die Berge Seiner sedimentumrandung. *Istanbul Univ. Fen Fak. Mecm., B23, 3-4.*

Blundy, J.D. & Holland, J.B. 1990. Calcic amphibole equilibria and a new amphibole-plagioclase geothermometer. *Contr. Min. Petrol., 104, 208-224.*

Blundy, J.D. & Shimizu, N. 1991. Trace element evidence for plagioclase recycling in calc-alkaline magmas. *Earth Planet. Sci. Lett., 102, 178-197.*

Bohlen, S.R., Peacor, D.R. & Essene, E.J. 1980. Crystal chemistry of a metamorphic biotite and its significance in water barometry. *Am. Min., 31, 275-299.*

Boyd, F.R. & England, J.L. 1965. The rhombic enstatite-clinoenstatite inversion. *Carnegie Inst. Washington, Ann. Rept. Dir. Geophys. Lab.,1964-65, 117-120.*

Boynton, W.W. 1984. Cosmochemistry of the rare earth elements. *In:* Henderson, P. (eds) *Rare Earth Geochemistry. Elseiver, Amsterdam, 63-107.*

Brandeis, G. & Jaupart, C. 1986. On the interaction between convection and crystallization in cooling magma chambers. *Earth Planet. Sci. Lett., 77, 354-361.*

Brandon, A.D. & Goles, G.G. 1988. A Miocene subcontinental plume in the Pacific Northwest: geochemical evidence. *Earth Planet. Sci. Lett., 88, 3-4, 273-283.*

Brazier, S., Sparks, R.S.J., Carey, S.N., Sigurdsson, H. & Westgate, J.A. 1983. Bimodal grain size distribution and secondary thickening in air-fall ash layers. *Nature, 301, 115-119.*

Brigatti, M.F., Galli, E. & Poppi, L. 1991. Effect of Ti substitution in biotite-1M crystal chemistry. *Am. Min., 76, 1174-1183.*

Brigatti, M.F. & Gregnanin, A. 1987. Crystal chemistry of igneous rock biotites. *Min. Petrol., 37, 323-341.*

Brinkmann, R. 1976. *Geology of Turkey. Ferdinand Enke. Stuttgart, 158p.*

Brique, L. & Lancelot, J.R. 1979. Rb-Sr systematics and crustal contamination models for calc-alkaline igneous rocks. *Earth Planet. Sci. Lett., 43, 385-396.*

Briqueu, L., Bougault, H. & Joron, J.L. 1984. Quantification of Nb, Ta, Ti, and V anomalies in magmas associated with subduction zones: petrogenetic implications. *Earth Planet. Sci. Lett., 68, 279-308.*

Brown, G.M. 1967. Mineralogy of basaltic rocks. *In:* Hess, H.H. & Poldervaart, A. (eds) *Mineralogy of Basaltic Rocks. I, Basalts. Interscience, New York, 103-162.*

Bryan, W.B., Finger, L.W. & Chayes, F. 1969. Estimating proportions in petrographic mixing equations by least squares approximation. *Science, 163, 926-927.*

Burnham, C.W. & Jahns, R.H. 1962. A method for determining the solubility of water in silicate melts. *Am. J. Sci., 260, 721-745.*

Burton, B.P. 1984. Thermodynamic analysis of the system Fe_2O_3-$FeTiO_3$. *Phys. Chem. Minerals., 11, 132-139.*

Cabanis, B. & Lecolle, M. 1989. Le diagramme La/10, Y/15, Nb/8: un outil pour la discrimination des series volcaniques et la mise en evidence des procussus de melanges et/ou de contamination crustale. *C.R. Acad. Sci. Paris, 309, 2023-2029.*

Cantagrel, J.M., Didier, J. & Gourgaud, A. 1984. Magma mixing, origin of intermediate rocks and 'enclaves' from volcanism to plutonism. *Phys. Earth Planet. Inter., 35, 65-76.*

Carey, S.N., Sigurdsson, H. & Sparks, R.S.J. 1988. Experimental studies of particle-laden plumes. *J. Geophys. Res., 93, 15314-15328.*

Carlson, R.W., Lugmair, G.W. & MacDougall, J.D. 1981. Columbia River volcanism: the question of mantle heterogeneity or crustal contamination. *Geochim. Cosmochim. Acta, 45, 2483-2499.*

Carmichael, I.S.E. & Nicholls, J. 1967. Iron-titanium oxides and oxygen fugacities in volcanic rocks. *Geophys. J. R. Astr. Soc., 72, 4665-4687.*

Carmichael, I.S.E., Turner, F.J. & Verhoogen, J. 1974. *Igneous Petrology. Mc Graw-Hill, New York, 739p.*

Carpenter, M.A. 1980. Composition and cation order variations in a sector-zoned blueschist pyroxene. *Am. Min., 65, 313-320.*

Cas, R.A.F. & Wright, J.V. 1987. *Volcanic Successions, Modern and Ancient. Allen and Unwin, London, 528p.*

Cerling, T.E., Brown, F.H. & Bowman, J.R. 1985. Low temperature alteration of volcanic glass: hydration, Na, K, ^{18}O and Ar mobility. *Chem. Geol., 52, 281-293.*

Chappell, B.W. 1978. Granitoids of the Moonbi district, New England Batholith, eastern Australia. *J. Geol. Soc. Aust., 25, 267-284.*

Chappell, B.W. & White, A.J.R. 1974. Two contrasting granite types. *Pacific. Geol., 8, 173-174.*

Chappell, B.W. & White, A.J.R. 1992. I- and S-type granites in the Lachlan Fold Belt. *Trans. Roy. Soc. Edinburg Earth Sci.,83, 1-26.*

Chatterjee, N.D. & Johannes, W. 1974. Thermal stability and standard thermodynamic properties of synthetic $2M_1$-Muscovite, $KAl_2[AlSi_3O_{10}(OH)_2]$. *Cont. Min. Petrol., 48, 89-114.*

Chauwel, C. & Jahn, B.M. 1984. Nd-Sr isotope and REE geochemistry of alkali basalts from the Massif Central, France. *Geochim. Cosmochim. Acta., 48, 93-110.*

Chawthorn, R.G. & O'Hara, M.J. 1976. Amphibole fractionation in calcalkaline magma genesis. *Am. J. Sci., 276, 309-329.*

Christiansen, E.H., Bikun, J.V., Sheridan, M.F. & Burt, D.M. 1984. Geological evolution of topaz rhyolites from the Thomas Range and Spor Mountain, Utah. *Am. Min., 69, 223-236.*

Christiansen, E.H., Burt, D.M., Sheridan, M.F. & Wilson, R.T. 1983. Petrogenesis of topaz rhyolites from the western United States. *Cont. Min. Petrol., 83, 16-30.*

Christiansen, E.H., Sheridan, M.F. & Burt, D.M. 1986. The geology and geochemistry of Cenozoic topaz rhyolites from the western United States. *Geol. Soc. Am. Spec. Paper, 205, 82p.*

Clague, D.A. & Frey, F.A. 1982. Petrology and trace element geochemistry of the Honolulu volcanic series Oahu: Implications for the oceanic mantle below Hawaii. *J. Petrol., 23, 447-504.*

Clarke, D.B. 1992. *Granitoid Rocks. Chapman&Hall, London, 280p.*

Clayton, R.N. & Mayeda, T.K. 1963. The use of bromine pentafluoride in the extraction of oxygen from oxides and silicates for isotopic analysis. *Geochim. Cosmochim. Acta, 27, 43-53.*

Clemens, J.D. 1990. The granulite-granite connexion. *In:* Vielzeuf, D. & Vidal, P. (eds) *Granulites and Crustal Evolution. Kluwer, Dordrecht, Netherlands, 25-36.*

Clemens, J.D. & Vielzuf, D. 1987. Constraints on melting and magma production in the crust. *Earth Planet. Sci. Lett., 86, 287-306.*

Clemens, J.D. & Wall, V.J. 1981. Crystallization and origin of some peraluminous(S-type) granitic magmas. *Can. Min. ,19, 111-132.*

Clemens, J.D. & Wall, V.J. 1984. Origin and evolution of a peraluminous silicic ignimbrite suite: the Vilolent Town Volcanics. *Cont. Min. Petrol., 88, 354-371.*

Conrad, W.K., Nicholls, I.A. & Wall, V.J. 1988. Water-saturated and undersaturated melting of metaluminous and peraluminous crustal compositions at 10 kb: evidence for the origin of silicic magmas in Taupo Volcanic Zone, New Zealand, and other occurrence. *J. Petrol., 29, 765-803.*

Coolley, S., Thompson, J., Wilson, T.R.S. & Higgs, N.C. 1984. Post-depositional migration of elements during diagenesis in brown clay and turbidite sequences in the northeast Atlantic. *Geochim. Cosmochim. Acta, 48, 1223-1236.*

Coombs, D.S. & Wilkinson, J.F.G. 1969. Lineages and fractionation trends in undersaturated volcanic rocks from the East Otago Volcanic Province(New Zealand) and related rocks. *J. Petrol., 10, 440-501.*

Cox, K.G., Bell, J.D. & Pankhurst, R.J. 1979. *The Interpretation of Igneous Rocks. George Allen and Unwin, London, 450p.*

Cox, K.G. & Hawkesworth, C.J. 1985. Chemical stratigraphy of the Deccan traps at Mahabaleshwar, Western Ghats, India, with implications for open system magmatic processes. *J. Petrol., 26, 355-377.*

Craig, H. 1961a. Standard for reporting concentrations of deuterium and oxygen-18 in natural waters. *Science, 133, 1833-1934.*

Crook, K.A.W. 1974. Lithogenesis and geotectonics: the significance of compositional variation in flysch arenite(greywackes). *Soc. Eco. Paleo. Min. Spec. Publ., 19, 304-310.*

Cullers, R.L. & Graf, J.H. 1984. Rare earth elements in igneous rocks of the continental crust: predominantly basic and ultrabasic rocks. *In:* Henderson, P. (eds) *Rare Earth Element Geochemistry. Elsevier, Amsterdam, 237-274.*

Cundari, A. 1979. Petrogenesis of leucite-bearing lavas in the Roman volcanic region, Italy. The Sabatini lavas. *Cont. Min. Petrol., 70, 9-21.*

Cuney, M., Autran, A., Burnal, L., Brouand, M., Dudoignon, P., Feybesse, J.L., Gagny, C., Jacquot, T., Kosakevitch, A., Martin, P., Meunier, A., Monier, G. & Tegyey, M. 1986. Resultants preliminaires apportes parle sondage GPF sur la coupole de granite albitique a topaze-lepidolite de Beauvoir(Massif Central, France). *C.R. Acad. Sci. Fr., 303, 569-574.*

Curtis, C.D. 1964. Application of the crystal field theory to the inclusions of trace-transition elements in minerals during magmatic differentiation. *Geochim. Cosmochim. Acta, 28, 389-403.*

Dallmeyer, R.D. 1974. The role of crystal structure in controlling the partitioning of Mg and Fe^{2+} between coexisting garnet and biotite. *Am. Min., 59, 201-203.*

Davidson, J.P. 1986. Isotopic and trace element constraints on the petrogenesis of subduction related lavas from Martinique, Lesser Antilles. *J. Geophys. Res.,91, 5943-4962.*

Davidson, J.P. & Harmon, R.S. 1989. Source enrichment and crustal contamination of volcanic rocks from Martinique, Lesser Antilles: the oxygen isotope perspective. *Earth Planet. Sci. Lett., 95, 255-270.*

Dawson, J.B. 1967. Geochemistry and origin of kimberlites. *In:* Wyllie, P.J. (eds) *Ultramafic and Related Rocks. 269-278.*

De Pieri, R., Gregnanin, A. & Piccirillo, E.M. 1978. Trachyte and rhyolite biotites in the Euganean Hills(North-Eastern Italy). *N. Jahrbuch. Min. Ab., 148, 55-82.*

De Silva, S.L. 1991. Styles of zoning in Central Andean ignimbrites; Insights into magma chamber processes. *In:* Harmon, R.S. & Rapela, C.W. (eds) *Andean Magmatism and Its Tectonic Setting. Geol. Soc. Am. Spec. Paper, 265, 217-232.*

De Silva, S.L. & Francis, P.W. 1989. Correlation of large ignimbrites-two case studies from the Central Andes of northern Chile. *J. Volcanol. Geotherm. Res., 37, 133-149.*

Deer, W.A., Howie, R.A. & Zussman, J. 1962a. *Rock-Forming Minerals. Sheet Silicates, 3, Longman, London, 270p.*

Deer, W.A., Howie, R.A. & Zussman, J. 1978. *Rock-Forming Minerals. Single-Chain Silicates, 2A, Longman, London, 668p.*

Deer, W.A., Howie, R.A. & Zussman, J. 1982. *Rock-Forming Minerals. Orthosilicates, Volume 1A, Longman, London, 919p.*

Deer, W.A., Howie, R.A. & Zussman, J. 1992. *An Introduction to the Rock-Forming Minerals. Longman, London, 696p.*

Defant, M.J. & Drummond, M.S. 1990. Derivation of some modern arc magmas by melting of young subducted lithosphere. *Nature, 347, 662-665.*

Defant, M.J. & Drummond, M.S. 1993. Mount St. Helens: Potential example of the partial melting of the subducted lithosphere in a volcanic arc. *Geology, 21, 547-550.*

Defant, M.J. & Nielsen, R.L. 1990. Interpretation of open-system petrogenetic processes: Phase equilibria constraints on magma evolution. *Geochim. Cosmochim. Acta, 54, 87-102.*

DePaolo, D.J. 1981. Trace element and isotopic effects of combined wallrock assimilation and fractional crystallization. *Earth Planet. Sci. Lett , 53, 189-202.*

DePaolo, D.J. 1983. Comment on Columbia river volcanism: the question of mantle heterogeneity or crustal contamination. *Geochim. Cosmochim. Acta, 47, 841-844.*

DePaolo, D.J. & Wasserburg, G.J. 1979a. Petrogenetic mixing models and Nd-Sr isotopic patterns. *Geochim. Cosmochim. Acta, 43, 615-627.*

DePaolo, D.J. & Wasserburg, G.J. 1979b. Neodymium isotopes in flood basalts from Siberian Platform and inferences about their mantle source. *Proc. Nat. Acad. Sci. USA, 76, 3056-3060.*

Dewey, J.F. 1984. Extensional collapse of orogens. *Tectonics, 7, 1123-1139.*

Dewey, J.F., Hempton, M.R., Kidd, W.S.F., Saroglu, F. & Sengor, A.M.C. 1986. Shortening of continental lithosphere: the neotectonics of Eastern Anatolia - a young collision zone. *In:* Coward, M.P. & Ries, A.C. (eds) *Collision Tectonics. Geol. Soc. London Spec. Publ.,19, 3-36.*

Dobson, P.F. & O'Neil, J.R. 1987. Stable isotope compositions and water contents of boninite series volcanic rocks from Chichi-Jima, Bonin Islands, Japan. *Earth Planet. Sci. Lett., 82, 75-86.*

Dodson, M.H. 1978. A linear method for second-degree interpolation in cyclical data collection. *J. Phys. Earth Sci. Inst., 11, 296.*

Donaldson, C.H. & Henderson, C.M.B. 1988. A new interpretation of round embayments in quartz crystals. *Min. Mag., 52, 27-33.*

Dosso, L. & Murthy, V.R. 1980. A Nd isotope study of the Kerguelen islands: inferences on enriched oceanic mantle sources. *Earth Planet. Sci. Lett.*, 48, 268-276.

Dostal, J., Dupuy, C., Carron, J.P., Le Guen de Kerneizon, M. & Maury, R.C. 1983. Partition coefficients of trace elements: application to volcanic rocks of St. Vincent, West Indies. *Geochim. Cosmochim. Acta, 47, 525-533.*

Dostal, J., Zentilli, M., Caeles, J.C. & Clark, A.H. 1977. Geochemistry and origin of volcanic rocks of the Andes(26-28°S). *Cont. Min. Petrol., 63, 113-128.*

Dowty, E. 1976. Crystal structure and crystal growth: II. Sector zoning in minerals. *Am. Min., 61, 460-469.*

Dowty, E. 1980b. Synneusis reconcidered. *Cont. Min. Petrol., 74, 75-84.*

Drake, M.J. 1975. The oxidation state of europium as an indicator of oxygen fugacity. *Geochim. Cosmochim. Acta., 39, 55-64.*

Drake, M.J. & Weill, D.F. 1975. Partition of Sr, Ba, Ca, Y, Eu^{+2}, Eu^{+3} and other REE between plagioclase feldspar and magmatic liquid: an experimental study. *Geochim. Cosmochim. Acta, 39, 689-712.*

Drummond, M.S. & Defant, M.J. 1990. A model for trondhjemite-tonalite-dacite genesis and crustal growth via slab melting: Archean to modern comparisons. *J. Geophy. Res., 95, 21503-21521.*

Dungan, M.A., Lindstrom, M.M., McMillan, N.J., Moorbath, S., Hoefs, J. & Haskin, L. 1986. Open system magmatic evolution of the Taos Plateau volcanic field, northern Mexico. I: The petrology and geochemistry of the Servilleta Basalt. *J. Geophys. Res., 91, 5999-6028.*

Dupuy, C. 1970. Contribution a'le'tude des fractionnements geochimiques des alcalins, des alcalino- terreux du gallium au cours des processus magmatiques. Exemple: less roches intrusives et effusives de Toscane et du Latium Septentrional(Italie). *Thesis, Univ. Montpellier, 339p.*

Dupuy, C. & Dostal, J. 1984. Trace element geochemistry of some continental tholeiites. *Earth Planet. Sci. Lett., 67, 1, 61-69.*

Dymek, R.F. 1983. Titanium, aluminum and interlayer cation distributions in biotite from high-grade gneisses, West Greenland. *Am. Min., 68, 880-899.*

Eby, G.N. 1990. The A-type granitoids: A review of their occurrence and chemical characteristics and speculations on their petrogenesis. *Lithos, 26, 115-134.*

Eggler, D.H. 1972a. Amphibole stability in H_2O-undersaturated calc-alkaline melts. *Earth Planet. Scie. Lett., 15, 28-34.*

Eggler, D.H. 1972b. Water-saturated and undersaturated melting relations in a Paricutin andesite and an estimate of water contents in the natural magma. *Cont. Min. Petrol., 34, 261-271.*

Eggler, D.H. & Burnham, C.W. 1973. Crystallization and fractionation trends in the system andesite-H_2O-CO_2-O_2 at pressures to 10 kb. *Geol. Soc. Am. Bull., 84, 2517-2532.*

Eichelberger, J.C. 1978. Andesitic volcanism and crustal evolution. *Nature, 275, 21-27.*

Eichelberger, J.C. 1981. Mechanism of magma mixing at Glass Mountain Medicine Lake Highland volcano, California. *In:* Johnson, D.A. & Donelly-Nolan, J. (eds) *Guides to Some Volcanic Terranes in Washington, Idaho, Oregon, and Northern California. U.S. Geol. Surv. Circular, 838, 183-189.*

Ellam, R.M. & Harmon, R.S. 1990. Oxygen isotope constraints on the crustal contribution to the subduction-related magmatism of the Aeolian Islands, southern Italy. *J. Volcanol. Geotherm. Res., 44, 105-122.*

Ellam, R.M., Hawkesworth, C.J., Menzies, M.A. & Rogers, N.W. 1989. The volcanism of southern Italy: the role of subduction and the relationship between potassic and sodic alkaline magmas. *J. Geophys. Res., 94, 4589-4601.*

Ellam, R.M., Menzies, M.A., Hawkesworth, C.J., Leeman, W.P., Rosi, M. & Serri, G. 1988. The transition from calc-alkaline to potassic orogenic magmatism in the Aeolian Islands, southern Italy. *Bull. Volc., 50, 386-398.*

Ellis, D.J. & Thompson, A.B. 1986. Subsolidus and partial melting reactions in the quartz-excess $CaO+MgO+Al_2O_3+SiO_2+H_2O$ system under water-excess and water deficient conditions to 10kb: some implication for the origin of peraluminous melt from mafic rocks. *J. Petrol., 27, 91-121.*

England, P.C. & Thompson, A.B. 1984. Pressure-temperature-time paths of regional metamorphism. Part I: Heat transfer during the evolution of regions of thickened continental crust. *J. Petrol., 25, 849-928.*

Ercan, T., Fujitani, T., Matsuda, J., Notsu, K., Tokel, S. & Ui, T. 1990. Dogu ve Guneydogu Anadolu Neojen-Kuvaterner volkanitlerine iliskin yeni jeokimyasal, radyometrik ve izotopik verilerin yorumu. *M.T.A. Bull., 110, 143-164.*

Ewart, A. 1976a. Mineralogy and chemistry of modern orogenic lavas-some statistics and implications. *Earth Planet. Sci. Lett., 31, 417-432.*

Ewart, A. 1979. A review of the mineralogy and chemistry of Tertiary-Recent dacitic, rhyolitic, and related salic volcanic rocks. *In:* Barker, F. (eds) *Trondhjemites, Dacites, and Related Rocks. Elsevier, Amsterdam, 13-121.*

Ewart, A. 1982. The mineralogy and petrology of Tertiary-Recent orogenic volcanic rocks: with special reference to the andesitic-basaltic compositional range. *In:* Thorpe, R.S. (eds) *Andesites: Orogenic Andesites and Related Rocks. John Wiley, New York, 25-95.*

Faure, G. 1986. *Principles of Isotope Geology. Wiley, New York, 589p.*

Ferrara, G. & Treuil, M. 1974. Petrological implications of trace element and Sr isotope distributions in basalt-pantellerite series. *Bull. Volc., 38, 548-574.*

Fink, J. 1983. Structure and emplacement of a rhyolitic obsidian flow: Little Glass Mountain, Medicine Lake Highland, northern California. *Geol. Soc. Am. Bull., 94, 362-380.*

Fink, J.H. & Manley, C.R. 1987. Origin of pumiceous and glassy textures in rhyolite flows and domes. *In:* Fink, J.H. (eds) *The Emplacement of Silicic Domes and Lava Flows. Geol. Soc. Am. Spec. Paper, 212, 77-88.*

Fisher, R.V. 1979. Models for pyroclastic surges and pyroclastic flows. *J. Volcanol. Geotherm. Res., 6, 305-318.*

Fisher, R.V. & Schmincke, H.-U. 1984. *Pyroclastic Rocks. Springer-Verlag, Berlin, 472p.*

Floyd, P.A. & Leveridge, B.E. 1987. Tectonic environment of the Devonian Gramscatho basin, south Cornwall: framework mode and geochemical evidence from turbiditic sandstones. *J. Geol. Soc. London, 144, 531-542.*

Floyd, P.A., Leveridge, B.E., Franke, W., Shail, R. & Dorr, W. 1990. Provenance and depositional environment of Rhenohercynian synorogenic greywackes from the Giessen nappe, Germany. *Geol. Runds., 79, 611-626.*

Floyd, P.A., Shail, R., Leveridge, B.E. & Franke, W. 1991b. Geochemistry and provenance of Rhenohercynian synorogenic sandstones: implications for tectonic environment discrimination. *In:* Morton, A.C., Todd, S. & Haughton, P.D.W. (eds) *Geol. Soc. London Spec. Publ., 57, 173-188.*

Floyd, P.A. & Winchester, J.A. 1975. Magma type and tectonic setting discrimination using immobile elements. *Earth Planet. Sci. Lett., 27, 211-218.*

Folk, R.L. 1962. Spectral subdivision of limestone types. *In:* Ham, W.E. (eds) *Classification of Carbonate Rocks. Mem. Am. Ass. Petrol. Geol. , 1, 62-84.*

Folk, R.L. 1965. Some aspects of recrystallization in ancient limestones. *In:* Pray, L.C. & Murray, R.C. (eds) *Dolomitization and Limestone Diagenesis: a Sysmposium. Soc. Econ. Palaeon. Min. Spec. Publ., 13,* 14-48.

Foster, M.D. 1960a. Layer charge relations in the dioctahedral and trioctahedral micas. *Am. Min., 45, 383-398.*

Foster, M.D. 1960b. Interpretation of the compositions of trioctahedral micas. *U.S. Geol. Surv. Professional Paper, 354-B, 11-48.*

France-Lanord, C. & Le Fort, P. 1988. Crustal melting and granite genesis during the Himalayan collision orogenesis. *Trans. Roy. Soc. Edinburg Earth Sci., 79, 183-195.*

Francis, P.W., Thorpe, R.S., Moorbath, S., Kretzschmar, G.A. & Hammil, M. 1980. Strontium isotope evidence for crustal contamination of calc-alkaline volcanic rocks from Cerro Galan, northwest Argentina. *Earth Planet. Sci. Lett., 48, 257-267.*

Frey, F.A., Green, D.H. & Roy, S.D. 1978. Integrated models of basalts petrogenesis: a study of quartz tholeiites to olivine melilitites from south Australia utilizing geochemical and experimental petrological data. *J. Petrol., 19, 463-513.*

Frey, F.A., Wise, W.S., Garcia, M.O., West, H., Kwon, S.T. & Kennedy, A. 1990. Evolution of Mauna Kea Volcano, Hawaii: Petrologic and geochemical constraints on postshield volcanism. *J. Geophys. Res., 95, 1271-1300.*

Frick, C. & Kont, L.E. 1984. Drift pumice in the Indian and South Atlantic Oceans. *Trans. Geol. Soc. S. Africa, 87, 19-33.*

Friedman, G.M. 1969. Trace elements as possible environmental indicators in carbonate sediments. *In:* Friedman, G.M. (eds) *Depositional Environments in Carbonate Rocks. Soc. Econ. Paleo. Min. Spec. Publ., 14, 193-198.*

Fuhrman, M.L. & Lindsley, D.H. 1988. Ternary-feldspar modelling and thermometry. *Am. Min., 73, 201-215.*

Fujimaki, H., Tatsumoto, M. & Aoki, K. 1984. Partition coefficients of Hf, Zr and REE between phenocrysts and groundmasses. Proceeding of the fourteenth lunar and planetary science conference, Part 2. *J. Geophys. Res., 89, Suppl. B662-B672.*

Galer, S.J.G. & O'Nions, R.K. 1986. Magmagenesis and the mapping of chemical and isotopic variations in the mantle. *Chem. Geol., 56, 45-61.*

Garcia, M.O. & Jacobson, S.S. 1979. Crystal clots, amphibole fractionation, and the evolution of calc-alkaline magmas. *Cont. Min. Petrol., 69, 319-327.*

Garlick, G.D. & Dymond, J.R. 1970. Oxygen isotope exchange between volcanic materials and ocean water. *Geol. Soc. Am. Bull., 81, 2137-2142.*

Gast, P.W. 1968. Trace element fractionation and the origin of tholeiitic and alkaline magma types. *Geochim. Cosmochim. Acta., 332, 1057-1086.*

Gealy, W.K. 1977. Ophiolite obduction and geologic evolution of the Oman mountains and adjacent areas. *Geol. Soc. Am. Bull., 88, 1183-1191.*

Genc, S. 1990. Petrography, metamorphism and genesis of metamorphics in the Cokekyazi Gokay(Hizan, Bitlis) area of the Bitlis Massif. *Geol. Bull. Turkey, 33, 1-14.*

Gerlach, D.C. & Grove, T.L. 1982. Petrology of Medicine Lake Highland volcanics: characterization of end members of magma mixing. *Cont. Min. Petrol., 80, 147-159.*

Giannetti, B. & Luhr, J.F. 1983. The White trachytic tuff of Roccamonfina Volcano(Roman Region, Italy). *Cont. Min. Petrol., 84, 235-252.*

Gibb, F.C.G. 1973. The zoned clinopyroxene of the Shiant Isles sill, Scotland. *J. Petrol., 14, 203-230.*

Gibbs, A.K., Montgomery, C.W., O'Day, P.A. & Erslev, E.A. 1986. The Archean-Proterozoic transition: evidence from the geochemistry of metasedimentary rocks of Guyana and Montana. *Geochim. Cosmochim. Acta, 50, 2125-2141.*

Gill, J.B. 1978. Role of trace element partition coefficients in models of andesite genesis. *Geochim. Cosmochim. Acta, 42, 709-724.*

Gill, J.B. 1981. *Orogenic Andesites and Plate Tectonics. Springer, Berlin, 390p.*

Glazner, A.F. & Farmer, G.L. 1992. Production of isotopic variability in continental basalts by cryptic crustal contamination. *Science, 255, 72-74.*

Glazner, A.F., Ussler, W. & Mathis, A.C. 1990. Interpretation of plagioclase texture in volcanic rocks. *Trans. Am. Geophys. Un.(EOS), 71, 1678.*

Glazner, A.F., Ussler, W. & Mies, J.W. 1988. Fate of granitic minerals in mafic magmas. *Trans. Am. Geophys. Un.(EOS), 69, 1504.*

Graf, D.L. 1962. Minor element distribution in sedimentary rocks. *Geochim. Cosmochim. Acta., 26, 849-856.*

Green, D.H., Edgar, A.D., Beasley, P., Kiss, E. & Ware, N.G. 1974. Upper mantle source for some hawaiites, mugearites and benmoreites. *Cont. Min. Petrol., 48, 33-43.*

Green, D.H. & Ringwood, A.E. 1967. The genesis of basaltic magmas. *Cont. Min Petrol., 15, 103-190.*

Green, T.H. 1972. Crystallization of calcalkaline andesite under controlled high-pressure conditions. *Cont. Min. Petrol., 34, 150-166.*

Green, T.H. 1976. Experimental generation of cordierite-, or garnet-bearing granitic liquids from a pelitic composition. *Geology, 4, 85-88.*

Green, T.H. & Pearson, N.J. 1983. Effect of pressure on rare earth element partition coefficients in common magmas. *Nature, 305, 414-416.*

Green, T.H. & Pearson, N.J. 1985. Experimental determination of REE partition coefficients between amphibole and basaltic to andesitic liquids at high pressure. *Geochim. Cosmochim. Acta, 49, 1465-1468.*

Green, T.H. & Pearson, N.J. 1986a. Ti-rich accessory phase saturation in hydrous mafic-felsic compositions at high P, T. *Chem. Geol., 54, 185-201.*

Green, T.H. & Pearson, N.J. 1986b. Rare-earth element partitioning between sphene and coexisting silicate liquid at high pressure and temperature. *Chem. Geol., 55, 105-119.*

Green, T.H. & Pearson, N.J. 1987. An experimental study of Nb and Ta partitioning between Ti-rich minerals and silicate liquids at high pressure and temperature. *Geochim. Cosmochim. Acta, 47, 925-939.*

Green, T.H., Sie, S.H., Ryan, C.G. & Cousens, D.R. 1989. Proton microprobe-determined partitioning of Nb, Ta, Zr, Sr and Y between garnet, clinopyroxene and basaltic magma at high pressure and temperature. *Chem. Geol., 74, 201-216.*

Green, T.H. & Watson, E.B. 1982. Crystallization of apatite to natural magmas under high pressure, hydrous conditions, with particular reference to "orogenic" rock series. *Cont. Min. Petrol., 79, 96-105.*

Gromet, L.P., Dymek, R.F., Haskin, L.A. & Korotev, R.L. 1984. The "North American shale composite": Its composition, major and trace element characteristics. *Geochim. Cosmochim. Acta,48, 2469-2482.*

Grove, L.L. & Kinzler, R.J. 1986. Petrogenesis of andesites. *Ann. Rev. Earth Planet. Sci., 14, 417-454.*

Grove, T.L. & Baker, M.B. 1984. Phase equilibrium controls on the tholeiitic versus calc-alkaline differentiation trends. *J. Geophys. Res., 89, 3253-3274.*

Grove, T.L. & Donnelly-Nolan, J.M. 1986. The evolution of young silicic lavas at Medicine Lake Volcano, California: Implications for the origin of compositional gaps in calc-alkaline series lavas. *Cont. Min. Petrol., 92, 281-302.*

Grove, T.L., Gerlach, D.C. & Sando, T.W. 1982. Origin of calcalkaline lavas at Medicine Lake volcano by fractionation, assimilation and mixing. *Cont. Min. Petrol., 80, 160-182.*

Guidotti, C.V. 1984. Micas in metamorphic rocks. *In:* Bailey, S.W. (eds) *Micas. Min. Soc. Am. Rev. Min., 13, 357-467.*

Guidotti, C.V., Cheney, J.T. & Conatore, P.D. 1975. Interrelationship between Mg/Fe ratio and octahedral Al content in biotite. *Am. Min., 60, 849-853.*

Guidotti, C.V., Cheney, J.T. & Guggenhein, S. 1977. Distribution of titanium between coexisting muscovite and biotite in pelitic schists from northwestern Maine. *Am. Min., 62, 438-448.*

Gulen, L. 1980. Strontium isotope geochemistry of Mount Ararat and Mount Suphan volcanics, Eastern Turkey. *Trans. Am. Geophys. Un.(EOS), 61, 412.*

Gulen, L. 1982. Sr, Nd and Pb systematics of Ararat and Suphan volcanoes, Eastern Turkey. *Trans. Am. Geophys. Un.(EOS), 63, 1145.*

Guner, L. 1984. Nemrut yanardaginin jeolojisi, jeomorfolojisi ve volkanizmasinin evrimi. *Jeomorfoloji Dergisi, 12, 23-65.*

Guner, Y. & Saroglu, F. 1987. Dogu Anadolu'da Kuvaterner volkanizmasi ve jeotermal enerji acisindan onemi. *Turkiye 7. Petrol Kongresi Bildiriler Kitabi, 371-383.*

Gust, D.A. & Perfit, M.R. 1987. Phase relations of a high-Mg basalt from the Aleutian Island Arc: implications for primary island arc basalts and high-Al basalts. *Cont. Min. Petrol., 97, 7-18.*

Haggerty, S.E. 1976. Opaque mineral oxides in terrestrial igneous rocks. *In:* Rumble, D. (eds) *Oxide Minerals. Min. Soc. Am. Rev. Min., 101-300.*

Hall, R. 1976. Ophiolite emplacement and the evolution of the Taurus suture zone, Southeastern Turkey. *Geol. Soc. Am. Bull., 87, 1078-1088.*

Hallam, A. 1976. Geology and plate tectonics interpretation of the sediments of the Mesozoic radiolarite-ophiolite complex in the Neyriz region, southern Iran. *Geol. Soc. Am. Bull., 87, 47-52.*

Hanson, G. 1978. The application of trace elements to the petrogenesis of igneous rocks of granitic composition. *Earth Planet. Sci. Lett., 38, 26-43.*

Hanson, G.N. 1980. Rare earth elements in petrogenetic studies of igneous systems. *Ann. Rev. Earth Planet. Sci., 8, 371-406.*

Hanson, G.N. 1989. An approach to trace element modeling using a simple igneous system as an example. *In:* Lipin, B.R. & McKay, M.G.A. (eds) *Geochemistry and Mineralogy of Rare Earth Elements. Min. Soc. Am. Rev. Min., 21, 79-97.*

Hargrove, H.R. 1982. Geology of the southern portion of the Montana Mountains, McDermitt caldera Nevada. *M.Sc. Thesis, Arizona State University, 202p.*

Harmon, R.S. & Hoefs, J. 1984. O-isotope relationships in Cenozoic volcanic rocks: evidence for a heterogeneous mantle source and open-system magmagenesis. *In:* Dungan, M.A., Grove, T.L. & Hildreth, W. (eds) *Proc. Conf. Open Magmatic Sys., Inst. Stud. Earth and Man, S.M.U. Spec. Publ., 69-71.*

Harmon, R.S., Hoefs, J. & Wedepohl, K.H. 1987. Stable isotope(O, H, S) relationships in Tertiary basalts and their mantle xenoliths from the Northern Hessian Depression, W. Germany. *Cont. Min. Petrol., 95, 350-369.*

Harmon, R.S., Kempton, P.D., Stosch, H.G., Hoefs, J., Kovalenko, V.I. & Eonov, D. 1986. $^{18}O/^{16}O$ ratios in anhydrous spinel lherzolite xenoliths from the Shavaryn-Tsaram volcano, Mongolia. *Earth Planet. Sci. Lett., 81, 193-202.*

Harmon, R.S., Thorpe, R.S. & Francis, P.W. 1981. Petrogenesis of Andean andesites from combined O-Sr isotope relationships. *Nature, 290, 396-399.*

Harmon, R.S., Barreiro, B.A., Moorbath, S., Hoefs, J., Francis, P.W., Thorpe, R.S., Deruelle, B., McHugh, J. & Viglino, J.A. 1984. Regional O-, Sr-, and Pb-isotope relationships in late Cenozoic calc-alkaline lavas of the Andean Cordillera. *J. Geol Soc. London, 141, 803-822.*

Harris, C. 1989. Covariance of initial $^{87}Sr/^{86}Sr$ ratios, $\delta^{18}O$, and SiO_2 in continental flood basalt suites: The role contamination and alteration. *Geology, 17, 634-636.*

Harris, C., Whittingham, A.M., Milner, S.C. & Amstrong, R.A. 1990. Oxygen isotope geochemistry of the silicic volcanic rocks of the Etendeka-Parana province: Source constraints. *Geology, 18, 1119-1121.*

Harris, N.B.W., Pearce, J.A. & Tindle, A.G. 1986. Geochemical characteristics of collision-zone magmatism. *In:* Coward, M.P & Ries, A.C. (eds) *Collision Tectonics. Geol. Soc. London Spec. Publ., 19, 67-81.*

Harrison, T.M., Watson, E.B. & Rapp, R.P. 1986. Does anatexis deplete the lower crust in heat-producing elements?. Implications from experimental studies.*Trans. Am. Geophys. Un.(EOS), 67, 386.*

Hart, W.K. & Carlson, R.W. 1987. Tectonic controls on magma genesis and evolution in the northwestern United States. *J. Volcanol. Geotherm. Res., 32, 119-135.*

Harvey, P.K., Taylor, D.M., Hendry, R.D. & Bancroft, F. 1973. An accurate fusion method for the analysis of rocks and chemically related minerals by X-ray fluorescence. *X-Ray Spectrometry, 2, 33-44.*

Haughton, P. 1988. A cryptic Caledonian flysch terrane in Scotland. *J. Geol. Soc. London, 145, 685-704.*

Hawkesworth, C.J. 1982. Isotope characteristics of magmas erupted along destructive plate margins. *In:* Thorpe, R.S. (eds) *Andesites: Orogenic Andesites and Related Rocks. John Wiley & Sons, 549-571.*

Hawkesworth, C.J., Marsh, J.S., Duncan, A.R., Erlank, A.J. & Norry, M.J. 1984. The role of continental lithosphere in the generation of the Karoo volcanic rocks: evidence from combined Nd- and Sr-isotope studies. *In:* Erlank, A.J. (eds) *Petrogenesis of the volcanic rocks of the Karoo Province. Geol. Soc. S. Afr. Spec. Publ., 13, 341-354.*

Hawkesworth, C.J., Norry, M.J., Roddick, J.C., Baker, P.E., Francis, P.W. & Thorpe, R.S. 1979a. $^{143}Nd/^{144}Nd$, $^{87}Sr/^{86}Sr$, and incompatible element variations in calc-alkaline andesites and plateau lavas from South America. *Earth Planet. Sci. Lett., 42, 45-57.*

Hawkesworth, C.J., Norry, M.J., Roddick, J.C. & Vollmer, R. 1979. $^{143}Nd/^{144}Nd$ and $^{87}Sr/^{86}Sr$ ratios from the Azores and their significance in LIL-element enriched mantle. *Nature, 280, 28-31.*

Hawkesworth, C.J., O'Nions, R.K. & Arculus, R.J. 1979b. $^{143}Nd/^{144}Nd$ and $^{87}Sr/^{86}Sr$ geochemistry of the alkalic rock suite, Grenada, Lesser Antilles. *Earth Planet. Sci. Lett., 45, 237-248.*

Hawkesworth, C.J. & van Calsteren, P.W.C. 1984. Radiogenic isotopes-some geological applications. *In:* Henderson, P. (eds) *Rare Earth Element Geochemistry. Elsevier, Amsterdam, 375-421.*

Hawkesworth, C.J. & Vollmer, R. 1979. Crustal contamination versus enriched mantle: $^{143}Nd/^{144}Nd$ and $^{87}Sr/^{86}Sr$ evidence from the Italian volcanics. *Cont. Min. Petrol., 69, 151-165.*

Heiken, G. & Eichelberger, J. 1980. Eruptions at Chaos Crags, Lassen Volcanic National Park, California. *J. Volcanol. Geotherm. Res., 7, 443-481.*

Heiken, G. & Wohletz, K. 1987. Tephra deposits associated with silicic domes and lava flow. *In:* Fink, J.H. (eds) *The Emplacement of Silicic Domes and Lava Flows. Geol. Soc. Am. Spec. Publ., 212, 55-76.*

Hellman, P.L. & Green, T.H. 1979. The role of sphene as an accessory phase in the high-pressure partial melting of hydrous mafic compositions. *Earth Planet.Science Lett., 42, 191-201.*

Helz, R.T. 1973. Phase relations of basalts in their melting range at PH_2O=5 kb as a function of oxygen fugacity. Part I. Mafic phases. *J. Petrol., 14, 249-302.*

Helz, R.T. 1976. Phase relations of basalts in their melting range at PH_2O=5 kb. Part II. Melt compositions. *J. Petrol., 17, 139-193.*

Heming, R.F. & Rankin, P.C. 1979. Ce-anomalous lavas from Rabaul caldera, Papua New Guinea. *Geochim. Cosmochim. Acta, 43, 1351-1355.*

Hempton, M.R. 1982. The North Anatolian Fault and complexities of continental escape. *J. Struct. Geol., 4, 502-504.*

Hempton, M.R. & Dewey, J.F. 1983. Eartquake induced deformational structures in young lacustrine sediments, East Anatolian Fault, Southeast Turkey. *Tectonophysics, 98, 7-14.*

Henderson, P. 1982. *Inorganic Geochemistry. Pergamon Press, Oxford, 353p.*

Henderson, P. 1984. General geochemical properties and abundances of the rare earth elements. *In:* Henderson, P. (eds) *Rare Earth Element Geochemistry. Elsevier, Amsterdam, 1-32.*

Hensen, B.J. & Green, D.H. 1973. Experimental study of the stability of cordierite and garnet in pelitic compositions at high pressures and temperatures. III. Synthesis of experimental data and geological applications. *Cont. Min. Petrol., 38, 151-166.*

Hewitt, D.A. & Wones, D.R. 1984. Experimental phase relations of the micas. *In:* Bailey, S.W. (eds) *Micas. Min. Soc. Am. Rev. Min., 13, 201-247.*

Hibbard, M.J. 1981. The magma mixing origin of mantled feldspars. *Cont. Min. Petrol., 76, 158-170.*

Hickey, R.L., Frey, F.A. & Gerlach, D.C. 1986a. Multiple sources for basaltic arc rocks from the southern volcanic zone of the Andes(34°-41°S): Trace element and isotopic evidence for contributions from subducted oceanic crust, mantle, and continental crust. *J. Geophy. Res., 91, 33-45.*

Hickey, R.L., Frey, F.A. & Gerlach, D.C. 1986b. Multiple sources for volcanic rocks from the southern volcanic zone of the Andes(39°-41°S): trace element and isotopic evidence for contributions from subducted oceanic material and continental crust. *J. Geophys. Res., 91, 5943-5962.*

Hildreth, E.W. 1977. The Magma Chamber of the Bishop Tuff: Gradients in temperature, pressure and composition. *Ph.D Thesis, Berkeley, University of California, 328p.*

Hildreth, W. 1979. The Bishop Tuff: Evidence for the origin of compositional zonation in silicic magma chambers. *Geol. Soc. Am. Spec. Paper, 180, 43-75.*

Hildreth, W. 1981. Gradients in silicic magma chambers: Implications for lithospheric magmatism:. *J. Geophys. Res., 86, 10153-10192.*

Hildreth, W. & Mahood, G. 1985. Correlation of ash flow tuffs. *Geol. Soc. Am. Bull., 96, 968-974.*

Hildreth, W.E. & Moorbath, S. 1988. Crustal contributions to arc magmatism in the Andes of Central Chile. *Cont. Min. Petrol., 98, 455-489.*

Hiscott, R.N. 1984. Ophiolitic source rocks for Taconic-age flysch: Trace element evidence. *Geol. Soc. Am. Bull., 95, 1261-1267.*

Hole, M.J., Saunders, A.D., Marriner, G.F. & Tarney, J. 1984. Subduction of pelagic sediments: implications for the origin of Ce-anomalous basalts from the Mariana Islands. *J. Geol. Soc. London, 141, 453-472.*

Holland, H.D. 1978. *The Chemistry of the Atmosphere and Oceans. Willey, New York, 351p.*

Hollister, L.S. & Gancarz, A.J. 1971. Compositional sector-zoning in clinopyroxene from the Naree area, Italy. *Am. Min., 56, 959-979.*

Hower, J., Eslinger, E.W., Hower, M.E. & Perry, E.A. 1976. Mechanism of burial metamorphism of argillaceous sediment. 1: Mineralogical and chemical evidence. *Geol. Soc. Am. Bull., 87, 725-737.*

Huebner, J.S. 1980. Pyroxene phase equilibria at low pressure. *In:* Prewitt, C.T. (eds) *Pyroxenes. Min. Soc. Am. Rev. Min.,7, 213-280.*

Huppert, H.E. & Sparks, R.S.J. 1984. Double-diffusive convection due to crystallization in magma. *Ann. Rev. Earth Planet. Sci., 12, 11-37.*

Huppert, H.E. & Sparks, R.S.J. 1985. Cooling and contamination of mafic and ultramafic magmas during ascent through continental crust. *Earth Planet. Sci. Lett., 74, 371-386.*

Huppert, H.E. & Sparks, R.S.J. 1988. The generation of granitic magmas by intrusion of basalt into continental crust. *J. Petrol., 29, 599-624.*

Iacumin, P., Piccirillo, E.M. & Longinelli, A. 1991. Oxygen isotopic composition of Lower Cretaceous tholeiites and Precambrian basement rocks from the Parana basin(Brazil): the role of water-rock interaction. *Chem. Geol., 86, 255-237.*

Inman, D.L. 1952. Measures for describing the size distribution of sediments. *J. Sed. Petrol., 22, 125-145.*

Innocenti, F., Manetti, P., Mazzuoli, R., Pasquare, G. & Villari, L. 1982a. Anatolia and Northwestern Iran. *In:* Thorpe, R.S. (eds) *Andesites: Orogenic Andesites and Related Rocks. Wiley, New York, 327-349.*

Innocenti, F., Mazzuoli, C., Pasquare, G., Serri, G. & Villari, L. 1980. Geology of the volcanic area North of Lake Van, Turkey. *Geol. Runds., 69, 292-322.*

Innocenti, F., Mazzuoli, R., Pasquare, G., Radicati di Brozola, F. & Villari, L. 1976. Evolution of the volcanism in the area of interaction between the Arabian, Anatolian and Iranian plates(Lake Van, Eastern Turkey). *J. Volcanol. Geotherm. Res., 1, 103-112.*

Innocenti, F., Mazzuoli, R., Pasquare, G., Radicati di Brozola, F. & Villari, L. 1982b. Tertiary and Quaternary volcanism of The Erzurum-Kars area(Eastern Turkey): geochronological data and geodynamic evolution. *J. Volcanol. Geotherm. Res., 13, 223-240.*

Innocenti, F., Mazzuoli, R., Pasquare, G., Radicati, F. & Villari, L. 1975. Neogene and Quaternary volcanism along the Taurus Belt: Inferences for a geodynamic model. *Rapp. Comm. Int. Mer. Medit., 23, 205-206.*

Irvine, T.N. & Baragar, W.R.A. 1971. A guide to the chemical classification of the common volcanic rocks. *Can. J. Earth Sci., 8, 523-548.*

Irving, A.J. 1974. Megacrysts from the Newer Basalts and other basaltic rocks of southeastern Australia. *Bull. Geol. Soc. Am., 85, 1503-1514.*

Irving, A.J. 1978. A review of experimental studies of crystal/liquid trace element partitioning. *Geochim. Cosmochim. Acta, 48, 1201-1221.*

Ito, E., White, W.M., Gopel, C., O'Hearn, J. & Melson, W.G. 1984. Isotope geochemistry of N-type and P-type MORB glasses. *Trans. Geophys. Un.(EOS), 65, 302.*

Jackson, J. & McKenzie, D.P. 1984. Active tectonics of the Alpine-Himalayan Belt between Western Turkey and Pakistan. *Geophys. J.R. Astr. Soc., 77, 185-264.*

Jahn, B.M., Sun, S.S. & Nesbitt, R.W. 1979. REE distribution and petrogenesis of the Spanish Peaks igneous complex, Colorado. *Cont. Min. Petrol., 70, 281-298.*

Jakes, P. & Gill, J.B. 1970. Rare earth elements and the island arc tholeiitic series. *Earth Planet. Sci. Lett., 9, 17-28.*

Jakes, P. & White, A.J.R. 1972. Major and trace element abundances in volcanic rocks of orogenic areas. *Geol. Soc. Am. Bull., 83, 29-40.*

James, D.E. 1981. The combined use of oxygen and radiogenic isotopes as indicators of crustal contamination. *An. Rev. Earth Planet. Sci. Lett., 9, 311-344.*

James, D.E. 1982. A combined O, Sr, Nd, and Pb isotopic and trace element study of crustal contamination in central Andean lavas. I. Local chemical variations. *Earth Planet. Sci. Lett., 57, 47-62.*

Jarvis, I. 1992. Sample preparation for ICP-MS. *In:* Jarvis, K.E., Gray, A.L. & Houck, R.S. (eds) *Handbook of Inductively Coupled Plasma Mass Spectrometry. Blakie, Glasgow, 172-224.*

Jarvis, K.E. 1988. Inductively coupled plasma mass spectrometry: A new technique for the rapid or ultra-trace level determination of the rare-earth elements in geological materials. *Chem. Geol., 68, 31-39.*

Jenkins, R. & De Vries, J.L. 1967. *Practical X-Ray Spectrometry. Centrex Eindhoven, 182p.*

Jensen, B.B. 1973. Patterns of trace element partitioning. *Geochim. Cosmochim. Acta, 37, 2227-2242.*

Jirka, G.H. & Katavola, D.S. 1979. Supercritical withdrawal from two-layered fluid systems. Part 2: Three-dimensional flow into a round intake. *J. Hydraulic Res., 17, 53-62.*

Johnson, M.C. & Rutherford, M.J. 1989. Experimental calibration of the aluminum in hornblende geobarometer with application to Long Valley caldera(California) volcanic rocks. *Geology, 17, 837-841.*

Joron, J.L. & Treuil, M. 1977. Utilisation des proprietes des elements fortement hygromagmaphiles pou l'etude de la composition chimique et de l'heterogeneite du manteau. *Bull. Soc. Geol. Fr., XIX, 6, 1197-1205.*

Kable, E.J.D., Fresq, H.W. & Gurney, J.J. 1975. The significance of the inter element relationships of some minor and trace elements in south African Kimberlites. *In:* Ahrens, L.H. (eds) *Physics and Chemistry of the Earth, 9, 709-734.*

Karamanderesi, I.H., Can, A.R., Coskun, B., Guner, A., Caglav, F., Polat, Z., Trakcioglu, H. & Yildirim, T. 1984. Zilanderesi(Van-Ercis) jeolojisi ve jeotermal enerji olanaklari. *M.T.A. Rap. No, 7793.*

Kay, R.W. 1977. Geochemical constraints on the origin of Aleutian magmas. *In:* III, M.T.a.W.C.P. (eds) *Island Arcs, Deep Sea Trenches and Back-Arc Basins. Maurice Ewing Ser. 1, AGU, Washington D.C.* 229-242.

Kay, R.W. & Gast, P.W. 1973. The REE content and origin of alkali-rich basalts. *J. Geology, 81, 653-682.*

Kay, S.M., Makasaev, V., Moscoso, R., Mpodozis, C., Nasi, C. & Gordillo, C.S. 1988. Tertiary Andean magmatism in Chile and Argentina between 28°S and 33°S: Correlation of magmatic chemistry with a changing Benioff zone. *J. South. Am. Earth Sci., 1, 21-38.*

Kelemen, P.B., Dick, H.J.B. & Quick, J.E. 1992. Formation of harzburgite by pervasive melt/rock reaction in the upper mantle. *Nature, 358, 635-641.*

Kelemen, P.B., Johnson, K.T.M., Kinzler, R.J. & Irving, A.J. 1990. High-field-strength element depletions in arc basalts due to mantle-magma interaction. *Nature, 345, 521-524.*

Kempton, P.D., Dungan, M.A. & Blanchard, D.P. 1987. Petrology and geochemistry of xenolith-bearing alkalic basalts from the Geronimo Volcanic Field, southeast Arizona: Evidence for polybaric fractionation and implications for mantle heterogeneity. *In:* Morris, E.M. & Pasteris, J.D. (eds) *Mantle Metasomatism and Alkaline Magmatism. Geol. Soc. Am. Spec. Publ., 215, 347-370.*

Kempton, P.D., Harmon, R.S., Stosch, H.G., Hoefs, J. & Hawkesworth, C.J. 1988. Open system O-isotope behaviour and trace element enrichment in the sub-Eifel mantle. *Earth Planet. Sci. Lett., 89, 273-287.*

Kennedy, G.C. 1955. Some aspects of the role of water in rock melts. *In:* Poldervaart, A. (eds) *Crust of the Earth. Geol. Soc. Am. Spec. Paper, 66, 489-504.*

Ketin, I. 1976. Main orogenic events and paleogeographical evolution of Turkey. *M.T.A. Bull., 88, 1-4.*

Kolisnik, A. 1990. Phenocrysts zoning and heterogeneity in andesites and dacites of Volcan Popocatepetl, Mexico. *M.Sc. Thesis, Qeen's University, Kingston, Ontario, Canada, 247p.*

Korringa, M.K. & Noble, D.C. 1971. Distribution of Sr and Ba between natural feldspar and igneous melt. *Earth Planet. Sci. Lett., 11, 147-151.*

Kremenetskiy, A.A., Yushko, N.A. & Budyanskiy, D.D. 1980. Geochemistry af rare alkalis in sediments and effusives. *Geochem. Int., 178, 4, 54-72.*

Kress, V.C. & Carmichael, I.S.E. 1991. The compressibility of silicate liquids containing Fe_2O_3 and the effect of composition, temperature, oxygen fugacity and pressure on their redox states. *Cont. Min. Petrol., 108, 82-92.*

Kretz, R. 1982. Transfer and exchange equilibria in portion of the pyroxene quadrilateral as deduced from natural and experimental data. *Geochim. Cosmochim. Acta, 46, 411-422.*

Kuno, H. 1950. Petrology of Hakone volcano and adjacent areas, Japan. *Geol. Soc. Am. Bull., 25, 957-1020.*

Kuno, H. 1966. Review of pyroxene relations in terrestrial rocks in the light of recent experimental work. *Min. J. Japan, 5, 21-43.*

Kuno, H. 1968. Differentiation of basalt magmas. *In:* Hess, H.H. & Poldervaat, A. (eds) *Basalts II. Interscience, New York, 623-688.*

Kuo, L. & Kirkpatrick, R.J. 1982. Pre-eruption history of phyric basalts from DSDP Legs 45 and 46: Evidence from morphology and zoning patterns in plagioclase. *Cont. Min. Petrol., 79, 13-27.*

Kushiro, I. 1960. Si-Al relations in clinopyroxenes from igneous rocks. *Am. J. Sci., 258, 548-554.*

Kyser, T.K. 1986. Stable isotope variations in the mantle. *In:* Valley, J.M., Taylor, H.P. & O'Neil, J.R. (eds) *Stable Isotopes in High Temperature Geological Processes. Min. Soc. Am. Rev. Min., 16, 141-164.*

Kyser, T.K., O'Neil, J.R. & Carmichael, I.S.E. 1981. Oxygen isotope thermometry of basic lavas and mantle nodules. *Cont. Min. Petrol., 77, 11-23.*

Kyser, T.K., O'Neil, J.R. & Carmichael, I.S.E. 1982. Genetic relations among basic lavas and ultramafic nodules: evidence from oxygen isotope compositions. *Cont. Min. Petrol., 81, 88-102.*

La Roche, H., Leterrier, J., Grand Claude, P. & Marchal, M. 1980. A classification of volcanic and plutonic rocks using R1-R2 diagrams and major element analyses-its relationship with current nomenclature. *Chem. Geol., 29, 183-210.*

Labotka, T.C. 1983. Analyses of the compositional variations of biotite in pelitic hornfelses from northeastern Minnesota. *Am. Min., 68, 900-914.*

Lambert, R.J., Holland, J.G. & Owen, P.F. 1974. Chemical petrology of a suite of calc-alkaline lavas from Mount Ararat, Turkey. *J. Geol., 82, 419-438.*

Lambert, R.S.J. & Holland, J.G. 1974. Yttrium geochemistry applied to petrogenesis utilizing calcium-yttrium relationships in minerals and rocks. *Geochim. Cosmochim. Acta, 38, 1393-1414.*

Lange, R.A. & Carmichael, I.S.E. 1990. Hydrous basaltic andesites associated with minette and related lavas in western Mexico. *J. Petrol., 31, 1225-1259.*

Langmuir, C.H., Vocke, R.D., Hanson, G.N. & Hart, S.R. 1978. A general mixing equations with applications to icelandic basalts. *Earth Planet. Sci. Lett., 37, 380-392.*

Le Bas, M.J., Le Maitre, R.W., Streckeisen, A. & Zanettin, B. 1986. A chemical classification of volcanic rocks based on the total alkali-silica diagram. *J. Petrol., 27, 745-750.*

Le Bas, N.J. 1962. The role of aluminium in igneous clinopyroxenes with relation to their parentage. *Am. J. Sci., 260, 267-288.*

Le Maitre, R.W. 1989. *A Classification of Igneous Rocks and Glossary of Terms. Blackwell, Oxford, 193p.*

Le Roex, A.P. 1987. Source regions of mid-ocean ridge basalts; evidence for enrichment processes. *In:* Menzies, A.M. & Hawkesworth, C.J. (eds) *Mantle Metasomatism. Academic Press, London, 389-422.*

Le Roex, A.P., Dick, H.J.B., Erlank, A.J., Reid, A.M., Frey, F.A. & Hart, S.R. 1983. Geochemistry, mineralogy and petrogenesis of lavas erupted along the south west Indian ridge between the Bouvet triple junction and 11°E. *J. Petrol., 24, 3, 267-318.*

Leake, B.E. 1978. Nomenclature of amphiboles. *Am. Min., 63, 1025-1052.*

Leake, B.E., Hendry, G.L., Kemp, A., Plant, A.G., Harrey, P.K., Wilson, J.R., Coats, J.S., Aucott, J.W., Lunel, T. & Howard, R.J. 1969. The chemical analysis of rock powders by automatic X-ray fluorescence. *Chem. Geol., 5, 7-86.*

Leat, P.T., Jackson, S.E., Thorpe, R.S. & Stillman, C.J. 1986. Geochemistry of bimodal basalt-subalkaline/peralkaline rhyolite provinences within the southern British Caledonides. *J. Geol. Soc. London, 143, 259-276.*

Leat, P.T., Macdonald, R. & Smith, R.L. 1984. Geochemical evolution of the Menangai Caldera Volcano, Kenya. *J. Geophys. Res., 89, 8571-8592.*

Leeman, W.P. 1981. The influence of crustal structure on composition of subduction-related magmas. *1981 IAVCEI symposium, Arc Volcanism Abst.,Tokyo, 203.*

Leeman, W.P. & Hawkesworth, C.J. 1986. Open magma systems: Trace element and isotopic constraints:. *J. Geophys. Res., 91, 5901-5912.*

Leeman, W.P. & Lindstrom, D.J. 1978. Partitioning of Ni^{+2} between basaltic melt and synthetic melts and olivines-an experimental study. *Geochim. Cosmochim. Acta, 42, 801-816.*

Leterrier, M. 1982. Clinopyroxene composition as a method of identification of the magmatic affinities of paleo-volcanic series. *Earth Planet. Sci. Lett., 59, 139-154.*

Lightfoot, P.C., Hawkesworth, C.J., Devey, C.W. & Rogers, N.W. 1990a. Source and differentiation of Deccan Trap lavas: implications of geochemical and mineral chemical variations. *J. Petrol., 31, 5, 1165-1200.*

Lindstrom, D.J. & Weill, D.F. 1978. Partitioning of transition metals between diopside and coexisting silicate liquids. I. Nickel, cobalt and manganese. *Geochim. Cosmochim. Acta, 42, 817-831.*

Lipman, P.W. 1971. Iron-titanium oxide phenocrysts in compositionally zoned ash-flow sheets from southern Nevada. *J. Geol., 79, 438-456.*

Lofgren, G. 1971. Experimentally produced devitrification textures in natural rhyolitic glass. *Geol. Soc. Am. Bull., 82, 111-124.*

Lofgren, G.E. & Norris, N. 1981. Experimental duplication of plagioclase sieve and overgrowth textures. *Geol. Soc.Am. Abstr. with Progr., 13, 498.*

Long, P.E. 1978. Experimental determination of partition coefficients for Rb, Sr and Ba between alkali feldspar and silicate liquid. *Geochim. Cosmochim. Acta, 42, 833-846.*

Loomis, T.P. 1982. Numerical simulations of crystallization processes of plagioclase in complex melts: The origin of major and oscillatory zoning in plagioclase. *Cont. Min. Petrol., 81, 219-229.*

Ludden, J.N. & Thompson, G. 1979. An evaluation of the behaviour of the rare earth elements during the weathering of sea-floor basalt. *Earth Planet. Sci. Lett., 43, 85-92.*

Luhr, J.F. & Carmichael, I.S.E. 1980. The Colima Volcanic Complex, Mexico. *Cont. Min. Petrol., 71, 343-372.*

Luhr, J.F. & Carmichael, I.S.E. 1981. The Colima Volcanic Complex, Mexico: II. Late-Quaternary cinder cones. *Cont. Min. Petrol., 71, 343-372.*

Luhr, J.F., Carmichael, I.S.E. & Varekamp, J.C. 1984. The 1982 eruptions of El Chichon Volcano, Chiapas, Mexico: Mineralogy and petrology of the anhydrite-bearing pumice. *J. Volcanol. Geotherm. Res., 23, 69-108.*

Luhr, J.F. & Giannetti, B. 1987. The brown leucitic tuff of Rocamonfina Volcano(Roman Region, Italy). *Cont. Min. Petrol., 95, 420-436.*

Luth, W.C., Jahns, R.H. & Tuttle, O.F. 1964. The granitic system at pressures of 4 to 10 kilobars. *J. Geophys. Res., 69, 759-773.*

Lyakhovich, V.V. & Lyakhovich, T.T. 1987. Geochemical features of biotite. *Geochem. Inter., 24, 10, 15-25.*

Maaløe, S. 1985. *Principles of Igneous Petrology. Springer Verlag, Berlin, 374p.*

MacDonald, G.A. & Katsura, T. 1964. Chemical composition of Hawaiian lavas. *J. Petrol., 5, 82-133.*

MacKenzie, W.S., Donaldson, C.H. & Guilford, C. 1982. *Atlas of Igneous Rocks and their Textures. Longman, Harlow, 148p.*

Mahoney, J., MacDougall, J.D., Lugmair, G.W., Murali, A.W., Sankar Das, M. & Gopalan, K. 1982. Origin of Deccan Trap flows at Mahabaleshwar inferred from Nd and Sr isotopic and chemical evidence. *Earth Planet. Sci. Lett., 60, 47-60.*

Mahood, G. 1981. Geochemical evolution of a Pleistocene rhyolitic center, Sierra La Primavera, Jalisco, Mexico. *Cont. Min. Petrol., 77, 129-149.*

Mahood, G. & Hildreth, W. 1983. Large partition coefficients for trace elements in high-silica rhyolites. *Geochim. Cosmochim. Acta, 47, 11-30.*

Manning, D.D.C. 1981. The effects of flurine on liquidus phase relationships in the system Qz-Ab-Or with excess water at 1 kb. *Cont. Min. Petrol., 76, 206-215.*

Matsuhisa, Y. 1979. Oxygen isotopic composition of volcanic rocks from the East Japan island arcs and their bearing on petrogenesis. *J. Volcanol. Geotherm. Res., 5, 271-286.*

Matsuhisa, Y. & Kurasawa, H. 1983. Oxygen and strontium isotopic characteristics of calcalkaline volcanic rocks from the central and western Japan arcs: evaluation of contribution of crustal component to the magmas. *J. Volcanol. Geotherm. Res., 18, 483-510.*

Maury, R.C. & Bizouard, H. 1974. Melting of acid xenoliths into a basanite: An approach to the possible mechanism of crustal contamination. *Cont. Min. Petrol., 48, 275-286.*

Maxcon, J.H. 1936. Turkiyenin krater golu Nemrut. *M.T.A. Mecmuasi Sene 1, Sayi 5.*

McBirney, A.R. 1980. Mixing and unmixing of magmas. *J. Volcanol. Geotherm. Res., 7, 357-371.*

McBirney, A.R. 1984. *Igneous Petrology. Freeman, Cooper, San Francisco, 509p.*

McBirney, A.R., Baker, B.H. & Nilson, R.H. 1985. Liquid fractionation. Part I: Basic principles and experimental simulations. *J. Volcanol. Geotherm. Res., 24, 1-24.*

McKenzie, D. 1976. The East Anatolian Fault: a major structure in Eastern Turkey. *Earth Planet. Sci. Lett., 29, 189-193.*

McKenzie, D.P. 1972. Active tectonics of the Mediterranean region. *Geophys. J.R. Astr. Soc., 30, 109-185.*

McLennan, S.M. 1989. Rare earth elements in sedimentary rocks: influence of provenance and sedimentary processes. *In:* Lipin, B.R. & McKay, G.A. (eds) *Geochemistry and Mineralogy of Rare Earth Elements. Min. Soc. Am., Rev. Min., 21, 169-200.*

McLennan, S.M., Nance, W.B. & Taylor, S.R. 1980. Rare earth element-thorium correlations in sedimentary rocks, and the composition of the continental crust. *Geochim. Cosmochim. Acta., 44, 1833-1840.*

McLennan, S.M., Taylor, S.R., McCulloch, M.T. & Maynard, J.B. 1990. Geochemical and Nd-Sr isotopic composition of deep sea turbidites: Crustal evolution and plate tectonic association. *Geochem. Cosmochim. Acta, 54,2015-2050*

McLennan, S.M., Taylor, S.R. & McGregor, V.R. 1984. Geochemistry of Archean metasedimentary rocks from west Greenland. *Geochim. Cosmochim. Acta., 48, 1-13.*

McMillan, N.J., Harmon, R.S., Moorbath, S., Lopez-Escobar, L. & Strong, D.F. 1989. Crustal sources involved in continental arc volcanism: A case study of volcan Mocho-Choshuenco, southern Chile. *Geology, 17, 1152-1156.*

Mensing, T.M., Faure, G., Jones, L.M., Bowman, J.R. & Hoefs, J. 1984. Petrogenesis of the Kirkpatrick Basalt, Solo Nunatak, North Victoria Land, Antartica. *Cont. Min. Petrol., 87, 101-108.*

Menzies, M. & Murthy, V.R. 1980a. Nd and Sr isotope geochemistry of hydrous mantle nodules and their host alkali basalts: Implications for local heterogeneties in metasomatically veined mantle. *Earth Planet. Sci. Lett., 46, 323-334.*

Menzies, M. & Murthy, V.R. 1980b. Mantle metasomatism as precursor to genesis of alkali magmas: Isotopic evidence. *Am. J. Sci., 280A, 622-638.*

Menzies, M.A. & Kyle, P.R. 1990. Continental volcanism: a crust-mantle probe. *In:* Menzies, M.A. (eds) *Continental Mantle. Clarendon Press, Oxford, 157-177.*

Menzies, M.A., Leeman, W.P. & Hawkesworth, C.J. 1984. Geochemical and isotopic evidence for the origin of continental flood basalts with particular reference to the Snake River Plain and Columbia River. *Phil. Trans. Roy. Soc. London, A310, 643-660.*

Merzbacher, C. & Eggler, D.H. 1984. A magmatic geohygrometer: application to Mount St. Helens and other dacitic magmas. *Geology, 12, 587-590.*

Michard, A., Whitechurch, H., Ricou, L.E., Montigny, R. & Yazgan, E. 1984. Tauric subduction(Malatya-Elazig province) and its bearing on tectonics of the Tethyan realmin Turkey. *In:* Robertson, A.H.F. & Dixon, J.E. (eds) *The Geological Evolution of the Eastern Mediterranean. Blackwell, Oxford, 361-373.*

Middlemost, E.A.K. 1980. A contribution to the nomenclature and classification of volcanic rocks. *Geol. Mag., 117(1), 51-57.*

Middlemost, E.A.K. 1988. *Magmas and Magmatic rocks: An Introduction to Igneous Petrology. Longman and Wiley, New York, 266p.*

Miller, C.F. & Mittlefehldt, D.W. 1982. Depletion of light rare earth elements in felsic magmas. *Geology, 10, 129-133.*

Minster, J.F. & Allegre, C.J. 1978. Systematic use of trace elements in igneous processes. Part III: Inverse problem of batch partial melting in volcanic studies. *Cont. Min. Petrol., 68, 37-52.*

Miyashiro, A. 1974. Volcanic rock series in island arcs and active continental margins. *Am. J. Sci., 274, 321-355.*

Moorbath, S. & Thompson, R.N. 1980. Strontium isotope geochemistry and petrogenesis of the early Tertiary lava pile of the Isle of Skye, Scotland, and other basic rocks of the British Tertiary Province: an example of magma-crust interaction. *J. Petrol., 21, 2, 295-321.*

Morimoto, M. 1988. Nomenclature of pyroxenes. *Min. Mag., 52, 535-550.*

Muehlenbachs, K. 1986. Alteration of the oceanic crust and the ^{18}O history of sea water. *In:* Valley, J.W., Taylor, H.P. & O'Neil, J.R. (eds) *Stable Isotopes in High Temperature Geological Processes. Min. Soc. Am. Rev. Min., 16, 425-444.*

Muehlenbachs, K. & Byerly, G. 1982. ^{18}O-enrichment of silicic magmas caused by fractional crystallization at the Galapagos spreading center. *Cont. Min. Petrol., 79, 76-79.*

Muehlenbachs, K. & Clayton, R.N. 1972. Oxygen isotope geochemistry of submarine greenstones. *Can. J. Earth. Sci., 9, 471-478.*

Muehlenbachs, K. & Kushiro, I. 1974. Oxygen isotope exchange and equilibrium of silicates with CO_2 or O_2. *Carnegie Inst. Washington Yearb., 73, 232-236.*

Musselwhite, D.S., DePaolo, D.J. & McCurry, M. 1989. The evolution of a silicic magma system: Isotopic and chemical evidence from the Woods, Mountains volcanic centre, eastern California. *Cont. Min. Petrol., 101, 19-29.*

Myers, R.E. & Breitkopf, J.H. 1989. Basalt geochemistry and tectonic settings: A new approach to relate tectonic and magmatic processes. *Lithos, 23, 53-62.*

Mysen, B.O. & Kushiro. 1977. Compositional variations of coexisting phases with degree of melting of peridotite in the upper mantle. *Am. Min., 62, 843-865.*

Nagasawa, H. 1970. Rare earth concentrations in zircons and apatites and their host dacites and granites. *Earth Planet. Sci. Lett., 9, 359-364.*

Nagashima, K., Miyawaki, R., Takase, J., Nakai, I., Sakurai, K., Matsubara, S., Kato, A. & Iwano, S. 1986. Kimuraite, $CaY_2(CO_3)_4$ $6H_2O$, a new mineral from fissures in an alkali olivine basalt from Soga Prefecture, Japan, and new data on lokkaite. *Am. Min., 72, 1028-1033.*

Nakada, S. 1991. Magmatic processes in titanite-bearing dacites, central Andes of Chile and Bolivia. *Am. Min., 76, 548-560.*

Nakamura, Y. 1973. Origin of sector-zoning in igneous clinopyroxenes. *Am. Min., 58, 986-990.*

Nakamura, Y. & Kushiro, I. 1970a. Compositional relations of coexisting orthopyroxene, pigeonite and augite in a tholeiitic andesite from Hakone volcano. *Cont. Min. Petrol., 26, 265-275.*

Nash, W.P. & Crecraft, H.R. 1985. Partition coefficients for trace elements in silicic magmas. *Geochim. Cosmochim. Acta, 49, 2309-2332.*

Nelson, D.O., Nelson, K.L., Reeves, K.D. & Mattison, G.D. 1987a. Geochemistry of Tertiary alkaline rocks of the eastern Trans-Pecos magmatic province, Texas. *Cont. Min. Petrol., 97, 72-92.*

Nelson, S.T. & Montana, A. 1992. Sieve-textured plagioclase in volcanic rocks produced by rapid decompression. *Am. Min., 77, 1242-1249.*

Nesbitt, H.W., Markovics, G. & Price, R.C. 1980. Chemical processes affecting alkalis and alkaline earth during continental weathering. *Geochim. Cosmochim. Acta, 44, 1659-1666.*

Nesbitt, H.W. & Young, G.M. 1982. Early Proterozoic climates and plate motions inferred from major element chemistry of lutites. *Nature, 299, 715-717.*

Newhall, C.G. & Melson, W.G. 1983. Explosive activity associated with the growth of volcanic domes. *J. Volcanol. Geotherm. Res., 17, 111-131.*

Nicholls, I.A. 1971. Petrology of Santorini volcano, Cyclades Greece. *J. Petrol., 12, 67-119.*

Nicholls, I.A. & Harris, K.L. 1980. Experimental rare earth element partition coefficients for garnet, clinopyroxene and amphibole coexisting with andesitic and basaltic liquids. *Geochim. Cosmochim. Acta, 44, 287-308.*

Nixon, G.T. 1988a. Petrology of the Younger andesites and dacites of Iztaccihuatl Volcano, Mexico: I. Disequilibrium phenocryst assemglages as indicators of magma chamber processes. *J. Petrol., 29, 213-264.*

Nixon, G.T. & Pearce, T.H. 1987. Laser-interforemetry study of oscillatory zoning in plagioclase: The record of magma mixing and phenocryst recycling in calc-alkaline magma chambers, Iztaccihuatl volcano, Mexico. *Am. Min., 72, 1144-1162.*

Noble, D.C., Bowman, H.R., Hebert, A.J., Silberman, M.L., Heropoulos, C.E., Fabbi, B.P. & Hedge, C.E. 1975. Chemical and isotopic constraints on the origin of low-silica latite and andesite from the Andes of Central Peru. *Geology, 3, 501-504.*

Noble, D.C., Vogel, T.A., Peterson, P.S., Landis, G.P., Grant, N.K., Jazek, P.A. & McKee, E.H. 1984. Rare-element-enriched, S-type ash-flow tuffs containing phenocrysts of muscovite, andalusite and sillimanite, southeastern Peru. *Geology, 12, 35-39.*

Nockolds, S.R. & Allen, R. 1953. The geochemistry of some igneous rock series. *Geochim. Cosmochim. Acta, 4, 105-142.*

Norman, M.D. & Leeman, W.P. 1990. Open-system magmatic evolution of andesites and basalts from the Salman Creek volcanics, southern Idaho, U.S.A. *Chem. Geol., 81, 3, 167-189.*

Norrish, K. & Chappell, B.W. 1977. X-ray fluorescence spectrometry. *In:* Zussman, J. (eds) *Physical Methods in Determinative Mineralogy. Academic Press, London, 201-272.*

Nowroozi, A.A. 1972. Focal mechanism of earthquakes in Persia, Turkey, west Pakistan and Afghanistan and plate tectonics of the Middle East. *Bull. Seismol. Soc. Am., 62, 832-850.*

O'Brien, H.E., Irving, A.J. & McCallum, I.S. 1988. Complex zoning and resorption of phenocrysts in mixed potassic mafic magmas of the Highwood Mountains, Montana. *Am. Min., 73, 1007-1024.*

O'Hara, M.J. 1968. The bearing of phase equilibria studies in synthetic and natural systems on the origin and evolution of basic and ultrabasic rocks. *Earth Sci. Rev., 4, 69-133.*

O'Hara, M.J. 1977. Geochemical evolution during fractional crystallization of periodically refilled magma chamber. *Nature, 266, 503-507.*

O'Hara, M.J. & Mathews, R.E. 1981. Geochemical evolution in an advancing, periodically replenished, periodically tapped, continuously fractionated magma chamber. *J. Geol. Soc. London, 138, 237-277.*

O'Neill, J.R. 1986. Theoretical and experimental aspects of isotopic fractionation. *In:* Valley, J.W., Taylor, H.P. & O'Neil, J.R. (eds) *Stable Isotopes in High Temperature Geological Processes. Min. Soc. Am. Rev. Min., 16, 1-40.*

Olesch, M. 1979. Ca-bearing phlogopite: Synthesis and solid solubility at high temperatures and pressures of 5 and 10 kilobars. *Bulletin de Mineralogie, 102, 14-20.*

Ongur, T., Karamanderesi, I.H., Unlu, M.R., Suludere, Y. & Yogurtcuoglu, A. 1974. Diyadin-Ercis jeotermal arastirma sahalarinin jeolojisine iliskin on rapor. *M.T.A.,*

Ormerod, D.S., Hawkesworth, C.J., Leeman, W.P. & Menzies, M.A. 1988. The identification of subduction-related and within-plate components in basalts from the western U.S.A. *Nature, 333, 349-353.*

Orton, G. 1992. Geochemical correlation of Ordovician flow tuffs in North Wales. *Geol. Journal, 27, 317-338.*

Osborn, E.F. 1962. Reaction series of subalkaline igneous rocks based on different oxygen pressure conditions. *Am. Min., 47, 211-226.*

Ozpeker, I. 1973. Nemrut yanardaginin volkanolojik incelenmesi. *Tubitak 4.Bilim Kongresi Yerbilimleri Seksiyonu Tebligler Kitabi, 1-17.*

Pankhurst, R.J. 1977. Open system fractionation and incompatible element variation in basalts. *Nature, 268, 36-38.*

Patchett, P.J. 1991. Isotope geochemistry and chemical evolution of the mantle and crust. *Rev. Geophys., 29, 457-470.*

Pearce, J.A. 1982. Trace element characteristics of lavas from destructive plate margins. *In:* Thorpe, R.S. (eds) *Andesites: Orogenic Andesites and Related Rocks. John Wiley, New York, 525-548.*

Pearce, J.A. 1983. Role of the sub-continental lithosphere in magma genesis at active continental margins. *In:* Hawkesworth, C.J. & Norry, M.J. (eds) *Continental Basalts and Mantle Xenoliths. Shiva, Cheshire, 230-249.*

Pearce, J.A., Bender, J.F., De Long, S.E., Kidd, W.S.F., Low, P.J., Guner, Y., Saroglu, F., Yilmaz, Y., Moorbath, S. & Mitchell, J.G. 1990. Genesis of collision volcanism in Eastern Anatolia, Turkey. *J. Volcanol. Geotherm. Res., 44, 189-229.*

Pearce, J.A. & Cann, J.R. 1973. Tectonic setting of basic volcanic rocks determined using trace element analyses. *Earth Planet. Sci. Lett., 19, 290-300.*

Pearce, J.A., Harris, N.B.W. & Tindle, A.G. 1984. Trace element discrimination diagrams for the tectonic interpretation of granitic rocks. *J. Petrol., 25, 956-983.*

Pearce, J.A. & Norry, M.J. 1979. Petrogenetic implications of Ti, Zr, Y, Nb variations in volcanic rocks. *Cont. Min. Petrol., 69, 33-47.*

Pearce, T.H. & Kolisnik, A.M. 1990. Observations of plagioclase zoning using interference imaging. *Earth Sci. Rev., 29, 9-26.*

Pearce, T.H., Russell, J.K. & Wolfson, I. 1987. Laser-interference and Nomarski interference imaging of zoning profiles in plagioclase from the May 18, 1980, eruption of Mount St. Helens. *Am. Min., 72, 1131-1143.*

Peccerillo, A. & Taylor, S.R. 1976. Geochemistry of Eocene calc-alkaline volcanic rocks from the Kastamonu area, Northern Turkey. *Cont. Min. Petrol., 58, 63-91.*

Perfit, M.R., Gust, D.A., Bence, A.R., Arculus, R.J. & Taylor, S.R. 1980. Chemical characteristics of island arc basalts: Implications for mantle sources. *Chem. Geol., 30, 227-256.*

Pettijohn, F.J., Potter, P.E. & Siever, R. 1973. *Sand and Sandstone. Springer-Verlag, Berlin, 617p.*

Philpotts, J.A. & Schnetzler, C.C. 1970. Phenocryst-matrix partition coefficients for K, Rb, Sr and Ba with applications to anorthosite and basalt genesis. *Geochim. Cosmochim. Acta, 34, 307-322.*

Pichavant, M., Boher, M., Stenger, J.F., Aissa, M. & Charoy, B. 1987b. Relations de phases des granites de Beavoir entre 1 et 3 kbar en conditions de saturation en H_2O. *Geol. France, 2-3, 77-86.*

Pichavant, M., Kontak, D.J., Briqueu, L., H.J., V. & Clark, A.H. 1988. The Miocene-Pliocene Macusani volcanics, SE Peru. II. Geochemistry and origin of a felsic peraluminous magma. *Cont. Min. Petrol., 100, 325-338.*

Pichavant, M. & Montel, J.M. 1988. Petrogenesis of a two-mica ignimbrite suite: the Macusani Volcanics, SE Peru. *Trans. Roy. Soc. Edinburg Earth Sci., 79, 197-207.*

Pichavant, M., Valencia Herrera, J., Boulmier, S., Briqueu, L., Joron, J.L., Juteau, M., Marin, L., Michard, A., S.M.F., S., Treuil, M. & Venet, M. 1987a. The Macusani glasses, SE Peru: evidence of chemical fractionation in peraluminous magmas. *In:* Mysen, B.O. (eds) *Magmatic Processes: Physicochemical Principles. Geochem. Soc. Spec. Publ., 1, 359-373.*

Pineau, F., Javoy, M., Hawkins, J.W. & Craig, H. 1976. Oxygen isotope variations in marginal basin and ocean-ridge basalts. *Earth Planet. Sci. Lett., 28, 299-307.*

Powell, R. 1984. Inversion of the assimilation and fractional crystallization(AFC) equations; characterization of contaminants from isotope and trace element relationships in volcanic suites. *J. Geol. Soc. London, 141, 447-452.*

Presnall, D.C., Dixon, S.A., Dixon, J.R., O'Donnell, T.H., Drennes, N.L., Schrick, R.L. & Dycus, D.W. 1978. Liquidus phase relations on the join diopside-forsterite-anorthite from 1 atm to 20 kb: Their bearing on the generation and crystallization of basaltic magma:. *Cont. Min. Petrol., 66, 203-220.*

Prestvik, T. 1980. Petrology of hybrid intermediate and silicic rocks from Oraefajokull, southeast Iceland. *Geol. Foreningens Stockholm Forhandl., 101, 299-307.*

Puchelt, H. & Emmermann, R. 1976. Bearing of rare earth patterns of apatites from igneous and metamorphic rocks. *Earth Planet. Sci. Lett., 31, 279-286.*

Pushkar, O., McBirney, A.R. & Kudo, A.M. 1972. The isotopic composition of strontium in Central American ignimbrites. *Bull. Volc., 35, 265-294.*

Ragland, P.C. 1989. *Basic Analytical Petrology. Oxford University Press, New York, 369p.*

Rapp, R.P., Watson, E.B. & Miller, C.F. 1991. Partial melting of amphibolite/eclogite and the origin of Archean trondhjemites and tonalites. *Precam. Res., 51, 1-25.*

Reagan, M.K., Gill, J.B., Malavassi, E. & Garcia, M.O. 1987. Changes in magma composition at Areal volcano, Costa Rica, 1968-1985: real-time monitoring of open-system differentiation. *Bull. Volc., 49, 1, 415-434.*

Reeder, R.J. & Grams, J.C. 1987. Sector zoning in calcite cement crystals: implications for trace element distributions in carbonates. *Geochim. Cosmochim. Acta, 51, 187-194.*

Reid, J.B., Evans, O.L. & Fates, D.G. 1983. Magma mixing in granitic rocks of the central Sierra Nevada, California. *Earth Planet. Scie Lett., 66, 243-261.*

Righter, K. & Carmichael, I.S.E. 1992. Hawaiites and related lavas in the Atenguillo graben, western Mexican Volcanic Belt. *Geol. Soc. Am. Bull., 104, 1592-1607.*

Riley, J.P. 1958. Simultaneous determination of water and carbon dioxide in rocks and minerals. *Analyst, 83/982, 42-49.*

Rimsaite, J. 1964. On micas from magmatic and metamorphic rocks. *Beitrage zur Mineralogie und Petrographie, 10, 152-183.*

Ringwood, A.E. 1975. *Composition and petrology of the Earth's Mantle. McGraw-Hill, New York, 618p.*

Ritchey, J.L. & Eggler, D.H. 1978. Amphibole stability in a differentiated calc-alkaline magma chamber: an experimental investigation. *Carnegie Inst. Washington Yearb., 77, 790-793.*

Robert, J.L. 1976. Titanium solubility in synthetic phlogopite solid solution. *Chem. Geol., 17, 213-227.*

Roberts, M.P. & Clemens, J.D. 1993. Origin of high-potassium, calc-alkaline, I-type granitoids. *Geology, 21, 825-828.*

Robertson, A.H.F. & Aktas, A.H.F. 1984. The Maden Complex, SE Turkey: evolution of a neotethyan active margin. *In:* Robertson, A.H.F. & Dixon, J.E. (eds) *The Geological Evolution of the Eastern Mediterranean. Blackwell, Oxford, 375-402.*

Roeder, P.L. 1974. Activity of iron and olivine solubility in basaltic liquids. *Earth Planet. Sci. Lett., 23, 397-410.*

Roeder, P.L. & Emslie, R.F. 1970. Olivine-liquid equilibrium. *Cont. Min. Petrol., 29, 275-289.*

Rogers, G. & Hawkesworth, C.J. 1989. A geochemical traverse across the North Chilean Andes: evidence for crust generation from the mantle wedge. *Earth Planet. Sci. Lett., 91, 271-285.*

Rogers, N.W., Hawkesworth, C.J., Mattey, D.P. & Harmon, R.S. 1987. Sediment subduction and the source of potassium in orogenic leucitites. *Geology, 15, 451-453.*

Rogers, N.W., Hawkesworth, C.J., Parker, R.J. & Marsh, J.S. 1985. The geochemistry of potassic lavas from Vulsini, central Italy, and implications for mantle enrichment processes beneath the Roman region. *Cont. Min. Petrol., 90, 244-257.*

Romick, J.D. 1987. Amphibole fractionation and magma mixing in andesites and dacites from the central Aleutians, Alaska. *Trans. Am. Geophy. Un.(EOS), 68, 461.*

Romick, J.D., Kay, S.M. & Kay, R.W. 1992. The influence of amphibole fractionation on the evolution of calcalkaline andesite and dacite tephra from the central Aleutians, Alaska. *Cont. Min. Petrol., 112, 101-118.*

Roser, B.P. & Korsch, R.J. 1988. Provenance signatures of sandstone-mudstone suites determined using discrimination function analysis of major element data. *Chem. Geol., 67, 119-139.*

Ross, M., Bence, A.E., Dwornik, E.J., Clark, J.R. & Papike, J.J. 1970. Mineralogy of the lunar clinopyroxene, augite and pigeonite. *Geochim. Cosmochim. Acta, 34, 1, 839-848.*

Rotstein, Y. & Kafka, A.L. 1982. Seismotectonics of the southern boundary of Anatolia, Eastern Mediterranean region: subduction, collision and arc jumping. *J. Geophys. Res., 87, 7694-7706.*

Rutherford, M.J. & Devine, J. 1986. Experimental petrology of recent Mount St. Helens dacites: amphibole, Fe-Ti oxides and magma chamber conditions. *Geol. Soc. Am. Abst. with. Prog., 18, 736.*

Rutherford, M.J. & Devine, J.D. 1988. The May 18, 1980 eruption of Mt. St. Helens: 3. stability and chemistry of amphibole in the magma chamber. *J. Geophys. Res., 93, 11949-11959.*

Rutherford, M.J., Sigurdsson, H., Carey, S. & Davis, A. 1985. The May 18, 1980 eruption of Mt. St. Helens; Melt, composition and experimental phase equilibra. *J. Geophys. Res., 90, 2929-2947.*

Sack, R.O., Walker, D. & Carmichael, I.S.E. 1987. Experimental petrology of alkalic lavas: Constraints on cotectics of multiple saturation in natural basic liquids. *Cont. Min. Petrol., 96, 1-23.*

Sarna-Wojcick, A.M., Morrison, S.D., Meyer, C.E. & Hillhouse, J.W. 1987. Correlation of upper Cenozoic tephra layers between sediments of the western United States and eastern Pacific ocean and comparison with biostratigraphic and magnetostratigraphic ice age data. *Geol. Soc. Am. Bull., 98, 207-223.*

Sarna-Wojcicki, A.M., Shipley, S., Waitt, R.B., Dzurisin, D. & Wood, S.H. 1981. Areal distribution, thickness, mass, volume and grain-size of air-fall ash from the six major

eruptions of 1980. *In:* Lipman, P.W. & Mullineaux, D.R. (eds) *U.S. Geol. Surv. Prof. Paper, 1250, 577-600.*

Saroglu, F. & Guner, Y. 1979. Tutak Fayi. *Yeryuvari ve Insan, 1/3, 11-15.*

Saroglu, F. & Guner, Y. 1981. Dogu Anadolu'nun jeomorfolojik gelisimine etki eden ogeler; jeomorfoloji, tektonik, volkanizma iliskileri. *Turkiye Jeoloji Kurumu Bulteni, 24, 2, 39-50.*

Saroglu, F., Guner, Y., Kidd, W.S.F. & Sengor, A.M.C. 1980. Neotectonics of Eastern Turkey: new evidence for crustal shortening and thickening in a collision zone. *Trans. Am. Geophys. Un.(EOS), 61, 17, 360.*

Saroglu, F. & Yilmaz, Y. 1984. Dogu Anadolu'nun Neotektonigi ve ilgili magmatizmasi. *Turkiye Jeoloji Kurumu Ketin Simpozyumu Bildiriler Kitabi, 149-162.*

Sato, H. 1975. Diffusion coronas around quartz xenocrysts in andesite and basalts from Tertiary volcanic region in northeastern Shikoku, Japan. *Cont. Min. Petrol., 50, 49-64.*

Saunders, A.D., Tarney, J. & Weaver, S.D. 1980. Transverse geochemical variations across the Antarctic Peninsula: Implications for the genesis of calcalkaline magmas. *Earth Planet. Sci. Lett., 46, 344-360.*

Savci, G. 1980. Dogu Anadolu volkanizmasinin neotektonik onemi. *Yeryuvari ve Insan, 5, 3-4, 46-49.*

Sawyer, E.W. 1986. The influence of source rock type, chemical weathering, and sorting on the geochemistry of clastic sediments from the Quetico metasedimentary belt, Superior Province, Canada. *Chem. Geol., 55, 77-95.*

Schairer, J.R. & Boyd, F.R. 1957. Pyroxenes: The join $MgSiO_3$-$CaMgSi_2O_6$. *Carnegie Inst. Washington, Ann. Rept. Dir.Geophys. Lab., 223-225.*

Schilling, J.G. 1971. Sea-floor evolution: rare earth evidence. *Phil. Trans. R. Soc. London., A268, 663-706.*

Schilling, J.G. & Whinchester, J.W. 1969. Rare earth contribution to the origin of Hawaiian lavas. *Cont. Min. Petrol., 23, 27-37.*

Schmid, R. 1981. Descriptive nomenclature and classification of pyroclastic deposits and fragments: recommendations of the IUGS subcommission on the systematics of igneous rocks. *Geology, 9, 41-43.*

Schnetzler, C.C. & Philpotts, J.A. 1970. Partition coefficients of rare earth elements between igneous matrix material and rock-forming mineral phenocrysts-II. *Geochim. Cosmochim. Acta, 34, 331-340.*

Schock, H.H. 1979. Distribution of rare-earth and other trace elements in magnetites. *Chem. Geol., 26, 119-133.*

Schreyer, W., Massonne, H.J. & Chopin, C. 1987. Continental crust subducted to depth near 100 km: implications for magma and fluids genesis in collision zones. *In:* Mysen, B.O. (eds) *Magmatic Processes: Physicochemical Principles. Geochem. Soc. Spec. Publ., 1, 155-163.*

Schumacher, J.C. 1991. Empirical ferric iron correction: necessity, assumptions, and effects on selected geothermobarometers. *Min. Mag., 55, 3-18.*

Sekine, T., Katsura, T. & Aramaki, S. 1979. Water saturated phase relations of some andesites with application to the estimation of the initial temperature and water pressure of the time of eruption. *Geochim. Cosmochim. Acta, 43, 1367-1376.*

Sengor, A.M.C. 1976. Collision of irregular continental margins: Implications for foreland deformation of Alpine-type orogens. *Geology, 4, 779-782.*

Sengor, A.M.C. & Kidd, W.S.F. 1979. Post-collisional tectonics of the Turkish-Iranian plateau and a comparison with Tibet. *Tectonophysics, 55, 361-376.*

Sengor, A.M.C. & Yilmaz, Y. 1981. Tethyan evolution of Turkey: a plate tectonic approach. *Tectonophysics, 75, 181-241.*

Senior, A. & Leake, B.E. 1978. Regional metasomatism and the geochemistry of the Dalradian metasediments of Connemara, western Ireland. *J. Petrol., 19, 585-625.*

Sewell, R.J., Darbyshire, D.P.F., Langford, R.L. & Strange, P.J. 1992. Geochemistry and Rb-Sr geochronology of Mesozoic granites from Hong-Kong. *Trans. R. Soc. Edinburg Earth Sci., 83, 269-280.*

Shand, S.J. 1947. *Eruptive Rocks. Their Genesis, Composition, Classification, and their Relation to Ore-Deposits. John Wiley, New-York, 488p.*

Shau, Y.-H., Yang, H.-Y. & Peacor, D.R. 1991. On oriented titanite and rutile inclusions in sagenitic biotite. *Am. Min., 76, 1205-1217.*

Shaw, D. 1968. A review of K-Rb fractionation trends by covariance analysis. *Geochim. Cosmochim. Acta, 32, 573-602.*

Shaw, D.M. 1970. Trace element fractionation during anatexis. *Geochim. Cosmochim. Acta, 34, 237-259.*

Shelley, D. 1993. *Igneous and Metamorphic Rocks Under The Microscope. Chapman and Hall, London, 445p.*

Sheppard, S.M.F. & Harris, C. 1985. Hydrogen and oxygen isotope geochemistry of Ascension Island lavas and granites: variation with crystal fractionation and interaction with seawater. *Cont. Min. Petrol., 19, 1-71.*

Sheridan, M.F. & Marshall, J.P. 1983. Interpretation of pyroclast surface features using SEM images. *J. Volcanol. Geotherm. Res., 16, 153-159.*

Shimizu, N. & Arculus, R.J. 1975. Rare earth element concentrations in a suite of basanitoids and alkali olivine basalts from Grenada, Lesser Antilles. *Cont. Min. Petrol., 50, 231-240.*

Sibley, D.F., Vogel, T.A., Walker, B.M. & Byerly, G. 1976. The origin of oscillatory zoning in plagioclase: A diffusion and growth controlled model. *Am. J. Sci., 276, 275-284.*

Sieh, K. 1983. Most recent eruption of the Mono Craters, eastern central California. *Trans. Am. Geophys. Un.(EOS), 64, 8, 889.*

Sigurdsson, H. & Sparks, R.S.J. 1981. Petrology of rhyolitic and mixed magma ejecta from the 1875 eruption of Askja, Iceland. *J. Petrol., 22, 41-84.*

Smith, D.R. & Leeman, W.P. 1987. Petrogenesis of Mount St. Helens dacitic magmas. *J. Geophys. Res., 92, 10313-10334.*

Smith, J.V. & Brown, W.L. 1988. *Feldspar Minerals. Volume I, Springer-Verlag, Berlin, 828p.*

Smith, R.K. & Lofgren, G.E. 1983. An analytical and experimental study of zoning in plagioclase. *Lithos, 1, 153-168.*

Smith, R.L. 1979. Ash-flow magmatism. *In:* Chapin, C.E. & Elston, W.E. (eds) *Ash-Flow Tuffs. Geol. Soc. Am. Spec. Paper, 180, 5-27.*

Sonder, L.J., England, P.C., Wernicke, B.P. & Christiansen, R.L. 1987. A physical model for Cenozoic extension of western North America. *In:* Coward, M.P. (eds) *Continental Extension Tectonics. Geol. Soc. London Spec. Publ., 28, 187-201.*

Sparks, R.S.J. 1976. Grain size variations in ignimbrites and implications for the transport of pyroclastic flows. *Sedimentology, 23, 147-188.*

Sparks, R.S.J. 1978. Gas release rates from pyroclastic flows: an assessment of the role of fluidisation in their emplacement. *Bull. Volc., 41, 1-9.*

Sparks, R.S.J., Hupper, H.E. & Turner, J.S. 1984. The fluid dynamics of evolving magma chambers. *Phil. Trans. R. Soc. London, 310A, 511-534.*

Sparks, R.S.J. & Marshall, L. 1986. Thermal and mechanical constraints on magma mixing between mafic and silicic magmas. *J. Volcanol. Geotherm. Res., 29, 99-124.*

Sparks, R.S.J., Self, S. & Walker, G.P.L. 1973. Products of ignimbrite eruptions. *Geology, 1, 115-118.*

Sparks, R.S.J., Sigurdsson, H. & Wilson, L. 1977. Magma mixing: a mechanism for triggering acid explosive eruptions. *Nature, 257, 315-318.*

Sparks, R.S.J. & Wilson, L. 1976. A model for the formation of ignimbrite by gravitational column collapse. *J. Geol. Soc. London, 132, 441-451.*

Sparks, R.S.J., Wilson, L. & Sigurdsson, H. 1981. The pyroclastic deposits of the 1875 eruption of Askja, Iceland. *Phil. Trans. R. Soc. London, A299, 241-273.*

Spear, F.S. & Kimball, K. 1984. RECAMP-A FORTRAN IV program for estimating Fe^{+3} contents in amphiboles. *Comp. Geosci., 10, 317-325.*

Speer, J.A. 1984. Micas in igneous rocks. *In:* Bailey, S.W. (eds) *Micas. Min. Soc. Am. Rev. Min., 13, 299-356.*

Spencer, K.I. & Lindsley, D.H. 1981. A solution model for coexisting iron-titanium oxides. *Am. Min., 66, 1189-1201.*

Spulger, S.D. & Rutherford, M.J. 1983. The origin of rhyolite and plagiogranite in oceanic crust: An experimental study. *J. Petrol., 24, 1-25.*

St. Seymour, K., Vlassopoulos, D., Pearce, T.H. & Rice, C. 1990. The record of magma chamber processes in plagioclase phenocrysts at Thera Volcano, Aegean Volcanic Arc, Greece. *Cont. Min. Petrol., 104, 73-84.*

Stern, R.A., Hanson, G.N. & Shirey, S.B. 1989. Petrogenesis of mantle-derived, LILE-enriched Archean monzodiorites and trachyandesites(sanukitoids) in southwestern Superior Province. *Can. J. Earth Sci.,*

Stewart, D.C. 1975. Crystal clots in calc-alkaline andesites as breakdown products of high-Al amphiboles. *Cont. Min. Petrol., 53, 195-204.*

Stimac, J.A. & Pearce, T.H. 1992. Textural evidence of mafic-felsic magma interaction in dacite lavas, Clear Lake, California. *Am. Min., 77, 795-809.*

Stolper, E. 1980. A phase diagram for mid-ocean ridge basalts: Preliminary results and implications for petrogenesis. *Cont. Min. Petrol., 74, 13-24.*

Storey, M., Wolff, J.A., Norry, M.J. & Marriner, G.F. 1989. Origin of hybrid lavas from Aqua de Pau volcano, Sao Miguel, Azores. *In:* Saunders, A.D. & Norry, M.J. (eds) *Magmatism in the Ocean Basins. Geol. Soc. London Spec. Publ., 42, 161-180.*

Stormer, J.C. & Nicholls, J. 1978. XLFRAC: A program for the interactive testing of magmatic differentiation models. *Comp. Geosci., 4, 143-159.*

Streckeisen, A. 1979. Classification and nomenclature of volcanic rocks, lamprohyres, carbonatites, and melilitic rocks. Recommendations and suggestions of the IUGS Subcommision on the systematics of igneous rocks. *Geology, 7, 331-335.*

Stuckless, J.S. & O'Neil, J.R. 1973. Petrogenesis of the Superstition-Superior volcanic area as inferred from strontium and oxygen-isotope studies. *Geol. Soc. Am. Bull., 84, 1987-1998.*

Sun, S. & McDonough, W.F. 1989. Chemical and isotopic systematics of oceanic basalts: implications for mantle composition and processes. *In:* Saunders, A.D. & Norry, M.J. (eds) *Magmatism in the Ocean Basins. Geol. Soc. London Spec. Publ.,42, 313-345.*

Sun, S.S. 1980. Lead isotope study of young volcanic rocks from mid-ocean ridges, ocean islands and island arcs. *Phil. Trans. R. Soc. London., A297, 409-455.*

Sun, S.S. 1982. Chemical composition and origin of the earth's primitive mantle. *Geochim. Cosmochim. Acta, 47, 179-192.*

Sun, S.S. & Hanson, G.N. 1975. Evolution of mantle: Geochemical evidence from alkali basalt. *Geology, 3, 297-302.*

Sun, S.S. & Nesbitt, R.W. 1977. Chemical heterogeneity of the archean mantle, composition of the earth and mantle evolution. *Earth Planet. Sci. Lett., 44, 429-448.*

Sun, S.S., Nesbitt, R.W. & Sharaskin, A.Y. 1979. Geochemical characteristics of mid-ocean ridge basalts. *Earth Planet. Sci. Lett., 44, 119-138.*

Swanson, S.E., Naney, M.T. & Westrich, H.R. 1989. Crystallization history of Obsidian Dome, Inyo Domes, California. *Bull. Volc., 51, 161-176.*

Tait, S.R., Worner, G., Vanden Bogaard, P. & Schmincke, H.-U. 1989. Cumulative nodules as evidence for convective fractionation in a phonolite magma chamber. *J. Volcanol. Geotherm. Res., 37, 21-37.*

Taskin, C. 1984. Van-Ercis-Meydandagi-Bitlis-Adilcevaz-Harmantepe koyu Agri-Patnos Koseler koyu perlit sahalari hakkinda jeoloji ve teknoloji raporu. *M.T.A. Rap. No, 7563.*

Tatar, Y. 1975. Tectonic structures along the North Anatolian Fault Fault Zone, north west of Refahiye(Erzincan). *Tectonophysics, 29, 401-410.*

Tatsumi, Y., Hamilton, D.L. & Nesbitt, R.W. 1986. Chemical characteristics of fluid phase released from a subducted lithosphere and origin of arc magmas: evidence from high-pressure experiments and natural rocks. *J. Volcanol. Geotherm. Res., 29, 293-309.*

Taylor, H.P. 1987. Comparison of hydrothermal systems in layered gabbros and granites and the origin of low ^{18}O magmas. *In:* Mysen, B.O. (eds) *Magmatic Processes: Physicochemical Principles. Geochem. Soc. Spec. Publ.,1, 337-358.*

Taylor, H.P. & Sheppard, S.M.F. 1986. Igneous rocks: I. Processes of isotopic fractionation and isotope systematics. *In:* Valley, J.W., Taylor, H.P. & O'Neil, R.J. (eds) *Stable Isotopes in High-Temperature Geological Processes. Min. Soc. Am. Rev. Min., 16, 227-271.*

Taylor, H.P.J. 1968. The oxygen isotope geochemistry of igneous rocks. *Cont. Min. Petrol., 19, 1-71.*

Taylor, H.P.J. 1980. The effects of assimilation of country rocks by magmas on $^{18}O/^{16}O$ and $^{87}Sr/^{86}Sr$ systematics in igneous rocks. *Earth Planet. Sci. Lett., 47, 243-254.*

Taylor, S.R. & McLennan, S.M. 1981. The composition and evolution of the continental crust: rare earth element evidence from sedimentary rocks. *Phil. Trans. R. Soc. London, A301, 381-399.*

Taylor, S.R. & McLennan, S.M. 1988. The significance of the rare earths in geochemistry and cosmochemistry. *In:* Gschneidner, Jr.K.A. & Eyring, L. (eds) *Handbook on the Physics and Chemistry of Rare Earths. Elseiver,11, 485-580.*

Taylor, Y. & McLennan, S.M. 1985. *The Continental Crust: its Composition and Evolution. Blackwell, Oxford, 312p.*

Tchalenko, J.S. 1977. A reconnaissance of the seismicity and tectonics at the Northern border of the Arabian plate(Lake Van region). *Rev. Geogr. Phys. Geol. Dyn., 19, 189-208.*

Tera, F., Brown, L., Morris, J., Sacks, I.S., Klein, J. & Middleton, R. 1986. Sediment incorporation in island arc magmas: inferences from ^{10}Be. *Geochim. Cosmochim. Acta, 50, 535-550.*

Thompson, M. & Walsh, J.W. 1989. *Handbook of Inductively Coupled Plasma Spectrometry. Blackie, London, 316p.*

Thompson, R.N. 1982. Magmatism of the British Tertiary volcanic province. *Scott. J. Geol., 18, 1, 49-107.*

Thompson, R.N., Morrison, M.A., Hendry, G.L. & Parry, S.J. 1984. An assessment of the relative roles of crust and mantle in magma genesis: An elemental approach. *Phil. Trans. R. Soc. London, A310, 549-590.*

Thorpe, R.S., Francis, P.W. & O'Callaghan, L. 1984b. Relative roles of source composition, fractional crystallization and crustal contamination in the petrogenesis of Andean volcanic rocks. *Phil. Trans. R. Soc. London, A310, 675-692.*

Tindle, A.G. & Pearce, J.A. 1983. Assimilation and partial melting of continental crust: evidence from the mineralogy and geochemistry of autoliths and xenoliths. *Lithos, 16, 185-202.*

Tokel, S. 1979. Erzurum-Kars yoresinde Neojen cokuntusuyle ilgili volkanizmanin incelenmesi. *Docentlik tezi, Karadeniz Teknik Universitesi, 106p.*

Tokel, S. 1980a. Dogu Anadolu'da Neojen volkanizmasinin jeokimyasi. *Turkiye Jeoloji Kurumu 34. Turkiye Jeoloji Bilimsel ve Teknik Kurultayi Bildiri Ozetleri Kitabi, 33.*

Tokel, S. 1980b. Iz ve ana element ayirtman diyagramlariyla Anadolu'da Neojen volkanizmasinin tektonik yerlesiminin incelenmesi. *Tubitak 7. Bilim Kongresi Yerbilimleri Seksiyonu Bildiriler Kitabi, 1-10.*

Tokel, S. 1984. Dogu Anadolu'da kabuk deformasyon mekanizmasi ve genc volkanitlerin petrojenezi. *Turkiye Jeoloji Kurumu Ketin Simpozyumu Bildiriler Kitabi, 121-130.*

Toscani, L., Venturelli, G., Barbieri, M., Capedri, S., Fernandez Soler, J.M. & Oddone, M. 1990. Geochemistry and petrogenesis of two-pyroxene andesites from Sierra de Gata(Spain). *Min. Petrol., 41, 199-213.*

Treuil, M., Billhot, M., Varet, J. & Barberi, F. 1971. Distribution of nickel, copper and zinc in the volcanic series of Erta Ale, Ethiopia. *Cont. Min. Petrol., 30, 84-94.*

Treuil, M. & Varet, J. 1973. Criteres volcanologiques, petrologiques et geochimiques de le genese et de la defferenciation des magmas basaltiques: exemple de l'Afar. *Bull. Soc. Geol. Fr., XV, 5-6, 506-540.*

Trial, A.J. & Spera, F.J. 1990. Mechanism for the generation of compositional heterogeneities in magma chambers. *Geol. Soc. Am. Bull., 102, 353-367.*

Tronnes, R.G., Edgar, A.D. & Arima, M. 1985. A high pressure-high temperature study of TiO_2 solubility in Mg-rich phlogopite: Implications to phlogopite chemistry. *Geochim. Cosmochim. Acta, 49, 2323-2329.*

Tsuchiyama, A. 1985. Dissolution kinetics of plagioclase in melt of the system diopside-albite-anorthite and the origin of dusty plagioclase in andesites. *Cont. Min. Petrol., 84, 1-16.*

Tsuchiyama, A. & Takahashi, E. 1983. Melting kinetics of a plagioclase feldspar. *Cont. Min. Petrol., 84, 345-354.*

Turcotte, D.L. 1983. Mechanism of crustal deformation. *J. Geol. Soc. London, 140, 701-724.*

Turcotte, D.L. & Emerman, S.H. 1983. Mechanism of active and passive rifting. *Tectonophysics, 79, 39-50.*

Turkunal, S. 1980. *Dogu ve Guneydogu Anadolu'nun jeolojisi. TMMOB Jeoloji Muhendisleri Odasi Yayini, 8, Ankara, 60p.*

Turner, J.S. & Gufstafson, L.B. 1981. Fluid motions and compositional gradients produced by crystallization or melting at vertical boundaries. *J. Volcanol. Geotherm. Res., 11, 93-125.*

Tuttle, O.F. & Bowen, N.L. 1958. Origin of Granite in the light of experimental studies in the system $NaAlSi_3O_8$-$KAlSi_3O_8$-SiO_2-H_2O. *Geol. Soc. Am. Mem.,74, 153.*

Twist, D. & Harmer, R.E.J. 1987. Geochemistry of contrasting siliceous magmatic suites in the Bushveld complex: Genetic aspects and the implications for tectonic discrimination diagrams. *J. Volcanol. Geotherm. Res., 32, 83-98.*

Van Weering, T.C.E. & Klaver, G.T. 1985. Trace element fractionation and distribution in turbidites, homogeneous and pelagic deposits: the Zaire Fan, southeast Atlantic Ocean. *Geomarine Letters, 5, 165-170.*

Vance, J.A. 1965. Zoning in igneous plagioclase; patchy zoning. *J. Geol., 73, 636-651.*

Vance, J.A. 1969. On synneusis. *Cont. Min. Petrol., 24, 7-29.*

Veizer, J. & Demovic, R. 1974. Strontium as a tool in facies analysis. *J. Sed. Petrol., 44, 93-115.*

Velde, D. 1969. Les micas des lamprophyres: Kersantites, minettes et lamproites. *Bull. Soc. Fran. Min. Cristall., 92, 203-223.*

Verhoogen, J. 1962. Distribution of titanium between silicates and oxides in igneous rocks. *Am. J. Sci.,* 260, 211-220.

Vidal, P., Cocherie, A. & Le Fort, P. 1982. Geochemical investigation of the origin of the Manaslu leucogranite(Himalaya, Nepal). *Geochim. Cosmochim. Acta, 46, 2279-2292.*

Vielzeuf, D. & Halloway, J.R. 1988. Experimental determination of the fluid-absent melting relations in the pelitic system. Consequences for crustal differentiation. *Cont. Min. Petrol., 98, 257-276.*

Villemant, B., Jaffrezic, H., Joron, J.L. & Treuil, M. 1981. Distribution coefficients of major and trace elements; fractional crystallization in the alkali basalt series of Chaine des Puys(Massif Central, France). *Geochim. Cosmochim. Acta, 45, 1997-2016.*

Vogel, T.A., Younker, L.W., Wilband, J.T. & Kamplmueller, E. 1984. Magma mixing; the Marsco suite, Isle of Skye, Scotland. *Cont. Min. Petrol., 87, 231-241.*

Walker, D., Shibata, T. & Delong, S.E. 1979. Abyssal tholeiites from the Oceanographer Fracture Zone. II. Phase equilibria and mixing. *Cont. Min. Petrol., 70, 111-125.*

Walker, G. 1971. Grain-size characteristics of pyroclastic deposits. *J. Geol., 79, 696-714.*

Walker, G.P.L. 1973. Explosive volcanic eruptions-a new classification scheme. *Geol. Runds., 62, 431-446.*

Walker, G.P.L. 1980. The Taupo pumice; product of the most powerful known(ultraplinian) eruption?. *J. Volcanol. Geotherm. Res., 8, 69-94.*

Walker, G.P.L. 1983. Ignimbrite types and ignimbrite problems. *J. Volcanol. Geotherm. Res., 17, 65-88.*

Walker, G.P.L. & McBroom, L. 1983. Mount St. Helens 1980 and Mount Pelee 1902 -Flow or surge?. *Geology, 11, 575-577.*

Wallace, P. & Carmichael, I.S.E. 1989. Minette lavas and associated leucitites from the western front of the Mexican Volcanic Belt: Petrology, chemistry and origin. *Cont. Min. Petrol., 103, 470-492.*

Wanless, H.R. 1979. Limestone response to stress: Pressure solution and dolomitization. *J. Sed. Petrol., 49, 437-462.*

Warshaw, C.M. & Smith, R.L. 1988. Pyroxenes and fayalites in the Bandelier Tuff, New Mexico: temperatures and comparison with other rhyolites. *Am. Min., 73, 1025-1037.*

Watson, E.B. 1982. Basalt contamination by continental crust: Some experiments and models:. *Cont. Min. Petrol., 80, 73-87.*

Watson, E.B. & Green, T.H. 1981. Apatite/liquid partition coefficients for the rare earth elements and strontium. *Ibid., 56, 405-421.*

Watson, E.B. & Jurewicz, S.R. 1985. Behaviour of alkalies during diffusive interaction of granitic xenoliths with basaltic magma. *J. Geol., 92, 121-131.*

Watson, E.B. & Ryerson, F.J. 1986. Partitioning of zircon between clinopyroxene and magmatic liquids of intermediate composition. *Geochim. Cosmochim. Acta, 50, 2523-2526.*

Weber, J.N. 1964. Trace element composition of dolostones and dolomites and its bearing on the dolomite problem. *Geochim. Cosmochim. Acta, 28, 1817-1868.*

Webster, J.D. & Duffield, W.A. 1991. Volatiles and lithophile elements in Taylor Creek Rhyolite: constraints from glass inclusion analysis. *Am. Min., 76, 1628-1645.*

White, A.J.R. & Chappell, B.W. 1977. Ultrametamorphism and granitoid genesis. *Tectonophysics, 43, 7-22.*

White, A.J.R. & Chappell, B.W. 1983. Granitoid types and their distribution in the Lachlan fold belt, southeastern Australia. *Geol. Soc. Am. Mem., 159, 21-33.*

White, W.M. & Dupre, B. 1986. Sediment subduction and magma genesis in the Lesser Antilles: Isotopic and trace element constraints. *J. Geophys. Res., 91, 5927-5941.*

White, W.M. & Patchett, J. 1984. Hf-Nd-Sr isotopes and incompatible element abundances in island arcs: Implications for magma origins and crust-mantle evolution. *Earth. Planet. Sci. Lett., 67, 167-185.*

Whitham, A.G. & Sparks, R.S.J. 1986. Pumice. *Bull. Volc., 48, 209-223.*

Whitney, J.A. 1975. The effects of pressure, temperature, and XH_2O on phase assemblages in four synthetic rock compositions. *J. Geol., 83, 1-27.*

Wilson, C.J.N. & Walker, G.P.L. 1982. Ignimbrite depositional facies; the anatomy of a pyroclastic flow. *J. Geol. Soc. London, 139, 581-592.*

Wilson, L. 1980. Relationships between pressure, volatile content and ejecta velocity in three types of volcanic explosion. *J. Volcanol. Geotherm. Res., 8, 297-314.*

Wilson, L., Sparks, R.S.J., Huang, T.C. & Watkins, N.D. 1978. The control of volcanic column heights by eruption energetics and dynamics. *J. Volcanol. Geotherm. Res., 83, 1829-1836.*

Wilson, L., Sparks, R.S.J. & Walker, G.P.L. 1980. Explosive volcanic eruptions-IV. The control of magma properties and conduit geometry on eruption column behaviour. *Geophys. J. R. Astr. Soc., 63, 117-148.*

Winchester, J.A. & Floyd, P.A. 1977. Geochemical discrimination of different magma series and their differentiation products using immobile elements. *Chem. Geol., 20, 325-343.*

Windley, B.F. 1991. Early Proterozoic collision tectonics, and rapakivi granites as intrusions in an extensional thrust-thickened crust: The Ketilidian orogen. *Tectonophysics, 195, 1-10.*

Wohletz, K.H. 1983. Hydrovolcanic explosions II: Evolution of basaltic tuff rings and tuff cones. *Am. J. Sci., 283, 385-413.*

Wohletz, K.H. & Sheridan, M.F. 1979. A model of pyroclastic surge. *In:* Chapin, C.E. & Elston, W.E. (eds) *Ash Flow Tuffs. Geol. Soc. Am. Spec. Paper,180, 177-194.*

Wolff, J.A. 1985. Zonation, mixing and eruption of silica undersaturated alkaline magma: a case study from Tenerife, Canary Islands. *Geol. Mag., 122, 641-647.*

Wolff, J.A. & Storey, M. 1984. Zoning in highly alkaline magma bodies. *Geol. Mag., 121, 6, 563-575.*

Wolff, J.A., Worner, G. & Blake, S. 1990. Gradients in physical parameters in zoned felsic magma bodies: implications for evolution and eruptive withdrawal. *J. Volcanol. Geotherm. Res., 43, 37-55.*

Wones, D.R. 1989. Significance of the assemblage titanite+magnetite+quartz in granitic rocks. *Am. Min., 74, 744-749.*

Wood, D.A. 1979. A variably melted sub-oceanic upper mantle: genetic significance for mid-ocean ridge basalts from geochemical evidence. *Geology, 7, 499-503.*

Wood, D.A., Joron, J.L. & Treuil, M. 1979a. A Re-appraisal of use of trace elements to classify and discriminate between magma series erupted in different tectonic settings. *Earth Planet. Sci. Lett., 45, 326-336.*

Woodhead, J.D. 1989. Geochemistry of the Mariana arc(western Pacific): source composition and processes. *Chem. Geol., 76, 1-24.*

Woodhead, J.D., Harmon, R.S. & Fraser, D.G. 1987. O, S, Sr and Pb isotope variations in volcanic rocks from the Northern Mariana Islands. *Earth Planet. Sci. Lett., 83, 39-52.*

Worner, G. & Schmincke, H.-U. 1984. Mineralogy and chemical zonation of the Laacher See tephra sequence(East Eifel, Germany). *J. Petrol., 25, 805-835.*

Worner, G. & Wright, T.L. 1984. Evidence for magma mixing within the Laacher See magma chamber(east Eifel, Germany). *J. Volcanol. Geotherm. Res., 22, 301-327.*

Worner, G., Zindler, A., Staudigel, H. & Schminche, H.-U. 1986. Sr, Nd and Pb isotope geochemistry of Tertiary and Quaternary alkaline volcanics from West Germany. *Earth Planet. Sci. Lett., 79, 1-2, 107-119.*

Wrafter, J.P. & Graham, J.R. 1989. Ophiolitic detritus in the Ordovician sediments of south Mayo, Ireland. *J. Geol. Soc. London., 146, 213-215.*

Wright, J.V., Smith, A.L. & Self, S. 1980. A working terminology of pyroclastic deposits. *J. Volcanol. Geotherm. Res., 8, 315-336.*

Wronkiewicz, D.J. & Condie, K.C. 1987. Geochemistry of Archean shales from the Witwatersrand Supergroup, south Africa: source area, weathering and provenance. *Geochim. Cosmochim. Acta, 51, 2401-2416.*

Wyborn, L.A.I., Wyborn, D., Warren, R.G. & Drummand, B.J. 1992. Proterozoic granite types in Australia; implications for lower crust composition, structure and evolution. *Trans. Roy. Soc. Edinburg Earth Sci., 83, 201-209.*

Wyers, G.P. & Barton, M. 1986. Petrology and evolution of transitional alkaline-subalkaline lavas from Patmos, Dodecanesos, Greece: Evidence for fractional crystallization, magma mixing and assimilation. *Cont. Min. Petrol., 93, 297-311.*

Wyllie, P.J. 1977. Crustal anatexis: An experimental review. *Tectonophysics, 43, 41-71.*

Wyllie, P.J. 1983. Experimental studies on biotite- and muscovite-granites and some crustal magmatic sources. *In:* Atherton, M.P. & Gribble, C.D. (eds) *Migmatites, Melting and Metamorphism. Shiva, Cheshire, 12-26.*

Yagi, K. & Onuma, K. 1967. The join $CaMgSi_2O_6$-$CaTiAl_2O_6$ and its bearing on the titanaugites. *J. Fac. Sci. Hokkaido Univ. Ser. 4, Geol. Min., 13, 463-483.*

Yamamoto, K., Suigisaki, R. & Arai, F. 1986. Chemical aspects of the alteration of acidic tuffs and their application to siliceous deposits. *Chem. Geol., 55, 61-76.*

Yilmaz, Y. 1984. Turkiye'nin jeolojik tarihinde magmatik etkinlik ve tektonik evrimle iliskisi. *Turkiye Jeoloji Kurumu Ketin Simpozyumu Bildiriler Kitabi, 63-81.*

Yilmaz, Y. 1990. Comparisons of the young volcanic associations of Western and Eastern Anatolia under compressive regime. *J. Volcanol. Geotherm. Res., 44, 69-87.*

Yilmaz, Y., Saroglu, F. & Guner, Y. 1987. Initiation of the neomagmatism in East Anatolia. *Tectonophysics, 134, 177-199.*

Yoder, H.S., Stewart, D.B. & Smith, J.R. 1957. Ternary feldspars. *Garnegie Inst. Washington Yearb., 56, 206-214.*

Yoder, H.S.J. & Tilley, C.E. 1962. Origin of basaltic magmas. An experimental study of natural and synthetic rock systems. *J. Petrol., 3, 342-532.*

Zanettin, B. 1984. Proposed new chemical classification of volcanic rocks. *Episodes, 7, 19-20.*

Zielinski, R.A. 1982. The mobility of uranium and other elements during alteration of rhyolitic ash to montmorillonite: a case study in the Troublesome Formation, Colarodo, USA. *Chem. Geol., 35, 185-204.*

APPENDIX 1. ANALYTICAL TECHNIQUES

1.1. Powder preparation for whole-rock analysis

In all cases, fresh rock samples were collected. Any weathered surfaces were discharged and the remainder crushed to around 0.5 cm in hardened steel jaw crusher. After cone and quartering, approximately 100 g of crushed rock were powdered to 150 and 250 mesh in agate "Tema" mill.

1.2. Separation of minerals for O-isotope analysis

After crushing the rock at least to the mineral grain-size, the minerals were separated using a Frantz isodynamic magnetic separator followed by a repeated separation in tetra-bromethane with density adjustment. Periodic checks of purity were carried out using XRD technique.

1.3. X-ray fluorescence technique for major and trace element analysis

Energy dispersive X-ray fluorescence(EDXRF) techniques were used to analyse major elements and the trace elements. Major elements were analysed using glass discs, made by mixing 2 g of Johnson Mattey lithium tetraborate spectroflux with 0.375 g of rock powder, dried overnight at 105°C. This mixture was fused in a Pt-Au alloy crucible in muffle furnace at 1200°C for 20 minutes. Loss on ignition data were obtained by heating pre-dried rock powder in crucible at 1000°C for 20 minutes. Trace element analyses were performed on pressed powder pellets made by thoroughly mixing 6 g of rock powder with a binding agent(organic resin), compressing into a 3 cm diameter disc using a hydraulic press and drying at 105°C for 30 minutes.

Samples were analysed using a Phillips PW 1450/20 automatic sequential X-ray spectrometer at the University of Glasgow with Cr and Mo tube targets. This consisted of a low power(maximum 49 W) silver anode side window X-ray tube operated in pulsed mode with maximum setting of 49 kV or 1 mA, and a Si(Li) detector with resolution of 165 keV at 5.9 keV. The EDXRF was calibrated using international standards covering a wide range of compositions. For major elements glass discs were counted in duplicate for 500 seconds at 10 kV, 0.2 mA with no primary beam filter. Pressed powder pellets were counted twice for 800 seconds at 45 keV, 0.3 mA with a 127 μm silver primary beam filter. All major element analyses were performed on duplicate discs prepared and analysed within the same batch of sample. Data presented are averages of duplicate analyses. The average detection limits for major(wt.%) and trace elements(ppm) as follows: SiO_2(0.09), TiO_2(0.09), Al_2O_3(0.09), Fe_2O_3(0.05), MnO(0.01), MgO(0.17), CaO((0.01), Na_2O(0.16), K_2O(0.01), P_2O_5(0.02), Zr(3), Y(1), Sr(2), Rb(2), Th(12), Pb(12), Ga(2), Zn(2), Cu(4), Ni(5), Co(3), Cr(2), Ce(3), Ba(12), La(4), Nb(7).

1.4. Ferrous iron determination

Ferrous iron in rock powders was determined using the method of Pratt(1894). Approximately 0.5 g of sample in a Pt crucible was carefully dissolved in a 49% HNO_3 - 50% H_2SO_4 mixture on the hotplate at 160°C for 15 minutes and analyzed for FeO content using

titration by potassium dichromate with indication to sodium diphenylamine. Based on the repeated analysis of Glasgow laboratory standards, the precision of FeO determination is about 0.1 wt%.

1.5. Electron microprobe and scanning electron microscope studies

Electron microprobe analyses of the main rock-forming minerals carried out on diamond polished and carbon-coated thin sections using a Cambridge Microscan 5 instrument(EDS) at the University of Glasgow. In order to produce spot analyses a focused beam of 20 kV and 30 nA was used. A cobalt metal target was used as a drift monitor and the current response was normalized against natural wollastonite, jadeite and K-feldspar standards. Contents of Si, Ti, Fe, Mn, Mg, Ca, Na and K were calculated from integrals of their Kα peaks collected for 100s. ZAF corrections for atomic number(Z), x-ray absorption(A) and secondary fluorescence(F) were employed using a built-in computer program(Link Analytical). Mineral formulas were calculated by stochiometry on the basis of assumed number of oxygen(F, Cl, OH, ...) atoms in a unit cell.

The SEM study of some minerals was carried out on the same samples using a Cambridge Stereoscan 360 electron microscope at the University of Glasgow fitted with 4 quadrant BSE detector. A beam of 20 kV and probe current of 6-12 nA were used.

1.6. ICP-MS technique for REE determination

The decomposition procedure of the whole-rock samples was similar to that suggested by Thompson and Walsh(1989) using exclusively Aristar grade chemicals. Approximately 0.250 g of 250 mesh rock powder was weighed into a PTFE beaker and a mixture of 4 ml of 70% HNO_3 + 1 ml of 70% $HCLO_4$ + 10 ml of 48% HF was added. The beaker was then heated on the hotplate on the following scheme: covered with a PTFE lid for 3 hours at 120°C, uncovered for 3 hours at 160°C and uncovered for 10 hours at 210°C. Dry salts in a PFTE beaker were then dissolved in 5% HNO_3 and heated on the hotplate at 50°C for 30 minutes. Precipitated hydroxides and hydre-oxides of Fe^{+2} were dissolved by adding few drops of concentrated H_2O_2 and solution was diluted to 100 ml and transferred to polyethylene flasks.

For the REE analysis, a VG Plasma Quad-I ICP-MS instrument at the SURRC, East Kilbridge was used. The external standards were made up by diluting Johnson Mattey specpure REE solutions. ^{104}Ru, ^{187}Re and ^{115}In were used as internal standards. The periodic checks of accuracy made against international geological reference materials yielded satisfactory results. The limits of quantitation(in $\mu g\ g^{-1}$) for an open digestion and dilution factor of 500(Jarvis, 1988; Jarvis, 1992) are as follows; La(0.125), Ce(0.17), Pr(0.15), Nd(0.35), Sm(0.25), Eu(0.10), Gd(0.15), Tb(0.05), Dy(0.20), Ho(0.05), Er(0.10), Tm(0.02), Yb(0.10), Lu(0.10).

1.7. Mass spectrometry technique for Sr- and O-isotope studies

1.7.1. General chemistry

All chemical separation and analysis was performed in a laboratory with small positive pressure generated by an air make-up unit with particle filters. Sample dissolution were

performed in teflon beakers(Savillex) within laminar cupboard. Teflon laboratory were cleaned by thorough washing in distilled water, soaker for 24 hours in concentrated HNO_3, followed by soaking in distilled water for 24 hours on a hotplate. RO water is supplied from a Mili Q reverse osmosis purification system. HCl and HNO3 were double distilled in quartz stills and further purified in sub-boiling teflon stills(TD). HF and HBr were purified in similar teflon stills.

1.7.2. Sr-isotope chemistry

Around 150 mg of rock powder was weighed into teflon beaker, a static charge gun was used to prevent loss of powder due to static charge build-up upon teflon. About 2 ml of 16M HNO3 and 5 ml of 40% HF was added and evaporated to dryness in a teflon oven at 80°C with clean air circulation. When dry a further 2 ml of 16M HNO3 was added and evaporated, after which 2 ml 6M HCl was added. At this stage the sample was closely inspected to ensure complete dissolution and the HCl was evaporated down. The sample was then redissolved in 2.5M HCl and left overnight an a covered beaker. Occasionally the dissolution process was repeated to achieve a complete digestion. On rare occasions complete dissolution was only achieved after 6M HCl treatment in a teflon bomb placed in a metal jacket in an oven at 180°C overnight. The sample, dissolved in 1 ml 2.5M HCl was then centrifuged to remove any residue and the solution was loaded onto a pre-conditioned cation exchange column containing 10 ml Bio-Rad AGW 50x8, 200-400 mesh resin. The sample was washed in with 2x1 ml 2.5M HCl and eluted with 40 ml 2.5M HCl. Sr was then collected in 10 ml 2.5M HCl in a clean teflon beaker, and evaporated to dryness.

1.7.3.O-isotope chemistry

Oxygen isotope analyses were performed using procedures described by Clayton and Mayeda(1963) as modified for ClF_3 rather than BrF_5. Prior to oxygen extraction, samples were heated under vacuum at 200°C for a minimum of one hour and briefly prefluorinated. The extracted oxygen was converted to CO_2 by reaction with hot graphite. The carbon dioxide was then analysed by isotope ratio mass spectrometry.

Sr was loaded in a filtered loading bay, laboratory coat and gloves were worn throughout. Sr was dissolved in a drop of TD H2O and loaded onto outgassed single Ta filament onto which about 1 µl of H_3PO_4 had been placed. A small current was passed through the filament to slowly dry the sample and then gradually increased until the H_3PO_4 fumed off and the filament glowed dull red. Loaded filaments were placed in a twelve sample turret and analysed automatically on a Vacuum Generators Isomass 54E thermal ionization mass spectrometer at the SURRC.

1.7.4. Isotope measurement

1.7.4.1. Sr isotopes

Sr isotope abundances were measured with a beam intensity of 15 pA at a filament current of 2.5 A. Peaks were counted for four periods of 1.28 seconds, after which the magnet

was stepped to the next position. The measuring cycle was 88, 87, 86, 85.5, 85, 84. The 84 peak was eliminated after the first set and the 85 peak when the Rb contribution to the 87 peak was less than 0.01%. Peak intensities were calculated using a double interpolation algorithm(Dodson, 1978) and were corrected for zero, dynamic memory and Rb interference where necessary. Mass fractionation was corrected for by assuming that $^{86}Sr/^{88}Sr=0.1194$ and that there is a linear dependence on mass difference. The isotopic ratios were stored in sets of ten and then the mean and error calculated for each set. Any ratios which did not satisfy were rejected and the mean and error re-calculated. Sets whose total error(1 sigma) was 100 ppm or more were rejected and those with total error of 500 ppm or greater were rejected but not those ignored, and a running mean was formed. The analysis continued until at least 100 ratios had been accepted and the error was 20 ppm or less.

1.7.4.2.O isotopes

$\delta^{18}O$ of CO_2 was performed on a VG Micromass 903 mass spectrometer with a reference gas calibrated against water, carbonate and silicate standards. For NBS 28 a value of $\delta^{18}O=9.6‰$(SMOW) was measured. Reproducibility is variable for the samples, but isotopically homogeneous mineral separates usually have precision $\pm 0.1‰(\sigma)$ by the technique. The isotopic data are presented as δ-values per mil relative to the SMOW standard defined as follows;

$$\delta^{18}O=\left[\frac{(^{18}O/^{16}O)_{sample}}{(^{18}O/^{16}O)_{standard}} -1\right] x\ 1000(‰)$$

Where standard is Standard Mean Ocean Water(SMOW; Craig, 1961a).

APPENDIX 2. SAMPLE LOCATIONS

SAMPLE NO	SAMPLE DESCRIPTION	SAMPLE LOCATION	GRID REFERENCE (Long.- Latid.)
MA-1	Trachyte(Meydan lava)	southwest of the Meydan caldera	42250 - 38875
MA-6A	Benmoreite(Meydan lava)	northeast of the Meydan caldera	45275 - 40675
MA-9	Hawaiite(Meydan lava)	near Pinarli village	44125 - 35625
MA-10	Trachyte(Meydan lava)	west of Meydan Deres	43125 - 38375
MA-11	Rhyolite(Gurgurbaba lava)	south of Gurgur Deres	44375 - 39250
MA-13	Trachyte(Meydan lava)	west of Cinpinari	43875 - 37875
MA-14	Trachyte(Meydan lava)	west of Cinpinari	43935 - 37685
MA-15	Hawaiite(Meydan lava)	near Molla pinari	47435 - 33560
MA-17	Rhyolite(Gurgurbaba lava)	north of Cagdas village	47375 - 35185
MA-18	Trachyte(Meydan lava)	south of Kilis pinari	44750 - 35060
MA-20	Alkali olivine basalt(Meydan lava)	east of Yayla Dere	41750 - 35310
MA-21	Alkali olivine basalt(Meydan lava)	east of Kalender Dere	41060 - 32560
MA-23	Alkali olivine basalt(Meydan lava)	near Gumusoluk village	40250 - 33500
MA-27	Alkali olivine basalt(Meydan lava)	south skirt of Topsini Tepe	39810 - 35560
MA-29B	Hawaiite(Meydan lava)	north of Goktas village	38685 - 45375
MA-31B	Rhyolite dyke	south of Kottepe	38935 - 41375
MA-33	Hawaiite(Meydan Lava)	southwest of Cerpinari	48435 - 39935
MA-34A	Benmoreite(Meydan lava)	Basri Tepe	46125 - 41310
MA-35	Benmoreite(Meydan lava)	southeast of Sait Tepe	45125 - 40500
MA-36	Hawaiite(Meydan lava)	Kucukdeveci Tepe	45875 - 42125
MA-37	Hawaiite(Meydan lava)	east of Kucukdeveci Tepe	46500 - 42075
MA-38A	Rhyolite dome	slope of Maruf Tepe	38750 - 42600
MA-38B	Rhyolite dome	slope of Maruf Tepe	38775 - 42650
MA-39	Trachyte(Meydan lava)	south Kurt Sirti	41950 - 38775
MA-40	Hawaiite(Meydan lava)	around Sait Tepe	44750 - 41450
MA-41	Alkali olivine basalt(Meydan lava)	north of Hirindes Yayla	40400 - 43800
MA-42A	Trachyte(Meydan lava)	north of Kurttepe	40950 - 41325
MA-43	Trachyte(Meydan lava)	summit of Kurttepe	40575 - 40700
MA-44	Mugearite(Meydan lava)	east of Buyukdeveci Tepe	47550 - 43025
MA-45	Ignimbrite	east of Buyukdeveci Tepe	47950 - 42925
MA-47	Mugearite(Meydan lava)	northwest of Goktas village	38225 - 45175
MA-48	Mugearite(Meydan lava)	east of Kuyruk Dere	39950 - 40800
MA-49A	Mugearite(Meydan lava)	west of Goktas village	38250 - 44850
MA-49B	Mugearite(Meydan lava)	west of Goktas village	38250 - 44875
MA-50	Rhyolite(Gurgurbaba lava)	near Gurgurdere	44625 - 39350
MA-51	Mugearite(Meydan lava)	west of Kuyruk Tepe	39250 - 41625
MA-52	Ignimbrite	west of Evbeyli village	46850 - 43850
MA-53	Mugearite(Meydan lava)	east of Kosehasan Tepe	46425 - 43675
MA-54	Mugearite(Meydan lava)	east of Kosehasan Tepe	46550 - 43850
MA-55A	Trachyte(Aladag lava)	near Ali Deresi	46425 - 45500
MA-55B	Trachyte(Aladag lava)	near Ali Deresi	46450 - 45525
MA-56B	Limestone(Kizildere formation)	north of Magara village	48100 - 44850
MA-56C	Sandstone(Kizildere formation)	north of Magara village	48125 - 44875
MA-56D	Sandstone(Kizildere formation)	north of Magara village	48150 - 44900
MA-56E	Sandstone(Kizildere formation)	north of Magara village	48150 - 44950
MA-57	Ignimbrite	east of Binbasi Dere	48250 - 45750
MA-58A	Rhyolite(Gurgurbaba lava)	southwest of Gurgurbaba Tepe	44750 - 39250
MA-59A	Perlite(Gurgurbaba lava)	south of Gurgurbaba Tepe	44625 - 38525
MA-59B	Perlite(Gurgurbaba lava)	south of Gurgurbaba Tepe	44650 - 38375
MA-62	Rhyolite dyke	north of Goktas village	38300 - 46275
MA-64	Hawaiite(Meydan lava)	south of Gultepe	39100 - 34250
MA-65	Trachyte(Aladag lava)	south skirt of Sevis Efendi Tepe	47400 - 46500
MA-66	Trachyte(Aladag lava)	around Sevis Efenti Tepe	47475 - 46575
MA-69	Hawaiite(Meydan lava)	summit of Sevis Efenti Tepe	47625 - 47175
MA-70	Hawaiite(Meydan lava)	south of Sevis Efendi Tepe	47950 - 46925
MA-71	Trachyte(Aladag lava)	east of Sevis Efendi Tepe	48400 - 46775

MA-73	Ignimbrite	southeast of Sevis Efendi Tepe	48550 - 46025
MA-74	Ignimbrite	southeast of Sevis Efendi Tepe	48875 - 45775
MA-75	Ignimbrite	southeast of Miletiris Tepe	49675 - 45050
MA-76	Limestone(Kizildere formation)	southeast of Miletiris Tepe	49950 - 44950
MA-78	Andesite	west of Kelle Tepe	50375 - 46275
MA-79	Andesite	west of Kelle Tepe	50425 - 46275
MA-83	Dacite	Kardogan Sirti	51450 - 46375
MA-84	Dacite	south of Kardogan Sirti	51350 - 46150
MA-85	Dacite	north of Merkez Tepe	51400 - 45950
MA-89	Limestone(Kizildere formation)	south of Kurutas Kayasi	50125 - 43900
MA-91	Dacite	around Omeraga Tepe	52650 - 45675
MA-93	Dacite	south of Omeraga Tepe	52950 - 45400
MA-94	Dacite	southeast of Sogutlu village	53275 - 45025
MA-96	Dacite	southwest of Sakiran Tepe	52475 - 43750
MA-98	Dacite	south of Sikevt Dere	52775 - 42675
MA-101	Sandstone(Kizildere formation)	summit of Berrus Tepe	51650 - 42600
MA-102	Sandstone(Kizildere formation)	slope of Berrus Tepe	51200 - 42725
MA-104	Sandstone(Kizildere formation)	north of Gelintasi Tepe	51775 - 41550
MA-105	Dolomitic limestone(Kizildere fm.)	northeast of Gelintasi Tepe	52250 - 41525
MA-107	Trachyandesite	north of Keragili	52450 - 40750
MA-109B	Limestone(Kizildere formation)	around Keragili	52550 - 40275
MA-110	Dolomitic limestone(Kizildere fm.)	east of Keragili	52950 - 40150
MA-111	Dolomitic limestone(Kizildere fm.)	east of Keragili	53125 - 39975
MA-113	Trachyandesite	near Karaagac Dere	53825 - 39825
MA-114	Trachyandesite	near Karaagac Dere	54375 - 39475
MA-115	Trachyandesite	east of Purnisin	54300 - 39025
MA-116	Trachyandesite	east of Purnisin	54025 - 39125
MA-117	Hawaiite(Meydan lava)	west of Magara Kayalari	49700 - 40850
MA-120	Andesite	southeast of Kose Deresi	48675 - 39125
MA-121	Andesite	west of Yesildere	49125 - 39200
MA-122	Dacite	summit of Alikalesi Tepe	49150 - 37700
MA-123	Dacite	southeast of Alikalesi Tepe	49400 - 37450
MA-125	Dacite	northeast of Kohkalesi Tepe	50025 - 36750
MA-126	Andesite	northeast of Kohkalesi Tepe	50425 - 36875
MA-127	Limestone(Kizildere formation)	southeast of Kavak Tepe	51625 - 38600
MA-129	Andesite(Kizildere lava)	north of Manikcesme Dere	54250 - 37125
MA-131	Andesite	southeast of Gecekayagi Dere	52875 - 36775
MA-132	Trachyandesite	northeast of Karakale Tepe	52575 - 36600
MA-134	Trachyandesite	east of Karakale Tepe	52725 - 35750
MA-135	Dacite	Karakale Tepe	52550 - 35650
MA-138	Andesite	around Misir Tepe	54225 - 35225
MA-139	Andesite	southeast of Kurttepe	54025 - 34050
MA-140	Hawaiite(Meydan lava)	northwest of Agacoren village	54100 - 33825
MA-141A	Andesite	south of Sehit Tepe	53350 - 32275
MA-142	Dacite	summit of Sehit Tepe	53325 - 32825
MA-143	Trachyandesite	west of Sehit Tepe	52625 - 33275
MA-146	Trachyandesite	around Kale Tepe	51250 - 32700
MA-148	Andesite	south of Kecitasi Tepe	50575 - 34200
MA-150	Trachyandesite	nort of Kurttepesi	49950 - 35300
MA-151	Dacite	southeast of Gullu Tepe	49125 - 35875
MA-152	Andesite	around Gullu Tepe	48925 - 35950
MA-153	Trachyte(Meydan lava)	north west of the Meydan caldera	41550 - 41575
MA-155	Mugearite(Meydan lava)	north west of the Meydan caldera	41250 - 41425
MA-157	Trachyte(Meydan lava)	west wall of the Meydan caldera	41275 - 40800
MA-159	Trachyte(Meydan lava)	west wall of the Meydan caldera	41775 - 39575
MA-160	Trachyte(Meydan lava)	west wall of the Meydan caldera	41575 - 39600
MA-161	Trachyte(Meydan lava)	west wall of the Meydan caldera	41375 - 39575
MA-163	Trachyte(Meydan lava)	east of Budak Yayla	40600 - 38725
MA-164	Hawaiite(Meydan lava)	around Kartepe	39850 - 38300
MA-166	Hawaiite(Meydan lava)	around Topsini Tepe	40025 - 35925
MA-168	Trachyte(Meydan lava)	south of Sait Tepe	44925 - 40750
MA-169	Hawaiite(Meydan lava)	south of Sait Tepe	45075 - 40950

MA-171	Hawaiite(Meydan lava)	around Kucukdeveci Tepe	45325 - 42250
MA-173	Trachyte(Meydan lava)	southwest of Kosehasan Tepe	44825 - 43050
MA-175	Hawaiite(Meydan lava)	south of Taht Dere	43375 - 46875
MA-176	Mugearite(Meydan lava)	north of Semi kayalari Sirti	45425 - 46125
MA-177	Mugearite(Meydan lava)	east of Semi kayalari Sirti	45875 - 45250
MA-178	Ignimbrite	southeast of Semi kayalari Sirti	46300 - 45075
MA-179	Trachyandesite	east of Seytan Dere	57325 - 40675
MA-180	Dacite	around Gunduk Tepe	56300 - 40825
MA-183	Dacite	west of Yukari seytan Dere	56375 - 42050
MA-185	Dacite	north of Asagi seytan Dere	55375 - 43675
MA-186	Ignimbrite	southwest of Sira kayalar Tepe	56475 - 44025
MA-187	Dacite	southwest of Sira kayalar Tepe	56650 - 43650
MA-188	Dacite	northeast of Yukari seytan Dere	56950 - 42775
MA-189	Dacite	east of Yukari seytan Dere	57175 - 42325
MA-190	Trachyandesite	southeast of Yukari seytan Dere	57525 - 41900
MA-192A	Hyalorhyolite(Kizildere lava)	around Varikani Yaylasi	59175 - 42625
MA-193	Andesite(Kizildere lava)	east of Varikani Yaylasi	59525 - 42875
MA-196	Sandstone(Kizildere formation)	south of Tavsan Tepe	59425 - 44200
MA-198A	Tuff(Kizildere formation)	north of Tavsan Tepe	59425 - 45150
MA-199	Andesite(Kizildere lava)	northwest of Tavsan Tepe	58775 - 45175
MA-200	Andesite(Kizildere lava)	south of Kuzubulak Golu	58575 - 45650
MA-201	Ignimbrite	north of Kuzubulak Golu	58200 - 46025
MA-202	Ignimbrite	north of Kuzubulak Yayla	57425 - 45850
MA-203	Dacite	southwest of Kuzubulak Yayla	57175 - 45400
MA-205	Andesite(Kizildere lava)	southeast of Sira kayalar Tepe	58125 - 44075
MA-206	Basaltic andesite(Kizildere lava)	southeast of Sira kayalar Tepe	58250 - 43875
MA-207	Trachyandesite	south of Varikani Yayla	58175 - 41625
MA-208	Sandstone(Kizildere formation)	west of Hasanaptal village	58275 - 41275
MA-210	Limestone(Kizildere formation)	north of Attepesi	57525 - 40050
MA-213	Andesite(Kizildere lava)	south of Hasanaptal village	59450 - 40125
MA-214	Andesite(Kizildere lava)	nort of Kurt Tepe	59025 - 39450
MA-215	Andesite(Kizildere lava)	summit of Kurt Tepe	58800 - 38875
MA-217	Andesite(Kizildere lava)	southeast of Kurt Tepe	59325 - 38175
MA-219	Andesite(Kizildere lava)	east of Hudut Dere	59575 - 37700
MA-220A	Tuff(Kizildere formation)	northeast of Isbasi village	59500 - 37525
MA-224	Limestone(Kizildere formation)	south of Attepesi	57600 - 38825
MA-226A	Zilan lava	around Attepesi	56325 - 38225
MA-228	Agglomerate clast	northwest of Demek Tepe	58175 - 34700
MA-229	Ignimbrite	northwest of Omeraga pinari	57675 - 34025
MA-230	Hawaiite(Meydan lava)	southeast of Omeraga pinari	58025 - 34025
MA-231	Andesite(Kizildere lava)	around Tandirbasi village	58300 - 38725
MA-232B	Pumice clast	along Ercis-Patnos road	38025 - 33250
MA-233A	Lithic clast in pumice deposits	along Ercis-Patnos road	38025 - 33250
MA-233B	Lithic clast in pumice deposits	along Ercis-Patnos road	38025 - 33250
MA-234A	Pumice clast	along Ercis-Patnos road	38250 - 32875
MA-239	Obsidian(Gurgurbaba lava)	northeast of Meydan village	43750 - 38675
MA-240A	Obsidian(Gurgurbaba lava)	northeast of Meydan village	43775 - 38650
MA-240B	Obsidian(Gurgurbaba lava)	northeast of Meydan village	43775 - 38650
MA-246	Andesite(Kizildere lava)	south of Cayirbicen village	47675 - 43375
MA-247	Limestone(Kizildere formation)	east of Magara village	49050 - 44150
MA-248	Tuff(Kizildere formation)	south of Koycuk village	51175 - 42475
MA-250	Hawaiite(Meydan lava)	summit of Maruf Tepe	38575 - 42750
MA-252	Hawaiite(Meydan lava)	summit of Kottepe	38750 - 42125
MA-253	Agglomerate clast	southwest of Demek Tepe	58125 - 34625
MA-254	Agglomerate clast	southwest of Demek Tepe	58125 - 34600
MA-255	Agglomerate clast	southwest of Demek Tepe	58120 - 34550
MA-256	Agglomerate clast	southwest of Demek Tepe	58100 - 34500
MA-262	Andesite(Kizildere lava)	west of Isbasi village	58150 - 37175
MA-263	Zilan lava	around Hasanaptal village	59100 - 41025

Note: Grid references are based on the 1000 m grid of the Turkey 1:25 000 topographical map series(Karakose -J50).

APPENDIX 3. MAJOR AND TRACE ELEMENT ANALYSES, CIPW NORMS AND NIGGLI VALUES

Sample	MA-1	MA-6A	MA-9	MA-10	MA-11	MA-13	MA-14	MA-15	MA-17
SiO_2	61.30	56.98	50.62	62.07	74.38	62.17	62.27	47.37	73.21
TiO_2	1.12	1.72	1.45	1.07	0.11	0.98	0.98	1.93	0.08
Al_2O_3	17.41	15.31	18.30	17.30	12.80	17.48	17.97	17.64	13.44
Fe_2O_3	3.42	8.37	4.90	2.86	0.00	4.25	2.72	5.11	0.89
FeO	1.48	1.16	4.44	1.76	1.44	0.20	1.39	6.02	0.44
MnO	0.18	0.18	0.13	0.10	0.14	0.16	0.11	0.11	0.11
MgO	1.17	1.54	5.90	1.56	0.41	0.98	1.38	5.87	0.71
CaO	2.90	3.55	9.05	3.15	0.38	2.32	2.45	8.59	2.21
Na_2O	6.07	5.49	4.84	8.23	5.31	6.92	7.10	5.42	6.17
K_2O	3.39	3.32	1.41	3.56	4.09	3.58	3.80	1.04	4.24
P_2O_5	0.46	0.73	0.51	0.46	0.03	0.33	0.36	0.52	0.03
LOI	0.55	0.71	0.50	0.44	0.50	0.84	0.42	0.39	0.85
Total	99.45	99.06	102.05	102.56	99.59	100.21	102.95	100.01	102.38
Zr	361	396	174	379	272	396	401	218	321
Y	52	63	31	51	63	50	55	36	50
Sr	410	302	689	460	23	343	382	715	27
U	bdl	bdl	bdl	bdl	bdl	bdl	bdl	bdl	bdl
Rb	106	114	18	106	163	95	121	8	221
Th	17	14	8	14	22	16	16	5	24
Pb	20	16	10	20	26	15	19	7	27
Ga	22	23	18	19	21	21	18	18	16
Zn	85	107	65	69	59	74	69	73	52
Cu	8	72	15	0	bdl	bdl	bdl	12	bdl
Ni	4	3	43	8	3	6	5	31	4
Co	0	13	46	10	1	2	8	52	6
Cr	4	17	78	10	32	38	29	53	3
Ce	119	133	65	135	70	114	146	61	77
Ba	932	680	637	846	79	787	1068	403	78
La	70	79	32	60	32	73	69	31	29
Nb	21	19	13	20	20	26	25	4	25
Ap	1.09	1.72	1.16	0.99	0.07	0.77	0.81	1.23	0.07
Il	2.15	2.47	2.64	1.94	0.02	0.39	1.79	3.65	0.15
Or	20.27	19.98	7.98	19.98	24.76	21.28	21.45	6.09	24.64
Ab	51.94	47.29	30.47	59.92	44.09	58.96	57.36	28.09	44.82
An	10.36	7.47	23.14	2.33	0.00	6.08	5.67	20.72	0.00
Mt	1.52	0.00	7.45	2.43	0.00	0.00	1.56	8.38	0.00
Hm	2.39	8.36	0.00	1.30	0.00	4.26	1.72	0.00	0.00
Di	0.86	3.19	16.91	7.55	1.02	0.50	2.84	14.53	5.03
Hy	2.54	2.43	0.00	0.00	0.57	2.23	1.97	0.00	0.00
Q	6.66	5.79	0.00	0.00	28.58	3.40	4.71	0.00	19.88
Ol	0.00	0.00	5.27	0.13	0.00	0.00	0.00	7.66	0.00
Ne	0.00	0.00	4.81	3.33	0.00	0.00	0.00	9.54	0.00
Cm	0.00	0.00	0.02	0.00	0.00	0.02	0.00	0.02	0.00
Mg#	29.27	22.35	50.57	35.36	33.65	28.25	35.57	45.46	47.47
SI	7.46	7.73	26.32	8.48	3.62	6.21	8.27	23.64	5.68
DI	78.87	73.06	43.26	83.23	97.43	83.64	83.52	43.72	89.34
al	38.07	30.36	24.70	35.28	46.22	38.72	37.88	23.82	37.53
fm	20.55	31.78	37.84	20.13	3.74	18.11	19.43	41.56	10.05
c	11.52	12.82	24.66	11.05	2.50	9.36	9.39	21.08	11.24
alk	29.86	25.03	12.79	33.54	47.54	33.81	33.30	13.54	41.18
si	227.36	191.77	118.26	209.65	455.58	233.60	236.93	108.51	346.94
k	0.27	0.28	0.16	0.22	0.34	0.25	0.26	0.11	0.31
ti	3.12	4.35	2.49	2.65	0.49	2.78	2.65	3.32	0.29
mg	0.31	0.24	0.53	0.38	1.00	0.30	0.38	0.48	0.50
w	0.67	0.86	0.52	0.62	0.00	0.95	0.65	0.46	0.65

Sample	MA-18	MA-20	MA-21	MA-23	MA-27	MA-29B	MA-31B	MA-33	MA-34A
SiO_2	62.82	48.94	47.99	48.00	50.28	48.51	73.51	47.11	49.73
TiO_2	0.93	1.18	1.18	1.19	0.99	1.52	0.39	1.74	1.64
Al_2O_3	16.87	18.80	17.51	18.02	14.91	18.20	14.82	17.45	19.04
Fe_2O_3	3.61	3.52	6.48	3.24	3.41	2.59	0.83	4.88	4.45
FeO	0.64	4.95	2.32	5.23	4.64	6.83	0.76	5.27	4.28
MnO	0.18	0.13	0.15	0.16	0.10	0.13	0.06	0.00	0.18
MgO	0.88	6.48	7.02	7.29	10.41	6.90	0.70	6.02	3.10
CaO	2.28	11.09	11.33	10.82	10.49	10.59	0.88	8.85	7.93
Na_2O	6.61	3.51	3.88	3.68	4.05	4.39	4.75	5.22	5.85
K_2O	3.65	0.78	0.75	0.78	1.08	1.33	5.22	1.60	2.16
P_2O_5	0.33	0.35	0.36	0.37	0.31	0.44	0.05	0.65	0.86
LOI	0.53	0.18	0.89	0.51	0.18	0.26	0.44	0.34	0.57
Total	99.33	99.91	99.86	99.29	100.85	101.69	102.41	99.13	99.79
Zr	396	123	117	129	131	185	268	216	269
Y	52	31	27	31	25	31	21	33	37
Sr	339	679	631	630	429	767	90	767	837
U	bdl	bdl	bdl	bdl	bdl	bdl	bdl	0	bdl
Rb	122	10	14	14	28	16	278	32	57
Th	17	5	8	5	11	4	37	11	10
Pb	22	5	6	0	6	7	22	11	11
Ga	20	15	18	17	17	15	14	19	21
Zn	102	52	55	66	66	61	24	93	84
Cu	5	31	45	45	51	20	bdl	28	74
Ni	4	62	59	57	216	49	6	31	17
Co	5	56	39	33	42	45	9	36	22
Cr	18	11	54	94	414	67	40	67	29
Ce	122	53	43	52	43	67	92	77	124
Ba	845	397	303	326	306	426	312	558	773
La	67	28	25	25	28	31	46	49	60
Nb	23	7	4	8	5	8	19	12	14
Ap	0.77	0.81	0.86	0.86	0.70	0.98	0.12	1.53	2.02
Il	1.35	2.26	2.32	2.30	1.84	2.79	0.70	3.34	3.13
Or	21.87	4.67	4.61	4.67	6.26	7.57	29.61	9.57	12.88
Ab	56.59	25.76	25.21	25.22	26.39	18.26	38.58	23.82	31.77
An	5.65	33.67	33.71	30.70	18.90	20.77	3.59	19.69	19.47
Mt	0.00	5.09	4.15	4.68	5.15	4.28	1.26	7.05	6.47
Hm	3.61	0.00	3.56	0.00	0.00	0.00	0.00	0.00	0.00
Di	2.22	15.80	17.10	16.97	23.85	21.81	0.23	16.25	11.49
Hy	1.19	0.00	3.85	0.00	0.00	0.00	1.58	0.00	0.00
Q	5.98	0.00	0.00	0.00	0.00	0.00	24.25	0.00	0.00
Ol	0.00	9.43	4.42	10.98	12.73	9.54	0.00	7.37	2.74
Ne	0.00	2.36	0.00	3.44	3.95	13.86	0.00	11.35	9.84
Cm	0.00	0.00	0.02	0.02	0.09	0.02	0.02	0.02	0.00
Mg#	26.85	56.30	58.74	59.07	67.79	53.56	41.77	50.13	37.56
SI	5.71	32.83	36.13	35.29	42.82	28.42	5.63	25.60	16.94
DI	84.44	32.79	29.82	33.33	36.60	39.69	92.44	44.74	54.49
al	38.75	25.60	24.10	24.17	18.78	23.10	43.73	23.99	29.30
fm	17.66	37.91	39.90	40.16	47.29	39.40	11.84	39.66	30.11
c	9.53	27.47	28.35	26.40	24.04	24.43	4.75	22.15	22.17
alk	34.06	9.02	7.65	9.26	9.89	13.06	39.69	14.20	18.42
si	244.90	110.79	109.72	109.30	109.61	106.57	378.13	109.95	129.80
k	0.27	0.13	0.15	0.12	0.15	0.14	0.42	0.17	0.20
ti	2.72	2.04	2.07	2.05	1.59	2.47	1.45	3.05	3.21
mg	0.29	0.59	0.61	0.62	0.70	0.56	0.44	0.53	0.40
w	0.83	0.39	0.71	0.35	0.41	0.29	0.51	0.45	0.48

Sample	MA-35	MA-36	MA-37	MA-38A	MA-38B	MA-39	MA-40	MA-41	MA-42A
SiO_2	58.67	47.60	48.70	71.15	69.75	62.26	49.42	47.56	62.06
TiO_2	1.80	1.90	1.80	0.41	0.38	1.06	1.35	1.50	0.90
Al_2O_3	15.46	18.79	18.27	14.35	13.84	17.18	17.96	18.32	17.28
Fe_2O_3	5.32	11.41	3.12	1.16	1.04	4.24	2.91	5.84	2.91
FeO	4.16	0.40	6.83	0.84	0.84	0.80	5.91	4.01	1.07
MnO	0.18	0.13	0.11	0.08	0.09	0.07	0.12	0.19	0.11
MgO	1.50	3.61	5.19	0.85	0.85	0.84	5.46	6.16	1.14
CaO	3.54	8.37	8.37	1.16	1.80	2.64	9.33	9.98	1.89
Na_2O	5.21	4.14	5.12	4.87	4.37	6.84	6.23	3.21	7.46
K_2O	3.37	1.58	1.60	5.26	4.88	3.50	1.67	1.27	3.74
P_2O_5	0.72	0.85	0.73	0.09	0.08	0.43	0.46	0.46	0.31
LOI	0.89	1.66	0.16	2.38	2.60	0.59	0.10	1.48	1.18
Total	100.82	100.44	100.00	102.60	100.52	100.45	100.92	99.98	100.05
Zr	389	248	220	290	253	388	206	173	438
Y	58	50	33	27	24	43	31	35	58
Sr	306	887	947	98	103	434	774	795	340
U	2	bdl	bdl	bdl	bdl	bdl	bdl	bdl	bdl
Rb	114	15	20	253	246	110	38	22	124
Th	14	4	4	38	35	16	7	7	16
Pb	16	7	10	24	23	21	10	9	20
Ga	24	17	19	15	14	19	20	18	19
Zn	101	82	70	27	27	67	72	83	70
Cu	28	16	16	0	bdl	3	10	24	0
Ni	8	46	23	4	4	13	32	55	7
Co	11	51	39	6	8	11	43	41	7
Cr	3	18	74	26	32	12	73	63	5
Ce	132	100	90	102	88	150	78	77	162
Ba	679	613	542	296	311	895	495	525	1001
La	61	62	48	48	46	65	38	37	86
Nb	18	12	13	21	19	24	9	18	23
Ap	1.67	1.99	1.70	0.21	0.19	0.99	1.05	1.09	0.70
Il	3.42	0.87	3.40	0.76	0.74	1.69	2.55	2.89	1.71
Or	19.92	9.46	9.34	30.08	29.73	20.74	9.75	7.62	22.34
Ab	44.07	35.53	28.39	39.93	38.15	57.95	21.01	27.58	63.70
An	8.85	28.40	22.02	4.33	3.87	5.85	15.97	32.37	2.65
Mt	7.79	3.62	5.89	1.48	1.57	0.00	4.39	8.42	0.91
Hm	0.00	0.00	0.00	0.17	0.00	4.25	0.00	0.00	2.48
Di	3.14	11.42	11.64	0.50	3.78	2.99	21.74	11.59	3.79
Hy	2.48	2.27	0.00	1.84	0.49	0.70	0.00	3.16	1.11
Q	8.46	2.12	0.00	20.62	21.39	4.32	0.00	0.00	0.50
Ol	0.00	4.16	9.65	0.00	0.00	0.00	9.51	5.05	0.00
Ne	0.00	0.00	7.86	0.00	0.00	0.00	16.91	0.00	0.00
Cm	0.00	0.00	0.02	0.0	0.00	0.00	0.02	0.02	0.00
Mg#	21.07	35.48	44.19	41.19	43.49	22.58	50.23	51.87	32.32
SI	7.45	17.18	22.01	6.45	7.04	5.15	23.74	29.60	6.87
DI	72.45	47.11	45.59	90.63	89.27	83.01	47.67	35.20	86.54
al	30.51	28.21	25.49	42.52	40.38	37.61	24.58	25.56	38.09
fm	32.67	36.16	39.15	13.68	13.68	18.98	35.73	39.86	18.36
c	12.70	22.83	21.23	5.83	9.56	10.49	23.21	25.31	7.58
alk	24.11	12.80	14.14	37.98	36.37	32.92	16.49	9.28	35.97
si	196.51	121.21	115.28	343.71	340.33	231.14	114.71	112.59	232.14
k	0.30	0.20	0.17	0.42	0.42	0.25	0.15	0.21	0.25
ti	4.53	3.65	3.21	1.46	1.41	2.96	2.36	2.66	2.51
mg	0.23	0.38	0.47	0.44	0.46	0.24	0.53	0.55	0.35
w	0.54	0.96	0.35	0.57	0.53	0.83	0.32	0.56	0.72

Sample	MA-43	MA-44	MA-45	MA-47	MA-48	MA-49A	MA-49B	MA-50	MA-51
SiO_2	62.36	53.44	67.98	52.62	51.03	52.02	52.42	75.63	52.50
TiO_2	1.10	2.11	0.68	1.96	2.15	1.38	1.50	0.12	1.37
Al_2O_3	17.67	18.32	15.88	19.81	16.31	17.74	18.66	14.26	18.45
Fe_2O_3	2.66	6.96	2.26	7.19	3.96	4.98	7.06	1.48	8.99
FeO	1.99	1.49	0.49	1.32	6.40	3.79	2.19	0.00	0.44
MnO	0.13	0.11	0.13	0.20	0.04	0.13	0.14	0.11	0.12
MgO	1.90	1.26	0.39	1.74	4.29	3.71	3.49	0.39	2.14
CaO	2.42	6.41	0.48	8.28	7.87	8.52	6.22	0.33	6.77
Na_2O	6.78	5.83	6.74	4.66	5.39	4.71	4.79	5.22	4.43
K_2O	3.57	2.07	4.01	1.87	1.57	1.60	1.62	4.54	1.65
P_2O_5	0.49	0.54	0.11	0.70	0.59	0.34	0.39	0.03	0.44
LOI	0.44	1.52	0.84	1.25	0.40	0.74	2.80	0.36	2.09
Total	101.51	100.06	99.99	101.60	100.00	99.66	101.28	102.47	99.39
Zr	443	261	576	221	251	201	186	323	220
Y	46	52	52	39	44	28	31	55	56
Sr	440	545	35	685	493	585	442	45	470
U	bdl	bdl	3	0	bdl	bdl	0	bdl	bdl
Rb	109	54	122	48	28	36	41	218	bdl
Th	17	9	14	10	6	8	7	22	bdl
Pb	22	11	17	8	6	10	9	32	bdl
Ga	22	18	22	22	17	14	22	18	19
Zn	64	74	58	60	93	68	80	55	86
Cu	bdl	67	4	57	20	39	34	bdl	34
Ni	2	19	7	23	11	15	14	3	21
Co	9	25	2	13	50	46	34	nd	17
Cr	14	63	1	29	40	63	26	nd	36
Ce	137	83	117	109	80	62	53	nd	69
Ba	750	547	628	731	429	459	440	nd	442
La	60	47	56	61	35	37	33	nd	40
Nb	15	13	nd	13	13	9	10	nd	12
Ap	1.09	1.28	0.26	1.63	1.37	0.79	0.91	0.07	1.05
Il	2.03	3.13	1.03	2.74	4.08	2.66	2.87	0.02	0.92
Or	20.39	12.35	23.88	10.99	9.28	9.57	9.63	25.89	10.05
Ab	55.49	49.83	57.53	39.25	37.62	40.35	40.78	46.38	38.58
An	7.05	17.95	1.29	27.52	15.66	22.78	24.74	0.00	26.38
Mt	3.05	0.00	0.00	0.00	6.44	7.21	2.68	0.00	0.00
Hm	0.64	7.37	2.20	7.21	0.00	0.00	6.22	0.00	8.99
Di	4.90	6.88	0.00	5.51	21.59	13.92	2.89	0.75	1.62
Hy	2.31	0.00	0.97	1.75	0.00	0.46	7.40	0.57	4.75
Q	2.87	0.00	12.37	1.93	0.00	0.00	1.71	24.89	5.23
Ol	0.00	0.00	0.00	0.00	5.49	2.11	0.00	0.00	0.00
Ne	0.00	0.00	0.00	0.00	4.28	0.00	0.00	0.00	0.00
Cm	0.00	0.02	0.00	0.00	0.02	0.02	0.00	0.02	0.02
Mg#	40.23	20.04	20.17	26.25	39.82	42.03	37.28	30.82	29.23
SI	11.01	6.95	2.72	10.25	18.83	19.40	14.14	3.07	12.26
DI	78.75	62.18	93.78	52.17	51.18	49.92	52.12	97.25	53.86
al	35.25	32.49	43.34	32.98	24.42	27.84	30.20	46.04	32.36
fm	22.43	25.91	12.18	25.81	38.35	32.97	35.90	3.13	30.14
c	12.40	20.65	2.41	25.08	21.42	24.30	18.29	1.95	21.60
alk	29.92	20.95	42.07	16.13	15.81	14.89	15.60	48.89	15.90
si	214.54	160.82	314.81	148.67	129.66	138.43	143.98	425.21	156.25
k	0.26	0.19	0.28	0.21	0.16	0.18	0.18	0.32	0.20
ti	2.81	4.77	2.35	4.16	4.11	2.77	3.10	0.47	3.06
mg	0.43	0.22	0.22	0.28	0.42	0.45	0.40	1.00	0.32
w	0.56	0.82	0.80	0.83	0.38	0.54	0.77	0.00	0.95

Sample	MA-52	MA-53	MA-54	MA-55A	MA-55B	MA-56B	MA-56C	MA-56D	MA-56E
SiO_2	65.24	52.50	51.33	65.96	65.38	2.73	64.41	59.08	64.20
TiO_2	0.65	2.11	1.63	0.82	0.85	0.04	0.25	0.31	0.43
Al_2O_3	16.07	18.91	17.16	15.92	15.65	0.57	10.94	11.05	12.78
Fe_2O_3	2.35	8.64	4.86	2.45	2.56	0.14	1.33	2.11	1.08
FeO	0.80	2.04	3.24	1.12	1.48	0.24	0.36	0.28	0.34
MnO	0.11	0.13	0.13	0.07	0.10	0.73	0.09	0.17	0.07
MgO	1.09	2.32	2.70	1.29	1.11	0.53	3.23	0.87	0.17
CaO	1.43	7.60	9.50	2.00	2.34	52.91	8.00	10.86	8.47
Na_2O	5.35	5.09	5.13	7.91	6.69	2.63	4.74	3.37	2.26
K_2O	4.41	1.87	1.71	4.08	4.17	0.07	1.49	1.93	3.05
P_2O_5	0.16	0.64	0.63	0.25	0.25	0.07	0.08	0.08	0.09
LOI	2.35	1.10	2.17	0.25	0.50	39.89	6.22	10.05	7.73
Total	100.01	102.95	100.19	102.12	101.08	100.48	102.14	100.16	100.67
Zr	544	252	377	506	519	12	141	145	154
Y	46	45	36	42	42	5	17	19	21
Sr	211	565	1199	206	185	514	134	142	255
U	bdl	bdl	bdl	bdl	bdl	5	5	0	3
Rb	176	13	202	149	146	1	65	71	77
Th	29	10	13	18	20	6	12	9	10
Pb	25	11	19	18	19	bdl	bdl	bdl	30
Ga	19	19	19	19	20	48	bdl	bdl	11
Zn	61	73	99	50	49	18	28	404	14
Cu	1	64	2	0	2	bdl	bdl	bdl	bdl
Ni	7	18	6	6	13	bdl	275	2	7
Co	11	25	35	12	16	1	4	4	7
Cr	12	57	41	28	41	bdl	bdl	bdl	bdl
Ce	177	105	131	132	109	bdl	37	31	28
Ba	894	612	698	624	615	1	578	231	275
La	86	51	59	61	49	bdl	16	19	23
Nb	33	11	10	20	23	6	4	7	8
Ap	0.37	1.46	1.51	0.56	0.56		0.19	0.21	0.23
Il	1.27	3.91	3.15	1.52	1.54		0.49	0.67	0.80
Or	26.71	10.82	10.34	23.64	23.76		9.22	12.94	19.80
Ab	46.36	42.13	38.99	58.01	54.56		41.79	32.48	21.06
An	6.20	22.78	19.14	0.00	2.97		4.38	10.62	17.32
Mt	0.70	0.42	5.84	0.22	2.25		0.40	0.02	0.00
Hm	1.85	8.42	0.78	0.00	1.08		1.03	2.06	1.07
Di	0.00	7.84	14.77	6.46	5.16		18.05	5.32	1.02
Hy	2.79	2.02	0.00	0.68	0.28		0.00	0.00	0.00
Q	13.34	0.03	0.00	2.10	7.73		18.72	17.38	31.86
Ol	0.00	0.00	0.00	0.00	0.00		0.00	0.00	0.00
Ne	0.00	0.00	2.90	0.00	0.00		0.00	0.00	0.00
Cm	0.00	0.02	0.02	0.00	0.02		0.000	0.00	0.00
Mg#	38.11	27.04	36.67	11.39	11.17				
SI	7.80	11.36	15.13	7.54	6.80				
DI	86.41	52.97	52.23	83.75	86.05				
al	41.17	29.90	27.61	35.31	37.16	0.54	24.24	25.49	37.90
fm	17.43	31.81	28.02	17.96	18.74	1.71	22.70	11.35	6.43
c	6.64	21.87	27.81	8.06	9.47	93.54	32.22	45.57	34.87
alk	34.77	16.42	16.56	38.67	34.64	4.20	20.83	17.60	20.80
si	283.60	140.81	140.17	248.37	255.09	6.04	245.67	223.45	323.06
k	0.35	0.19	0.18	0.25	0.29	0.02	0.17	0.27	0.47
ti	2.14	4.24	3.34	2.31	2.39	0.05	0.70	0.90	1.62
mg	0.41	0.29	0.39	0.40	0.33	0.75	0.79	0.45	0.20
w	0.72	0.80	0.57	0.67	0.62	0.25	0.76	0.85	0.72

Sample	MA-57	MA-58A	MA-59A	MA-59B	MA-62	MA-64	MA-65	MA-66	MA-69
SiO_2	68.75	62.12	71.51	73.46	69.87	49.96	65.49	67.73	48.72
TiO_2	0.65	0.54	0.15	0.10	0.41	0.92	0.83	0.87	1.46
Al_2O_3	16.03	16.51	14.25	12.26	14.89	14.67	16.55	16.12	17.51
Fe_2O_3	1.86	3.90	0.81	0.83	1.25	3.21	4.32	3.95	3.26
FeO	0.80	0.60	0.81	0.64	0.56	4.41	0.29	0.48	6.19
MnO	0.08	0.12	0.07	0.07	0.07	0.12	0.13	0.07	0.16
MgO	0.78	2.24	0.00	0.08	0.64	9.65	0.91	1.21	6.02
CaO	0.72	4.85	0.41	0.31	1.08	10.21	2.19	2.34	9.88
Na_2O	6.03	4.90	3.61	3.77	4.35	5.11	4.84	5.01	4.37
K_2O	4.54	2.20	4.61	4.50	4.71	1.16	3.92	3.95	1.28
P_2O_5	0.16	0.20	0.02	0.04	0.09	0.26	0.25	0.27	0.39
LOI	1.20	1.83	3.73	3.04	1.88	0.31	0.29	0.11	0.10
Total	101.60	100.01	99.98	99.10	99.80	99.99	100.01	102.10	99.34
Zr	728	167	292	294	265	127	478	480	171
Y	57	20	55	63	27	27	45	68	32
Sr	53	472	41	23	105	502	183	183	718
U	bdl	bdl	13	11	bdl	bdl	bdl	4	1
Rb	133	67	174	185	221	14	136	138	35
Th	21	11	29	26	43	4	16	17	5
Pb	20	14	30	34	25	6	12	18	7
Ga	21	17	20	19	16	14	20	21	16
Zn	64	52	60	66	29	56	52	61	67
Cu	bdl	21	bdl	bdl	bdl	32	15	12	39
Ni	5	15	149	17	9	222	9	9	50
Co	8	20	2	2	8	64	9	4	35
Cr	33	49	bdl	bdl	53	449	9	23	55
Ce	122	70	64	69	92	48	102	156	56
Ba	618	749	130	16	284	396	675	645	500
La	55	38	32	27	45	26	58	88	37
Nb	29	11	36	25	20	9	33	23	12
Ap	0.35	0.47	0.05	0.09	0.21	0.60	0.58	0.60	0.93
Il	1.20	1.05	0.30	0.21	0.80	1.75	0.61	0.97	2.83
Or	26.18	13.24	28.25	27.72	28.72	6.80	23.34	22.69	7.74
Ab	49.83	42.13	31.72	33.25	37.98	22.48	41.28	41.20	23.79
An	2.49	16.85	2.05	1.38	4.92	13.67	9.28	9.56	24.86
Mt	0.68	0.36	1.09	1.19	0.64	5.54	0.00	0.00	4.58
Hm	1.41	3.90	0.00	0.00	0.79	0.00	3.98	3.66	0.00
Di	0.00	4.91	0.00	0.00	0.00	27.70	0.00	0.00	18.12
Hy	1.89	3.38	0.66	0.55	1.64	0.00	2.27	2.94	0.00
Q	15.61	13.59	33.05	34.81	23.28	0.00	17.03	17.93	0.00
Ol	0.00	0.00	0.00	0.00	0.00	10.09	0.00	0.00	9.43
Ne	0.00	0.00	0.00	0.00	0.00	11.11	0.00	0.00	7.51
Cm	0.00	0.02	0.00	0.00	0.02	0.10	0.00	0.00	0.02
Mg#	32.99	45.68	0.00	8.84	38.63	99.73	21.48	23.18	99.68
SI	5.50	15.91	0.00	0.79	5.56	39.16	6.43	7.93	27.74
DI	91.62	68.96	93.02	95.78	89.98	40.39	81.65	81.82	39.04
al	42.45	34.78	50.91	47.11	45.08	18.70	40.86	38.92	24.31
fm	14.78	24.66	7.38	8.07	11.91	45.34	19.15	20.63	38.84
c	3.45	18.57	2.75	2.21	5.92	23.67	9.81	10.24	24.94
alk	39.32	21.99	38.96	42.61	37.09	12.29	30.18	30.20	11.90
si	317.98	221.96	433.28	479.21	353.87	108.05	274.25	281.57	112.40
k	0.33	0.23	0.46	0.44	0.42	0.13	0.35	0.34	0.16
ti	2.18	1.45	0.70	0.52	1.57	1.50	2.63	2.69	2.59
mg	0.35	0.48	0.00	0.09	0.41	0.69	0.29	0.36	0.54
w	0.68	0.86	0.45	0.53	0.66	0.44	0.92	0.88	0.31

Sample	MA-70	MA-71	MA-73	MA-74	MA-75	MA-76	MA-78	MA-79	MA-83
SiO_2	50.82	64.42	65.66	66.78	65.81	0.00	62.35	65.47	64.83
TiO_2	1.60	0.84	0.70	0.71	0.63	0.05	0.58	0.51	0.47
Al_2O_3	16.82	15.69	16.65	16.56	15.64	0.52	16.76	16.34	16.62
Fe_2O_3	5.62	3.49	2.80	2.98	2.55	0.05	4.51	4.53	3.31
FeO	3.66	0.94	0.24	0.40	0.56	0.18	0.98	0.16	0.72
MnO	0.19	0.12	0.06	0.05	0.07	0.03	0.06	0.07	0.05
MgO	2.65	0.65	0.58	0.94	0.95	1.28	1.88	1.52	1.27
CaO	9.77	2.08	1.20	1.41	1.27	56.01	5.12	3.36	3.90
Na_2O	4.15	5.70	5.33	4.39	4.38	1.65	3.50	3.47	4.20
K_2O	1.83	3.65	4.60	4.62	5.05	0.00	2.05	2.39	2.54
P_2O_5	0.56	0.32	0.20	0.27	0.19	0.03	0.28	0.17	0.18
LOI	1.93	0.66	0.89	0.89	2.89	40.49	1.13	1.55	1.57
Total	99.60	98.56	100.71	100.00	99.99	100.29	99.20	99.54	99.66
Zr	334	480	518	526	510	7	155	152	151
Y	43	44	54	49	55	4	18	17	19
Sr	1125	218	195	191	160	507	469	344	381
U	16	5	3	3	5	bdl	1	1	bdl
Rb	145	130	142	142	154	bdl	69	66	80
Th	8	17	23	23	24	2	10	9	9
Pb	22	20	25	26	26	7	11	14	17
Ga	39	21	22	21	19	bdl	17	17	18
Zn	209	57	69	62	63	bdl	55	43	48
Cu	6	12	5	1	1	bdl	31	28	34
Ni	10	11	6	5	8	bdl	35	24	14
Co	26	7	5	4	1	2	11	8	12
Cr	36	9	8	2	37	bdl	69	24	38
Ce	101	105	168	130	167	bdl	42	45	54
Ba	738	687	884	922	888	1	615	667	579
La	54	68	89	76	94	5	27	36	36
Nb	17	26	35	42	36	4	15	7	13
Ap	1.42	0.77	0.47	0.63	0.47		0.70	0.40	0.42
Il	3.13	1.65	0.51	0.85	1.19		1.14	0.34	0.91
Or	11.11	22.34	27.78	27.66	30.79		12.65	14.60	15.31
Ab	36.12	49.83	46.10	37.56	38.32		30.96	30.37	36.29
An	22.49	6.68	4.80	5.28	5.24		24.58	16.10	18.57
Mt	7.32	0.64	0.00	0.00	0.00		1.53	0.00	0.98
Hm	0.27	2.93	2.72	2.87	2.41		3.26	4.33	2.53
Di	14.67	1.42	0.00	0.00	0.00		0.00	0.00	0.00
Hy	0.00	1.03	1.47	2.37	2.47		4.88	3.91	3.24
Q	1.38	12.57	14.43	20.10	17.86		20.05	27.09	21.37
Ol	0.00	0.00	0.00	0.00	0.00		0.00	0.00	0.00
Ne	0.00	0.00	0.00	0.00	0.00		0.00	0.00	0.00
Cm	0.02	0.00	0.00	0.00	0.02		0.02	0.00	0.02
Mg#	99.73	19.35	25.57	33.80	36.25		38.45	37.26	35.86
SI	14.60	4.51	4.28	7.06	7.12		14.70	12.74	10.51
DI	48.61	84.74	88.31	85.32	86.97		63.66	72.06	72.97
al	27.18	39.27	44.06	43.82	42.42	0.46	36.87	40.72	39.95
fm	29.90	17.94	13.74	17.06	16.84	3.10	25.10	23.42	19.82
c	28.68	9.46	5.79	6.75	6.31	94.06	20.48	15.19	17.03
alk	14.23	33.34	36.40	32.36	34.43	2.38	17.55	20.66	23.20
si	139.27	269.26	294.79	299.84	302.95	0.00	225.33	272.64	264.30
k	0.22	0.30	0.36	0.41	0.43	0.00	0.28	0.31	0.28
ti	3.31	2.69	2.38	2.40	2.18	0.06	1.61	1.63	1.44
mg	0.36	0.23	0.28	0.37	0.39	0.92	0.42	0.41	0.39
w	0.56	0.76	0.91	0.86	0.79	0.13	0.79	0.96	0.80

Sample	MA-84	MA-85	MA-89	MA-91	MA-93	MA-94	MA-96	MA-98	MA-101
SiO_2	63.81	65.83	27.49	63.68	66.52	66.87	66.24	67.32	65.88
TiO_2	0.48	0.48	0.19	0.52	0.47	0.46	0.49	0.38	0.91
Al_2O_3	16.94	16.10	3.73	16.41	16.05	15.45	16.48	16.89	25.19
Fe_2O_3	4.45	3.64	0.84	2.56	2.98	2.71	3.07	2.86	0.13
FeO	0.04	0.42	0.96	1.12	0.22	0.36	0.34	0.18	0.00
MnO	0.08	0.05	0.15	0.08	0.06	0.06	0.08	0.06	0.00
MgO	1.27	1.32	1.93	2.29	1.46	1.79	1.53	0.67	0.00
CaO	4.26	3.80	35.37	4.69	3.86	3.63	3.87	3.13	0.00
Na_2O	3.28	4.25	1.28	4.69	3.59	3.44	4.24	4.25	0.72
K_2O	2.45	2.63	0.50	2.14	2.27	2.32	2.28	2.63	0.06
P_2O_5	0.17	0.19	0.14	0.18	0.18	0.17	0.18	0.15	0.34
LOI	2.67	0.95	28.57	0.70	1.45	2.09	0.63	1.03	6.60
Total	99.90	99.66	101.15	99.06	99.11	99.35	99.43	99.55	99.83
Zr	154	157	17	173	168	160	172	149	86
Y	16	19	10	16	16	15	15	14	2
Sr	345	382	1215	435	430	366	419	404	3206
U	2	1	127	1	0	bdl	bdl	bdl	1
Rb	80	90	17	65	69	71	71	78	bdl
Th	12	10	2	10	10	8	8	10	9
Pb	15	18	4	17	16	14	12	15	56
Ga	16	18	5	17	18	16	15	15	38
Zn	44	50	24	47	48	42	48	41	bdl
Cu	20	20	17	25	15	14	18	16	32
Ni	12	13	51	13	5	9	11	6	bdl
Co	14	6	9	11	5	6	7	6	94
Cr	38	20	67	20	26	17	19	9	31
Ce	45	58	3	43	39	37	49	51	70
Ba	557	589	77	495	475	559	535	537	261
La	28	36	bdl	24	32	32	32	29	44
Nb	17	17	3	13	15	18	20	12	4
Ap	0.42	0.44		0.44	0.42	0.42	0.42	0.37	
Il	0.07	0.91		1.03	0.47	0.71	0.72	0.38	
Or	15.25	15.96		13.00	13.89	14.24	13.83	16.13	
Ab	29.27	36.88		40.86	31.47	30.29	36.80	37.31	
An	21.09	17.51		17.88	18.67	17.58	18.52	14.33	
Mt	0.00	0.00		2.11	0.00	0.00	0.00	0.00	
Hm	4.26	3.51		1.05	2.89	2.64	2.98	2.78	
Di	0.00	0.44		3.77	0.00	0.00	0.00	0.04	
Hy	3.34	3.16		4.13	3.79	4.63	3.91	1.72	
Q	25.12	21.10		15.65	26.97	28.13	22.20	26.37	
Ol	0.00	0.00		0.00	0.00	0.00	0.00	0.00	
Ne	0.00	0.00		0.00	0.00	0.00	0.00	0.00	
Cm	0.02	0.00		0.00	0.00	0.00	0.00	0.00	
Mg#	34.49	36.97		52.36	45.44	50.91	44.69	28.66	
SI	11.21	10.81		17.86	13.98	16.84	13.38	6.35	
DI	69.64	73.94		69.51	72.33	72.66	72.83	79.81	
al	39.70	39.12	4.81	36.08	41.17	40.15	40.12	41.61	95.26
fm	20.98	20.16	9.03	23.07	19.41	21.47	19.67	15.01	0.00
c	19.28	16.80	82.77	18.77	17.99	17.16	17.17	15.90	0.00
alk	20.04	23.92	3.39	22.08	21.43	21.22	23.04	27.48	4.74
si	265.40	267.38	60.05	233.77	285.15	290.38	269.56	319.09	416.34
k	0.33	0.29	0.21	0.23	0.29	0.31	0.26	0.29	0.06
ti	1.54	1.48	0.31	1.47	1.55	1.53	1.52	1.37	4.41
mg	0.38	0.40	0.70	0.55	0.49	0.55	0.48	0.32	0.00
w	0.99	0.88	0.36	0.66	0.92	0.87	0.88	0.93	0.00

Sample	MA-102	MA-104	MA-105	MA-107	MA-109B	MA-110	MA-111	MA-113	MA-114
SiO_2	49.61	58.31	0.14	68.33	17.33	19.54	26.49	67.38	66.38
TiO_2	0.63	0.63	0.03	0.44	0.07	0.02	0.17	0.38	0.42
Al_2O_3	16.03	17.53	0.57	15.88	1.32	0.63	4.05	16.16	16.72
Fe_2O_3	2.41	3.20	0.53	2.66	0.76	0.25	0.85	2.62	2.87
FeO	0.16	2.87	0.81	0.36	0.38	1.48	2.48	0.22	0.24
MnO	0.01	0.12	0.31	0.06	0.30	0.34	0.30	0.06	0.01
MgO	0.63	3.00	19.51	0.50	1.24	14.21	11.88	0.45	1.01
CaO	0.28	4.06	30.31	2.87	44.11	23.74	20.56	2.82	3.28
Na_2O	1.67	4.35	1.58	3.72	2.24	2.86	2.24	5.62	3.76
K_2O	1.26	0.24	0.02	2.71	0.19	0.01	0.57	2.66	2.73
P_2O_5	0.15	0.14	0.05	0.19	0.04	0.03	0.39	0.14	0.16
LOI	20.74	5.06	46.37	1.36	33.73	37.02	31.16	0.92	1.84
Total	93.58	99.51	100.23	99.08	101.71	100.13	101.14	99.43	99.42
Zr	131	133	17	154	18	23	51	150	153
Y	7	29	4	15	10	bdl	19	30	13
Sr	373	339	47	389	273	33	86	390	408
U	3	bdl	1	2	3	0	bdl	0	bdl
Rb	1	7	bdl	87	4	23	bdl	84	80
Th	12	7	2	12	6	1	bdl	9	11
Pb	309	10	41	20	5	9	bdl	17	17
Ga	bdl	16	0	17	2	4	3	15	17
Zn	bdl	133	125	43	1	0	19	45	48
Cu	bdl	3	bdl	16	bdl	bdl	bdl	16	29
Ni	bdl	7	154	7	bdl	bdl	7	11	5
Co	5	14	10	8	4	2	5	6	4
Cr	53	3	bdl	4	bdl	1	39	17	43
Ce	69	22	bdl	49	bdl	bdl	1	73	37
Ba	288	140	bdl	621	144	8	31	598	563
La	24	16	bdl	33	12	3	7	65	30
Nb	13	10	3	11	3	4	4	11	17
Ap				0.44				0.35	0.40
Il				0.76				0.44	0.52
Or				16.43				15.96	16.73
Ab				32.23				48.30	32.99
An				13.34				11.20	15.76
Mt				0.00				0.00	0.00
Hm				2.59				2.55	2.79
Di				0.00				1.14	0.00
Hy				1.30				0.62	2.62
Q				30.67				18.96	26.96
Ol				0.00				0.00	0.00
Ne				0.00				0.00	0.00
Cm				0.00				0.00	0.02
Mg#				22.90				22.21	37.11
SI				5.03				3.92	9.54
DI				79.33				83.22	76.68
al	64.47	36.46	0.52	45.16	1.48	0.73	5.06	42.27	42.32
fm	16.91	32.78	46.59	14.28	4.85	44.07	42.89	12.24	17.05
c	2.06	15.36	50.49	14.83	89.33	49.76	46.69	13.45	16.04
alk	16.56	15.40	2.40	25.73	4.34	5.44	5.36	31.85	24.59
si	338.55	205.72	0.22	329.53	36.55	38.20	56.15	300.46	303.10
k	0.33	0.03	0.01	0.32	0.05	0.00	0.14	0.24	0.32
ti	3.32	1.68	0.04	1.59	0.10	0.03	0.28	1.29	1.46
mg	0.38	0.48	0.97	0.26	0.72	0.94	0.88	0.25	0.40
w	0.91	0.50	0.24	0.86	0.55	0.09	0.18	0.91	0.91

Sample	MA-115	MA-116	MA-117	MA-120	MA-121	MA-122	MA-123	MA-125	MA-126
SiO_2	65.45	67.00	47.38	63.90	61.56	67.23	66.51	62.80	64.33
TiO_2	0.53	0.45	1.77	0.51	0.61	0.33	0.34	0.59	0.48
Al_2O_3	16.91	16.01	17.59	16.48	17.47	16.47	16.56	17.01	16.41
Fe_2O_3	5.79	2.69	8.64	4.69	4.43	2.54	2.32	4.90	2.96
FeO	0.14	0.36	2.48	0.24	1.17	1.10	0.24	0.44	0.44
MnO	0.07	0.06	0.18	0.08	0.07	0.06	0.06	0.13	0.02
MgO	0.58	0.59	5.75	0.91	1.73	0.98	1.41	1.72	0.95
CaO	2.52	3.36	8.50	4.62	5.27	2.87	3.38	4.96	4.18
Na_2O	5.17	4.86	4.46	3.50	4.14	3.65	3.99	4.37	5.87
K_2O	0.39	2.59	1.58	2.24	2.22	2.56	2.73	2.13	2.84
P_2O_5	0.11	0.15	0.68	0.13	0.22	0.13	0.23	0.10	0.17
LOI	1.69	1.02	0.30	1.84	1.11	1.50	1.73	1.09	1.18
Total	99.35	99.14	99.31	99.14	100.00	99.42	99.50	99.15	99.83
Zr	100	144	215	145	152	172	166	153	150
Y	29	13	34	24	29	13	11	27	28
Sr	268	420	875	416	430	441	472	441	374
U	bdl	0	0	bdl	3	bdl	bdl	0	3
Rb	11	85	35	79	60	85	80	60	79
Th	10	11	8	11	14	11	10	12	14
Pb	8	15	8	13	14	18	17	13	16
Ga	10	17	18	17	20	19	19	19	17
Zn	20	36	83	45	58	39	37	60	37
Cu	20	17	28	24	16	18	17	35	17
Ni	10	2	29	15	12	8	6	9	12
Co	7	6	36	9	14	6	3	13	8
Cr	4	15	21	17	20	13	17	14	13
Ce	33	44	78	49	51	60	51	42	54
Ba	181	542	604	529	557	703	569	566	578
La	18	24	43	28	37	37	33	29	38
Nb	10	107	18	10	13	12	13	13	11
Ap	0.26	0.37	1.60	0.30	0.51	0.33	0.56	0.47	0.40
Il	0.29	0.76	3.42	0.50	1.16	0.19	0.53	0.95	0.93
Or	2.42	15.78	9.52	13.65	13.30	15.78	16.84	12.71	17.02
Ab	46.02	33.67	30.32	30.54	35.53	32.23	35.28	37.31	50.33
An	12.43	16.17	23.69	22.82	22.91	13.92	15.99	20.76	10.16
Mt	0.00	0.00	2.91	0.00	2.07	0.00	0.00	0.00	0.00
Hm	5.47	2.62	5.95	4.48	2.64	2.48	2.27	4.67	3.00
Di	0.00	0.00	11.49	0.00	1.71	0.00	0.00	1.89	5.16
Hy	1.52	1.49	0.00	2.34	3.62	2.54	3.69	3.43	0.00
Q	28.30	27.84	0.00	24.79	16.47	30.29	24.23	17.41	11.64
Ol	0.00	0.00	6.48	0.00	0.00	0.00	0.00	0.00	0.00
Ne	0.00	0.00	4.43	0.00	0.00	0.00	0.00	0.00	0.00
Cm	0.00	0.00	0.00	0.00	0.00	0.00	0.00	0.00	0.00
Mg#	15.23	26.02	99.62	25.04	36.22	40.59	50.28	36.42	33.47
SI	4.85	5.91	24.88	7.98	12.79	10.04	13.27	12.67	7.28
DI	76.74	77.29	17.37	38.94	65.30	78.30	76.35	67.43	78.99
al	42.16	43.86	25.08	39.94	36.83	44.09	41.04	36.69	37.67
fm	22.03	14.31	39.94	19.86	23.58	16.10	17.65	23.43	15.62
c	12.14	16.76	22.05	20.38	20.19	14.83	16.23	19.44	17.46
alk	23.67	25.07	12.92	19.83	19.40	24.98	25.08	20.45	29.24
si	289.88	311.42	114.68	262.67	220.21	324.95	293.21	229.73	250.63
k	0.05	0.31	0.19	0.30	0.26	0.32	0.31	0.24	0.24
ti	1.80	1.59	3.22	1.59	1.62	1.18	1.13	1.63	1.42
mg	0.18	0.28	0.52	0.28	0.39	0.44	0.53	0.40	0.35
w	0.97	0.86	0.74	0.94	0.75	0.95	0.89	0.90	0.86

Sample	MA-127	MA-129	MA-131	MA-132	MA-134	MA-135	MA-138	MA-139	MA-140
SiO_2	1.00	60.02	60.34	59.39	59.96	58.33	57.33	64.09	43.62
TiO_2	0.05	0.57	0.57	0.60	0.61	0.59	0.61	0.47	2.30
Al_2O_3	0.87	16.93	15.34	16.97	16.70	15.70	16.56	16.70	14.20
Fe_2O_3	0.00	4.58	3.90	4.99	3.72	4.47	5.01	3.03	8.68
FeO	0.34	2.04	1.78	0.58	1.99	1.08	1.99	1.24	3.26
MnO	0.19	0.13	0.11	0.16	0.12	0.11	0.16	0.09	0.21
MgO	1.11	2.34	3.31	3.18	3.36	2.82	2.79	2.47	6.38
CaO	54.79	6.35	6.12	6.21	6.02	5.02	6.15	4.63	14.27
Na_2O	2.39	4.18	4.51	3.77	4.05	3.60	3.92	3.17	4.54
K_2O	0.01	1.78	2.47	2.45	2.46	2.35	1.66	2.58	1.17
P_2O_5	0.05	0.13	0.20	0.19	0.23	0.18	0.16	0.14	1.12
LOI	40.67	0.51	1.06	1.35	0.85	1.16	1.76	1.28	0.86
Total	101.47	99.56	99.71	99.84	100.21	99.04	99.00	99.89	100.61
Zr	16	119	141	140	155	146	134	132	241
Y	6	27	24	27	22	23	32	21	37
Sr	295	363	618	668	666	580	288	373	1232
U	1	bdl	17	1	2	1	18	1	bdl
Rb	bdl	48	88	65	79	86	61	71	25
Th	3	11	16	16	17	16	2	7	10
Pb	bdl	8	26	17	19	16	5	13	7
Ga	0	16	32	17	19	18	29	18	17
Zn	49	51	141	65	53	57	132	46	114
Cu	bdl	28	23	22	27	25	33	13	84
Ni	bdl	7	45	39	47	41	0	19	47
Co	207	19	18	19	15	20	17	9	39
Cr	bdl	77	86	118	129	108	21	67	123
Ce	381	32	72	64	64	64	26	49	129
Ba	bdl	495	772	730	709	841	403	540	678
La	5	18	44	39	36	47	21	28	65
Nb	4	10	10	10	7	16	7	16	17
Ap		0.30	0.47	0.47	0.54	0.44	0.40	0.35	2.62
Il		1.10	1.10	1.20	1.16	1.18	1.20	0.93	4.43
Or		10.64	14.77	15.07	14.66	14.66	10.17	15.66	6.97
Ab		35.70	38.66	33.16	34.43	32.06	33.58	27.49	8.59
An		22.37	14.51	20.22	18.39	20.80	24.06	21.54	15.04
Mt		4.94	4.03	0.08	4.65	1.81	4.85	2.66	3.82
Hm		1.21	1.17	4.70	0.54	3.46	1.87	1.11	5.36
Di		6.68	11.64	8.23	8.72	3.28	5.08	0.85	34.65
Hy		2.78	2.95	4.43	4.37	5.88	4.87	5.91	0.00
Q		14.12	10.51	12.25	12.38	16.25	13.76	23.39	0.00
Ol		0.00	0.00	0.00	0.00	0.00	0.00	0.00	0.00
Ne		0.00	0.00	0.00	0.00	0.00	0.00	0.00	16.40
Cm		0.02	0.02	0.03	0.03	0.03	0.00	0.02	0.03
Mg#		38.64	51.76	51.08	52.04	47.97	42.19	50.55	99.74
SI		15.68	20.96	21.46	21.82	19.81	18.48	19.73	26.14
DI		60.46	65.07	60.48	61.47	62.97	57.51	66.54	31.96
al	0.78	32.60	29.26	31.43	30.38	32.94	31.79	35.85	17.80
fm	2.93	28.21	30.26	28.91	30.46	30.15	31.26	26.60	38.71
c	92.74	22.23	21.23	22.25	21.48	19.15	21.46	19.26	32.53
alk	3.55	16.96	19.25	17.41	17.68	17.76	15.50	18.28	10.96
si	1.52	196.11	195.38	194.97	194.91	209.85	186.65	248.29	92.81
k	0.00	0.22	0.26	0.30	0.29	0.30	0.22	0.35	0.14
ti	0.06	1.41	1.39	1.52	1.47	1.58	1.48	1.39	3.69
mg	0.86	0.40	0.53	0.55	0.53	0.50	0.43	0.54	0.52
w	0.00	0.67	0.66	0.88	0.63	0.79	0.69	0.68	0.69

Sample	MA-141A	MA-142	MA-143	MA-146	MA-148	MA-150	MA-151	MA-152	MA-153
SiO_2	58.33	60.21	59.25	59.74	60.22	60.78	62.40	61.31	65.21
TiO_2	0.60	0.45	0.63	0.60	0.52	0.59	0.49	0.56	0.79
Al_2O_3	15.45	14.84	16.32	14.44	16.78	16.67	16.28	16.61	16.26
Fe_2O_3	5.21	2.88	4.31	4.12	4.87	3.85	4.06	4.67	3.39
FeO	0.58	0.62	1.44	1.76	0.16	1.30	0.52	0.59	0.66
MnO	0.11	0.06	0.12	0.12	0.09	0.09	0.06	0.11	0.15
MgO	3.58	1.23	3.71	3.37	1.94	1.95	1.35	2.17	1.05
CaO	6.81	7.75	6.42	6.53	6.13	5.89	4.59	5.39	2.42
Na_2O	5.08	5.14	3.89	5.81	4.80	4.10	3.92	4.33	5.91
K_2O	2.41	2.38	2.44	2.51	2.06	2.08	2.58	2.00	3.28
P_2O_5	0.20	0.30	0.20	0.23	0.18	0.20	0.13	0.21	0.26
LOI	1.27	3.59	0.71	0.93	1.38	1.33	2.26	1.53	0.52
Total	99.63	99.45	99.44	100.16	99.13	98.83	98.64	99.48	99.85
Zr	161	200	139	149	159	166	137	162	375
Y	28	21	22	22	22	18	19	23	53
Sr	643	461	666	613	414	415	327	452	245
U	1	0	18	bdl	1	1	1	1	1
Rb	54	52	89	76	69	70	91	65	111
Th	15	10	16	13	6	8	16	9	12
Pb	14	11	22	12	13	11	18	13	18
Ga	19	18	31	17	18	18	17	16	21
Zn	50	43	116	50	59	59	42	64	66
Cu	26	19	20	33	18	15	25	19	4
Ni	42	9	51	37	11	10	9	10	4
Co	17	6	20	13	12	13	8	15	4
Cr	113	10	123	107	44	29	23	49	0
Ce	63	59	75	52	56	52	41	47	88
Ba	723	537	762	780	540	518	660	752	619
La	39	39	48	35	30	29	45	36	45
Nb	12	17	11	14	14	11	13	12	28
Ap	0.47	0.72	0.47	0.54	0.44	0.49	0.30	0.51	0.60
Il	1.16	0.04	1.22	1.14	0.35	1.16	0.99	1.10	1.39
Or	14.48	14.66	14.77	14.95	12.77	12.77	16.08	12.35	19.50
Ab	43.65	45.34	33.75	49.49	33.75	35.95	34.85	29.52	50.33
An	12.44	10.86	20.41	5.97	23.74	21.67	17.90	25.61	8.19
Mt	0.07	0.66	2.88	3.90	0.00	2.55	0.20	0.30	0.00
Hm	5.24	2.54	2.14	1.46	4.64	2.23	3.76	4.25	3.41
Di	16.02	6.88	8.54	18.27	0.37	5.61	0.00	0.72	1.58
Hy	1.64	0.00	5.53	0.00	4.88	2.42	3.54	5.32	1.91
Q	4.65	9.67	10.12	3.39	18.06	15.02	21.43	20.16	12.78
Ol	0.00	0.00	0.00	0.00	0.00	0.00	0.00	0.00	0.00
Ne	0.00	0.00	0.00	0.00	0.00	0.00	0.00	0.00	0.00
Cm	0.03	0.00	0.03	0.03	0.02	0.00	0.00	0.02	0.00
Mg#	52.66	38.85	53.33	51.33	41.73	40.86	35.12	43.03	31.87
SI	21.30	10.07	23.44	19.38	15.38	14.81	10.96	17.20	7.34
DI	62.78	69.67	58.64	67.83	64.58	63.74	72.36	62.03	82.61
al	27.93	31.17	30.45	26.32	36.99	34.67	39.78	36.26	38.83
fm	29.88	16.09	30.92	29.68	23.75	24.33	21.68	25.68	18.92
c	22.38	29.58	21.78	21.64	20.56	22.27	15.96	21.38	10.53
alk	19.82	23.16	16.85	22.36	18.71	18.73	22.58	16.69	31.71
si	178.95	214.60	184.33	184.74	225.30	211.01	258.73	223.27	264.30
k	0.24	0.23	0.29	0.22	0.26	0.25	0.30	0.28	0.27
ti	1.38	1.21	1.48	1.38	1.45	1.56	1.54	1.54	2.39
mg	0.55	0.41	0.57	0.52	0.45	0.42	0.38	0.47	0.34
w	0.89	0.81	0.72	0.68	0.96	0.73	0.87	0.87	0.82

Sample	MA-155	MA-157	MA-159	MA-160	MA-161	MA-163	MA-164	MA-166	MA-168
SiO_2	50.05	60.55	61.32	60.85	60.57	61.49	50.38	51.02	57.21
TiO_2	1.61	1.09	1.08	1.15	1.14	1.08	1.22	1.22	1.72
Al_2O_3	19.24	17.05	17.39	17.48	17.45	17.63	18.51	18.81	15.00
Fe_2O_3	5.41	3.12	4.48	4.89	3.66	2.94	2.89	6.34	5.02
FeO	4.04	1.77	0.62	0.44	1.96	2.02	5.29	2.27	5.20
MnO	0.18	0.18	0.21	0.20	0.14	0.14	0.15	0.12	0.20
MgO	2.74	1.35	0.77	1.32	1.34	1.41	5.68	4.55	1.47
CaO	8.07	2.83	2.78	2.75	2.47	2.91	8.79	8.81	3.54
Na_2O	5.27	6.09	7.35	6.54	5.00	5.80	4.90	4.27	6.35
K_2O	2.23	3.32	3.57	3.35	3.31	3.31	1.27	1.31	3.52
P_2O_5	0.79	0.45	0.38	0.40	0.45	0.43	0.42	0.43	0.66
LOI	0.69	1.48	0.62	1.24	1.23	0.36	0.00	0.24	0.46
Total	100.35	99.28	100.57	100.61	98.72	99.52	99.50	99.39	100.35
Zr	283	369	356	380	379	357	158	151	412
Y	36	51	44	46	41	42	23	28	67
Sr	805	404	398	327	295	374	628	618	305
U	1	1	1	bdl	14	2	19	18	19
Rb	62	86	109	81	124	105	40	40	141
Th	10	13	10	12	17	14	bdl	bdl	23
Pb	11	17	14	17	20	14	10	11	26
Ga	20	20	20	21	37	23	32	33	37
Zn	107	77	75	80	141	67	144	142	187
Cu	46	3	5	bdl	bdl	4	29	28	89
Ni	16	7	5	6	5	8	68	76	bdl
Co	24	3	7	3	0	4	33	33	17
Cr	18	13	bdl	7	5	7	58	41	12
Ce	126	120	130	139	98	107	44	54	138
Ba	685	801	877	721	769	792	332	382	801
La	56	72	69	66	67	62	29	37	80
Nb	19	26	25	23	28	24	9	13	22
Ap	1.84	1.11	0.88	0.93	1.09	1.05	0.98	0.99	1.53
Il	3.08	2.17	1.29	0.91	2.24	2.15	2.32	2.34	3.27
Or	13.24	20.51	20.92	19.74	20.21	20.39	7.51	7.86	20.80
Ab	33.87	45.01	61.59	55.16	43.74	42.30	32.16	36.63	53.80
An	22.33	11.55	3.88	10.98	9.58	12.09	24.93	28.64	2.04
Mt	7.87	2.66	0.00	0.00	3.08	3.53	4.07	3.83	7.29
Hm	0.00	1.20	4.44	4.87	1.65	0.43	0.00	3.32	0.00
Di	9.93	0.00	4.08	0.00	0.00	0.00	13.01	9.96	9.17
Hy	0.00	3.54	0.00	3.29	3.46	3.66	0.00	0.00	1.73
Q	0.00	10.98	1.45	3.19	12.44	13.34	0.00	0.00	0.14
Ol	1.77	0.00	0.00	0.00	0.00	0.00	9.66	1.42	0.00
Ne	5.90	0.00	0.00	0.00	0.00	0.00	5.17	0.00	0.00
Cm	0.00	0.00	0.00	0.00	0.00	0.00	0.02	0.02	0.00
Mg#	35.03	33.09	21.40	30.78	30.51	33.43	99.76	99.73	21.26
SI	14.20	9.24	4.60	8.00	8.87	9.69	27.51	24.00	6.99
DI	53.01	76.50	83.96	78.09	76.39	76.03	44.84	44.49	74.74
al	29.79	38.94	37.06	38.42	39.14	38.37	26.69	28.72	28.20
fm	30.32	22.01	18.19	21.25	24.34	22.95	36.68	33.95	32.92
c	22.72	11.75	10.75	10.40	10.05	12.20	23.04	24.43	12.08
alk	17.17	27.30	34.00	29.93	26.47	26.48	13.59	12.90	26.80
si	131.50	230.77	225.28	214.64	227.43	236.85	123.23	132.12	182.42
k	0.22	0.30	0.24	0.25	0.30	0.31	0.14	0.17	0.27
ti	3.19	3.18	2.94	3.06	3.27	3.19	2.23	2.36	4.12
mg	0.35	0.36	0.23	0.33	0.31	0.36	0.56	0.52	0.21
w	0.55	0.60	0.87	0.91	0.63	0.55	0.32	0.70	0.46

Sample	MA-169	MA-171	MA-173	MA-175	MA-176	MA-177	MA-178	MA-179	MA-180
SiO_2	49.52	47.82	61.21	49.33	50.08	50.90	65.35	66.45	64.24
TiO_2	1.53	1.79	0.79	1.40	1.54	1.62	0.64	0.44	0.45
Al_2O_3	17.62	18.33	17.60	16.35	16.73	17.14	16.32	17.13	15.69
Fe_2O_3	5.02	10.92	3.62	3.93	7.11	8.66	2.74	2.63	2.88
FeO	4.99	0.44	0.42	6.66	2.94	1.00	0.38	0.44	0.60
MnO	0.18	0.18	0.15	0.17	0.26	0.17	0.11	0.03	0.08
MgO	5.46	3.77	1.34	6.02	3.61	2.42	0.92	0.51	1.40
CaO	8.88	8.88	2.15	9.52	9.20	9.23	1.37	3.47	3.79
Na_2O	3.64	4.46	6.32	4.27	4.26	4.32	4.09	4.52	7.42
K_2O	1.67	1.61	3.61	1.28	1.33	1.69	4.48	3.39	2.62
P_2O_5	0.49	0.60	1.64	0.41	0.35	0.59	0.18	0.19	0.22
LOI	0.20	1.01	0.65	0.50	2.21	2.04	3.14	0.54	1.50
Total	99.20	99.81	99.50	99.84	99.61	99.78	99.72	99.74	100.89
Zr	239	236	365	163	178	350	475	190	144
Y	34	31	49	31	38	43	61	18	11
Sr	660	796	216	705	459	1135	208	419	382
U	1	2	3	14	bdl	1	4	bdl	19
Rb	45	38	119	40	26	108	146	65	93
Th	10	10	17	bdl	8	15	22	9	10
Pb	10	7	17	8	5	17	24	14	27
Ga	20	17	21	34	17	23	19	17	30
Zn	87	92	60	136	76	114	68	40	108
Cu	15	22	4	32	59	6	3	17	16
Ni	24	29	6	63	32	4	9	7	5
Co	31	37	6	33	35	24	2	3	10
Cr	35	32	10	36	52	45	21	49	7
Ce	78	79	91	59	55	100	180	51	36
Ba	565	511	641	536	428	694	839	519	614
La	48	48	44	38	26	53	93	39	28
Nb	14	16	21	14	10	17	37	12	19
Ap	1.16	1.44	3.90	0.98	0.84	1.42	0.42	0.44	0.51
Il	2.94	0.97	0.91	2.74	3.04	2.17	0.80	0.87	0.86
Or	9.87	9.87	21.87	7.74	8.16	10.34	27.42	14.60	15.42
Ab	31.22	33.84	54.82	25.50	37.39	37.73	35.87	39.42	62.52
An	27.21	26.23	0.06	22.24	23.43	23.14	5.87	16.52	1.77
Mt	6.93	0.00	0.00	5.86	5.14	0.00	0.00	0.13	0.59
Hm	0.00	9.84	3.49	18.99	3.82	7.97	2.67	2.47	2.46
Di	11.25	8.34	0.00	0.00	14.56	13.43	0.00	0.00	7.47
Hy	4.30	0.00	3.41	0.00	0.00	0.00	2.37	1.32	0.00
Q	0.00	0.00	8.81	9.44	2.12	1.87	21.41	23.96	5.82
Ol	4.93	4.11	0.00	6.31	0.00	0.00	0.00	0.00	0.00
Ne	0.00	2.84	0.00	0.00	0.00	0.00	0.00	0.00	0.00
Cm	0.02	0.00	0.00	0.02	0.02	0.02	0.00	0.02	0.00
Mg#	99.73	99.68	37.37	99.70	32.24	31.05	34.81	22.73	42.17
SI	25.64	17.96	8.78	28.03	14.52	13.43	7.31	4.83	9.42
DI	31.22	46.55	85.50	42.68	47.67	49.94	84.70	77.98	83.76
al	25.74	27.86	38.47	22.78	27.09	28.46	44.70	42.90	34.35
fm	39.31	33.84	19.30	41.37	32.15	28.86	16.81	13.59	17.65
c	23.59	24.52	9.05	24.13	27.08	27.84	6.82	16.81	17.07
alk	11.36	13.78	33.18	11.72	13.68	14.83	31.68	26.70	32.93
si	122.78	120.73	240.65	111.91	137.57	143.37	303.66	299.96	242.34
k	0.23	0.19	0.27	0.16	0.17	0.21	0.42	0.26	0.19
ti	2.85	3.48	2.34	2.49	3.19	3.42	2.22	1.52	1.26
mg	0.51	0.43	0.41	0.51	0.33	0.35	0.38	0.25	0.44
w	0.46	0.95	0.88	0.35	0.68	0.87	0.86	0.83	0.81

Sample	MA-183	MA-185	MA-186	MA-187	MA-188	MA-189	MA-190	MA-192A	MA-193
SiO_2	68.29	68.80	66.24	67.13	68.10	66.48	63.50	75.28	64.25
TiO_2	0.32	0.39	0.48	0.50	0.43	0.41	0.56	0.14	0.49
Al_2O_3	16.55	16.02	17.94	16.19	16.31	16.40	16.63	15.85	15.90
Fe_2O_3	1.72	2.39	2.17	3.10	2.40	2.43	5.11	0.61	4.46
FeO	0.38	0.45	0.41	0.42	0.48	0.40	0.40	0.16	0.46
MnO	0.04	0.05	0.02	0.06	0.04	0.03	0.06	0.00	0.09
MgO	1.23	1.12	0.56	1.21	0.88	0.57	1.45	0.13	2.22
CaO	3.30	3.30	4.07	3.79	3.02	3.31	5.34	0.70	4.07
Na_2O	4.58	3.95	4.00	4.11	4.30	4.89	3.37	2.36	3.98
K_2O	2.45	2.76	2.04	2.43	2.58	2.42	2.15	2.06	2.38
P_2O_5	0.13	0.15	0.16	0.19	0.24	0.16	0.18	0.04	0.15
LOI	0.99	0.80	1.89	1.05	0.96	2.20	0.99	1.81	1.44
Total	99.98	100.18	99.98	100.18	99.74	99.70	99.74	99.14	99.89
Zr	153	158	166	165	188	192	148	88	125
Y	13	13	15	19	17	16	24	34	23
Sr	375	379	580	416	383	389	443	80	393
U	bdl	1	bdl	bdl	bdl	2	1	1	0
Rb	75	87	55	70	73	65	56	38	68
Th	6	11	9	11	9	8	14	bdl	12
Pb	16	17	14	16	15	15	16	11	13
Ga	16	16	19	16	17	18	18	12	16
Zn	31	45	47	42	39	39	53	22	39
Cu	12	15	5	20	20	11	17	2	9
Ni	2	4	9	12	4	6	16	0	7
Co	3	6	4	8	5	5	12	0	14
Cr	1	25	8	9	18	26	21	bdl	25
Ce	29	39	53	46	38	43	54	18	51
Ba	493	489	796	508	491	503	619	91	498
La	21	29	37	33	28	32	30	10	27
Nb	9	14	11	13	9	17	13	11	14
Ap	0.30	0.37	0.40	0.44	0.56	0.40	0.42	0.09	0.35
Il	0.61	0.74	0.82	0.86	0.84	0.46	0.84	0.29	0.95
Or	14.66	16.49	12.35	14.48	15.48	14.77	13.06	12.77	14.30
Ab	39.17	33.75	34.52	35.11	36.88	42.81	29.27	20.90	34.26
An	15.72	15.48	19.53	17.76	13.61	13.37	24.55	3.41	18.88
Mt	0.30	0.32	0.00	0.00	0.27	0.00	0.00	0.11	0.03
Hm	1.39	2.05	2.07	3.01	2.16	2.51	4.86	0.53	4.25
Di	0.00	0.00	0.00	0.00	0.00	1.46	0.80	0.00	0.57
Hy	3.11	2.81	1.44	3.04	2.22	0.79	3.34	0.35	5.36
Q	24.01	27.20	26.56	24.78	26.39	22.59	22.46	54.68	20.93
Ol	0.00	0.00	0.00	0.00	0.00	0.00	0.00	0.00	0.00
Ne	0.00	0.00	0.00	0.00	0.00	0.00	0.00	0.00	0.00
Cm	0.00	0.00	0.00	0.00	0.00	0.00	0.00	0.00	0.00
Mg#	52.24	41.83	28.48	37.84	35.11	21.89	32.17	24.01	44.90
SI	11.97	10.57	6.14	10.72	8.26	4.95	11.66	4.28	16.16
DI	77.84	77.44	73.43	74.37	78.75	80.17	64.79	88.35	69.49
al	43.11	42.01	46.28	40.52	43.44	41.42	37.39	61.44	36.11
fm	14.75	16.86	11.90	18.70	15.60	13.73	23.11	5.81	26.38
c	15.63	15.93	19.13	17.27	14.63	16.17	21.91	5.69	16.82
alk	26.51	25.21	22.69	23.51	26.32	28.68	17.70	27.07	20.69
si	301.72	310.02	290.03	285.27	307.85	303.47	238.42	566.77	247.48
k	0.26	0.32	0.25	0.28	0.28	0.25	0.30	0.37	0.28
ti	1.05	1.31	1.58	1.58	1.48	1.39	1.59	0.81	1.42
mg	0.55	0.45	0.31	0.41	0.38	0.28	0.36	0.26	0.48
w	0.79	0.82	0.82	0.86	0.81	0.85	0.91	0.76	0.89

Sample	MA-196	MA-198A	MA-199	MA-200	MA-201	MA-202	MA-203	MA-205	MA-206
SiO_2	65.98	74.83	66.50	62.97	69.29	65.12	69.78	64.67	55.05
TiO_2	0.19	0.14	0.54	0.56	0.66	0.55	0.40	0.62	0.92
Al_2O_3	6.01	13.18	16.97	16.69	15.17	16.12	16.04	16.40	16.80
Fe_2O_3	0.70	0.57	3.42	3.39	1.93	3.67	2.19	3.36	6.67
FeO	0.20	0.12	0.40	0.20	0.52	0.20	0.36	0.32	2.76
MnO	0.06	0.02	0.03	0.03	0.06	0.08	0.02	0.02	0.16
MgO	0.32	0.00	0.75	0.67	0.45	1.55	0.64	1.65	3.59
CaO	13.04	0.71	3.45	3.61	0.41	4.23	2.90	4.06	7.75
Na_2O	0.11	0.60	3.74	8.36	5.69	4.91	5.61	4.25	3.74
K_2O	1.57	6.52	2.37	2.36	4.13	2.31	2.75	2.27	1.44
P_2O_5	0.14	0.01	0.20	0.22	0.11	0.19	0.16	0.22	0.33
LOI	11.47	2.74	1.63	1.16	1.52	1.16	0.96	2.19	1.60
Total	99.79	99.44	100.00	100.44	99.94	100.09	100.81	100.03	100.81
Zr	47	160	176	175	595	170	141	171	140
Y	11	22	23	19	60	20	13	19	33
Sr	318	141	406	461	48	459	412	398	651
U	16	0	bdl	bdl	2	bdl	14	1	23
Rb	41	145	69	45	132	57	94	65	44
Th	bdl	27	10	9	20	12	12	8	11
Pb	19	16	14	16	21	14	27	11	24
Ga	6	15	16	18	22	19	34	18	35
Zn	14	3	48	33	97	49	94	54	145
Cu	1	bdl	16	8	bdl	13	13	14	38
Ni	10	1	9	5	8	10	bdl	8	40
Co	bdl	bdl	7	9	2	8	4	7	19
Cr	116	7	7	5	bdl	21	25	0	89
Ce	23	63	52	57	118	51	54	48	89
Ba	1465	601	508	596	568	574	541	488	791
La	13	33	57	37	77	32	32	32	52
Nb	4	nd	15	19	34	13	11	15	12
Ap	0.37	0.02	0.47	0.51	0.26	0.44	0.37	0.51	0.77
Il	0.39	0.25	0.87	0.86	1.10	0.42	0.74	0.63	1.77
Or	10.64	40.25	14.30	14.07	24.82	13.77	16.13	13.71	8.57
Ab	1.10	5.33	32.23	71.23	48.90	41.96	47.04	36.71	31.89
An	9.76	3.66	16.11	1.04	1.37	15.30	10.37	19.15	24.99
Mt	0.00	0.00	0.00	0.00	0.00	0.00	0.00	0.00	6.25
Hm	0.70	0.57	3.31	3.41	1.84	3.71	2.17	3.43	2.41
Di	1.98	0.00	0.00	3.60	0.00	2.74	2.21	0.00	9.03
Hy	0.00	0.00	1.89	0.00	1.15	2.64	0.55	4.21	4.83
Q	49.52	45.85	28.21	0.53	19.51	18.10	20.35	21.16	9.31
Ol	0.00	0.00	0.00	0.00	0.00	0.00	0.00	0.00	0.00
Ne	0.00	0.00	0.00	0.00	0.00	0.00	0.00	0.00	0.00
Cm	0.00	0.00	0.00	0.00	0.00	0.00	0.00	0.00	0.02
Mg#	38.79	0.00	25.92	23.67	25.30	41.80	30.90	44.52	41.51
SI	11.03	0.00	7.02	4.41	3.58	12.26	5.54	13.92	20.28
DI	61.26	91.43	74.74	85.83	93.23	73.83	83.52	71.58	49.77
al	15.42	56.31	43.99	36.15	44.72	37.24	41.72	38.91	27.95
fm	5.79	3.73	17.13	14.29	12.35	20.55	12.79	21.18	35.79
c	72.98	5.58	16.25	14.23	2.21	17.79	13.74	17.52	23.44
alk	5.81	34.38	22.63	35.33	40.71	24.42	31.75	22.40	12.83
si	344.69	535.41	292.54	231.46	346.41	255.35	307.99	260.28	155.39
k	0.90	0.88	0.29	0.16	0.32	0.24	0.24	0.26	0.20
ti	0.75	0.78	1.79	1.54	2.51	1.63	1.34	1.87	1.96
mg	0.43	0.00	0.29	0.25	0.27	0.44	0.33	0.47	0.42
w	0.73	0.80	0.88	0.88	0.76	0.94	0.84	0.90	0.69

Sample	MA-207	MA-208	MA-210	MA-213	MA-214	MA-215	MA-217	MA-219	MA-220A
SiO_2	62.34	53.25	0.75	62.13	58.62	65.40	67.57	63.73	73.87
TiO_2	0.54	0.66	0.07	0.54	0.55	0.52	0.53	0.52	0.80
Al_2O_3	16.96	15.67	1.26	16.39	16.54	16.48	16.40	16.03	15.19
Fe_2O_3	5.34	4.31	1.75	4.48	4.67	3.37	4.25	2.64	0.33
FeO	0.20	2.87	0.22	0.60	1.42	0.30	0.18	1.04	0.14
MnO	0.07	0.16	0.13	0.09	0.15	0.04	0.05	0.05	0.02
MgO	1.85	1.86	0.75	1.98	2.85	1.31	0.40	1.43	1.05
CaO	4.67	7.96	52.46	5.06	4.65	4.17	0.40	4.75	0.07
Na_2O	4.40	2.69	3.33	3.94	6.65	4.28	2.39	4.86	0.23
K_2O	2.30	1.41	0.20	2.29	1.90	2.36	2.39	2.40	2.00
P_2O_5	0.84	0.20	0.12	0.20	0.32	0.23	0.16	0.22	0.05
LOI	2.16	8.95	40.85	1.63	2.29	1.14	5.19	1.79	5.19
Total	101.67	99.99	101.89	99.33	100.72	99.60	99.91	99.46	98.94
Zr	144	126	5	150	159	206	162	198	168
Y	22	25	6	24	27	12	27	10	22
Sr	447	206	527	431	298	418	80	427	21
U	2	1	1	bdl	2	bdl	bdl	20	5
Rb	62	36	3	59	50	80	67	87	54
Th	13	bdl	2	13	9	10	11	15	bdl
Pb	16	17	7	15	10	13	13	21	48
Ga	18	17	bdl	17	17	17	17	31	16
Zn	52	42	6	47	60	61	19	117	0
Cu	18	12	bdl	7	11	24	2	15	bdl
Ni	18	3	21	15	4	14	2	16	bdl
Co	14	18	2	11	11	11	3	11	bdl
Cr	41	32	bdl	33	5	58	bdl	19	7
Ce	47	32	bdl	55	52	53	46	52	51
Ba	607	289	12	632	367	508	246	526	122
La	24	14	bdl	38	23	40	28	35	26
Nb	9	11	6	14	9	18	14	13	15
Ap	1.95			0.49	0.77	0.54	0.40	0.53	0.12
Il	0.39			1.06	1.06	0.62	0.38	1.01	0.32
Or	13.71			14.01	11.41	14.18	14.89	14.54	6.44
Ab	37.48			25.80	58.12	36.80	21.32	42.13	2.12
An	17.88			24.67	9.30	19.12	0.97	15.16	0.07
Mt	0.00			0.38	2.95	0.00	0.00	1.88	0.00
Hm	5.07			4.03	2.71	3.26	4.49	1.40	0.33
Di	0.00			0.00	9.31	0.00	0.00	5.80	0.00
Hy	4.63			5.13	2.88	3.34	1.05	0.95	2.86
Q	17.70			23.93	1.29	21.68	45.99	16.54	73.17
Ol	0.00			0.00	0.00	0.00	0.00	0.00	0.00
Ne	0.0			0.00	0.00	0.00	0.00	0.00	0.00
Cm	0.02			0.00	0.00	0.02	0.00	0.00	0.00
Mg#	37.22			41.54	46.06	38.98	13.29	41.48	79.96
SI	13.08			16.27	16.33	11.30	3.96	11.62	38.16
DI	68.89			63.74	70.82	72.66	82.20	73.21	81.73
al	36.44	31.60	1.15	37.22	31.01	39.69	54.07	36.67	74.56
fm	24.43	27.22	3.26	25.31	28.43	18.92	22.07	19.32	17.07
c	18.25	29.19	90.39	20.88	15.84	18.30	2.39	19.75	0.70
alk	20.88	12.00	5.20	16.59	24.72	23.10	21.47	24.26	7.67
si	227.24	178.83	1.16	239.35	186.51	267.26	378.14	247.48	658.64
k	0.26	0.26	0.04	0.34	0.16	0.27	0.40	0.25	0.74
ti	1.47	1.70	0.08	1.56	1.32	1.60	2.23	1.51	5.41
mg	0.41	0.35	0.53	0.45	0.47	0.42	0.15	0.43	0.82
w	0.96	0.54	0.82	0.86	0.75	0.90	0.96	0.70	0.66

Sample	MA-224	MA-226A	MA-228	MA-229	MA-230	MA-231	MA-232B	MA-233A	MA-233B
SiO_2	10.80	6270	61.34	68.80	47.81	60.59	70.52	46.71	50.74
TiO_2	0.16	1.10	0.57	0.64	1.59	0.53	0.11	1.55	1.56
Al_2O_3	3.64	15.81	17.10	15.50	17.26	16.46	12.52	17.04	16.70
Fe_2O_3	1.03	4.12	5.62	2.28	4.14	3.03	1.07	6.94	8.50
FeO	1.78	1.12	1.02	0.60	7.09	2.04	0.66	3.68	1.64
MnO	0.19	0.08	0.13	0.07	0.18	0.09	0.07	0.17	0.21
MgO	3.43	1.09	2.39	0.52	5.86	1.54	0.35	4.84	3.77
CaO	41.12	3.87	6.06	0.39	9.16	5.11	0.40	9.97	10.69
Na_2O	1.53	5.34	3.39	5.19	5.39	5.81	4.16	4.26	4.37
K_2O	0.15	2.70	1.26	4.11	1.16	2.36	4.52	1.37	0.60
P_2O_5	0.16	0.35	0.12	0.08	0.53	0.21	0.02	0.43	0.21
LOI	36.09	0.94	1.46	1.56	0.04	2.47	4.85	1.46	1.63
Total	100.08	99.22	100.46	99.74	100.21	100.24	99.24	98.42	100.62
Zr	24	178	125	592	199	128	262	216	145
Y	14	31	29	59	32	22	61	40	68
Sr	286	332	281	36	673	332	21	776	349
U	2	1	bdl	2	3	bdl	1	bdl	bdl
Rb	9	78	60	130	37	65	175	31	16
Th	bdl	12	8	17	8	8	18	10	4
Pb	3	13	7	17	8	11	27	6	0
Ga	2	17	15	21	18	15	19	19	17
Zn	23	68	59	67	61	47	68	78	103
Cu	bdl	15	16	bdl	25	13	bdl	18	71
Ni	14	4	6	10	34	6	7	39	42
Co	3	10	14	1	34	8	bdl	42	36
Cr	23	10	21	3	53	66	bdl	19	191
Ce	6	51	23	114	63	47	74	65	27
Ba	373	396	438	470	417	437	49	463	202
La	9	29	21	56	40	23	41	34	26
Nb	7	19	6	35	14	13	31	10	9
Ap		0.84	0.28	0.19	1.23	0.49	0.05	1.05	0.49
Il		2.13	1.10	1.25	3.02	1.03	0.23	3.10	2.98
Or		16.25	7.57	24.99	6.86	14.12	28.60	8.51	3.61
Ab		45.94	29.10	45.26	24.51	49.74	37.65	22.88	37.31
An		11.41	28.09	1.46	19.44	12.01	2.00	24.55	24.41
Mt		0.39	1.60	0.09	5.99	4.45	1.67	7.71	0.68
Hm		3.92	4.22	2.17	0.00	0.00	0.00	1.99	8.11
Di		4.50	1.23	0.00	18.15	8.99	0.00	19.16	20.47
Hy		0.68	5.46	1.35	0.00	0.00	1.08	0.00	0.00
Q		13.84	21.20	21.11	0.00	8.69	28.54	0.00	1.03
Ol		0.00	0.00	0.00	9.23	0.00	0.00	2.68	0.00
Ne		0.00	0.00	0.00	11.39	0.00	0.00	8.19	0.00
Cm		0.00	0.00	0.00	0.02	0.02	0.00	0.00	0.04
Mg#		27.49	38.88	24.25	99.61	35.91	27.16	45.66	40.23
SI		7.64	17.40	4.06	25.56	10.54	3.24	23.34	20.13
DI		76.03	57.87	91.36	42.76	72.55	94.79	39.58	41.95
al	3.91	35.81	34.73	45.41	23.26	33.93	44.44	24.34	25.04
fm	12.96	21.75	28.79	14.48	40.66	21.97	11.31	37.62	34.08
c	80.25	15.94	22.36	2.07	22.44	19.14	2.59	25.90	29.13
alk	2.88	26.50	14.11	38.04	13.64	24.97	41.65	12.14	11.75
si	25.14	240.83	211.38	337.05	109.32	215.43	418.90	108.40	129.09
k	0.06	0.25	0.20	0.34	0.12	0.21	0.42	0.17	0.08
ti	0.22	3.18	1.48	2.39	2.74	1.40	0.51	2.82	2.98
mg	0.72	0.29	0.43	0.27	0.49	0.37	0.27	0.47	0.42
w	0.26	0.77	0.82	0.76	0.34	0.57	0.59	0.63	0.82

Sample	MA-234A	MA-239	MA-240A	MA-240B	MA-246	MA-247	MA-248	MA-250	MA-252
SiO_2	72.55	73.63	73.50	73.28	65.48	24.54	64.90	49.35	53.22
TiO_2	0.11	0.09	0.09	0.07	0.42	0.31	0.89	1.30	1.17
Al_2O_3	12.22	12.75	13.48	13.07	14.96	5.79	19.35	17.97	17.57
Fe_2O_3	0.34	0.77	0.63	0.64	2.96	1.06	0.10	6.36	3.76
FeO	1.08	0.80	0.84	0.84	0.70	1.64	0.24	3.67	4.57
MnO	0.03	0.07	0.08	0.08	0.06	0.08	0.00	0.16	0.16
MgO	0.31	0.00	0.00	0.24	0.95	3.76	3.76	5.61	4.63
CaO	0.45	0.28	0.32	0.27	2.75	32.69	0.26	10.06	7.65
Na_2O	4.46	5.01	3.81	3.44	4.09	1.29	1.25	2.99	3.39
K_2O	4.51	4.22	4.53	4.47	2.94	1.32	0.34	0.73	1.78
P_2O_5	0.03	0.05	0.08	0.01	0.28	0.16	0.26	0.38	0.39
LOI	3.55	0.34	1.12	1.45	4.04	28.02	5.33	1.29	1.37
Total	99.64	99.01	98.48	97.86	99.63	100.66	96.68	99.87	99.66
Zr	105	314	305	312	136	24	133	99	168
Y	26	64	54	57	28	11	7	27	27
Sr	17	20	20	22	279	845	151	553	551
U	bdl	10	13	9	5	2	5	0	3
Rb	146	184	217	212	88	51	4	14	57
Th	14	17	19	15	bdl	bdl	bdl	bdl	bdl
Pb	21	37	39	39	22	5	209	4	16
Ga	16	21	19	21	15	5	26	16	19
Zn	31	70	71	70	47	54	bdl	62	59
Cu	bdl	bdl	bdl	bdl	18	22	bdl	45	26
Ni	1	bdl	3	0	12	79	0	59	40
Co	0	bdl	0	0	8	7	bdl	39	24
Cr	bdl	21	19	24	19	99	14	71	55
Ce	61	74	66	71	53	21	18	41	72
Ba	384	45	38	47	587	205	605	312	539
La	27	27	40	28	36	13	2	20	38
Nb	9	33	32	35	13	7	10	11	16
Ap	0.07	0.12	0.19	0.02	0.70		0.65	0.91	0.93
Il	0.21	0.17	0.17	0.13	0.86		1.88	2.53	2.28
Or	27.72	25.59	27.48	27.72	18.44		2.19	4.73	10.82
Ab	39.25	43.06	33.16	30.54	36.63		11.51	25.80	29.52
An	0.03	0.00	1.12	1.32	12.48		0.44	34.11	28.35
Mt	0.51	0.95	0.91	0.93	1.08		0.00	8.20	5.25
Hm	0.00	0.00	0.00	0.00	2.13		0.10	0.33	0.00
Di	1.78	0.99	0.00	0.00	0.00		0.00	11.09	6.51
Hy	1.48	0.29	0.91	1.60	2.52		10.14	9.11	12.42
Q	29.91	28.45	34.01	35.45	24.32		55.11	3.41	3.72
Ol	0.00	0.00	0.00	0.00	0.00		0.00	0.00	0.00
Ne	0.00	0.00	0.00	0.00	0.00		0.00	0.00	0.00
Cm	0.00	0.00	0.00	0.00	0.00		0.00	0.00	0.00
Mg#	29.54	0.00	0.00	23.25	31.98		95.19	99.74	99.76
SI	2.91	0.00	0.00	2.50	8.18		66.09	29.60	26.19
DI	95.88	97.10	94.65	93.71	79.39		68.81	33.94	44.06
al	43.67	45.27	49.54	49.06	40.75	7.09	60.08	26.10	28.51
fm	9.77	7.40	7.24	9.66	18.68	15.70	30.91	39.04	36.78
c	2.93	1.83	2.15	1.82	13.9	72.86	1.46	26.57	22.55
alk	43.63	45.50	41.07	39.45	26.98	4.35	7.56	8.29	12.16
si	439.90	443.50	458.30	460.56	297.94	51.05	341.78	121.63	143.70
k	0.40	0.36	0.44	0.46	0.32	0.40	0.15	0.14	0.26
ti	0.48	0.40	0.41	0.32	1.48	0.49	3.55	2.42	2.41
mg	0.28	0.00	0.00	0.23	0.35	0.74	0.95	0.53	0.52
w	0.22	0.45	0.40	0.40	0.78	0.29	0.26	0.59	0.41

Sample	MA-253	MA-254	MA-255	MA-256	MA-262	MA-263
SiO_2	59.96	61.51	66.69	64.41	60.10	62.42
TiO_2	0.60	0.55	0.52	0.54	0.59	1.31
Al_2O_3	17.40	17.56	15.31	16.84	16.72	17.83
Fe_2O_3	6.19	5.67	5.21	6.21	3.29	3.61
FeO	0.52	0.18	0.46	0.16	2.48	1.27
MnO	0.14	0.04	0.06	0.08	0.09	0.09
MgO	1.34	1.22	1.28	1.17	4.90	0.67
CaO	7.15	5.50	4.33	5.31	4.95	3.19
Na_2O	2.43	2.97	2.57	2.52	3.39	4.93
K_2O	1.34	2.73	2.02	1.76	2.16	3.75
P_2O_5	0.13	0.16	0.10	0.13	0.20	0.53
LOI	2.26	1.22	1.62	0.70	1.64	0.39
Total	99.46	99.31	100.17	99.83	100.51	99.99
Zr	124	133	112	127	107	510
Y	25	35	25	27	23	58
Sr	307	305	238	284	355	308
U	4	2	1	6	7	6
Rb	61	44	62	42	72	111
Th	bdl	bdl	bdl	bdl	bdl	1
Pb	11	10	13	14	15	24
Ga	16	17	15	16	14	23
Zn	53	68	79	56	53	95
Cu	17	16	8	15	18	8
Ni	1	bdl	3	3	0	bdl
Co	15	10	11	11	12	2
Cr	17	18	12	19	36	9
Ce	32	35	30	27	47	122
Ba	478	438	439	544	431	670
La	14	15	12	12	26	63
Nb	5	12	4	9	10	31
Ap	0.30	0.40	0.23	0.30	0.47	1.23
Il	1.16	0.40	0.99	0.34	1.14	2.51
Or	8.27	10.58	12.12	10.52	12.94	22.34
Ab	21.49	26.06	22.08	21.57	29.10	41.96
An	31.05	27.17	21.23	25.84	23.60	12.46
Mt	0.00	0.00	0.00	0.00	4.63	0.30
Hm	5.83	5.37	4.95	5.85	0.00	3.14
Di	0.00	0.00	0.00	0.00	0.00	0.00
Hy	3.49	3.14	3.24	2.96	13.36	1.72
Q	27.10	25.29	33.79	30.70	14.44	13.10
Ol	0.00	0.00	0.00	0.00	0.00	0.00
Ne	0.00	0.00	0.00	0.00	0.00	0.00
Cm	0.00	0.00	0.00	0.00	0.00	0.00
Mg#	26.47	27.16	28.82	24.68	61.18	53.85
SI	11.43	10.40	11.13	9.91	30.66	25.83
DI	56.86	61.93	67.99	62.79	56.47	77.40
al	38.44	39.64	38.59	39.07	31.18	40.92
fm	24.85	22.49	25.44	24.52	37.21	17.86
c	24.69	22.60	19.85	22.40	16.81	13.30
alk	12.02	15.27	16.12	14.02	14.79	27.92
si	224.80	235.57	285.29	253.65	190.28	242.92
k	0.27	0.28	0.34	0.31	0.30	0.33
ti	1.70	1.59	1.67	1.61	1.41	3.84
mg	0.30	0.31	0.32	0.28	0.62	0.22
w	0.91	0.96	0.90	0.97	0.53	0.70

APPENDIX 4. RARE EARTH ELEMENT ANALYSES

	MA-180	MA-234A	MA-132	MA-192A	MA-208	MA-56C	MA-232B	MA-220A	MA-256
La	18.12	5.68	41.28	2.29	15.06	17.75	6.42	15.82	16.87
Ce	39.69	19.11	78.42	7.37	36.36	34.66	24.57	41.25	33.82
Pr	4.21	2.03	8.30	0.93	4.46	3.58	2.62	4.14	4.02
Nd	13.12	7.04	25.51	3.41	15.65	10.64	9.28	13.45	13.43
Sm	3.31	2.28	5.59	1.20	4.17	3.13	2.57	2.35	3.77
Eu	1.15	0.49	1.80	0.36	1.34	1.12	0.22	0.36	1.31
Gd	1.08	0.64	2.10	0.30	1.28	0.99	0.87	1.17	1.30
Tb	0.29	0.24	0.53	0.12	0.44	0.27	0.36	0.25	0.42
Dy	0.72	0.68	1.39	0.30	1.20	0.72	1.12	0.67	1.16
Ho	0.21	0.29	0.43	0.12	0.45	0.27	0.51	0.20	0.51
Er	0.53	0.67	1.10	0.25	0.99	0.65	1.14	0.55	1.15
Tm	0.09	0.14	0.20	0.05	0.20	0.13	0.27	0.10	0.25
Yb	0.53	1.01	1.30	0.37	1.29	0.94	1.87	0.70	1.73
Lu	0.09	0.16	0.20	0.06	0.20	0.16	0.30	0.11	0.29

	MA-263	MA-121	MA-213	MA-240B	MA-201	MA-199	MA-230	MA-23	MA-27
La	43.84	30.92	29.82	18.61	43.45	38.78	27.03	22.30	21.51
Ce	100.48	50.97	56.94	52.98	85.80	45.10	60.15	47.31	44.31
Pr	11.77	7.23	6.29	6.02	11.59	9.01	6.91	5.63	5.19
Nd	39.72	23.47	19.47	20.04	36.60	29.51	22.87	21.75	19.77
Sm	9.21	5.60	4.62	4.96	8.52	6.03	5.09	4.15	3.81
Eu	2.77	1.84	1.53	0.30	2.18	1.81	1.75	1.43	1.27
Gd	3.19	1.65	1.61	1.80	2.83	1.77	1.88	4.04	3.82
Tb	1.11	0.55	0.45	0.72	1.01	0.60	0.61	0.58	0.57
Dy	3.04	1.42	1.20	2.15	2.83	1.51	1.67	3.59	3.33
Ho	1.17	0.44	0.41	0.95	1.09	0.39	0.60	0.66	0.63
Er	2.64	1.09	0.97	2.15	2.49	0.99	1.38	1.90	1.84
Tm	0.52	0.18	0.18	0.48	0.49	0.15	0.25	0.27	0.25
Yb	3.60	1.22	1.26	3.29	3.40	1.01	1.68	1.76	1.69
Lu	0.57	0.19	0.19	0.52	0.53	0.15	0.26	0.25	0.24

	MA-29B	MA-40	MA-166	MA-175	MA-226	MA-140	MA-53	MA-54	MA-34B
La	27.54	33.28	30.02	30.83	25.11	56.53	40.99	51.12	51.23
Ce	57.98	69.08	56.36	60.27	54.67	120.23	84.65	106.04	103.39
Pr	6.75	7.86	7.25	7.23	5.86	14.41	10.27	11.99	11.44
Nd	25.42	29.11	27.25	27.17	21.57	54.33	39.11	43.70	40.65
Sm	4.89	5.19	5.07	5.18	4.32	10.11	7.37	7.74	6.81
Eu	1.67	1.67	1.59	1.80	1.35	3.04	2.24	2.28	2.17
Gd	4.88	5.00	5.03	5.22	4.32	9.46	7.43	7.41	6.49
Tb	0.70	0.73	0.73	0.74	0.64	1.15	1.08	1.03	0.88
Dy	4.17	4.29	4.34	4.33	3.88	6.41	6.44	6.11	5.06
Ho	0.78	0.80	0.82	0.84	0.73	1.05	1.18	1.15	0.94
Er	2.28	2.35	2.36	2.44	2.15	2.89	3.39	3.42	2.72
Tm	0.32	0.33	0.33	0.35	0.31	0.37	0.47	0.50	0.39
Yb	2.19	2.29	2.18	2.28	2.09	2.33	3.02	3.44	2.63
Lu	0.32	0.32	0.30	0.32	0.30	0.32	0.42	0.50	3.64

	MA-10	MA-43	MA-65	MA-58A	MA-17	MA-38	MA-31	MA-73	MA-52
La	56.54	48.47	53.88	32.52	30.97	41.55	42.52	61.47	72.33
Ce	115.91	101.84	106.39	59.21	60.47	80.32	82.42	131.16	142.55
Pr	12.53	11.68	12.09	6.59	10.07	8.22	8.27	13.90	15.87
Nd	45.16	42.20	42.59	22.98	30.09	25.98	26.20	48.17	53.56
Sm	8.00	7.59	7.81	3.96	4.11	4.44	4.39	8.54	9.17
Eu	2.50	2.32	1.94	1.20	1.03	0.69	0.76	2.12	2.30
Gd	7.76	7.27	7.35	3.54	1.68	4.37	4.18	7.87	8.38
Tb	1.14	1.09	1.09	0.47	1.04	0.66	0.62	1.03	1.22
Dy	6.86	6.35	6.56	2.61	1.23	4.19	3.78	6.00	7.10
Ho	1.32	1.19	1.23	0.47	1.02	0.83	0.74	1.01	1.31
Er	3.99	3.61	3.66	1.37	1.11	2.70	2.28	2.99	3.89
Tm	0.59	0.53	0.54	0.20	1.02	0.41	0.36	0.40	0.57
Yb	4.07	3.68	3.75	1.33	1.02	2.96	2.61	2.69	3.96
Lu	0.61	0.54	0.53	0.19	1.08	0.44	0.39	0.37	0.55

	MA-186	MA-228	MA-84	MA-94	MA-122	MA-135	MA-143	MA-141A	MA-223
La	27.13	15.58	27.87	19.23	27.14	36.60	37.41	32.26	32.17
Ce	49.78	32.08	52.33	35.39	53.92	65.97	70.95	58.45	58.21
Pr	5.47	38.56	5.59	3.96	52.80	7.46	7.79	6.93	6.46
Nd	19.23	14.88	19.02	14.08	17.60	26.24	27.70	24.52	22.34
Sm	3.42	3.26	3.53	2.62	3.05	4.67	4.75	4.36	4.10
Eu	1.19	1.03	1.05	0.82	0.90	1.38	1.44	1.32	1.18
Gd	3.13	3.40	3.28	2.42	2.68	4.47	4.14	3.98	3.95
Tb	0.37	0.55	0.42	0.31	0.32	0.58	0.56	0.53	0.52
Dy	1.93	3.41	2.45	1.75	1.78	3.34	3.16	3.14	3.19
Ho	0.29	0.68	0.40	0.28	0.28	0.61	0.56	0.53	0.56
Er	0.81	1.99	1.24	0.82	0.78	1.83	1.66	1.71	1.67
Tm	0.09	0.30	0.17	0.11	0.10	0.26	0.24	0.24	0.24
Yb	0.61	2.09	1.15	0.69	0.68	1.74	1.58	1.62	1.68
Lu	0.08	0.31	0.16	0.09	0.09	0.26	0.23	0.23	0.24

	MA-193
La	26.76
Ce	51.25
Pr	5.54
Nd	18.92
Sm	3.50
Eu	1.04
Gd	3.49
Tb	0.47
Dy	2.79
Ho	0.51
Er	1.53
Tm	0.21
Yb	1.47
Lu	0.21

Note: Major elements are in wt.%, trace and rare earth elements are in ppm. CIPW normative mineralogy is in wt.% and calculated from the major element oxide data after normalizing the totals to 100 % on a volatile free basis.

$Mg^{\#}$(Mg-number)=100xMg/(Mg+Fe)

SI(Solidification index)=100xMgO/(MgO+FeO+Na_2O+K_2O)*

DI(Differentiation index)=q+or+ab+ne+lc+kp

APPENDIX 5

GEOLOGICAL MAP OF MEYDAN-ZILAN(ERCIS-VAN, TURKEY) AREA

Mehmet ARSLAN, 1992

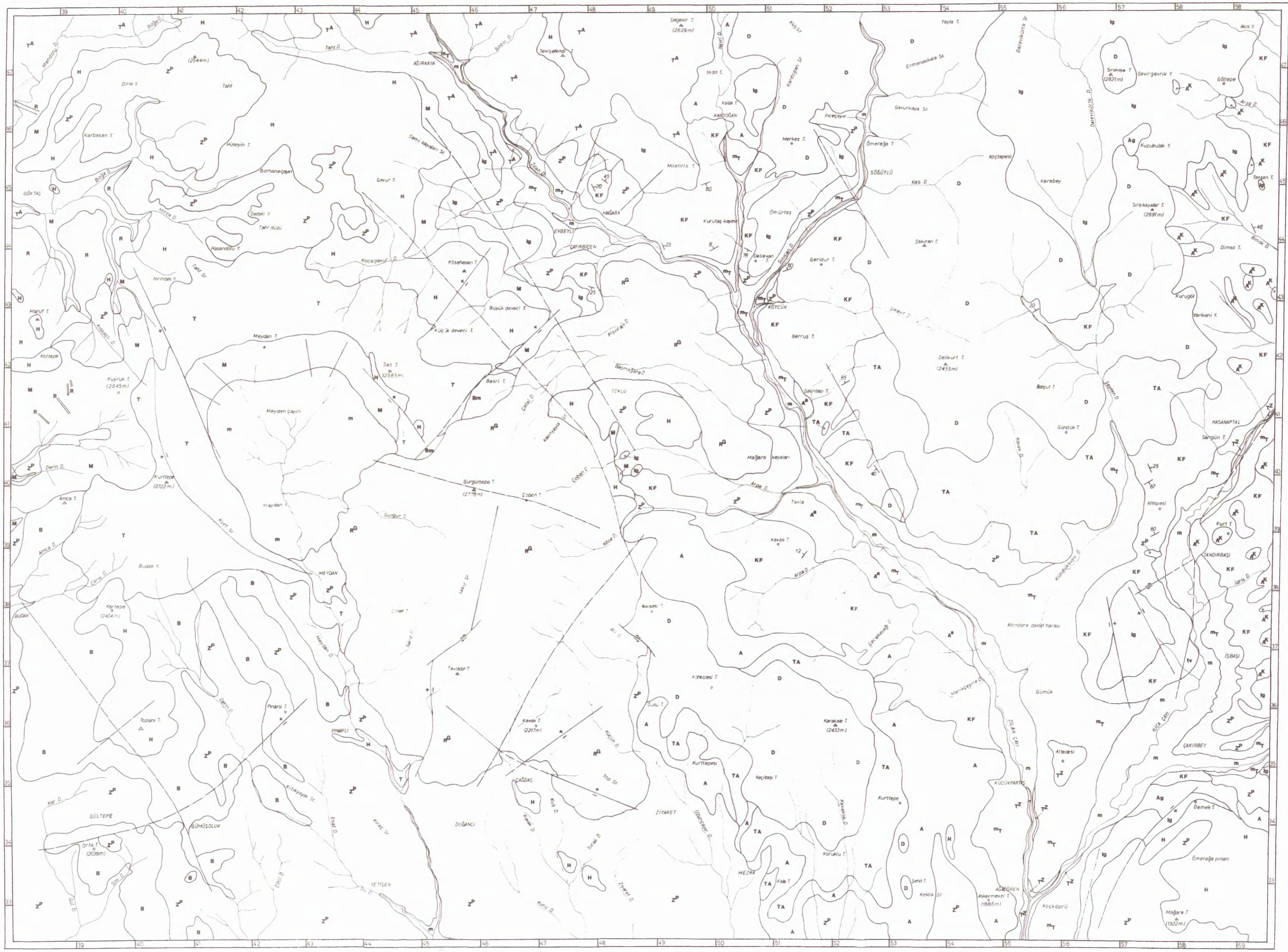

SYMBOLS

⟋	Formation Boundary
⟋	Dip Slip Fault
⫽	Strike Slip Fault
⟋	Possible Fault
⟋25	Strike and Dip
△ (1920m)	Triangulation Point
⟋	Stream

N

0 1 Km
SCALE

EXPLANATIONS

Age	Symbol	Unit
QUATERNARY	m	Alluvium
	m_T	Old Alluvium
	tv	Travertine
	τ^Z	Zilan Lava
	R^G	Gurgurbaba Lava
	Z^P	Pumice and Tuff Deposits
	R	Rhyolite Dome and Dykes
PLIOCENE	T	Trachyte
	Bm	Benmoreite
	M	Mugearite
	H	Hawaiite
	B	Alkali Olivine Basalt
	Ig	Ignimbrite
	Ag	Agglomerate
PLIOCENE	τ^A	Aladag Lava
	D	Dacite
MIOCENE	TA	Trachyandesite
	A	Andesite
	A^K	Kızıldere Lavas
	KF	Kızıldere Formation
	A^a	Altered Andesite

APPENDIX 5

GEOLOGICAL MAP OF MEYDAN-ZILAN(ERCIS-VAN, TURKEY) AREA

Mehmet ARSLAN, 1992